ADCHEM 2006

International Symposium on Advanced Control of Chemical Processes

Gramado, Brazil, April 2-5, 2006

Preprints Volume I

Papers of the 1st (Sunday) and 2nd (Monday) days

EDITORS

Francis J. Doyle III
University of California, Santa Barbara, CA, USA

Jorge O. Trierweiler
Federal University of Rio Grande do Sul, Brazil

Argimiro R. Secchi
Federal University of Rio Grande do Sul, Brazil

ASSISTANT EDITORS

Mehmet Mercangoz
University of California, Santa Barbara, CA, USA

Luciane S. Ferreira
Federal University of Rio Grande do Sul, Brazil

The ADCHEM Organizing Committees
gratefully acknowledges the support of:

Diamond Sponsor

PETROBRAS
www.petrobras.com.br

Gold Sponsors

Braskem
Petroquímica Brasileira de Classe Mundial
www.braskem.com.br

REFAP
Alberto Pasqualini - Refap S/A
www.refapsa.com.br

Silver Sponsors

ARACRUZ
www.aracruz.com.br

chemtech
A Siemens Company
PAVILION TECHNOLOGIES
www.chemtech.com.br

COPESUL
COMPANHIA PETROQUÍMICA DO SUL
www.copesul.com.br

Bronze Sponsors

aspentech
www.aspentech.com

Ipiranga Petroquímica
www.ipq.com.br

Support

UCSB
doyle.chemengr.ucsb.edu

UFRGS
UNIVERSIDADE FEDERAL DO RIO GRANDE DO SUL
www.eng.ufrgs.br/gimscop

Brazilian National Funding Agencies

CAPES
www.capes.gov.br

CNPq
Conselho Nacional de Desenvolvimento Científico e Tecnológico
www.cnpq.br

INTERNATIONAL PROGRAM COMITTEE

Francis J. Doyle III, USA—Chairman

Program Area Chairmen

Optimization and Scheduling
Stratos Pistokopoulos, UK

Batch Process Modeling and Control
Richard Braatz, USA

Process Control Applications
Robert Parker, USA

Model Based Control
Martin Guay, Canada

Modeling and Identification
Mayuresh V. Kothare, USA

Process and Control Monitoring
Dale Seborg, USA

MEMBERS

Allgöwer, Frank (Germany)
Alvarez, Jesus (Mexico)
Araujo, Ofélia (Brazil)
Arkun, Yaman (Turkey)
Bandoni, José A. (Argentina)
Barolo, Max (Italy)
Bequette, Wayne (USA)
Bonvin, Dominique (Switzerland)
Brambilla, Alessandro (Italy)
Christophides, Panagiotis (USA)
Cinar, Ali (USA)
Daoutidis, Prodromos (USA)
De Souza Jr., Mauricio (Brazil)
Edgar, Tom (USA)
Engell, Sebastian (Germany)
Forbes, Fraser (Canada)
Foss, Bjarne (Norway)
Gao, Furong (Hong Kong)
Gatzke, Edward P. (USA)
Georgakis, Christos (USA)
Giudici, Reinaldo (Brazil)
Hahn, Jürgen (USA)
Hasebe, Shinji (Japan)
Henson, Mike (USA)
Hoo, Karlene (USA)
Huang, Biao (Canada)
Jacobsen, Elling (Sweden)
Jorgensen, Sten Bay (Denmark)
King, Rudibert (Germany)
Kravaris, Costas (Greece)
Lee, Jay (USA)
Lee, Peter (Australia)
Lewin, Danny (Israel)
Lima, Enrique (Brazil)
Maciel Filho, Rubens (Brazil)
Marchetti, Jacinto (Argentina)
Marlin, Thomas E. (Canada)
Marquardt, Wolfgang (Germany)
McAvoy, Thomas (USA)
Morari, Manfred (Switzerland)
Moro, Lincoln F. (Brazil)
Nikolaou, Mike (USA)
Ogunnaike, Babatunde A. (USA)
Ohshima, Masahiro (Japan)
Nascimento, Claudio O. (Brazil)
Palazoglu, Ahmet (USA)
Park, Sunwon (Korea)
Perrier, Michel (Canada)
Preisig, Heinz (Norway)
Qin, Joe (USA)
Rawlings, Jim (USA)
Romagnoli , Jose (Australia)
Scali, Claudio (Italy)
Shah, Shirish L. (Canada)
Skogestad, Sigurd (Norway)
Soroush, Masoud (USA)
Swartz, Chris (Canada)
Thornhill, Nina (U.K.)
Ydstie, Erik (USA)
Yoon, En Sup (Korea)
Young, Robert E. (USA)
Yu, Cheng-Ching (Taiwan)

NATIONAL ORGANIZING COMITTEE

Jorge Otávio Trierweiler, Brazil — Chairman

Argimiro R. Secchi (UFRGS)
Darci Odloak (USP)
Luciane S. Ferreira (UFRGS)
Marcelo Farenzena (UFRGS)

ADCHEM 2006

The ADCHEM 2006 (International Symposium on Advanced Control of Chemical Processes) was held in Gramado, Brazil from April 2 to 5, 2006 and was organized under the auspices of International Federation of Automatic Control (IFAC) and Brazilian Society for Automation (SBA). The ADCHEM is a continuing series of international symposia held most recently in Hong Kong, China (2003/2004), in Pisa, Italy (2000), Banff, Canada (1997), Kyoto, Japan (1994), and Toulouse, France (1991). These meetings focus on advances in methods for modeling and control for all types of chemical processes. They are part of a three year rotation of IFAC meetings, which also include the IFAC DYCOPS Symposium Series (recently held in Boston, USA) and the IFAC World Congress.

Promoter Organizations:

IFAC

http://www.ifac-control.org/

http://www.sba.org.br/

Contents of Volume I – Sunday and Monday Program

Plenary Session

Keynotes 1 and 2

Session 1.1 - Applications of State Estimation and Monitoring

Session 1.2 - Advances in Modeling and Identification

Session 1.3 - Model Predictive Control

Keynotes 3 and 4

Session 2.1 - Optimization and Control of Biological Systems

Session 2.2 - Batch Processes

Session 2.3 - Optimization and Scheduling

Session 3.1 - Batch Processes

Session 3.2- Model Based Control

Session 3.3 - Process Control Applications

ADCHEM 2006

International Symposium on Advanced Control of Chemical Processes
Gramado, Brazil – April 2-5, 2006

SYSTEM ARCHITECTURE FOR PROCESS AUTOMATION: REVIEW AND TRENDS

Tariq Samad*, Paul McLaughlin, and Joseph Lu*****

*Honeywell Labs, 3660 Technology Drive, Minneapolis, MN 55418, U.S.A.,
tariq.samad@honeywell.com
**Honeywell Process Solutions, 1100 Virginia Drive, Fort Washington, PA 19034, U.S.A.,
paul.f.mclaughlin@honeywell.com
***Honeywell Process Solutions, 2500 W. Union Hills Drive, Phoenix, AZ 85027, U.S.A.,
joseph.lu@honeywell.com

Abstract: New developments in information technologies are radically transforming process automation. Their impact and benefit derive both from these technologies individually and from their convergence in new system architecture concepts. This paper reviews how process automation system architectures have evolved and discusses future trends. We draw an analogy between the synergistic new technologies being developed today and the technology landscape of the early 1970s—characterized by the near-simultaneous appearance of microprocessors, communication networks, CRT displays—that resulted in the first DCS system (the Honeywell TDC2000). Emerging technologies highlighted include wireless, embedded devices, service-oriented architecture, and application infrastructures.

Keywords: Architectures, process control, process automation, systems engineering, distributed control systems (DCSs), communication networks, information technology

1. INTRODUCTION

A process plant is a complex, multifaceted entity, a structured organization of physical elements, operated for economic and other criteria that are often industry-specific, and with a number of different stakeholders who can affect and/or are affected by its operation. Critical to the operation of the vast majority of plants today is an automation system that performs control and other advanced functions including, but not limited to, optimization, scheduling, and planning. The automation system ensures that appropriate parameters are measured, operational situations analyzed, more profitable opportunities explored and control actions calculated and taken, plant personnel kept informed and their knowledge and capabilities exploited, abnormal situations identified and addressed, and business processes integrated. The components and devices of the automation system perform functions that are essential for safe and efficient process operation, but it is the system architecture—the logical organization of the components and associated infrastructure—that often dictates choices of components and determines key system performance features such as reliability, capability, throughput, scalability, and cost. The system architecture also dictates how well applications are integrated, deployed and supported throughout their life-cycles, and in what manner the application functionality is delivered. A major theme for a system architecture is thus (1) to devise infrastructures, services, components, and their organizational schemes for best delivering the automation functions including advanced application capabilities; and (2) to integrate—to cohesively combine seemingly disparate components into an effective and consistent whole. It's the architecture that makes a system more than the sum of its parts.

System architecture is a hard thing to define crisply, let alone discuss in any depth. It is not a component, even an abstract one. It has enormous impact on how, and how well, we operate our plants, but its "emergent" nature is somewhat at odds with the research community's typical focus on specific technologies and their applications. Individual technology developments relevant to process automation are often discussed in depth, but we seldom examine how multifarious developments can result in the synthesis that is architecture.

This paper focuses on architecture for process automation systems. We first discuss the key issues related to process plant operations that are affected by automation system architecture. Next, we briefly review the history of process automation with

specific reference to the development of distributed control systems (DCSs). Several technology developments are likely to dramatically transform process automation architectures in the near future; we highlight some of these developments. We conclude with a comment on the connection between system architecture and research topics in the controls community. Readers seeking a broader architectural perspective on the process industries as enterprises may find the Purdue Enterprise Reference Architecture of interest (www.pera.net).

2. THE IMPACT OF ARCHITECTURE

Architectural choices can profoundly impact how well we manage and control industrial processes—indeed the scale and complexity of the typical plant elevates the importance of architecture. Here we briefly discuss the connection between system architecture and each of several "critical to quality" (CTQ) criteria.

2.1 Applications Capability

The number, the variety, and the sophistication of advanced software applications for process automation continue to grow, and the automation system architecture determines how rapidly and cost-effectively they can be developed, implemented, and maintained. Architecture impacts applications through functions and features such as support for data types, interprocess communication mechanisms, on-process migration, real-time scheduling policies, and componentization and interoperability of modular blocks.

Four classes of avanced applications can be differentiated:

- *Process effectiveness* applications provide better control/optimization, increase throughput, reduce operating cost and waste, improve product quality, and ensure regulatory compliance.
- *Asset effectiveness* applications predict and pre-empt asset malfunctions, reduce maintenance costs, prevent asset decay (e.g., corrosion), and enhance asset security
- *Business effectiveness* applications respond to seasonal change or volatility in markets. They optimize what to produce, when, and in what quantity.
- *People effectiveness* applications improve operator proficiency, reduce/avoid unplanned capacity loss, implement/audit best work practices, and turn data into actionable information or knowledge for plant staff.

2.2 Reliability

It is inevitable that automation components—sensors, transmitters, actuators, displays, panels, wires, routers, etc.—will fail or require offline maintenance. Given the quantity of automation equipment in a plant, in fact, it is a virtual impossibility that every piece of equipment is functioning correctly at any instant. Yet we expect—and generally realize—high levels of process uptime. In large part, this is because of reliability features that have been designed into the automation architecture. A number of architectural approaches that can help improve reliability have been adopted. We note four here:

- Reliability can be achieved via redundancy—e.g., parallel, dual communication networks.
- Fundamental to system reliability is the ability to diagnose for faults and to annunciate these faults to both plant personnel and operational logs. An undiagnosed fault in a redundant element means that the availability of the solution is no better than having a nonredundant element.
- A distributed system (if appropriately designed) can improve reliability over a centralized system by collocating (or more closely locating) critical components. Distributed systems are not universally more reliable than centralized ones, however; the former can be easier to maintain and upgrade and synchronization and consistency issues are of less concern.
- Aspects of system architecture beyond the physical also influence reliability. Thus communication semantics in process automation include "failure" signals that are separate from the "values" being communicated. A failure signal can trigger automatic reconfiguration or promptly raise an alarm for an operator.

2.3 Lowest Total Installed Cost (LTIC)

LTIC is an important decision criterion for new and upgrade installation of automation systems. With proprietary automation systems largely giving way to open ones, plant owners and managers have many more supplier options. The cost and ease of integration can vary substantially among alternatives. LTIC includes the product cost itself, as delivered, plus the cost of installing it in the plant and configuring it so that it can be brought online and integrated with the process automation system. The automation system architecture affects both installation and configuration. Wireless is now widely seen as a game changer in industrial automation, principally because it removes the need to run wire to every new device—especially valuable for upgrades to existing plants where the cost to add wiring is prohibitive. For a typical sensor installation today, the wiring cost handily exceeds the cost of the component itself, so wireless-enabled devices can command a premium if the process automation system architecture is wireless-capable. Often power and communication wiring are separately installed or power may be available at the point of installation anyway, so substantial savings are to be gained even if the wireless capability on a device is only for communication.

In addition to the physical installation and software installation and administration, configuration is also required. Whether hardware or software or a combination of both, a device will have parameters, methods, and other settings whose appropriate values must be specified. In many cases this configuration will require the use of purpose-built tools. The software architecture of the automation system in particular can affect ease of configuration. Autodiscovery features, Web servers and Web services, and shared semantic models are some features that can reduce configuration cost—by enabling, for example, a high-school-graduate operator to do the job instead of a trained engineer, by enabling the configuration to be performed remotely, and by reducing the time required for it.

We're not quite there yet, but we can envision a not-too-distant future in which a new device can be physically plugged into a network and be automatically discovered by the system and auto-configured, with only minimal human supervision.

2.4 Maintenance and Migration

A large continuous process will remain operational for decades, and any maintenance to or migration of the computer and control system components must be done in an online operational manner. This necessity presents a significant technical challenge for the automation system design team and for the end-user.

Online modification of the configuration of the system is a key requirement. Examples of online modifications include adding or removing new sensors, actuators and their interconnection to the control and monitoring system; adding new basic, supervisory or optimization controls; adding or upgrading human-machine interaction (HMI) consoles; loop tuning; and modifying the alarm and event reporting schema.

Online upgrade of all or part of the core system or application software is also a fundamental requirement; software releases can occur much more frequently (.5 to 2 years) than process shutdown cycles (3 to 8 years). View or control of any loops cannot be lost during software and system migration. Online upgrade typically depends on redundant computer and control components. In general, a secondary node is loaded with new software and is manually commanded to become the primary, while the primary remains in a passive backup state, with the original system software but able to resume its prior role. This capability is referred to as "load and go back."

Another significant migration and maintenance challenge for current DCS providers is the increased use of commercial-off-the-shelf (COTS) components, such as personal computers, servers, and network switches and routers. It is assumed by DCS customers that the supplier will ensure that the initial set of components will operate together correctly; it is also understood that the vendor shall provide methods for the customer to upgrade and replace these components over time while maintaining consistent online operations. The pace of change and obsolescence in PC and network technology far exceeds that of traditional DCS "proprietary" hardware.

2.5 Real-time Properties

Ultimately, what distinguishes a process automation system from an office automation system is the former's connection with a complex, dynamic physical system, an industrial process or plant. The process automation system is required for accurately and conveniently monitoring, controlling, and super-vising the operation of the process. Continuous processes pose particular challenges in this regard, in particular since the timing of measurements and actions will influence not just the timing of the process's evolution but its very nature. The right action but with timing off by a few seconds (or less) can be ineffective or potentially even disastrous.

Two timing properties that are especially crucial for feedback control are latency and jitter. Latency refers to end-to-end delays associated with communication, computation, and actuation. In general, the greater the latency the poorer the quality of control that can be achieved—actions can only respond to delayed measurements, not current ones. For disturbance rejection, excessive latency can result in larger disturbance perturbation and performance degeneration. Worse yet, there is no control design or tuning that can improve the rejection performance within the latency band. For discrete logic and/or safety control, long latency can result in a disqualification of the control system.

Jitter refers to the variability of latency measurement. For feedback control (or any discrete-time application) it is the end-to-end jitter that is important. Even if a required sampling rate is maintained on average, for example, jitter is undesirable. During design and simulation of feedback controllers, jitter is difficult to consider because almost all the formulas and theorems of discrete-time mathematics used in control design assume jitter-less sampling. If encountered in the online system, control quality can be significantly poorer than suggested by the simulation results.

2.6 Scalability

In that a distributed system has a large degree of variability with respect to how it is assembled and organized, it is imperative that the system be designed to ensure that overall performance targets, capacity limits, and topology deployments be considered in the up-front design. It is very difficult to scale a "small" system into a large system, and likewise, very difficult to scale a system designed to

be “large” into a cost-efficient and feature-bundled “small” system. An example of a small system would be one intended to control one piece of process equipment, and be constituted with a single HMI station, a single controller, and a small quantity of I/O (conventional or fieldbus-based). An example of a large system would be one designed to cover a large refinery, including all process elements (both continuous and discrete), all human-machine operations, and all business management functions.

2.7 Security

Security would not have been considered a “CTQ” a decade or two ago, beyond simple user classification and authentication (e.g. keys), but times and technologies have changed since. Both cyber and physical security are now top-of-mind considerations for automation systems. Computers in plants are now connected to the Internet. In some cases “air gaps” may be designed between the process-connected and Internet-connected parts of the automation system; in other cases the protection is a firewall. Wireless is already being adopted for some applications. Fortunately we do not know of any major accidents caused by cyberattacks, but “successful” pranks and inadvertent unauthorized accesses have been reported.

Unauthorized physical accesses are also a topic of concern, and there is increasing interest in access security, biometrics, and video surveillance. Integration within one automation infrastructure is the desired goal, not only for reasons of complexity and cost but also because of the synergy possibilities. For example, in addition to a password, a biometric recognition device could provide a second, automatic check for automation system access.

3. THE EVOLUTION OF SYSTEM ARCHITECTURE FOR PROCESS AUTOMATION

Process system architecture has gone through dramatic transitions since automation began to be applied on a broad scale to process plants, and we can already anticipate future revolutions. In this section we provide a brief and selective review of significant developments in process system architecture. Much of this section is derived from Przybylski (1989), James and Weir (1989), and Dallimonti (1985). The specific examples we discuss are largely Honeywell products and solutions since those are the ones we are most familiar with.

Not only were the first process automation systems not computerized, they did not even rely on electricity. All sensing and control was done pneumatically, with small-bore metal tubing used to convey pressurized air through the plant. Sensors would transform a measurement to an air pressure, actuators typically employed metal bellows to transform pressure to mechanical movement, and control was implemented via pneumatic devices.

The pneumatic system continued to serve as the model even after electrification. Instead of air pressure, a 4-20 mA current became the signal representation, but connections (now with wires) were point-to-point and controllers were assembled from discrete electronic components such as operational amplifiers, resistors, and capacitors.

Digital computers started to be used in industrial control in the 1950s, when the Ramo Woolridge Company (the precursor of TRW) won a contract to develop a computer control system for a catalytic polymerization unit at the Texaco Port Arthur, Texas refinery (Moore, 2003). At first, the computer was used only for data-logging, alarming, offline efficiency calculations and operator guidance. Process control was still done the old-fashioned way, with analog equipment.

The first completely digital computer-controlled systems relied on a centralized CPU, although analog controllers continued to be used for backup for reliability. With the advent of DCSs digital control began to be widely adopted.

3.1 The First DCS

Honeywell’s TDC 2000 (see Fig. 1) is generally recognized as the first digital distributed control system. Its development started with an internal proposal process in 1969 and culminated with the announcement of the system on November 11, 1975.

The TDC 2000 was revolutionary in its adoption and extension of new technologies:

- Board-based small programmable digital computers were developed that could serve as multiloop process controllers. The TDC 2000 featured the first 16-bit microprocessor in a commercial product. Each controller had 8 outputs, 8 control slots, and 16 inputs. It contained 16K × 10 bits ROM for the firmware and ran at a frequency of 3 Hz—thus 24 loops/sec. Control strategies that previously required a central minicomputer, with attendant reliability issues, could now be implemented on microprocessors. Timing, communication, and scheduling problems were greatly ameliorated.
- A serial digital communication network called the “Data Hiway” was used to link the controllers, the operator interfaces, and computers. This network was a primitive but pioneering local area network (although the term had not been coined and no such commercial technology existed then) with redundant media. (At the release event for the TDC 2000, the reliability of the Data Hiway was demonstrated

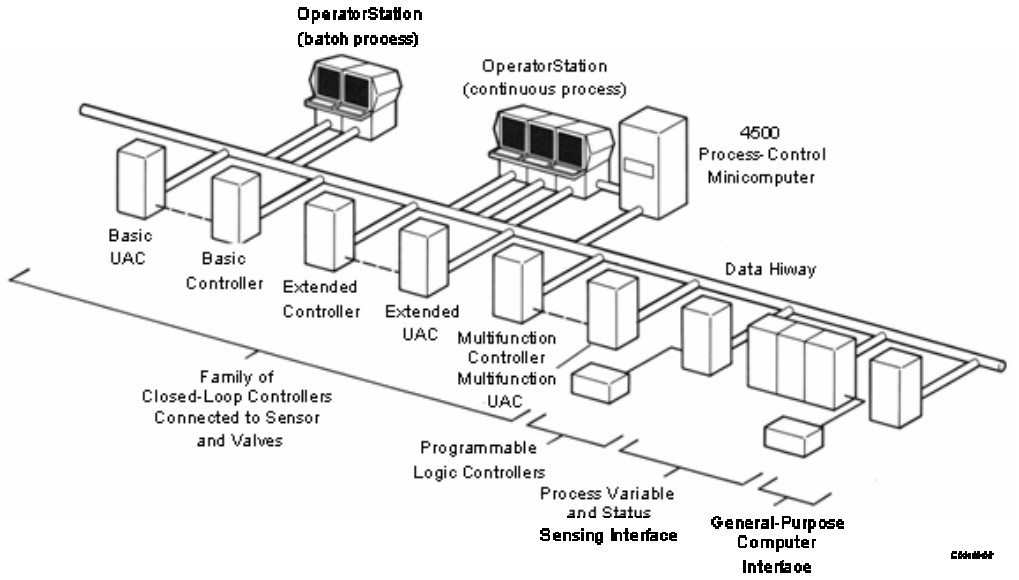

Fig. 1. The system architecture for the Honeywell TDC 2000 distributed control system. From (Dallimonti, 1985)

by severing a cable with an axe. Because of the redundant design, the system continued to function normally.) Communication was at 250 kb/sec and controlled by a central scheduler. The replacement of point-to-point wiring with one digital network resulted in huge savings in installation costs—up to a million dollars for large jobs.

- Instead of large instrument panels, the TDC 2000 featured desk-size consoles with several CRT displays in the control room (Fig. 2). The CRT-based operator console allowed easy configuration of displays without any programming by end users and for the first time enabled the combination of process operations, alarms, and configuration into a console. The operator station was a precursor to the graphical user interface (GUI), which would later appear in the Apple Lisa and Microsoft Windows. The majority of customers were skeptical of the CRT console innovation when it was first released, and the operator stations could be ordered with analog displays for a more familiar look.

The initial TDC 2000 release included the basic controller, the Data Hiway redundant network, the basic operator station, and the supporting systems infrastructure—cabinets, power systems, battery backup, and a number of options called "analog modules." The analog modules made the digital controller look like a traditional panel board and provided a level of backup capability. Later releases provided several enhancements, including the Data Hiway Port (DHP) that allowed non-Honeywell devices such as Modicon and Allen-Bradley PLCs to be interfaced to the TDC 2000 and a firmware enhancement to support sequence capability using SOPL (Sequence-Oriented Programming Language)—this was the first time a control-engineer-friendly language became available in a controller.

The TDC 2000 was introduced with the theme "A System You Can Start With, Live With, And Grow With." The basic controller, now 30+ years old, is still running many refineries worldwide. It has not been withdrawn from sale. The hardware platform has been recreated, due to parts obsolescence among other issues, as the "Universal Controller" product.

3.2 The TDC 3000

The first generation of distributed control systems were process *control* systems rather than process *automation* systems. Other limitations included a lack of discrete-event handling capability and the use of two separate operator interfaces (one for the supervisory computer and another for the basic controllers). The TDC 3000 (see Fig. 3) was Honeywell's next major DCS release and intended to address these limitations. The TDC 3000 subsumed the TDC 2000; multiple data hiways and distributed controllers and transmitters could be integrated within one TDC 3000 system. A "universal station" replaced the different operator stations. The TDC 3000 also included a node which tied all automation activities together—the Application Module (AM). The AM was an advanced, supervisory, and direct digital controller capable of spanning multiple low-level control products. A much faster (5 Mbps) fully redundant local area network for control, called the Local Control Network (LCN), was also included.

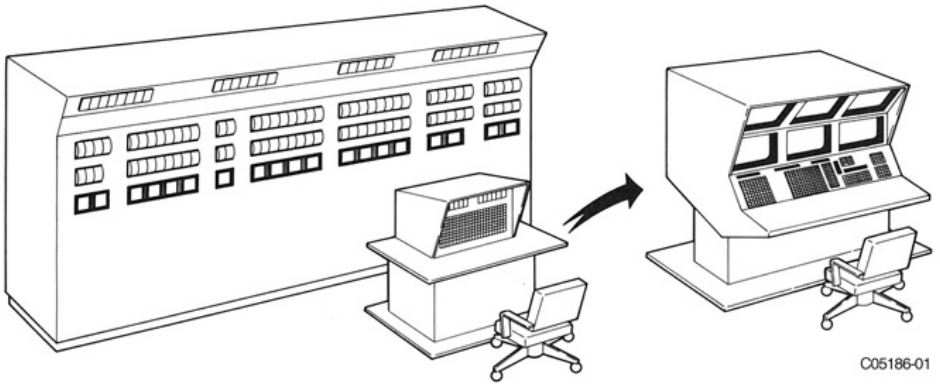

Fig. 2. TDC 2000 innovations included the replacement of the traditional instrument panel with analog displays (left) with a multi-CRT console (right). From (Dallimonti, 1985)

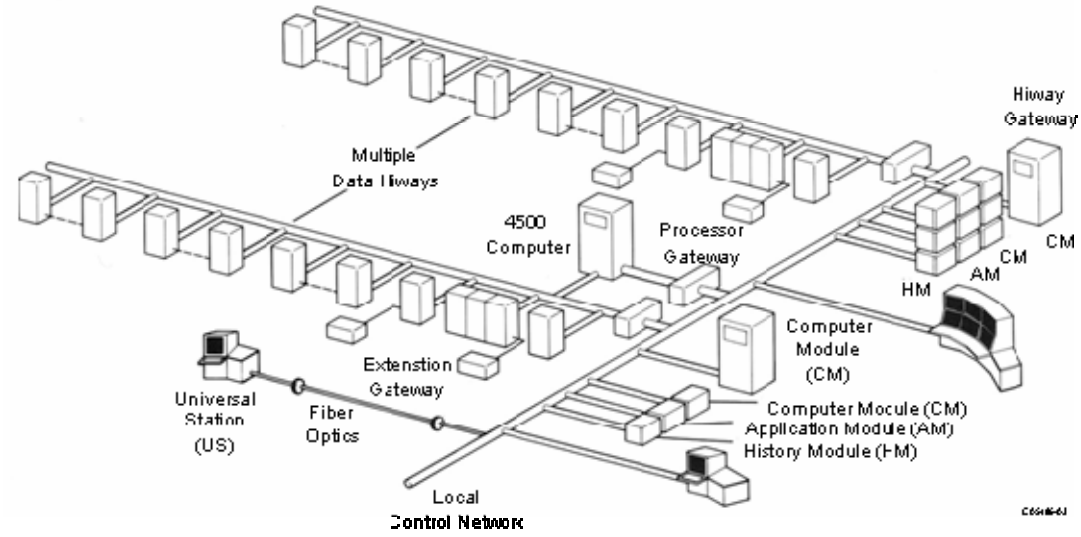

Fig. 3. The original system architecture for the Honeywell TDC 3000. The Local Control Network was introduced to integrate multiple TDC 2000 Data Hiways. The computer modules could be used for production scheduling and other information management tasks as well as for process control. From (Dallimonti, 1985)

A significant release of the TDC 3000 was R210, introduced in September, 1988. This brought in the Process Manager (PM) controller, the Universal Control Network (UCN), and the Network Interface Module (NIM). The PM controller featured dual redundant Motorola 68000 microprocessors and performed 160 loops/sec (with the R500 release of the High-Performance Process Manager with 68040 processors, the execution bandwidth increased to 800 loops/sec). The UCN was used to network PMs into the TDC system with the NIM serving as the LCN/UCN gateway.

With the TDC 3000, one automation system could be used to oversee and regulate the operation not just of a process but of an entire facility.

3.3 Recent Architectural Developments

More recent architectural, or architecturally relevant, developments in process automation include the following:

- Process control has historically been considered a continuous control application with occasional and limited need for discrete or event-based control, and specialized devices have generally been used. With the emergence of hybrid control applications, a need for controllers that integrate different time- and event-based control has arisen. Hybrid control in this context encompasses regulatory, discrete, batch, logic, and sequence control.
- Proprietary systems (such as the TDC) have given way to "open" systems, typically based on PCs running variations of Windows. PCs are not hosting closed-loop control for safety-critical applications, but they are now in widespread use for supervisory functions and advanced applications. Even for these purposes, extensions have been made to off-the-shelf systems, such as an ability to designate windows that cannot be occluded on the desktop.
- A related development is the popularity of fieldbuses—device-level digital communication networks that conform to established standards.

Several fieldbuses are now in widespread use, including Foundation Fieldbus, ControlNet, Profibus, and Modbus.

- In another related development, fieldbus technology has led to devices becoming more sophisticated. Sensor transmitters can have compression and scaling algorithms built in, and actuators can include processors on which control calculations can be executed. The control system has become even more distributed, with the potential for negative impact on overall system latency and jitter.
- With Moore's Law continuing its seemingly inexorable progress, more and more computing power has steadily become available at all levels of the automation architecture. Small multivariable model-predictive control (MPC) has migrated from level 3 (supervisory) to level 2 (regulatory) controllers, the difference being that the latter are embedded. This trend will continue, but we believe the emphasis will shift toward highly available MPC with easy-to-use interfaces and tools. Level 2 controllers are typically designed for hosting PIDs and their users are traditionally instrumentation technicians, unit operators, foremen, and supervisors. Architectural modification is needed before MPC and its supporting tools can be "natively" integrated into the embedded controller to further lower the knowledge required for implementing advanced control in closer-to-the-process controllers.
- Recent technology revolutions such as the World Wide Web are now finding their way into process automation systems. For example, process industry customers can subscribe to Honeywell's Loop Scout service (www.loopscout.com) and have process data automatically collected, communicated over the Web to a remote server, and analyzed by algorithms hosted on the server. Reports are then delivered to the customer via the Web (Fig. 4). The Web and the Internet are also enabling support for remote access and operation.

These and other recent developments are already making their way into commercial DCS offerings. For example, Honeywell's Experion PKS (www.experionpks.com) permits the integration of non-Honeywell process control and safety systems, interfaces with multiple fieldbus protocols, and uses Web technologies to provide a unified facilitywide view for local or distant staff.

Experion PKS also includes a control solution framework called the Control Execution Environment (CEE) which addresses hybrid control requirements. The CEE evolved from the marriage of process industry needs and emerging computer science theory—object oriented analysis and design. It was recognized that early DCSs forced users to think in terms of the control systems themselves and not of the process under control. Instead of thinking in "natural" terms of pumps, boilers, reactors and the like, process engineers were forced to model and design in terms of "points" and "parameters". The CEE approach was to apply object orientation to control system design so that users could design their automation configuration in the "natural paradigm," using function blocks organized in hierarchical control structures that mapped 1:1 to process elements and which could be templatized and reused for much faster and more reliable engineering.

In its latest version, CEE features a backplane-less design, using Fault-Tolerant Ethernet and a new I/O link as the basis for joining peer and subordinate devices. This packaging allows for much greater flexibility and mix of traditional and emerging IO devices, especially the various fieldbus networks and devices (Foundation, ProfiBus, HART, et al.).

The flexible, graphically oriented design paradigm that is exemplified by CEE is not the only approach that is needed for process control. Especially for larger-scale applications—e.g., model-predictive control for a unit or an optimization application—an ability to design and analyze at more aggregated levels is also essential. To this end, in the next section we discuss advanced application infrastructure as an emerging technology.

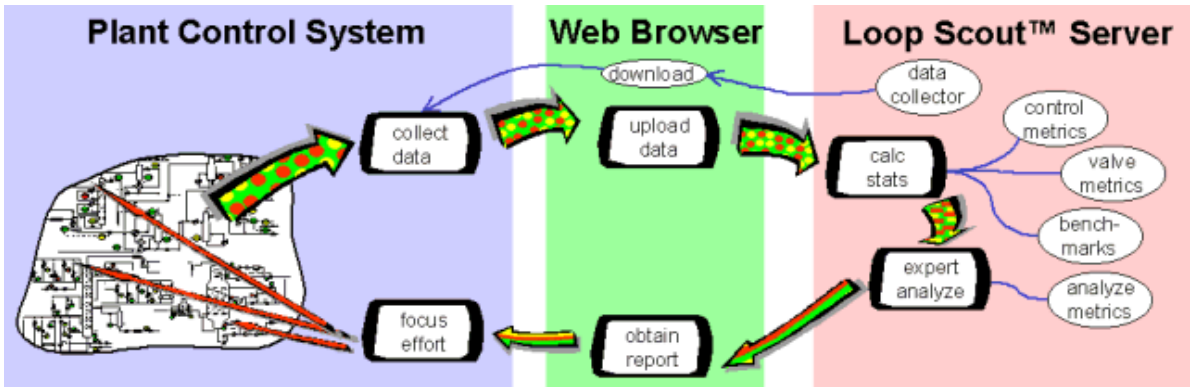

Fig. 4. Information flow for LoopScout™ (www.loopscout.com).

4. EMERGING TECHNOLOGIES FOR PROCESS AUTOMATION

4.1 Wireless

The replacement of wired communication with wireless may not seem a transformational change, but it is. Wireless enables substantial reduction in installation cost, it enables untethered mobility for humans and machines, and it enables measurement and monitoring of a quality and scale that could not previously have been envisioned.

The cost of wiring in an industrial plant has been estimated at up to $100 per foot and up to $2000 per foot for specialized applications (DOE, 2002). As noted above, the cost of equipment such as a sensor is generally substantially less than the wiring cost associated with installation. With broad-based adoption of wireless savings in the millions of dollars are likely to be realized.

Wireless is an architectural innovation that begets others. Today access to the control system is obtained from the control room or offices, through fixed displays. Already, portable wireless terminals are available in the market and being used in process plants. These devices provide limited functionality compared to what is available in the control room today, but we can envision a future where operators and other staff can obtain much the same information that is available to them in the control room virtually anywhere in the plant—for example, at the location of a potential problem. In effect, the control room will likely become distributed.

Although we measure the variables that we need to measure for effective operation of a plant, there are many gaps in our measurements that limit performance and reliability. With sensors becoming increasingly miniaturized and wireless promising an order-of-magnitude-plus reduction in installation cost, we can foresee much more use of sensing. Wireless may be a harbinger of a "pervasive sensing" paradigm in process automation. Sensors could also be installed on a temporary basis for asset management—e.g., when there is an early indication of degradation, to defer replacement until necessary with minimum down time.

Wireless technology has to progress significantly before these visions can be realized. Two challenges in particular are critical to overcome for process industry applications: power management and reliability. With thousands of potential wireless devices, battery lifetimes on the order of a year or so will require full-time staff just for battery replacement. Better energy storage and harvesting technologies as well as more intelligent power usage approaches are needed. In the foreseeable future, wireless devices may often be line-powered—communication, not power supply, may be wireless. The reliability problem would also be ameliorated in this case, since higher-power transmission would exact less operational cost.

4.2 Intelligent Network Devices

Automation architectures are often structurally complex and hierarchical because of the variety of different protocols and communication media used for different functions. Integration requires extensive use of a variety of bridges and gateways. Recently, a new class of network devices have appeared that can directly connect to multiple networks and serve as unified intelligent gateways (Tridium, 2003). Ports for multiple types of network connectors and protocol conversion between a supervisory IP (Internet protocol) network and a variety of control networks including Modbus, Cnet, LON, and BACnet can be integrated within one device.

Network-connected devices now also increasingly feature embedded Web servers. Through any Internet connection, these devices can serve up Web pages including graphics, parameter values, and configuration screens. Lower-level sensor and control equipment that is connected to these devices can then be directly configured and monitored from a browser anywhere through a secure connection.

This technology is first making its mark in building management systems (Fig. 5), but it is relevant (with appropriate caveats or modifications) for industrial automation as well.

We note an intriguing research challenge in this context. A representation formalism needs to be developed for the process industries that can capture the variety and complexity of process equipment in a structured way that explicitly records semantics, relationships, and dependencies.

4.3 Service-Oriented Architecture

Today's automation systems deliver much of their functionality through software programs: monitoring, estimation, control, and optimization algorithms; visualization, trending, and other operator aids; integration bridges with business and supplier databases; etc. We often refer to such software as "applications," but this term has connotations—packaged, stand-alone, purposefully obtained—that can be misleading as new software architectures are developed and adopted.

An exciting example of a new software architecture methodology is service-oriented architecture (SOA) (Reekie and McAdam, in preparation). SOA is founded on the provision and consumption of "services," which are software programs in a distributed computing environment. Applications become much more loosely bound to one another through exposed service contracts as opposed to the

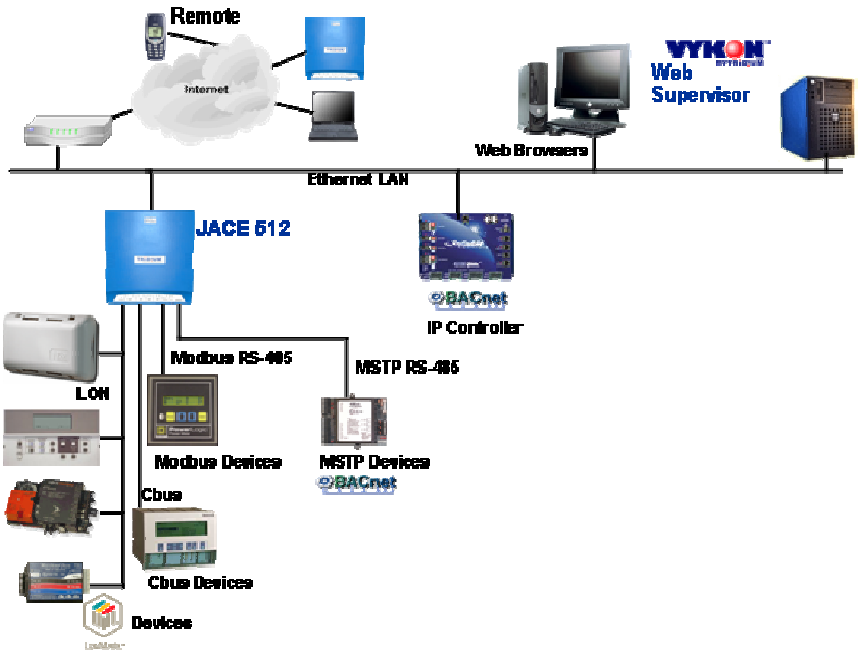

Fig. 5. A new architecture for building management systems, with intelligent network devices featuring embedded Web servers and multiprotocol capabilities (www.tridium.com).

prior model of application programming interfaces (APIs). These programs can be resident on a remote, connected site (typically via the Web). They are autonomous in the sense that they can serve useful functions on their own, yet they can be composed with other services when needed; their functions and interfaces are well-defined in an explicit modeling language (e.g., some XML variant or extension) with the result that other programs can automatically reason about them and compose them. SOAs also provide automated discovery and publishing, with the result that new services can be developed and integrated at any time with as much (or as little) human supervision as desired. In principle at least, a university team could develop a new monitoring or visualization tool and "publish" it on its Web site. It could be discovered by the automation system of a plant which would recognize that an improved monitoring service is needed. A trial version could be downloaded for offline testing. Once verified, it could be brought online. Commercial service providers would be able to provide a pay-per-use service which could be automatically negotiated and engaged. Plantwide models could automatically be composed from component models developed by different vendors, with tuning to the actual plant done through another service. Thus, among other benefits, SOAs open up new possibilities for business delivery and collaboration models.

The main challenge in the broad-based adoption of SOA is in how loosely coupled, widely distributed services can be integrated in an automation system in a way that is consistent with architectural qualities such as reliability, availability, manageability, migration/upgrade, and security.

4.4 Infrastructure for Advanced Applications

The automation system is being envisioned as the control and decision support centre for just-in-time manufacturing. It is asked to handle not only basic and advanced control, economic optimization, production/maintenance scheduling, and long-term planning, but also asset management, decision support, best practices implementation, and overall business agility improvement. The trend is also driven by the desire for broader participation from users, vendors, consultants, and third parties in various automation activities and practices.

An aspect of system architecture that relates to the ability of the automation system to serve these functions and stakeholders is the infrastructure that the architecture provides for developing, deploying, and maintaining advanced software applications.

The attributes required for an advanced application infrastructure include (a partial list):

- support for resources and services that can handle a mix of "hard" real-time, "soft" real-time and non-real-time applications;
- efficient execution of a mix of continuous, discrete, and transaction-based applications;
- a suitable namespace and organizational scheme;
- an ability to process complex data in system components and services, including communication schemes, data integrity, and presentations and timely updating of complex data;
- support for version control, application deployment, update, and migration;
- ability to isolate an application crash from the rest of the system—particularly needed for customer-created applications;
- support for application "plug & play" and componentization.

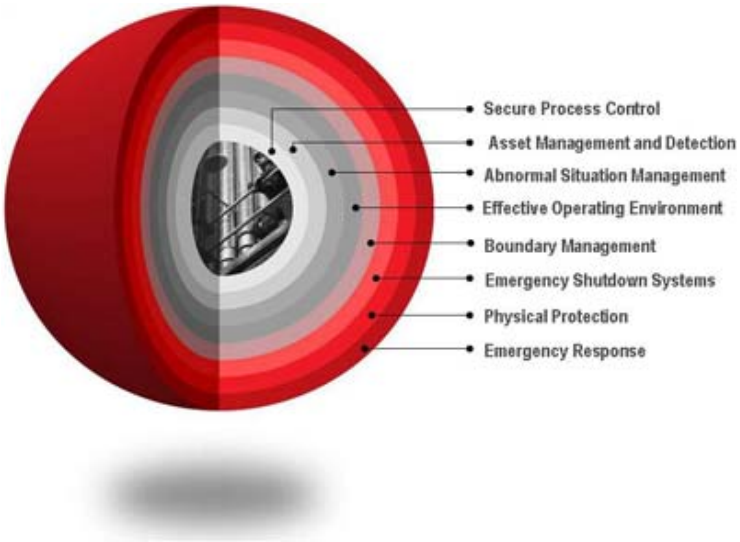

Fig. 6. A layered protection framework for integrated process safety. From (Honeywell, 2005)

See Horn et al. (2005) for a recent application infrastructure development, Uniformance Real Time (URT), that addresses several such issues and Havlena and Lu (2005) for examples of how the development and deployment of advanced applications can benefit from such infrastructure.

5. INFORMATION TECHNOLOGIES AND PROCESS AUTOMATION

Progress in automation architecture since the advent of computer-based control has steadily loosened constraints of collocation, bandwidth, integration, and access. But it seems only a slight overstatement to say that recent technology developments promise to completely remove such constraints. Trends in system architecture portend connectivity on demand, boundaryless systems, and global information access. This is not to say that future process automation systems will not impose any restrictions on human-automation-process interactions, but that the restrictions may be based on functional and operational requirements, not derived from technological limitations.

In our prognostications we must not forget that we are concerned with process automation, not office automation. The "CTQs" we noted earlier cannot be ignored. Reliability or real-time responsiveness cannot be compromised when we are considering process-connected equipment. Installation cost concerns will continue to often trump technology innovation. Whether through "loops-per-operator" or (more likely) some other metric, staff size will remain a point of scrutiny. The trends we have highlighted did not arise in the process control space; as with microprocessors, CRTs, and communication networks they are being borrowed and extended from more general information technology developments.

The security challenge is worth emphasizing. With process automation evolving toward open, integrated, wireless, nonlocalized system architectures, there are potentially many more points of access and hence vulnerability. Hackers, phishers, spammers, not to mention terrormongers must be guarded against. But the intersection of the physical and the IT world that is represented by process automation implies that cyber and physical security must be coordinated and that safety and security must be jointly considered. Thus, there is no single solution or silver bullet. Multiple protections and a holistic perspective are necessary. In this context, Fig. 6 illustrates a layered framework for process safety and security, with different levels of protection and response available to manage a variety of problems. Today's automation systems already have footprints that extend into cyberspace beyond the control system per se and into physical space beyond the plant perimeter (e.g., wireless signals). A sophisticated, multifaceted approach is recommended, and will, with appropriate extensions, be essential as economics and performance considerations drive us toward even more open and globally connected architectures.

6. CONCLUSIONS

Research in process control has by and large been an algorithmic enterprise. Variations of PID, automatic tuning, loop shaping, model-predictive control, filtering and estimation, inferential sensing, statistical process monitoring, sensor validation... developments in these areas are the marks and milestones of progress. It is not just in the research literature where these contributions in algorithms and theory have made an impact; industrial processes operate more reliably, more efficiently, and more productively as a result of this knowledge base.

It is easy to overlook the role of automation system architecture in the advancement of process control

practice. Enhancements in computation and memory, communication networks, operator interfaces and interaction modalities, sensing and actuation infrastructure, software technologies, and design, development, and deployment capabilities have been necessary preconditions for deriving operational benefits from research results.

Developments in information technologies continue apace. Indeed, we have claimed in this paper that the convergence of new technologies today is reminiscent of an earlier convergence, one from three decades ago and that led to the development of the first DCS with all the attendant benefits of that revolutionary advance. This assertion raises interesting questions, in particular: What new research directions in process control will be motivated by these architectural innovations and what dramatic practical improvements can be envisioned? These questions will be answered in course, but by anticipating the answers the research community can help shrink the research/practice gap and expedite the process of achieving economic impact.

ACKNOWLEDGEMENTS

We thank R. McAdam for contributions to the material on service-oriented architecture.

REFERENCES

Dallimonti, R (1985). The development of TDC 2000. *Scientific Honeyweller*, **vol 6**, no. 4, pp. 23-28.

DOE (2002). Industrial Wireless Technology for the 21st Century. Office of Energy Efficiency and Renewable Energy, U.S. Department of Energy. Available online at http://www.eere.energy.gov/industry/sensors_automation/pdfs/wireless_technology.pdf

Havlena, V. and J. Lu (2005). A distributed automation framework for plant-wide control, optimisation, scheduling and planning. In *Selected Plenaries, Milestones and Surveys, 16th IFAC World Congress*, P. Horacek et al. (ed.), pp. 80-95.

Honeywell (2005). Integrated safety. Available online at http://hpsweb.honeywell.com/Cultures-/en-US/Services/IndustrialSecurity/Cyber-Security/default.htm.

Horn, B. et al. (2005). Platform for advanced control applications. *Proc. 16th IFAC World Congress*, Prague.

Moore, J.F. (2003). Creating profit with computers: my life as CEO of Bonner & Moore Associates. *Annals of the History of Computing*, **vol. 25**, no. 3, July-Sept. 2003 pp.30 - 47.

Przybylski, F. (1989). Industrial control: a tutorial. *Scientific Honeyweller*, vol. 10, no. 1, pp. 6-18.

Reekie, J. and R. McAdam (in preparation). *A Software Architecture Primer*.

Tridium (2003). *Unifying Automation Systems with a Web-enabled Software Platform: The Need for an Automation Framework.* White paper. Available online at http://www.tridium.com/library/whitepaper/UnifyingAutomationSystemsWithWebEnabledPlatformWP.pdf.

ADCHEM 2006

International Symposium on Advanced Control of Chemical Processes
Gramado, Brazil – April 2-5, 2006

FEEDBACK CONTROL FOR OPTIMAL PROCESS OPERATION

Sebastian Engell

Lehrstuhl für Anlagensteuerungstechnik (Process Control Laboratory)
Department of Biochemical and Chemical Engineering
Universität Dortmund
D-44221 Dortmund, Germany
astwww.bci.uni-dortmund.de

Abstract: Starting from the statement that the purpose of process control is to achieve optimal process operations and that optimal tracking of setpoints is in most cases only a means to this end, different approaches how to realize optimal process operation by feedback control are reviewed. The emphasis is on direct optimizing control by optimizing an economic cost criterion online on a finite horizon where the usual control specifications in terms of e.g. product purities enter as constraints and not as setpoints. The potential of this approach is demonstrated by its application to a complex process which combines reaction with chromatographic separation. Issues for further research are outlined in the final section.

Keywords: Process control, online optimization, predictive control, optimizing control, real-time optimization, finite horizon optimization, chromatography.

1. INTRODUCTION

From a process engineering point of view, the purpose of automatic feedback control (and that of manual control) is *not* primarily to keep some variables at their setpoints as well as possible or to nicely track setpoint changes but to operate the plant such that the net return is maximized in the presence of disturbances and while the model used for plant design does not represent the real process exactly so that an operating regime that was optimized for the plant model will not lead to an optimal operation of the real plant, exploiting the available measurements. This has been pointed out in a number of papers (e. g. Morari, et al., 1980, Narraway, et al., 1991, Narraway and Perkins, 1993, Zheng, et al., 1999, Skogestad, 2000) but nonetheless almost all of the literature on automatic control and controller design for chemical processes is concerned with the task to make certain controlled variables track given setpoints or setpoint trajectories while assuring closed-loop stability. In chemical process control, however, good tracking of setpoints is mostly of interest for lower level control tasks. This is one reason why managers and process engineers often consider the choice and the tuning of controllers as a subordinate task, comparable to the procurement and maintenance of pumps or valves for a predefined purpose.

In their plenary lecture at ADCHEM 2000, Backx, Bosgra and Marquardt (2000) stressed the need for dynamic operations in the process industries in a increasingly marked-driven economy where plant operations are embedded in flexible supply chains striving at just-in-time production in order to maintain competitiveness. Minimizing operation cost while maintaining the desired product quality in such an environment is considerably harder than in a continuous production with infrequent changes, and this cannot be achieved solely by experienced operators and plant managers using their accumulated experience about the performance of the plant. Profitable agile operation calls for a new look on the integration of process control with process operations. In this contribution, we give a review of the state of the art in integrated process optimization and control of continuous processes and highlight the option of direct or online optimizing control (also called 1-layer approach (Zanin, et al., 2002) or full optimizing control (Rolandi and Romagnoli, 2005)).

First the idea to implement the optimal plant operation by conventional feedback control, termed "self-optimizing control", is discussed in Section 2. In highly automated plants, the goal of economically optimal operation is usually addressed by a two-layer structure (Marlin and Hrymak, 1997). On the upper layer, the operating point of the plant is optimized based upon a rigorous nonlinear stationary plant model (real-time optimization, RTO). The optimal operating point is then characterized by setpoints for a set of controlled variables that are passed to lower-level controllers that keep the chosen variables as close to their setpoints as possible by manipulating the available degrees of freedom of the process within certain bounds. The two-layer structure has certain drawbacks. As the optimization is only performed intermittently, the adaptation of the operating conditions is slow. The manipulated variables cannot be kept at their constraints if they are used to reduce the variations of the controlled variables, thus the operating point cannot be at the constraints but some margin must be reserved for the feedback control layer. Thirdly, different models are used leading to inconsistencies. These issues are partly addressed by schemes in which the economic optimization is integrated within a linear MPC controller on the lower level, as discussed in section 4.

Recent progress in numerical simulation and optimization algorithm enables to move from the two-layer architecture to direct online optimizing control. In this approach, the available degrees of freedom of the process are directly used to optimize an economic cost functional over a certain prediction horizon based upon a rigorous nonlinear process model. The regulation of quality parameters, which is usually formulated as a tracking or disturbance rejection problem, can be integrated into the optimization by means of additional constraints that have to be satisfied over the prediction horizon. The applicability of this integrated approach is demonstrated for the operation of simulated moving bed chromatographic processes. Finally, open issues and possible lines of future research are discussed.

2. OPTIMIZATION BY REGULATION (SELF-OPTIMIZING CONTROL)

The idea behind what was termed self-optimizing control by Skogestad (2000) was outlined already in Morari, et al. (1980): a feedback control structure should have the property that the adjustments of the manipulated variables that are enforced by keeping some function of the measured variables constant are such that the process is operated at the economically optimal steady state in the presence of disturbances. Morari et al. explicitly stated that the objective in the synthesis of a control structure is "*to translate the economic objectives into process control objectives*", a point of view that has thereafter found surprisingly little attention in the literature on control structure selection. Skogestad formulated the goal somewhat more modestly: to select the regulatory control structure of a process such that if the selected controlled variables are driven to suitably chosen setpoints, steady-state optimality of process operations is realized to the maximum extent possible. The selection is done with respect to the stationary process performance only, the consideration of the dynamics of the controlled loops follows as a second step. This reflects that from a plant operations point of view, a control structure that yields nice transient responses and tight control of the selected variables may be useless or even counterproductive if keeping these variables at their setpoints does not improve the economic performance of the process. The goal of the control structure selection is that in the steady state a similar performance is obtained as would be realized by optimizing the stationary values of the operational degrees of freedom of the process for known disturbances and parameter variations. Thus the relation between the manipulated variables $\underline{u}$ and the disturbances $\underline{d}$ $\underline{u}_{con}=f(\underline{y}_{set},\underline{d}_i)$ which is (implicitly) realized by regulating the chosen variables to their setpoints should be an approximation of the optimal input $\underline{u}_{opt}(\underline{d}_i)$. The application of this idea to the selection of control structures has been demonstrated in a number of application papers (Larsson, et al., 2001, 2003, Scharf and Engell, 2005).

The effect of feedback control on the profit function J in the presence of disturbances can be expressed as (Scharf and Engell, 2005)

$$\begin{aligned}\Delta J = {} & J(\underline{u}_{nom}, d=0) - J(\underline{u}_{nom}, \underline{d}_i) \\ & + J(\underline{u}_{nom}, \underline{d}_i) - J(\underline{u}_{opt}, \underline{d}_i) \\ & + J(\underline{u}_{opt}, \underline{d}_i) - J(\underline{u}_{con}, \underline{d}_i).\end{aligned} \tag{1}$$

The first term is the loss that would be realized if the manipulated variables were fixed at their nominal values, the second term represents the effect of an optimal adaptation of the manipulated variables to the disturbance $\underline{d}_i$, and the third term is the difference of the optimal compensation of the disturbance and the compensation which is achieved by the chosen feedback control structure. If the first term in (1) is much larger than the second one, or if all terms are comparatively small, then a variation of the manipulated variables offers no advantage, and neither optimization nor feedback control are required for this disturbance. If the third term is not small compared to the attainable profit for optimized inputs for all possible regulating structures, then online optimization or an adaptation of the setpoints should be performed rather than just regulation of the chosen variables to fixed pre-computed setpoints.

Eq. (1) represents the loss (which may also be negative, i.e. a gain) of profit for one particular disturbance $\underline{d}_i$ and a fixed control structure. The economic performance of a control structure can then be measured by

$$\Delta J = \int_{-d_{1,\max}}^{d_{1,\max}} \cdots \int_{-d_{n,\max}}^{d_{n,\max}} w(d)\left(J(u_{nom},d) - J(u_{con},d)\right) dd_1 \ldots dd_n \tag{2}$$

where $w(\underline{d})$ is the probability of the occurrence of the disturbance $\underline{d}$, neglecting the effect of potential constraint violations. As feedback control is based on measurements, errors in the measurements of the controlled variables must be taken into account. A variable may be very suitable for regulatory control in the sense that the resulting inputs are a good approximation of the optimal inputs, but due to a large measurement error or a small sensitivity to changes in the inputs, the resulting values $\underline{u}_{con}$ may differ considerably from the desired values. This was discussed in a qualitative fashion by checking the sensitivity of the profit with respect to the controlled variables in (Skogestad, 2000). An alternative is to consider the worst case control performance for regulation of the controlled variables to values in a range around the nominal set-point $\underline{y}_{set}$ which is defined by the measurement errors (Scharf and Engell, 2005). For a disturbance scenario $\underline{d}_i$, the performance measure of a control structure is:

$$\begin{aligned} &\min_{\underline{u}} J(\underline{u},\underline{d}_i,\underline{x}) \\ &s.t.: \dot{\underline{x}} = \underline{f}(\underline{u},\underline{d}_i,\underline{x}) = 0 \\ &\quad \underline{y} = \underline{m}(\underline{x}) = \underline{M}(\underline{u},\underline{d}_i) \\ &\quad \underline{y}_{set} - \underline{e}_{sensor} < \underline{y} < \underline{y}_{set} + \underline{e}_{sensor}, \end{aligned} \tag{3}$$

where $\underline{f}$ represents the plant dynamics. A regulatory control structure that yields a comparatively small value of the minimal profit is not able to guarantee the desired performance of the process in the presence of measurement errors and hence is not suitable. This formulation includes the practically relevant situation where closed-loop control leads to a *worse* result than keeping the manipulated variables constant at their nominal value. This will usually happen for small disturbances, as illustrated by Fig. 1 where the effect of disturbances of different magnitudes on the performance of a process is illustrated for fixed nominal inputs, optimized inputs, and feedback control with and without measurement errors. For small disturbances, keeping the controlled inputs at their setpoints is better than reacting to disturbed measurements. It is therefore important to include scenarios with small disturbances and not only those with very large ones into the set of disturbances that are considered in the analysis of the self-optimizing capacity of a control structure.

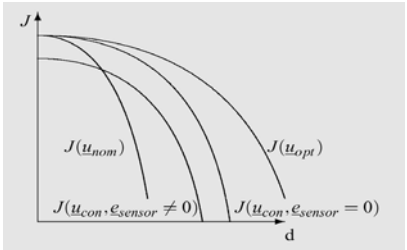

Figure 1: Schematic representation of the influence of a disturbance on the profit for different control approaches in the presence of measurement errors

Application studies have shown that the profit loss that is obtained by using regulation instead of steady-state optimization can be quite low for suitably chosen control structures. E.g., in (Larsson, et al., 2001) a performance loss of less than 5% is reported for the Tennessee Eastman benchmark problem (Downs and Vogel, 1993). The above analysis and subsequent control structure selection so far are limited to disturbances or variations of the plant behavior that persist over a very large horizon compared to the plant dynamics. The inclusion of disturbances with a higher bandwidth is an open issue.

3. REAL-TIME OPTIMIZATION (RTO)

The established approach to create a link between regulatory control and optimization of the economics of the unit or the plant under control is *real-time optimization* (RTO) (see e. g. Marlin and Hrymak, 1997, and the references therein). An RTO system is a model-based, upper-level control system operated in closed-loop that provides setpoints to the lower-level control systems in order to maintain the process operation as close as possible to the economic optimum. The general structure of an RTO system is shown in Figure 2. Its hierarchical structure follows the ideas put forward already in the 1970's (Findeisen, et al., 1980).

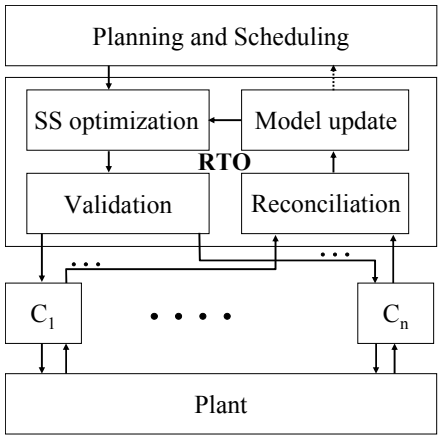

Figure 2: Elements of real-time optimization (RTO)

The planning and scheduling system provides production goals (e. g. demands of products, quality parameters), parameters of the cost function (e. g. prices of products, raw materials, energy costs) and constraints (e. g. availability of raw materials), and the process control layer provides plant data on the actual values of all relevant variables of the process. This data is first analyzed for stationarity of the process and, if a stationary situation is confirmed, reconciled using material and energy balances to compensate for systematic measurement errors. The reconciled plant data is used to compute a new set of model parameters (including unmeasured external inputs) such that the plant model represents the plant as accurately as possible at the current (stationary) operating point. Then new values for critical state variables of the plant are computed that optimize an economic cost function while meeting the technical constraints of the process and the economic constraints imposed by the plant management system. These values are then

filtered by a supervisory system (which often includes the plant operators) (e. g. checked for plausibility, mapped to ramp changes, clipped to avoid large changes) (Miletic and Marlin, 1996) and forwarded to the process control layer which uses these values as set-points and implements appropriate moves of the operational degrees of freedom (manipulated variables). The implementation of the optimal steady states by linear model predictive controllers was discussed in detail in (Rao and Rawlings, 1999).

As the RTO system employs a stationary process model and the optimization is only performed if the plant is approximately in a steady state, the time between successive RTO steps must be large enough for the plant to reach a new steady state after the last commanded move. Thus the sampling period must be several times the largest time-constant of the controlled process. Reported sampling times are usually on the order of magnitude of several (4 to 8) hours or once per day.

The introduction of an RTO system provides a clear separation of concerns and of time-scales between the RTO system and the process control system. The RTO system optimizes the plant economics on a medium time-scale (shifts to days) while the control system provides tracking and disturbance rejection on shorter time-scales from seconds to hours. Often the control system is again divided into separate layers to handle different speeds of response and to structure the system into smaller modules. This separation of concerns from a management point of view may be misunderstood that the process control layer is a necessary piece of equipment to run the process but the RTO system and the plant management system help to earn money. Consequently, the control system is just a part of the cost and any "luxury" on this layer should be avoided.

In (Forbes and Marlin, 1996, Zhang and Forbes, 2000), a performance metric for RTO systems, called design cost, was introduced where the profit obtained by the use of the RTO system is compared to an estimate of the theoretical profit obtained from a hypothetical delay-free static optimization and immediate implementation of the optimal setpoints without concern for the plant dynamics. The cost function consists of three parts:

- the loss in the transient period before the layered system consisting of the RTO system and the process control layer has reached a new steady state,
- the loss due to model errors in the steady state,
- the loss due to the propagation of stochastic measurement errors to the optimized setpoints.

The last factor advocates a filtering of the changes before they are applied to the real plant to avoid inefficient moves (Miletic and Marlin, 1998, Zhang et al., 2001). The issue of model fidelity was discussed in detail in (Zhang and Forbes, 2000, Yip and Marlin, 2004). In general, the use of a rigorous model is recommended. Adequacy of a model requires that the gradient and the curvature of the profit function are described precisely whereas the absolute value is not critical (Forbes, et al., 1994, Forbes and Marlin, 1995). As parameter estimation is a core part of an RTO system, the commanded set-point changes have an influence on the model accuracy and hence on the closeness to the true optimum. Yip and Marlin (2003) made the very interesting proposal to include the effect of set-point changes on the accuracy of the parameter estimates into the RTO optimization. Nonetheless, plant-model mismatch will always be an important issue. Cheng and Zafiriou (2000) proposed a modification of an SQP optimization algorithm (Zhou, et al., 1997) for steady-state optimization on the RTO layer such that the available measurement information is taken into account when the search direction and the step size are computed. In this fashion, convergence to the optimum can be assured even for considerable structural plant-model mismatch, resulting from the use of simplified process models that do not satisfy the conditions for a sufficiently accurate model as formulated in (Forbes, et al., 1994). Their algorithm avoids the need to determine gradients of the cost function and of the constraints by perturbations of the input to the real plant (and hence long periods of sub-optimal operation) as required by the algorithms proposed by Roberts and co-workers (Roberts 1979, Brdys, et al., 1987, Zhang and Roberts, 1990).

Duvall and Riggs (2000) in the evaluation of the performance of their RTO scheme for the Tennessee Eastman Challenge Problem pointed out: *"RTO profit should be compared to optimal, knowledgeable operator control of the process to determine the true benefits of RTO. Plant operators, through daily control of the process, understand how process setpoint selection affects the production rate and/or operating costs*". In particular, they argue that the operators would most likely know which variables should be kept at their bounds but will not be able to optimize setpoints within their admitted ranges according to the disturbances encountered. This practically results in the same comparison as assuming that a "self-optimizing" regulatory control scheme according to Skogestad (2000) is used on the lower level.

Quoting the famous Dutch soccer player and coach Johan Cruyff, *"every advantage is also a disadvantage"*. The advantage of the RTO/MPC structure is that it provides a clear separation between the tasks of the control and the optimization layer. This separation is performed with respect to time-scales as well as to models. Rigorous nonlinear models are used only on the steady-state optimization layer. Such models nowadays are often available from the plant design phase, so the additional effort to develop the model is not very high. The control algorithms are based upon linear models (or no models at all if conventional controllers are tuned on-site) which can be determined from plant data. As pointed out by e. g. (Backx, et al., 2000), (Sequeira et al., 2002) this implies however that the models on the optimization layer and on the control layer will in general not be

fully consistent, in particular their steady-state gains will differ.

The main disadvantage of the RTO approach is the delay of the optimization which is inevitably encountered because of the steady-state assumption. After the occurrence of a disturbance the optimization has to be delayed until the controlled plant has settled into a new steady state. To detect whether the plant is in a steady state itself is not a simple task (see e.g. Jiang, et al., 2003).

Suppose a step disturbance occurs in some unmeasured external input to the plant. Then first the control system will regulate the plant (to the extent possible) to the setpoints that were computed before the disturbance occurred. After all control loops have settled, the RTO optimizer can be started, and after the results have been computed (which may also require a considerable amount of time, depending on the complexity of the model used) and validated, the control layer can start to regulate the plant to the new setpoints. Thus it will take several times the settling time of the control layer to drive the plant to the new optimized mode of operation. In the first phase, the control system will try hard to maintain the previously optimal operating conditions even if without fixing the controlled variables to their setpoints the operation of the plant would have been more profitable. If the disturbance persists for one sampling period of the RTO system plus one settling time of the regulatory layer, the use of the RTO system on the average recovers about half of the difference between the profit obtained by the regulatory system alone (with fixed setpoints) and an online-optimizing controller that implements the optimal setpoints within the settling time of the regulatory control layer. The combined RTO/regulatory control structure will work satisfactorily for infrequent step changes of feeds, product specifications or product quantities but it will provide no benefit for changes that occur at time scales below the RTO sampling period.

Marlin and Hrymak (1997) listed several areas for improvement of RTO systems. Two important ones are addressed in the remainder of this paper: the integration with the process control layer, and the extension to unsteady-state operation. They pointed out that instead of sending set-points to the control layer, an ideal RTO system should output a design (i.e. tuning parameters or even a choice of the control structure) of the control system that leads to an optimized performance under the current long-term operating conditions.

4. REDUCING THE GAP BETWEEN REGULATION AND RTO

4.1 Frequent RTO

As a consequence of the drawback of RTO to work with rather long sampling periods, several authors have proposed schemes that work with smaller sampling times on the optimizing layer. E.g., Sequeira et al. (2002) propose to change the set-points for the regulatory layer in much shorter intervals (in the case study presented 1/50 of the settling time of the plant) and to perform a "real-time evolution" of the set-points by heuristic search (used here to reduce the computation time) based upon the stationary process model and the available measurements. To avoid overshooting behavior, the steps of the decision variables are bounded in each step. In the example shown, this scheme outperforms steady state RTO with regulatory control especially for non-stationary disturbances and in the first phase after a disturbance occurs which is not too surprising. The idea that a "step in the right direction" should be better than to wait until the process has settled to a new steady-state is convincing, however the approach suffers from neglecting the dynamic aspects. This concerns two aspects: the interaction of the set-point change with the regulatory control layer and the assumption that a steady-state optimization performed at an instationary operating point yields the right move of the set-points. In the same line of thinking, Basak, et al. (2002) discussed an on-line optimizing control scheme for a complex crude distillation unit. They proposed to perform a steady-state optimization of the unit for an economic cost function under constraints on the product properties with respect to the operational degrees of freedom and a model parameter update at a sampling rate of 1-2 hours and to apply the computed manipulated values directly to the plant. If the update of the manipulated variables is based solely on information on the plant inputs and the economics, such a scheme will react to disturbances only via the model parameter update. If dynamic variables enter the optimization, the resulting dynamics of the controlled plant will be unpredictable from the stationary behavior. The idea to perform updates of the operating point using a stationary model more frequently than every few settling times of the plant but to limit the size of the changes that are applied to the plant such that quasi-stationary transients are realized is also used in industrial practice. This leads to the implementation of the optimal set-point changes by ramps rather than steps or, in other terms, of a nonlinear integral controller, causing slow moves of the overall system.

The fast sampling approach is similar to gain scheduling control because a projection of the actual dynamic state on a corresponding stationary point that is defined by the values of the measured, actuated or demanded variables during transients is performed. It shares the potential of stability problems with gain scheduling controllers that usually can only be avoided if "slow", quasi-stationary set-point changes are realized (Shamma and Athans, 1992, Lawrence and Rugh, 1995).

4.2 Integration of steady-state optimization into model-predictive control

The so-called LP-MPC and QP-MPC two-stage MPC structures that are frequently used in industry to narrow the gap between the low-frequency nonlinear

steady-state optimization performed on the RTO layer and the relatively fast MPC layer (Morshedi, et al., 1985, Brosilow and Zhao, 1988, Yousfi and Tournier, 1991, Muske, 1997, Sorensen and Cutler, 1998, Nath and Alzein, 2000) were analyzed by Ying and Joseph (1999). The task of the upper MPC layer is to compute the setpoints (targets) both for the controlled variables and for the manipulated inputs for the lower MPC layer by solving a constrained linear or quadratic optimization problem, using information from the RTO layer and from the MPC layer. The optimization is performed with the same sampling period as the lower-level MPC controller (see Fig. 3). This structure addresses the following issues:

- A faster change of the setpoints after the occurrence of disturbances is realized;
- Inconsistency of the nonlinear steady-state model on the RTO layer and the linear steady-state model used on the MPC layer is reduced;
- Large infrequent setpoint changes that may drive the linear controllers unstable are avoided;
- The distribution of the offsets from the desired targets that are realized by the MPC controller is explicitly controlled and optimized.

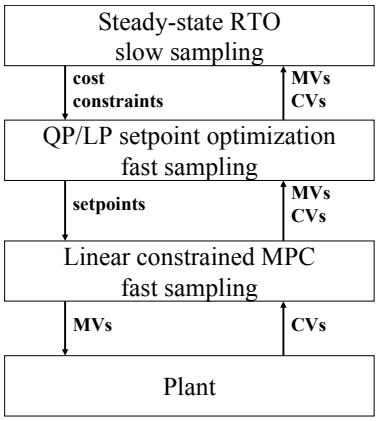

Figure 3: Two-layer MPC with setpoint optimization

The plant model and the disturbance estimate used on the intermediate optimization layer is the same as that used (and eventually updated) on the MPC layer, thus avoiding inconsistencies, whereas the weights in the cost function and the linear constraints are chosen such that they approximate the nonlinear cost function and the constraints on the RTO layer around the present operating point. As long as this approximation is good, optimal operations are ensured.

A simpler approach to the integration of steady-state optimization and model predictive control is to optimize those tuning parameters of a DMC or QDMC controller that determine the steady-state behavior of the controller (setpoints of the regulated variables, targets of the manipulated variables, weights on the deviations of the regulated variables from the setpoints and on the deviations of the of the manipulated variables from the targets) such that the profit obtained is maximized over a number of disturbance scenarios as proposed by (Kassidas, et al., 2000). In the parameter optimization, a full nonlinear steady-state plant model is used. Note that this optimization is only performed once (off-line), whereas only the usual computations of the DMC or QDMC controller moves employing linear plant models have to be performed online. The approach was compared to rigorous steady-state optimization (similar to what a RTO layer working together with a zero-offset controller would yield) of the purity setpoints and to a controller that controls the plant to fixed pre-computed purity setpoints (also optimized over the various disturbance scenarios) for a simple distillation example. The optimization approach led to a considerable variation of the controlled outputs over the different scenarios, while when the process is regulated to fixed setpoints, this variation is mapped to the manipulated variables. The optimally tuned DMC controller implements a compromise between these extremes and realizes about 70% of the average additional profit that results for rigorous optimization. Even better results can be expected for examples where the optimal operation is mostly determined by the constraints.

4.3 Integration of nonlinear steady-state optimization in the linear MPC controller.

Zanin, et al. (2000, 2002) reported the formulation, solution and industrial implementation of a combined MPC/optimizing control scheme for an FCC unit. The plant has 7 manipulated inputs and 6 controlled variables. The economic cost used is the amount of LPG produced. The optimization problem that is solved in each controller sampling period is formulated in a mixed manner: range control MPC with a fixed linear plant model (imposing soft constraints on the controlled variables by a quadratic penalty term that only becomes active when the constraints are violated) plus a quadratic control move penalty plus an economic objective that depends on the values of the manipulated inputs at the end of the control horizon. The economic objective value is computed using a nonlinear steady-state process model. As only the first move of the controller is implemented, a penalty term is added that penalizes the deviation of the first values of the manipulated variables from their final values within the control horizon. Several variants for this penalty term are investigated. The different components of the cost function are weighted such that the economic criterion and the MPC part have a similar influence on the values of the overall cost.

This combined optimizing/MPC controller was implemented and tested at a real plant with a sampling rate of 1 minute, a control horizon of 2 steps and a prediction horizon of 20 steps. An impressive performance is reported, both in terms of the economic performance and of the smoothness of the transients, pushing the process to its limits. The integrated control scheme performed substantially better than the conventional scheme where the operators chose setpoints based on their experiences that were then implemented by a conventional MPC scheme. The final weights of the different contributions to the cost function were determined by experiments. Simulations also showed that the one-layer approach compared

favorably to a two-layer approach in which the economic optimization provided setpoints for a linear MPC scheme in terms of dynamic response. A similar control scheme was experimentally validated in (Costa, et al., 2005).

5. DIRECT FINITE HORIZON OPTIMIZING CONTROL

5.1 General ideal

For demanding applications, the replacement of linear MPC controllers by nonlinear model predictive control is a promising option and industrial applications are reported in particular in polymerization processes (Qin and Badgewell, 2003, Bartusiak, 2005, Naidoo, et al., 2005). If nonlinear model-based control is used to implement optimal set-points or optimal trajectories at a plant, it is only a small step to replace the traditional quadratic cost criterion that penalizes the deviations of the controlled variables from the reference values and the input variations by an economic criterion. Constraints on outputs (e.g. strict product specifications) as well as process limitations can then be included directly in the optimization problem. This approach has several advantages over a combined steady-state optimization/ linear MPC scheme:

- Fast reaction to disturbances, no waiting for the plant to reach a steady state is required;
- Regulation of constrained variables to setpoints that implies a safety margin between these setpoints and the constraints is avoided, the exact constraints can be implemented for measured variables and only the model error has to be taken into account for unmeasured constrained variables;
- Over-regulation is avoided, no variables are forced to fixed setpoints and all degrees of freedom can be used to optimize process performance;
- No inconsistency arises from the use of different models on different layers;
- Economic goals and process constraints do not have to be mapped to a control cost whereby inevitably economic optimality is lost and tuning is difficult;
- The overall scheme is structurally simple.

An important point in favor of using an economic cost criterion and formulating restrictions of the process and the product properties as constraints is that this largely reduces the need for tuning of the weights in less explicit formulations. In contrast, Exxon's technology for NMPC employs a combination of criteria that represent reference tracking, operating cost and control moves (Bartusiak, 2005).

In the next section, it will be demonstrated that direct online optimizing control can successfully be applied to control problems that are hard to tackle by conventional control techniques. Other application studies have been reported e. g. by (Singh, et al., 2000) and Johansen and Sbarbaro (2005) for blending processes and by (Busch, et al., 2005) for a waste-water treatment plant.

5.2 Case Study: Control of reactive simulated moving bed chromatographic processes

Process Description. Chromatographic separations are a widespread separation technology in the fine chemicals, nutrients and pharmaceutical industry. Chromatography is applied for difficult separation tasks, in particular if the volatilities of the components are similar or if the valuable components are sensitive to thermal stress. The separation of enantiomers (molecules that are mirror images of each other) is an example where chromatography is the method of choice. The standard chromatographic process is the batch separation where pulses of the mixture that has to be separated are injected into a chromatographic column followed by the injection of pure solvent. The components travel through the column at different speeds and can be collected at the end of the column in different purified fractions. In the batch mode, the adsorbent is not used efficiently and it usually leads to highly diluted products.

The goal of a continuous operation of chromatographic separations with a counter-current movement of the solid phase and the liquid phase led to the development of the Simulated Moving Bed (SMB) process (Broughton 1961). It is gaining increasing attention in industry due to its advantages in terms of productivity and solvent consumption (Guest 1997, Juza, et al. 2000). An SMB process consists of several chromatographic columns connected in series which constitute a closed loop. An effective counter-current movement of the solid phase relative to the liquid phase is achieved by periodically and simultaneously moving the inlet and outlet lines by one column in the direction of the liquid flow (see Fig. 4).

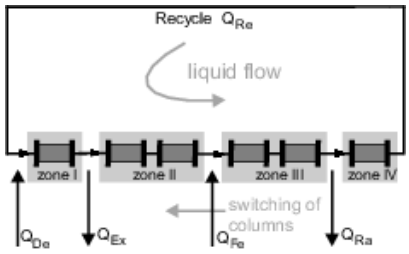

Figure 4: Simulated Moving Bed principle

After a startup phase, SMB processes reach a cyclic steady state (CSS). The length of a cycle is equal to the duration of a switching period times the number of columns, but relative to the port positions, the profiles are repeated every switching period. Fig. 5 shows the concentration profiles of a binary separation along the columns plotted for different time instants within a switching period.

Control of SMB processes. Classical feedback control strategies are not directly applicable to SMB processes due to their mixed discrete and continuous dynamics, spatially distributed state variables with steep slopes, and slow and strongly nonlinear responses of the concentrations profiles to changes of the operating parameters. A summary of different approaches to

control of SMB processes can be found in (Engell and Toumi 2005, Toumi and Engell, 2005).

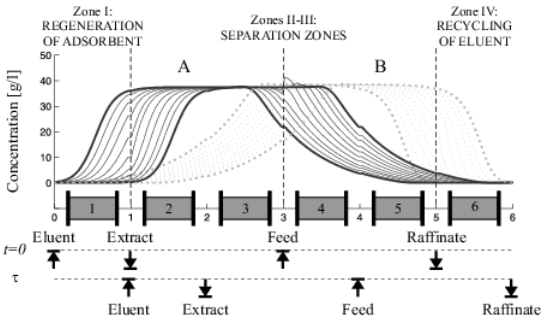

Figure 5: Concentration profiles of an SMB process

Klatt, et al. (2002) proposed a two-layer control architecture similar to the RTO/MPC scheme where the optimal operating trajectory is calculated at a low sampling rate by dynamic optimisation based on a rigorous process model. The model parameters are adapted based on online measurements. The low-level control task is to keep the process near the optimal cyclic steady state despite disturbances, plant degradation and plant/model mismatch by controlling the front positions. The controller is based on input/output models that are identified using simulation data produced by the rigorous process model near the optimal cyclic steady state (Klatt, et al., 2002, Wang, et al., 2003). A disadvantage of this two-layer concept is that keeping the front positions at the values obtained from the rigorous optimization does not guarantee the product purities if structural plant/model mismatch occurs. Thus an additional purity controller is required, and the overall scheme becomes quite complex without actually ensuring optimality.

Online optimizing control. As the progress in efficient numerical simulation and optimization enabled a dynamic optimization of the process within one switching period, Toumi and Engell (2004a) proposed a direct finite horizon optimizing control scheme that employs the same rigorous nonlinear process model that is used for process optimization and applied it to a 3-zones reactive SMB process for glucose isomerisation (Toumi and Engell 2004a,b) The key feature of this approach is that the production cost is minimised on-line over a finite horizon while the product purities are considered as constraints, thus a real online optimisation of all operational degrees of freedom is performed, and there is no tracking of any precomputed setpoints or reference trajectories. In (Toumi, et al. 2005), this control concept was extended to the more complex processes VARI*COL* (Ludemann-Homburger, et al., 2000 Toumi, et al., 2003) and PowerFeed (Kearney and Hieb 1992) where the ports are switched asynchronously and the flow rates are varied in the subintervals of the switching period. These process variants offer an even larger number of degrees of freedom that can be used for the optimization of the process economics while satisfying the required product purities. In the optimizing control scheme of Toumi, et al. (2004a,b), the states of the process model are determined by forward simulation starting from measurements in the recycle stream and in the product streams.

A different optimization-based approach to the control of SMB processes was proposed by (Erdem, et al., 2004a, Erdem, et al., 2004b, Abel, et al., 2005). In their work, a moving horizon online optimization is performed based on a linear reduced-order model that is obtained from linearizing a rigorous model around the periodic steady state. The state variables of the model are estimated by a Kalman Filter that processes the product concentration measurements. Due to the use of repetitive MPC (Natarajan and Lee, 2000) the switching period is kept fixed although it has a considerable influence on the process performance.

The Hashimoto reactive SMB process. The integration of chemical reactions into chromatographic separations offers the potential to improve the conversion of equilibrium limited reactions. By the simultaneous removal of the products, the reaction equilibrium is shifted to the side of the products. This combination of reaction and chromatographic separation can be achieved by packing the columns of the SMB process uniformly with adsorbent and catalyst, this leads to the reactive SMB (SMBR) process. The SMBR process can be advantageous in terms of higher productivity in comparison to a sequential arrangement of reaction and separation units (Borren and Fricke, 2005). However, for reactions of the type A <=> B, a uniform catalyst distribution in the SMBR promotes the backward reaction near the product outlet which is detrimental to the productivity, further, the renewal of deactivated catalyst is difficult when it is mixed with adsorbent pellets, and the same operating conditions must be chosen for separation and reaction what may lead to either suboptimal reaction or suboptimal separation. The Hashimoto SMB process (Hashimoto, et al., 1983) overcomes the disadvantages of the SMBR by performing separation and reaction in separate units that contain only adsorbent or only catalyst. In this configuration, the conditions for reaction and for separation can be chosen separately and the reactors can constantly be placed in the separation zones of the SMB process by appropriate switching. The structure of a Hashimoto SMB process is shown in Fig. 6. The dynamics of this class of processes is highly complex.

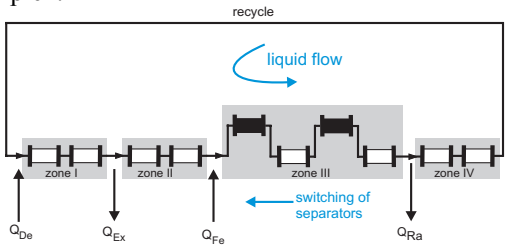

Figure 6: Four-zones Hashimoto SMB process

Optimizing controller application. The example process considered in (Küpper and Engell, 2005) is the racemization of *Tröger's Base (TB)* in combination with chromatographic separation for the production of *TB*- that is used for the treatment of cardiovascular

diseases. The solvent is an equimolar mixture of acetic acid that acts as the catalyst for the reaction and 2-propanole that increases the solubility of the mixture. The Tröger's Base system is described by an adsorption isotherm that is of multi component Langmuir type:

$$q_i = \frac{H_i c_{p,i}}{1 + \sum_k b_{i,k} c_{p,k}}, \; \mathrm{k} = +, - . \qquad (4)$$

The reaction takes place in plug flow reactors that are operated at 80°C whereby the catalyst is thermally activated. In the chromatographic columns that have a temperature of 25°C the catalyst is virtually deactivated. In the simulation run shown below, a four-zones Hashimoto process with 8 chromatographic columns, 2 reactors, and a column distribution as shown in Fig. 6 is considered. The objective of the optimizing controller is to minimize the solvent consumption Q_D for a constant feed flow and a given purity requirement of 99% in the presence of a plant/model mismatch. The inevitable mismatch between the model and the behavior of the real plant is taken into account by feedback of the difference of the predicted and the measured product purities. A regularization term is added to the objective function to obtain smooth trajectories of the input variables. The controller has to respect the purity requirement for the extract flow which is averaged over the prediction horizon, the dynamics of the Hashimoto SMB model and the maximal flow rate in zone I due to limited pump capacities. In order to guarantee that at least 70% of the mass of the components fed to the plant averaged over the prediction horizon leaves the plant in the extract product stream, an additional productivity requirement was added. The resulting mathematical formulation of the optimization problem is:

$$\begin{aligned}
&\min_{\beta_I,\beta_{II},\beta_{III},\beta_{IV}} \sum_{i=1}^{H_P} Q_i + \Delta\beta\, R\, \Delta\beta \\
s.t. \quad &\begin{cases} \tilde{x}^k_{smb} = x^k_{smb} + \int_{t=0}^{\tau} f_{smb}(x_{smb}(t, u_{smb}(t), p))dt \\ x^{k+1}_{smb} = P\tilde{x}^k_{smb}, \end{cases} \\
&\frac{\sum_i^{H_{P1}} Pur_{Ex,i}}{H_{P1}} \geq (Pur_{Ex,\min} - \Delta Pur_{Ex}) \qquad (5) \\
&\frac{\sum_i^{H_{P1}} m_{Ex,i}}{H_{P1}} \geq 0.7 m_{Fe} - \Delta m_{Ex} \\
&Q_I \leq Q_{\max} \\
&Q_{De}, Q_{Ex}, Q_{Fe}, Q_{\mathrm{Re}} \geq 0,
\end{aligned}$$

where the purity error and the mass error are calculated according to

$$\begin{aligned}
\Delta Pur_{Ex} &= Pur_{Ex,plant,i-1} - Pur_{Ex,\mathrm{mod}el,i-1}, \qquad (6) \\
\Delta m_{Ex} &= m_{Ex,plant,i-1} - m_{Ex,\mathrm{mod}el,i-1}.
\end{aligned}$$

The model of the plant consists of rigorous dynamic models of the individual columns of the plant, the node equations and the port switching. The chromatographic columns are described accurately by the general rate model (Guichon, et al., 1994) which accounts for all important effects of a radially homogeneous column, i.e. mass transfer between the liquid and the solid phase, pore diffusion, and axial dispersion. The pdes are discretized using a Galerkin approach on finite elements for the bulk phase and orthogonal collocation for the particle phase (Gu, 1995). The reactors consist of 3 columns in series. Each column is discretized into 12 elements, yielding an overall model with 1400 dynamic states. For the solution of the optimization problem, the feasible path solver FFSQP (Zhou, et al., 1997) is applied. It first searches for a feasible operating point and then minimizes the objective function. The number of iterations of the SQP solver was limited to 8 because the optimizer performs this number of iterations within one cycle of the process (8 switching periods), as required for online control.

In the simulation scenario, an exponential decrease of the catalyst activity was assumed that occurs in the case of a disturbance in the heating system. A model/plant mismatch was introduced by disturbing the initial Henry coefficients H_A and H_B of the model by +10% and -15%. The parameters of the controller are displayed in Table 1.

Table 1: Controller parameters

Sampling time		8 periods = 1 cycle
Prediction horizon	H_P	6 cycles
Control horizon	H_C	1 cycle
Regularization	R	[0.3 0.3 0.3 0.3]
Controller start		72nd period
Estimator start		72nd period

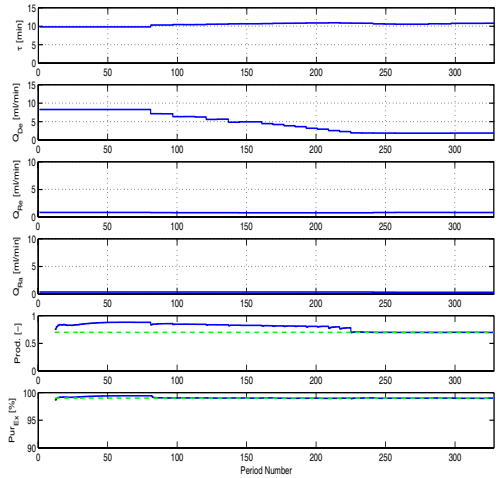

Figure 7: Simulation of the optimizing controller of the Hashimoto reactive SMB process

The performance of the controller is illustrated by Fig. 7. The controller manages to keep the purity and the productivity above their lower limits, while it im-

proves the economical operation of the plant by reducing the solvent consumption. As reported in (Toumi and Engell, 2004a,b) the optimizing controller has been implemented at a medium scale commercial SMB plant using a PLC-based process control system and an additional PC for optimization and parameter estimation.

5.3 Numerical Aspects.

In the example described above, a relatively simple numerical approach using direct simulation, computation of the gradients by perturbation and a feasible path SQP algorithm for the computation of the optimal controls was used. By using more advanced numerical techniques, much shorter computation times can be realized. Diehl, et al. (2002) proposed a scheme for the solution of nonlinear model-predictive control problems with large plant models where the multiple shooting method (Bock and Plitt, 1984) with a tailored SQP algorithm is used and only one iteration of the SQP-problem is performed in each sampling interval. Moreover, the steps performed in the algorithm are ordered such that a new output is computed fast immediately after a new measurement became available and the remainder of the computations is done thereafter, thus reducing the reaction time to disturbances considerably. A further improvement of the speed of the solution of the optimization problem is presented in (Schäfer, et al., 2006). The maximum time needed for the solution of a quadratic NMPC problem for a distillation column modeled by a rigorous DAE model of order 106+159 and prediction and control horizons of 36 sampling intervals is reported to be less than 20 s for a Pentium 4 computer. Diehl, et al. (2005) proved convergence of the real-time iteration scheme to the optimal solution for general cost functions.

An alternative to the multiple shooting approach is to apply full discretization techniques were similar progress has been reported (e. g. Biegler, et al., 2002, Grossmann and Biegler, 2004). Jockenhövel, et. al. (2003) reported the application of conventional NMPC with a quadratic cost criterion to the Tennessee Eastman challenge problem with 30 dynamic and 149 algebraic states, 11 control variables, several constraints on state variables, and control and prediction horizons of 60 steps. Using full discretization and an interior point method, a reliable solution well within the sampling time of 100 s is achieved. It can thus be concluded that online optimizing control is computationally feasible nowadays for models with several hundred state variables and for long prediction horizons.

6. OPEN ISSUES

Modeling. In a direct optimizing control approach accurate dynamic nonlinear process models are needed. While nonlinear steady-state models are nowadays available for control purposes for many processes because they are used extensively in the process design phase, there is still a considerable effort required to formulate, implement and validate nonlinear dynamic process models. The recent trend towards the use of training simulators may alleviate this problem. Training simulators are increasingly ordered together with new plants and are available before the real plant starts production. The models inside the training simulator represent the plant dynamics faithfully even for states far away from the nominal operating regime (e.g. during start-up and shut-down) and can be used also for optimization purposes. Such rigorous models may however include too much detail from a control point of view. It does not seem to be necessary to include dynamic phenomena that effect the behavior only on time scales much longer than the prediction horizon or shorter than the sampling time of the controller. However, the appropriate simplification of nonlinear models still is an unresolved problem (Lee, 2000, Marquardt, 2002). The alternative to use black-box or grey-box models as proposed frequently in nonlinear model-predictive control (e.g. Draeger and Engell, 1995, Wang, et al., 2003, Camacho and Bordons, 2005) does not seem appropriate for optimizing control with performance requirements formulated as constraints.

Stability. Optimization of a cost function over a finite horizon in general neither assures optimality of the complete trajectory nor stability of the closed-loop system. Closed-loop stability has been addressed extensively in the theoretical research in nonlinear model-predictive control. There is a pronounced difference in the attention that practitioners and researchers pay to this issue – practitioners will usually tend to say that if suffices to choose sufficiently long prediction and control horizons which, for stable plants, will work indeed. Nonetheless, the theoretical discussion has led to a clear understanding of what is required to ascertain stability of a nonlinear model predictive control scheme and clearly pointed out the deficiencies of less sophisticated schemes. Stability results so far have been proven for regulatory NMPC where stability means convergence to the desired equilibrium point. Stability can be assured by proper choice of the stage cost within the prediction horizon and the addition of a cost on the terminal state and the restriction of the terminal state to a suitable set (Chen and Allgöwer, 1998, Mayne, et al, 2000). If the stage cost is an economic cost function, bounded cost will in general not ensure boundedness of the difference of the states to the equilibrium state because economic cost functions often involve only few process variables, mostly inputs and mass flows leaving the physical system. Moreover, there is no fixed equilibrium state.

An optimizing control algorithm with guaranteed stability in principle can be designed if in addition to the direct optimizing controller a steady-state optimization is performed to determine the desired terminal state. Then the cost function can be extended by a terminal cost that penalizes the distance of the state at the end of the prediction horizon from the optimal steady state and by a (small) quadratic penalty term on the deviation of the state (or of suitable outputs)

from the terminal state within the prediction horizon. If a suitable constraint on the terminal state is added, this will provide a stabilizing control scheme. It has been demonstrated recently that algorithms of this type are computationally feasible even for very large nonlinear plant models (Nagy, et al., 2005). The constraint on the terminal state has to be computed for each update of the optimal terminal state what is computationally demanding but should be feasible on the steady-state optimization layer. By the choice of the weighting terms, a compromise between optimizing process performance over a limited horizon at a fast sampling rate and long-term performance under the assumption that no major disturbance occurs can be established. This leads to a hierarchical scheme similar to the RTO/MPC scheme where the upper layer provides the terminal state and the terminal region and the lower layer now is "cost-conscious" and no longer purely regulatory. In contrast to the RTO/MPC-scheme, the optimization goals as well as the models used are consistent in this structure.

An alternative approach to guaranteeing stability of an optimizing controller is applied in (Johansen and Sbarbaro, 2005) to a linear process with a static nonlinearity at the output, based on an augmented control Lyapunov function.

State estimation. For the computation of economically optimal process trajectories based upon a rigorous nonlinear process model, the state variables of the process at the beginning of the prediction horizon must be known. As not all states will be measured in a practical application, state estimation is a key ingredient of a directly optimizing controller. The state estimation problem is of the same complexity as the optimization problem, unless simple approaches as predicting the state by simulation of a process model are employed. The natural approach is to formulate the state estimation problem also as an optimization problem on a moving horizon (Jang, et al., 1986, Muske and Rawlings, 1994, Rao, et al., 2000). Parameter estimation can be included in this formulation. Experience with the application of moving horizon state estimation however still is quite limited to date. Simpler and computationally less demanding schemes as the constrained extended Kalman filter (CEKF) may provide a comparable performance (Gesthuisen, et al., 2001). As accurate state estimation is at least as critical for the performance of the closed-loop system as the exact tuning of the optimizer, more attention should be paid to the investigation of the performance of state estimation schemes in realistic situations with non-negligible model-plant mismatch.

Measurement-based optimization. In the scheme described in section 5, feedback of the measured variables is only realized via the updates of the state and of the parameters and by a bias term in the formulation of the constraints and possibly in the cost criterion. As discussed in the section on RTO, a near-optimal solution requires that the gradients provided by the model and the second derivatives are accurate and in such a scheme there is no feedback present to establish optimality despite the presence of model errors. This can be addressed by the solution of a modified optimization problem (Roberts 1979, Brdys, et al., 1987). As shown by Tatjewski (2002), optimality can be achieved without parameter update and for structural plant-model mismatch by correcting the optimization criterion based on gradient information derived from the available measurements. This idea was extended to handling constraints and applied to batch chromatography in (Gao and Engell, 2005) and should be explored in the continuous case as well. An alternative to implement measurement-based optimization is to formulate the optimization problem (partly) as the tracking of necessary conditions which are robust against model mismatch (Srinivasan, et al., 2002, Chatzidoukas, et al., 2005, Kadam, et al., 2005).

Reliability and transparency. As discussed above, relatively large nonlinear dynamic optimization problems can be solved in real-time nowadays, so this issue does not prohibit the application of a direct optimizing control scheme to complex units. A practically very important issue however is that of reliability and transparency. It is hard, if not impossible to rule out that a nonlinear optimizer does not provide a solution which at least satisfies the constraints and gives a reasonable performance. While for RTO an inspection of the commanded setpoints by the operators may be feasible, they can hardly act as filters in direct optimizing control of complex units. Hence automatic result filters are necessary as well as a backup scheme that stabilizes the process in the case where the result of the optimization is not considered safe. But the operators will still have to supervise the operation of the plant, so a control scheme with optimizing control should be structured into modules which are not too complex. The concept of adding a cost term that represents steady-state optimality as described above provides a solution for the dynamic online optimization of larger complexes based on decentralized optimizing control of smaller units. The co-ordination of the units is performed by the steady state real-time optimization that sends the desired terminal states plus adequate penalty terms to the lower level controls. These penalty terms must reflect the sensitivity of the global optimum with respect to local deviations, i.e. how an economic gain on the local level within the optimization horizon is traded against a global loss due to not steering the plant to the globally optimal steady state. Still, acceptance by the operators and plant managers will be a major challenge. Good interfaces to the operators that display the predicted moves and reactions and enable comparisons with their intuitive strategies are believed to be essential for practical success.

Effort vs. performance. Of course, the complexity of the control scheme has to be traded against the gain in performance. If a carefully chosen standard regulatory control layer leads to a close-to-optimal operation, there is no need for optimizing control. If the disturbances that affect profitability and cannot be handled well by the regulatory layer (in terms of eco-

nomic performance) are slow, the combination of regulatory control and RTO is appropriate. In a more dynamic situation or for complex nonlinear multivariable plants, the direct optimizing control idea should be explored. As for an NMPC controller that is designed for reference tracking, a successful implementation will require careful engineering such that as many uncertainties as possible are compensated by simple feedback controllers and only the key dynamic variables are handled by the optimizing controller based on a rigorous model of the essential dynamics and of the stationary relations of the plant without too much detail.

REFERENCES

Abel, S., G. Erdem, M. Amanullah, M. Morari, M. Mazzotti and M. Morbidelli (2005). Optimizing control of simulated moving beds-experimental implementation. *J Chromatography A*, **1092** (1), 2-16.

Backx, T., O. Bosgra and W. Marquardt (2000). Integration of Model Predictive Control and Optimization of Processes. *Proc. IFAC Symposium ADCHEM*, Pisa, 249-260.

Bartusiak, R.D. (2005). NMPC: A platform for otpimal control of feed- or product-flexible manufacturing. *Preprints Int. Workshop on Assessment and Future Directions of NMPC, Freudenstadt,* 3-14.

Basak, K., K.S. Abhilash, S. Ganguly and D.N. Saraf (2002). On-line Optimization of a Crude Distillation Unit with Constraints on Product Properties. *Ind. Eng. Chem. Res.,* **4**1, 1557-1568.

Biegler, L.T., A.M. Cervantes and A. Wächter (2002). Advances in simultaneous strategies for dynamic process optimization. *Chem. Eng. Sci.,* **57**, 575-593.

Bock, H.G. and K.J. Plitt. (1984). A multiple shooting algorithm for direct solution of optimal control problems. *Proc. 9th IFAC World Congress*, Pergamon Press, Oxford, 243-247.

Borren, T. and J. Fricke (2005). Chromatographic Reactors. Chapter 8 in *Preparative Chromatography*, Schmidt-Traub, H., (Ed.), Wiley-WCH, Weinheim, 371-400.

Brdys, M., J.E. Ellis and P.D. Roberts (1987). Augmented integrated system optimization and parameter estimation technique: Derivation, optimality and convergence. *Proc. IEE,* **134**, 201-209.

Brosilow, C. and G.Q. Zhao (1988). A Linear Programming Approach to Constrained Multivariable Process Control. *Contr. Dyn. Syst.,* **27**, 14l.

Broughton, D. and C. Gerhold (1961). Continuous sorption process employing fixed bed of sorbent and moving inlets and outlets. US Patent 2985586.

Busch, J., M. Santos, J. Oldenburg, A. Cruse and W. Marquardt (2005). A Framework for the Mixed Integer Dynamic Optimisation of Waste Water Treatment Plants using Scenario-Dependent Optimal Control. *Proc. ESCAPE 15*, Elsevier, 955-960.

Camacho, E.F. and C. Bordons. (2005). Nonlinear Model Predictive Control: An Introductory Survey. *Preprints Int. Workshop on Assessment and Future Directions of NMPC, Freudenstadt.* 15-30.

Chatziodoukas, C., C. Kiparissides, B. Srinivasan and D. Bonvin (2005). Optimisation of grade transitions in an industrial gas-phase olefin polymerization fluidized bed reactor via NCO tracking. *16th IFAC World Congress,* Prague.

Chen, H. and F. Allgöwer (1998). A quasi-infinite horizon nonlinear model predictive control scheme with guaranteed stability. *Automatica,* **14**, 1205-1217.

Cheng, J.H. and Zafiriou, E. (2000). Robust Model-Based Iterative Feedback Optimization of Steady-State Plant Operations. *Ind. Eng. Chem. Res.,* **39**, 4215-4227.

Costa, C.E.S., F.B. Freire, N.A. Correa, J.T. Freire and R.G. Correa (2005). Two-layer real-time optimization of the drying of pastes in a spouted bed: experimental implementation. *16th IFAC World Congress*, *Prague*.

Diehl, M., H.G. Bock, J.P. Schlöder, Z., Nagy and F. Allgöwer (2002). Real-time optimization and nonlinear model predictive control of processes governed by differential-algebraic equations. *J. Proc. Contr.,* **12**, 577-585.

Diehl, M., H.G. Bock and J.P. Schlöder (2005). A real-time iteration scheme for nonlinear optimization in optimal feedback control. *SIAM J. Control Optim.,* **43**, 1714-1736.

Downs, J.J. and E.F. Vogel (1993). A plant-wide industrial process control problem. *Comp. Chem. Eng.,* **17**, 245-255.

Draeger, A. and S. Engell (1995). Nonlinear model predictive control using neural net plant models. *Methods of Model Based Process Control*, Berber, R., (Ed.), Kluwer Academic Publishers, 627-639.

Duvall, P.M. and J.B. Riggs (2000). On-line optimization of the Tennessee Eastman challenge problem. *J. Process Control,* **10**, 19-33.

Engell, S. and A. Toumi (2005). Optimization and control of chromatography. *Comp. Chem. Eng.,* **29**, 1243-1252.

Erdem, G., S. Abel, M. Morari, M. Mazzotti and M. Morbidelli (2004a). Automatic control of simulated moving beds. Part I: Linear isotherms. *Ind. Eng. Chem. Res.,* **43**, 405-421.

Erdem, G., S. Abel, M. Morari, M. Mazzotti and M. Morbidelli (2004b). Automatic control of simulated moving beds. Part II: Nonlinear isotherms. *Ind. Eng. Chem. Res.* **43**, 3895-3907.

Findeisen, W., F.N. Bailey, M. Brdys, K. Malinowski, P. Wozniak and A. Wozniak (1980). Control and Coordination in Hierarchical Systems. John Wiley, New York.

Forbes, J.F., T.E. Marlin and J. MacGregor (1994). Model Selection Criteria for Economics-Based Optimizing Control. *Comp. Chem. Eng.,* **18**, 497-510.

Forbes, J.F. and T.E. Marlin (1995). Model Accuracy for Economic Optimizing Controllers: The Bias Update Case. *Ind. Eng. Chem. Fund.,* **33**, 1919-1929.

Forbes, J.F. and T.E. Marlin (1996). Design Cost: A Systematic Approach to Technology Selection for Model-Based Real-Time Optimization Systems. *Comp. Chem. Eng.,* **20**, 717.

Gao, W. and S. Engell (2005). Iterative set-point optimisation of batch chromatography. *Comp. Chem. Eng.,* **29**, 1401-1410.

Gesthuisen, R., K.-U. Klatt and S. Engell (2001). Optimization-based state estimation – a comparative study fort the batch polycondensation of PET. *Proc. ECC 2001*, Porto, 1062-1067.

Grossmann, I. E. and L.T. Biegler (2004). Future perspective on optimization. *Comp. Chem. Eng.,* **28**, 1193-1218.

Gu, T. (1995). *Mathematical Modelling and Scale Up of Liquid Chromatography.* Springer, New York.

Guest, D. W. (1997). Evaluation of simulated moving bed chromatography for pharmaceutical process development, *Journal of Chromatography A* **760,** 159–162.

Guiochon, G., S. Golshan-Shirazi and A. Katti (1994). *Fundamentals of Preparative and Nonlinear Chromatography*. Academic Press, Boston.

Hashimoto, K., S. Adachi, H. Noujima and Y. Ueda (1983). A new process combining adsorption and enzyme reaction for producing higher-fructose syrup. *J. Biotechnol. Bioeng*. **25**, 2371-2393.

Jang, S.-S., B. Joseph and H. Mukai (1986). Comparison of two approaches to online parameter and state estimation of nonlinear systems. *Ind. Eng. Chem. Proc. Des. Developm.* **25**, 809-814.

Jiang, T., B. Chen, X. He and P. Stuart (2003). Application of steady-state detection method based on wavelet transform. *Comp. Chem. Eng*., **27**, 569-578.

Jockenhövel, T., L.T. Biegler and A. Wächter (2003). Dynamic optimization of the Tennessee Eastman process using the OptControlCentre. *Comp. Chem. Eng.,* **27**, 15l3-l53l.

Johansen, T.A. and D. Sbarbaro (2005). Lyapunov-Based Optimizing Control of Nonlinear Blending Processes. *IEEE Tr. on Control Systems Technology,* **13**, 4, 631-638.

Juza, M., M. Mazzotti and M. Morbidelli. (2000). Simulated moving-bed chromatography and its application to chirotechnology, *Trends in Biotechnology* **18,** 108–118.

Kadam, J.V., M. Schlegel, B. Srinivasan, D. Bonvin and W. Marquardt (2005). Dynamic real-time optimization: From off-line numerical solution to measurement-based implementation. *16th IFAC World Congress,* Prague.

Kassidas, A, J. Patry and T. Marlin (2000). Integration of process and controller models for the design of self-optimizing control. *Comp. Chem. Eng.,* **24**, 2589-2602.

Kearney, M. and K. Hieb (1992). Time variable simulated moving bed process. US Patent 5.102.553.

Klatt, K-U., F. Hanisch, G. Dünnebier and S. Engell (2000). Model-based optimization and control of chromatographic processes. *J. Process Control,* **24**, 1119-1126.

Küpper, A. and S. Engell (2005). Non-linear model predictive control of the Hashimoto simulated moving bed process, *Int. Workshop on Assessment and Future Directions of NMPC, Freudenstadt.*

Larsson, T., K. Hestetun, E. Hovland and S. Skogestad (2001). Self-optimizing control of a large-scale plant: The Tennessee Eastman process. *Ind. Eng. Chem. Res.,* **40,** 4889-4901.

Larsson, T., S. Govatsmark and S. Skogestad. (2003). Control structure selection for reactor, separator, and recycle processes. *Ind. Eng. Chem. Res.,* **42,** 1225-1234.

Lawrence, D.A. and W.J. Rugh (1995). Gain scheduling dynamic linear controllers for a nonlinear plant. *Automatica,* **31**, 381-390.

Lee, J.H. (2000). Modeling and identification in nonlinear model predictive control. *Nonlinear Model Predictive Control,* Allgöwer, F. and A. Zheng (Eds.), Birkhäuser, Basel, 269-293.

Ludemann-Hombourger, O. and R.M. Nicoud (2000). The VARlCOL process: A new multicolumn continuous separation process. *Separation Science and Technology,* **35,** 1829-1862.

Marlin, T.E. and A.N. Hrymak (1997). Real-time Operations Optimization of Continuous Processes. *Proc. CPC V*, AIChE Symposium Series*,* **93,** 156-164.

Mayne, D.Q., J.B. Rawlings, C.V. Rao and P.O.M. Scokaert (2000). Constrained model predictive control: Stability and optimality, *Automatica,* **36,** 789-814.

Miletic, I. and T.E. Marlin (1996). Results Analysis for Real-Time Optimization (RTO): Deciding when to change the plant operation, *Comp. Chem. Eng.,* **20,** 1077.

Miletic, I. and T.E. Marlin (1998). On-line statistical results analysis in real-time operations optimization. *Ind. Eng. Chem. Res.,* **37,** 3670-3684.

Morari, M., G. Stephanopoulos and Y. Arkun (1980). Studies in the Synthesis of Control Structures for Chemical Processes, Part I. *AIChE Journal,* **26,** 220-232.

Morshedi, A. M., C.R. Cutler and T.A. Skrovanek (1985). Optimal Solution of Dynamic Matrix Control with Linear Programming Techniques. *Proc. American Control Conference,* 208.

Muske, K. R. (1997). Steady-State Target Optimization in Linear Model Predictive Control, *Proc. American Control Conference,* 3597.

Muske, K.R. and J. B. Rawlings (1995). Nonlinear Moving Horizon State Estimation. *Methods of Model Based Process Control*, Berber, R., (Ed.), Kluwer Academic Publishers, 349-365.

Naidoo, K., J. Guiver, P. Turner, M. Keenan and M. Harmse (2005). Experiences with Nonlinear MPC in Polymer Manufacturing. *Preprints Int. Workshop on Assessment and Future Directions of NMPC, Freudenstadt*. 335-345.

Narraway, L.T., J.D. Perkins and G.W. Barton (1991). Interaction between process design and process control economic analysis of process dynamics. *J. Process Control,* **1**, 243-250.

Narraway, L.T. and J.D. Perkins (1993). Selection of Process Control Structure Based on Linear Dy-

namic Economics. *Ind. Eng. Chem. Res*., **32**, 2681-2692.

Natarajan, S. and J.H.Lee (2000). Repetitive model predictive control applied to a simulated moving bed chromatography system. *Comp. Chem. Eng*., **24**, 1127-1133.

Nath, R. and Z. Alzein (2000). On-line dynamic optimization of olefins plants, *Comp. Chem. Eng.,* **24,** 533-538.

Qin, S.J. and Badgewell, T. (2003). A survey of industrial model predictive control technology. *Contr. Eng. Pract.,* 11, 733-764.

Rao, C.V. and J.B. Rawlings (1999). Steady States and Constraints in Model Predictive Control. *AIChE Journal,* **45,** 1266-1278.

Rao, C.V., J.B. Rawlings and D.Q. Mayne (2003). Constrained State Estimation for Nonlinear Discrete-time Systems. *IEEE Tr on AC*, **48**, 246-258.

Roberts, P. D. (1979). An algorithm for steady-state system optimization and parameter estimation. *Int. J. Syst. Sci*. **10**, 719-734.

Rolandi, P.A. and J.A. Romagnoli. (2005). A Framework for On-line Full Optimising Control of Chemical Processes. *Proc. ESCAPE 15*, Elsevier, 1315-1320.

Roman, R., Z.K. Nagy, F. Allgöwer. and S.P. Agachi, (2005). Dynamic Modeling and Nonlinear Model Predictive Control of a Fluid Catalytic Cracking Unit. *Proc. ESCAPE 15*, Elsevier, 1363-1368.

Schäfer, A., P. Kühl, M. Diehl, J.P. Schlöder. and H.G. Bock (2006). Fast reduced multiple shooting methods for nonlinear model predictive control. Submitted to *Chemical Engineering and Processing.*

Scharf, T. and S. Engell (2005). A methodology for control structure selection based on rigorous process models. 16th *IFAC World Congress*, Tu-E14-T0/6.

Sequeira, E., M. Graells and L. Puigjaner (2002). Real-time Evolution of On-line Optimization of Continuous Processes. *Ind. Eng. Chem. Res.* **41,** 1815-1825.

Shamma, J.S. and M. Athans (1992). Gain Scheduling: Potential Hazards and Possible Remedies. *IEEE Control Systems Magazine,* **12** (3)**,** 101-107.

Singh, A, J.F. Forbes, P.J. Vermeer and S.S. Woo (2000). Model-based real-time optimization of automotive gasoline blending operations. *J. Process Control,* **10,** 43-58.

Skogestad, S. (2000). Plantwide control: The search for the self-optimizing control structure. *J. Process Control* **10**, 487-507.

Sorensen, R. C. and C. R. Cutler (1998). LP integrates economics into dynamic matrix control. *Hydrocarbon processing,* **9,** 57-65.

Srinivasan, B., D. Bonvin, E. Visser and S. Palanki (2002). Dynamic optimization of batch processes II. Role of measurements in handling uncertainty. *Comp. Chem. Eng.* **27**, 27-44.

Tatjewski, P. (2002). Iterative optimizing set-point control - the basic principle redesigned. *15th IFAC World Congress*. Barcelona.

Toumi, A., S. Engell, O. Ludemann-Hombourger, R.M. Nicoud and M. Bailly (2003). Optimization of simulated moving bed and Varicol processes. *J. Chromatography A,* **1006** (1-2), 15-31.

Toumi, A. and S. Engell (2004a). Optimal operation and control of a reactive simulated moving bed process. *Preprints IFAC Symposium ADCHEM, Hong Kong,* 243-248.

Toumi, A. and S. Engell (2004b). Optimization-based control of a reactive simulated moving bed process for glucose isomerization. *Chem. Eng. Sci.,* **59,** 3777-3792.

Toumi, A, M. Diehl, S. Engell, H.G. Bock and J.P. Schlöder (2005). Finite horizon optimizing of control advanced SMB chromatographic processes. 16th *IFAC World Congress,* Fr-M06-TO/2.

Toumi, A. and S. Engell (2005). Advanced Control of Simulated Moving Bed Processes. Chapter 9 in: *Preparative Chromatography*, Schmidt-Traub, H., (Ed.), Wiley-WCH, Weinheim, 401-416.

Wang, C., K.-U. Klatt., G. Dünnebier, S. Engell and F. Hanisch (2003). Neural network-based identification of SMB chromatographic processes. *Contr. Eng. Pract.,* **11,** 949-959.

Yip, W. S. and T. E. Marlin (2003). Designing plant experiments for real-time optimization systems. *Contr. Eng. Pract.,* **11,** 837-845.

Yip, W. S. and T. E. Marlin (2004). The effect of model fidelity on real-time optimization performance. *Comp. Chem. Eng.,* **28***,* 267-280.

Yousfi, C. and R. Tournier (1991). Steady-State Optimization Inside Model Predictive Control, *Proc. American Control Conference,* 1866.

Zanin, A.C., M. Tvrzska de Gouvea, and D. Odloak, (2000). Industrial implementation of a real-time optimization strategy for maximizing prouction of LPG in a FCC unit. *Comp. Chem. Eng.,* **24,** 525-531.

Zanin, A.C., M. Tvrzska de Gouvea, and D. Odloak (2002). Integrating real-time optimization into the model predictive controller of the FCC system. *Contr. Eng. Pract.,* **10,** 819-831.

Zhang, H., and P.D. Roberts (1990). On-line steady-state optimization of nonlinear constrained processes with slow dynamics. *Trans. Inst. Meas. Contr.*, **12,** 251-261.

Zhang, Y. and J. F. Forbes (2000). Extended design cost: A performance criterion for real-time optimization systems, *Comp. Chem. Eng.,* **24,** 1829-1841.

Zhang, Y., D. Nadler and J.F. Forbes (2001). Results analysis for trust constrained real-time optimization. *J. Process Control, **11,*** 329-341.

Zhang, Y., D. Monder and J.F. Forbes (2002). Real-time optimization under parametric uncertainty: A probability constrained approach, *J. Process Control,* **12,** 373-389.

Zheng, A., R.V. Mahajannam and J.M. Douglas (1999). Hierarchical Procedure for Plantwide Control System Synthesis. *AIchE Journal,* **45**, 1255-1265.

Zhou, J., A. Tits and C. Lawrence (1997). User's Guide for *FFSQP* Version 3.7: University of Maryland.

Keynote 1

Advances and New Directions in Plant–Wide Controller Performance Assessment

N. F. Thornhill and A. Horch,
University College London

Keynote 2

Good or Bad? When is Plant Nonlinearity an Obstacle for Control?

T. Schweickhardt and F. Allgöwer
University of Stuttgart

ADCHEM 2006

International Symposium on Advanced Control of Chemical Processes
Gramado, Brazil – April 2-5, 2006

ADVANCES AND NEW DIRECTIONS IN PLANT-WIDE CONTROLLER PERFORMANCE ASSESSMENT

Nina F. Thornhill* and Alexander Horch+

**Department of Electronic and Electrical Engineering, UCL, UK*
+ABB Corporate Research Centre, Ladenburg, Germany

Abstract: This article reviews advances in detection and diagnosis of plant-wide control system disturbances in chemical processes and discusses new directions that look promising for the future. Causes of plant-wide disturbances include non-linear limit cycles in control loops, controller interactions and tuning problems. The diagnosis of non-linearity, especially when due to valve stiction, has been an active area. Detection of controller interactions and disturbances due to plant structure remain open issues, however, and will need new approaches. For the future, the linkage of data-driven analysis with a qualitative model of the process is an exciting prospect that now looks within reach. Finally, the paper offers some comments about emerging applications.

Keywords: fault detection; nonlinear time-series analysis; oscillation, performance analysis; plantwide, process monitoring; process operation.

1. INTRODUCTION

Single-input-single-output control loop performance assessment (CLPA) and benchmarking is well established in the process industries [1,2]. The SISO approach has a shortcoming, however, because control loops are not isolated from one another. Specifically, the reason for poor performance in one control loop might be that it is being upset by a disturbance originating elsewhere.

The basic idea of process control is to divert process variability away from key process variables into places that can accommodate the variability such as buffer tanks and plant utilities [3]. Unfortunately, process variability is often *not* accommodated and it may just move elsewhere. The reason for this is that modern industrial processes have reduced inventory and use recycle streams and heat integration. The interactions are strong in such processes because the amount of buffer capacity is small and the opportunities to exchange heat energy with plant utilities are restricted.

A plant-wide approach means that the distribution of a disturbance is mapped out and the location and nature of the cause of the disturbance is determined with a very high probability of being right first time. The alternative is a time consuming procedure of testing each control loop in turn until the root cause is found. Some key requirements (e.g. see[4]) are:

- Detection of the presence of one or more periodic oscillations;
- Detection of non-periodic disturbances and plant upsets;
- Determination of the locations of the various oscillations/disturbances in the plant and their most likely root causes.

A wish-list from [2] included:

- Automated, non-invasive stick-slip detection in control valves;
- Facility-wide approaches including behaviour clustering;
- Automated model-free causal analysis;
- Incorporation of process knowledge such as the role of each controller.

The paper gives an overview of our own and others' work in detection and diagnosis of plant-wide control system disturbances. Detection of plant-wide disturbances is covered in Section 2 and the isolation

and diagnosis of the root causes in Section 3. Both attempt a logical and structured classification and a comparative review of methods as well as highlighting open issues and unsolved problems. They are illustrated with a case study from a refinery. Section 4 discusses tests for sticking valves while Section 5 describes a new research direction involving the linkage of process information with data driven analysis using computer aided design data. Finally, Section 6 outlines some potential new areas of application.

2. PLANT-WIDE DIAGNOSIS

2.1 A classification of disturbances

Timescales: The first distinction in a classification of plant-wide disturbances concerns the timescale, which may be (a) slowly-developing, e.g. catalyst degradation or fouling of a heat exchanger, (b) persistent and dynamic, and (c) abrupt, e.g. a compressor trip. The focus of this paper is on (b), dynamic disturbances that persist over a time horizon of hours to days. The approach is typically one of process auditing in which a historical data set is analysed off-line. The off-line approach gives opportunities for advanced signal processing methods such as integral transforms and non-causal filtering.

Oscillating and non-oscillating disturbances. Figure 1 shows a family tree of methods for the detection of plant-wide disturbances and cites the references. The vertical placements in the tree are of no significance, they have been adjusted in order to make the text fit. The main sub-division is between oscillating and non-oscillating behaviours. An oscillation is clear in both the time domain and as a peak in the frequency domain suggesting that either might be exploited for detection. The time trends of a non-oscillating disturbance often look somehow similar but in a way that is hard to characterize because the localised behaviour is not strongly coordinated. The frequency domain, on the other hand, shows the similarity well and therefore the spectra are exploited for detection of non-oscillating disturbances. Some dynamic disturbances are not stationery. For instance, an oscillation may come and go or may change in magnitude. The localisation in time means wavelet methods should be used for such cases.

2.2 Detection of oscillating disturbances

Methods for detection of oscillation fall into three main classes namely those which use the time domain, those using autocovariance function (ACF), and spectral peak detection. Filtering or some other way of dealing with noise is usually needed in the time domain applications. A benefit of using the ACF is that the ACF of random noise appears at zero lag leaving a clean signal for analysis at other lags. All the methods [5-10] should be able to detect the oscillations whose time domain, ACF and spectra are shown in Figure 3.

Most of the methods are off-line and exploit the off-line advantages, such as the use of the whole data set to determine a spectrum or autocovariance function. The oscillation monitor of Hägglund [5] is an on-line method and was implemented industrially in the ECA400 PID controller from Alfa Laval Automation which gave an alarm when as oscillation is detected.

The cited methods in [5-8] and [10] achieve the detection of an oscillation one measurement at a time, but more is needed for plant-wide detection than the detection of oscillations in individual control loops. It requires the recognition that an oscillation in one measurement is the same as the oscillation in another measurement, even though the shape of the waveform may differ and when interferences such as other oscillations are present. A characterization and grouping step is needed as well as oscillation detection. The method in [9] automated the detection of clusters of similar oscillations. An agglomerative classification algorithm from [16] detects the tags within each cluster and issues a report, an example of which is given in Table 1.

2.3 Detection of non-oscillating disturbances

Persistent non-oscillatory disturbances are generally characterized by their spectra which may have broad-band features or multiple spectral peaks. The plant-wide detection problem requires (a) a suitable distance measure by which to detect similarity and (b) determination and visualization of clusters of measurements with similar spectra.

In spectral principal component analysis (PCA) [11] the rows of the data matrix $\mathbf{X}$ are the power spectra $P(f)$ of the signals and a PCA decomposition reconstructs the $\mathbf{X}$ matrix as a sum over p

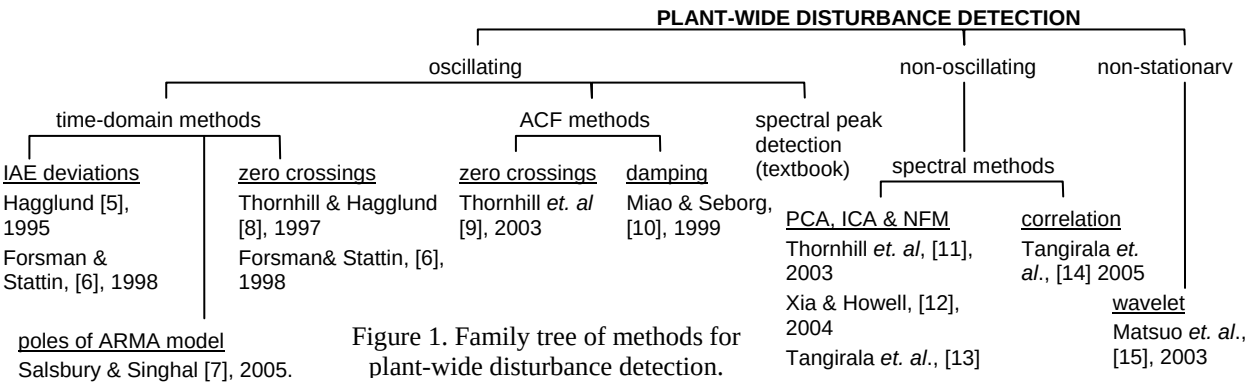

Figure 1. Family tree of methods for plant-wide disturbance detection.

orthonormal basis functions $\mathbf{w}'_1$ to $\mathbf{w}'_p$ which are spectrum-like functions each having N frequency channels arranged as a row vector:

$$\mathbf{X} = \begin{pmatrix} t_{1,1} \\ \dots \\ t_{m,1} \end{pmatrix} \mathbf{w}'_1 + \begin{pmatrix} t_{1,2} \\ \dots \\ t_{m,2} \end{pmatrix} \mathbf{w}'_2 + \dots + \begin{pmatrix} t_{1,p} \\ \dots \\ t_{m,p} \end{pmatrix} \mathbf{w}'_p + \mathbf{E}$$

The i'th spectrum in $\mathbf{X}$ maps to a spot having the co-ordinates $t_{i,1}$ to $t_{i,p}$ in a p-dimensional space. Similar spectra have similar t-coordinates and form clusters which can be detected using the Euclidian distance or the angles between lines connecting each spot to the origin. Methods for display include hierarchical tree or a colour map [13]. Independent Component Analysis (ICA) is a decomposition of a data matrix that minimises statistical dependence between the basis vectors. It gives basis functions with a good one-to-one relationship with the physical sources of signals, as shown by Xia and Howell [12] who gave the first application of ICA to process spectra. Non-negative matrix factorization (NMF) was introduced in the area of image recognition [17]. The authors described it as follows: "The basis images for PCA are *eigenfaces* … which resemble distorted versions of whole faces. The NMF basis … are localized features that correspond with … the parts of faces." The first report of the use of NMF for plant-wide disturbance analysis is [13].

2.4 Case study example[1]

The upper panel in Figure 3 plots mean centred and normalized data from the refinery separation unit of Figure 2 showing a large amplitude oscillation in steam flow, analyser and temperature controller errors (*err*) and outputs (*op*) Measurements from upstream and downstream pressure controllers PC1 and PC2 are also included. The lower panel shows the power spectra. The sampling interval was 20s. The steam sensor in FC1 was faulty. Condensate collected on the upstream side of the orifice plate until it reached a critical level, and the accumulated liquid would then periodically clear itself by siphoning through the orifice causing the plant-wide oscillation that can be seen in the data.

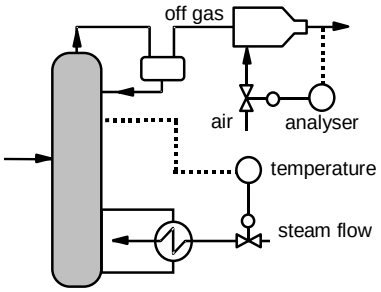

Figure 2. Process schematic.

[1] The methods illustrated in the case study are being productized in a joint ABB/University project [18].

Table 1 gives the results of plant-wide oscillation analysis using [9]. Two plant-wide oscillations are reported because the most regularly oscillating tags in each group (those with the smallest standard deviation) have oscillation periods that are different by more that the standard deviation of either (Tag 4 has 18.9 ± 1.5 and Tag 7 has 21.1 ± 1.1).

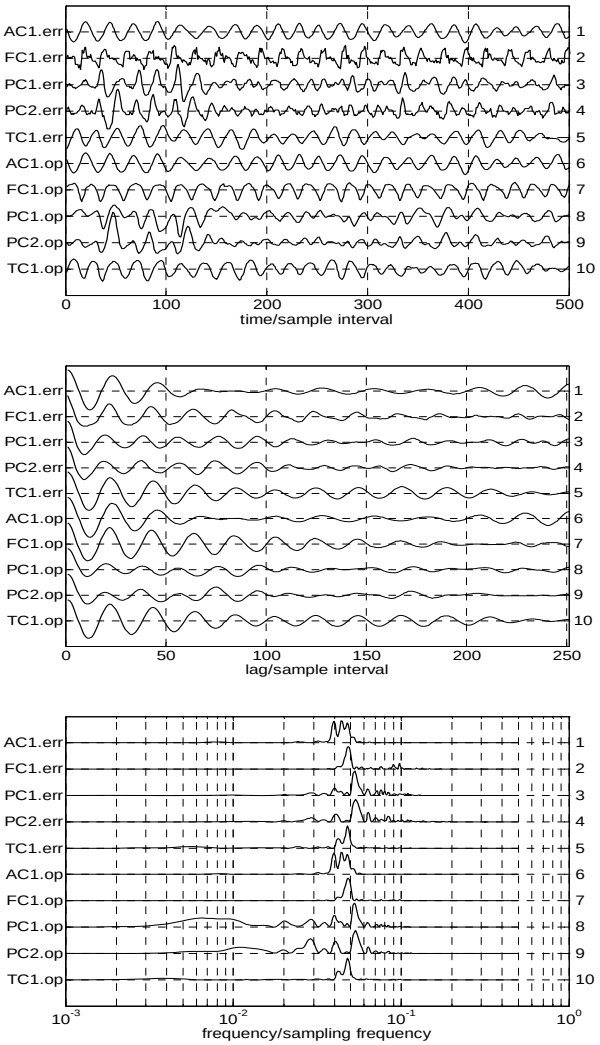

Figure 3. Data set. Upper panel: time trends. Middle panel: ACF. Lower panel: power spectra.

Table 1. Oscillation analysis for the industrial case study.

tag analysis

tag no	period	tag no	period
1	20.4 ± 4.3	6	20.4 ± 4.3
2	20.9 ± 2.5	7	21.1 ± 1.1
3	19.1 ± 1.8	8	18.7 ± 5.5
4	18.9 ± 1.5	9	18.9 ± 3.9
5	20.9 ± 1.1	10	20.7 ± 1.4

cluster analysis

period	tags
18.9	4 3 9 8
20.7	7 5 10 2 6 1

The results of spectral principal component analysis are shown in the form of a hierarchical tree in Figure 4 in which the spectrum of each tag is represented as

a square on the horizontal axis. Spectra form a cluster if they are connected to each other by short vertical lines and are well separated from all other spectra. The tree shows Tags 3, 4, 8 and 9 have similar spectra (PC1 and PC2), as do 1, 2, 5, 6, 9, and 10 (FC1, TC1 and AC1). The wide separation of the spectral PCA clusters shows that the groups are distinctly different thus confirming the finding from oscillation analysis. Tags 1 and 6 are the controller error and controller output of AC1. AC1 at the top of the column is physically well separated from FC1 and TC1 (Tags 2, 5, 7 and 10), however, it shares similar dynamic behaviour.

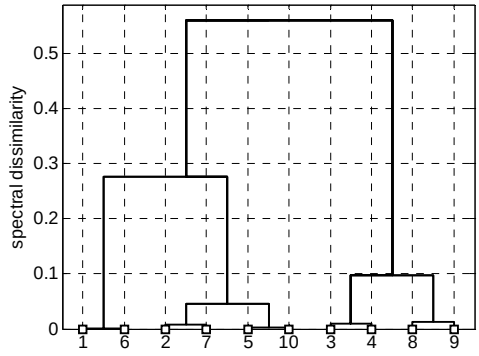

Figure 4 Spectral classification tree.

3. ROOT CAUSE DIAGNOSIS

Figure 5 is a family tree of methods for the diagnosis of a plant-wide disturbance. The main distinction is between *non-linear* and *linear* sources. Examples of non-linear sources include:

- Control valves with excessive static friction;
- On-off and split-range control;
- Sensors faults;
- Process non-linearities leading to limit cycles;
- Hydrodynamic instability such as slugging flows.

The diagnosis problem decomposes into two parts. Firstly the root cause of each plant-wide disturbance should be distinguished from the secondary propagated disturbances which will be solved without any further work when the root cause is addressed. The second stage is testing of the candidate root cause loop to confirm the diagnosis.

3.1 Finding a non-linear root cause of a plant-wide disturbance

Examples of plant-wide disturbances caused by non-linearity were discussed in [21]. They included a faulty steam flow sensor and a hydrodynamic instability caused by foaming in an absorber column. Other examples include the stop-start nature of flow from a funnel feeding molten steel into a rolling mill [37] and variations in consistency of pulp in a mixing process [24]. The point of these examples is to show that disturbances due to non-linearity are not just confined to control valve problems.

Non-linear time series analysis: A non-linear time series means a time series that was generated as the output of a non-linear system, and a distinctive characteristic is the presence of phase coupling between different frequency bands. Non-linear time series analysis uses concepts that are quite different from linear time series methods and are covered in the textbook of Kantz and Schreiber [38]. For example, surrogate data are times series having the same power spectrum as the time series under test but with the phase coupling removed by randomization of phases. A key property of the test time series is compared to that of its surrogates and nonlinearity is diagnosed if the property is significantly different in the test time series. Another method of nonlinearity detection uses higher order spectra because these are sensitive to certain types of phase coupling. The bispectrum and the related bicoherence have been used to detect the presence of nonlinearity in process data [19]. Root cause diagnosis based on non-linearity has been reported [20,21,39] on the assumption that the measurement with the highest non-linearity is closest to the root cause.

Limit cycles and harmonics: Sustained limit cycles are common in non-linear systems. The waveform in a limit cycle is periodic but non-sinusoidal and therefore has harmonics which can be used to detect non-linearity. It is not always true, however, that the time trend with the largest harmonic content is the

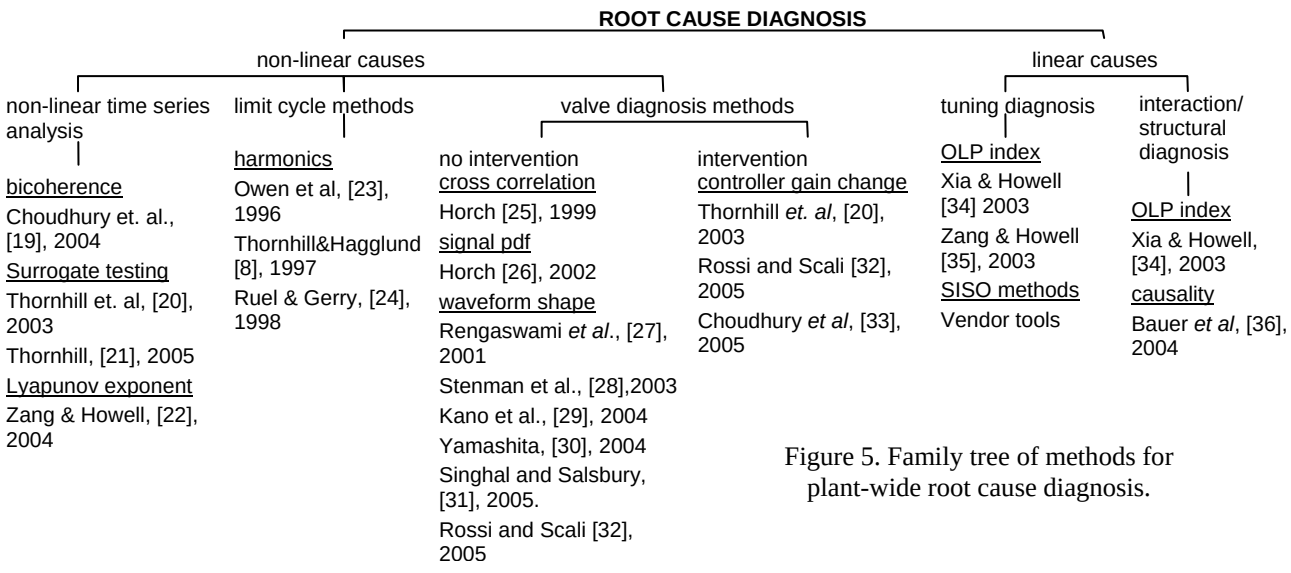

Figure 5. Family tree of methods for plant-wide root cause diagnosis.

root cause. The second and third harmonics of a non-sinusoidal oscillatory disturbance are sometimes amplified in the secondary disturbance when a control loop compensates for higher harmonics in an external disturbance. In that case the harmonic content of the manipulated variable may be higher than that of either the disturbance or the controlled variable, even though non-linearity tests show the manipulated variable to be more linear [40].

Disturbance propagation: The reason why the non-linearity is strongest nearest to the source of a disturbance is that the plant acts as a mechanical filter. As the limit cycle propagates to other variables such as levels, compositions and temperatures the waveforms generally become more sinusoidal and more linear because plant dynamics destroys the phase coupling and removes the harmonics. Empirically, non-linearity measures do very well in isolation of non-linear root causes. However, a full theoretical analysis is missing at present of why and how the various measures change as a disturbance propagates, and this remains open research question.

Case study example: Non-linearity testing using [21] showed the group of tags in Table 1 with the 21 samples per cycle oscillation period had non-linearity in the FC1 controller output, FC1 controller error and the TC1 controller output which points unambiguously to the FC1 slave control loop as the source of the oscillation. This is the correct result, the FC1 control loop was in a limit cycle because of its faulty steam flow sensor. There was no non-linearity present in tags 3, 4, 8 and 9 associated with PC1 and PC2 and a root cause other than non-linearity has to be sought for their oscillation. A controller interaction is suspected because set point changes in PC1 (not shown) initiated oscillatory transient responses in both pressure controllers.

3.2 Finding a linear root cause of a plant-wide disturbance

A poll of industrial process control engineers at a June 2005 IEE Seminar in the UK suggested the most common root causes, after non-linearity, are poor controller tuning, controller interaction and structural problems involving recycles. The detection of poorly tuned loops SISO loops is routine using commercial CLPA tools, but the question of whether an oscillation is generated by the controller or is external has not yet been solved satisfactorily. Promising approaches to date require some knowledge of the transfer function [34].

There has been little academic work to address the diagnosis of controller interaction and structural problems using only data from routine process operations. Some progress in being made, however, by cause and effect analysis of the process signals using a technique that is sensitive to directionality to find the origin of a disturbance [36,41,42]. The methods are sensitive to time delays, attenuation and the presence of noise and further disturbances that affect the propagating signals. The outcome of the analysis is a qualitative process model showing the causal relationships between variables.

An example: The analysis can be a help to an experienced process control engineer who has good knowledge of the process. A joint study between BP and UCL used the method of transfer entropy with data from a process with a recycle, Figure 6. None of the time trends was non-linear and the causal map implicated the recycle because all the variables in the recycle were present in the order of flow. Knowing that the problem involves the recycle rather than originating with any individual control loop suggested the need for an advanced control solution.

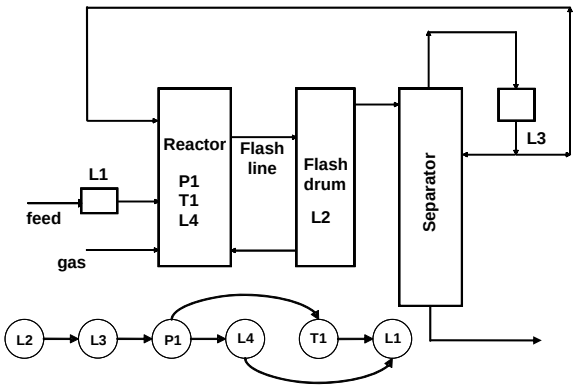

Figure 6. Cause and effect in a process with recycle (courtesy of A. Meaburn and M. Bauer).

4. VALVE TESTS

If a root cause has been isolated to a particular part of the plant then further tests are usually carried out before maintenance action is requested. Also, some alleviating actions may be taken to minimise the impact of the problem. Figure 5 cites references for useful methods which have been reviewed in detail elsewhere [43]. Some general observations are discussed here.

Stiction in valves: A problem with control valves is the dead band and stick-slip behaviour (stiction) caused by excessive statistic friction [44]. *Deadband* arises when a finite force is needed before the valve stem starts to move, *stick-slip* behaviour happens when the maximum static friction required to start the movement exceeds the dynamic friction once the movement starts [44, 45, 46;47].

Control valve diagnosis is straightforward if the controller output signal, *op*, and either the flow through the valve, *mv*, or the valve position are measured. A *op-mv* plot is a straight line at 45 degrees for a healthy linear valve, and any deviations such as deadband can be easily diagnosed by visual inspection. Unfortunately the flow through the control valve is frequently *not* measured unless it is in a flow control loop. Similarly, the position, while it may be measured on a modern valve with a positioner, is not always available in the data historian. The challenge in analysis of valve problems, then, is to determine and quantify the type

of fault present using *op* and *pv* data only. The *pv* is the measurement or controlled variable of the control loop, for instance the level in the case of a level control loop. The major difficulty is that the process dynamics (integration in the case of a level loop) greatly interfere with the analysis. It is encouraging that several of the methods reviewed in depth in [43] are able to utilize *op* and *pv* data successfully.

The impact of the controller on the limit cycle: It has been known for many years that control loops with sticking valves do not always have a limit cycle [48,49]. Table 2 lists the behaviour depending on the process, controller and the presence or not of deadband and stick-slip. A short-term solution is to change the controller to *P*-only. The oscillation should disappear in a non-integrating process and while it may not disappear in an integrating process its amplitude will probably decrease.

A further observation is that changing the controller gain changes the amplitude and period of the limit cycle oscillation. In fact, observing such a change is a good test for a faulty control valve [20]. The aim is to reduce the magnitude of the limit cycle in the short term until maintenance can be carried out. In practice, since the expected change in amplitude and period is complicated to work out, one tries a 50% reduction in gain first or a similar increase in gain if the trends seems to be going the wrong way.

Table 2 Limit cycles in control loops.

process and controller	deadband only	stick-slip
integrating, PI	limit cycle	limit cycle
integrating, P-only	no limit cycle	limit cycle
non-integrating, PI	no limit cycle	limit cycle
non-integrating, P-only	no limit cycle	no limit cycle

5. USE OF PROCESS INFORMATION

Qualitative process information is implicitly used in diagnosis when an engineer analyses the results from a data-driven analysis. An exciting possibility is to capture and make automated use of such information. Qualitative models include signed digraphs (SDG) [50, 51] and Multilevel Flow Modelling [52]. Chiang and Braatz [53] and also [54] showed enhanced diagnosis using signal based analysis if a qualitative model is available.

We believe that qualitative models of processes will in future become almost as readily available as the historical data. The new technology that will generate such models is already in place in Computer Aided Engineering tools such as ComosPT (Innotec) and Intools (Intergraph). The object-oriented representation of process diagrams can be exported in a text based format that describes equipments and the connections between them. In Europe, the Standard is a (Pre)Norm DIN V 44366:2004-12 called Computer Aided Engineering Exchange (CAEX). ISO-15926-7 is a similar standard.

A prototype tool that links a CAEX description with a data-driven analysis has been demonstrated in a joint project between UCL and ABB. Its aim is to parse and draw conclusions from an electronic process schematic. When linked with data-driven signal analysis of process measurements the end result is a powerful diagnostic tool for isolating the root causes of disturbances. The features are:

- Capture of a process connectivity description using CAEX;
- Parsing and manipulation of the description;
- Linkage of plant description and results from data-driven analysis;
- Testing of root cause hypotheses through falsification;
- Logical tools to give root cause diagnosis and process insights.

The CAEX file describes items of equipment in the plant such as tanks, pipes, valves and instruments and how they are linked together physically and/or through electronic control signals. The data file gives information about the plant disturbances, for instance the period of oscillation, its intensity and regularity, the measurement points where it was detected and any non-linearity detected in the time trends.

A reasoning engine finds physical paths and control paths in the plant and connections between equipments, and determines root causes for plant-wide disturbances. For example, detection of non-linearity in the time series of the process measurements suggests a non-linear root cause such as a sticking valve. In the case of ambiguity then the reasoning engine highlights the one further upstream as the more likely root cause. It can also verify that there is a feasible propagation path between a candidate root cause and all the other locations in the plant where secondary disturbances have been detected. A further capability is to suggest the best proxy measurement point for an unmeasured flow.

6. NEW APPLICATION AREAS

Plant-wide detection and diagnosis is starting to have an impact in areas outside process systems such as power plants, supply chains and electricity transmission systems. The techniques map across without difficulty after adjustments for the timescales, for instance inter-area oscillation in electricity transmission typically have periods of 2 to 5 seconds while in manufacturing supply chains the oscillation have periods of weeks to months. The main challenge in successful transfer of the methods is in knowing what faults are typical of the target systems, and the business needs and drivers.

Power plant applications: The heart of the power generation process is a recycle. Power plants are well-equipped with sensors and instrumentation is generally well maintained. Typical disturbances therefore are linear root-causes rather than actuator and instrument problems. The density of instrumentation means that many measurements

share similar disturbance patterns which increases the complexity of the task to be solved. On the other hand, due to the dense instrumentation, it should be possible to locate possible root causes rather exactly.

Supply chain: Business needs include detection and diagnosis of rogue seasonality and demand amplification. Rogue seasonality is oscillation in inventory, orders and deliveries to customers induced by internal business practices. Demand amplification (also known as bullwhip) occurs in multi-echelon chains when replenishment rules magnify small variations in end-customer demands into large amplitude variations for upstream suppliers. Business data are often presented as weekly averages, meaning that only 52 data points are generated per year for each measured variable.

Electricity transmission: A requirement for daily operation is for on-line assessment of the damping status of a transmission network, and methods already exist to do this task.. The tools described in this paper are for off-line auditing, nevertheless they have promise for the analysis and diagnosis immediately after an operational problem. Data collection is challenging. One issue is the accurate time-stamping of data collected over a very wide area, another is the compilation of data from different commercial organizations. Generating companies own the measurements of generator speed and rotor angle, while the transmission company owns the voltage, current and bus angle measurements.

7. SUMMARY

Section 1 listed some industrial requirements and a wish-list for plant-wide controller performance assessment. The work reviewed in this paper has showed good progress towards these targets especially in detection of plant-wide disturbances and behaviour clustering. Non-linear root causes can now be located and distinguished from the secondary propagated disturbances using analysis of signals from routine operation, with a high chance of being right first time. Stiction detection in valves has had much attention with several methods starting to perform well even in the difficult situation where no manipulated variable is measured. The isolation of linear root causes such as controller interactions and recycle dynamics is an open area still needing attention, however. Finally, we believe the linkage of plant layout information with signal analysis is due to take a big step forward using new Standards for description of plant layouts.

8. ACKNOWLEDGMENTS

The first author gratefully acknowledges the support of the Royal Academy of Engineering (Global Research Award) and of ABB Corporate Research.

9. REFERENCES

1 Qin, S.J. (1998). Control performance monitoring - a review and assessment. *Computers and Chemical Engineering*. **23** 173-186.
2 Desborough, L. and R. Miller (2002). Increasing customer value of industrial control performance monitoring – Honeywell's experience. *AIChE Symposium Series* No 326. **98**, 153-186.
3 Luyben, W.L., B.D. Tyreus and M.L. Luyben (1999). *Plantwide Process Control*. McGraw-Hill.
4 Paulonis, M.A. and J.W. Cox (2003). A practical approach for large-scale controller performance assessment, diagnosis, and improvement. *Journal of Process Control*. **13**, 155-168.
5 Hägglund, T. (1995). A control-loop performance monitor. *Control Engineering Practice*. **3**, 1543-1551.
6 Forsman, K. and A. Stattin, (1999). A new criterion for detecting oscillations in control loops. *European Control Conference*, Karlsruhe, Germany.
7 Salsbury, T.I. and A. Singhal, (2005). A new approach for ARMA pole estimation using higher-order crossings. *Proceedings of ACC 2005*, Portland, USA.
8 Thornhill, N.F. and T. Hägglund (1997). Detection and diagnosis of oscillation in control loops. *Control Engineering Practice*. **5**, 1343-1354.
9 Thornhill, N.F., B. Huang, and H. Zhang (2003). Detection of multiple oscillations in control loops. *Journal of Process Control*. **13**, 91-100.
10 Miao, T. and D.E. Seborg (1999). Automatic detection of excessively oscillatory feedback control loops. *IEEE Conference on Control Applications*. Hawaii, 359-364
11 Thornhill, N.F., S.L. Shah, B. Huang, and A. Vishnubhotla (2002). Spectral principal component analysis of dynamic process data. *Control Engineering Practice*. **10**, 833-846.
12 Xia, C. and J. Howell (2005). Isolating multiple sources of plant-wide oscillations via spectral independent component analysis. *Control Engineering Practice*. **13**, 1027-1035.
13 Tangirala, A.K. and S.L. Shah (2005). Non-negative matrix factorization for detection of plant-wide oscillations. *Submitted to IEEE Transactions on Knowledge and Data Mining*.
14 Tangirala, A.K., S.L. Shah and N.F. Thornhill (2005). PSCMAP: A new measure for plant-wide oscillation detection. *Journal of Process Control*. **15**, 931-941.
15 Matsuo, T. H. Sasaoka and Y. Yamashita (2003). Detection and diagnosis of oscillations in process plants. *Lecture Notes in Computer Science*. **2773**, 1258-1264.
16 Chatfield, C. and A.J. Collins (1980) *Introduction to Multivariate Analysis*. Chapman and Hall, London, UK
17 Lee, D.D. and H.S. Seung (1999). Learning the parts of objects by non-negative matrix factorization. *Nature*. **401**,788-791.
18 Horch, A., V. Hegre, K. Hilmen, H. Melbø, L. Benabbas, E.N. Pistikopoulos, N.F. Thornhill and N. Bonavita (2005). Root Cause - Computer-aided plant auditing made possible by successful university cooperation. *ABB Review* 2/2005. Online: http://www.abb.com/abbreview
19 Choudhury, M.A.A.S., S.L., Shah and N.F. Thornhill (2004). Diagnosis of poor control loop performance using higher order statistics. *Automatica*. **40**, 1719–1728.
20 Thornhill, N.F., J.W. Cox and M. Paulonis (2003). Diagnosis of plant-wide oscillation through data-driven

analysis and process understanding. *Control Engineering Practice*. **11**, 1481-1490.
21 Thornhill, N.F. (2005). Finding the source of nonlinearity in a process with plant-wide oscillation. *IEEE Transactions on Control System Technology*. **13**, 434-443
22 Zang, X. and J. Howell (2004). Correlation dimension and Lyapunov exponents based isolation of plant-wide oscillations. *DYCOPS* 7, Boston July 5-7.
23 Owen, J.G., D. Read, H. Blekkenhorst and A.A. Roche (1996). A mill prototype for automatic monitoring of control loop performance. *Proceedings of Control Systems 96*, Halifax, Novia Scotia, 171-178.
24 Ruel, M. and J. Gerry (1998). Quebec quandary solved by Fourier transform. *Intech* (*August*), 53-55.
25 Horch, A. (1999). A simple method for detection of stiction in control valves. *Control Engineering Practice*. **7**, 1221-1231.
26 Horch, A., 2002, Patents WO0239201 and US2004/0078168
27 Rengaswamy, R., T. Hägglund and V. Venkatasubramanian (2001). A qualitative shape analysis formalism for monitoring control loop performance. *Engineering Applications of Artificial Intelligence*. **14**, 23-33.
28 Stenman, A., F., Gustafsson and K. Forsman (2003). A segmentation-based method for detection of stiction in control valves. *International Journal of Adaptive Control and Signal Processing*. **17**, 625-634.
29 Kano, M., H. Maruta, H. Kugemoto and K. Shimizu (2004). Practical model and detection algorithm for valve stiction. *DYCOPS* 7, Boston, USA, July 5-7.
30 Yamashita, Y. (2004). Qualitative analysis for detection of stiction in control valves. *Lecture Notes in Computer Science*. **3214**, Part II, 391-397.
31 Singhal, A. and T.I. Salsbury (2005). A simple method for detecting valve stiction in oscillating control loops. *Journal of Process Control*. **15**, 371-382.
32 Rossi, M. and C. Scali (2005). A comparison of techniques for automatic detection of stiction: simulation and application to industrial data. *Journal of Process Contro*l. **15**, 505-514.
33 Choudhury, M.A.A.S., V. Kariwala, S.L. Shah, H. Douke, H. Takada and N.F. Thornhill (2005). A simple test to confirm control valve stiction. *IFAC World Congress* 2005, July 4-8, Praha.
34 Xia, C. and J. Howell (2003). Loop status monitoring and fault localisation. *Journal of Process Control*. **13**, 679-691.
35 Zang, X. and J. Howell (2003). Discrimination between bad turning and non-linearity induced oscillations through bispectral analysis. *Proceedings of SICE Annual Conference*, Fukui, Japan.
36 Bauer, M., N.F. Thornhill and A. Meaburn (2004). Specifying the directionality of fault propagation paths using transfer entropy. *DYCOPS* 7 *conference*, Boston, July 5-7, 2004.
37 Graebe, S.F., G.C. Goodwin and G. Elsley (1995). Control design and implementation in continuous steel casting. *IEEE Control Systems Magazine*. **15**(4), 64-71.
38 Kantz, H. and T. Schreiber (1997). *Nonlinear Time Series Analysis*. Cambridge University Press.
39 Zang, X. and J. Howell (2005). Isolating the root cause of propagated oscillations in process plants. *International Journal of Adaptive Control Signal Processing*, **19**, 247-265.
40 Matsuo, T., I. Tadakuma and N.F. Thornhill (2004). Diagnosis of a unit-wide disturbance caused by saturation in a manipulated variable, *IEEE Advanced Process Control Applications for Industry Workshop*,. Vancouver, April 26-28 2004.
41 Huang, B., N.F. Thornhill, S.L. Shah and D. Shook (2002). Path analysis for process troubleshooting. *Proceedings of AdConIP 2002*, Kumamoto, Japan, 149-154.
42 Schreiber, T. (2000). Measuring information transfer. *Physical Review Letters*. **85**, 461-464.
43 Horch, A. (2006). Benchmarking control loops with oscillations and stiction. In: *Process Control Performance Assessment*. (Ordys, A., Uduehi, D and Johnson, M.A, Eds), Springer, Guildford, UK.
44 Choudhury, M.A.A.S., N.F. Thornhill and S.L. Shah (2005). Modelling of valve stiction. *Control Engineering Practice.* **13**, 641-658.
45 Olsson, H. (1996). *Control Systems With Friction*. PhD thesis, Lund Institute of Technology, Sweden
46 Karnopp, D. (1985). Computer simulation of stick-slip friction in mechanical dynamical systems. *Journal of Dynamic Systems, Measurement, and Control*. **107**, 100–103.
47 Kayihan, A. and F.J. Doyle III (2000). Friction compensation for a process control valve. *Control Engineering Practice*. **8**, 799–812.
48 McMillan, G. K. (1995). Improve control valve response. *Chemical Engineering Progress*. **91**(6), 76-84.
49 Piipponen, J. (1996). Controlling processes with nonideal valves: Tuning of loops and selection of valves. *Proceedings of Control Systems 96, Halifax, Nova Scotia, Canada*, 179–186.
50 Venkatasubramanian, V., R. Rengaswamy and S.N. Kavuri (2003). A review of process fault detection and diagnosis Part II: Qualitative model and search strategies. *Computers and Chemical Engineering*. **27**, 313-326.
51 Maurya MR, R. Rengaswamy and V. Venkatasubramanian (2004). Application of signed digraphs-based analysis for fault diagnosis of chemical process flowsheets. *Engineering Applications of Artificial Intelligence*. **17**, 501-518.
52 Petersen, J. (2000). Causal reasoning based on MFM. *Proceedings of Cognitive Systems Engineering in Process Control* (CSEPC 2000), Taejon, Korea, 36-43.
53 Chiang, L.H. and R.D. Braatz (2003). Process monitoring using causal map and multivariate statistics: fault detection and identification. *Chemometrics and Intelligent Laboratory Systems*. **65**, 159-178.
54 Lee GB, S.O. Song, and E.S. Yoon (2003). Multiple-fault diagnosis based on system decomposition and dynamic PLS. *Industrial & Engineering Chemistry Research*. **42**, 6145-6154.

ADCHEM 2006

International Symposium on Advanced Control of Chemical Processes
Gramado, Brazil – April 2-5, 2006

GOOD OR BAD – WHEN IS PLANT NONLINEARITY AN OBSTACLE FOR CONTROL?

Tobias Schweickhardt * **Frank Allgöwer** *

* *Institute for Systems Theory and Automatic Control, University of Stuttgart, Germany*

Abstract: Virtually every real process is a nonlinear system. Nevertheless, linear system analysis and linear controller design methods have proven to be adequate in many applications. On the other hand, there are nonlinear processes that require or benefit from nonlinear control. Therefore, recognizing a system as being nonlinear does not suffice, but the extent and severity of a system's inherent nonlinearity is the crucial characteristic in order to decide whether linear system analysis and controller synthesis methods are adequate. The introduction of nonlinearity measures is an attempt to systematically approach this problem. In this contribution, we review existing approaches to nonlinearity assessment, we state the most important results and we give a glance ahead to what might be expected from this field in the future. *Copyright © 2006 IFAC*

Keywords: Nonlinear control, robust control, nonlinearity

1. INTRODUCTION

Linear techniques for systems analysis and controller design are well developed. For many control-related engineering problems, methods are available that are theoretically sound as well as practically implementable. Due to the diverse qualitative behaviour of nonlinear systems, tools for nonlinear systems analysis and control will probably never reach the same level of generality. To cope with nonlinear control problems, there are two alternative approaches. For highly nonlinear systems, special methods have to be developed that rely upon certain physical properties of the application or upon mathematical properties of a certain system class, like energy-shaping methods for mechanical control systems or feedback linearization. For mildly nonlinear systems, one can attempt to use a linear model and linear controller design methods, hoping that the nonlinear distortion is not large enough to destabilize destabilize the closed-loop system or to deteriorate closed-loop performance.

However, there are no mathematical definitions of "mildly nonlinear" and "highly nonlinear" process behaviour, and it is often difficult to decide whether a control problem at hand is a candidate for the application of linear or nonlinear controller design techniques. The area of quantitative nonlinearity assessment aims at filling that gap by deriving systematic methods to evaluate the degree of nonlinearity inherent to a plant, and its impact on the control design task. In particular it is of interest to ask the questions

(1) How good can a linear model for a given nonlinear process be?
(2) How good can a linear controller for a given nonlinear process be?
(3) How can a suitable linear controller for a given nonlinear process actually be designed?

The aim of this paper is to introduce the field of nonlinearity assessment and to present recent developments. To this end, we first give a brief overview on existing approaches to nonlinearity assessment in Section 2. Giving a comprehensive treatment of some well-known facts and some recent results, we then

study questions (1) and (3) in greater detail. Some approaches to answer question (2) can be found in (Stack and Doyle III, 1997*b*; Schweickhardt *et al.*, 2003; Shastri *et al.*, 2004). In Section 3 we introduce nonlinearity measures as a means to quantify the best achievable quality of a linear model for a nonlinear process. We review the properties of nonlinearity measures and discuss ways to compute the values of nonlinearity measures for practical systems. The material of this Section also provides a basis for the subsequent presentation. In Section 4 an approach is presented that integrates nonlinearity assessment and the design of linear controllers for nonlinear systems based on linear robust control techniques and based on the nonlinearity measures introduced earlier. The paper concludes with Section 5.

2. A LITERATURE REVIEW

Nonlinearity measures appeared for the first time in (Desoer and Wang, 1980), where the induced gain of the difference between a nonlinear system and its best linear model is considered. This viewpoint is also adopted in (Allgöwer, 1995) and will be considered in greater detail in Section 3. The basic idea of this approach is to consider the input/output-behaviour of a system, and how closely it can be reproduced by linear models. In (Desoer and Wang, 1980) also the norm of the error signal itself is proposed as a nonlinearity measure and in (Sourlas and Manousiouthakis, 1992; Sourlas and Manousiouthakis, 1998) a method is given to compute this measure for second order discrete-time Volterra models with any desired precision.

The idea of linear modeling for nonlinear systems is further developed for the discrete-time case in (Partington and Mäkilä, 2002). System gains for nonlinear systems are defined and an upper bound on the modeling error $\left\|\tilde{G} - G\right\|_{i,\infty}$ for discrete-time piecewise linear systems is given. In (Mäkilä and Partington, 2003), the best linear models for discrete-time bi-gain systems is given with respect to the l_∞-norm and the existence of a best linear model for nonlinear finite impulse response filters is proven. The relative induced error $\left\|\tilde{G} - G\right\|_{i,\infty} / \|G\|_{i,\infty}$ as a measure of nonlinearity is mentioned. It is also of interest to study the achievable approximation quality for one given input only (Mäkilä, 2003; Mäkilä and Partington, 2004; Mäkilä, 2004). It can be shown that there are situations in which the best linear model defined this way is better suited for controller design than the model obtained by linearization around an equilibrium (or trajectory) (Mäkilä and Partington, 2004). A generalization of such a nonlinearity measure to (continuous-time) batch processes can be found in (Helbig *et al.*, 2000). It is also possible to consider not only linear models, but for instance Hammerstein systems, Wiener systems or Volterra series expansions as models for a general nonlinear system, and to quantify the suitability of the respective model class (Menold *et al.*, 1997*a*; Pearson *et al.*, 1997; Menold *et al.*, 1997*b*). A common property of all nonlinearity measures based on system gains is that they are only defined for stable systems.

A rather geometric viewpoint is taken in (Guay *et al.*, 1995; Guay, 1996), where the curvature of the steady state map is introduced as a measure of nonlinearity. A very interesting result is that two components of nonlinearity can be discerned, a tangential component that can be compensated for by input transformations and a normal component that can only be affected by coordinate transformations or feedback. The curvature measure can be extended to dynamic systems using Fréchet derivatives of operators (Guay *et al.*, 1997*b*; Guay, 1996). Again, these measures can only be calculated for stable processes.

A third approach is presented by Hahn and Edgar (2001*a*; 2001*b*), who introduce empirical controllability and observability Gramians in order to quantify the degrees of input-to-state and state-to-output nonlinearity respectively.

All approaches so far consider process nonlinearity as some kind of inherent process property that stands for itself. On the other hand, nonlinearity assessment, like robustness analysis, needs further specification in order to be meaningful. In robustness analysis we want a certain property (to be specified) of the system to be robust under a certain type of uncertainty or disturbance (to be specified). In a similar way, we have to specify the task we want to perform in order to decide whether process nonlinearity is of importance: for the same process, the tasks of process control, process design, process monitoring and model or parameter identification may be affected in very different ways by the nonlinear behaviour.

So far, only identification of nonlinear systems (see e.g. (Haber and Unbehauen, 1990; Dobrowiecki and Schoukens, 2001; Schoukens *et al.*, 2002; Enqvist and Ljung, 2002; Enqvist and Ljung, 2004)) and control-relevant nonlinearity assessment have received considerable attention in the literature. The notion of control-law nonlinearity was introduced by Guay *et al.* (1995; 1996). As the inverse process steady-state map can be used to achieve perfect set-point tracking, it is analyzed by the curvature measure in order to obtain a measure of control law nonlinearity. Similar to the open-loop steady-state map curvature measure, the control-law nonlinearity measure captures only static effects and is defined only for stable systems. In (Guay *et al.*, 1997*a*; Guay, 1996), the approach of the control law nonlinearity measure is extended to a nonlinear interaction measure representing a generalization of the *relative gain array (RGA)* (Bristol, 1966).

Stack and Doyle III (1997*b*) emphasize that not only the plant dynamics and the operating region determine the control-law nonlinearity analysis, but the

performance objective plays an important role as well. Therefore they suggest to measure the nonlinearity of the optimal controller given by the classical optimal control theory. The controller structure is not restricted in advance but only the optimization criterion must be specified. In order to circumvent the derivation of the exact solution for the optimal state feedback controller, Stack and Doyle III define the so-called Optimal Control Structure (OCS). By this means, interesting questions can be examined like the dependence of control-relevant nonlinearity on the set-point and region of operation (Stack and Doyle III, 1997*a*), the relation between nonlinearity and controller aggressiveness (Stack and Doyle III, 1997*b*; Hernjak *et al.*, 2002) and the severity of certain classes of nonlinear behaviour (Hernjak *et al.*, 2002). Extensions to measurement feedback have also been made (Stack and Doyle III, 1997*a*; Hernjak *et al.*, 2002). This method is further developed in (Schweickhardt *et al.*, 2003) to the Optimal Control Law (OCL) nonlinearity measure that is better suited for numeric treatment and allows for processes with both stable and unstable modes. A case study of a chemical reactor is treated in (Shastri *et al.*, 2004).

The framework of nonlinear internal model control provides also a basis for control-relevant nonlinearity assessment. This approach is taken e.g. in (Stack and Doyle III, 1999; Eker and Nikolaou, 2002; Hernjak *et al.*, 2003).

Instead of analyzing the nonlinearity numerically in the whole region of operation, one can attempt to quantify the sensitivity of the closed loop performance on process nonlinearity locally at the operating point. First steps in this direction are presented in (Dier *et al.*, 2004; Guay and Forbes, 2004; Guay *et al.*, 2005).

3. NONLINEARITY MEASURES AND LINEAR MODELS FOR NONLINEAR SYSTEMS

In this chapter, we define different nonlinearity measures, specify some of their properties and discuss computational schemes to derive numerical values of the measures.

3.1 Definition and basic properties of nonlinearity measures

The fundamental setup of the input/output-based nonlinearity measures is depicted in Fig. 1. A general nonlinear (i.e. not necessarily linear) stable dynamical system N, described by the transfer operator $N : u \mapsto y = Nu$ is compared to a linear model G described by the linear transfer operator $G : u \mapsto \tilde{y} = Gu$ that approximates the dynamic behaviour of N. The signals u, y and $\tilde{y}$ represent input and output trajectories of the systems N and G respectively. Without loss of generality it is assumed that $N0 = 0$. The

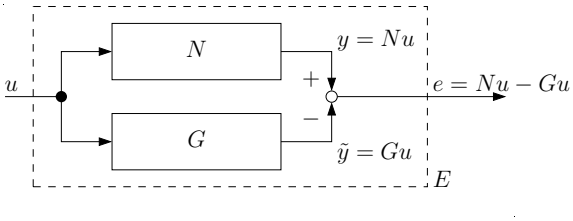

Fig. 1. Setup for comparison of a nonlinear system N with a linear system G.

error signal e is the difference between the output y of the nonlinear system and the output $\tilde{y}$ of the linear system. In order to quantify this error, a signal norm like $\|e\|_p = \left(\int_0^\infty |e(t)|^p \,\mathrm{d}t\right)^{1/p} < \infty$ for $0 \le p < \infty$ or $\|e\|_\infty = \operatorname{ess\,sup}_{t\ge 0} |e(t)| < \infty$ for $p = \infty$ ("peak norm") will be used, where $|\cdot|$ denotes the Euclidean vector norm. In the sequel, we will simply write $\|\cdot\|$, leaving the type of norm unspecified when any choice is possible. The required type of stability for the plant N is always the corresponding (finite-gain) L_p-stability (Vidyasagar, 2002).

Yet the norm of the error itself, $\|e\| = \|Nu - Gu\|$ is not the best quantity to look at, as it heavily depends on the magnitude of the input. Therefore, for any causal, L_p-stable system $N : \mathcal{U} \subseteq L_p^m \to L_p^n$ we define the *error-gain nonlinearity measure of N on* $\mathcal{U}$ as

$$\gamma_N^{\mathcal{U}} \triangleq \inf_{G\in\mathcal{G}} \sup_{u\in\mathcal{U}} \frac{\|Nu - Gu\|}{\|u\|}. \qquad (1)$$

This nonlinearity measure gives the gain of the error system E (see Fig. 1), when the worst case input signal $u \in \mathcal{U}$ is considered. The best linear approximation G is chosen among the set of all causal stable linear (convolution) operators $\mathcal{G}$ such that the resulting worst case gain is minimized.

As can be seen from its definition, the error-gain nonlinearity measure $\gamma_N^{\mathcal{U}}$ depends on the system N and on the set of considered inputs $\mathcal{U}$. The set $\mathcal{U}$ usually describes the region of operation in which the nonlinearity of the system N is to be assessed. In this case $\mathcal{U}$ contains e.g. only signals not exceeding a certain maximal amplitude.

In Section 4 the error gain nonlinearity measure will turn out to be useful for controller design. But for analysis purposes, there are two reasons for the error gain nonlinearity measure not being the only quantity we are interested in. Firstly, the measure is not bounded by definition. For different systems, different values indicate a "high degree of nonlinearity". For example, an additional scalar gain in the I/O-behaviour of a system changes the error gain nonlinearity measure, although the type and qualitative behaviour of the nonlinear system do not change. Secondly, the error gain nonlinearity measure can only be computed for stable systems in general while we might want to quantify the degree of nonlinear distortion also for unstable

systems. Thus, for the analysis of nonlinear systems we introduce a second quantity.

Let therefore N be as above, but instead of stability we only require that the system does not exhibit a finite escape time (i.e. $\|(Nu)_T\| < \infty$ for all $T > 0$ and $u \in \mathcal{U}$). We define the *relative nonlinearity measure of N on $\mathcal{U}$* by

$$\varphi_N^{\mathcal{U}} \triangleq \inf_{G\in\mathcal{G}} \sup_{u\in\mathcal{U}} \limsup_{T\to\infty} \frac{\|(Nu - Gu)_T\|}{\|(Nu)_T\|} \qquad (2)$$

where the definitions of $\mathcal{G}$ and $\mathcal{U}$ are as above. An important property of the measure $\varphi_N^{\mathcal{U}}$ is that its value is bounded by one (Allgöwer, 1995), a value close to one corresponding to a highly nonlinear system. We can thus compare the degree of nonlinearity of different systems on a unified scale. The value of $\varphi_N^{\mathcal{U}}$ corresponds to the percent-wise deviation of the output of the best linear approximation G from the output of the nonlinear system N.

There are two more properties that both nonlinearity measures have in common. Firstly, if the measures are zero then the I/O-behaviour of the system N can exactly be reproduced by a linear system for the considered inputs, and N is said to be *linear in $\mathcal{U}$*. Conversely, if N is linear, then the best linear approximation is $G = N$ and thus the nonlinearity measures vanish. Secondly, it has already been said that $\mathcal{U}$ can characterize the region of operation. Note that the nonlinearity measure can not decrease when additional inputs are considered (when $\mathcal{U}$ is made bigger). This fact is mathematically expressed by

$$\mathcal{U}_1 \subseteq \mathcal{U}_2 \Rightarrow \gamma_N^{\mathcal{U}} \leq \gamma_N^{\mathcal{U}} \qquad (3)$$

and the equivalent relationship holds for $\varphi_N^{\mathcal{U}}$. The practical meaning is intuitively clear: if a larger operating regime is considered, the nonlinearity measure will increase or stay constant, but will not decrease. But $\mathcal{U}$ can have other significances as well. In Sec. **??** we discuss how $\mathcal{U}$ can reflect the effect of feedback for control-relevant nonlinearity characterization.

3.2 Nonlinearity measures and steady-state behaviour of nonlinear systems

In this section we consider the evaluation of nonlinearity measures based on the steady-state behaviour of nonlinear dynamic systems. Therefore, we assume that the system under consideration has a unique steady state for all inputs in the considered operating regime. The steady-state locus is a (static) function that maps the steady-state inputs to the steady-state outputs. In order to make statements about the nonlinearity measures of dynamic systems based on their steady-state locus, we first have to obtain results for nonlinearity measures of (static) functions.

To this end, we consider memoryless systems of the form

$$N_f : u \mapsto y : \; y(t) = f(u(t)) \; \forall t \qquad (4)$$

where $f : \mathcal{V} \to \mathbb{R}^n$ is a function satisfying $|f(v)| < \infty$ for all $v \in \mathcal{V}$. Here, the set $\mathcal{V} \subseteq \mathbb{R}^m$ determines the set of allowed input values (i.e. the region of operation), that is we define $\mathcal{U} = \{u \in L_p^m | u(t) \in \mathcal{V} \, \forall t\}$. We then have the following equivalences

$$\gamma_{N_f}^{\mathcal{U}} = \inf_{K\in\mathbb{R}^{n\times m}} \sup_{v\in\mathcal{V}} \frac{|f(v) - Kv|}{|v|} \qquad (5)$$

$$\varphi_{N_f}^{\mathcal{U}} = \inf_{K\in\mathbb{R}^{n\times m}} \sup_{v\in\mathcal{V}} \frac{|f(v) - Kv|}{|f(v)|}. \qquad (6)$$

Note that this equality holds regardless of the norm used, i.e. for all $p \in [1, \infty]$, and the value of the nonlinearity gain of N_f does not depend on p for our definition of the L_p-norms. The above equalities have the following significance:

(1) When we want a linear model for a memoryless nonlinear system, a dynamic linear model has no advantage over a memoryless linear system (which is a gain matrix).
(2) Instead of a signal set $\mathcal{U}$, we only need to consider the maximum over a set of real numbers (or vectors) $\mathcal{V}$. We thus end up with a much easier optimization problem.

The computation of the measure for static functions can be done analogously to the procedure described in (Allgöwer, 1995). We therefore discretize the set $\mathcal{V}$ that describes the operating regime in terms of admissible values for the input signals. We then calculate the corresponding steady-state responses. This way, a finite number of points $(u_{SS,i}, y_{SS,i})$ on the steady state locus are obtained. Then we have to solve the optimization problem

$$\gamma_{N_f}^{\mathcal{U}} = \min_{z\in\mathbb{R}, K\in\mathbb{R}^{n\times m}} z$$
$$\text{s.t.} \; \frac{\left|y_{SS,i} - Ku_{SS,i}\right|}{\left|u_{SS,i}\right|} - z \leq 0 \; \forall i$$

where $u_{SS,i}$ in the denominator must be replaced by $y_{SS,i}$ for the calculation of $\varphi_{N_f}^{\mathcal{U}}$.

In the case of a scalar function $f : \mathbb{R} \to \mathbb{R}$ the nonlinearity measures of memoryless systems can be obtained even simpler by using the sector bounds on f. Consider therefore a function f that lies in the sector $[k^-, k^+]$ for all $v \in \mathcal{V}$, but may lie outside for $v \neq \mathcal{V}$ (see Fig. 2 with $\mathcal{V}$ an interval on the v-axis). It can be seen that the slopes of the straight lines that bound the sector are given by

$$k^+ = \sup_{v\in\mathcal{V}\setminus\{0\}} \frac{f(v)}{v} \text{ and } k^- = \inf_{v\in\mathcal{V}\setminus\{0\}} \frac{f(v)}{v}.$$

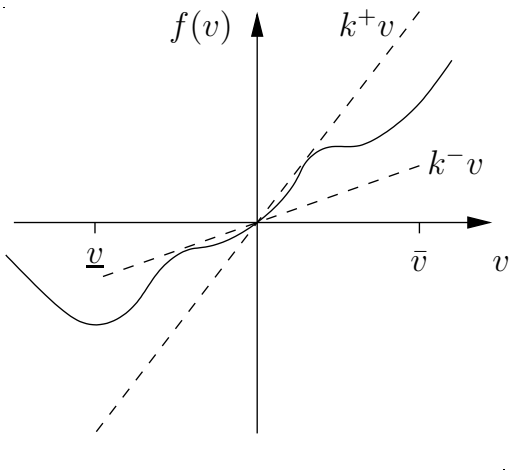

Fig. 2. A nonlinear function and its sector bounds for $\mathcal{V} = [\underline{v}, \bar{v}]$.

Given this information, we can determine the error gain nonlinearity measure by

$$\gamma_{N_f}^{\mathcal{U}} = \begin{cases} \frac{1}{2}(k^+ - k^-) & \text{if } |k^+|, |k^-| < \infty \\ \infty & \text{else} \end{cases}$$

and the best linear model is the straight line with slope $k^* = \frac{1}{2}(k^+ + k^-)$ if $\gamma_{N_f}^{\mathcal{U}}$ is finite. In a similar way we get

$$\varphi_{N_f}^{\mathcal{V}} = \begin{cases} \left|\frac{k^+ - k^-}{k^+ + k^-}\right| & \text{if } 0 < k^+k^-, |k^+|, |k^-| < \infty \\ 0 & \text{if } k^+ = k^- = 0 \\ 1 & \text{else} \end{cases}$$

for the relative nonlinearity measure and the best linear model with respect to the latter is given by

$$\begin{cases} \frac{1}{k^*} = \frac{1}{2}\left(\frac{1}{k^+} + \frac{1}{k^-}\right) & \text{if } 0 < k^+k^-, |k^+|, |k^-| < \infty \\ k^* = 0 & \text{else.} \end{cases}$$

Now let us assume we have calculated the nonlinearity measure of the steady-state locus. Recall that we assumed that the steady-state response is unique, i.e. $y(t) = (Nu)(t) \to f(v)$ whenever $u(t) \to v$ for $t \to \infty$. Then, the nonlinearity measures of the (dynamic) plants are bounded below by the respective quantities of the steady-state locus:

$$\gamma_N^{\mathcal{U}(\mathcal{V})} \geq \gamma_{N_f}^{\mathcal{V}} \text{ and } \varphi_N^{\mathcal{U}(\mathcal{V})} \geq \varphi_{N_f}^{\mathcal{V}}.$$

Proofs of the facts given in this section can be found in (Schweickhardt and Allgöwer, 2005). Next, we turn our attention to the computation of the nonlinearity measure for general dynamic systems.

3.3 Computation of nonlinearity measures

In the literature, different schemes can be found to approximately compute the nonlinearity measure. A lower bound can be calculated by considering only harmonic input signals (Allgöwer, 1995). Approximate computational scheme are given in (Allgöwer, 1996) for the general case, and in (Sourlas and Manousiouthakis, 1992; Sourlas and Manousiouthakis, 1998) an approach to derive a value for the absolute measure from (Desoer and Wang, 1980) is developed for a class of discrete-time systems. In (Kihas and Marquez, 2004) a quantity very similar to nonlinearity measures is considered. A procedure is proposed to approximately compute the L_2-gain of the error system defined as the difference between a nonlinear system and its Jacobi-linearization (both in continuous time). To this end, a Hamilton-Jacobi inequality is approximated at a finite number of points in a given region of the state space. Then the input-to-state- and L_∞-gain of the nonlinear process and its linearization respectively are calculated in order to estimate an upper bound on $\|u\|$ that guarantees that the system remains in the given region of the state-space. For all approaches, the most difficult part in obtaining accurate values for the nonlinearity measure is the computation of gains (Nikolaou and Manousiouthakis, 1989; Choi and Manousiouthakis, 2000; van der Schaft, 2000). Nonetheless, the mentioned approximation procedures often give sufficiently accurate results. We will not go into further detail but concentrate on the main ideas of nonlinearity assessment.

4. LINEAR CONTROL OF NONLINEAR SYSTEMS – A SMALL GAIN APPROACH

Once we have decided that linear controller design is adequate for the nonlinear control problem at hand, we turn the attention to the design of a suitable controller. The usual approach to the design of linear controllers for nonlinear systems is to use the linearization around the operating point as a linear model, design a linear controller and analyze (e.g. by simulation) the stability and performance of the closed loop with the nonlinear plant. By this method, no stability and performance guarantees can be made and the degree of nonlinearity of the plant is not taken into account in the controller design step. In this Section, a novel approach is presented that integrates nonlinearity analysis and linear controller design for nonlinear systems in order to

(1) decide for a given control problem whether linear controller design is adequate,
(2) derive a suitable linear model (not necessarily equivalent to the local linearization)
(3) describe a linear controller design procedure that guarantees stability (and possibly performance) of the closed loop containing the nonlinear process.

The suggested method in this Section will deal with stable nonlinear systems exhibiting a finite gain $\gamma(N) := \sup_u \frac{\|Nu\|}{\|u\|}$. The idea is to use the small gain theorem in order to maintain stability despite a non-

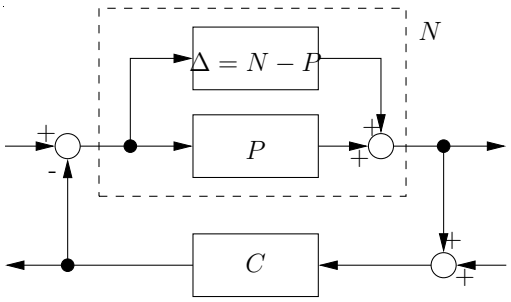

(a) Linear closed loop with nonlinear uncertainty

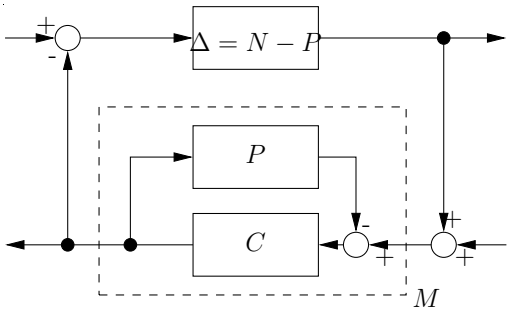

(b) Reformulation for use with small gain theorem

Fig. 3. Formulation of the nonlinear control problem as linear control problem with norm bounded nonlinear uncertainty.

linear uncertainty (for the small gain theorem, see e.g. (Vidyasagar, 2002)). With the help of the small gain theorem, a controller C that satisfies $\gamma(N)\gamma(C) < 1$, where N is the plant, will achieve closed loop stability, see Fig. 3 (a). While stability can be achieved this way, it remains unclear how performance requirements can be met and how the controller should look like apart from the requirement $\gamma(C) < \gamma(N)^{-1}$. In particular, this approach excludes controllers with integral action as the controller has to be stable itself. To circumvent these problems, a different approach is taken. We therefore split the nonlinear system N into a (stable) linear part P and a (stable) nonlinear part $\Delta = N - P$ and use linear techniques to design a (not necessarily stable) linear controller C for the linear part P.

With the help of the loop transformation theorem (Vidyasagar, 2002, Ch. 6), we can reorder the closed loop as depicted in Fig. 3 (b). Now, let the linear closed loop transfer operator be $M = CS = C(I + PC)^{-1}$. The small gain theorem then states that if the gains of M and Δ satisfy

$$\gamma(\Delta)\gamma(M) < 1$$

the closed loop system is stable. Moreover, the linear controller can be designed such that the performance requirements are met at least for the linear model P and integral action is possible. In order to get the best results, the linear model must be chosen such that the gain of the model uncertainty $\gamma(\Delta)$ takes the least possible value. This is achieved by choosing P such that $\gamma(\Delta) = \gamma(N - P)$ is minimized. But this procedure exactly corresponds to the definition of the error gain nonlinearity measure $\gamma_N^{\mathcal{U}} = \inf_G \gamma(N - P)$. We call a model P^* with $\gamma(N - P^*) = \gamma_N^{\mathcal{U}}$ the best linear model. Whenever no such P^* exists we choose a $\tilde{P}^*$ for which $\gamma(N - \tilde{P}^*) \approx \gamma_N^{\mathcal{U}}$. The nonlinearity assessment then consists of (i) computing $\gamma_N^{\mathcal{U}}$ and P^* and (ii) check with linear H_∞-techniques whether $\gamma(M) < 1/\gamma_N^{\mathcal{U}}$ is achievable. If so, P^* gives a suitable linear model and linear controller design can be done to optimize customized performance objectives. In principal, any controller design method can be utilized as long as the constraint $\gamma_N^{\mathcal{U}}\gamma(M) < 1$ is guaranteed to be satisfied.

We will illustrate the presented approach with a small example. Consider the system

$$\dot{y} = -y - y^3 + u$$

in the operating range $|u(t)| < 2\,\forall t$. Using the steady-state locus, which is easy to compute, and using the formulas given in Section 3, we can immediately give the lower bound of $\gamma_N^{\mathcal{U}} \geq 0.25$ for the nonlinearity measure. Indeed, the numeric computations of the dynamic nonlinearity measure results in a value of 0.271. The corresponding best linear approximation is of order 10 and can be reduced to obtain the model

$$P^*(s) = \frac{0.040s + 0.796}{s + 1.025}$$

as opposed to the linearization around the steady state which yields

$$P_{lin}(s) = \frac{1}{s + 1}.$$

For both models we design a controller such that the closed loop (with the model) has a first order delay behaviour with a bandwidth of $3rad/s$. As discussed above the error between the best linear model P^* and the true nonlinear process can be taken into consideration and it is guaranteed that the nonlinear closed loop is stable. This is accomplished by verifying that for the controller based on the best model P^* we have $\gamma_N^{\mathcal{U}}\gamma(M) = 0.271 \cdot 3.298 = 0.892 < 1$. For P_{lin} the size of the error is not known and therefore no guarantees can be given. In fact P^* is the linear model that makes the error smallest and thus will give rise to the lowest conservativeness which, with all due caution, is related to a better performance. This can also be seen from the closed loop simulations. In Fig. 4, step responses of the closed loops containing the nonlinear plant and the controllers based on the best linear model and based on the local linearization respectively are plottet.

Due to integral action, both controllers achieve vanishing steady state errors. But it can be seen that for this simple system already the proposed procedure not only guarantees stability, but also leads to a better performance when compared to the conventional approach. More details on the approach and

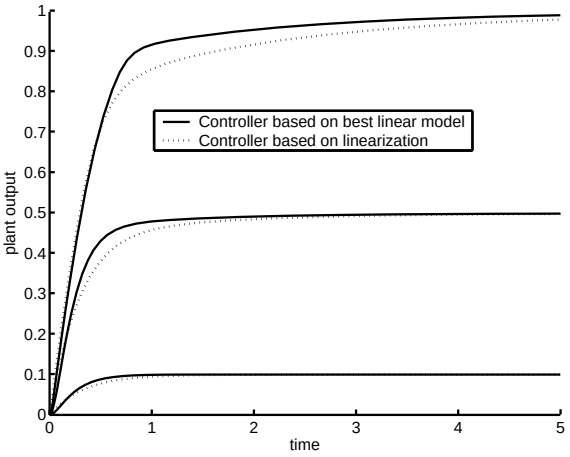

Fig. 4. Responses of the closed loops to steps in the reference signal of different height. The solid line corresponds to the controller based on the best linear model, the dotted line to the controller based on the local linearization.

more complex worked out examples can be found in (Schweickhardt and Allgöwer, 2006).

5. CONCLUSIONS

The development of advanced controller design techniques for nonlinear processes requires much effort. Linear controller design can be implemented much more easily and fortunately leads to satisfactory results in many practical situations. Thus, one requires to have tools in order to determine prior to controller design whether linear controller design is adequate or whether nonlinear techniques have to be used. It is interesting to observe that similar studies are taking place in the area of empirical modeling, where process nonlinearity can obstruct identification of linear models, or render the identified models obsolete.

In this note, we presented an introduction to recent results on the input/output-based approach to nonlinearity assessment. Useful formulas to quickly determine lower bounds of nonlinearity measures based on the steady-state process behaviour were given. We motivated the necessity of control-relevant nonlinearity assessment and introduced the corresponding optimal control law nonlinearity measure. We then presented a novel approach that combines nonlinearity assessment and controller design by using linear robust control methods and nonlinearity measures. An example was given that showed the usefulness of the proposed approach.

In the future, two directions of further investigations are expected to play an important role. Firstly, it is desirable to get methods that more precisely quantify how much performance can be gained by using nonlinear controller design techniques instead of linear ones. Secondly, the proposed method for linear controller design of nonlinear systems is only a first step. Many other approaches can be imagined, and once easily realizable and reliable methods are developed that also guarantee a certain level of performance they are expected to have a tremendous impact on process control practice.

REFERENCES

Allgöwer, F. (1995). Definition and computation of a nonlinearity measure. In: *3rd IFAC Nonlinear Control Systems Design Symposium*. Lake Tahoe, CA. pp. 279–284.

Allgöwer, F. (1996). *Näherungsweise Ein-/Ausgangs-Linearisierung nichtlinearer Systeme*. Fortschr.-Ber. VDI Reihe 8 Nr. 582, VDI Verlag. Düsseldorf.

Bristol, E. H. (1966). On a new measure of interaction for multivariable process control. *IEEE Trans. Automat. Contr.* **AC-11**, 133–134.

Choi, J. and V. Manousiouthakis (2000). On a measure of bounded input/initial state bounded output stability over ball. *Chem. Eng. Sci.* **55**, 6059–6070.

Desoer, C. A. and Y.-T. Wang (1980). Foundations of feedback theory for nonlinear dynamical systems. *IEEE Trans. on Circuits and System* **CAS-27**(2), 104–123.

Dier, R., M. Guay and P. J. McLellan (2004). Effect of process nonlinearity on linear quadratic regulator performance. In: *Proc. of IFAC Symp. Advanced Contr. of Chem. Proc. ADCHEM 2003*. Hong Kong.

Dobrowiecki, T. P. and J. Schoukens (2001). Bounds on modeling error due to weak non-linear distorsions. In: *IEEE Instr. Meas. Tech. Conf., Budapest, Hungary*. Vol. 1. pp. 14–19.

Eker, S. A. and M. Nikolaou (2002). Linear control of nonlinear systems: Interplay between nonlinearity and feedback. *AIChE J.* **48**(9), 1957–80.

Enqvist, M. and L. Ljung (2002). Estimating nonlinear systems in a neighborhood of LTI-approximants. In: *Proc. 41th IEEE Conf. Decision Contr.*. Las Vegas, Nevada, USA. pp. 1005–1009.

Enqvist, M. and L. Ljung (2004). LTI approximations of slightly nonlinear systems: some intriguing examples. In: *Proc. of IFAC Symp. on Nonlinear Control Systems NOLCOS*. Stuttgart.

Guay, M. (1996). Measurement of Nonlinearity in Chemical Process Control. PhD thesis. Dept. of Chemical Engineering, Queen's University. Kingston, Canada.

Guay, M. and J. F. Forbes (2004). Effect of nonlinearity on linear quadratic regulator performance. In: *Proc. 43rd IEEE Conf. Decision Contr.*. Vol. 3. pp. 2267 – 2272.

Guay, M., P. J. McLellan and D. W. Bacon (1995). Measurement of nonlinearity in chemical process control systems: The steady state map. *Can. J. Chem. Eng.* **73**, 868–882.

Guay, M., P. J. McLellan and D. W. Bacon (1997*a*). Measure of closed-loop nonlinearity and interaction for nonlinear chemical processes. *AIChE J.* **43**(9), 2261–2278.

Guay, M., P. J. McLellan and D. W. Bacon (1997*b*). Measurement of dynamic nonlinearity in chemical process control. In: *Proc. of IFAC Symp. Advanced Contr. of Chem. Proc. ADCHEM'97, Banff, Canada*. pp. 589–594.

Guay, M., R. Dier, J. Hahn and P. J. McLellan (2005). Effect of process nonlinearity on linear quadratic regulator performance. *J. Proc. Contr.* **15**(1), 113–124.

Haber, R. and H. Unbehauen (1990). Structure identification of nonlinear dynamic systems. *Automatica* **26**(4), 651–677.

Hahn, J. and T. F. Edgar (2001*a*). A Gramian based approach to nonlinearity quantification and model classification. *Ind. Eng. Chem. Res.* **40**, 5724–31.

Hahn, J. and T. F. Edgar (2001*b*). Nonlinearity quantification and model classification using gramians and other covariance matrices. In: *AIChE Annual Meeting, Reno, NV, paper no. 286d*.

Helbig, A., W. Marquardt and F. Allgöwer (2000). Nonlinearity measures: definition, computation and applications. *J. Proc. Contr.* **10**, 113–123.

Hernjak, N., F. J. Doyle III and R. K. Pearson (2002). Control-relevant characterization of nonlinear classes of process systems. In: *Proc. 15th IFAC World Congress, Barcelona, Spain*.

Hernjak, N., F.J. Doyle III, F. Allgöwer and T. Schweickhardt (2003). Relationship between control-relevant nonlinearity and performance objective. In: *IFAC Symposium on Advanced Control of Chemical Processes (ADCHEM)*. Hong Kong. pp. 543–548.

Kihas, D. and H. J. Marquez (2004). Computing the distance between a nonlinear model and its linear approximation: an l_2 approach. *Comp. and Chem. Eng.* **28**(12), 2659–2666.

Mäkilä, P. M. (2003). Squared and absolute errors in optimal approximation of nonlinear systems. *Automatica* **39**, 1865–1876.

Mäkilä, P. M. (2004). On optimal LTI approximation of nonlinear systems. *IEEE Trans. Automat. Contr.* **49**(7), 1178–1182.

Mäkilä, P. M. and J. R. Partington (2003). On linear models for nonlinear systems. *Automatica* **39**(1), 1–13.

Mäkilä, P. M. and J. R. Partington (2004). Least-squares LTI approximation of nonlinear systems and quasistationarity analysis. *Automatica* **40**(7), 1157–1169.

Menold, P. H., F. Allgöwer and R. K. Pearson (1997*a*). On simple representations of distillation dynamics.. In: *Proc. of the First European Congress on Chemical Engineering – ECCE-1*. Florenz. pp. 1363–1366.

Menold, P.H., R.K. Pearson and F. Allgöwer (1997*b*). Nonlinear structure identification of chemical processes. *Comp. and Chem. Eng.* **21**, 137–142.

Nikolaou, M and V. Manousiouthakis (1989). A hybrid approach to nonlinear system stability and performance. *AIChE J.* **35**(4), 559–572.

Partington, J. R. and P. M. Mäkilä (2002). On system gains for linear and nonlinear systems. *Systems & Control Letters* **46**, 129–136.

Pearson, R. K., F. Allgöwer and P. H. Menold (1997). Stochastic suitability measures for nonlinear structure identification. In: *Proc. of the 4th European Control Conference, ECC'97*. Brüssel. Paper FR-A F4.

Schoukens, J., R Pintelon and T. Dobrowiecki (2002). Linear modeling in the presence of nonlinear distorsions. *IEEE Trans. Instrum. Meas.* **51**(4), 786–792.

Schweickhardt, T. and F. Allgöwer (2005). Linear modeling error and steady-state behaviour of nonlinear dynamical systems. In: *Proc. 44th IEEE Conf. Decision Contr.*. Seville, Spain. pp. 8150–8155.

Schweickhardt, T. and F. Allgöwer (2006). A robustness approach to linear control of nonlinear processes. submitted.

Schweickhardt, T., F. Allgöwer and F. J. Doyle III (2003). Nonlinearity quantification for the optimal state feedback controller. In: *European Control Conference (ECC)*. Cambridge, U.K. Paper #056.

Shastri, Y., T. Schweickhardt and F. Allgöwer (2004). Plant and control-relevant nonlinearity analysis of a CSTR: a case study. In: *7th Int. Symp. on Dynamics and Control of Process Systems (DYCOPS)*. Paper #123.

Sourlas, D. and V. Manousiouthakis (1992). Development of linear models for nonlinear plants. In: *AIChE Annual Meeting, Miami, FL*. paper 125c.

Sourlas, D. and V. Manousiouthakis (1998). On the computation of the nonlinearity measure. In: *Proc. 37th IEEE Conf. Decision Contr.*. pp. 1434–39.

Stack, A. J. and F. J. Doyle III (1997*a*). Application of a control-law nonlinearity measure to the chemical reactor analysis. *AIChE J.* **43(2)**, 425–439.

Stack, A. J. and F. J. Doyle III (1997*b*). The optimal control structure: an approach to measuring control-law nonlinearity. *Comp. and Chem. Eng.* **21(9)**, 1009–1019.

Stack, A. J. and F. J. Doyle III (1999). Local nonlinear performance assessment for single-controller design. In: *Proc. 14th IFAC World Congress, Beijing, China*.

van der Schaft, A. J. (2000). *L_2-Gain and Passivity Techniques in Nonlinear Control*. Springer. London.

Vidyasagar, M. (2002). *Nonlinear Systems Analysis (2nd ed.)*. SIAM. Philadelphia, PA.

Session 1.1

Applications of State Estimation and Monitoring

Monitoring the Physiological State of Mammalian Cell Perfusion Processes by On–Line Estimation of Intracellular Fluxes

O. Henry, A. Kamen and M. Perrier,
Ecole Polytechnique de Montreal

Observer Design using Boundary Injections for Pipeline Monitoring and Leak Detection

O. M. Aamo, J. Salvesen and B. A. Foss,
Norwegian University of Science and Technology

First Principles Invariants for Asymptotic Observers in Chemical Reactors

F. Couenne, C. Jallut and D. Dochain,
Université Claude Bernard Lyon
Universite Catholique de Louvain Batiment

Control of Continuous Reactors with Non–Monotonic Reaction Rate

J. Alvarez, J. Diaz–Salgado and J. Moreno,
Universidad Autónoma de Madrid

Rotary Kiln Product Quality Forecasting Based on Flame Imaging

C. Duchesne, A. Desbiens and G. Szatvanyi,
Universite Laval

ADCHEM 2006

International Symposium on Advanced Control of Chemical Processes
Gramado, Brazil – April 2-5, 2006

MONITORING THE PHYSIOLOGICAL STATE OF MAMMALIAN CELL PERFUSION PROCESSES BY ON-LINE ESTIMATION OF INTRACELLULAR FLUXES

O. Henry[1,2], A. Kamen[2], M. Perrier[1]

[1]*École Polytechnique de Montréal, Montréal, Québec, Canada.*
[2]*Institut de Recherche en Biotechnologie, CNRC, 6100 avenue Royalmount, Montréal, Québec H4P 2R2, Canada*
**Email of corresponding author: michel.Perrier@polymtl.ca*

Abstract: Rapid assessment of the cells physiological state during a culture is essential for bioprocess optimization and the design of effective control strategies. In this work, an approach was developed to provide an online estimation of the intracellular flux distribution of cells grown in perfusion cultures, based on a comprehensive metabolic network involving 40 biochemical reactions and 46 components. The specific uptake and production rates were evaluated from daily nutrient and metabolite concentration measurements, using an extended Kalman-filter for noise reduction and rate estimation. The biosynthetic rates were determined from an on-line estimate of the specific growth rate using a recursive least-squares method. Our results demonstrate that this approach allows monitoring of the cells metabolic activity and can be a useful tool for process development.

Keywords : monitoring, bioprocess, perfusion culture, metabolic flux analysis

1. INTRODUCTION

The design of efficient monitoring techniques and control strategies is instrumental for the rapid development and optimization of bioprocesses. For these methods to be truly effective in detecting the cellular response to environmental changes or operating conditions, they must be based on a profound knowledge of the cell metabolism. With proper assessment of the physiological state of the cells, the optimization can consist in selecting the appropriate operating conditions so as to maintain or drive the culture towards a desirable productive state (Konstantinov, 1996).

To date, most of the on-line monitoring tools derive knowledge on the physiological state indirectly, from extracellular measurements. Cell concentration and respiration are the parameters commonly measured on-line to monitor the metabolic activity of a culture. Flow injection analysis techniques have also allowed real-time monitoring of various nutrients and metabolites concentrations, such as glucose, glutamine, lactate and ammonia (Blankenstein, *et al.*, 1994; Siegwart, *et al.*, 1999).

However useful for monitoring a production, these process variables only give an incomplete estimate of the metabolic state of the cells. To complement the information of extracellular measurements, intracellular data must be considered as well. This constitute a challenging task, hampered by the lack of available measurements and the limited applicability of mathematical models, in turn due to the complexity of animal cell systems.

Advances in the development and application of techniques such as NMR, mass spectroscopy and radioactive tracers have permitted the development of more accurate metabolic model. Metabolic flux analysis is an approach that allows to take into account the intracellular reaction rates and has become an established tool to study the metabolism of cells. However, to date, metabolic flux analysis applied to animal systems was mostly confined to a descriptive tool, for *a posteriori* assessment of cellular response to culture changes. This can be mainly attributed to the large number of measurements required to carry the analysis (nutrients, metabolite products, cellular composition, etc).

In the present work, an approach was developed to provide daily estimates of the intracellular fluxes, based on on-line and off-line measurements and assuming a constant cellular composition. To illustrate this approach, the time courses of metabolic fluxes in two perfusion cultures performed under different feeding strategies were analyzed. Our results demonstrate intimate links between the intracellular flux distribution, culture productivity and the operating conditions. By allowing to monitor the physiological status of a culture, this approach can provide a systematic tool for process optimization and control.

2. MATERIALS AND METHODS

2.1 Cell Line, Bioreactor System and Culture Conditions

Experiments were conducted using the HEK-293 cells and a low-protein serum-free proprietary medium formulation. The cultures were performed in a controlled 3.5 L bioreactor equipped with 3 surface baffles and two marine impellers. The temperature was maintained at 37 °C and the pH was controlled at 7.2. The agitation was kept constant at 80 RPM and the dissolved oxygen was maintained at 40 % air saturation. Cells were retained in the reactor using a BioSep 10L acoustic filter (Applikon Inc., Foster City, Ca). The feed and harvest rates were controlled by two peristaltic pumps.

2.2 Analytical Methods

Viable and total cells were counted using a haemacytometer (Hausser Scientific, Horshaw, PA). Viability was assessed by dye exclusion method using erythrosine B. The Biolyzer (Kodak, New Haven, Connecticut) was used for the analysis of glucose, lactate and ammonia. Amino acid analysis was performed by HPLC. DNA analysis and dry weight estimation have been performed as described in Nadeau et al. (Nadeau, *et al.*, 2002). Extracellular proteins were assayed using the Dc Protein Assay (Bio-Rad, Hercules, CA) and total proteins were analysed using the BCA kit (Pierce, Rockford, IL).

2.3 Estimation of the Specific Growth Rate

An estimation of the growth rate is required to evaluate the biosynthetic rates. From a mass balance on viable cells, we obtain the following equation for a bioreactor operated in perfusion mode:

$$\mu = \frac{1}{X}\left(\frac{dX}{dt} + DX_H\right) \quad (1)$$

where D is the perfusion rate, X the concentration inside the bioreactor and X_H the concentration of cells in the outflow. In perfusion cultures, growth rate determination is particularly subject to noise due to the imprecision of cell counting and fluctuations in cell retention efficiency. This was addressed by using a biomass probe allowing real-time monitoring of the culture capacitance. The later is proportional to the concentration of viable cells. Based on this measurements, on-line estimation of the specific growth rate was performed using a discrete least-square estimator as described in (Bastin and Dochain, 1990). The algorithm is given by:

$$\hat{\mu}_t = \hat{\mu}_{t-1} + \Delta t \gamma_t X_{t-1}\left[X_t - X_{t-1} - \Delta t \hat{\mu}_{t-1} X_{t-1} + \Delta t D_{t-1} X_{Ht-1}\right] \quad (2)$$

where Δt is the sampling rate. The covariance (γ) is updated by the following equation:

$$\gamma_t = \frac{\gamma_{t-1}}{\lambda + T^2 X_{t-1}{}^2 \gamma_{t-1}} \quad (3)$$

The forgetting factor, λ, is a tuning parameter. The concentration of cells in the harvest (X_H) and the dilution rate (D) were re-evaluated at each sample and the values were assumed constant in between experimental measurements. The linear relation assumed between the capacitance signal and the cell concentration was also updated at each off-line measurement by linear regression on current and previous data points. This procedure allowed to re-calibrate on-line the biomass monitor system.

2.4 Nutrient uptake/Metabolite production rate estimation

In contrast with biomass, only few measurements of substrate and metabolite concentrations are available, typically once or twice a day. The specific uptake and production rates can be calculated using material balances around the bioreactor to yield the following equations:

$$\frac{dS}{dt} = -q_S X + D(S_{in} - S) \quad (4)$$

$$\frac{dP}{dt} = -q_P X + DP \quad (5)$$

where D is the perfusion rate, q_S and q_P are the specific consumption and production rates, S is the nutrient concentration in the reactor, S_{in} is the nutrient concentration in the feed and P is the metabolite concentration in the reactor.

Due to the large sampling rate, calculation using direct difference from current and past measurement is prone to error. Instead, an extended Kalman filter was employed for rate estimation and noise reduction. In the "continuous-discrete" form of the filter, the correction is made only at discrete times (t_k).

Prediction step:

$$\left.\begin{aligned} \frac{dS}{dt} &= qX + D(S_{in} - S) \\ \frac{dq}{dt} &= 0 \end{aligned}\right\} \; t_k \le t \le t_{k+1} \quad (6)$$

Whenever a new measurement is available, the predicted specific rate is corrected by a term proportional to the difference between the measured (S_M) and predicted (S) nutrient/product concentrations according to the following equation:

Correction step:

$$\begin{bmatrix} S \\ q \end{bmatrix}_F = \begin{bmatrix} S_M \\ q \end{bmatrix} + K(t)\left[S_M - \hat{S}\right] \quad (7)$$

where K is the filter gain optimized at each measurement time:

$$K = P(t)H^T(t)\left[H(t)P(t)H^T(t) + R\right]^{-1} \quad (8)$$

The error covariance is also updated according to:

$$P_F(t) = \left[I - K(t)H(t)\right]P(t) \quad (9)$$

The trade off between confidence in the measurements and confidence in the model is determined by the measurement error and the process model covariances (R and Q, respectively).

3. METABOLIC MODEL

The metabolic model used in this study was developed by Nadeau *et al.* (2002). The reactions considered in this biochemical network are shown in Table I. The metabolic model involves 46 components and 40 fluxes, which include the catabolism pathways of glucose, glutamine and 18 amino acids.

Evaluation of the metabolic flux vector F is performed using a weighted linear least-squares:

$$F = (M^T \psi^{-1} M) M^T \psi^{-1} q \quad (10)$$

where q is the vector of measured nutrient uptake and metabolite production rates, M contains the stoichiometric coefficients and ψ is the variance-covariance matrix associated with the measured rate.

Table I. Listing of biochemical reactions included in the metabolic network

1	Glc + ATP → Fruct6P
2	Fruct6P + ATP → 2 GAP
3	GAP → Pyr + 2 ATP + NADH + H^+
4	Pyr + NADH + H^+ → Lac
5	mPyr + CoA → ACCoA + NADH + CO_2 + H^+
6	Pyr + Glu → Ala + ∝KG
7	OAA + Glu → Asp + ∝KG
8	mGln + H_2O → mGlu + NH_3
9	2 Gln + 5/4 Asp + Rib5P + ½ Gly + 27/4 ATP + 5/8 NADPH → ADN|ARN + ¾ NADH + ¾ Fum + 2 Glu
10	mMal + 2ATP → mPyr + CO_2 + NADPH + H^+
11	Asp + Gln + ATP → Asn + Glu
12	Glu + ATP + 2 NADPH + 2 H^+ → Pro
13	2 Gly → Ser + NH_3
14	G6P + ATP → 1/3 Rib5P + 2/3 Xu5P + 2 NADPH + H^+ + CO_2
15	R5P + 2 Xu5P → 2 Fruct6P + GAP
16	2 (9 Cit + 17 ATP + 9 CoA + 16 NADPH) → AcOLE + 18 OAA
17	Extracellular Proteins → ΣAA
18	ΣAA → Intracellular Proteins
19	Lys + 2 m∝KG + NADPH → 2 AcCoA + 2 CO_2 + 4 NADH + 3 H^+ + $FADH_2$ + 2 mGlu
20	Leu + m∝KG + ATP → 3 AcCoA + mGlu + CO_2 + NADH + H^+ + $FADH_2$
21	Ile + m∝KG + ATP → SuCoA + AcCoA + CO2 + 2 NADH + 2 H^+ + $FADH_2$ + mGlu
22	Thr → CO_2 + 2 NADH + 2 H^+ + $FADH_2$ + NH_3 + mPyr
23	Val + m∝KG + ATP → SuCoA + 3 NADH + H^+ + $FADH_2$ + 2CO_2 + mGlu
24	Met + Ser + 2 ATP → Cte + SucCoA + NADH + H^+ + CO_2 + NH_3
25	Phe + O_2 + NADPH + H^+ → Tyr
26	Tyr + m∝KG + 2O_2 → Fum + 2 AcCoA + m Glu
27	Arg + m∝KG → mGlu + NADH + H^+
28	His → mGlu + NH_3
29	mOAA + AcCoA → Cit
30	Cit → m∝KG + CO_2 + NAPH + H^+
31	m∝KG → SuCoA + NADH + H^+ + CO_2
32	SuCoA → Fum + ATP + $FADH_2$
33	Fum → mMal
34	mMal → mOAA + NADH + H^+
35	NADH + ½ O_2 → 3 ATP
36	Pyr → mPyr
37	Glu + mAsp → mGlu + Asp
38	Gln → mGln
39	mMal + ∝KG → Mal + m∝KG
40	mGlu + mOAA → mAsp + m∝KG

4. RESULTS AND DISCUSSION

4.1 Growth Rate Estimation

Figure 1 illustrates one example of growth rate estimation from a raw capacitance signal (Fig 1A). Cells in the midexponential phase from a seed culture were inoculated at a concentration of $2x10^5$ cells/mL (Fig 1B). The culture was grown in batch mode for two days before the perfusion rate was initiated and kept constant at 1 vol/d. As evident from the reduced initial growth kinetics, the culture underwent a lag phase. The results demonstrate the ability of the estimator to track the changes in cellular growth as the cell entered exponential phase in a later stage (Fig 1C).

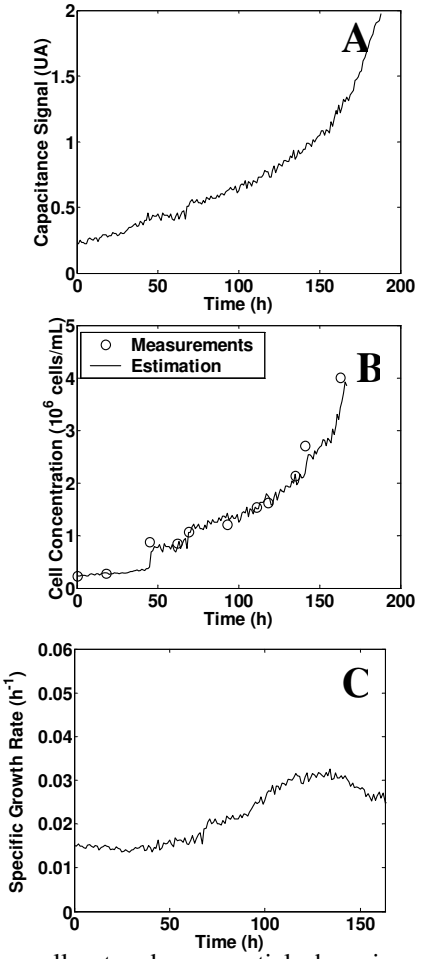

Fig.1. Real-time estimation of the specific growth rate (C) from on-line capacitance (A) and off-line cell count measurements (B) during a perfusion culture.

4.2 Estimation of Metabolic Fluxes

Based on the online estimate of the specific growth rate and the determination of specific uptake/production rates, the 40 intracellular fluxes of the metabolic network were computed online. Figure 2 illustrates how changes in cellular metabolism can be observed as they happen during the course of a culture. In this experiment, the perfusion rate was kept constant at 1 Vol/d throughout the culture (Fig 2A).

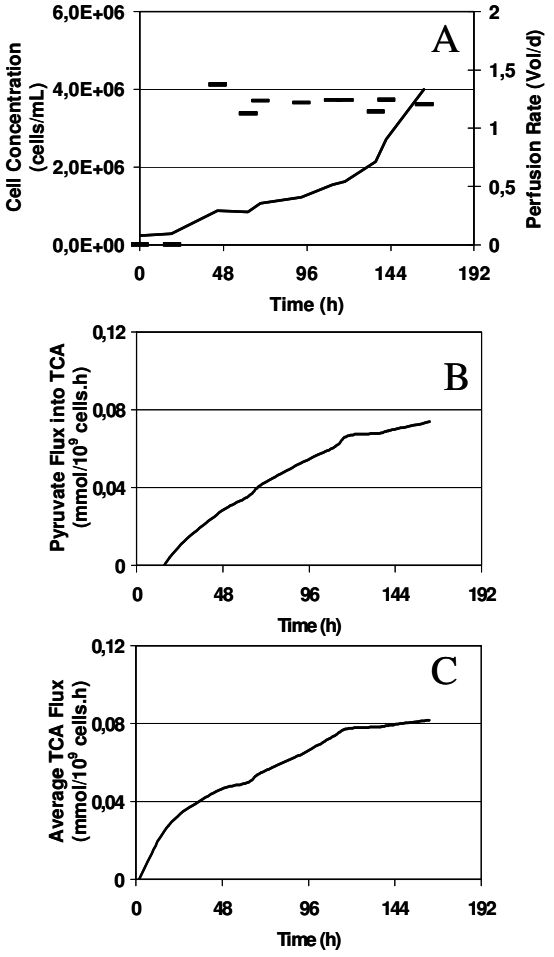

Fig.2. Estimation of intracellular fluxes during a perfusion culture. A) Cell concentration and perfusion rate profiles. B) Glycolytic flux. C) Pyruvate to TCA flux. D) Avergae TCA flux

The time profiles of selected intracellular fluxes are shown (Fig 2C & D). These key fluxes were identified as good indicators of the overall metabolic activity of the cells. Analysis of the flux distribution revealed that as the cell concentration increases over time, cells are shifting towards a more efficient utilization of the main substrate. However, the productivity of the cells tends to decrease with increasing cell concentrations (data not shown). Thus, it is critical to assess the physiological status of the cells and to maintain a culture in a favourable state. This can be accomplished through the manipulation of the perfusion rate as will be shown in the next section.

4.3 Effect of the Perfusion Rate

To evaluate the effect of the perfusion rate on the intracellular flux distribution, another experiment was conducted in which the feed rate was adjusted with increasing cell concentrations (Fig. 3A). This feeding strategy allowed to maintain relatively constant nutrient concentrations inside the bioreactor. In turn, the estimated intracellular fluxes remained very similar throughout the experiment (Fig. 3C & D). To investigate how this would affect the specific productivity, cells were harvested from the bioreactor at different cell concentrations (Fig. 3A) and inoculated into shake-flasks to measure their productivity. As shown in Fig 3D, no significant difference can be discerned in terms of cell specific productivity. These results demonstrate that cells can be maintained in a desirable productive state by manipulating the feed rate so as to meet their nutritional requirements.

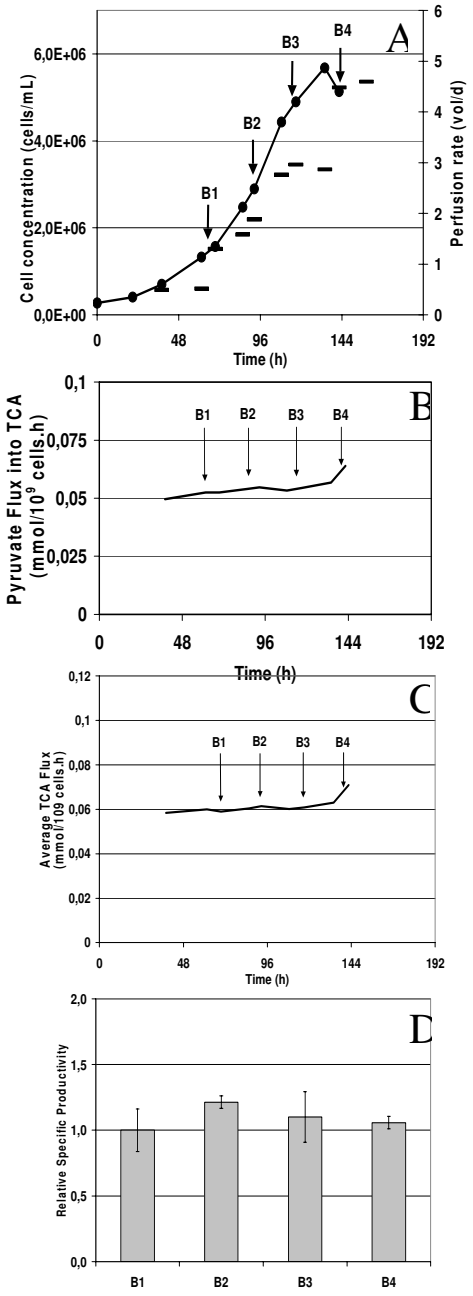

Fig. 3 A) Cell concentration and perfusion rate profiles. B) Pyruvate flux into TCA cycle. C) Average TCA flux. D) Relative cell specific productivity at different times during the perfusion.

CONCLUSIONS

The trend in bioprocess monitoring is towards strategies which are based on the physiological status of the organism in the bioprocess. An approach was developed to provide online estimates of metabolic fluxes of cells grown in perfusion mode. With a constant perfusion rate, intracellular fluxes were varying as cells were exposed to ever-changing environmental conditions (cell, nutrient and waste concentrations). However, by adjusting the perfusion rate with increasing cell concentrations, it allowed to maintain cells in a similar physiological status throughout a perfusion run. Monitoring the physiological state of the cells can be helpful to rapidly establish the conditions favouring the growth or resulting in enhanced productivities. Future efforts are aimed at incorporating this approach into a control scheme.

REFERENCES

Bastin, G., Dochain, D. 1990. On-line estimation and adpative control of bioreactors. Amsterdam, The Netherlands: Elsevier Science Publishers.

Blankenstein, G., Spohn, U., Preuschoff, F., Thommes, J., Kula, M.R., 1994. Multi-channel flow injection analysis biosensor system for on-line monitoring of glucose, lactate, glutamine, glutamate and ammonia in animal cell culture. Biotechnol. Appl. Biochem. 20, 291-307.

Konstantinov, K., 1996. Monitoring and Control of the Physiological State of Cell Cultures. Biotechnol. Bioeng. 52, 271-289.

Nadeau, I., Gilbert, P.A., Jacob, D., Perrier, M., Kamen, A., 2002. Low-protein medium affects the 293SF central metabolism during growth and infection with adenovirus. Biotechnol. Bioeng. 77, 91-104.

Siegwart, P., Cote, J., Male, K., Luong, J.H.T., Perrier, M., Kamen, A., 1999. Adaptive control at low glucose concentration of HEK-293 cell serum-free cultures. Biotechnol. Prog. 15, 608-616.

ADCHEM 2006

International Symposium on Advanced Control of Chemical Processes
Gramado, Brazil – April 2-5, 2006

OBSERVER DESIGN USING BOUNDARY INJECTIONS FOR PIPELINE MONITORING AND LEAK DETECTION

Ole Morten Aamo, Jørgen Salvesen, and Bjarne A. Foss

Department of Engineering Cybernetics
Norwegian University of Science and Technology
N-7491 Trondheim

Abstract: We design a leak detection system consisting of an adaptive Luenberger-type observer based on a set of two coupled one dimensional first order nonlinear hyperbolic partial differential equations governing the flow dynamics. It is assumed that measurements are only available at the inlet and outlet of the pipe, and output injection is applied in the form of boundary conditions. For the linearized model without friction and leak, exponential convergence of the state estimates to the plant state is shown by Lyapunovs method. The observer design is performed for the continuum model, ensuring that convergence properties established theoretically are not an artifact of the method of discretization. Heuristic update laws for adaptation of the friction coefficient and leak parameters are given, and simulations demonstrate their ability to detect, quantify and locate leaks.

Keywords: Partial differential equations; Observers; Adaptive systems; Pipeline leaks

1. INTRODUCTION

Transportation of liquids in pipelines requires monitoring to detect malfunctioning such as leaks. In the petroleum industry, leaks from pipelines may potentially cause environmental damage, as well as economic loss. These are motivating factors, along with requirements from environmental authorities, for developing efficient leak detection systems. While some leak detection methods are hardware-based, relying on physical equipment being installed along the pipeline, the focus of this paper is on software-based methods that work for cases with limited instrumentation. In fact, instrumentation in the petroleum industry is usually limited to the inlet and outlet of pipelines, only. This calls for sophisticated signal processing methods to obtain reliable detection of leaks. Some software-based leak detection methods perform statistical analysis on measurements (black box), while others incorporate models based on physical principles. Our method falls into the latter category, in that we will use a dynamic model of the pipe flow based on a set of two coupled hyperbolic partial differential equations.

There have been numerous studies on model based leak detection. We mention here the most relevant ones with regard to our work. Based on a discretized pipe flow model, Billman and Isermann (1987) designed an observer with friction adaptation. In the event of a leak, the outputs from the observer differs from the measurements, and this is exploited in a correlation technique that detects, quantifies and locates the leak. Verde (2001) used a bank of observers, computed by the method for fault detection and isolation developed by Hou and Müller (1994). The underlying model is a linearized, discretized pipe flow model on a grid of N nodes. The observers are designed in

such a way that all but one will react to a leak. Which one of the N observers that does not react to the leak depends on the position of the leak, and this is the mechanism by which the leak is located. The outputs of the remaining observers are used for quantifying the leak. The bank of observers are computed using the recursive numerical procedure suggested by Hou and Müller (1994), however it was shown in Salvesen (2005) that due to the simple structure of the discretized model, the observers may be written explicitly. This is important, because it removes the need for recomputing the bank of observers when the operating point of the pipeline is changed. Verde (2004) also proposed a nonlinear version, using an extremely coarse discretization grid.

Several companies offer commercial solutions to pipeline monitoring with leak detection. Fantoft (2005) uses a transient model approach in conjunction with the commercial pipeline simulator OLGA2000, while EFA Technologies (1987, 1990, 1991) uses an event detection method that looks for signatures of no-leak to leak transitions in the measurements.

The detection method of Verde (2001) using a bank of observers, can potentially detect multiple leaks. However, multiple simultaneous leaks is an unlikely event, so the complex structure of a bank of N observers seems unnecessary. In this paper, we instead employ ideas from adaptive control, treating the size and location of a single point leak as constant unknown parameters. This differs from the method of Billman and Isermann (1987), since we will model the leak in the observer, thereby obtaining state estimates also in a leak situation. Another important aspect of our method is that the observer is designed for the continuum model, ensuring that convergence properties established theoretically are not an artifact of the method of discretization. Our leak detection system consists of an adaptive Luenberger-type observer, based on a set of two coupled one dimensional first order nonlinear hyperbolic partial differential equations governing the flow dynamics. It is assumed that measurements are only available at the inlet and outlet of the pipe, and output injection is applied in the form of boundary conditions. Heuristic update laws for adaptation of the friction coefficient and the two leak parameters are suggested.

2. MATHEMATICAL MODEL

2.1 Physical Model

For liquid flow in a pipe we have the mass conservation

$$\frac{\partial p}{\partial t} + u\frac{\partial p}{\partial x} + \rho c^2 \frac{\partial u}{\partial x} = 0, \tag{1}$$

and the momentum conservation (ignoring friction for now)

$$\frac{\partial u}{\partial t} + u\frac{\partial u}{\partial x} + \frac{1}{\rho}\frac{\partial p}{\partial x} = 0, \tag{2}$$

for $(x,t) \in (0,L) \times (0,\infty)$, and where u is flow velocity, p is pressure, and ρ is density. The relation between pressure and density is modelled as (Nieckele et al. (2001))

$$\rho = \rho_{ref} + \frac{p - p_{ref}}{c^2}, \tag{3}$$

where ρ_{ref} is a reference density at reference pressure p_{ref}, and c is the speed of sound. Equation (1)–(2) also describes gas flow in a pipe, simply by replacing (3) with the ideal gas law. Under the conditions we consider, we assume c is sufficiently large to ensure $\rho > 0$. In compact form, we have

$$\frac{\partial}{\partial t}\begin{bmatrix} p \\ u \end{bmatrix} + A(p,u)\frac{\partial}{\partial x}\begin{bmatrix} p \\ u \end{bmatrix} = 0, \tag{4}$$

where, using (3),

$$A(p,u) = \begin{bmatrix} u & k+p \\ \dfrac{c^2}{k+p} & u \end{bmatrix}, \tag{5}$$

$$k = c^2\rho_{ref} - p_{ref}, \tag{6}$$

and the boundary conditions are

$$u(0,t) = u_0(t), \tag{7}$$

$$p(L,t) = p_L(t). \tag{8}$$

The eigenvalues of A are

$$\lambda_1 = u - c,\ \lambda_2 = u + c. \tag{9}$$

Assuming that $u \ll c$, which is always the case in the applications we are considering, the eigenvalues are distinct and satisfy

$$\lambda_1 < 0 < \lambda_2. \tag{10}$$

The system is therefore strictly hyperbolic. Steady state solutions $(\bar{p}, \bar{u})$ of (4), must satisfy

$$A(p,u)\frac{\partial}{\partial x}\begin{bmatrix} p \\ u \end{bmatrix} = 0. \tag{11}$$

Since $A(p,u)$ is invertible ($\lambda_i \neq 0$), we have that

$$\frac{\partial \bar{p}}{\partial x} = 0,\ \frac{\partial \bar{u}}{\partial x} = 0, \tag{12}$$

so $\bar{p}$ and $\bar{u}$ are constant. The boundary conditions (7)–(8) yield $\bar{p} = p_L$ and $\bar{u} = u_0$.

2.2 Model in Characteristic Form

Consider now the change of coordinates

$$\alpha(p,u) = c\ln\left(\frac{k+p}{k+\bar{p}}\right) + u - \bar{u}, \tag{13}$$

$$\beta(p,u) = -c\ln\left(\frac{k+p}{k+\bar{p}}\right) + u - \bar{u}, \quad (14)$$

which clearly is defined for all physically feasible p and u. It is easy to see that it's inverse is

$$p(\alpha,\beta) = (k+\bar{p})\exp\left((\alpha-\beta)/(2c)\right) - k, \quad (15)$$
$$u(\alpha,\beta) = \bar{u} + (\alpha+\beta)/2. \quad (16)$$

Notice that the fixed point $(\bar{p},\bar{u})$ corresponds to $(0,0)$ in the new coordinates. The time derivative of (13)–(14) is

$$\alpha_t = c\frac{p_t}{k+p} + u_t, \quad (17)$$
$$\beta_t = -c\frac{p_t}{k+p} + u_t. \quad (18)$$

Inserting for p_t and u_t from (4) yields

$$\begin{aligned}\alpha_t &= -c\frac{up_x + (k+p)u_x}{k+p} - \left(\frac{c^2}{k+p}p_x + uu_x\right)\\ &= -(u+c)\left(c\frac{p_x}{k+p} + u_x\right)\\ &= -(u+c)\alpha_x, \quad (19)\\ \beta_t &= c\frac{up_x + (k+p)u_x}{k+p} - \left(\frac{c^2}{k+p}p_x + uu_x\right)\\ &= -(u-c)\left(-c\frac{p_x}{k+p} + u_x\right)\\ &= -(u-c)\beta_x. \quad (20)\end{aligned}$$

Using (16), we obtain

$$\alpha_t + (\bar{u} + c + (\alpha+\beta)/2)\alpha_x = 0, \quad (21)$$
$$\beta_t + (\bar{u} - c + (\alpha+\beta)/2)\beta_x = 0. \quad (22)$$

The boundary conditions are obtained from (15)–(16), and are

$$\alpha(0,t) + \beta(0,t) = 0, \quad (23)$$
$$\alpha(L,t) - \beta(L,t) = 0. \quad (24)$$

The characteristic form (21)–(22) is convenient for the observer design carried out in the next section.

3. OBSERVER DESIGN

In reality, input signals to pipelines are usually choke openings at the inlet and outlet. Here, we instead view $u_0(t)$ and $p_L(t)$ in (7)–(8) as inputs to the process, and construct the copy of the plant dynamics (4)

$$\frac{\partial}{\partial t}\begin{bmatrix}\hat{p}\\ \hat{u}\end{bmatrix} + A(\hat{p},\hat{u})\frac{\partial}{\partial x}\begin{bmatrix}\hat{p}\\ \hat{u}\end{bmatrix} = 0, \quad (25)$$

with boundary conditions

$$\hat{u}(0,t) = u_0(t), \quad (26)$$
$$\hat{p}(L,t) = p_L(t). \quad (27)$$

Notice that the input to (4)–(8) is also copied in (25)–(27). Equation (25)–(27) can be viewed as a Luenberger-type observer, and convergence is guaranteed when the process is operated at asymptotically stable fixed points, which is usually the case for pipelines. However, we look for alternatives to the boundary conditions (26)–(27) which yield better convergence properties. Taking $p_0(t) = p(0,t)$ and $u_L(t) = u(L,t)$ as process measurements, we may apply output injection to (25)–(27). In transformed coordinates, we obtain

$$\hat{\alpha}_t + \left(\bar{u} + c + \left(\hat{\alpha}+\hat{\beta}\right)/2\right)\hat{\alpha}_x = 0, \quad (28)$$
$$\hat{\beta}_t + \left(\bar{u} - c + \left(\hat{\alpha}+\hat{\beta}\right)/2\right)\hat{\beta}_x = 0, \quad (29)$$

with boundary conditions (we omit the argument t for brevity)

$$\hat{\alpha}(0) + \hat{\beta}(0) = b_0\Big(\alpha(0),\beta(0),\hat{\alpha}(0),\hat{\beta}(0),\alpha(L),\beta(L),\hat{\alpha}(L),\hat{\beta}(L)\Big), \quad (30)$$

$$\hat{\alpha}(L) - \hat{\beta}(L) = b_L\Big(\alpha(0),\beta(0),\hat{\alpha}(0),\hat{\beta}(0),\alpha(L),\beta(L),\hat{\alpha}(L),\hat{\beta}(L)\Big), \quad (31)$$

where b_0 and b_L are functions to be designed. Notice that the boundary injections (30)–(31) may be any function of the known signals at both ends of the pipe. For convergence analysis, we consider the linearization of (21)–(22) and (28)–(29) around $(0,0)$ and form the dynamics of the observer error, defined as $\tilde{\alpha} = \alpha - \hat{\alpha}$, $\tilde{\beta} = \beta - \hat{\beta}$. We obtain

$$\frac{\partial}{\partial t}\begin{bmatrix}\tilde{\alpha}\\ \tilde{\beta}\end{bmatrix} + \Lambda\frac{\partial}{\partial x}\begin{bmatrix}\tilde{\alpha}\\ \tilde{\beta}\end{bmatrix} = 0, \quad (32)$$

with boundary conditions

$$\tilde{\alpha}(0) + \tilde{\beta}(0) = -b_0\Big(\alpha(0),\beta(0),\hat{\alpha}(0),\hat{\beta}(0),\alpha(L),\beta(L),\hat{\alpha}(L),\hat{\beta}(L)\Big), \quad (33)$$

$$\tilde{\alpha}(L) - \tilde{\beta}(L) = -b_L\Big(\alpha(0),\beta(0),\hat{\alpha}(0),\hat{\beta}(0),\alpha(L),\beta(L),\hat{\alpha}(L),\hat{\beta}(L)\Big), \quad (34)$$

where

$$\Lambda = \begin{bmatrix}\bar{u}+c & 0\\ 0 & \bar{u}-c\end{bmatrix}. \quad (35)$$

Following Xu and Sallet (2002) and Coron et al. (2004), consider the Lyapunov function candidate

$$V = \frac{1}{c+\bar{u}}\int_0^L \tilde{\alpha}^2 e^{-\mu x/(c+\bar{u})}dx + \frac{1}{c-\bar{u}}\int_0^L \tilde{\beta}^2 e^{\mu x/(c-\bar{u})}dx, \quad (36)$$

recalling the assumption that $c \gg |\bar{u}|$. The time derivative of V along solutions of (32)–(34) is

$$\dot{V} = -\mu V + \tilde{\alpha}^2(0) - \tilde{\beta}^2(0) - \tilde{\alpha}^2(L)\, e^{-\mu L/(c+\bar{u})} + \tilde{\beta}^2(L)\, e^{\mu L/(c-\bar{u})}. \quad (37)$$

At this point we need to select b_0 and b_L such that $\tilde{\alpha}^2(0) - \tilde{\beta}^2(0)$ and $-\tilde{\alpha}^2(L)\, e^{-\mu L/(c+\bar{u})} + \tilde{\beta}^2(L)\, e^{\mu L/(c-\bar{u})}$ are negative. We adopt the particularly simple choice made in Coron et al. (2004), and select b_0 and b_L such that

$$\tilde{\alpha}(0) = k_0 \tilde{\beta}(0), \quad (38)$$

$$\tilde{\beta}(L) = k_L \tilde{\alpha}(L), \quad (39)$$

in which case

$$\dot{V} = -\mu V - \left(1 - k_0^2\right)\tilde{\beta}^2(0) - \left(e^{-\mu L/(c+\bar{u})} - k_L^2 e^{\mu L/(c-\bar{u})}\right)\tilde{\alpha}^2(L). \quad (40)$$

So, if

$$|k_0| \leq 1 \text{ and } |k_L| \leq e^{-\mu L/c} \quad (41)$$

then

$$\dot{V} \leq -\mu V. \quad (42)$$

Since (36) defines a norm equivalent to the L_2 norm on $[0, L]$, it follows that system (32) with (38)–(39) is exponentially stable at the origin in the L_2 norm. Notice that (41) implies that whenever $|k_L| < 1$, there exists $\mu > 0$ for which (42) holds. Replacing (26)–(27) with the new boundary conditions, the observer becomes

$$\frac{\partial \hat{p}}{\partial t} + \hat{u}\frac{\partial \hat{p}}{\partial x} + (k + \hat{p})\frac{\partial \hat{u}}{\partial x} = 0, \quad (43)$$

$$\frac{\partial \hat{u}}{\partial t} + \frac{c}{k+\hat{p}}\frac{\partial \hat{p}}{\partial x} + \hat{u}\frac{\partial \hat{u}}{\partial x} = 0, \quad (44)$$

with boundary conditions

$$\hat{u}(0) = u(0) + c\frac{1-k_0}{1+k_0}\ln\left(\frac{k+p(0)}{k+\hat{p}(0)}\right), \quad (45)$$

$$\hat{p}(L) = (k + p(L)) \times \exp\left(\frac{k_L - 1}{c(1+k_L)}\left(u(L) - \hat{u}(L)\right)\right) - k. \quad (46)$$

When $k_0 = 1$ and $k_L = 1$, (45)–(46) reduces to (26)–(27). It is interesting to notice that the above Lyapunov analysis does not provide exponential convergence in this case. Another interesting observation to make is that the design is independent of the working condition $(\bar{u}, \bar{p})$. Figure 1 shows the observer error in terms of evolution in time of the $L_2(0, L)$ norm of $u(x,t) - \hat{u}(x,t)$ for the cases with and without output injection (the L_2 norm of $p(x,t) - \hat{p}(x,t)$ looks qualitatively the same).

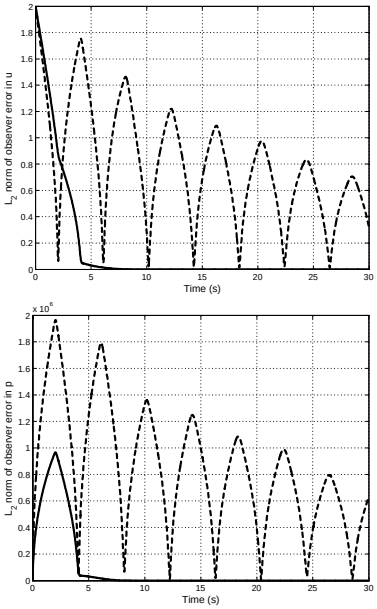

Fig. 1. Observer error with (solid) and without (dashed) output injection.

4. ADAPTATION OF FRICTION COEFFICIENT

Adding friction to the model (4), we have the mass balance

$$\frac{\partial p}{\partial t} + u\frac{\partial p}{\partial x} + (k+p)\frac{\partial u}{\partial x} = 0, \quad (47)$$

and momentum conservation

$$\frac{\partial u}{\partial t} + u\frac{\partial u}{\partial x} + \frac{c^2}{k+p}\frac{\partial p}{\partial x} = -(1+\Delta)\frac{f}{2}\frac{|u|\,u}{D}, \quad (48)$$

where D is the pipe diameter, and Δ is considered an unknown constant that accounts for uncertainty in the friction coefficient f, which is given by Schetz and Fuhs (1996)

$$\frac{1}{\sqrt{f}} = -1.8\log_{10}\left[\left(\frac{\epsilon/D}{3.7}\right)^{1.11} + \frac{6.9}{\mathrm{Re}_d}\right]. \quad (49)$$

ϵ/D is the pipe relative roughness, Re_d is the Reynolds number defined as

$$\mathrm{Re}_d = \frac{\rho u D}{\mu}, \quad (50)$$

and μ is the fluid viscosity. The observer is then

$$\frac{\partial \hat{p}}{\partial t} + \hat{u}\frac{\partial \hat{p}}{\partial x} + (k+\hat{p})\frac{\partial \hat{u}}{\partial x} = 0, \quad (51)$$

$$\frac{\partial \hat{u}}{\partial t} + \hat{u}\frac{\partial \hat{u}}{\partial x} + \frac{c^2}{k+\hat{p}}\frac{\partial \hat{p}}{\partial x} = -\left(1+\hat{\Delta}\right)\frac{\hat{f}}{2}\frac{|\hat{u}|\,\hat{u}}{D}, \quad (52)$$

which incorporates an estimate $\hat{\Delta}$ of Δ, and with boundary conditions (45)–(46). Consider the heuristic parameter update law

$$\dot{\hat{\Delta}} = -\kappa_\Delta\left(\tilde{\alpha}(L) + \tilde{\beta}(0)\right), \quad (53)$$

where κ_Δ is a strictly positive constant. In physical coordinates, equation (53) corresponds to

$$\dot{\hat{\Delta}} = -\kappa_\Delta\left(\varphi_1 + \varphi_2\right), \quad (54)$$

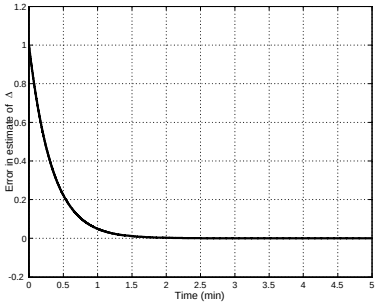

Fig. 2. Error in estimated friction factor, that is $\Delta - \hat{\Delta}$.

where

$$\varphi_1 = u(0) - \hat{u}(0) + c \ln\left(\frac{k + \hat{p}(0)}{k + p(0)}\right), \quad (55)$$

$$\varphi_2 = u(L) - \hat{u}(L) + c \ln\left(\frac{k + p(L)}{k + \hat{p}(L)}\right). \quad (56)$$

Figure 2 shows the evolution of $\Delta - \hat{\Delta}$ when the initial friction in the observer is twice that of the plant.

5. LEAK DETECTION

Adding a leak to the model (47)–(48), with $\Delta = 0$, we have the mass balance

$$\frac{\partial p}{\partial t} + u\frac{\partial p}{\partial x} + (k+p)\frac{\partial u}{\partial x} = -\frac{c^2}{A} f_l(x), \quad (57)$$

and the momentum conservation

$$\frac{\partial u}{\partial t} + u\frac{\partial u}{\partial x} + \frac{c^2}{k+p}\frac{\partial p}{\partial x} = -\frac{f}{2}\frac{|u|\,u}{D} + \frac{1}{A}\frac{c^2}{k+p} u f_l(x), \quad (58)$$

where A is the pipe cross sectional area. Assuming a point leak, we select $f_l(x)$ as

$$f_l(x) = w_l \delta(x - x_l), \quad (59)$$

where w_l and x_l are the size of the leak and position of the leak, respectively, and δ denotes the Dirac distribution. The observer is then

$$\frac{\partial \hat{p}}{\partial t} + \hat{u}\frac{\partial \hat{p}}{\partial x} + (k+\hat{p})\frac{\partial \hat{u}}{\partial x} = -\frac{c^2}{A}\hat{w}_l \delta(x - \hat{x}_l), \quad (60)$$

$$\frac{\partial \hat{u}}{\partial t} + \hat{u}\frac{\partial \hat{u}}{\partial x} + \frac{c^2}{k+\hat{p}}\frac{\partial \hat{p}}{\partial x} = -\frac{\hat{f}}{2}\frac{|\hat{u}|\,\hat{u}}{D} + \frac{1}{A}\frac{c^2}{k+\hat{p}}\hat{u}\hat{w}_l \delta(x - \hat{x}_l), \quad (61)$$

which incorporates estimates of the leak size and position, $\hat{w}_l$, $\hat{x}_l$. Consider the heuristic parameter update laws

$$\dot{\hat{w}}_l = -\kappa_w\left(\tilde{\beta}(0) - \tilde{\alpha}(L)\right), \quad (62)$$

and

$$\dot{\hat{x}}_l = -\kappa_x \varphi_{\alpha\beta}\left|\varphi_{\alpha\beta}\right|^{\frac{1}{\gamma}-1}, \quad (63)$$

where

$$\varphi_{\alpha\beta} = \tilde{\alpha}(L) + \tilde{\beta}(0), \quad (64)$$

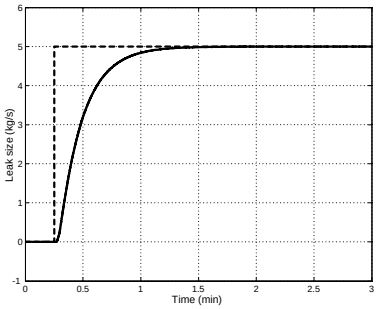

Fig. 3. Estimated size of leak (solid) and actual size of leak (dashed).

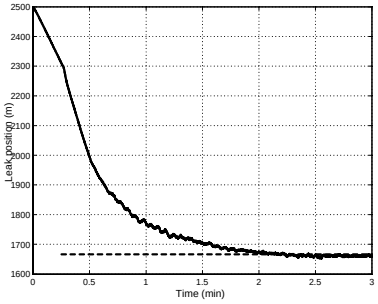

Fig. 4. Estimated position of leak (solid) and actual position of leak (dashed).

and κ_w, κ_x and γ are strictly positive constants. In physical coordinates, equation (62)–(63) corresponds to

$$\dot{\hat{w}}_l = -\kappa_w(\varphi_1 - \varphi_2), \quad (65)$$

$$\dot{\hat{x}}_l = -\kappa_x(\varphi_1 + \varphi_2)\left|\varphi_1 + \varphi_2\right|^{\frac{1}{\gamma}-1}, \quad (66)$$

where φ_1 and φ_2 are given in (55)–(56). Figures 3–4 show the evolution of the estimates (65)–(66) for a leak occuring at $t = 0.25$ minutes.

6. SIMULATIONS WITH OLGA

The leak detection test in the previous section was a nominal test, where the plant dynamics and the observer dynamics were identical (except for output injection, of course). Here, we perform more realistic tests, replacing the plant dynamics by the state-of-the-art flow simulator OLGA2000 [1]. For two different cases, summarized in Table 1, we run our leak detection scheme (60)–(63) with (45)–(46). In the table, w_{in} denotes the mass rate of fluid at the inlet. Figure 5 shows that the leaks are quantified very accurately, while localization is somewhat noisy. However, the average error in position taken over the last 15 seconds shown in the Figure, is within 0.25% and 0.36% of the pipe length for Cases I and II, respectively.

[1] OLGA2000 is a commercially available flow simulator widely used by the petroleum industry. It is developed by Scandpower AS.

Parameter	Case I	Case II	Unit
L	990	8000	m
D	0.10	0.51	m
c	$1.26e3$	$1.2e3$	m/s
k	$1.38e9$	$1.24e9$	Pa
μ	0.0063	0.0056	Pa s
ϵ	0	0	m
$\hat{\Delta}$	0.13	0.028	-
w_l	4.9	12.5	kg/s
x_l	505	4000	m
w_{in}	70	300	kg/s

Table 1. Numerical coefficients.

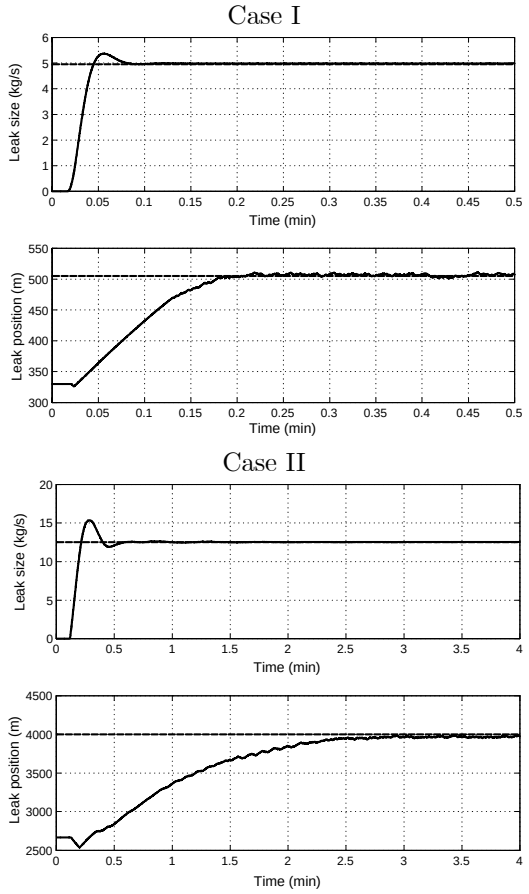

Fig. 5. Leak detection applied to OLGA simulations.

7. CONCLUDING REMARKS

We have designed a leak detection system for pipelines consisting of an adaptive Luenberger-type observer and heuristic update laws for the parameters characterizing a point leak. The only available process information is flow velocity and pressure at the inlet and outlet of the pipe. Simulations with a state-of-the-art flow simulator as process, demonstrate accurate quantification and localization in two test cases.

ACKNOWLEDGEMENTS

We gratefully acknowledge the support from the Gas Technology Center at NTNU, Statoil, and the Norwegian Research Council.

REFERENCES

L. Billmann and R. Isermann, "Leak detection methods for pipelines," *Automatica*, vol. 23, no. 3, pp. 381–385, 1987.

J.-M. Coron, B. d'Andrea-Novel, and G. Bastin, "A strict Lyapunov function for boundary control of hyperbolic systems of conservation laws," *Proceedings of the 43rd IEEE Conference on Decision and Control*, Paradise Island, Bahamas, December 14-17, 2004.

EFA Technologies, Inc., "Events at a leak," Technical paper available from EFA on request, 1987.

EFA Technologies, Inc., "Effect of pressure measurement resolution on PPA leak detection," Technical paper available from EFA on request, 1990.

EFA Technologies, Inc., "PPA event suppression capability," Technical paper available from EFA on request, 1991.

Fantoft, "D-SPICE overview: Production management systems," Fantoft Process Technologies, 2005.

J.-M. Greenberg and T.-t. Li, "The effect of boundary damping for the quasilinear wave equations," *Journal of Differential Equations*, vol. 52, pp. 66-75, 1984.

J. de Halleux, C. Prieur, J.-M. Coron, B. d'Andrea-Novel, and G. Bastin, "Boundary feedback control in networks of open channels," *Automatica*, vol. 39, pp. 1365–1376, 2003.

M. Hou and P. Müller, "Fault detection and isolation observers," *International Journal of Control*, vol. 60, no. 5, pp. 827–846, 1994.

A.O. Nieckele, A.M.B. Brage, and L.F.A. Azevedo, "Transient pig motion through gas and liquid pipelines," *Journal of Energy Resources Technology*, vol. 123, no. 4, 2001.

J. Salvesen, *Leak Detection by Estimation in an Oil Pipeline*, MSc Thesis, NTNU, 2005.

J.A. Schetz and A.E. Fuhs, *Handbook of Fluid Dynamics and Fluid Machinery, Volume 1, Fundamentals of Fluid Mechanics*, John Wiley & Sons, 1996.

D.N. Shields, S.A. Ashton, and S. Daley, "Design of nonlinear observers for detecting faults in hydraulic sub-sea pipelines," *Control Engineering Practice*, vol. 9, pp. 297–311, 2001.

C. Verde, "Multi-leak detection and isolation in fluid pipelines," *Control Engineering Practice*, vol. 9, pp. 673–682, 2001.

C. Verde, "Minimal order nonlinear observer for leak detection," *Journal of Dynamic Systems, Measurement and Control*, vol. 126, pp. 467–472, 2004.

C.-Z. Xu and G. Sallet, "Exponential stability and transfer functions of processes governed by symmetric hyperbolic systems," *ESAIM Journal on Control, Optimisation and Calculus of Variations*, vol. 7, pp. 421-442, 2002.

ADCHEM 2006

International Symposium on Advanced Control of Chemical Processes
Gramado, Brazil – April 2-5, 2006

FIRST PRINCIPLES INVARIANTS FOR ASYMPTOTIC OBSERVERS IN CHEMICAL REACTORS

Françoise Couenne * **Christian Jallut** *
Denis Dochain **

* *LAGEP, UCB Lyon 1, UMR CNRS 5007*
ESCPE, Bat 308 G, 43 Bvd du 11 Nov 1918
69622 Villeurbanne cedex, France
** *CESAME, Universite Catholique de Louvain Batiment*
EULER 4, av. Georges Lemaitre, B-1348
Louvain-la-Neuve, Belgium

Abstract: In this paper, a method to build asymptotic estimators for continuous stirred tank reactor in the case of constant pressure and constant volume liquid phase is proposed. The estimator is based on the measurement of temperature and some concentrations. This method works for highly nonlinear reactions, with realistic thermodynamic properties and is based on the preservation of two fundamental conserved quantities: the mass and the energy. Simulations results for an example are proposed and discussed.

Keywords: Estimators, continuous stirred tank reactor, conservation laws

1. INTRODUCTION

Observers or estimators for nonlinear systems were much studied in the last ten years: so a very important literature exists for the construction of observers or estimators for chemical reactions occurring in a continuous stirred tank reactor (*CSTR*) (see (Dochain *et al.*, 1992), (Dootingh *et al.*, 1992), (Gibon-Fargeot *et al.*, 1994), (Alvarez-Ramirez, 1995) and (Gibon-Fargeot *et al.*, 2000)).

In this paper, it is shown how the so-called asymptotic observer presented in (Dochain *et al.*, 1992) can be reformulated so that the reconstructed variables correspond to fundamental conserved quantities: the mass conservation and the energy conservation.

2. THE MODEL

This section is devoted to establishing the model used in this study. The material balance and the energy balance are successively presented.

Consider a liquid phase perfectly mixed continuous stirred tank reactor. The liquid phase chemical reactions and the jacketed reactor in which the reaction takes place are modeled with the following assumptions:

- The heat flux exchanged with the jacket is represented by Φ_{jac}. It is assumed to be depending on to the temperatures of the jacket and of the mixture T in the reactor.
- At the inlet of the reactor, the pure components are injected separately at the same temperature T_e.
- r independent reactions involving S species are occurring in the CSTR.

- It is supposed that the reactional volume remains constant as well as the pressure.

3. THE INVARIANTS IN CHEMICAL REACTION SYSTEMS

The material balance for each specie is given by:

$$\frac{d\mathbf{n}}{dt} = (\mathbf{QC})_e - \frac{Q}{V}\mathbf{n} + V\mathcal{N}^T\mathcal{R}(\mathbf{n}, T, V) \qquad (1)$$

with $\mathbf{n}$ the component mole number vector, $(\mathbf{QC})_e$ the molar flow rate vector at the inlet: the i^{th} element is given by Q_{ei} where Q_{ei} is the volumetric inlet flow rate for the i^{th} specie and C_{ei}, the concentration at the inlet for the i^{th} specie, $\mathbf{Q}$ the total volumetric flow rate at the outlet, $\mathcal{N}$ the stoichiometric matrix, $\mathcal{R}$ the vector of the reaction rate, V the reactional volume and T the temperature of the mixture.

We first present the invariants for chemical reactions relative to the mass balance. The aim is to use these invariants in order to express a part of the differential equations of the species balance in such a way that the reaction terms disappear.

Up to some permutations of the state vector $\mathbf{n}$ and as presented in (Dochain *et al.*, 1992) or in (Villermaux, 1985; Makila and Waller, 1981; Srinivasan *et al.*, 1998) there exists a linear transformation:

$$\mathbf{z} = \begin{bmatrix} z_1 \\ z_2 \end{bmatrix} = \begin{bmatrix} \left(\mathbf{I}_R \mid 0 \ \dots \ 0 \right) \mathbf{n} \\ \mathbf{P}^T\mathbf{n} \end{bmatrix}$$

for chemical reaction systems which leads to the following system with $z_1 \in \mathbb{R}^R$ and $z_2 \in \mathbb{R}^{S-R}$:

$$\frac{dz_1}{dt} = \left(\mathbf{I}_R \mid 0 \ \dots \ 0 \right) (\mathbf{QC})_e - \frac{\mathbf{Q}}{V} z_1 + V\mathcal{N}\mathcal{R}(\mathbf{z}, V) \qquad (2)$$

$$\frac{dz_2}{dt} = \mathbf{P}^T(\mathbf{QC})_e - \frac{\mathbf{Q}}{V} z_2 \qquad (3)$$

z_2 is related to the conservation of atoms in the chemical processes.

The energy balance is extensively used in modeling purposes. In general, this balance is often expressed with a constant specific heat capacity for the mixture. In this presentation we do not assume this hypothesis. Let us express the energy balance in terms of temperature as it is usually the case:

$$\begin{aligned} \frac{dT}{dt} = & \frac{(\mathbf{QC})_e^T(\mathbf{h}_e - \left[\frac{\partial H(\mathbf{n},T)}{\partial \mathbf{n}}\right])}{\frac{\partial H(\mathbf{n},T)}{\partial T}} \\ & - \frac{\frac{Q}{V}(H(\mathbf{n},T) - \left[\frac{\partial H(\mathbf{n},T)}{\partial \mathbf{n}}\right]^T \mathbf{n})}{\frac{\partial H(\mathbf{n},T)}{\partial T}} \\ & - \frac{\Phi_{jac}}{\frac{\partial H(\mathbf{n},T)}{\partial T}} \\ & - \frac{\left[\frac{\partial H(\mathbf{n},T)}{\partial \mathbf{n}}\right]^T V\mathcal{N}^T\mathcal{R}(\mathbf{n},T,V)}{\frac{\partial H(\mathbf{n},T)}{\partial T}} \end{aligned} \qquad (4)$$

where the vector h_e represents the molar enthalpy of each species at the inlet, the species being injected separately at the same temperature T_e. $H(\mathbf{n},T) = \sum_i n_i hi(n,T)$ represents the total enthalpy of the mixture present in the CSTR. In this energy balance (4), the reaction rates appears explicitly as it is well known.

However by the use of the invariant concept, the reaction rates can be eliminated from (4) leading straight to the enthalpy formulation (5). Actually the energy is a conserved quantity and in the case of constant volume and pressure it also corresponds to the enthalpy: this conservation principle leads for open systems to the following conservation equation where only terms expressing energy exchange with the environment:

$$\frac{dU}{dt} = \frac{dH}{dt} = (\mathbf{QC})_e^T\mathbf{h}_e - \frac{Q}{V}H - \Phi_{jac} \qquad (5)$$

The equation (3) and (5) express variables z_2 and H that are not affected by reaction. These variables can be used to construct asymptotic observers as soon as $R-1$ complementary variables from (2) are measured as well as the temperature.

4. THE ASYMPTOTIC OBSERVER

In this section, we briefly recall the conditions under which it is possible to construct the asymptotic observers.

So let us assume that:

- The first $R-1$ components mole numbers issued from z_1 are available for on-line measurements as well as the temperature of the reactor.
- The outlet flow rate as well as the volume are known.
- The stoichiometry of the reactions is known.
- A model is available to calculate the molar enthalpy for the mixture.

Let us call $\overline{n}_2$ the vector formed by n_2 and the last element of n_1 and consider the notation: $P = \left[P_1 \mid P_2 \right]$ where P_1 is a $R-1 \times S-R$ matrix corresponding to the measures states variables.

Finally let us call n_{1mes} the vector of measures and $\mathcal{P}$ the physical domain of $\overline{n}_2$.

Theorem 1. Under the previous assumptions and if the input $\frac{Q}{V}$ is regularly persistent, the system formed by

$$\begin{aligned}\frac{dz_2}{dt} &= \mathbf{P}^T(\mathbf{QC})_e - \frac{Q}{V}z_2 \\ \frac{dH}{dt} &= (\mathbf{QC})_e^T\mathbf{h}_e - \frac{Q}{V}H - \Phi_{jac}\end{aligned} \tag{6}$$

is an asymptotic observer of the non measured states of $\mathbf{n}$ if the mapping

$$\psi : \begin{array}{ccc}\mathcal{P} \subset \mathbb{R}^{S-R+1} & \longrightarrow & \mathbb{R}^{S-R+1} \\ \overline{n}_2 & \longrightarrow & \begin{pmatrix} H(n_{1mes}, \overline{n}_2) \\ P_2^T \begin{pmatrix} n_{1mes} \\ \overline{n}_2 \end{pmatrix} \end{pmatrix}\end{array}$$

is injective.

The proof of this theorem is given in (Dochain *et al.*, 1992).

Remark 2. Since H is not necessarily linear with respect to $\overline{z}_2$, the explicit inversion is not always possible. For example, in the case that the non-ideality of the mixture is represented by an excess model as in (Sandler, 1999), the molar enthalpy of the mixture h is given by:

$$h = \left(\mathbf{h}(T,P)^T\mathbf{x}\right) + \Delta h^{ex}(T,P,\mathbf{x}) \tag{7}$$

with $\mathbf{h}$ the vector of the molar enthalpy of pure ideal species, $\mathbf{x}$ the vector of molar fractions and $\Delta h^{ex}(T,P,\mathbf{x})$ the excess term. Following the mixture, this term can give rise different forms and no general results can be deduced.

In the case of an ideal mixture, we obtain

$$h = \left(\mathbf{h}(T,P)^T\mathbf{x}\right) \tag{8}$$

Consider the following partition: $\mathbf{h}^T = \left[\, \overline{h}_1 \mid \overline{h}_2 \,\right]$ where $\overline{h}_1$ is a $R-1\times 1$ matrix formed by the molar enthalpies $\left(\, h_1 \;\ldots\; h_{R-1} \,\right)$ and $\overline{h}_2 = \left(\, h_R \;\ldots\; h_S \,\right)$ and we can state:

Corollary 3. Under the previous assumptions and if the input $\frac{Q}{V}$ is regularly persistent , the system formed by (6) is an asymptotic observer of the non measured states of $\mathbf{n}$ if $\begin{pmatrix} \overline{h}_2 \\ P_2 \end{pmatrix}$ has a left inverse. The estimated vector $\widehat{n}$ is given by:

$$\widehat{n}(t) = \begin{pmatrix} \overline{h}_2 \\ P_2 \end{pmatrix}^+ \left(\begin{pmatrix} H(t) \\ z_2(t) \end{pmatrix} - \begin{pmatrix} \overline{h}_1 \\ P_1 \end{pmatrix} n_{1mes}(t) \right) \tag{9}$$

Remark 4. It can be noticed that in this formulation the enthalpy of the reaction does not appear as a parameter but is related to the formation enthalpies of the species h_{iref}.

5. ILLUSTRATION EXAMPLE

Let us illustrate the method with the following simple reaction scheme involving three chemical species X_1, X_2 and X_3:

$$\nu_1 X_1 \xrightarrow[r_1 = k_1(T)C_1^2]{} \nu_2 X_2 \xrightarrow[r_2 = k_2(T)C_2]{} \nu_3 X_3$$

with the stoichiometric coefficients (ν_1, ν_2, ν_3). where C_1, C_2 and C_3 are respectively the concentrations in the species X_1, X_2 and X_3. r_{v1} and r_{v2} represent the reaction rate of the two consecutive reactions.

Moreover we consider that the molar enthalpy for each specie is $h_i = c_{pi}\left(T - T_{ref}\right) + h_{iref}$ and that the mixture is ideal. In this case the model is represented by:

$$\begin{aligned}\frac{dn_1}{dt} &= Q_{e1}C_{e1} - \frac{Q}{V}n_1 - \nu_1 r_1(n1,T,V)V \\ \frac{dn_2}{dt} &= Q_{e2}C_{e2} - \frac{Q}{V}n_2 + \nu_2 r_1(n1,T,V)V \\ &\quad -\nu_2 r_2(n2,T,V)V \\ \frac{dn_3}{dt} &= Q_{e3}C_{e3} - \frac{Q}{V}n_3 + \nu_3 r_2(n2,T,V)V \\ \frac{dT}{dt} &= \frac{\sum_{i=1}^3 Q_{ei}C_{ei}c_{pi}(Tei - T) - \Phi_{jac}}{\left(\sum_{i=1}^3 n_i c_{pi}\right)} \\ &\quad - \frac{\left(\nu_2 h_2 - \nu_1 h_1\right) r_1 V}{\left(\sum_{i=1}^3 n_i c_{pi}\right)} \\ &\quad - \frac{\left(\nu_3 h_3 - \nu_2 h_2\right) r_2 V}{\left(\sum_{i=1}^3 n_i c_{pi}\right)}\end{aligned} \tag{10}$$

Let us consider the following variables: $z_1 = \nu_1 n_1 + \frac{\nu_1}{\nu_2}n_2 + \frac{\nu_1}{\nu_3}n3$ and $z_2 = \sum_{i=1}^3 n_i h_i(T)$. Finally let us choose that n_1 is measured and let us call this measure n_{1m}. Let us express the model in the new system of coordinates.

$$\begin{aligned}\frac{dz_1}{dt} &= \nu_1 Q_{e1}C_{e1} + \frac{\nu_1}{\nu_2}Q_{e2}C_{e2} + \frac{\nu_1}{\nu_3}C_{e3} - \frac{Q}{V}z_1 \\ \frac{dz_2}{dt} &= \sum_{i=1}^{S} Q_{ei}C_{ei}h_{ei} - \frac{Q}{V}z_2 - \Phi_{jac}\end{aligned} \tag{11}$$

From the knowledge of the invariants z_1 and z_2, the construction of the estimate $\hat{n}_2$ and $\hat{n}_3$ is easily performed:

$$\frac{\nu_1}{\nu_2}\hat{n}_2 + \frac{\nu_1}{\nu_3}\hat{n}_3 = z_1 - \nu_1 n_{1m}$$

$$\begin{aligned}&\left(c_{p2}\left(T - T_{ref}\right) + h_{2ref}\right)\hat{n}_2 + \\ &\quad \left(c_{p3}\left(T - T_{ref}\right) + h_{3ref}\right)\hat{n}_3 \\ &\qquad = z_2 - n_{1m}\left(c_{p1}\left(T - T_{ref}\right) + h_{1ref}\right)\end{aligned} \tag{12}$$

Let us apply these equations to the the example treated by (Dochain *et al.*, 1992). For the reaction the stoichiometric coefficient are equal to 1. The reaction rate vector is given by:

$$\begin{pmatrix} r_1 \\ r_2 \end{pmatrix} = \begin{pmatrix} k_1 e^{-\frac{E_1}{RT}} \left(\frac{n_1}{V}\right)^2 \\ k_2 e^{-\frac{E_2}{RT}} \left(\frac{n_2}{V}\right) \end{pmatrix}$$

with

$$k_1 = 1.1\,10^{-3} m^3\,mol^{-1}\,s^{-1}, k_2 = 172.2 s^{-1}$$
$$E_1 = 2.09\,10^4 J\,mol^{-1},\ E_2 = 4.18\,10^4 J\,mol^{-1}$$
$$R = 8.3143 J\,mol^{-1}\,K^{-1}.$$

The heat flux with the jacket is expressed as follows:

$$\phi_{jac} = h\,A_c\,(T - T_{jac}) \tag{13}$$

with

$$h = 5\,10^3 J\,s^{-1}\,m^{-2},\ A_c = 170 m^2$$

and the temperature of the jacket $T_j = 350K$. The parameters and input variables are chosen as :

$$V = 10 m^3,\ T_e = 350K,\ C_{e1} = 10^4 mol\,m^{-3}$$
$$C_{e2} = C_{e3} = 0,\ Q_{e1} = 0.1 m^3 s^{-1}$$

Let us define the values for the computation of the enthalpy:

$$T_{ref} = 350K,\ c_{p1} = 1000 J\,mol^{-1}\,K^{-1}$$
$$c_{p2} = 1000 J\,mol^{-1}\,K^{-1},\ c_{p3} = 1000 J\,mol^{-1}\,K^{-1}$$
$$h_{1ref} = 0 J\,mol^{-1},\ h_{2ref} = -20.18\,10^4 J\,mol^{-1}$$
$$h_{3ref} = -45.18\,10^4 J\,mol^{-1}$$

In the present example the initial states are set to the following values :

$$n_1(0 = 10^4 mol,\ n_2(0) = 5\,10^4 mol$$
$$n_3(0) = 0 mol,\ T(0) = 360K$$

and for the estimator:

$$z_2(0) = 0.9(n_1(0) + n_2(0) + n_3(0))$$
$$H(0) = 0.9 \sum_{i=1}^{3} n_i(0)(c_{pi}(T(0) - T_{ref}) + h_{iref}).$$

For the computation of Q, the molar volume v_i of species are necessary: $v_1 = v_2 = v_3 = 0.167\,10^{-4}$.

The simulation results presented below correspond to the following profile of Q_{e1}:
from t=0 to 300s $Q_{e1} = 0.1$,
from t=300 to 600s $Q_{e1} = 0.2$ and
from t=600s $Q_{e1} = 0.1$.

Figures 1 and 2 respectively give the profile of the measurements: the temperature and n_1. These values are injected in the estimator. Finally, figures 3 and 4 give the profile of n_2 and n_3 and of their estimates.

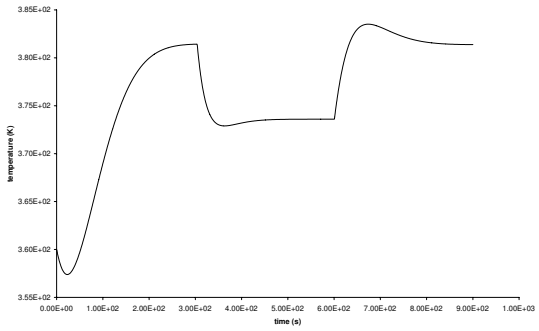

Fig. 1. The temperature profile.

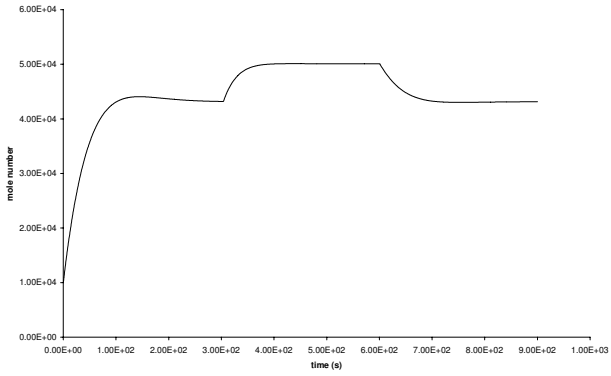

Fig. 2. n_1 profile.

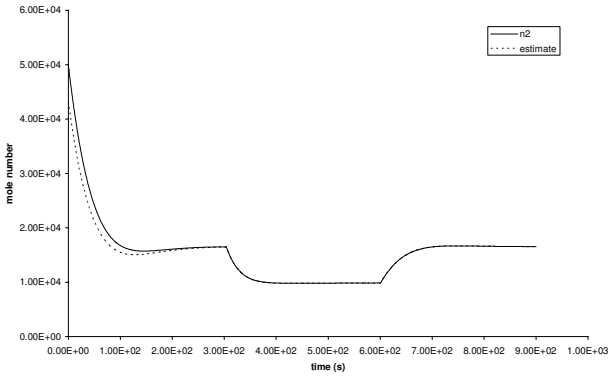

Fig. 3. n_2 profile and its estimation.

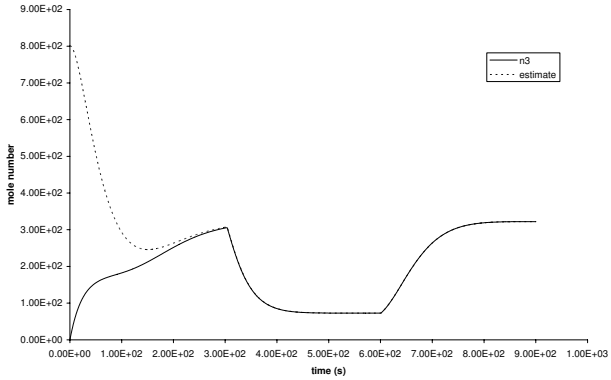

Fig. 4. n_3 profile and its estimation.

6. CONCLUSION

The estimator presented in this paper is based on the first principle invariants: mass invariants and the energy invariant. The use of the enthalpy is clarified with respect to previous works (Dochain *et al.*, 1992) on asymptotic observers. It permits to present how to use the conserved quantities for models of chemical reactions. This work can be applied to gaseous phase reaction. The important hypothesis is that the volume remains constant. The generalization to non ideal mixture is theoretically possible and will necessitate the use of differential algebraic methods.

REFERENCES

Alvarez-Ramirez, J. (1995). Observers for a class of continuous tank reactors via temperature measurement. *Chemical Engineering Science*.

Dochain, D., M. Perrier and B.E. Ydstie (1992). Asymptotic observers for stirred tank reactors. *Chemical Engineering Science*.

Dootingh, M. Van, F. Viel, D. Rakotopara, J. P. Gauthier and P. Hobbes (1992). Nonlinear deterministic observer for state estimation: Application to a continuous free radical polymerization reactor. *Computers and Chemical Engineering*.

Gibon-Fargeot, A.M., F. Celle-Couenne and H. Hammouri (2000). Cascade estimation design for cstr models. *Computers and Chemical Engineering*.

Gibon-Fargeot, A.M., H. Hammouri and F. Celle (1994). Nonlinear observers for chemical reactors. *Computers Engineering Science*.

Makila, P.M. and K. V. Waller (1981). The energy balance in modeling gas-phase chemical reactor dynamics. *Chemical Engineering Science*.

Sandler, S.I. (1999). *Chemical and engineering thermodynamics*. Wiley.

Srinivasan, B., M. Amrhein and D. Bonvin (1998). Reaction and flow variants/invariants in chemical reaction systems with inlet and outlet streams. *AIChE Journal*.

Villermaux, J. (1985). *Génie de la réaction chimique: conception et fonctionnement des réacteurs*. Lavoisier, second edition. Paris.

ADCHEM 2006

International Symposium on Advanced Control of Chemical Processes
Gramado, Brazil – April 2-5, 2006

CONTROL OF CONTINUOUS REACTORS WITH NON-MONOTONIC REACTION RATE

Jorge Díaz-Salgado [**] **Jesus Alvarez** [*]
Jaime Moreno [**]

[*] *Universidad Autónoma Metropolitana Iztapalapa, México D.F. jac@xanum.uam.mx* [1]
[**] *Universidad Nacional Autónoma de México. {JDiazS, JMorenoP}@iingen.unam.mx*

Abstract: In this paper, the problem of controlling a (possibly open-loop unstable) continuous exothermic chemical reactor with non-monotonic reaction rate, maximum production rate specification, and temperature measurements is addressed. The problem difficulty resides in the lack of reactor local observability at the nominal steady-state. A nonlocal constructive design approach leads to a passivated control scheme with linearity, decentralization and reduced model dependency features as well as nonlocal closed-loop behavior. The resulting control scheme resembles industrial type components: a linear PI cascade temperature controller, and a ratio inventory-based feedforward concentration controller. The approach is tested with a typical case example through numerical simulations.

Keywords: Reactor Control, Process Control.

1. INTRODUCTION

Reactors with non-monotonic kinetic rate dependency on concentration constitute an important class of reactors (Lapidus, 1977; Elnashaie, et al., 1990). These reactors may exhibit strongly nonlinear behavior, like steady-state multiplicity, limit cycling and parametric sensitivity. To obtain the maximum product yield, these reactors must be operated at a steady-state with maximum reaction rate, a concentration that is not locally observable from a temperature measurement. From a local control design viewpoint, this lack of observability means that, in spite of being able to control the temperature, it is not possible to know if the reactor concentration is in the isotonic or antitonic branch of the reaction rate function. This problem has been tackled by choosing a nominal concentration sufficiently below the one of the maximum rate (Smets, et al., 2002). So that locally: the reaction rate becomes monotonic, the steady-state is observable, and the concentration can be estimated and/or controlled. However, in the theoretical systems estimation literature is well known that lack of local (linear) observability does not necessarily imply lack of nonlocal (nonlinear) observability (Hermann and Krener, 1977), and this motivates the question addressed in the present work; on whether it is possible to nonlocally control a continuos reactor with non-monotonic reaction rate about a prescribed (possibly open-loop unstable) steady-state with maximum reaction rate. On the other hand, in a recent control study for an exothermic polymer reactor with monotonic reaction rates, the combination of feedfordward, passivity and observability ideas yielded an output feedback cascade

[1] Apdo. 55534 Dpto. Ing. de Procesos e Hidráulica, UAM-I, Av. Purísima y Michoacán s/n, Col. Vicentina, México, D.F. C.P. 09340 Tel.58-04-49-58

controller with (Gonzalez and Alvarez, 2005): (i) linearity, decentralization and model independency features, (ii) industrial-like (linear PI, ratio and inventory) components, and (iii) behavior recovery of an exact model-based nonlinear state-feedback (SF) passivated controller. In this paper, the problem of controlling a (possibly open-loop unstable) continuous exothermic chemical reactor with non-monotonic reaction rate, maximum production rate specification, temperature measurements, and heat exchange and reactant dosage rate as manipulated variables is addressed. Having as point of departure the above discussed PI-inventory reactor control scheme, the combination nonlocal of passivity, observability and stability notions within robustness-oriented constructive control framework yields a measurement-driven dynamic control scheme that non-locally stabilizes the non-monotonic rate reactor about a steady state with maximum reaction rate. The resulting controller has two parts that resemble industrial conventional control components: (i) a PI temperature controller with a measurement noise filter, and (ii) a feedforward-like ratio controller for the reactant dosage rate. The proposed approach is tested with a case example through numerical simulations.

2. CONTROL PROBLEM

Consider a continuous chemical reactor where an exothermic reaction takes place, the volume is kept constant with suitable level control loop, heat exchange is enabled via a cooling jacket, by manipulating its temperature T_j, in the understanding that T_j is the set-point signal to drive a secondary control loop in a cascade configuration. Since the secondary temperature control loop design can be performed with existing techniques (Alvarez-Ramirez, et al., 2002; Gonzalez and Alvarez, 2005), here we will circumscribe to address the design of the primary temperature controller, in coordination with a composition regulation component. From standard mass and energy conservation arguments the reactor model is given by (Lapidus, 1977):

$$\begin{aligned} \dot{c} &= -\rho(c,T,p) + \theta(c_e - c) \\ \dot{T} &= \beta\rho(c,T,p) + \theta(T_e - T) - \upsilon(T - T_j) \\ y &= T, z_c = c, z_T = T, d_T = T_e, d_c = c_e \end{aligned} \quad (1)$$

Where c is the reactant dimensionless concentration T is the reactor temperature, T_j is the jacket temperature, θ is the dilution rate, υ is the heat transfer coefficient, and β is the adiabatic temperature rise (i.e., the heat of reaction divided by the reactor heat capacity). The *states* are the concentration c and the temperature T. The *control inputs* are the dilution rate θ and the jacket temperature T_j. The *regulated outputs* (z_c and z_T) are the concentration c and the temperature T. The *measured output* (y) is the temperature T. In other words, only one (the temperature) of the two regulated outputs is measured. The exogenous load disturbance inputs (d_T and d_c) are the measured feed temperature T_e and the unmeasured feed concentration c_e.

The strictly positive scalar function $\rho(c,T,p)$ describes the non-monotonic kinetic rate dependency on c and T, p is a parameter vector, and $\rho(c,T,p)$ has a maximum in the curve

$$\Omega = (c,T) \mid \frac{\partial \rho(c,T,p)}{\partial c} := \rho_c(c,T,p) = 0 \quad (2)$$

implying that the pair (T,p) uniquely determines a concentration value c^* where the reaction rate is maximum, this is,

$$c^* = \kappa(T,p) \ni \rho_c[\kappa(T,p),T,p] = 0$$

The reactor must operate about a (possibly open loop unstable) steady-state $\bar{x} = (\bar{c},\bar{T})^T$, and the nominal concentration $\bar{c}$ must yield the maximum reaction rate at $\bar{T}$, according to the steady-state expressions

$$\begin{aligned} 0 &= -\rho(\bar{c},\bar{T},p) + \theta(\bar{c}_e - \bar{c}), \;\; \rho_c(\bar{c},\bar{T},p) = 0 \\ 0 &= \beta\rho(\bar{c},\bar{T},p) + \theta(\bar{T}_e - \bar{T}) - \upsilon(\bar{T} - \bar{T}_j) \end{aligned} \quad (3)$$

where $\bar{c}_e$(or $\bar{T}_e$) is the nominal feed concentration (or temperature). In compact vector notation, the reactor (1) is written as follows

$$\dot{x} = f(x,d,u,p), \quad y = c_y x, \quad z = x$$

where
$x = [c,T]^T, d = [c_e,T_e]^T, c_y = [0,1], u = [\theta,T_j]$.

The controllability ($\mathcal{C}$) and observability ($\mathcal{O}$) matrix ranks of the linear reactor approximation about the prescribed steady-state ($\bar{x}$) are:

$$rank[\mathcal{C}] = 2 \Leftrightarrow \upsilon \neq 0, \bar{c}_e \neq \bar{c} \; ; \;\; \mathcal{C} = [B, AB]$$
$$rank[\mathcal{O}] = 2 \Leftrightarrow \rho_c(c,T,p) \neq 0 \; ; \;\; \mathcal{O} = [c_y, c_y A]^T$$

where $A = f_x(\bar{x},\bar{d},\bar{u},p)$, $B = f_u(\bar{x},\bar{d},\bar{u},p)$.

Observe that: (i) at $\bar{x}$ the linear reactor approximation is controllable but not observable, (ii) when $x \neq \bar{x}$ the linear approximation is controllable and observable, and (iii) nowhere the reactor is nonlinearly instantaneously observable (Hermann and Krener, 1977; Alvarez, 2000) because, given $(T,\dot{T},T_j,T_e)$ the heat equation $\rho(c,T,p) = [\dot{T} - \theta(T_e - T) - \upsilon(T - T_j)]/\beta$ admits two concentration solutions. This signifies that a nonlinear high-gain Luenberguer observer cannot be employed (Zeitz, 1987), because the related observability matrix is singular at the curve Ω (2). Technically speaking, our problem is the following: given a prescribed steady-state operation (3), that is optimal in the sense that maximizes the production rate at $\bar{T}$, design an output-feedback

controller that, driven by measured output (y) and input (d_T) temperature measurements (without measuring the concentration), manipulates the dilution rate (θ) and the jacket temperature (T_j) to maintain the concentration (c) and temperature (T) outputs about their prescribed (possibly open loop unstable) steady-state values. In particular, we are interested in drawing a control design that: (i) is robust with respect to modeling and measurement uncertainties, and (ii) yields a robust closed-loop behavior with a suitable tuning scheme.

3. CONTROLLER CONSTRUCTION

3.1 State-feedback controller

For the moment, assume the *state* x, the *exogenous input* d, the model function, and the model parameters are known. Enforce the prescribed regulated output error dynamics

$$\dot{e}_c = -k_c e_c, \quad e_c = c - \bar{c} \qquad (4)$$
$$\dot{e}_T = -k_T e_T, \quad e_T = T - \bar{T}$$

combine (4) with (1), and obtain the SF static controller

$$\theta = [-k_c(c - \bar{c}) + \rho(c, T, p)]/[c_e - c] \qquad (5)$$
$$T_j = T + [-k_T(T - \bar{T}) - \beta\rho(c, T, p) - \theta(T_e - T)]/\upsilon$$

which is passive because it is underlain by a model (1) with relative degree pair $(1, 1)$, and without zero-dynamics.

3.2 Output feedback controller

Given that the temperature pair (T, T_e) is measured, the feed concentration (c_e) is nearly constant about its nominal value, and the thermodynamic-transfer parameter pair (β, υ) is reasonably known [in fact, υ can be on-line estimated, as part of the temperature secondary control design (Gonzalez and Alvarez, 2005)], the implementation of the nonlinear SF controller (5) needs an estimate $\hat{c}$ of the reactor concentration and the reaction rate function $\rho(c, T, p)$. To avoid the need of $\rho(c, T, p)$, let us assume that the reaction rate is in slowly changing regime with respect to the underlying estimation error dynamics, meaning that the time derivative $\dot{r}(t) \approx 0$ of the reactor rate function $\rho(c(t), T(t), p(t)) = r(t)$ is approximately zero (Alvarez-Ramirez, et al., 2002). Combine this assumption with the dynamic heat balance to obtain the estimation model, write the corresponding calorimetric estimator (Alvarez-Ramirez, et al., 2002; Gonzalez and Alvarez, 2005) (6), incorporate the mass balance with $\rho(c, T, p)$ replaced by its estimate $\hat{r}$, and obtain the estimator

$$\dot{\hat{T}} = \beta\hat{r} + \theta(\hat{T}_e - \hat{T}) - \upsilon(\hat{T} - T_j) + 2\zeta_T\omega_T(y - \hat{T})$$
$$\dot{\hat{r}} = (\omega_T^2/\beta)(y - \hat{T}) \qquad (6)$$
$$\dot{\hat{c}} = -\hat{r} + \theta(c_e - \hat{c}), \quad \hat{c}(0) = \hat{c}_0 \qquad (7)$$

that yields exponentially convergent estimates, with adjustable (or fixed) rate ω_T/ζ_T (or $\sim \theta$) for the reaction rate (or concentration) (Flores, et al., 2005; Gonzalez and Alvarez, 2005)

$$\hat{r} \overset{\omega_T/\zeta_T}{\longrightarrow} r, \quad \hat{c}(t) \overset{\sim\theta}{\longrightarrow} c(t)$$

The nonlinear SF controller (5) with the preceding estimator yields the output-feedback (OF) dynamic controller

$$\dot{\hat{c}} = -\hat{r} + \theta(\hat{c}_e - \hat{c}) \qquad (8)$$
$$\dot{\hat{T}} = \beta\hat{r} + \theta(\hat{T}_e - \hat{T}) - \upsilon(\hat{T} - T_j) + 2\zeta_T\omega_T(y - \hat{T}) \qquad (9)$$
$$\dot{\hat{r}} = (\omega_T^2/\beta)(y - \hat{T}) \qquad (10)$$
$$T_j = \hat{T} + [-k_T(\hat{T} - \bar{T}) - \beta\hat{r} - \theta(\hat{T}_e - \hat{T})]/\upsilon \qquad (11)$$
$$\theta = [-k_c(\hat{c} - \bar{c}) + \hat{r}]/(\hat{c}_e - \hat{c}) \qquad (12)$$

This controller has been employed to track an optimal transition between two open-loop steady-states, in a reactor of class (1) with monotonic reaction rate (Flores, et al., 2005). It must be pointed out that: (i) the implementation of the preceding output-feedback controller does not need the reaction rate function $\rho(c, T, p)$, (ii) the temperature controller (9,10,11) is linear and can be realized as the combination of a linear PI controller with a filter (Gonzalez and Alvarez, 2005), and (iii) the concentration controller is basically a material balance-based ratio control component that sets θ proportionally to $\hat{r}$ (Gonzalez and Alvarez, 2005).

3.3 Redesigned output-feedback controller

The preceding controller has been designed within a local dynamical framework assuming that the closed-loop reactor operates in a sufficiently small neighborhood of the open-loop unstable and partially observable prescribed steady-state. Accordingly, the concentration estimator component (7) has been designed without measurement injection because the temperature measurement does not contains meaningful information. However, from a nonlocal design perspective two considerations must be made: (i) due to typical state and/or exogenous load disturbances, the reactor state may find itself away from a small neighborhood of the steady-state, and (ii) in such case the onset of the complete observability feature offers the possibility of improving the concentration estimator behavior via temperature measurement injection. Thus, the corresponding nonlocal control redesign problem amounts to redesigning the concentration estimation to exploit the far-from equilibrium innovation capability. In principle, two estimator approaches can be employed to perform the joint reaction rate-concentration estimation task: (i) the Luenberguer-like geometric estimator (GE) (Alvarez, 2000), and (ii) the extended Kalman filter (EKF) (Jazwinski, 1970)(Gelb, et al., 1974).

The GE approach is discarded because its observability matrix is singular or equivalently its gain is infinite in the curve Ω (2) (where $\rho_c = 0$) where the nominal steady-state is, and the EKF is disregarded because its observability index equal to two is against the robustness specification of the control design. Instead, a constructive-like hybrid GE-EKF concentration estimation approach will be pursued according to the following rationale: (i) retain the passive-like reaction rate estimation structure (6), and (ii) in a way that is analogous to the design of robust nonlinear controllers via passivation by backstepping using a virtual control to overcome the high relative (say two) obstacle (Krstic, 1995), regard the (quick) reaction rate estimate $\hat{r}$ (10) as a virtual measurement for the concentration dynamics, according to the expressions

$$\dot{\hat{c}} = -\hat{r} + \theta(\hat{c}_e - \hat{c}) \qquad \hat{r} = \rho(\hat{c}, \hat{T}, \hat{p})$$

The corresponding passivated EKF is given by

$$\begin{aligned} \dot{\hat{c}} &= -\hat{r} + \theta(\hat{c}_e - \hat{c}) + g(\hat{c}, \hat{T}, \hat{p}) \left[\hat{r} - \rho(\hat{c}, \hat{T}, \hat{p})\right] \\ \dot{s} &= -2\theta s + \nu - \rho_c^2(\hat{c}, \hat{T}, \hat{p}) s^2, \quad s(0) = s_0 \qquad (13) \\ s &= \sigma / q_r, \quad g(\hat{c}, \hat{T}, \hat{p}) = s\rho_c(\hat{c}, \hat{T}, \hat{p}), \quad \nu = q_c / q_r \end{aligned}$$

where q_c (or q_r) is the model (or measurement) noise intensity, σ is the concentration error covariance, and g is the estimator gain. The variable s and the intensity noise quotient ν have been introduced to have ν as the single tuning parameter. It must be pointed out that the gain g vanishes at the curve Ω ($\rho_c = 0$) and is positive (or negative) in the iso(or anti)tonic branch of the reaction rate, where $\rho_c > (or <) 0$, this is,

$$\begin{aligned} g(c^*, \hat{T}, \hat{p}) = 0, \quad g(c < c^*, \hat{T}, \hat{p}) < 0 \\ g(c > c^*, \hat{T}, \hat{p}) > 0, \quad c^* = \kappa(T, p) \end{aligned}$$

These vanishing-gain switching properties ensure the estimator nonlocal convergence, and imply that, as expected, the estimator injection ceases as the reactor approaches the curve Ω that lacks instantaneous nonlinear and local (linear) observability or, equivalently, the estimator behaves in open-loop regime.

Recall the OF controller (8) replace its open-loop estimator by the passivated EKF (13), and obtain the redesigned OF controller:

$$\begin{aligned} \dot{\hat{T}} &= \beta\hat{r} + \hat{\theta}(\hat{T}_e - \hat{T}) - \upsilon(\hat{T} - \hat{T}_j) + 2\zeta_T\omega_T(y - \hat{T}) \\ \dot{\hat{r}} &= (\omega_T^2/\beta)(y - \hat{T}) \\ \dot{\hat{c}} &= -\hat{r} + \hat{\theta}(\hat{c}_e - \hat{c}) + s\rho_c(\hat{c}, \hat{T}, \hat{p}) \left[\hat{r} - \rho(\hat{c}, \hat{T}, \hat{p})\right] \\ \dot{s} &= -2\hat{\theta}s + \nu - \rho_c^2(\hat{c}, \hat{T}, \hat{p}) s^2 \\ \hat{T}_j &= \hat{T} + [-k_T(\hat{T} - \bar{T}) - \beta\hat{r} - \hat{\theta}(\hat{T}_e - \hat{T})]/\upsilon \\ \hat{\theta} &= [-k_c(\hat{c} - \bar{c}) + \hat{r}]/(\hat{c}_e - \hat{c}) \qquad (14) \end{aligned}$$

4. CLOSED LOOP STABILITY AND TUNING

The application of the EKF output feedback controller (14) to the reactor yields the closed-loop dynamics(k_c and k_T and have been defined in (4), and $A_{T,r}$,q_{ϵ_h},q_σ,q_{ϵ_c},q_T,q_c,λ_c are defined on Appendix A):

$$\begin{aligned} \dot{\epsilon}_h =& A_{T,r}\epsilon_h + \\ & q_{\epsilon_h}\left(c, T, r, c_e, T_e, k_c, k_T; e_T, e_c, \epsilon_c, \tilde{c}_e, \tilde{T}_e\right) \qquad (15) \\ \dot{s} =& -2\theta s + q_\sigma(c, T, \nu, s;\ \epsilon_c) \qquad (16) \\ \dot{\epsilon_c} =& -\lambda_c\tilde{c} + q_{\epsilon_c}(c, T, r, c_e, k_c, \nu; \epsilon_h, \epsilon_c, e_c, \tilde{p}, \tilde{c}_e) \qquad (17) \\ \dot{e}_T =& -k_T e_T + q_T\left(k_c, k_T; \epsilon_h, \epsilon_c, \tilde{p}, \tilde{c}_e, \tilde{T}_e\right) \qquad (18) \\ \dot{e}_c =& -k_c e_c + q_c\left(k_c, k_T; \epsilon_h, \epsilon_c, \tilde{p}, \tilde{c}_e, \tilde{T}_e\right) \qquad (19) \end{aligned}$$

where $\epsilon_h = (\tilde{T}, \tilde{r})$, $\tilde{T} = \hat{T} - T$, $\tilde{r} = \hat{r} - r$, $e_c = c - \bar{c}$, $e_T = T - \bar{T}$, $\epsilon_c = \tilde{c} = \hat{c} - c$.

the perturbation terms vanish as follows:

$$\begin{aligned} q_{\epsilon_h}(c, T, r, c_e, T_e, k_c, k_T; 0, 0, 0, 0, 0) &= 0 \\ q_{\epsilon_c}(c, T, r, c_e, k_c, \nu; 0, 0, 0, 0, 0) &= 0 \\ q_T(k_c, k_T; 0, 0, 0, 0, 0) &= 0 \\ q_c(k_c, k_T; 0, 0, 0, 0, 0) &= 0 \\ q_\sigma(c, T, \nu, s; 0) &= 0 \end{aligned}$$

Observe that: (i) equation (18,19) with $(q_T, q_c) = 0$ is the closed-loop reactor dynamics with the exact SF controller (5), (ii) equation (15) [or (17)] describes the temperature-reaction rate [or concentration] estimation error dynamics, and (iii) the Riccati equation (16) enters only the concentration estimation error dynamics. From the application of standard results in Input-to-State (IS) stability analysis (Isidori, 1995; Sontag, 2000), the next proposition follows:

Proposition 1. (Proof sketch in Appendix B)

The closed-loop reactor is IS stable if the control (k_c, k_T) and estimator (ν, ω_T) gains ($\zeta_T = 1.5$) are chosen so that the following low and high gain conditions are met:

i) $k_c, k_T > 0$, ii)$\nu^-(k_c) < \nu < \nu^+(k_c^{-1})$

iii)$\omega_T^-(k_c, k_T) < \omega_T < \omega_T^+(k_c^{-1}, k_T^{-1})$

where $\nu^-, \nu^+, \omega_T^-, \omega_T^+$ are monotonic functions of their arguments. ■

Condition i) says that feedback is necessary for closed loop reactor stability. Condition ii) says that the estimation gain ν(or ω_T) need to be chosen within interval $[\nu^-, \nu^+]$(or $[\omega_T^-, \omega_T^+]$), with bounds depending on (k_c, k_T). Observe that the lower (or upper) limits ν^- and ω_T^- (or ν^+ and ω_T^+) depend proportionally (inversely proportionally) on the control gains k_c and k_T. In other words, the stability conditions can be met by choosing the control gains (k_c, k_T) sufficiently small. From the preceding closed-loop stability discussion the next tuning guidelines follow:

1. Set the control gains equal to the nominal dilution rate, this is: $k_c \approx k_T \approx \theta$ and choose the temperature and concentration estimation gains about three times faster, this is, $\omega_T \approx 3k_T$, $\nu \approx [3k_c]^{\frac{1}{2}}$.

2. Increase ω_T and ν until the behavior becomes oscillatory, at gain pair $(\omega_T, \nu)^*$. Back off and set$(\omega_T, \nu) \approx (\omega_T, \nu)^* /3$.

3. Increase k_c and k_T until the response behavior becomes oscillatory at $(k_c, k_T)^*$. Back off and set $(k_c, k_T) \approx (k_c, k_T)^*/3$.

4. If necessary, adjust the estimator gains.

5. APPLICATION EXAMPLE

The application example was built by recalling the non-monotonic kinetic function from a previous catalytic reactor estimation study (López, et al., 2002), with a modification to obtain a case where the unstable steady-state coincided with the point that yielded the maximum reaction rate at a prescribed temperature. The non-monotonic reaction function is given by:

$$\rho(c,T,p) = cke^{-\gamma/T} / \left(1+\sigma c\right)^2, \quad c^* = 1/3$$

The operation conditions are listed in Table 1. There are three steady-states, two stable ones S_I(ignition) and S_E(extinction), and one unstable U. The related phase portrait is presented in Fig. B.1. The control input θ(or T_j) is constrained to take values in [0.1,1.2] (or [300,500]). The application of the tuning guidelines yielded the gains: $\zeta_T = 1.5$, $\omega_T = 16$, $k_c = 3$, $k_T = 3$, and $\nu = 3.7$. The reactor was ran from different initial conditions in growing regions about the nominal steady-state $\bar{x}$ finding that: (i) the controller without saturation stabilized the reactor in a rather ample region of initial states (x_0) about $\bar{x}$ ($T_0 \in [416, 456], c_0 \in [0.1, 0.39]$), (ii) with a more sluggish response, the saturated control stabilized the reactor over a rather large region of initial conditions, (iii) in the cold-reactant deficit region the open-loop (OL) and EKF concentration estimator-based controllers exhibited the same behavior, and (iv) in the hot-reactant surplus region the controller with the EKF outperforms its OL concentration-based counterpart. As expected, the controller with the EKF concentration observer has the (non-local) capability of improving its behavior when the reactor finds itself in the dangerous high temperature region. This situation is illustrated in fig B.2, with initial condition $T_0 = \bar{T} + 6$ and $c_0 = \bar{c} - 0.063$. As it can be seen, both controllers yield the same temperature response, the controller with the OL (or EKF) composition estimator causes the reactor concentration to reach its set point in a 98% setting time in 4 (or 1.25) time units. In other words, in this region the passivated EKF yields a concentration response that is about three times faster than the one of the passive OL (i.e. asymptotic) estimator.

Table 1. Steady states and operation conditions

$k = e^{25}, \gamma = 10e4, \sigma = 3, \theta = 0.989$ $\upsilon = c_e = 1, T_e = T_j = 370, \beta = 200$			
steady states	S_E	U	S_I
concentration [mol/L]	0.991	0.333	0.033
temperature [K]	370.88	436.02	465.25
local condition	stable	unstable	stable

6. CONCLUSIONS

The problem of controlling a continuous reactor with non-monotonic reaction rate, about a (possibly open-loop unstable) steady state with maximum rate and lack of local observability was addressed within a nonlocal constructive design framework. The resulting output-feedback controller was made of passive components: (i) a calorimetric PI temperature controller combined with a linear filter, (ii) a feedforward-like ratio concentration controller driven by the reaction rate estimate, or equivalently, by the integral action of the temperature controller. The unmeasured concentration was regulated via a material balance-based inferential scheme. The lack of local observability and the presence of away-from-equilibrium concentration observability were handled by a passivated concentration EKF driven by the quickly convergent reaction rate estimate acting as a virtual measurement. The closed-loop behavior of a representative case through simulations corroborated the nonlocal robust functioning of the proposed controller.

Appendix A. NONLINEAR MAPS

$$A_{T,r} = \begin{bmatrix} -k_T - 2\zeta_T\omega_T & \beta \\ 0 & -\frac{\omega_T^2}{\beta} \end{bmatrix}, \quad \lambda_c = k_c\left(1+\frac{1}{c_e-c}\right) + \hat{g}\,\mathrm{sec}_{\tilde{c}}^{\rho}$$

$$\mathrm{sec}_c^{\rho} = \frac{\rho\left(c+\tilde{c},T,p\right)-\rho\left(c,T,p\right)}{\tilde{c}}, \quad q_{\epsilon_h} = [q_T, q_r]^T$$

$$q_T = (T-T_e)\left(\hat{\theta}-\theta\right) + \gamma\left(\hat{T}_j - T_j\right)$$

$$q_r = \rho_c(c,T,p)k_c(e_c+\tilde{c}) - \rho_c(c,T,p)q_c(c,T,r,c_e;\tilde{c},\tilde{T},\tilde{r},\tilde{c}_e)$$

$$q_\sigma = \nu + \rho_c(c-\hat{c},T,\hat{p}), \quad q_{e_c} = -\tilde{r} + \left(\hat{\theta}-\theta\right)(\tilde{c}_e - \tilde{c})$$

$$q_{\epsilon_c} = -g(\hat{c},\hat{T},\nu)\left[\rho(\hat{c},\hat{T},p+\tilde{p}) - \rho(\hat{c},T,p)\right] - \tilde{r} - (\tilde{c}_e)\left(\hat{\theta}-\theta\right)$$

$$q_{e_T} = \beta\tilde{r} + \left(\hat{\theta}-\theta\right)\left(\tilde{T}_e - \tilde{T}\right) - \delta\left(\tilde{T}+\tilde{T}_j\right)$$

Appendix B. SKETCH OF THE PROOF OF PROPOSITION 1.

The proof of Proposition 1 follows from the application of two well known results:

Theorem 1. (Sontag, 2000) The system

$$\dot{x} = f(x,u),\ f(0,0) = 0 \qquad \text{(B.1)}$$

is IS stable if: (a) the zero input system $x = f(x,0)$ is zero-stable, and (b) the system with input has an asymptotic gain λ_u^x. ■

Theorem 2. (Small gain) (Isidori, 1995) Consider two IS stable systems (with convergence parameters λ_x and λ_y) $\dot{x} = f(x, y, u)$ λ_x $\dot{y} = g(x, y, u)$ λ_y The interconnection of the systems is IS stable if:

$$(a_x L_y^f /)(a_y L_x^g /) < 1 \quad .\blacksquare$$

where L_y^f denotes the Lipschitz constant of f with respect to y. Further technical details on the application of the theorems can be seen in (Gonzalez and Alvarez, 2005), here we circumscribe ourselves to sketch the proposition proof: (i) Apply Theorem 1 to ensure the stability for each subsystem of the error dynamics (15-17). (ii) Successively apply Theorem 2 to draw the stability condition for the closed-loop reactor dynamics (15-19).■

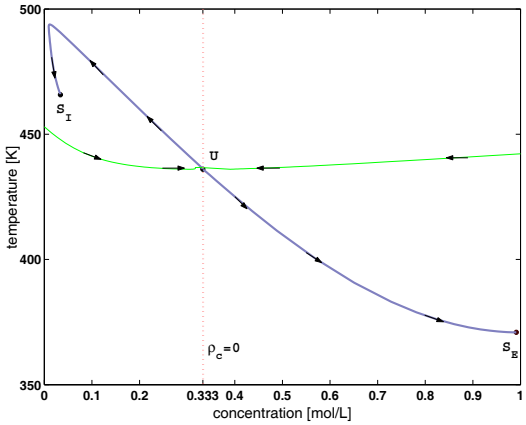

Fig. B.1. Open-loop reactor behavior

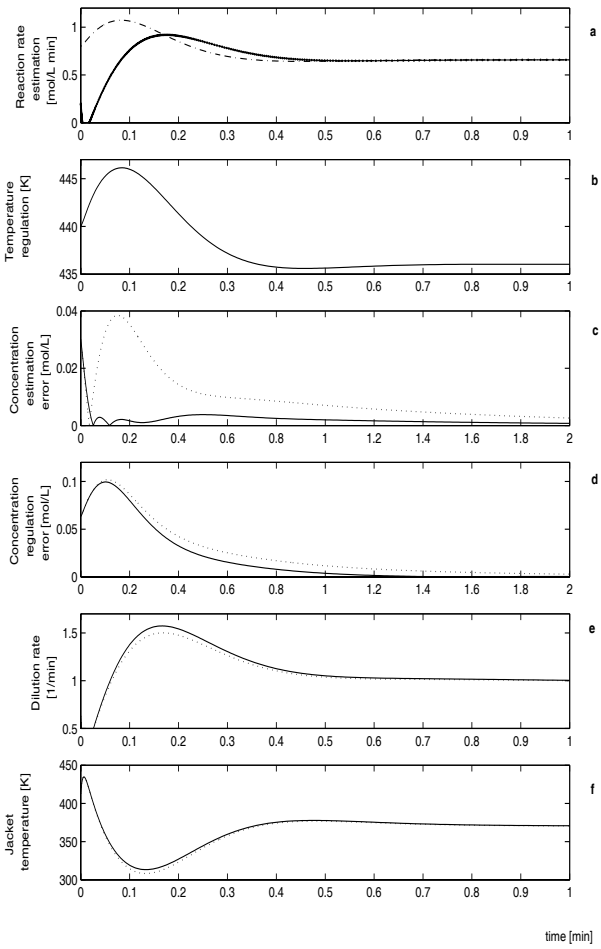

Fig. B.2. (a) Actual (-·) and reaction rate estimators with passive OL (–) and passive EKF (··) concentration estimator. (b) Temperature regulation. (c-f) Closed loop with OL (··) and EKF (–) passive concentration observers

REFERENCES

Alvarez, J., Nonlinear state estimation with robust convergence, *J. of Process Control*, v 10, n 1, p 59-71, 2000.

Alvarez-Ramirez, J., Alvarez, J., Morales, A., An adaptive cascade control for a class of chemical reactors, *I. J. of Adaptive Control and Signal Processing.* 16:681-701, 2002.

Elnashaie, S., Abashar, M., The implication of non-monotonic kinetics on the design of catalytic reactors, *Ch. Eng. Sc.* Vol. 45, No. 9, pp. 2964-2967, 1990.

Flores-Tlacuahuac, A., Alvarez, J., Saldivar-Guerra E., Oaxaca, G., Optimal transition and robust control design for exothermic continuous reactors, *AIChEJ.* Vol. 51, Is. 3, 2005.

Gelb, A., Kasper, J., Nash, R., Price, C., Sutherland, A., *Applied Optimal Estimation.* MIT press cambridge, MA, 1974.

González, P., Alvarez, J., Combined PI-inventory control of solution homopolymerization reactors, *Ind. & Eng. Chem. Res. J.* 2005.

Hermann, R., Krener, A.J., Nonlinear controllability and observability, *Trans. on Aut. Control.* IEEE, p 728-740, 1977.

Isidori, A., *Nonlinear Control Systems.*, Spinger, New York, 1995.

Jazwinski, A.H., *Stochastic Processes and Filtering Theory.* Academic Press, New York, 1970.

Krstic, M., Kanellakopoulos, I., Kokotovic, P., *Nonlinear and Adaptive Control Design.*Wiley, New York, 1995.

Lapidus, L.,Amundson, N. Editors *Chemical Reactor Theory.* Prentice Hall, New jersey, 1977.

Lopez, T., Tronci, S., Baratti, R., Alvarez, J., State estimation in a Catalytic Reactor via a Constructive Approach, *15th Triennial World Congress*, 2002.

Smets, I., Bastin, G., Van Impe, J., Feedback Stabilization of Fed-Batch Bioreactors: Non-Monotonic Growth Kinetics, *Biothecnol. Prog.* 18,p. 1116-1125, 2002.

Sontag, E.D., The ISS Phylosophy as a unifying Framework for Stability-like Behavior, in Nonlinear Control in the year 2000, Vol 2., *Lecture Notes in Control and Information Sciences.* Berlin, 2000.

Zeitz, M., The extended Luenberger observer for nonlinear systems, *Systems & Control Letters.* 9 pp. 149-156, 1987.

ADCHEM 2006

International Symposium on Advanced Control of Chemical Processes
Gramado, Brazil – April 2-5, 2006

ROTARY KILN PRODUCT QUALITY FORECASTING BASED ON FLAME IMAGING

Carl Duchesne [**,1] **André Desbiens** [***,1]
Gerard Szatvanyi [**]

LOOP (Laboratoire d'observation et d'optimisation des procédés - Process observation and optimization laboratory)
[**] *Department of Chemical Engineering*
[***] *Department of Electrical and Computer Engineering*
Université Laval, Pavillon Adrien-Pouliot
Québec City (Québec), Canada G1K 7P4
Email: Carl.Duchesne@gch.ulaval.ca

Abstract: For most applications, the rotary kiln product quality control problem is to apply a certain temperature profile to the solids within the kiln through direct contact with a hot flue gas produced by combustion. Since it is very difficult to measure the solids temperature profile in the kiln, due to the harsh environment and the rotating motion of the shell, quality control is often achieved in practice by controlling the solids discharge temperature close to some target value. The rational behind that is twofold: 1) the solids discharge temperature is often highly correlated to

Keywords: Image analysis, Multivariate quality control, Industrial control, Prediction, Forecasts

1. INTRODUCTION

Rotary kilns are frequently used in the chemical and mineral processing industries since they can accommodate the production of various kinds of products over a wide range of operating conditions. These very versatile process equipments are used for the calcination of lime and coke, the pyrolysis of various kinds of wastes, and for ore roasting and sintering. They are also used to dry a wide variety of products, such as fish and Soya meal, minerals, sawdust, and grain, bark, coal, fertilizer, and other aggregates. Rotary kilns are, however, very complex systems involving simultaneous solid-gas heat and mass transfer coupled to chemical reactions and solids transportation problems. Fundamental modelling of these systems to improve understanding and operational practices is still a very active research area (Finnie *et al.*, 2005).

For most applications, the rotary kiln product quality control problem is to apply a certain temperature profile to the solids within the kiln through direct contact with a hot flue gas produced by combustion. Since it is very difficult to measure the solids temperature profile in the kiln, due to the harsh environment and the rotating motion of the shell, quality control is often achieved in practice by controlling the solids discharge temperature close to some target value. The rational behind that is twofold: 1) the solids discharge temperature is often highly correlated to product quality measured in the laboratory,

[1] Supported by NSERC (Canada).

and 2) this temperature is easier to measure with good accuracy using IR pyrometers, which also provides more frequent measurements than laboratory quality analyses (in the order of seconds instead of a few times per day). The typical quality control strategy is to maintain the solids discharge temperature above a lower limit, below which product quality starts degrading (production loss), and below an upper limit, above which the kiln automatically shuts down for safety reasons. In the latter case, several minutes are required to restart the kiln and also involve production losses. Achieving a solids discharge temperature within these limits is, however, no longer sufficient due to constantly increasing fuel costs and the pressure to reduce CO_2 emissions (e.g. Kyoto agreement) and other combustion pollutants such as CO, NO_x and SO_2. The solution to simultaneously reduce gaseous emissions and fuel consumption while maintaining the desired product quality is to reduce temperature variations as much as possible to bring its target value closer to the lower temperature limit (i.e. reduce overheating).

Reducing discharge temperature variability is difficult since this amount in reducing variations in the heat released by the combustion process. In most rotary kiln applications, turbulent non-premixed combustion is used, which means that combustion and mixing of the fuel and the oxidizer (e.g. air) occur simultaneously, at the burner tip. This type of combustion process is more chaotic and difficult to control than when the fuel and air are premixed and then burned (Yu and MacGregor, 2004). Moreover, the secondary air flow rate is not always measured (but changed using fans), and several rotary kilns are operated using multiple sources of fuel having different heats of combustion.

Implementing feedback controllers on such a rotary kiln to control the discharge temperature using, for example, total fuel flow rate as the manipulated variable is the first step in reducing variability. However, these kilns have long dead-times and slow dynamics and are affected by several sources of unmeasured disturbances, several of them introduced by the combustion process itself. To further reduce discharge temperature (quality) variability ones need to predict the impact of these unmeasured disturbance and to forecast them in the future. This is very difficult to do with the actual instrumentation due to the absence of internal state measurements. The main contribution of this work is to provide one such internal state sensor to forecast product quality using images of the combustion flame taken within the kiln. This new sensor could be used in conjunction with any process control strategy and would fit particularly well into a Model Predictive Control (MPC) framework. It can also be of great help to operators when the kilns are manually controlled, as is often the case in industry.

Flame imaging has already been investigated in the past, but most of these contributions were performed on laboratory scale combustion systems and premixed flames, and their approach was to compute geometrical and luminous properties of the flame extracted from gray scale images and use them to either classify the flame into arbitrarily defined states (Bertucco *et al.*, 2000; Victor *et al.*, 1991) or to predict various quantities such as flicker rate (Huang *et al.*, 1999), unburnt carbon, CO_2 and NO_x emissions (Shimoda *et al.*, 1990; Lu *et al.*, 1999; Yan *et al.*, 2002) or fuel and air flow rates (Tao and Burkhardt, 1995). Only a few past investigations were extracting the flame features from RGB color images (Wang *et al.*, 2002; Keyvan, 2003) and were taking advantage of the three wavelengths to estimate the flame temperature distribution using the bicolor method. Finally, a few research works analyzed the flames using spectrometers (Keyvan, 2003) from which it is possible to extract more precise chemical information about the radicals present in the flame. An additional limitation of these approaches consists of extracting the flame visual features directly from the image space. Since the flame is turbulent, it bounces around continuously and hence, extracting the flame visual characteristics requires finding the location of the flame boundaries for each image. This step increases computation time and might cause difficulties for on-line monitoring of highly turbulent flames. This problem has recently been addressed by Yu and MacGregor (Yu and MacGregor, 2004) who applied the Multivariate Image Analysis (MIA) technique to RGB images of non-premixed turbulent flames from an industrial boiler. This method will be used in this work to build a dynamic model between the flame image and solids discharge temperature.

The rest of this paper is organized as follows: the industrial rotary kiln system is presented in Section 2, as well as the data and flame images collected from it. In Section 3, Multivariate Image Analysis and Regression (MIA and MIR) methods to extract the features of flame images and to regress them against discharge temperature (product quality) are presented. Three approaches for forecasting the product quality are described and compared in Section 4: forecasts based on flame images, on an autoregressive model and finally by combining both preceding techniques with a Kalman filter. Finally, some conclusions are drawn in Section 5.

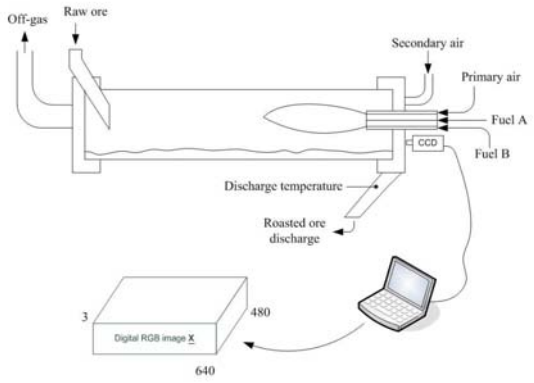

Fig. 1. Rotary kiln and imaging system setup

2. INDUSTRIAL PROCESS AND COLLECTED DATA AND IMAGES

The rotary kiln studied in this work is shown in Figure 1, along with the flame monitoring system. A total of four of these kilns are currently operated by QIT-Fer et Titane inc. (Sorel-Tracy, Qubec, Canada), each of them are about 220 ft long and have a diameter of about 12 ft. The kiln is used to apply a heat treatment to raw ore by a direct contact with a hot gas flowing in countercurrent with the solids. The mean residence time of the solids within the kiln is currently about 80 minutes as determined by the rotational speed and the inclination of the kiln, as well as the solids throughput. A number of thermocouples are inserted through the kiln shell at different locations along the kiln length. However, these are considered unreliable by operators and engineers. They are located in an extremely harsh environment and would require frequent maintenance to ensure reliable readings, which can be performed only during shutdowns since they rotate with the shell. Only the roasted ore (final product) discharge temperature obtained using an IR pyrometer is considered to be a reliable solids temperature measurement. The solids discharge temperature is strongly related to roasted ore quality and is currently used by operators for quality control since laboratory quality measurements are only available every few hours and are obtained from a composite sample of all the kilns. It is the variations in the discharge temperature that will be modeled using flame imaging.

The combustion takes place at the solids discharge end of the kiln. Two types of fuel as well as primary air are fed to the burner tip from three concentric pipes without premixing. The flow rates of primary air and the two fuel types are measured on-line. Fuel A is produced in another part of the plant and both its flow rate and heat of combustion vary. The flow rate of fuel B (supplied to the plant) is adjusted to maintain heat released by the combustion, based on a relationship involving the ratio of standard heat of combustion of each fuel. Finally, secondary air is also blown in the kiln to support complete combustion and to maintain a certain amount of excess oxygen in off-gas for safety considerations. Secondary air flow rate is not currently measured, but changed using fans.

Periods	Date	Number of frames
1	May 2004	2526
2	June-July 2004	6730
3	August 2004	1839
4	November 2004	23134
5	February 2005	46229
	Total:	80458

Table 1. Summary of collected images

The color CCD video camera (JVC TK-C1380) is installed in a small opening just behind the burner. An air-cooling device is used to protect the CCD from damage caused by high temperatures. The output signal of the camera is sent to a portable computer located in the control room, where the frames are digitized using a frame grabber card. Each of the resulting digital image forms a three way array or a "cube" of data consisting of 640 x 480 pixels (spatial dimensions) and, for each of these pixels, the light intensity in the red (R), the green (G), and the blue (B) colors are stored in the third dimension of the cube (i.e. the spectral dimension is 3). The RGB light intensities vary between 0 and 255 with a resolution of 24 bytes.

To develop prediction models for solids discharge temperature (quality), a total of 80458 such images were collected over time at a rate of 1 frame every 10 seconds. Images were intentionally gathered at different periods during year 2004-2005 to capture any seasonal variations and to test the robustness of the prediction models. Table 1 summarizes the five image collection periods.

On-line kiln operation data was also collected and synchronized with the flame images. About 50 measurements currently are available around the kilns. However, the most relevant measurements for this work were solids throughput and discharge temperature, as well as the following combustion related variables: fuel (A and B) and primary air flow rates, fuel ratio and total fuel flow rate, and the shutter position of the secondary air blower.

3. FEATURE EXTRACTION AND REGRESSION BASED ON MIA AND MIR

3.1 Extraction of Flame Image Features using MIA

Prior to developing models between flame images and solids discharge temperature, ones needs to extract the features of flame images in order to formulate the regression problem. It has been shown

by Yu and MacGregor (Yu and MacGregor, 2004) that flame color features can be efficiently extracted using a MIA technique, since it classifies the image pixels according to their spectral characteristics (e.g. combinations of RGB intensities) without considering their spatial position. This means that flames having a similar coloration (i.e. similar heat release) will be projected in a similar region of the MIA low dimensional feature space even if they are located differently in the image. This is a very useful characteristic since the objective of this work is to develop a model between heat released by the flames (i.e. flame color) and product quality rather than tracking the position of highly turbulent flames that bounce around constantly. MIA therefore allows extracting flame information without first locating the flame within the image. This is a major advantage compared to conventional flame image analysis techniques used in previous research working directly in the image space, hence requiring additional computing time.

The MIA technique will be briefly discussed here, but for more details the reader is referred to Geladi and Grahn (Geladi and Grahn, 1996) and to a few of papers (Yu *et al.*, 2003) using this technique for various quality control applications. MIA essentially consists in performing a Multi-Way Principal Component Analysis (MPCA) on a digital multivariate image. This involves two steps. First, the digital image $\underline{\boldsymbol{X}}$ is unfolded from a three-way array to a two-way matrix $\boldsymbol{X}$:

$$\underline{\boldsymbol{X}}_{(\boldsymbol{N_{row}},\boldsymbol{N_{col}},\boldsymbol{N_{spect}})} \overset{unfold}{\longrightarrow} \boldsymbol{X}_{(N_{row}\times N_{col},N_{spect})} \tag{1}$$

where N_{row} and $_{Ncol}$ correspond to the spatial dimensions of the image (640 and 480 in this study), whereas the third dimension or spectral dimension is identified by N_{spect}. Since the images have three spectral channels (R, G, and B), N_{spect} equals 3. This unfolding operation collects the RGB intensities of each pixel row wise in matrix $\boldsymbol{X}$. Second, PCA is performed on the unfolded digital image $\boldsymbol{X}$:

$$\boldsymbol{X} = \sum_{a=1}^{K} \boldsymbol{t_a}\boldsymbol{p_a}^T + \boldsymbol{E} \tag{2}$$

where K is the number of principal components, the $\boldsymbol{t_a}$ vectors are the score vectors, and the corresponding $\boldsymbol{p_a}$ vectors are the loading vectors. For RGB images, the maximum number of components is 3. If $K < 3$, then $\boldsymbol{E}$ contains the residuals of the PCA decomposition. A kernel algorithm is typically used to compute this decomposition since $\boldsymbol{X}$ has a very large number of rows ($N = 640480 = 307200$) and a small number of columns (3). In this algorithm, the loadings vectors ($\boldsymbol{p_a}$) are obtained from a singular value decomposition (SVD) of the very low dimensional kernel matrix $\boldsymbol{X}^T\boldsymbol{X}$ (only 3×3 for an RGB image). The score vectors are then computed using $\boldsymbol{t_a} = \boldsymbol{X}\boldsymbol{p_a}$. The MIA technique as described previously is used for the analysis of a single image. When MIA is to be used for the analysis of a set of J images, then the kernel matrix is calculated as $\sum_{i=1}^{J} \boldsymbol{X_i}^T\boldsymbol{X_i}$ and then SVD is performed on that summation matrix to calculate the loading vectors.

As for the analysis of data matrices using PCA, the interpretation of image features is performed using score plots, and particularly $t_1 - t_2$ score plots since in most MIA applications using RGB images, the first two principal components explain most of the variance (Yu and MacGregor, 2004). However, due to the very large number of score values typically encountered in image analysis (total number of pixels or 307200 for a 640×480 image), the score plots are usually displayed as 2-D density histograms and shown as images themselves to enhance their visual appearance. To obtain such a score histogram, denoted as $\boldsymbol{TT}$, the $t_1 - t_2$ score plots is first divided into a number of bins, usually 256×256, and the pixels falling into each bin are then counted and stored in matrix $\boldsymbol{TT}$ at the corresponding bin location. After selecting a proper color map proportional to the pixel density in each bin, the 2-D score density histogram $\boldsymbol{TT}$ ($256 \times 256 \times 1$) can be displayed as an image. When a set of images are analyzed using MIA, a common scaling range is used for the scores prior to compute the density histograms. This scaling range corresponds to the minimum and maximum values of all t_1 and t_2 score vectors of the set of images.

An alternative way to interpret the image information is to refold the $\boldsymbol{t_a}$ ($N_{row} \times N_{col} \times 1$) score vectors in a three-way array $\boldsymbol{T_a}$ ($N_{row} \times N_{col} \times 1$) according to the same spatial coordinates as in the original image $\underline{\boldsymbol{X}}$ (i.e. pixel locations), and then show each $\boldsymbol{T_a}$ as a univariate image. This is useful to visually identify the information extracted from the original image by each principal component (Yu and MacGregor, 2004).

3.2 Multivariate Image Regressionsubsec:MIR)

The aim of this work is to build a dynamic model between the flame color features extracted from each image and the corresponding solids discharge temperature measurement (i.e. quality variable). This can be accomplished using Multivariate Image Regression (MIR), which refers to a family of techniques used for regressing quality or response variables on image features. Image regression problems can be formulated in several ways, depending on the image feature extraction method. In this study, solids discharge temperature is regressed on the $t_1 - t_2$ score density histograms (i.e. distribution features) obtained from

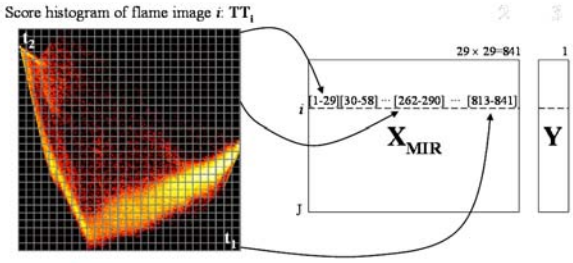

Fig. 2. Multivariate Image Regression (MIR) problem formulation

flame images using MIA (see previous section). However, prior to build regression models, one needs to solve the dimensionality issue arising from the fact that for each score histogram (i.e. a matrix of dimension $N_{bt1} \times N_{bt2}$) correspond a single temperature measurement (i.e. a scalar). Dimensions N_{bt1} and N_{bt2} are the number of bins dividing the score plot along the t_1 and t_2 score axes respectively. This problem was addressed by storing the elements of each score histogram matrix (i.e. number of pixels falling into each bin) row wise in a new matrix $\boldsymbol{X_{MIR}}$ as follows:

$$\begin{aligned} &\boldsymbol{X_{MIR}}(i, 1 : N_{bt1} \times N_{bt2}) = \\ &\quad [\boldsymbol{TT_i}(1, 1 : N_{bt1}) \;\; \boldsymbol{TT_i}(2, 1 : N_{bt1}) \;\; \dots \\ &\quad \dots \;\; \boldsymbol{TT_i}(N_{bt2}, 1 : N_{bt1})] \\ &i = 1, 2, \dots, J \end{aligned} \tag{3}$$

This procedure is schematically shown in Figure 2 for the score histogram of flame image i ($\boldsymbol{TT_i}$) with $N_{bt1} = N_{bt2} = 29$ (i.e. score histogram divided using a grid of 29×29). In this way, the $t_1 - t_2$ score density histogram information obtained for image i is all contained in row i of $\boldsymbol{X_{MIR}}$ whereas the corresponding quality measurement is stored in the i^{th} row of the quality matrix $\boldsymbol{Y}$. Any appropriate regression method can then be used to build a model between $\boldsymbol{X_{MIR}}$ and $\boldsymbol{Y}$, such as Ordinary Least Squares (OLS), Partial Least Squares (PLS), etc. For this regression to be meaningful, however, one must absolutely make sure that a common scaling range has been applied to the $t_1 - t_2$ score density histograms before storing their elements in $\boldsymbol{X_{MIR}}$, and that these elements are always stored in the same order to preserve information congruency.

Finally, dividing score plots using a grid of 256×256 is appropriate for image interpretation and visualization using MIA as discussed in Section 3.1. For image regression purposes, however, such a resolution is often unnecessarily high, and would unduly increase computing time and memory requirements. Most previous work on MIR make use of a 32×32 grid. After some testing, a grid of 29×29 bins was selected for convenience, but no further improvements in the results were obtained by increasing the grid resolution.

Model	A	B	C	D
Forecast (min)	0	+5	+10	+15
$R^2_{X,cum}$ (%)	59.8	59.9	59.9	59.8
$R^2_{Y,cum}$ (%)	79.7	76.4	71.9	68.3
$Q^2_{X,cum}$ (%)	77.8	74.4	69.4	66.0
RMSEP	16.22	17.35	18.20	19.10
Model	E	F	G	H
Forecast (min)	+20	+40	+60	+80
$R^2_{X,cum}$ (%)	52.9	53.3	53.3	53.2
$R^2_{Y,cum}$ (%)	61.8	49.1	37.2	28.3
$Q^2_{X,cum}$ (%)	60.3	47.1	34.8	25.3
RMSEP	20.13	22.82	25.30	27.01

Table 2. Summary statistics for the various dynamic models between flame images and solids discharge temperature

4. PREDICTION RESULTS

A subset of the data discussed in Section 2 was used to build dynamic models between the color features of flame images and solids discharge temperature. After removing outliers, only the data for which no operation disruption (kiln shutdown) occurred within an 80 minutes window from current time was kept for model development. From the 80458 original images, only 53300 satisfied the above criteria and were kept for model building and validation.

The summary statistics for each prediction model are presented in Table reftab:stats. It shows the number of PLS components (A) used for each MIR model determined by cross-validation, three cumulative multiple correlation coefficients ($R^2_{X,cum}$, $R^2_{Y,cum}$, and $Q^2_{X,cum}$), and the root mean square prediction errors (RMSEP). The $R^2_{X,cum}$ statistics correspond to the percentage of the total variance in the image information (X) used to explain Y whereas $R^2_{Y,cum}$ gives the percentage of the total variance of Y explained by the model. The cumulative $Q^2_{X,cum}$ value is the percentage of the total variance of Y that can be predicted by the models using a leave-one-out cross validation procedure. Model A shows a very interesting result which is about 80% of the discharge temperature variations are explained by the flame color features, and hence are related to variations in the combustion process. The remaining 20% may be caused by feed disturbances (i.e. changes in moisture content and solids composition and feed rate) and measurement noise. This confirms that stabilizing the combustion process could significantly reduce temperature variations and therefore shows the importance of monitoring the flame and kiln walls. As the forecast horizon increases from 0 to 80 minutes in the future, the rate of increase in the RMSEP is lower than linear. Predicting discharge temperature $t + 80$ minutes in the future using as the only the image color feature at time t as the only source of information still allow to explain as much as 30% of the variations.

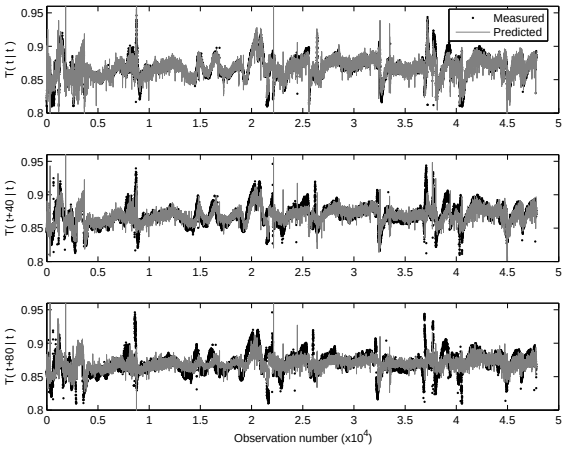

Fig. 3. Measured and predicted discharge temperature at time t, $t + 40$ and $t + 80$ minutes in the future using the flame image collected at time t (model A, F, and H respectively)

Figure 3 shows the prediction performance of models A, F, and H on a validation data set, consisting of 48000 images not used for model building (only 5300 images were used for model development). A very good agreement between the time series, even for model H. .....

5. CONCLUSION

When ran simultaneously, models A-H will provide a temperature forecast from time t to time $t + 80$ minutes, which will be very useful for kiln operators to take appropriate control decisions, when the kiln is manually operated. This set of temperature predictions could also be incorporated into various predictive control schemes when automatic kiln control is preferred. In future work, ways to improve discharge temperature forecasts by adding past images to that one collected at time t will be investigated. This is not trivial since each image contains large amounts of information. Combining the current prediction models with past temperature measurements into an ARMA time series models framework is considered. How to used the image information for combustion control and discharge temperature (quality) control will also be investigated.

REFERENCES

Bertucco, L., A. Fichera, G. Nunnari and A. Pagano (2000). A cellular neural networks approach to flame image analysis for combustion monitoring. In: *Proceedings of the 6th IEEE International Workshop on Cellular Neural Networks and Their Applications*. pp. 455–459.

Finnie, G.J., N.P. Kruyt, M. Ye, C. Zeilstra and J.A.M. Kuipers (2005). Longitudinal and transverse mixing in rotary kilns: A discrete element method approach. *Chemical Engineering Science* **60**, 4083–4091.

Geladi, P. and H. Grahn (1996). *Multivariate Image Analysis*. Wiley. Chichester, UK.

Huang, Y., Y. Yan, G. Lu and A. Reed (1999). On-line flicker measurement of gaseous flames by image processing and spectral analysis. *Meas. Sci. Technol.* **10**, 726–733.

Keyvan, S. (2003). Diagnostics and control of natural gas fired furnaces via flame image analysis. In: *Sensors and Automation FY03 Annual Review Meeting*. Office of Industrial Technologies, Energy Efficiency and Renewable Energy. US Department of Energy.

Lu, G., Y. Yan, Y. Huang and A. Reed (1999). An intelligent vision system for monitoring and control of combustion flames. *Measurement and Control* **32**, 164–168.

Shimoda, M., A. Sugano, T. Kimura, Y. Watanabe and K. Ishiyama (1990). Prediction methods of unburnt carbon for coal fired utility boiler using image processing technique of combustion flame. *IEEE Transactions on Energy Conversion* **5**, 640–645.

Tao, W. and H. Burkhardt (1995). Vision-guided flame control using fuzzy logic and neural networks. *Particle and Particle System Characterisation* **12**, 87–94.

Victor, J., J. Costeira, J. Tomé and J. Sentieiro (1991). A computer vision system for the characterization and classification of flames in glass furnaces. In: *Conference Record of the IEEE Industry Applications Society Annual Meeting*. pp. 1109–1117.

Wang, F., X.J. Wang, Z.Y. Ma, J.H. Yan, Y. Chi, C.Y. Wei, M.J. Ni and K.F. Cen (2002). The research on the estimation for the nox emissive concentration of the pulverized coal by the flame image processing technique. *Fuel* **81**, 2113–2120.

Yan, Y., G. Lu and M. Colechin (2002). Monitoring and characterisation of pulverized coal flames using digital imaging techniques. *Fuel* **81**, 647–656.

Yu, H. and J.F. MacGregor (2004). Monitoring flames in an industrial boiler using multivariate image analysis. *AIChE J.* **50**, 1474–1483.

Yu, H., J.F. MacGregor, G. Haarsma and W. Bourg (2003). Digital imaging for on-line monitoring and control of industrial snack food processes. *Ind. Eng. Chem. Res.* **42**, 3036–3044.

Session 1.2

Advances in Modeling and Identification

ADCHEM 2006

International Symposium on Advanced Control of Chemical Processes
Gramado, Brazil – April 2-5, 2006

A COMBINED APPROACH TO SYSTEM IDENTIFICATION OF A CLASS OF HYBRID SYSTEM

Egbunonu Patrick, **Guay Martin** [1]

Department of Chemical Engineering, Queen's University,
Kingston, Ontario, K7L 3N6 , Canada

Abstract: Hybrid Systems consist of continuous time and/or discrete time processes interfaced with some logical or decision making process. In this paper, a class of hybrid systems - switched linear systems is considered. It is shown that for this class of hybrid systems, it is possible to combine subspace methods with mixed integer programming. While most approaches are based on an input-output framework, we a state space identification approach is advocated. The states of the system are extracted from input-output data using sub-space methods. Once these states are known, the switched system is re-written as a mixed logical dynamical (MLD) system and the model parameters are solved for via mixed integer programming. An example is reported at the end of this paper.

Keywords: Hybrid Systems, System Identification, Subspace Identification, Mixed Integer Programming

1. INTRODUCTION

Most existing methods for system identification make use of an input-output framework where the input signals, $u(t)$ to the system, and the output signals, $y(t)$, from the system are observed data. For linear systems, a set of already established algorithms, are available in literature, with the prediction error method (Ljung, 1999) being very common. In this paper we focus on the development of system identification techniques for hybrid systems. Hybrid systems consist of a family of continuous/discrete-time subsystems and a rule that orchestrates the switching between them. In the particular case where all the individual subsystems are linear, a switched linear system is obtained. Considerable work has been performed in the area of hybrid system iden-

[1] corresponding author. email: guaym@chee.queensu.ca

tification (Trecate *et al.*, 2003; Bemporad *et al.*, 2001; Roll, 2003; Del Vecchio *et al.*, 2003; Vidal *et al.*, 2003; Huang *et al.*, 2004).

While most existing techniques are based on an input-output framework, the approach proposed in this paper advocates a state- space construction. A recent work by Huang *et al.* (2004) also looks at solving this problem using a state space approach. A major difference is that we approach this problem by advocating the combination of two different algorithms. Using a subspace identification technique, the identification problem is formulated in matrix form and the states of the system are then extracted. A basic assumption in this work is that the order of the system has a known upper bound, and the number of discrete states is known a priori. We assume that the states of the system is not known a-priori and focus on showing that for a very simple class of hybrid systems, it is possible to combine subspace methods with mixed integer programming. This paper is structured as follows: In section 2, we consider the class of hybrid system we are dealing with. In section 3, we present the contributions of this work, together with an example. Finally, we draw our conclusions in Section 4.

2. THE CLASS OF HYBRID SYSTEMS

Hybrid Systems are a class of systems that exhibit discrete/logical and continuous dynamics. Hybrid systems are ubiquitous in nature with most research work focusing on modeling and control of such systems. Examples of hybrid systems include the dynamics of a car, elevator, etc. Many chemical processes, which are not inherently hybrid, make use of hybrid controllers. An example can be found in Lennartson *et al.* (1996),where a hybrid controller is designed for a chemical mixing process.

In this paper we consider a special class of hybrid system, switched linear system. These consists of linear (state space) sub-models with a rule that determines which of the sub-models is active at any time t. A general form for the deterministic, discrete time switched linear systems is as follows:

$$x_{t+1} = A(\Upsilon_t)x_t + B(\Upsilon_t)u_t \quad (1)$$
$$y_t = C(\Upsilon_t)x_t + D(\Upsilon_t)u_t \quad (2)$$

where $x_t \in \mathbb{R}^n$, $u_t \in \mathbb{R}^m$ and $y_k \in \mathbb{R}^l$ are the states, inputs and measured outputs of the system respectively. Υ_t, which we refer to as the active mode at time t, assumes its values in the set $\{1, ..., n_s\}$ [2] , so that the system parameters $A(\Upsilon_t) \in \mathbb{R}^{n\times n}$, $B(\Upsilon_t) \in \mathbb{R}^{n\times m}$, $C(\Upsilon_t) \in \mathbb{R}^{l\times n}$ and $D(\Upsilon_t) \in \mathbb{R}^{l\times m}$ switch among n_s different discrete states. The evolution of the discrete state Υ_t is modeled as a polyhedral partition of the hybrid state space (Bemporad and Morari, 1999).

Prior to solving this problem, we make the following assumptions:

Assumption 1. The system to be reformulated can be represented or approximated by the following equations

$$x_{t+1} = A(\Upsilon_t)x_t + Bu_t \quad (3)$$
$$y_t = Cx_t + Du_t \quad (4)$$

Assumption 2. Each of the modes is persistently excited for a long time in the data available.

Assumption 3. Each of the sub-linear system is controllable ,observable, and of the same order n

Assumption 4. The order, n, and the number of discrete states, n_s,of the system is known a priori

Remark 5. Assumptions 1, 3 and 4 are non-trivial as the purpose of this paper is to demonstrate and motivate -using a simple class of hybrid systems- the use of subspace and integer methods. Assumption 2 makes sure that all the modes are excited, enabling the different possible states to be identified. With

[2] $n_s \in \mathbb{R}$ is the number of discrete states in the the hybrid system

Assumption 3, we have that the controllability and observability matrices are full rank.

Remark 6. Comparing these assumptions with other methods; we note that in most of the methods mentioned earlier (Vidal *et al.*, 2003), the assumption is that the number of discrete states is not known. A major difference is that we use a state space framework, and look for a way of combining two algorithms.

The hybrid system deterministic identification problem is therefore as follows:

Problem 7. Given s measurements of the input $u_k \in \mathbb{R}^m$ and the output $y_k \in \mathbb{R}^l$ generated by the unknown deterministic system (3)-(4)of order n, and n_s discrete states, determine:

- The states of the system
- The system matrices $A(\Upsilon) \in \mathbb{R}^{n\times n}$, $B \in \mathbb{R}^{n\times m}$,$C \in \mathbb{R}^{l\times n}$,and $D \in \mathbb{R}^{l\times m}$.

To solve this problem, we first extract the states of the system from input-output data using subspace methods(VanOverschee and Moor, 1996). Once these states are known, the switched system is re-written as a mixed logical dynamical (MLD) system (Bemporad *et al.*, 2001)and the model parameters computed.

3. MATRIX ANALYSIS

In this section, we re-write the system described by (3)-(4) in Matrix form, and show how we can extract the states and the parameters of the system. We conclude this section with a relevant example. Let us define the following parameters:

Definition 8.

$$\begin{aligned}\widehat{\mathbb{A}}_L^K &= A(\Upsilon_{t_L})A(\Upsilon_{t_{L-1}})A(\Upsilon_{t_{L-2}}) \\ &\quad \ldots A(\Upsilon_{t_{K+1}})A(\Upsilon_{t_K}) \qquad (5)\\ \widehat{\mathbb{A}}_K^K &= A(\Upsilon_{t_K}) \\ &= \widehat{\mathbb{A}}^K \qquad (6)\end{aligned}$$

where $\widehat{\mathbb{A}}_L^K \in \mathbb{R}^{n\times n}$.

Using results analogous to VanOverschee and Moor (1996), we define the Hankel Matrix $\overbrace{Y_0^{2i}} \in \mathbb{R}^{2il\times j}$ containing the outputs $y_{t_i} \in \mathbb{R}^l$, as,

$$\overbrace{Y_0^{2i}} := \begin{bmatrix} y_{t_0} & y_{t_1} & y_{t_2} & \cdots & y_{t_{j-1}} \\ y_{t_1} & y_{t_2} & y_{t_3} & \cdots & y_{t_j} \\ \cdots & \cdots & \cdots & \cdots & \cdots \\ y_{t_{i-1}} & y_{t_i} & y_{t_{i+1}} & \cdots & y_{t_{i+j-2}} \\ \cdots & \cdots & \cdots & \cdots & \cdots \\ y_{t_i} & y_{t_{i+1}} & y_{t_{i+2}} & \cdots & y_{t_{i+j-1}} \\ y_{t_{i+1}} & y_{t_{i+2}} & y_{t_{i+3}} & \cdots & y_{t_{i+j}} \\ \cdots & \cdots & \cdots & \cdots & \cdots \\ y_{t_{2i-1}} & y_{t_{2i}} & y_{t_{2i+1}} & \cdots & y_{t_{2i+j-2}} \end{bmatrix} \qquad (7)$$

$$\overbrace{Y_0^{2i}} := \begin{bmatrix} Y_p \\ \cdots \\ Y_f \end{bmatrix} \qquad (8)$$

$Y_p \in \mathbb{R}^{il\times j}$, and $Y_f \in \mathbb{R}^{il\times j}$ are Hankel matrices containing past and future output data respectively. i, l, and k are parameters defined by the user. We also define the *time-dependent 'hybrid observability matrix'*, $\widehat{\mathcal{O}}_w^r \in \mathbb{R}^{l(w-r+1)\times n}$, between times t_w and t_r,(irrespective of whether switching occurs or not) as

$$\widehat{\mathcal{O}}_w^r := \begin{bmatrix} C \\ C\widehat{\mathbb{A}}^r \\ C\widehat{\mathbb{A}}_{r+1}^r \\ \vdots \\ C\widehat{\mathbb{A}}_{w-2}^r \\ C\widehat{\mathbb{A}}_{w-1}^r \end{bmatrix} \qquad (9)$$

w and r are user defined indexes.

Let

$$\mathbf{U}_0 = \begin{bmatrix} u_{t_0} & 0 & 0 & \dots & 0 \\ 0 & u_{t_1} & 0 & \dots & 0 \\ 0 & 0 & u_{t_2} & \dots & 0 \\ \vdots & \vdots & \dots & \ddots & \vdots \\ 0 & 0 & 0 & \dots & u_{t_{j-1}} \\ u_{t_1} & 0 & 0 & \dots & 0 \\ 0 & u_{t_2} & 0 & \dots & 0 \\ 0 & 0 & u_{t_3} & \dots & 0 \\ \vdots & \vdots & \dots & \ddots & \vdots \\ 0 & 0 & 0 & \dots & u_{t_j} \\ \dots & \dots & \dots & \dots & \dots \\ u_{t_{i-1}} & 0 & 0 & \dots & 0 \\ 0 & u_{t_i} & 0 & \dots & 0 \\ 0 & 0 & u_{t_{i+1}} & \dots & 0 \\ \vdots & \vdots & \dots & \ddots & \vdots \\ 0 & 0 & 0 & \dots & u_{t_{i+j-2}} \end{bmatrix} \tag{10}$$

and

$$\mathbf{U}_i = \begin{bmatrix} u_{t_i} & 0 & 0 & \dots & 0 \\ 0 & u_{t_{i+1}} & 0 & \dots & 0 \\ 0 & 0 & u_{t_{i+2}} & \dots & 0 \\ \vdots & \vdots & \dots & \ddots & \vdots \\ 0 & 0 & 0 & \dots & u_{t_{i+j-1}} \\ u_{t_{i+1}} & 0 & 0 & \dots & 0 \\ 0 & u_{t_{i+2}} & 0 & \dots & 0 \\ 0 & 0 & u_{t_{i+3}} & \dots & 0 \\ \vdots & \vdots & \dots & \ddots & \vdots \\ 0 & 0 & 0 & \dots & u_{t_{i+j}} \\ \dots & \dots & \dots & \ddots & \dots \\ u_{t_{2i-1}} & 0 & 0 & \dots & 0 \\ 0 & u_{t_{2i}} & 0 & \dots & 0 \\ 0 & 0 & u_{t_{2i+1}} & \dots & 0 \\ \vdots & \vdots & \dots & \ddots & \vdots \\ 0 & 0 & 0 & \dots & u_{t_{2i+j-2}} \end{bmatrix} \tag{11}$$

and define the matrix

$$\hat{\mathcal{X}}_i = \begin{bmatrix} x_{t_i} & 0 & 0 & \dots & 0 \\ 0 & x_{t_{i+1}} & 0 & \dots & 0 \\ 0 & 0 & x_{t_{i+2}} & \dots & 0 \\ \vdots & \vdots & \ddots & \dots & \vdots \\ 0 & 0 & 0 & 0 & x_{t_{i+j-1}} \end{bmatrix} \in \mathbb{R}^{nj \times j} \tag{12}$$

where $x_{t_i}, x_{t_i+1}, .., x_{t_{i+j-1}}$ are the states and t_i is the first element of the state sequence. Similar to past outputs, we define $\mathcal{X}_p \in \mathbb{R}^{nj \times j}$ (contains the past states $x_{t_0}, x_{t_1}, .., x_{t_{j-1}}$), and $\mathcal{X}_f \in \mathbb{R}^{nj \times j}$ (containing the future state sequence $x_{t_i}, x_{t_i+1}, .., x_{t_{i+j-1}}$) as:$\mathcal{X}_p = \hat{\mathcal{X}}_0, \mathcal{X}_f = \hat{\mathcal{X}}_i$. also $\mathcal{U}_p \in \mathbb{R}^{mj(i-1) \times j}$ and $\mathcal{U}_f \in \mathbb{R}^{mj(i-1) \times j}$ as the matrix of past inputs and future inputs respectively,and

$$\mathcal{U}_p = \mathbf{U}_0 \tag{13}$$
$$\mathcal{U}_f = \mathbf{U}_i \tag{14}$$

The results in this section of the paper can be summarized by the following theorem which shows how the switched linear state space system of (3)-(4) can be reformulated in matrix form.

Proposition 9. If the switched linear system of (3)-(4) satisfies assumptions (1)-(6), the system can be represented by the following Matrix input-output equations(Egbunonu, 2005).

$$Y_p = \Delta_0 \mathcal{X}_p + \mathbf{\Gamma}_0 \mathcal{U}_p \tag{15}$$
$$Y_f = \Delta_i \mathcal{X}_f + \mathbf{\Gamma}_i \mathcal{U}_f \tag{16}$$
$$\mathbb{I}_i \mathcal{X}_f = \mathcal{A} \mathcal{X}_p + \mathfrak{F} \mathcal{U}_p \tag{17}$$

where

$$\Delta_i = \begin{bmatrix} \widehat{\mathcal{O}}^i_{i+k-1} & \widehat{\mathcal{O}}^{i+1}_{i+k} & \widehat{\mathcal{O}}^{i+2}_{i+k+1} & \dots & \widehat{\mathcal{O}}^{i+j-1}_{i+k+j} \end{bmatrix} \in \mathbb{R}^{lk \times nj}$$

and

$$\mathbf{\Gamma}_i = \begin{bmatrix} D & \dots & 0 \\ CB & \dots & 0 \\ C\widehat{\mathbb{A}}^{i+1}B & \dots & 0 \\ \dots & \dots & \dots \\ C\widehat{\mathbb{A}}^{i+1}_{i+k-2}B & \dots & D \end{bmatrix} \tag{18}$$

$$\mathfrak{F} := \begin{bmatrix} \widehat{\mathbb{A}}^1_{i-1}B & \widehat{\mathbb{A}}^i B & \widehat{\mathbb{A}}^{i+1}B & \dots & \widehat{\mathbb{A}}^{i+j-2}B & \dots & B \end{bmatrix}$$

$$\mathbb{I}_i := \begin{bmatrix} I & I & I & \dots & I \end{bmatrix} \tag{19}$$

where $\mathfrak{F} \in \mathbb{R}^{n \times mjk}, \mathbf{\Gamma}_i \in \mathbb{R}^{lk \times mjk}, I \in \mathbb{R}^{n \times n}$ is the identity matrix and $\mathbb{I}_i \in \mathbb{R}^{n \times nj}$

3.1 Extraction of The States of the Hybrid System

Once our system is reformulated into matrix form, using the Theorems from the preceding section, we extract the states of the hybrid system by making use of the following simple technique (VanOverschee and Moor, 1996; Egbunonu, 2005) summarized in the following theorem

Theorem 10. Given (15) to (17) and assuming that the row space of the future inputs and the row space of the past states is empty, we have that(Egbunonu, 2005)

(1) The matrix Δ_i is equal to

$$\Delta_i = L.S_1 \tag{20}$$

(2) The matrix $\mathcal{X}_f$ is equal to

$$\mathcal{X}_f = \Delta_i^{\dagger} W_i \tag{21}$$

(3) The state sequence $\mathbb{X}_f$ is equal to

$$\mathbb{I}_i \mathcal{X}_f \tag{22}$$

$W_i \in \mathbb{R}^{li \times j}$, $L \in \mathbb{R}^{li \times li}$,and $S \in \mathbb{R}^{li \times j}$

3.2 Mixed Logical Dynamical Systems

After extracting the states, we now re-formulate our system of (3)-(4) as a Mixed Logical Dynamical (MLD) systems (Bemporad and Morari, 1999) i.e. we can re-write equation (3)-(4) in MLD form as

$$x(t+1) = \sum_{i=1}^{n_s} z_i(t) \tag{23}$$

where

$$\begin{aligned} z_i(t) &\leq M\delta_i(t) \\ z_i(t) &\geq m\delta_i(t) \\ z_i(t) &\leq A_i x(t) + B_i u(t) - m(1-\delta_i(t)) \\ z_i(t) &\geq A_i x(t) + B_i u(t) - M(1-\delta_i(t)) \end{aligned} \tag{24}$$

$\delta_i(\mathrm{t})$ are $0-1$ variables and the vectors $M = [M_1, \dots, M_n]'$, $m = [m_1, ..., m_n]'$ are defined as

$$M_j \triangleq \max_{i=1,\dots,n_s} \left\{ \max_{[x \quad u]' \in \Im} A_i^j x + B_i^j u \right\} \tag{25}$$

$$m_j \triangleq \min_{i=1,\dots,n_s} \left\{ \max_{[x \quad u]' \in \Im} A_i^j x + B_i^j u \right\} \tag{26}$$

With this formulation, we can now solve for the parameters of the system, using least squares method. The result is a Mixed Integer Programming Problem. One must mention here that this method has a drawback which is its computational complexity. The branch and bound method utilized in solving the problem, increases the computational time and makes the solution algorithm potentially more complex. To aid the algorithm, several bounds and assumptions are introduced.

3.3 Example

In this section we look at an example of a linear hybrid system and how we can use the Matrix Form of the system to extract the states of the system.

Example 11. Consider the discrete switched linear systems shown below:

$$x(t+1) = A_{n_a} x + \begin{bmatrix} 0.4 \\ 0.2 \end{bmatrix} u \tag{27}$$

$$y = \begin{bmatrix} -2 & 1 \end{bmatrix} x + 5u \tag{28}$$

where $x \in \mathbb{R}^2$, $u \in \mathbb{R}$, $y \in \mathbb{R}$, $A \in \mathbb{R}^{2\times 2}$ $n_a = \{1, 2\}$, and

$$A_1 = \begin{bmatrix} -0.3 & -0.2 \\ -0.1 & 0.5 \end{bmatrix} \text{ if } K_1 x + J_1 u \leq T_1 \tag{29}$$

$$A_2 = \begin{bmatrix} -0.5 & -0.4 \\ -0.1 & 0.3 \end{bmatrix} \text{ if } K_2 x + J_2 u \leq T_2 \tag{30}$$

$K_1 = \begin{bmatrix} 0.2 & 0.3 \end{bmatrix}$; $K_2 = \begin{bmatrix} -0.2 & -0.3 \end{bmatrix}$;$J_1 = 5$;$J_2 = -5$, $T_1 = 0.8$, $T_2 = -0.8$

Using the methods described in the previous sections, coupled with the aforementioned assumptions, we are able to extract the states of the system, and generate a set of parameters describing the system. (Results were generated by using the TOMLAB/Xpress software to solve the mixed integer problem). Figure 1 shows a validation graph of the outputs generated by the actual and predicted system, with mean error value of -0.006.

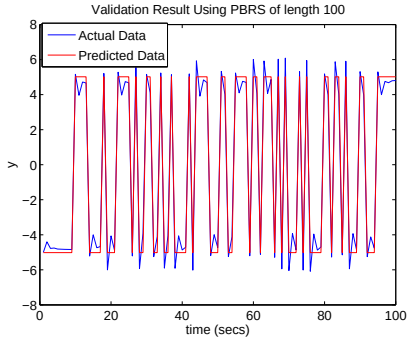

Fig. 1. Validation of Predicted Switched Linear System (2)

4. CONCLUSIONS

In this paper, we have proposed a combined subspace and mixed integer methods for identification of a set of switched linear systems. We made use of a state space modeling framework, and assumed that the order of our system and the number of discrete states where known. We also assumed a deterministic model. Open issues includes the performance of the algorithm in the presence of noise and/or disturbances. Also, a possible extension of the algorithm would be to cases where the order of the system and perhaps the number of discrete states are unknown. A positive note is that since we are dealing with a state space model, the availability of tested algorithm for analysis and control of linear systems makes this option very applicable and use-able.

REFERENCES

Bemporad, A. and M. Morari (1999). Control of systems integrating logic, dynamics, and constraints. **35**(3), 407–427.

Bemporad, Alberto, Jacob Roll and L. Ljung (2001). Identification of hybrid systems via mixed-integer programming. Proceedings of the IEEE Conference on Decision and Control, Orlando, Florida, USA, pp. 786-792.

Del Vecchio, Domitila., Richard M. Murray and P. Perona (2003). Decomposition of human motion into dynamcs based primitives with application to drawing tasks. **39**(12), 2085–2098.

Egbunonu, P. (2005). Identification of hybrid systems using subspace and integer methods. MSc. Thesis, Queen's University.

Huang, K., A. Wagner and Y. Ma (2004). Identification of hybrid linear time-invariant systems via subspace embedding and segmentation. *In Proc. 43st IEEE Conf. on Decision and Control* **3**, 3227–3234.

Lennartson, B., M. Tittus, B. Egardt and S. Pettersson (1996). Hybrid systems in process control. Control Systems Magazine, IEEE, Volume: 16 Issue: 5. 45-56.

Ljung, Lennart (1999). *System Identification-Theory For The User*. Prentice Hall. Upper Saddle River, New Jersey.

Roll, Jacob (2003). Local and piecewise affine approaches to system identification. Ph.D. Thesis, Linköping University, Sweden.

Trecate, G.F., M. Muselli, D. Liberati and M. Morari (2003). Identification of piecewise affine and hybrid systems. **39**(2), 205–217.

VanOverschee, P. and B. De Moor (1996). *Subspace Identification for Linear Systems Theory, Implementation, Applications*. Kluwer Academic Publishers. London.

Vidal, Rene., Y. Soatto, Y. Ma and S. Sastry (2003). An algebraic gemetric approach to the identification of a class of hybrid systems. Proceedings of the IEEE Conference on Decision and Control.

ADCHEM 2006

International Symposium on Advanced Control of Chemical Processes
Gramado, Brazil – April 2-5, 2006

PARAMETER AND DELAY ESTIMATION OF CONTINUOUS-TIME MODELS FROM IRREGULARLY SAMPLED OUTPUT

Salim Ahmed [*] **, Biao Huang** [*,1] **and Sirish L. Shah** [*]

[*] *Department of Chemical and Materials Engineering*
University of Alberta, Edmonton, AB, Canada T6G 2G6

Abstract: Linear filter approach might be the most commonly used method for continuous-time identification. Recently we have proposed a new linear filter method for simultaneous estimation of time delay and other parameters of continuous-time models in (Ahmed *et al.*, 2006). The proposed method involves choice of filter parameters and the filter structure is restricted to all real pole form. In this paper, the linear filter method is presented for a general structure of the filter. Also the filter parameters are updated iteratively. Next, an algorithm is prescribed to make this method applicable when the output is sampled irregularly. To demonstrate the performance of the proposed algorithm, results from a simulation example as well as an experimental example are presented.

Keywords: Linear filter, time delay, irregular data.

1. INTRODUCTION

Time delay estimation is an important part of system identification. In process control, it is even more important to consider time delay because of the common occurrence of the delay and its significant bearings on the achievable performance of control systems. However, both in continuous-time(CT) and discrete-time(DT) identification, the development of time delay estimation methods lags behind the advancement of the estimation techniques for other model parameters. For example, linear filter methods are commonly used for CT model parameter estimation and a significant development have taken place over the last few decades, see e.g. (Fairman, 1971; Garnier *et al.*, 2003; Saha and Rao, 1983; Wang and Gawthrop, 2001; Young, 2002). In linear filter approach, the most commonly used algorithm to estimate the time delay is based on a comprehensive search routine as used in (Rao and Sivakumar, 1976; Saha and Rao, 1983; Young, 2002) where process parameters are estimated for a set of time delays within a certain range and a predefined cost function is calculated for every set of estimated parameters. Finally the delay that gives the optimum value of the cost function is chosen. This procedure is computationally expensive specially for rapidly sampled data. Other popular approaches are approximation of the delay by a rational transfer function such as the Padé approximation as in Agarwal and Canudas (1987) and the Laguerre expansion or by a polynomial approximation. Such approaches require estimation of more parameters and an unacceptable approximation error may occur for systems having large delay (Wang and Zhang, 2001). Most of the methods to directly estimate the delay along with other model parameters are based on step response data see e.g. (Wang and Zhang, 2001; Ingimundarson and Hagglund, 2001). It is well recognized that a step input may not provide a sufficient excitation.

An important issue related to many of the time

[1] author to whom all correspondence should be addressed.
E-mail: biao.huang@ualberta.ca, Tel: 1-780-492-9016

delay estimation methods is that the delay is expressed in terms of number of sampling interval. The problem arises when the sampling interval is not constant. For such a case, the time delay becomes time varying and most of the methods fail to estimate such a parameter.

A more general problem that prevents many identification algorithms to be applicable in real industrial processes is the irregularity in data. By irregular data we refer to a data set that contains measurements of all variables at some time instants, but at others, measurements of only some variables are available. The unavailable elements are often termed as missing data. In chemical processes, data can be missing for two basic reasons: failures in the measurement devices and errors in data management. Sometimes data may be missing because of the strategy of sampling. For example, from a time and cost consideration, concentrations are less frequently measured than temperatures and pressures. For such multi-rate data the intermediate values of the slow sampled variables may be considered as missing. In some cases, where it requires time consuming lab analysis, frequency of measurements may be irregular (Imtiaz *et al.*, 2004).

In this paper, the linear filter method proposed in (Ahmed *et al.*, 2006) is presented for a more general filter structure. Also in this approach the filter parameters are updated iteratively within the iteration steps for time delay estimation. Thus it does not need any additional step in the algorithm and the user needs to specify only the initial values of the filter parameters. The final estimates of the process parameters are found to have little or no effect on the initial choice of filter parameters. For identification from irregular data we prescribe a procedure based on the idea of iterative prediction.

2. THE LINEAR FILTER METHOD

Let us consider a linear single input single output (SISO) system with time delay described by

$$\mathbf{a}_n \mathbf{y}^{(n)}(t) = \mathbf{b}_m \mathbf{u}^{(m)}(t-\delta) + e(t) \qquad (1)$$

where,

$$\mathbf{a}_n = [a_n \; a_{n-1} \cdots a_0] \in \mathbb{R}^{1\times(n+1)}$$
$$\mathbf{b}_m = [b_m \; b_{m-1} \cdots b_0] \in \mathbb{R}^{1\times(m+1)}$$
$$\mathbf{y}^{(n)}(t) = \left[y^{(n)}(t) \; y^{(n-1)}(t) \cdots y^{(0)}(t)\right]^T$$
$$\mathbf{u}^{(m)}(t-\delta) = \left[u^{(m)}(t-\delta) \cdots u^{(0)}(t-\delta)\right]^T$$

$y^{(i)}$ and $u^{(i)}$ are i^{th} order time derivatives of y and u and $e(t)$ is the error term. Taking Laplace transformation on both sides of eqn(1), considering that both input and output are initially at rest, we can write

$$\mathbf{a}_n \mathbf{s}^n Y(s) = \mathbf{b}_m \mathbf{s}^m U(s) e^{-\delta s} + E(s) \qquad (2)$$

$Y(s)$, $U(s)$ and $E(s)$ are the Laplace transforms of $y(t)$, $u(t)$ and $e(t)$, respectively, and

$$\mathbf{s}^n = \left[s^n \; s^{n-1} \cdots s^0\right]^T \in \mathbb{R}^{(n+1)\times 1} \qquad (3)$$

Now, consider a causal filter described in Laplace domain as $F(s)$. If we apply the filtering operation on both sides of eqn(2) we end up with the formulation

$$\mathbf{a}_n \mathbf{s}^n F(s) Y(s) = \mathbf{b}_m \mathbf{s}^m F(s) U(s) e^{-\delta s} + F(s) E(s) \qquad (4)$$

To estimate the time delay along with other parameters, in (Ahmed *et al.*, 2006) a filter of the form $F(s) = \frac{\beta^n}{s(s+\lambda)^n}$ is proposed where the parameters λ and β are to be specified by the user. Here, we propose a filter having a first order integral dynamics along with a lag dynamics which is the denominator of the process transfer function i.e.

$$F(s) = \frac{1}{sA(s)} \qquad (5)$$

where, $A(s) = \mathbf{a}_n \mathbf{s}^n$ is the denominator of the process transfer function. The objective of using such a filter structure is to have the delay, δ, as an element of the parameter vector. The integrator generates an integration term of delayed input. This integrated delayed input signal, which represent a certain area under the input curve, can be expressed by subtracting two sub-areas from the integrated input signal. By doing so, δ becomes an explicit parameter in the estimation equation. To describe the necessary mathematical formulation let us define $\underline{Y}(s)$ as

$$\underline{Y}(s) = \frac{Y(s)}{A(s)} \qquad (6)$$

By defining $\underline{U}(s)$ in the same way as $\underline{Y}(s)$ is defined in eqn(6), we can express eqn(4) as

$$\mathbf{a}_n \mathbf{s}_+^{n-1} \underline{Y}(s) = \mathbf{b}_m \mathbf{s}_+^{m-1} \underline{U}(s) e^{-\delta s} + \xi(s) \qquad (7)$$

where, the subscript $(\bullet_+)$ means that the $\mathbf{s}^{n-1}$ vector has been augmented by $\frac{1}{s}$, i.e.,

$$\mathbf{s}_+^{n-1} = \left[s^{n-1} \; s^{n-2} \cdots s^0 \; \frac{1}{s}\right] \qquad (8)$$

Now using partial fraction expansion the transfer function of the filter, $1/sA(s)$, can be expressed as

$$\frac{1}{sA(s)} = \frac{C(s)}{A(s)} + \frac{1}{s} \qquad (9)$$

where, $C(s) = -(a_n s^{n-1} + a_{n-1} s^{n-2} + \cdots + a_1)$. Eqn(9) can be used to represent the filtered input as

$$\begin{aligned} U_F(s) &= \frac{C(s)}{A(s)} U(s) + \frac{1}{s} U(s) \\ &= C(s)\underline{U}(s) + U_I(s) \end{aligned} \qquad (10)$$

Applying eqn(9) and (10), we can restructure eqn(7) to give a standard least-square form

$$\underline{Y}_I(s) = -\bar{\mathbf{a}}_n \mathbf{s}^{n-1}\underline{Y}(s) + \bar{\mathbf{b}}_m \mathbf{s}^{m-1}\underline{U}(s)e^{-\delta s} + b_0\left[C(s)\underline{U}(s) + U_I(s)\right]e^{-\delta s} + \xi(s) \quad (11)$$

where,
$\bar{\mathbf{a}}_n$: $\mathbf{a}_n$ with its last column removed, $\bar{\mathbf{a}}_n \in \mathbb{R}^{1\times n}$
$\bar{\mathbf{b}}_m$: $\mathbf{b}_m$ with its last column removed,$\bar{\mathbf{b}}_m \in \mathbb{R}^{1\times m}$

Taking inverse Laplace Transform, we get the time domain expression for any time $t = t_k$

$$\underline{y}_I(t_k) = -\bar{\mathbf{a}}_n \underline{\mathbf{y}}^{n-1}(t_k) + \bar{\mathbf{b}}_m \underline{\mathbf{u}}^{m-1}(t_k - \delta) + b_0\left[\underline{u}_c(t_k - \delta) + u_I(t_k - \delta)\right] + \zeta(t_k) \quad (12)$$

with

$$\underline{y}_I(t_k) = L^{-1}\left[\frac{\underline{Y}(s)}{s}\right]$$
$$\underline{u}_c(t_k - \delta) = L^{-1}\left[C(s)\underline{U}(s)e^{-\delta s}\right]$$
$$u_I(t_k - \delta) = L^{-1}\left[\frac{1}{s}U(s)e^{-\delta s}\right]$$

At any time $t = t_k$, the integrated input and the integrated delayed input can be expressed as

$$u_I(t_k) = \int_0^{t_k} u(t)dt \quad (13)$$

$$u_I(t_k - \delta) = \int_0^{t_k} u(t)dt - \int_{t_k-\delta}^{t_k}[u(t) - u(t_k)]dt - u(t_k)\delta \quad (14)$$

Applying eqn(14) in eqn(12)and rearranging it to give a standard least square form we get

$$\underline{y}_I(t_k) = -\bar{\mathbf{a}}_n \mathbf{y}^{n-1}(t_k) + \mathbf{b}_m \underline{\mathbf{u}}_+^{m-1}(t_k - \delta) + b_0 u(t_k)\delta + \zeta(t_k) \quad (15)$$

where,

$$\underline{\mathbf{u}}_+^{m-1}(t_k - \delta) = \begin{bmatrix} \underline{u}^{m-1}(t_k - \delta) \\ \cdots \\ \underline{u}(t_k - \delta) \\ u_+(t_k - \delta) \end{bmatrix}$$

$$u_+(t_k - \delta) = \underline{u}_c(t_k - \delta) + u_I(t_k) - \int_{t_k-\delta}^{t_k}[u(t) - u(t_k)]dt$$

Or equivalently

$$\gamma(t_k) = \phi^T(t_k)\theta + \zeta(t_k) \quad (16)$$

where,

$$\gamma(t_k) = \underline{y}_I(t_k)$$
$$\phi(t_k) = \begin{bmatrix} -\underline{\mathbf{y}}^{n-1}(t_k) \\ \underline{\mathbf{u}}_+^{m-1}(t_k - \delta) \\ u(t_k) \end{bmatrix}$$
$$\theta = [\bar{\mathbf{a}}_n \;\; \mathbf{b}^m \;\; b_0\delta]^T$$

Eqn(16) can be written for $t_k = t_{d+1}, t_{d+2}\cdots t_N$ where $t_d \le \delta < t_d + 1$ and be combined to give

$$\mathbf{\Gamma} = \mathbf{\Phi}\theta + \zeta \quad (17)$$

From θ we can directly get $\bar{\mathbf{a}}_n$ and $\mathbf{b}_m$. δ is obtained as $\delta = \theta(n+m+2)/\theta(n+m+1)$. But to estimate θ solving eqn(17), we need to know $A(s)$ and δ, which are of course unknowns. This problem can be solved by applying an iterative procedure that adaptively adjust an initial choice of $A(s)$ and δ until they converge. The least-square estimate of θ that minimizes the sum of the squared errors is given by

$$\hat{\theta}^{LS} = \left[\mathbf{\Phi}^T\mathbf{\Phi}\right]^{-1}\Phi^T\mathbf{\Gamma} \quad (18)$$

However, the least-square solution does not give unbiased estimate in the presence of general forms of measurement noise such as colored noise. A popular bias elimination procedure is to use the instrumental variable (IV) method. A bootstrap estimation of IV type where the instrumental variable is built from an auxiliary model (Young, 1970) is considered here. The instrumental variable is defined as

$$\psi(t_k) = \begin{bmatrix} -\hat{\underline{\mathbf{x}}}^{n-1}(t_k) \\ \underline{\mathbf{u}}_+^{m-1}(t_k - \delta) \\ u(t_k) \end{bmatrix} \quad (19)$$

where $\hat{x}(t) = \hat{G}(p, \hat{\theta}^{LS})u(t-\delta)$ and $\hat{G}(p, \hat{\theta}^{LS})$ is the process model estimated from least-square solution. The IV-based bias-eliminated parameters are given by

$$\hat{\theta}^{IV} = \left[\mathbf{\Psi}^T\mathbf{\Phi}\right]^{-1}\mathbf{\Psi}^T\mathbf{\Gamma} \quad (20)$$

The IV estimate can also be calculated in a recursive or recursive/iterative manner. The iterative iteration procedure is summarized in *Algorithm 1.*

Algorithm 1: Iterative procedure for parameter and delay estimation.

Step 1: Initialization Choose an initial estimate $A_0(s)$ and δ_0.

Step 2: LS step i =1 Construct Γ and Φ by replacing $A(s)$ and δ by $A_0(s)$ and δ_0 and get the LS solution of θ as

$$\hat{\theta}^{LS} = (\mathbf{\Phi}^T\mathbf{\Phi})^{-1}\mathbf{\Phi}^T\mathbf{\Gamma} \quad (21)$$

$\hat{\theta}^1 = \hat{\theta}^{LS}$. Get $\hat{A}_1(s)$, the process numerator $\hat{B}_1(s)$ and $\hat{\delta}_1$ from $\hat{\theta}^1$.

Step 3: IV step $i = i + 1$. Construct $\mathbf{\Gamma}$, $\mathbf{\Phi}$ and $\mathbf{\Psi}$ by replacing $A(s)$, $B(s)$ and δ by $\hat{A}_{i-1}(s)$,$\hat{B}_{i-1}(s)$ and $\hat{\delta}_{i-1}$ and get the IV solution of θ as

$$\hat{\theta}^i = (\mathbf{\Psi}^T\mathbf{\Phi})^{-1}\mathbf{\Psi}^T\mathbf{\Gamma} \quad (22)$$

Obtain $\hat{A}_i(s)$,$\hat{B}_i(s)$ and $\hat{\delta}_i$ from $\hat{\theta}^i$ and repeat **step 3** until $\hat{A}_i$ and $\hat{\delta}_i$ converge.

Step 4: Termination When $\hat{A}_i$ and $\hat{\delta}_i$ converge, the corresponding $\hat{\theta}^i$ is the final estimate of parameters.

Though there is no theoretical proof available, extensive simulation studies show that the iterative procedure converges monotonically except for non-minimum phase (NMP) processes. However, for NMP processes it exhibits monotonic divergence. Based on this, for such processes, we suggest an *ad hoc* procedure that defines $\Delta\delta = \delta_{i-1} - \delta_i$ and in the $(i+1) - th$ stage of iteration the guessed value is taken as $\delta_i + \Delta\delta$. The iteration steps otherwise remain the same.

3. IDENTIFICATION FROM IRREGULAR DATA

3.1 *The Algorithm*

For identification with irregular data, we propose an algorithm based on iterative prediction. However, it is not possible to develop a single algorithm that can deal with every types of data irregularity. We will consider here a specific type of irregular data where the input is available at all time instants but not necessarily in regular interval while the output is available at some time instants and missing at others. As the initialization of the iterative procedure, a so called input only method is applied. A distinguished feature of these methods is that the current output is expressed in terms of only current and previous input. So the parameter estimation equation can be formulated only at the time instants when output is available. The estimated model is then used to predict the missing values to get a complete data set. Next, this complete data set is used to estimate the parameters of the continuous time model using the procedure described in section 2. This model is then used to predict the missing outputs. This procedure is carried on iteratively by replacing the prediction from previous model by that from the current one until some convergence criteria are met. The iteration algorithm is presented in *Algorithm 2* and the different steps of the iteration procedure are detailed below.

3.2 *Input only modeling*

A number of input only approaches, both in discrete-time and continuous-time, are available in literature. In this work, we adopt one of the orthogonal basis function approach, the Laguerre polynomial model in continuous time for the initial prediction. The use of Laguerre functions in identification goes back to Wiener (1956). In the transform domain, the Laguerre functions are given as (Lee, 1932)

$$L_j(s) = \sqrt{2p}\frac{(s-p)^j}{(s+p)^{j+1}} \tag{23}$$

Let $z_j(t)$ be the output of the $j-th$ Laguerre function, with $u(t)$ as input, i.e.

$$Z_j(s) = L_j(s)U(s) \tag{24}$$

where, $Z_j(s)$ and $U(s)$ represent the Laplace transform of $z_j(t)$ and $u(t)$, respectively. The output of a stable plant with input $u(t)$ can be approximated by a truncated $l-th$ order Laguerre polynomial model as

$$y(t) = \sum_{j=0}^{l} \alpha_j z_j(t) \tag{25}$$

where, $\alpha = [\alpha_0, \alpha_1 \cdots \alpha_l]^T$, is the parameter vector for the Laguerre model. Theories and proofs of the convergence of the Laguerre model can be found in (Makila, 1990; Parington, 1991; Wang and Cluett, 1995). In the initial prediction stage using Laguerre polynomial model, the estimation equation (eqn(25)) is formulated only at the time instants when the output is available i.e.,

$$y(t_i^{obs}) = \sum_{j=0}^{l} \alpha_j z_j(t_i^{obs}) \tag{26}$$

Next, eqn(26) can be formulated for t_i^{obs} with $i = 1, 2 \cdots M$, where, M is the number of available output, to give an equation in least square form as

$$\mathbf{Y}_{obs} = \mathbf{Z}_{obs}\alpha \tag{27}$$

where,

$$\mathbf{Y}_{obs} = [y(t_1^{obs}) \;\; y(t_2^{obs}) \cdots y(t_M^{obs})]^T \tag{28}$$

$$\mathbf{Z}_{obs} = \begin{bmatrix} z_0(t_1^{obs}) & z_1(t_1^{obs}) & \cdots & z_l(t_1^{obs}) \\ z_0(t_2^{obs}) & z_1(t_2^{obs}) & \cdots & z_l(t_2^{obs}) \\ \cdots & \cdots & \cdots & \cdots \\ z_0(t_M^{obs}) & z_1(t_M^{obs}) & \cdots & z_l(t_M^{obs}) \end{bmatrix} \tag{29}$$

Finally the parameter vector can be estimated as

$$\hat{\alpha} = (\mathbf{Z}_{obs}^T\mathbf{Z}_{obs})^{-1}\mathbf{Z}_{obs}^T\mathbf{Y}_{obs} \tag{30}$$

Now, the missing elements of the output can be obtained as

$$\hat{y}(t_i^{mis}) = \sum_{j=0}^{l} \hat{\alpha}_j z_j(t_i^{mis}) \tag{31}$$

The estimated value of the missing elements can then be inserted into the output vector to get a complete data set.

3.3 *Criterion for convergence*

The iterative procedure described here is based on the idea of iterative prediction. Consequently, a natural option for criterion of convergence is the prediction error. As the output has missing elements, we can define the mean squared error at $i-th$ stage of iteration as

$$MSE_i^{obs} = \frac{1}{M}\sum_{k=1}^{M}\left[y(t_k^{obs}) - \hat{y}_i(t_k^{obs})\right]^2 \tag{32}$$

where, $\hat{y}_i$ is the prediction of the model obtained in the $i-th$ stage of iteration. Convergence of this MSE criterion is equivalent to the convergence of the model prediction and the model parameters.

4. SIMULATION RESULTS

To demonstrate the applicability of the proposed methods, we consider here a second order process having the following transfer function

$$G(s) = \frac{-4s+1}{9s^2+2.4s+1}e^{-0.615s} \tag{33}$$

A complete data set of 2000 samples is generated using a random binary signal (RBS) as input with

Algorithm 2: Algorithm for parameter estimation from irregular data.

Step 1: Initial Prediction Using only the observed output, estimate the parameters of the input only model using eqn(30). Predict the missing element of the output using eqn(31). Use these predicted values, $\hat{y}^0_{mis}$ to replace y_{mis}. $i = 0$.

Step 2: Iterative Prediction $i = i + 1$. Using *Algorithm1* Estimate the continuous time model parameters with the complete data set $y = [y_{obs} \quad \hat{y}^{i-1}_{mis}]$. Use the estimated model, θ^i, to get the $i-th$ prediction of the missing values, $\hat{y}^i_{mis}$. Replace $\hat{y}^{i-1}_{mis}$ by $\hat{y}^i_{mis}$

Step 3: Comparison Compare MSE^i_{obs} with MSE^{i-1}_{obs}. If their is significant improvement, go back to step 2 and repeat the iteration.

Step 4: Termination When MSE^i_{obs} converges, the corresponding θ^i is the final estimate of parameters.

a uniform sampling interval of 30 milliseconds (ms). Discrete time white noise is added to get the noisy output signal. The signal to noise ratio (NSR) is 10%. Table 1 summarizes the parameter estimation results for 100 Monte Carlo simulations (MCS) when all the data are available.

Table 1. Estimation results when all data are available

		Estimated parameters	
Parameter	True value	Mean	Variance
a_2	9.00	9.0068	0.0387
a_1	2.40	2.4309	0.0465
b_1	-4.00	-4.0201	0.0570
b_0	1.00	1.0109	0.0068
δ	0.615	0.6302	0.0253

Next, to test the performance of the algorithm proposed for irregular data, we generate three sets of irregular data that differ in terms of their amount of data missing. Every 3rd samples are taken out to generate a data set for 33% missing data, every 2^{nd} for 50% missing and every 2^{nd} and 3^{rd} for 67%. The model estimated using the iterative algorithm is compared with the model estimated using only the available data i.e. data at the time instants when both input and output are available. To compare different models with a single index we define a total error criterion that is measure of bias and variance together. We denote it by E_{total} where

$$E_{total} = \frac{1}{N_\theta} \sum_{i=1}^{N_\theta} \frac{(\hat{\theta}_i - \theta_i)^2 + \mathrm{var}(\hat{\theta}_i)}{\theta_i^2} \qquad (34)$$

θ_i is the true values of the i^{th} parameter and $\hat{\theta}_i$ is its estimated value. N_θ is the number of parameters. Figure 1 shows the total error for 100 MCS study. The estimated value is the mean of 100 estimates. The error corresponding to 0% missing data refers to the model estimated using the entire data set and can be taken as a benchmark. When 33% of the data are missing, the model estimated using only the available data has error comparable with the benchmark value and the iterative algorithm has little room to improve.

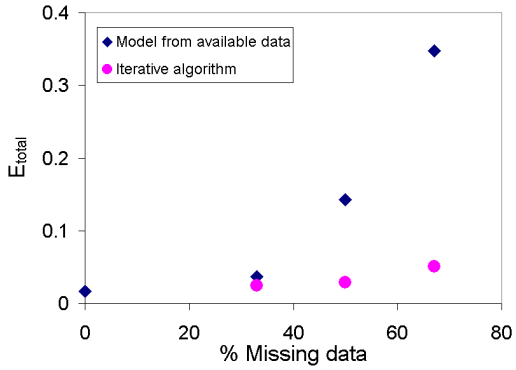

Fig. 1. Improvement of model quality using the iterative algorithm for the simulation example

This suggests that the available data are enough to give a good model. Consequently the error level of the model estimated using the iterative algorithm remains almost the same. However, when more data are missing the error corresponding to the model estimated using the available data is much higher than the benchmark value and the iterative algorithm reduces the error to a level comparable with the benchmark.

5. EXPERIMENTAL EVALUATION

The iterative prediction algorithm is evaluated using an experimental data set from a mixing process. The set-up consists of a continuous stirred tank used as a mixing chamber having two input streams fed from two tanks. A salt solution and pure water run from the feed tanks and mixed together in the mixing chamber. The output is the concentration of salt in the tank. The input is that in the feed. The electrical conductivity of the solutions are used as measure of their concentration. The volume of liquid in the stirred tank and its temperature are maintained at a constant level. The concentration of the feed is manipulated by adjusting the ratio of the flow rate of the feed salt solution and the flow rate of water. The total input flow i.e., the combined salt solution inlet and water inlet is kept constant which ensures a constant outlet flow.The input signal is a random binary signal. The sampling period is 20 seconds. A total of 955 data points are used for this study. To study the effect of % data missing and evaluate the performance of the iterative prediction algorithm, missing data were chosen on a random basis and the algorithm was applied. The study is carried out for 30%, 50% and 70% missing data. To generate a certain data set, say with 30% of its elements missing, 30% of the available output data are taken out on a random basis. The identification algorithm is then applied with the remaining 70% data points. The same procedure is applied 100 times with a different data set chosen each

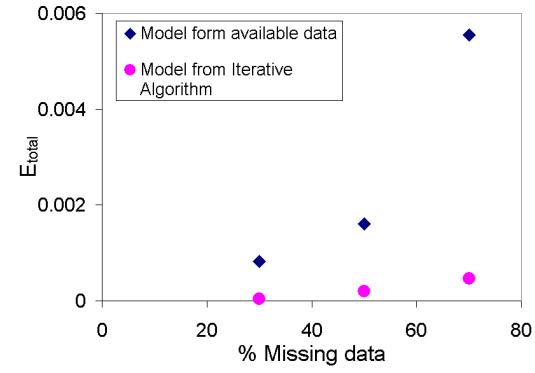

Fig. 2. Improvement of model quality using the iterative algorithm for the mixing process.

time containing 70% of the total data. Finally we get 100 estimates of the parameters. The total error is then calculated from the estimated mean and variance of the 100 estimates. To calculate the bias error, the model estimated using the entire data set is taken as the nominal or true value. Figure 2 shows the performance of the proposed iterative algorithm for the mixing process data. While the error levels for models estimated only the available data points are high, the iterative algorithms gives final estimates of the parameters with a much lower levels of error.

6. CONCLUSION

Identification from irregular data has been considered in discrete-time identification but mainly for multi-rate data. In continuous-time identification, it is assumed that the methods are capable of dealing with irregular data by nature. However, the inherent assumption of inter-sample behavior resulting in certain arbitrary interpolation introduces errors in the estimation of continuous-time parameters. In this paper, a simple algorithm is presented to deal with irregular output sampling. It has been demonstrated both using simulated and experimental data that the quality of the model estimated using the proposed model based prediction algorithm is much better than the quality of the model estimated using only the available output data. Also we present a recently proposed linear filter method for a more general filter structure.

7. REFERENCES

Agarwal, M. and C. Canudas (1987). On-line estimation of time-delay and continuous-time process parameters. *International Journal of Systems Science* **46**(1), 295–311.

Ahmed, S., B. Huang and S.L. Shah (2006). Parameter and delay estimation of continuous-time models using a linear filter. *Journal of Process Control* **16**(4), 323–331.

Fairman, F.W. (1971). Parameter estimation for a class of multivariate nonlinear processes. *International Journal of Control* **1**(3), 291–296.

Garnier, H., M. Mensler and A. Richard (2003). Continuous-time model identification from sampled data: Implementation and performance evaluation. *International Journal of Control* **76**(13), 1337–1357.

Imtiaz, S.A., S.L. Shah and S. Narasimhan (2004). Missing data treatment using IPCA and data reconciliation. *Proc. of the 7th IFAC Symposium on Dynamics and Control of Process Systems, Boston, USA, July 4-7 2004.*

Ingimundarson, A. and T. Hagglund (2001). Robust tuning procedure of dead-time compensating controllers. *Control Engineering Practice* **9**, 1195–1208.

Lee, Y.W. (1932). Synthesis of electrical networks by means of Fourier transform of Laguerre functions. *J. Math. Phys.* **11**, 83–113.

Makila, P.M. (1990). Approximation of stable systems by Laguerre filters. *Automatica* **26**(2), 333–345.

Parington, J.R. (1991). Approximation of delay systems by Fourier-Laguerre series. *Automatica* **27**(3), 569–572.

Rao, G.P. and L. Sivakumar (1976). Identification of deterministic time-lag systems. *IEEE Transactions on Automatic Control* **21**, 527–529.

Saha, D.C. and G.P. Rao (1983). *Identification of Continuous Dynamical Systems - The Poisson Moment Functional Approach.* first ed.. Springer-Verlag.

Wang, L. and P. Gawthrop (2001). On the estimation of continuous-time transfer functions. *International Journal of Control* **74**(9), 889–904.

Wang, L. and W.R. Cluett (1995). Building transfer function models from noisy step response data using Laguerre network. *Chemical Engineering Science* **50**(1), 149–161.

Wang, Q.G. and Y. Zhang (2001). Robust identification of continuous systems with dead-time from step response. *Automatica* **37**(3), 377–390.

Wiener, N. (1956). *Modern mathematics for the engineer.* Chap. The theory of prediction. McGraw-Hill. Scarborough, CA.

Young, P.C. (1970). An instrumental variable method for real time identification of noisy process. *Automatica* **6**, 271–287.

Young, P.C. (2002). Optimal IV identification and estimation of continuous-time TF models. *Proceedings of the 15th IFAC Triennial World Congress, Barcelona, Spain* **25**(5), 337–358.

ADCHEM 2006

International Symposium on Advanced Control of Chemical Processes
Gramado, Brazil – April 2-5, 2006

DATA-BASED UNCERTAINTY MODELING BY CONVEX OPTIMIZATION TECHNIQUES

Kurt E. Häggblom

Process Control Laboratory, Faculty of Technology,
Åbo Akademi University, FI-20500 Turku, Finland

Abstract: A procedure based on convex optimization techniques for deriving norm-bounded uncertainty models for MIMO systems is presented. The procedure is developed for unstructured additive uncertainty models, but in principle this is no limitation since any uncertainty model of LFT type can be transformed into such a model. The models are determined by matching to process data available in the form of frequency responses of a set of individual models or sets of input-output data. Conditions for the existence of solutions to the data-matching problems are defined by LMIs. Uncertainty models that tightly match the data are obtained by minimizing an ellipsoidal uncertainty region. An application to distillation is included.

Keywords: Uncertainty modeling, linear multivariable systems, convex optimization, linear matrix inequalities, determinant minimization, robust control, distillation columns.

1. INTRODUCTION

Many robust control design methods are based on a linear transfer function model incorporating a weighted norm-bounded uncertainty description. The construction of a non-conservative uncertainty model from process data is a significant problem.

The generation of useful process data for uncertainty modeling is a nontrivial task. This task is especially difficult if the system is multivariable and ill-conditioned or nonlinear. In practice, the dynamics of such a system cannot be captured in a single linear model without some advanced uncertainty modeling.

An appealing approach to uncertainty modeling is first to determine a set of individual models, then to construct an uncertainty model that encompasses all these models. In this way "difficult" dynamics, which may be hard to include in a single model, can be split between several models. Furthermore, the use of several models may facilitate the task of separating noise and dynamics so that noise and bias largely can be excluded from the model set (Häggblom and Böling, 1998).

One way of constructing a norm-bounded uncertainty model from a set of individual models is to employ model-matching techniques. The basis of this method is that the uncertainty model should be capable of reproducing every model in the model set. Such a technique has been used by Hindi *et al*. (2002). However, if the identification has given several models, it is because different input sequences and operating points generate different models. It is then valid to assume that a model only applies to the input sequence used to generate the data from which the model was determined. This suggests derivation of an uncertainty model using input-output matching instead of model matching. It can be shown that model matching cannot produce a model less conservative than input-output matching for a given model structure (Nyström *et al.*, 2003) .

An important aspect in uncertainty modeling is the choice of objective function to be minimized so as to obtain a non-conservative uncertainty model, which "tightly" matches the known data. A natural choice is to minimize the largest possible discrepancy between a nominal model and the uncertainty model. This results in a norm-minimization problem and has been used, e.g., by Hindi *et al*. (2002).

In this paper it is argued that a less conservative uncertainty model is obtained by minimizing the size of the ellipsoidal region that the deviations between the outputs from the uncertainty model and a nominal model cover. This results in a determinant-minimization problem.

A significant task is also the development of a suitable numerical procedure for solving the problem. Generally, convex optimization methods are desired. In this paper it is shown that the determinant-minimization problem can be formulated as a convex optimization problem, where the various data-matching requirements and certain norm-related constraints can be expressed as linear matrix inequalities (LMIs). Both model matching and input-output matching as well as methods based on norm minimization can be handled by essentially the same procedure.

An application to uncertainty modeling of a distillation column is included.

2. PROBLEM FORMULATION

2.1 Uncertainty Description

We consider linear multiple-input multiple-output (MIMO) uncertainty models of the form

$$G(s) = G_0(s) + W_1(s)\Delta(s)W_2(s), \quad \|\Delta\|_\infty \le 1 \qquad (1)$$

where $G_0(s)$ is a stable nominal transfer matrix model, $W_1(s)$ and $W_2(s)$ are stable transfer matrix filters acting as uncertainty weights, and $\Delta(s)$ is a norm-bounded uncertainty matrix. Only uncertainty with an unstructured Δ matrix is considered in this paper.

Structurally, model (1) is an additive uncertainty model, but obviously multiplicative input and output uncertainties can be handled by including G_0 in W_1 or W_2. In fact, general linear fractional transformation (LFT) models

$$\hat{G} = \hat{G}_0 + \hat{W}_1\hat{\Delta}\left(I - \hat{W}_3\hat{\Delta}\right)^{-1}\hat{W}_2, \quad \left\|\hat{\Delta}\right\| \le 1, \left\|\hat{W}_3\right\| < 1 \qquad (2)$$

can be cast in the form of (1) (Chen and Gu, 2000; Hindi *et al*., 2002). Thus, (1) can represent a large class of uncertainty model types.

2.2 Data Matching in the Frequency Domain

We wish to determine W_1 and/or W_2 so that the uncertainty model (1) can reproduce sets of known frequency-response data with a minimum amount of conservatism. This means that any reduction of the region of uncertainty covered by the model would result in some data being irreproducible.

We shall use data matching as the technique for determining a non-conservative uncertainty model. It is assumed that frequency-response data are known at a number of relevant frequencies $\omega \in \Omega$ for a number of data sets k, $k = 1,\ldots,N$, either as (a) smoothed (noise-free) input-output data $\{u_k(\mathrm{j}\omega), y_k(\mathrm{j}\omega) : \omega \in \Omega\}$ or (b) transfer matrix data $\{G_k(\mathrm{j}\omega) : \omega \in \Omega\}$. In addition, a nominal model $G_0(\mathrm{j}\omega)$ may be known in either case. In the sequel, the argument "$\mathrm{j}\omega$" is omitted for convenience.

In practice, the data may be obtained from a number of identification experiments k, $k = 1,\ldots,N$. In case (a), the smoothing of output data can be accomplished by fitting a model G_k to data and using the output from this model as the output y_k, i.e.,

$$y_k = G_k u_k, \ \forall k \qquad (3)$$

This is a convenient way of excluding noise and retaining "difficult" dynamics, which cannot easily be included in a single model (e.g., due to nonlinearity), in the model set (Böling *et al*., 2004; Häggblom *et al*., 2003). The modeling technique to be described does not require a nominal model G_0 to be known initially, but if such a model is used, it can be obtained, e.g., by fitting a single model to all available input-output data.

Since the uncertainty modeling is based on data obtain, e.g., through identification, it is important that the identification experiments are thoroughly exciting and that they adequately cover the relevant operating region. We think that this requirement is of greater concern than, e.g., the possible uncertainty associated with the individual models G_k. Therefore, we do not take such uncertainty into account.

2.3 Input-Output Matching vs Model Matching

Case (a), mentioned above, can be considered an input-output matching problem and case (b) a model matching problem. Insofar as these kinds of techniques have been used for uncertainty modeling, model matching seems to be the predominant choice (see Hindi *et al.*, 2002; Farag and Werner, 2004). However, model matching generally results in an uncertainty model having a larger region of uncertainty than a model determined by input-output matching (Nyström *et al.*, 2003).

This can be explained by the fact that in model matching, every model G_k, $k = 1,\ldots,N$, is assumed to apply for all possible inputs, whereas only a single input-output pair (u_k, y_k) is associated with G_k in input-output matching. If the identification experiments have resulted in a set of models, it is because different input sequences (as well as different operating points and conditions) give different models. Thus, it is realistic to assume that a model applies only to the input sequence used for generating the data, from which the model was determined.

Because of this, we propose input-output matching as the main method for uncertainty modeling. However,

because both methods have merit, and only model data might be available in a given case, we do consider both methods in this paper. Furthermore, the techniques for input-output matching and model matching are quite similar.

3. UNCERTAINTY MODELING BY CONVEX OPTIMIZATION

3.1 Minimizing the Region of Uncertainty

Calculations for the uncertainty modeling are performed "frequency-by-frequency" for a set of relevant frequencies $\omega \in \Omega$. At each frequency, we desire a non-conservative norm-bounded uncertainty description

$$G = G_0 + W_1 \Delta W_2, \quad \bar{\sigma}(\Delta) \le 1 \tag{4}$$

where $\bar{\sigma}(\Delta)$ is the maximum singular value of Δ.

As a result of the optimization, we will obtain frequency responses of W_1 and W_2, and possibly of a new G_0, at all frequencies considered. A model of the form (1) requires that transfer function matrices are fitted to these frequency responses. Although the frequency responses are determined subject to appropriate data-matching conditions, the same data-matching conditions should again be enforced during the fitting so as not to introduce unnecessary conservatism or violation of constraints. However, we shall not consider this part of the problem in this paper.

Although the uncertainty modeling is based on certain frequency-response data, a model relevant for arbitrary (norm-bounded) inputs u, $\|u\| \le 1$, is desired. Here, $\|u\|$ denotes the Euclidean 2-norm of u. For such an input, the deviation e between the output from the uncertainty model and the nominal model is a measure of the uncertainty. This deviation is given by

$$e := (G - G_0)u = W_1 \Delta W_2 u \tag{5}$$

Here, $W_2 u$ is an input to the uncertainty block Δ. An unstructured uncertainty Δ, $\bar{\sigma}(\Delta) \le 1$, can then produce any output x bounded by $\|x\| \le \|W_2 u\|$. When x varies over its range of possible values, the deviation $e = W_1 x$ covers an ellipsoidal region. This interpretation may not be immediately obvious when the entities are complex valued, but it can be justified (Häggblom, 2005a). When W_1 has full row rank (which is necessary for arbitrary data matching), the size (volume) of this ellipsoid is proportional to $\det(W_1 W_1^*)^{1/2} \|x\|^n$, where n is the size of the matrix $W_1 W_1^*$ (equal to the number of outputs) and superscript $*$ denotes complex-conjugate transpose. We are interested in minimizing the size of this ellipsoid for the worst input u. This gives the objective function

$$J = \det(W_1 W_1^*)^{1/2} \|W_2\|^n \tag{6}$$

to be minimized subject to appropriate data-matching and other constraints.

The scaling factor $\|W_2\|$ introduces a potential problem in the minimization of J. However, since the values of the right-hand sides of (4) and (6) do not change if one of the weights is multiplied by a positive scalar and the other weight is divided by the same scalar, W_2 can, without loss of generality, be required to have a given norm and can thus be excluded from (6).

If possible, we require the objective function to be convex. The determinant in (6) is the determinant of a positive definite matrix, but it is not a convex function. Fortunately, it can be transformed to an equivalent convex function and one way of doing it is to take the logarithm of the determinant (Vandenberghe *et al.*, 1998). However, this results in a convex objective function for a maximization problem. Since we want to minimize the determinant, we need to use the inverse of the positive definite matrix. We thus want to

$$\text{minimize} \ \log\det Y^{-1} \tag{7}$$

where

$$Y := (W_1 W_1^*)^{-1/2} \succ 0 \tag{8}$$

Here, "$\succ$" denotes "positive definite".

An obvious alternative to the minimization of $\det Y^{-1}$ is minimization of $\|W_1\|$. This would minimize the largest possible deviation of e, but the size of the resulting uncertainty region would generally be larger than that obtained by determinant minimization. In norm minimization, a scalar weight would in fact be sufficient (Böling *et al.*, 2004).

For robustness reasons in controller design, it might be desirable to restrict $\|W_1\|$ even when $\det Y^{-1}$ is minimized. Let us introduce the restriction

$$\|W_1\| \le \gamma_1 \tag{9}$$

This is equivalent with the matrix inequalities

$$(W_1 W_1^*)^{1/2} = Y^{-1} \preccurlyeq \gamma_1 I \quad \Leftrightarrow \quad \gamma_1 I - I Y^{-1} I \succcurlyeq 0 \tag{10}$$

or

$$\begin{bmatrix} Y & I \\ I & \gamma_1 I \end{bmatrix} \succcurlyeq 0 \tag{11}$$

which can be used as a constraint when $\det Y^{-1}$ is minimized.

We note that although we do not try to minimize the largest deviation e, we do consider the most harmful input u, $\|u\| \le 1$. Since the input $W_2 u$ to Δ also covers an ellipsoidal region when u, $\|u\| \le 1$, varies over its admissible range of values, a reasonable alternative would be to minimize the product of the sizes of the two ellipsoids (Häggblom, 2005b).

Next we shall derive constraints imposed by data matching requirements. For ease of presentation, we start with model matching.

3.2 Model Matching

In model matching it is required that every $G = G_k$ can be reproduced by some allowed perturbation $\Delta = \Delta_k$ in accordance with (4). We thus require a condition which guarantees that

$$E_k := G_k - G_0 = W_1 \Delta_k W_2 , \quad \bar{\sigma}(\Delta_k) \le 1 \tag{12}$$

can be satisfied exactly. In principle, we can construct such a Δ_k explicitly, but we shall here use a result from the literature.

Let $E_k \in \mathbb{C}^{n\times m}$, $W_1 \in \mathbb{C}^{n\times p}$, $W_2 \in \mathbb{C}^{q\times m}$, $n \le p$, $q \ge m$. Then there is a $\Delta_k \in \mathbb{C}^{p\times q}$, $\bar{\sigma}(\Delta_k) \le 1$, if and only if (Poolla *et al.*, 1994; Chen and Gu, 2000)

$$\begin{bmatrix} W_1 W_1^* & E_k \\ E_k^* & W_2^* W_2 \end{bmatrix} \succcurlyeq 0 \tag{13}$$

We note that this condition does not require any of the matrices to be square; it is only required that the dimensions of Δ_k are not less than those of E_k.

In order to be useful for our purposes, the data matching condition should be linear with respect to the optimization variables. As given, (13) is not linear with respect to Y, defined in (8). However, (13) can be reformulated in various ways (see, e.g., VanAntwerp and Braatz, 2000). The condition is equivalent with

$$W_1 W_1^* \succ 0 , \quad W_2^* W_2 - E_k^* (W_1 W_1^*)^{-1} E_k \succcurlyeq 0 \tag{14}$$

If we introduce Y according to (8) and define

$$X := W_2^* W_2 \succcurlyeq 0 \tag{15}$$

the latter part of (14) can be written

$$X - E_k^* Y^* Y E_k \succcurlyeq 0 \tag{16}$$

This, in turn, can be written as the linear matrix inequality (LMI)

$$\begin{bmatrix} I & YE_k \\ (YE_k)^* & X \end{bmatrix} \succcurlyeq 0 \ , \quad \forall k \tag{17}$$

which is linear in Y and X.

If we want to optimize also with respect to G_0, (17) has to be modified slightly. By defining

$$Z := YG_0 \tag{18}$$

(17) can be written as

$$\begin{bmatrix} I & YG_k - Z \\ (YG_k - Z)^* & X \end{bmatrix} \succcurlyeq 0 \ , \quad \forall k \tag{19}$$

which is linear in Y, Z and X.

As discussed in the previous section, $\|W_2\|$ needs to be restricted. Otherwise, (16) can always be satisfied by a sufficiently large X regardless of Y. Let us thus introduce the restriction

$$\|W_2\| \le \gamma_2 \tag{20}$$

This is equivalent with the matrix inequalities

$$W_2^* W_2 = X \preccurlyeq \gamma_2^2 I \quad \Leftrightarrow \quad \gamma_2^2 I - X X^{-1} X \succcurlyeq 0 \tag{21}$$

or

$$\begin{bmatrix} X & X \\ X & \gamma_2^2 I \end{bmatrix} \succcurlyeq 0 \tag{22}$$

In principle, arbitrary structures can be imposed on W_1 and W_2, resulting in corresponding structures for Y and X. These structures would most commonly be block-diagonal ones. If desired, the structure of Z could also be constrained, thus affecting the structure of the estimated G_0.

More generally, Y, X and Z may belong to certain sets $\mathcal{Y}$, $\mathcal{X}$ and $\mathcal{Z}$, respectively. The general optimization problem based on model matching can then be formulated as follows:

$$\begin{aligned} &\underset{Y\in\mathcal{Y}, X\in\mathcal{X}, Z\in\mathcal{Z}}{\text{minimize}} \ \det Y^{-1} , \forall \omega \in \Omega \\ &\text{subject to (19), (22), (11)} \end{aligned} \tag{23}$$

3.2 Input-Output Matching

In the case of input-output matching we require

$$e_k := y_k - G_0 u_k = W_1 \Delta_k W_2 u_k , \quad \bar{\sigma}(\Delta_k) \le 1 \tag{24}$$

Similarly as above, we can derive the LMIs

$$\begin{bmatrix} I & Ye_k \\ (Ye_k)^* & u_k^* X u_k \end{bmatrix} \succcurlyeq 0 , \quad \forall k \tag{25}$$

and

$$\begin{bmatrix} I & Yy_k - Zu_k \\ (Yy_k - Zu_k)^* & u_k^* X u_k \end{bmatrix} \succcurlyeq 0 , \quad \forall k \tag{26}$$

where the latter is used if G_0 is to be updated.

The general optimization problem based on input-output matching can now be formulated as follows:

$$\begin{aligned} &\underset{Y\in\mathcal{Y}, X\in\mathcal{X}, Z\in\mathcal{Z}}{\text{minimize}} \ \det Y^{-1} , \forall \omega \in \Omega \\ &\text{subject to (26), (22), (11)} \end{aligned} \tag{27}$$

3. APPLICATION TO DISTILLATION

A distillation column is a multivariable system usually characterized by a strong directionality, which means that the transfer matrix is ill-conditioned and nearly singular. In order to be useful for controller design, a model must provide a good description of the directionality properties.

It tends to be almost impossible to capture these properties with sufficient accuracy in a single linear model determined through system identification. The nonlinearity of the plant further complicates the

matter. Therefore, an appealing approach in the modeling of a distillation column is to determine a set of linear models. Such a set has been determined by Häggblom and Böling (1998) and will be used in this application.

The distillation column is a pilot-scale two-product column, which was identified by applying a series of step changes in the high- and low-gain input directions. From these experiments, a nominal model as well as six additional models were determined as transfer matrix models composed of second-order transfer functions with deadtime (Häggblom and Böling, 1998). The models have two outputs (distillate and bottoms composition) and two inputs (reflux and vapor to the reboiler).

Various types of "simple" uncertainty models have been considered for this column and a multiplicative output uncertainty model of the form

$$G = (I + W_1\Delta)G_0 \tag{28}$$

was found adequate in previous studies (Nyström *et al.*, 2003; Böling *et al.*, 2004; Häggblom, 2005b). In these studies, the 2×2 weight matrix W_1 was determined frequency by frequency by matching to input-output data using determinant minimization. Transfer function filters were also determined by fitting to the calculated weights. The possibility of adjusting the nominal model so as to reduce the conservatism of the uncertainty model was not considered.

The convex optimization formulation presented in this paper was not available in the previous works. Thus, the optimizations were non-convex with various numerical problems. By the present formulation it is straightforward to solve the problem. The calculation of a nominal model and other types of uncertainty models can be handled within the same framework.

In this paper, we shall compare the uncertainty models obtained by determinant minimization with models obtained by minimization of the maximum singular value of the weight matrix. We shall consider full weight matrices, diagonal weight matrices and scalar weights. We shall also illustrate how the uncertainty model can be improved by optimizing the nominal model. For simplicity, we only illustrate the results by steady-state data.

Table I shows the nominal model obtained by fitting to all input-output data in Table II. Experiments 1–3 are step changes in the low-gain direction and experiments 4–6 step changes in the high-gain direction of the distillation column.

Figure 1 shows the experimental data points as the coordinates of the components of the deviation

$$e_k = y_k - G_0 u_k \tag{29}$$

normalized by $\|u_k\|$. Because the data points farthest away from the origin are close to the coordinate axes, it is sufficient to use a diagonal uncertainty weight

TABLE I

Nominal Steady-State Model

$$G_0(0) = \begin{bmatrix} -0.04229 & 0.09349 \\ 0.11733 & -0.27858 \end{bmatrix}$$

TABLE II

Steady-State Data of Individual Experiments

Exp. #	u_1	u_2	y_1	y_2
1	10.0	5.0	0.06180	–0.23315
2	–20.0	–10.0	–0.09280	0.42640
3	10.0	5.0	0.04135	–0.20590
4	0.5	–1.0	–0.11513	0.50204
5	–1.0	2.0	0.22997	–0.76869
6	0.5	–1.0	–0.17393	0.33254

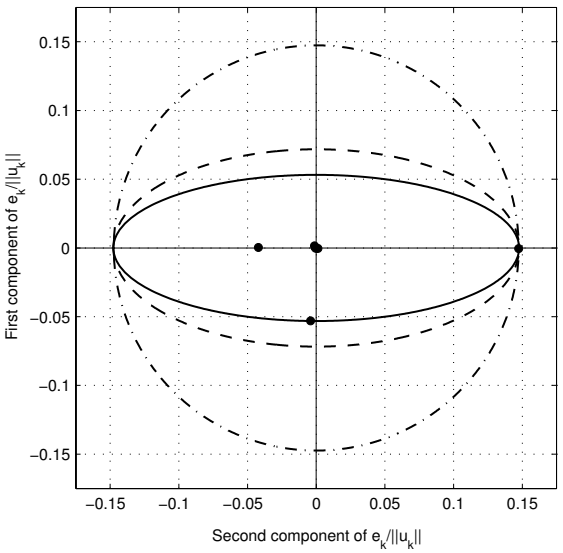

Fig. 1. Normalized output deviations of experimental points with uncertainty regions at steady state: smallest region (——), region with smallest norm (— — —), smallest region with scalar weight (— · —).

matrix W_1 in the uncertainty model (28). The smallest ellipse in Fig. 1 illustrates the uncertainty region of model (28) obtained when the size (i.e., area) of this region is minimized. The uncertainty model can generate any point inside the ellipse. As can be seen, all experimental points are in the region and it cannot be made smaller, using a diagonal weight and the given nominal model, without excluding some experimental point.

Figure 1 also shows the uncertainty region obtained by minimizing the maximum singular value of the diagonal weight W_1 as well as the uncertainty region for an optimal scalar weight. Clearly, these are larger than the uncertainty obtained by minimizing the size of the uncertainty region. It can also be mentioned that the uncertainty region obtained by model matching is an order of a magnitude larger than the one obtained by data matching.

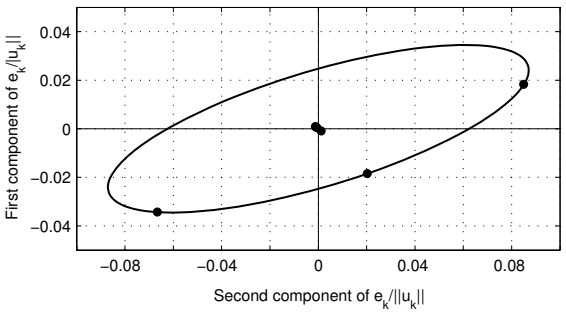

Fig. 2. Experimental points and uncertainty region for full optimal weight and nominal model.

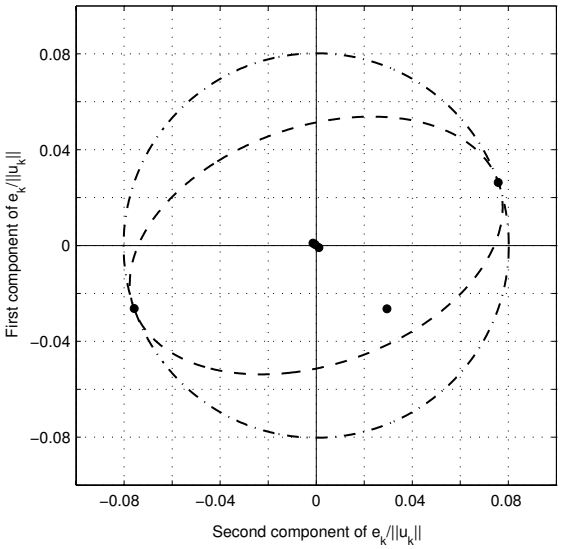

Fig. 3. Experimental points and uncertainty regions for full weight with smallest norm (— —) and smallest scalar weight (— · —) with optimal nominal model.

The experimental points in Fig. 1 indicate that the uncertainty regions could be reduced by adjusting the nominal model. Figure 2 shows the result of such an adjustment obtained by solving the problem defined in Eq. (27). Note that the positions of the experimental points are changed because the nominal model affects the deviations e_k. Note also the differences between the scales in Fig. 1 and Fig. 2.

Figure 3 shows the corresponding result for the cases when the maximum singular value of a full weight matrix W_1 is minimized and when an optimal scalar weight is used. Even though the nominal model is adjusted so as to minimize these weights, the resulting models have uncertainty regions significantly larger than that of the model obtained by solving Eq. (27).

4. CONCLUSIONS

A procedure based on convex optimization techniques for deriving norm-bounded uncertainty models for MIMO systems has been presented. The procedure applies for uncertainty models with a norm-bounded unstructured uncertainty, but otherwise quite general model types (additive, multiplicative, LFT uncertainty) as well as placement and structures of weights can be handled. Data for the uncertainty modeling may be available as sets of input-output data or a number of deterministic models. Generally, input-output data is preferable since it gives a less conservative uncertainty model. The uncertainty modeling is based on data (or model) matching in the frequency domain, for which necessary and sufficient conditions are expressed by LMIs. The size (area, volume) of an ellipsoidal uncertainty region, or its norm (largest distance from the origin), may be minimized. As indicated by an application to distillation modeling, minimization of the size of the uncertainty region tends to be the superior approach. The uncertainty models contain a nominal model, which strongly affects the size of the uncertainty region, and which may be adjusted so as to minimize this region.

Acknowledgment

Financial support from the Academy of Finland under grant number 206750 is gratefully acknowledged.

REFERENCES

Böling, J.M., K.E. Häggblom and R.H. Nyström (2004). Multivariable uncertainty estimation based on multimodel output matching. *J. Process Control*, 14, 293–304.

Chen, J. and G. Gu (2000). *Control-Oriented System Identification: An H_∞ Approach.* Wiley-Interscience, New York.

Farag. A. and H Werner (2004). Constructing tight LFT uncertainty models for robust controller design. *Proc. 43rd IEEE Conf. on Decision and Control*, pp. 406–410, Nassau, Bahamas.

Häggblom, K.E. (2005a). Real-field formulation of norm-related problems in the frequency domain. *Proc. 4th Int. DCDIS Conf. on Engineering Applications and Computational Algorithms*, pp. 635–640, Guelph, Ontario, Canada.

Häggblom, K.E. (2005b). Derivation of unstructured MIMO uncertainty models via data matching. Presented at the *44th IEEE Conf. on Decision and Control, and European Control Conf. ECC'05*, Seville, Spain. Available at http://www.abo.fi/fak/ktf/rt/pro0009.html.

Häggblom, K.E. and J.M Böling (1998). Multimodel identification for control of an ill-conditioned distillation column. *J. Process Control*, **8**, 209–218.

Häggblom, K.E., R.H. Nyström and J.M. Böling (2003). Uncertainty estimation for MIMO systems via multimodel identification. Presented at *AIChE Annual Meeting*, paper 436d, San Francisco, CA, USA.

Hindi, H., C.-Y. Seong and S. Boyd (2002). Computing optimal uncertainty models from frequency domain data. *Proc. 41st IEEE Conf. on Decision and Control*, pp. 2898–2905, Las Vegas, NV, USA.

Nyström R.H., K.E. Häggblom and J.M. Böling (2003). Derivation and selection of norm-bounded uncertainty descriptions based on multiple models. *Int. J. Control*, **76**, 717–727.

Poolla, K., P. Khargonekar, A. Tikku, J. Krause and K. Nagpal (1994). A time-domain approach to model validation. *IEEE Trans. Autom. Control*, **39**, 951–959.

VanAntwerp, J.G. and R.D. Braatz (2000). A tutorial on linear and bilinear matrix inequalities. *J. Process Control*, **10**, 363–385.

Vandenberghe, L., S. Boyd and S.-P. Wu (1998). Determinant maximization with linear matrix inequality constraints. *SIAM J. Matrix Analysis and Applications*, **19**, 499–533.

ADCHEM 2006

International Symposium on Advanced Control of Chemical Processes
Gramado, Brazil – April 2-5, 2006

CLOSED LOOP CONTINUOUS-TIME FOPTD IDENTIFICATION USING TIME-FREQUENCY DATA FROM RELAY EXPERIMENTS

George Acioli Jr. , Marcus A. R. Berger and Péricles R. Barros

Dep. de Eng. Elétrica, Univ. Fed. de Campina Grande, Cx.P. 10105, Campina Grande, PB – BRAZIL.
E-mail: georgeacioli@yahoo.com.br,marcusarb@yahoo.co.uk, prbarros@dee.ufcg.edu.br

Abstract: In this work the identification of first-order plus dead-time models from a relay experiment is considered. The relay excitation is applied to the closed-loop. Alternative techniques for identification are examined and simple algorithms are proposed for dealing with the dead-time. Simulation examples are used to illustrate the techniques.

Keywords: Continuous-time identification; Process identification; Closed-loop identification; Time delay process; Relay excitation.

1. INTRODUCTION

The estimation of continuous-time models from sampled data has received some attention in last years, motivated by the need of such models to recover physical parameters or to allow the use of design techniques developed for continuous-time controllers. An extensive list of references on the subject can be found in (Mensler, 1999), in which a detailed survey discusses the advantages of a direct approach in relation to the indirect estimation of a discrete-time model plus a later transformation into a continuous-time model. Several papers have been presented in recent conferences (for instance, 13th IFAC Symposium on System Identification (SYSID 2003) and 16th IFAC World Congress 2005) to report new developments and applications.

The continuous-time results reported in the literature mainly address finite-dimensional systems. But dead-time is present in several industrial processes so that simple models such as first and second order dead-time continuous time one are widely used to tune industrial controllers. In the design of PID controllers the process model that receives most attention is first-order plus dead-time model (FOPDT) (Sudaresan and Krishnaswamy, 1977). There are a few methods to estimate parameters for this model. Among them one can mention the graphics and the area methods (Åström and Hägglund, 1995). A method less sensitive to noise is proposed in (Wang *et al.*, 1999) which uses least-squares method to estimate the parameters of FOPDT model. Variants of this methods are used in (Wang and Zhang, 2001) and (Wang *et al.*, 2000). Other method for open loop unstable processes is presented in (Marchetti and Lewin, 2001). For such simple models the results are remarkably good and motivated the present work. Methods of closed-loop identification have been used in industrial applications (Forssell and Ljung, 1999). The closed-loop identification doesn't cause stops in system operation comparing with the open-loop identification. Besides this reason, there are others to do experiments of closed-loop identification which are:

demands of safety in the operation of the process or because the process has unstable behavior in open-loop, which are found in many industrial processes (Ljung, 1999). There are situations where the plants are stable but restrictions in production are strong reasons not to allow experiments in open-loop. An additional consideration to accomplish experiments in closed-loop is that the dynamic exhibited by the plant with the old controller must be more important to design a high performance controller than the dynamic of the plant in open-loop.

In this paper three techniques for the estimation of continuous-time systems from discrete-time measurements with data obtained from relay based closed-loop experiments are compared.

The first technique is the one presented in ((Coelho and Barros, 2003)) where least-squares minimization is used with a search for a initial dead-time estimate. The second technique uses an approximated model. Both techniques use only time-domain data.The third one is a constrained least-squares minimization which uses frequency data obtained from a relay experiment.

This paper is organized as follows. In Section 2, the problem statement is presented. The relay closed loop experiment used to obtain time and frequency information is presented in Section 3. The continuous-time identification of FOPTD techniques are presented in Section 4. In Section 5 the techniques are compared using simulations of examples and, finally, conclusions are presented in Section 6.

2. THE PROBLEM STATEMENT

In this paper it is considered the identification of first-order plus dead-time (FOPDT) continuous-time models represented by

$$G(s) = \frac{b}{s+a} e^{-Ls}. \qquad (1)$$

It is assumed closed-loop operation and that the excitation is generated from a relay-based experiment. In this paper is considered a closed-loop with transfer function $T(s)$, process transfer function $G(s)$, controller $C(s)$, and loop gain $L(s)$. Although it is desired to estimate a continuous-time model, the available data to the estimation is discrete-time. The aim of the paper is to evaluate the improvements obtained, for such simple models, with the introduction of frequency domain information as constraints in the minimization problem.

The frequency domain information is obtained by using a relay based test as described in the sequel.

3. THE LOOP GAIN RELAY EXPERIMENT

A basic procedure for the estimation of a general frequency point of the loop gain transfer function using a relay feedback is presented in (de Arruda and Barros, 2003). The feedback structure applied for loop transfer function estimation is presented in Fig. 1. The conditions of the limit cycle operation are defined by the following proposition.

Consider the closed loop relay system shown in Fig (1). Assume that for a stable closed loop $T(s)$ and a real positive number r, the transfer function

$$F(s) = \frac{2}{r} \frac{T(s)}{T(s)\left(\frac{1-r}{r}\right) + 1} - 1 \qquad (2)$$

is also stable. Then if a limit cycle is present it oscillates at a frequency ω_o such that

$$|L(j\omega_o)| \approx r \; .$$

See (de Arruda and Barros, 2003).

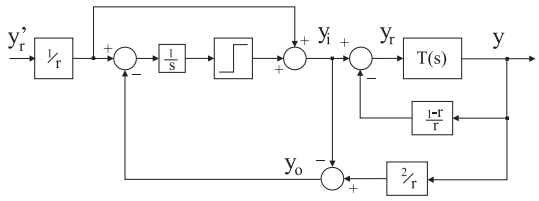

Fig. 1. Relay Closed Loop Experiment for Loop Transfer Function Estimation.

Selecting $r = 1$, the current loop gain crossover frequency ω_g can be estimated. This estimate is denoted $\hat{\omega}_g$. In this case the scheme reduces to the one presented in (Schei, 1992).

The setpoint $y_r(t)$ is the loop gain experiment excitation applied to the closed loop $T(s)$ formed by the process $G(s)$ with controller $C(s)$. The process transfer function at the crossover frequency is estimated computing the DFT of one period of the process input u and output y when the relay oscillation is present and steady. This loop gain relay excitation is used at all examples.

4. TECHNIQUES USED FOR THE IDENTIFICATION OF FOPDT MODELS

In this Section the identification techniques are described.

4.1 Technique 1: Identification of FOPDT Model with Dead-Time Search

This technique is the one presented in ((Coelho and Barros, 2003)) for a closed-loop step response

In this paper the excitation used is the one obtained from the loop gain relay experiment with $r = 1$.

Under mild conditions the process model (1)can be written as

$$y(t) = -a\int_0^t y(\tau)\,d\tau + b\int_0^{t-L} u(\tau)\,d\tau. \quad (3)$$

It can also be rewritten as

$$y(t) = -a\int_0^t y(\tau)\,d\tau + b\int_0^t u(\tau)\,d\tau - b\int_{t-L}^t u(\tau)\,d\tau. \quad (4)$$

Then, define

$$\phi(t) = \left[-\int_0^t y(\tau)\,d\tau \;\; \int_0^t u(\tau)\,d\tau \;\; -\int_{t-L}^t u(\tau)\,d\tau \right]^T,$$
$$\theta = \left[a \;\; b_1 \;\; b_2 \right]^T. \quad (5)$$

and Eq.(4) can be written in regression form

$$y(t) = \phi(t)\,\theta. \quad (6)$$

Unfortunately, the value of L is not known. In this case, a straightforward procedure is to search for the best fit among several values of L. An algorithm presented in ((Coelho and Barros, 2003)) is used to avoid estimate a L which is a multiple of the sampling period. Its motivation comes from the fact that $b_1 = b_2$ for the true value of L. Is choose a range for the dead-time, $[L_{\min}, L_{\max}]$, with $L_{\min} = k_{\min}T_s$ and $L_{\max} = k_{\max}T_s$. Using a regression model the parameters for each value of k in $[k_{\min}, k_{\max}]$ are estimated. For each value $i = k - k_{\min} + 1$ estimate $\hat{\theta}^i$ is computed

$$\begin{bmatrix} a^i \\ b_1^i \\ b_2^i \end{bmatrix} = \begin{bmatrix} \hat{\theta}^i(1) \\ \hat{\theta}^i(2) \\ \hat{\theta}^i(3) \end{bmatrix}. \quad (7)$$

an estimate of L, say L_1, is recovered

$$L_1 = \hat{k}T_s \quad \text{with} \quad \hat{k} = \min_i \left| b_1^i - b_2^i \right|.$$

So, applying the estimator to the regression vector

$$\phi(t) = \begin{bmatrix} -\int_0^t y(\tau)\,d\tau \\ \int_0^t u(\tau)\,d\tau \\ -\frac{1}{L_1}\int_{t-L_1}^t u(\tau)\,d\tau \end{bmatrix}, \quad (8)$$

$$\theta = \left[a \;\; b \;\; \beta \right]^T, \quad (9)$$

the final estimate $\left\{ \hat{a}, \quad \hat{b}, \quad \hat{L} = \hat{\beta}/\hat{b} \right\}$ are obtained and the corresponding model $G_{LS1}(s)$.

4.2 Technique 2: Identification of FOPTD Model using Approximation

In this second technique, the following approximation for model 1 is used:

$$G(s) = \frac{b(1 - sL)}{s + a} \quad (10)$$

the process model (10) can be written as

$$y(t) = -a\int_0^t y(\tau)\,d\tau + b\int_0^t u(\tau)\,d\tau - bLu(t). \quad (11)$$

Define

$$\phi(t) = \left[-\int_0^t y(\tau)\,d\tau \;\; \int_0^t u(\tau)\,d\tau \;\; u(t) \right]^T,$$
$$\theta = \left[a \;\; b \;\; \beta \right]^T. \quad (12)$$

This case is equivalent to choose $L_1 = T_s$ in the first technique. The final estimate $\left\{ \hat{a}, \quad \hat{b}, \quad \hat{L} = \hat{\beta}/\hat{b} \right\}$ are obtained and the corresponding model $G_{LS2}(s)$.

4.3 Technique 3: Identification of FOPTD Model with Frequency Domain Constraints

In the third technique, equality constraints are used with the least-squares minimization ((Nelles, 2001)). The procedure solves a time least-squares problem submitted to a constraint on frequency. The constraint is obtained through the process frequency response on the first harmonic of the relay experiment signal. The frequency response is obtained computing the DFT of process input and output. In this frequency, the loop gain has approximately magnitude one. Assuming the data is grouped in a vector from yielding matrices Y and $\hat{\theta}$. The least-squares optimization problem is given by

$$J = \left(Y - \Phi\hat{\theta} \right)^T \left(Y - \Phi\hat{\theta} \right) \quad (13)$$

submitted to the

$$M\theta = \gamma. \quad (14)$$

which express the equality constraints in the time and frequency domains in a linear form.

The equality constraint is defined through the following regression vector which is obtained using the linear form 14 given by:

$$\hat{z} = x^T(\omega)\,\hat{\theta}$$

with

$$\hat{z} = j\omega\hat{G}(j\omega); \quad x^T(j\omega) = \left[-\hat{G}(j\omega) \;\; 1 \;\; -j\omega \right]$$
$$\theta = \left[a \;\; b \;\; \beta \right]^T$$

where ω is the crossover frequency estimated using the relay experiment. More frequencies points may have been used.

In this case, the least-squares optimization problem with constraint is equivalent to minimize in relation to $\hat{\theta}$ and λ the cost function given by

$$J = \left(Y - \Phi\hat{\theta}\right)^T \left(Y - \Phi\hat{\theta}\right) + \lambda(\gamma - M\theta) \quad (15)$$

By defining

$$E = 2\Phi^T\Phi$$
$$F = 2\Phi^T Y$$

The optimal solution has a closed-form

$$\begin{bmatrix} E & -M^T \\ M & 0 \end{bmatrix} \begin{bmatrix} \theta \\ \lambda^T \end{bmatrix} = \begin{bmatrix} F \\ \gamma \end{bmatrix}$$

which can be solved explicitly as

$$\lambda^T = \left[ME^{-1}M^T\right]^{-1}\left[\gamma - ME^{-1}F\right]$$
$$\hat{\theta} = [E]^{-1}\left(F + M^T\lambda^T\right)$$

The final estimate $\left\{\hat{a}, \quad \hat{b}, \quad \hat{L} = \hat{\beta}/\hat{b}\right\}$ are obtained and the corresponding model $G_{LS3}(s)$.

5. SIMULATION EXAMPLES

In this section the closed loop identification algorithms are applied to three processes. The cost function used to compare the estimates is

$$\varepsilon = \frac{1}{N}\sum_{k=0}^{N-1}\left[y(kT_s) - \widehat{y}(kT_s)\right]^2$$

where $y(kT_s)$ is the actual process output (with noise), while $\widehat{y}(kT_s)$ is the estimated process output from a closed loop simulation with the same controller and under the same step setpoint. In all experiments $T_s = 0.1s$, $k_{\max} = 50$ samples $(= 5s)$, $k_{\min} = 5$ samples $(= 0.5s)$, and the controller used is $C_1 = 1 + \frac{0.1}{s}$. White noise is added only to the output of the process. The processes and the results are shown below.

5.1 Example 1

In the first example it is used a FOPDT model

$$G_1(s) = \frac{0.14}{s + 0.12}e^{-0.95s}.$$

The noise variance is 0.02. The estimates are

$$G_{LS1}(s) = \frac{0.1329}{s + 0.1099}e^{-0.6397s}$$
$$G_{LS2}(s) = \frac{0.1354}{s + 0.1144}e^{-0.8381s}$$
$$G_{LS3}(s) = \frac{0.1368}{s + 0.1164}e^{-0.8326s}.$$

The mean squared errors are

$$\varepsilon_1 = 7.549e{-}05,\ \varepsilon_2 = 1.562e{-}05,\ \varepsilon_3 = 1.009e{-}05.$$

The estimated crossover frequency is $\widehat{w}_g = 0.1017$ and the processes have the following magnitudes in this frequency

$$|G_1(j\widehat{w}_g)| = 0.8901$$
$$|G_{LS1}(j\widehat{w}_g)| = 0.8878$$
$$|G_{LS2}(j\widehat{w}_g)| = 0.8848$$
$$|G_{LS3}(j\widehat{w}_g)| = 0.8851.$$

All techniques yields good results. The nyquist plot is shown in Fig. (2).

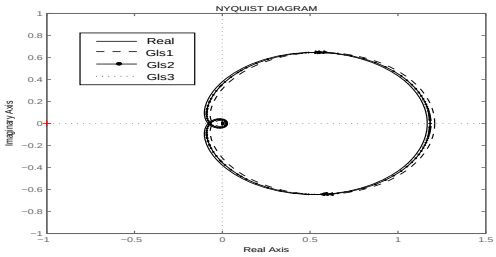

Fig. 2. Nyquist plot for process 1

In other simulation for the same $G_1(s)$, the noise variance is increased to 0.05. The estimates are

$$G_{LS1}(s) = \frac{0.1255}{s + 0.1001}e^{-0.3302s}$$
$$G_{LS2}(s) = \frac{0.1335}{s + 0.1133}e^{-0.9368s}$$
$$G_{LS3}(s) = \frac{0.1379}{s + 0.1179}e^{-0.9043s}.$$

The mean squared errors are

$$\varepsilon_1 = 2.83e{-}04,\ \varepsilon_2 = 2.93e{-}05,\ \varepsilon_3 = 2.532e{-}06.$$

The estimated crossover frequency is $\widehat{w}_g = 0.1018$. The process magnitude in this frequency are

$$|G_1(j\widehat{w}_g)| = 0.8901$$
$$|G_{LS1}(j\widehat{w}_g)| = 0.8786$$
$$|G_{LS2}(j\widehat{w}_g)| = 0.8762$$
$$|G_{LS3}(j\widehat{w}_g)| = 0.8849.$$

Increasing the noise variance the third technique provides a better fitting in the crossover frequency and the decreasing of the quadratic error. The loop gain experiment and nyquist plot are shown in Fig. (3) and (4).

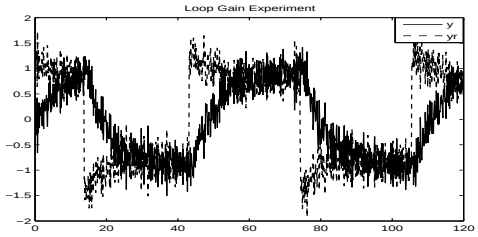

Fig. 3. Loop Gain Experiment for process 1.

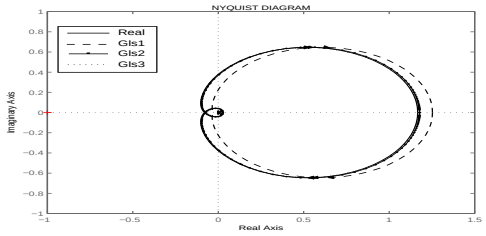

Fig. 4. Nyquist plot for process 1

5.2 Example 2

The process is now given by

$$G_2(s) = \frac{0.14}{(s+0.12)(s+1)} e^{-0.95s}.$$

The noise variance is 0.02. The estimates are

$$G_{LS1}(s) = \frac{0.1314}{s+0.1093} e^{-1.5325s}$$
$$G_{LS2}(s) = \frac{0.1276}{s+0.1057} e^{-1.4075s}$$
$$G_{LS3}(s) = \frac{0.1299}{s+0.1074} e^{-1.3854s}.$$

The mean squared errors are

$$\varepsilon_1 = 7.693e{-}05,\ \varepsilon_2 = 1.255e{-}04,\ \varepsilon_3 = 1.365e{-}04.$$

The estimated crossover frequency is $\widehat{w}_g = 0.0983$ and the process magnitudes

$$|G_2(j\widehat{w}_g)| = 0.8981$$
$$|G_{LS1}(j\widehat{w}_g)| = 0.8939$$
$$|G_{LS2}(j\widehat{w}_g)| = 0.8836$$
$$|G_{LS3}(j\widehat{w}_g)| = 0.8922.$$

Although there was a better fitting in the crossover frequency if compared with the second technique, the error have increased because the use of the constraint. The nyquist plot is shown in Fig. (5).

In other simulation for the same $G_2(s)$, the noise variance is increased to 0.05. The estimates are

$$G_{LS1}(s) = \frac{0.1254}{s+0.1017} e^{-1.2603s}$$
$$G_{LS2}(s) = \frac{0.1275}{s+0.1076} e^{-1.5736s}$$
$$G_{LS3}(s) = \frac{0.1319}{s+0.1104} e^{-1.5193s}.$$

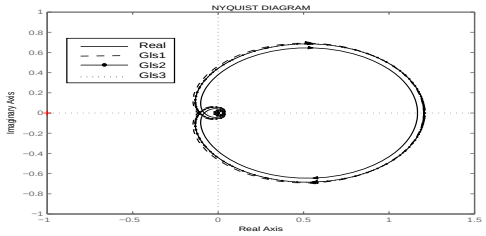

Fig. 5. Nyquist plot for process 2.

The mean squared errors are

$$\varepsilon_1 = 2.143e{-}04,\ \varepsilon_2 = 7.22e{-}05,\ \varepsilon_3 = 7.975e{-}05.$$

The estimated crossover frequency is $\widehat{w}_g = 0.0985$. The process magnitude in this frequency are

$$|G_2(j\widehat{w}_g)| = 0.8975$$
$$|G_{LS1}(j\widehat{w}_g)| = 0.8858$$
$$|G_{LS2}(j\widehat{w}_g)| = 0.8741$$
$$|G_{LS3}(j\widehat{w}_g)| = 0.8914.$$

Increasing the noise variance the third technique provides a better fitting in the crossover frequency and the decreasing of the quadratic error if compared with the first technique. The loop gain experiment and nyquist plot are shown in Fig. (6) and (7).

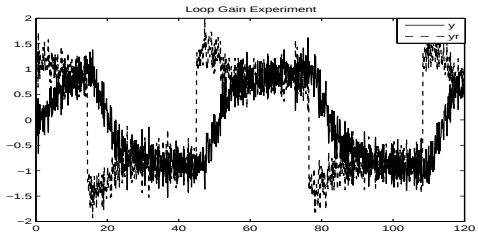

Fig. 6. Loop Gain Experiment for process 2.

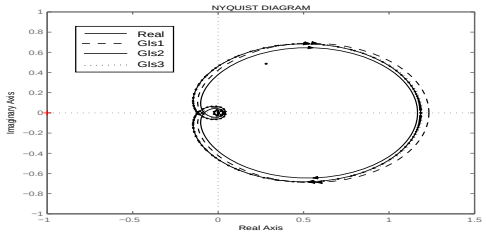

Fig. 7. Nyquist plot for process 2

5.3 Example 3

The process is now given by

$$G_3(s) = \frac{1}{(s+1)^8}.$$

The noise variance is 0.001.The estimates are

$$G_{LS1}(s) = \frac{0.2978}{s + 0.2929} e^{-4.8819s}$$
$$G_{LS2}(s) = \frac{0.1529}{s + 0.1357} e^{-2.8747s}$$
$$G_{LS3}(s) = \frac{0.1737}{s + 0.1569} e^{-2.3721s}.$$

The mean squared errors are

$$\varepsilon_1 = 0.0021,\ \varepsilon_2 = 0.0124,\ \varepsilon_3 = 0.0154.$$

In this case, the estimated crossover frequency is $\widehat{w}_g = 0.0985$ and the process magnitudes are

$$|G_3(j\widehat{w}_g)| = 0.9621$$
$$|G_{LS1}(j\widehat{w}_g)| = 0.9639$$
$$|G_{LS2}(j\widehat{w}_g)| = 0.9120$$
$$|G_{LS3}(j\widehat{w}_g)| = 0.9377.$$

The constrained least-square minimization if compared with the second technique produces a data fitting with a larger quadratic error despite a closer model in the crossover frequency to the real process. The loop gain experiment and nyquist plot are shown in Fig. (8) and (9).

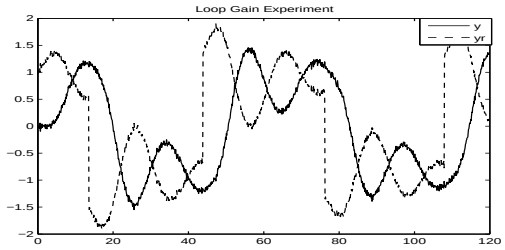

Fig. 8. Loop Gain Experiment for process 3.

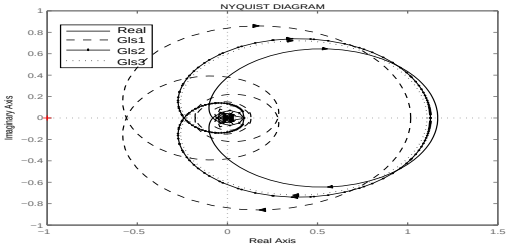

Fig. 9. Nyquist plot for process 3.

6. CONCLUSIONS

In this paper three techniques for the identification of continuous-time FOPTD models from closed loop step response was presented. One of the techniques use frequency domain information as equality constraints. Structures for identification in closed loop were also discussed. The use of constrains provided a better fitting in the crossover frequency, a good issue in closed loop identification and controller design.

REFERENCES

Åström, Karl Johan and Tore Hägglund (1995). *PID Controllers: Theory, Design and Tuning*. 2nd ed.. Instrument Society of America. Research Triangle Park, North Carolina.

Coelho, F. S. and P. R. Barros (2003). Continuous-time identification of first-order plus dead-time models from step response in closed loop. 13th IFAC Symposium on System Identification. Rotterdam (The Netherlands).

de Arruda, Gustavo Henrique Machado and Péricles Rezende Barros (2003). Transfer function relay based frequency points estimation. *Automatica* **39**(2), 309–315.

Forssell, U. and L. Ljung (1999). Closed-loop identification revistited. *Automatica* **35**(7), 1215–1241.

Ljung, Lennart (1999). *System Identification: Theory for the User*. 2nd ed.. Prentice Hall. Upper Saddle River, NJ.

Marchetti, G., C. Scali and D. R. Lewin (2001). Identification and control of open-loop unstable processes by relay methods. *Automatica* **37**, 2049–2055.

Mensler, M. Mensler (1999). Analyse et étude comparative de méthodes d'identification des systèmes à represéntation continue. Développement d'une boîte à outilis logicielle. Thèse du doctorad. Université Henry Poincaré Nancy 1. Nancy,France.

Nelles, Oliver (2001). *Nonlinear System Identification*. 1st ed.. Springer-Verlag. Berlin, Germany.

Schei, Tor Steinar (1992). A method for closed loop automatic tuning of PID controllers. *Automatica* **28**(3), 587–591.

Sudaresan, K.R. and P.R. Krishnaswamy (1977). Estimation of time delay time constant parameters in time, frequency, and laplace domains. India.

Wang, Q.G. and Y. Zhang (2001). Robust identification of continuous systems with dead-time from step responses. *Automatica* **37**(3), 377–390.

Wang, Q.G., Q. Bi, W.J. Cai, E.L. Lee, C.C. Hang and Y. Zhang (1999). Robust identification of first-order plus dead-time model from step response.. *Control Engineering Practice* (7), 71–77.

Wang, Qing-Guo, Bin Hwang and Xin Guo (2000). Auto-tuning of tito decoupling controllers from step tests. *ISA Transactions* **39**, 407–418.

ADCHEM 2006

International Symposium on Advanced Control of Chemical Processes
Gramado, Brazil – April 2-5, 2006

SENSITIVITY OF BIFURCATION TRAITS TO MODEL PARAMETERS IN POLY-ß-HYDROXYBUTRYRATE PRODUCTION

Mark A. Pinto *,1 Charles D. Immanuel *,2

Centre for Process Systems Engineering, Department of Chemical Engineering, Imperial College London, Exhibition Road, London SW7 2AZ, United Kingdom

Abstract: There is growing interest in the chemical engineering community in the development of environmentally friendly products such as biopolymers. Poly-ß-hydroxybutyrate (PHB) is an important biopolymer whose commercial application is still limited due to the high costs associated with its production. This paper examines a continuous bioreactor proposed for the production of PHB. The in.uence of minor variations in the kinetic parameters of a simple cybernetic model formulated is examined. It is shown that minor variations in these parameters can have signi.cant impacts on the bifurcation analyses obtained.

Keywords: Biopolymers, Continuous Process, Bifurcation Analysis, Cybernetic Modelling

1. INTRODUCTION

Over the past few decades, society's dependence on man-made materials, and polymers in particular, has increased dramatically. However, the non-biodegradable nature of these products has resulted in a situation where we are now generating millions of tons of municipal waste every year. A promising solution to this problem is to use biodegradable materials which do not need recycling and could be disposed off in landfills without fear of soil contamination. Biopolymers are among the important biodegradable materials being produced today. They are polymers produced from biological sources such as plants and micro-organisms. An important class of biopolymers is that of the natural polyesters, polyhydroxyalkanoates (PHAs). Since they were first discovered, PHAs have become one of the largest groups of thermoplastic polymers known with over 100 different types currently produced from a variety of monomers (Williams *et al.*, 1999). They have a wide range of applications from biodegradable plastics to biomedical engineering. As a result, they are the subject of much attention within the chemical engineering community and a lot of research has been undertaken towards improving the production of these biopolymers (Lee *et al.*, 1999).

The metabolic processes by which PHAs are accumulated by bacterial cells is reasonably well understood. Bacteria synthesise PHAs as a carbon and energy reserve material when their growth is limited due to the unavailability of a nutrient such as nitrogen, sulphur or phosphorous (Anderson and Dawes, 1990). Although in theory, PHB production can be triggered by engineering a deficiency in one of several nutrients, it is normal practice to employ ammonia as the limiting nutrient under excess glucose (Anderson and Dawes, 1990). Under these conditions, the cells tend to accumulate a large amount of the polymer.

In spite of the significant amount of research that has been undertaken, the industrial production of PHB has been limited. One of the problems preventing the wide-spread commercial application of PHB is its high production cost, the most significant expense being that of the carbon source (Lee *et al.*, 1999). Therefore, recent efforts have focussed on genetically modifying microorganisms such as *Escherichia coli* to produce PHB. The advantages of using such microorganisms are that they grow fast and can be lysed easily, thereby reducing production time and costs (Madison and Huisman, 1999).

[1] Supported by Universities UK through the Overseas Research Students Awards Scheme (ORSAS)
[2] Corresponding Author: Fax: +44 (0)20 7594 6606 email: *c.immanuel@imperial.ac.uk*

While the genetic modifications described above hold significant promise, efforts at maximising the efficiency of existing processes for producing PHB are also invaluable as insights into these processes may help in the formulation of future PHB production strategies. Progress in the fields of flow cytometry and nonlinear model predictive control is enabling improved process monitoring and control. However, for these developments to significantly improve the efficiency of a process, a systematic analysis needs to be undertaken to determine the operating conditions under which maximum productivity is obtained.

Bifurcation theory is a very useful tool in this regard as it provides insight into features such as steady states and limit cycles which can in turn help determine the optimal operating conditions for a given process. A bifurcation analysis employs a mathematical model of the process being studied to predict stable and unstable stationary and periodic steady states. An implicit assumption is that the model employed 'is' the process, *i.e.* the model is an ideal and exact representation of the process. A mathematical model of any process relies on certain parameters to qualitatively and quantitatively simulate experimental observations. These parameters are usually estimated from a given set of experimental data. However, unmeasurable process disturbances often reduce the accuracy of the data and minor discrepancies are often observed between the model predictions and the experimental data. A second consideration is that, unlike parameters in empirical models that are estimated using a wealth of data, parameters in mechanistic models are often obtained from a limited data set.

Bifurcation analysis has been employed to study a range of biological processes. In these cases, the results obtained from the bifurcation analysis corresponded at least qualitatively with experimentally observed phenomena. Based on the successes of these studies, one might be tempted to accept the findings of a bifurcation analysis of a particular process without performing sufficient experiments. The objective of this paper is to demonstrate the potential dangers of making such a decision by examining the effect of variations in parameter values on predictions of the bifurcation analysis.

2. CYBERNETIC MODELLING OF PHB ACCUMULATION

While several approaches are available to model PHB production, one modelling approach that has been very successful in describing biological systems is the cybernetic modelling approach (Kompala *et al.*, 1986) which was originally formulated to describe 'the Diauxie effect' first observed by Monod. In this approach, cells are construed to be optimal strategists that seek to maximise a particular goal (usually cell growth) given the existing environmental conditions. Two cybernetic models of PHB synthesis in microorgranisms are available in the literature (Yoo and Kim, 1994; Gadkar *et al.*, 2003). The first model (Yoo and Kim, 1994) assumes that cells are composed of two components, namely residual biomass and PHB. Though this model was successful in predicting PHB production in the bacterium *Alcaligenes eutrophus*, it failed to take into consideration the underlying metabolic processes. In order to address this deficiency, Gadkar and co-workers (Gadkar *et al.*, 2003) formulated a detailed cybernetic model that takes into consideration the metabolic pathways by which the carbon and nitrogen sources are utilised for cell growth and PHB synthesis. In this paper, a model of intermediate complexity was formulated accounting for the underlying metabolic processes.

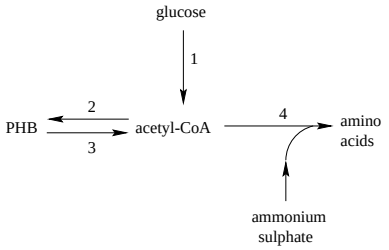

Fig. 1. New cybernetic model of PHB synthesis in *Alcaligenes eutrophus*.

The model formulated here (see Figure 1) considers four reactions, each representing one of the pathways in the detailed model described above (Gadkar *et al.*, 2003). In this scheme, the first reaction represents the glycolytic pathway and accounts for glucose assimilation and conversion to acetyl CoA. The second reaction represents the PHB synthesis pathway while the third reaction represents the reverse phenomenon. The last reaction accounts for nitrogen assimilation and conversion, together with acetyl CoA, to amino acids. Cells are assumed to be comprised of PHB and residual biomass. Residual biomass is defined as all metabolites excluding PHB present in the cell. Acetyl-CoA and amino acids are assumed to be the precursors for cell growth. The rates of these reactions and for the reaction producing residual biomass are assumed to follow variations of Monod's kinetics.

Two sets of cybernetic variables are employed in the model. The first set seeks to maximise the production of acetyl-CoA from reactions 1 and 3. The second set of cybernetic variables seeks to maximise the production of PHB and residual biomass from reactions 2 and 4. However, in defining the corresponding variables, the reaction rates

corresponding to glucose and ammonium sulphate assimilation are employed. This strategy was used with the reasoning that, from a biological perspective, the choice of which reaction to maximise is dependent not on the rates of production of PHB and amino acids from acetyl-CoA but on the availability of glucose and ammonium sulphate.

The kinetic parameters were first selected so that the model was in qualitative agreement with the biology of the process. A continuous bioreactor was then considered and bifurcation diagrams were constructed with the dilution rate as the chosen bifurcation parameter. The aim of this exercise was to evaluate the ability of the chosen model structure to capture intricate bifurcation behaviour. In constructing these diagrams, a steady state was first identified by simulation. The steady state locus around this point was traced using the bifurcation analysis software AUTO (Doedel, 2001). The bifurcation diagrams thus obtained for different glucose feed concentrations are shown in Figures 2. The ammonium sulphate feed concentration was kept constant at 2.54 g/l. From Figure 2a, it can be seen that at low glucose feed concentrations, the reactor rapidly undergoes washout while at higher glucose feed concentrations the residual biomass concentration remains relatively constant. Further, multiple steady states are observed separated by a region of instability. With respect to the process productivity, from Figure 2b it can be seen that the productivity increases sharply with an increase in the glucose feed concentration. This result is in qualitative agreement with the biology of the system as when the bacteria are exposed with an excess of glucose, the excess substrate is channeled into PHB. Based on the results of these analyses, it can be concluded that the model, though relatively simple, is capable of explaining complex bifurcation phenomena such as steady-state multiplicity.

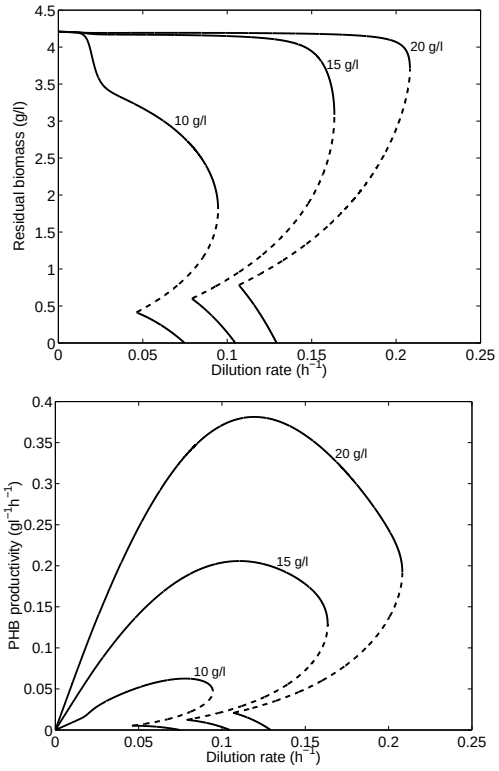

Fig. 2. Bifurcation diagrams for the model formulated for different feed glucose concentrations. Randomly selected values for the kinetic parameters are used.

3. BIFURCATION ANALYSIS OF A CONTINUOUS REACTOR PRODUCING PHB

In order for the model to be quantitatively accurate, reasonable values of the model parameters must be used. The experimental data of Yoo and Kim (Yoo and Kim, 1994) (56 experimental data points) were used as a reference in finding the values of the 11 kinetic parameters in the model. Values were initially obtained by trial-and-error and were refined using least squares parameter estimation in gPROMS^{TM} (Process Systems Enterprise) (see Figures 3).

In this process, the two main control variables are the dilution rate and the ratio of the concentrations of glucose and ammonium sulphate in the feed stream. A bifurcation analysis was first undertaken with the glucose feed concentration as the bifurcation parameter. The bifurcation diagrams thus obtained are shown in Figures 4. The dilution rate and the feed concentration of ammonium sulphate were kept constant at 0.01 h^{-1} and 2.54 g/l respectively. From Figure 4a, it can be seen that when the feed concentration of glucose is very low, there exists no stable steady state for the model. This is consistent with the biology of the system as if insufficient glucose is provided to the cells, then the growth rate of cells will be less

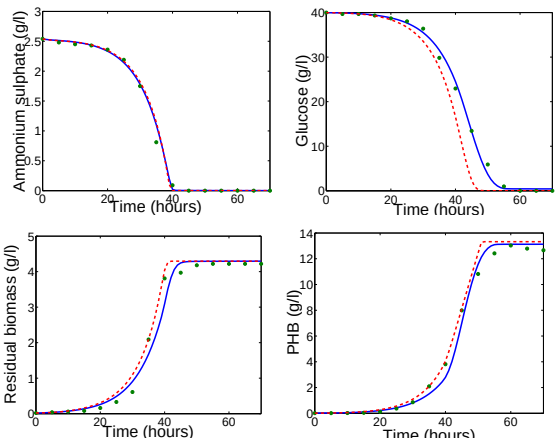

Fig. 3. Comparison of the simulation results of the formulated model with published experimental data. Legend: —— estimated parameters, - - - modified parameters.

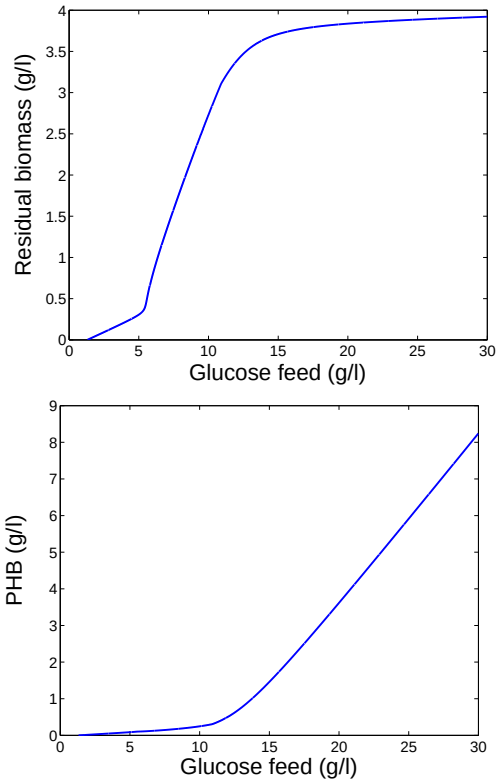

Fig. 4. Bifurcation diagrams for a single reactor producing PHB with respect to the feed concentration of glucose.

than that required to prevent reactor wash out. Beyond a threshold glucose concentration, the concentration of residual biomass in the reactor increases sharply with an increase in the glucose feed concentration while from Figure 4b it can be seen that very little, if any, PHB accumulation takes place. This is again reasonable as when the carbon source is not in excess, in general, no PHB accumulation takes place. Further, under these conditions, an increase in the amount of substrate available corresponds to a proportional increase in the growth rate of the cells.

Above a second threshold glucose concentration, the behaviour of the system undergoes a significant change as can be seen from Figures 4. At these high feed concentrations of glucose, the concentration of residual biomass remains relatively independent of the glucose feed concentration while the PHB concentration increases linearly. This is, again, a perfectly reasonable observation as these high glucose feed concentrations correspond to an excess of carbon source. Under such conditions, the cells channel the excess substrate to produce PHB while the residual biomass content remains relatively constant. It has been observed that glucose concentrations need to be maintained in the region of 10 to 20 g/l to achieve high cell and PHB concentrations (Kim *et al.*, 1994). As this is evident from Figures 4, it

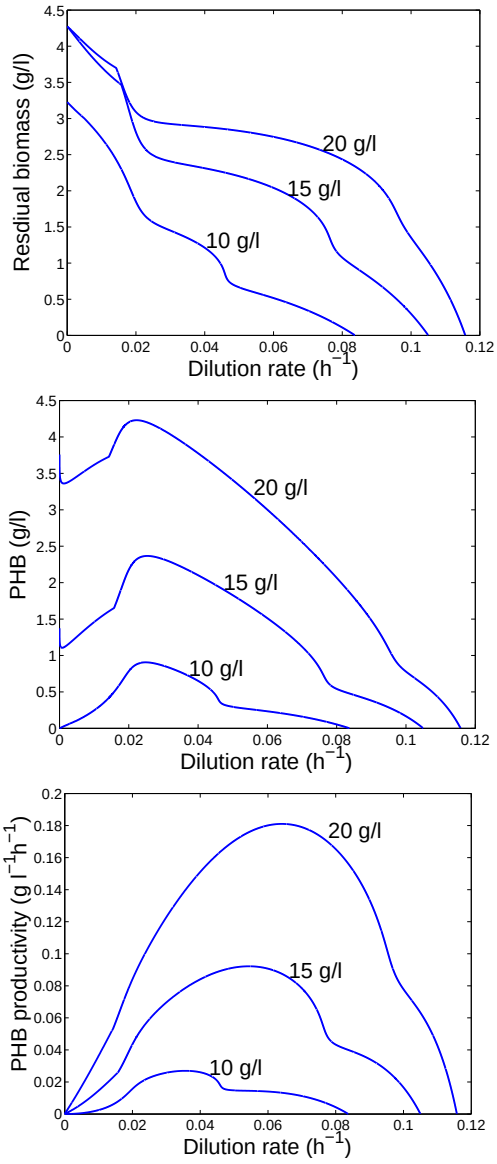

Fig. 5. Bifurcation diagrams for a single reactor producing PHB for different feed concentrations of glucose with respect to the dilution rate.

can be said that the model formulated here is a reasonably accurate representation of the process under consideration.

A bifurcation analysis of the model formulated was then undertaken with the dilution rate to the reactor as the bifurcation parameter. The bifurcation diagrams obtained for different feed concentrations of glucose are depicted in Figures 5. The feed concentration of ammonium sulphate was again kept constant at 2.54 g/l. Figure 5a shows the dependence of the concentration of residual biomass on the dilution rate. It can be seen that, for a given feed concentration of glucose, the concentration of residual biomass decreases with an increase in the dilution rate until the reactor undergoes washout. Further, in this model, the rate at which the residual biomass decreases is not regular. The reason for this unusual behaviour

has not been ascertained. Another important observation is that multiple steady states are not encountered in any region. This observation was validated by undertaking exhaustive simulations, each starting at a different initial condition. Also, decreasing the glucose feed concentration resulted in a decrease in the residual biomass concentration for a given dilution rate. This is perfectly reasonable as decreasing the amount of glucose fed to the reactor has a proportional and direct effect on the growth rate of cells.

The variation of PHB concentration in the reactor with dilution rate is qualitatively different from that of the residual biomass, as seen in Figure 5b. In this case, the concentration of PHB first increases with an increase in the dilution rate before undergoing a decrease. However, the decrease is more rapid than for the case of residual biomass. Given the reaction network adopted for this system, this behaviour is reasonable as it is similar to that of intermediates and products in series reactions occurring in continuous reactors. Also, as expected, decreasing the glucose feed concentration has a significant effect on the PHB concentration in the reactor. This is reasonable as, when faced with lower glucose concentrations, cells tend to accumulate less PHB. This result shows that the model, though relatively simple, is qualitatively accurate.

From the point of view of process design and control, the most important variable is the PHB productivity, which is the rate at which PHB is produced in the reactor. From Figure 5c, it can be seen that, initially, the PHB productivity increases with an increase in the dilution rate before undergoing a rapid decrease at high dilution rates. Further, by comparing Figures 5b and 5c, it can be seen that the dilution rate at which the PHB productivity is maximum does not necessarily correspond to the dilution rate at which the PHB concentration in the reactor is maximum. These observations are reasonable as the productivity of a reactor is dependent not just on the concentration of the desired product in the reactor, but also on the dilution rate. The effects of reducing the glucose feed concentration to the reactor are best observed in Figure 5c. It can be seen that at high glucose feed concentrations, doubling the glucose feed concentration results in a corresponding increase in PHB productivity. However, at low glucose concentrations, *i.e.* when glucose is not in excess or barely so, there is almost no production of PHB.

4. INFLUENCE OF MODEL PARAMETERS ON BIFURCATION ANALYSES

Two important considerations in fitting a model to experimental data are the amount and quality of the available data and the number of model parameters to be estimated. The quality of available data is dependent on the accuracy of the measurement techniques and reproducibility of the experiments. While the latter is usually rigorously accounted for, unmeasurable disturbances in the operating conditions can result in minor variations in the measured data. These variations introduce uncertainty into the estimated values of the parameters and, consequently, possible inaccuracies in the bifurcation analyses. Secondly, a sufficient amount of data is necessary in order to obtain confidence in the estimated values of parameters. If insufficient data is available, then multiple sets of parameter values may be obtainable giving the same accuracy with respect to the ability of the model to reproduce experimental observations.

In this section, the sensitivity of the bifurcation behaviour to uncertainty in the model parameters is discussed. The parameter values are of the same order of magnitude as those used in the model above with the exception of the constants used in the residual biomass growth rate (data not shown). While the glucose concentration shows the largest difference, the inaccuracy is still not very significant (see Figures 3). Therefore the model can be said to be almost as accurate as the model used above.

The bifurcation diagrams obtained for the case of a single reactor using these parameter values are shown in Figures 6. Here, the dilution rate is the chosen bifurcation parameter. The feed concentrations of glucose and ammonium sulphate are kept constant at 20 g/l and 2.54 g/l respectively. The most significant difference between this analysis and that depicted in Figures 5 is with respect to the concentration of residual biomass in the reactor. In the previous case, the concentration of residual biomass only decreased with an increase in the dilution rate, irrespective of the range of the dilution rate. However, in this case, the residual biomass first increases to a maximum before decreasing. Further, the dilution rate at which washout occurs is greater than that in the earlier case.

The bifurcation diagrams with respect to both PHB concentration and PHB productivity are qualitatively similar for both cases. However, in this case, the maximum productivity achievable is almost 50% greater than that achievable in the first case. This is an extremely important difference as analyses such as these could possibly be used in the early stages of process design. Inaccurate predictions in process variables at these times could significantly affect the estimated operating costs. In the worst case, a significant overprediction could result in financial losses. This simple analysis thus shows how important it is

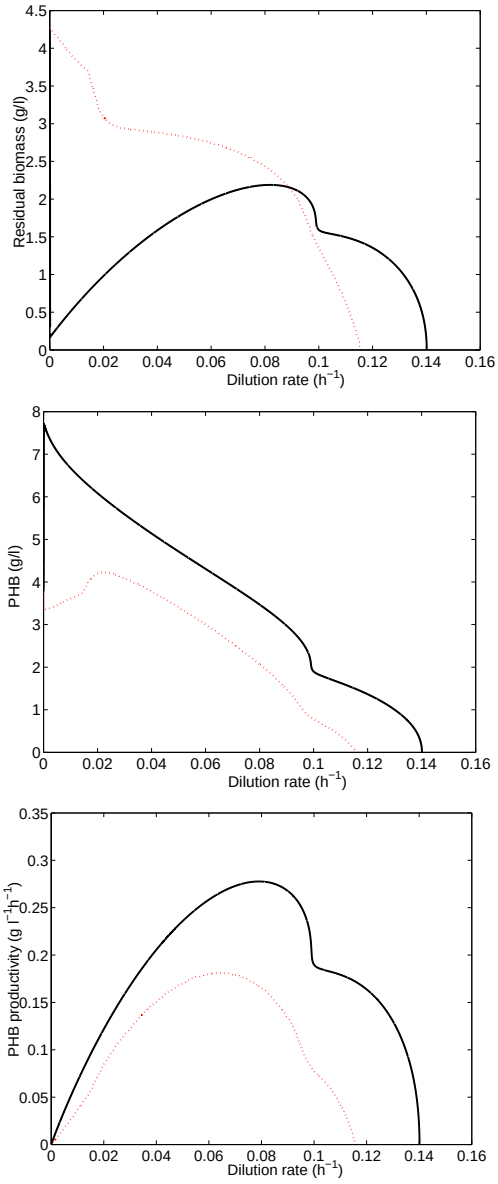

Fig. 6. Bifurcation diagrams for a single reactor producing PHB using the model with modified kinetic parameters. The dotted lines correspond to the model with estimated parameters.

to have accurate values for the model parameters and hence the importance of both detailed experimentation and robustness considerations in design and control.

5. CONCLUSIONS

Biopolymers are gaining increasing importance due to the various advantages they offer over synthetic polymers. However, their commercial application is still limited due to the high costs associated with their production and a careful analysis of the production processes available needs to be undertaken in order to determine the optimal operating conditions. Bifurcation analysis is a useful tool for conducting such an analysis. In undertaking a bifurcation analysis, a dynamic model is usually employed to represent the process. In this study, a cybernetic modelling framework was adopted. The model structure employed has the capabilities of identifying complex and intricate bifurcation behaviour should they occur in the process (depending on model parameters and design/operation variables). Bifurcation studies were performed for the production of PHB, with the dilution rate as the bifurcation variable. Further, the influence of model parameters on bifurcation results was examined. It was observed that minor variations in the values of the kinetic parameters had a significant effect on the predictions obtained. These results evince the importance, on the one hand, of detailed experimentation for model validation and parameter estimation and, on the other hand, robustness considerations in design and control.

REFERENCES

Anderson, A. J. and E. A. Dawes (1990). Occurrence, metabolism, metabolic role, and industrial uses of bacterial polyhydroxyalkanoates. *Microbiol. Rev.* **54**, 450–472.

Doedel, E. J. (2001). *AUTO 2000*. http://indy.cs.concordia.ca/auto/.

Gadkar, K. G., F. J. Doyle, T. J. Crowley and J. D. Varner (2003). Cybernetic model predictive control of a continuous bioreactor with cell recycle. *Biotech. Prog.* **19**, 1487–1497.

Kim, B. S., S. C. Lee, S. Y. Lee, H. N. Chang, Y. K. Chang and S. I Woo (1994). Production of poly(3-hydroxybutyric acid) by fed-batch culture of *Alcaligenes eutrophus* with glucose concentration control. *Biotech. Bioeng.* **43**, 892–898.

Kompala, D. S., D. Ramkrishna, N. B. Jansen and G. T. Tsao (1986). Investigation of bacterial growth on mixed substrates: experimental evaluation of cybernetic models. *Biotech. Bioeng.* **28**, 1044–1055.

Lee, S. Y., J. Choi and H. H. Wong (1999). Recent advances in polyhydroxyalkanoate production by bacterial fermentation: mini-review. *Int. J. Biol. Macromol.* **25**, 31–36.

Madison, L. L. and G. W. Huisman (1999). Metabolic engineering of poly(3-hydroxyalkanoates): From DNA to plastic. *Microbiol. Mol. Biol. Rev.* **63**, 21–53.

Williams, S. F., D. P. Martin, D. M. Horowitz and O. P. Peoples (1999). PHA applications: addressing the price performance issue. I. Tissue engineering. *Int. J. Biol. Macromol.* **25**, 111–121.

Yoo, S. and W.-S. Kim (1994). Cybernetic model for synthesis of poly-β-hydroxybutyric acid in *Alcaligenes eutrophus*. *Biotech. Bioeng.* **43**, 1043–1051.

Session 1.3

Model Predictive Control

An Analytical Solution to Multivariable Nonlinear MPC for Second–Order Laguerre Systems

A. L. Antoine and R. S. Parker
University of Pittsburgh

Feasible Model Predictive Control with Bounded Disturbances

M. Hovd
Norwegian University of Science and Technology

Nonconvex Optimization and Robustness in Realtime Model Predictive Control

D. DeHaan and M. Guay
Queen's University

Extended Robust Model Predictive Control for Integrating Systems

A.H. González, J.L. Marchetti and D. Odloak
Universidad Nacional del Litoral
University of São Paulo

Generalized Predictive Control in Fast–rate Single–rate and Input Multiplex Type Multirate System

T. Sato and A. Inoue
University of Hyogo

ADCHEM 2006

International Symposium on Advanced Control of Chemical Processes
Gramado, Brazil – April 2-5, 2006

AN ANALYTICAL SOLUTION TO MULTIVARIABLE NONLINEAR MPC FOR SECOND-ORDER LAGUERRE SYSTEMS

Abigale L. Antoine * **Robert S. Parker** *,1

* *Department of Chemical and Petroleum Engineering, University of Pittsburgh, Pittsburgh, PA*

Abstract: An analytical solution to the multivariable (two-input, two-output) nonlinear model predictive control (NMPC) problem was derived for systems represented by (Volterra-)Laguerre models. The standard two-norm squared NMPC objective function was employed, and the minimization was carried out with $m = 1$ and over the prediction horizon, p. The polynomial structure of the system model yielded a polynomial objective function for the NMPC problem. Differentiation of this scalar objective function with respect to the manipulated input variables provided the first-order necessary conditions for optimality: a set of n_u (equal to the number of inputs) coupled polynomials. Via Gröbner basis transformation, this set of polynomials was converted to a structured set of higher-order polynomials solvable via roots calculations and back-substitution. The algorithm was tested using a two-input two-output polymerization case study.

Keywords: nonlinear model predictive control, Volterra models, Laguerre functions, Gröber basis, multivariable systems

1. INTRODUCTION

Model predictive controllers are a class of high-performance control algorithms garnering intense academic and industrial interest (Kouvaritakis and Cannon, 2001). Algorithms based on linear models may effectively control some nonlinear systems (Stack and Doyle III, 1997; Hernjak and Doyle III, 2004). However, a higher degree of performance may be achieved by employing a nonlinear algorithm, and hence a nonlinear model, on the grounds that model quality is correlated with achievable controller performance (Morari and Zafiriou, 1989). Nonlinear models, and hence, nonlinear algorithms are especially necessary for systems displaying input multiplicity (or other even-order polynomial-like behavior), as linear integrating controllers cannot stabilize these processes at the process optimum (Morari, 1983). The construction of nonlinear models, from the fundamental process physics, is an active research area (Doyle III *et al.*, 2002*a*; Daoutidis and Henson, 2002), but these models may take significant time to develop. Furthermore, the structure of these models may make the implicit inversion problem of NMPC more complicated due to their size or by generating performance objectives that are nonconvex. This, in turn, may lead to algorithms that become trapped in local minima (Zheng, 1997). Objective function and model nonlinearities, the root cause of the aforementioned nonconvexity, may inherently limit the ability of an NMPC algorithm to deliver optimal performance.

The ability to analytically solve optimization problems eliminates the above nonconvexity concerns. Careful selection of the objective function, as well as the system model structure, leads to nonlinear optimization problems with desirable properties. This is the nonlinear analog to the original use of step

[1] To whom correspondence should be addressed: rparker@pitt.edu; +1-412-624-7364; 1249 Benedum Hall, Pittsburgh, PA 15261 USA

response models for linear MPC – the model structure facilitates the solution of the optimization problem. The use of models with polynomial structure, such as the Volterra or Laguerre models, allows the explicit expansion of the optimization objective as a polynomial in the manipulated variables (Dumont and Fu, 1993*a*; Dumont *et al.*, 1994; Parker and Doyle III, 2001; Parker, 2002*b*). In the single-input single-output (SISO) case, NMPC for (Volterra-)Laguerre systems has been previously posed and solved (semi-)analytically in a variety of formulations. Dumont and co-authors employed a steady state tracking objective (minimize error at the end of the prediction horizon) with $m = 1$ (where m is the manipulated variable move horizon in MPC) and did not weight the manipulated variable (1993*a*; 1994). This work was extended by Parker and Doyle III to the case with input penalty and error calculation over the entire prediction horizon (2001). Further extensions to the $m > 1$ case were discussed by Parker using: (i) local linearization for future input moves (2002*a*); and analytical solution for $m = 2$ using Gröbner basis transformation (2002*b*). The present work extends the Gröbner basis NMPC solution methodology for MIMO (Volterra-)Laguerre systems

2. LAGUERRE MODEL STRUCTURE

The present work focuses on second-order multivariable systems of Laguerre structure. This includes Laguerre models that are derived from Volterra series models (Zheng and Zafiriou, 1995), the so-called Volterra-Laguerre models. The multivariable discrete time Laguerre model has the following state space structure (Schetzen, 1980):

$$\ell(k+1) = A(\alpha)\ell(k) + B(\alpha)u(k) \quad (1)$$

$$y(k) = C\ell(k) + L_b^T(k)DL(k) \quad (2)$$

Here $\ell(k)$, $u(k)$, and $y(k)$ are vectors of dimension n_ℓ, n_u, and $n_y \times 1$, respectively. The parameter α is the Laguerre pole, taking on values in the range $[0,1)$, and establishes the dominant time constant of the system. Matrix A is square and of dimension n_ℓ. The input matrix B is of dimension $n_\ell \times n_u$, and the linear output matrix, C^T is of dimension $n_y \times n_\ell$. The second-order output term is composed of matrix $D = blockdiag\{D_1, D_2\}$, where the subscripts denote the output corresponding to the second-order effect. The vector $L(k) = \left[\ell^T(k), \ell^T(k), ..., \ell^T(k)\right]^T$ is composed of n_y $\ell(k)$ terms stacked vertically, thereby having dimension $n_\ell \bullet n_y \times 1$. $L_b(k)$ is the block diagonal version of $L(k)$, where the $\ell(k)$ vectors are along the diagonal, rather than vertically stacked, and $L_b(k)$ has dimension $n_\ell \bullet n_y \times n_y$. It is straightforward to convert (1) to a Δu formulation, as follows:

$$\ell(k+1) = A(\alpha)\ell(k) + B(\alpha)u(k-1) + B(\alpha)\Delta u(k) \quad (3)$$

This structure facilitates controller synthesis as the state equations can be written in terms of two contributions: (i) variables whose values are known at time k; and (ii) the input changes at time k, as follows:

$$\ell(k+1) = \begin{bmatrix} A & B \end{bmatrix} \begin{bmatrix} \ell(k) \\ u(k-1) \end{bmatrix} + B\Delta u(k) \quad (4)$$

The future state prediction, over a future horizon of length p, is constructed as follows (similar to (Muske and Rawlings, 1993)):

$$\begin{bmatrix} \ell(k+1|k) \\ \ell(k+2|k) \\ \vdots \\ \ell(k+p|k) \end{bmatrix} = \begin{bmatrix} A & \bar{A}_1 B \\ A^2 & \bar{A}_2 B \\ \vdots & \vdots \\ A^p & \bar{A}_p B \end{bmatrix} \begin{bmatrix} \ell(k) \\ u(k-1) \end{bmatrix} + \begin{bmatrix} \bar{A}_1 B \\ \bar{A}_2 B \\ \vdots \\ \bar{A}_p B \end{bmatrix} \Delta u(k) \quad (5)$$

$$\mathscr{L}(k+1|k) = \mathscr{A}H(k) + \mathscr{B}\Delta u(k) \quad (6)$$

$$\bar{A}_n = \sum_{i=1}^{n} A^{i-1} \quad \forall n \geq 1 \quad (7)$$

Similarly, the output prediction over a similar horizon is given as:

$$\mathscr{Y}(k+1|k) = \mathscr{C}^T\mathscr{L}(k+1|k) + \mathscr{L}_b^T(k+1|k)\mathscr{D}\mathscr{L}(k+1|k) \quad (8)$$

Here, $\mathscr{Y}(k+1|k) = [y(k+1)\, y(k+2) \ldots y(k+p)]^T$ and the matrices $\mathscr{C}^T$ and $\mathscr{D}$ are block-diagonal matrices composed of p C^T and D matrices, respectively. The matrix $\mathscr{L}_b^T(k+1|k)$ is a block-diagonal matrix having n_y repetitions of $\ell(k+i|k)$ per sub-block, with p total sub-blocks (*i.e.*, $i \in [1,p]$).

3. CONTROLLER SYNTHESIS

The present work employs the following standard two-norm squared objective function based on the input change, $\Delta\mathscr{U}(k|k)$:

$$\min_{\Delta\mathscr{U}(k|k)} \|\Gamma_y[\mathscr{R}(k+1) - \mathscr{Y}(k+1|k)]\|_2^2 + \|\Gamma_u\Delta\mathscr{U}(k|k)\|_2^2 \quad (9)$$

The vector $\mathscr{R}(k+1)$ is the output reference trajectory, over the horizon p, and the n_u manipulated variables are given by $\Delta\mathscr{U}(k|k)$. Setpoint tracking and manipulated variable movement are weighted by Γ_y and Γ_u, respectively. Substituting (6) into (8), and the result into (9), yields the following optimization problem:

$$\min_{\Delta\mathscr{U}(k|k)} F\left(\Delta\mathscr{U}(k|k), \ell(k), u(k-1), r(k+1), y_m(k)\right) \quad (10)$$

At each time, $y_m(k)$ is measured from the process, $\ell(k)$ is known from the process model, $u(k-1)$ is the

input value implemented at the previous time step, and $r(k+1)$ is specified (thereby specifying $\mathscr{R}(k+1)$). The scalar objective function $F(\bullet)$ is composed of a collection of matrix multiplications dependent on the Laguerre model (6) and (8).

Equation (10) is a nonlinear programming (NLP) problem, which is solvable by standard NLP techniques (Biegler, 1998). In some cases, these NLP solution techniques may fail to converge to the global optimum; this is most easily observed for SISO systems having input multiplicity (Parker and Doyle III, 2001). Hence, an analytical solution to (10) could provide superior performance. Differentiating $F(\bullet)$ with respect to $\Delta\mathscr{U}(k|k)$ and setting the resulting equations equal to zero yields the points at which the objective function has zero slope, *i.e.* its minima, maxima, and saddle points. In the present case, with $m=1$, the differentiation yields a number of equations equal to the number of manipulated variables, each having the following structure:

$$\begin{aligned} f_i = {} & p_{i30}\Delta u_1^3(k|k) + p_{i20}\Delta u_1^2(k|k) + p_{i10}\Delta u_1(k|k) \\ & + p_{i21}\Delta u_1^2(k|k)\Delta u_2(k|k) + p_{i01}\Delta u_2(k|k) + p_{i00} \\ & + p_{i11}\Delta u_1(k|k)\Delta u_2(k|k) + p_{i02}\Delta u_2^2(k|k) \\ & + p_{i12}\Delta u_1(k|k)\Delta u_2^2(k|k) + p_{i03}\Delta u_2^3(k|k) \\ = {} & 0 \quad \forall i \in [1, n_u] \end{aligned} \tag{11}$$

The polynomial coefficients p_{ivw}, where v and w denote the polynomial order of $\Delta u_1(k|k)$ and $\Delta u_2(k|k)$, respectively, are functions of $\ell(k)$, $u(k-1)$, and $r(k+1)$. The i subscript denotes the manipulated variable with respect to which the partial derivative ($f_i = \frac{\partial F}{\partial \Delta u_i}$) was taken. At each sample time the polynomial coefficients are recalculated. The explicit functionality of these coefficients is omitted from the present work due to space constraints. It is interesting to note that the polynomial equations (11) are structurally similar to the corresponding equations resulting from a SISO $m=2$ analysis (Parker, 2002*b*), with $\Delta u_2(k|k)$ corresponding to $\Delta u_1(k+1|k)$, partial derivatives taken with respect to the n_u manipulated variables rather than the m-length horizon of input changes, and different numerical values for the p_{ivw}'s.

To identify the input values leading to process extrema, the set of coupled nonlinear polynomials (11) must be solved simultaneously. While there is no general solution to this set of equations, the Gröbner basis transformation, an analytical geometry technique, can be used to solve the set of polynomials above in a straightforward fashion.

4. GRÖBNER BASIS TRANSFORMATION

It is beyond the scope of the present work to provide a full background on Gröbner basis (GB) transformation methods. Interested readers are referred to (Fröberg, 1997; Cox *et al.*, 1997). Among other problems, Gröbner basis techniques can solve systems of polynomial equations. In fact, solution by Gröbner bases provides all the solutions in k^n of the system of polynomial equations (Cox *et al.*, 1997):

$$g_i(x_1, \ldots, x_n) = 0 \quad \forall i \in [1, n] \tag{12}$$

Here the functions g_i lie on the polynomial ring k^n; the coefficients (such as p_{ivw} in (11)) determine the field, k. General background on fields and polynomial rings can also be found in (Fröberg, 1997; Cox *et al.*, 1997). For the present work, the focus is on the field of rational numbers, ($\mathbb{Q} = \frac{\mathbb{Z}_{num}}{\mathbb{Z}_{den}}$), although integers ($\mathbb{Z}$), reals, and complex numbers are also feasible choices. Under this selection, the NMPC problem equations (11) can be posed as a Gröbner basis problem:

Problem 1. (**NMPC Optimization).** Find all common solutions on the ring $\mathbb{Q}^2[\Delta u_1(k|k), \Delta u_2(k|k)]$ of the system of polynomial equations:

$$f_1(\Delta u_1(k|k), \Delta u_2(k|k)) = f_2(\Delta u_1(k|k), \Delta u_2(k|k)) = 0$$

While the coefficients of most NMPC problems are generally of type real ($p_{ivw} \in \mathbb{R}$), these can be rationalized to place them in $\mathbb{Q}$. The key driving force for this modification is that many Gröbner solution algorithms are more efficient when handling rationals than reals (*e.g.*, groebner::gbasis in MuPAD 3.1.1, ©2005, SciFace Software).

The algorithm that is commonly employed in the solution of the **NMPC Optimization** problem is Buchberger's Algorithm (Buchberger, 1985; Cox *et al.*, 1997). Given a polynomial ideal, such as the equations (11), in $\mathbb{Q}^2$, a Gröbner basis for the ideal can be constructed in a finite number of steps. In practice, a reduced Gröbner basis (rGB) is employed because it is unique for a given ideal where a GB is not necessarily unique (Cox *et al.*, 1997). In employing the GB solution method, an elimination order can be selected for the unknown variables ($\Delta u_i(k|k)$). In the present case, order is not particularly important, aside from the fact that variable ordering alters the polynomial coefficients, p_{ivw}. Hence, $\Delta u_1(k|k) > \Delta u_2(k|k)$ was chosen arbitrarily, where $>$ denotes an order of removal. For this ordering, the variable $\Delta u_1(k|k)$ is removed preferentially from the equations. The resulting set of rGB polynomials contain the following: (i) a set of (one or more) polynomials containing only $\Delta u_2(k|k)$; and (ii) a second set of polynomials with both $\Delta u_2(k|k)$ and $\Delta u_1(k|k)$ appearing. Ordering is more relevant to the $m > 1$ problem, where, for the SISO case, $\Delta u(k+1|k) > \Delta u(k|k)$ was chosen (Parker, 2002*b*) to yield one polynomial in $\Delta u(k|k)$ alone, and a second polynomial in $\Delta u(k|k)$ and $\Delta u(k+1|k)$.

Implementation of the GB solution algorithm has off-line and on-line components. Prior to on-line

execution, the ideal (11) is calculated analytically (*e.g.*, symbolically, using MATLAB ©2005, The Mathworks, Natick, MA). The dynamic variables, $\Delta u(k)$, $\ell(k)$, $u(k-1)$, and $r(k+1)$ are retained within the ideal so that they may be updated at each sample time. The solution of the ideal is accomplished using a specialized GB solution routine within a symbolic or numerical package (*e.g.*, MuPAD). The known variables at a point in time are converted from real to rational form and are passed to the MuPAD subroutine which computes the rGB. For the case study in Section 5.1, the rGB had the following structure:

$$q_{19}\Delta u_2^9(k|k) + \ldots + q_{11}\Delta u_2(k|k) + q_{10} = 0 \quad (13)$$

$$\Delta u_1(k|k) = \sum_{z=0}^{8} q_{2z}\Delta u_2^z(k|k) \quad (14)$$

The original problem, (11), which had no easily identified solution has been transformed to an rGB which is straightforward to solve. The univariate polynomial (13) is solved using a command such as *roots* in MATLAB. For each real root, a candidate for $\Delta u_2(k|k)$, the corresponding $\Delta u_1(k|k)$ candidate is calculated from (14). Roots with imaginary component are discarded because the manipulated variables are physical quantities, and hence, the solutions must be real-valued. Each pair of candidate solutions is simulated over the prediction horizon, which is a straightforward matrix multiplication for the Laguerre system using (1) and (2). The objective function value is calculated for each simulation profile, and the input move combination resulting in the lowest objective function value is implemented as $\Delta\mathscr{U}(k|k)$. This process repeats at each sample time with the dynamic updating of the ideal, rGB solution, candidate move identification, and move selection.

5. RESULTS

5.1 Polymerization Case Study

The case study employed in this work is the multivariable polymerization reactor of Hidalgo and Brosilow (1990), including the addition of number average molecular weight (NAMW) as a controlled variable and operation about the low-conversion steady state point, as made by Doyle *et al.* (2002*b*). Monomer (Q_i) and cooling water (Q_c) flow rates are manipulated to control polymer NAMW and temperature. It is assumed that (Doyle III *et al.*, 2002*b*): (i) monomer disappearance is driven primarily by propagation, rather than chain transfer to another monomer; (ii) that the rate constant of overall polymer chain termination is the sum of combination and disproportionation contributions (Schmidt and Ray, 1981); and a constant volume fraction of solvent is maintained such that the gel effect can be neglected (Choi, 1986).The full process description, including state space formulation and model parameters, can be found in (Doyle III *et al.*, 2002*b*). The inputs and outputs were scaled as follows:

$$W_u = \begin{bmatrix} 108 & 0 \\ 0 & 471.6 \end{bmatrix} \qquad W_y = \begin{bmatrix} 2500 & 0 \\ 0 & 0.5 \end{bmatrix}$$

Doyle *et al.* (2002*b*) developed a MIMO second-order Volterra model for this process via Carlemann linearization (Rugh, 1981). This model was projected onto the Laguerre basis using a least-squares approach similar to (Parker and Doyle III, 1998). The projection was accomplished over a range of α values ($\alpha \in [0.01, 0.99]$), and the C and D matrices of the Volterra-Laguerre model were calculated for each α. The α, C, D combination that provided the best fit to the original Volterra model was employed in the model. This resulted in each input channel having a different Laguerre pole value, such that the monomer flow rate used $\alpha = 0.76$ and the cooling water flow rate had $\alpha = 0.81$. The state space matrices for this model are as follows:

$$A = \begin{bmatrix} 0.76 & 0 & 0 & 0 & 0 & 0 \\ 0.422 & 0.76 & 0 & 0 & 0 & 0 \\ -0.321 & 0.422 & 0.76 & 0 & 0 & 0 \\ 0 & 0 & 0 & 0.81 & 0 & 0 \\ 0 & 0 & 0 & 0.344 & 0.81 & 0 \\ 0 & 0 & 0 & -0.279 & 0.344 & 0.81 \end{bmatrix}$$

$$B = \begin{bmatrix} 0.65 & 0 \\ -0.494 & 0 \\ 0.375 & 0 \\ 0 & 0.586 \\ 0 & -0.475 \\ 0 & 0.385 \end{bmatrix} \qquad C^T = \begin{bmatrix} -2.997 & 1.571 \\ -3.01 & 1.44 \\ -0.108 & 0.04 \\ 0.602 & -2.012 \\ 1.095 & -1.884 \\ 0.438 & -0.063 \end{bmatrix}$$

$$D_1 = \begin{bmatrix} 0.412 & 0.508 & 0.072 \\ 0.508 & 0.470 & 0.010 \\ 0.072 & 0.010 & -0.072 \\ -0.019 & 0.041 & 0.037 \\ 0.041 & 0.056 & 0.036 \\ 0.037 & 0.036 & 0.001 \end{bmatrix}$$

$$D_2 = \begin{bmatrix} 0.043 & 0.078 & 0.032 \\ 0.078 & 0.108 & 0.016 \\ 0.032 & 0.016 & -0.058 \\ 0.244 & 0.223 & 0.001 \\ 0.223 & 0.345 & 0.086 \\ 0.001 & 0.086 & 0.131 \end{bmatrix}$$

5.2 Controller Evaluation

An NMPC controller was synthesized using the method in Section 3. Controller tuning parameters were $m = 1$ and $p = 20$, with the weighting matrices as follows (Doyle III *et al.*, 2002*b*):

$$\Gamma_y = \begin{bmatrix} 2 & 0 \\ 0 & 1 \end{bmatrix} \qquad \Gamma_u = \begin{bmatrix} 0 & 0 \\ 0 & 0 \end{bmatrix} \quad (15)$$

For comparison, a gradient-based NMPC algorithm was synthesized and solved using the *fmincon*

function in MATLAB. The objective function surface, calculated from equation (9), using a setpoint value of $r(k+1) = [0 \quad 0]^T$ for the mismatch case is shown in Figure 1. This objective function surface has a

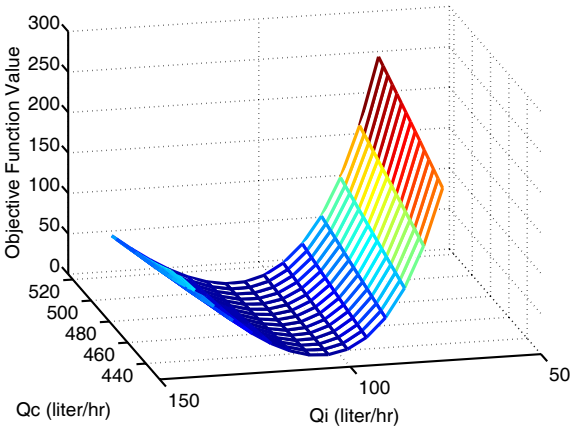

Fig. 1. Objective function surface for the polymerization case study at the nominal conditions and the reference trajectory $R(k+1) = [0 \quad 0]^T$.

global minimum, with no local minima. Given the smooth convex nature of the surface, the gradient-based algorithm should track the desired setpoint. The performance of the analytical NMPC algorithm in response to setpoint changes, therefore, should be within optimizer numerical accuracy to that of the gradient-based solution.

In the nominal case, where the plant and model are both described by the Volterra-Laguerre equations, the system was subjected to a reference change of $[+21519 \quad 0]^T$ (deviation from nominal) [results not shown]. The gradient-based algorithm tracks the desired reference trajectory, and the performance of the Gröbner NMPC algorithm is nearly identical. The output profiles overlay; as such, differentiation between the responses is not significant with respect to measurement noise associated with NAMW or temperature sensing devices.

Simulations using the nonlinear ODEs (Hidalgo and Brosilow, 1990; Doyle III *et al.*, 2002*a*) as the process description, with the controller synthesized from the Volterra-Laguerre model, return similar results to those above. As an additional test in the mismatch case, a normally-distributed noise signal ($\mu = 0, \sigma = \begin{bmatrix} 2400 & 0 \\ 0 & 0.5 \end{bmatrix}$, corresponding to 5% measurement noise on average for the NAMW channel) was added to the plant output. The closed-loop performance under both NMPC algorithms is shown in Figure 2. The gradient-based and analytical controllers again provide similar levels of closed-loop performance.

6. DISCUSSION AND SUMMARY

An analytical solution to the multivariable nonlinear MPC problem was developed for two-

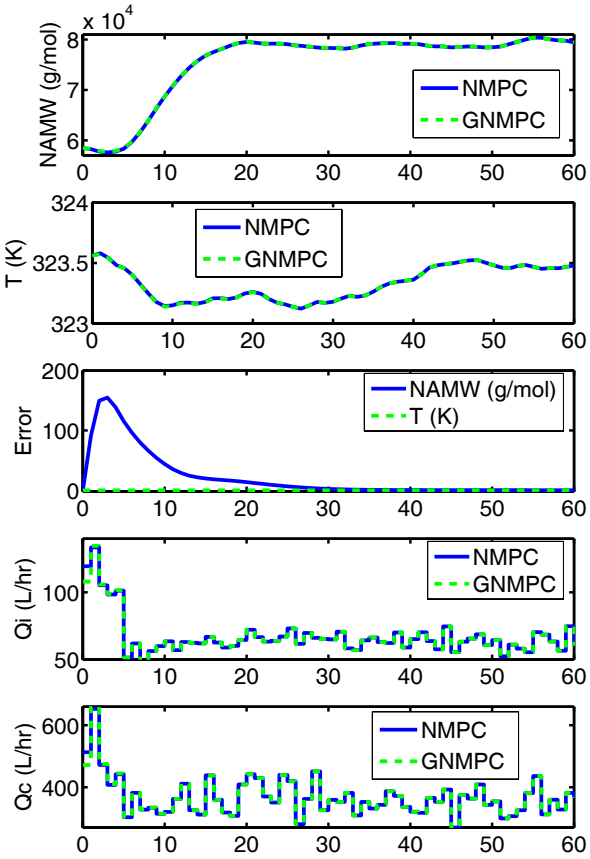

Fig. 2. Closed-loop NMPC on the mismatch system in response to a setpoint of $\mathscr{R}(k+1) = [80{,}000 \quad 0]^T$ (absolute variables) at time = 5 hr in the presence of measurement noise. Controller response curves generally overlay in panes 1, 2, 4, and 5. Note: GNMPC = Gröbner NMPC.

input two-output systems modeled with second-order (Volterra-)Laguerre equations. The future model predictions were posed in terms of information available at the current time. The NMPC objective function, and its derivatives with respect to the input vector, were precalculated symbolically off-line using the model prediction equations. The matrix polynomial corresponding to the first-order necessary condition for an optimum, which was previously limited to numerical solution in the multivariable case, was transformed using Gröbner bases to an easily solvable form. The resulting equations provided candidate input move combinations calculated by a combination of polynomial roots calculations and back-substitution. For systems with smooth convex objective functions, the closed-loop performance was shown to be equivalent to that obtained using gradient-based NMPC solution algorithms.

While performance advantages were not observed for the multivariable polymerization case study above, this was not surprising. Previous work with analytical NMPC solutions on SISO systems (Dumont and Fu, 1993*b*; Parker and Doyle III, 2001; Parker, 2002*b*) has demonstrated the advantage exists primarily when the system displays a nonconvex objective function surface. Bioreactor and chip refiner case studies

that have "unreachable" setpoints (*i.e.*, second-order systems having setpoints above the steady state locus) or input multiplicity are problematic for gradient-based algorithms. In the latter case, the gradient-based routine may become trapped on one side of the optimum, which may result in suboptimal performance (especially in the presence of input constraints, as shown in (Parker, 2002*b*)).

The present work complements the SISO $m > 1$ analytical NMPC work of (Parker, 2002*b*) in demonstrating the utility of Gröbner basis transformation for the solution of MIMO NMPC problems. In fact, the $m = 2$ SISO solution has identical structure to that of equations (13) and (14). While these studies have focused on second-order problems, the extension to third-order (Volterra-)Laguerre systems is ongoing in our laboratory. Also of interest is the coupling of the MIMO and $m > 1$ analytical solution problems in a unified algorithm construction. It is worth noting that there is no theoretical limit on either the size of m or the input-output dimension of the multivariable system that can be formulated using the Gröbner basis technique. The limitation of this solution method lies in the Gröbner transformation routine, where the total number of manipulated variable moves ($m \bullet n_u$) characterizes the complexity of the problem and its possible solution. Increasing m, n_u, or polynomial order will lead to: (i) an increased number (due to m or n_u) of higher-order (due to polynomial order) polynomial equations (11); (ii) a larger number of variables (due to m or n_u) in the Gröbner problem (12); and (iii) potential roots calculation issues, such as identifiability and numerical stability, in the larger number of potentially higher-order solution equations, akin to (13) and (14). Items (i) and (ii) can likely be addressed with sufficient computational power (CPU speed, memory/swap, etc.). More theoretical issues, which remain open at present, include limitation (iii) as well as a proof of Gröbner NMPC algorithm stability.

7. ACKNOWLEDGMENT

Support for this work was provided by the National Science Foundation CAREER Award Program (CTS #0134129).

REFERENCES

Biegler, L. T. (1998). Efficient solution of dynamic optimization and NMPC problems. In: *International Symposium on Nonlinear Model Predictive Control: Assessment and Future Directions*. Ascona, Switzerland. pp. 46–63.

Buchberger, B. (1985). Groebner bases: An algorithmic method in polynomial ideal theory. In: *Multidimensional Systems Theory* (N. K. Bose, Ed.). pp. 184–232. D. Reidel Publishing Company, Dordrecht.

Choi, K. Y. (1986). Analysis of steady state of free radical solution polymerization in a continuous stirred tank reactor. *Polymer Engng. and Sci.* **26**(14), 975–981.

Cox, D., J. Little and D. O'Shea (1997). *Ideals, Varieties, and Algorithms*. second ed.. Springer-Verlag. New York.

Daoutidis, P. and M. A. Henson (2002). Dynamics and control of cell populations in continuous bioreactors. In: *Proceedings of CPC VI*. AIChE Symposia Series. CACHE Corporation.

Doyle III, F. J., M. Soroush and C. Cordeiro (2002*a*). Control of product quality in polymerization processes. In: *Proceedings of CPC VI*. AIChE Symposia Series. CACHE Corporation.

Doyle III, F. J., R. K. Pearson and B. A. Ogunnaike (2002*b*). *Identification and Control Using Volterra Models*. Springer-Verlag.

Dumont, G. A. and Y. Fu (1993*a*). Non-linear adaptive control via Laguerre expansion of Volterra kernels. *Int. J. Adaptive Control Sig. Proc.* **7**, 367–382.

Dumont, G. A., Y. Fu and G. Lu (1994). Nonlinear adaptive generalized predictive control and applications. In: *Advances in Model–based Predictive Control* (D. Clarke, Ed.). pp. 498–515. Oxford University Press.

Dumont, G.A. and Y. Fu (1993*b*). An optimum time scale for discrete laguerre network. *IEEE Transactions on Automatic Control* **38**(6), 934–938.

Fröberg, R. (1997). *An Introduction to Gröbner Bases*. John Wiley & Sons. Chichester.

Hernjak, N. and F. J. Doyle III (2004). Assessment of performance limitations due to nonlinearity in the model of a human with diabetes. In: *Proc. Am. Cont. Conf.*. IEEE Press. Piscataway, NJ.

Hidalgo, P. M. and C. B. Brosilow (1990). Nonlinear model predictive control of styrene polymerization at unstable operating points. *Comput. Chem. Eng.* **14**(4/5), 481–494.

Kouvaritakis, B. and Cannon, M., Eds.) (2001). *Nonlinear Predictive Control: Theory and Applications*. The Institution of Electrical Engineers. London.

Morari, M. (1983). Robust stability of systems with integral control. In: *Proceedings of the IEEE Conference on Decision and Control*. IEEE Press. San Antonio, TX. pp. 865–869.

Morari, M. and E. Zafiriou (1989). *Robust Process Control*. Prentice-Hall, Englewood Cliffs, NJ.

Muske, K. R. and J. B. Rawlings (1993). Model predictive control with linear models. *AIChE J.* **39**(2), 262–287.

Parker, R. S. (2002*a*). Efficient nonlinear model predictive control: Exploiting the Volterra–Laguerre model structure. In: *Proceedings of CPC VI*. CACHE Corporation. AIChE Symposia Series.

Parker, R. S. (2002*b*). Nonlinear model predictive control of a continuous bioreactor using approximate data–driven models. In: *Proc. American Control Conf.*. Anchorage, AK.

Parker, R. S. and F. J. Doyle III (1998). Nonlinear model predictive control of a continuous bioreactor at near–optimum conditions. In: *Proc. American Control Conf.*. New York, NY. Philadelphia, PA. pp. 2549–2553.

Parker, R. S. and F. J. Doyle III (2001). Optimal control of a continuous bioreactor using an empirical non-linear model. *Ind. Eng. Chem. Res.* **40**, 1939–1951.

Rugh, W. J. (1981). *Nonlinear System Theory - The Volterra/Wiener Approach*. The Johns Hopkins University Press, Baltimore, MD.

Schetzen, M. (1980). *The Volterra and Wiener Theories of Nonlinear Systems*. John Wiley & Sons, New York, NY.

Schmidt, A. D. and W. H. Ray (1981). The dynamic behavior of continuous polymerization reactors-I. *Chem. Eng. Sci.* **36**, 1401–1410.

Stack, A. J. and F. J. Doyle III (1997). The optimal control structure approach to measuring control-relevant nonlinearity. *Comput. Chem. Eng.* **21**, 1009–1019.

Zheng, A. (1997). A computationally efficient nonlinear MPC algorithm. In: *Proc. American Control Conf.*. Albuquerque, NM. pp. 1623–1627.

Zheng, Q. and E. Zafiriou (1995). Nonlinear system identification for control using Volterra-Laguerre expansion. In: *Proc. American Control Conf.*. Seattle, WA. pp. 2195–2199.

ADCHEM 2006

International Symposium on Advanced Control of Chemical Processes
Gramado, Brazil – April 2-5, 2006

FEASIBLE MODEL PREDICTIVE CONTROL WITH BOUNDED DISTURBANCES

Morten Hovd *,1

* *Engineering Cybernetics Department, Norwegian University of Technology and Science, N-7491 Trondheim, Norway*

Abstract: This paper shows how to calculate feasible regions, parameterized in terms for the present state x_k, for MPC controllers for constrained linear systems. The dependence of the feasible region on the prediction horizon is also made clear. It is also shown how the procedure may be modified to find guaranteed feasible regions in the presence of unknown, bounded disturbances. These 'robust' feasible regions are used to propose a very simple MPC controller which achieves robust feasibility. *Copyright© 2005 Author*

Keywords: Model predictive control, feasible region, prediction horizon, disturbances.

1. INTRODUCTION

Model Predictive Control (MPC) has been a remarkable industrial success.A distinguishing feature of MPC controllers is the relative ease with which constraints in both states/outputs and inputs are handled. This paper starts by addressing the calculation of feasible regions and corresponding required prediction horizon for MPC. It is then shown how to calculate feasible regions that are robust to unkonwn, bounded disturbances. Subsequently, the parametrization of the robustly feasible regions are used to propose a simplified MPC controller. We start from a fairly typical MPC formulation:

$$\min_{u_0,u_1,\cdots,u_{N-1}} \sum_{k=0}^{N-1} \left(u_k^T R u_k + x_k^T Q x_k\right) + x_N^T Q_f x_N \tag{1}$$

with constraints

$$Gx_k + Hu_k \leq b, k \in [0,\ldots,N,\ldots,N+j] \tag{2}$$

$$x_{k+1} = Ax_k + Bu_k, \;\; x_0 = given \tag{3}$$

$$Q \succeq 0, \; Q_f \succeq 0 \; R \succ 0 \tag{4}$$

Input constraints are normally present in in real-life problems, these are usually the only constraints in (2) that are enforced at $k = 0$ (the corresponding rows in G are zero). For (2) to be meaningful, i.e., for the constraints to be fulfilled for a time horizon beyond the prediction horizon N, the control action in the interval $N \leq k \leq N+j$ needs to be defined. Here the common assumption is made that the infinite horizon LQ-optimal controller for the weighting matrices R and Q is used, and that Q_f is the solution of the corresponding algebraic Riccati equation. Additional assumptions are

A1 The system described by (3) is stabilizable.
A2 $(Q^{1/2}, A)$ is observable.
A3 The constraints defined by (2) constitute a closed and bounded polyhedron in the space

[1] To whom correspondence should be addressed. e-mail: morten.hovd@itk.ntnu.no

spanned by $\{x, u\}$, and $\{0, 0\}$ is in the interior of this polyhedron.

A1 and A2 are necessary to guarantee closed loop stability, A1 is implied by the assumption that a (stabilizing) LQ-optimal controller can be found. A3 is not very restrictive. Manipulated variables in practice have a limited range of manipulation. In cases where the physical constraints do not impose constraints on all states, artificial constraints can be added so far from the origin that operation in the region of the added constraints is unlikely and/or represent unacceptably poor performance.

The purpose of extending the constraint horizon in (2) from N to $N + j$ is to ensure that the (unconstrained) LQ-optimal controller K will not violate any constraints. When these constraints are fulfilled, applying at each time step u_0 from the solution of (1) and applying the LQ-optimal controller K will result in the same closed loop trajectories for states and manipulated variables after time $k = N$. Closed loop stability of the MPC controller then follows from the stability of the LQ-optimal controller (since the constraints never become active for time steps $k \geq N$), see (Scokaert and Rawlings, 1998) for a proof. The matrices Q and R play much the same role in MPC as in conventional LQ-optimal control, and Q_f and K follow from Q and R. Issues that are particular to MPC (or, constrained LQ regulation) are

I1 The determination of j in (2).
I2 Efficient representation of the constraints for the period $N \leq k \leq N + j$, since many of the constraints in (2) may be redundant.
I3 Determination of the prediction horizon N , and the relationship between N and the feasible region.

The focus of this paper is on issue 3 above, and will be addressed in section 3. However, tackling this issue will require that issues 1 and 2 have been addressed first. For completeness, section 2 will therefore address issues 1 and 2, by specializing the results of (Gilbert and Tan, 1991) to constrained linear systems. The calculations involved in addressing issues 1-3 can be performed off-line, at the design stage when there is presumably ample time for computations. The focus in this paper will therefore be on the clarity of presentation rather than finding the computationally most efficient algorithms.

In (Grieder *et al.*, 2004), it is stated that no method for calculating N is known, and a method of calculating the prediction horizon and associated feasible region was proposed, based on an explicit MPC formultion. The method described next only aims at describing the relationship between the prediction horizon N and the feasible region, without engaging the machinery of explicit MPC. In this author's opinion, explicit MPC is one of the most exciting developments in advanced control in recent years, but nevertheless the majority of applications still rely on on-line solution of optimization problems. The authors of (Grieder *et al.*, 2004) are prominent in the MPC community. Although well known mathematical tools are used in this paper, it is therefore fair to assume that the application of these tools in the present context is not generally understood by the MPC community.

2. MAXIMAL OUTPUT ADMISSIBLE SETS FOR CONSTRAINED LINEAR SYSTEMS

In (Rawlings and Muske, 1993) a conservative criterion for estimating a value for j in (3) was proposed. This criterion depends on the predicted value of x_N, and is thus impractical for on-line use. While the criterion in (Rawlings and Muske, 1993) makes it simple to check on-line whether a sufficiently large parameter j is in use, it is hard to know at the design stage what will be a sufficiently large value for j. Introducing assumption A3 above allows us to determine a non-conservative value for j at the design stage, and also to simplify the quadratic programming problem by removing redundant constraints, i.e., constraints that are always fulfilled whenever other constraints are fulfilled.

Applying the state feedback controller $u_k = Kx_k$ for $k \geq N$, the resulting closed loop system can be considered as an unforced linear system provided constraints are not active for $k \geq N$. The largest set of initial conditions for which an unforced linear system satisfies all constraints for all future times is called the Maximal Output Admissible Set, often denoted $\mathcal{O}_\infty$. Correspondingly, the set of initial conditions for which all constraints are fulfilled up until time t is denoted $\mathcal{O}_t$. Obviously, $\mathcal{O}_\infty \subseteq \mathcal{O}_{t+1} \subseteq \mathcal{O}_t$. The determination of output admissible sets was addressed in (Gilbert and Tan, 1991). We will apply their results to linear systems subject to linear inequality constraints. Assumption 3 above, together with the fact that the system is stable in closed loop, allow us to use some of the results of Gilbert and Tan (Gilbert and Tan, 1991) in the following:

R1 $\mathcal{O}_\infty$ is closed and bounded (and is convex due to the linearity of the constraints).
R2 $\mathcal{O}_\infty$ is *finitely determined* if $\mathcal{O}_\infty = \mathcal{O}_t$ for finite t. For the cases studied here, $\mathcal{O}_\infty$ is finitely determined by construction.
R3 If $\mathcal{O}_t = \mathcal{O}_{t+1}$ then $\mathcal{O}_\infty = \mathcal{O}_t$.

In our case, we are interested in the set to which x_N must belong in order for (2) to hold for all

$k \geq N$, assuming that the inputs are determined by $u_k = Kx_k$. We will in the following denote the set of states x_N for which all inequality constraints (2) are fulfilled for $N \leq k \leq N + t$ by $\mathcal{O}_t$. A straight forward way of determining the maximal output admissible set is therefore given by Algorithm 1.

Algorithm 1. Maximal Output Admissible Set.

(1) Set $t = 0$, and let $\mathcal{O}_0$ be parameterized by (2) for $k = N$.
(2) Increment the time index t, and express the constraints at time t in terms of x_N, using the system model (3) and the equation for the state feedback controller.
(3) Remove any redundant constraints for time t. If all constraints for time index t are redundant, $\mathcal{O}_{t-1} = \mathcal{O}_t$, and hence $\mathcal{O}_\infty = \mathcal{O}_{t-1}$. Stop. Otherwise, augment the set of constraints describing $\mathcal{O}_{t-1}$ by the non-redundant constraints for time t to define $\mathcal{O}_t$. Go to Step 2.

Due to R2 above, this algorithm will terminate in finite time for the problems considered here. Checking for redundancy of constraints is also straight forward for linear systems subject to linear inequality constraints.

Checking redundancy at step 3 in Algorithm 1 above does not necessarily guarantee that the final set of constraints is minimal (i.e., does not contain any redundant constraints). Redundant constraints may still be present in the description of $\mathcal{O}_\infty$ due to the possible presence of redundant constraints in the description of the original polyhedron, or because a constraint that was not redundant at time i was made redundant by adding constraints at later times. Clearly, it is simple to identify and remove any such redundant constraints in the description of $\mathcal{O}_\infty$, if necessary.

3. FEASIBLE REGIONS FOR MPC CONTROLLERS

With the description of the 'terminal set' $\mathcal{O}_\infty$ within which the predicted state at time N must lie, we are ready to address the issue of determining the feasible region for an MPC controller, and how this feasible region depends on the value of N. To this end, we will use what is known as Fourier-Motzkin elimination. This is a procedure for eliminating variables from sets of inequalities, originally discovered by Fourier in the first half of the 1800's. The use of Fourier-Motzkin elimination has been proposed in the control literature previously (e.g., (Keerthi and Gilbert, 1987), (Kerrigan and Maciejowski, 2000)), and it should be well known to people working with invariant sets (also in the MPC context). Nevertheless, as argued above, recent literature show that its application in the present context is not widely known.

3.1 Application to MPC controllers

When applying Fourier-Motzkin elimination in the design and analysis of MPC controllers, we assume that we start from a description of the maximal output admissible set $\mathcal{O}_\infty$, as well as a predefined feasible region (2) and the model equations (3). A typical problem may then be to find the required prediction horizon N such that a feasible solution to the MPC QP problem exists for all x_0 such that

$$\mathcal{A}_r x_0 \leq b_r \tag{5}$$

Naturally, it is assumed that the required feasible region is consistent with the constraints in (2). The most straight forward approach would then be to guess at a value for N, use (3) to eliminate x_k from the constraints (in (2) as well as $\mathcal{O}_\infty$) for all $k > 0$, use Fourier-Motzkin elimination to eliminate $u_0, \cdots, u_{N-1}$, and finally check whether the resulting feasible region is sufficiently large. Instead, we will work 'backwards' from the prediction horizon, as this will allow a stage-wise removal of redundant constraints, and allows terminating the analysis once a sufficiently large feasible region has been found. The stage-wise removal of redundant constraints is important in this context, as it reduces the complexity of the description of the feasible region. The resulting algorithm is as follows:

Algorithm 2. Calculating the required prediction horizon N.

(1) Start with $N = 0$ (ordinary LQ-optimal control) and corresponding feasible region $\mathcal{O}_\infty$.
(2) Check whether the feasible region is sufficiently large. If yes, terminate.
(3) Set $N \leftarrow N+1$ and correspondingly $x_0 \leftarrow x_1$.
(4) Use (3) to express the 'new' x_1 in the constraints in terms of x_0 and u_0.
(5) Use Fourier-Motzkin elimination to remove u_0 from the constraints.
(6) Remove any redundant constraints. Go to Step 2.

For Algorithm 2 to terminate in a finite number of steps is clearly critically dependent on the assumption that the desired feasible region is consistent with the constraints in (2). For unstable systems, this assumption also implies that the desired feasible region is within the region that can be stabilized by constrained inputs.

Applying Algorithm 2 now only requires a method for checking whether the feasible region is sufficiently large. A simple way of checking this is to

check that all the constraints defining the feasible region are 'redundant' relative to the desired feasible region described by (5).

Example 1.
We will here consider the example in (Grieder *et al.*, 2004). The system is given by

$$x_{k+1} = \begin{bmatrix} 0.7326 & -0.0861 \\ 0.1722 & 0.9909 \end{bmatrix} x_k + \begin{bmatrix} 0.0609 \\ 0.0064 \end{bmatrix} u_k$$

The system should be regulated to the origin while adhering to the constraints $|u_k| \leq 2\ \forall k \geq 0$ The desired feasible region is given by $|x_{k,i}| \leq 1000$ and we want to determine the parameters N in (1) and j in (2) such that this feasible region is achieved. To fulfill assumption A3 above we add the artificial constraints $|x_{k,i}| \leq 2000$. The weight matrices are set to $Q = I$ and $R = 0.01$.

Applying Algorithm 1, we find that the parameter j in (2) should be set to $j = 3$, and that the maximal output admissible set $\mathcal{O}_\infty$ is defined by eight inequalities. These inequalities all arise from the constraints in the manipulated variable, and are hence not influenced by the artificial constraints. Performing the Fourier Motzkin elimination, starting from the previously calculated $\mathcal{O}_\infty$, we get that the prediction horizon N needs to be set to $N = 68$ to achieve the desired feasible region. Note that $N + j = 71$, which is the same as the required horizon found in (Grieder *et al.*, 2004).

4. ROBUSTNESS TO DISTURBANCES

The methods presented in sections 2 and 3 do not consider disturbances, and are hence quite idealized and optimistic. In this section, we will describe how the methods can be modified to account for disturbances. In a similar fashion as done above, the maximal output admissible set (in the face of disturbances) will be considered first, since $\mathcal{O}_\infty$ is the starting point for calculating prediction horizons N and corresponding feasible regions. Maximal output admissible sets with disturbance inputs has been studied previously in (Kolmanovsky and Gilbert, 1995), whereas accounting for disturbances when calculating prediction horizons and feasible regions represents an extension of the results in (Grieder *et al.*, 2004). The same MPC formulation as in Section 1 will be used, with the modifications that (3), is replaced by

$$x_{k+1} = Ax_k + Bu_k + Ed_k, \quad x_0 = given \tag{6}$$

Clearly, bounded control can guarantee neither feasibility nor performance with unbounded disturbances. We therefore assume that the disturbances are bounded, and are confined to a polytope defined by the linear inequalities

$$\mathcal{A}_d d_k \leq b_d \tag{7}$$

The zero disturbance, $d_k = 0$, is assumed to lie in the interior of this polytope.

4.1 Robust output admissible sets

Application of the state feedback controller $u_k = Kx_k$ to the system described by (6) yields

$$x_{k+l} = (A + BK)^l x_k + \sum_{i=0}^{l-1} (A + BK)^i E d_{k+l-i-1} \tag{8}$$

Substituting (8) into (2) gives for timestep $k + l$

$$\begin{aligned} (G + HK)(A + BK)^l x_k &\leq b \\ -(G + HK) \sum_{i=0}^{l-1} (A + BK)^i E d_{k+l-i-1} & \end{aligned} \tag{9}$$

Clearly, the right hand side of (9) cannot be evaluated at time k without advance knowledge of the disturbances. However, to ensure feasibility of the constraints, we need only consider worst case disturbances (Kolmanovsky and Gilbert, 1995), i.e., the sequence of disturbances that minimizes the RHS of (9). Note that the worst case disturbances may be different for different constraints in (9), and we thus need to solve one LP for each of these constraints. Thus, we introduce the vector h, where $h = [h_1 \cdots h_m \cdots]^T$ and

$$h_m = \max_{[d_k, \cdots, d_{k+l-1}]} \sum_{i=0}^{l-1} \left[(A + BK)^i E \right]_m d_{k+l-i-1} \tag{10}$$

subject to the inequality (7) being fulfilled. Here the subscript m on the matrices $(A + BK)^i E$ indicates *row* number m of these matrices. Having modified the constraints accordingly, we can still use Algorithm 1 to determine the (robust) maximal output admissible set $\mathcal{O}_\infty$, and **R3** above still serves as a test for identifying $\mathcal{O}_\infty$ (Kolmanovsky and Gilbert, 1995). However, it is no longer obvious *a priori* that $\mathcal{O}_\infty$ is non-empty. We therefore assumed that $b - h > 0$, otherwise the state feedback controller cannot guarantee feasible operation even if $x_k = 0$. If this assumption is violated, it will be necessary either to change weights Q and R to retune the controller, or to take other measures (other than feedback control) to reduce the effects of the disturbances.

4.2 Robust feasible regions

The Fourier-Motzkin elimination can easily be used to calculate feasible regions that are robust to disturbances. The necessary modifications are:

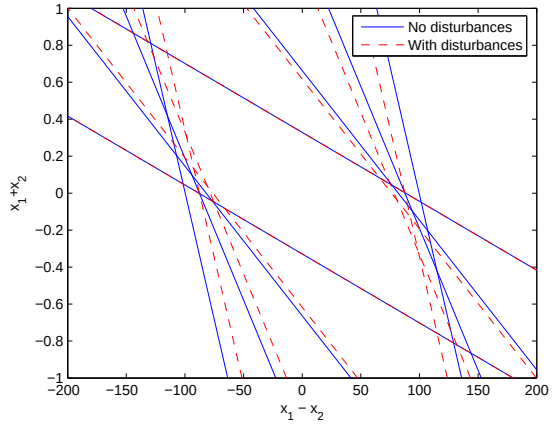

Fig. 1. Maximal output admissible sets $\mathcal{O}_\infty$ for Example 2 with and without disturbances.

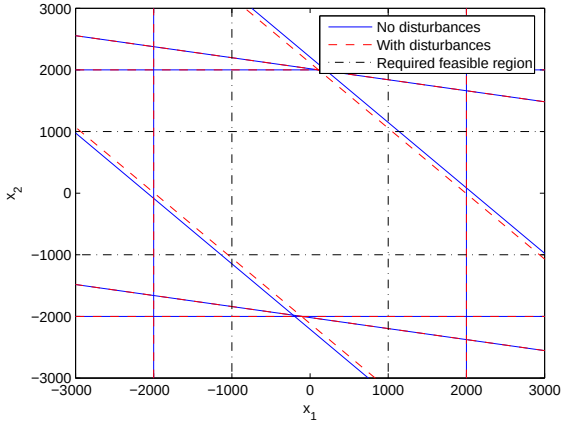

Fig. 2. Feasible regions for Example 2 with and without disturbances.

- Begin the calculations from the *robust* output admissible set $\mathcal{O}_\infty$, calculated as described above.
- The set of constraints used at each stage of Fourier-Motzkin elimination should be the intersection of the constraint sets over the vertices of the disturbance set. Since (8) is linear, the set of states for which there exists a feasible solution for all vertices of the constraint set will also admit a feasible solution for disturbances in the interior or along the edges of the disturbance set.

To illustrate the effects of considering disturbances in the calculation of output admissible sets and feasible regions, we modify Example 1 above by introducing disturbances, with $E = \mathrm{diag}(0.02, 0.003)$ in (6), and $|d_{k,i}| \leq 1$. Calculating j in (2), we still get $j = 3$, just as for the disturbance free case, but the maximal output admissible set is somewhat smaller. This can be seen from Fig. 1, where the two maximal output admissible sets are compared. Requiring the same feasible region as in the disturbance free case, we find that with disturbances we must increase the prediction horizon n from 68 to 69 to account for the disturbances. The resulting feasible regions are compared in Fig. 2.

5. A SIMPLE, ROBUSTLY FEASIBLE MPC

The MPC criterion in 1, when used with the plant model (6) cannot be optimized without *a priori* knowledge of the disturbances. This is clearly not realistic in most cases. Possible modifications include optimizing the *worst case* value of the criterion (leading to a *min-max* formulation), or optimizing the *expected value* of the MPC criterion 1. Both these modifications lead to very complex controllers with high computational load for linear constrained systems. Next, a very simple MPC controller is proposed, which retains the robust feasibility of a more complex formulation, while the control performance may be reduced during transients. Assume the following are given:

(1) A stabilizing controller K for the unconstrained linear system.
(2) The corresponding robust output admissible set, represented by linear inequalities $\mathcal{A}_0 x_k \leq b_0$.
(3) Robust feasible regions for MPC controllers of horizon N, represented by $\mathcal{A}_N x_k \leq b_N; N \in [1, \ldots, \bar{N}]$, where $\bar{N}$ is large enough for the corresponding feasible region to cover the required operating region.

The robust feasible region for the horizon-N controller is known from the calculations described above, and is parametrized by

$$\mathcal{A}_N x_k \leq b_N \tag{11}$$

At each timestep k, it is then very simple to identify the smallest prediction horizon N_k such that x_k lies within the corresponding feasible region. The basic idea behind the simplified MPC is then to use a prediction horizon of 1, but to constrain the optimization such that x_{k+1} is known to lie within the feasible region for an MPC of prediction horizon $N_k - 1$. Note that it is not sufficient to add the constraint

$$\mathcal{A}_{N_k-1} x_{k+1} \leq b_{N_k-1},$$

rather one has to ensure that that this constraint is fulfilled for all possible disturbances - but without knowledge of the actual disturbance values. With x_k given, (6) then gives

$$\mathcal{A}_{N_k-1} B u_k \leq b_{N_k-1} - \mathcal{A}_{N_k-1} A x_k - \mathcal{A}_{N_k-1} E d_k \tag{12}$$

In the same way as for the calculation in (10), solving a set of LP is (in general) needed to maximize the last term in (12). Let the results of these LP's be collected in the vector h_{N_k-1}. Thus, we get

$$\min_{u_0} \quad \left(u_0^T R u_0 + x_{k+1}^T Q_f x_{k+1}\right) \tag{13}$$

$$s.t. \quad \mathcal{A}_{N_k-1} A x_k + \mathcal{A}_{N_k-1} B u_k \leq b_{N_k-1} - h_{N_k-1}, \tag{14}$$

$$H_0 u_k \leq b_0 \tag{15}$$

where (15) represents the input constraints for $k = 0$ in (2). MPC controllers with robust feasibility in the face of bounded disturbances have also been proposed in previous works (Chischi *et al.*, 2001), (Sakizlis *et al.*, 2004). The controllers in these works use a prediction horizon of a fixed length N (as is common in predictive control), and constraints that are formulated to account for the worst possible disturbance sequence. In contrast, the controller proposed here uses a prediction horizon of 1, while the constraints are formulated to ensure that a feasible solution will exist also at future times if a feasible solution is found initially. The main advantage with the robust MPC formulation proposed here is that it requires the solution of quite small QP problems (whether solved on-line or *a priori* using parametric programming). The *worst case* performance is likely to be better with the controllers in (Chischi *et al.*, 2001), (Sakizlis *et al.*, 2004), since performance is optimized over an extended horizon N.

The idea of using a 'one step' controller to guarantee constraint fulfillment for an infinite horizon was recently proposed in the context of piecewise affine systems in (Grieder *et al.*, 2005). In some ways, the 'one step' controller proposed here is a specialization of their controller to linear systems. However, in order to achieve stability (Grieder *et al.*, 2005) assumes the origin to be an equilibrium state, which precludes the possibility of persistent bounded disturbances. The robust output admissible set is control invariant, and hence stability is guaranteed also in the face of bounded persistent disturbances for the 'one step' controller in this work.

6. CONCLUSIONS

This paper uses well known mathematical tools for determining the required prediction horizon in constrained linear MPC to guarantee a specified feasible region. It is shown how the calculation of the prediction horizon and feasible region can be modified to account for bounded disturbances. A simple MPC formulation is then proposed, which uses the robustly feasible regions to guarantee robust feasibility while keeping the computational load very low. The simple MPC controller does not guarantee any form of optimality during transients (when constraints are active), but at steady state it will inherit the optimality properties of the state feedback controller.

ACKNOWLEDGEMENTS

The many constructive comments of Dr. J. A. Rossiter of the University of Sheffield are gratefully acknowledged.

REFERENCES

Chischi, L., J. A. Rossiter and G. Zappa (2001). Systems with persistent disturbances: predictive control with restricted constraints. *Automatica* **37**, 1019–1028.

Gilbert, E.G. and K.T. Tan (1991). Linear systems with state and control constraints: The theory and application of maximal output admissible sets. *IEEE Trans. Autom. Contr.* **36**, 1008–1020.

Grieder, P., F. Borrelli, F. Torrisi and M. Morari (2004). Computation of the constrained infinite time linear quadratic regulator. *Automatica* **40**, 701–708.

Grieder, P., M. Kvasnica, M. Baotic and M. Morari (2005). Stabilizing low complexity feedback control of constrained piecewise affine systems. *Automatica* **41**, 1683–1694.

Keerthi, S. S. and E. G Gilbert (1987). Computation of minimum-time feedback control laws for discrete-time systems with state-control constraints. *IEEE Transactions on Automatic Control* pp. 432–435.

Kerrigan, E. C. and J. M. Maciejowski (2000). Soft constraints and exact penalty functions in model predictive control. In: *Proceedings of the UKACC International Conference (CONTROL 2000).*

Kolmanovsky, I. and E. G. Gilbert (1995). Maximal output admissible sets for discrete-time systems with disturbance inputs. In: *Proceedings of the American Control Conference.* pp. 1995–1999.

Rawlings, J. B. and K. R. Muske (1993). The stability of constrained receding horizon control. *IEEE Transactions on Automatic Control* **38**(10), 1512–1516.

Sakizlis, V., N. M. P. Kakalis, V. Dua, J. D. Perkins and E. N. Pistikopoulos (2004). Design of robust model-based controllers via parametric programming. *Automatica* **40**, 189–201.

Scokaert, P. O. M. and J. B. Rawlings (1998). Constrained linear quadratic regulation. *IEEE Trans. Auto. Contr.* **43**, 1163–1169.

ADCHEM 2006

International Symposium on Advanced Control of Chemical Processes
Gramado, Brazil – April 2-5, 2006

NONCONVEX OPTIMIZATION AND ROBUSTNESS IN REALTIME MODEL PREDICTIVE CONTROL

Darryl DeHaan, [1] **Martin Guay** [2]

Department of Chemical Engineering, Queen's University, Kingston, ON, Canada K7L 3N6

Abstract: Recent works in the nonlinear MPC literature have presented "realtime" optimization approaches based upon incremental updating of input parameters using local descent directions of the cost functional. The main downside to these methods is their strong dependence upon the values used to initialize the input parameters. In this note we study the robustness issues associated with non-local search methods in continuous-time MPC, and demonstrate a framework for robustly incorporating these approaches in a realtime setting.

Keywords: nonlinear model predictive control, robustness, nonlinear systems, realtime optimization

1. INTRODUCTION

The flexibility of model predictive control (MPC) for dealing with constraints has lead to its rapid emergence as the advanced control method of choice in the process industries. However, computational complexity remains the main limitation preventing the use of MPC in many applications.

Current application of nonlinear MPC is limited to so-called "perfect model" implementations, which rely on nominal robustness guarantees such as discussed in (Magni and Sepulchre, 1997; Grimm *et al.*, 2004; Grimm *et al.*, 2003). In particular, in (Grimm *et al.*, 2004) it is shown that continuity of *either* the value function *or* the MPC feedback policy are sufficient for nominal robustness to disturbance inputs; while the feedback policy may generally be discontinuous for nonlinear problems, the value function can be made continuous using appropriate inner approximations of the constraint limits.

[1] Work supported by the National Sciences and Engineering Research Council of Canada.
[2] Corresponding author. email: guaym@chee.queensu.ca.

However, as discussed in (Coron and Rosier, 1994), discontinuous feedback policies for continuous-time systems are potentially non-robust to measurement error in the feedback loop. While (Messina *et al.*, 2005) show that *discrete-time* MPC exhibits nominal robustness to measurement noise, (Tuna *et al.*, 2005) demonstrate that this nominal robustness may approach zero for systems with fast sampling.

In this work, we demonstrate that realtime MPC methods based on gradient-driven local optimization are automatically nominally robust to measurement errors. Furthermore, we proceed to demonstrate a means by which non-local optimization methods can be incorporated into a realtime framework without violating nominal robustness. This work is organized as follows. Section 2 discusses the lack of robustness in the standard definition of MPC, while Section 3 reviews the basic ideas of realtime MPC and presents robustness results. Section 4 discusses the incorporation of nonconvex optimization into a realtime framework, and a simulation example is included in Section 5.

1.1 Preliminaries

Throughout this work, $\|s\|_\infty$ denotes a vector $\infty-$norm, whereas the space $\mathcal{L}^\infty_{\mathcal{I}}$ of bounded functions on domain $\mathcal{I}$ have norm $\|s(\cdot)\|_{\mathcal{L}^\infty}$. A function $\gamma : [0,\infty) \to \mathbb{R}_{\geq 0}$ is of class $\mathcal{K}$ if it is monotone increasing from $\gamma(0) = 0$. The notations $\overline{\mathbb{S}}$, $\mathring{\mathbb{S}}$, $\partial\mathbb{S}$, co$\{\mathbb{S}\}$, and $\mu(\mathbb{S})$ respectively denote the closure, interior, boundary (i.e. $\overline{\mathbb{S}} \setminus \mathring{\mathbb{S}}$), convex hull, and Lebesgue measure of a set $\mathbb{S}$. We define the distance $d_{\mathbb{S}}(s) \triangleq \inf_{s' \in \mathbb{S}} \|s - s'\|$ and the ball $\mathcal{B}(\mathbb{S}, \varepsilon) \triangleq \{s \mid d_{\mathbb{S}}(s) \leq \varepsilon\}$. Finally, a function $f \in C^{p+}$ if $f \in C^p$, with all $\nabla^p f$ locally Lipschitz.

The system of interest is any nonlinear dynamic

$$\dot{x} = f(x,u), \qquad x(0) = x_0 \tag{1}$$

subject to pointwise constraints of the form $(x,u) \in \mathbb{X}\times\mathbb{U} \subseteq \mathbb{R}^n \times \mathbb{R}^m$, such that $\mu(\mathbb{X}\times\mathbb{U}) > 0$. The control objective is regulation of x to a (not necessarily connected) target set $\Sigma_x \subset \mathbb{X}$, which is weakly invariant under (1) for $(x,u) \in \Sigma \triangleq \Sigma_x \times \Sigma_u(x)$. Performance is measured by the function

$$J(x, \mathbf{u}_{[0,T]}) = \int_0^T L(x^p, u)\; d\tau + W(x^p(T)) \tag{2a}$$

$$s.t. \quad \dot{x}^p = f(x^p(\tau), u(\tau)), \quad x^p(0) = x \tag{2b}$$

$$(x^p(\tau), u(\tau)) \in \mathbb{X} \times \mathbb{U}, \quad \forall \tau \in [0,T] \tag{2c}$$

$$x^p(T) \in \mathcal{X}_f \tag{2d}$$

Unless stated otherwise, the functions $f(\cdot,\cdot)$, $L(\cdot,\cdot)$, and $W(\cdot)$ are assumed C^{0+}, and there exists $\gamma_1, \gamma_2 \in \mathcal{K}$ such that $L(x,u) \geq \gamma_1(d_\Sigma(x,u))$ and $W(x) \geq \gamma_2(d_{\Sigma_x}(x))$. It is assumed that $\mathcal{X}_f$ and W satisfy sufficient conditions for stability as detailed in (Mayne *et al.*, 2000), and x_0 is feasibly open-loop stabilizable to the origin.

2. CONTINUOUS-TIME MPC AND MEASUREMENT ERRORS

A generic continuous-time MPC feedback $u = k_{mpc}(x)$ which minimizes (2) is given by

$$k_{mpc}(x) = \lim_{\tau \downarrow 0} \mathbf{u}^*_{[0,T]}(\tau) \tag{3a}$$

$$\mathbf{u}^*_{[0,T]} = \arg\min_{\mathbf{u}_{[0,T]}} J(x, \mathbf{u}_{[0,T]}) \tag{3b}$$

$$J^*(x) \triangleq J(x, \mathbf{u}^*_{[0,T]}) \; . \tag{3c}$$

The minimization (3b) is over piecewise continuous functions $\mathbf{u}_{[0,T]} \in \mathcal{L}^\infty_{[0,T]}$, and solutions are not necessarily unique, so $k_{mpc} : \mathbb{X} \to \mathbb{U}$ is a possibly discontinuous and set-valued mapping.

The closed-loop dynamics therefore properly take the form of the differential inclusion

$$\dot{x} \in f(x, k_{mpc}(x)) \; . \tag{4}$$

A uniformly continuous function $x(t)$ is a *classical solution* on the interval $t \in [0,T)$ if it satisfies (4) for almost all $t \in (0,T)$. Traditional MPC stability proofs, such as (Mayne *et al.*, 2000; Chen and Allgower, 1998), correspond to showing $J^*(x)$ is nonincreasing over all classical solutions to (4).

It follows from (Grimm *et al.*, 2003) that if the state constraint in (2) is replaced with one of the form $x(\tau) \in \mathbb{X}'(\tau)$, where $\mathcal{X}_f \subset \mathbb{X}'(t_2) \subset \mathbb{X}'(t_1) \subset \mathbb{X}$ for all $0 \leq t_1 < t_2 \leq T$, then there exists a $\delta > 0$ such that for $\|d\|_{\mathcal{L}^\infty} \leq \varepsilon$, global asymptotic stability (GAS) of classical solutions to (4) implies the same for

$$\dot{x} \in f(x, k_{mpc}(x)) + d(t) \, . \tag{5}$$

In contrast, arbitrarily small measurement error

$$\dot{x} \in f(x, k_{mpc}(x + e(t))) \; . \tag{6}$$

can cause k_{mpc} to "dither" around a discontinuity, generating trajectories which may differ greatly from any classical solution of (4). This illustrates the notion of *Filippov* solutions to (4), defined as any trajectory $x(t)$ satisfying $\dot{x} \in \mathcal{F}(x)$, $\mathcal{F}(x) \triangleq \text{co}\{\overline{f(x, k_{mpc}(x))}\}$, for almost all $t \in (0,T)$. This type of dithering can induce directions of motion not even in the span of $\nabla_u f(x,\cdot)$, and hence not covered by the standard stability proof for k_{mpc}.

To demonstrate the potential impact of measurement noise, in similar spirit to (Tuna *et al.*, 2005) we offer the following extension of (Coron and Rosier, 1994, Prop. 1.4). First, it is necessary to (loosely) define the *Clarke normal cone* $N^C_{\mathbb{S}}(s)$ at $s \in \partial\mathbb{S}$ as the convex hull of every vector normal to $\mathbb{S}$ at arbitrary s', with $s' \to s$ (Clarke *et al.*, 1998).

Lemma 1. Assume all classical solutions to (4) are GAS. Define $\mathcal{H} = \{x \in \mathbb{X} \,|\, \overline{k_{mpc}(x)} \setminus k_{mpc}(x) \neq \emptyset\}$, and for each $z_0 \in \mathcal{H}$, let $\mathcal{Z}(z_0)$ denote the set of Filippov solutions $z : \mathcal{I} \to \mathbb{R}^n$ to (4) with $z(0) = z_0$ and $\mathcal{I} \subseteq [0,\infty)$ maximal. Then any initial state $x(0) \in \mathcal{H}_u$

$$\mathcal{H}_u \triangleq \{z_0 \in \mathcal{H} \,|\, \sup_{z(\cdot) \in \mathcal{Z}(z_0)} \lim_{t \uparrow \partial\mathcal{I}} d_\Sigma(z(t)) > 0\}$$

can be prevented from reaching Σ_x by arbitrarily small measurement error. Furthermore, if the set

$$\mathcal{H}^o_u \triangleq \{z_0 \in \mathcal{H}_u \,|\, \forall \xi \in N^C_{\mathcal{H}_u}, \; \exists \nu \in \mathcal{F}(z_0) \; s.t. \; \langle \xi, \nu \rangle > 0\}$$

is nonempty, then $\exists \delta(\cdot) \in \mathcal{K}$ and a neighbourhood $\mathfrak{H}$ of $\mathcal{H}^o_u$ with measure $\mu(\mathfrak{H}) \geq \delta(\varepsilon) > 0$ such that any initial state $x(0) \in \mathfrak{H}$ can be prevented from reaching Σ by a measurement error $\|e\|_{\mathcal{L}^\infty} \leq \varepsilon$.

The first claim is essentially a direct application of (Coron and Rosier, 1994, Prop. 1.4). The second claim is an extension, which essentially states that if Filippov solutions span every outward direction, then measurement error can induce flows back *towards* $\mathcal{H}^o_u$ from any point sufficiently close (i.e.

with x and $x+e$ on "opposite sides" of $\mathcal{H}_u^o$). This is relatively straightforward given $f \in C^{0+}$.

Within the context of chemical processes, there is potential for this type of effect any time a controller must make a choice between two distinct paths. One major instance in which this occurs is when x is near the threshold at which a profitable trajectory becomes infeasible with respect to state constraints, and must be abandoned for a less profitable one.[3] Another situation of interest is when pieces of equipment must be arbitrarily selected from a group for some type of preferential treatment (e.g. starting up parallel pumps in sequence to avoid electrical trips, applying activation heat to parallel reactors sequentially due to steam limitations, etc). This is of particular concern when responding to unplanned events requiring decisive response to mitigate losses.

3. DESCENT-BASED REALTIME METHODS

It is apparent from Section 2 that robustness issues due to measurement noise stem from the assumed globality of the minimization in (3). In practice, however, only local solutions can be guaranteed online; in fact, precisely locating even a local minimum within one sampling period can be difficult. For this reason, a variety of "realtime" approaches such as (Ohtsuka, 2004; Cannon and Kouvaritakis, 2000; DeHaan and Guay, 2005) allow the optimization parameters to evolve incrementally within the same timescale as the dynamics. In this section, we study whether these approaches suffer the same lack of robustness to measurement error discussed in Section 2. Our presentation will follow the method of (DeHaan and Guay, 2005), reviewed briefly,[4] but an effort is made to generalize whenever possible.

3.1 Description of Realtime Method

The approach in (DeHaan and Guay, 2005) allows for piecewise parameterization of the control input using a parameter vector $\omega^T = [\pi;\, \theta]$, consisting of an ordered time support $\pi \in \mathbb{R}^{N+1}_{\geq 0}$ and vectors $\theta_i \in \mathbb{R}^p$ for each of the N intervals. Using a preselected basis ϕ (e.g. polynomial, exponential), the input trajectory is parameterized piecewise as

$$u^p(\tau,\omega) = \begin{cases} \phi(\tau,\theta_1) & \tau \in [0,\, \pi_1] \\ \phi(\tau-\pi_{i-1},\, \theta_i) & \tau \in (\pi_{i-1},\, \pi_i], \quad i \in \{2 \dots N\} \end{cases} \quad (7)$$

which is substituted for $u(\tau)$ in (2), to define $J(x,\omega)$ in an obvious manner. The closed-loop system evolves continuously as

$$\dot{x} = f(x, k_{rt}(\omega)), \quad k_{rt}(\omega) = u^p(\pi_0, \theta_1) \quad (8a)$$
$$\dot{\omega} = g(x,\omega) \quad (8b)$$
$$\text{while } h(\omega) \triangleq \pi_1 - \pi_0 > 0 \quad (8c)$$

where $\omega(0) = \omega_0$ is assumed to be chosen as a feasible (but sub-optimal) parameterization with respect to (2b,c). Upon equality $h(\omega) = 0$ (i.e. the first switching point of (7) is reached), the reset

$$\omega^+ = \begin{cases} \pi_i^+ = \begin{cases} 0 & i = 0 \\ \pi_{i+1} & 1 \leq i < N \\ \pi_N + \delta(x^p(\pi_N)) & i = N \end{cases} \quad (9a) \\ \theta_i^+ = \begin{cases} \theta_{i+1} & 1 \leq i < N \\ \kappa(x^p(\pi_N)) & i = N \end{cases} \end{cases}$$
$$\text{when } h(\omega) \triangleq \pi_1 - \pi_0 = 0 \quad (9b)$$

occurs, where $\delta : \mathcal{X}_f \to \mathbb{R}_{>0}$ and $\kappa : \mathcal{X}_f \to \mathbb{R}^p$ are C^{0+} functions representing a local control law which feasibly initializes the parameters for the new interval being augmented to the horizon. This makes the closed-loop behaviour that of a hybrid system[5]. Stability is proven by the invariance principle, using the strict decrease of $J(x,\omega)$ under (8), the non-increase under (9)[6], and the fact that $h(\omega) \equiv 0$ is not invariant.

The precise definition of $g(x,\omega)$ in (8) varies somewhat between methods, in particular depending on the manner by which the constraints (2c,d) are enforced. We thus distinguish between two classes of approach. In all cases, gradients of J are ensured to exist by strengthening the assumptions on $L(\cdot,\cdot)$, $W(\cdot)$, $f(\cdot,\cdot)$ to C^{1+}.

3.1.1. Interior-point Approaches In the approach of (DeHaan and Guay, 2005), the constraints (2c,d) are replaced by an augmented cost $J^a(x,\omega)$ which incorporates C^{1+} barrier functions into $L(x,u)$ and $W(x)$. Then $g(x,\omega)$ is of the form

$$g(x,\omega) = \mathcal{G}(\omega,\upsilon), \quad \upsilon \triangleq -k\nabla_\omega J^a(x,\omega) \quad (10)$$

where υ represents the nominal descent-update, while $\mathcal{G}$ is a locally Lipschitz operator, possibly including such operations as projecting υ to keep ω in a desired convex set, limiting the growth rate of ω, etc. In particular, $\mathcal{G}$ ensures both $\langle \nabla_\omega J^a, \mathcal{G}(\omega,\upsilon)\rangle \leq 0$ and $\lim_{h(\omega)\downarrow 0}(\dot{\pi}_1 - \dot{\pi}_0) < 0$ (so event (9b) is well defined under small perturbations). Stability follows using J^a as a Lyapunov function, since $\frac{dJ^a}{dt} \leq -L(x,k_{rt}(\omega)) + \langle \nabla_\omega J^a, \mathcal{G}(\omega,\upsilon)\rangle < 0$. The open interior of all constraints is rendered invariant, thus preserving feasibility given feasible initial conditions.

[3] this is *still possible* even if (2b) is nominally robust with respect to $d(t)$, and $\mathbb{X}(\tau)$ is nested as discussed previously.
[4] for omitted details, see (DeHaan and Guay, 2005)
[5] While (Ohtsuka, 2004; Cannon and Kouvaritakis, 2000) do not include hybrid behaviour, they are still encompassed in (7)-(9) by simply defining $\dot{\pi} \equiv 1$, $\pi_0(0) \neq \pi_1(0)$.
[6] guaranteed by conditions on the design of $\kappa(x)$ and $\delta(x)$

3.1.2. Active set-based Approaches In the approach of (Cannon and Kouvaritakis, 2000), the update law is of the form (10), but with $\nabla_\omega J$ instead of $\nabla_\omega J^a$. Constraint feasibility is ensured by incorporation a parameter projection into the definition of $\mathcal{G}$, which removes components of v directed out of the (x-dependent) feasible set for ω. Since the feasible parameter set is impractical to calculate online, this approach corresponds to testing along the length of the prediction $x^p(\tau)$ for constraint violation. Effectively, this is comparable to incorporating a lagrange-multiplier trajectory $\lambda(\tau)$ into the minimization. For robustness, this approach must include a τ-varying constraint $\mathbb{X}'(\tau)$ of the form discussed in Section 2.

3.2 Robustness of Descent-based Methods

The question of robustness for the class of descent-based approaches discussed in Section 3.1 is answered by the following Lemma. Measurement errors in (8)-(10) are interpreted as (2) taking the form $J(x+e(t),\omega)$ when evaluating $\nabla_\omega J$ and $x^p(\pi_N)$ in the feedbacks.

Lemma 2. Assume $f(\cdot,\cdot), L(\cdot,\cdot), W(\cdot) \in C^{1+}$. For any initial condition (x_0,ω_0) such that predictions (2b-d) are strictly feasible, global asymptotic stability of the target Σ_x under closed-loop dynamics (8)-(9) is nominally robust to additive disturbances and measurement errors.

Sketch of Proof: By standard results, the prediction $x^p(\tau)$ of (2b) is Lipschitz with respect to small changes in its initial condition x. Then for interior-point approaches, $\nabla_\omega J^a(x,\omega)$ is C^{0+} in x, as are the dynamics of (8), (9) and the jump condition $h(\omega)$. If $z(t)$ is any closed-loop solution from $z(0)=x(0)$, perturbed by $\|d,e\|_{\mathcal{L}^\infty} \leq \varepsilon$, then it follows that $x(t)$ and $z(t)$ are "close" in the sense $\lim_{\varepsilon \downarrow 0}\{\max_{s\in\mathbb{R}^+}\min_{s'\in\mathbb{R}^+}\|x(s)-z(s')\|\} = 0$. Feasibility and approximate-GAS of $z(\cdot)$ for sufficiently small $\varepsilon>0$ follow by the *strict* feasibility and asymptotic stability of $x(\cdot)$. A similar argument works for active-set approaches. ■

The robustness margins discussed above may be quite small, since the proof makes no use of the update (8b) to compensate by adjusting the input parameterization (since it cannot be guaranteed that this is possible, when $\nabla_\omega J \approx 0$). However, it is important to note that any method based upon achieving minimizing solutions (as opposed to incremental improvement) must necessarily be implemented in a sampled-data framework, with significantly slower sampling rates than used by realtime methods. Such methods then require an equally restrictive assumption of open-loop robustness between sampling instances.

4. ROBUSTLY INCORPORATING NONCONVEX METHODS

Since descent-based realtime methods evolve continuously within connected neighbourhoods of their initial conditions, they do not generate differential inclusions (assuming C^{1+} process dynamics). As such, a local descent-based method automatically exhibits nominal robustness to measurement errors, unlike global approaches. The obvious downside is that performance depends strongly upon the quality of the initial condition.

One simple approach to reducing the impact of ω_0 is to instead allow for multiple initial conditions to be specified; i.e. to allow for multiple independent sets of parameters to be (locally) minimized in parallel. It will first be shown how this can be done in a manner robust to measurement noise, after which we will provide discussion on more sophisticated extensions of this approach.

4.1 Modified Realtime Dynamics

Let $q \geq 1$ denote the number of independent input parameter sets calculated online, denoted ω^i, $i \in \{1,\dots q\}$. For convenience it is assumed all parameterizations use the same basis ϕ, although each ω^i contains an independent time support π^i, potentially of length $N^i \neq N^j$ intervals. The flows (8) then take the form

$$\dot{x} = f(x, k_{rt}(\omega^{i^*})),\ \ k_{rt}(\omega^{i^*}) = u^p(\pi_0^{i^*}, \theta_1^{i^*}) \quad (11a)$$

$$\dot{\omega}^i = \begin{cases} g^i(x,\omega^i) & i = i^* \\ \mathrm{g}^i(x,\omega^i) & i \neq i^* \end{cases} \quad \forall i \in \{1\dots q\} \quad (11b)$$

$$\text{while}\ \ \pi_1^{i^*} - \pi_0^{i^*} > 0, \quad \text{and} \quad (11c)$$

$$\text{while}\ \ J(x,\omega^{i^*}) < (1+\epsilon)J(x,\omega^i),\ \forall i \neq i^* \quad (11d)$$

where $\epsilon > 0$ is a design constant, and $i^* \in \mathbb{N}$ is an additional state of the system identifying which one of the parameter sets is "active". The vectorfields $g^i(x,\omega^i)$ are of the form discussed in Section 3, while g^i reflects that a different update law may be desired if ω^i is not active.

Equality of (11c) triggers the reset (9) (for ω^{i^*} only). Meanwhile, equality of (11d) triggers

$$(i^*)^+ = \text{choose}\left\{\arg\min_{i\in\{1\dots q\}} J(x,\omega^i)\right\} \quad (12)$$

in which "choose" represents any arbitrary convention for selecting between multiple minimizers. If an interior-point approach is used for the $g^i(x,\omega^i)$, then (11d) and (12) are interpreted using $J^a(x,\omega^i)$; regardless, we adopt the convention that $J(x,\omega^i) = +\infty$ if either (2c,d) do not hold.

Using $J(x,\omega^{i^*})$ as a Lyapunov function, the previous stability arguments still hold in light of the strict decrease of $J(x,\omega^{i^*})$ under reset (12). The

robustness of this stability to small measurement errors $e(t)$ hinges on the fact that $\epsilon > 0$ in (11d); i.e. for $\epsilon = 0$, (11a) becomes a differential inclusion with $u = k_{rt}(\Omega)$, $\Omega = \{\omega^i \,|\, J(x,\omega^i) = \min_j J(x,\omega^j)\}$, and is no longer robust to arbitrarily small measurement errors. The nominal robustness of (11) can therefore be summarized:

Claim 3. $\exists \varepsilon(\cdot) \in \mathcal{K}$ s.t. (11) is robust to measurement errors $\|e\|_{\mathcal{L}^\infty} \leq \varepsilon(\epsilon)$, with ϵ from (11d)

4.2 Possible Extensions

It is crucial to note that stability depends upon feasible update and resets of the *active* parameterization ω^{i^*} only. Infeasibility of any w^i, $i \neq i^*$, simply results in that parameterization being (temporarily) excluded from consideration as a candidate in (12). Likewise, arbitrary reset mappings of the form $(\omega^i)^+ = \mathfrak{h}^i(x,\omega^1,\ldots,\omega^p)$, $i \neq i^*$ can be executed at any time without impacting stability. To discuss the wide variety of optimization approaches that could be used to design g^i and $\mathfrak{h}^i$ is beyond the scope of this note. Instead, we simply highlight a few possible approaches that could be used,[7] and postpone analysis of their relative merits to future research.

Infeasible-point approaches: The likelihood of identifying the global (or at least a better) minimum significantly increases if the optimization is allowed to temporarily pass through infeasible regions. Thus, the $\mathrm{g}^i(x,\omega^i)$ update laws may be based upon infeasible-point methods without any weakening of guaranteed feasibility of $x(t)$.

Quasi-Global Search Methods: Several methods exist for generating a continuous search trajectory which attempts to visit many or all of the minima on the surface. This includes augmenting the search with extra velocity dynamics to help escape shallow minima, or methods which switch between ascent and descent phases. The $\mathrm{g}^i(x,\omega^i)$ could be based on any one of these.

Deterministic Resetting If $\left\|\nabla_{\omega^i} J(x,\omega^i)\right\|$, $i \neq i^*$, becomes sufficiently small without triggering (11d), then it may be desirable to reset ω^i. One could, for example, generate a *very* crude branch-and-bound (off-line, or in a slower timescale) to identify new values for ω^i showing potential as minimizers, differing sufficiently from other ω^j.

Stochastic Resetting Similar to the above, there are many stochastic approaches which could be used to reset ω^i. This can be done in conjunction with a deterministic master, which shapes the statistical distribution to target regions of interest or rule out regions which are not.

[7] references regrettably omitted for space considerations

5. SIMULATION EXAMPLE

In order to illustrate the approach, we consider a simple exothermic reaction $A \rightarrow B$ taking place in a non-isothermal, gas-phase CSTR. The system is comprised of three states; although many equivalent coordinate systems can be used, the equations are most clear for the choice: n (total moles of gas in reactor), n_A (moles of A), and T (reactor temperature). The control objective is specified as regulation to the target $(n, n_A, T)_{ss} = (2.5kmol,\ 0.25kmol,\ 500K)$, corresponding to an ideal gas pressure of $1040kPa$, from the initial state $(n, n_A, T)_0 = [2,\ 0.5,\ 350]$. Manipulated variables are the outlet molar flow F_{out}, and rate of heat removal $\dot{Q}$. Using several simplistic assumptions, the system equations are

$$\dot{n} = F_{in} - F_{out} \tag{13a}$$

$$\dot{n}_A = F_{in} - \frac{n_A}{n} F_{out} - k(T) n_A \tag{13b}$$

$$\dot{T} = F_{in}\frac{T_{in}-T}{n} - k(T)\frac{\Delta H_r}{\overline{c_p}}\frac{n_A}{n} + \frac{\dot{Q}}{\overline{c_p}\, n} \tag{13c}$$

where $k(T) = k_0 e^{-\frac{E}{RT}}$. System parameters are

$$\Delta H_r = -5000\frac{kJ}{kmol} \qquad R = 8.314\frac{m^3\,kPa}{kmol\,K}$$

$$V = 10m^3 \quad E = 8000\frac{m^3\,kPa}{kmol} \quad \overline{c_p} = 10\frac{kJ}{kmol\,K}$$

$$T_{in} = 300K \quad k_0 = 6.2s^{-1} \quad F_{in} = 0.25kmol\,s^{-1}$$

An important objective of the controller is to ensure the system trajectories avoid passing through the shaded region in the $P-T$ plane shown in Figure 1, for example to avoid undesireable thermodynamic behaviour of other components in the gas stream which occurs in that region. Using the ideal gas law, this constraint was incorporated as (2c) in the form $g(n,T) \leq 0$.

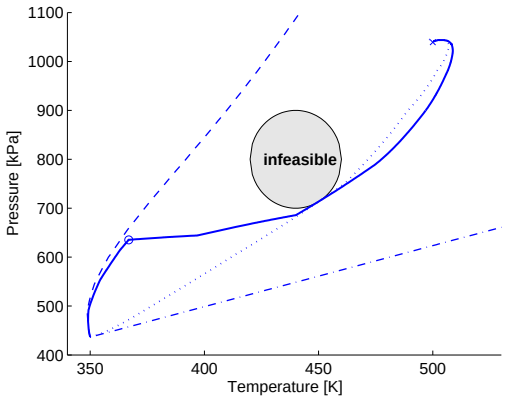

Fig. 1. System trajectories in the $P-T$ plane: closed loop (solid), optimal (dots), initializations ω_0^1 (dash), ω_0^2 (dash-dot). Small circle indicates switch in active ω^i.

The cost function was assumed to be $L(x,u) = x^T\mathrm{diag}(10,\ 10,\ 1\text{e-}3)x + u^T\mathrm{diag}(0.2,\ 0.5)u$, where

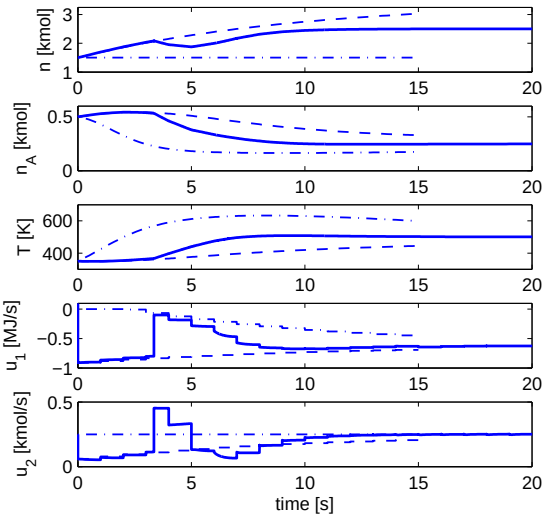

Fig. 2. System trajectories: closed loop (solid), initializations ω_0^1 (dash), ω_0^2 (dash-dot)

$x^T = [n, n_A, T]_{dev}$ and $u^T = [\dot{Q}, F_{out}]_{dev}$ are deviations from the indicated steady state. The terminal penalty $W(x)$ is the quadratic solution to an algebraic Ricatti equation for the linearized (13), and the local control law $\kappa(x)$ was derived from the optimal linear controller using the method presented in (DeHaan and Guay, 2005).

Using simple piecewise constant parameterizations, two sets of parameters ω^1 and ω^2 (both with $N = 15$, $\delta(x) \equiv 1s$, shown in Figure 2) were adapted online. The initializations ω_0^1 and ω_0^2 corresponded to different paths around the constraint region in the P-T plane (whose image is a skewed infinite cylinder in the x-space). As can be seen in Figure 1, neither initialization was very close to the infinite-horizon optimal solution. The controller initially selected the active parameterization ω^1 (i.e. "over" the constraint in Fig. 1), but as the dynamics and adaptation progressed, the active parameterization switched to ω^2 in time to feasibly pass under the constraint region.

6. CONCLUSIONS

Using existing results concerning discontinuous feedbacks, it has been demonstrated that a naive implementation of global search methods creates a robustness concern with respect to measurement noise for continuous-time (i.e. fast-sampled) MPC. While purely local realtime methods do not exhibit this characteristic, any mechanism for evaluating alternative paths generates a potential robustness concern. By incorporating hysteresis in the decision making, a framework has been created for improving the performance of realtime approaches in a nominally robust manner.

REFERENCES

Cannon, M. and B. Kouvaritakis (2000). Continuous-time predictive control of constrained nonlinear systems. In: *Nonlinear Model Predictive Control: Assessment and Future Directions for Research* (F. Allgower and A. Zheng, Eds.). Birkhauser-Verlag.

Chen, H. and F. Allgower (1998). A computationally attractive nonlinear predictive control scheme with guaranteed stability for stable systems. *Journal of Process Control* **8**(5-6), 475–485.

Clarke, F.H., Y.S. Ledyaev, R.J. Stern and P.R. Wolenski (1998). *Nonsmooth Analysis and Control Theory*. Grad. Texts in Math. 178, Springer-Verlag. New York.

Coron, J.M. and L. Rosier (1994). A relation between continuous time-varying and discontinuous feedback stabilization. *Journal of Mathematical Systems, Estimation, and Control* **4**(1), 67–84.

DeHaan, D. and M. Guay (2005). A new real-time method for nonlinear model predictive control. In: *International Workshop on Assessment and Future Directions of Nonlinear Model Predictive Control*. Freudenstadt-Lauterbad, Germany. pp. 73–84.

Grimm, G., M. Messina, S. Tuna and A. Teel (2003). Nominally robust model predictive control with state constraints. In: *Proc. IEEE Conf. on Decision and Control*. pp. 1413–1418.

Grimm, G., M. Messina, S. Tuna and A. Teel (2004). Examples when model predictive control is non-robust. *IEEE Trans. Automat. Contr.* **40**(10), 1729–1738.

Magni, L. and R. Sepulchre (1997). Stability margins of nonlinear receding-horizon control via inverse optimality. *Systems and Control Letters* **32**, 241–245.

Mayne, D. Q., J. B. Rawlings, C. V. Rao and P. O. M. Scokaert (2000). Constrained model predictive control: Stability and optimality. *Automatica* **36**, 789–814.

Messina, M., S. Tuna and A. Teel (2005). Discrete-time certainty equivalence output feedback: allowing discontinuous control laws including those from model predictive control. *Automatica* **41**(4), 617–628.

Ohtsuka, T. (2004). A continuation/GMRES method for fast computation of nonlinear receding horizon control. *Automatica* **4**(40), 563–574.

Tuna, S., R. Sanfelice, M. Messina and A. Teel (2005). Hybrid MPC: Open-minded but not easily swayed. In: *International Workshop on Assessment and Future Directions of Nonlinear Model Predictive Control*. Freudenstadt-Lauterbad, Germany. pp. 169–180.

ADCHEM 2006

International Symposium on Advanced Control of Chemical Processes
Gramado, Brazil – April 2-5, 2006

EXTENDED ROBUST MODEL PREDICTIVE CONTROL FOR INTEGRATING SYSTEMS

A. H. González*, J. L. Marchetti* and D. Odloak[+]

[*] *Institute of Technological Development for the Chemical Industry (INTEC), CONICET - Universidad Nacional del Litoral (U.N.L.). Güemes 3450, (3000) Santa Fe - Argentina.*

[+] *Department of Chemical Engineering, University of São Paulo, Av. Prof. Luciano Gualberto, trv. 3, n. 380, 05508-900 São Paulo, Brazil*

Abstract: This paper proposes a robust model predictive control for systems with stable and integrating poles. The approach combines the methods developed in Odloak (2004) and Carrapiço and Odloak (2005) to obtain a robust controller for integrating systems when multi-plant uncertainty is considered. The key idea in this development is to separate the control problem in two sub-problems, each of which takes into account the required robust constraints. Nominal stability is achieved by using an infinite output horizon, and the whole method is based on a state space model formulation that leads to an offset free MPC. The simulation examples illustrate the performance and robustness of the proposed approach and demonstrate that it can be implemented in real applications.

Keywords: Model Predictive Control, Integrating Systems, Infinite Horizon, Robustness.

1. INTRODUCTION

Robust stability is still one of the main weaknesses of the available MPC technology (Qin and Badgwell, 2003). However, this subject has been extensively treated in the control literature (Kothare et al., 1996, Mayne et al., 2000; Morari and Lee, 1999, Ralhan and Badgwell, 2000, Lee and Yu, 1997). A robust controller is meant to guarantee closed loop stability for different process operating conditions. It is well known that numerous chemical processes are nonlinear but they can be approximated by a set of linear models, where each linear model represents the process locally, around a specific operating condition. If the controller is based on a single linear model, it is desirable to assure that this controller will remain stable for the whole family of models that represent the process.

The standard form to get stability in MPC is the strategy known as infinite horizon. However, this formulation requires additional features in order to achieve offset free tracking. Rodrigues and Odloak (2003) present an incremental state-space model formulation that produces offset free MPC. This formulation adds integrating modes to the system, that must be zeroed at the end of the control horizon in order to keep the infinite cost bounded. If, in addition, the system to be controlled has already integrating modes, a set of constraints must be added to the original problem to compensate both, the original and new unstable modes. As a result, the optimization problem may become infeasible, and the convergence of the cost to zero may be deteriorated.

In this paper, we first present the general model formulation for systems with stable and integrating modes. Then, a single infinite horizon MPC problem is presented as a tutorial to introduce a two-step formulation, which should result more reliable to prevent infeasibilities. This two-step formulation is extended to deal with a multi-model representation of the real plant and the convergence of the method is analyzed. Finally, we provide some simulation results and the conclusions.

2. INFINITE HORIZON MPC FOR INTEGRATING SYSTEMS

2.1 Model Formulation

We assume at first a MIMO system with *nu* inputs and *ny* outputs. For each pair (y_i, u_j), there is a transfer function model

$$G_{i,j}(z) = \frac{b_{i,j,1}z^{-1} + \cdots + b_{i,j,nb}z^{-nb}}{\left(1 + a_{i,j,1}z^{-1} + \cdots + a_{i,j,na}z^{-na}\right)\left(1 - z^{-1}\right)}, \quad (1)$$

where $\{na, nb \in \mathbb{N}\}$. When the poles of the system are non-repeated, the k^{th} coefficient of the step response can be calculated as follows:

$$S_{i,j}(k) = d^0_{i,j} + \sum_{l=1}^{na}\left[d^d_{i,j,l}\right] r_l^k + d^i_{i,j} k\Delta t \qquad (2)$$

where r_l, $l=1, 2, \ldots, na$ are the non-integrating poles of the system, Δt is the sampling time and the coefficients $d^0_{i,j}, d^d_{i,j,l}, d^i_{i,j}$ are obtained by partial expansion of $G_{i,j}$. A state-space model that produces an offset free MPC can be expressed in the following form:

$$x(k+1) = Ax(k) + B\Delta u(k) \qquad (3)$$

$$y(k) = Cx(k) \qquad (4)$$

where

$$[x] = \begin{bmatrix} x^s \\ x^d \\ x^i \end{bmatrix} \in \mathbb{C}^{nx}, \quad nx = 2ny + nd, \quad nd = ny.nu.na,$$

$$x^s \in \mathbb{R}^{ny}, \quad x^d \in \mathbb{C}^{ny.nu.na}, \quad x^i \in \mathbb{R}^{ny}$$

$$A = \begin{bmatrix} I_{ny} & 0 & \Delta t\, I_{ny} \\ 0 & F & 0 \\ 0 & 0 & I_{ny} \end{bmatrix} \in \mathbb{C}^{nx\times nx}, B = \begin{bmatrix} D^0 + \Delta t D^i \\ D^d F N \\ D^i \end{bmatrix} \in \mathbb{R}^{nx\times nu},$$

$$[y] = \begin{bmatrix} y_1 & \cdots & y_{ny} \end{bmatrix}^T, \quad C = \begin{bmatrix} I_{ny} & \Psi & 0_{ny} \end{bmatrix},$$

$$\begin{bmatrix} x^s \end{bmatrix} = \begin{bmatrix} x^s_1 & \cdots & x^s_{ny} \end{bmatrix}^T, \quad \begin{bmatrix} x^i \end{bmatrix} = \begin{bmatrix} x^i_1 & \cdots & x^i_{ny} \end{bmatrix}^T,$$

$$\begin{bmatrix} x^d \end{bmatrix} = \begin{bmatrix} x^d_{1,1,1} & \cdots & x^d_{1,1,na} & x^d_{1,2,1} & \cdots & x^d_{1,2,na} \\ \cdots & x^d_{2,1,1} & \cdots & x^d_{2,1,na} & \cdots & x^d_{ny,1,na} & \cdots & x^d_{ny,nu,na} \end{bmatrix}^T$$

$$D^0 = \begin{bmatrix} d^0_{1,1} & \cdots & d^0_{1,nu} \\ \vdots & \ddots & \vdots \\ d^0_{ny,1} & \cdots & d^0_{ny,nu} \end{bmatrix} \in \mathbb{R}^{ny\times nu},$$

$$D^i = \begin{bmatrix} d^i_{1,1} & \cdots & d^i_{1,nu} \\ \vdots & \ddots & \vdots \\ d^i_{ny,1} & \cdots & d^i_{ny,nu} \end{bmatrix} \in \mathbb{R}^{ny\times nu}$$

$$F = \mathrm{diag}\left(r_{1,1,1}\cdots r_{1,1,na}\cdots r_{1,nu,1}\cdots r_{1,nu,na}\cdots r_{ny,1,1}\cdots r_{ny,1,na}\cdots r_{ny,nu,1}\cdots r_{ny,nu,na}\right) \in \mathbb{C}^{nd\times nd}$$

$$D^d = \mathrm{diag}\left(d^d_{1,1,1}\cdots d^d_{1,1,na}\cdots d^d_{1,nu,1}\cdots d^d_{1,nu,na}\cdots d^d_{ny,1,1}\cdots d^d_{ny,1,na}\cdots d^d_{ny,nu,1}\cdots d^d_{ny,nu,na}\right) \in \mathbb{C}^{nd\times nd}$$

$$N = \begin{bmatrix} J_1 \\ J_2 \\ \vdots \\ J_{ny} \end{bmatrix} \in \mathbb{R}^{nd\times nu}, \; J_i = \begin{bmatrix} 1 & 0 & \cdots & 0 \\ \vdots & \vdots & \ddots & \vdots \\ 1 & 0 & \cdots & 0 \\ & & \ddots & \\ 0 & 0 & \cdots & 1 \\ \vdots & \vdots & \ddots & \vdots \\ 0 & 0 & \cdots & 1 \end{bmatrix} \in \mathbb{R}^{nu\, na\times nu},$$

$i = 1, \ldots, ny$, $\quad \Psi = \begin{bmatrix} \Phi & & 0 \\ & \ddots & \\ 0 & & \Phi \end{bmatrix} \in \mathbb{R}^{ny\times nd}$,

$$\Phi = \begin{bmatrix} 1 & \cdots & 1 \end{bmatrix} \in \mathbb{R}^{nu\, na}.$$

In this model formulation, x^s corresponds to the integrating states introduced by the incremental form of the inputs, x^d corresponds to the stable states and x^i corresponds to the original integrating states of the system.

2.2 Infinite Prediction Horizon

The cost function of the infinite horizon MPC can be written as follows

$$V_{1,k}(\Delta u_k) = \sum_{j=1}^{\infty} e(k+j)^T\, Qe(k+j) + \sum_{j=0}^{m-1} \Delta u(k+j)^T\, R\Delta u(k+j) \qquad (5)$$

where $Q \in \mathbb{R}^{ny\times ny}$ is positive definite and $R \in \mathbb{R}^{nu\times nu}$ is positive semi-definite, $e(k+j) = y(k+j) - y^r$ is the error of the predicted output at sampling time $k+j$ including the effect of future control actions, y^r is the desired output reference and m is the control horizon (as usual in MPC, beyond the control horizon, the input moves are assumed equal to zero). As was described by Carrapiço and Odloak (2005), the cost function (5) would become unbounded since the model formulation described earlier contains integrating modes. To avoid this difficulty, it is necessary to include the following constraints into the optimization problem

$$e^s(k) + \left(D^0_m - D^i_{2m}\right)\Delta u_k = 0 \qquad (6)$$

$$x^i(k) + D^i_{1m}\Delta u_k = 0, \qquad (7)$$

where

$$e^s(k) = x^s(k) - y^r$$

$$D^0_m = \begin{bmatrix} D^0 & \cdots & D^0 \end{bmatrix} \in \mathbb{R}^{ny\times m.nu}$$

$$D^i_{1m} = \begin{bmatrix} D^i & \cdots & D^i \end{bmatrix} \in \mathbb{R}^{ny\times m.nu}$$

$$D^i_{2m} = \begin{bmatrix} 0 & \Delta t D^i & \cdots & (m-1)\Delta t D^i \end{bmatrix} \in \mathbb{R}^{ny\times m.nu}$$

$$\Delta u_k = \begin{bmatrix} \Delta u(k)^T & \cdots & \Delta u(k+m-1)^T \end{bmatrix}^T \in \mathbb{R}^{m.nu}$$

Now, substituting eqs. (6) and (7) into eq. (5) and rearranging the infinite term, the IHMPC can be formulated as follows

Problem P1

$$\min_{\Delta u_k} V_{1,k}(\Delta u_k) = \sum_{j=0}^{m-1} e(k+j)^T\, Qe(k+j) + x^d(k+m)^T\, \bar{Q} x^d(k+m) + \sum_{j=0}^{m-1} \Delta u(k+j)^T\, R\Delta u(k+j) \qquad (8)$$

subject to:
(6), (7), and

$$\Delta u(k+j) \in U, \quad j = 0, 1, \cdots, m-1 \qquad (9)$$

$$U = \left\{ \Delta u(k+j) \;\middle|\; \begin{array}{c} -\Delta u^{\max} \le \Delta u(k+j) \le \Delta u^{\max} \\ u^{\min} \le \Delta u(k-1) + \sum_{i=0}^{j} \Delta u(k+i) \le u^{\max} \end{array} \right\}$$

where $\bar{Q}$ is obtained from the solution of the well known Lyapunov equation

$$\bar{Q} - F^T \bar{Q} F = F^T \Psi^T Q \Psi F , \qquad (10)$$

and $\Delta u^{\max}, u^{\min}, u^{\max}$ are: the maximum input increment, and the minimum and maximum input values respectively.

2.3 Preventing Infeasibilities

As long as Problem P1 remains feasible, the convergence of the closed loop system can be guaranteed. However, depending on the size of the disturbance or the set point change, a conflict between constraints (6), (7) and (9) may arise. This is so because in practice the control horizon may be short to reduce the computer effort, and the maximum control move may be small to produce a smooth operation of the system. Carrapiço and Odloak (2005) presented two methods to extend the feasibility range of the infinite horizon controller for integrating systems with incremental state space model. One of these strategies, that includes slack variables to relax the constraints (6), (7) and (9) in Problem P1, is based on an optimization technique developed by Lee and Xiao (2000). The latter propose a two-step approach to solve the problem of including the steady state economic optimization in the conventional MPC of stable and integrating systems represented by step response models. Following this idea, the extended controller is obtained as the solution of the two following problems:

Problem P2a

$$\min_{\delta_k^i, \Delta u_{a,k}} \; V_{2a,k} = {\delta_k^i}^T S_2 \delta_k^i + \Delta u_{a,k}^T \bar{R} \Delta u_{a,k}$$

subject to

$$\Delta u_a(k+j) \in U, \;\; j \geq 0$$
$$x^i(k) + \delta_k^i + D_{1m}^i \Delta u_{a,k} = 0 \qquad (11)$$

where

$\Delta u_{a,k} = \left[\Delta u_a(k)^T \quad \cdots \quad \Delta u_a(k+m-1)^T \right]^T$, $\bar{R}$ and S_2 are positive definite matrices, and $\delta_k^i \in \mathbb{R}^{ny}$ is a vector of slack variables for the integrating states that provides extra degrees of freedom.

Let the optimal solution to Problem P2a be designated $\left(\delta_k^{i*}, \Delta u_{a,k}^*\right)$ and consider the resultant input increment

$$u^*(k+m-1) - u(k-1) = \sum_{j=0}^{m-1} \Delta u_a^*(k+j) . \qquad (12)$$

This optimal input increment is passed to a second problem, which is solved within the same time step:

Problem P2b

$$\min_{\Delta u_{b,k}, \delta_k^s} V_{2b,k} = \sum_{j=0}^{\infty} \left(e(k+j) + \delta_k^s \right)^T Q \left(e(k+j) + \delta_k^s \right) + \sum_{j=0}^{m-1} \Delta u_b(k+j)^T R \Delta u_b(k+j) + {\delta_k^s}^T S_1 \delta_k^s$$

subject to:

$$\Delta u_b(k+j) \in \mathrm{U}, \;\; j \geq 0$$
$$e^s(k) + \delta_k^s + (D_{2,m}^i - D_m^0) \Delta u_{b,k} = 0 \qquad (13)$$
$$u^*(k+m-1) - u(k-1) = \sum_{j=0}^{m-1} \Delta u_b(k+j)$$

where $\Delta u_{b,k} = \left[\Delta u_b(k)^T \quad \cdots \quad \Delta u_b(k+m-1)^T \right]^T$, S_1 is a positive definite matrix and $\delta_k^s \in \mathbb{R}^{ny}$ is a new vector of slack variables.

The control law obtained through the sequential solution of problems P2a and P2b above leads to the convergence of the system output to the reference value.

3. PLANT UNCERTAINTY DESCRIPTION

In order to characterize the model uncertainty, we assume that matrices D^0, D^d and F of the model represented in (3) are not exactly known but they lie within a set Ω. This set is composed by a finite number of integrating models with the same dimensions, that is,

$$\Omega = \left\{ \theta_1 \quad \cdots \quad \theta_L \right\} , \qquad (14)$$

where $\theta \triangleq (A, B)$ designate each individual plant of the set, and matrices A and B depend on matrices D^0, D^d and F. Note that matrix D^i is assumed to be known, which may be acceptable in many practical applications.

In addition, let us assume that the true plant θ_T lies within the set Ω, and there exist a most likely plant (also laying in Ω), which is named nominal plant (θ_N).

4. COST CONTRACTING MPC FOR INTEGRATING SYSTEMS

Badgwell (1997) developed a robust linear quadratic regulator for the multi-plant uncertainty described in (14). Combining Problems P2a and P2b with Badgwell's results, an extended cost contracting robust MPC for integrating systems can be obtained as the solution of the following sequence of optimization problems:

Problem P3ar

$$\min_{\Delta u_{a,k}, \delta_k^i(\theta_N)} V_{3a,k}\left(\Delta u_{a,k}, \delta_k^i(\theta_N)\right) = \delta_k^i(\theta_N)^T S_2 \delta_k^i(\theta_N) + \Delta u_{a,k}^T \bar{R} \Delta u_{a,k} \qquad (15)$$

subject to:

$$\Delta u_a(k+j) \in U, \quad j = 0, 1, ..., m-1 \qquad (16)$$
$$x^i(k) + \delta_k^i(\theta_N) + D_{1m}^i(\theta_N) \Delta u_{a,k} = 0, \qquad (17)$$

where

$$\Delta u_{a,k} = \left[\Delta u_a(k)^T \quad \cdots \quad \Delta u_a(k+m-1)^T \right]^T ,$$

Now, the optimal input increment is passed to the second problem through the constraint

$$\sum_{j=0}^{m-1} \Delta u_b(k+j) = \sum_{j=0}^{m-1} \Delta u_a^*(k+j) .$$

Problem P3br

$$\min_{\Delta u_{b,k},\delta_k^s(\theta_N)} V_{3b,k}\left(\Delta u_{b,k},\delta_k^s(\theta_N),\theta_N\right)$$
$$=\sum_{j=0}^{\infty}\left(e(k+j)+\delta_k^s(\theta_N)\right)^T Q\left(e(k+j)+\delta_k^s(\theta_N)\right)$$
$$+\sum_{j=0}^{m-1}\Delta u_b(k+j)^T R\Delta u_b(k+j)+\delta_k^s(\theta_N)^T S_1\delta_k^s(\theta_N) \quad (18)$$

subject to:

$$\Delta u_b(k+j)\in U,\quad j=0,1,...,m-1 \quad (19)$$
$$e^s(k)+\delta_k^s(\theta)+\left(D_m^0(\theta)-D_{2m}^i(\theta_N)\right)\Delta u_{b,k}=0,\ \theta\in\Omega \quad (20)$$
$$\sum_{j=0}^{m-1}\Delta u_b(k+j)=\sum_{j=0}^{m-1}\Delta u_a^*(k+j) \quad (21)$$
$$V_{3b,k}\left(\Delta u_{b,k},\delta_k^s(\theta),\theta\right)\le V_{3b,k}\left(\Delta\tilde{u}_{b,k},\tilde{\delta}_k^s(\theta),\theta\right),\qquad \theta\in\Omega \quad (22)$$

where $\Delta u_a^*(k+i)$ stands for the optimal solution obtained in Problem P3ar,

$$\Delta\tilde{u}_{b,k}=\left[\Delta u_b^*(k)^T\ \cdots\ \Delta u_b^*(k+m-2)^T\ \ 0\right]^T,$$

and $\tilde{\delta}_k^s(\theta)$ are such that:

$$e^s(k)+\tilde{\delta}_k^s(\theta)+\left(D_m^0(\theta)-D_{2m}^i(\theta_N)\right)\Delta\tilde{u}_{b,k}=0,\ \theta\in\Omega \quad (23)$$

Remarks

* Note that in Problem P3ar, since we assume that all models have the same matrix D^i, only the nominal one is considered.

* Equations (20), (22) and (23) represent L constraints each (as many as models are considered), that has to be satisfied by the same Δu_k, and by $\delta_k^s(\theta_1)\cdots\delta_k^s(\theta_L)$. Despite both, Δu_k and δ_k^s are optimization variables, only Δu_k is actually independent of the model since a given input sequence generates one output steady state offset per model.

* $x^s(k)$ and $x^i(k)$ are measured states and then correspond to the actual plant θ_T.

* Variable $\Delta\tilde{u}_{b,k}$ is the optimal control sequence obtained at time step *k-1* and translated to time *k*.

4.1 Convergence of the method

The following theorem shows that the control algorithm produced by the solution of Problem P3r provides convergence of the true system output to the reference value.

Theorem 1: Consider an integrating system whose true model is unknown but lies within the set Ω. Assume that in the control objective $V_{3b,k}$, the weight S_1 is large enough to prevent offset in the system output.

Assume also that Problem P3r is feasible at time steps *k, k+1, k+2, ...* and the system outputs are not saturated. Then, the control law obtained as the solution of Problem P3r drives the true system to the reference value.

Proof

First stage

Let the optimal solution to Problem P3ar be $\Delta u_{a,k}^*,\delta_k^{i*}$ [1]; and let the optimal solution to Problem P3br, be $\Delta u_{b,k}^*,\delta_k^{s*}(\theta)$, $\theta\in\Omega$. Note that for every optimal input sequence, there is one slack variable per model. The first control move $\Delta u_b^*(k)$ is injected into the true process and the time is moved to *k+1*. Because of equation (21), it can be shown that $\Delta\tilde{u}_{a,k+1}=\left[\Delta u_b^*(k+1)^T\ \cdots\ \Delta u_b^*(k+m-1)^T\ \ 0\right]^T$ and $\delta_{k+1}^i=\delta_k^{i*}$ is a feasible solution to Problem P3ar. Now, considering that $\bar{R}$ is negligible in comparison to S_2, the corresponding value of the objective function of Problem P3ar at time *k*+1 is still $V_{3a,k}^*$. Consequently, the optimal solution of Problem P3ar will be $V_{3a,k+1}^*\le V_{3a,k}^*$. Since we have selected $\bar{R}<<S_2$, the objective function of Problem P3ar will converge to zero, which corresponds to $\delta_k^i=0$.

Second stage

Now, for a large *k*, $\delta_k^i(\theta_T)=0$; that is[2]:

$$x^i(k)+D_{1m}^i\Delta u_{a,k}^*=0. \quad (24)$$

Take again the solution $\Delta u_{b,k}^*,\delta_k^{s*}(\theta)$, $\theta\in\Omega$. For the true model the corresponding cost is:

$$V_{3b,k}\left(\Delta u_{b,k}^*,\delta_k^{s*}(\theta_T),\theta_T\right)$$
$$=\sum_{j=1}^{\infty}\left(e(k+j)+\delta_k^s(\theta_T)\right)^T Q\left(e(k+j)+\delta_k^s(\theta_T)\right)$$
$$+\sum_{j=0}^{m-1}\Delta u_b(k+j)^T R\Delta u_b(k+j)+\delta_k^s(\theta_T)^T S_1\delta_k^s(\theta_T)$$

Assume that we inject the first control action $\Delta u_b^*(k)$ into the true plant and move time to *k+1*. At this time, the objective for $\left(\Delta\tilde{u}_{b,k+1},\tilde{\delta}_{k+1}^s(\theta_T),\theta_T\right)$, is:

$$V_{3b,k+1}\left(\Delta\tilde{u}_{b,k+1},\tilde{\delta}_{k+1}^s(\theta_T),\theta_T\right)=$$
$$V_{3b,k}\left(\Delta u_{b,k}^*,\delta_k^{s*}(\theta_T),\theta_T\right)-\left(e(k+1)+\delta_k^{s*}(\theta_T)\right)^T$$
$$Q\left(e(k+1)+\delta_k^{s*}(\theta_T)\right)-\Delta u_b^*(k)^T R\Delta u_b^*(k),$$

[1] There is only one slack δ_k^i for all the models because D^i is known.

[2] Note that who decides the value of the slack $\delta_k^i(\theta_T)$ (which is zero in this case) is the complete increment $\sum_{j=0}^{m-1}\Delta u_a(k+j)$, and not the individual increments $\Delta u_a(k+j)$.

(25)

where

$$\Delta\tilde{u}_{b,k+1} = \left[\Delta u_b^*(k+1)^T \quad \cdots \quad \Delta u_b^*(k+m-1)^T \quad 0 \right]^T$$

and $\tilde{\delta}_{k+1}^s(\theta_T)$ is such that

$$e^i(k+1) + \tilde{\delta}_{k+1}^s(\theta_T) + \left(D_m^0(\theta_T) - D_{2m}^i\right)\Delta\tilde{u}_{b,k+1} = 0.$$

Note that, since the state at time *k+1* corresponds to the true plant, and $\delta_k^i = 0$; then $\tilde{\delta}_{k+1}^s(\theta_T) = \delta_k^{s^*}(\theta_T)$. Since no new input increments are added in $\Delta\tilde{u}_{b,k+1}$, the predicted output (in the absence of integrating modes) will be the same as in the case of using $\Delta u_{b,k}^*$, for the true models.

Now assume that the optimal solution to problem P3br is found at time *k+1*. We know that the plant lies in the family Ω, so the robustness constraint (22) must be satisfied for the true plant at time *k+1*. That is:

$$V_{3b,k+1}\left(\Delta u_{b,k+1}^*, \delta_{k+1}^{s^*}(\theta_T), \theta_T\right) \leq V_{3b,k+1}\left(\Delta\tilde{u}_{b,k+1}, \tilde{\delta}_{k+1}^s(\theta_T), \theta_T\right) \tag{26}$$

Combining (25) with (26) we obtain:

$$\begin{aligned} V_{3b,k+1}\left(\Delta u_{b,k+1}^*, \delta_{k+1}^{s^*}(\theta_T), \theta_T\right) - V_{3b,k}\left(\Delta u_{b,k}^*, \delta_k^{s^*}(\theta_T), \theta_T\right) \\ \leq -\left(e(k+1) + \delta_k^{s^*}(\theta_T)\right)^T Q\left(e(k+1) + \delta_k^{s^*}(\theta_T)\right) \\ - \Delta u_b^*(k)^T R \Delta u_b^*(k) \end{aligned}$$

This shows that the sequence of optimal cost is non-increasing. Finally, since we assume that S_1 is large enough to prevent output offset, the error converges to zero for the true plant.

5. SIMULATION RESULTS

The system adopted to test the robust controller is based on the ethylene oxide reactor system presented by Rodrigues and Odloak (2003). This is a typical example of the chemical process industry that exhibits stable and integrating poles. The following transfer matrix represents the system

$$G(s) = \begin{bmatrix} \dfrac{-0.19}{s} & \dfrac{-1.7}{19.5s+1} \\ \dfrac{-0.763}{31.8s+1} & \dfrac{0.235}{s} \end{bmatrix},$$

and the translation into the model formulation presented in section 2, can be seen in Carrapiço and Odloak (2005).

We focus on a case in which both, the stable gains and the time constants are uncertain parameters. The true plant has a larger gain and a smaller time constant than the nominal model used in the controller, which is a quite critical situation. The set Ω contains the five models indicated in Table 1.

The differences between the nominal model and the true plant were selected so that the nominal controller becomes unstable.

Table 1: Parameters of the Models used in the Test.

	Mo 1	Mo 2	Mo 3	Mo 4	Nom	True
d^0_{12}	-4.68	-4.68	-0.17	-0.17	-1.7	-4.68
d^0_{21}	-2.10	-0.08	-2.10	-0.08	-0.76	-2.10
r_{12}	.8787	.9738	.9262	.9738	.9500	.8787
r_{21}	.8963	.9448	.9932	.9932	.9690	.8963

Figures I, II and III show the simulation responses when a set point change of 2 and 3 units is made on output 1 and 2 respectively. In Figure I, it can be seen that the input constraint $\Delta u_{\max}$, u_{min} and u_{max} become active during the transient states. This shows the capability of the controller to handle input constraints, together with the additional robust requirements. Another property to remark is the flexibility of the controller to tolerate a short control horizon. This is a critical parameter to reduce the computational cost.

Figures IV and V, show the responses for the same system when the robust constraints are not added to the MPC formulation (nominal controller). In this case the manipulated variables saturates giving oscillatory system behaviour. The tuning parameters of the robust controller are shown in Table 2.

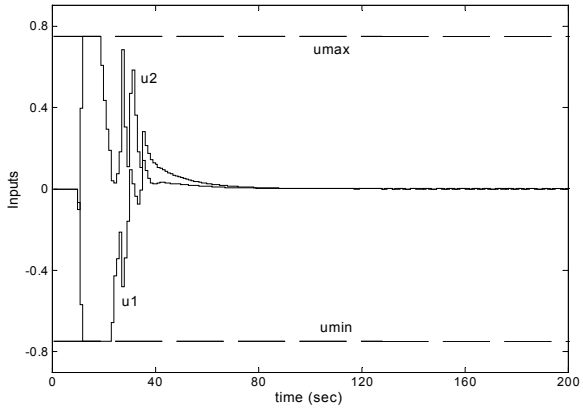

Figure I. Input responses of the robust controller.

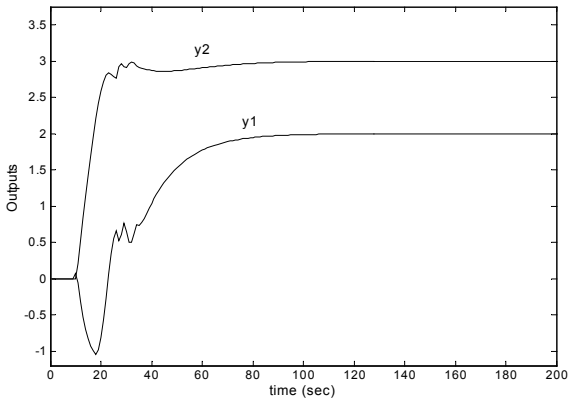

Figure II. Output responses of the robust controller.

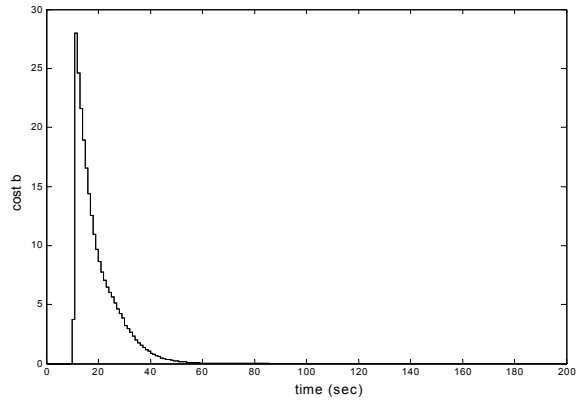

Figure III. Secondary cost of the robust controller.

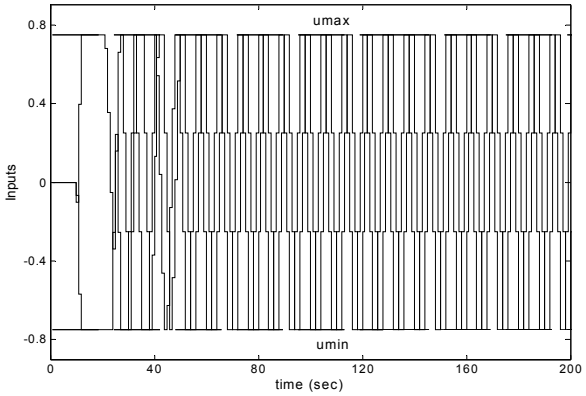

Figure IV. Input responses of the nominal controller, maintaining the same tuning parameters.

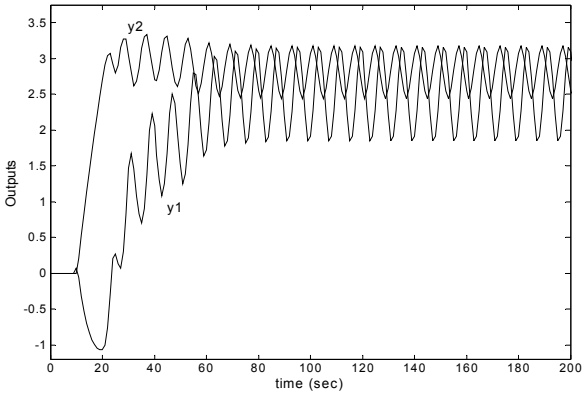

Figure V. Output responses of the nominal controller, maintaining the same tuning parameters.

Table 2: Controller parameters.

T	m	Δu_{max}	u_{max}	u_{min}
1	3	0.5	0.75	-0.75

Q	R	$\overline{R}$	S_1	S_2
0.1	0.1	0.1	2.5	1000

6. CONCLUSION

In this paper we have presented a method to extend a particular robust MPC controller to the case of systems containing stable and integrated modes. Robust stability is achieved by assembling cost contracting constraints with the constraints necessary to compensate the unstable modes of the system. On the other hand, the control formulation allows dealing with problems that cannot be reduced to the regulator problem due to unknown disturbances or model non-linearities, and can be directly implemented in real applications. A representative example shows the capability of the controller to handle significant uncertainty in both, the stable gains and the time constants of the system, in the case that inputs constraints become active during the transient states.

REFERENCES

Badgwell T.A. (1997). Robust model predictive control of stable linear systems. *International Journal of Control*, 68, 797-818.

Carrapiço O.L. and D. Odloak. (2005). A stable model predictive control for integrating process. *Computers and Chemical Engineering,* 29, 1089-1099.

Kothare M.V., V. Barakrishnan and M. Morari. (1996). Robust constrained model predictive control using linear matrix inequalities. *Automática*, 32, 1361-1379.

Lee J.H. and J. Xiao. (2000). Use of two-stage optimization in model predictive control of stable and integrating systems. *Computer and Chemical Engineering*, 23, 1591-1596.

Lee J.H. and Z. Yu. (1997). Worst case formulation of model predictive control for systems with bounded parameters. *Automatica*, 33(5), 763-781.

Mayne, D.Q., J. B. Rawlings, C.V. Rao and P. O. Scokaert. (2000). Constrained model predictive control: stability and optimality. *Automatica*, 36, 789–814.

Morari M. and J.H. Lee. (1999). Model predictive control: past, present and future. *Computer and Chemical Engineering,* 23, 667-682.

Odloak D. (2004). Extended Robust Model Predictive Control. *AIChE Journal*., 50 (8) 1824-1836.

Qin S.J. and T.A. Badgwell. (2003). A Survey of Industrial Model Predictive Control Technology. *Control Engineering Practice*, 11 (7) 733-764.

Ralhan S. and T.A. Badgwell. (2000). Robust control of stable linear systems with continuous uncertainty. *Computer and Chemical Engineering*, 24, 2533-2544.

Rodrigues, M.A. and D. Odloak. (2003). An infinite horizon model predictive control for stable and integrating processes. *Computer and Chemical Engineering,* 27, 1113-1128.

ADCHEM 2006

International Symposium on Advanced Control of Chemical Processes
Gramado, Brazil – April 2-5, 2006

GENERALIZED PREDICTIVE CONTROL IN FAST-RATE SINGLE-RATE AND INPUT MULTIPLEX TYPE MULTIRATE SYSTEM

Takao Sato * **Akira Inoue** **

* *Division of Mechanical System, Department of Mechanical Engineering, Graduate School of Engineering, University of Hyogo, 2167 Shosha, Himeji, Hyogo, 671-2201 JAPAN*
** *Division of Industrial Innovation Sciences, Graduate School of Natural Science and Technology, Okayama University, 3-1-1, Tsushima-naka, Okayama, 700-8530 JAPAN*

Abstract: This paper discusses the designs of Generalized Predictive Control (GPC) scheme. GPC is designed in two cases; the first is a multirate system, where the sampling interval of a plant output is an integer multiple of the holding interval of a control input, and the second is a fast-rate single-rate system, where both the holding and sampling intervals are equivalent to the holding interval of the multirate system. Furthermore, the relation between them is investigated. This study gives the conditions that the fast-rate single-rate and the multirate GPC become equivalent.

Keywords: generalized predictive control, single-rate system, multirate system, lifting, fast-rate system, single-rate system

1. INTRODUCTION

In digital control a system is called a single-rate system, where the holding interval of a control input is equal to the sampling interval of a plant output. On the other hand, a system is called a multirate system, where these intervals are not equal. The multirate system is also called as a dual-rate system. This paper discusses a single-input single-output multirate linear time-invariant system, where the sampling interval of a plant output is an integer multiple of the holding interval of a control input. In this case, a control input is updated at a fast-rate, but a plant output is sampled at a slow-rate.

Generally, a fast-rate single-rate system, where input and output intervals are equivalent and are sampled or updated at a fast-rate, is superior to a slow-rate single-rate system, where input and output intervals are equivalent and are sampled or updated at a slow-rate. However, these intervals cannot be always set arbitrarily due to constraints or specifications of actuators or sensors. Then, a fast-rate single-rate system cannot be obtained, but only a slow-rate single-rate or a dual-rate system can be realized. In that case it is expected that a multirate system is better than the slow-rate single-rate system. The design of the dual-rate system is obtained by a similar way to the design of the slow-rate single-rate system, that is, first, the dual-rate system can be transformed into a multi-input single-output slow-rate single-rate system using the lifting (Chen and Francis, 1995), then the dual-rate system is designed the same as the slow-rate single-rate system.

However, in the dual-rate system, since ripples may emerge between sampled outputs (Tangirala *et al.*, 1999), and the ripples should be suppressed. Generalized Predictive Control (GPC) (Clarke *et al.*, 1987*a*; Clarke *et al.*, 1987*b*) in a multirate system was proposed (Scattolini, 1992), and the ripples can be suppressed by using this multirate GPC because an integrator is included in the process of the design. Sheng *et al.* extended the design method of GPC considering intersample performance (Masuda *et al.*, 1997) into a multirate system (Sheng *et al.*, 2001*a*). Because this design method takes care of intersample output, the ripples are suppressed. In this paper, to suppress the ripples, GPC is designed considering the variation in control input between sampled instants. This paper also discusses the relation between the fast-rate single-rate and the dual-rate GPC and shows the conditions that the fast-rate single-rate and the dual-rate GPC are equivalent. This study results in an unified design method of the fast-rate single-rate and the dual-rate GPC.

This paper is organized as follows. In section 2, a plant model is given. A fast-rate single-rate and a dual-rate GPC law are derived in section 3 and 4, respectively. By comparing the GPC laws in the fast-rate single-rate and the dual-rate system, the relation between them is shown in section 5.

2. PLANT MODEL

Consider a plant with the following discrete-time model

$$\bar{\boldsymbol{x}}[k+1] = \bar{A}\bar{\boldsymbol{x}}[k] + \bar{\boldsymbol{b}}u[k] \tag{1}$$

$$y[k] = \bar{\boldsymbol{c}}^T\bar{\boldsymbol{x}}[k] \tag{2}$$

where, $u[k]$ and $y[k]$ the control input and the plant output, and n-th order vector $\bar{\boldsymbol{x}}[k]$ is the state variable. $\bar{A}$, $\bar{\boldsymbol{b}}$ and $\bar{\boldsymbol{c}}^T$ are an $n \times n$ matrix and n-th vectors, respectively.

The extended model with an integrator is given as (Scattolini, 1992)

$$\boldsymbol{x}[k+1] = A\boldsymbol{x}[k] + \boldsymbol{b}\Delta u[k] \tag{3}$$

$$y[k] = \boldsymbol{c}^T\boldsymbol{x}[k] \tag{4}$$

where,

$$A = \begin{bmatrix} \bar{A} & \bar{\boldsymbol{b}} \\ \boldsymbol{0}_{1,n} & 1 \end{bmatrix} \tag{5}$$

$$\boldsymbol{b} = \begin{bmatrix} \bar{\boldsymbol{b}} \\ 1 \end{bmatrix} \tag{6}$$

$$\boldsymbol{c}^T = \begin{bmatrix} \bar{\boldsymbol{c}}^T & 0 \end{bmatrix} \tag{7}$$

$$\boldsymbol{x}[k] = \begin{bmatrix} \bar{\boldsymbol{x}}[k] \\ u[k-1] \end{bmatrix} \tag{8}$$

$$\Delta = 1 - z^{-1}. \tag{9}$$

z^{-1} is the one-step backward shift operator.

When the plant output is sampled every step and the control input is updated every step, the control system is called a fast-rate single-rate system, and when both of the intervals are l steps, the system is called a slow-rate single-rate system. On the other hand, the system is called a dual-rate system when the control input is updated every step, but the plant output is sampled at interval of l steps.

The following are assumed in this paper.

[A.1] The model of a plant is known.
[A.2] A reference input is given as a step type.
[A.3] The control input is updated every step.
[A.4] In the fast-rate single-rate system, the plant output is sampled every step.
[A.5] In the dual-rate system, the plant output is sampled every l steps.

The fast-rate single-rate system is simply described as the single-rate system hereafter.

3. SINGLE-RATE GPC

In this section a GPC law is derived in the single-rate system.

3.1 Performance function

The performance function of the single-rate GPC is given by the following

$$J_s = E\left[\sum_{j=N_{s,1}}^{N_{s,2}} \mu_{s,j}\{y[k+j] - w[k+j]\}^2 + \sum_{j=1}^{N_{s,u}} \lambda_{s,j}\Delta u[k+j-1]^2\right] \tag{10}$$

where, $N_{s,1}$, $N_{s,2}$ and $N_{s,u}$ are minimum prediction horizon, maximum prediction horizon and control horizon, respectively. $\mu_{s,j}$ is a weighting factor of the error between the reference input $w[k+j]$ and the plant output, and $\lambda_{s,j}$ is a weighting factor of the variation in the control input, respectively. A GPC law minimizing J_s is derived in the single-rate system.

3.2 Reference Input

The reference input in the single-rate GPC is given as follows (Clarke *et al.*, 1987*a*).

$$w[k] = y[k] \tag{11}$$

$$w[k+j] = (1-\alpha_s)r + \alpha_s w[k+j-1] \quad (0 \le \alpha_s < 1) \tag{12}$$

where, r is the set-point, and α_s is a design parameter. The future reference input is rewritten

by (13) when the set-point is given as step type (Sato and Inoue, 2006).

$$w[k+j] = \alpha_s^j y[k] + (1-\alpha_s^j) r \tag{13}$$

3.3 Predictive Output

One step and two steps forward predictive output are given as

$$y[k+1] = \boldsymbol{c}^T A \boldsymbol{x}[k] + \boldsymbol{c}^T \boldsymbol{b} \Delta u[k] \tag{14}$$

$$y[k+2] = \boldsymbol{c}^T A^2 \boldsymbol{x}[k] + \boldsymbol{c}^T A \boldsymbol{b} \Delta u[k] + \boldsymbol{c}^T \boldsymbol{b} \Delta u[k+1]. \tag{15}$$

Repeating these calculations, j steps forward predictive output is calculated by

$$y[k+j] = \boldsymbol{c}^T A^j \boldsymbol{x}[k] + \boldsymbol{c}^T \sum_{i=0}^{j-1} A^i \boldsymbol{b} \Delta u[k+j-1-i]. \tag{16}$$

3.4 Derivation of Control Law

The future control input series minimizing (10) is given as follows.

$$\Delta \boldsymbol{u}_s[k] = (G_s^T M_s G_s + \Lambda_s)^{-1} \times G_s^T M_s (\boldsymbol{w}_s[k] - H_s \boldsymbol{x}[k]) \tag{17}$$

where,

$$\Delta \boldsymbol{u}_s[k] = \begin{bmatrix} \Delta u[k] \\ \Delta u[k+1] \\ \vdots \\ \Delta u[k+N_{s,u}-1] \end{bmatrix} \tag{18}$$

$$\boldsymbol{w}_s[k] = \begin{bmatrix} w[k+N_{s,1}] \\ w[k+N_{s,1}+1] \\ \vdots \\ w[k+N_{s,2}] \end{bmatrix} \tag{19}$$

$$H_s = \begin{bmatrix} \boldsymbol{c}^T A^{N_{s,1}} \\ \boldsymbol{c}^T A^{N_{s,1}+1} \\ \vdots \\ \boldsymbol{c}^T A^{N_{s,2}} \end{bmatrix} \tag{20}$$

$$\Lambda_s = \mathrm{diag}\{\lambda_{s,1}, \lambda_{s,2}, \cdots, \lambda_{s,N_{s,u}}\} \tag{21}$$

$$M_s = \mathrm{diag}\{\mu_{s,N_{s,1}}, \mu_{s,N_{s,1}+1}, \cdots, \mu_{s,N_{s,2}}\} \tag{22}$$

$$(i,j) \text{ element of } G_s = \begin{cases} \boldsymbol{c}^T A^{N_{s,1}+i-1-j} \boldsymbol{b} & (N_{s,1}+i-1-j \geq 0) \\ 0 & (N_{s,1}+i-1-j < 0) \end{cases}. \tag{23}$$

The standard single-rate GPC utilizes only the first element of the obtained control inputs $\Delta \boldsymbol{u}_s[k]$ because of the use of Receding Horizon.

On the other hand, in order to show the relation with the dual-rate GPC derived in the next section, the first l elements ($\Delta \boldsymbol{u}[k]$) of $\Delta \boldsymbol{u}_s[k]$ are utilized in this paper; therefore the following control law is obtained.

$$\Delta \boldsymbol{u}[k] = \begin{bmatrix} I_l & \boldsymbol{0}_{l,(N_{s,u}-l)} \end{bmatrix} (G_s^T M_s G_s + \Lambda_s)^{-1} \times G_s^T M_s (\boldsymbol{w}_s[k] - H_s \boldsymbol{x}[k]) \tag{24}$$

where,

$$\Delta \boldsymbol{u}[k] = \begin{bmatrix} \Delta u[k] \\ \Delta u[k+1] \\ \vdots \\ \Delta u[k+l-1] \end{bmatrix}. \tag{25}$$

4. DUAL-RATE GPC

In the dual-rate system, the plant output is sampled every l steps due to the assumption. Hence, the dual-rate system is transformed into the slow-rate single-rate system by using the lifting (Chen and Francis, 1995), and a GPC law is derived as l-inputs single-output single-rate system.

4.1 Lifted System

Using the lifting (Chen and Francis, 1995), single-input single-output fast-rate single-rate system (3) and (4) is transformed into the following l-inputs single-output slow-rate single-rate system.

$$\boldsymbol{x}[k+l] = A_l \boldsymbol{x}[k] + B_l \Delta \boldsymbol{u}[k] \tag{26}$$

$$y[k] = \boldsymbol{c}^T \boldsymbol{x}[k] \tag{27}$$

where,

$$A_l = A^l \tag{28}$$

$$B_l = \begin{bmatrix} A^{l-1}\boldsymbol{b} & A^{l-2}\boldsymbol{b} & \cdots & A\boldsymbol{b} & \boldsymbol{b} \end{bmatrix}. \tag{29}$$

The dual-rate GPC is designed using this lifted single-rate system.

4.2 Performance function

The dual-rate GPC derives future control input series minimizing the following performance function.

$$J_m = E\left[\sum_{j=N_{m,1}}^{N_{m,2}} \mu_{m,j} \{y[k+jl] - w[k+jl]\}^2 + \sum_{j=1}^{N_{m,u}} ||\Delta \boldsymbol{u}[k+(j-1)l]||^2_{\bar{\Lambda}_{m,j}} \right] \tag{30}$$

$$\bar{\Lambda}_{m,j} = \mathrm{diag}\{\lambda_{m,(j-1)l+1}, \lambda_{m,(j-1)l+2}, \cdots, \lambda_{m,jl}\} \tag{31}$$

where, $N_{m,1}$, $N_{m,2}$ and $N_{m,u}$ are minimum prediction horizon, maximum prediction horizon and control horizon of the dual-rate GPC, respectively. $\mu_{m,j}$ and $\lambda_{m,j}$ are weighting factors of the error and the variation in the control input, respectively.

4.3 Reference Input

In designing the dual-rate GPC, a reference input is given by the following.

$$w[k] = y[k] \tag{32}$$

$$w[k+jl] = (1-\alpha_m)r + \alpha_m w[k+(j-1)l] \quad (0 \le \alpha_m < 1) \tag{33}$$

The reference input in the dual-rate system is rewritten by (34) (Sato and Inoue, 2005).

$$w[k+jl] = \alpha_m^j y[k] + (1-\alpha_m^j)r \tag{34}$$

4.4 Predictive Output

In the dual-rate system, the plant output is sampled at interval of l steps, and l steps and $2l$ steps forward predictive output are given as

$$y[k+l] = \boldsymbol{c}^T A_l \boldsymbol{x}[k] + \boldsymbol{c}^T B_l \Delta \boldsymbol{u}[k] \tag{35}$$

$$y[k+2l] = \boldsymbol{c}^T A_l^2 \boldsymbol{x}[k] + \boldsymbol{c}^T A_l B_l \Delta \boldsymbol{u}[k] + \boldsymbol{c}^T B_l \Delta \boldsymbol{u}[k+l]. \tag{36}$$

Repeating these calculations, jl steps forward predictive output of the lifted system is calculated by

$$y[k+jl] = \boldsymbol{c}^T A_l^j \boldsymbol{x}[k] + \boldsymbol{c}^T \sum_{i=0}^{j-1} A_l^i B_l \Delta \boldsymbol{u}[k+(j-1-i)l]. \tag{37}$$

4.5 Derivation of Control Law

With the predictive output (37), the future control input series minimizing the performance function is obtained by the followings (Sheng *et al.*, 2001*b*).

$$\Delta \boldsymbol{u}_m[k] = (G_m^T M_m G_m + \Lambda_m)^{-1} \times G_m^T M_m (\boldsymbol{w}_m[k] - H_m \boldsymbol{x}[k]) \tag{38}$$

where,

$$\Delta \boldsymbol{u}_m[k] = \begin{bmatrix} \Delta \boldsymbol{u}[k] \\ \Delta \boldsymbol{u}[k+l] \\ \vdots \\ \Delta \boldsymbol{u}[k+(N_{m,u}-1)l] \end{bmatrix} \tag{39}$$

$$\boldsymbol{w}_m[k] = \begin{bmatrix} w[k+N_{m,1}l] \\ w[k+(N_{m,1}+1)l] \\ \vdots \\ w[k+N_{m,2}l] \end{bmatrix} \tag{40}$$

$$H_m = \begin{bmatrix} \boldsymbol{c}^T A_l^{N_{m,1}} \\ \boldsymbol{c}^T A_l^{N_{m,1}+1} \\ \vdots \\ \boldsymbol{c}^T A_l^{N_{m,2}} \end{bmatrix} \tag{41}$$

$$\Lambda_m = \text{block diag}\{\bar{\Lambda}_{m,1}, \bar{\Lambda}_{m,2}, \cdots, \bar{\Lambda}_{s,N_{m,u}}\} \tag{42}$$

$$M_m = \text{diag}\{\mu_{m,N_{m,1}}, \mu_{m,N_{m,1}+1}, \cdots, \mu_{m,N_{m,2}}\} \tag{43}$$

(i,j) block of block matrix G_m =

$$\begin{cases} \boldsymbol{c}^T A_l^{N_{m,1}-1+i-j} B_l & (N_{m,1}+i-1-j \ge 0) \\ \boldsymbol{0}_{1,l} & (N_{m,1}+i-1-j < 0) \end{cases}. \tag{44}$$

Because the lifted single-rate system is l-inputs system, the first l elements of $\Delta \boldsymbol{u}_m[k]$, that is $\Delta \boldsymbol{u}[k]$, are utilized. Thus, multiplying both sides of (38) by $[I_l \ \ \boldsymbol{0}_{l,(N_{m,u}-1)}]$ from the left, the next dual-rate GPC law is obtained.

$$\Delta \boldsymbol{u}[k] = \left[I_l \ \ \boldsymbol{0}_{l,(N_{m,u}-1)} \right] (G_m^T M_m G_m + \Lambda_m)^{-1} \times G_m^T M_m (\boldsymbol{w}_m[k] - H_m \boldsymbol{x}[k]) \tag{45}$$

5. CONDITIONS

In this section, we give the conditions that the performance functions in the single-rate and the dual-rate system become equivalent.

With (16), jl steps forward of the prediction output in the single-rate system is rewritten as

$$y[k+jl] = \boldsymbol{c}^T A^{jl} \boldsymbol{x}[k] + \boldsymbol{c}^T \sum_{i=0}^{jl-1} A^i \boldsymbol{b} \Delta u[k+jl-1-i]. \tag{46}$$

Further the second term in the right hand of (46) is rewritten as

$$\begin{aligned} &\boldsymbol{c}^T \sum_{i=0}^{jl-1} A^i \boldsymbol{b} \Delta u[k+jl-1-i] \\ &= \boldsymbol{c}^T \sum_{i=0}^{j-1} \sum_{h=il}^{(i+1)l-1} A^h \boldsymbol{b} \Delta u[k+jl-1-h] \\ &= \boldsymbol{c}^T \sum_{i=0}^{j-1} A_l^i B_l \Delta \boldsymbol{u}[k+(j-1-i)l]. \end{aligned} \tag{47}$$

Hence, it follows from (46) and (47) that jl steps forward predictive outputs of the fast-rate single-rate and the dual-rate GPC are equivalent.

It follows from (13) and (34) that the weighting factor of the reference input is determined by

$$\alpha_s^l = \alpha_m. \tag{48}$$

Then, the reference input in the single-rate and the dual-rate system are equivalent.

In the dual-rate system, because the plant output is sampled at interval of l steps, the weighting factor $\mu_{s,j}$ of the single-rate GPC is designed as (49) so as to evaluate the control error between the

reference input and the future predictive output at the same step as the dual-rate system.

$$\mu_{s,j} = \begin{cases} \mu_{m,j/l} & (\mathrm{rem}(j,l)=0) \\ 0 & (\text{others}) \end{cases} \tag{49}$$

where j is divisible by l with remainder $\mathrm{rem}(j,l)$.

The following conditions of prediction and control horizon are required so that the performance functions of the dual-rate and the single-rate GPC become equivalent.

$$N_{s,1} = lN_{m,1} \tag{50}$$
$$N_{s,2} = lN_{m,2} \tag{51}$$
$$N_{s,u} = lN_{m,u} \tag{52}$$

(53) gives the condition that the weighting factor of the control input in the single-rate and the dual-rate system are equivalent.

$$\lambda_{s,j} = \lambda_{m,j} \quad (j = 1, \cdots, N_{s,u}) \tag{53}$$

where $N_{s,u}$ is designed so that (52) is satisfied.

If the design parameters of GPC satisfy the conditions (48) $\sim$ (53), the single-rate and the dual-rate GPC law become equivalent. As mentioned above, the dual-rate GPC law can be taken as the fast-rate single-rate GPC law satisfying the conditions. Further, l control inputs of the dual-rate GPC designed as the slow-rate single-rate system using the lifting can be equivalent to the first l elements of the future control input series of the fast-rate single-rate GPC.

6. NUMERICAL EXAMPLE

Consider a plant described by the following linear time-invariant continuous-time model.

$$\dot{\boldsymbol{x}}(t) = \begin{bmatrix} -0.14 & -0.0040 \\ 1.00 & 0 \end{bmatrix} \boldsymbol{x}(t) + \begin{bmatrix} 1 \\ 0 \end{bmatrix} u(t) \tag{54}$$
$$y(t) = \begin{bmatrix} 0 & 0.0040 \end{bmatrix} \boldsymbol{x}(t) \tag{55}$$

We will show the responses with the single-rate and the dual-rate GPC. The simulation length is $50[s]$, and the set-point r is 1. The control input is updated at interval of $1[s]$, but the plant output is sampled at interval of $2[s]$. The dual-rate GPC is designed first, and then the single-rate GPC whish is equivalent to the dual-rate GPC is designed.

The design parameters are set as: $N_{m,1} = 1$, $N_{m,2} = 5$, $N_{m,u} = 2$, $\alpha_m = 0.75^2$, $\lambda_{m,j} = 0.005$ $(j = 1, \cdots, N_{m,u})$, $\mu_{m,j} = 1$ $(j = N_{m,1}, \cdots, N_{m,2})$. With these parameters the dual-rate GPC law is given by the following.

$$\begin{aligned} \Delta \boldsymbol{u}[k] = & \begin{bmatrix} 0.71 & 1.6 & 1.9 & 1.6 & 0.98 \\ -0.20 & 0.20 & 0.64 & 1.1 & 1.5 \end{bmatrix} \\ & \times \left(\begin{bmatrix} 0.56y[k] + 0.44r \\ 0.32y[k] + 0.68r \\ 0.18y[k] + 0.82r \\ 0.10y[k] + 0.90r \\ 0.056y[k] + 0.94r \end{bmatrix} \right. \\ & \left. - \begin{bmatrix} 0.0070 & 0.0040 & 0.0073 \\ 0.012 & 0.0039 & 0.027 \\ 0.016 & 0.0038 & 0.055 \\ 0.019 & 0.0036 & 0.089 \\ 0.020 & 0.0035 & 0.13 \end{bmatrix} \boldsymbol{x}[k] \right) \end{aligned} \tag{56}$$

Next, the single-rate GPC law is designed using (48) $\sim$ (53). The design parameters of the single-rate GPC is set as: $N_{s,1} = 2$, $N_{s,2} = 10$, $N_{s,u} = 4$, $\alpha_s = 0.75$, $\lambda_{s,j} = 0.005$ $(j = 1, \cdots, N_{s,u})$,

$$\mu_{s,j} = \begin{cases} 1 & (\mathrm{rem}(j,2)=0) \\ 0 & (\text{others}) \end{cases} \tag{57}$$

$(j = N_{s,1}, \cdots, N_{s,2})$. Then, the dual-rate GPC law is given by the following.

$$\begin{aligned} \Delta \boldsymbol{u}[k] = & \begin{bmatrix} 0.71 & 0 & 1.63 & 0 & 1.9 & 0 & 1.6 & 0 & 0.98 \\ -0.20 & 0 & 0.20 & 0 & 0.64 & 0 & 1.1 & 0 & 1.5 \end{bmatrix} \\ & \times \left(\begin{bmatrix} 0.56y[k] + 0.44r \\ 0 \\ 0.32y[k] + 0.68r \\ 0 \\ 0.18y[k] + 0.82r \\ 0 \\ 0.10y[k] + 0.90r \\ 0 \\ 0.056y[k] + 0.94r \end{bmatrix} \right. \\ & \left. - \begin{bmatrix} 0.0070 & 0.0040 & 0.0073 \\ 0 & 0 & 0 \\ 0.012 & 0.0039 & 0.027 \\ 0 & 0 & 0 \\ 0.016 & 0.0038 & 0.055 \\ 0 & 0 & 0 \\ 0.019 & 0.0036 & 0.089 \\ 0 & 0 & 0 \\ 0.020 & 0.0035 & 0.13 \end{bmatrix} \boldsymbol{x}[k] \right) \end{aligned} \tag{58}$$

Using the derived control laws the plant is controlled. Output and input results are illustrated in Fig. 1 and Fig. 2, respectively. The sampled outputs in the single-rate and the dual-rate system are plotted by dot and circle in Fig. 1, respectively. Because the dual-rate and the single-rate GPC law calculate the same control inputs shown in Fig. 2, the sampled outputs at interval of $2[s]$ are the same. It follows from the simulation results that the single-rate GPC law is designed equivalent to the dual-rate GPC law using (48) $\sim$ (53).

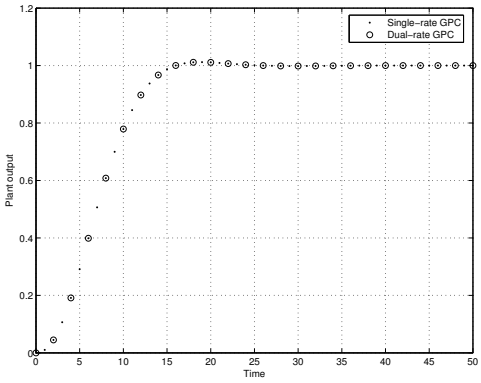

Fig. 1. Output results with the single-rate and the dual-rate GPC

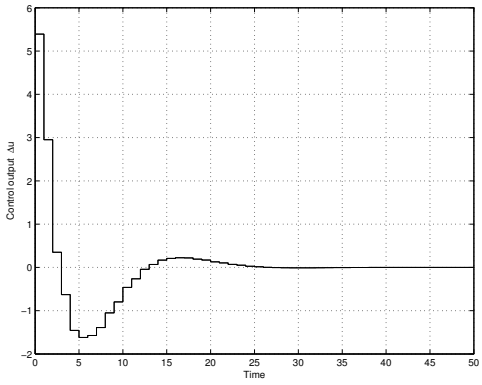

Fig. 2. Input results with the single-rate and the dual-rate GPC

7. CONCLUSION

We designed GPC in both a fast-rate single-rate and a dual-rate system and discussed the relation between them, and the conditions for identifying the fast-rate single-rate GPC as the dual-rate GPC were shown. It follows from our research result that the fast-rate single-rate GPC can be equivalent to the dual-rate GPC by selecting the design parameters. Consequently, the dual-rate GPC can be designed by the same way as the standard single-rate system. Further, the relation between the fast-rate single-rate and the dual-rate GPC is made clear. Finally, in order to illustrate the effectiveness of the proposed method, the numerical examples have been shown.

REFERENCES

Chen, T. and B. Francis (1995). *Optimal Sampled-Data Control Systems*. Springer-Verlag.

Clarke, D.W., C. Mohtadi and P.S. Tuffs (1987*a*). Generalized predictive control – part I. the basic algorithm. *Automatica* **23**(2), 137–148.

Clarke, D.W., C. Mohtadi and P.S.Tuffs (1987*b*). Generalized predictive control – part II. extensions and interpretations. *Automatica* **23**(2), 149–160.

Masuda, S., A. Inoue, Y. Hirashima and R. M. Miller (1997). Intersample performance improvement in generalized predictive control. In: *IFAC International Symposium on Advanced Control of Chemical Processes*. pp. 139–144.

Sato, T. and A. Inoue (2005). Reference trajectory improvement in i-pd controller based on generalized predictive control in input multiplex type multirate system. In: *Joint Automatic Control Conference*. Vol. 48. pp. 663–666. (in Japanese).

Sato, T. and A. Inoue (2006). Improvement of tracking performance in self-tuning pid controller based on generalized predictive control. *The International Journal of Innovative Computing, Information and Control*. (to be appreared).

Scattolini, R. (1992). Multi-rate self-tuning predictive controller for multi-variable systems. *Int. J. Systems Sci.* **23**(8), 1347–1359.

Sheng, J., T. Chen and S. L. Shah (2001*a*). Multirate generalized predictive control for sampled-data systems. *Dynamics of Continuous, Discrete and Impulsive Systems* **Series B**(Applications & Algorithms 8), 485–499.

Sheng, J., T. Chen and S.L. Shah (2001*b*). On stability robustness of dual-rate generalized predictive control systems. In: *Proceedings of the American Control Conference*. pp. 3415–3420.

Tangirala, A.K., D. Li, R. Patwardhan, S.L. Shah and T. Chen (1999). Issues in multirate process control. In: *Proceedings of the American Control Conference*. pp. 2771–2775.

8. ACKNOWLEDGMENT

We would like to acknowledge the helpful comments and suggestions of the reviewers.

This research was supported by Education & Research Special Grant of University of Hyogo.

Keynote 3

Industrial Challenges in Modeling Of Processes and Model Reduction

T. Backx, O. Bosgra, and W. Marquardt
Eindhoven University of Technology
RWTH Aachen Univeristy

Keynote 4

Short–Term Scheduling of Chemical Process Including Uncertainty

M. G. Ierapetritou and Z. Jia,
Rutgers University

ADCHEM 2006

International Symposium on Advanced Control of Chemical Processes
Gramado, Brazil – April 2-5, 2006

INDUSTRIAL CHALLENGES IN MODELING OF PROCESSES AND MODEL REDUCTION

Ton Backx[1)], Okko Bosgra[1)], Wolfgang Marquardt[2)]

[1)] *Eindhoven University of Technology, Electrical Eng. Dept.,*
P.O.Box 513, 5600MB Eindhoven, The Netherlands
e-mail: ton.backx@hetnet.nl
[2)]*RWTH Aachen, Turmstrasse 46, D-52064 Aachen, Germany*

Abstract: Currently a shift of focus towards 6-sigma quality and market responsive operation has been initiated in the chemical processing industries. The fast evolution of products and processes enforced by fierce global competition and by tightening legislation are major forces for new application development approaches and for new technologies. The need of high performance non-linear model based control, optimization, monitoring and soft sensing applications and the cost driven necessity of re-use of models and results of earlier engineering effort will be explained to be the drivers for the current and future industrial challenges in (hybrid) modelling and system identification. These market developments require more extensive application of (non-linear) rigorous models extended with empirical model components to achieve the model accuracy requirements, the coverage of wide process operating ranges and minimization of engineering costs, which cannot be attained by application of pure black box modelling approaches. Besides the techniques applied for hybrid modelling and parameter estimation, the paper also discusses the techniques needed for model reduction, model tracking and state estimation to make the high performance model based applications work properly. An overview with some results is given of the techniques applied and tested in our current R&D industrial pilot projects.

Keywords: Model reduction, Process Control, Model Based Control, Industrial Automation, Plantwide Optimization, Chemical Processing Industry, Process Operations, Manufacturing Execution Systems

1. INTRODUCTION

Over the past decades processing industries have been facing significant changes, both in the marketplace as well as in society. The marketplace has turned from a quasi-infinite market, with only limited and mostly local competition in the 1970s, to an almost completely saturated and extremely competitive global world market at present. Society has become well aware of the limitations of our earth's ecosphere in handling the effects of our rapid consumption of fossil fuel reserves and large growth of emissions. Industries are confronted today with ever tightening legislation with respect to the environmental impact of their production, the use of natural resources, and the disposal or recycling of their products. They are getting full responsibility for all future effects of their production processes as well as of their products and by-products on people and environment. Hence, industries have to move towards a competitive and sustainable production on demand at tight operating constraints as well as product quality and variability specifications in order to cope with these changes.

To get a clear understanding of the problems process industry is facing, an analysis needs to be made of the way processes are operated today in comparison with market demand and market opportunities (Backx et al, 2000; Pantelides et al. 2004; Britt et al., 2004).
At present the Chemical Processing Industries are still largely operating their production facilities in a supply driven mode of operation. This implies that no direct link exists in most companies between actual market demand and actual production. Products are to a large extent produced cyclically in fixed sequences. Delivery of orders is mostly handled from stock of finished products or from intermediates that only require finishing.

The highly competitive market on the contrary imposes a strong need for flexibility with respect to the production of a broad variety of product types and grades at time-varying capacities. Good prices can only be made during those time periods where a product is asked for in the market. Hence, production capacity and product quality must become predictably controlled to enable and support market driven marketing and sales. On-time delivery of the right product at the right quality at a competitive price at the right location must be guaranteed as a minimum. Despite the need for high flexibility, delivery on demand has to be achieved by the industries without building up large stock volumes of intermediates or products. In addition price pressure enforces producers to process a broad variety of market available feedstock materials and utilities at loosely specified properties for producing products at tight -6-sigma- quality specifications.

Examples from two different industries are presented next in order to illustrate the trends. Supply of polymer products to the automotive industries is taken as a first example. Currently, most of the polymer suppliers work with yearly renewable, preferred supplier type contracts. These contracts settle the base prices as a function of the ultimately requested volume of delivered product. Detailed orders for specific deliveries are placed up to just a few weeks before the requested moment of delivery. Significant penalties are agreed upon for late or off-spec deliveries.
Considering the broad range of polymer grades requested by the market, flexibility in manufacturing and tight quality control are absolute requirements for polymer suppliers to stay in business. Capital productivity and hence economic success highly depend on their manufacturing flexibility.

A second example is taken from the oil refining industries. Tightening legislation on fuels and permitted exhaust gas composition has resulted in more detailed and tighter fuel composition specifications. Consequently, complexity of fuel manufacturing has been increasing. At the same time, legislation on waste reduction and market pressure has forced refineries to further process heavy residues. Since crude feedstock quality is slowly degrading over time, high quality feedstock prices are increasing rapidly. Consequently, cheaper feedstock materials of lower and diverse quality are going into the market. Feedstock switch frequency is increasing to exploit economic opportunities in processing low priced raw materials. Economic performance of refineries is depending more and more on their flexibility to being able to handle and quickly change-over between a wide range of feedstock materials driven by availability, price and opportunities to meet delivery at market demand. Operating point switching facilitates the processing of a variety of feedstocks to minimize raw material cost, the processing of heavy residues to reduce waste streams, and the production of the right product qualities on demand. Capital productivity is continuously driven to its maximum by pushing total throughput despite of continuously varying operating conditions.

The examples clearly demonstrate the need to enable production plants to be operated in a deliberately dynamic mode, covering feasible, wide operating ranges. Today many companies produce products at lowest possible costs in a lean operation with minimum overhead costs and no significant investments in upgrade of operation support technologies that focus on market driven production and innovation. Longer term these enterprises will experience that the average residence time of products in their warehouses will be long in comparison with the average residence time of products in warehouses of companies that have strongly invested in directly linking production to market demand and innovation. Margins will continuously be under extreme pressure for a significant part of the volume produced due to market saturation effects and due to mismatch between market demand and supply from stored products. The average capital turnaround cycle time will remain poor, despite a limitation of the number of grades produced per plant. This will continue putting pressure on the ultimate business results of these companies.
Only those enterprises will be successful in the longer run, which will be able to exploit opportunities by quickly adapting to market dynamics. Critical issues are flexibility with respect to volume, type and grade of products, transition time and cost, predictability of production, reproducibility of transitions and tight quality control. Consequently, manufacturing will have to move from largely steady-state operation to an intentionally dynamic operation of the plant (Koolen, 1994; Backx et al., 1998). Companies that have invested in flexible and innovative operation are the ones that are setting the scene for turning around the way of working in the Chemical Processing Industries (CEFIC, 2004-1,2). These companies are doing the same as the ultimately successful companies in the Consumer Electronics and Automotive Industries did 20-30 years earlier: Operate production directly driven by market demand to the extent feasible. Companies doing so now are facing tough times however, as their total production costs, due to their focus on flexibility and innovation, initially appear to be higher. They have to make significant investments in adapting their operations, production and internal organisation to enable the flexible operation. Ultimately, these companies will see their overall performance rapidly improve due to the increase of capital turnaround, the better margins related to improved flexibility, their ability to better adapt to changing market conditions and their capability to timely deliver at (changing) specifications and varying volumes of product demand. A significant

improvement of economic performance results when the response of production to orders received is coupled directly. This of course requires predictable performance in manufacturing. Focussing operations on enabling market driven operation of processes opens up the opportunity for best economic performance. It ultimately ensures that production of ordered products starts after orders have been received and that the products are delivered to customers immediately after production so enabling shortest possible capital turnaround and significantly improved capital productivity.
Innovation in future process technologies must in the first place aim at a high degree of adaptability of manufacturing to fluctuations in market demand covering operations as well as process and equipment design. The constraints imposed upon production result in increasing complexity of processes and of their operations. More sophisticated, model based operation support systems will be required to exploit freedom available in process operation (Backx et al., 1998).

2. MODELING REQUIREMENTS IN THE CONTEXT OF MARKET DRIVEN PROCESS OPERATIONS

Two challenges have to be faced in order to move towards intentional dynamic and supply chain conscious market driven plant operation:

- Fully integrated technologies are needed that make transparent operation of plants and their processes as part of supply chains feasible to enable the implementation of dynamic operation in industrial practice. In addition also a significant change in the culture of operators and plant management will be required. Dynamics has to be accepted as a further opportunity for performance improvement rather than considered as a strange, undesired and even dangerous phenomenon outside the scope of normal process operations.
- In addition, built up knowledge of processes and plants has to be condensed preferably in re-usable, well documented, generally applicable so called Reference Models, which are continuously updated and refined to reflect state-of-the-art understanding of plant and process behaviour (Foss, et al., 1998; Pantelides, 2003). These reference models at their turn may form the basis for highly automated updating of applied model based (dynamic) optimisation systems, (non-) linear control systems, process monitoring systems, soft sensing systems, etc. In these systems information on operational objectives and manufacturing status must be transparent at all levels of the automation hierarchy, since the operators will ultimately become the proprietors of the process (Clark, et al. 1995; Han, et al., 1995). Instead of merely executing process operation tasks targeting at process variables, operators will move towards making productivity decisions on the basis of real-time business variables derived from actual and model based process measurements and enterprise policy.

Market driven process operation puts extremely high requirements on predictability and reproducibility in process operation. One needs to be able to produce products at adjustable specifications in predefined, tight time slots and in changing volumes. Flexibility and timing are key parameters that drive performance. Technologies that support such process operation have to provide the functionality to operate processes this way.

The problems faced by process industries to turnover production control from supply driven process operation to market driven process operation may be summarized by the following problem statement:

Given an industrial scale production plant that forms one link in a supply chain, provide the model based technologies for this plant that:

- *Enable flexible, dynamic operation of the plant in such a way that imposed operating constraints related to safety, ecology, plant lifetime and plant economics are always satisfied*
- *Support continuous improvement of the plant and its operations to drive the plant towards conditions that comply with supply chain optimum operation within a pre-defined, feasible operating envelope for the plant*
- *Operate the plant in accordance with process conditions that push for maximization of capital productivity of the company the plant belongs to.*
- *Exploit freedom in plant operation to maximize capital productivity of the plant over plant lifetime*

Assuming that best performance is achieved, if plants are operated in an anticipative way by exploiting detailed knowledge of dynamic behaviour of the plants, this problem definition clearly links to the following set of sub-problems related to modelling and model reduction (cf. fig. 2.1):

- Enable fast and accurate modelling of application relevant dynamic process behaviour using detailed knowledge of processing equipment, materials and chemistry (Marquardt, 1995; Pantelides, 2003): apply *Reference Models* to make cost effective and market responsive, innovative operation feasible
- Extract application relevant information for various model based applications (e.g. model based optimisers, model based control systems, model based soft sensors, model based monitoring systems, model based research and development of processes and equipment, …) in fast and robustly computing approximate models in a highly automated way: enable development of *Reduced Models* that robustly and accurately reflect relevant system characteristics.

- Realize continuous improvement of knowledge of processing equipment, materials and chemistry stored in *Libraries*. These libraries have to contain model building components that represent the state-of-the-art of the knowledge that should be applied throughout the company for R&D, Design, Process & Systems Engineering, Monitoring, Maintenance and Operations.
- Create model adaptation mechanisms that enable closed loop adjustment of specific approximate model parts to overcome remaining inaccuracies and imperfections of the applied reduced complexity, approximate models.

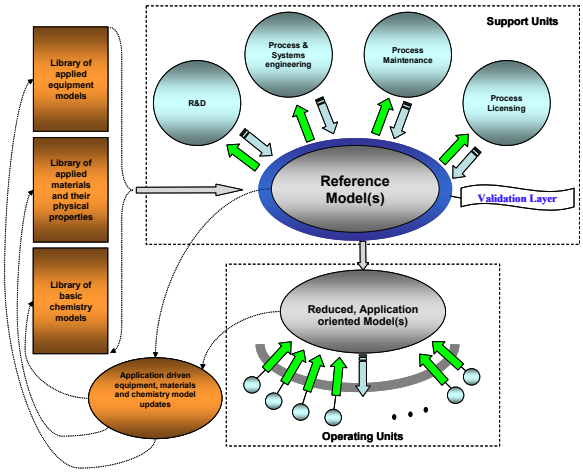

Fig. 2.1 The Reference Model concept

The model based applications have to use all freedom available in plant operation for continuously driving the plant to the operating conditions that best comply with a selected balance of most of the time mutually conflicting objectives.

3. STATE-OF-THE-ART IN MODELLING AND MODEL REDUCTION

Model based applications require the models to satisfy very specific properties. The specific requirements imposed depend on the application. Most of the literature on modelling and model reduction is related to specific applications discussed. No structuring of modelling and model reduction techniques has been discussed in literature yet.

Two types of modelling approaches are applied in the (petro-)chemical processing industry for the development of model based applications:

– Empirical modelling (black box modelling)

– First principles based modelling

Empirical modelling techniques are the techniques that are applied extensively in industry for the development of model predictive control systems, inferential control systems and soft sensors. The process identification techniques applied for empirical modelling have been given broad research attention the past two decades in a predominantly linear model context covering model structure (Ho et al., 1966; Willems, 1986, 1987; Ljung, 1987; Backx et al., 1992), parameter estimation (Åström et al., 1971; Eykhoff, 1974; Richalet et al., 1978; Ljung, 1987; Söderström et al., 1989; Heuberger, 1990; Verhaegen et al., 1992; Van Overschee et al., 1993; Zhu et al., 1993; Falkus, 1994; Van den Hof et al., 1994; Van Overschee, 1995; De Vries et al., 1998), model reduction (Ho et al., 1966; Zeiger et al., 1974; Moore, 1981; Pernebo et al., 1982; Backx, 1987; Heuberger, 1990), closed loop identification (Forssell et al., 2000; Van Donkelaar et al., 2000; Zhu, 2003) and parametrization and estimation of model uncertainty (Ljung, 1987; Zhu, 1991; Falkus, 1994; Hakvoort, 1994; Van den Hof et al., 1994; De Vries, 1994; Reinelt, et al. 2002). Process identification techniques focus on accurate modelling of process dynamics, which are relevant for process control. The techniques applied –model parameter estimation on the basis of input-output process data generated by persistent excitation of process inputs during sufficiently long time- result in models that have both good observability and good controllability. The models obtained reflect the approximated linear dynamic behaviour of the processes observed during the data generation. The models are valid for the operating window covered during testing, but in general cannot be applied reliably for operating conditions, which have not been covered during testing.

First principles based modelling techniques apply basic physical/chemical/biological laws and mechanisms –mass balances, energy balances, momentum balances extended with constitutive equations- to construct models. As the models are based on basic laws, they have wide range validity in general. A main problem in creating models that accurately reflect actual process behaviour is stemming from the fact that no direct process information is used to select the mechanisms included in the models. Especially accurate modelling of process chemistry appears difficult due to inaccurate knowledge of main reaction complexes and reaction kinetics. Physics related process behaviour of applied equipment can be modelled accurately in general by application of the conservation laws. Accurate modelling of physical properties of materials mostly results in complex models with much redundancy. Model inaccuracies always remain due to inaccurately known physical properties, reaction complexes and reaction kinetics. Models resulting from first principles modelling therefore always will require adaptation to align them with actually observed process behaviour (Briesen et al., 2000). This implies that adjustments of the models based upon actual process measurements are a necessity to assure that the applied models reflect actual process behaviour. The actual model accuracy and model content requirements are a function of the specific application of the models: Model based research and development, model based (dynamic) optimization, model predictive control, inferential control, model based soft sensing, model based process monitoring, process performance analysis ….

The requirements involve the range of dynamics covered (time scale), the operating range covered, specific process mechanisms covered and model components applied for model adaptation.
State-of-the-art model reduction techniques in general focus on two main requirements imposed on the reduced model:

- Extraction of model behaviour relevant for the application (relevant range of dynamics, applied operating window)
- Reduction of model complexity to enable faster simulations (relevant process mechanisms, restriction to the actual operating window, approximate modelling)

In general closed loop applications impose restrictions on the range of dynamics covered by the reduced model, the operating window covered and the condition number of the reduced model. Due to limitations in the range of dynamics, accuracy and reproducibility of actuators and sensors only two decades of dynamics can be handled in most industrial model predictive control applications. As model predictive control systems predominantly are focussing on disturbance rejection (time varying) linear models can be applied for actual control in general. This also applies for model based control systems for transition control and batch control. In addition the models applied in model predictive control and closed loop optimization applications may not contain too small gain directions. If a model would contain very small gain components, the controller or optimizer would directly use these directions for achieving its objectives by generating large input amplitudes in these small gain directions. Even small model inaccuracies in these directions result in very poor controller or optimizer performance due to the large input amplitudes applied in not exactly right directions.
Similar requirements apply for soft sensing, inferential control and observer applications to achieve robust performance (Marquardt, 2001; Antoulas, 2005).

4. INITIAL STRUCTURING OF THE MODEL REDUCTION TECHNIQUES

In order to support minimum effort design and maintenance of model based applications in chemical processing, the reference model concept may be applied. This concept assumes that a reference model is developed and maintained that reflects all process knowledge available from R&D, process and systems engineering, process operations, process control and optimization. The reference model reflects all relevant process knowledge available at any time first principles based, if necessary extended with empirical model components. The reference model only approximates actual process behaviour. Therefore it always will be inaccurate to some extend and on-line adaptation of the derived model on the basis of measured process behaviour will be necessary.
The reference model will become too complex on the other hand for most applications as it will be based on rather generic library components that reflect knowledge obtained from a wide range of research, development, design, monitoring, maintenance and operation activities. Model approximation and model reduction techniques are required to extract the relevant behaviour for specific applications in sub-models. To derive approximate models that match the needs, specific model reduction and model approximation procedures need to be developed for this purpose. Such model reduction procedures do not exist yet. The EC funded 6th Framework Program Marie-Curie Training Network project PROMATCH focuses on the development of these techniques. To enable appropriate model reduction aiming at approximate initial process models that reflect all application relevant process dynamics with minimum complexity, a procedure will be elaborated on based on a selection of the following categorized techniques:

- Selection of main process mechanisms in a well balanced way by application of physical/chemical model reduction (Tatrai, et al. 1994; Androulakis, 2000; Vora et al., 2001; Petzold et al., 1999; Briesen et al., 2000; Maas et al., 1992; Ganguly et al., 1993).
- Selection of relevant operating windows and relevant dynamics by using projection methods (Inertial methods, Galerkin projection methods, Proper Orthogonal Decomposition methods) and Krylov subspace methods (Armaou et al., 2001; Rathinam et al., 2003; Adrover, et al. 2002; Kunisch et al., 2002; Shvartsman, et al. 2000; Novo, et al. 2001; Garcia-Archilla, et al. 1999; Bai, 2002; Jaimoukha, 1997; Heres, 2005)
- Reduction of the model complexity by non-linear model reduction (Löffler et al., 1991; Lohmann, 1995; Lall, et al. 2002; Mossayebi, et al. 1992; Desrochers et al., 1980)
- Selection of relevant process dynamics by application of numerical reduction methods (Baldea et al., 2006; Lee, et al. 2000; Carpanzano, 2000; Kumar, et al. 1998; Sun et al., 2005; Hedengren et al., 2005)

In addition to the direct use of the techniques summarized above, it seems important to evaluate these techniques additionally under closed-loop conditions imposed by real-time feedback control and feedback optimization algorithms.

5. EXAMPLE

MPC control based upon detailed CFD models of a glass forehearth is used to demonstrate the rigorous model based approach. This example has been worked on as part of a research project funded by the Dutch government (REGLA project funded by the E.E.T. program).

The objective of the controller is to stabilize the temperature of the glass that is delivered to the forming machines in order to improve the so-called workability of the glass. The workability of glass, or the ease with which the glass can be used for forming the final product, depends largely on the viscosity and therefore on the temperature and temperature distribution of the glass melt.
A new approach to set-up control models:

- The approach starts with setting up a separate CFD model for the feeder under consideration. This model is validated, as the performance of the controller will depend largely on the quality of this underlying model.
- Subsequently, dynamic tests are performed upon the CFD model. The simulation tests couple the response of temperatures and flows in the feeder to changes in the input. Proper Orthogonal Decomposition (POD) is applied for model reduction.
- The resulting approximate model is used to achieve constant temperatures and setpoints at the exit of the feeder even for the case of disturbances in the melt entering the feeder or disturbances in the feeder itself.

The resulting control model, which is derived from these CFD simulation tests, can be used for a large set of working points (e.g. a large range of loads) instead of for one single working point, as the response of the feeder to large variations in disturbances and process settings is determined. Consequently, the control model does not have to be rebuilt when a different working point for the feeder/furnace is selected due to e.g. the production of a different product (as long as the type of glass does not change). It is a fast way of setting up a complete control model without any risk for production.

The resulting control scheme for the industrial feeder is shown in figure 5.1. The temperatures in the feeder are controlled via the set-points of three PID controllers that adjust the fuel supply to the three zones in the feeder. These PID set-points are the result of the MPC, which reads the values of the 9-grid thermocouple at the feeder exit. Based on the fast reduced model describing the dynamic behavior of the feeder, the MPC determines the optimal values of the PID set-points such that the desired temperature (homogeneity) at the feeder exit is attained. Next to the control objectives (desired temperature and temperature homogeneity at the feeder exit), also several constraints are imposed to the MPC: the glass melt temperatures in the feeder may not exceed and drop below certain values; also the rate of fuel adaptation is constrained to avoid instabilities in the feeder. These constraints limit the flexibility of the feeder operation and hamper the identification of the optimal feeder settings (optimal PID set-points to ensure stable production at the desired glass melt temperature (homogeneity)) when CFD models are not consulted.

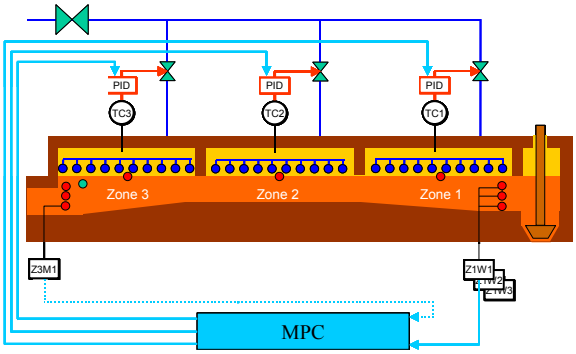

Figure 5.1: Control scheme for the industrial feeder.

Although the feeder entrance temperature (homogeneity) is measured continuously, in the field test of the MPC this information has not been taken into account. Incorporation of the entrance temperatures in the MPC (indicated by the dotted line in figure 5.1) would allow the MPC to anticipate in the feeder (by adjusting the PID set-points) on temperature disturbances from the refiner.
The application of the described MPC feeder control has been extensively tested on various production campaigns for a production feeder in emerald green container glass manufacturing. Figure 5.2 shows the impact of the controller on the average 9-point grid temperature, which is the main objective for the controller. In manual control mode, deviations in temperature in the 9-grid exceed +/ 2.5 degrees C, in some instances even more. It is clearly seen that the feeder temperatures become very stable (+/ 0.5 degrees C) once the controller is switched on. It should be noted, that the smallest change in temperature that is detected by the thermocouples is 0.2 degrees C, which makes the capabilities of the controller even clearer. Besides the increased stability, changes in set points are realized within a short period of time. Even automated transitions between largely different operating points (95 ton/day – 135 ton/day; different glass gob temperatures) have been performed successfully.

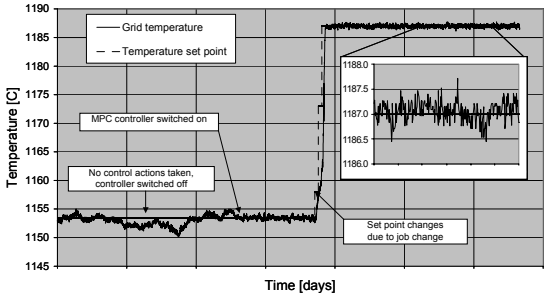

Fig. 5.2 Wide operating range POD reduced model based controller performance

6. CONCLUDING REMARKS

Changing market conditions enforce chemical processing industries to better utilize process capabilities. Process operation needs to be closer tied with market demand to improve capital productivity. Model based techniques require dedicated models that reflect application relevant dynamics with sufficient accuracy for the relevant operating range. New concepts have been discussed that are based on the development of a reference model and subsequent derivation of approximate, reduced process models. The approximate models are derived from the reference model by using an adequate model reduction/ model approximation method. This requires a highly automated, minimum engineering effort model reduction technology.

REFERENCES

Adrover A., G.Continillo, S.Crescitelli (2002). Construction of approximate inertial manifold by decimation of collocation equations of distributed systems. Computers and Chemical Engineering, 26 (2002), 1, pp. 113-123

Androulakis I.P. (2000), Kinetic mechanism reduction based on an integer programming approach AIChE Journal, 46(2000), 2, pp. 361-371

Antoulas, A.C. (2005), Approximation of Large-Scale Dynamical Systems. Soc. Industr. Appl. Mathematics, Philadelphia, PA, 2005 ISBN:[[0-89871529-6]

Armaou A., P.D.Christofides (2001), Computation of empirical eigenfunctions and order reduction for nonlinear parabolic PDE systems with time-dependent spatial domains. Nonlinear Analysis Theory Methods and Applications, 47 (2001), 4, pp. 2869-2874

Åström, K.J. and P. Eykhoff (1971). System identification - a survey. Automatica, **7**, pp. 123-162.

Backx, A.C.P.M. (1987). Identification of an industrial process: A Markov parameter approach. PhD Thesis, Eindhoven University of Technology, Eindhoven, The Netherlands, 1987.

Backx A.C.P.M. and A.H. Damen (1992). Identification for the control of MIMO processes. IEEE Trans. AC, **37**, pp. 980--986.

Backx T., O. Bosgra, and W. Marquardt (1998). Towards intentional dynamics in supply chain conscious process operations. FOCAPO 1998 conf., Snowbird Resort Utah, July 5-10.

Backx, T., O. Bosgra and W. Marquardt (2000), Integration of Model Predictive Control and Optimization of Processes, proc. AdChem 2000, June 2000, Pisa, Italy

Bai Z.J. (2002), Krylov subspace techniques for reduced-order modeling of large-scale dynamical systems Applied Numerical Mathematics, 43(2002), 1-2, pp. 9-44

Baldea M., P. Daoutidis (2006), Model reduction and control of reactor-heat exchanger networks. Journal of Process Control, Vol 16, Issue 3, March 2006, pp. 265-274

Briesen H., W.Marquardt (2000), Adaptive model reduction and simulation of thermal cracking of multicomponent hydrocarbon mixtures Computers and Chemical Engineering. 24(2000), 2-7, pp. 1287-1292

Britt, H., C-C Chen, V. Mahalec and A. McBrien, (2004). Modeling and simulation in 2004: An industrial perspective. Proc. of FOCAPD 2004, Princeton University, Princeton, New Jersey, July 11-16, 2004

CEFIC study report (2004). Chemical Industry 2015: Roads to the future. Study by the European Chemical Industry Council (CEFIC). www.cefic.org

CEFIC executive summary (2004). Horizon 2015: Perspectives for the European Chemical Industry. www.cefic.org

Clark, D., Scarlett, J. (1995), What will a typical process plant look like in the year 2005? Honeywell Inc., http:/www.iac.honeywell.com/Pub/Journal/a9504plant2005.html,.

De Vries D. (1994). Identification of Model Uncertainty for Control Design. PhD Thesis, Delft University of Technology, Delft, The Netherlands, 1994.

De Vries, D, P. van den Hof (1998), Frequency domain identification with generalized orthonormal basis functions. IEEE Trans. A.C., Vol. AC-43, no. 5, pp. 656-669.

Desrochers A.A., G.N.Saridis (1980), A model reduction technique for nonlinear systems. Automatica, 16(1980), 3, pp. 323-329

Eykhoff P. (1974). System Identification; Parameter and State Estimation. John Wiley & Sons.

Falkus H. (1994). Parametric Uncertainty in System Identification. PhD Thesis, Eindhoven University of Technology, Eindhoven, The Netherlands, 1994.

Forssell U., L. Ljung (2000), A projection method for closed-loop identification. IEEE Transactions on Automatic Control, Vol AC-45, pp 2101 - 2106.

Foss, B., B. Lohmann and W. Marquardt, (1998). A field study of the industrial modelling process. Journal of Process Control, 8, 1998, pp. 325-337.

Garcia-Archilla B., J.Novo, E.S.Titi (1999), An approximate inertial manifolds approach to postprocessing the Galerkin method for the Navier-Stokes equations Mathematics of Computation, 68 (1999), 227, pp. 893-911

Carpanzano E. (2000), Order reduction of general nonlinear DAE systems by automatic tearing. Math. and Computer Modelling of Dynamical Systems, 6(2000), 2, pp. 145-168

Ganguly S., D.N.Saraf (1993), A semi-rigorous dynamic distillation model for on-line optimization and nonlinear control Journal of Process Control, 3(1993), 3, pp. 153-161

Hakvoort R.G. (1994). System Identification for Robust Process Control, Nominal Models and Error Bounds. PhD Thesis, Delft University of Technology, Delft, The Netherlands, 1994.

Han, C., Stephanopoulos, G. (1995), Integration of information, management and control in process industries. In: R. Berber (Ed.): "Methods of Model Based Process Control". NATO ASI Series E, Vol. 293, Kluwer, pp. 715-751.

Hedengren J.D., T.F.Edgar (2005), Order reduction of large scale DAE models Computers and Chemical Engineering, 29(2005), pp. 2069-2077

Heres, P. (2005), Robust and efficient Krylov subspace methods for model order reduction. PhD Thesis, Eindhoven University of Technology, 13 Dec 2005

Heuberger P.S.C. (1990). On Approximate System Identification with System-based Othonormal Functions. PhD Thesis, Delft University of Technology, Delft, The Netherlands, 1990.

Ho B.L. and R.E. Kalman (1966). Effective construction of linear state-variable models from input/output functions. Regelungstechnik, 14, pp. 545-548.

Jaimoukha I.M. (1997), A general minimal residual Krylov subspace method for large-scale model reduction. IEEE Transactions on Automatic Control, 42(1997), 10, pp. 1422-1427

Koolen, J. (1994). Plant operation in the future. Computers Chem. Eng., Suppl. pp. 477-481

Kumar A., P.D.Christofides, P.Daoutidis (1998), Singular perturbation modeling of nonlinear processes with nonexplicit time-scale multiplicity Chemical Engineering Science, 53(1998), 8, pp. 1491-1504

Kunisch K., S.Volkwein (2002) Galerkin proper orthogonal decomposition methods for a general equation in fluid dynamics. SIAM Journal on Numerical Analysis, 40(2002), 2, pp. 492-515

Lall S., J.E.Marsden, S.Glavaski (2002), A subspace approach to balanced truncation for model reduction of nonlinear control systems. Internat. Journal of Robust and Nonlinear Control, 12(2002), 6, pp. 519-535

Lee K.S., Y.Eom, J.W.Chung (2000), A control-relevant model reduction technique for nonlinear systems Computers and Chemical Engineering, 24(2000), 2-7, pp. 309-315

Ljung L. (1987). System Identification: Theory for the User. Prentice Hall, Englewood Cliffs, NJ.

Löffler H.P., W.Marquardt (1991) Order reduction of nonlinear differential-algebraic process models Journal of Process Control, 1(1991), 1, pp. 32-40

Lohmann B., (1995), Order reduction and determination of dominant state variables of nonlinear systems. Mathematical Modelling of Systems, 1(1995), 2, pp. 77-90

Maas U., S.B.Pope (1992), Simplifying chemical kinetics: intrinsic low-dimensional manifolds in composition space Combustion and Flame, 88(1992), pp. 239-264

Marquardt, W. (1995), Towards a Process Modeling Methodology. In: R. Berber: Methods of Model-Based Control, NATO-ASI Ser. E, Applied Sciences, Vol. 293, 3-41, Kluwer Academic Pub., Dordrecht, 1995

Marquardt W. (2001), Nonlinear model reduction for optimization based control of transient chemical processes preprint, 34 pp. Oct. 2001

Moore B.C. (1981). Principal component analysis in linear systems: Controllability, observability and model reduction. IEEE Trans. A.C., **26**, pp. 7-32.

Mossayebi F., T.T.Hartley, J.A.Deabreu-Garcia (1992), A fundamental theorem for the model reduction of nonlinear systems Journal of the Franklin Institute, 329(1992), 1, pp. 145-153

Novo J., E.S.Titi, S.Wynne (2001), Efficient methods using high accuracy approximate inertial manifolds Numerische Mathematik, 87 (2001), 3, pp. 523-554

Pantelides C., (2003). Process Modelling and Model-Based Automation. INCOOP workshop, 23 January 2003, Düsseldorf, Germany.

Pantelides, C. and Z.E. Urban, (2004). Process modelling technology: A critical review of recent developments. Proc. of FOCAPD 2004, Princeton University, Princeton, New Jersey, July 11-16, 2004

Pernebo L.and L.M. Silverman (1982). Model reduction via balanced state space representations. IEEE Trans. AC., **27**, pp. 382-387.

Petzold L., W.J.Zhu (1999), Model reduction for chemical kinetics: An optimization approach AIChE Journal, 45(1999), 4, pp. 869-886

Rathinam M., L.R.Petzold (2003) A new look at proper orthogonal decomposition. SIAM Journal on Numerical Analysis, 41(2003), 5, pp. 1893-1925

Reinelt W., A. Garulli, L. Ljung (2002), Comparing different approaches to model error modeling in robust identification. Automatica, Vol 38, pp 787-803.

Richalet, J., A. Rault, J.L. Testud, and J. Papon (1978). Model predictive heuristic control: Applications to industrial processes. Automatica, **14**, pp. 413-428.

Shvartsman S.Y, C.Theodoropoulos, R.Rico-Martinez (2000), Order reduction for nonlinear dynamic models of distributed reacting systems. Journal of Process Control, 10 (2000), 2-3, pp. 177-184

Söderström T. and P. Stoica (1989). System Identification. Prentice Hall, UK.

Sun C., J. Hahn (2005), Reduction of stable differential-algebraic equation systems via projections and system identification Journal of Process Control, 15(2005), pp. 639-650

Tatrai F.Z., P.A.Lant, P.L.Lee (1994), Control relevant model reduction: A reduced order model for 'Model IV' fluid catalytic cracking unit Journal of Process Control. 4(1994), 1, pp. 3-14

Van den Hof P.M.J., P.S.C. Heuberger, and J. Bokor (1994). Identification with generalized orthonormal

basis functions - statistical analysis and error bounds. In: Proc. IFAC conf. System Identification and Parameter Estimation, Copenhagen.
Van Donkelaar E., P. van den Hof (2000), Analysis of closed loop identification with a tailor made parametrization. European Journal of Control, Vol. 6, no. 1, pp. 54-62.
Van Overschee P. (1995). Subspace Identification, Theory-Implementation-Application. PhD thesis, Katholieke Universiteit Leuven, Leuven, Belgium, 1995.
Van Overschee P. and B. de Moor (1993). Subspace algorithms for the stochastic identification problem. Automatica, **29**, pp. 649-660, 1993.
Verhaegen, M. and P. Dewilde (1992). Subspace model identification. part i: The output-error state space model identification class of algorithms / part ii: Analysis of the elementary output-error state space model identification algorithm. Int.J.Contr., **56**, pp. 1187-1241.
Vora N., P. Daoutidis (2001), Nonlinear model reduction of chemical reaction systems AIChE Journal, 47(2001), 10, pp. 2320-2332
Willems. J.C (1986). From time series to linear systems; part i: Finite dimensional linear time invariant systems. Automatica, **22**, pp. 561-580.
Willems J.C. (1986). From time series to linear systems; part ii: Exact modelling. Automatica, **22**, pp. 675-694.
Willems J.C. (1987). From time series to linear systems; part iii: Approximate modelling. Automatica, **23**, pp. 87-115.
Zeiger J.G. and A.J. McEwen (1974). Approximate linear realisations of given dimension via Ho's algorithm. IEEE Trans. AC., **19**, pp. 585-601.
Zhu Y.C. (1991). Identification and MIMO Control of Industrial Processes, An Integration Approach. PhD Thesis, Eindhoven University of Technology, Eindhoven, The Netherlands, 1991.
Zhu Y.C. and T. Backx (1993). Identification of Multivariable Industrial Processes for Simulation, Diagnosis and Control. Springer Verlag.
Zhu, Y.C. (2003). New development in industrial MPC identification. Preprints of ADCHEM 2003, International Symposium on Advanced Control of Chemical Processes. 11-14 January, 2004, Hong Kong, P.R. China.

ADCHEM 2006

International Symposium on Advanced Control of Chemical Processes
Gramado, Brazil – April 2-5, 2006

SHORT-TERM SCHEDULING OF CHEMICAL PROCESS INCLUDING UNCERTAINTY

Marianthi G. Ierapetritou and Zhenya Jia

Chemical and Biochemical Engineering Department,
Rutgers University

Abstract: This paper addresses the short-term scheduling of chemical process with uncertainty considerations. A multiobjective robust optimization method is proposed to identify Pareto optimal solutions, where Normal boundary intersection (NBI) technique is utilized in order to trace the Pareto optimal surface in the objective space, on which each point represents a trade-off between the various objectives. The issue is also addressed using parametric mixed integer linear programming (pMILP) analysis where uncertain parameters are present on the right hand side (RHS) of the constraints. For the case of multiple uncertain parameters, a new algorithm of multiparametric linear programming (mpLP) is proposed that does not require the construction of the LP tableaus but relies on the comparison between solutions at leaf nodes. Given the range of uncertain parameters, the output of this proposed framework is a set of optimal integer solutions and their corresponding critical regions and optimal functions.

Keywords: scheduling, uncertainty, robust optimization, parametric MILP.

1. INTRODUCTION

Substantial benefits can be achieved through the use of optimization techniques in plant operations by improving the resource utilization at different levels of decision making process. However, uncertainty exists in realistic manufacturing environment due to lack of accurate process models and variability of process and environment data. The presence of uncertainty can substantially reduce or eliminate the advantages of optimization approaches. Therefore, it is of great importance to develop systematic methods to address the problem of uncertainty in process operations.

Although there has been a substantial amount of work addressing the problem of design and planning under uncertainty, a detailed literature review of which can be found in Cheng et al. (2003), the issue of uncertainty in scheduling problems has received relatively little attention. Existing work mainly includes stochastic programming approaches involving chance constraints and two-stage programming (Bonfill *et al*., 2005, Jia and Ierapetritou, 2004), as well as robust optimization methods (Basset *et al*., 1997; Lin *et al*., 2004; Vin and Ierapetritou, 2001). A brief overview of these approaches are presented here. Ierapetritou and Pistikopoulos (1996) addressed the scheduling of single-stage and multistage multiproduct continuous plants with a single production line at each stage when uncertainty in product demands is involved. They used Gaussian quadrature integration to evaluate the expected profit and formulated the problem as a MILP models. Lin et al (2004) proposed a robust optimization method to address the problem of scheduling with uncertain processing times, market demands, or prices. The robust optimization model was derived from its deterministic model considering the worst-case values of the uncertain parameters, and a certain infeasibility tolerance was introduced to allow constraint violations. Vin and Ierapetritou (2001) addressed the problem of multiproduct batch plant scheduling under demand uncertainty. They introduced a robustness metric based on deviations from the expected performance including the infeasible scenarios. Robust schedules are generated based on a multiperiod approach. Balasubramanian and Grossmann (2002) considered uncertain processing times in scheduling of multistage flowshop plants. They also proposed a multiperiod MILP model and proposed a special branch and bound algorithm with aggregated probability model to select the sequence of jobs with minimum expected makespan. Recently, Bonfill et al. (2005) used a two-stage stochastic approach to address the robustness in scheduling batch processes with uncertain operation times. The objective is to minimize a weighted combination of the expected makespan and wait times. Basset et al. (1997) proposed a framework considering uncertainties in processing times,

equipment reliability, process yields, demands and manpower changes. They generate random instances by Monte Carlo sampling, and determine the schedules for these instances. The solutions are then analyzed to derive a number of operating policies. Orcun et al. (1996) presented an approach to deal with uncertain processing times in batch processes and utilized chance constraints to take into consideration the violation of operation time constraints under certain conditions. In our earlier work (Jia and Ierapetritou, 2004), we developed a branch-and-bound solution framework to determine a set of alternative schedules for a given range of uncertain parameters. The idea of inference based sensitivity analysis for MILP problems was employed that has the advantage of not substantially increasing the complexity compared with the deterministic formulation.

A number of problems from the area of process design and operations are commonly formulated as mixed integer linear programming (MILP) problems. One way to incorporate uncertainty into these problems is using MILP sensitivity analysis and parametric programming methods. The main limitation of most existing methods is that they can only be applied to problems with a single uncertain parameter or several uncertain parameters varying in a single direction. A number of approaches have been developed for parametric integer programming problems that involve a single parameter/scalar variation, basically including implicit enumeration methods (Roodman, 1972; Piper and Zoltners, 1976), branch and bound methods (Roodman, 1974}, Marsten and Morin (1977), Ohtake and Nishida (1985), and cutting plane methods (Holm and Klein, 1984), Jenkins and Peters, 1987), etc. A detailed literature review can be found in Jenkins (1990).

Jenkins' approach is extended by Crema (2002) for the multiparametric 0-1 integer linear programming (ILP) problem considering the perturbation of the constraint matrix, the objective function and the RHS vector. The proposed algorithm iteratively solves a nonlinear problem, which can be converted to an equivalent MILP formulation, in order to obtain a complete multiparametric analysis.

Acevedo and Pistikopoulos (1997) proposed a parametric programming approach for the analysis of linear process engineering problems under uncertainty. The procedure solves the multiparametric linear programming (mpLP) at each node of the B&B tree, then compares and identifies the different optimal integer solutions and their corresponding optimal value functions. Pertsinidis et al. (1998) developed an algorithm for MILP sensitivity analysis. At each iteration, the LP sensitivity analysis results and a cut that excludes the current integer solution are incorporated to a MILP problem so as to find the breaking point and the successor optimal integer solution. Their ideas were extended by Dua and Pistikopoulos (2000), by decomposing the mp-MILP into two subproblems and then iterating between them. The first subproblem is obtained by fixing the integer variables, resulting in a mpLP problem, whereas the second subproblem is obtained by relaxing the parameters as variables, leading to a MILP problem.

The problem of RHS multiparametric linear problem was first addressed by Gal and Nedoma (1972). Their algorithm is based on the Simplex algorithm for deterministic LPs. It starts with an initial optimal basis at a feasible point and moves to each of its possible neighbor bases by one dual step to determine the new optimal solution. This procedure is repeated until there is no optimal basis that still has unexamined neighbors. A geometric approach is proposed by Borrelli et al. (2003), which is based on the direct exploration of the parameter space and their definition of critical regions is not associated with bases but with the set of active constraints.

Our work towards addressing the problem of uncertainty in scheduling has been evolved around two different directions based on the variable information about uncertainty. For the cases where uncertainty is well characterized, robust optimization can be used to simultaneously optimize the different objectives in the face of uncertainty, such as expected profitability, flexibility, robustness. However, when there is not enough information, parametric programming can be employed to generate a set of alternative schedules to cover the whole uncertainty space.

This paper is organized as follows. Section 2 presents the multiobjective robust optimization model for short-term scheduling, whereas the details of the proposed parametric MILP approach for the cases of single and multiple uncertain parameters are presented in section 3. Section 4 is used to present the effectiveness of the proposed methods through the solution of one case study whereas section 5 summarizes the work and present some of the ideas for future developments.

2. ROBUST OPTIMIZATION

A wide variety of problems arising in design and operation of engineering systems require simultaneous optimization of more than one objective function. A solution that optimizes all the objectives most likely doesn't exist, thus we need to find out solutions that trade-off the different objectives.

This type of problems are known as multiobjective, multicriteria or vector optimization problems, which consist of two or more conflicting objective functions with a set of constraints taken into consideration. Optimization of these problems is to identify the set of Pareto optimal solutions.

A solution is Pareto optimal if improvement in one objective can only be achieved at the expense of some other objectives. In mathematical terms, for a general multiobjective optimization problem:

$$\min_{x \in C} F(x) = \begin{bmatrix} f_1(x) \\ f_2(x) \\ \vdots \\ f_n(x) \end{bmatrix} \qquad n \geq 2 \qquad \text{(MOP)}$$

where $C = \{x : h(x) = 0, g(x) \leq 0, a \leq x \leq b\}$

A point $x^* \in C$ is Pareto optimal (or non-dominated) for multiobjective optimization problem (MOP) if and only if there is no $x \in C$ such that $f_i(x) \leq f_i(x^*)$ for all $i \in 1,2,..,n$, with at least one strict inequality.

Classical approaches for MOP are the weighting method (1963) and the ε-constraint method (Haimes, 1973). Weighting method minimizes a positively weighted sum of the individual objectives, where the choice of appropriate weighting coefficients is left to the users. For this method the objective takes the following form:

$$\sum_i \alpha_i f_i(x), \qquad \alpha_i > 0, i = 1,2,...,n$$

where α_i are the weights for the different objectives. ε-constraint method (Haimes, 1973) minimizes a primary objective $f_p(x)$, and constrains the upper bounds for the remaining objectives as follows:

$$\min_{x \in C} f_p(x)$$

$$\text{subject to } f_i(x) \leq \varepsilon_i \quad i = 1,..,n \quad i \neq p$$

Hillermeier (1995) proposed a homotopy method that considers the set of Pareto candidates as a differentiable manifold and constructs a local chart which is fitted to the local geometry of that Pareto manifold. New Pareto candidates are generated by evaluating the local chart numerically.

The normal boundary intersection (NBI) (Das and Dennis, 1998) method uses a geometrically intuitive parametrization to produce an even distributed set of points on the Pareto surface, even for poorly scaled problems. This method is utilized in this chapter to generate the Pareto surface of multiobjective scheduling problem. The details of this approach are provided in section 2.3 after the presentation of deterministic and robust scheduling in sections 2.1 and 2.2, respectively.

2.1 Deterministic Scheduling Formulation

In this section, the mathematical model for batch plant scheduling proposed by Ierapetritou and Floudas (1998) is adopted. It follows the main idea of event based continuous time formulation and involves the following constraints:

$$\min H \quad \text{or} \quad \max \sum_{s,n} price_s d_{s,n} \qquad (1)$$

$$\text{subject to } \sum_{i \in I_j} wv_{i,j,n} \leq 1 \qquad (2)$$

$$st_{s,n} = st_{s,n-1} - d_{s,n} - \sum_{i \in I_j} \rho^P_{s,i} \sum_{j \in J_i} b_{i,j,n} + \sum_{i \in I_j} \rho^C_{s,i} \sum_{j \in J_i} b_{i,j,n-1} \qquad (3)$$

$$st_{s,n} \leq st^{\max}{}_s \qquad (4)$$

$$v^{\min}_{i,j} wv_{i,j,n} \leq b_{i,j,n} \leq v^{\max}_{i,j} wv_{i,j,n} \qquad (5)$$

$$\sum_n d_{s,n} \geq r_s \qquad (6)$$

$$Tf_{i,j,n} = Ts_{i,j,n} + \alpha_{i,j} wv_{i,j,n} + \beta_{i,j} b_{i,j,n} \qquad (7)$$

$$Ts_{i,j,n+1} \geq Tf_{i,j,n} - U(1 - wv_{i,j,n}) \qquad (8)$$

$$Ts_{i,j,n} \geq Tf_{i',j,n} - U(1 - wv_{i,'j,n}) \qquad (9)$$

$$Ts_{i,j,n} \geq Tf_{i',j',n} - U(1 - wv_{i,'j',n}) \qquad (10)$$

$$Ts_{i,j,n+1} \geq Ts_{i,j,n} \qquad (11)$$

$$Tf_{i,j,n+1} \geq Tf_{i,j,n} \qquad (12)$$

$$Ts_{i,j,n} \leq H \qquad (13)$$

$$Tf_{i,j,n} \leq H \qquad (14)$$

In the above formulation, allocation constraints (2) state that only one of the tasks can be performed in each unit at an event point (n). Constraints (3) represent the material balances for each state (s) expressing that at each event point (n) the amount $st_{s,n}$ is equal to that at event point (n-1), adjusted by any amounts produced and consumed between event points (n-1) and (n), and delivered to the market at event point (n). The storage and capacity limitations of production units are expressed by constraints (4) and (5). Constraints (6) are written to satisfy the demands of final products. Constraints (7) to (14) represent time limitations due to task duration and sequence requirements in the same or different production units. Parameters $\alpha_{i,j}$ and $\beta_{i,j}$ are defined as: $\alpha_{i,j} = \frac{2}{3}\overline{T}_{i,j}$, $\beta_{i,j} = \frac{2}{3}\overline{T}_{i,j} / (v^{\max}_{i,j} - v^{\min}_{i,j})$ wher $\overline{T}_{i,j}$ is mean processing time of task (i) in unit (j). This is based on the assumption that there is 33% variability of the processing time around the mean value to accommodate different batch sizes, although different processing times functions can be easily adapted. When $wv_{i,j,n}$ equals to 0, the last two terms in constraints (7) are equal to zero due to capacity constraints. Otherwise, the last two terms are added to $Ts_{i,j,n}$. Therefore, the duration of task (i) at unit (j) at event point (n) depends on the amount of material being processed. The remaining timing constraints (8) - (14) represent the production recipe constraints and should be satisfied to impose the correct task sequence.

There is a lot of discussion in the literature recently regarding different modeling attempts of the deterministic scheduling problem. Maravelias and Grossmann (2003) discussed different time representation schemes and proposed a general continuous time MILP formulation for the short-term scheduling of multipurposes batch plants. In this chapter, we select the above presented model since it has been shown to perform well for different case

studies. However, the approach as presented in this paper to address the issue of uncertainty can be utilized independent of the scheduling formulation adopted.

2.2 Multiobjective Robust Optimization Model

In the proposed model, demand uncertainty is described by a number of scenarios (k), each of which is associated with probability p^k. The optimal schedule of the deterministic scheduling formulation presented in the previous subsection will be robust with respect to optimality if it remains close to the optimal solution for any realization of scenario $k \in K$. This solution is called *solution robust*. The schedule is also robust with respect to feasibility if it remains almost feasible for any realization of k, which is called *model robust*. Our aim is to find robust schedules in the face of uncertainty that can help the decision maker to select the optimal solution.

In order to incorporate these two objectives, a multiobjective robust optimization formulation is proposed, which has the following form for the case of uncertain demands:

$$\mathbf{min}\begin{bmatrix}\sum_{k} \mathrm{p}^{\mathrm{k}}\mathrm{H}^{\mathrm{k}} \\ \sum_{s,k} \mathrm{p}^{\mathrm{k}}\mathrm{slack}_{\mathrm{s}}^{\mathrm{k}} \\ \sum_{k} \mathrm{p}^{\mathrm{k}}\Delta^{\mathrm{k}}\end{bmatrix} \quad (15)$$

$$\text{subject to} \sum_{i\in I_j} wv_{i,j,n} \le 1 \quad (16)$$

$$st^k_{s,n} = st^k_{s,n-1} - d^k_{s,n} - \sum_{i\in I_j} \rho^P_{s,i} \sum_{j\in J_i} b^k_{i,j,n} + \sum_{i\in I_j} \rho^c_{s,i} \sum_{j\in J_i} b^k_{i,j,n-1} \quad (17)$$

$$st^k_{s,n} \le st^{\max}_s \quad (18)$$

$$v^{\min}_{i,j} wv_{i,j,n} \le b^k_{i,j,n} \le v^{\max}_{i,j} wv_{i,j,n} \quad (19)$$

$$\sum_n d^k_{s,n} + slack^k_s \ge r^k_s \quad (20)$$

$$Tf^k_{i,j,n} = Ts^k_{i,j,n} + \alpha_{i,j} wv_{i,j,n} + \beta_{i,j} b^k_{i,j,n} \quad (21)$$

$$Ts^k_{i,j,n+1} \ge Tf^k_{i,j,n} - U(1-wv_{i,j,n}) \quad (22)$$

$$Ts^k_{i,j,n} \ge Tf^k_{i',j,n} - U(1-wv_{i',j,n}) \quad (23)$$

$$Ts^k_{i,j,n} \ge Tf^k_{i',j',n} - U(1-wv_{i',j',n}) \quad (24)$$

$$Ts^k_{i,j,n+1} \ge Ts^k_{i,j,n} \quad (25)$$

$$Tf^k_{i,j,n+1} \ge Tf^k_{i,j,n} \quad (26)$$

$$Tf^k_{i,j,n} \le H^k \quad (27)$$

$$\Delta^k \ge H^k - \sum_k p^k H^k \quad (28)$$

$$\Delta^k \ge 0,\ H^k \le U \quad (29)$$

The first objective is minimizing the expected makespan, which is derived from the original objective in deterministic formulation. Model robustness is represented by the second objective that minimizes the expected unsatisfied demands, which is computed by introducing the artificial variables $slack^k(s)$ in the demand constraints (20).

Standard Deviation (SD) is one of the most commonly used metrics to evaluate the robustness of a schedule. To evaluate the SD, the deterministic model with a fixed sequence of tasks $wv_{i,j,n}$ is solved for different realizations of uncertain parameters that define the set of scenarios k which results in different makespans H_k. The SD is then defined as:

$$SD_{avg} = \sqrt{\sum_k \frac{(H_k - H_{avg})^2}{P_{tot} - 1}},\ H_{avg} = \frac{\sum_k H_k}{P_{tot}}$$

where H_{avg} is the average makespan over all the scenarios, and p_{tot} denotes the total number of scenarios. A detailed discussion of different robustness metrics can be found in Samsatli et al. (1998). Vin and Ierapetritou (2001) proposed a robustness metric taking into consideration the infeasible scenarios. In case of infeasibility, the problem is solved to meet the maximum demand possible by incorporating slack variables in the demand constraints. Then the inventory of all raw materials and intermediates at the end of the schedule are used as initial conditions in a new problem with the same schedule to satisfy the unmet demand. The makespan under infeasibility H_{corr} is determined as the sum of those two makespans. Their proposed robustness metric is defined as: $SD_{corr} = \sqrt{\sum_k \frac{(H_{act} - H_{avg})^2}{P_{tot} - 1}}$ where $H_{act} = H_k$, if scenario k is feasible and $H_{act} = H_{corr}$, if scenario k is infeasible. The concept of upper partial mean (UPM) introduced by Ahmed and Sahinidis is used in the third objective function in order to optimize the solution robustness. They define the variance measure $\overline{\Delta}$ as follows: $\overline{\Delta} = \sum_k p^k \Delta^k \quad \Delta^k = \max\{0, H^k - \sum_k p^k H^k\}$

where Δ^k corresponds to the positive deviation of makespan under scenario k from the expected value.

The main advantage of using UPM instead of variance is that it can avoid introducing nonlinearities in the formulation. Thus, the resulting model remains a mixed-integer linear programming (MILP) problem.

Comparing to the deterministic problem, in this formulation, the binary variables $wv_{i,j,n}$ that represent the task sequences remain the same over all scenarios, while the continuous variables that correspond to the batch sizes, and the starting and finishing times can vary to accommodate the realization of different scenarios. Thus, the schedules obtained by solving this multiobjective optimization problem include robust assignments that can accommodate the demand uncertainty.

Note that this robust optimization model is written for a general batch plant scheduling problem where the objective is to minimize the makespan. However, other scheduling problems can have different

objectives and constraints. In these cases, the above formulation has to be modified to accommodate the different objectives.

2.3 Normal Boundary Intersection

NBI is a solution methodology developed by Das and Dennis (1998) for generating Pareto surface in nonlinear multiobjective optimization problems. It is proved that this method is independent of the relative scales of the objective functions and is successful in producing an evenly distributed set of points in the Pareto surface given an evenly distributed set of parameters, which is an advantage compared to the most common multiobjective approaches - weighting method and the ε-constraint method.

The *anchor point* F_i^*, is obtained when the *ith* objective is minimized independently, while f_i^* represents the individual minima of the *ith* objective. The shadow minimum (utopia point) F^*, is defined as the vector containing the individual global minima of the objectives, i.e. $F^* = [f_1^*, f_2^*, ..., f_n^*]^T$.

2.4 Robust Scheduling

The basic steps of NBI in the context of robust production scheduling are as follows:

Step 1: Determine the anchor points: The robust optimization model for scheduling problems as presented in section 2.2 has three objectives, which are the expected value of makespan, unsatisfied demand (model robustness), and the upper partial mean of the makespan (solution robustness). In order to determine the anchor points, the robust optimization formulation is solved with one objective function being minimized each time. The expected makespan, model robustness, and solution robustness is minimized with respect to constraints (16) - (29) individually, and the minimum value and the values of the other two objectives are saved. Since the makespan requirement is imposed through the inequality in constraint (27), when the problem is solved to minimize the model robustness or solution robustness, the makespan that corresponds to each scenario H^k obtained may not be equal to the finishing time of the last task. Thus, in order to get the optimal value of expected makespan at the anchor points, if model or solution robustness is optimized first, the following step is required.

Step 2: Tighten the anchor points: When model or solution robustness is minimized first, they are fixed at the optimal values and the problem of minimizing the expected makespan is solved again. Thus, the resulting points are the real anchor points that contain the optimal value of the expected makespan corresponding to the finishing time of the last performed task and utopia point F^* is correctly determined.

Step 3: Formulate and solve problem (NBI_ω) iteratively for different values of ω.

The convex hull of individual minima (CHIM) has the following definition: let x_i^* be the respective minimizer of $f_i(x), i = 1,\ldots,n$ for $x \in C$. Let $F_i^* = F(x_i^*), i = 1,\ldots,n$, Φ be the $n \times n$ matrix whose i^{th} column is $F_i^* - F^*$. Then the set of points in ∂R^n that are convex combinations of $F_i^* - F^*$, i.e., $\{\Phi\omega : \omega \in \partial R^n, \sum_i \omega_i = 1, \omega_i \geq 0\}$ is referred to as the CHIM. The set of attainable objective vectors: $\{F(x) : x \in C\}$ is denoted by Φ so C is mapped onto Φ by F. The space ∂R^n which contains Φ is referred to as objective space. The boundary of Φ is denoted by $\partial\Phi$. NBI method determines the portion of $\partial\Phi$ which contains the Pareto optimal points solving problem (NBI_ω). The principal idea behind this approach is that the intersection point between the boundary $\partial\Phi$ and the normal pointing towards the origin ($\Phi\omega + t\hat{n}$, where ω is a convex weighting) emanating from any point in the CHIM ($\Phi\omega$ is a point on the portion of $\partial\Phi$ containing the efficient points. This point is guaranteed to be a Pareto optimal point if the trade-off surface is convex. Each of the points represents a trade-off solution between the expected performance, feasibility and deviation from the mean.

3. PARAMETRIC MILP APPROACH

As mentioned in the introduction for the case where there is not enough information about uncertainty characteristics, parametric MILP can be used to generate alternative schedules that can be then evaluated in the face of uncertainty. In this section, the parametric MILP problem is discussed.

For the general mixed integer problem:

$$\begin{aligned} &\min z = cx \\ \text{subject to} \quad &Ax \geq \theta \qquad\qquad (P1) \\ &x \geq 0, \quad x_j \text{ integer}, \ j = 1,..,k \end{aligned}$$

Assuming a perturbation of problem RHS parameter values such that: $Ax \geq \theta + \Delta\theta$

The aim of is to investigate the effect of Δθ on the optimal solution *x* and objective value *z*.

3.1 Single Uncertain Parameter

For the case of single uncertain parameter, the proposed approach follows the basic ideas of the interactive reference point approach proposed by Alves and Climaco (2000) presented for multiple objective MILP problems. The proposed framework is shown in Figure 1.

First the problem is solved at the nominal values of the uncertain parameters using a branch and bound solution approach, and the dual information λ^p, z^p is collected at each leaf node.

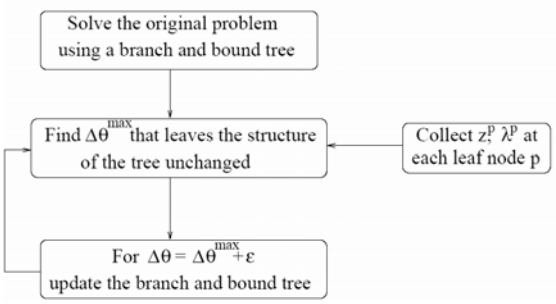

Figure 1. Flow chart of the proposed approach

Assuming that the optimal solution is found at node 0, the LP sensitivity analysis is then performed at node 0 to determine the range $\Delta\theta^{basis}$ within which the current optimal basis does not change.

We need to find the perturbation $\Delta\theta^{max}$ beyond which the structure of the branch and bound may not remain the same. $\Delta\theta^{max}$ can be found through the following equation: $\Delta\theta^{\max} = \min\{\Delta\theta^{basis}, \min\{\frac{z^p - z^0}{\lambda^0 - \lambda^p}\}\}$:

where z^0 and λ^0 are the objective value and dual multiplier at the optimal node 0, respectively. Note that only the positive $\frac{z^p - z^0}{\lambda^0 - \lambda^p}$ need to be considered, because the negative one means that node p can never provide a better solution than node 0 at a certain point.

3.2 Multiple Uncertain Parameters

This subsection presents the detailed steps (Figure 2) of the proposed approach to deal with the case of multiple uncertain parameters. Assuming for simplicity in the presentation that we want to investigate two parameters, θ_a and θ_b, changing in the range of $[a_0, a_0 + \Delta a]$ and $[b_0, b_0 + \Delta b]$. The MILP problem is first solved at (a_0, b_0) using branch and bound algorithm and the optimal solution is found at node 1 (Figure 3). Other leaf nodes of the B&B tree are denoted as node 2, node 3, ..., node n. Note that only the information at the leaf nodes is required.

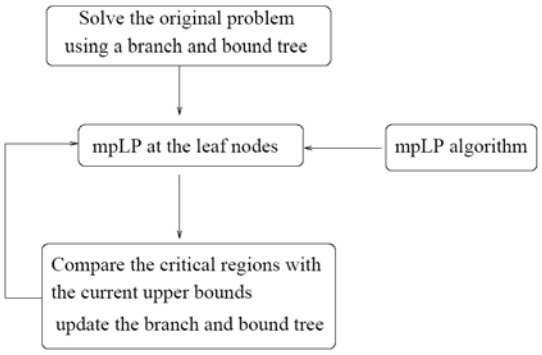

Figure 2. Flow chart of proposed approach for multiple uncertain parameters case

This is true since if at another set of uncertain parameters (a', b'), there exists a new optimal solution, it can always be uncovered by checking or continuing the branching procedure on the current leaf nodes. Let's assume for example that the new optimal solution can be provided by a non-leaf node (node A). With the original data, the relaxed LP problem of node A must have a partial integer solution, otherwise it is a leaf node. With the perturbed data, the LP problem of node A gives the optimal integer solution. According to our proposed method, all the current leaf nodes are examined that include the subsequent nodes of node A (node 2 and 3). Apparently, if node A yields an integer solution, either node 2 or 3 should provide that solution too. Thus, it is true that only the leaf nodes need to be examined at each iteration.

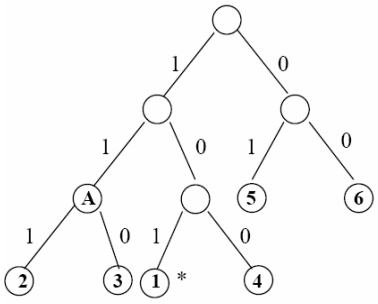

Figure 3. Branch and bound tree

Then the multiparametric linear programming is solved at each of the leaf nodes including node 1, so as to identify the optimal value functions and their corresponding critical regions in the region of $[a_0, a_0 + \Delta a]$ and $[b_0, b_0 + \Delta b]$. In this work, a new algorithm is proposed for the solution of mpLP. When the mpLP procedure is completed, the output will be a set of optimal functions $z = z^k + \lambda^k \theta_a + \beta_k \theta_b$, $k = 1, \ldots, K$, where K is the number of critical regions. For any point (θ_a, θ_b) in the range of $[a_0, a_0 + \Delta a]$ and $[b_0, b_0 + \Delta b]$, the objective value cx^* of the relaxed LP problem of that node can be expressed by $\max\{z^k + \lambda^k \theta_a + \beta_k \theta_b, k = 1, \ldots, K\}$. If the procedure is not complete, then there must exist a point (θ_a, θ_b), such that $\max_k\{z^k + \lambda^k \theta_a + \beta_k \theta_b\}$ is less than cx^*. Thus a bilevel programming problem is formulated as shown in problem (P2). It is proved that linear bilevel programming problems (BLPP) are strongly NP-hard (Bard 1998). In order to avoid solving a BLPP, we propose to first convert the relaxed LP problems (inner problem in (P2)) at the leaf nodes to its dual form, so that the uncertain parameters appear in the objective function and substitute the inner problem in problem (P1).

$$\max \quad \{\min cx \mid Ax \geq \theta\} - z \qquad \text{(P2)}$$

$$\text{subject to} \quad z \geq z^{(k)} + \lambda^{(k)}\theta_a + \beta^{(k)}\theta_b, k = 1,..K$$

$$a_0 \leq \theta_a \leq a_0 + \Delta a$$

$$b_0 \leq \theta_b \leq b_0 + \Delta b$$

In problem (P3), the objective function is to

maximize the gap between the optimal objective value θy at any point in the uncertain range and the maximum value of the optimal function, which is $\max_k\{z^k + \lambda^k\theta_a + \beta_k\theta_b\}$. Note that the problem is nonlinear due to the bilinear term in the objective function. The constraints contain the original constraints and the current optimal functions $z = z^k + \lambda^k\theta_a + \beta_k\theta_b$, hence all the constraints are linear. If the objective value of the (P3) model is nonzero, it means that there exists at least one point (θ_a, θ_b) at which its real objective value cannot be represented by any of the current objective value functions. Therefore, the objective value function at that point is $z = z' + \lambda'\theta_a + \beta'\theta_b$ and should be included in the next iterations. This procedure terminates when the objective value for problem (P3) is 0, which means that the entire uncertain parameter range is covered by the existing objective value functions. Since (P3) is a nonconvex problem, a global optimization algorithm should be utilized such as GAMS/BARON (Sahinidis, 1996), which relies on *branch-and-reduce* algorithm. Therefore, by performing mpLP at each leaf node p, a number of critical regions (k), $CR_p^1, CR_p^2, \ldots, CR_p^K$ are identified and in each $CR_p^k, k = 1, \ldots, K$, the optimal value z_p^{*k} is expressed as $z_p^{*k} = z_p^k + \lambda_p^k\theta_a + \beta_p^k\theta_b$. The next step is to update the B&B tree. The main procedure involves to compare the critical regions of the leaf nodes with the current upper bounds and finally identify a set of new critical regions, and their corresponding objective function values and optimal integer solutions. At the beginning, the upper bounds CR_p^{UB} are set to be the critical regions of the current optimal node (node 1), which are $CR_1^{(1)}, CR_1^{(2)}, \ldots, CR_1^{(K)}$. Assuming that we want to compare critical regions CR_1^{UB} and CR_2^{UB}, which have intersection CR^{int}, the following constraint is defined: $z_1^{UB} \geq z_2^{*2}$ and a redundancy test for this constraint is solved in CR^{int} as shown in problem (P4) (Acevedo and Pistikopoulos 1997). The solution of this problem provides the optimal functional form in CR^{int}.

$$\begin{aligned} &\max\ \theta y && \text{(P3)}\\ &\text{subject to}\ A^T y \leq c\\ &a_0 \leq \theta_a \leq a_0 + \Delta a\\ &b_0 \leq \theta_b \leq b_0 + \Delta b\\ &y \geq 0 \end{aligned}$$

$$\Downarrow$$

$$\begin{aligned} &\max\ \theta y - z\\ &\text{subject to}\ A^T y \leq c \end{aligned}$$

$$\begin{aligned} &z \geq z^{(k)} + \lambda^{(k)}\theta_a + \beta^{(k)}\theta_b, k = 1,..K\\ &a_0 \leq \theta_a \leq a_0 + \Delta a\\ &b_0 \leq \theta_b \leq b_0 + \Delta b\\ &y \geq 0 \end{aligned}$$

At each iteration, the new leaf nodes in the updated B&B tree will be compared to the current upper bounds, so as to determine the new optimal functions in their intersected region. This procedure stops when no further branching is required and the uncertainty analysis of the entire uncertain space can be presented by a number of critical regions that contain their corresponding optimal functions and integer solutions.

$$\begin{aligned} &\max\ \varepsilon && \text{(P4)}\\ &\text{subject to}\ z_1^{UB} = z_2^{*(2)} + \varepsilon\\ &z_1^{UB} = z_1^{UB} + \lambda_1^{UB}\theta_a + \beta_1^{UB}\theta_b\\ &z_2^{(2)} = z_2^{(2)} + \lambda_2^{(2)}\theta_a + \beta_2^{(2)}\theta_b\\ &b_0 \leq \theta_b \leq b_0 + \Delta b\\ &\theta_a, \theta_b \in CR^{ubt} \end{aligned}$$

Comparing to the existing approach (Acevedo and Pistikopoulos 1997), the proposed method solves the mpLP at only the leaf nodes in the B&B tree instead of every node during the branch and bound procedure, and consequently reduces the computational efforts significantly as will be shown in the preliminary results in the next section. Moreover, the new mpLP approach can efficiently determine the optimal function with respect to the uncertain parameters and the critical regions without having to retrieve the optimal tableaus and investigate the neighboring bases.

4. CASE STUDY

In this section a case study is presented and the results evaluated to assess the viability and efficiency of the proposed approach. High quality solutions were found efficiently, which provides confidence that the proposed approach will also be effective on new problems and extensions.

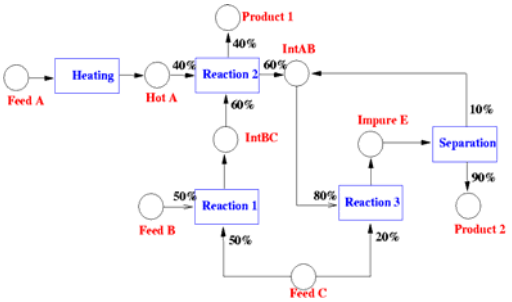

Figure 4. STN for example problem

To present the main steps, the first example is considered here as described through the STN representation in Figure 4. The data for this example can be found in Ierapetritou and Floudas (1997). The problem is solved at the initial demand value (50). A

branch and bound tree is constructed to determine the optimal schedule, which is found to be schedule 1 with makespan 7.04 hours. It is provided by two nodes 1A and 1B that represent equivalent schedules. Performing linear sensitivity analysis on the optimal nodes, we get $\Delta\theta^{max} = 6.92$ which is the change allowed in the demand for which the B&B structure remains the same. For a slight change in $\Delta\theta = \Delta\theta^{max} + \varepsilon = 7$, nodes 1A(B) still yield optimal solution with objective value of 7.08 hours, but the basis changes. For the second iteration, LP sensitivity analysis is performed on nodes 1A(B). This results in $\Delta\theta^{basis}$=26.03, which is the value of change of demand where the basis remains unchanged, and there is no leaf node at which this value is intersected which is determined by examining the value of $(z^p - z^0)/(\lambda^0 - \lambda^p)$ where z^p is the objective value at node p and λ^p the corresponding lagrange multiplier, and found to be larger than 26.03 for all leaf nodes. Therefore $\Delta\theta^{max} = 26.03$. For a small perturbation away from this value $\Delta\theta = \Delta\theta^{max} + \varepsilon = 27$, the tree is updated and the optimal solution is provided by nodes that correspond to equivalent schedules 2A(B, C, D). Nodes 2A(B, C, D) are intersected by another two nodes 3A(B) in the next iteration, then nodes 3A(B) continue to provide the optimal schedule but with a different basis in the following iteration. After that, the problem becomes infeasible when the demand is greater than 87.5. The three operations schedules are presented in Figure 5 and Figure 6 presents how the makespan and optimal schedule change with the demand.

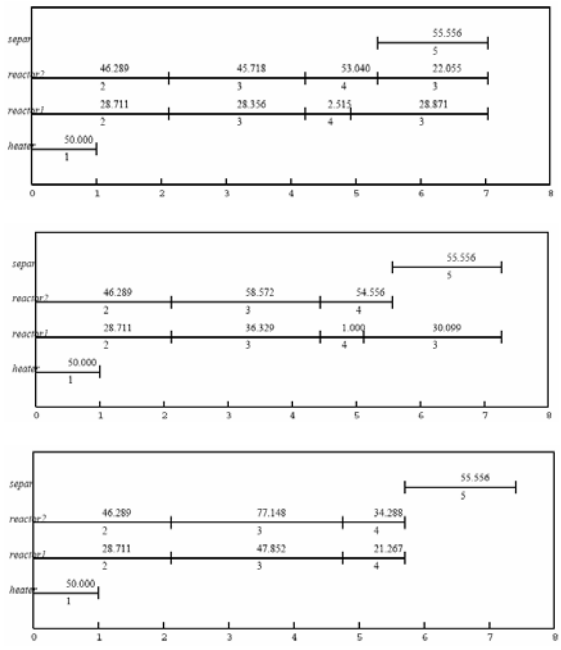

Figure 5: Gantt charts of schedules 1,2,3

For the multiobjective approach, the nominal demand for both products 1 and 2 is 80 and is assumed to exhibit a variability of ±50%. 5 scenarios (40, 60, 80, 100, 120) are selected to represent the uncertain demand for each product and thus result to a total of 25 scenarios. 10% demand satisfaction is also assumed for this example.

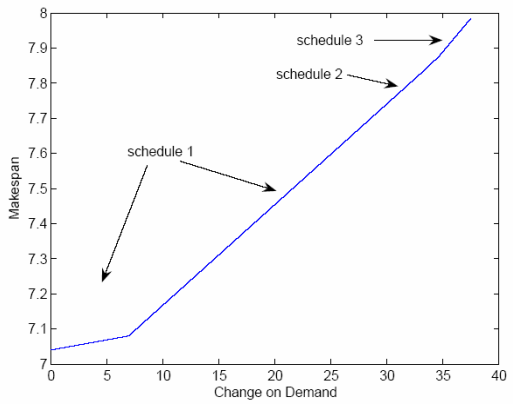

Figure 6. Parametric solution for example problem

Following the proposed approach presented in Section 3.2, the individual minimum points are obtained as follows: $f_1(x^*) = (5.005,\ 143.65,\ 0.045)$, $f_2(x^*) = (10.56,\ 0,\ 0.696)$, $f_3(x^*) = (5.236, 143.55, 0)$. Therefore, the utopia point is $F^* = (5.055, 0, 0)$ and the matrix $\Phi = \begin{pmatrix} 0 & 5.501 & 0.181 \\ 143.65 & 0 & 143.55 \\ 0.045 & 0.696 & 0 \end{pmatrix}$. In order to generate different values of ω, let's assume that for a n-objective problem, δ_j is the uniform spacing between two consecutive ω_j values for $j = 1, \ldots, n-1$. The possible values that can be taken by ω_1 are: $[0, \delta_1, 2\delta_1, \ldots, 1]$. Given a particular value of ω_i, $i = 1, \ldots, j-1$, the possible values of ω_j, $j = 1, \ldots, n-1$ are: $[0, \delta_j, 2\delta_j, \ldots, k_j\delta_j]$ where $k_j = I\left[\frac{1 - \sum_i \omega_i}{\delta_j}\right]$. The last component of ω_n is defined as: $\omega_n = 1 - \sum_i \omega_i$. For this example the step sizes are chosen to be $\delta_1 = 0.1$ and $\delta_2 = 0.05$, and NBI_ω problem is formulated and solved for different values of ω. The resulting Pareto optimal surface is shown in Figure 7, which contains 8 different schedules. Taking a closer look at the optimal Pareto solutions, a number of interesting observations can be made. For example, focusing on two points A and B as shown in Figure 6 point A which is obtained with ω= (0, 1, 0) is in the area of solutions that prefer model robustness. The three objective values for this point are 10.56, 0, 0.70 for expected makespan, model robustness, and solution robustness, respectively. On the other hand, point B represents the optimal solution for ω = (0.6, 0.4, 0),

which corresponds to a different schedule. Comparing to the schedule A, this solution corresponds to a decision that favors the expected makespan and solution robustness, the values of which are 6.82 and 0.25, respectively, at the expense of low model robustness, which is 64.39. For the nominal demand of (80, 80), schedule A requires 9.83hr and schedule B prefers having a shorter makespan of 8.46hr. However, at the maximum demand value (120, 120), schedule A focuses more on meeting the demands and can produce the required amount within 13.32hr, while schedule B results in an unsatisfied amount of 33.33 units for product 1 and 32.25 units for product 2.

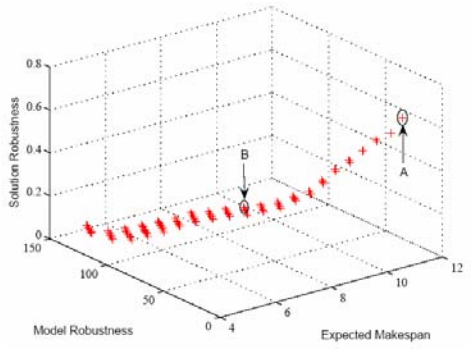

Figure 7. Pareto set of solutions for example 1

These results indicate that the proposed methods can be extended to meet all research objectives. The parametric analysis generates alternative solutions to cover the uncertainty space whereas the multiobjective optimization provides solutions according to decision maker's position towards risk.

5. CONCLUSIONS AND FUTURE WORK

A multiobjective robust optimization model is proposed to deal with the problem of uncertainty in scheduling considering the expected performance, model robustness and solution robustness. NBI technique is utilized to solve the multiobjective model and successfully produce Pareto optimal surface that captures the trade-off among different objectives in the face of uncertainty.

The issue is also addressed through parametric MILP analysis. An integrated framework is developed that allows the parameters in the RHS of the MILP formulation to vary independently. It mainly consists of two steps: LP/mpLP sensitivity analysis and updating the B&B tree. For the case of mpLP, a novel algorithm is proposed which solves a set of NLP problems iteratively using the commercially available global optimization solver BARON.

The work can be further extended to investigate the cases where preferences exist among the objectives, so as to generate more meaningful Pareto optimal solutions. This will help reducing the computational complexity of the proposed approach. In addition, there are cases that instead of unique anchor points, anchor curves are found due to the fact that the objectives are not entirely conflicting with each other. For these cases, it will be of interest to study how the selection of anchor points can affect the Pareto surface.

The parametric MILP approach can be further developed to enable the analysis of uncertainty in the constraints coefficients and the case that uncertainty exists in the objective function coefficients, constraints coefficients and the RHS parameter at the same time. In that case, a linear bilevel programming problem, which is similar to (P2), will be formed and solved using appropriate algorithms.

Acknowledgement

The authors gratefully acknowledge financial support from the National Science Foundation under the NSF CAREER program CTS-9983406.

REFERENCES

Acevedo, J. and Pistikopoulos, E.N. (1997). A multiparametric programming approach for linear process engineering problems under uncertainty. *Ind. Eng. Chem. Res*., **36**, 717.

Alves, M.J. and Climaco, J. (2000), An interactive reference point approach for multiobjective mixed-integer programming using branch-and-bound. *Eur. J. Oper. Res*.,**124**, 478.

Balasubramanian, J. and Grossmann, I.E. (2002). A novel branch and bound algorithm for scheduling flowshop plants with uncertain processing times. *Comput. Chem. Eng.*, **26**, 41.

Basset, M.H., Perkny, J.F. and Reklaitis, G.V. (1997). Obtaining realistic production plans for a batch production facility. *Comput. Chem. Eng*., **21**, S1203.

Bonfill, A., Espuna, A. and Puigjaner, L. (2005). Addressing robustness in scheudling batch processes with uncertain operations times. *Ind. Eng. Chem. Res.,* **44**, 1524.

Borrelli, F., Bemporad, A., and Morari, M. (2003). Geometric approach for multiparametric linear programming. *J. Optimization Theroy and Applications,* **118**, 515.

Cheng, L., Subramanian, E., and Westerbeger, A.W. (2003). Design and planning under uncertainty: issues on problem formulation and solution. *Comput. Chem. Eng.,* **27**, 781.

Crema, A. (2002). The multiparametric 0-1 integer linear programming problem: a unified approach. *Eur. J. Oper. Res.,***139**, 511.

Das, I. and Dennis, J.E. (1998). Normal boundary intersection: a new method for generating Pareto optimal points in multicriteria optimization problems *SIAM J. on Optimization,* **8**, 631.

Dua, V. and Pistikopoulos, E.N. (2000). An algorithm for the solution of multiparametric mixed integer linear programming problems. *Ann. Oper. Res.,***99**, 123.

Gal, T. and Nedoma J. (1972). Multiparametric linear programming. *Management Sci.*, **18**, 406.

Haimes, Y.Y. (1973). Integrated system identification and optimization. *Control and Dynamic Systems: Advances in Theory and Applications*, **10**, 435.

Hillermeier, C. (1995). Generalized homotopy approach to multiobjective optimization. *J. Optimization Theory and Applications,* **19**, 1089.

Holm, S. and Klein, D. (1984). Three methods for post-optimal analysis in integer linear programming. *Math. Prog. Study,* **21**, 97.

Ierapetritou, M.G. and Floudas, C.A. (1998) Effective continuous-time formulation for short-term scheduling. 1. Multipurpose batch processes. *Ind. Eng. Chem. Res.,* **37**, 4341.

Ierapetritou, M.G. and Pistikopoulos, E.N. (1996). Batch plant design and operations under uncertainty. *Ind. Eng. Chem. Res*., **35**, 772.

Jenkins, L. (1990). Parametric methods in integer linear programming. *Ann. Oper. Res*., **27**, 77.

Jenkins, L. and Peters, D. (1987). A computational comparison of Gomory and knapsack cuts. *Compt. Oper. Res*., **14**, 449.

Jia, Z. and Ierapetritou, M.G. (2004). Short-tem scheduling under uncertainty using MILP sensitivity analysis. *Ind. Eng. Chem. Res.,* **43**, 3782.

Lin, X., Janak, S.L. and Floudas, C.A. (2004). A new robust optimizaton approach for scheduling under uncertainty: I. Bounded Uncertainty. *Comput. Chem. Eng*., **28**, 1069.

Maravelias, C.T. and Grossmann, I.E. (2003). New Continuous-Time State Task Network Formulation for the Scheduling of Multipurpose Batch Plants. *Ind. Eng. Chem. Res*., **42**, 3056.

Marsten, R.E. and Morin, T.L. (1977). Parametric integer programming: the right-hand side case. *Ann. Discr. Math*., **1**, 375.

Ohtake, Y. and Nishida, N. (1985). A branch-and-bound algorithm for 0-1 parametric mixed integer programming. *Oper. Res. Lett.,* **4**, 41.

Orcun, S.,Altinel, I.K. and Hortacsu, O.J. (1996). Scheduling of batch processes with operational uncertainties. *Comp. Chem. Eng*., **20**, S1191.

Pertsinidis, A., Grossmann, I.E. andMcRae, G.J. (1998). Parametric optimization of MILP programs and a framework for the parametric optimization of MINLPs. *Comp. Chem. Eng*., **22**, S205.

Piper, C.J. and Zoltners, A.A. (1976). Some easy postoptimality analysis for zero-one programming. *Management Sci.,* **22**, 759.

Roodman, G.M. (1972). Postoptimality analysis in zero-one programming by implicit enumeration. *Naval Res. Log. Quarterly*, **19**, 435.

Roodman, G.M. (1974). Postoptimality analysis in integer programming by implicit enumeration: the mixed integer case. *Naval Res. Log. Quarterly*, **21**, 595.

Samsatli, N.J., Papageorgiou, L.G. and Shah, N. (1998) Robustness metrics for dynamic optimization models under parameter uncertainty. *AICHE J*, **44**, 1993.

Vin, J.P.,Ierapetritou, M.G. (2001). Robust short-term scheduling of multiproduct batch plants under demand uncertainty. *Ind. Eng. Chem. Res.*, **40**, 4543.

Zadeh, L. (1963). Optimality and nonscalar-valued performance criteria. *IEEE Transactions on Automatic Control*, **8**,59.

Session 2.1

Optimization and Control of Biological Systems

Dynamic Analysis and Control of Chemical and Biochemical Reaction Networks

I. Otero–Muras, G. Szederkényi, A. A. Alonso and K. M. Hangos
Spanish Council for Scientific Research

A Risk Management Criterion for an Unstable Wastewater Treatment Process

J. Hess, O. Bernard and M. Djuric
French Research Institute of Computer Science and Automatic Control

Control of High–Solids Saccharification using a Model–Based Methodology for Fed–Batch Operation

D. B. Hodge, M. N. Karim, D. J. Schell and J. D. McMillan
National Renewable Energy Laboratory
Texas Tech University

ITSE Observers for Batch Processes. A Wastewater Treatment Case Study

G. Acuna and D. Dochain
Universidad de Santiago de Chile

Robust Adaptive Control of Yeast Fed–Batch Cultures

F. Renard, A. VandeWouwer and M. Perrier
Faculté Polytechnique de Mons

Output Tracking of Bioprocesses Through Recirculation with Unknown Input Concentration

A. Rapaport, F. Mazenc and J. Harmand
French National Institute for Agricultural Research

ADCHEM 2006

International Symposium on Advanced Control of Chemical Processes
Gramado, Brazil – April 2-5, 2006

DYNAMIC ANALYSIS AND CONTROL OF CHEMICAL AND BIOCHEMICAL REACTION NETWORKS

Irene Otero-Muras * **Gábor Szederkényi** **
Antonio A. Alonso * **Katalin M. Hangos** **

* *Department of Process Engineering, IIM-CSIC, Eduardo Cabello 6 36208 Vigo, Spain*
** *Process Control Research Group, Computer and Automation Research Institute, H-1518 Budapest P.O.Box 63, Hungary*

Abstract: Metabolic or cell signalling pathways are examples of biochemical networks exhibiting possible complex dynamics in the form of steady-state multiplicity, sustained oscillations or even deterministic chaos. The origin of these nonlinear phenomena is not always well understood, nor it can be systematically predicted beyond a case by case basis. Despite considerable progress in dynamic aspects, efforts are still needed to develop efficient and robust methods of stabilization and control of reaction networks. In this work, we combine concepts and tools from irreversible thermodynamics and systems theory to explore the underlying dynamic properties of a general class of chemical and biochemical networks. Lyapunov and passivity based methods are given for the systematic design of globally stabilizing feedback controllers in both the concentration space and a novel minimal description of the kinetic networks dynamics: the reaction space.

Keywords: biochemical reaction networks, passivity, nonlinear control, entropy.

1. INTRODUCTION

Complex dynamics of biochemical networks in the form of steady-state multiplicities or sustained oscillations is a recurring theme in the literature due to its decisive role in physiology of living organisms (Thomas and Kaufman, 2001). In this contribution, we make use of concepts and tools from irreversible thermodynamics and systems theory to devise efficient control schemes capable of network stabilization of steady states.

On the one hand, irreversible thermodynamics gives us the necessary physical insight in exploring reaction networks dynamics, which evolution as dissipative systems occurs in terms of the combined action of entropy production and entropy flux. The mass action law establishes the macroscopic reaction rates as proportional to microscopic reactive collisions, connecting in a particular form the concentrations of species with the entropy, and imposing strict constraints on the concentration space (Feinberg, 1979). On the other hand, Lyapunov theory and other control system methods such as passivity which is proved to be useful in process system analysis and control (Alonso and Ystdie, 2001), will allow us to explore the intrinsic dynamic properties of chemical and biochemical reaction networks. Furthermore, these methods will be used to construct control configurations ensuring steady state stabilization.

The paper is organized as follows. In Section 2 we explore the structural properties of biochemical networks characterizing them as dissipative systems and define an entropy based Lyapunov function candidate. Connections between thermodynamics and nonlinear stabilizing control are also established here. In Section 3 we define a minimal representation of reaction networks which, being based on a potential structure, will allow us to derive connections with passivity and generalized Hamiltonian systems.

2. THE DISSIPATIVE NATURE OF REACTION SYSTEMS

2.1 The class of systems under study

In order to rigorously apply thermodynamic based tools to the dynamic analysis and control of chemical and biochemical systems, we must distinguish between closed and open networks depending on whether there is or not material exchange with the environment. By properly setting the boundary of the domain one defines the control volume of the system. This volume corresponds in classical reaction problems with the volume of the chemostat whereas regarding intra-cell processes it may be enclosed by a virtual boundary.

The general class of systems under study comprises those pure chemical reaction networks and those metabolic, genetic and signalling pathways, which satisfy the following assumptions: *i*) the reaction rates of the kinetic mechanisms obey the *mass action law*, *ii*) the spatial distribution of products can be neglected, *iii*) the process takes place in isothermal conditions, *iv*) all the kinetic steps are reversible, so that irreversible steps will be considered as inflow-outflow terms acting through the control volume.

At this point it is important to note that kinetics of Michaelis-Menten type are in fact reduced order models derived from original mass action law mechanisms.

2.2 The basic structure of reaction kinetic networks

In describing the underlying dynamic structure of reaction networks, we adopt the notation employed in (Gorban *et al.*, 2004). Let us first consider a closed and homogeneous isotherm system where n species participate on a r-step reaction network, represented by the following stoichiometric mechanism:

$$\sum_{i=1}^{n} \alpha_{ij} A_i \rightleftarrows \sum_{i=1}^{n} \beta_{ij} A_i \quad for\ j = 1, ...r \qquad (1)$$

with α_{ij}, β_{ij} being the constant stoichiometric coefficients for specie A_i in the reaction step j. All reactions are assumed to be reversible, with reaction rates obeying the *mass action law*:

$$W_j = W_j^+ - W_j^- = k_j^+ \prod_{i=1}^{n} x_i^{\alpha_{ij}} - k_j^- \prod_{i=1}^{n} x_i^{\beta_{ij}} \qquad (2)$$

where k_j^+ and k_j^- are the constants of the direct and inverse rates of the j-th reaction step, respectively, and $x_i \geq 0$ represents the concentration of the specie A_i. Each concentration evolves in time according to the ordinary differential equation:

$$\dot{x}_i = \sum_{j=1}^{r} \nu_{ij} (W_j^+ - W_j^-) \qquad (3)$$

where $\nu_{ij} = \alpha_{ij} - \beta_{ij}$ is positive or negative depending on whether the specie i is a product or a reactant in the reaction j. The dynamic evolution of the network can be then represented by a set of ordinary differential equations which in compact matrix form is written as:

$$\dot{x} = \mathcal{N} \cdot W(x) \qquad (4)$$

where $\mathcal{N} = [\nu_{ij}]$ is the $n \times r$ coefficient matrix whose columns are the linearly independent stoichiometric vectors $\nu_j = \beta_j - \alpha_j$, and $W(x) \in \mathbb{R}^r$ denotes the vector of reaction rates.

The reaction simplex. In a closed network the amount of each chemically unaltered component $\mathcal{C}_k$ $(k = 1, ..., m)$ remains constant and the corresponding component mass balances satisfy the following set of algebraic equations:

$$\mathcal{C}_k^0 = c_k^T \cdot x \qquad for\ \ k = 1, ..., m \qquad (5)$$

where entries of the vector $c_k \in \mathbb{N}^n$ represent the units of $\mathcal{C}_k$ in each specie, and $\mathcal{C}_k^0 = c_k^T \cdot x_0$ with $x_0 = x(0)$. The intersection of the positive orthant (i.e. $\mathbb{R}_+^n$) with the set of m conservation laws defines the *reaction simplex*:

$$\Omega(x_0) = \left\{ x \in \mathbb{R}_n^+ / c_k^T (x - x_0) = 0, \quad k = 1, ..., m \right\} \qquad (6)$$

that is invariant for the system dynamics. The set of vectors $[c_k]$ forms a basis of $\ker(\mathcal{N}^T)$ and consequently the number r of linearly independent reactions in a reaction network is determined by the difference between species and its elementary constituents, i.e. $r = n - m$. In addition, it follows that the minimal representation of a chemical reaction system (4) is r-dimensional, where $r \leq n$.

The equilibrium manifold. The relationships $\dot{x} = 0 \Leftrightarrow W(x) = 0$ determine the set of equilibrium points of the closed system. As it will be shown next by means of a direct Lyapunov argument, in a closed reaction network the equilibrium point is unique for every initial condition belonging to the same reaction simplex.

Example 1. Let us consider two connected reversible reactions involving four chemical species AB, A, A_2B and B, with concentrations defined

by the state vector $x = [x_1, x_2, x_3, x_4]$. These species are composed by two classes of atoms A and B representing the chemical unaltered components. The kinetic mechanism is described by two steps with respective rates W_1 and W_2 obeying the mass action law:

$$AB + A \underset{k_1^-}{\overset{k_1^+}{\rightleftarrows}} A_2B \qquad W_1 = k_1^+ x_1 \cdot x_2 - k_1^- x_3$$

$$A_2B + B \underset{k_2^-}{\overset{k_2^+}{\rightleftarrows}} 2AB \qquad W_2 = k_2^+ x_3 \cdot x_4 - k_2^- x_1$$

The state space description in compact matrix form (4) becomes:

$$\dot{x} = \begin{bmatrix} -1 & 2 \\ -1 & 0 \\ 1 & -1 \\ 0 & -1 \end{bmatrix} \cdot \begin{bmatrix} W_1 \\ W_2 \end{bmatrix} \tag{7}$$

and the atomic conservation balances (5) for this case read:

$$\mathcal{C}_A^0 = c_A^T x = x_1 + x_2 + 2x_3 \ , \ \mathcal{C}_B^0 = c_B^T x = x_1 + x_3 + x_4 \tag{8}$$

where $\mathcal{C}_A^0$ and $\mathcal{C}_B^0$ represent the concentrations of each atomic species. Vectors c_A and c_B can be grouped into the following matrix:

$$C^T = \begin{bmatrix} 1 & 1 & 2 & 0 \\ 1 & 0 & 1 & 1 \end{bmatrix} \tag{9}$$

which defines a basis for $\ker \mathcal{N}^T$ so that $C^T \mathcal{N} = 0$. Consequently, each vector $C^0 = (\mathcal{C}_A^0, \mathcal{C}_B^0)$ is constant along (7) and defines a specific reaction simplex $\Omega(x_0)$ for every initial condition x_0 satisfying $C^0 = C^T x_0$. For this example, the reaction simplex $\Omega(x_0)$, defined by the intersection of (8) with the positive orthant is two dimensional. A particular reaction simplex for $\mathcal{C}_A^0 = 10$ and $\mathcal{C}_B^0 = 8$ is depicted in Fig. 1 in the $x_1 - x_3$ space.

2.3 Stability of the equilibrium manifold

The second law of thermodynamics establishes an evolution criterion based on a concave function (the entropy) which never decreases in isolated systems and achieves its maximum at equilibrium. Isolated dissipative systems evolve to equilibrium through irreversible processes that produce entropy, being the rate of entropy production a way to quantify dissipation. The second law formulated as an entropy maximum principle has their counterparts in minimum principles of the thermodynamic potentials. The expression of the corresponding potential that we will use as an entropy-like function is the following function of the species concentrations:

$$S = \sum_{i=1}^{n} x_i \cdot (\ln x_i - 1) = \sum_{i=1}^{n} (x_i \ln x_i - x_i) \tag{10}$$

This expression can be derived by starting from the normalized potential for isothermal systems at a constant volume proposed in (Gorban *et al.*, 2004) in combination with the Euler expression for the thermodynamic entropy (Callen, 1980).

In addition, we have that the right hand side term in (4) is Lipschitz continuous. This implies, as discussed in (Alonso *et al.*, 2004), that for any arbitrary reference x_1 there exists a nonnegative function $L_\lambda(x, x_1)$ associated to a constant $\lambda \geq 0$, such that the following relation holds:

$$[\mu(x) - \mu(x_1)]^T \mathcal{N} \cdot W(x) + L_\lambda(x, x_1) = \lambda [\mu(x) - \mu(x_1)]^T (x - x_1) \tag{11}$$

where $\mu = \nabla_x S = \ln x$. Systems which, in addition, satisfy that $L_0(x, x_1) \geq 0$, are *purely dissipative*. Closed reaction networks are a class of purely dissipative systems for a state x_1 being the equilibrium reference. This can be easily shown by noting that for $\lambda = 0$ and $x_1 = x^*$ in (11):

$$L_0(x, x^*) = -(\mu - \mu^*)^T \sum_{j=1}^{r} \nu_j W_j \tag{12}$$

Equation (12) can be written in terms of the direct and inverse reaction rates (2) as:

$$L_0(x, x^*) = \sum_{j=1}^{r} \ln \frac{W_j^+}{W_j^-} \cdot (W_j^+ - W_j^-) \tag{13}$$

Since each term at the right hand side of (13) is non-negative we conclude that $L_0(x, x^*) \geq 0$.

In order to derive the stability conditions for closed reaction networks we define a positive definite and convex function $B(x)$, constructed as the difference between $S(x)$ and its supporting hyperplane at the equilibrium reference x^*:

$$B(x, x^*) = \sum_{i=1}^{n} x_i \left(\ln \frac{x_i}{x_i^*} - 1 \right) + x_i^* \tag{14}$$

Taking the time-derivative $B(x, x^*)$ along (14) and using (11) with $\lambda = 0$ we obtain:

$$\dot{B} = (\mu - \mu^*)^T \sum_{j=1}^{r} \nu_j W_j = -L_0(x, x^*) \tag{15}$$

Since by (13) $L_0 \geq 0$ we have that $\dot{B} \leq 0$. Consequently, B is a legitimate Lyapunov function which ensures the structural asymptotic stability for the general class of reaction networks under study at the equilibrium reference. In addition, this Lyapunov function B coincides with the one used by (Feinberg, 1979) in developing the *Chemical Reaction Network Theory* (Gunawardena, 2003). The contours of B and $L_0(x, x^*)$, corresponding to the Example 1 in the reaction simplex $\Omega(x_0)$ are presented in Fig. 1, where it can be seen that B is convex and $L_0(x, x^*)$ negative definite although not convex when far from the equilibrium reference.

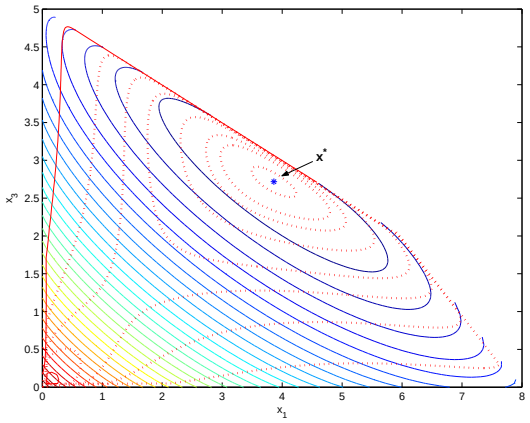

Fig. 1. Reaction simplex and contours of B (solid lines) and L_0 (dotted lines) for Example 1, where x^* is the equilibrium point.

2.4 Direct passivation of open reaction systems

The state-space representation of an open reaction system, i.e. a system which exchanges mass with its environment, is constructed by adding a set of input and output convection terms (Hangos and Cameron, 2001) to the closed reaction system (4). In order to handle standard operation conditions in chemostats, we further assume that the overall mass of the system is kept constant by having the same input and output overall mass flow Φ. In this way, the set of ordinary differential equations governing the evolution of states becomes:

$$\dot{x} = \mathcal{N} \cdot W(x) + \phi(x^0 - x) \qquad (16)$$

where $\phi = \Phi/V$, (with V being the volume of the chemostat), denotes the inverse of the residence time and x^0 is the inlet concentration vector. Regarding intra-cell reaction networks, degradation and generation of components appear to be accomodated in (16) substituting the chemostat by the appropriate control volume.

The material throughput flow introduces non-dissipative contributions in the system, by adding an entropy flux term in the entropy balance. In our formalism, this balance is obtained by computing the time derivative of B as defined in (14) along (16):

$$\dot{B} = (\mu - \mu^*)^T \sum_{j=1}^{r} \nu_j W_j + (\mu - \mu^*)^T \phi(x^0 - x) \quad (17)$$

The second term in the right hand side of (17) corresponds with entropy flux and may compensate or even override the natural entropy dissipation, thus undermining the inherent global asymptotic stability of the system. At this point, it should be noted the direct relationship between entropy flux and dynamical complexity. Therefore, in stabilizing open complex reaction systems it seems crucial to act on the non-dissipative contributions by appropriate control configurations.

A simple way of stabilizing steady states is summarized in the following proposition:

Proposition 1. *Any stationary solution x^* of (16) can be rendered exponentially stable by a control law of the form $x^0 = x^{0*} - \omega(x - x^*)$ with $\omega \geq (\lambda - \phi - \alpha)/\phi > 0$ and $\alpha > 0$*

Proof: First, let us construct a B function as in (14) with respect to the stationary solution x^* associated to the input concentration vector x^{0*}. Defining $\overline{x} = x - x^*$, $\overline{x}^0 = x^0 - x^{0*}$ and computing the time derivative of B along (16) we get:

$$\dot{B} = (\mu - \mu^*)^T \mathcal{N}(W(x) - W(x^*)) + \phi(\mu - \mu^*)^T(\overline{x}^0 - \overline{x}) \quad (18)$$

Since $B(x, x^*)$ is convex, we also have the following inequality:

$$B(x, x^*) \geq (\mu - \mu^*)^T \overline{x} \qquad (19)$$

Substituting (11) and the control law in (18):

$$\dot{B} = -L_\lambda + (\lambda - \phi - \phi\omega)(\mu - \mu^*)^T \overline{x} \qquad (20)$$

Since $L_\lambda > 0$ and B satisfies (19), equation (20) becomes $\dot{B} \leq \alpha B$ and the result follows. □

As a corollary, note that any open network can be made globally exponentially stable by defining a mass flow $\phi < \lambda$.

3. THE POTENTIAL STRUCTURE OF THE REACTION SPACE

3.1 The dynamics in the reaction space

Systems derived from a potential conform an interesting class of dynamic systems where powerful methods for control design, such as those based on passivity, directly apply. In this section, we demonstrate that a complex reaction network possesses an underlying potential structure on a state space that will be referred to as the *reaction space*, that is homeomorphic to the concentration space in the reaction simplex and is described by defining a new set of variables:

$$z_j = \ln \frac{p_j}{q_j} \qquad for \quad j = 1, ..., r \qquad (21)$$

with p_j and q_j being the direct and reverse rates associated to the reaction rate j (W_j^+ and W_j^-). In the new variables, the equation (2) becomes:

$$W_j = p_j - q_j = q_j(e^{z_j} - 1) \qquad (22)$$

The right hand side of Eq. (12) can then be transformed through appropriate manipulations into the form:

$$\ell(z, q) = -\sum_{j=1}^{r} z_j \; q_j(e^{z_j} - 1) = -z^T W \qquad (23)$$

Function ℓ can be easily connected with the so called dissipation function as it is the product of

thermodynamic fluxes (reaction rates) and thermodynamic forces (chemical affinities). In this way, it seems natural to explore the properties of chemical reaction network dynamics in the *reaction space* defined by z-variables. To that purpose, let us introduce the following notation:

$$S = \mathcal{N}^T \Gamma \mathcal{N} \tag{24}$$

$$\Gamma = diag\left[\frac{1}{x_1}, ..., \frac{1}{x_i}, ... \frac{1}{x_n}\right] \tag{25}$$

The particular structure of the reactor vector elements (22) suggests the definition of the potential:

$$H(z) = \sum_{j=1}^{r} (e^{z_j} - z_j) - 1 \tag{26}$$

and re-writing the vector of reaction rates as:

$$W = F(q) H_z \tag{27}$$

where $F(q) = diag[q_1, \ ... \ , q_j, \ ... \ , q_r]$ is a positive definite diagonal matrix and H_z represents the gradient of (26). Note that by construction, the potential H is convex and positive definite everywhere except at the equilibrium point $z^* = 0$, where $H(0) = 0$. Defining $J = SF(q)$ we obtain the following potential dynamic description:

$$\dot{z} = -JH_z \tag{28}$$

where H_z is the gradient of H. Provided that the matrix $J^T + J$ (and consequently J) is a positive definite matrix, Eqn.(28) matches the dynamics in the reaction space with a generalized Hamiltonian system (Van der Shaft, 2000). It is clear from (28) that H is decreasing in time if the state-dependent matrix $J^T + J$ is always positive definite. In this case, H is a Lyapunov-function for the reaction system proving global asymptotic stability in the reaction space. However, it can be shown that there are cases when $J^T + J$ is positive definite only in a neighborhood (denoted by U) of the selected stable equilibrium point of the reaction system.

3.2 Passivity and global stabilization in the reaction space

The dynamic evolution of the open reaction network (16) in the reaction space is described as:

$$\dot{z} = -JH_z - \mathcal{N}^T \Gamma \phi(x^0 - x) \tag{29}$$

The potential structure of (28) allows us to establish a straightforward connection with passivity:

Proposition 2. *If $J^T + J$ is globally positive definite, then the system (29) endowed with the function H (26) is passive with $y = H_z$ and $u = \mathcal{N}^T \Gamma \phi(x - x^0)$.*

Proof: We compute the time derivative of the potential (26) along (29) to obtain:

$$\dot{H} = -{H_z}^T J H_z - {H_z}^T \mathcal{N}^T \Gamma \phi(x^0 - x) \tag{30}$$

that with the selected inputs and outputs reads:

$$\dot{H} = -{H_z}^T J H_z + y^T u \tag{31}$$

Since the first term on the right hand side is negative definite, we obtain by integrating (31) in the time interval $(t, t+\tau)$ the following inequality:

$$H(t+\tau) - H(t) \leq \int_t^{t+\tau} y^T(s) u(s) ds \tag{32}$$

which coincides with the well-known passivity inequality (Van der Shaft, 2000). □

Remark 1. If $J^T + J$ is not globally positive definite, then open reaction networks can be globally stabilized in the reaction space with a control Lyapunov function H by nonlinear control laws of the form:

$$u = \mathcal{N}^T \Gamma (\mathcal{N} F + K \Gamma \mathcal{N}) y \tag{33}$$

where $K \in \mathbb{R}^{n \times n}$ is an appropriate matrix. The supply rate is then given by:

$$y^T u = H_z^T \underbrace{\mathcal{N}^T \Gamma \mathcal{N} F}_{J} H_z + H_z^T \mathcal{N}^T \Gamma K \Gamma \mathcal{N} H_z \tag{34}$$

and substituting (34) in (31) we get:

$$\dot{H} = y^T \mathcal{N}^T \Gamma K \Gamma \mathcal{N} y$$

which is clearly negative if K is negative definite (or zero if K is skew-symmetric).

Remark 2. It must be pointed out that the feedback (33) requires the measurement of the full state vector in the general case. The dimension of the artificial input u is equal to the dimension of the reaction space (i.e. r). However, the physically meaningful manipulable inputs for the system are the elements of either ϕ or x^0. If a value for u is computed from (33) then the values of the real physical inputs can be calculated from the relation (see Proposition 2):

$$u = \mathcal{N}^T \Gamma \phi (x - x^0) \tag{35}$$

which is linear separately in ϕ and x^0 (if one of them is arbitrarily fixed). It is clear from the above, that the required number of physical inputs for the stabilization is also r which is generally less than (or at most equal to) n. This result is in good agreement with (Sontag, 2001) although the control Lyapunov function is different from H.

Example 2. We use as an example the following Michaelis Menten mechanism of enzymatic catalysis with substrate inhibition:

$$E + S \underset{k_1^-}{\overset{k_1^+}{\rightleftarrows}} ES \qquad ES \underset{k_2^-}{\overset{k_2^+}{\rightleftarrows}} E + P \qquad ES + S \underset{k_3^-}{\overset{k_3^+}{\rightleftarrows}} ESS \tag{36}$$

This mechanism is shown to present multiplicities for the open case and a particular range of the rate constants. The dynamics of the open loop system can be described by the following set of differential equations of the form (4), where

$$N = \begin{bmatrix} -1 & -1 & 1 & 0 & 0 \\ 1 & 0 & -1 & 0 & 1 \\ 0 & -1 & -1 & 1 & 0 \end{bmatrix}^T , \quad (37)$$

$$w_1(x) = k_1^+ x_1 x_2 - k_1^- x_3 \quad (38)$$

$$w_2(x) = k_2^+ x_3 - k_2^- x_1 x_5 \quad (39)$$

$$w_3(x) = k_3^+ x_2 x_3 - k_3^- x_4 \quad (40)$$

and the state vector x contains the concentrations of the species E, S, ES, ESS and P, respectively. In this example, the values for all the kinetic constants $k_{\{1,2,3\}}^{\{+,-\}}$ were chosen as 1. The initial value of the state vector was $x(0) = [0.01 \quad 0.15 \quad 0.01 \quad 0.01 \quad 0.01]^T$. We assumed that the manipulable variables are the three inlet concentrations x_1^0, x_2^0 and x_3^0 (see eq. (16)). The value of the flux ϕ was 0.01, while the gain matrix K for the controller was $-0.1 \cdot I^{5\times 5}$. As it is shown in fig. 2, the proposed feedback (33) significantly improves the time-domain performance of the reaction-kinetic system.

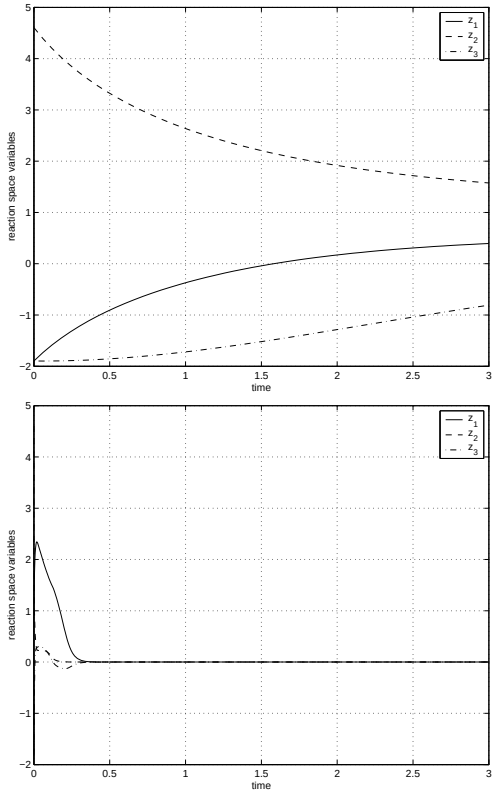

Fig. 2. Reaction space variables in the a) open-loop and b) closed-loop case

4. CONCLUSIONS

In this work, we combined concepts and tools from irreversible thermodynamics and systems and control theory to explore the underlying dynamic properties of a general class of kinetic networks. As a result, we firstly have shown how entropy or a related thermodynamic potential can be employed as a legitimate Lyapunov function candidate to derive stability conditions for kinetic networks in closed systems. A potential-like structure has been extracted from the network which conducts the evolution of the reaction rates. This enabled us to construct a local Hamiltonian description of the open reaction kinetic system in the reaction space. These results involving entropy and non-linear control design are applied to the efficient stabilization of arbitrary steady-states in open chemical and biochemical networks.

Acknowledgements The authors acknowledge financial support from the Spanish Government (MCyT Projects PPQ2001-3643 and DPI2004-07444-C04-03), Xunta de Galicia (PGIDIT02-PXIC40209PN) and grants no. T042710, F046223, of the Hungarian Research Fund. The second author is a grantee of the Bolyai János Research Scholarship of the Hungarian Academy of Sciences.

REFERENCES

Alonso, A. A. and B. E. Ystdie (2001). Stabilization of distributed systems using irreversible thermodynamics. *Automatica* **37(11)**, 1739–1755.

Alonso, A.A., C.V. Fernandez and J.R. Banga (2004). Dissipative systems: From physics to robust nonlinear control. *Int. J. of Robust and Nonlinear Control* **14**, 157–159.

Callen, H. B. (1980). *Thermodynamics and an introduction to thermostatistics*. John Wiley and Sons. New York.

Feinberg, M. (1979). *Lectures on chemical reaction networks*. Lectures given at the Mathematics Research Center, University of Wisconsin.

Gorban, A. N., I.V. Karlin and A.Y. Zinovyev (2004). Invariant grids for reaction kinetics. *Physica A* **33**, 106–154.

Gunawardena, J. (2003). *Chemical network theory for in-silico biologists*. Lecture given at the Bauer Center for Genomics Research, Harvard University.

Hangos, K.M. and I.T. Cameron (2001). *Process Modelling and Model Analysis*. Academic Press. London.

Sontag, E. (2001). Structure and stability of certain chemical networks and applications to the kinetic proofreading model of t-cell receptor signal transduction. *IEEE Trans. Autom. Control* **46**, 1028–1047.

Thomas, R. and M. Kaufman (2001). Multistationarity, the basis of cell differentiation and memory: Structural conditions of multistationarity and other nontrivial behaviour. *Chaos* **11**, 170–179.

Van der Shaft, A. (2000). *L_2-Gain and Passivity Techniques in Nonlinear Control*. Springer.

ADCHEM 2006

International Symposium on Advanced Control of Chemical Processes
Gramado, Brazil – April 2-5, 2006

A RISK MANAGEMENT CRITERION FOR AN UNSTABLE WASTEWATER TREATMENT PROCESS

Jonathan Hess [*,1] **Olivier Bernard** [*] **Malcolm Djuric**

[*] *French Research Institute of Computer Science and Automatic Control. COMORE Research Team. Sophia Antipolis 06902, France. e-mail : olivier.bernard@inria.fr, jonathan.hess@inria.fr*

Abstract: In this paper we consider an unstable biological process used for wastewater treatment. This anaerobic digestion ecosystem can have 2 locally stable steady states and one unstable steady state. We first study the model and characterise the attraction basin associated to the normal operating mode. In a second step we estimate the size of this attraction basin by using a simplified criterion that turns out to be a good approximation. Finally we apply the approach on a real anaerobic digestion plant, and we show that the proposed criterion allows to rapidly detect the conditions of a destabilisation.

Keywords: Haldane model, Anaerobic digestion, Nonlinear systems diagnosis

1. INTRODUCTION AND MOTIVATION

Control of biological systems is a very delicate problem since one has to deal with highly nonlinear systems described by poor quality models. In some cases this control issue can be really crucial when the system is unstable. This is especially the case for the anaerobic digestion process: a biological system in a bioreactor used to treat wastewater. This complex ecosystem involves more than 140 bacterial species (Delbès *et al.*, 2001). It progressively degrades the organic matter into CO_2 and methane CH_4. However this process is known to be very delicate to manage since it is unstable (Fripiat *et al.*, 1984): an accumulation of intermediate compounds can lead to the crash of the digester.

To solve this problem, many authors have proposed controllers (Perrier and Dochain, 1993; Steyer *et al.*, 1999; Mailleret *et al.*, 2004) that were able to warranty the local or even the global stability of the system using the dilution rate of the bioreactor as input. For various reasons (necessity of a storage tank, lack of online sensors, lack of robustness,...) these control laws are very seldom applied in practice. As a consequence, the controllers are often disconnected at the industrial scale and the plant manager manually operates the process trying both to avoid process destabilisation and wastewater storage.

The approach that we propose has the objective to provide the operator with a risk index associated to his management strategy. The idea is therefore to determine from the global analysis of the nonlinear system whether the process has been triggered to a dangerous working mode. This risk index can also be used in parallel controller.

[1] J.Hess is funded both by ADEME and by the Provence-Alpes-Cotes-d'Azur Region. This work has also been carried out with the support provided by the European commission, Information Society Technologies programme, Key action I Systems & Services for the Citizen, contract TELEMAC number IST-2000-28256.

The paper is composed as follows:in the second section a dynamical model of an anaerobic digestion process is recalled. The third part puts the emphasis on the analysis of the model dynamics. A simple criterion to assess the stability of the process is set in the fourth section, and finally this criterion is applied to a real experiment to determine its destabilisation risk.

2. MODEL PRESENTATION

We consider a simplified macroscopic model of the anaerobic process based on 2 main reactions (Bernard *et al.*, 2001), where the organic substrate (S_1) is degraded into volatile fatty acids (VFA denoted S_2) by acidogenic bacteria (X_1), and then the VFA are degraded into methane CH_4 and CO_2 by methanogenic bacteria (X_2):

- Acidogenesis:

$$k_1 S_1 \overset{\mu_1(S_1)X_1}{\longrightarrow} X_1 + k_2 S_2$$

- Methanogesis:

$$k_3 S_2 \overset{\mu_2(S_2)X_2}{\longrightarrow} X_2 + k_4 CH_4$$

Where $\mu_1(S_1)$ and $\mu_2(S_2)$ represent the bacterial growth rates associated to these 2 bioreactions.

The mass balance model in the CSTR (Continuous Stirred Tank Reactor) can then straightforwardly be derived:

$$\dot{X_1} = \mu_1(S_1)X_1 - \alpha D X_1 \tag{1}$$

$$\dot{S_1} = -k_1\mu_1(S_1)X_1 + D(S_{1in} - S_1) \tag{2}$$

$$\dot{X_2} = \mu_2(S_2)X_2 - \alpha D X_2 \tag{3}$$

$$\dot{S_2} = -k_3\mu_2(S_2)X_2 + k_2\mu_1(S_1)X_1 + D(S_{2in} - S_2) \tag{4}$$

D is the dilution rate, S_{1in} and S_{2in} are respectively the concentrations of influent organic substrate and of influent VFA. The 'k_is' are pseudo-stoichiometric coefficients associated to the bioreactions. Parameter $\alpha \in (0\ 1]$ represents the fraction of the biomass which is not attached in the digester. We denote by $\xi = (X_1,\ S_1,\ X_2,\ S_2)^T$ the state vector.

In the sequel, we will consider the rather generic mappings μ_1 and μ_2, satisfying the following properties:

Assumption 1. μ_1 **is an increasing function of** S_1**, with** $\mu_1(0) = 0$**.**

Assumption 2. μ_2 **is a function of** S_2 **which increases until a concentration** S_2^M **and then decreases, with** $\mu_2(S_2^M) = \mu_M$ **and** $\mu_2(0) = 0$**.**

In the mathematical analysis of this system, assumption is made that the environment of the bacteria remains constant and we will thus assume that D, S_{1in} and S_{2in} are positive constants. In the same way all the initial conditions are assumed to be positive.

3. MODEL ANALYSIS

3.1 Analysis of the acidogenic dynamics

The subsystem (1,2) is close to a classical Monod model but slightly modified by the term α. This makes the study of this system less straightforward than for Monod model (with $\alpha = 1$) (Smith and Waltman, 1995). However its behaviour is simple as stated in the following Property:

Property 1. System (1,2) with initial conditions in $\mathbb{R}^2_+$ *admits a single globally stable equilibrium. If* $\alpha D < \mu_1(S_{1in})$ *this equilibrium is in the interior domain.*

Proof: For sake of space limitation only the sketch of the proof is presented here.

The positivity of this system is trivial. To demonstrate the boundedness in a compact set of $\mathbb{R}^2_+$we consider the quantity $Z = S_1 + k_1 X_1$, and use the positivity of the variables.

The considered system (1,2) has 2 steady states: the trivial washout steady state $X_1^\dagger = 0,\ S_1^\dagger = S_{1in}$ which exists for any D, and another steady state in the positive domain if and only if $\alpha D < \mu_1(S_{1in})$ (ensuring $S_1^\star < S_{1in}$ and thus $X_1^\star > 0$) given by:

$$\begin{cases} S_1^\star = \mu_1^{-1}(\alpha D) \\ X_1^\star = \frac{1}{k_1\alpha}\left(S_{1in} - S_1^\star\right) \end{cases} \tag{5}$$

The study of the trace and of the determinant the Jacobian matrix of (1,2) at the two equilibria informs us that only the useful working point $(X_1^\star, S_1^\star)$ is an attractor, the washout steady state being a saddle point.

To conclude the proof and determine the global behaviour of (1,2) we change variables (X_1, S_1) to (X_1, Z). With this reformulation the system becomes :

$$\begin{cases} \dot{X_1} = \mu_1(Z - k_1 X_1)X_1 - \alpha D X_1 \\ \dot{Z} = D\left(S_{in} - Z\right) + (1-\alpha)\, k_1 X_1 \end{cases}$$

It follows directly that this system is cooperative. Furthermore the system is asymptotically bounded in a compact closure of $\mathbb{R}^2_+$. Hence from *Theorem* 2.2 in (Smith, 1995) for two-dimensional systems, the limit can only be a stable equilibrium

point. Since the washout equilibrium is unstable the system cannot converge towards it.

The useful working point of system (1,2) being globally asymptotically stable we have the following property:

Property 2. After a transient time T, system (1,2) satisfies the inequality $k_1\,\mu_1(S_1)X_1 \leq DS_{1in}$.

Remark: in practice this condition is often met at initial time or the transient time T is small.

3.2 Analysis of the methanogenic dynamics

Now we will consider the second system after a period greater than T (*cf. Property 2*). The total concentration of VFA available for the second step of the process is

$$S_{2in} + \frac{k_2}{D}\mu_1\left(S_1\right)X_1 \leq S_{2in} + \frac{k_2}{k_1}S_{1in} = \tilde{S}_{2in}.$$

In order to study the methanogenesis as a stand-alone process we consider $\tilde{S}_{2in}$ as a pessimistic upper bound of the total concentration of VFA in the reactor.

Thus the methanogenic system is reduced to a one-stage process independent of the acidogenic phase:

$$\begin{cases} \dot{X}_2 = \mu_2(S_2)X_2 - \alpha D X_2 \\ \dot{S}_2 = D(\tilde{S}_{2in} - S_2) - k_3\mu_2(S_2)X_2 \end{cases} \tag{6}$$

This system is close to a generic Haldane model but, as for the acidogenic subsystem, it is modified by the term α.

Property 3. System (6) with initial conditions in $\Omega = \mathbb{R}_+^* \times \mathbb{R}_+$ *admits a globally exponentially stable equilibrium in the interior domain for* $\alpha D < \mu_2\left(\tilde{S}_{2in}\right)$. *If* $\mu_2\left(\tilde{S}_{2in}\right) < \alpha D < \mu_M$ *it becomes locally exponentially stable and the washout equilibrium is also l.e.s. For* $\alpha D > \mu_M$ *the washout equilibrium becomes g.e.s. (see Tab. 1 for more details)*

Proof: For sake of brevity only the main steps are presented here.

We study the boundedness of the variables X_2 and S_2 in the same way as for the acidogenic phase, considering the quantity $Z_2 = S_2 + k_3X_2$. The trivial steady state corresponding to the bioreactor washout is given by $X_2^\dagger = 0,\ S_2^\dagger = \tilde{S}_{2in}$

Now we are going to explore the other steady states. They are solutions of the following system:

$$\begin{cases} \mu_2(S_2^\star) = \alpha D \\ X_2^\star = \frac{1}{\alpha k_3}(\tilde{S}_{2in} - S_2^\star) \end{cases} \tag{7}$$

Note that they must verify $S_2^\star \leq \tilde{S}_{2in}$ to have $0 \leq X_2^\star$.

First remark that, if $\tilde{S}_{2in} \leq S_2^M$ then μ_2 is an increasing function on the admissible domain $\left[0, \tilde{S}_{2in}\right]$. As a consequence the study of system (6) is identical to the study of equations (1,2). We will then focus now on the other case where $\tilde{S}_{2in} > S_2^M$.

As illustrated on Fig. 1, five cases are possible, depending on parameters values.

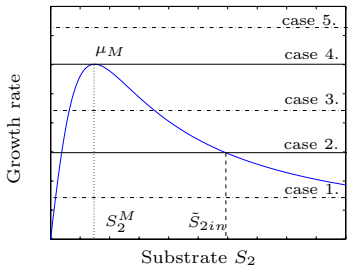

Fig. 1. Possible solutions for $\mu_2(S) = \alpha D$

cases 1. and 2. $\alpha D \in \left(0, \mu_2(\tilde{S}_{2in})\right]$: then the equation $\mu_2(S_2) = \alpha D$ has a single solution for $S_2 \in \left[0, \tilde{S}_{2in}\right)$:

$$(X_2^\star, S_2^\star) = \left(\frac{\tilde{S}_{2in} - \mu_2^{-1}(\alpha D)}{\alpha k_3}, \mu_2^{-1}(\alpha D)\right) \text{ (unique)}$$

case 3. $\alpha D \in \left(\mu_2(\tilde{S}_{2in}), \mu_M\right)$: here the equation $\mu_2(S_2) = \alpha D$ has two solutions for $S_2 \in \left[0, \tilde{S}_{2in}\right)$. Let us denote $S_2^{1\star}$ and $S_2^{2\star}$ such that $\mu_2(S_2^{1\star}) = \mu_2(S_2^{2\star}) = \alpha D$:

$$0 < S_2^{1\star} < S_2^M < S_2^{2\star} < \tilde{S}_{2in}$$

with $i = 1$ for the useful working point $\left(X_2^{1\star}, S_2^{1\star}\right)$ and $i = 2$ for the unstable equilibrium $\left(X_2^{2\star}, S_2^{2\star}\right)$.

then the two possible equilibria are:

$$\begin{cases} S_2^{1\star} < S_2^M \\ X_2^{1\star} = \frac{1}{\alpha k_3}(\tilde{S}_{2in} - S_2^{1\star}) \end{cases} \text{ and } \begin{cases} S_2^{2\star} > S_2^M \\ X_2^{2\star} = \frac{1}{\alpha k_3}(\tilde{S}_{2in} - S_2^{2\star}) \end{cases}$$

case 4. $\alpha D = \mu_M$: there is a unique solution to equation $\mu_2(S_2) = \alpha D$:

$$(X_2^\star, S_2^\star) = \left(\frac{\tilde{S}_{2in} - S_2^M}{\alpha k_3}, S_2^M\right)$$

case 5. $\alpha D > \mu_M$: here there is no solution to the equation $\mu_2(S_2) = \alpha D$. In this case there is no other equilibrium than the washout point.

3.3 Study of equilibria stability

The stability of system (6) is easy to assess by computing the trace and the determinant of the Jacobian matrix for all the considered cases:

- For the interior steady states $X_2^\star > 0$:

$$\text{trace}(\mathcal{J}) = -D - k_3 X_2^\star \frac{\partial \mu_2}{\partial S_2}(S_2^\star)$$
$$\det(\mathcal{J}) = k_3 \alpha D X_2^\star \frac{\partial \mu_2}{\partial S_2}(S_2^\star)$$

- For the washout steady states $X_2^\star = 0$:

$$\text{trace}(\mathcal{J}) = \mu_2(\tilde{S}_{2in}) - (1+\alpha)D$$
$$\det(\mathcal{J}) = -D(\mu_2(\tilde{S}_{2in}) - \alpha D)$$

It straightforwardly leads to the classification proposed in Table 1 [2].

Table 1. Possible equilibria together with parameter values

Case #	Conditions	**int.**	**wash.**
1)	$\alpha D < \mu_2(\tilde{S}_{2in})$	g.e.s.	un.
2)	$\alpha D = \mu_2(\tilde{S}_{2in})$	l.e.s.	un†.
3)	$\alpha D \in]\mu_2(\tilde{S}_{2in}), \mu_M[$	$S_2^{1\star}$ l.e.s. $S_2^{2\star}$ un.	l.e.s.
4)	$\alpha D = \mu_M$	un†.	l.e.s.
5)	$\alpha D > \mu_M$	/	g.e.s.

Remark: the 2 cases denoted by 'un†.' corresponding to non hyperbolic equilibria are:

- Case 2: $\left(0, \tilde{S}_{2in}\right)$ for $\alpha D = \mu_2(\tilde{S}_{2in})$. Let us remark that the region $\{S_2 \leq \tilde{S}_{2in},\ X_2 \geq 0\}$ is positively invariant. Moreover X_2 is increasing in the sub-domain $\{X_2 > 0,\ S_2^{1\star} \leq S_2 \leq \tilde{S}_{2in}\}$. The only way to reach the washout $X_2^\star = 0$ from the region $\{S_2 \leq \tilde{S}_{2in}\}$ is thus to start with a zero initial condition. This proves that $\left(0, \tilde{S}_{2in}\right)$ is unstable.
- Case 4: $(X_2^\star, S_2^\star)$ for $\alpha D = \mu_M$. It is clear that in this case $\dot{S}_2 \leq 0$, and therefore the point is unstable (there is however a region above $X_2 = X_2^\star$ converging toward this steady-state).

3.4 Concluding remarks on stability

This study highlighted a special case of interest, for $\tilde{S}_{2in} > S_2^M$ and $\alpha D \in \left(\mu_2(\tilde{S}_{2in}), \mu_M\right)$. Here there are 2 steady states in the interior domain, one of which together with the washout are stable. In this case, illustrated on Fig. 2a), the asymptotic state of the system is *a priori* not predictable, and depends on the initial state. The set of initial conditions leading to the interior steady state $\xi_2^{1\star} = (X_2^{1\star}, S_2^{1\star})$ corresponds to the **basin of attraction**.

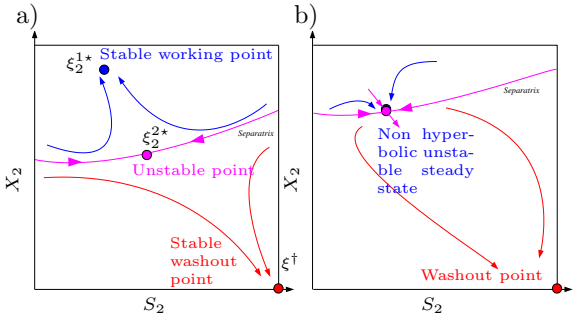

Fig. 2. Possible orbits in the phase plan: a) case 3, b) case 4

The next section will consist in characterising the size of the attraction basin in this specific case.

4. ATTRACTION BASIN OF THE NORMAL OPERATING MODE AND STABILITY CRITERIA

We still focus on the methanogenic step to establish a stability criterion associated to a process control action. In this part we assume the following specific forms for $\mu_1(S_1)$ and $\mu_2(S_2)$ satisfying *Assumptions* 1 and 2:

$$\mu_1(S_1) = \bar{\mu}_1 \frac{S_1}{S_1 + K_{S1}} \quad (Monod)$$
$$\mu_2(S_2) = \bar{\mu}_2 \frac{S_2}{S_2 + K_{S2} + \frac{S_2{}^2}{K_{I2}}} \quad (Haldane) \qquad (8)$$

In the sequel ξ denotes the state vector of the methanogenic phase (X_2, S_2).

4.1 Definition of the Attraction Basin and of the stability criterion

We have shown in the previous section that ξ remains bounded. We thus consider the acceptable domain as follows:

$$\mathcal{K} = \left(0, \frac{\tilde{S}_{2in}}{\alpha k_3}\right] \times \left[0, \tilde{S}_{2in}\right] \qquad (9)$$

For $\xi^{1\star} = \left(X_2^{1\star}, S_2^{1\star}\right)$, the interior critical point of system (6), we define its basin of attraction Λ as the set of initial conditions in $\mathcal{K}$ converging asymptotically towards it.

$$\Lambda\left(D, \xi_{in}\right) = \left\{\xi_0 \in \mathcal{K} \mid \lim_{t \to +\infty} \xi(\xi_0, t) = \xi^{1\star}\right\},$$

The main idea of this paper is to characterise the stability of the system by the area of the attraction basin Λ. The process stability can then be assessed by the relative surface of Λ in $\mathcal{K}$ (10).

However, from the previous study (see Tab. 1) it is worth noting that there still exists a non empty

[2] (ss: steady state, l.e.s.: locally exp. stable, g.e.s.: globally exp. stable, un.: unstable, int.: interior, wash: washout).

attraction basin $\Lambda^\star = \Lambda\left(\frac{\mu_M}{\alpha}, \xi_{in}\right)$ associated to case 4 ($\alpha D = \mu_M$) where the interior equilibrium is unstable (see Fig. 2b). This case should correspond to a zero stability index. For this reason we define the following criterion, which is simply the relative area of the attraction basin on the domain $\mathcal{K} \setminus \Lambda^\star$:

$$\mathcal{I}_\mathcal{S}\left(D, \tilde{S}_{in}\right) = \frac{\mathcal{S}\left(\Lambda\left(D, \xi_{in}\right) \setminus \Lambda^\star\right)}{\mathcal{S}\left(\mathcal{K} \setminus \Lambda^\star\right)} \qquad (10)$$

Where application $\mathcal{S}$ is the area of the considered domain.

4.2 Numerical computation of the stability index

The separatrix can be computed numerically by integrating System (6) in inverse time along the stable direction of the saddle point $\left(X_2^{2\star}, S_2^{2\star}\right)$ starting very close to it. The computation of the attraction basin area follows straightforwardly.

However the numerical computation of $\mathcal{I}_\mathcal{S}$ does not provide any analytical expression of the stability index that would base a management strategy. In the following section we seek a simpler criterion related to $\mathcal{I}_\mathcal{S}$.

4.3 Overloading tolerance of the process: a simple criterion

If the dilution rate is increased from zero, the interior equilibrium will remain g.e.s. until $D = \frac{\mu_2\left(\tilde{S}_{2in}\right)}{\alpha}$. Then the second (unstable) steady state appears in the interior domain together with a separatrix associated to the attraction basin $\Lambda\left(D, \xi_{in}\right)$ that does no longer occupy all the domain. The size of $\Lambda\left(D, \xi_{in}\right)$ will then decrease and finally vanish for $D \geq \frac{\mu_M}{\alpha}$. It is worth noting that the distance between the 2 interior steady states follows a rather comparable scheme: it will decrease from a maximum distance when $D = \frac{\mu_2\left(\tilde{S}_{2in}\right)}{\alpha}$ to zero for $D \geq \frac{\mu_M}{\alpha}$.

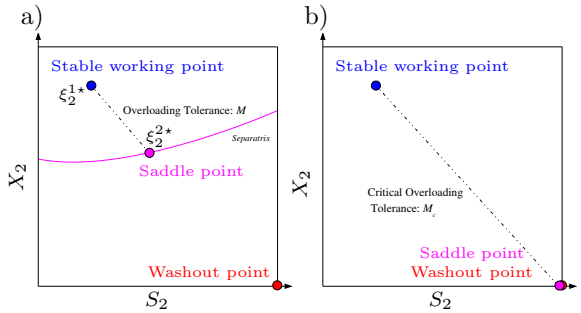

Fig. 3. Definition of a) the Overloading and b) the Critical Overloading Tolerance in the phase plan

From this consideration we define, for $\alpha D \in \left[\mu_2(\tilde{S}_{2in}), \mu_M\right]$, the notion of **Overloading Tolerance (OT)**, $\boldsymbol{M}$ which is simply the distance between the 2 interior steady states (see Fig 3a):

$$M\left(D\right) = \|\xi_2^{2\star} - \xi_2^{1\star}\| \qquad (11)$$

We also define the **Critical Overloading Tolerance (COT)** M_c, which is the maximum value of the overloading tolerance obtained for $D = \frac{\mu_2\left(\tilde{S}_{2in}\right)}{\alpha}$.

The approximate stability criterion that we will consider (named **Relative Overloading Tolerance**, **ROT**) is then defined as follows:

$$m(D, \xi_{in}) = \begin{cases} 0 & \text{for } \alpha D > \mu_M \\ \frac{M(D)}{M_c(\xi_{in})} & \text{for } \alpha D \in [\mu_2(\tilde{S}_{2in}), \mu_M] \\ 1 & \text{for } \alpha D < \mu_2(\tilde{S}_{2in}) \end{cases} .$$

The distance M between the 2 interior steady states can be computed straightforwardly from equations (7) and (8):

$$M(D) = 2\sqrt{1 + \frac{1}{\alpha^2 {k_3}^2}}\sqrt{\left(\frac{K_{I2}}{2}\left(\frac{\bar{\mu}_2}{\alpha\, D} - 1\right)\right)^2 - K_{I2}K_{S2}}$$

From this relation, we can see that the OT is a strictly decreasing function of the dilution rate and that it is independent from conditions (S_{1in}, S_{2in}). The COT is then:

$$M_c\left(\xi_{in}\right) = \sqrt{1 + \frac{1}{\alpha^2 {k_3}^2}}\left(\tilde{S}_{2in} - \frac{K_{I2}\, K_{S2}}{\tilde{S}_{2in}}\right)$$

4.4 Comparison between stability index and relative tolerance

Using model parameters presented in (Bernard *et al.*, 2001), we have computed the stability index $\mathcal{I}_\mathcal{S}$ and the ROT associated with many working conditions (D, S_{1in} and S_{2in}).

As it can be seen on Fig. 4 the ROT represents a good approximation of the stability index $\mathcal{I}_\mathcal{S}$ based on the real computation of the attraction basin size.

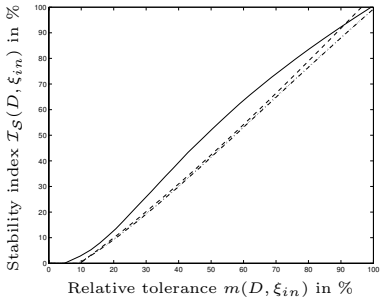

Fig. 4. Relation between $S_{BA^\star}$ and the ROT m for various couples $(S_{1in}, \tilde{S}_{2in})$: (3,30), (0,25), (15,20), (30,30)

The relative tolerance appears then as a simple but relevant criterion to assess the stability of an anaerobic digester.

From this criterion we define now the **"risk index"** which is simply $r = 1 - m$, and which will on-line indicate to the operator the destabilisation risk he is taking.

In the next section we use this operational criterion to assess the management strategy of a real anaerobic digester.

5. APPLICATION TO THE ON-LINE DETERMINATION OF THE DESTABILISATION RISK

In this section we apply the proposed index to a real experiment performed at the LBE-INRA in Narbonne, France. The process is an up-flow anaerobic fixed bed reactor with a useful volume of 0.948 m^3. The reactor is highly instrumented and many variables were measured during the experiments (Bernard *et al.*, 2001). The experiments were performed with raw industrial wine distillery vinasses.

The risk index has been computed with parameters of (Bernard *et al.*, 2001). Nevertheless, in order to favour a prudent strategy, and in the framework of a "worst case analysis" the parameter K_{I2} defining the inhibition level has been multiplied by a security constant δ (we have chosen $\delta = 0.7$).

The risk estimation is presented on Fig. 5 for an experiment conducted on the pilot scale fixed bed reactor at the LBE.

It is worth noting that the regimes associated with acid accumulation are all characterised by a very high risk. More surprising, some a priori less dangerous working mode are indeed also associated to a non zero risk. A very important point is that the risk index increases immediately while it takes time for the VFA to accumulate and even more time for the pH to decrease (not shown here).

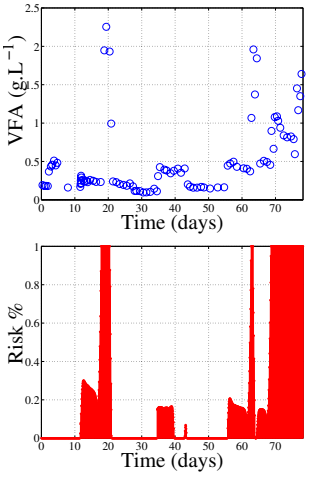

Fig. 5. Measured VFA and computed risk for an experiment performed at INRA LBE.

6. CONCLUSION

From the analysis of the nonlinear system describing the anaerobic process we have proposed a criterion that assesses the risk associated to an operating strategy. This index is highly correlated to the relative size of the normal working mode attraction basin.

The criterion turns out to be relevant to diagnose an operation strategy since it can predict very early a future accumulation of acids. It can thus be run as an indicator that helps an operator, or even diagnoses the strategy of an automatic controller which would not ensure global stability.

Next step would consist in estimating on-line the parameters in order to take into account the biological evolution of the system in the risk index computation.

REFERENCES

Bernard, Olivier, Z. Hadj-Sadok, D. Dochain, A. Genovesi and J.-P. Steyer (2001). Dynamical model development and parameter identification for an anaerobic wastewater treatment process. *Biotech.Bioeng.* **75**, 424–438.

Delbès, C., R. Moletta and J.-J. Godon (2001). Bacterial and archaeal 16s rdna and 16s rrna dynamics during an acetate crisis in an anaerobic digestor ecosystem. *FEMS Microbiology Ecology* **35**, 19–26.

Fripiat, J.L., H. Naveau T. Bol, R. Binot and E.J. Nyns (1984). A strategy for the evaluation of methane production from different types of substrate biomass. In: *Biomethane, Production and uses* (R. Buvet, M.F. Fox and D.J. Picker, Eds.). pp. 95–105. Roger Bowskill ltd. Exeter, UK.

Mailleret, L., O. Bernard and J.P. Steyer (2004). Nonlinear adaptive control for bioreactors with unknown kinetics. *Automatica* **40**(8), 1379–1385.

Perrier, M. and D. Dochain (1993). Evaluation of control strategies for anaerobic digestion processes. *Int. J. Adapt. Contr. Sign. Proc.* **7**, 309–321.

Smith, Hal L. (1995). *Monotone Dynamical Systems: an introduction to the theory of competitive and cooperative systems.* Vol. 41 of *Mathematical Surveys and Monographs.* American Mathematical Society. Providence, Rhode Island.

Smith, Hal L. and Paul Waltman (1995). *The theory of the chemostat: dynamics of microbial competition.* Cambridge University Press.

Steyer, J.-Ph., P. Buffiere, D. Rolland and R. Moletta (1999). Advanced control of anaerobic digestion processes through disturbances monitoring. *Wat. Res.* **9**, 2059–2068.

ADCHEM 2006

International Symposium on Advanced Control of Chemical Processes
Gramado, Brazil – April 2-5, 2006

Control of High-Solids Saccharification using a Model-Based Methodology for Fed-Batch Operation

David B. Hodge, M. Nazmul Karim, Daniel J. Schell, James D. McMillan

Abstract—This work utilizes both insights obtained from experimental work and kinetic modeling to develop an optimization strategy for high-solids cellulose saccharification, which presents a problem for the operation of stirred tank reactors (STRs) at insoluble solids levels greater than ~15%. In this work, a previously developed model for enyzmatic hydrolysis of cellulose was modified to consider the effects of feeding a stream of pretreated corn stover (PCS) solids and cellulase for a fed-batch process. By solving the set of model differential equations while controlling for a feed stream, it was possible to develop an open-loop control feeding profile that controls the insoluble solids at a constant or manageable level throughout the course of the reaction. This prevents any difficulties that would otherwise be encountered in mixing high-solids slurries. Experimental application of two fed-batch feeding policies in bench-scale STRs resulted in similar cellulose conversion profiles to batch shake flasks, with final cellulose conversions reaching ~80% for fed-batch STRs fed at the equivalent of 25% initial insoluble solids.

I. Introduction

A. Models for Enzymatic Hydrolysis

Process modeling is ultimately motivated by one of two objectives. The first objective is to demonstrate an understanding of a physical process by proposing a model structure that suitably fits the experimental data. Another goal is to develop an application-based model for process design, simulation, or control. An application-based model could be either mechanistic or empirical. Many kinetic models of both types have been developed for the enzymatic hydrolysis of cellulose or cellulosic biomass to glucose and cellobiose [1]-[7].

B. Reactor Considerations for High-Solids

Biomass conversion technologies for high solids operation are ultimately motivated by favorable economics. Positive economic advantages associated with a high-solids saccharification process over a conventional low solids process include: lower capital costs due to the reduced volume; lower operating costs due to less energy required for heating and cooling; lower downstream processing costs due to higher product concentrations; reduced disposal and treatment costs due to lower water usage [8].

High-solids slurries of pretreated lignocellulosic biomass are challenging to manage due to the increasingly high viscosities and non-Newtonian rheological properties [9]. This rheology results in increased problems with mixing (mass transfer) and temperature control (heat transfer). A variety of reactors have been used to deal with these problems during high-solids enzymatic hydrolysis. Examples include fermentation shake flasks [10]-[12], the paddle-impeller reactor of Tengborg et al. [13], a horizontally revolving reactor developed from a laboratory ball mill [8]. Currently, all of these laboratory-scale reactors require either a large reservoir of temperature controlled air (incubator) or water (water bath) to circumvent the problem of accurate temperature measurement and feedback control. Additionally, high power requirements for agitation may also be a limiting factor in many types of high-solids reactor.

Fed-batch processes combine the benefits of both batch and continuous processes to improve reaction conditions. A fed-batch methodology is commonly applied in fermentation for the purposes of minimizing effects of inhibitors, maximization of growth associated products, and induction of desired products with a feed stream [14]. Several approaches have been applied in the past for the fed-batch enzymatic saccharification of cellulose, although all of these were based on ad hoc approaches to feeding rather than a rigorous design methodology. These process-derived motivations fall into three general categories, the first of which is enzyme recycle. Pristavka et al. [15] used an approach similar to fed-batch for high-solids saccharification of steam-exploded willow. For this, a high-solids slurry was saccharified, the liquid phase removed, and more solids added to the solids fraction such that a large portion of enzyme adsorbed to the solids could be reused. Total sugar concentrations averaged 120 g/L including glucose and hemicellulosic sugars from pretreatment. Another enzyme recycle approach is to add only pretreated solids but no enzymes. As the cellulose is hydrolyzed, enzymes should be released to back into liquid such that

Manuscript submitted October 5, 2005. This work was supported in part by the U.S. Department of Energy Office of the Biomass Programs.

D.B. Hodge is with the National Bioenergy Center at the National Renewable Energy Laboratory (NREL), Golden, CO, 80401 (email: david_hodge@nrel.gov).

M.N. Karim is with the Department of Chemical Engineering, Texas Tech University, Lubbuck, TX USA (e-mail: naz.karim@coe.ttu.edu).

D.J. Schell is with the National Bioenergy Center at the National Renewable Energy Laboratory (NREL), Golden, CO, 80401 (email: dan_schell@nrel.gov).

J.D. McMillan is with the National Bioenergy Center at the National Renewable Energy Laboratory (NREL), Golden, CO, 80401 (email: jim_mcmillan@nrel.gov).

more cellulosic biomass could be added to reactor as these enzymes are released.

The second category uses fed-batch SSF [16]-[17] to mitigate the inhibitory effects of compounds in hydrolyzate liquors on the fermentative microorganism. Effective insoluble solids were also increased from 3% to 5% or to 8.4% for the two studies, respectively.

The third motivation for fed-batch saccharification is to utilize feeding to increase the equivalent insoluble solids level during saccharification to overcome rheological limitations in the reactor as in the work of Ballesteros *et al.* (2002) for SSF by *Kluyveromyces marxianus*. In this work, the insoluble solids were increased from 10% to 20%, which the reactor would have been incapable of handling initially, as well as reducing the effects of inhibitors in the hydrolyzate. Due to problems encountered in mixing wet oxidation pretreated corn stover at insoluble solids greater than 12%, Varga *et al.* [10] used a fed-batch hybrid hydrolysis and fermentation (HHF) approach to achieve 17% insoluble solids with high ethanol yields. Mohagheghi *et al*. [8] compared batch to fed-batch SSF and determined that the feeding of various combinations of pretreated biomass, media nutrients, and fresh inocula did not improve either ethanol yield or productivity in high-solids SSF for the ball-mill reactor system used.

C. Mathematical Approaches to Fed-Batch

In order to develop only a feeding policy without requiring online measurements of insoluble solids, an open-loop approach can be used. This doesn't rely on feed-back from process measurements, but rather is based only on the model predictions. Since open-loop control schemes rely solely on process models or speculation on the physical parameters governing the process, these control methods are only as good as the model.

Using a system of model differential equations, an exact analytical solution for a feeding profile can be obtained by developing and solving an optimal control problem. Optimal control fed-batch operation has been applied to cell cultures in bioreactors for a variety of objectives such as to maximize the production of cell mass, penicillin, amino acids, enzymes, and bioengineered products such as penicillin, ethanol, and recombinant proteins [14], [18], [19]. There are two general classes of methods to determine a numerical solution to this problem [20]. The first of these applies Pontryagin's maximum principle for determining the necessary conditions for the optimizer, which takes the form of a multi-point boundary problem for state and adjoint equations. The points at which the solution enters the boundary of the set of feasible conditions must be known *a priori* resulting in either singular or nonsingular control schemes. The second class of methods involves the discretization of the optimal control problem into a nonlinear programming (NLP) problem [20], which is solvable by optimization methods. For this method, as the number of time steps is increased, the calculated profile approaches the continuous optimal profile [18].

A general form for the continuous-time nonlinear system that is approximated by the model system in the optimal control problem can be described by the following system of equations as:

$$\dot{x} \equiv \frac{dx}{dt} = f(x(t),u(t)) \tag{1}$$

where $x(t)$ is the vector of state variables and $u(t)$ contains the controlled variables. A continuous form for the objective function for this algorithm seeks to minimize the difference between the desired process trajectory and the predicted process trajectory giving the minimization algorithm as:

$$\min_{u(t)} \Phi(x) = \int_0^{t_f} [r(t) - x_i(t)]^2 \, dt \tag{2}$$

subject to:

$$\begin{cases} \dot{x} = f(x(t),u(t),t) \\ t \in [0,t_f], x(0) = x_0 \end{cases}$$

where $r(t)$ is the desired output trajectory of the controlled variable and $x_i(t)$ is the controlled variable. The optimal path for $u(t)$ can be determined by reformulating the problem in terms of a Hamiltonian equation and developing a set of adjoint equations in order to solve the optimization problem under the conditions of the Pontryagin maximum principle [21]. Another approach is to discetize this continuous form of the objective function by subdividing the time region into K equal intervals as:

$$\mathbf{\Phi} = [\phi_1,\ldots,\phi_{k-1},\phi_k,\ldots,\phi_K] \tag{3}$$

and the discretized form of the minimization algorithm generated becomes a series of optimization tasks as:

$$\min_{u(k)} \phi_k = [r(k) - x_i(t_k)]^2 \tag{4}$$

subject to:

$$\begin{cases} \dot{x} = f(x(t),u(k),t) \\ t \in [t_{k-1},t_k], x(t_{k-1}) = x_{k-1} \end{cases}$$

Using this approach, only K values for the control variable $u(k)$ are required, and these are fixed over each time interval, resulting in a straightforward optimization problem.

II. MATERIALS AND METHODS

A. Shake Flask CSS

Corn stover was pretreated with dilute sulfuric acid in NREL's Sunds vertical pulp digester as the batch designated PS030312CS. The solids are composed of 53.2% cellulose by dry mass, and are washed with >10 times the mass of DI water as solids and centrifuged at 15800 x g. Washed solids are used to minimize any inhibition effects from background sugars entrained in the solids. The final glucose concentration in the wash water is verified to be less than 0.1 g/L.

The cellulase / β-glucosidase enzyme mixture used for this study was Spezyme CP (Genencor International, Lot # 301-00348-257). Total protein was assayed at 106.6 mg/mL (Bio-Rad assay) and the activity was determined to be 0.27 FPU/mg of protein using the NREL protocol LAP-006. For the modeling work, cellulase : β-glucosidase is assumed to

be 0.975:0.025. 1 M citrate buffer is prepared by adjusting the pH to 4.8 with NaOH, and is used as 5% of the total mass to yield an effective molality of 0.05 mol/kg. Enzyme, DI water, and citrate buffer are filter sterilized before use. PCS is added to the shake flasks and weighed before autoclaving. After autoclaving the shake flasks are weighed again so that any water lost could be made up. Water loss to evaporation in addition to reactor mass changes associated with feeding and sampling are tracked by weighing each flask before and after sampling and feeding.

B. Bench-Scale STR Fed-Batch Saccharification

Bench-scale fed-batch saccharification is performed using the same PCS substrates and enzymes as the shake flask reactors. Washed PCS is air-dried at ambient conditions to ~45% insoluble solids and the insoluble solids content is determined in triplicate using the 105ºC oven. New Brunswick Bioflo 3000 (7 L vessel size) reactors are autoclaved empty and allowed to cool in a sterile biological hood. The appropriate amounts of solids are measured and autoclaved and the amount of water lost is determined. Solids and other sterile components are next added to the reactors and allowed to mix and reach steady-state temperature before enzyme is added. Feeding policies are determined based on the solution to the optimal control problem as outlined in the **RESULTS AND DISCUSSION.** Feeding is performed by adding both autoclaved solids and filter-sterilized enzyme at discrete times. The solids and enzyme feeding policy is determined from the model kinetic equations in MATLAB to control the reactors using two feeding policies (F1 and F2). For F1, the actual insoluble solids level is increased from 12% to 15% as the reaction proceeds proportionally to the sugar produced. For F2 the insoluble solids are maintained at 15% insoluble solids. For both cases the feeding is continued until the reactors reach the equivalent of 25% initial insoluble solids. HPLC measurements for the reactor are taken both prior to and after feeding. Temperature is maintained at 45ºC by water circulating to a heating jacket from a temperature controlled water bath (maximum T = 52ºC). Enzyme loading is 40 mg protein / g cellulose (10.7 FPU / g cellulose), and enzyme is fed proportionally to the amount of PCS solids added. This can be considered as equivalent to the same amount of enzyme required for a given amount of PCS as would be used in an equivalent batch reaction. New Brunswick reactors are insulated and equipped with two marine impellers (d/D = 0.68) maintained at 400 rpm. Cellulose conversion for fed-batch reactors is determined based on the percentage of the final cumulative cellulose converted to glucose and cellobiose rather than only the initial or currently fed cellulose.

C. Sampling and Data Analysis

For the batch mode reactors, samples are taken approximately every 24 hours. Samples are removed with 5 mL pipettes (Falcon, Inc.) that had the tips broken off in order to accommodate the high level of insoluble solids. These are transferred to 2.5 mL microcentrifuge tubes and the pH is measured. The samples are next centrifuged at 10000 rpm for 5 minutes. The supernatant is decanted and diluted 1:5 and syringe filtered into HPLC vials for subsequent HPLC analysis. HPLC analysis is performed on all saccharification samples to determine the glucose, xylose, and cellobiose concentrations. An Agilent 1100 series HPLC equipped with a differential refractive index detector is used. This is equipped with a Bio-Rad HPX-87H organic acid column operating at 55^{o}C with a 0.01 N H_2SO_4 mobile phase at a flow rate of 0.6 mL/min. Component concentrations obtained from HPLC measurement are converted to g/kg concentrations based on the estimated insoluble solids level in the reactor. For fed-batch and CSS, cellulose conversions are based on cellulose converted to glucose and cellobiose, while for SSF conversions are based on cellulose converted to glucose, cellobiose, and ethanol.

III. RESULTS AND DISCUSSION

A. Development of Optimal Control Problem

The mechanistic model of Kadam *et al.* (2004) was used in this study. This model is based on the enzymatic hydrolysis of dilute acid pretreated corn stover (PCS) and considers the adsorption of β-glucosidase and that of CBH/EG enzymes separately while including an inhibition term for xylose. The kinetic model was implemented in MATLAB, and was modified to consider changes in volume for fed-batch operation, as well as introducing several new state variables. New state variables that need to be added include insoluble solids, enzyme concentration, and total reactor working mass. In addition to these new variables, all of the other differential equations needed modification to account for the rate changes associated with feeding and the change in reactor working mass for fed-batch operation. A new variable that needs to be introduced for systems where reactor working mass and/or concentrations is changing due to a feed stream is the dilution rate (D). This term can be defined as the feed flow rate / reactor volume, and can be considered the inverse of the reactor residence time.

All of the expressions for rate terms used in this model and the parameters within the rate terms can be in found in Kadam *et al.* [1]. It is important to note that enzyme inactivation is not considered in this model, and should be more significant for fed-batch operation when there is a large disparity between the ages of the enzymes and fractional utilization of substrates in the reactor.

B. Fed-Batch Saccharification Model Simulation

One barrier to developing a high-solids saccharification process in stirred tank reactors (STRs) is rheological limitations manifested as problems in mass and heat transfer. In our previous unpublished work, we demonstrated that the saccharification reaction is scalable from the shake flask to the bench scale STRs at insoluble solids levels of 15% or less using PCS solids. Above this level, STRs encounter problems with mixing and temperature control, which is primarily correlated to the amount of free water in the slurry. Based on this finding, the fed-batch approach control objective is to optimize reactor conditions (insoluble solids levels) to facilitate sufficient

mixing and temperature control. A large number of variables exist that can be altered to achieve this objective., although during the process of feeding, the feed rate is the only variable that is free to be changed.

Using the kinetic model, a feeding policy can be developed based on controlling the insoluble solids below a defined critical value during the saccharification reaction. This is possible by feeding a stream of PCS solids and cellulase at a rate that approximately matches the rate at which cellulose in the reactor is depolymerized and solubilized. Using the model equations, the rate of change for insoluble solids can be determined based on a set of initial operating conditions and a feed rate.

To determine a solution for the feeding policy, the set of equations must be integrated over time with the value for feed rate free in order to satisfy the control objectives of insoluble solids. For this, the insoluble solids rate equation can be either set to 0 as:

$$\frac{dS_I}{dt} = D \cdot \left(S_{IF} - S_I\right) - r_1 - r_2 = 0 \qquad (5)$$

or set the insoluble solids level (S_I) to a specified trajectory $(S_{I,SP}(t))$ as a function of the sugar level:

$$S_{I,SP}(t) = f(G, CB, S_I) \qquad (6)$$

since sugar level can be correlated to the substrate conversion and consequently to slurry rheology. To achieve the control objectives of both (5) and (6), the objective function of the optimization problem of (4) becomes:

$$\min_{F(k)} \phi_k = \left[S_I(k \mid k-1) - S_{I,SP}(k)\right]^2 \qquad (7)$$

while the constraints become the system of model equations.

Using this optimal control algorithm, fed-batch feeding policies can be developed, and a related set of feeding curves over various process objectives and initial conditions can be generated to determine the theoretical physical limitations and potential for using this type of fed-batch approach. Ultimately, physical limitations exist that limit the equivalent insoluble solids level to which a reactor under given initial conditions can be fed. The two important variables for this are reactor volume (V, or in dimensionless form as V/V_0) and insoluble solids level in the feed (x_{sf}). As the reactor is fed, the level of equivalent initial insoluble solids increases. The equivalent initial insoluble solids is defined as the level of initial insoluble solids that would be present if all of the solids were added initially and the reactor was operated in batch mode.

Simulations were performed using an enzyme loading of 40 mg protein / g cellulose (10.7 FPU / g cellulose for Spezyme CP). These simulation results in Fig. 1 show that higher solids levels in the feed result in both smaller reactor volumes and shorter residence times to achieve the same feeding objectives. The reason for this is that feeding a lower solids stream adds more water and is effectively diluting the product in the reactor.

Another option for a feeding policy is to use a non-constant insoluble solids level for the control trajectory. This could be based on our previous findings that cellulose removal affects the mixing behavior in STRs by allowing higher levels of glucan-depleted solids to be mixed effectively relative to the same level of glucan-rich solids. For this scheme, insoluble solids are initially maintained at 12% and are allowed to increase to about 15% during feeding as the equivalent cumulative solids approach 25%. The rate of increase in the insoluble solids set point ($S_{I,SP}$) is proportional to the amount of glucose produced. Estimating the final sugar concentration when the feeding was complete resulted in the development of the following relation:

$$S_{I,SP} = S_{I0} + (G + CB) / 4800 \qquad (8)$$

This approach (F1) was one of the two feeding policies selected for experimental validation of the modeling results. The other (F2) was based on controlling the insoluble solids at 15%, which was shown in simulation to have relatively rapid performance for 45% insoluble solids in the feed. Fig. 2 shows the two feeding policies (F1 and F2) chosen for experimental testing in the bench-scale STRs (New Brunswick Bioflo 3000). As seen in Fig. 2, by maintaining the insoluble solids level at 15% as in F2, solids can be fed up to 25% equivalent within a reasonable timeframe.

C. Experimental Validation of Theoretical Results

The two feeding policies chosen in Fig. 2 were performed experimentally in the bench-scale STRs. Batch saccharification shake flasks are also performed as controls in triplicate at 25% initial insoluble solids under similar conditions to determine maximum saccharification potential. The shake flask data is meant to be applied as a "best case" condition for these reaction conditions since these can be assumed to have demonstrated uniform temperature throughout the saccharification due to the reaction being performed in an air-temperature controlled shaking incubator. However, concentration gradients and rate limitations due to problems with diffusion of sugars and enzymes cannot be ruled out in shake flasks.

Fig. 3 shows that the glucose and cellobiose time profiles for both F1 and F2 meet the profiles for the batch shake flask reactors at approximately the end of the feeding, indicating that this fed-batch feeding policy will not require significantly higher residence times than a batch reaction. The "sawtooth" pattern for the fed-batch reactors is due to the change in volume and subsequent dilution of reactor components after addition of the feed. The reactor using feeding policy F1 is slower due to the slower feeding rate, while F2 shows more rapid rates as was predicted in simulation. From this work it was concluded that the fed-batch approach could allow STRs to saccharify the equivalent of 25% insoluble solids without significantly different residence times than shake flask reactors operating in batch mode at 25% solids. Interestingly, the much faster rate in batch predicted by the kinetic model was found not be consistent with experimental data, which show approximately equivalent rates for both batch and fed-batch reactors.

The implications of this work are that fed-batch saccharification enables high solids levels to be hydrolyzed at high conversions without the drawbacks associated with mixing, temperature, and pH control that would limit level

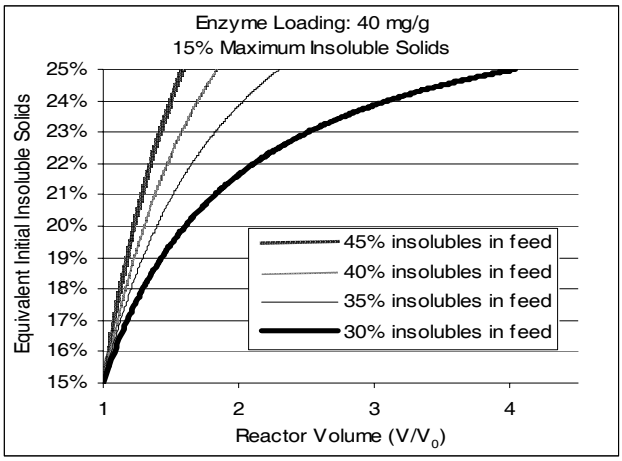

Figure 1: Effect of insoluble solids in the feed on equivalent initial insoluble solids; Reactors are fed to maintain insoluble solids at 15%.

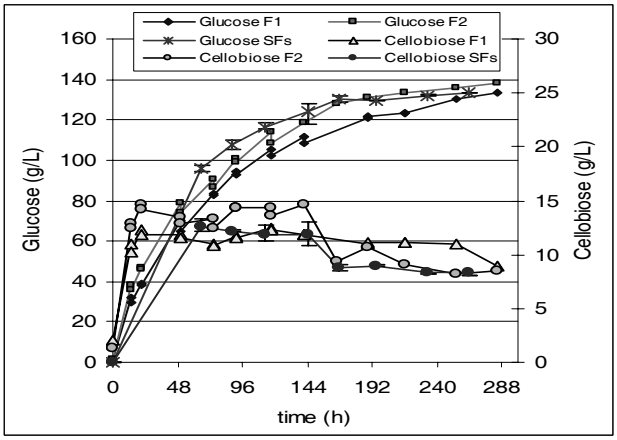

Figure 3: Glucose and cellobiose for the bench-scale STRs using the fed-batch feeding policies F1 and F2 and compared to batch CSS in shake flasks.

of solids used in stirred tank reactors. Final glucose concentrations >130 g/L and estimated cellulose conversions of 80% are achieved in both reactors, which is very promising economically. These high sugar levels are significant in that previous high-solids enzymatic saccharification work [8], [10] assumes that sugar inhibition will be a severely limiting factor, necessitating an SSF approach. Not only does this work show that current enzyme preparations are capable of robust activity at these high glucose levels, but that fed-batch can be used to perform these reactions at reasonable insoluble solids levels in STRs.

IV. CONCLUSIONS

The results of this work were significant in that it was demonstrated that through fed-batch, a reactor capable of handling approximately 15% insoluble solids, was able to achieve high cellulose conversions at 25% equivalent initial insoluble solids. It was also demonstrated that a kinetic model could be applied in an offline optimal control scheme

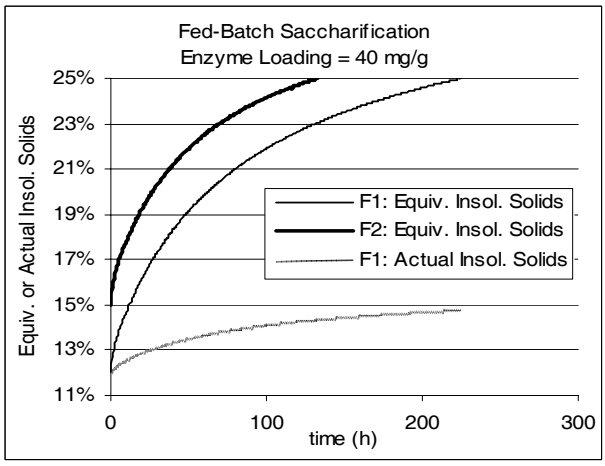

Figure 2: Equivalent total solids based on calculated feeding profiles for fed-batch operation at an enzyme loading of 40 mg/g and 45% insoluble solids in the feed stream.

to determine a fed-batch feeding policy capable of facilitating mixing and temperature control within the reactor, while achieving these high equivalent insoluble solids levels. When compared to batch saccharification results obtained in shake flask reactors, the overall rates in fed-batch reactors were slower due to the shorter cumulative residence times, although the final conversion results were similar. This is significant since slurry handling by process equipment (pumping, mixing, temperature, and pH control) is greatly simplified by operating at a lower solids level while gaining the economic advantages of a high-solids process.

V. REFERENCES

[1] Kadam KL, Rydholm EC, McMillan JD. (2004) Development and validation of a kinetic model for enzymatic saccharification of lignocellulosic biomass. *Biotechnol Prog.* 20(3):698-705.

[2] Chang VS and Holtzapple MT (2000). Fundamental Factors Affecting Biomass Enzymatic Reactivity. *Appl Biochem Biotechnol.* 84-86:5-37.

[3] Schell DJ, Ruth M, Tucker M (1999). Modeling the Enzymatic Hydrolysis of Dilute-Acid Pretreated Douglas Fir. *Appl Biochem Biotechnol.* 77-79:67-81

[4] Philippidis GP and Hatzis C (1997). Biochemical Engineering Analysis of Critical Process Factors in the Biomass-to-Ethanol Technology. *Biotech Prog.* 13(3):222 – 231.

[5] Gusakov AV, Arkady PS (1992). A Theoretical Analysis of Cellulase Product Inhibition: Effect of Cellulase Binding Constant, Enzyme/Substrate Ratio, and β-Glucosidase Activity on the Inhibition Pattern. *Biotech Bioeng*. 40(6):665-671.

[6] Ooshima H, Kurakak M, Kato J, Harano Y (1991). Enzyme Activity of Cellulase Adsorbed on Cellulose and its Change During Hydrolysis. *Appl Biochem Biotechnol.* 31(3):253-266.

[7] Converse AO, Ooshima H, Burns DS (1990). Kinetics of Enzymatic Hydrolysis of Lignocellulosic Materials Based on Surface Area of Cellulose Accessible to Enzyme and Enzyme Adsorption on Lignin and Cellulose. *Appl Biochem Biotechnol.* 24-25:67-73.

[8] Mohagheghi A, Tucker M, Grohmann K, Wyman C (1992). High Solids Simultaneous Saccharification and Fermentation of Pretreated Wheat Straw to Ethanol. *Appl Biochem Biotechnol.* 33:67-81.

[9] Pimenova NV and Hanley TR (2003). Measurement of Rheological Properties of Corn Stover Suspensions. *Appl Biochem Biotechnol*. 105-108:383-392.

[10] Varga E, Klinke HB, Réczey K, Thomsen AB. (2004). High solid simultaneous saccharification and fermentation of wet oxidized corn stover to ethanol. *Biotechnol Bioeng*. 88(5):567-574.

[11] Ballesteros I, Oliva JM, Negro MJ, Manzanares P, Ballesteros M (2002). Ethanol Production from Olive Oil Extraction Residue Pretreated with Hot Water. *Appl Biochem Biotechnol.* 98-100:717-731.

[12] Spindler DD, Wyman CE, Mohagheghi A, Grohmann K (1988). Thermotolerant Yeast for Simultaneous Saccharification and Fermentation of cellulose to Ethanol. *Appl Biochem Biotechnol.* 17:279-293.

[13] Tengborg C, Galbe M, Zacchi G (2001). Influence of Enzyme Loading and Physical Parameters on the Enzymatic Hydrolysis of Steam-Pretreated Softwood. *Biotechnol Prog*. 17:110-117.

[14] Hong J (1986). Optimal Substrate Feeding Policy for a Fed Batch Fermentation with Substrate and Product Inhibition Kinetics. *Biotech Bioeng* 28:1421-1431.

[15] Pristavka AA, Salovarova VP, Zacchi Z, Berezin IV, Rabinovich ML. (2000) Enzyme regeneration during hydrolysis of steam-pretreated willow and requirement for cellulase complex composition (Article in Russian) *Prikl Biokhim Mikrobiol.* 36(3):278-86.

[16] Söderström J, Galbe M, Zacchi G (2004). Effect of washing on yield in one- and two-step steam pretreatment of softwood for production of ethanol. *Biotechnol Prog.* 20(3):744-9.

[17] Wingren A, Söderström J, Galbe M, Zacchi G (2004). Process Considerations and Economic Evaluation of Two-Step Steam Pretreatment for Production of Fuel Ethanol from Softwood. *Biotechnol. Prog.* 20(5):1421-1429.

[18] Lee JH, Lim HC, Yoo YJ, Park YH (1999). Optimization of feed rate profile for the monoclonal antibody production. *Bioproc Eng* 20:137-146.

[19] Modak J, Lim H, Tayeb Y. (1986) General Characteristics of Optimal Feed Rate Profiles for Various Fed-Batch Fermentation Processes. *Biotech Bioeng* 18:1396-1407.

[20] Griesse R and Walther A (2004) Evaluating Gradients in Optimal Control: Continuous Adjoints versus Automatic Differentiation. *J Optim Theo Control*. 122(1):63-86.

[21] Gamkrelidze, RV (1978). *Principles of Optimal Control Theory.* Plenum Press, New York.

ADCHEM 2006

International Symposium on Advanced Control of Chemical Processes
Gramado, Brazil – April 2-5, 2006

ITSE OBSERVERS FOR BATCH PROCESSES. A WASTEWATER TREATMENT CASE STUDY

Gonzalo Acuña[1] and Denis Dochain[2]

[1]*Departamento de Ingeniería Informática, Universidad de Santiago de Chile, USACH, Av. Ecuador 3659 Santiago, CHILE, gacuna@usach.cl*
[2] *Cesame, Université Catholique de Louvain, Bâtiment Euler, 4-6 Av. Georges Lemaitre, 1348 Louvain-la-Neuve, Belgium, dochain@csam.ucl.ac.be*

Abstract: This paper deals with the design of observers for batch processes and the tuning of the observer gains with the objective to guarantee fast convergence of the state estimates. The approach followed in the present proposes to use an ITSE (Integral of the Time-weighted Square Error) criterion. The approach is illustrated on a batch process used in wastewater treatment, sequencing batch reactor (SBR).

Keywords: State observer, batch process, ITSE

1. INTRODUCTION

A key question in process control is how to monitor reactant and product concentrations in a reliable and cost effective manner. However, it appears that, in many practical applications, only some of the concentrations of the components involved and critical for quality control are available for on-line measurement. For instance, dissolved oxygen concentration in bioreactors, temperature in non-isothermal reactors and gaseous flow rates are available for on-line measurement while the values of the concentrations of products, reactants and/or biomass are often available via off-line analysis. An interesting alternative which circumvents and exploits the use of a model in conjunction with a limited set of measurements is the use of state observers. The design and application of state observers in (bio)processes has been an active area over the past decades (Doyle, 1997; Dochain, 2003a).

The design and application of state observers and parameter estimators to batch processes poses specific challenging questions, typically related to the time limitation of the batch operation. The question has been largely discussed in (Agrawal and Bonvin, 1989). It is obviously closely related to the control of the process, which is basically a finite-time optimal control problem, as it is nicely explained in (Bonvin *et al*., 2001).

One specific challenge of state observation and parameter estimation in batch processes is to design algorithms that are able to provide reliable estimates very quickly after the beginning of the batch. The problem is that so far the performance of parameter and state estimators are basically analyzed on the basis of the asymptotic behaviour of the related algorithms.

Bonvin and his coworkers (Agrawal and Bonvin, 1989; Agrawal and Bonvin, 1991; DeVallière and Bonvin, 1990) have identified several factors for the limitation of the extended Kalman filter when it is used to estimate both state variables and process parameters. These factors that are closely related to the inherent linearization of the estimator, are the following ones :

1) the bad knowledge about the key reaction parameters (these must be usually estimated, often with poor initial guesses);
2) the large variations of the operating conditions (particularly in batch);
3) the inaccuracy of the initial estimates of the state variables;
4) the imprecise measurement of the amounts of added agents;

5) the sensitivity of the reaction systems to trace certain species (e.g. impurities in polymerisation reactions)

These works suggest that, beyond the proposed improvements, there is a room to develop new tools for the design and analysis of state observers that are better appropriate to the specific features of batch processes. So far the scientific literature seems to very silent to what is often mentioned as a key question in process control today.

An appealing approach, developed in particular in (Bonné and Jorgensen, 2001) and (Bonvin *et al*., 2001), is the batch to batch improvement of the estimation and control algorithms. In (Bonné and Jorgensen, 2001), the emphasis is put on a model-based iterative learning control. In this approach, Model Predictive Control (MPC) is applied for trajectory tracking on the basis of a dynamical model of the batch process obtained by identification of Finite Impulse response (FIR) models or of AutoRegressive models with eXogenous inputs (ARX). Regularization is used in order to reduce the large dimensionality of the identification. In order to limit the negative effect of regularization (biased estimates), regularization weights are considered. A survey on optimal control in a large sense (the authors prefer the words "dynamic optimization") in batch processes is presented in (Bonvin *et al*., 2001). The batch-to-batch improvement is presented in the context of measurement-based optimization (MBO). MBO can include in particular parameter and state estimation as well as model refinement. Typically, when state and parameter is considered, one of the techniques described before is used. Improvement of the performance of the estimation of state variables and parameter can be obtained by considering for instance the recommendations given by (Agrawal and Bonvin, 1989) and (DeVallière and Bonvin, 1990) and summarized here above.

Beside the batch-to-batch improvement idea, new avenues should be traced in the design of state and parameter estimators. One of the main problem of the design of the presently available techniques is that it is based on *asymptotic* properties of the algorithms. In other words, the key issue usually addressed in the design of state observers and parameter estimators is to guarantee that for a time sufficiently large (tending to infinity!), the estimates will converge to the true values or within a bounded area close to these. But this approach is obviously inappropriate in the context of batch and semi-batch processes where one cannot wait very long before obtaining reliable estimates. The need to have rapidly reliable estimates is a crucial issue in batch and semi-batch operation. One possible suggestion would be to use, in the selection of the design parameters, criteria like the ITSE (Integral of the Time-weighted Square Error) criterion or other criteria that penalize remaining errors after a defined period of time. Such an approach has been followed in the present work. We have considered as a case study the model of sequencing batch reactors (SBR's) used in wastewater treatment, that are in particular under study in the framework the EOLI EC project.

The paper is organized as follows. The next section will introduce the model of the SBR under study. Then the observer equations and the ITSE observer parameter calibration procedure are introduced. Finally the ITSE observer performance are illustrated via simulation results.

2. PROCESS DESCRIPTION

The aerobic treatment of domestic and industrial wastewaters by activated sludge is a common process, but the characteristics of many industrial discharges often cause operational problems in continuous flow systems. Therefore, discontinuous processes, as sequencing batch reactors (SBR's), will be considered in this project because, in terms of investment and operation costs, process stability, and operation reliability, they are better than the conventional continuous activated sludge process. In dairy plants, SBR could be applied to raw wastewater with low organic load and intermittent production of wastewater or as post treatment after an anaerobic process when the organic load is high. When the flow rate of wastewater is continuous it is possible to use more than one SBR or a variation of SBR with continuous inflow of wastewater and intermittent outflow. Different carbon/nitrogen ratio and different type of carbon to be removed are obtained in each case. SBR is a promising system to treat these effluents. It is cheaper than other aerobic systems, it allows carbon removal and denitrification in the same reactor, and also phosphorus removal. A typical SBR process cycle with aerobic and anoxic phases to achieve nitrification and denitrification is composed by filling, mixing-aeration, sedimentation, draining and idle phases. In the following SBR model, we concentrate on the two successive batch steps : the anoxic phase followed by the aerobic phase. The model refers explicitly to these two phases. For the present process, one denitrification step and one step nitrification are considered in the anoxic and aerobic phases, respectively. Therefore the reaction scheme considered here is the following.

Anoxic phase
Denitrification : $S_C + S_{NO} \rightarrow X_h + N_2$
Ammonification : $S_N \rightarrow S_{NH}$

Aerobic phase
Nitrification : $S_O + S_{NH} \rightarrow X_a + S_{NO}$
C-removal : $S_C + S_O \rightarrow X_h$
Ammonification : $S_N \rightarrow S_{NH}$

The dynamics of the process are given by the following mass balance equations.

Anoxic phase

$$\frac{dX_h}{dt} = \mu_{hN} X_h \qquad (1)$$

$$\frac{dS_C}{dt} = -k_1 \mu_{hN} X_h \quad (2)$$

$$\frac{dS_{NO}}{dt} = -k_2 \mu_{hN} X_h \quad (3)$$

$$\frac{dS_{NH}}{dt} = k_3 r_N \quad (4)$$

$$\frac{dS_N}{dt} = -r_N \quad (5)$$

Aerobic phase

$$\frac{dX_h}{dt} = \mu_h X_h \quad (6)$$

$$\frac{dX_a}{dt} = \mu_a X_a \quad (7)$$

$$\frac{dS_C}{dt} = -k_4 \mu_h X_h \quad (8)$$

$$\frac{dS_O}{dt} = -k_5 \mu_h X_h - k_6 \mu_a X_a + k_L a(S_{O\max} - S_O) \quad (9)$$

$$\frac{dS_{NO}}{dt} = k_7 \mu_a X_a \quad (10)$$

$$\frac{dS_{NH}}{dt} = k_3 r_N - k_8 \mu_a X_a \quad (11)$$

$$\frac{dS_N}{dt} = -r_N \quad (12)$$

Where S_c, S_{NH}, S_{NO}, S_N, S_O, X_h and X_a are the biodegradable substrate concentration (carbon, mgCOD/L), the ammonia nitrogen concentration (mgN/L), the nitrate and nitrite concentration (mgN/L), the soluble organic nitrogen (mgN/L), the concentration of the dissolved oxygen (DO) in the water (mg/L) and the concentration of the digester biomasses (heterotrophs and autotrophs)(mgVSS/L), respectively.

And $k_1 = \frac{1}{Y_{hN}}$; $k_2 = \frac{1 - Y_{HN}}{2.86\, Y_{HN}}$; $k_4 = \frac{1}{Y_h}$;

$k_5 = \frac{1 - Y_h}{Y_h}$; $k_6 = \frac{\beta_1}{Y_a}$; $k_7 = \frac{\beta_2}{Y_a}$; $k_8 = \frac{1}{Y_a}$

With their values identified in the framework of the EC EOLI project (Betancur et al, 2003) and the following kinetic expressions:

$$\mu_{hN} = \mu_{hN\max} \frac{S_C - S_{C\min}}{K_{C1} + S_C - S_{C\min}} \frac{S_{NO}}{K_{NO} + S_{NO}} \quad (13)$$

$$r_N = \mu_0 (S_N - S_{N\min}) \quad (14)$$

$$\mu_h = \mu_{h\max} \frac{S_C - S_{C\min}}{K_{Ch} + S_C - S_{C\min}} \frac{S_O}{K_{Oh} + S_O} \quad (15)$$

$$\mu_a = \mu_{a\max} \frac{S_{NH}}{K_{NHa} + S_{NH}} \frac{S_O}{K_{Oa} + S_O} \quad (16)$$

3. ITSE OBSERVER

If we consider the following state space model of order n:

$$\frac{dx}{dt} = f(x,u) \quad (17)$$

where the measured variables y are related to the state variables x and the inputs u by:

$$y = h(x,u) \quad (18)$$

the general structure of a state observer can be written as:

$$\frac{d\hat{x}}{dt} = f(\hat{x},u) + K(\hat{x})(y - \hat{y}) \quad (19)$$

where $\hat{x}$ and $\hat{y}$ are the on-line estimates of x and y given by:

$$\hat{y} = h(\hat{x}) \quad (20)$$

with $K(\hat{x})$ the observer gain.

It is well known that the design of classical observers consists of choosing an appropriate gain, $K(\hat{x})$, such that the error dynamics has some desired properties (Dochain, 2003a). In the case of the extended Luenberger observer (ELO), the objective is to select $K(\hat{x})$ such that the linearised error dynamics around the process dynamics observation error e ($e = x - \hat{x}$) is asymptotically stable.

On the other hand the problem of choosing the appropriate gain $K(\hat{x})$ for ITSE observers becomes an optimisation problem. It consists on finding $K(\hat{x})$ that minimizes the following objective function J:

$$J = \int_0^T t\, e^2(t)\, dt \quad (21)$$

With T being an appropriate window of time. In this way the design of the observer includes minimization of the observation error together with better convergence rates.

3.1 Simulation Results

First of all the ITSE observer was tested for a simple CSTR process with Monod kinetics (Dochain, 2003b).

The model dynamics is described by the following equations:

$$\frac{dS}{dt} = -k_1 \mu X + D S_{in} - DS \quad (22)$$

$$\frac{dX}{dt} = \mu X - D X \quad (23)$$

With k_1, μ, D and S_{in} being the yield coefficient, the specific growth rate (h^{-1}), the dilution rate (h^{-1}) and

the influent substrate concentration (gL^{-1}) respectively.

$\mu = \frac{\mu_{max} S}{K_S + S}$ being a Monod kinetics with μ_{max} the maximum specific growth rate (h^{-1}) and K_S the saturation constant (gL^{-1}).

The observer equations become:

$$\frac{d\hat{S}}{dt} = -k_1 \mu_{max} \frac{\hat{S}}{K_S + \hat{S}} \hat{X} + D S_{in} - D\hat{S} + K_1 (S - \hat{S}) \quad (24)$$

$$\frac{d\hat{X}}{dt} = \mu_{max} \frac{\hat{S}}{K_S + \hat{S}} \hat{X} - D\hat{X} + K_2 (S - \hat{S}) \quad (25)$$

Considering the value of the parameters included in (Dochain 2003a) and the following initial values X(0)=1 (gL^{-1}), $\hat{X}(0)$= 5 (gL^{-1}), S(0)=30 (gL^{-1}) and $\hat{S}(0)$=50 (gL^{-1}) the ITSE observer performance can be seen in Figure 1

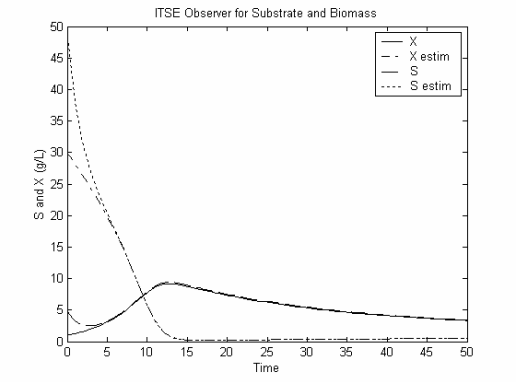

Fig 1. ITSE observer for biomass (X) and substrate (S) concentrations for a simple CSTR process

The ITSE performance was then compared with an ELO observer with gains K_1 and K_2 selected as indicated in (Dochain, 2003b) with $\lambda_1=\lambda_2$= -0.1 being the selected poles of the error dynamics (see Figure 2).

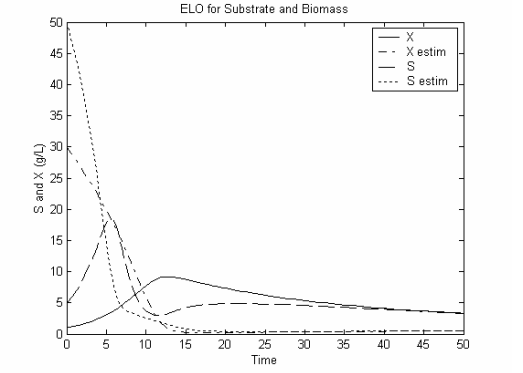

Fig. 2. Extended Luenberger Observer for biomass (X) and substrate (S) concentrations for a simple CSTR process

It can be noticed that the ITSE observer performs better than ELO with very good convergence properties.

4. APPLICATION TO THE WASTEWATER TREATMENT PROCESS

In order to illustrate the performance of the ITSE observer in the SBR with perturbed initial conditions, we first proceed with the anoxic phase.

4.1 *ITSE Observer for the Anoxic Phase*

In a first step and taking into account that the system of equations (1)-(2)-(3) is not observable with only one measurement (S_{NO}) (the observability matrix constructed from the Jacobian of system (1)-(2)-(3) is of rank 2), we started by developing an asymptotic observer for S_c as follows :

Let $$Z = \frac{-k_2}{k_1} S_C + S_{NO} \quad (26)$$

Then the asymptotic observer which is independent from the specific kinetics is written as follows :

$$\frac{d\hat{Z}}{dt} = 0 \text{ and } \hat{S}_C = \frac{-k_1}{k_2} (\hat{Z} - S_{NO}) \quad (27)$$

Then, by considering the already determined $\hat{S}_C$ in a second step, we developed the following observer :

$$\frac{d\hat{X}_h}{dt} = \hat{\mu}_{hN} \hat{X}_h + K_1 (\hat{S}_{NO} - S_{NO}) \quad (28)$$

$$\frac{d\hat{S}_{NO}}{dt} = -k_2 \hat{\mu}_{hN} \hat{X}_h + K_2 (\hat{S}_{NO} - S_{NO}) \quad (29)$$

with

$$\hat{\mu}_{hN} = \mu_{hN\max} \frac{\hat{S}_C - S_{C\min}}{K_{C1} + \hat{S}_C - S_{C\min}} \frac{\hat{S}_{NO}}{K_{NO} + \hat{S}_{NO}} \quad (30)$$

Considering the parameter values of the EOLI project (Betancur et al, 2003) and the following initial values: $X_h(0)$=1; $\hat{X}_h(0)$= 1.2; $S_C(0)$= $S_C(0)$ = 200 (carbon, mg COD/L); $S_{NO}(0)$= $\hat{S}_{NO}(0)$ =0.5 (mg N/L) which correspond to a 20% error in the initial observed value of X_h . The ITSE observer performs as shown in Figure 3.

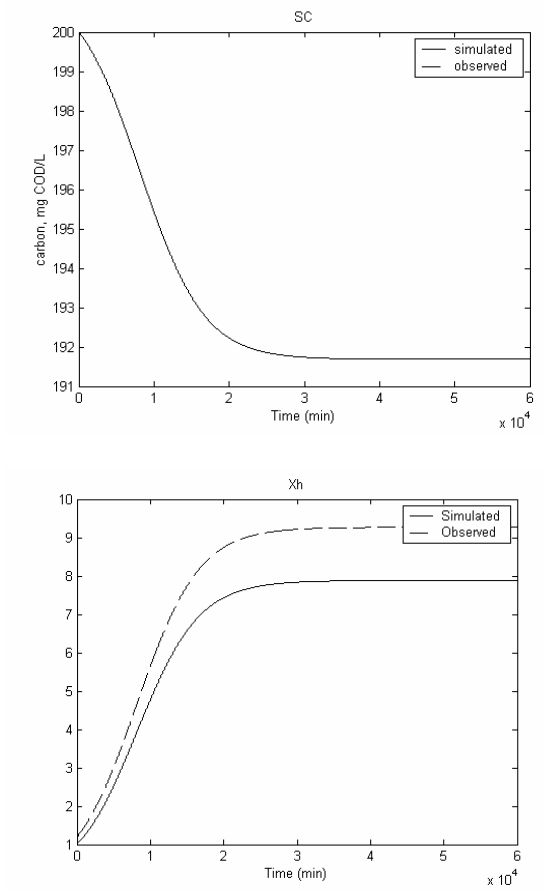

Fig. 3. ITSE Observer for S_c and X_h during the anoxic phase of the wastewater treatment process with a 20% error in the initial condition of X_h

As it can be seen in Figure 3, the ITSE is biased for X_h observation. In fact it happens that X_h can be poorly observed from S_{NO} measurements. The observability test shows that the observability matrix constructed from the Jacobian of system equations (1) and (3) is of rank 2 if and only if $\mu_{hN} >> 0$ which is not at all the case. This is also the reason why the equivalent ELO performs in a very unstable way. It can be proved that the gain K_1 of the ELO has μ_{hN} in a denominator.

4.*2 ITSE Observer for the Anoxic and AerobicPhase*

In a first step we begun by developing an asymptotic observer for X_a as follows :

$$\text{Let} \quad Z = k_7 X_a - S_{NO} \tag{31}$$

Then the asymptotic observer which is independent from the specific kinetics is written as follows :

$$\frac{d\hat{Z}}{dt} = 0 \quad \text{and} \quad \hat{X}_a = \frac{1}{k_7}(\hat{Z} + S_{NO}) \tag{32}$$

By considering the estimated value of $\hat{X}_a$ given by the asymptotic observer, the observer for the other state variables considering that S_O, S_{NO} and S_{NH} are measured variables is given by the following set of equations :

$$\frac{d\hat{S}_N}{dt} = -\hat{r}_N + K_1(\hat{S}_{NH} - S_{NH}) \tag{33}$$

$$\frac{d\hat{S}_{NH}}{dt} = k_3\,\hat{r}_N - k_8\,\hat{\mu}_a\,\hat{X}_a + K_2(\hat{S}_{NH} - \hat{S}_{NH}) \tag{34}$$

$$\frac{d\hat{X}_h}{dt} = \hat{\mu}_h\,\hat{X}_h + K_3(\hat{S}_O - S_O) \tag{35}$$

$$\frac{d\hat{S}_C}{dt} = -k_4\,\hat{\mu}_h\,\hat{X}_h + K_4(\hat{S}_O - S_O) \tag{36}$$

$$\frac{d\hat{S}_O}{dt} = -k_5\hat{\mu}_h\,\hat{X}_h - k_6\hat{\mu}_a\hat{X}_a + k_L a(S_{O\max} - \hat{S}_O) + K_5(\hat{S}_O - S_O) \tag{37}$$

a nd the following kinetic expressions:

$$\hat{\mu}_{hN} = \mu_{hN\max}\,\frac{\hat{S}_C - S_{C\min}}{K_{C1} + \hat{S}_C - S_{C\min}}\,\frac{\hat{S}_{NO}}{K_{NO} + \hat{S}_{NO}} \tag{38}$$

$$\hat{r}_N = \mu_0(\hat{S}_N - S_{N\min}) \tag{39}$$

$$\hat{\mu}_h = \mu_{h\max}\,\frac{\hat{S}_C - S_{C\min}}{K_{Ch} + \hat{S}_C - S_{C\min}}\,\frac{\hat{S}_O}{K_{Oh} + \hat{S}_O} \tag{40}$$

$$\hat{\mu}_a = \mu_{a\max}\,\frac{\hat{S}_{NH}}{K_{NHa} + \hat{S}_{NH}}\,\frac{\hat{S}_O}{K_{Oa} + \hat{S}_O} \tag{41}$$

Taking into account that S_{NO} is a measured variable we shall only consider that:

$$\frac{d\hat{S}_{NO}}{dt} = k_7\,\hat{\mu}_a\,\hat{X}_a \tag{42}$$

Considering the value of the parameters included in (Betancur et al, 2003) and the following initial values: $X_h(0)=1$; $\hat{X}_h(0)= 1.2$; $S_C(0)= \hat{S}_C(0) = 200$; $S_{NO}(0)= \hat{S}_{NO}(0) =0.5$; $S_{NH}(0)=0.1$; $\hat{S}_{NH}(0)=0.12$; $S_N(0)=20$; $\hat{S}_N(0)=24$; $X_a(0)=1$; $\hat{X}_a(0)=1.2$; $S_O(0)=0.010$; $\hat{S}_O(0)=0.012$. The ITSE observer performs as shown in Figure 4.

It is worth noting that the ITSE performs very well even with the important initial errors in some of the observed variables. Another advantage over the ELO is that the observer gains are easy to determine which is not the case for the ELO when the system is of high order as it is the case for the wastewater treatment process.

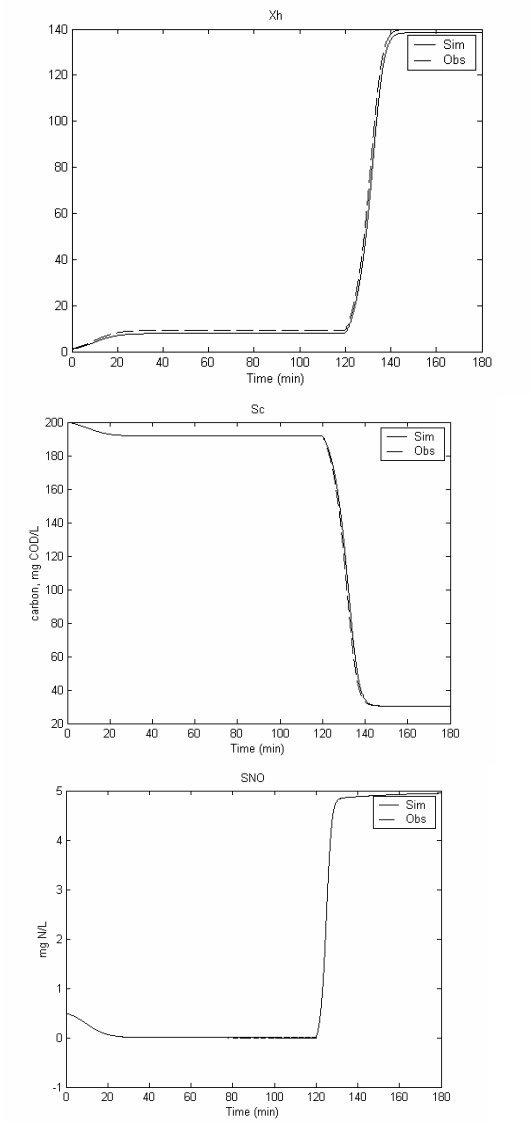

Fig. 4. ITSE Observer for S_c , X_h and S_{NO} during the anoxic and aerobic phase of the wastewater treatment process with a 20% error in the initial condition of $X_{h,,}$ S_{NH}, S_N, X_a *and* S_O

5. CONCLUSIONS

In this paper, we have handled the question designing state observers that can possibly account for the limited time duration of batch processes by considering the design of ITSE observers in which the observer gains are computed via an ITSE criterion. The results of the observer have been illustrated first with a simple microbial growth model, then with the model of a SBR process, a process used in wastewater treatment.

Acknowledgments

This paper presents research results of the Belgian Programme on Inter-University Poles of Attraction initiated by the Belgian State, Prime Minister's office for Science, Technology and Culture. The scientific responsibility rests with its authors. It includes results of the EOLI project that is supported by the INCO program of the European Community (Contract number ICA4-CT-2002-10012).

REFERENCES

Agrawal M. and D. Bonvin (1989). Limitations of the extended Kalman filter for batch reactors. *Proc. IFAC Symp. DYCORD'89*, 299-306.

Agrawal M. and D. Bonvin (1991). Improved state estimator in the face of unreliable parameters. *J. Process Control*, **1***, 251-257.*

Betancur M., D. Dochain and H. Fibrianto (2003). WP 2 : model selection and parameter identification. Deliverable D2.3 : validated model. EC EOLI project, contract Number ICA4-CT-2002-10012.

Bonné and S.B. Jorgensen (2001). Batch to batch improving control of yeast fermentation. *Proc. ESCAPE11*, Kolding, Denmark.

Bonvin D., B. Srinivasan and D. Ruppen (2001). Dynamic optimization in the batch chemical industry. *Preprints CPC6*, Tucson, Arizona, 283-307.

De Vallière Ph. and D. Bonvin (1990). Application of estimation techniques to batch reactors - III. Modelling refinements which improve the quality of state and parameter estimation. *Comp. Chem. Eng*., **14** (7), 799-808.

Dochain D. (2003a). State and parameter estimation in chemical and biochemical processes : a survey. *Journal of Process Control*, **13** (8), 801-818

Dochain D. (2003b). State observers for processes with uncertain kinetics. *Int. J. Control*, **76** (15), 1483-1492

Doyle III F.J. (1997). Nonlinear inferential control for process applications. *Proc. ADCHEM'97*, 170-18

ADCHEM 2006

International Symposium on Advanced Control of Chemical Processes
Gramado, Brazil – April 2-5, 2006

ROBUST ADAPTIVE CONTROL OF YEAST FED-BATCH CULTURES

F. Renard [*,1] **A. Vande Wouwer** [*] **M. Perrier** [**]

[*] *Service d'Automatique, Faculté Polytechnique de Mons, Boulevard Dolez 31, B-7000 Mons, Belgium*
[**] *Departement de Génie Chimique, Ecole Polytechnique de Montréal, Canada*

Abstract: A robust controller combining a feedforward compensator (for the measured disturbance) and a feedback *RST* controller is designed for the control of *S. cerevisiae* cultures. The controller is based on the linearization of Sonnleitner's model allowing a simple transfer function model to be derived, which describes the relation between the ethanol concentration, the substrate feed and a measurable disturbance - image of the substrate demand for cell growth. This control scheme is made robust to neglected high frequency dynamics (of glucose and oxygen) and uncertain stoichiometry coefficients using the observer polynomial. This control scheme, whose performance is demonstrated in simulation, requires only the on-line measurements of the ethanol concentration and bioreactor volume, estimation of the oxygen transfer rate, and minimal *a priori* process knowledge, i.e. only one stoichiometric coefficient. *Copyright 2006 IFAC.*

Keywords: Robust control; Adaptive control; Fed-batch fermentation; Biotechnology;

1. INTRODUCTION

Due to their robustness and ability to utilize cheap materials for growth and production, *Saccharomyces cerevisiae* strains are among the most popular industrial microorganisms. Recently, with the achievement of modern gene technology, *S. cerevisiae* have been increasingly used as host organisms for producing recombinant proteins (production of insulin, vaccines, ...).

To ensure optimal operating conditions (i.e. to maximize biomass productivity), a commonly used method consists in regulating the ethanol concentration at a low value. Several control schemes, which have been tested in genuine industrial applications, have been proposed to this end (see, e.g. Chen *et al.*, 1995; Pomerleau, 1990; Pomerleau and Viel, 1992; Axelsson, 1988). These controllers result from the linearizing control theory (Bastin and Dochain, 1990), where the control law can be viewed as a proportional controller acting around a trajectory representing the substrate demand for cell growth. In (Chen *et al.*, 1995), this trajectory is deduced from an on-line biomass estimation while in (Pomerleau, 1990), it is deduced from the measurement of the oxygen transfer rate (*OTR*). In this connection, nonlinear parameter adaptation techniques are used to estimate uncertain parameters.

In this contribution, a simplified model is derived by linearization of the global nonlinear model of Sonnleitner and Käppeli (1986) around the above-mentioned trajectory. This transfer-function model depicts the relationship between the ethanol concentration and the substrate feed and a measured disturbance representing the substrate demand for cells growth. An adaptive feedforward controller is used in combination with a feedback RST controller to regulate the ethanol concentration. This approach allows the use of linear control theory and a simple design of a robust controller. For instance, requirements in terms

[1] Author to whom correspondence should be addressed:
e-mail: Frederic.Renard@fpms.ac.be
phone: +32 (0)65374131 fax: +32 (0)65374136

of measurement noise attenuation or robustification to neglected high frequency dynamics can easily be incorporated. In comparison with the linearizing control theory, the purely linear control framework, into which the suggested control algorithm is developed, allows the robustness issues to be easily taken into account.

2. MODELING OF YEAST FED-BATCH CULTURES

2.1 *Nonlinear dynamic model*

The metabolism of yeast depends strongly on the culture conditions. During the aerobic growth, glucose and ethanol can be used as carbon sources according to the following reaction scheme :

$$\text{Glucose oxidation :} \quad \mathrm{G} + k_5\,\mathrm{O} \xrightarrow{r_1} k_1\,\mathrm{X} + k_7\,\mathrm{P} \quad (1a)$$

$$\text{Glucose fermentation :} \quad \mathrm{G} \xrightarrow{r_2} k_2\,\mathrm{X} + k_4\,\mathrm{E} + k_8\,\mathrm{P} \quad (1b)$$

$$\text{Ethanol oxidation :} \quad \mathrm{E} + k_6\,\mathrm{O} \xrightarrow{r_3} k_3\,\mathrm{X} + k_9\,\mathrm{P} \quad (1c)$$

where X, G, E, O, P are, respectively, the concentration in the culture medium of biomass, glucose, ethanol, dissolved oxygen and dissolved carbon dioxide, and k_i are the pseudo-stoichiometric coefficients.

The reaction rates associated with these reactions are :

$$r_1 = \min\left(r_G, \frac{r_{Omax}}{k_5}\right) \quad (2)$$

$$r_2 = \max\left(0, r_G - \frac{r_{Omax}}{k_5}\right) \quad (3)$$

$$r_3 = \max\left(0, \min\left(r_E, \frac{r_{Omax} - k_5 r_G}{k_6}\right)\right) \quad (4)$$

The kinetic terms associated with the glucose consumption r_G, the respiratory capacity r_{Omax} and the potential ethanol oxidative rate r_E are :

$$r_G = \mu_G \frac{\mathrm{G}}{\mathrm{G} + K_G},\ r_{Omax} = \mu_O \frac{\mathrm{O}}{\mathrm{O} + K_O},\ r_E = \mu_E \frac{\mathrm{E}}{\mathrm{E} + K_E}$$

where μ_G, μ_O and μ_E are the maximal values of specific growth rates, K_G, K_O and K_E are the saturation constants of the corresponding substrate.

This kinetic model is based on the bottleneck hypothesis developed by Sonnleitner and Käppeli (1986). It assumes a limited oxidation capacity of yeast, leading to the formation of ethanol under conditions of oxygen limitation and/or high glucose concentration. The glucose concentration corresponding to the oxidative capacity is denoted G_{crit}, and is such that $r_G = r_{Omax}/k_5$. According to the glucose concentration value, two different operating regimes can be distinguished. At low glucose concentrations ($G \leq G_{crit}$), the system is in respiratory regime. The glucose consumption rate is smaller than the maximal respiratory capacity ($r_G \leq r_{Omax}/k_5$) and the rate of the oxidative glucose metabolism is determined by the glucose consumption rate (2). Ethanol can be oxidized in parallel with glucose and the rate of the oxidative ethanol metabolism depends on the excess of respiratory capacity and the available ethanol (4). At high glucose concentrations ($G \geq G_{crit}$), the system is said in respiro-fermentative regime. The glucose consumption rate is larger than the maximal respiratory capacity ($r_G \geq r_{Omax}/k_5$) and the respiratory capacity of the cells determines the rate of the oxidative glucose metabolism (2). The excess of glucose is metabolized by the fermentative metabolism (3). Under oxygen starvation conditions, the fermentative metabolic pathway always predominates.

Based on the reaction scheme (1), the following macroscopic mass balances can be derived :

$$\frac{d(VX)}{dt} = (k_1 r_1 + k_2 r_2 + k_3 r_3) XV \quad (5a)$$

$$\frac{d(VG)}{dt} = -(r_1 + r_2) XV + F_{in} G_{in} \quad (5b)$$

$$\frac{d(VE)}{dt} = (k_4 r_2 - r_3) XV \quad (5c)$$

$$\frac{d(VO)}{dt} = -(k_5 r_1 + k_6 r_3) XV + V\,OTR \quad (5d)$$

$$\frac{dV}{dt} = F_{in} \quad (5e)$$

where G_{in} is the substrate concentration in the feed, F_{in} is the inlet feed rate, V is the culture medium volume and D is the dilution rate ($D = F_{in}/V$).

2.2 *Simplified linear model*

In (Valentinotti *et al.*, 2004), it is shown that maximization of biomass productivity corresponds to a feeding strategy which exactly fills the bottleneck. Hence, the optimal operating conditions correspond to the boundary between the respiro-fermentative and the respiratory regimes ($G = G_{crit}$). The nonlinear model (5) can be linearized around this optimal point, i.e. in the respiro-fermentative or respiratory regime, with $G \to G_{crit}$. For both regimes, it is assumed that there is no accumulation of glucose and oxygen in the culture medium so that the dynamics of the total amount of these substrates can be neglected. Along the optimal trajectory, where G is maintained at a low concentration ($G_{crit} \approx 0.02\,g/l$), glucose is the limiting substrate and the biomass assimilates very quickly the glucose fed to the bioreactor (so that $(r_1 + r_2)XV \approx F_{in} G_{in}$ and $d(VG)/dt \approx 0$). Moreover, the oxygen solubility in the culture medium is low and the dynamics associated to the oxygen transfer from the gaseous to the liquid phase is fast compared to the time constant of the biological process, so that the dynamics of the total amount of oxygen VO in the culture medium can be neglected ($d(VO)/dt \approx 0$).

In the respiro-fermentative regime, the nonlinear model is given by (5) where the rate of ethanol oxidation $r_3 = 0$. Based on (5b) and (5d), the previous assumptions yield :

$$\frac{d(VG)}{dt} \approx 0 \qquad \Rightarrow \qquad r_2 XV = F_{in} G_{in} - r_1 XV \quad (6)$$

$$\frac{d(VO)}{dt} \approx 0 \qquad \Rightarrow \qquad r_1 X = \frac{OTR}{k_5} \quad (7)$$

Substitution into (5c) gives (using also (5e)) :

$$\frac{dE}{dt} = \frac{F_{in}}{V}(k_4 G_{in} - E) - \frac{k_4}{k_5} OTR \quad (8)$$

The nominal trajectory is characterised by a constant ethanol concentration E^* and, in turn, by a dilution profile $D^* = F_{in}^*/V^*$ satisfying the following relation :

$$D^* = \frac{1}{k_4 G_{in} - E^*} \frac{k_4}{k_5} OTR \quad (9)$$

Linearizing (8) around the nominal trajectory and neglecting the variations of E and V gives :

$$\frac{dE}{dt} = F_{in} \frac{k_4 G_{in} - E^*}{V^*} - \frac{k_4}{k_5} OTR \quad (10)$$

For the respiratory operating regime, similar developments give :

$$\frac{dE}{dt} = F_{in} \frac{\frac{k_5}{k_6} G_{in} - E^*}{V^*} - \frac{OTR}{k_6} \quad (11)$$

Finally, for both operating regimes, the ethanol dynamics can be expressed by the same discrete transfer function :

$$E(k) = \frac{q^{-1}}{1 - q^{-1}} \left[b F_{in}(k) - \alpha OTR(k) \right] \quad (12)$$

where q^{-1} is the backward shift operator and the parameters b and α listed in Table 1 depend on the operating regime (T_s is the sampling time).

The block diagram of Fig. 1 shows the schematic representation of the simplified fed-batch fermentation model. The measured perturbation αOTR represents the glucose demand for cells growth. If the feeding flux $b F_{in}$ is higher or lower than the measured perturbation, there is production or consumption of ethanol, respectively.

Around the optimal trajectory, the system is modeled by the same transfer function for both operating regimes. The only difference lies in the b and α values which change with the operating regime. For controller design, the b variation according to the operating regime and the neglected dynamics of glucose and oxygen can be considered as modeling uncertainties, with respect to which the controller has to be robust. Moreover, the gain b evolving widely with the volume, a robust and adaptive control strategy is needed.

3. CONTROL STRATEGY

3.1 *Controller design*

Based on the linear model (12), where the notation $\hat{A}(q^{-1}) = 1 - q^{-1}$ and $\hat{B}(q^{-1}) = b\, q^{-1}$ is used, a linear controller can be designed. The control scheme

Table 1. Parameters expressions of linear discrete model (12).

	Respiro-fermentative regime	respiratory regime
b	$T_s \frac{k_4 G_{in} - E^*}{V^*}$	$T_s \frac{\frac{k_5}{k_6} G_{in} - E^*}{V^*}$
α	$T_s \frac{k_4}{k_5}$	$T_s \frac{1}{k_6}$

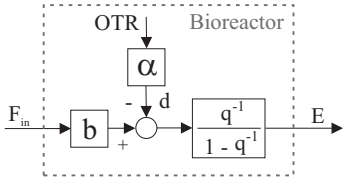

Fig. 1. Schematic representation of the simplified (linear) fed-batch fermentation model.

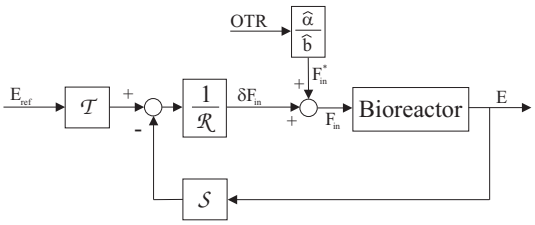

Fig. 2. Closed-loop diagram. A feedback RST controller is used in combination with an adaptive feedforward controller in order to cancel the measured disturbance d effect on the ethanol concentration E.

developed in this work consists of a feedback RST controller and a feedforward controller canceling the measured disturbance effect on the output. The corresponding block diagram is shown in Fig. 2. The feedback RST controller compensates deviations from the nominal trajectory defined by (12) when E is equal to a constant setpoint E_{ref} :

$$F_{in}^*(k) = \frac{\hat{\alpha}(k)}{\hat{b}(k)} OTR(k) \quad (13)$$

where $\hat{\alpha}(k)$ and $\hat{b}(k)$ are the adapted values of the corresponding parameters.

The control law is written as follows :

$$\mathcal{R}(q^{-1}) \delta F_{in}(k) = -\mathcal{S}(q^{-1}) E(k) + \mathcal{T}(q^{-1}) E_{ref}(k)$$

$$F_{in}(k) = \delta F_{in}(k) + \frac{\hat{\alpha}(k)}{\hat{b}(k)} OTR(k)$$

where δF_{in} is the controller output which represents the variation of the feed rate around the nominal trajectory F_{in}^*, E_{ref} is the desired ethanol setpoint and $\mathcal{R}$, $\mathcal{S}$ and $\mathcal{T}$ are polynomials in backward-shift operator q^{-1}.

For the sake of simplicity, the RST controller polynomials are computed by a pole-placement procedure (Astrom and Wittenmark, 1997). Let the reference model be given by :

$$H_m(q^{-1}) = \frac{B(q^{-1}) P(1)}{B(1) P(q^{-1})} \quad (14)$$

where $P(q^{-1})$ allows the poles of the tracking closed-loop transfer function to be chosen.

Let assume that the controller must ensure zero-steady-state error with respect to a step disturbance acting on the process input. This deterministic disturbance $d(k)$ can be modeled by the following dynamical system :

$$A_d(q^{-1})d(k) = C(q^{-1})\delta(k) \qquad (15)$$

where $\delta(k)$ is the unit pulse, $A_d(q^{-1}) = \Delta(q^{-1}) = 1 - q^{-1}$ and $C(q^{-1}) = T(q^{-1})$ is an observer polynomial, which can be used to robustify the control law as it is common practice for predictive controllers (see e.g. Soeterboek, 1992; Clarke, 1996).

With the previous reference and disturbance models, the following $\mathcal{R}$, $\mathcal{S}$ and $\mathcal{T}$ polynomials can be selected :

$$\mathcal{R} = \Delta P, \qquad \mathcal{S} = \mathcal{S}' P, \qquad \mathcal{T} = T\,\frac{P(1)}{\hat{B}(1)} \qquad (16)$$

where $\mathcal{S}'$ is the solution of $T = \Delta\hat{A} + \hat{B}\mathcal{S}'$.

Note that, in this way, an integrator is introduced in the controller. In practice, the integral action must be implemented with an anti-reset windup mechanism in case of saturation of the control action. In fact, at the beginning of a culture, the flow rate is very small and any deviation from the nominal trajectory can lead to negative flow rates which are not allowed. An anti-reset windup mechanism avoid amplifying oscillations when saturation occurs.

If the process model is correctly estimated, the closed loop transfer function can be written as follows :

$$\begin{aligned} E &= \frac{B\mathcal{T}}{A\mathcal{R} + B\mathcal{S}}\,E_{ref} + \frac{\mathcal{R}q^{-1}}{A\mathcal{R} + B\mathcal{S}}\,d \\ &= \frac{BP(1)}{\hat{B}(1)P}\,E_{ref} + \frac{\Delta q^{-1}}{T}\,d \end{aligned} \qquad (17)$$

Note that P does not appear in the transfer function related to the disturbance. Thus, the tracking and rejection behaviors can be adjusted independently in selecting the roots of the polynomials P and T, respectively. Note also that Δ appears in the numerator of the rejection transfer function. Therefore, the internal model principle (Francis and Wonham, 1976) ensures that a step of a process input disturbance will be rejected asymptotically by the controller (16).

The proposed controller can be tuned by selecting appropriate P and T polynomials. The overall time constant of the bioprocess is quite big and it is reasonable to choose a sampling time T_s of 0.1 h. The P polynomial is designed to achieve a first-order tracking behavior with a time constant of 1 h, i.e. P is given by $P(q^{-1}) = 1 - 0.9q^{-1}$. The observer polynomial T is designed in order to achieve a trade-off between the rejection performance and robustness. If the adapted gain $\hat{b}(k)$ corresponds to the actual process gain, the controller (16) yields a corrected open-loop transfer

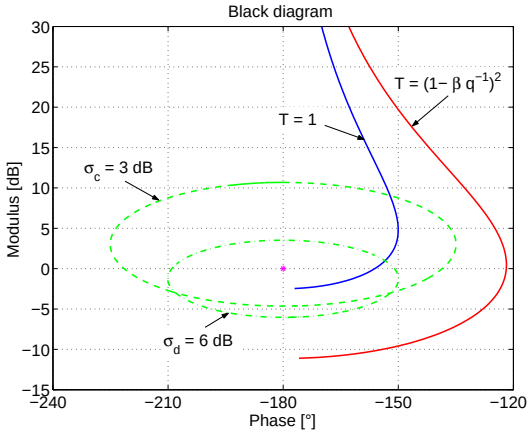

Fig. 3. Black diagram of the controlled system before robustification ($T(q^{-1}) = 1$) and after robustification ($T(q^{-1}) = (1-\beta q^{-1})^2$). σ_c and σ_d are the complementary and direct sensitivity functions.

function $\frac{B\mathcal{S}}{A\mathcal{R}}$, which depends only on the T polynomial, and whose stability robustness can be directly adjusted by choosing the T roots. The design rules of predictive controllers (see e.g. Soeterboek, 1992; Clarke, 1996) can be used and lead to $T(q^{-1}) = (1 - \beta q^{-1})^2$. The robustness margin is monotonically increasing when the value of the parameter β increases. Obviously, the rejection performance decreases in the same way and, for this application, $\beta = 0.7$ leads to a good trade-off.

Fig. 3 shows the Black diagrams of control schemes without robustification ($T(q^{-1}) = 1$) and with robustification ($T(q^{-1}) = (1-\beta q^{-1})^2$). It is well known that ensuring a modulus lower than 6 dB for the direct sensitivity function σ_d and lower than 3 dB for the complementary sensitivity function σ_c provides a good stability robustness. It is apparent that, before robustification, the controller shows bad robustness at high frequencies, whereas a good robustness margin is required in this frequency range because the oxygen and glucose dynamics have been neglected. Robustification provides the desired margins.

In addition, robustification allows the influence of the noise corrupting the ethanol concentration measurement on the control signal to be strongly attenuated (noise on the control signal affects the pump wear).

3.2 *Adaptation scheme*

An indirect adaptation scheme is used. Considering (17), it can be shown that cancellation of the T polynomial in the tracking transfer function is effective only if the process gain is correctly estimated. Therefore, adaptation of the parameter b is required for constant tracking performance during a culture. The parameter b can be directly adapted using the measurements of E and V. The measurement of the volume can obtained from a measurement of the bioreactor weight. If a weight measurement is not available, the volume

can be estimated on-line from all liquid additions and withdrawals such as evaporation, sampling, base addition for pH control, etc. Therefore, the adapted b parameter is given by :

$$\hat{b}(k) = T_s \frac{k_4 G_{in} - E(k)}{V(k)} \tag{18}$$

Because, in practice, the α parameter is not known exactly, it must also be estimated on-line to ensure perfect cancellation of the measured disturbance. To this end, the discrete model (12) can be written as a linear regression :

$$\varepsilon_1(k) = \varepsilon_2(k)\,\alpha \tag{19}$$

where $\varepsilon_1(k) = \hat{b}(k-1)F_{in}(k-1) - A(q^{-1})E(k)$ and $\varepsilon_2(k) = OTR(k-1)$.

Linear regression (19) can be solved on-line by an appropriate algorithm (see e.g. Ljung, 1999) taking into account that ε_1 and ε_2 are corrupted with noise because these signals are computed from measurements. In practice, ε_1 and ε_2 are filtered by $P(1)/P(q^{-1})$ to remove the mutual correlation and a recursive least-squares (RLS) algorithm proves to give a satisfactorily unbiaised estimation of α.

Remark In (Pomerleau, 1990), the suggested nonlinear controller appears as a special case of the design procedure developed in this study. In fact, if $A_d(q^{-1}) = 1$, $C(q^{-1}) = 1$, and $T(q^{-1}) = 1$, i.e. there is no disturbance model nor observer polynomial, then the pole-placement procedure (Astrom and Wittenmark, 1997) based on the same reference model $H_m(q^{-1})$, gives :

$$\mathcal{R} = 1\,; \quad \mathcal{S} = \mathcal{T} = \frac{P(1)}{\hat{B}(1)} \tag{20}$$

Equations (14) can then be written as :

$$F_{in}(k) = \frac{\gamma\,(E_{ref}(k) - E(k)) + \hat{\alpha}(k)\,OTR(k)}{\hat{b}(k)} \tag{21}$$

where $\gamma = P(1)$.

This controller can be interpreted as a proportional controller acting around the nominal trajectory given by (13). In (Pomerleau, 1990), the parameter α is not estimated thanks to a RLS algorithm but with a nonlinear estimation technique. An observer based estimator (Bastin and Dochain, 1990) is designed based on the differential equation (8) and the observer parameters are tuned so as to make the estimation dynamics independent of the process dynamics (Perrier *et al.*, 2000). Note that the same nonlinear estimation technique could be used in the present study.

4. SIMULATION RESULTS

The control algorithm described in Section 3 is implemented in simulation on the nonlinear process model presented in Section 2.1. When the ethanol concentration is regulated to the setpoint E_{ref} = 1 g/l, the process operates in respiro-fermentative regime. Thus, the only non operational parameter required to compute the controller is the stoichiometric coefficient k_4. The value proposed by Sonnleitner and Käppeli (1986) is chosen, k_4 = 0.48 [g of E/g of G]. The operational parameters are given as follows : G_{in} = 500 g/l; V_0 = 5 l; X_0 = 0.4 g/l; E_0 = 0.5 g/l, where the subscript 0 denotes an initial value. The design polynomials for the controller are given by $P(q^{-1}) = 1 - 0.9q^{-1}$ and $T(q^{-1}) = (1 - 0.7q^{-1})^2$ so that the polynomials $\mathcal{R}$, $\mathcal{S}$ and $\mathcal{T}$ can be computed from (16).

A setpoint step is imposed at t = 10 h in order to evaluate the tracking performance. For simulation purposes, OTR is computed using a well established model of the oxygen transfer, i.e., $OTR = K_l a \cdot (O_{sat} - O)$, where O_{sat} is the saturation oxygen concentration and $K_l a$ is the volumetric mass transfer coefficient. A low value of $K_l a$ is chosen in order to simulate a substrate limitation by oxygen. In industrial yeast culture, this kind of limitation is very frequent because the oxygen transfer coefficient of industrial bioreactors is generally low. Thus, the controller must keep on performing well in this situation.

Simulation results are shown on Fig. 4 and 5, demonstrating that the control algorithm is able to regulate E at the setpoint. When the setpoint step occurs, the tracking behavior is in accordance with the reference model H_m (first order system with 1 h time constant). Fig. 5 shows that the maximum oxygen transfer rate is achieved at about 16 h. From that time on, the oxidation capacity decreases gradually as the biomass grows. In spite of this metabolism change, almost no deviation of the E signal from the setpoint is observed, i.e. the controller decreases the feed rate in order to prevent excessive formation of ethanol. As the OTR signal is a good image of the glucose demand for cell growth, the fluctuations of this demand can be instantaneously compensated to follow the nominal trajectory.

5. CONCLUSIONS

Linearization of Sonnleitner's model around a nominal trajectory allows a simple linear model of the fed-batch fermentation process of *Saccharomyces cerevisae* to be derived. This model describes the main macroscopic phenomena taking place in the bioreactor, i.e. it includes a transfer function between the substrate feed and the ethanol concentration, and a measured disturbance. This disturbance, which can be measured on-line via the OTR signal, is the image of the substrate demand for cell growth. As explained by the linear model, the production or consumption of ethanol results from the excess or deficit of feed rate applied to the system, as compared to the substrate demand for growth. The advantage of using a linear

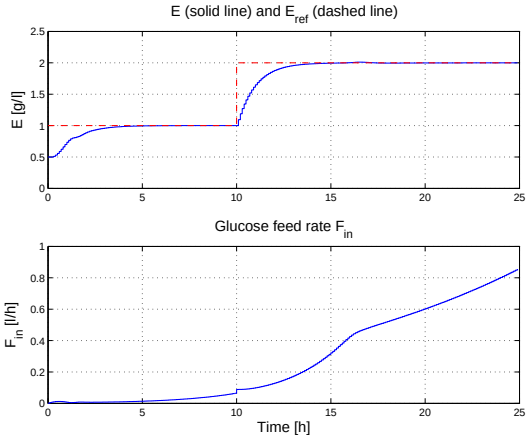

Fig. 4. Simulation results of a yeast fed-batch fermentation controlled with the algorithm proposed in Section 3. Ethanol concentration E and inlet flow rate F_{in}.

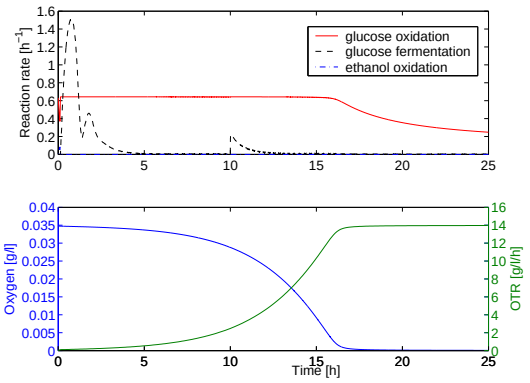

Fig. 5. Simulation results of a yeast fed-batch fermentation controlled with the algorithm proposed in Section 3. Reaction rates, dissolved oxygen concentration O and oxygen transfer rate OTR.

model (in contrast with the usual non linear models used for bioprocess simulation) is the possibility to easily develop a robustness analysis based on linear control theory.

In order to cancel the measured disturbance effect on the ethanol concentration, a feedforward controller is used in combination with a feedback RST controller. When developing the simplified process model, several high frequencies dynamics are neglected and the numerical values of some stoichiometric coefficients can be uncertain. Therefore, particular attention is paid to the design of a robust controller, allowing a separate (independent) tuning of the tracking performance and of the stability margins. As the process parameters can evolve during a culture, an indirect adaptive scheme is used to update on-line the controller parameters. The proposed control scheme can be viewed as a generalisation of the controller proposed in (Pomerleau, 1990).

The control algorithm requires only two on-line measurements : E and OTR. OTR measurements are commonly available and reliable E sensors are now becoming available at reasonable costs. Moreover, the V signal is also needed, which can be estimated by integration of all the liquid fluxes or via simple bioreactor weight measurements. With these on-line signals at hand, the implementation of control algorithm is quite simple. Tests in simulation are presented in the present paper, and these preliminary results demonstrate the ability of the controller to maintain the desired ethanol setpoint even when oxygen limitation occurs (as it is frequent in many industrial applications).

6. REFERENCES

Astrom, K. J. and B. Wittenmark (1997). *Computer Controlled Systems Theory and Design*. Information and System Sciences. Prentice Hall.

Axelsson, J.P. (1988). On the role of adaptive controllers in fed-batch yeast production. ADCHEM 1988. Copenhagen.

Bastin, G. and D. Dochain (1990). *On-line estimation and adaptive control of bioreactors*. Elsevier. Amsterdam.

Chen, L., G. Bastin and V. van Breusegem (1995). A case study of adaptive nonlinear regulation of fed-batch biological reactors. *Automatica* **31**(1), 55–65.

Clarke, D. W. (1996). Adaptive predictive control. *Annual Reviews in Control* **20**, 83–94.

Francis, B. A. and W. M. Wonham (1976). The internal model principle of control theory. *Automatica* **12**, 457–465.

Ljung, L. (1999). *System identification : Theory for the user*. Prentice-Hall Inc.

Perrier, M., S. Feyo de Azevedo, E. C. Ferreira and D. Dochain (2000). Tuning of observer-based estimators: theory and application to the on-line estimation of kinetic parameters. *Control engineering Practice* **8**, 377–388.

Pomerleau, Y. (1990). Modélisation et commande d'un procédé fed-batch de culture des levures pain. PhD thesis. Département de génie chimique. Université de Montréal.

Pomerleau, Y. and G. Viel (1992). Industrial application of adaptive nonlinear control for bakers' yeast production. ICCAFT 4. Keystone, CO, USA.

Soeterboek, R. (1992). *Predictive Control : A Unified Approach*. Systems and Control Engineering. Prentice Hall.

Sonnleitner, B. and O. Käppeli (1986). Growth of *saccharomyces cerevisiae* is controlled by its limited respiratory capacity : Formulation and verification of a hypothesis. *Biotechnol. Bioeng.* **28**, 927–937.

Valentinotti, S., C. Cannizzaro, B. Srinivasan and D. Bonvin (2004). An optimal operating strategy for fed-batch fermentations by feeding the overflow metabolite. ADCHEM 2004. Hong Kong.

ADCHEM 2006

International Symposium on Advanced Control of Chemical Processes
Gramado, Brazil – April 2-5, 2006

OUTPUT TRACKING OF BIOPROCESSES THROUGH RECIRCULATION WITH UNKNOWN INPUT CONCENTRATION[1]

Alain Rapaport * **Frédéric Mazenc** *
Jérôme Harmand **

* *UMR Analyse des Systèmes et Biométrie, INRA, 2 place Pierre Viala, 31060 Montpellier Cedex 1, France*
** *Laboratoire de Bitechnologie de l'Environnement, INRA, Avenue des étangs, 11100 Narbonne, France*

Abstract: In a recent work, a new regulator of the output of a continuous auto-catalytic bioprocess, by means of recirculation loop, has been presented. It was shown that controlling the recirculation flow rate allows the stabilization of the output in presence of an uncontrolled input flow rate. In the present paper, we extend this result when the input substrate concentration is unknown. For this purpose, we propose the design of an observer of the input concentration which, coupled with a slightly different control law reminiscent of the one used in the case where the input concentration is known, guarantees the regulation of the output.

Keywords: bioprocess, recirculation loop, output regulation, nonlinear control, unknown input observer.

1. INTRODUCTION

1.1 Context

In a recent work (cf. (Harmand *et al.*, 2005)), a new control law for regulating the output of a continuous auto-catalytic process was proposed. While most of the available studies of the literature use the input flow rate Q as the control variable, it was proposed to control the process through a recirculation loop. Among others, advantages are that no storage tank is needed anymore at the entrance of the process and that the flow rate has not to be known perfectly. The particular process configuration considered to do so is described in Fig. 1 where $\alpha \in [0, 1]$ and $\beta \geq 0$ are the manipulated variables.

[1] This work was supported by the french INRA-INRIA project "MERE".

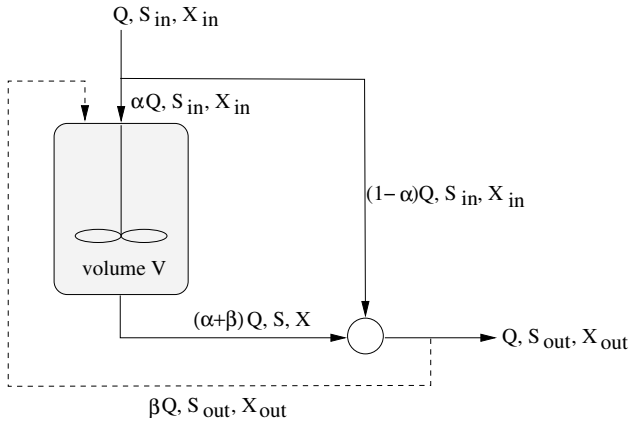

Fig. 1. General view of the bioprocess configuration under interest.

1.2 Modeling

The function $D(t) = Q(t)/V$ be given, the model of this system described in Figure 1 can be written as it follows:

$$\begin{aligned} \dot{X} &= \mu(S)X + uD(t)\,(X_{in} - X) \\ \dot{S} &= -\frac{\mu(S)}{Y}X + uD(t)\,(S_{in} - S) \end{aligned} \tag{1}$$

where S and X stand for the biomass and the substrate concentrations (in mg/l) in the reactor and $u = \frac{\alpha+\beta}{1+\beta} \in [0,1]$ is the control variable. $\mu(S)$ is the reaction rate (in t^{-1}), Y the conversion yield (in mg of substrate consumed by mg of biomass formed) and V the volume of the reactor (in l). All these quantities are assumed to be known.

S_{in} and X_{in} are the unknown input substrate and biomass concentrations (in mg/l), possibly time varying but bounded:

$$(X_{in}(t), S_{in}(t)) \in [\underline{X}_{in}, \overline{X}_{in}] \times [\underline{S}_{in}, \overline{S}_{in}],\ \forall t \geq 0,$$

where $\overline{X}_{in} \geq \underline{X}_{in} \geq 0$ and $\overline{S}_{in} \geq \underline{S}_{in} > 0$ are known numbers.

The control problem investigated in the paper is the regulation of the output

$$S_{out} = uS + (1-u)S_{in} \tag{2}$$

even though S_{in} is unknown. We consider a time-varying reference trajectory to be tracked, that we denote $S^\star_{out}(\cdot)$, and we introduce the following hypothesis.

Hypothesis H0. There exist numbers $\overline{S}^\star_{out} \geq \underline{S}^\star_{out} > 0$ such that $S^\star_{out}(t) \in [\underline{S}^\star_{out}, \overline{S}^\star_{out}]$ for all $t \geq 0$, with

$$\overline{S}^\star_{out} < \underline{S}_{in}\ .$$

1.3 Regulation of S_{out} when S_{in} is known

In this section, we recall the result we obtained when S_{in} is perfectly known (Harmand *et al.*, 2005). We introduce usual assumptions on the growth function $\mu(\cdot)$.

Hypothesis H1. The function $\mu(\cdot)$ is a non-negative Lipschitz continuous function with $\mu(0) = 0$ and $\mu(\underline{S}^\star_{out}) > 0$, that fulfills

$$\mu(S) \geq \mu(\underline{S}^\star_{out}), \quad \forall S \in [\underline{S}^\star_{out}, \overline{S}_{in}] \tag{3}$$

Contrary to usual approaches for which the input flow rate D is a manipulated variable, D is here imposed but we assume that it is bounded, with known bounds.

Hypothesis H2. There exist numbers $\underline{D} \leq \overline{D}$ and $T \geq 0$ such that $D(t) \in [\underline{D}, \overline{D}]$ for all $t \geq T$, with $\underline{D} > 0$ and

$$\overline{D} < \mu(\underline{S}^\star_{out}) \frac{\underline{X}_{in} + Y(\underline{S}_{in} - \underline{S}^\star_{out})}{Y(\overline{S}_{in} - \underline{S}^\star_{out})}\ . \tag{4}$$

Then we have the following result (cf. (Harmand *et al.*, 2005)):

Proposition 1. Assume H0-H1-H2 are satisfied by the system (1). Then for any initial condition such that $X(0) > 0$ and $0 \leq S(0) < \overline{S}_{in}$, the feedback

$$u^\star(t, S, S_{in}) = \frac{S_{in} - S^\star_{out}(t)}{S_{in} - \min(S^\star_{out}(t), S)} \tag{5}$$

drives the output $S_{out}(\cdot)$, defined in (2), at $S^\star_{out}(\cdot)$ in finite time.

On the one hand, it is supposed here that the substrate concentration S inside the reactor: it is the case in many biotechnological industries, in particular in those where the input characteristics are not well known (biological Wastewater Treatment Plants for instance). Here, we consider the problem of controlling such bioprocesses. On the other hand, the measurement of X is also necessary: as it will be seen, it is rather a technical requirement and it can be argued that this measurement can be difficult to obtain in practice (it is part of the perspectives to develop a version of the proposed controller that will not need the measurement of X). Finally, when dealing with these biosystems, S_{in} is usually considered as an unknown input. While the above results were valid when S_{in} is measured, we show in the remaining part of the paper how to construct an observer for S_{in} under some mild assumptions (Section 2). Then we show how to couple this estimation with the control law (5) to achieve the regulation of the output (Section 3). Simulation results are presented and discussed in Section 4 while conclusions and perspectives are drawn in Section 5.

2. INPUT CONCENTRATION OBSERVER

In most of known approaches, the regulation of the substrate concentration at the output of a bioprocess requires the knowledge of the substrate concentration at the input of the process (in a sense, most of the available nonlinear approaches, as for example the well known adaptive controller by (Bastin and Dochain, 1990), should be considered as feedforward-feedback controllers rather than as feedback controllers). However, a number of practical and economical reasons makes the measurement of the input substrate concentration a difficult task. Thus, for control as well as for monitoring and diagnosis purposes, an accurate

estimation of this exogenous input is appreciated. To our best knowledge, only very few approaches have been specifically proposed for estimating unknown input concentrations of biosystems (cf. (Aubrun *et al.*, 2001), (Sperandio and Queinnec, 2004), (Theilliol *et al.*, 2002) and (Theilliol *et al.*, 2003)).

We propose here a new observer, which is of interest by itself, independently of our control objective:

$$\begin{aligned}\dot{\widehat{S}} &= -\frac{\mu(S)}{Y}X + uD(t)(\widehat{S}_{in} - S) \\ &\quad + uD(t)(\theta+\theta^2)(S-\widehat{S}) \\ \dot{\widehat{S}}_{in} &= uD(t)\theta^3(S-\widehat{S})\end{aligned} \tag{6}$$

where $\theta > 1$ is a parameter to be tuned. The only assumption on the unknown function $S_{in}(\cdot)$ we require is to have a bounded first derivative.

Hypothesis H3. $S_{in}(\cdot)$ is differentiable and there exists $M < +\infty$ such that $|\dot{S}_{in}(t)| \leq M$, for any time t.

Proposition 2. Under Hypothesis H3, for any control law $u(\cdot)$ such that $\inf_{t\geq 0} u(t)D(t) = \gamma > 0$ and any non-negative initial conditions of (1)–(6) such that $\widehat{S}(0) = S(0)$ and $\widehat{S}_{in}(0) \in [\underline{S}_{in}, \overline{S}_{in}]$, then the estimation of S_{in} provided by (6) fulfills the following inequality, for any $t \geq 0$

$$\begin{aligned}|\widehat{S}_{in}(t) - S_{in}(t)| \leq \frac{2M}{\theta-1} \\ + \frac{\theta}{\theta-1}(\overline{S}_{in} - \underline{S}_{in})e^{-\gamma\theta t}.\end{aligned} \tag{7}$$

Remark 3. When the unknown S_{in} is constant ($M = 0$), the convergence (7) of the observer is exact. In face of unknown variations of $S_{in}(\cdot)$, the convergence (7) is practical (by practical, it is meant that, tuning parameters, one can ensure that the error variables enter an arbitrary small neighborhood of the origin).

Proof. Define the error variables $e_S = \widehat{S} - S$ and $e_{S_{in}} = \widehat{S}_{in} - S_{in}$, whose dynamics can straightforwardly be written as follows

$$\frac{d}{dt}\begin{bmatrix} e_S \\ e_{S_{in}} \end{bmatrix} = u(t)D(t)A\begin{bmatrix} e_S \\ e_{S_{in}} \end{bmatrix} - \begin{bmatrix} 0 \\ \dot{S}_{in} \end{bmatrix}$$

with

$$A = \begin{bmatrix} -\theta-\theta^2 & 1 \\ -\theta^3 & 0 \end{bmatrix}$$

One can easily check that the eigenvalues of A are $-\theta$ and $-\theta^2$. Remark also that due the choice of initial conditions of (6), one has

$$e_S(0) = 0, \quad |e_{S_{in}}(0)| \leq \overline{S}_{in} - \underline{S}_{in} \tag{8}$$

Consider the time parameterization

$$\tau := \int_0^t u(s)D(s)ds \geq \gamma t, \quad t \geq 0 \tag{9}$$

and define the function

$$\psi(\tau) = \frac{\frac{dS_{in}}{dt}(\tau)}{u(\tau)D(\tau)} \in \left[-\frac{M}{\gamma}, \frac{M}{\gamma}\right]. \tag{10}$$

This leads to write the dynamics

$$\frac{d}{d\tau}\begin{bmatrix} e_S \\ e_{S_{in}} \end{bmatrix} = A\begin{bmatrix} e_S \\ e_{S_{in}} \end{bmatrix} - \begin{bmatrix} 0 \\ \psi(\tau) \end{bmatrix} \tag{11}$$

Consider the change of variables

$$z_1 = \theta e_S - e_{S_{in}}, \quad z_2 = -\theta^2 e_S + e_{S_{in}}. \tag{12}$$

One can readily check that

$$\frac{dz_1}{d\tau} = -\theta z_1 + \psi(\tau), \quad \frac{dz_2}{d\tau} = -\theta^2 z_2 - \psi(\tau),$$

which implies the following inequalities, using (10)

$$|z_i(\tau)| \leq \frac{M}{\gamma\theta^i} + |z_i(0)|e^{-\theta^i\tau} \quad (i = 1, 2) \tag{13}$$

From equations (12) and (13), one obtains easily the inequality

$$|e_{S_{in}}(\tau)| \leq \frac{(\theta+\theta^{-1})\frac{M}{\gamma} + \theta^2(|z_1(0)| + |z_2(0)|)e^{-\theta\tau}}{\theta^2-\theta}$$

Finally, from (8), one has $|z_i(0)| \leq \overline{S}_{in} - \underline{S}_{in}$ ($i = 1, 2$), and the announced estimation of the error is guaranteed

$$|\widehat{S}_{in}(t) - S_{in}(t)| \leq \frac{2M}{\theta-1} + \frac{\theta}{\theta-1}(\overline{S}_{in} - \underline{S}_{in})e^{-\gamma\theta t}.$$

3. COUPLING THE OBSERVER WITH THE FEEDBACK CONTROL LAW

Let us first define the saturation function $sat_{[\underline{S}_{in}, \overline{S}_{in}]}$ as follows

$$sat_{[\underline{S}_{in}, \overline{S}_{in}]}(\sigma) = \max(\underline{S}_{in}, \min(\overline{S}_{in}, \sigma)).$$

Then, coupling the feedback law (5) with the observer (6) leads to the following result.

Proposition 4. Under Hypotheses H0-H1-H2-H3, for any initial condition $X(0) > 0$, $\widehat{S}(0) = S(0) \in [0, \overline{S}_{in}[$ and $\widehat{S}_{in}(0) \in [\underline{S}_{in}, \overline{S}_{in}]$, the dynamic output feedback law

$$\widetilde{u}^*(t, S, \widehat{S}_{in}) := u^*(t, S, sat_{[\underline{S}_{in}, \overline{S}_{in}]}(\widehat{S}_{in})) \tag{14}$$

where $u^*(\cdot)$ is defined in (5) and $\widehat{S}_{in}$ is given by (6) possesses the following property

$$\limsup_{t\geq 0} |S_{out}(t) - S^*_{out}(t)| \leq \Omega$$

with

$$\Omega = \frac{2M}{\theta - 1}\left(1 - \frac{\underline{S}_{in} - \overline{S}^*_{out}}{\overline{S}_{in}}\right).$$

Remark 5. Notice that $\widetilde{u}^*(\cdot)$ is well defined because of the saturation and Hypothesis H0.

Proof. From Hypothesis H1, it is immediate to check that the domain $\mathcal{D} = \Re^*_+ \times [0, \overline{S}_{in}[$ is invariant under the dynamics (1), for any non-negative control law $u(\cdot)$. Fix an initial condition $(X(0), S(0)) \in \mathcal{D}$ and denote $(X(\cdot), S(\cdot))$ the solution of system (1) with the dynamic output feedback (14). Denote also

$$\widetilde{u}(t) = \widetilde{u}^*(t, S(t), \widehat{S}_{in}(t))$$

Observe that from assumptions H0 and H2 one has the inequality

$$\widetilde{u}(t) \geq \underline{u} = (1 - \overline{S}^*_{out}/\underline{S}_{in}) > 0.$$

Consequently, there exists $T' > 0$ such that $S(t) \leq S^*_{out}(t)$ for any $t \geq T'$ (see Lemma 1 in Appendix). Posit $\widetilde{S}_{in}(t) = sat_{[\underline{S}_{in}, \overline{S}_{in}]}(\widehat{S}_{in}(t))$ and $\widetilde{e}_{S_{in}}(t) = \widetilde{S}_{in}(t) - S_{in}(t)$ and it follows, for any $t \geq T'$,

$$\begin{aligned} S_{out}(t) &= \frac{\widetilde{S}_{in}(t) - S^*_{out}(t)}{\widetilde{S}_{in}(t) - S(t)}(S(t) - S_{in}(t)) \\ &\quad + S_{in}(t) \\ &= S^*_{out}(t) \\ &\quad - \widetilde{e}_{S_{in}}(t) \underbrace{\left(1 - \frac{\widetilde{S}_{in}(t) - S^*_{out}(t)}{\widetilde{S}_{in}(t) - S(t)}\right)}_{\Gamma(t)} \end{aligned}$$

where $0 \leq \Gamma(t) \leq \overline{\Gamma} = 1 - (\underline{S}_{in} - \overline{S}^*_{out})/\overline{S}_{in}$. Then

$$|S_{out}(t) - S^*_{out}(t)| \leq |\widehat{S}_{in}(t) - S_{in}(t)|\overline{\Gamma}, \quad (15)$$

for all $t \geq T'$. Finally, notice that $u(t)D(t) \geq \gamma = \underline{u}\,\underline{D} > 0$, for $t \geq T$, and one conclude from Proposition 2:

$$|S_{out}(t) - S^*_{out}(t)| \to \left[0, \frac{2M}{\theta - 1}\overline{\Gamma}\right] \text{ as } t \to +\infty.$$

4. SIMULATIONS

Numerical simulations were performed using the control law presented here above, with a Monod growth function: $\mu(S) = \mu_{\max} S/(K_S + S)$. Variables S and X were measured online. The following model parameters were used: $\mu_{max} = 0.045$, $K_S = 10$, $Y = 0.05$, $V = 40$, D is the sum of a constant ($\bar{D} = 0.02\ 1/h$) and of three other signals:

i) a sinusoid of magnitude 0.0025 and of frequency 0.02,
ii) a sinusoid signal of magnitude 0.001 and of frequency 0.0002,
iii) a square signal of magnitude 0.0015 and of frequency 0.015.

Thus, at $t = 100$, a set point step was simulated. The input substrate concentration is measured and is built as follows. It consists of the sum of:

i) a constant equal to 475 mg/l
ii) a sinusoid of magnitude 25 and of frequency 0.01
iii) a sinusoid of magnitude 15 and of frequency 0.005

The objective is to regulate the output substrate concentration S_{out} between $S^\star_{out} = 30\ mg/l$ and 50 mg/l. First, it was verified that condition (4) holds given the extreme expected values of D, S_{in} and $S^\star_{out}$. The simulations were performed over

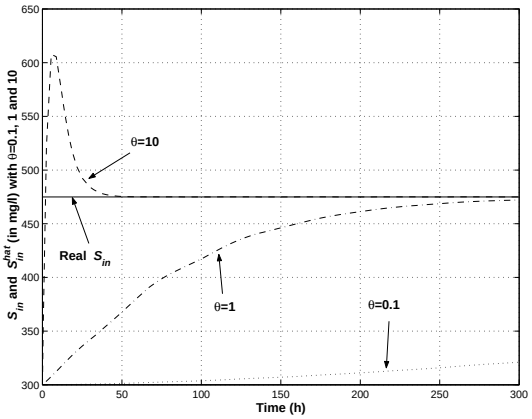

Fig. 2. S_{in} is an unknown constant: S_{in} and estimations with different values of θ.

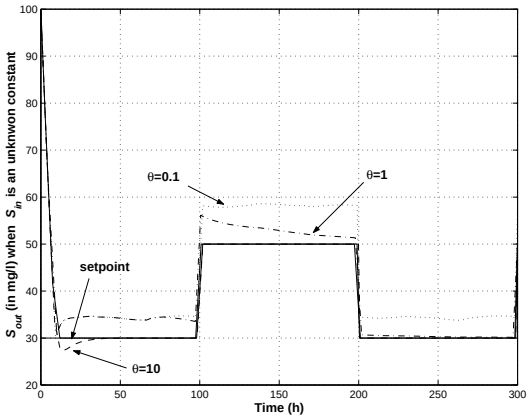

Fig. 3. S_{in} is an unknown constant: S_{out} with different estimations of S_{in}.

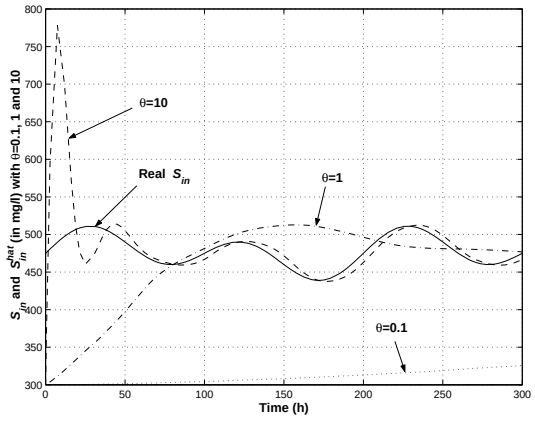

Fig. 4. S_{in} is time-varying: S_{in} and estimations with different values of θ.

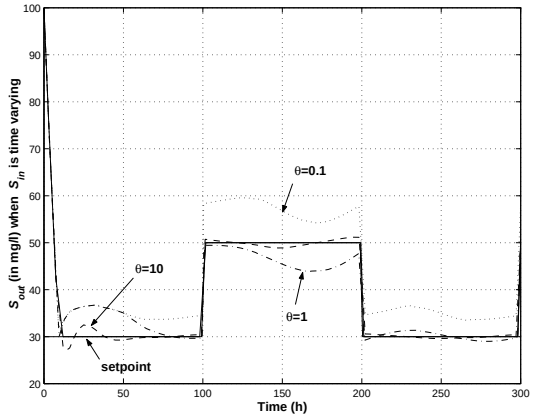

Fig. 5. S_{in} is time-varying: S_{out} with different estimations of S_{in}.

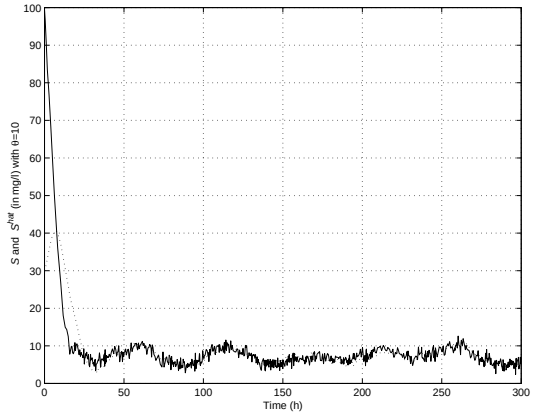

Fig. 6. S and $\hat{S}$ in presence of a measurement noise (S_{in} is time-varying).

a period of 300 hours. The results are shown in Figures 2 to 5.

Obviously, simulation results are in accordance with theoretical developments. It should be noticed that the regulation exhibits good performance whatever the case investigated: S_{in} constant (in this case, the convergence of the observer is exact) and S_{in} variable (in which case the convergence is practical).

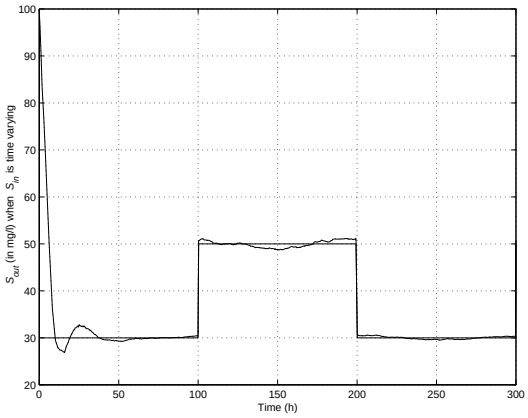

Fig. 7. S_{out} in presence of measurement noise on S (S_{in} is time-varying).

In presence of a 10 % measurement noise on S (cf. Figure 6), it can be seen in Figure 7 that the performance of the controller remains correct, even when S_{in} is time-varying.

5. CONCLUSIONS AND PERSPECTIVES

This paper proposed a new observer of an unknown input substrate concentration. It was shown that it exhibits an exact convergence property if S_{in} is constant while it is practical when S_{in} is time varying a bounded first derivative. The coupling of this estimator to a control law first proposed in (Harmand *et al.*, 2005), allows us to track any bounded reference trajectory. However, it should be stressed that, while in its original form only S and S_{in} were necessary, in the present paper, the measurement of S and X are required. Thus, extension of the present approach to cases where X is unmeasured is under investigation.

6. APPENDIX

Lemma 6. Under Hypotheses H0-H1-H2, for any initial condition $(X(0), S(0)) \in \Re_+^* \times [0, \overline{S}_{in}[$ and any control law such that $\underline{u} = \inf_{t\geq 0} u(t) > 0$, S stays below $\underline{S}_{out}^*$ after a finite time.

Proof. From Hypothesis H1, we immediately deduce that the domain $\Re_+^* \times [0, \overline{S}_{in}[$ is invariant by the dynamics (1), for any non-negative control law $u(\cdot)$. Make the change of variable $(S, Z) = (S, X + YS)$:

$$\begin{aligned} \dot{S} = F(t,S,Z) &= u(t)D(t)(S_{in}(t) - S) \\ &\quad -\frac{\mu(S)}{Y}(Z - YS) \\ \dot{Z} &= -u(t)D(t)(Z - Z_{in}(t)) \end{aligned}$$

where $Z_{in} = X_{in} + YS_{in}$. Remark that, for any $t \geq 0$, $Z_{in}(t) \in [\underline{Z}_{in}, \overline{Z}_{in}]$, where $\underline{Z}_{in} =$

$\underline{X}_{in} + Y\underline{S}_{in}$ and $\overline{Z}_{in} = \overline{X}_{in} + Y\overline{S}_{in}$. Thus, from $u(t)D(t) \geq \underline{u}\,\underline{D} > 0$, we infer that $Z(t)$ converges exponentially towards $[\underline{Z}_{in}, \overline{Z}_{in}]$.

Remark that $S \in [\underline{S}^*_{out}, \overline{S}_{in}[$ implies the following inequality, for any $t \leq T$

$$F(t,S,Z) \leq (\overline{D} - \mu(\underline{S}^\star_{out}))(\overline{S}_{in} - S) - \frac{\mu(S)}{Y}(\underline{Z}_{in} - Y\overline{S}_{in}) + \frac{\mu(S)}{Y}(\underline{Z}_{in} - Z) \quad (16)$$

At $S = \underline{S}^*_{out}$, one has

$$F(t,\underline{S}^*_{out},Z) \leq -\delta + \frac{\mu(\underline{S}^*_{out})}{Y}(\underline{Z}_{in} - Z)$$

where $\delta = \mu(\underline{S}^\star_{out})(\underline{Z}_{in} - Y\underline{S}^\star_{out})/Y - \overline{D}(\overline{S}_{in} - \underline{S}^\star_{out})$ (notice that condition (4) ensures $\delta > 0$). But the convergence of Z towards the interval $[\underline{Z}_{in}, \overline{Z}_{in}]$ implies the existence of $T_1 \geq T$ such that

$$F(t,\underline{S}^*_{out},Z) \leq -\frac{\delta}{2} < 0, \quad t \geq T_1$$

Then, the existence of a finite time $T_2 \geq T_1$ such that $S(T_2) \leq \underline{S}^*_{out}$ implies that the variable $S(t)$ stays below $\underline{S}^*_{out}$ for any future time $t \geq T_2$. We show now that such a time T_2 necessarily exists.

If such a time T_2 does not exist, then $S(t) > \underline{S}^*_{out}$ for any $t \geq T_1$. We distinguish three cases:

Case 1. $\underline{Z}_{in} > Y\overline{S}_{in}$ and $\overline{D} \leq \mu(\underline{S}^\star_{out})$ (note that condition (4) is necessarily fulfilled), then from (16) and the convergence of $Z(\cdot)$ towards $[\underline{Z}_{in}, \overline{Z}_{in}]$, we deduce the existence of $T_3 \geq T_1$ such that

$$F(t,S,Z(t)) \leq -\frac{1}{2}\frac{\mu(\underline{S}^\star_{out})}{Y}(\underline{Z}_{in} - Y\overline{S}_{in}) < 0$$

for all $t \geq T_3$. We conclude that $S(\cdot)$ reaches $\underline{S}^\star_{out}$ in finite time, thus a contradiction.

Case 2. If $\underline{Z}_{in} > Y\overline{S}_{in}$ and $\overline{D} > \mu(\underline{S}^\star_{out})$, we obtain the following inequality from (16) and (4)

$$F(t,S,Z) \leq -\delta + \frac{\mu(S)}{Y}(\underline{Z}_{in} - Z)\ .$$

The asymptotic properties of $Z(\cdot)$ allow then to write

$$F(t,S,Z(t)) \leq -\frac{\delta}{2} < 0, \quad t \geq T_3'$$

for a certain $T_3' \geq T_1$. Thus we obtain again a contradiction.

Case 3. If $\underline{Z}_{in} \leq Y\overline{S}_{in}$, then condition (4) ensures $\overline{D} < \mu(\underline{S}^\star_{out})$. One can then write, from (1) and (3), the following inequalities for all $t \geq T_1$

$$\begin{aligned}\dot{X} &\geq (\mu(\underline{S}^\star_{out}) - \overline{D})X\ ,\\ \dot{S} &\leq -(\mu(\underline{S}^\star_{out}) - \overline{D})\frac{X}{Y} + \frac{\overline{D}}{Y}(Y\overline{S}_{in} - \underline{Z}_{in}) + \frac{\overline{D}}{Y}(\underline{Z}_{in} - Z(t)).\end{aligned}$$

Since $X(T_1)$ is positive, $X(\cdot)$ is increasing, and there exist $\gamma > 0$, $T_1' \geq T_1$ such that $(\mu(\underline{S}^\star_{out}) - \overline{D})X(t) > \overline{D}(Y\overline{S}_{in} - \underline{Z}_{in}) + \gamma$ for all $t \geq T_1'$. From the convergence of $Z(\cdot)$, we deduce that there exists $T_3'' \geq T_1'$ such that

$$\dot{S}(t) \leq -\frac{\gamma}{2Y} < 0, \quad t \geq T_3''$$

that leads again to a contradiction.

REFERENCES

Aubrun, C., D. Theilliol, J. Harmand and J.P. Steyer (2001). Software sensor design for cod estimation in an anaerobic fluidized bed reactor. *Water Science and Technology* **43**, 115–122.

Bastin, G. and D. Dochain (1990). *On-Line Estimation and Adaptive Control of Bioreactors*. Elsevier.

Harmand, J., A. Rapaport and F. Mazenc (2005). About feedback stabilization of continuous bioprocesses through recirculation. In: *16th IFAC World Congress*. Prague.

Sperandio, M. and I. Queinnec (2004). On-line estimation of wastewater nitrifiable nitrogen, nitrification and denitrification rates using orp and do dynamics. *Water Science and Technology* **49**, 31–38.

Theilliol, D., C. Aubrun, J.C. Ponsart and J. Harmand (2002). On line estimation of unmeasured inputs for anaerobic process based on a multiple model scheme. In: *b'02 IFAC World Congress*. Barcelona, Spain.

Theilliol, D., J.C. Ponsart, J. Harmand, C. Join and P. Gras (2003). On line estimation of unmeasured inputs for anaerobic wastewater treatment processes. *Control Engineering Practice* **11**, 1007–1019.

Session 2.2

Batch Processes

Fault Detection and Diagnosis in Industrial Fed-Batch Cell Culture

J. C. Gunther, D. E. Seborg and J. S. Conner
University of California, Santa Barbara

Batch Process Monitoring using Multiblock Multiway Principal Component Analysis

S. Perk and A. Cinar
Illinois Institute of Technology

2D Model Predictive Iterative Learning Control Schemes for Batch Processes

J. Shi, F. Gao and T. J. Wu
Hong Kong University of Science and Technology

Scale-Up of Batch Processes via Decentralized Control

A. Marchetti, D. Bonvin and M. Amrhein
Ecole Polytechnique Fédérale de Lausanne

Real-Time Dynamic Optimization of Non-Linear Batch Systems

N. Peters, M. Guay and D. DeHaan
Queen's University

ADCHEM 2006

International Symposium on Advanced Control of Chemical Processes
Gramado, Brazil – April 2-5, 2006

FAULT DETECTION AND DIAGNOSIS IN INDUSTRIAL FED-BATCH CELL CULTURE

Jon C. Gunther * **Dale E. Seborg** *
Jeremy S. Conner **

* *Department of Chemical Engineering, University of California, Santa Barbara*
** *Amgen, Inc., Thousand Oaks, California*

Abstract: *Multivariate statistical process monitoring* techniques are applied to pilot-plant, cell culture data for the purpose of fault detection and diagnosis. Data from 23 batches, 20 *normal operating conditions* (NOC) and three abnormal, were available. A PCA model was constructed from 19 NOC batches, while the remaining NOC batch was used for model validation. Subsequently, the model was used to successfully detect (both offline and online) abnormal process conditions and to diagnose the root causes.

Keywords: Monitoring, cell culture processes, batch control, process control, biocontrol, biotechnology, multivariable systems

1. INTRODUCTION

Protein production cell culture has progressed significantly in recent years and is now a major source of industrially produced therapeutic agents. Because this process is sensitive to environmental conditions, successful cell culture requires precise maintenance of critical process variables (e.g., temperature, pH, and dissolved oxygen). In addition, the pharmaceutical industry is under increasing governmental pressure, such as the *Process Analytical Technology* (PAT) initiative (U.S. Food and Drug Administration, 2004), to reduce process variability.

Data-driven monitoring approaches, such as *Principal Component Analysis* (PCA), have proven to be an effective method for detecting abnormal process conditions and reducing process variability (Kourti, 2005). A particularly valuable feature of PCA is its compatibility with many of the methods available in *multivariate statistical process control* (MSPC). This statistical methodology provides a means to detect the appearance, magnitude, and duration of a process fault that causes a process to depart from proper operation (Cinar *et al.*, 2003). Also, the source of the fault can be diagnosed, assuming that the fault is observable from process data.

The objective of this research is to apply PCA and MSPC to industrial fed-batch cell culture data (courtesy of Amgen, Inc.) in an attempt to detect and diagnose abnormal process conditions using both offline and online analysis. These abnormal conditions were indicated during discussion with Amgen engineers.

2. BACKGROUND

Consider a batch process, where J process variables are measured at K instances of time. In batch MSPC applications, it is assumed that I batches conducted at *normal operating conditions* (NOC) are available for the development of a PCA model. These data are typically represented in a three-dimensional data array $\underline{\mathbf{X}}$ $(I \times J \times K)$.

For standard PCA analysis, three-dimensional array data are *unfolded* into a two-dimensional matrix. Several groups have evaluated different unfolding strategies (Nomikos and MacGregor, 1995; Wold *et al.*, 1998). The two primary unfolding techniques preserve either the I direction (i.e., batches) or the J direction (i.e., variables) of the data. For variable-wise unfolding (i.e., unfolding the data into $\mathbf{X}$ $(IK \times J)$), the nonlinear, time-varying trajectories of these data are preserved (Westerhuis *et al.*, 1999). Because batch-wise unfolding avoids this complication, it was chosen for this research. Hence, $\underline{\mathbf{X}}$ was unfolded into a matrix $\mathbf{X}$ $(I \times JK)$, such that each $I \times J$ slice is located side by side, starting with the first sampling instant. Subsequently, these data were *autoscaled* (i.e., the columns of $\mathbf{X}$ were mean-centered and scaled to unit variance) in an attempt to remove the dominance of large magnitude measurements and the nonlinear trajectories of the data from the PCA model.

For PCA $\mathbf{X}$ is expressed as the summation of the product of a score matrix $\mathbf{T}$ $(I \times A)$ and a transposed loadings matrix $\mathbf{P}^{'}$ $(A \times JK)$ plus a residual matrix $\mathbf{E}$ $(I \times JK)$, where A denotes the number of principal components, which is typically selected through a process of cross-validation (Wold, 1978):

$$\mathbf{X} = \mathbf{T}\mathbf{P}^{'} + \mathbf{E} \tag{1}$$

A major advantage of PCA modeling is its ability to compare new batch data, $\mathbf{x}_{new}$ $(1 \times JK)$, to the NOC data in a systematic fashion. PCA achieves this comparison by projecting this new data set on the PCA model generated from NOC data in order to determine the new batch scores, $\mathbf{t}_{new}$ $(1 \times A)$:

$$\mathbf{t}_{new} = \mathbf{x}_{new}\mathbf{P}(\mathbf{P}^{'}\mathbf{P})^{-1} \tag{2}$$

2.1 Offline Monitoring

For offline PCA analysis, Eq. 2 can be used to calculate $\mathbf{t}_{new}$. Note that $\mathbf{P}^{'}\mathbf{P}$ is by definition the identity matrix due to the orthonormality of $\mathbf{P}$ (Nomikos and MacGregor, 1995). After determining $\mathbf{t}_{new}$, Eq. 3 can be used to calculate the new batch residual, $\mathbf{e}_{new}$ $(1 \times JK)$.

$$\mathbf{e}_{new} = \mathbf{x}_{new} - \mathbf{t}_{new}\mathbf{P}^{'} \tag{3}$$

Two statistical metrics are widely used to monitor disparities between the new batch and the NOC batches. *Hotelling's* T^2 statistic captures differences in the systematic part of the PCA model (i.e., $\mathbf{T}\mathbf{P}^{'}$). It is defined as follows:

$$T^2_{new} = \mathbf{t}_{new}(\mathbf{S})^{-1}\mathbf{t}^{'}_{new} \tag{4}$$

$$\mathbf{S} = \frac{\mathbf{T}^{'}\mathbf{T}}{I-1} \tag{5}$$

where $\mathbf{S}$ is the covariance matrix of the model score matrix, $\mathbf{T}$, (cf. Eq. 1) and I is the number of NOC batches. If the $\mathbf{X}$ data are from a multivariate normal distribution, T^2 follows an F distribution and α confidence limits can be calculated accordingly (Westerhuis *et al.*, 2000):

$$T^2_{\alpha} = \frac{A(I^2-1)}{I(I-A)}F_{A,I-A,\alpha} \tag{6}$$

A second metric, the *Sum of Squared Residuals* Q, captures the information in the residuals,

$$Q_{new} = \mathbf{e}_{new}\mathbf{e}^{'}_{new} \tag{7}$$

where Q_{new} is assumed to be χ^2 distributed. A method for approximating α confidence limits based upon this assumption (Jackson and Mudholkar, 1979) is used in this paper:

$$\begin{aligned} Q_{\alpha} &= \theta_1[1 - \frac{\theta_2 h_0(1-h_0)}{\theta_1^2} + \\ &\quad \frac{z_{\alpha}(2\theta_2 h_0^2)^{1/2}}{\theta_1}]^{1/h_0} \\ \mathbf{V} &= \frac{\mathbf{E}\mathbf{E}^{'}}{I-1} \\ \theta_i &= trace(\mathbf{V}^i) \text{ for } i = 1, 2, \text{ and } 3 \\ h_0 &= 1 - \frac{2\theta_1\theta_3}{3\theta_2^2} \end{aligned} \tag{8}$$

2.2 Online Monitoring

From an operational perspective, it is preferable to monitor the batch online, as it progresses, so that corrective or terminative action can be taken in a timely manner. However, to evaluate process data from a new batch using Eqs. 2-8, the new batch is required to have the same number of columns as the NOC data (i.e., JK columns). This is not possible when the batch is incomplete and thus future measurements are missing from the new batch (i.e., $\mathbf{x}_{new}$ only has Jk columns where $k \leq K$). For the unfinished new batch, the missing future data must be estimated in order to proceed. Several solutions to this problem have been proposed and evaluated (Nomikos and MacGregor, 1995). The *PCA Projection* method is used in this paper. It only uses the portion of the loading matrix corresponding to the elapsed time period until the current sampling instant k to calculate the new score vector, $\mathbf{t}_{new}(k)$ $(1 \times Jk)$:

$$\mathbf{t}_{new}(k) = \mathbf{x}_{new,1:Jk}\mathbf{P}_{1:Jk}(\mathbf{P}^{'}_{1:Jk}\mathbf{P}_{1:Jk})^{-1} \tag{9}$$

For online monitoring, the term $\mathbf{P}^{'}_{1:Jk}\mathbf{P}_{1:Jk}$ in Eq. 9 is not necessarily identity until $k = K$. At

sample k, $\mathbf{e}_{new}(k)$ and $T^2_{new}(k)$ can be evaluated in a manner similar to Eqs. 3 and 4 noting that $T^2_{new}(k)$ is calculated from a time-varying scores covariance matrix, $\mathbf{S}(k)$. To monitor the residuals, the *Squared Prediction Error*, $SPE_{new}(k)$, was utilized:

$$SPE_{new}(k) = \sum_{j=1}^{J} \mathbf{e}_{new,jk}(k)^2 \tag{10}$$

Another significant benefit of PCA is its ability to determine process variable contributions from $T^2_{new}(k)$ and $SPE_{new}(k)$. These contributions can then be used for fault diagnosis. For online monitoring, the contributions can be calculated in the following manner (Westerhuis *et al.*, 2000):

$$C_{T^2_{jk}} = \sum_{a=1}^{A} \mathbf{S}^{-1}_{k,aa} \mathbf{t}_{new,a}(k) \mathbf{x}_{new,jk} \mathbf{P}_{jk,a} \tag{11}$$

$$C_{SPE_{jk}} = \mathbf{e}_{new,jk}(k)^2 \tag{12}$$

where $\mathbf{S}_{k,aa}$ is the ath diagonal element of the time-varying covariance matrix and the subscripts j and k represent a single process variable and a single sampling instant, respectively. Confidence limits for $C_{SPE_{jk}}$ are determined in the same way as for $SPE_{new}(k)$. However, confidence limits for $C_{T^2_{jk}}$ are calculated in a *jackknife* procedure. In this approach, each NOC batch is omitted in a sequential manner and contributions for each batch are calculated. The estimated mean and standard deviation are then used as 3σ limits (Westerhuis *et al.*, 2000).

3. PROCESS DESCRIPTION

The fed-batch cell culture experiments were performed at Amgen Process Development. A controlled environment within the reactor was maintained with cascaded PID feedback loops for DO and pH. The key process variables used in this PCA research are summarized in Table 1.

Data for 23 batches were available. These batches were all conducted at nearly identical process conditions and possessed approximately equal time duration. NOC batches 1-19 were used in PCA model development, while NOC batch 20 was used for model validation and batches 21-23 were used for detection of abnormal situations. Amgen personnel categorized batches 21-23 as abnormal due to irregular thermal heating (21), DO controller problems (22), and agitator problems that led to a future device failure (23).

Table 1. Process variable measurements used in the PCA model.

Variable	Abbreviation
Agitation	AG
Agitation controller output	AGc
Inlet air flow	AF
Inlet air flow controller output	AFc
Inlet CO_2 flow	CO2
Inlet CO_2 flow controller output	CO2c
Dissolved oxygen	DO
Dissolved oxygen controller output	DOc
Inlet O_2 flow	O2
Inlet O_2 flow controller output	O2c
Vessel temperature	T
Vessel temperature controller output	Tc
pH	pH
pH controller output	pHc

4. RESULTS

A PCA model was constructed using NOC batches 1-19 data for the 14 process variables in Table 1. Cross-validation was performed in order to select an appropriate number of principal components, three.

To evaluate the ability of the PCA model to detect process abnormalities and reject false positives, overall batch T^2 and Q values were determined (see Figs. 1 and 2). It is clear that abnormal batches 21-23 exceed the 99% confidence limits for Q, while NOC validation batch 20 does not.

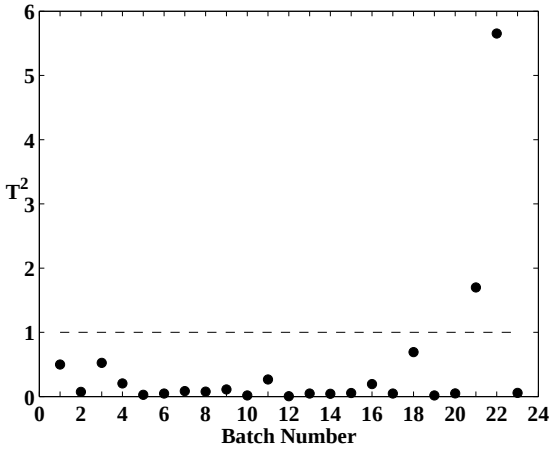

Fig. 1. Overall batch T^2. Batches 1-19 were calibration, batch 20 was validation, and batches 21-23 were abnormal. The dashed line denotes the 99% confidence limits.

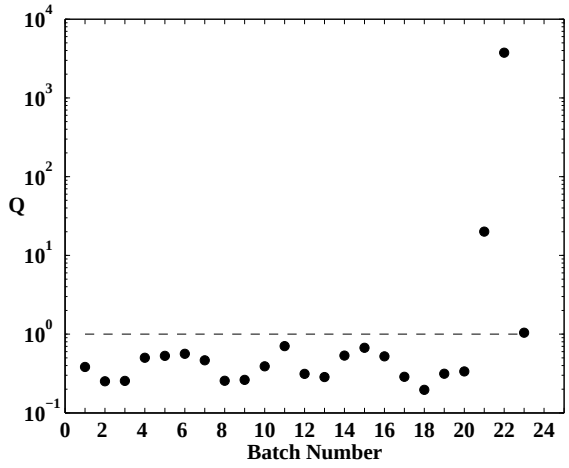

Fig. 2. Overall batch Q. Note that a semilog scale is used. Batches 1-19 were calibration, batch 20 was validation, and batches 21-23 were abnormal. The dashed line denotes the 99% confidence limits.

From an operational perspective, it is desirable to detect the onset of abnormal operation before the batch is finished. To fulfill this objective, online $T^2(k)$ and $SPE(k)$ were calculated. In Figure 3 the results for validation batch 20 are displayed. The $T^2(k)$ confidence limit is not violated, while the seven $SPE(k)$ confidence limit violations that occur are not exceptional for 1966 samples.

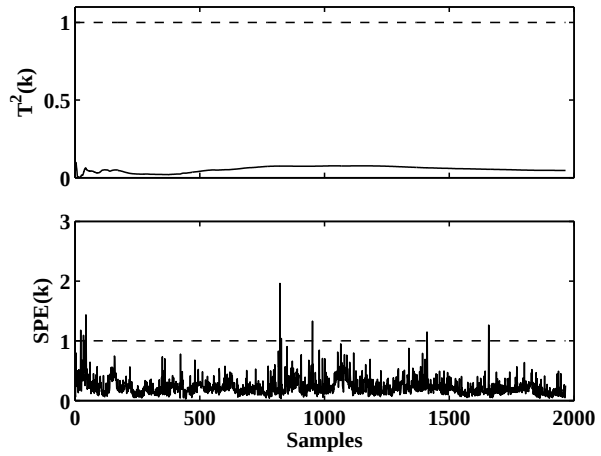

Fig. 3. Online normalized $T^2(k)$ and $SPE(k)$ for batch 20. The dashed lines denote the 99% confidence limits.

In Figure 4 it is evident that the $SPE(k)$ confidence limits are violated for batch 21 for the entire duration of the batch, while a sustained $T^2(k)$ violation occurs for all samples $k < 1100$. To diagnose the cause of this abnormal situation, a contribution plot (Fig. 5) was generated and identifies the temperature controller output as being the major source of abnormal process conditions. From inspection of the vessel temperature controller output (Tc) time-series data in Figure 6, it is clear that batch 21 is abnormal in comparison to the average NOC batch trajectory for batch 21. Amgen engineers indicated that for batch 21 the reactor possessed a unique thermal heating jacket that resulted in elevated Tc values.

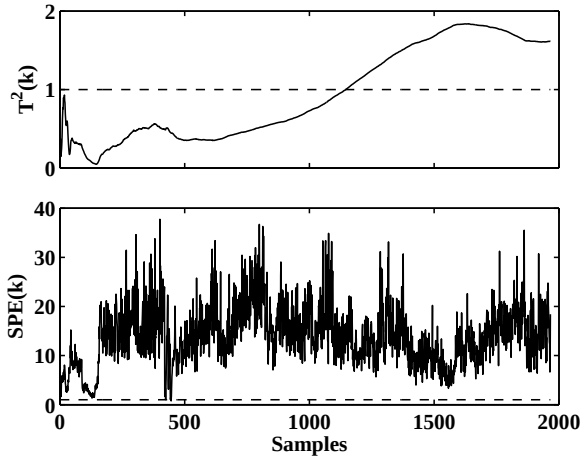

Fig. 4. Online normalized $T^2(k)$ and $SPE(k)$ for batch 21. The dashed lines denote the 99% confidence limits.

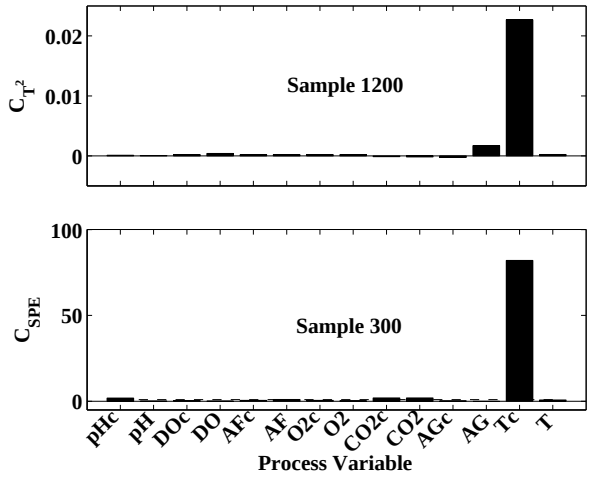

Fig. 5. Process variable contributions to online $T^2(k)$ and $SPE(k)$ at designated samples for batch 21.

For batch 22 the $T^2(k)$ and $SPE(k)$ confidence limits in Figure 7 are violated from the onset of the batch. From the contribution plot in Figure 8, it is obvious that DO was abnormal in both the score and residual spaces. Figure 6 reveals that for the early period of operation ($k < 700$) the DO values were indeed large in comparison to the average NOC batch trajectory.

For batch 23 the abnormal process conditions are more difficult to detect. An abnormally large number of confidence limit violations occur for $SPE(k)$ in Figure 9, but none occur for $T^2(k)$. However, in Figure 10 the contribution plot clearly indicates abnormal agitation. In Figure 6 batch

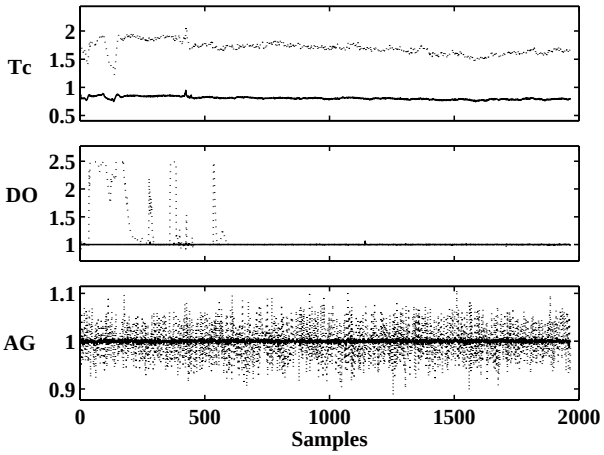

Fig. 6. Time-series plots for process variables most affected by abnormal process conditions for batches 21 (top), 22 (middle), and 23 (bottom). Solid line represents average NOC batch trajectory, while the dotted line represents the particular batch.

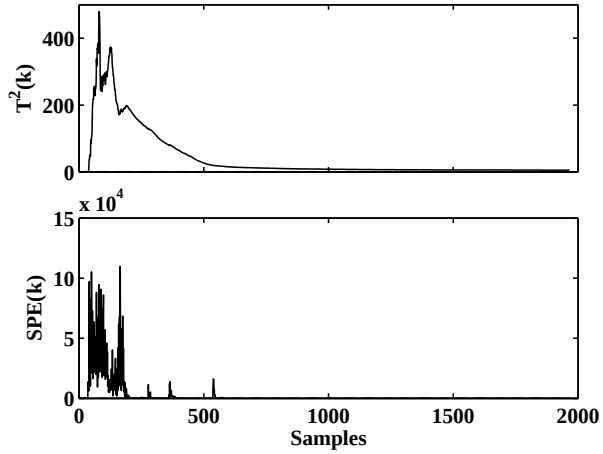

Fig. 7. Online normalized $T^2(k)$ and $SPE(k)$ for batch 22. The dashed lines denote the 99% confidence limits.

23 appears to possess considerably more agitation variation than the average batch trajectory. Amgen engineers reported that the agitator for this reactor failed during the next period of operation.

5. CONCLUSIONS

In this paper, MSPC and PCA techniques are applied to industrial fed-batch cell culture data. It was shown that a PCA model can successfully detect abnormal process conditions resulting from differences in the equipment (batch 21), operational issues (batch 22), and imminent device failure (batch 23). Analysis of contribution plots indicated that abnormal Tc levels, elevated DO values, and large agitation variation were the major sources of abnormal process conditions

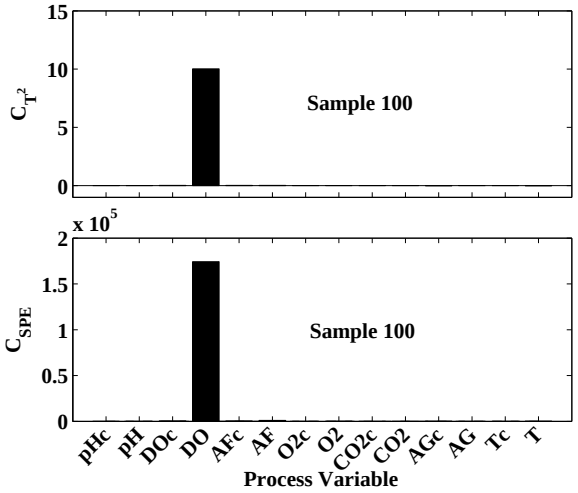

Fig. 8. Process variable contributions to online $T^2(k)$ and $SPE(k)$ at designated samples for batch 22.

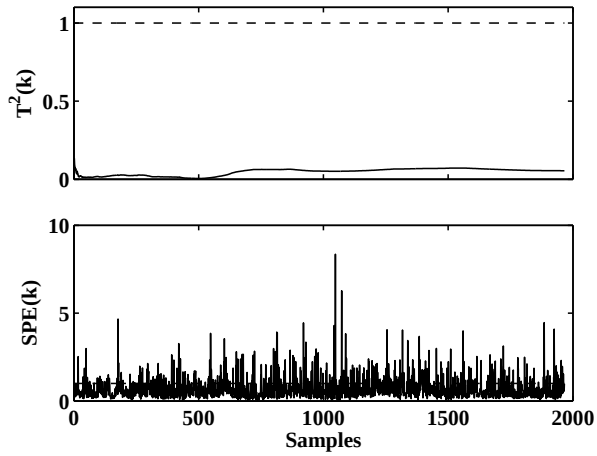

Fig. 9. Online normalized $T^2(k)$ and $SPE(k)$ for batch 23. The dashed lines denote the 99% confidence limits.

found in batches 21, 22, and 23 respectively. The PCA explanation of these process abnormalities is consistent with the process behavior reported by Amgen engineers.

ACKNOWLEDGEMENTS

Financial and technical support provided by Amgen, Inc. is gratefully acknowledged.

REFERENCES

Cho, H.-W. and K.-J. Kim (2003). A method for predicting future observations in the monitoring of a batch process. *J. Qual. Tech.* **35**(1), 59–69.

Cinar, A., S. J. Parulekar, C. Ündey and G. Birol (2003). *Batch Fermentation: Modeling, Monitoring, and Control.* Marcel Dekker. New York.

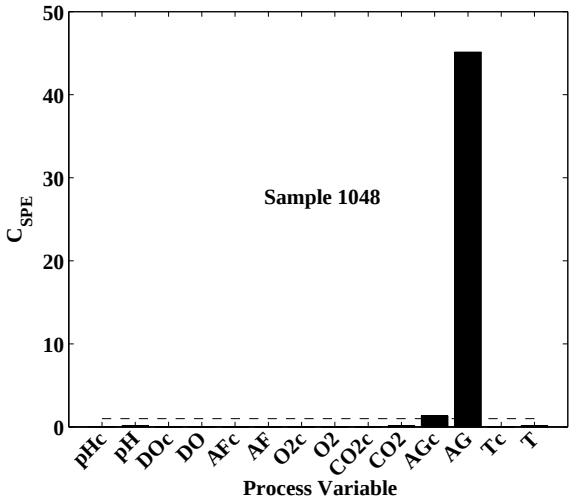

Fig. 10. Process variable contributions to online $T^2(k)$ and $SPE(k)$ at designated samples for batch 23.

Jackson, J. E. and G. S. Mudholkar (1979). Control procedures for residual associated with principal component analysis. *Technometrics* **21**(3), 341–349.

Kourti, T. (2005). Application of latent variable methods to process control and multivariate statistical process control in industry. *Internat. J. Adapt. Control Signal Process.* **19**, 213–246.

Nomikos, P. and J. F. MacGregor (1995). Multivariate SPC charts for monitoring batch processes. *Technometrics* **37**(1), 41–59.

U.S. Food and Drug Administration (2004). Guidance for industry PAT: A framework for innovative pharmaceutical development, manufacturing, and quality assurance.

Vinci, V. A. and S. R. Parekh (2003). *Handbook of Industrial Cell Culture*. Humana Press. Totowa, New Jersey.

Westerhuis, J. A., S. P. Gurden and A. K. Smilde (2000). Generalized contribution plots in multivariate statistical process monitoring. *Chemom. Intell. Lab. Syst.* **51**, 95–114.

Westerhuis, J. A., T. Kourti and J. F. MacGregor (1999). Comparing alternative approaches for multivariate statistical analysis of batch process data. *J. Chemometrics* **13**, 397–413.

Wold, S. (1978). Cross-validatory estimation of the number of components in factor and principal components models. *Technometrics* **20**(4), 397–405.

Wold, S., N. Kettaneh, H. Fridén and A. Holmberg (1998). Modelling and diagnostics of batch processes and analogous kinetic experiments. *Chemom. Intell. Lab. Syst.* **44**, 331–340.

ADCHEM 2006

International Symposium on Advanced Control of Chemical Processes
Gramado, Brazil – April 2-5, 2006

BATCH PROCESS MONITORING USING MULTIBLOCK MULTIWAY PRINCIPAL COMPONENT ANALYSIS

Sinem Perk * **and Ali Çınar** *

* *Illinois Institute of Technology, Department of Chemical and Environmental Engineering, 10 West 33rd Street, Chicago, IL, 60616, USA*

Abstract: Batch process monitoring to detect the existence and magnitude of changes that cause a deviation from the normal operation has gained considerable attention in the last decade. There are some batch processes that occur as a single step, whereas many others include multiple phases due to operational or phenomenological regimes or multiple stages where different processing units are employed. Having a single model for all different phases/stages with different covariance structures may not give a sufficient explanation of the system behavior and fault detection and diagnosis can be more challenging with increasing model size. Multiblock methods have been recently proposed to improve the capabilities of the existing statistical monitoring models. In this study, a multiblock algorithm based on concensus principal component analysis is applied to the benchmark fed-batch penicillin fermentation simulator data. The results of a static multiblock model and a sliding window multiblock model are compared. The need for data synchronization, and the effect of block size are discussed. Multiblock multiway principal component analysis methods are found to be effective in fault detection and localization.

Keywords: Batch monitoring, Fault detection and diagnosis, Multiblock models

1. INTRODUCTION

As the importance of batch processes in chemical and biotech process industries has increased in recent years, different modeling, monitoring, diagnosis and control techniques have been proposed by researchers. Since batch data has an additional dimension of batch number, the existing statistical control models, namely principal component analysis (PCA) and partial least squares (PLS) have been improved to account for the additional batch dimension. Nomikos and MacGregor (1994) and Kourti *et al.* (1995) presented process analysis, monitoring and diagnosis procedures based on multiway PCA and multiway PLS methods (Nomikos and MacGregor, 1995*b*), which are widely adopted by the chemical industry. To account for the multistage/ multiphase batch processes multiblock methods based on PCA and PLS have been developed. Valuable information about the multiblock methods is available in the literature. A good summary and comparison of the popular multiblock methods is provided (Smilde *et al.*, 2003). In addition, these algorithms have been applied to monitoring, fault detection and diagnosis of continuous processes and new definitions for control limits for multiblock algorithms have been developed (Qin *et al.*, 2001). MacGregor *et al.* (1994) applied multiblock PLS methods on a multisection tubular reactor for the production of low density polyethylene and Kourti *et al.* (1995) divided the process variables into multiple blocks

and simultaneously related to the quality variables. A batch monitoring algorithm based on hierarchical PCA was proposed and evaluated on an industrial batch polymerization process (Rännar *et al.*, 1998). In their work, variables from each time slot are blocked in the corresponding time block, resulting in as many blocks as the batch time points. Another application of multiblock PCA algorithm is presented, where, an adaptive multiblock PCA for the monitoring of a sequencing batch reactor was proposed (Lee and Vanrolleghem, 2003). In this work, multiblock PCA based on consensus PCA is applied to a multiphase penicillin fermentation process. Monitoring, fault detection and diagnosis using a multiblock algorithm is studied.

2. MULTIWAY MONITORING

2.1 Principal Component Analysis (PCA) and Concensus PCA

PCA is a multivariable statistical technique that can extract the essential information from a data set reported as a single block of data such as process measurements. PCA decomposes the data matrix into a score matrix times a loading matrix plus a residual matrix. This decomposition is useful to explain the information contained in the data using fewer dimensions. In the PCA computations, mostly the SVD algorithms for simultaneous or the NIPALS algorithm for sequential computation of the dominant principal components is used (Wold *et al.*, 1987).

The consensus PCA algorithm for multiple blocks, based on a series of NIPALS steps is given in (Westerhuis *et al.*, 1998). The method was introduced to compare several blocks of variables measured on the same objects. The data are divided into B blocks. A column of one of the block is selected as a starting super score and this vector is regressed on all block data to find the block loadings, from which the block scores for all blocks are calculated. All block scores are augmented in a super block. The super score is then regressed on the super block to give the super weight. The super weight is normalized and used to calculate a new super score vector. If this new super scores converges to a predefined criteria, the iteration stops. Then, each block is deflated using the super scores and the procedure repeats for the next principal component dimension. Otherwise, the iteration continues until the super score vector converges. For monitoring purposes, the statistics can be calculated for both the super level and for lower block level.

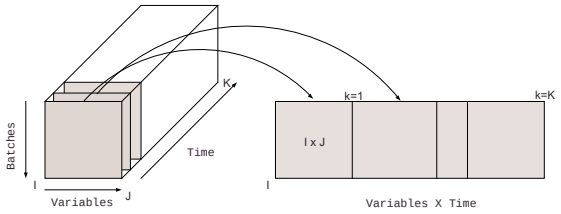

Fig. 1. Batch data representation and unfolding process.

2.2 Multiway Principal Component Analysis

Batch processes usually generate three-way data X ($I \times J \times K$), where I is the number of batches, J is the number of variables and K is the number of sampling times in a batch. MPCA is equivalent to performing ordinary PCA on an unfolded and properly scaled two-way array. Unfolding of the batch data can be done in six possible ways. For instance, each of its vertical slices ($I \times J$) is put side by side to the right starting with the slice corresponding to the first time interval forming an ($I \times JK$) dimensional matrix (Figure 1). This particular unfolding enables the analysis of variability amongst batches (Nomikos and MacGregor, 1994). Mean centering of the unfolded matrix, in other words subtraction of the mean trajectories from each variable, removes most of the nonlinearity contained in the data. And after proper scaling, PCA is applied. The ith elements of the score vectors correspond to the ith batch with respect to the other batches in the database over the entire history of the batch. The loadings matrices summarize the time variation of the measured variables about their average trajectories.

The statistics used for monitoring multivariate batch processes are the statistical distance T^2, also known as the D-statistic in literature when it is based on batch process data scores, and the squared prediction error, SPE (Nomikos and MacGregor, 1995a). If a new batch is good and consistent with the normal batches, its scores should fall within the normal range and the SPE of Q-statistic should be small.

2.3 Multiblock Consensus PCA

In the multiblock MPCA the data matrix is divided into blocks in the time dimension according to the start and end times of the different phases. In other words, each block data is $I \times J \times K_b, b = 1, ..., B$ (B : *total number of blocks*) (Figure 2). These three-way block data are unfolded and scaled for consensus PCA calculation.

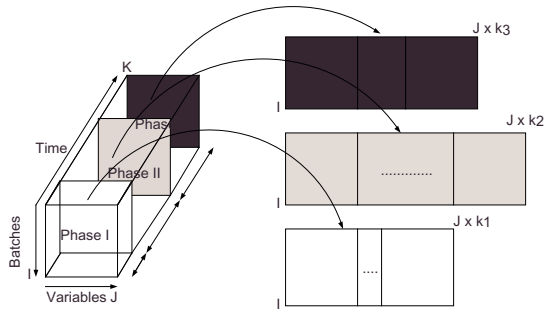

Fig. 2. Multiphase batch data unfolding.

3. PENICILLIN FERMENTATION SIMULATOR: PENSIM

The penicillin fermentation simulator was developed by Birol *et al.* (2002) and has been used as a testbed for process monitoring. More information is given in Çınar *et al.* (2002). The nonlinear dynamics and multiphase characteristics of the process also make it a good candidate for multiblock model applications.

The effects of environmental variables such as pH and temperature, and input variables such as aeration rate, agitation power, feed flow rate of substrate on biomass formation have been considered for completeness. Biomass growth, CO_2, penicillin production, substrate consumption and heat generation are included in the model equations.

In a typical penicillin fermentation process the formation of the target product, the antibiotic, is usually not associated with cell growth. It is common practice to grow the cells in a batch culture followed by a fed-batch operation with continuous glucose addition to promote the synthesis of the antibiotic.

The data from the simulator have three phases. The first phase is the batch culture. Simulator can switch to the fed-batch mode either manually at a preset time or after a threshold value for the glucose is reached. The fed-batch mode consists of two phases the exponential growth phase and the stationary phase where the penicillin concentration reaches and stays at the maximum value. These three phases are shown in Figure 3.

4. MULTIBLOCK PROCESS MONITORING AND DATA ANALYSIS

Two different approaches based on multiblock consensus PCA algorithm are applied to the monitoring of the fermentation simulation data. The multiblock consensus PCA, as described above, is called the static model. Here, the reference batches from normal operation are used in the

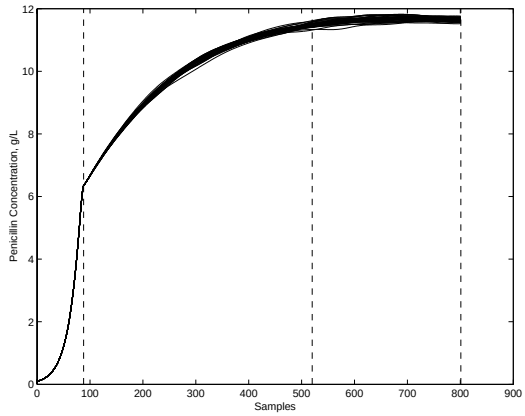

Fig. 3. Different phases of penicillin production.

model building and a new batch is projected on to this model. It is called static model because only one multiblock model is formed and used in fault detection and diagnosis. In the sliding window model, a window of batches is slid on the reference data. A model is formed using only the batches in the window. The new batch is projected onto this model and if the system does not give an out-of-control signal, the new batch is included in the model and the first batch in the window is excluded from the model. In the following cases, both methods are employed. Each model is built using the first four dominant principal components and each block is given equal weight in the calculations.

4.1 Case 1: Multiblock monitoring with equal batch lengths

Fifty normal operating batches with small random variations are generated. The phase change times are the same for all batches. Total batch duration is 400hr and sampling time is 0.5hr, making 801 samples, including the initial conditions. The data are broken into three phases based on the preset time points and the blocks are formed. A -2% step change in aeration rate (variable 1) is introduced at 70hr and the disturbance stays in the system until the 90th hour. Since the batch/fed-batch switch takes place at 44hr, this change should affect mostly the second block, and thus second block model should signal. For the static model, all of the normal operation batches are employed in the model development. In the sliding window model, a window size of forty batches is slid through the data.

In order to detect the occurrence of a fault in a process, super model control charts are the first ones to look at. If an alarm is given at the super level, block diagnostics are the second information source to check and find out where the fault is originating from. Block contributions to the statistics is also used to detect the blocks that

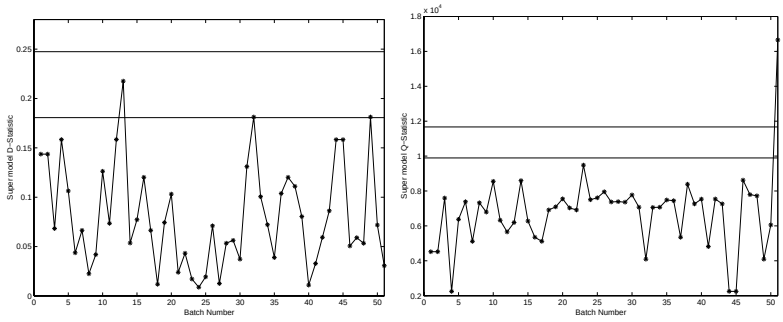

(a) (b)

Fig. 4. Case 1:Statistics for the equal length batch super model (a) D-Statistic (b) Q-Statistic.

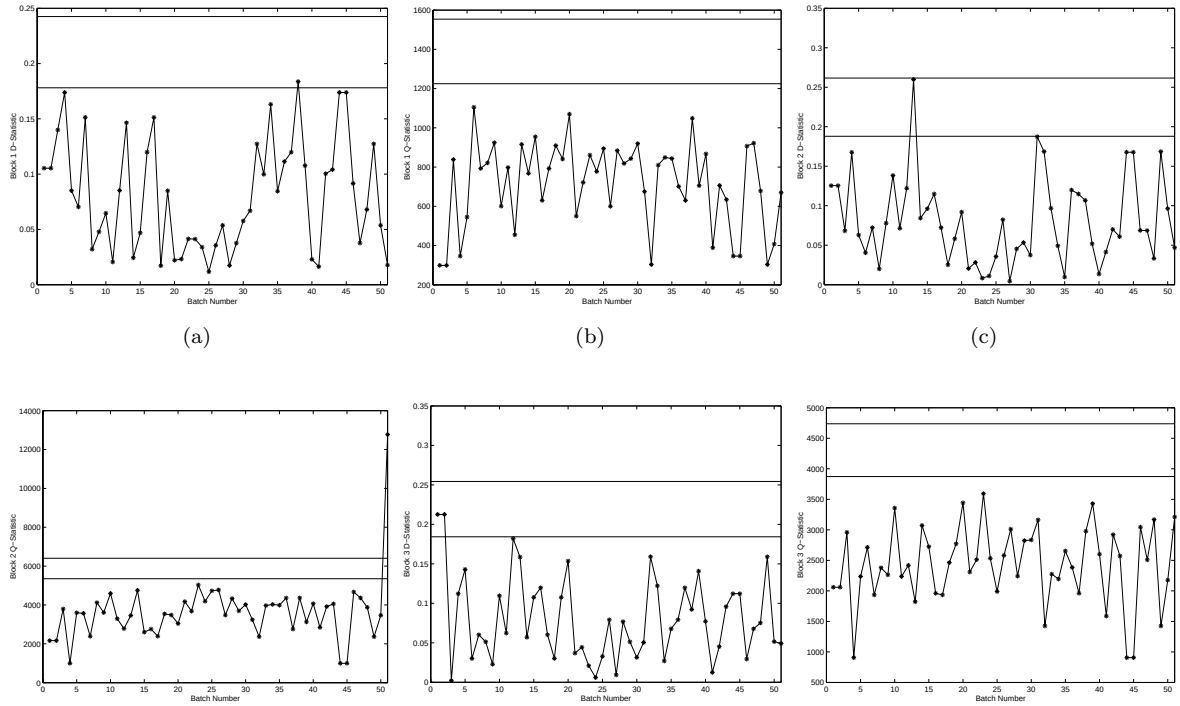

(a) (b) (c)

(d) (e) (f)

Fig. 5. Case 1:Static block models for equal length batch data (a)D-Statistics for Block 1,(b) Q-Statistics for Block 1, (c)D-Statistics for Block 2,(d) Q-Statistics for Block 2, (e)D-Statistics for Block 3,(f) Q-Statistics for Block 3.

are mainly contributing to the fault. The variable that is responsible for the fault and the variables that are affected most are found from the variable contribution charts. Super model diagnostics are given in Figure 4, the corresponding block diagnostics are shown in Figure 5, the time of occurrence of the fault for the faulty batch is given in Figure 6 and the contribution plots are provided in Figure 7. From these graphics, it is easy to conclude that the fault is in the second phase and variable 1 is the main cause of the fault.

Sliding window model generally gives better results than a static model in the sense of false alarms. On the other hand, a poor choice of window length can result in an insensitive model, since a slow drift of batches from normal operation can be missed in a small window. In this study, sliding window model also detects the fault and correctly identifies the main contributors to the fault. Because of space concerns the sliding window model results are not shown.

In these calculations, the blocks were given equal weight. If the block containing the fault is given a smaller weight compared to the other blocks, it leads to missed alarms. Looking at the super level diagnostics one can think the system is in-control, however, in the lower level one of the blocks may be experiencing a disturbance that need to be corrected as soon as possible. Block

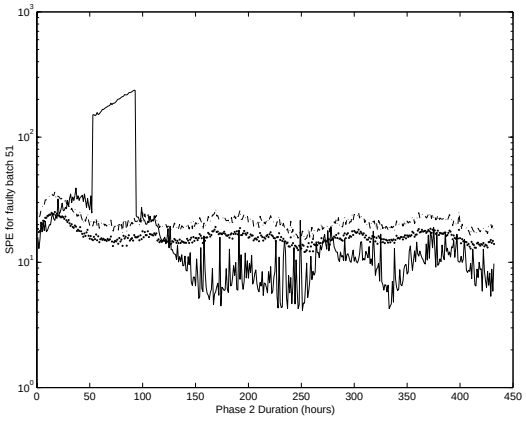

Fig. 6. Case 1: SPE for the faulty batch during the evolution of the batch.

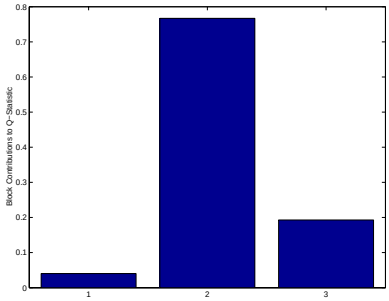

(a)

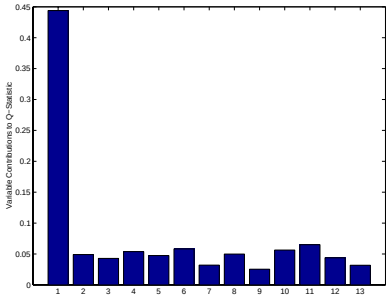

(b)

Fig. 7. Contribution plots for equal length batch data: (a)Block contributions to Q-Statistic and (b)Variable contributions to Q-Statistic.

weighting should be given extra attention to build a reliable model.

4.2 Case 2: Multiblock monitoring with different batch lengths

Forty normal operating batches with different batch/fed-batch switch times and different durations are simulated with small random variations. The system automatically switches to the fed-batch mode after the glucose concentration drops to a threshold value, 0.3g/l. Because of the random variations introduced, each batch has a different batch/fed-batch switch time. Also, the

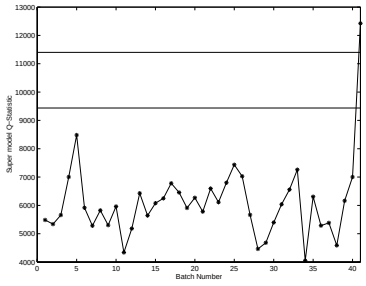

(a)

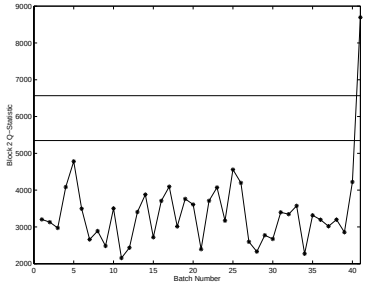

(b)

Fig. 8. Case 2:Statistics for the static block models for unaligned batch data (a)Super model Q-Statistics, (b) Block 2 Q-Statistic.

time required to reach the maximum penicillin concentration varies from batch to batch. For the penicillin fermentation it is easy to detect the phase-change points in time, since they correspond to the changes in measured variables of the system. The second phase starts with substrate addition and the third phase starts when penicillin concentration reaches its maximum value.

MPCA model development requires batches having the same length. However, in most processes, variations in process operation yield batch data of unequal length. In order to form the three-way array and apply batch monitoring tools, batch lengths should be equalized. Batch length equalization methods should also account for the alignment of process landmarks. Dynamic time warping (DTW) locally translates, compresses and expands the patterns so that similar features are aligned (Kassidas *et al.*, 1998; Ündey and Çınar, 2002).

In our case study, the start and end times for each phase during each batch are recorded at the end of a simulation. Then, each batch is divided into three different phases. Each batch in each phase is synchronized using DTW and equalized batches are put in their respective blocks.

A faulty batch is generated and projected on the models, and statistical control charts are employed to see if the fault is detected. A -2% step change is introduced to the aeration rate (variable 1) between samples 140 and 180 (correspond to

samples 50 and 90 in the second block) and a window length of thirty batches is used in the sliding window model. The fault is detected and correctly diagnosed by both methods.

Super model Q-Statistics detects the fault and block statistics in Figure 8 show that the fault is again originated from the second phase and variable 1 is diagnosed as the main cause of the fault (not shown).

5. CONCLUSION

The multiblock PCA algorithm based on consensus PCA is used on a multiphase batch/fed-batch penicillin fermentation simulator data for monitoring, fault detection and diagnosis purposes. A static model and a constantly updating sliding window model are built on two different batch data. Both methods were effective in detecting and localizing the fault in the system, However, none of them proved to be superior to the other.

Original MPCA is applied to both data sets considering the whole batch as a single block data, and the results proved that MPCA is an effective tool for multiphase/ multistage data as well. The benefit of multiblock algorithms in localizing and isolating the fault can be better experienced in very large processes involving many processing units with many process variables. With multiblock methods, the overall process and also each different unit or subsections of a unit can be monitored. This enables the isolation of the processing unit in which the deviation occurred and detection of the major contributors to the event.

REFERENCES

Birol, G., C. Ündey and A. Çınar (2002). A modular simulation package for fed-batch fermentation: penicillin production. *Computers and Chemical Engineering* **26**, 1553–1565.

Çınar, A., S.J. Parulekar, C. Ündey and Í. Birol (2002). *Batch Fermentation: Modeling, Monitoring and Control*. Marcel Dekker.

Kassidas, A., J.F. MacGregor and P.A. Taylor (1998). Synchronization of batch trajectories using dynamic time warping. *AIChE Journal* **44**, 864–875.

Kourti, T., P. Nomikos and J.F. MacGregor (1995). Analysis, monitoring and fault diagnosis of batch processes using multiblock, multiway PLS. *Journal of Process Control* **5**, 277–284.

Lee, D.S. and P.A. Vanrolleghem (2003). Monitoring of a sequencing batch reactor using adaptive multiblock principal component analysis. *Biotechnology and Bioengineering* **82**, 489–497.

MacGregor, J.F., C. Jaeckle, C. Kiparissides and M. Koutoudi (1994). Process monitoring and diagnosis by multiblock PLS methods. *AIChE Journal* **40**, 826–838.

Nomikos, P. and J.F. MacGregor (1994). Monitoring batch processes using multiway principal component analysis. *AIChE Journal* **40**, 1361–1375.

Nomikos, P. and J.F. MacGregor (1995*a*). Multivariate SPC charts for batch processes. *Technometrics* **37**, 41–59.

Nomikos, P. and J.F. MacGregor (1995*b*). Multiway partial least squares in monitoring batch processes. *Chemometrics and Intelligent Laboratory Systems* **30**, 97–108.

Qin, S.J., S. Valle and M.J. Piovoso (2001). On unifying multiblock analysis with application to decentralized process monitoring. *Journal of Chemometrics* **15**, 715–742.

Rännar, S., J.F. MacGregor and S. Wold (1998). Adaptive batch monitoring using hierarchical PCA. *Chemometrics and Intelligent Laboratory Systems* **41**, 73–81.

Smilde, A.K., J.A. Westerhuis and S. de Jong (2003). A framework for sequential multiblock component methods. *Journal of Chemometrics* **17**, 323–337.

Ündey, C. and A. Çınar (2002). Statistical monitoring of multistage, multiphase batch processes. *IEEE Control Systems Magazine* **22**(5), 40–52.

Westerhuis, J.A., T. Kourti and J.F. MacGregor (1998). Analysis of multiblock and hierarchical PCA and PLS models. *Journal of Chemometrics* **12**, 301–321.

Wold, S., P. Geladi, K. Esbensen and J. Öhman (1987). Multi-way principal components and PLS analysis. *Journal of Chemometrics* **1**, 41–56.

ADCHEM 2006

International Symposium on Advanced Control of Chemical Processes
Gramado, Brazil – April 2-5, 2006

2D MODEL PREDICTIVE ITERATIVE LEARNING CONTROL SCHEMES FOR BATCH PROCESSES

Jia Shi[1,2], **Furong Gao**[1], **Tie-Jun Wu**[2]

[1]*Deptment of Chemical Engineering, Hong Kong University of Science & Technology, Hong Kong, China*
[2]*Institute of Intelligent Systems and Decision Making, Zhejiang University, Hangzhou, 310027, China*

Abstract: Iterative learning control (ILC) system is modelled and treated as a 2D system in this paper. Based on single-batch and multi-batch cost functions, 2D model predictive iterative learning control (2D-MPILC) schemes are developed in the framework of model predictive control (MPC) for the 2D system. Structure analysis shows that the resulted 2D-MPILC laws are causal and they implicitly combine a time-wise MPC law with a cycle-wise ILC law to ensure the optimal control in 2D sense. To eliminate oscillating input, 2D control penalty is introduced to the 2D-MPILC design. The simulation results show that the proposed schemes are effective.

Keywords: Iterative methods, Learning control, Two-dimensional (2D) system, Model-based control, Predictive control, Batch control.

1. INTRODUCTION

Iterative learning control (ILC) was originally developed for the manipulation of an industrial robot to repetitively perform a given task (Arimoto *et al.*, 1984). Since then, it has been widely studied and extended to applications on processes with repetitive or cyclic nature (Xu *et al.*, 1998).

The conventional ILC scheme (Arimoto *et al.*, 1984), which uses only the information of previous cycles for control input refinement, is only a batch-to-batch control that may not be able to guarantee the control performance along time index. For this reason, real-time feedback control is often combined with the conventional ILC to ensure the control performance not only along the time but also along the cycle. In the early works using such a combination (Xu *et al.*, 1998), however, the separate designs of real-time feedback control and cycle-wise ILC were performed; this may not be able to guarantee optimal performance for both directions. Norm-optimal ILC that implicitly combines a state feedback control with a feed-forward ILC was proposed by Amann *et al.* (1995, 1996) based on the performance index defined over one cycle. Their extended method includes prediction over future cycles (Owens *et al.*, 2000), the resulted feedback control law also in state form, however, is non-causal, and the computation load may be heavy for long batch duration. Base on a quadratic performance defined over one cycle, Lee *et al.* (2000) proposed a model-based ILC scheme.

*Corresponding author: Telephone: +852-2358 7139. Fax: +852-2358 0054. Email: kefgao@ust.hk.

An ILC system essentially is a two-dimensional (2D) system, where dynamic behaviour along the time is determined by the process and the feedback control, while ILC introduces dynamics along the cycle. Model and design ILC system as a 2D system can result in a united design of time-wise feedback control and cycle-wise ILC, guaranteeing the control performance in 2D sense. The above reviewed methods did not treat the optimizations of ILC design directly in 2D sense. While the existing 2D based methods (Geng *et al.*, 1990; Kurek *et al.*, 1993; Shi *et al.*, 2005) consider only the convergence and/or robustness of the system, leading to, sometime, a conservative control law.

In this paper, the iterative learning control design is treated from the 2D system viewpoint. Single-batch and multi-batch objective functions are defined and optimized in the framework of model predictive control (MPC) for the 2D system, resulting in a single-batch and a multi-batch 2D model predictive iterative learning control (2D-MPILC) schemes. Structure analysis is conducted to give insight of the resulted 2D control system. It shows that the resulted 2D-MPILC schemes consist of two types of controls: one is an MPC that uses the real-time input-output information to ensure the control performance within cycle, and the other is batch-wise ILC that improves the control performance from cycle to cycle. The united design of these two types of controls ensures the optimal control in terms of the defined 2D cost functions. The computation of the methods depends on the design parameters that can be balanced by the practitioner, and the resulted control laws are casual

for practical implementation. 2D input change penalty terms can also be easily introduced to the design to ensure a smooth control. Simulation results show that the proposed methods are very effective.

2. PROBLEM FORMULATIONS

For simplicity, it is assumed in this paper that the underlying process is a SISO system. All the results can be extended to MIMO cases.

2.1 Batch processes and ILC law

A batch process, repetitively performing a given task over finite time duration, called a batch or cycle, is described by the following linear model

$$\Sigma_{BP}: \quad A(q^{-1})y_k(t) = B(q^{-1})u_k(t) + w_k(t) \qquad (1)$$
$$t = 0,1,...,T; \quad k = 1,2,...$$

where t is time and k represents the batch/cycle index, $u_k(t)$, $y_k(t)$ and $w_k(t)$ are, respectively, the input, output and disturbance of the process at time t in the k th cycle, q^{-1} indicates the *unit backward-shift operator*, and $A(q^{-1})$ and $B(q^{-1})$ are both operator polynomials

$$A(q^{-1}) = 1 + a_1 q^{-1} + a_2 q^{-2} + \cdots + a_n q^{-n} \qquad (2)$$
$$B(q^{-1}) = b_1 q^{-1} + b_2 q^{-2} + \cdots + b_m q^{-m} \qquad (3)$$

For the above batch process, introduce an ILC law with the form

$$u_k(t) = u_{k-1}(t) + r_k(t), \qquad u_0(t) = 0, \quad t = 1,2,...,T \qquad (4)$$

where $r_k(t)$ is referred as the *updating law* to be determined, and $u_0(t)$ is the *initial profile* of iteration.

2.2 2D representation and cost functions

Substituting (4) into (1) leads to the following input-output model

$$\Sigma_{2D}: A(q^{-1})y_k(t) = B(q^{-1})r_k(t) + A(q^{-1})y_{k-1}(t) + \Delta w_k(t) \quad (5)$$

where $r_k(t)$ and $y_k(t)$ are, respectively, the input and output of the model, and $\Delta w_k(t) = w_k(t) - w_{k-1}(t)$ is viewed as the disturbance.

Due to the combination of the batch-wise dynamic introduced by ILC law (4), model (5) is a 2D input-output model describing the dynamics of the ILC system. To design updating law $r_k(t)$, two cost functions are introduced, depending on the number of cycles involved.

- Single-batch cost function

$$J(t,k,n_1,n_2) = \sum_{i=1}^{n_1}\alpha(i)\left(\hat{e}_{k|k}(t+i\,|\,t)\right)^2 + \sum_{j=1}^{n_2}\beta(j)\left(r_k(t+j-1)\right)^2 \qquad (6)$$

- Multi-batch cost function

$$J(t,k,n_1,n_2,n_3) = \sum_{l=1}^{n_3}\lambda(l)\left(\sum_{i=1}^{n_1}\alpha(i)\left(\hat{e}_{k+l-1|k}(t+i\,|\,t)\right)^2 + \sum_{j=1}^{n_2}\beta(j)\left(r_{k+l-1}(t+j-1)\right)^2\right) \qquad (7)$$

where $\hat{e}_{k+l|k}(t+i\,|\,t) = y_r(t+i) - \hat{y}_{k+l|k}(t+i\,|\,t)$ and $\hat{y}_{k+l|k}(t+i\,|\,t)$ represents the estimated output at time $(t+i)$ of the $(k+l)$th cycle based on the measurements before time t of kth cycle, $y_r(t)$, $t = 0,1,...,T$ is the desired trajectory to be tracked, $\alpha(i) \ge 0$, $\beta(j) > 0$ and $\lambda(l) > 0$ are the weighting factors indicating the importance of each cost term, integers $n_1, n_2 (n_1 \ge n_2 > 0)$ are, respectively, referred as the *time-wise prediction horizon* and *control horizon*, and n_3 is called the *batch-wise optimization horizon*.

Obviously, the single-batch cost function (6), where the prediction tracking errors and the updating control effort within specified horizons along one cycle are penalized, is a special case of multi-batch cost function (7) which takes the predicted control performances over several cycles within specified horizons into account. The objective of this paper is to find, at time t of the kth cycle, updating control laws in the MPC framework to minimize the cost functions (6) and (7).

3. 2D-MPILC SCHEMES

3.1 2D prediction model

In MPC framework, the derivation of control scheme requires a prediction model to provide output estimation over the future horizon. According to 2D model (5), at any time t the input and output information of the process can be divided into known and unknown two parts governed by:

$$(\boldsymbol{A}_1 \;\; \boldsymbol{A}_2)\begin{pmatrix}\boldsymbol{y}_k\left(\begin{smallmatrix}t-n+1\\ t\end{smallmatrix}\right)\\ \boldsymbol{y}_k\left(\begin{smallmatrix}t+1\\ t+n_1\end{smallmatrix}\right)\end{pmatrix} = (\boldsymbol{B}_1 \;\; \boldsymbol{B}_2)\begin{pmatrix}\boldsymbol{r}_k\left(\begin{smallmatrix}t-m+1\\ t-1\end{smallmatrix}\right)\\ \boldsymbol{r}_k\left(\begin{smallmatrix}t\\ t+n_1-1\end{smallmatrix}\right)\end{pmatrix} + (\boldsymbol{A}_1 \;\; \boldsymbol{A}_2)\begin{pmatrix}\boldsymbol{y}_{k-1}\left(\begin{smallmatrix}t-n+1\\ t\end{smallmatrix}\right)\\ \boldsymbol{y}_{k-1}\left(\begin{smallmatrix}t+1\\ t+n_1\end{smallmatrix}\right)\end{pmatrix} + \boldsymbol{\Delta w}_k\left(\begin{smallmatrix}t+1\\ t+n_1\end{smallmatrix}\right) \qquad (8)$$

where

$$\boldsymbol{f}_k\left(\begin{smallmatrix}t_1\\ t_2\end{smallmatrix}\right) = \left(f_k(t_1) \;\; f_k(t_1+1) \;\cdots\; f_k(t_2)\right)^T, \;\; \boldsymbol{f} \in \{\boldsymbol{y}, \boldsymbol{r}, \boldsymbol{\Delta w}\} \qquad (9)$$

$$(\boldsymbol{A}_1 \,|\, \boldsymbol{A}_2) = \left(\begin{array}{ccccc|ccccc} a_n & a_{n-1} & a_{n-2} & \cdots & a_1 & 1 & 0 & \cdots & 0 & 0\\ 0 & a_n & a_{n-1} & \cdots & a_2 & a_1 & 1 & \cdots & 0 & 0\\ 0 & 0 & a_n & \cdots & a_3 & a_2 & a_1 & \cdots & 0 & 0\\ \vdots & \vdots & \vdots & \ddots & \vdots & \vdots & \vdots & \ddots & \vdots & \vdots\\ 0 & 0 & 0 & \cdots & * & * & * & \cdots & a_1 & 1 \end{array}\right) \qquad (10)$$

$$(\boldsymbol{B}_1 \,|\, \boldsymbol{B}_2) = \left(\begin{array}{ccccc|ccccc} b_m & b_{m-1} & b_{m-2} & \cdots & b_2 & b_1 & 0 & \cdots & 0 & 0\\ 0 & b_m & b_{m-1} & \cdots & b_3 & b_2 & b_1 & \cdots & 0 & 0\\ 0 & 0 & b_m & \cdots & b_4 & b_3 & b_2 & \cdots & 0 & 0\\ \vdots & \vdots & \vdots & \ddots & \vdots & \vdots & \vdots & \ddots & \vdots & \vdots\\ 0 & 0 & 0 & \cdots & * & * & * & \cdots & b_2 & b_1 \end{array}\right) \qquad (11)$$

Since $\boldsymbol{A}_2$ is a nonsingular matrix and $\boldsymbol{\Delta w}_k\left(\begin{smallmatrix}t+1\\ t+n_1\end{smallmatrix}\right)$ depends on the disturbances of the future, generally assumed to be Gaussian, the best prediction of the outputs over the prediction horizon is therefore

$$\hat{\boldsymbol{y}}_{k|k}\left(\begin{smallmatrix}t+1\\ t+n_1\end{smallmatrix}\,|\,t\right) = \boldsymbol{A}_2^{-1}\boldsymbol{B}_2\boldsymbol{r}_k\left(\begin{smallmatrix}t\\ t+n_1-1\end{smallmatrix}\right) + \boldsymbol{y}_{k-1}\left(\begin{smallmatrix}t+1\\ t+n_1\end{smallmatrix}\right) + \boldsymbol{A}_2^{-1}\boldsymbol{B}_1\boldsymbol{r}_k\left(\begin{smallmatrix}t-m+1\\ t-1\end{smallmatrix}\right) - \boldsymbol{A}_2^{-1}\boldsymbol{A}_1\boldsymbol{y}_k\left(\begin{smallmatrix}t-n+1\\ t\end{smallmatrix}\right) + \boldsymbol{A}_2^{-1}\boldsymbol{A}_1\boldsymbol{y}_{k-1}\left(\begin{smallmatrix}t-n+1\\ t\end{smallmatrix}\right) \qquad (12)$$

Let

$$\boldsymbol{G} = \boldsymbol{A}_2^{-1}\boldsymbol{B}_2, \quad \boldsymbol{H}_k(t) = \boldsymbol{y}_{k-1}\left(\begin{smallmatrix}t+1\\ t+n_1\end{smallmatrix}\right) + \boldsymbol{F}_k(t) \qquad (13)$$

$$\boldsymbol{F}_k(t) = \boldsymbol{A}_2^{-1}\boldsymbol{B}_1\boldsymbol{r}_k\left(\begin{smallmatrix}t-m+1\\ t-1\end{smallmatrix}\right) - \boldsymbol{A}_2^{-1}\boldsymbol{A}_1\boldsymbol{y}_k\left(\begin{smallmatrix}t-n+1\\ t\end{smallmatrix}\right) + \boldsymbol{A}_2^{-1}\boldsymbol{A}_1\boldsymbol{y}_{k-1}\left(\begin{smallmatrix}t-n+1\\ t\end{smallmatrix}\right) \qquad (14)$$

Prediction model (12) can be rewritten as

$$\hat{\boldsymbol{y}}_{k|k}\left(\begin{smallmatrix}t+1\\ t+n_1\end{smallmatrix}\,|\,t\right) = \boldsymbol{G}\boldsymbol{r}_k\left(\begin{smallmatrix}t\\ t+n_1-1\end{smallmatrix}\right) + \boldsymbol{H}_k(t) = \boldsymbol{G}\boldsymbol{r}_k\left(\begin{smallmatrix}t\\ t+n_1-1\end{smallmatrix}\right) + \boldsymbol{y}_{k-1}\left(\begin{smallmatrix}t+1\\ t+n_1\end{smallmatrix}\right) + \boldsymbol{F}_k(t) \qquad (15)$$

Note that $\boldsymbol{H}_k(t)$ and $\boldsymbol{F}_k(t)$ depend on the available input and output information of current cycle and last cycle. If $\boldsymbol{r}_k\left(\left|_{t+n_1-1}^{t}\right.\right)=\boldsymbol{0}$, one has

$$\boldsymbol{H}_k(t)=\hat{\boldsymbol{y}}_{k|k}\left(\left|_{t+n_1}^{t+1}\right.|\,t\right),\quad \boldsymbol{F}_k(t)=\hat{\boldsymbol{y}}_{k|k}\left(\left|_{t+n_1}^{t+1}\right.|\,t\right)-\boldsymbol{y}_{k-1}\left(\left|_{t+n_1}^{t+1}\right.\right) \quad (16)$$

which show that $\boldsymbol{H}_k(t)$ is the estimation of the system response over the prediction horizon when the control input is not updated, while $\boldsymbol{F}_k(t)$ represents the estimated variation of outputs along the cycle direction.

Prediction model (15) is a 2D model which can be directly extended to estimate the outputs in the following batches, that is,

$$\begin{aligned}\hat{\boldsymbol{y}}_{k+l|k}\left(\left|_{t+n_1}^{t+1}\right.|\,t\right)&=\boldsymbol{G}\boldsymbol{r}_{k+l}\left(\left|_{t+n_1-1}^{t}\right.\right)+\hat{\boldsymbol{H}}_{k+l|k}(t)\\&=\boldsymbol{G}\boldsymbol{r}_{k+l}\left(\left|_{t+n_1-1}^{t}\right.\right)+\hat{\boldsymbol{y}}_{k+l-1|k}\left(\left|_{t+n_1}^{t+1}\right.|\,t\right)+\hat{\boldsymbol{F}}_{k+l|k}(t)\end{aligned} \quad (17)$$

where

$$\hat{\boldsymbol{H}}_{k+l|k}(t)=\hat{\boldsymbol{y}}_{k+l-1|k}\left(\left|_{t+n_1}^{t+1}\right.|\,t\right)+\hat{\boldsymbol{F}}_{k+l|k}(t) \quad (18)$$

$$\begin{aligned}\hat{\boldsymbol{F}}_{k+l|k}(t)=&\boldsymbol{A}_2^{-1}\boldsymbol{B}_1\boldsymbol{r}_k\left(\left|_{t-1}^{-m+1}\right.\right)-\boldsymbol{A}_2^{-1}\boldsymbol{A}_1\hat{\boldsymbol{y}}_{k+l|k}\left(\left|_{t}^{t-n+1}\right.|\,t\right)\\&+\boldsymbol{A}_2^{-1}\boldsymbol{A}_1\hat{\boldsymbol{y}}_{k+l-1|k}\left(\left|_{t}^{t-n+1}\right.|\,t\right)\end{aligned} \quad (19)$$

If it is assumed that the batch-wise steady control performance have been achieved before time t in the $(k+l)$th ($l>0$) cycle, in other word, that $\boldsymbol{r}_{k+l}\left(\left|_{t-1}^{0}\right.\right)=\boldsymbol{0}$, leading to $\hat{\boldsymbol{F}}_{k+l|k}(t)=\boldsymbol{0}$, then, from the prediction model (17), the following simplified prediction model can be obtained

$$\hat{\boldsymbol{y}}_{k+l|k}\left(\left|_{t+n_1}^{t+1}\right.|\,t\right)=\boldsymbol{G}\boldsymbol{r}_{k+l}\left(\left|_{t+n_1-1}^{t}\right.\right)+\hat{\boldsymbol{y}}_{k+l-1|k}\left(\left|_{t+n_1}^{t+1}\right.|\,t\right),\ l>0 \quad (20)$$

Models (15) and (20) are suitable for the output estimation when the prediction horizon and control horizon are equal, otherwise, the following modifications should be given to matrix $\boldsymbol{G}$ to accommodate the specified configuration of input signal $\boldsymbol{r}_k(\left|_{t+n_1-1}^{t+n_2}\right.)$:

- If $r_k(t+i)=0$ for $i=n_2,...,n_1-1$, then the last n_1-n_2 columns of matrix $\boldsymbol{G}$ are deleted;
- If $r_k(t+i)=r_k(t+n_2-1)$ for $i=n_2,...,n_1-1$, then the last n_1-n_2 columns of matrix $\boldsymbol{G}$ are added to the n_1th column.

Now, the 2D prediction models (15) and (20) are generalized as follows

$$\hat{\boldsymbol{y}}_{k|k}\left(\left|_{t+n_1}^{t+1}\right.|\,t\right)=\boldsymbol{G}\boldsymbol{r}_k\left(\left|_{t+n_2-1}^{t}\right.\right)+\boldsymbol{y}_{k-1}\left(\left|_{t+n_1}^{t+1}\right.\right)+\boldsymbol{F}_k(t) \quad (21)$$

$$\hat{\boldsymbol{y}}_{k+l|k}\left(\left|_{t+n_1}^{t+1}\right.|\,t\right)=\boldsymbol{G}\boldsymbol{r}_{k+l}\left(\left|_{t+n_1-1}^{t}\right.\right)+\hat{\boldsymbol{y}}_{k+l-1|k}\left(\left|_{t+n_1}^{t+1}\right.|\,t\right),\ l>0 \quad (22)$$

In the next subsection, the 2D-MPILC schemes will be derived based on these prediction models.

3.2 2D-MPILC schemes

- Single-batch 2D-MPILC scheme

The cost function (6) can be written in a matrix form

$$\begin{aligned}&J(t,k,n_1,n_2)\\&=\hat{\boldsymbol{e}}_{k|k}^T\left(\left|_{t+n_1}^{t+1}\right.|\,t\right)\boldsymbol{Q}\hat{\boldsymbol{e}}_{k|k}\left(\left|_{t+n_1}^{t+1}\right.|\,t\right)+\boldsymbol{r}_k^T\left(\left|_{t+n_2-1}^{t}\right.\right)\boldsymbol{R}\boldsymbol{r}_k\left(\left|_{t+n_2-1}^{t}\right.\right)\end{aligned} \quad (23)$$

where $\hat{\boldsymbol{e}}_{k|k}\left(\left|_{t+n_1}^{t+1}\right.|\,t\right)=\boldsymbol{y}_r\left(\left|_{t+n_1}^{t+1}\right.\right)-\hat{\boldsymbol{y}}_{k|k}\left(\left|_{t+n_1}^{t+1}\right.|\,t\right)$, and

$$\boldsymbol{Q}=diag\{\alpha(1),\alpha(2),...,\alpha(n_1)\} \quad (24)$$

$$\boldsymbol{R}=diag\{\beta(1),\beta(2),...,\beta(n_2)\} \quad (25)$$

Clearly, $\boldsymbol{R}>0$, $\boldsymbol{Q}\geq 0$.

It follows from prediction model (21) and optimization algorithm that the cost function (23) is minimized by the following optimal control

$$\boldsymbol{r}_k^*\left(\left|_{t+n_2-1}^{t}\right.\right)=(\boldsymbol{R}+\boldsymbol{G}^T\boldsymbol{Q}\boldsymbol{G})^{-1}\boldsymbol{G}^T\boldsymbol{Q}\left(\boldsymbol{y}_r\left(\left|_{t+n_1}^{t+1}\right.\right)-\boldsymbol{H}_k(t)\right) \quad (26)$$

The positivity of matrix $\boldsymbol{R}$ guarantees the nonsingularity of matrix $\boldsymbol{R}+\boldsymbol{G}^T\boldsymbol{Q}\boldsymbol{G}$. Now, let $\boldsymbol{K}$ be the first row of matrix $(\boldsymbol{R}+\boldsymbol{G}^T\boldsymbol{Q}\boldsymbol{G})^{-1}\boldsymbol{G}^T\boldsymbol{Q}$, the single-batch 2D-MPILC scheme is obtained from definition (13), that is

$$\begin{aligned}\Sigma_{SB-MPILC}:\ u_k(t)&=u_{k-1}(t)+\boldsymbol{K}\left(\boldsymbol{y}_r\left(\left|_{t+n_1}^{t+1}\right.\right)-\boldsymbol{H}_k(t)\right)\\&=u_{k-1}(t)+\boldsymbol{K}\left(\boldsymbol{e}_{k-1}\left(\left|_{t+n_1}^{t+1}\right.\right)-\boldsymbol{F}_k(t)\right)\end{aligned} \quad (27)$$

where $\boldsymbol{e}_{k-1}\left(\left|_{t+n_1}^{t+1}\right.\right)=\boldsymbol{y}_r\left(\left|_{t+n_1}^{t+1}\right.\right)-\boldsymbol{y}_{k-1}\left(\left|_{t+n_1}^{t+1}\right.\right)$ is the tracking error vector over the prediction horizon. It is noted from the first equality that the control signal will not be refined if the model-based estimation of the system response over the prediction horizon is the same as desired trajectory.

- Multi-batch 2D-MPILC scheme

Rewrite multi-batch cost function (7) in the following matrix form

$$\begin{aligned}J(t,k,n_1,n_2,n_3)=\sum_{l=1}^{n_3}\lambda(l)\Big(&\hat{\boldsymbol{e}}_{k+l-1|k}^T\left(\left|_{t+n_1}^{t+1}\right.|\,t\right)\boldsymbol{Q}\hat{\boldsymbol{e}}_{k+l-1|k}\left(\left|_{t+n_1}^{t+1}\right.|\,t\right)\\&+\boldsymbol{r}_{k+l-1}^T\left(\left|_{t+n_2-1}^{t}\right.\right)\boldsymbol{R}\boldsymbol{r}_{k+l-1}\left(\left|_{t+n_2-1}^{t}\right.\right)\Big)\end{aligned} \quad (28)$$

where $\hat{\boldsymbol{e}}_{k+l-1|k}\left(\left|_{t+n_1}^{t+1}\right.|\,t\right)=\boldsymbol{y}_r\left(\left|_{t+n_1}^{t+1}\right.\right)-\hat{\boldsymbol{y}}_{k+l-1|k}\left(\left|_{t+n_1}^{t+1}\right.|\,t\right)$ representing the prediction of the tracking error over the prediction horizon, matrices $\boldsymbol{Q}$ and $\boldsymbol{R}$ are defined by (24) and (25), respectively.

To derive the multi-batch 2D-MPILC scheme, the batch-wise *dynamic programming* will be conducted. Firstly, consider the cost function of the last cycle in the batch-wise optimization horizon

$$\begin{aligned}J(t,k+n_3-1,n_1,n_2)=&\lambda(n_3)\hat{\boldsymbol{e}}_{k+n_3-1|k}^T\left(\left|_{t+n_1}^{t+1}\right.|\,t\right)\boldsymbol{Q}\hat{\boldsymbol{e}}_{k+n_3-1|k}\left(\left|_{t+n_1}^{t+1}\right.|\,t\right)\\&+\lambda(n_3)\boldsymbol{r}_{k+n_3-1}^T\left(\left|_{t+n_2-1}^{t}\right.\right)\boldsymbol{R}\boldsymbol{r}_{k+n_3-1}\left(\left|_{t+n_2-1}^{t}\right.\right)\end{aligned} \quad (29)$$

It follows from prediction model (22) that the above cost function is minimized by the following optimal control

$$\begin{aligned}&\boldsymbol{r}_{k+n_3-1}^*\left(\left|_{t+n_2-1}^{t}\right.\right)\\&=\left(\lambda(n_3)\boldsymbol{R}+\boldsymbol{G}^T\lambda(n_3)\boldsymbol{Q}\boldsymbol{G}\right)^{-1}\boldsymbol{G}^T\lambda(n_3)\boldsymbol{Q}\hat{\boldsymbol{e}}_{k+n_3-2|k}\left(\left|_{t+n_1}^{t+1}\right.|\,t\right)\end{aligned} \quad (30)$$

with the minimal cost defined by

$$\begin{aligned}J^*(t,k+n_3-1,n_1,n_2)=&\lambda(n_3)\left(\hat{\boldsymbol{e}}_{k+n_3-2|k}\left(\left|_{t+n_1}^{t+1}\right.|\,t\right)\right)^T\\&\bullet\left(\boldsymbol{Q}+\boldsymbol{Q}\boldsymbol{G}\left(\boldsymbol{R}+\boldsymbol{G}^T\boldsymbol{Q}\boldsymbol{G}\right)^{-1}\boldsymbol{G}^T\boldsymbol{Q}\right)\bullet\left(\hat{\boldsymbol{e}}_{k+n_3-2|k}\left(\left|_{t+n_1}^{t+1}\right.|\,t\right)\right)\end{aligned} \quad (31)$$

Let $\boldsymbol{P}_{n_3-1}=\lambda(n_3)\left(\boldsymbol{Q}+\boldsymbol{Q}\boldsymbol{G}\left(\boldsymbol{R}+\boldsymbol{G}^T\boldsymbol{Q}\boldsymbol{G}\right)^{-1}\boldsymbol{G}^T\boldsymbol{Q}\right)$, and from the principle of optimality, the minimal cost over the last two cycles within the batch-wise optimization horizon is

$$\begin{aligned}&J^*(t,k+n_3-2,n_1,n_2,2)\\&=\min_{\substack{\boldsymbol{r}_{k+n_3-2}\left(\left|_{t+n_2-1}^{t}\right.\right)\\ \boldsymbol{r}_{k+n_3-1}\left(\left|_{t+n_2-1}^{t}\right.\right)}}\sum_{l=n_3-1}^{n_3}\lambda(l)\Big(\hat{\boldsymbol{e}}_{k+l-1|k}^T\left(\left|_{t+n_1}^{t+1}\right.|\,t\right)\boldsymbol{Q}\hat{\boldsymbol{e}}_{k+l-1|k}\left(\left|_{t+n_1}^{t+1}\right.|\,t\right)\\&\qquad+\boldsymbol{r}_{k+l-1}^T\left(\left|_{t+n_2-1}^{t}\right.\right)\boldsymbol{R}\boldsymbol{r}_{k+l-1}\left(\left|_{t+n_2-1}^{t}\right.\right)\Big)\\&=\min_{\boldsymbol{r}_{k+n_3-2}\left(\left|_{t+n_2-1}^{t}\right.\right)}\lambda(n_3-1)\Big(\hat{\boldsymbol{e}}_{k+n_3-2|k}^T\left(\left|_{t+n_1}^{t+1}\right.|\,t\right)\boldsymbol{Q}\hat{\boldsymbol{e}}_{k+n_3-2|k}\left(\left|_{t+n_1}^{t+1}\right.|\,t\right)\\&\quad+\boldsymbol{r}_{k+n_3-2}^T\left(\left|_{t+n_2-1}^{t}\right.\right)\boldsymbol{R}\boldsymbol{r}_{k+n_3-2}\left(\left|_{t+n_2-1}^{t}\right.\right)\Big)+J^*(t,k+n_3-1,n_1,n_2)\end{aligned}$$

$$= \min_{\boldsymbol{r}_{k+n_3-2}\left(\left|_{t+n_2-1}\right.\right)} \Big(\hat{\boldsymbol{e}}^T_{k+n_3-2|k}\left(\left|^{t+1}_{t+n_1}\right.|\,t\right)\left(\lambda(n_3-1)\boldsymbol{Q}+\boldsymbol{P}_{n_3-1}\right)\hat{\boldsymbol{e}}_{k+n_3-2|k}\left(\left|^{t+1}_{t+n_1}\right.|\,t\right)$$

$$+\lambda(n_3-1)\boldsymbol{r}^T_{k+n_3-2}\left(\left|^{t}_{t+n_2-1}\right.\right)\boldsymbol{R}\boldsymbol{r}_{k+n_3-2}\left(\left|^{t}_{t+n_2-1}\right.\right)\Big) \quad (32)$$

Let $Q_{n_3-1} = \lambda(n_3-1)\boldsymbol{Q}+\boldsymbol{P}_{n_3-1}$. Then the optimal control law is given by

$$\boldsymbol{r}^*_{k+n_3-2}\left(\left|^{t}_{t+n_2-1}\right.\right)$$

$$=\left(\lambda(n_3-1)\boldsymbol{R}+\boldsymbol{G}^T\boldsymbol{Q}_{n_3-1}\boldsymbol{G}\right)^{-1}\boldsymbol{G}^T\boldsymbol{Q}_{n_3-1}\hat{\boldsymbol{e}}_{k+n_3-3|k}\left(\left|^{t+1}_{t+n_1}\right.|\,t\right) \quad (33)$$

The above procedure can be repeated backward along the batch index until the $(k+1)$ th cycle, leading to the optimal control law

$$\boldsymbol{r}^*_{k+1}\left(\left|^{t}_{t+n_2-1}\right.\right)=\left(\lambda(2)\boldsymbol{R}+\boldsymbol{G}^T\boldsymbol{Q}_2\boldsymbol{G}\right)^{-1}\boldsymbol{G}^T\boldsymbol{Q}_2\hat{\boldsymbol{e}}_{k|k}\left(\left|^{t+1}_{t+n_1}\right.|\,t\right) \quad (34)$$

and minimal cost of last n_3-1 cycles in the batch-wise optimization horizon computed by

$$J^*(t,k+1,n_1,n_2,n_3-1)=\hat{\boldsymbol{e}}^T_{k|k}\left(\left|^{t+1}_{t+n_1}\right.|\,t\right)\boldsymbol{P}_1\hat{\boldsymbol{e}}_{k|k}\left(\left|^{t+1}_{t+n_1}\right.|\,t\right) \quad (35)$$

where matrices $\boldsymbol{Q}_2$ and $\boldsymbol{P}_1$ are determined by the following *backward recursive algorithm*

$$\boldsymbol{P}_{n_3}=\boldsymbol{0}, \qquad \boldsymbol{Q}_l=\lambda(l)\boldsymbol{Q}+\boldsymbol{P}_l \quad (36)$$

$$\boldsymbol{P}_l=\boldsymbol{Q}_{l+1}+\boldsymbol{Q}_{l+1}\boldsymbol{G}\left(\lambda(l+1)\boldsymbol{R}+\boldsymbol{G}^T\boldsymbol{Q}_{l+1}\boldsymbol{G}\right)^{-1}\boldsymbol{G}^T\boldsymbol{Q}_{l+1} \quad (37)$$

$$l=n_3,n_3-1,\ldots,1$$

Now, for the k th cycle, the following optimal control law is yielded from prediction model (21)

$$\boldsymbol{r}^*_k\left(\left|^{t}_{t+n_2-1}\right.\right)=\left(\lambda(1)\boldsymbol{R}+\boldsymbol{G}^T\boldsymbol{Q}_1\boldsymbol{G}\right)^{-1}\boldsymbol{G}^T\boldsymbol{Q}_1\left(\boldsymbol{e}_{k-1}\left(\left|^{t+1}_{t+n_1}\right.\right)-\boldsymbol{F}_k(t)\right) \quad (38)$$

where $\boldsymbol{Q}_1$ is also determined by the backward recursive algorithm (36)(37). Let $\boldsymbol{K}$ be the first row of matrix $\left(\lambda(1)\boldsymbol{R}+\boldsymbol{G}^T\boldsymbol{Q}_1\boldsymbol{G}\right)^{-1}\boldsymbol{G}^T\boldsymbol{Q}_1$, then the multi-batch 2D-MPILC scheme is defined

$$\Sigma_{MB-MPILC}: u_k(t)=u_{k-1}(t)+\boldsymbol{K}\left(\boldsymbol{e}_{k-1}\left(\left|^{t+1}_{t+n_1}\right.\right)-\boldsymbol{F}_k(t)\right) \quad (39)$$

Remark 3.1. Note from (27) and (39) that both single-batch and multi-batch 2D-MPILC laws have same formulation, and, at any time t, the updating laws depend on the input and output information of current cycle before time t, the output information of last cycle before time t and the tracking errors of last cycle over the prediction horizon.

Remark 3.2. Similar to MPC scheme, the computational burdens for both single-batch and multi-batch 2D-MPILC schemes are dependent on the values of n_1, n_2 and n_3, which can be balanced by practitioner in terms of computational load and control performance.

Remark 3.3. Single-batch 2D-MPILC scheme which takes only the control performance of current cycle into account is more suitable for the case when large control errors exist in the last cycle, such as the first cycle of the batch process. Multi-batch 2D-MPILC scheme which takes the control performances of several cycles into account can provides faster convergence along the batch index.

Remark 3.4. The proposed design methods can be extended to general cases of MIMO time-varying linear processes with input time delay. Proper selection of time-varying weighting matrices $\boldsymbol{Q}$ and $\boldsymbol{R}$ can also be used to accommodate time-varying dynamic characteristics of the processes.

4. STRUCTURE ANALYSIS

In a 2D system view, the resulted closed-loop system is composed of a 2D process Σ_{2D} and a controller $\Sigma_{SB-MPILC}$ or $\Sigma_{MB-MPILC}$, as shown in Figure 1(a), where the dot-arrow lines indicate the information flows of the last cycle from the storages, while the solid-arrow lines indicate the real-time information flows. Plant Σ_{2D} is a 2D system consisting of a batch process Σ_{BP} and an iteration loop, while $\Sigma_{SB-MPILC}$ or $\Sigma_{MB-MPILC}$ is a 2D model predictive control scheme.

In an ILC system view, ILC law (27) or (39) can be reformulated as

$$u_k(t)=u_{k-1}(t)$$

$$+\boldsymbol{K}\left(\boldsymbol{I}\;\; \boldsymbol{A}_2^{-1}\boldsymbol{A}_1\;\; -\boldsymbol{A}_2^{-1}\boldsymbol{B}_1\right)\begin{pmatrix}\boldsymbol{e}_{k-1}\left(\left|^{t+1}_{t+n_1}\right.\right)\\ \boldsymbol{y}_k\left(\left|^{t-n+1}_{t}\right.\right)-\boldsymbol{y}_{k-1}\left(\left|^{t-n+1}_{t}\right.\right)\\ \boldsymbol{u}_k\left(\left|^{t-m+1}_{t-1}\right.\right)-\boldsymbol{u}_{k-1}\left(\left|^{t-m+1}_{t-1}\right.\right)\end{pmatrix} \quad (40)$$

Let $\left(\boldsymbol{K}_1\;\; \boldsymbol{K}_2\;\; \boldsymbol{K}_3\right)=\boldsymbol{K}\left(\boldsymbol{I}\;\; \boldsymbol{A}_2^{-1}\boldsymbol{A}_1\;\; -\boldsymbol{A}_2^{-1}\boldsymbol{B}_1\right)$, then the above ILC law can be decomposed as

$$u_k(t)=u_{ilc,k}(t)+u_{mpc,k}(t) \quad (41)$$

where $u_{ilc,k}(t)$ and $u_{mpc,k}(t)$ are described by

$$\Sigma_{ILC}: \qquad u_{ilc,k}(t)=u_{ilc,k-1}(t)+\boldsymbol{K}_1\boldsymbol{e}_{k-1}\left(\left|^{t+1}_{t+n_1}\right.\right) \quad (42)$$

$$\Sigma_{MPC}: \qquad u_{mpc,k}(t)=\boldsymbol{K}_2\boldsymbol{y}_k\left(\left|^{t-n+1}_{t}\right.\right)+\boldsymbol{K}_3\boldsymbol{u}_k\left(\left|^{t-m+1}_{t-1}\right.\right) \quad (43)$$

It is clear that Σ_{ILC} is an ILC law for the improvement of control performance from batch to batch, while Σ_{MPC} is an MPC law ensuring control performance over time of each cycle. The 2D based design framework gives a united design of these two types of control laws. The equivalent structure of the closed-loop system is shown as Figure 1(b), where the triangular blocks represent the proportional controllers.

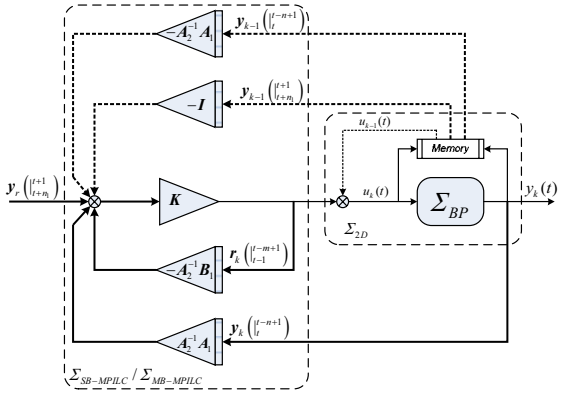

(a)

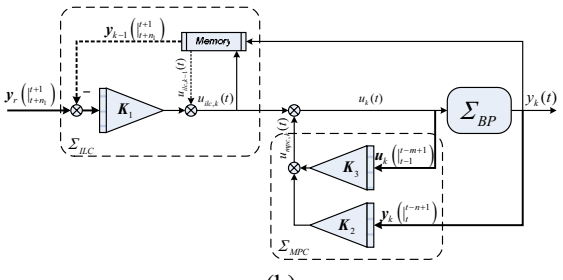

(b)

Fig 1. Equivalent system structures: (a) 2D system structure; (b) ILC system.

5. 2D-MPILC SCHEMES BASED ON 2D CONTROL PENALTY

In cost functions (6) and (7), the tracking errors and the change of control variable along the batch index are penalized. Theoretically, for any desired trajectory, the optimal control driving the cost function (6) and (7) approaching to zero can be achieved gradually by refining the control signal iteratively. An ILC strategy, in essence, searches for process input by inversing the process dynamic to generate the desired trajectory. For a non-minimum phase system, however, the inversion of the process is unstable; this can result in that the optimal control may not be physically realizable. One way to solve this problem is to place hard restrictions on the control variable, leading to a quadratic programming problem for the controller design (Lee *et al.*, 2000). Another method is to introduce a penalty to the change of the control variable along the time axis into the cost functions as well, resulting in the following cost functions with 2D control penalty,

- Single-batch cost function

$$J(t,k,n_1,n_2)=\sum_{i=1}^{n_1}\alpha(i)\left(\hat{e}_{k|k}(t+i\,|\,t)\right)^2+\sum_{j=1}^{n_2}\beta(j)\left(r_k(t+j-1)\right)^2+\sum_{j=1}^{n_2}\gamma(j)\left(\Delta u_k(t+j-1)\right)^2 \quad (44)$$

- Multi-batch cost function

$$J(t,k,n_1,n_2,n_3)=\sum_{l=1}^{n_3}\lambda(l)\left(\sum_{i=1}^{n_1}\alpha(i)\left(\hat{e}_{k+l-1|k}(t+i\,|\,t)\right)^2+\sum_{j=1}^{n_2}\beta(j)\left(r_{k+l-1}(t+j-1)\right)^2+\sum_{j=1}^{n_2}\gamma(j)\left(\Delta u_{k+l-1}(t+j-1)\right)^2\right) \quad (45)$$

where $\Delta u_k(t)=u_k(t)-u_k(t-1)$, indicating the change of the control variable along the time index, $\gamma(j)\ge 0$ is the weighting factor.

In this section, single-batch 2D-MPILC scheme will be developed based on the cost function (44). By using dynamic programming, the multi-batch case can be developed in a similar way.

Clearly, cost function (44) can be written in matrix form as

$$J(t,k,n_1,n_2)=\hat{\boldsymbol{e}}_{k|k}^T\left(\left|{}_{t+n_1}^{t+1}\,|\,t\right.\right)\boldsymbol{Q}\hat{\boldsymbol{e}}_{k|k}\left(\left|{}_{t+n_1}^{t+1}\,|\,t\right.\right)+\boldsymbol{r}_k^T\left(\left|{}_{t+n_2-1}^{t}\right.\right)\boldsymbol{R}\boldsymbol{r}_k\left(\left|{}_{t+n_2-1}^{t}\right.\right)+\Delta\boldsymbol{u}_k^T\left(\left|{}_{t+n_2-1}^{t}\right.\right)\boldsymbol{S}\Delta\boldsymbol{u}_k\left(\left|{}_{t+n_2-1}^{t}\right.\right)$$

$$=\begin{pmatrix}\hat{\boldsymbol{e}}_{k|k}\left(\left|{}_{t+n_1}^{t+1}\,|\,t\right.\right)\\ \Delta\boldsymbol{u}_k\left(\left|{}_{t+n_2-1}^{t}\right.\right)\end{pmatrix}^T\begin{pmatrix}\boldsymbol{Q}&\boldsymbol{0}\\ \boldsymbol{0}&\boldsymbol{S}\end{pmatrix}\begin{pmatrix}\hat{\boldsymbol{e}}_{k|k}\left(\left|{}_{t+n_1}^{t+1}\,|\,t\right.\right)\\ \Delta\boldsymbol{u}_k\left(\left|{}_{t+n_2-1}^{t}\right.\right)\end{pmatrix}+\boldsymbol{r}_k^T\left(\left|{}_{t+n_2-1}^{t}\right.\right)\boldsymbol{R}\boldsymbol{r}_k\left(\left|{}_{t+n_2-1}^{t}\right.\right)$$

where $\boldsymbol{S}=diag\{\gamma(1),\gamma(2),...,\gamma(n_2),\}$. From relation

$$\Delta u_k(t)=r_k(t)-r_k(t-1)+\Delta u_{k-1}(t) \quad (46)$$

we have

$$\Delta\boldsymbol{u}_k\left(\left|{}_{t+n_2-1}^{t}\right.\right)=\boldsymbol{H}\boldsymbol{r}_k\left(\left|{}_{t+n_2-1}^{t}\right.\right)+\Delta\boldsymbol{u}_{k-1}\left(\left|{}_{t+n_2-1}^{t}\right.\right) \quad (47)$$

where

$$\boldsymbol{H}=\begin{pmatrix}1&0&0&\cdots\\ -1&1&0&\cdots\\ 0&-1&1&\cdots\\ \vdots&\vdots&\vdots&\ddots\end{pmatrix}_{n_2\times n_2} \quad (48)$$

Together with 2D prediction model (21), the following augmented 2D prediction model is obtained

$$\begin{pmatrix}\hat{\boldsymbol{e}}_{k|k}\left(\left|{}_{t+n_1}^{t+1}\,|\,t\right.\right)\\ \Delta\boldsymbol{u}_k\left(\left|{}_{t+n_2-1}^{t}\right.\right)\end{pmatrix}=\begin{pmatrix}-\boldsymbol{G}\\ \boldsymbol{H}\end{pmatrix}\boldsymbol{r}_k\left(\left|{}_{t+n_2-1}^{t}\right.\right)+\begin{pmatrix}\boldsymbol{e}_{k-1}\left(\left|{}_{t+n_1}^{t+1}\right.\right)\\ \Delta\boldsymbol{u}_{k-1}\left(\left|{}_{t+n_2-1}^{t}\right.\right)\end{pmatrix}+\begin{pmatrix}-\boldsymbol{F}_k(t)\\ \boldsymbol{0}\end{pmatrix}$$

Based on optimization algorithm, the optimal control law is obtained as

$$\boldsymbol{r}_k^*\left(\left|{}_{t+n_2-1}^{t}\right.\right)=-\left(\boldsymbol{R}+\begin{pmatrix}-\boldsymbol{G}\\ \boldsymbol{H}\end{pmatrix}^T\begin{pmatrix}\boldsymbol{Q}&\boldsymbol{0}\\ \boldsymbol{0}&\boldsymbol{S}\end{pmatrix}\begin{pmatrix}-\boldsymbol{G}\\ \boldsymbol{H}\end{pmatrix}\right)^{-1}\begin{pmatrix}-\boldsymbol{G}\\ \boldsymbol{H}\end{pmatrix}^T\begin{pmatrix}\boldsymbol{Q}&\boldsymbol{0}\\ \boldsymbol{0}&\boldsymbol{S}\end{pmatrix}\cdot\left(\begin{pmatrix}\boldsymbol{e}_{k-1}\left(\left|{}_{t+n_1}^{t+1}\right.\right)\\ \Delta\boldsymbol{u}_{k-1}\left(\left|{}_{t+n_2-1}^{t}\right.\right)\end{pmatrix}+\begin{pmatrix}-\boldsymbol{F}_k(t)\\ \boldsymbol{0}\end{pmatrix}\right)$$

$$=\left(\boldsymbol{R}+\boldsymbol{G}^T\boldsymbol{Q}\boldsymbol{G}+\boldsymbol{H}^T\boldsymbol{S}\boldsymbol{H}\right)^{-1}\left(\boldsymbol{G}^T\boldsymbol{Q}\left(\boldsymbol{e}_{k-1}\left(\left|{}_{t+n_1}^{t+1}\right.\right)-\boldsymbol{F}_k(t)\right)-\boldsymbol{H}^T\boldsymbol{S}\Delta\boldsymbol{u}_{k-1}\left(\left|{}_{t+n_2-1}^{t}\right.\right)\right) \quad (49)$$

Let $\boldsymbol{K}_1$ and $\boldsymbol{K}_2$ indicate respectively the first row of matrices $\left(\boldsymbol{R}+\boldsymbol{G}^T\boldsymbol{Q}\boldsymbol{G}+\boldsymbol{H}^T\boldsymbol{S}\boldsymbol{H}\right)^{-1}\boldsymbol{G}^T\boldsymbol{Q}$ and $-\left(\boldsymbol{R}+\boldsymbol{G}^T\boldsymbol{Q}\boldsymbol{G}+\boldsymbol{H}^T\boldsymbol{S}\boldsymbol{H}\right)^{-1}\boldsymbol{H}^T\boldsymbol{S}$, then the single-batch 2D-MPILC law can be formulated as

$$u_k(t)=u_{k-1}(t)+\boldsymbol{K}_1\left(\boldsymbol{e}_{k-1}\left(\left|{}_{t+n_1}^{t+1}\right.\right)-\boldsymbol{F}_k(t)\right)+\boldsymbol{K}_2\Delta\boldsymbol{u}_{k-1}\left(\left|{}_{t+n_2-1}^{t}\right.\right) \quad (50)$$

Different from 2D-MPILC law (27), the above control law has an additional term depending on the changes of control signal in last cycle over the prediction horizon. As the change of the control variable along both time and cycle directions are penalized, weighting factors $\beta(\bullet)$ and $\gamma(\bullet)$ should be designed properly to ensure the feasible and necessary variation of control signal along both time and cycle indices.

6. EXAMPLES

Injection molding process is a typical repetitive process (Gao *et al.*, 2001; Shi *et al.*, 2005), where many process variables need to be controlled to follow certain profiles repetitively to ensure the product quality. To illustrate the effectiveness of the proposed schemes, a simulation is performed on the following the injection velocity control process

$$\Sigma_{BP}: P_k(q^{-1})=\frac{2.651q^{-1}+5.298q^{-2}+0.5805q^{-3}}{1-1.454q^{-1}+0.5285q^{-2}-0.04736q^{-3}} \quad (51)$$

The designs of control schemes are based on the following simplified model

$$\Sigma_{MBP}: \quad M_k(q^{-1})=q^{-1}\frac{13.81q^{-1}}{1-0.9524q^{-1}} \quad (52)$$

For cost functions (6) and (7) with parameters

$$n_1=10,\ n_2=10,\ n_3=3,\ \alpha=1,\ \beta=100,\ \lambda=1 \quad (53)$$

single-batch and multi-batch 2D-MPILC laws are designed, and their set-point tracking results are shown in Figure 2 and Figure 3, respectively. In both cases, MPC control law guarantees a good tracking performance even in the first cycle and the control performance improves by the ILC from cycle to cycle. As process (51) has an unstable zero, significant oscillations of control input signal are required for the perfect tracking, as seen in the control signals of the 30th cycle shown in Figure 2 and Figure 3. This may be not practical. To solve this problem, single-batch 2D-MPILC law (50) is designed based on the cost function (44) with weighting factor $\gamma=10$. The simulation results are

shown in Figure 4. It is clearly seen that the oscillation of control signal are reduced with the satisfactory control performance maintained. The sum of tacking errors over each cycle for different control schemes are shown in Figure 5, indicating that multi-batch 2D-MPILC scheme has the best convergence along the cycle index.

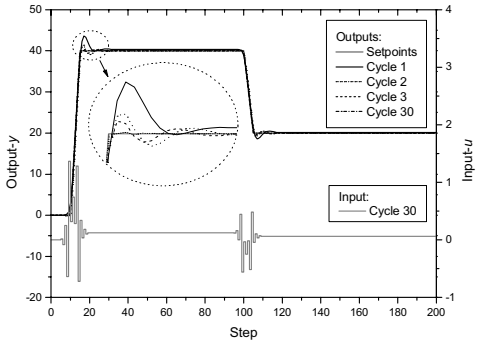

Fig 2. Output responses and control signal of single-batch 2D-MPILC scheme.

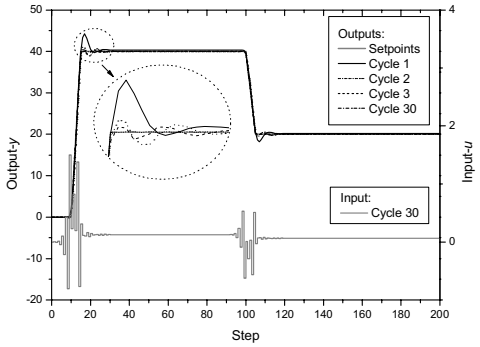

Fig 3. Output responses and control signal of multi-batch 2D-MPILC scheme.

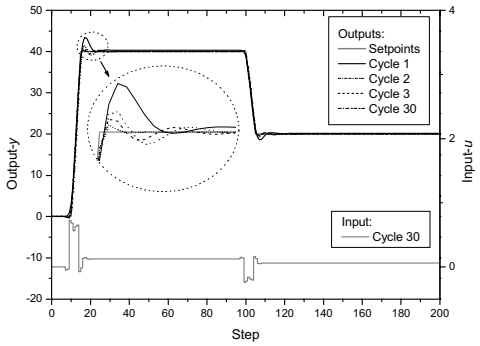

Fig 4. Output responses and control signal of single-batch 2D-MPILC scheme based on 2D control penalty.

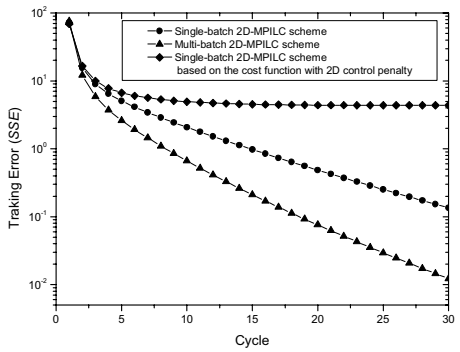

Fig 5. Tracking errors of different control schemes.

7. CONCLUSIONS

In this paper, iterative learning control design problem has been modelled and solved from the 2D system viewpoint. Single-batch and multi-batch 2D-MPILC schemes have been developed in the framework of MPC of a 2D system problem. The resulted 2D-MPILC laws implicitly combine an MPC along time with an ILC along cycle to ensure the optimal control in 2D sense. The computational load and performance of the proposed design methods can be balanced by proper selection of design parameters in the defined cost functions. 2D control penalty can be further introduced to the 2D-MPILC design to ensure non-oscillatory operation.

REFERENCES

Amann, N., Owens, D.H., Rogers, E. (1995). Iterative learning control for discrete time systems using optimal feedback and feedforward actions. *Proceedings of the 34th Conference on Decision and Control, New Orleans, LA*, pp1696-1701.

Amann, N., Owens, D.H., Rogers, E. (1996). Iterative learning control using optimal feedback and feedforward actions. *Int. J. Control*, Vol. 65(2), 277-293.

Arimoto, S., Kawamura, S., Miyazaki, F. (1984). Bettering operation of robots by learning. *Journal of Robotic Systems*, Vol.1(2), pp123-140.

Gao, F., Yang, Y., Shao, C. (2001). Robust iterative learning control with applications to injection molding process. *Chemical Engineering Science*, Vol.56, pp7025-7034.

Geng, Z., Carroll, R., Xie, J. (1990) Two-dimensional model and algorithm analysis for a class of iterative learning control systems. *Int. J. Control*, Vol. 52(4), pp833-862.

Kurek, J.E., Zaremba, M.B. (1993). Iterative learning control synthesis based on 2-D system theory. *IEEE Transactions on Automatic Control*, Vol.38(1), pp121-125.

Lee, J.H., Lee, K.S., Kim, W.C. (2000). Model-based iterative learning control with a quadratic criterion for time-varying linear systems. *Automatica*, Vol.36, pp641-657.

Owens, D.H., Amann, N., Rogers, E., French, M. (2000). Analysis of linear iterative learning control schemes – a 2D system/repetitive processes approach. *Multidimensional Systems and Signal Processing*, Vol.11, pp125-177.

Shi, J., Gao, F., Wu, T.-J. (2005). Robust design of integrated feedback and iterative learning control of a batch process based on a 2D Roesser system. *Journal of Process Control*, Vol.15, pp907-924.

Xu, J.-X., Bien, Z.Z. (1998). The frontiers of iterative learning control. In: *Iterative Learning Control: Analysis, Design, Integration and Application.* Kluwer Academic Publishers, Boston/Dordrecht/London, pp9-35.

ADCHEM 2006

International Symposium on Advanced Control of Chemical Processes
Gramado, Brazil – April 2-5, 2006

SCALE-UP OF BATCH PROCESSES VIA DECENTRALIZED CONTROL

A. Marchetti, M. Amrhein, B. Chachuat and D. Bonvin

Laboratoire d'Automatique
Ecole Polytechnique Fédérale de Lausanne (EPFL)
CH-1015 Lausanne, Switzerland

Abstract: The economic environment in the specialty chemicals industry requires short times to market and thus the ability to develop new products and processes rapidly. This, in turn, calls for large scale-ups from laboratory to production. Due to scale-related differences in operating conditions, direct extrapolation of conditions obtained in the laboratory is often impossible, especially when terminal objectives must be met and path constraints respected. This paper proposes a decentralized control scheme for scaling-up the operation of batch and semi-batch processes. The targets to be reached are either taken directly from laboratory experiments or adjusted to account for production constraints. Some targets are reached on-line within a given run, while others are implemented on a run-to-run basis. The methodology is illustrated in simulation via the scale-up of a semi-batch reactor.

Keywords: Scale-up, Batch processes, Decentralized control, Batch control, Iterative learning control, Run-to-run control

1. INTRODUCTION

The production of a wide variety of specialty chemicals, pharmaceutical products, food and agricultural products, dyes, composites and polymers calls for small production volumes and variable requirements, which has made batch or semi-batch processing the prime mode of operation. The production of specialty chemicals in batch reactors typically involves following conservative recipes that have been developed in the laboratory with the objective to achieve satisfactory productivity and meet safety and quality requirements. The extrapolation of these recipes to large-scale operation is often made difficult by differences in both equipment and scale. Of particular importance are differences in mass and heat transfer characteristics, residence time distributions, surface-to-volume ratios and heat removal, which can lead to considerable performance degradation and constraint violations (Bisio and Kabel, 1985).

Until recently, conservative approaches to scale-up have been used, mainly performing experiments at intermediate scales of operation before going to large-scale production. However, since the production of specialty chemicals is the subject of intense competition, it has become imperative to go as quickly as possible from a limited number of laboratory experiments to batch production campaigns. Dynamic simulation is avoided because it is often difficult and time consuming to develop sufficiently accurate models (Bonvin, 1998). Current industrial practice uses reaction calorimeters to perform screening experiments and obtain a sound chemical knowledge regarding the reac-

tion phases, the solvent and the type of catalyst. Then, statistical experimental design techniques are used to 'optimize' the process. The key factors (e.g., solvent, type of catalyst, temperatures, reactant concentrations, feed rates, pH, reaction time) that affect the main outcome of the process (e.g., conversion, purity, reaction time, safety indicators) are identified (Roberge, 2004). A limited number of experiments is usually performed, leading to some empirical model that describes the cause-effect relationship in the process, e.g. in the form of a quadratic response surface as a function of the key factors.

When the initial investigations reveal the presence of scale-dependent effects, the experimental design study should be carried out at a larger (pilot plant) scale. However, since there is often only limited time and resources for pilot-plant design, construction and operation, batch processes are often scaled-up directly to production scale by setting some of the independent factors to conservative levels for safety reasons.

Ideally, one wishes to obtain similar performance by extrapolating the laboratory recipe to production scale. However, due to the aforementioned scale-dependent uncertainty, different (and often lesser) performance is obtained and part of the operational requirements may be violated. Fortunately, measurements can be used to compensate the effect of uncertainty by adjusting the available manipulated variables consisting of independent factors and manipulated profiles. With the availability of measurements, scale-up can be considered as a control problem, i.e. the setpoints correspond to the desired specifications and the manipulated variables are the free elements of the batch operation.

Batch processes are characterized by two types of outputs, the run-time outputs (quantities that can be measured on-line) and the run-end outputs (quantities that are only available at final time). Hence, the control problem has many facets: It is multivariable and involves meeting objectives (setpoints) both during the batch and at final time. By appropriately defining the manipulated variables (independent factors and input profiles) and assigning them to the different performance objectives, there results a decentralized control scheme.

The paper is organized as follows. Section 2 reviews the available control approaches for batch processes. The scale-up problem and the formulation of a decentralized control problem are presented in Section 3. The methodology is illustrated in simulation via the scale-up of a semi-batch reactor in Section 4, and conclusions are drawn in Section 5.

2. CONTROL OF BATCH PROCESSES

The control of batch processes differs from that typically found in continuous processes for two main reasons: (i) Batch processes have no steady-state operating point, and (ii) they are characterized by two 'time' variables, the run time t and the run index k. The first reason implies the presence of time-varying profiles for the setpoints and the manipulated variables. The second reason provides additional degrees of freedom for meeting the control objectives since the work does not necessarily have to be completed in a single batch but can be distributed over several batches. However, this brings into picture an additional type of outputs that need to be controlled, i.e. the run-end outputs z. The main difficulty is that these outputs are only available at the end of the run.

The model of a batch process, including the two time variables t and k and the run-end outputs z, can be written generically as:

$$\dot{x}_k(t) = F(x_k(t), u_k(t)), \qquad x_k(0) = x_{0,k} \quad (1)$$

$$y_k(t) = H(x_k(t), u_k(t)) \quad (2)$$

$$z_k = Z(x_k[0, t_f], u_k[0, t_f]) \quad (3)$$

where t refers to the run time and the subscript $(.)_k$ to the run index. x represents the state vector, u the input vector, and t_f the final time. F and H are vector functions and Z is a vector operator. There are two types of outputs, the run-time outputs $y(t)$ –or, equivalently, the complete profiles $y[0, t_f]$– that are measured on-line, and the run-end outputs z evaluated at the end of the batch. The corresponding setpoints express the control objectives, i.e. the desired run-time output profiles $y_{\mathrm{sp}}(t)$ or $y_{\mathrm{sp}}[0, t_f]$ and the desired run-end output values z_{sp}.

Accordingly, there are two types of control objectives, and also different ways of reaching them as illustrated in Figure 1 and discussed next (Bonvin *et al.*, 2005).

Implementation aspect	*Control objectives*	
	Run-time setpoints $y_{sp}(t)$ or $y_{sp}[0,t_f]$	Run-end setpoints z_{sp}
On-line	1 On-line control $u(t) \rightarrow y(t) \rightarrow y[0,t_f]$ (PID)	2 Predictive control $u[t,t_f] \rightarrow z_{pred}(t)$ (MPC)
Run-to-run	3 Iterative learning control $u_k[0,t_f] \rightarrow y_k[0,t_f]$ (ILC)	4 Run-to-run control $\mathcal{U}(\pi_k) = u_k[0,t_f] \rightarrow z_k$ (R2R)

Fig. 1. Control approaches to meet run-time and run-end objectives.

2.1 On-line control of run-time outputs

The approach is similar to that used in continuous processing. However, though certain controlled variables such as temperature may be constant, the key process characteristics such as process gain and time constants can vary considerably. Hence, the need to provide adaptation or efficient feedforward control to handle the main part of the expected variations. Control is typically done using PID techniques or more sophisticated alternatives whenever necessary. Formally, this controller can be written as:

$$u_k(t) = \mathcal{K}(y_k(t), y_{\mathrm{sp}}(t)) \tag{4}$$

where $\mathcal{K}$ is the on-line controller run-time outputs and $y_{\mathrm{sp}}(t)$ the setpoint at time instant t.

2.2 On-line control of run-end outputs

With this approach, it is necessary to predict the run-end outputs based on measurement of the run-time outputs. Model predictive control (MPC) is well suited to that task (Nagy and Braatz, 2003). Note, however, that the (mechanistic) process models needed for prediction are often very simplified and thus of limited accuracy in batch processes. The controller can be written as:

$$u_k(t) = \mathcal{P}(z_{\mathrm{pred},k}(t), z_{\mathrm{sp}}) \tag{5}$$

where $\mathcal{P}$ is the on-line controller for run-end outputs and $z_{\mathrm{pred},k}(t)$ the prediction of z available at time instant t.

2.3 Run-to-run control of run-time outputs

The manipulated variable profiles can be generated using Iterative Learning Control (ILC) that exploits information from previous runs (Moore, 1993). Clearly, this strategy exhibits the limitations of open-loop control for run-time operation, in particular the fact that there is no feedback correction for run-time disturbances. Yet, this scheme is highly efficient for generating a feedforward input term. The controller has the following structure:

$$u_{k+1}[0, t_f] = \mathcal{I}(y_k[0, t_f], y_{\mathrm{sp}}[0, t_f]) \tag{6}$$

where $\mathcal{I}$ is the iterative learning controller for the run-time outputs. It processes the entire profile of the current run to generate the entire manipulated profile for the next run.

2.4 Run-to-run control of run-end outputs

The input profiles are parameterized using the input parameters π_k, i.e. $u_k[0, t_f] = \mathcal{U}(\pi_k)$. This way, the batch process can be seen as a static map between the input parameters π_k, which are set before the run starts, and the run-end outputs z_k. Control can then be implemented using discrete integral control laws, i.e. $\pi_{k+1} = \pi_k + K(z_{\mathrm{sp}} - z_k)$ (François *et al.*, 2005). Formally, the controller can be written as:

$$u_{k+1}[0, t_f] = \mathcal{U}(\pi_{k+1}), \;\; \pi_{k+1} = \mathcal{R}(z_k, z_{\mathrm{sp}}) \tag{7}$$

where $\mathcal{R}$ is the run-to-run controller for the run-end outputs and $\mathcal{U}$ the input parametrization.

Of course, it is possible to combine on-line (feedback) and run-to-run (feedforward) control for either of the outputs. Except for predictive control that involves prediction, all the other control approaches use measurements only, i.e. they do not necessitate a process model for implementation – a very nice feature for the scale-up of batch processes.

3. SCALE-UP PROBLEM

3.1 Operational requirements

Because of differences in equipment and scale, the bounds on time-dependent quantities (also called path constraints) are generally different in production and in the laboratory. Examples of such path constraints include the maximum pressure in a pump, the heat removal capacity of a reactor and the maximum flowrate through a valve. Other constraints are inherent to the chemical system and do not depend on the equipment scale, such as the maximum temperature to prevent decomposition of a chemical compound. Beside path constraints, the operation of batch processes requires satisfying terminal requirements such as quality specifications or some economic perfomance. The path constraints and the terminal requirements constitute the *operational requirements* that have to be respected in production.

3.2 Recipe from the laboratory

The chemist investigates the possible synthesis routes in the laboratory and selects the key chemical parameters such as the solvent and the catalyst. The study of reaction systems in reaction calorimeters or automated laboratory reactors gives valuable information for the selection of a recipe that satisfies the operational requirements. A recipe is characterized by a set of parameters ρ_{lab} and time-varying input variables $u_{lab}(t)$. ρ_{lab} typically includes the feed concentration, the initial conditions and the amount of catalyst, while $u_{lab}(t)$ corresponds to the feed-rate policy and/or the reactor temperature profile.

So far as possible, the laboratory experiments are run in such a way that they respect operational requirements equivalent to those of production via

a *scale-down approach*. Conservatism is typically introduced in recipes so that these requirements can be met also in the presence of (slightly) different conditions. In practice, this is not always possible due to the presence of large uncertainties. The control objective is then to stir the system to the specified operational requirements.

3.3 Control problem

The formulation of the control problem involves the selection of the manipulated and controlled variables. All the elements of the recipe not being chosen as manipulated variables constitute the fixed part of the recipe and are applied without feedback from the process.

The manipulated variable profiles $u(t)$ are parameterized by time-varying arcs and the switching times between the various arcs. The resulting manipulated variables in the control problem consist of a number of arcs $\eta(t)$, and parameters π (including some of the ρ-parameters). The controlled variables include the run-time outputs $y(t)$ and the run-end ouputs z. An objective of the controlled system is to reach the corresponding setpoints, $y_{\rm sp}(t)$ and $z_{\rm sp}$, after as few batch runs as possible.

The number of manipulated variables in the control problem is chosen equal to the number of controlled variables, thus leading to a square multivariable control problem:

- Manipulated variables (MV): $\eta(t)$, π
- Controlled variables (CV): $y(t)$, z
- Control setpoints (SP): $y_{\rm sp}(t)$, $z_{\rm sp}$

A control scheme is proposed in Figure 2, where $y(t)$ is controlled on-line with the on-line controller $\mathcal{K}$ (feedback) and run-to-run with the ILC-controller $\mathcal{I}$ (feedforward). Furthermore, z is controlled on a run-to-run basis using the R2R-controller $\mathcal{R}$. Note that this control scheme does not require a mechanistic process model.

The control problem must be robust towards uncertainty in the sense that the setpoints must remain reachable in the presence of perturbed operating conditions. In practice, flexibility can be introduced by choosing conservative setpoint values for a number of extensive controlled variables such as the batch duration or the productivity (e.g., by backing-off the values obtained from the laboratory experiments). Only those set-points corresponding to controlled variables not dictated by 'hard' operational requirements can be relaxed though. This is illustrated through a semi-batch reactor example in the following section.

4. APPLICATION TO A SEMI-BATCH REACTOR

4.1 Reaction system and operational requirements

Consider the following parallel reaction scheme:

$$A + B \longrightarrow C, \qquad 2\,B \longrightarrow D. \tag{8}$$

The desired product is C, while D is undesired. The reactions are exothermic. A jacketed reactor of 7.5 $\rm m^3$ will be used in production. This reaction scheme represents one step of a rather long synthesis route, and the reactor assigned to this step is part of a multi-purpose plant. Allocation of the different operations in the plant requires that the reaction duration does not exceed 240 min. The final selectivity of D, $y_D(t_f)$ defined below, should not exceed $y_{D,max}$=18%. The lowest achievable cooling jacket temperature is $T_{j,min} = 10$°C. The manipulated input profiles are the feed rate F, and the flowrate of coolant through the jacket F_j. With this, the operational requirements are:

$$T_j(t) \geq 10\text{°C} \tag{9}$$

$$y_D(t_f) = \frac{2\ n_D(t_f)}{n_C(t_f) + 2\ n_D(t_f)} \leq 0.18 \tag{10}$$

where n_C and n_D denote the number of moles of C and D in the reactor, respectively.

4.2 Recipe from the laboratory

In the laboratory, a 1.5 l reaction calorimeter is used. The reactor is initially filled with A, and B is added at the constant feed rate $\bar{F}$. The reaction is performed isothermally at $T_r = 40$°C. Though the cooling rate q_c is not a limitation in the laboratory, a scale-down of the production path constraint (9) is proposed as:

$$[q_{c,max}]_{\rm lab} = [(T_r - T_{j,min})UA]_{\rm prod}\,/r, \tag{11}$$

where $r = 5000$ is the scale-up factor and $UA = 3.7 \times 10^4$ J/mol °C the estimated heat transfer capacity of the production reactor. With $(T_r - T_{j,min}) = 30$°C, the maximum cooling rate, $q_{c,max}$, is 222 J/min. Note that $q_{c,max}$ restricts the value of $\bar{F}$.

The fixed part of the recipe includes the initial concentrations of A and B, c_{A_o} and c_{B_o}, the feed concentration of B, $c_{B_{in}}$, the reactor temperature T_r, and the initial volume V_o. The numerical values of the recipe are given in Table 1. The results obtained for a batch run in the laboratory are given in Table 2. Notice the conservatism in the recipe with respect to the operational requirements $y_{D,max}$ and $q_{c,max}$.

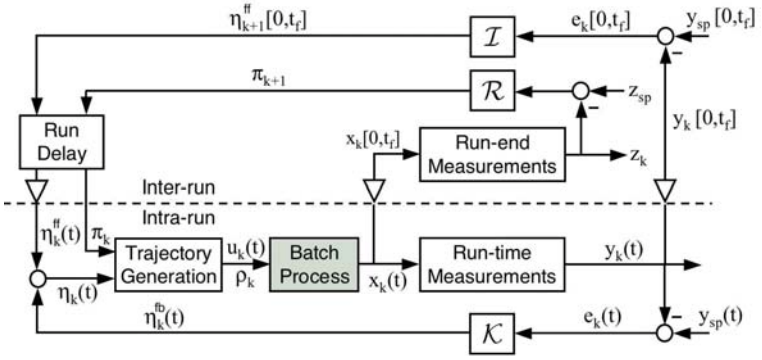

Fig. 2. Control scheme for scale-up implementation. Notice the distinction between intra-run and inter-run activities. The symbol $\triangledown$ is used to indicate a change in viewing the time argument, e.g. from a trajectory to an instantaneous value when going downward and conversely when going upward.

Table 1. Recipe for the laboratory.

T_r	40	°C	$c_{B_{in}}$	5	mol/l
c_{A_o}	0.5	mol/l	c_{B_o}	0	mol/l
V_o	1	l	t_f	240	min
$\bar{F}$	0.0004	l/min			

Table 2. Laboratory results.

$n_C(t_f) = 0.346$ mol	$\max_t(q_c(t)) = 182.6$ J/min
$y_D(t_f) = 0.1706$	

4.3 Control problem for production

Temperature control is achieved via a cascade control scheme, with a slave and a master loop as shown in Figure 3. The master loop receives the reactor temperature setpoint $T_{r,\mathrm{sp}}$, and computes the feedback part of the jacket temperature setpoint $T^{\mathrm{fb}}_{j,\mathrm{sp}}$, while the slave loop adjusts F_j so as to track the jacket temperature setpoint $T_{j,\mathrm{sp}}(t) = T^{\mathrm{ff}}_{j,\mathrm{sp}}(t) + T^{\mathrm{fb}}_{j,\mathrm{sp}}(t)$. The feedforward term for the jacket temperature setpoint $T^{\mathrm{ff}}_{j,\mathrm{sp}}$, is constant at 20°C. Alternatively, an ILC controller could be used to adjust $T^{\mathrm{ff}}_{j,\mathrm{sp}}(t)$. This does not seem necessary here as the feedback action alone allows satisfactory control of the reactor temperature (see Figure 4 below).

The goal of the scale-up is to reproduce in production the final selectivity obtained in the laboratory, while guaranteeing a given productivity of C. Therefore, $n_C(t_f)$ and $y_D(t_f)$ are chosen as the controlled variables. If the laboratory results were directly extrapolated to production, the final productivity of C would be: $[n_C(t_f)]_{\mathrm{prod}} = r \times [n_C(t_f)]_{\mathrm{lab}} = 1730$ mol. However, due to scale-related uncertainty, a certain backoff is introduced on the productivity setpoint to make the control problem more flexible. Two manipulated parameters are needed to control these two run-end outputs. Hence, the feed rate profile $F[0, t_f]$ is parameterized using a 2-stage piecewise-constant approximation (with parameters F_1 and F_2). Overall, the control problem reads:

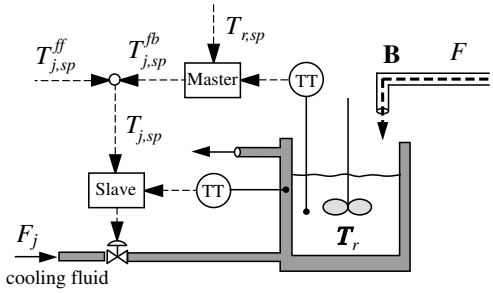

Fig. 3. Cascade structure for temperature control.

- MV: $\eta(t) = T_{j,\mathrm{sp}}(t), \quad \pi = \left[\, F_1,\ F_2 \,\right]^T$
- CV: $y(t) = T_r(t),\ z = \left[\, n_C(t_f),\ y_D(t_f) \,\right]^T$
- SP: $y_{\mathrm{sp}}(t) = 40°\mathrm{C},\ z_{\mathrm{sp}} = \left[\, 1530 \text{ mol},\ 0.17 \,\right]^T$

The proposed control scheme includes the following elements: (i) A cascade scheme, with master controller $\mathcal{K}$, that controls the reactor temperature in real time , and (ii) an integral run-to-run controller $\mathcal{R}$ that controls z by adjusting π:

$$\text{(i)}\ T^{\mathrm{fb}}_{j,\mathrm{sp}}(t) = k_{\mathcal{K}} \left(e(t) + \frac{1}{\tau_{I,\mathcal{K}}} \int_0^t e(\tau) d\tau \right) \quad (12)$$

$$\text{(ii)}\quad \pi_{k+1} = \pi_k + G^{-1} K_{\mathcal{R}} [z_{\mathrm{sp}} - z_k] \quad (13)$$

with $e(t) = T_{r,\mathrm{sp}}(t) - T_r(t)$, $k_{\mathcal{K}}$ the scalar proportional gain, and $\tau_{I,\mathcal{K}}$ the integral time constant of the PI master controller. The integral term of the run-to-run controller is based on the sensitivities of the run-end output errors with respect to π, i.e. $G = \partial(z_{sp} - z)/\partial\pi$, which are estimated experimentally from laboratory or process data (François *et al.*, 2005). Notice that G is a 2×2 matrix, and $K_{\mathcal{R}}$ is the diagonal controller gain matrix.

4.4 Production results

The recipe given in Table 1 is applied in production by scaling-up the extensive variables V_o and $\bar{F}$. Here, $V_o = 5$ m^3 (for all runs), and $F_1 = F_2 = \bar{F}\, r = 2$ l/min for $k = 1$ (subsequently adapted

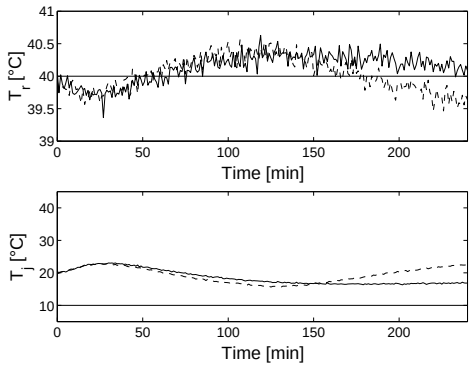

Fig. 4. Temperature profiles for the first and last batches. Top: T_r; bottom: T_j. Solid: k=1; dashed: k=20.

according to (13) for $k > 1$). For the simulation of the production reactor, the kinetic rate constants of the first and second reactions are reduced by 25% and 20%, respectively. Also, Gaussian noise with standard deviation of 0.001mol/l is introduced for the measurement of the final concentrations $c_C(t_f)$ and $c_D(t_f)$, and with standard deviation of 0.1°C for the measurement of $T_r(t)$.

On applying the recipe directly to production, one gets $n_C(t_f) = 1637$ mol and $y_D(t_f) = 0.198$. Therefore, the final selectivity of D violates the operational requirements in the first batch. The batch-to-batch evolution of the run-end outputs $n_C(t_f)$ and $y_D(t_f)$ is shown in Figure 5. It is seen that the requirement on $y_D(t_f)$ is fulfilled after about 5 batches, and the region where the adaptation is within the noise level is attained after 8-10 batches. During the adaptation, parameter F_2 takes a lower value than F_1.

On the other hand, the profiles of T_r and T_j during runs 1 and 20 are shown in Figure 4. Note in particular that the minimum jacket temperature is not reached during the operation, i.e. the operational requirement on $T_{j,min}$ is satisfied.

Clearly, the batch operation is suboptimal in this example, since the productivity is regulated at a somewhat conservative value. A higher production of C could be obtained, e.g., by pushing the operation towards the active operational constraints (9) and (10). However, this self-optimizing alternative should be studied in the context of NCO-tracking (tracking the Necessary Conditions of Optimality) (Srinivasan *et al.*, 2003) and falls beyond the scope of the present paper.

5. CONCLUSIONS

The formulation of a multivariable control problem that is implemented in a two-'time' space has been presented for meeting run-time and run-end objectives for batch processes. This work shows how to construct and operate such a decentralized

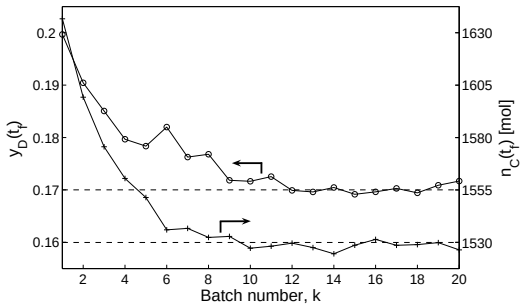

Fig. 5. Approaching the run-end setpoints in a run-to-run manner. (+): $n_C(t_f)$; (∘): $y_D(t_f)$; dashed lines: setpoints.

control approach for scaling-up the operation of batch processes. A control scheme that includes an on-line controller, an ILC controller and a R2R-controller has been proposed. It is illustrated through a simple scale-up example of a semi-batch reactor.

Future work will address the interaction between on-line and run-to-run control activities, as well as the use of self-optimizing decentralized control for the scale-up of batch processes. For this last point, the NCO-tracking methodology will be implemented.

REFERENCES

Bisio, A. and R. L. Kabel (1985). *Scaleup of Chemical Processes. Conversion from Laboratory Scale Tests to Successful Commercial Size Design*. John Wiley.

Bonvin, D. (1998). Optimal operation of batch reactors - A personal view. *J.Process.Contr.* **8**(5-6), 355–368.

Bonvin, D., B. Srinivasan and D. Hunkeler (2005). Control and optimization in the batch chemical industry. In: *IEEE Control Systems Magazine (CSM), Submitted*.

François, G., B. Srinivasan and D. Bonvin (2005). Use of measurements for enforcing the necessary conditions of optimality in the presence of constraints and uncertainty. *J.Process.Contr.* **15**(6), 701–712.

Moore, K. L. (1993). *Iterative Learning Control for Deterministic Systems*. Springer-Verlag, Advances in Industrial Control. London.

Nagy, Z. K. and R. D. Braatz (2003). Robust nonlinear model predictive control of batch processes. *AIChE J.* **49**(7), 1776–1786.

Roberge, D. (2004). An integrated approach combining reaction engineering and design of experiments for optimizing reactions. *Org.Proc.Res.Dev.* **8**, 1049–1053.

Srinivasan, B., D. Bonvin, E. Visser and S. Palanki. (2003). Dynamic optimization of batch processes: II. Role of measurements in handling uncertainty. *Comp.Chem.Eng.* **27**, 27–44.

ADCHEM 2006

International Symposium on Advanced Control of Chemical Processes
Gramado, Brazil – April 2-5, 2006

REAL-TIME DYNAMIC OPTIMIZATION OF NON-LINEAR BATCH SYSTEMS

Nathaniel Peters * **Martin Guay** * **Darryl DeHaan** *

* *Queen's University, Kingston, Ontario, Canada*

Abstract: In this paper a methodology for designing and implementing a real time optimizing controller for nonlinear batch processes is discussed. The controller is used to optimize the system input and state trajectories according to a cost function. An interior point method with penalty function is used to incorporate constraints into a modified cost functional, and a Lyapunov based extremum seeking approach is used to compute the trajectory parameters. This technique was previously proposed for optimizing differentially flat systems in a cascade implementation. Smooth trajectories were generated with reduced computing time compared to many optimizations in literature. In this paper the theory is extended to general non-flat nonlinear systems in a true on-line optimization.

Keywords: real-time optimization, batch optimization, on-line optimization

1. INTRODUCTION

Industrial chemical processes can be divided into two categories of production: continuous and fed-batch. Continuous processes are designed to run at steady-state. Examples include oil refining, gas processing, and many chemical processes. To maximize the efficiency and profits from these processes, it is necessary to keep the plant in the operating range under disturbances. The optimization task required to operate such processes is usually performed to achieve disturbance rejection, designing con- trollers to reach and maintain set-point effectively, and keeping the down time to a minimum. Since the operating range is generally very narrow, the system dynamics can often be approximated by linear dynamics. Batch processing, however, provides some very unique challenges. Batch processes have a finite operating time, rather than a continuous operation. The control objective in batch processing is not to reach steady state, but to reach some desired objective by the end of the batch. This usually involves movement through a very wide operating range, and nonlinearities in the system can be very strong. Batch optimization focuses on maximizing the performance objective by finding the corresponding system trajectories. Since batch production is usually of low volume, high value production, optimization of its operation is critical to make the process viable. Examples include pharmaceuticals, specialty chemicals, biological processes, and food production.

To determine the optimal profiles for a batch process, an off-line optimization is often performed to design the best possible profiles to be followed by the batch process. Typically, this is accomplished using some sort of nonlinear programming method. The computations are usually very extensive and must be performed off-line and then implemented with a feedback controller for tracking. However if there are changes to the plant, such as the initial conditions, plant dynamics, or disturbances then the off-line trajectory may no longer correspond to the optimal. Under these circumstances it is desirable to make on-line adjustments to the desired trajectories to reach the new optimal performance.

A significant amount of research has been done in the area of so called on-line optimization. Numerous methods have been investigated including dynamic programming (Hestenes, 1966), (Bellman, 1957), discretization, (Cuthrell and Biegler, 1987), and parametrization, (Visser *et al.*, 2000); and these have been incorporated with a variety of model structures and optimization routines.

Dynamic or nonlinear programming is often used to attempt on-line optimization. The heavy demand for computing time restricts the frequency of updates, and consequently these methods usually result in very discrete on-line changes (look at (Noda *et al.*, 2000), (Zuo and Wu, 2000), (Arpornwichanop *et al.*, 2005), (Loeblein *et al.*, 1999), (Fournier *et al.*, 1999), and (Zhang and Rohani, 2003)). This has been termed a pseudo on-line optimization. To try and compensate for the amount of computing time required, the profiles may be parameterized to known trajectories that have met with success (see (Visser *et al.*, 2000)). In a series of papers by Palanki and Rahman (Palanki *et al.*, 1993), (Palanki and Rahman, 1994), (Rahman and Palanki, 1996), and (Rahman and Palanki, 1998) a method is introduced that provides a geometric approach to handling batch optimization. They show how to develop feedback laws for end-point optimization problems under a variety of state space variations.

Gattu (Gattu and Zafiriou, 1999) used a steepest descent method to define a parameter update law for the system trajectories and then tracked it via a controller. This is an example of the application of gradient methods to batch optimization and forms the basis for the theory presented here. The gradient is used to determine the parameters over the whole batch and introduced measurement feedback through a low level tracking controller. Control design may be difficult depending on the system, so it is desirable to incorporate measurement feedback into the optimization routine.

While the development of this methodology comes from the extremum seeking literature, the methodology is quite close to that of Non-linear Model Predictive Control (DeHaan and Guay, n.d.), (Fontes, 2001), (Magni and Scattolini, 2004). Work has been done on the use of receding horizon NMPC for batch systems (Nagy and Braatz, 2003), (Helbig *et al.*, 1998) and a Lyapunov based approach was used in (Jadbabaie *et al.*, 2001).

In the next section the theory is outlined for a true on-line optimization for general nonlinear dynamical control systems. This theory has been developed from the earlier cascade optimization done in (Guay and Peters, n.d.) for flat systems. This theory outlines the design of a true on-line controller based on the current conditions, and extended to a general non-flat nonlinear case.

2. ON-LINE OPTIMIZATION

We consider a general class of nonlinear dynamical systems of the form:

$$\dot{x} = f(x, u) \tag{1}$$

where $x \in \mathbf{R^n}$ are the state variables and $u \in \mathbf{R^p}$ is the vector of input variables, $f(x) : \mathbf{R^n} \rightarrow \mathbf{R^n}$ is a smooth continuous functions of x. There is a vector $u(t) = [u_1 ... u_p]$ of p input variables.

The optimization centers around finding a system trajectory that minimizes the dynamic optimization problem for some cost function. The cost function is expressed as follows

$$J(x, u) = \int_0^T q(x(t), u(t))dt \tag{2}$$

subject to the dynamics in 1 and the following constraints on the path and end-point variables

$$w(x(t), u(t)) \geq 0 \tag{3}$$

$$x(0) = x_0 \tag{4}$$

$$x(T) = x_f \tag{5}$$

It is assumed that a continuous control, $u(t)$ exists that can steer the states from x_0 to x_f over the batch interval $t \in [0, T]$. Although T can be treated as a time-varying parameter, in the following discussion T is considered to be fixed.

The input trajectories are parameterized

$$u(t) = \left[u_1 \ \dots \ u_p(t) \right] \tag{6}$$

where

$$u_i(t) = \sum_{i=1}^{N} \theta_{ij} \Xi_{ij}(t) \tag{7}$$

where Ξ are the basis functions and θ_i for $i = 1, \dots, N$ and $j = 1, \dots, p$ are the parameters to be determined. The state space equations can be rewritten in terms of θ and the initial conditions. If the input is defined as a polynomial then

$$u_i = \theta^T \phi(t) \tag{8}$$

where the parameters and basis functions are expressed as follows

$$\theta = \left[\theta_1 \ \dots \ \theta_N \right] \tag{9}$$

$$\phi(t) = \left[1 \ t \ \dots \ t^{N-1} \right]. \tag{10}$$

The states can be expressed as a function of the input trajectories and the current conditions

$$x^p = \alpha(\theta^T \phi(\tau), x^m(t)) \tag{11}$$

where the superscript m denotes a measured quantity, and the superscript p denotes a predicted quantity. An analytical solution for the states may not exist, so the system of differential equations must be solved to determine x^p.

Having defined the structure of admissible input trajectories, the following assumptions are necessary to construct the optimization problem. The constraint set

$$\Omega_c = \{x \in \mathbf{R^n}, u \in \mathbf{R^p} | w(x,u) \geq 0\} \tag{12}$$

describes a convex subset of $\mathbf{R^n}$. It is assumed that the input trajectories evolve on a compact subset Ω of $\mathbf{R^n}$. The cost functional $J : \Omega \rightarrow \mathbf{R}$ is assumed to be convex and continuously differentiable on Ω_c. The cost function $q(x,u)$ is assumed to be sufficiently smooth.

The dynamic optimization problem is now expressed in terms of the parameters as followa

$$\min_{\theta} J = \int_0^T q(\alpha(\theta^T\phi(t), x_0^m), \theta^T\phi(t))dt \tag{13}$$

$$w(\alpha(\theta^T\phi(t), x_0^m), \theta^T\phi(t)) \geq 0 \tag{14}$$

$$\alpha(\theta^T\phi(0), x_0^m) = x_0^m \tag{15}$$

$$\alpha(\theta^T\phi(T), x_0^m) = x_f^p. \tag{16}$$

As in (Guay and Peters, n.d.) an interior point method with penalty function is used to include the constraint costs. An interior point method incorporating a log barrier function enforces the state and input constraints. The boundary conditions are incorporated through a terminal penalty function. In the remaining equations obvious notation has been omitted.

Let the path cost with the log barrier function be expressed as follows

$$L = q - \sum_{i=1}^{\rho} \mu_i log(w_i + \epsilon) \tag{17}$$

The new cost functional with interior point inclusion and a penalty function is defined as follows

$$J_{ip} = \int_0^T Ld\tau + M(\alpha(\theta^T\phi(T), x^m(0)) - x_f)^2 \tag{18}$$

where $\mu_i > 0$, $\epsilon_i > 0$ and $M > 0$ are the tuning parameters of the cost functional, with μ and ϵ being taken as small as possible, and M taken as large as possible. It is assumed that the constraint set described by 14 is convex over a set Ω and is also convex over a set Υ in the parameter space. While the focus of this paper is convex problems, if the constraint set is not convex, an infeasible interior-point method can be used. Further details can be found in (Benson *et al.*, 2000*b*), (Benson *et al.*, 2000*a*) and (Benson *et al.*, 2002).

To make the optimization based on the current conditions, the cost needs to be split up into the elapsed and remaining costs.

$$J_{ip} = \int_0^t L^m d\tau + \int_t^T L^p d\tau + M(x^p(T) - x_f)^2 \tag{19}$$

where the first integral represents the actual cost being calculated from the measured states, and the second integral is the predicted cost remaining using the current parameters. The measured cost can be thought of as another state of the system, z, such that

$$z = \int_0^t L^m d\tau \tag{20}$$

and

$$\dot{z} = L^m \tag{21}$$

This leaves a modified cost

$$J_{ip} = z + \int_t^T L^p dt + M(x^p(T) - x_f))^2 \tag{22}$$

A Lyapunov-based approach is used to solve the optimization problem (Guay and Peters, n.d.). Assuming that the cost functional is convex with respect to θ over Υ, then the first order conditions can be applied such that at the optimal parameter set θ^*

$$\nabla J_{ip}(\theta^*) = 0 \tag{23}$$

The Lyapunov function is defined as the cost functional

$$V = J_{ip} \tag{24}$$

and the time derivative is given by

$$\dot{V} = \frac{\partial J_{ip}}{\partial t} + \frac{\partial J_{ip}}{\partial x}\dot{x} + \frac{\partial J_{ip}}{\partial \theta}\dot{\theta} + \frac{\partial J_{ip}}{\partial z}\dot{z} \tag{25}$$

where

$$\frac{\partial J_{ip}}{\partial t} = \int_t^T \frac{\partial L}{\partial x^p}\frac{\partial x^p}{\partial t}d\tau + M(x^p(T) - x_f)\frac{\partial x^p}{\partial t} - L(x^p, u^p)|_t \tag{26}$$

and

$$\frac{\partial J_{ip}}{\partial x}\dot{x} = \int_t^T \frac{\partial L}{\partial x^p}\frac{\partial x^p}{\partial x}\dot{x}d\tau + M(x^p(T) - x_f)\frac{\partial x^p}{\partial x}\dot{x} \quad (27)$$

$$\frac{\partial J_{ip}}{\partial z}\dot{z} = \dot{z} = L(x^m, u^m)|_t \quad (28)$$

where $\frac{\partial J_{ip}}{\partial \theta} == \nabla_\theta J_{ip}$.

The expression (25) can be simplified. Given the current time and conditions the predicted dynamics are subject to the following differential equation

$$\frac{\partial x^p}{\partial \tau} = f(x^p, u^p) \quad (29)$$

with the initial conditions $x^p(t) = x$. Perturbing either of the initial conditions will perturb the solution vectors tangent to the original unperturbed solution. This can be represented by the following simplifying expression.

$$\frac{\partial x^p}{\partial t} + \frac{\partial x^p}{\partial x}\dot{x} = 0 \quad (30)$$

Using this simplification, $\dot{V}$ becomes

$$\dot{V} = \nabla_\theta J_{ip}\dot{\theta} + L^m|_t - L^p|_t \quad (31)$$

By definition $x^p(t) = x^m(t)$ and ensuring that $u^p(t) = u^m(t)$ then

$$\dot{V} = \nabla_\theta J_{ip}\dot{\theta} \quad (32)$$

Using a straightforward steepest descent approach for the parameter update law

$$\dot{\theta} = -k\nabla_\theta J_{ip}. \quad (33)$$

Then the final form of the Lyapunov function is

$$\dot{V} = -k\nabla_\theta J_{ip}^T \nabla_\theta J_{ip}. \quad (34)$$

The Lyapunov function is strictly decreasing except when the gradient is zero (which occurs at the minima, and at the end of the batch).

To avoid divergence of the update law, a projection algorithm was introduced to ensure the parameters remain in a convex set. The properties of the projection algorithm are discussed in (Krstic *et al.*, 1995) and is given below

$$\dot{\theta} = Proj(\theta, \Upsilon) = \begin{cases} \Upsilon, & \text{if} \|\theta\| < \omega_n \\ & \text{or}(\|\theta\| = \omega_n \text{and} \\ & \nabla P(\theta) \leq 0) \\ \Psi, & \text{otherwise} \end{cases} \quad (35)$$

where $\Psi = \Upsilon - \Upsilon\frac{\varsigma\nabla P(\theta)\nabla P(\theta)^T}{\|\nabla P(\theta)\|_\varsigma^2}, \Upsilon = -k\nabla_\theta J_{ip}$, $P(\theta) = \theta^T\theta - \omega_m \leq 0$, θ is the vector of parameter estimates and ω_m is chosen such that $\| \theta \| \leq \omega_m$.

In the next section an example is explored via simulation. In this example it is assumed that the model is perfect and that there is full state feedback.

3. BIOREACTOR SIMULATION

3.1 Problem Definition

The optimization problem deals with a batch bioreactor discussed in (Mahadevan *et al.*, 2001). The state space equations modelling the reaction are given as follows

$$\dot{x_1} = \frac{\mu_m x_1 x_2}{K_m + x_2} - \frac{u x_1}{x_3}$$
$$\dot{x_2} = \frac{u(S_f - x_2)}{x_3} - \frac{\mu_m x_1 x_2}{Y_{xs}(K_m + x_2)}$$
$$\dot{x_3} = u$$

where x_1 and x_2 are the concentrations of the biomass and substrate respectively; x_3 is the volume, and u is the feed rate. The optimization scheme is to maximize the amount of biomass formed at the end of the batch. The optimization problem is described as follows

$$\min_\theta J = \int_0^T -\left(\frac{\mu_m x_1 x_2}{K_m + x_2} - \frac{u x_1}{x_3}\right) dt$$

$$u_1 \geq 0$$
$$x_3 \leq 10$$
$$10 - u_1 \geq 0$$

The system parameters are summarized in Table 1.

Table 1. Parameters and Initial Conditions

Parameters	Values
S_f	15g/L
K_m	1.2g/L
Y_{xs}	0.4g/g
μ_m	0.5/h
T	7.8h
Initial Conditions	Values
x_{10}	1g/L
x_{20}	0g/L
x_{30}	2L
Algorithm Parameters	Values
μ_1	1E−20
ϵ	1E−8
k	10

3.2 Parametrization

In (Mahadevan *et al.*, 2001), the input profile was parameterized by subdividing the batch into a

number of intervals and representing each interval by a fifth order polynomial. The optimization was modified to include the constraint that the volume must reach its maximum value by the end of the batch. The initial guess of the parameters was taken from the solution of a highly constrained problem. The optimization was solved using nonlinear programming.

In this paper, a simple fifth order polynomial profile was arbitrarily selected for the input, with the initial parameters set to zero. The goal here is to show that the optimization can be performed with reasonable computing time, and no off-line analysis of the feasible profile or initial guesses. The input was defined as follows

$$u(t) = \sum_{i=1}^{6} \theta_i \left(\frac{t}{7.8} \right)^{i-1}$$

3.3 Modified Cost

Having selected the parametrization, the next step is to construct the modified cost. The volume constraint is incorporated as a terminal cost, while the input constraints are implemented with log barrier functions. The modified cost function is described below

$$\min_{\theta} J = \int_0^T -\left(\frac{\mu_m x_1 x_2}{K_m + x_2} - \frac{u x_1}{x_3} \right) - \mu(log(u_1 + \epsilon) + log(10 - u_1 + \epsilon))d\tau + (x_3(T) - 10)^2$$

The gradient was computed as discussed in the theory, the details are not included here. The next section will discuss the tuning and algorithm issues. The algorithm parameters for this simulation are in Table 1.

3.4 Algorithm and Computing Issues

Computing time is always an issue when an ODE solver is needed to determine the prediction and sensitivities. The Fortran package ODESSA was used to calculate the model prediction and the first order sensitivities. MATLAB was used to perform the simulation of the closed-loop system.

The run time for this 7.8 hour simulation was approximately 10 seconds, using a 1.6 GHz Centrino Processor, using cost gradient as the update law.

3.5 Results

The dynamic optimization technique was applied to the nominal case presented above. The resulting simulation of the state and input variables profiles can be found in Figure 1. As in (Mahadevan *et al.*, 2001), the optimal final biomass concentration obtained was 4.8 g/L. The technique performs as expected without the need for complex parameterizations and the requirement for partial flatness.

To verify the effect of initial conditions and parameters, various initial batch conditions were tested. Under various parameter guesses, the overall performance was unchanged. New initial conditions resulted in new optimal profiles. Table 2 shows the initial and final cost for several different initial conditions. The method used here provided

Table 2. Cost Summary

x_{10} (g/L)	x_{20}g/L (g/L)	x_{30}L (L)	Final Cost
1	0	2	4.8
2	0.5	4	4.5
0.5	0.7	0.5	0.8
4	0.2	7	4.7

results comparable to those used in (Mahadevan *et al.*, 2001). However no initial understanding of the optimal structure was needed. A simpler structure was used with all the initial parameters set to zero. Less analysis was needed before running the batch, and the overall algorithm was simpler. This technique can be applied to a variety of problems, with minimal pre-batch analysis.

4. CONCLUSION AND FUTURE WORK

In this paper, we proposed a new on-line optimizing controller for nonlinear dynamical systems. Smooth trajectories were generated on-line with feasible computing time to construct optimal trajectories without the need for off-line analysis. In future work, we plan to study the impact of imperfect state measurements and parametric uncertainties.

REFERENCES

Arpornwichanop, A., P. Kittisupakorn and I.M. Mujtaba (2005). On-line dynamic optimization and control strategy for improving the performance of batch reactors. *Chemical Engineering and Processing* **44**(1), 101–114.

Bellman, R.E. (1957). *Dynamic Programming*. Princeton University Press. Princeton.

Benson, H.Y., D.F. Shanno and R.J. Vanderbei (2000*a*). Interior-point methods for nonconvex nonlinear programming: Filter methods and merit functions. Technical Report ORFE-00-06. Princeton University.

Benson, H.Y., D.F. Shanno and R.J. Vanderbei (2000*b*). Interior-point methods for nonconvex nonlinear programming: Jamming and

comparative numerical testing. Technical Report ORFE-00-02. Princeton University.

Benson, H.Y., D.F. Shanno and R.J. Vanderbei (2002). Interior-point methods for nonconvex nonlinear programming: Complementarity constraints. Technical Report ORFE-02-02. Princeton University.

Cuthrell, J.E. and L.T. Biegler (1987). On the optimization of differential algebraic process systems. *AIChE Journal* **33**(8), 1257–1270.

DeHaan, D. and M. Guay (n.d.). A real-time framework for model predictive control of continuous-time nonlinear systems. In: *Proc. IEEE Conf. on Decision and Control*. accepted for publication.

Fontes, F. (2001). A general framework to design stabilizing nonlinear model predictive controllers. *Systems and Control Letters* **43**(2), 127–143.

Fournier, F., M.A. Latifi and G. Valentin (1999). Methodology of dynamic optimization and optimal control of batch electrochemical reactors. *Chemical Engineering Science* **54**(13-14), 2707–2714.

Gattu, G. and E. Zafiriou (1999). Methodology for on-line setpoint modification for batch reactor control in the presence of modelling error. *Chemical Engineering Journal* **75**(1), 21–29.

Guay, M. and N. Peters (n.d.). Real-time dynamic optimization of nonlinear systems: A flatness-based approach. In: *Proc. IEEE Conf. on Decision and Control*. accepted for publication.

Helbig, A., O. Abel and W. Marquardt (1998). Model predictive control for on-line optimization of semi-batch reactors. In: *Proceedings of the American Control Conference*. pp. 1695–1699.

Hestenes, M. R. (1966). *The calculus of variations and optimal control theory*. Wiley. New York.

Jadbabaie, A., J. Yu and J. Hauser (2001). Unconstrained receding-horizon control of nonlinear systems. *IEEE Transactions on Automatic Control* **46**(5), 776–782.

Krstic, M., I. Kanellakopoulos and P. Kokotovic (1995). *Nonlinear and Adaptive Control Design*.

Loeblein, C., J.D. Perkins, B. Srinivasan and D. Bonvin (1999). Economic performance analysis in the design of on-line batch optimization systems. *Journal of Process Control* **9**(1), 61–78.

Magni, L. and R. Scattolini (2004). Model predictive control of continuous-time nonlinear systems with piecewise constant control. *IEEE Trans. Automat. Contr.* **49**(6), 900–906.

Mahadevan, R., S.K. Agrawal and F.J. Doyle (2001). Differential flatness based nonlinear predicted control of fed-batch bioreactors. *Control Engineering Practice* **9**, 889–899.

Nagy, Z. and R. Braatz (2003). Robust nonlinear model predictive control of batch processes. *AIChE* **49**(7), 1776–1786.

Noda, M., T. Chida, S. Hasebe and I. Hashimoto (2000). On-line optimization system of pilot scale multi-effect batch distillation system. *Computers and Chemical Engineering* **24**(2), 1577–1583.

Palanki, S. and S.A.K.M Rahman (1994). State feedback synthesis for on-line optimization of batch reactors with a non-affine manipulated input and free terminal time. In: *Proceedings of the American Control Conference*. Vol. 3. pp. 3076–3079.

Palanki, S., C. Kravaris and H.Y. Wang (1993). Synthesis of stated feedback laws for end-point optimization in batch processes. *Chemical Engineering Science* **48**(1), 135–151.

Rahman, A.K.M.S. and S. Palanki (1996). On-line optimization of batch processes with nonlinear manipulated input. *Chemical Engineering Science* **51**(3), 449–459.

Rahman, S. and S. Palanki (1998). State feedback synthesis for on-line optimization of batch reactors with multiple manipulated inputs. *Computers and Chemical Engineering* **22**(10), September.

Visser, E., B. Srinivasan, S. Palanki and D. Bonvin (2000). Feedback-based implementation scheme for batch process optimization. *Journal of Process Control* **10**(5), 399–410.

Zhang, G.P. and S. Rohani (2003). On-line optimal control of a seeded batch cooling crystallizer. *Chemical Engineering Science* **58**(9), 1887–1896.

Zuo, K. and W.T. Wu (2000). Semi-realtime optimization and control of a fed-batch fermentation system. *Computers and Chemical Engineering* **24**(2), 1105–1109.

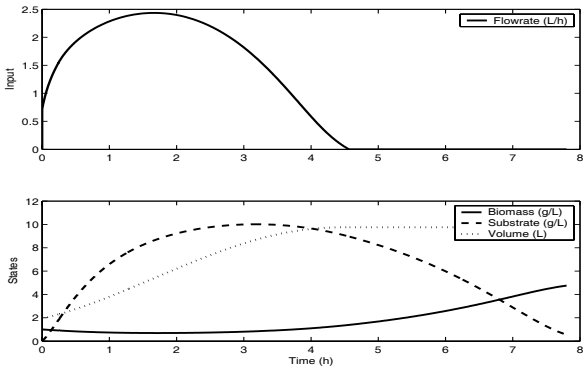

Fig. 1. Bioreactor Optimization Profiles

Session 2.3

Optimization and Scheduling

Optimal Operation of Ethylene Polymerization Reactors for Tailored MWD

M. Asteasuain and A. Brandolin
Planta Piloto de Ingenieria Quimica

Optimal Operation of an LNG Plant

J. B. Jensen and S. Skogestad
Norwegian University of Science and Technology

Facility Location Problems: Model, Algorithm, and Application to Compressor Allocation

E. Camponogara, M. P. de Castro and A. Plucenio
Federal University of Santa Catarina

Capacity Management in the Chemical Supply Chain

P. K. Naraharisetti, I. A. Karimi, and R. Srinivasan
Institute of Chemical and Engineering Sciences

Process Optimization and Control Under Uncertainty: A Chance Constrained Programming Approach

H. Arellano-Garcia, T. Barz and G. Wozny
Berlin University of Technology

Optimal Grade Transition in Polymerization Reactors: A Comparative Case Study

N. Padhiyar, S. Bhartiya and R. D. Gudi
Indian Institute of Technology Bombay

ADCHEM 2006

International Symposium on Advanced Control of Chemical Processes
Gramado, Brazil – April 2-5, 2006

OPTIMAL OPERATION OF ETHYLENE POLYMERIZATION REACTORS FOR TAILORED MWD

Mariano Asteasuain Adriana Brandolin [1]

Planta Piloto de Ingeniería Química (Universidad Nacional del Sur - CONICET), Camino La Carrindanga km 7, C.C. 717, (8000) Bahía Blanca, Argentina

Abstract: A comprehensive steady-state model of the high-pressure ethylene polymerization in a tubular reactor that is able to calculate the complete molecular weight distribution (MWD) as function of the reactor axial distance is presented. MWD is calculated by means of the probability generating function technique. The model is implemented in gPROMS and included in an optimization framework that is used to determine optimal operating conditions for producing a polymer with tailored MWD. Two application examples are presented, the first involves maximization of conversion while maintaining the original MWD, and the second consists in finding the operating conditions needed to produce a polymer with a bimodal MWD.

Keywords: Polyethylene, Polymerization, Molecular weight distribution, Mathematical models, Optimization, Tubular reactor

1. INTRODUCTION

Polyethylene is a commodity polymer with one of the most important markets among the commercial polymers, with a world annual production of about 35 million tons (Kim and Iedema, 2004). Low density polyethylene (LDPE), one of the members of the polyethylene family, is produced by high-pressure free-radical polymerization in tubular or autoclave reactors. This work focuses on the polymerization in tubular reactors to produce low density polyethylene. This is a widely used industrial process, which is carried out under rigorous operating conditions. For instance, axial velocities are usually around 11 m/s, pressures range from 1800 to 2800 bar, and temperatures are between 50°C at the reactor entrance and 335°C at the peaks. A typical reactor has a main feed consisting of ethylene monomer, a mixture of modifiers, inerts, and oxygen initiator. In addition, there are lateral injections of peroxide initiator mixtures, which may be accompanied by monomer and/or modifiers. The reactor is divided in heating/cooling jacket zones in order to reach an appropriate reaction temperature or to control the exothermic reaction. Pressure pulsing of the reactor is sometimes applied to control polymer build-up at the reactor walls.

Driven by commercial reasons, several studies have been performed on the optimization of LDPE tubular reactors, most of which used simplified models. For instance, Mavridis and Kiparissides (1985) presented an optimization strategy using a theoretical model to find the best values of the operative parameters, so as to obtain the maximum conversion for a polyethylene of certain molecular weight. Yoon and Rhee (1985) determined optimal temperature profiles that maximized conversion. They used a simplified model without includ-

[1] Author to whom correspondence should be addressed

ing molecular properties requirements. Kiparissides *et al.* (1994) carried out an on-line optimization of a LDPE tubular reactor taking into account requirements on the polymer melt index and density. In a series of papers (Brandolin *et al.*, 1991; Asteasuain *et al.*, 2001*a*), a rigorous model of the reactor was used to determine optimal operating policies and reactor design features for an industrial reactor, while keeping average molecular properties within desired values.

A very important molecular property to which less attention has been paid is the complete molecular weight distribution (MWD). Optimization of the reactor operation while tailoring the MWD is a very useful application of a mathematical model, because a number of processing and end-use properties of the polymer are strongly dependent on the breadth and shape of the MWD. For example, high molecular weight tails and *shoulders* can increase the sensitivity of melt viscosity to shear rate (Wells and Ray, 2005). Several methods have been proposed to predict the complete MWD in different systems. However, applications for tailoring the MWD are not frequent. In the case of the high-pressure ethylene polymerization in tubular reactors, there are few works dealing with the calculation of the complete MWD (Wells and Ray, 2005; Schmidt *et al.*, 2005; Kim and Iedema, 2004), but none of them attempted to tailor this property in an optimization framework.

This work presents a comprehensive steady-state model of the high-pressure ethylene polymerization in a tubular reactor that is able to calculate the complete MWD as function of the reactor axial distance, and its application in optimizing the reactor operation while producing a polymer with tailored MWD. A previous model (Brandolin *et al.*, 1996) is extended to calculate the complete MWD by means of the probability generating function (pgf) technique developed by the authors (Asteasuain *et al.*, 2002*a*; Asteasuain *et al.*, 2002*b*). This technique allows modelling the MWD easily and efficiently, in spite of the reactor model complexity. Detailed modelling capabilities of the previous model are kept. The rigorous model of the polymerization reactor presented here is implemented in gPROMS (Process Systems Enterprise, Ltd.), and included in an optimization framework that is used to determine optimal operating conditions for producing a polymer with specific MWD. To the best of our knowledge, this is the first work dealing with the optimization of this process in which a tailored shape for the MWD is included. Two application examples are presented, the first involves maximization of conversion while maintaining the original MWD, and the second consists in finding the operating conditions needed to produce a polymer with a bimodal MWD.

2. MODEL DESCRIPTION

The reactor configuration is displayed in figure 1. It corresponds to a typical industrial reactor, with 8 jacket zones and 2 lateral feedings. Some of the design features are shown in the figure. The mathematical model of the polymerization reactor is based on a previous model by the authors (Brandolin *et al.*, 1996), which was extended to calculate the complete MWD. It assumes plug flow and supercritical reaction mixture; besides, it considers variation of physical and transport properties along the axial distance, calculated with rigorous correlations. Detailed calculation of the heat-transfer coefficient along the axial distance is also included (Lacunza *et al.*, 1998).

Polymer properties of interest in this work are the complete MWD and the average molecular weights. Therefore, only the reactions of the former kinetic mechanism (Brandolin *et al.*, 1996) that are crucial for the prediction of the mentioned properties, as well as the conversion and temperature profiles, were kept. The kinetic mechanism is shown in table 1.

Table 1. Kinetic mechanism.

Peroxide Initiation
$I_k \xrightarrow{k_{ik}} 2R(0) \quad k = 1, 2$
Oxygen Initiation
$O_2 + M \xrightarrow{k_o} 2R(0)$
Monomer thermal initiation
$3M \xrightarrow{k_{mi}} R(1) + R(2)$
Generation of inert
$O_2 + R(m) \xrightarrow{f_o k_o} X$
Propagation
$R(m) + M \xrightarrow{k_p} R(m+1)$
Termination by combination
$R(n) + R(m) \xrightarrow{k_{tc}} R(n+m)$
Thermal degradation
$R(m) \xrightarrow{k_{tdt}} P(m) + R(0)$
Chain transfer to monomer
$R(m) + M \xrightarrow{k_{trm}} P(m) + R(1)$
Chain transfer to polymer
$R(n) + P(m) \xrightarrow{m\,k_{trp}} P(n) + R(m)$
Chain transfer to modifier
$R(m) + S \xrightarrow{k_{trs}} P(m) + R(0)$

Symbols M, I, O_2 and S stand for ethylene monomer, peroxide initiator, oxygen and modifier, respectively; $P(m)$ and $R(m)$ are polymer and living radical molecules, respectively, of chain length m.

In order to avoid iterative calculations that increase the computational burden, the jacket temperature at each one of the eight reaction zones was assumed constant, and the pressure pulse was neglected. Besides, peroxide and modifier mixtures are treated as single fictitious species. These simplifications were validated in a subsequent work by the authors (Asteasuain *et al.*, 2001*b*),

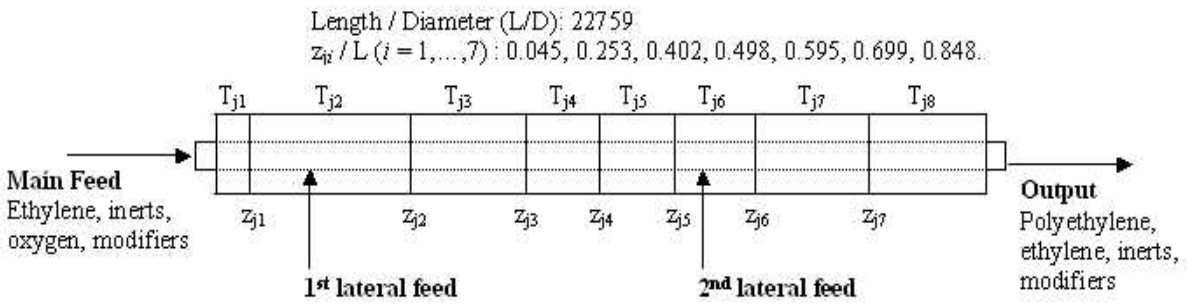

Fig. 1. Tubular reactor for high-pressure ethylene polymerization

against several data sets from an industrial tubular reactor. The set of kinetic constants obtained in Asteasuain *et al.* (2001*b*) are used here.

The set of the main model equations is listed in table 2. In these equations, ρ and $C_{\rm p}$ are the density and heat-capacity of the reaction mixture, v is the axial velocity, T and $T_{\rm j}$ are the reactor and jacket temperatures, and P is the reactor pressure; U, D, ΔH, $f_{\rm f}$ and Mw_j are the global heat-transfer coefficient, reactor internal diameter, propagation reaction enthalpy, friction factor and molecular weight of the j component; λ_a and μ_a are the ath order moments of the radical and polymer chain length distribution; r_j and r_Ψ are the generation rate of the j and Ψ entities, respectively; $r_{\rm pm}$ is the reaction rate of the propagation reaction; $F_{\rm main}$ is the global mass flow at the reactor entrance; $\bar{F}_j$ is the molar flow per unit length of the j component; $\phi_{a,l}$ and $\varphi_{a,l}$ are the probability generating functions (pgf) of the radical and polymer chain length distribution (a = 0, 1, 2 is related to the MWD expressed in number, weight and chromatographic (mass times the molecular weight) fraction, respectively, as shown in table 2, and l is the dummy variable of the pgf); $n(m)$, $w(m)$ and $c(m)$ are the number, weight and chromatographic fraction of the macromolecule of chain length m. Expressions corresponding to the terms r_j and r_Ψ can be found elsewhere (Asteasuain and Brandolin, 2005). The molar flows per unit length $\bar{F}_j$ are used to model the lateral feedings to the reactor (Asteasuain and Brandolin, 2005).

The innovation of the present model is the addition of the calculation of the complete MWD along the axial distance. The MWD is calculated, independently, in number, weight and chromatographic fraction. This is performed by means of the probability generating function (pgf) technique developed by the authors (Asteasuain *et al.*, 2002*a*; Asteasuain *et al.*, 2002*b*) . With this technique, first the mass balances of the generic species $R(m)$ and $P(m)$ are transformed into the pgf domain, obtaining the balance equations for $\phi_{a,l}$ and $\varphi_{a,l}$. Then, from the solution of these equations and an appropriate numerical inversion of the pgfs, the complete MWDs are obtained. The inversion step is represented by function $f\left(\varphi_{a,l}(z)\right)$ in table 2. The inversion of the pgfs is carried out using Stehfest's algorithm (Asteasuain *et al.*, 2002*a*). The pgf technique allowed modelling the MWD easily and efficiently, in spite of the complexity of the reactor model. The resulting model also keeps the capabilities of the former model to calculate the following quantities along the axial distance: monomer conversion, reaction mixture temperature and pressure, mass fraction of oxygen, peroxides, monomer, radicals and polymer; average molecular weights; Peclet, Nusselt, Reynolds and Prandtl numbers, global heat-transfer coefficient, velocity, viscosity and specific heat. As mentioned before, the LDPE reactor model was implemented in gPROMS (Process Systems Enterprise, Ltd.)

Table 2. Main model equations.

Global mass balance
$\rho(z)\,v(z) = F_{\rm main} + \int_0^z \left(\sum_j \bar{F}_j(z)\,\mathrm{Mw}_j\right) dz$
Mass balances of components
$\frac{d\left(C_j(z)\,v(z)\right)}{d\,z} = -r_j(z) + \bar{F}_j(z)$
$j = O_2, M, I_k\ (k = 1, 2), S$
Mass balances of moments and pgfs
$\frac{d(\Psi(z)\,v(z))}{d\,z} = -r_\Psi(z)$
$\Psi = \lambda_a, \mu_a,\ \phi_{a,l}, \varphi_{a,l} (a = 0, 1, 2)$
Energy balance
$\rho(z)\,v(z)\,C_{\rm p}(z)\,\frac{d\,T(z)}{d\,z} = -\frac{4\,U(z)\,(T(z)-T_{\rm j})}{D} +$
$+ r_{\rm pm}(z)\,(-\Delta H) + \check{C}_{\rm p}\,(T_{\rm inlet} - T(z)) * \sum_j \bar{F}_j\,Mw_j$
Pressure drop
$\frac{d\,P(z)}{d\,z} = -\rho(z)\left(v(z)\frac{d\,v(z)}{d\,z} + \frac{2\,f_{\rm f}\,v(z)^2}{D}\right)$
Number average molecular weight
$\mathrm{Mn}(z) = \mathrm{Mw}_M\,\frac{\lambda_1(z)+\mu_1(z)}{\lambda_0(z)+\mu_0(z)}$
Weight average molecular weight
$\mathrm{Mw}(z) = \mathrm{Mw}_M\,\frac{\lambda_2(z)+\mu_2(z)}{\lambda_1(z)+\mu_1(z)}$
Monomer conversion
$x(z) = \frac{\mu_1(z)}{\mu_1(z)+C_M(z)}$
Polymer MWDs
$n(m,z) = f\left(\varphi_{0,l}(z)\right),\ w(m,z) = f\left(\varphi_{1,l}(z)\right)$
$c(m,z) = f\left(\varphi_{2,l}(z)\right)$

3. OPTIMIZATION OF THE LDPE TUBULAR REACTOR

3.1 First case study

The first case study involved the optimization of the base case operating conditions in order to maximize conversion, while keeping the production of a polymer with the same MWD. A set of 19 optimization variables was considered, involving flow rates of different components in the main and lateral feedings, the inlet temperature and pressure and location of the lateral feedings. Optimization variables are listed in table 3. Base case operating conditions, corresponding to the production of a typical commercial polyethylene in an actual industrial reactor, are shown in the same table. Two optimization problems were solved: in the first one the lateral feedings should be at the same temperature of the main feed stream (*cold* lateral feedings); in the second, the temperature was assumed to be equal to the reactor temperature at the injection point (*hot* lateral feedings). The maximum allowed deviation with respect to the original MWD was specified by adding the constraints shown in equations 1 and 2 to the optimization problem.

$$\sum_i \left(\frac{w_{\text{new}}(m_i, z_{\max}) - w_{\text{orig}}(m_i)}{w_{\text{orig}}(m_i)} \right)^2 \leq 0.01 \quad (1)$$

$$\sum_i \left(\frac{c_{\text{new}}(m_i, z_{\max}) - c_{\text{orig}}(m_i)}{c_{\text{orig}}(m_i)} \right)^2 \leq 0.01 \quad (2)$$

An upper bound was imposed on the reaction mixture temperature along the axial distance to ensure safe operating conditions (thermal runaway occurs at 345°C) (Kiparissides *et al.*, 1994):

$$T(z) \leq 335^{\circ}\text{C} \quad (3)$$

Besides, an upper bound was also considered for the reactor temperature at the reactor exit, required for downstream process units:

$$T(z_{\max}) \leq 285^{\circ}\text{C} \quad (4)$$

A constraint in the total monomer feed to the reactor (main feed plus lateral feedings) was applied, so as to keep the same flow rate as in the base case:

$$A \left(F_{M,\text{main}} + \int_0^z \bar{F}_M(z)\, \text{Mw}_M dz \right) = 11 \frac{\text{kg}}{\text{s}} \quad (5)$$

where A is the cross-sectional area of the reactor. Lower and upper bounds for the optimization variables were selected according to the usual operating conditions of an industrial reactor. Finally, the optimization problem involved maximizing conversion at the reactor exit ($x(z_{\max})$) subject to the reactor model and the constraints shown in equations 1–5. The optimization was solved using the commercial software gPROMS (Process Systems Enterprise, Ltd.).

3.2 Second case study

The second case study involved the optimization of the operating conditions in order to synthesize a polymer with a tailored MWD. A bimodal distribution was selected as the *target* distribution because it is very difficult to obtain under usual operating conditions. For instance, in a set of 31 operating cases taken from an actual industrial reactor, only polyethylene with monomodal distribution was produced. In order to show the flexibility of this approach to determine the *target* MWD, only the existence of a local minimum, a necessary condition for a bimodal distribution, and its approximate location were specified (equations 6 and 7). Chain length values m_1, m_2 and m_3 were selected so that the corresponding molecular weights ($m_i\, Mw_M$) were, respectively, 44380, 224000 and 280000 g/mol. The objective function of the optimization problem (equation 8) was meant to increase the height of the right shoulder of the distribution.

$$c(m_2, z_{\max}) - c(m_1, z_{\max}) \leq 0 \quad (6)$$

$$c(m_2, z_{\max}) - c(m_3, z_{\max}) \leq 0 \quad (7)$$

$$FO = \min c(m_2, z_{\max}) - c(m_3, z_{\max}) \quad (8)$$

Equations 6 and 7 replace equations 1 and 2 in the optimization formulation. Besides, a lower bound on the monomer conversion was added to avoid uneconomical operation:

$$x(z_{\max}) \geq 0.2 \quad (9)$$

The same set of optimization variables as in the previous case was used, plus the possibility of adding a lateral injection of modifier.

4. RESULTS AND DISCUSSION

Optimization results for the first case study are shown in table 3. It can be seen that the monomer conversion has been significantly increased. The success in maintaining the original MWD can be

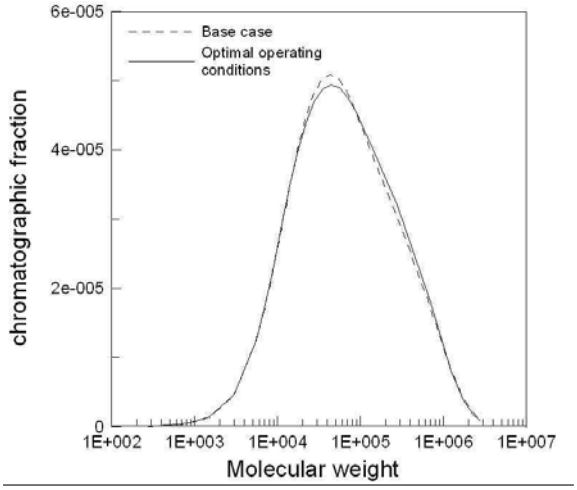

Fig. 2. Comparison of the original and final MWD. First case study

observed in figure 2, in which the original and final chromatographic MWDs are depicted. An even closer matching was obtained for the weight MWD.

Table 3. Optimal operating conditions. First case study.

Variable	Base Case	Optimal
Inlet temperature (°C)	77	72
Inlet pressure (bar)	2300	2800
Oxygen flow rate (kg/s)	$6.9\,10^{-5}$	$7.7\,10^{-5}$
Modifier flow rate (kg/s)	0.00762	0.2
Peroxide. 1^{st} injection (kg/s)	0.00102	$6.1\,10^{-4}$
Peroxide. 2^{nd} injection (kg/s)	$1.57\,10^{-4}$	$8.3\,10^{-5}$
Monomer. Main feed (kg/s)	11	11
Monomer 1^{st} injection (kg/s)	0	0
Monomer 2^{nd} injection (kg/s)	0	0
Location of 1^{st} injection (m)	160	49
Location of 2^{nd} injection (m)	840	833
Jacket temp. Zones 1-8 (°C)	170-225	153-249
	170-170	150-150
	170-170	150-150
	170-170	150-150
Conversion	**25%**	**30%**

Figure 3 shows the temperature profiles corresponding to the base case and to the optimal operating conditions. Notice that the path and end point constraints on the reactor temperature (equations 3 and 4) are satisfied.

Optimization results were the same when using *cold* or *hot* lateral feedings. This is an expected result, as the optimal point involves only initiator lateral addition, which for its small amount does not contribute significantly to the reaction mixture enthalpy. Notice that the whole monomer feed is used in the main stream, and that the first injection point has been moved nearer to the reactor entrance. Besides, a higher solvent flow rate is used to achieve the same molecular properties in spite of the conversion increase. These results are consistent with previous studies on this reactor (Asteasuain *et al.*, 2001*a*).

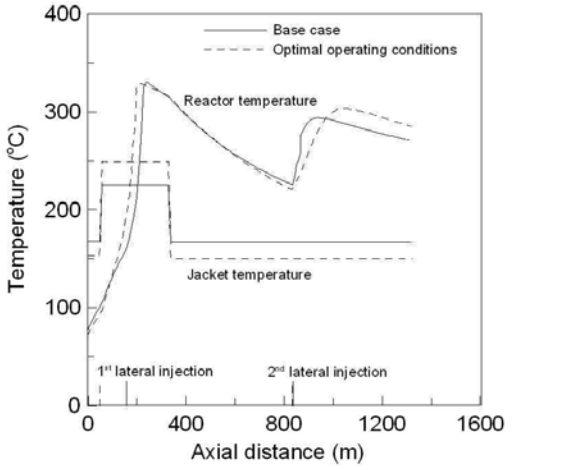

Fig. 3. Temperature profiles corresponding to the base case and to the optimal operating conditions. First case study

Figure 4 shows the resulting MWD for the second case study. A comparison of the distributions after the first reaction zone and at the reactor exit is presented. A clear bimodality at the reactor exit can be observed, showing the success of the optimization procedure. The set of the optimal operating conditions are shown in table 4.

Table 4. Optimal operating conditions. Second case study.

Variable	Base Case	Optimal
Inlet temperature (°C)	77	70
Inlet pressure (bar)	2300	2800
Oxygen flow rate (kg/s)	$6.9\,10^{-5}$	$5.9\,10^{-5}$
Modifier. Main feed (kg/s)	0.00762	0.12
Modifier. 1^{st} injection (kg/s)	0	$3.5\,10^{-3}$
Modifier. 2^{nd} injection (kg/s)	0	0.9
Peroxide. 1^{st} injection (kg/s)	0.00102	$2.4\,10^{-4}$
Peroxide. 2^{nd} injection (kg/s)	$1.57\,10^{-4}$	$8.6\,10^{-5}$
Monomer. Main feed (kg/s)	11	9.4
Monomer. 1^{st} injection (kg/s)	0	0.6
Monomer. 2^{nd} injection (kg/s)	0	1
Location of 1^{st} injection (m)	160	41
Location of 2^{nd} injection (m)	840	498
Jacket temp. Zones 1-8 (°C)	170-225	154-150
	170-170	270-226
	170-170	176-170
	170-170	270-270
Conversion	**25%**	**25%**

The operating scenario is very different to the previous ones. Notice that now the monomer feed is split between the two lateral injections, and that side injections of modifiers are also used, with an important addition in the second injection. This radical change in the process conditions was not unexpected since a polymer with a very different MWD was to be produced. Other authors (Kim and Iedema, 2004) have also found that lateral additions of modifiers are necessary to obtain bimodal MWDs in tubular reactors.

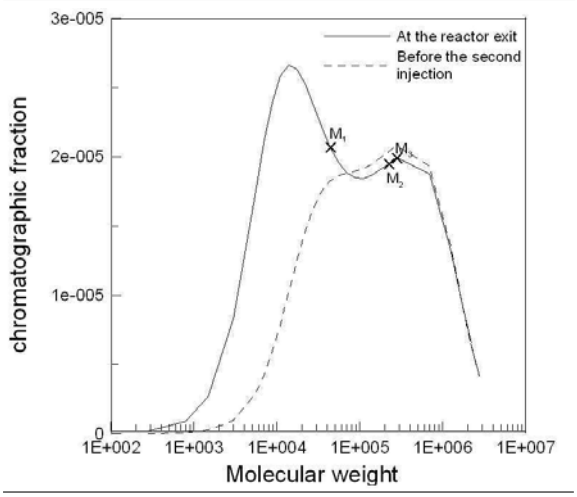

Fig. 4. Bimodal MWD. Second case study

It is interesting to see in figure 4 that the polymer formed after the first lateral injection is of high molecular weight, contributing with the right shoulder of the distribution, while the lower molecular weight polymer produced after the second injection (which involves an important addition of modifier) is responsible for the left shoulder of the distribution.

5. CONCLUSIONS

In this work we present a comprehensive steady-state model of the high-pressure ethylene polymerization in a tubular reactor that is able to calculate the complete MWD as function of the reactor axial distance, and its application in optimizing the reactor operation while producing a polymer with tailored MWD. This is performed via an optimization approach that allows great flexibility for specifying the *target* MWD and other process constraints. The two case studies presented here, the first involving maximization of conversion while maintaining the original MWD, and the second consisting in finding the operating conditions necessary to produce a polymer with a bimodal MWD, show the potential benefits of using this tool.

6. ACKNOWLEDGEMENTS

The authors wish to thank Universidad Nacional del Sur (Bahía Blanca, Argentina) and CONICET (Argentina) for financial support.

REFERENCES

Asteasuain, M., A. Brandolin and C. Sarmoria (2002*a*). Recovery of molecular weight distributions from transformed domains. Part II: application of numerical inversion methods. *Polymer* **43**, 2529–2541.

Asteasuain, M. and A. Brandolin (2005). Comprehensive mathematical model for a high-pressure ethylene polymerization reactor developed in gPROMS. Submitted to Comput. Chem. Eng.

Asteasuain, M., C. Sarmoria and A. Brandolin (2002*b*). Recovery of molecular weight distributions from transformed domains. Part I: application of pgf to mass balances describing reactions involving free radicals. *Polymer* **43**, 2513–2527.

Asteasuain, M., P.E. Ugrin, M.H. Lacunza and A. Brandolin (2001*a*). Effect of multiple feedings in the operation of a high-pressure polymerization reactor for ethylene polymerization. *Polym. React. Eng.* **9**, 163–182.

Asteasuain, M., S. Pereda, M.H. Lacunza, P.E. Ugrin and A. Brandolin (2001*b*). Industrial high pressure ethylene polymerization initiated by peroxide mixtures: a reduced mathematical model for parameter adjustment. *Polym. Eng. Sci.* **41**, 711–726.

Brandolin, A., E.M. Valles and J.N. Farber (1991). High pressure tubular reactor for ethylene polymerization. Optimization aspects. *Polym. Eng. Sci.* **31**, 381–390.

Brandolin, A., M.H. Lacunza, P.E. Ugrin and N.J. Capiati (1996). High pressure polymerization of ethylene. An improved mathematical model for industrial tubular reactors. *Polym. React. Eng.* **4**, 193–241.

Kim, D. and P.D. Iedema (2004). Molecular weight distribution in low-density polyethylene polymerization; Impact of scission mechanisms in the case of a tubular reactor. *Chem. Eng. Sci.* **59**, 2039–2052.

Kiparissides, C., G. Verros and A. Pertsinidis (1994). On-line optimization of a high-pressure low-density polyethylene tubular reactor. *Chem. Eng. Sci.* **49**, 5011–5024.

Lacunza, M.H., P.E. Ugrin, A. Brandolin and N.J. Capiati (1998). Heat transfer coefficient in a high pressure tubular reactor for ethylene polymerization. *Polym. Eng. Sci.* **38**, 992–1013.

Mavridis, H. and C. Kiparissides (1985). Optimization of a high-pressure polyethylene reactor. *Polym. Proc. Eng.* **3**, 263–290.

Schmidt, C., M. Busch, D. Lilge and M. Wulkow (2005). Detailed molecular structure modeling – a path forward to designing application properties of ldPE. *Macromol. Mater. Eng.* **290**, 404–414.

Wells, G.J. and W.H. Ray (2005). Prediction of polymer properties in ldpe reactors. *Macromol. Mater. Eng.* **290**, 319–346.

Yoon, B.J. and H.K. Rhee (1985). A study of the high-pressure polyethylene tubular reactor. *Chem. Eng. Commun.* **34**, 253–265.

ADCHEM 2006

International Symposium on Advanced Control of Chemical Processes
Gramado, Brazil – April 2-5, 2006

OPTIMAL OPERATION OF A SIMPLE LNG PROCESS

Jørgen Bauck Jensen & Sigurd Skogestad [1]

Department of Chemical Engineering, NTNU, Trondheim, Norway

Abstract: Considering the large amount of work that goes into the design of LNG processes there is surprisingly little attention to the subsequent operation. This probably comes from the misconception that optimal design and optimal operation is the same, but this is usually not true. In this paper we are studying optimal operation of a relatively simple LNG process, namely the PRICO process.

Keywords: Self-optimizing control, optimization, operation

1. INTRODUCTION

Large amounts of natural gas are found at locations that makes it infeasible or not economical to transport it in gaseous state (in pipelines or as compressed natural gas) to the customers. The most economic way of transporting natural gas over long distances is to first produce liquefied natural gas (LNG) and then transport the LNG by ships. LNG has approximately 600 times the density of gaseous natural gas.

At atmospheric pressure LNG has a temperature of approximately $-162\,^{\circ}\mathrm{C}$, so the process of cooling and condensing the natural gas requires large amounts of energy. Several different process designs are used and they can be grouped roughly as follows:

- Pure fluid cascade process: Several pure refrigerant cycles are used to limit the mean temperature difference in the heat exchange
- Single mixed refrigerant: The refrigerant composition is adjusted to match the cooling curve of the natural gas. Some are designed with a separate pre-cooling cycle
- Mixed fluid cascade process: Energy efficiency is further improved by using several mixed refrigerant cycles

The process considered in this paper is a single mixed refrigerant process, namely the PRICO process (Stebbing and O'Brien, 1975) and (Price and Mortko, 1996). This is the simplest configuration utilizing mixed refrigerant, but it provides valuable insight also applicable to more complex configurations. The PRICO process is optimized in several publications ((Lee *et al.*, 2002) and (Del Nogal *et al.*, 2005)), but only with respect to design.

2. PROCESS DESCRIPTION

Figure 1 shows a simplified flowsheet of the PRICO process.

Nominal conditions:

- The natural gas enters with a pressure of 55 bar and a temperature of $25\,^{\circ}\mathrm{C}$ after pretreatment
- Natural gas flow rate is $1\,\mathrm{kmol\,s^{-1}}$
- Composition of natural gas: 89.7 % methane, 5.5 % ethane, 1.8 % propane, 0.1 % n-butane and 2.8 % nitrogen

[1] Corresponding author skoge@chemeng.ntnu.no

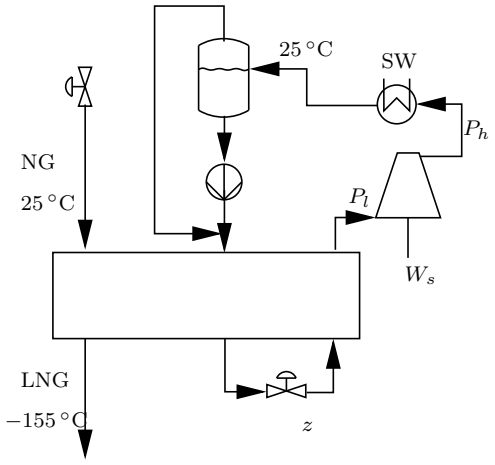

Fig. 1. Simplified flowsheet of the PRICO process

- Pressure drops:
  - 5 bar in natural gas stream
  - 0.1 bar in SW cooler
  - 4 bar for hot refrigerant in main heat exchanger
  - 1 bar for cold refrigerant in main heat exchanger
- Constant heat transfer coefficients
- The refrigerant is a mix of nitrogen (N_2), methane (C_1), ethane (C_2), propane (C_3) and n-butane (nC_4) and the composition is used in optimization
- Cooling of refrigerant to 25 °C in SW cooler
- Vapour to compressor is super-heated 10 °C
- The compressor has a fixed isentropic efficiency of 80 %
- In design the minimum temperature difference in the heat exchanger (ΔT_{min}) is 1.2 °C

Using the above conditions the cycle in Figure 1 is working as follows: After compression the mixed refrigerant is cooled to 25 °C in a sea water (SW) cooler before it is further cooled together with the natural gas through the main heat exchanger. The high pressure sub-cooled liquid is then sent through a choke valve to give a low temperature two-phase mixture which is vaporized in the main heat exchanger to provide the necessary cooling duty. The vapour is slightly super-heated (10 °C) before it is compressed back to the high pressure.

2.1 Model

The SRK equation of state is used both for the natural gas and the refrigerant. The main heat exchanger is a distributed model, which has been discretized into 100 cells.

2.2 Manipulated inputs

There are in total 9 manipulated inputs (degrees of freedom):

- Compressor power W_s
- Choke valve opening z
- Flow of sea water (SW) in SW cooler
- Flow of natural gas (can also be considered a disturbance)
- Composition of refrigerant (4 independent inputs)
- Active charge (within the heat exchangers). The active charge can be manipulated by altering liquid level in a receiver in the cycle, or by having an external filling/emptying system. Here it may be changed by the liquid pump after the refrigerant separator

2.3 Constraints during operation

There are some constraints that must be satisfied during operation.

- Super-heating: The vapour entering the compressor must be at least 10 °C super-heated
- T_{LNG}^{out}: Natural gas temperature out of the main heat exchanger must be −155 °C or colder
- Pressure: Must be within certain bounds (not considered in this paper)
- Compressor outlet temperature must be below a given temperature (not considered in this paper)
- Compressor power (W_s) maximum 20 MW

2.4 Active constraints

Using some general knowledge of the process we are able to identify constraints that will be active at optimum. In total there are 3 active constraints:

- Super-heating should be minimized (e.g. see (Jensen and Skogestad, 2005), and for this case this means controlling $\Delta T_{sup} = 10$ °C. Note that measuring the degree of super-heating directly requires knowledge of the refrigerant composition.
- Excess cooling is costly so $T_{LNG} = -155$ °C
- Maximum cooling: Assume $T = 25$ °C after SW cooler

2.5 Degrees of freedom

After implementing the three active constraints using three of the nine manipulated inputs, we are left with six degrees of freedom. For this steady state analysis the pairing of inputs and outputs is insignificant, so say we are left with the following subset of manipulated inputs:

- Pressure P_h (could correspond to the liquid pump as physical input)
- Four refrigerant compositions

- Flow of natural gas (can also be considered a disturbance)

These variables should be adjusted to optimize the operation.

3. OPTIMI ATION RESULTS

In this section we will show that the most common method for designing heat exchangers, the specification of the minimum approach temperature ΔT_{min}, has a major drawback in terms of finding the true optimum.

3.1 Design versus operation

In design it is common to specify ΔT_{min} for each heat exchanger in order to get a balance between capital costs (favored by a large ΔT_{min}) and operational costs (favored by a small ΔT_{min}). In operation however, ΔT_{min} is free to vary. This gives rise to two different optimization problems. One for design

$$\begin{aligned} &\min(W_s) \qquad (1)\\ \text{such that} \quad &\Delta T - \Delta T_{\min} \geq 0 \end{aligned}$$

and one for operation

$$\begin{aligned} &\min(W_s) \qquad (2)\\ \text{such that} \quad &A_{\max} - A \geq 0 \end{aligned}$$

In both cases we have as optimization degrees of freedom, the pressure P_h and four compositions. The feed rate of NG is assumed given. The A_{max} used for operation is obtained as a result of solving the design problem.

Table 1 shows the difference between design and optimal operation at the conditions listed in section 2. In design, we specify $\Delta T_{min} = 1.2\,^{\circ}\mathrm{C}$ (which is the same as reported in (Del Nogal *et al.*, 2005) and (Lee *et al.*, 2002)). In operation, with areas found by design, ΔT_{min} is reduced to $0.537\,^{\circ}\mathrm{C}$ and we are able to find a new operating point (with the same heat exchanger area) with 2.60 % less compressor power (Case I in Table 1). This is possible by altering the composition of the refrigerant and the pressure. The pressure ratio (P_h/P_l) is actually increased slightly from 5.93 to 6.87, but this is more than compensated for by the reduction in refrigerant flow rate (from 3.118 to $2.773\,\mathrm{kmol\,s^{-1}}$). In Case II, we vary only the pressure (and fix the composition in operation to the value found in the design), and we are able to reduce the shaft work by 1.89 % compared to design. Similar results have also been reported for an ammonia cycle (Jensen and Skogestad, 2005). Note that althoug the savings depend on the value for ΔT_{min}, the fact that there are savings do not.

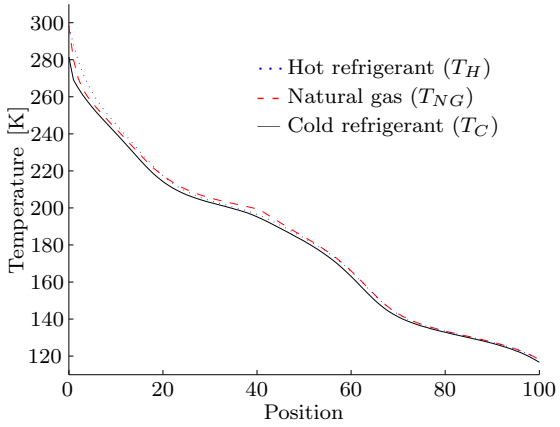

Fig. 2. Temperature profile in the main heat exchanger as function of position for optimal operation (Case I)

Table 1. Difference between design with fixed ΔT_{min} and optimal operation with free refrigerant composition (Case I) and with composition as design (Case II)

	Design *	**Case I** **	**Case II** *
$\mathbf{\Delta T_{min}}$ [°C]	1.200	0.537	0.642
$\mathbf{W_s}$ [MW]	17.404	16. 50	17.075
$\mathbf{P_h}$ [bar]	1 .124	23.617	23.811
$\mathbf{P_l}$ [bar]	3.226	3.438	3.05
Flow [kmol s ^{1}]	3.118	2.773	2.621

* Composition [%]:
N_2: 7.72, C_1: 23.65, C_2: 3 .4 , C_3: 0.00, C_4: 2 .14
** Composition [%]:
N_2: 7.45, C_1: 25.86, C_2: 38.5 , C_3: 0.00, C_4: 28.11

We generally find a smaller ΔT_{min} in optimal operation, because the temperature difference varies more throughout the heat exchanger. Only at the limit when ΔT_{min} is zero (infinite heat transfer areas) is ΔT_{min} for design and optimal operation equal. Note that the savings actually increase with decreasing heat transfer areas (increasing ΔT_{min}).

The temperature profile in the main heat exchanger is given in Figure 2. Note the very close match of the cooling and heating curves. To see this more clearly, the temperature difference profile in optimal design and optimal operation are shown in Figure 3. The two optimums are also illustrated in pressure-enthalpy diagrams in Figure 4. Note that since the composition of the refrigerant is changed, the pressure enthalpy diagrams are actually different.

The obtained values for W_s, both for design (17.40 MW) and optimal operation (16.95 MW), are better than the results reported by (Del Nogal *et al.*, 2005) 24.53 MW and (Lee *et al.*, 2002) 26.60 MW. It is unclear if this is because of differences in the optimization or in the conditions.

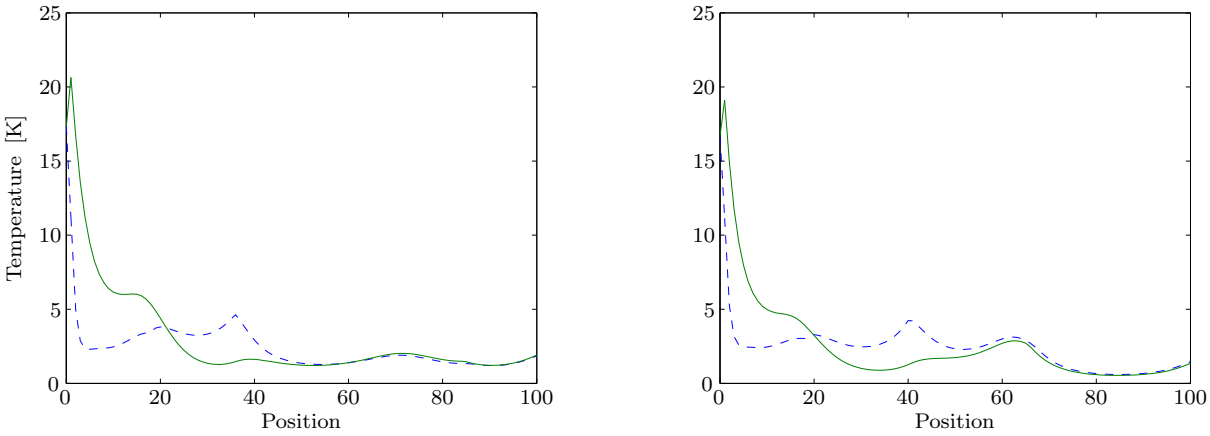

(a) Design (b) Case I

Fig. 3. Temperature difference profile in the main heat exchanger as function of position for design ($\Delta T_{min} = 1.2\,^{\circ}$C) and optimal operation (Case I). Dashed line - $T_{NG} - T_C$. Solid line - $T_H - T_C$

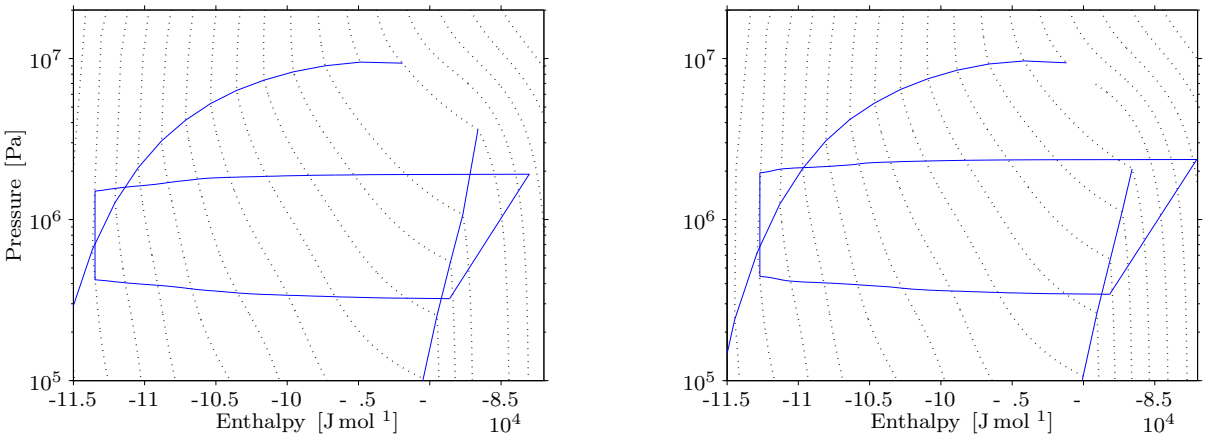

(a) Design (b) Case I

Fig. 4. Pressure-enthalpy diagram for both (a) design and (b) optimal operation (Case I)

4. IMPLEMENTING OPTIMAL OPERATION

We have now identified the optimum for the PRICO process, but how should we control the process to maintain close to optimal operation when the process is exposed to disturbances? This is related to selection of controlled variables, which is presented below.

4.1 Operating strategies

In general, there are two main modes of operation of a plant:

(1) Throughput (of NG) given, minimize operating cost (here W_s) (studied in previous section)
(2) Maximize throughput given operational constraints (in this case the bottleneck will be W_s^{max} where W_s^{max} is given by design).

For our case study the bottleneck (W_s) is identical to the operating cost, so optimal operation in modes (1) and (2) are identical. This follows since $\frac{\partial W_s}{\partial F} \geq 0$, so increasing F will also increase W_s (which is not possible).

4.2 Self optimizing control

Self optimizing control is when we can achieve acceptable loss with constant setpoint values for the controlled variables (without the need to re-optimize when disturbances occur) (Skogestad, 2000).

We will use the procedure in (Halvorsen *et al.*, 2003) to identify controlled variables that may result in self optimizing control. First we use a linear model (scaled both in input and output direction) to locate promising controlled variables.

The most promising candidates are then tested on the non-linear model using full disturbances.

Outline of the linear procedure:

(1) With fixed active constraints, obtain a linear model (G) from the unconstrained inputs (u) to outputs (candidate controlled variables):

$$y = Gu$$

(2) Scale the linear model in the inputs such that the effect of all inputs on the objective function is equal.
(3) Scale the linear model in the outputs so their expected variety (sum of span y and implementation error n) is equal.
(4) We are looking for controlled variables that maximize the minimum singular value of the scaled linear gain matrix.

From this point on we assume that the refrigerant composition is maintained constant and that the natural gas flow is determined by an upstream or downstream process (a disturbance). So we are left with one unconstrained degree of freedom for optimization, e.g. P_h. Since there is only one input it is not necessary to scale with respect to the input, and the procedure of finding the set of controlled variables that maximize the minimum singular value reduces to picking outputs with high linear scaled gains.

4.3 Linear analysis of controlled variables (CV)

Two obvious controlled candidates are the pressures P_h and P_l. Other candidate controlled variables can be a temperature somewhere in the main heat exchanger or after some unit. It is also possible to control a linear combination of two measurements, such as the degree of sub-cooling of refrigerant at outlet of main heat exchanger ($\Delta T_{sub} = T - T_{sat}$) or a temperature difference at some position ($\Delta T_j(i) = T_j(i) - T_C(i)$).

To get the optimal span y we consider the variance of y using 1 % of the expected disturbances (given in Table 2).

The results of the linear method for the most promising controlled variables are given in Table 3. Table 3 shows the scaled linear gain from the input (P_h) to some candidate controlled variables. Only a subset of all the variables are given We are looking for candidates with a high scaled linear gain $|G'|$ so P_l looks like a poor choice with $|G'|$=0.69. P_h is much better with $|G'|$=6.41. The theoretical loss is inversely proportional to $|G'|^2$ so controlling the high side pressure P_h instead of the low side pressure P_l would reduce the loss by a factor $(6.41/0.69)^2 = 86.3$. Other variables in Table 3 are also promising, including temperature

Table 2. Nominal, minimum and maximum values for the disturbances

	Nominal	Min	Max
NG flow [kmol s ^{1}]	1	0.5	1.1
NG P [bar]	55	50	60
SW T [°C]	25	20	30
REF C_1 [%]	25.86	15.86	35.86
REF C_2 [%]	38.5	28.5	48.5
REF C_4 [%]	28.11	18.11	38.11
REF N_2 [%]	7.45	0.00	17.45

in the main heat exchanger, refrigerant flow and temperature out of the compressor.

Table 3. Linear analysis of controlled variables

CV	G	span y	n *	G' 1 6
P_h [Pa]	1	56036	1e5	6.41
P_l [Pa]	-3.76e-2	4175	5e4	0.6
ΔT_{sub} [°C]	-2.24e-5	2.0	1.5	6.24
$T_H(12)$ ** [°C]	-1.80e-5	1.66	1	6.78
$T_{NG}(12)$ [°C]	-1.5 e-5	1.62	1	6.0
$T_C(12)$ [°C]	-1.74e-5	1.82	1	6.18
$T_{NG}(50)$ [°C]	-2.5 e-5	11.3	1	2.10
$T_H(50)$ [°C]	-2.53e-5	11.0	1	2.11
$T_C(50)$ [°C]	-2.5 e-5	14.	1	1. 6
$F \quad w$ [mol]	-8.46e-4	73.5	10	10.13
T_o^{ou} [°C]	2.80e-5	1.51	1	11.16
W_s [MW]	8.30e-8	0.21	1e-4	0.40
$\Delta T_{NG}(41)$ [°C]	7.66e-6	0.55	1.5	3.74
$\Delta T_H(21)$ [°C]	-3.7 e-6	0.28	1.5	2.13

* Implementation error
** (i): Position in heat exchanger (see Figure 2)

This linear approach is only valid close to the nominal point so the most promising controlled variables must be checked using the non-linear model with full disturbances. This will reveal feasibility problems together with large reduction in performance caused by non-linearities.

4.4 Non-linear analysis of promising CV's

In the linear analysis we assumed composition disturbances of 10 % (absolute) for each component, but in practice this turns out to be infeasible because of excessive compressor work. From this we see that the composition when filling the system is vital to achieving good performance, and make-up should be added to stay at the desired composition.

In the following we assume that the steady state disturbance in the composition is 2 % for each component. From the linear analysis we found that P_l is a poor controlled variable, and this is verified in the non-linear brute force evaluation where we find that a constant P_l is infeasible for several of the disturbances. Temperatures within the main heat exchanger look promising from the

Table 4. Maximum loss with implementation error and disturbance; d1 - all variables (Table 2) except composition. d2 - also composition (2 %)

CV	Maximum loss	
	d1 *	d2 **
ΔT_{sub}	0.62 %	0.62 %
P_h	0.74 %	2.58 %
T_o^{ou}	0.81 %	0.88 %

* No disturbance in refrigerant composition
** 2 % disturbance in refrigerant compositions

linear analysis, but these are affected by nonlinearities and proves to be poor in practice. This is also the case for refrigerant flow. Table 4 shows the losses of the three best candidate controlled variables (CV's). We have used the disturbances from Table 2, (except that we use only ±2 % in refrigant composition) and implementation errors (n) from Table 3. Simultaneous disturbances have not been considered.

Note that controlling ΔT_{sub} requires knowledge about the composition of the refrigerant, so it may be better to control the compressor outlet temperature with only 0.26 % extra loss.

4.5 Proposed control structure

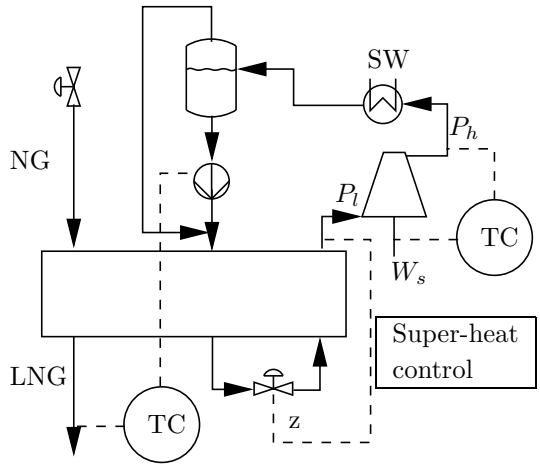

Fig. 5. Proposed control structure

First of all we should control the active constraints:

- Control T_{NG}^{out} with liquid pump
- Control ΔT_{sup} with choke valve

The remaining degree of freedom could be used to control either of the three candidates listed above (ΔT_{sub}, P_h or T_{om}^{out}).

In Figure 5 we choose to:

- Control T_{om}^{out} with compressor power W_s

Note that we in this steady state study we can only say what variables that should be maintain constant during operation.

5. CONCLUSION

We have shown that the design method specifying ΔT_{min} to design heat exchanger will result in a operating point that is not optimal. Even for a small design ΔT_{min} of 1.2 °C, the compressor power can be reduced by as much as 2.60 %. For a process that requires the large amounts of energy, such as LNG processes, this is a significant saving.

For the PRICO LNG process we have found that there will be one unconstrained degree of freedom. This degree of freedom may be used to control P_h, ΔT_{sub} or T_{om}^{out} as this will lead to self-optimizing control. Controlling ΔT_{sub} gives smaller loss, but controlling T_{om}^{out} or P_h may be easier in practice.

REFERENCES

Del Nogal, F.L, J. Kim, R. Smith and S. J. Perry (2005). Improved design of mixed refrigerant cycles using mathematical programming. *Gas Processors Association (GPA) Europe Meeting, Amsterdam.*

Halvorsen, I. J., S. Skogestad, J. C. Morud and V. Alstad (2003). Optimal selection of controlled variables. *Ind. Eng. Chem. Res.* **42**, 3273–3284.

Jensen, J. B. and S. Skogestad (2005). Control and optimal operation of simple heat pump cycles. In: *European Symposium on Computer Aided Process Engineering (ESCAPE) 15, arcelona.*

Lee, G. C., R. Smith and X. X. hu (2002). Optimal synthesis of mixed-refrigerant systems for low-temperature processes. *Ind. Eng. Chem. Res.* **41**(20), 5016–5028.

Price, B. C. and R. A. Mortko (1996). PRICO - a simple, flexible proven approach to natural gas liquefaction. In: *GASTECH, LNG, Natural Gas, LPG international conference , Vienna.*

Skogestad, S. (2000). Plantwide control: the search for the self-optimizing control structure. *J. Process Contr.* **10**(5), 487–507.

Stebbing, R. and J. O'Brien (1975). An updated report on the PRICO (TM) process for LNG plants. In: *GASTECH, LNG, Natural Gas, LPG international conference , Paris.*

ADCHEM 2006

International Symposium on Advanced Control of Chemical Processes
Gramado, Brazil – April 2-5, 2006

THE FACILITY LOCATION PROBLEM: MODEL, ALGORITHM, AND APPLICATION TO COMPRESSOR ALLOCATION

Eduardo Camponogara [*,1],
Melissa Pereira de Castro [*,2],
Agustinho Plucenio [*,2]

[*] *Department of Automation and Systems, Federal University of Santa Catarina, Cx.P. 476, 88040-900 Florianópolis, SC, Brazil*

Abstract: Unlike other problems found in the oil industry, the allocation of compressors to gas-lifted oil wells lacks formal models and algorithms capable of delivering globally optimal assignments. To this end, this paper casts the compressor allocation problem as a facility location problem. Owing to the special structure of the target problem, an efficient (polynomial time) algorithm is conceived by applying the framework of dynamic programming. An example illustrates the inner-workings of the algorithm. Connections between the polyhedron of feasible solutions and integer-programming theory are established.

1. MOTIVATION

The prospection for oil reserves, the recovery of oil, and the distillation into final products are complex processes that rely heavily on technology. Since the inception of the oil industry, production and decision processes have been automated, in part to cut costs and improve efficiency in response to the mounting pressure from competitive markets, but also due to the continuous transformation of scientific advances into technology (Jahn et al., 2003). For instance, a plan to recover oil from a reservoir takes into account geological studies of the formation, data from seismic analysis, and predictions from simulators. A plan will pinpoint the locations for drilling, along with the technology and apparatus to artificially lift hydrocarbons from the reservoir to surface facilities, where they are separated into oil, water, and gas. Among the artificial lifting techniques (Nishikiori et al., 1995; Buitrago et al., 1996), continuous gas-lift is a favored technique for its relatively low installation and maintenance costs, wide range of operating conditions, and robustness. Continuous gas-lift works by injecting high pressure gas at the bottom of the production tubing to reduce the weight of the oil column, thereby forcing the flow of fluid to surface facilities. In view of the complexity of planning and operating the production processes of an oil field as a whole, the overall task is invariably broken down to smaller, tractable sub-problems that can be solved more efficiently with the aid of models and algorithms. In particular, two relevant sub-problems are lift-gas allocation and compressor scheduling.

Lift-gas allocation concerns the distribution of a limited gas rate to the oil wells, while respecting lower and upper bounds for gas injection at each well, maximum compressing capacity, and surface facility constraints with the aim of minimizing production costs. A number of models and algorithms appeared in the literature (Kanu et al., 1981; Buitrago et al., 1996; Alarcón et al., 2002), but more recently globally optimal algorithms

[1] Partially supported by CNPq
[2] Supported by the Brazilian Agency of Petroleum (ANP)

have been developed to handle discrete decisions and the non-linear nature of well performance curves (Camponogara and Nakashima, 2006b,a).

On the other hand, compressor scheduling concerns the allocation of compressors to meet the pressure levels set down by the (oil field) recovery plan for each oil well. Setting up compressor facilities to precisely meet the pressure needs of each well is not only inconvenient, but the installation costs are also excessive. In a typical situation, the decision-maker has to trade-off the installation costs and energy-loss costs incurred by reducing the pressure yielded by the scheduled compressor to the well's level. The task of deciding which compression levels (*facilities*) will be installed and how they will supply lift-gas to the wells (*clients*) so as to minimize the overall cost gives rise to the compressor allocation problem (CAP). Unlike lift-gas allocation, the compressor allocation problem has received little attention, lacking formal models and provably optimal algorithms. This works is a first attempt to bridge the gap between industry and academia, having the aim of formally stating the problem, developing a baseline algorithm, and pointing out directions for further research.

2. PROBLEM FORMULATION

Roughly speaking, in the facility location problem one has to decide upon the location of facilities and how these facilities supply clients' demands, while minimizing the aggregated cost incurred by installing facilities and transporting goods to clients (Wolsey, 1998; Cornuejols et al., 1977). $N = \{1, \ldots, n\}$ is the set of potential sites for facilities and $M = \{1, \ldots, m\}$ is the set of clients. A fixed cost a_j is charged to set up facility j, while c_{ij} is the cost to fulfill the whole demand of client i from facility j. Because clients have special needs, a client i can be serviced only by a subset $N_i \subseteq N$ of the facilities. Let $M_j = \{i \in M : j \in N_i\}$ be the subset of potential clients of facility j. The problem can be cast in mathematical programming as follows:

$$P : \text{Minimize } J = \sum_{j=1}^{n} a_j y_j + \sum_{i=1}^{m} \sum_{j \in N_i} c_{ij} x_{ij} \quad (1a)$$

Subject to :

$$x_{ij} \leqslant y_j, \ i \in M, \ j \in N_i \quad (1b)$$

$$\sum_{j \in N_i} x_{ij} = 1, \ i \in M \quad (1c)$$

$$y_j \in \{0, 1\}, \ j \in N \quad (1d)$$

$$x_{ij} \in \{0, 1\}, \ i \in M, \ j \in N_i \quad (1e)$$

Despite its clear statement and simple model, the computational solution of the facility location problem is intrinsically hard, that is to say, a polynomial-time algorithm for P would entail solving the class of NP-Hard problems in polynomial time (Garey and Johnson, 1979). One such problem is set covering (Nemhauser and Wolsey, 1988): given a set S, a family $\{S_j\}_{j=1}^{n}$ of subsets of S, and the cost c_j for each S_j, the problem rests on finding a subset $U \subseteq \{1, \ldots, n\}$ that minimizes $\sum_{j \in U} c_j$ and such that $\cup_{j \in U} S_j = S$ (i.e., the selected subsets induce a cover of S), which gives the name to the problem. It is a straightforward exercise to reduce set covering to the facility location problem in polynomial time and space—just associate each facility j with a subset S_j, model each client i as an element of S, equate M_j to S_j and define N_i accordingly, set a_j as c_j, and set $c_{ij} = 0$ for all i and j; the optimal solution to the facility location problem is precisely a minimum cost cover for S.

Not surprisingly, the target application of compressor allocation can be framed as a facility location problem, with the facilities representing the potential pressure levels for compressor pools, whereas the clients represent the oil wells. In this scenario, compressing station j yields lift-gas flow at pressure p_j^c. The problem arises from the allocation of these pressure levels to the oil wells so as to meet the recovery plan of the oil field, according to which lift-gas should be injected in well i at pressure p_i^w. Henceforth, this problem will be referred to as *compressor allocation problem* (CAP). Since pressure can only be reduced without energy gain, but invariably incurring energy losses, pressure p_j^c must be greater than or equal to pressure p_i^w for compressor j to be allocated to well i.

Assumption 1. An instance of CAP satisfies the properties:

(1) $p_1^c > p_2^c > \ldots > p_n^c$;
(2) $p_1^w \geqslant p_2^w \geqslant \ldots \geqslant p_m^w$;
(3) $p_1^c \geqslant p_1^w$, implying that demands from wells can be fulfilled;
(4) for all $i \in M$ and $j, k \in N_i, j < k$, $c_{ij} \geqslant c_{ik}$, expressing that the energy-loss cost to drop compressor pressure p_j^c to p_i^w, c_{ij}, is not lower than dropping from p_k^c, c_{ik}, because $p_j^c > p_k^c$.

The assumptions made above are typical of instances of the compressor allocation problem and, therefore, do not limit the developments hereafter but rather bring out the intrinsic structure of the problem. This structure can be exploited to develop specially-tailored algorithms that are far more efficient than general-purpose algorithms for the facility location problem. Actually, we will design a polynomial-time algorithm for facility location problems arising from instances of the compressor allocation problem.

3. DYNAMIC PROGRAMMING ALGORITHM

3.1 Background

Dynamic programming (DP) is a framework for breaking up problems in a set of smaller, easier to solve sub-problems arranged in a sequence (Bertsekas, 1995). The decisions are made in stages, each regarding a decision at the present time and its future consequences.

In a deterministic situation, the consequences are fully predictable whereas, in a stochastic situation, the outcomes are ruled by chance and modeled by random variables. The goal is to reach decisions that minimize the cumulative cost stretching from the current time until the end of the time horizon. Because each decision influences future outcomes, the decision-maker has to balance the desire of low costs at the current time and the undesirability of high future costs. Dynamic programming balances the trade-off between current and future costs: at each stage, the decisions are ranked according to the sum of the present cost and future costs, assuming optimal decision making over the subsequent stages, also known as *cost-to-go* (from the next state until termination).

For the stochastic scenario, the costs are expected values over the distributions of the random variables. DP has been successfully applied to a wide range of problems, including optimal control and discrete optimization problems.

In the domain of control theory, the typical task is to minimize system's state distance from a desired trajectory while factoring in the control-action costs and balancing the present and future costs. The system's state evolves over time according to discrete-time dynamic equations that might have random variables, such as the number of service requests arriving at a shop, random disturbances, or the number of units ordered from clients. Because an optimal control policy can only be determined after the observation of the random variables, the algorithmic solution is structured backward, working from the terminal stage toward the current time.

In the domain of optimization, the typical task is not unlike in control theory, where the system's state might represent the quantity of resources available at the moment, such as the remaining budget to pay for tolls to reach the destination or the remaining capacity in a knapsack. The applications in discrete optimization abound, including resource-constrained shortest-path problems, knapsack-like problems, and string matching (Cormen et al., 1990; Wolsey, 1998).

3.2 Recursive Formulation

Here, we take advantage of the structure of CAP, as formalized in Assumption 1, to break P into a sequence $\{P_m(s_m), P_{m-1}(s_{m-1}), \ldots, P_1(s_1)\}$ of sub-problems. $P_i(s_i)$ is a restricted form of P in which one has to allocate facilities to a subset of clients, namely $\{i, i+1, \ldots, m\}$, given that the facilities in $\{1, \ldots, s_i - 1\}$ are unavailable, facility s_m has been installed, and the installation of the facilities from $\{s_i+1, \ldots, n\}$ are to be decided. Let $J_i(s_i)$ be the value of an optimal solution to $P_i(s_i)$. Parameter s_i acts as the "*state of the system*" at stage i. Note that $P_1(0)$ is equivalent to P.

Rather than solving $\{P_i(s_i)\}$, we recursively solve the sequence $\{\hat{P}_i(s_i)\}$ given below, taking advantage of the problem structure to reduce the search for an optimal solution dramatically. The first problem of the sequence $\{\hat{P}_i(s_i)\}$ is expressed in mathematical programming as:

$$\hat{P}_m(s_m):$$

$$\hat{J}_m(s_m) = \text{Min} \sum_{j \in N_m^+} a_j y_j + \sum_{j \in N_m^-} c_{mj} x_{mj} \quad (2a)$$

S. to :

$$x_{mj} \leqslant y_j,\ j \in N_m^+ \quad (2b)$$

$$\sum_{j \in N_m^-} x_{mj} = 1 \quad (2c)$$

$$y_j \in \{0,1\},\ j \in N_m^+ \quad (2d)$$

$$x_{mj} \in \{0,1\},\ j \in N_m^- \quad (2e)$$

where:

- $N_m^+ = N_m \cap \{s_m + 1, \ldots, n\}$;
- $N_m^- = N_m \cap \{s_m, \ldots, n\}$; and
- $s_m \in \{0\} \cup N$ is the index of the lowest pressure level already installed.

In case $\{s_m, s_m + 1, \ldots, n\} \cap N_m = \emptyset$, $\hat{J}_m(s_m)$ becomes $+\infty$ as neither facility level s_m nor its succeeding levels can service client m. In case $s_m = 0$, one can choose the facility that induces the lowest combined cost of installation and transportation, that is, $\min\{a_j + c_{mj} : j \in N_m\}$.

For the remaining stages, the problem at stage i accounts for the cost to service client i and the clients in $\{i+1, \ldots, m\}$ (*cost-to-go* from the current stage and state to the terminal state), given that facilities $\{1, \ldots, s_i - 1\}$ are decommissioned and facility s_i is in service (if $s_i > 0$). The problem encompassing the decisions from stage i till termination is cast as follows:

$\hat{P}_i(s_i)$:

$$\hat{J}_i(s_i) = \text{Min} \sum_{j \in N_i^+} a_j y_j + \sum_{j \in N_i^-} c_{ij} x_{ij} + \hat{J}_{i+1}(s_{i+1}) \quad (3a)$$

S. to :

$$x_{ij} \leqslant y_j,\ j \in N_i^+ \quad (3b)$$

$$\sum_{j \in N_i^-} x_{ij} = 1 \quad (3c)$$

$$s_{i+1} = \max\{s_i, j : y_j = 1\} \quad (3d)$$

$$y_j \in \{0,1\},\ j \in N_i^+ \quad (3e)$$

$$x_{ij} \in \{0,1\},\ j \in N_i^- \quad (3f)$$

The purpose and interpretation of $s_i \in \{0\} \cup N$ is the same as in $\hat{P}_m(s_m)$. In equation (3d), if no facility is installed at stage i then s_{i+1} takes on value s_i, or else s_{i+1} becomes the index of the facility that has been installed. In the event of $\hat{P}_i(s_i)$ being infeasible, which occurs when $\{s_i, s_i+1, \ldots, n\} \cap N_i = \emptyset$, then $\hat{J}_i(s_i)$ becomes $+\infty$.

An effective DP algorithm can be designed to solve $\hat{P}_1(0)$ by recursively solving the problem family $\{\hat{P}_i(s_i)\}$ in an appropriate sequence, and skipping the instances that are clearly infeasible.

Dynamic Programming Algorithm

For $s_m = 0, \ldots, n$ do
  Solve $\hat{P}_m(s_m)$ to compute $\hat{J}_m(s_m)$
  Let $(x_m(s_m), y_m(s_m))$ be a solution to
    $\hat{P}_m(s_m)$ if $\hat{J}_m(s_m) < +\infty$, that is,
    $x_m(s_m) = (m, j)$ for which $x_{mj} = 1$ and
    $y_m(s_m) = 0$ if $j = s_m$ or else $y_m(s_m) = j$
For $i = m-1, \ldots, 1$ do
  For $s_i = 0, \ldots, n$ do
    Solve $\hat{P}_i(s_i)$ to compute $\hat{J}_i(s_i)$
    Let $(x_i(s_i), y_i(s_i))$ be the solution to
      $\hat{P}_i(s_i)$ which can be obtained as
      delineated above

Let $\hat{J}_i = \{\hat{J}_i(s_i) : s_i \in \{0\} \cup N_i\}$ be the table with the values of solutions to all the sub-problems at stage i, with the exception of the infeasible ones. The algorithm works by computing $\hat{J}_m$, $\hat{J}_{m-1}$, and so forth until reaching $\hat{J}_1$.

Of course, the decision maker needs the optimal solution, not only the optimal values. The algorithm outlined above bookkeeps the optimal decisions in tables $X_i = \{x_i(s_i) : s_i \in \{0\} \cup N_i\}$ and $Y_i = \{y_i(s_i)\}$, even though the decisions could be inferred from the tables $\hat{J}_i$, for the sake of simplicity. At termination, the optimal solution can be produced by the algorithm given below.

Optimal Solution Computation

Let y be a list of facilities to be installed
Let x be a list of client-facility pairs
$y \leftarrow \emptyset$, $x \leftarrow \emptyset$, and $s_1 \leftarrow 0$
For $i = 1, \ldots, m$ do
  $(i', j') \leftarrow x_i(s_i)$
  $x \leftarrow x \cup \{(i', j')\}$
  If $j' = s_i$
    then $s_{i+1} = s_i$
    else $s_{i+1} = j'$
      $y \leftarrow y \cup \{j'\}$

The procedure above outputs in y the indexes of the facilities to be installed and, in x, which facilities will be servicing which clients. The correctness of the dynamic programming is established below by showing that the recursive formulation $\{\hat{P}_i(s_i)\}$, given in (2a)–(2e) and (3a)–(3f), is equivalent to $\{P_i(s_i)\}$.

Lemma 1. $\hat{J}_i(s_i) = J_i(s_i)$ if Assumption 1 holds.

Proof: (By induction in i) For the basis, $i = m$, $\hat{P}_i(s_i)$ is obviously equivalent to $P_i(s_i)$ because only the facilities from N_m^+ may be installed, implying that $\hat{J}_m(s_m) = J_m(s_m)$.

For the induction step, $i < m$, suppose facility s_{i+1} services client i, where s_{i+1} must belong to N_i^-. Because $c_{kj} \geqslant c_{ks_{i+1}}$ for each $k \in \{i+1, \ldots, m\}$ and all $j \in N_k \cap \{s_i, \ldots, s_{i+1} - 1\}$ (refer to Assumption 1), and $a_j \geq 0$ for all j, the facilities in the set $N_k \cap \{s_i+1, \ldots, s_{i+1}-1\}$ do not need to be installed in an optimal solution. Consequently, $J_i(s_i) = c_{i,s_{i+1}} + J_{i+1}(s_{i+1}) = c_{i,s_{i+1}} + \hat{J}_{i+1}(s_{i+1}) = \hat{J}_i(s_i)$ by induction hypothesis if $s_{i+1} = s_i$ and, similarly, $J_i(s_i) = a_{s_{i+1}} + c_{i,s_{i+1}} + J_{i+1}(s_{i+1}) = a_{s_{i+1}} + c_{i,s_{i+1}} + \hat{J}_{i+1}(s_{i+1}) = \hat{J}_i(s_i)$ by induction hypothesis if $s_{i+1} > s_i$, completing the demonstration. ■

Corollary 1. $\hat{P}_1(0)$ is equivalent to P and $\hat{J}_1(0) = J$ is the value of an optimal solution.

Corollary 2. P can be solved in polynomial time.

Proof: The DP algorithm performs $\Theta(mn)$ steps each taking $O(n)$ steps to solve $\hat{P}_i(s_i)$. Thus, the algorithm runs in $O(mn^2) \in O(\max\{m,n\}^3)$ time and its memory usage is $\Theta(mn)$. ■

3.3 An Illustrative Example

The purpose of the material herein is to crystallize the concepts and illustrate the DP algorithm in a simple context. The scenario consists of $n = 4$ pressure levels (*facilities*) and $m = 4$ oil wells that

Table 1. Compressor and well data

Compressors				Oil wells		
j	p_j^c	a_j	M_j	i	p_i^w	N_i
1	10	8	$\{1,2,3,4\}$	1	9	$\{1\}$
2	8	6	$\{2,3,4\}$	2	8	$\{1,2\}$
3	6	10	$\{4\}$	3	7	$\{1,2\}$
4	4	4	$\{4\}$	4	3	$\{1,2,3,4\}$

Table 2. Energy loss costs

Energy loss cost: c_{ij}				
$i\backslash j$	1	2	3	4
1	8			
2	6	4		
3	10	8		
4	6	4	3	1

Table 3. Dynamic programming algorithm: sub-problem objective values

	$\hat{J}_i(s_i)$				
$i\backslash s_i$	0	1	2	3	4
1	37	29			
2	22	21	16		
3	18	15	12		
4	5	5	4	3	1

are operated via continuous gas-lift (*clients*). The pressure output of the compressors, the pressure demand of the wells, and the costs to install banks of compressors appear in Table 1. The penalties due to the energy loss resulting from pressure reduction are depicted in Table 2. This data comprises an instance of CAP.

3.4 Applying the DP Algorithm

The application of the dynamic programming algorithm to the instance given above yields the set $\hat{J} = \{\hat{J}_i : i \in M\}$ depicted in Table 3. The missing entries of the table have value $+\infty$, the default value for an infeasible sub-problem. Notice that $\hat{J}_4(s_4)$ is feasible for all s_4 given that client 4 can be serviced by all facilities. However, $\hat{J}_2(s_2)$ and $\hat{J}_3(s_3)$ take on value $+\infty$ when $s_2, s_3 \in \{3,4\}$ because neither facility 3 nor facility 4 can supply clients 2 and 3. The DP algorithm fills in the entries of client 4's row by solving $\hat{P}_m(s_m)$. The remaining lines are computed by solving $\hat{P}_i(s_i)$ for $i = 3,2,1$. The value of the optimal solution is therefore $\hat{J}_1(0) = 37$. Simultaneously, the solutions to these sub-problems are recorded in Table 4 for posterior retrieval. The optimal solution is obtained as follows: $x_1(0) = (1,1)$ and $y_1(0) = 1$ state that facility 1 should installed to service client 1; $x_2(1) = (2,1)$ and $y_2(1) = 0$ indicate that facility 1 services client 2; $x_3(1) = (3,1)$ and $y_3(1) = 0$ indicate that facility 1 services client 3; and $x_4(1) = (4,4)$ and $y_4(1) = 4$ indicate that facility 4 should be installed to supply client 4.

Table 4. Dynamic programming algorithm: optimal solutions

	$x_i(s_i)/y_i(s_i)$				
i	$s_i = 0$	1	2	3	4
1	$x_{11} = 1$	$x_{11} = 1$			
	$y_1 = 1$				
2	$x_{22} = 1$	$x_{21} = 1$	$x_{22} = 1$		
	$y_2 = 1$				
3	$x_{32} = 1$	$x_{31} = 1$	$x_{32} = 1$		
	$y_2 = 1$				
4	$x_{44} = 1$	$x_{44} = 1$	$x_{42} = 1$	$x_{43} = 1$	$x_{44} = 1$
	$y_4 = 1$	$y_4 = 1$			

3.5 Remarks

The particular structure of the compressor allocation problem allowed us to design an efficient, polynomial-time dynamic programming algorithm. A standing issue is whether or not this algorithm is optimal—put another way, the issue is whether $\Omega(mn^2)$ is a lower bound for the problem. If the problem data is given in matrix form, then the input size is of the order $\Theta(mn)$, and the issue is whether or not there exists an algorithm with running time between $\Theta(mn)$ and $\Theta(mn^2)$.

Another issue regards the design of a simpler, more efficient algorithm that would run in linear time regardless of the input size. The greedy algorithm, however, may fail to produce the optimal solution, as illustrated in the following scenario. Take the heuristic that scans the clients from 1 to m, deciding at each stage i whether to install a new facility or else service i with one of the existing facilities. The greedy choice would pick the least costly option. For the instance with $n = 2$, $a_1 = 10$, $a_2 = 8$, $N_1 = \{1\}$, $N_i = \{1,2\}$ for $i = 2,\ldots,m$, $c_{11} = 1$, $c_{i1} = 2$ and $c_{i2} = 0$ for $i = 2,\ldots,m$, the greedy heuristic fails when $m \geqslant 6$. It will install facility 1 and service all clients from this facility, incurring a total cost of $11+2(m-1)$, whereas the optimal solution installs facilities 1 and 2 with a total cost of 19. Likewise, the greedy heuristic that works in the opposite direction, from client m toward 1, may fail as well.

A feature of the dynamic programming algorithm is its simplicity: the algorithm is devoid of complex data structures and can be implemented in virtually any computer language. A second feature is the potential to use a parallel computer: because the computation of the values $\hat{J}_i(s_i)$ can be carried out in parallel for all $s_i \in \{0\} \cup N_i$, the algorithm may run in $O(mn)$ time when $\Theta(n)$ processors are available, thereby inducing maximum speed-up.

Let $\mathcal{P} = \{z \in \mathbb{R}^p : Az \leqslant b, 0 \leqslant z \leqslant 1\}$, $z = (x,y)$, be the polyhedron corresponding to a formulation of P, where $p = n + \sum_{j=1}^{n} |M_j|$ and matrix A consists of the constraints (1b) and (1c). Notice that P can be recast as $\max\{c^T z : z \in X\}$ where $X = \mathcal{P} \cap \mathbb{Z}^p$ and c is a suitable vector, this way giving $\mathcal{P}$ the status of a formulation.

From integer-programming theory (Nemhauser and Wolsey, 1988; Wolsey, 1998), follows that the convex hull of X, $conv(X)$, is also a polyhedron $\tilde{\mathcal{P}} = \{z \in \mathbb{R}^p : \tilde{A}z \leqslant \tilde{b}\} = conv(X)$ known as integer polyhedron. If $(\tilde{A}, \tilde{b})$ were known, one could instead solve $\max\{c^T z : \tilde{A}z \leqslant \tilde{b}\}$ with linear programming which, in turn, can be solved in polynomial time if the size of $(\tilde{A}, \tilde{b})$ is polynomial or if separation [3] can be performed in polynomial time. It so happens that certain problems have a formulation that is itself an integer polyhedron, that is, $\mathcal{P} = \tilde{\mathcal{P}}$. Examples include the matching and network-flow polyhedron. It has been established that the linear program $\max\{c^T z : Az \leqslant b, z \in \mathbb{R}^n_+\}$ has an integral solution for all integer vectors b for which it has a finite optimal value if and only if A is totally unimodular. A matrix A is totally unimodular (TU) if every square submatrix of A has determinant $+1, -1$, or 0. From a preliminary analysis, it appears that the matrix A arising from the constraints (1b) and (1c) is TU if the conditions of Assumption 1 hold, but this property is yet to be confirmed. An early result states that A is TU if, and only if, for every (square) *Eulerian* [4] submatrix B of A the sum of the entries of B divides by 4 (Camion, 1965). It seems plausible to use this result in trying to show that A is totally unimodular.

4. CONCLUSIONS AND FUTURE WORKS

The paper has formally stated the problem of allocating compressors to oil wells and framed it as a facility location problem. The special structure of the target problem enabled us to design an efficient, polynomial-time algorithm for an otherwise NP-Hard problem. A simple, but illustrative example helped to crystallize the concepts and the recursive principles upon which the algorithm was conceived. The polynomial-time solution of the compressor allocation problem raised the possibility of the constraint matrix being totally unimodular.

Future research will extend CAP to account for potential capacities of the compressors and time-dependent pressure demands for the oil wells.

ACKNOWLEDGMENTS

This research was funded by Agência Nacional de Petróleo (ANP) and Financiadora de Estudos e Projetos (FINEP), by means of a grant from Programa de Recursos Humanos da ANP para o Setor de Petróleo e Gás PRH-34 ANP/MCT.

[3] Let $S = \{\tilde{a}_i^T z \leqslant \tilde{b}_i, i = 1, \ldots, m\}$ be the set of constraints defined by $(\tilde{A}, \tilde{b})$. Given a fractional solution z, $z \notin \mathcal{P} \cap \mathbb{Z}^p$, the separation problem is to find a constraint i that is not respected by z, that is, $\tilde{a}_i^T z \not\leqslant \tilde{b}_i$.

[4] A matrix is said to be *Eulerian* if the sum of the entries of its lines and the sum of the entries of its columns are both even.

REFERENCES

G. A. Alarcón, C. F. Torres, and L. E. Gómez. Global optimization of gas allocation to a group of wells in artificial lift using nonlinear constrained programming. *ASME Journal of Energy Resources Technology*, 124(4):262–268, December 2002.

D. P. Bertsekas. *Dynamic Programming and Optimal Control*, volume I. Athena Scientific, Belmont, MA, 1995.

S. Buitrago, E. Rodríguez, and S. D. Espin. Global optimization techniques in gas allocation for continuous flow gas lift systems. In *Proc. SPE Gas Technology Conference*, pages 375–379, Calgary, Canada, 1996. Paper SPE 15616.

P. Camion. Characterization of totally unimodular matrices. *Proceedings of the American Mathematical Society*, 16, 1965.

E. Camponogara and P. H. R. Nakashima. Optimizing gas-lift production of oil wells: Piecewise linear formulation and computational analysis. *IIE Transactions*, 38, 2006a. 10 pages.

E. Camponogara and P. H. R. Nakashima. Solving a gas-lift optimization problem by dynamic programming. *Accepted to appear in European Journal of Operational Research*, 2006b.

T. H. Cormen, C. E. Leiserson, and R. L. Rivest. *Introduction to Algorithms*. MIT Press, Cambridge, MA, 1990.

G. Cornuejols, M. L. Fisher, and G. L. Nemhauser. On the uncapacitated location problem. *Annals of Discrete Mathematics*, 1:163–177, 1977.

M. R. Garey and D. S. Johnson. *Computers and Intractability: A Guide to the Theory of NP-Completeness*. W. H. Freeman and Co., 1979.

F. Jahn, M. Cook, and M. Graham. *Hydrocarbon Exploration and Production*. Elsevier, 2003.

E. P. Kanu, J. M. Mach., and K. E. Brown. Economic approach to oil production and gas allocation in continuous gas lift. *Journal of Petroleum Technology*, pages 1887–1892, October 1981.

G. L. Nemhauser and L. A. Wolsey. *Integer and Combinatorial Optimization*. John Wiley & Sons, New York, NY, 1988.

N. Nishikiori, R. A. Redner, D. R. Doty, and Z. Schmidt. An improved method for gas lift allocation optimization. *ASME Journal of Energy Resources Technology*, 117:87–92, 1995.

L. A. Wolsey. *Integer Programming*. John Wiley & Sons, New York, NY, 1998.

CAPACITY MANAGEMENT IN THE CHEMICAL SUPPLY CHAIN

P. K. Naraharisetti[1], I. A. Karimi[2,*], R. Srinivasan[1,2]

[1]Institute of Chemical and Engineering Sciences, 1 Pesek Road, Jurong Island, Singapore 627833
[2]Department of Chemical & Biomolecular Engineering, National University of Singapore, 4 Engineering Drive 4, Singapore 117576

Abstract: Long term capacity planning involves locating and allocating the production capacities and inventory capacities, and short term capacity planning involves the production allocation and distribution of materials. Most existing literature deals with them individually and also consider only investments in capacities and do not consider disinvestment. Combining the above problems into one would give a holistic picture of the entire supply chain and allows in better planning, leading to greater efficiency in terms of reduced costs or increased profit. In this work, we present a new deterministic capacity management model, which considers facility location, (dis)investment in capacity, production allocation, distribution of materials and regulatory factors among others. Also, we have improved the formulation of existing literature by using fewer binary variables.

Keywords: capacity, planning, distribution, discrete time, linear programming, optimization

1. INTRODUCTION

Capacity planning involves locating and allocating capacities, process planning, and allocating production. Long term capacity planning deals with (dis)investment in facilities (also called the location allocation problem) and short term capacity planning deals with production allocation and distribution (also called production distribution problem). Capacity management involves both long term and short term capacity planning.

Organizations strive towards meeting the customer demand, both in order to maintain good customer satisfaction and make profit. In an ever changing world, the demand for products changes with time. New products are introduced, old products are improved technologically, and some are no longer manufactured as customer demand drops. Hence, it is important for an organization to expand existing capacity or invest in new capacity in order to meet increased demand for existing products or to explore new markets, invest in new capacity for new products, disinvest old plants that no longer meet the latest technological specifications or if there is no demand. In order to remain profitable while meeting customer satisfaction, these decisions are to be made appropriately.

Previous work in the area of production allocation and distribution problem includes those of Arntzen, et al. (1995), Bradley and Arntzen (1999), Cohen and Lee (1989), Gjerdrum et al. (2001), Goetschalckx, et al. (2002), Pyke and Cohen (1994), Ryu and Pistikopoulos (2005), Tsiakis et al. (2001). These do not consider the location of new facilities and expansion of the existing facilities. Levis and Papageorgiou, (2004), Oh and Karimi (2004), Papageorgiou et al. (2001), have considered the issue of new facility location; however, there is only partial or no representation of the production allocation and distribution issue. In all of the above, disinvestment was not considered.

In this work we consider only the location and allocation of capacities and allocation of production, while not explicitly considering process planning (for further information on process planning, the readers are referred to Ahmed and Sahinidis, 2000). A multi echelon supply chain network is considered and a new deterministic model, which combines both of the location allocation problem and production distribution problem into an integrated location allocation production distribution problem (LAPD problem), is presented. The problem is formulated as a novel mixed integer linear programming (MILP) model with the ability to incorporate production changeover costs, depreciation, tax and regulatory factors among others, and is solved as maximizing the net present value of the profit. To the best of our knowledge, this is the first study that includes disinvestment, and we use fewer binary variables as compared to Oh and Karimi (2004).

2. PROBLEM STATEMENT

The supply chain of a multinational corporation (MNC) is considered in this work (Fig. 1). Let P be the set of all existing and future production facilities (p), I be the set of input inventories at production facilities (i), O be the set of output inventories (o), S be the set of existing and future suppliers of raw materials (s), D be the set of existing and future inventories at distribution centres (d) and C be the set of existing and future inventories at customer

* To whom correspondence should be addressed:
Tel: +65-6874-6359, Fax: +65-6779-1936
Email: cheiak@nus.edu.sg

locations (c). Given the demand profiles for all products from all customers, raw material availability profiles from all suppliers, price forecasts for raw materials and products, and other supply chain information and costs, the desired capacity management model should determine the location, timing and amount of change in capacity, purchase-distribution-sales of material such that the profit (net present value-NPV) is maximized.

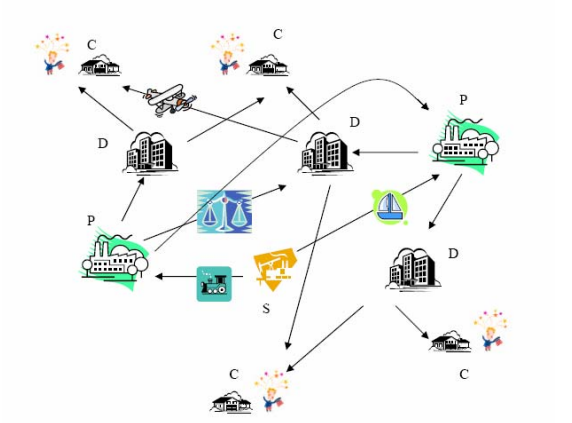

Fig. 1. Schematic representation of a chemical supply chain of an MNC.

To address this problem we make the following assumptions: 1.) Each production facility represents a specific process of producing products from the raw materials. Several such processes may exist at a single location and each is considered a distinct facility. 2.) Each production facility processes several materials and all materials are taken into consideration in mass balance. The utilization of capacity is the total weight of all the material in the facility at that time. 3.) The limits on transportation, production, and expansion polices are all known (ex: a facility may not expand more than thrice in the planning horizon). 4.) The time in between the starting of construction and starting of operation of a plant (cl_p) /inventory is fixed and is known. It may be different for different plants and inventories. Expansion does not affect the production and an expansion/construction cannot be started while a previous expansion/construction is in process. 5.) An existing capacity may expand by small amounts, but the first addition for a possible new facility have to be above a certain minimum, once this exists, it can expand in small increments. 6.) A facility is disinvested completely and this cannot be done partially. 7.) A facility once disinvested cannot be purchased again 8.) Interval is a few periods. A production facility can operate for only a fixed number of periods (op) in any given interval (ex: 11 periods in any given 12 periods) to allow time for maintenance. 9.) Costs of transportation from the point of purchase of raw materials from suppliers to the point of customer location are born by the MNC. 10.) Inventory (+ve) is carried forward from one period to another and there is no allowance for negative inventory or back orders i.e., material can be sold only when it is available. 11.) All costs and income are considered to be linear functions. 12.) The amount of investment that can be made in a given interval (in, di) is limited and is known, similarly constraints apply on disinvestment (IB, DR) (ex: the amount of investment that can be made in a year is one billion). 13.) Throughput is the product of throughput factor and capacity.

3. PROBLEM FORMULATION

A chemical supply chain, which consists of raw material suppliers, production facilities, input and output inventories at the production facilities, inventories at the distribution centres and customer locations is considered. The strategic plan should decide the timing, amount and location attributes of each of the variables under consideration such as the capacity change and utilization of a facility, and purchase/sales of raw materials/products and distribution of the same. Additional features like depreciation, interest rate and after tax profit are taken into account and tax at customer location for sales is born by the customer. To address this problem, the following formulation is presented as a.) Capacity Change Constraints, b.) Capacity Constraints, c.) Inventory Balance Constraints, d.) Costs and Income constraints.

1.1 *Constraints on Capacity Change*

The number of times that a plant may expand in the horizon is limited (np).

$$\sum_{t} PY_{pt} \le np \qquad 1a$$

where, PY is the plant expansion variable.

An expansion cannot start while a previous expansion is in process.

$$\sum_{t-cl_p+1}^{t} PY_{pt} \le 1 \qquad (t \ge cl_p) \qquad 1b$$

The following constraints relate plant expansion variable PY, plant disinvestment variable PX, plant existence variable PEY and plant sold off variable PSY (PY, PX are binary variables and PEY, PSY are 0-1 continuous variables).

$$PEY_{pt} \ge PY_{pt} \qquad 1c$$

$$PEY_{p(t-1)} \le PEY_{pt} + PSY_{pt} \qquad 1d$$

$$PEY_{pt} \le PEY_{p(t-1)} + PY_{pt} \qquad 1e$$

Once, the plant is sold off, it does not exist any more and this is indicated by the variable PSY, also, it is not possible for the plant to simultaneously exist and be sold off.

$$PSY_{pt} \ge PSY_{p(t-1)} \qquad 1f$$

$$PEY_{pt} + PSY_{pt} \le 1 \qquad 1g$$

A plant once disinvested cannot be purchased.

$$PY_{pt} \le 1 - PSY_{pt} \qquad 1h$$

A plant may be sold off only once in the given horizon. This is taken care of by the variable PX as

this can be '1', only if the plant existed in the previous period.

$$PSY_{pt} \geq PX_{pt} \qquad 1i$$

$$PEY_{p(t-1)} \geq PX_{pt} \qquad 1j$$

$$PSY_{pt} \leq PSY_{p(t-1)} + PX_{pt} \qquad 1k$$

A plant may add capacity at an existing location or a new location and there are different minimum limits on expansion at existing location and construction of new facility. No additions are possible at plant (p) at time (t) if it is slated for disinvestment at that time. PA, a positive variable, is the amount of capacity added in any period. $Pcap_{pt}$ is the capacity of a plant (p) at time (t), PA_p^{LN} is the lower limit of capacity addition for a new plant and PA_p^{LO} is the lower limit of capacity addition for an old plant.

$$Pcap_{pt} - Pcap_{p(t-1)} \leq PA_{pt} \leq Pcap_{pt} - Pcap_{p(t-1)} + Pcap_p^U PSY_{pt} \qquad (t \geq 2)$$

$$PA_{pt} \leq Pcap_p^U PY_{pt} \qquad 2a,b$$

$$Pcap_{pt} \leq Pcap_p^U (1 - PSY_{pt}) \qquad 2c$$

$$PA_{pt} \geq PA_p^{LN} (PY_{pt} - PEY_{p(t-1)}) + PA_p^{LO} (PEY_{p(t-1)} + PY_{pt} - 1) \qquad 2d$$

Similarly, $Icap_{it}$, $Ocap_{ot}$ and $Dcap_{dt}$ are written and similar constraints are written for inventories.

1.2 *Capacity Constraints*

There are limits on transportation and the transportation time is negligible compared to a period. The total amount of raw material (m) purchased at supplier (s) and sent to all inventories (i) at time (t) does not exceed the amount of the raw material available for purchase. SI_{msit} is the amount of material (m) purchased at supplier (s) and sent to inventory (i) at time (t). Similarly, OI, OD and DC are written. SM_{mst} is the amount of material (m) available for purchase from supplier (s) at time (t).

$$\sum_i SI_{msit} \leq SM_{mst} \qquad 3$$

The total amount of materials that an inventory (i) can receive in a time (t) is less than or equal to its throughput.

$$\sum_{m \in mi_i, s} SI_{msit} + \sum_{m \in mi_i, o} OI_{moit} + \sum_{m \in mi_i, p \in ipi_i} PI_{mpit} \leq tfI_{it} Icap_{it} \qquad 4a$$

where, tfI_{it} is the throughput factor of inventory (i) at time (t), mi_i is the set of all materials that an inventory (i) may hold and ipi_i is the set of plants (p) that an inventory (i) supplies material to. The subscript and the first letter of the set indicate the particular facility, second and third letters indicate 'from' and 'to' facility. Similarly, tfO_{ot}, mp_p, mo_o, md_d, mc_c, ioi_i, pip_p, ppo_p, ppi_p, opo_o and ooi_o are written.

Similar equations for throughput are written for the throughput of (o), (d) and (c). However, the corresponding terms for SI, OI, PI in equation 4a are modified to reflect the incoming materials appropriately ((o) receives material only from plants (p), (c) receives material only from distribution centres (d)).

$$\sum_{m \in md_d, o} OD_{modt} \leq tfD_{dt} Dcap_{dt} \qquad 4b$$

The amount of the materials in an inventory (i) at time (t) does not exceed the holding capacity in that period.

$$\sum_{m \in mi_i} IM_{mit} \leq Icap_{it} \qquad 4c$$

IM_{it} is the total amount of all the materials present in inventory (i) at time (t). Similar equations are written for the material in (o), (d) and (c).

The amount of material that a plant can accept and process in any time period is within the utilization limits. PZ is the binary variable for plant operation.

$$\sum_{m \in mp_p, i \in pip_p} IP_{mipt} \leq Pcap_{pt} \qquad 5a$$

$$\sum_{m \in mp_p, i \in pip_p} IP_{mipt} \geq ut_{pt} Pcap_{pt} - Pcap_p^U (1 - PZ_{pt}) \qquad 5b$$

$$\sum_{m \in mp_p, i \in pip_p} IP_{mipt} \leq Pcap_p^U PZ_{pt} \qquad 5c$$

where, mp_p is the set of materials that a plant (p) can process. pip_p is the set of inventory (i) that supplies material to plants (p), ut_{pt} is the utilization of plant (p) at time (t)

A plant may operate only if it exists.

$$PEY_{pt} \geq PZ_{pt} \qquad 6a$$

The number of periods that a plant may operate in any given interval is known.

$$\sum_{t-op_p^p+1}^{t} PZ_{pt} \leq op_p \qquad (t \geq op_p^p) \qquad 6b$$

1.3 *Inventory Balance Constraints*

Inventory balance equations are written for each of the inventories and stoichiometry is written for the plants. The amount of material (m) in an inventory ((i), (o), (d) or (c)) at time (t) is equal to the amount of the material at time (t-1) plus the amount of material that came in at time (t) minus the amount of material that went out at time (t). Initialization is done appropriately.

$$IM_{mit} = IM_{mi(t-1)} - \sum_{p \in ipi_i} IP_{mipt} + \sum_{p \in ipi_i} PI_{mpit} + \sum_{s} SI_{msit} + \sum_{o \in ioi_i} OI_{moit} \quad (7a)$$

$$\frac{\sum_i IP_{mipt}}{st^{ip}_{mp}} = \frac{\sum_i IP_{m'ipt}}{st^{ip}_{mp}} = \frac{\sum_o PO_{m''pot}}{st^{po}_{mp}} = \frac{\sum_i PI_{m'''pit}}{st^{pi}_{mp}} \quad (m \neq m' \neq m'' \neq m''') \quad (7b)$$

$$OM_{mot} = OM_{mo(t-1)} - \sum_d OD_{modt} + \sum_{p \in opo_o} PO_{mpot} - \sum_{i \in ooi_o} OI_{moit} \quad (7c)$$

$$DM_{mdt} = DM_{md(t-1)} - \sum_c DC_{mdct} + \sum_o OD_{modt} \quad (7d)$$

$$CM_{mct} = CM_{mc(t-1)} - Sa_{mct} + \sum_d DC_{mdct} \quad (7e)$$

$$Sa_{mct} \leq DE_{mct} \quad (7f)$$

where, IP_{mipt} is the amount of material (m) transferred from inventory (i) to plant (p) in time (t), st_{mp} is the stoichiometry coefficient of material (m) in plant (p), DE_{mct} is demand and Sa_{mct} is sales of material (m) at customer location (c) at time (t). Similarly, PO is written.

1.4 *Constraints on Costs and Income*

The cost incurred in the purchase of raw materials is proportional to the amount of raw material purchased.

$$RC_{mst} = \sum_{i,r \in rsi_{si}} SI_{msirt} msC_{mst} \quad (8)$$

Where, RC_{mst} is the raw material purchase cost and, msC is the unit cost of raw material.

The costs due to transportation are born by the inventory at the arrival location. Storage costs and production costs include fixed operational costs irrespective of the amount of material and costs related to the amount of material handled. Similarly, they are written for distribution centres and customer locations while production costs are only written for the production facilities.

$$TCI_{i,t} = \sum_{m \in mi_i, s} TCmsi_{msit} SI_{msit} + \sum_{m \in mo_o, o} TCmoi_{moit} OI_{moit} \quad (9)$$

$$SCI_{i,t} = fiC_{it} IEY_{it} + \sum_{m \in mi_i} Cmi_{mit} IM_{mit} \quad (10)$$

$$PC_{p,t} = fpC_{pt} PEY_{pt} + Cmp_{pt} \sum_{m \in mp_p, i \in pip_p} IP_{mipt} \quad (11)$$

where TCI is the transportation cost paid by inventory, TCmsi and TCmoi are unit transportation costs for (s) to (i) and (o) to (i), SCI is storage cost at inventory, fiC is fixed inventory operation cost, miC is unit material handling cost at inventory, fpC is fixed plant operation costs, mpC is unit material processing costs and PC is production costs.

Plants incur a change-over cost due to stopping or starting production. s1, s2 are starting and stopping (changeover) costs.

$$Csw1_{pt} \geq s1_{pt}(POpe_{pt} - POpe_{p(t-1)}) \quad (t \geq 2)$$

$$Csw2_{pt} \geq s2_{pt}(POpe_{p(t-1)} - POpe_{pt}) \quad (t \geq 2)$$

$$Csw_{p,t} = Csw1_{pt} + Csw2_{pt} \quad (t \geq 2) \quad (12a,b,c)$$

The revenue (R) from sales is directly proportional to the amount of sales. mr is unit price of the product.

$$R_{c,t} = \sum_{m \in mc_c} Sa_{mct} mr_{mct} \quad (13)$$

The depreciation cost due to an existing capacity and a new addition are calculated based on different rates of depreciation and it is calculated only for a plant that exists. Similarly depreciation is calculated for all inventories.

$$PDC_{p,t} \leq Pcap_{p1} DP_{pt} rdpo_{pt} + (Pcap_{pt} - Pcap_{p1}) DP_{pt} rdpn_{pt} \quad (t \geq 2) + Pcap^U_p DP_{pt}(1 - PEY_{pt}) \quad (14a)$$

$$PDC_{p,t} \geq Pcap_{p1} DP_{pt} rdpo_{pt} + (Pcap_{pt} - Pcap_{p1}) DP_{pt} rdpn_{pt} \quad (t \geq 2) \quad (14b)$$

$$-Pcap^U_p DP_{pt}(1 - PEY_{pt})$$

$$PDC_{p,t} \leq Pcap^U_p DP_{pt} PEY_{pt} \quad (t \geq 2) \quad (14c)$$

$$IDC_{i,t} = Icap_{i1} DI_{it} rdio_{it} + (Icap_{it} - Icap_{i1}) DI_{it} rdin_{it} \quad (t \geq 2) \quad (14d)$$

where, PDC is the plant depreciation costs, DP is the value of plant considered in depreciation (depreciated plant value), rdpo is rate of depreciation of plant for old section, rdpn is for new section of the plant.

There are fixed and variable costs due to an investment. The total investment in any interval (in) cannot exceed IB. Similarly, disinvestment in any interval (di) cannot exceed DR.

$$CI_t = \sum_p fcip_{pt} PY_{pt} + \sum_p vcip_{pt} PA_{pt} + \sum_i fcii_{it} IY_{it} + \sum_i vcii_{it} IA_{it} + \sum_o fcio_{ot} OY_{ot} + \sum_o vcio_{ot} OA_{ot} \quad (t \geq 2) + \sum_d fcid_{dt} DY_{dt} + \sum_d vcid_{dt} DA_{dt} + \sum_c fcic_{ct} CY_{ct} + \sum_c vcic_{ct} CA_{ct} \quad 15a$$

$$\sum_{t-in+1}^{t} \left(\begin{array}{l} \sum_p fcip_{pt} PY_{pt} + \sum_p vcip_{pt} PA_{pt} \\ + \sum_i fcii_{it} IY_{it} + \sum_i vcii_{it} IA_{it} + \\ \sum_o fcio_{ot} OY_{ot} + \sum_o vcio_{ot} OA_{ot} \\ + \sum_d fcid_{dt} DY_{dt} + \sum_d vcid_{dt} DA_{dt} \\ + \sum_c fcic_{ct} CY_{ct} + \sum_c vcic_{ct} CA_{ct} \end{array} \right) \leq IB \quad (t \geq in) \quad 15b$$

where, fcip is fixed capital investment at plant and vcip is variable capital investment at plant. Similarly, fcii, fcio, fcid and fcic, vcii, vcio, vcid, and vcic are written.

cip is the fixed capital investment for the addition of a capacity, which is divided into fixed cost for the addition at a new location and fixed cost for the addition at an existing location as follows. *cip* is a positive variable and it is always kept to a minimum as this is a maximizing NPV problem.

$$cip_{pt} \geq fcip^{n}_{pt} (PY_{pt} - PEY_{p(t-1)}) + fcip^{o}_{pt} (PEY_{p(t-1)} + PY_{pt} - 1) \quad 15c$$

where, n (o) represents new (old) plant.

There is an income from the sales of an asset/capacity

$$RDP_{pt} \leq Pcap_{pt} ap_{pt} \quad 16a$$

$$RDP_{pt} \geq Pcap_{pt} ap_{pt} - Pcap^{U}_{p} ap_{pt} (1 - PX_{p(t-1)}) \quad 16b$$

$$RDP_{pt} \leq Pcap^{U}_{p} ap_{pt} PX_{p(t-1)} \quad 16c$$

$$RD_t = \sum_p RDP_{pt} \quad 16d$$

$$\sum_{t-di+1}^{t} RDP_t \leq DR \quad (t \geq di) \quad 16e$$

where, RDP is the revenue from disinvestment of a plant, ap is the unit asset price of the plant that is realized on disinvestment and RD is total revenue from disinvestment at time (t).

The taxable income is calculated based on the nation (n) in which the facilities fall.

$$CT_{n,t} \geq \sum_{(s \in sn_n, i \in in_n, p \in pn_n, o \in on_n, d \in dn_n, c \in cn_n)} CTx\, TR_{n,t} \quad 17a$$

where,

$$CTx = R_{c,t} - RC_{s,t} - PC_{pt} - Csw_{pt} - TCI_{it} - TCD_{dt} - TCC_{ct} - SCI_{it} - SCO_{ot} - SCD_{dt} - SCC_{ct} - PDC_{pt} - IDC_{it} - ODC_{it} - DDC_{dt} - CDC_{ct} \quad 17b$$

$$NPV = \sum_t \frac{NPVt}{(1 + ir(t))^{(yr(t)-1)}} \quad 18a,b$$

where,

$$NPVt = \sum_c R_{c,t} - \sum_s RC_{s,t} - \sum_p PC_{pt} - \sum_p Csw_{pt} - \sum_i TCI_{it} - \sum_d TCD_{dt} - \sum_c TCC_{ct} - \sum_i SCI_{it} - \sum_o SCO_{ot} - \sum_d SCD_{dt} - \sum_c SCC_{ct} - CI_t + \sum_p RDP_{pt} - \sum_n CT_{nt}$$

4. ILLUSTRATION

LAPD is a challenging problem and preliminary analysis on the above formulation is a first step to address the problem and a further improvement of the formulation is required in order to improve the efficiency.

To analyze the performance of the formulation, we considered an example with five raw materials, six intermediates, and seven products. Two suppliers supply all the raw materials and the intermediates, however, the plants can also manufacture the intermediates. Eight existing production plants and six potential locations for new plants, five existing input and output inventories at plants are considered. For case 1, three existing distributions centres, three customer locations, and two new possible inventories at each of these locations are considered. For case 2, five existing distribution centres, fifteen customer locations, five possible new distribution centres, and fifteen possible new customer locations are considered. We consider the disinvestment of plants only in this example for simplicity. However, both plants and inventories are considered for investment. A horizon of sixty one-month periods is considered. It takes two years and one year respectively for the plants and inventories to begin operation; hence, no new expansion can start operation at 6^{th}, 12^{th}, and 18^{th} month for plants and 6^{th} month for inventories. A plant can expand at 24^{th}, 30^{th}, 36^{th}, 42^{nd}, 48^{th}, and 54^{th} months only. Furthermore, a plant can be sold between 18^{th} and 48^{th} months only. Also, there is no incentive in beginning any operation at the end of the horizon (i.e., 60^{th} month). The model was solved using CPLEX 9.0 solver within GAMS 21.7 on

Windows XP workstation with an Intel Xeon dual (3.6GHz) processor. The model statistics are given in the Table 1 and preliminary results related to (dis)investment for Case 1 are presented in Table 2. It shows that some plants are disinvested at time forty eight, while there is no investment in plants. However, there is investment in the inventories at various locations.

Table 1 Computational statistics for the capacity management model

	Case 1	Case 2
Variables	732933	1169733
Constraints	575009	905549
Binary variables	1258	1498
Non-zeros	3191745	5223055
CPU Time (h)	10	6
% Gap	8.6	291.4

Table 2 Expansion and disinvestment variables indicating investment and disinvestment

p,o,d,c \t	Plant disinvestment	Input inventory	Output inventory	Customer location inventory
1	48	-	-	-
2	48	-	-	-
3	48	-	-	-
4	48	-	-	12
6	-	-	12	-
7	-	12	12	-
8	-	-	12	-
9	-	-	12	-
10	-	-	12	-

From the above preliminary results, it can be seen that the model appropriately considers capacity expansion and contraction. Though the model considers these for all inventories at all time periods, we have limited it to consider disinvestment only for plants, and investment at certain times only in order to reduce solution time and highlight the various features of the formulation. It may be noted that regulatory factors and insurance may be incorporated appropriately in the transportation cost parameters. The results indicate that selling the plants at the 48^{th} period is more profitable than using them to make products. The remaining plants are operated in order to make profit from the sale of products. In the case of the investment in inventory, the investment is made early in order to capture the high demand for the products. Since, the earliest the inventory can start operation is the 12^{th} month; they do so in order to capture the demand at the earliest.

5. CONCLUSION

We have presented a new formulation to address various aspects such as the capacity expansion and contraction, distribution of materials, regulatory factors and depreciation among others in strategic planning for a deterministic case in an end-to-end supply chain for a single MNC. However, the formulation and analysis are only preliminary. Improvements need to be done in order to increase the efficiency of the formulation such that it can handle larger problems in reasonable computational time. A decomposition procedure or a heuristic to solve such large problems may be an appropriate way to apply this model in practice.

REFERENCES

Ahmed S, N. V. Sahinidis (2000). Analytical investigations of the process planning problem. *Computers and Chemical Engineering,* **23**, 1605-1621.

Arntzen, B. C, G. G. Brown, T. P. Harrison, L. L. Trafton (1995). Global supply chain management at digital equipment corporation. *Interfaces*, **25**, 69-93.

Bradley, J. R, B. C. Arntzen (1999).The simultaneous planning of production, capacity, and inventory in seasonal demand environments. *Operations Research, **47**,* 795-806.

Cohen, M. A, H. L. Lee (1989). Resource deployment analysis of global manufacturing and distribution networks. *Journal of Manufacturing and Operations Management*, **2**, 81-104.

Gjerdrum, J, N. Shah, L. G. Papageorgiou (2001). Transfer prices for multienterprise supply chain optimization. *Industrial and Engineering Chemistry Research,* **40**, 1650-1660.

Goetschalckx, M, C. Vidal, K. Dogan (2002). Modeling and design of global logistics systems: A review of integrated strategic and tactical models and design algorithms. *European Journal of Operational Research,* **143**, 1-18.

Levis, A. A, L. G. Papageorgiou (2004). A hierarchical solution approach for multi-site capacity planning under uncertainty in the pharmaceutical industry. *Computers and Chemical Engineering,* **28**, 707-725.

Oh, H. C, I. A. Karimi (2004). Regulatory factors and capacity-expansion planning in global chemical supply chains. *Industrial and Engineering Chemistry Research,* **43**, 3364-3380.

Papageorgiou, L. G, G. E. Rotstein, N. Shah (2001). Strategic supply chain optimization for the pharmaceutical industries. *Industrial and Engineering Chemistry Research,* **40**, 275-286.

Pyke, D. F, M. A. Cohen (1994). Multiproduct integrated production distribution systems. *European Journal of Operational Research,* **74**, 18-49.

Ryu, J. H, E. N. Pistikopoulos (2005). Design and operation of an enterprise-wide process network using operation policies. 1. Design. *Industrial and Engineering Chemistry Research*, **44**, 2174-2182.

Tsiakis, P, N. Shah, C. C. Pantelides (2001). Design of multi-echelon supply chain networks under demand uncertainty. *Industrial and Engineering Chemistry Research*, **40**, 3585-3604.

ADCHEM 2006

International Symposium on Advanced Control of Chemical Processes
Gramado, Brazil – April 2-5, 2006

PROCESS OPTIMIZATION AND CONTROL UNDER UNCERTAINTY: A CHANCE CONSTRAINED PROGRAMMING APPROACH

Harvey Arellano-Garcia*, Tilman Barz, Günter Wozny

Department of Process Dynamics and Operation
Berlin University of Technology, Sekr. KWT-9, D-10623 Berlin, Germany

Abstract: A novel chance constrained programming approach for process optimization of large-scale nonlinear dynamic systems and control under uncertainty is proposed. The stochastic property of the uncertainties is explicitly considered in the problem formulation in which some input and state constraints are to be complied with predefined probability levels. This incorporates the issue of feasibility and the contemplation of trade-off between profitability and reliability. The approach considers a nonlinear relation between the uncertain input and the constrained variables. It also involves novel efficient algorithms both to consider time-dependent uncertainties and to compute the probabilities and, simultaneously, their gradients. To demonstrate the performance of the proposed method, a chance constrained NMPC scheme for the online optimization of a batch reactor under safety restrictions, and the optimal operation and control of a coupled two-pressure column system are discussed to show the efficiency and potential for optimization and control under uncertainty.

Keywords: uncertainty, chance constraints, dynamic real-time optimization, NMPC

1. INTRODUCTION

For a quantitative understanding and control of time varying phenomena in process system, it is essential to relate the observed dynamical behaviour to mathematical models. These models usually depend on a number of parameters whose values are unknown or only known roughly. Furthermore, often only a part of the system's dynamics can be measured. Therefore, a plant model unavoidably involves uncertainties. They are either endemic due to the external disturbances or introduced into the model to account for imprecisely known dynamics. However, uncertainty and variability are inherent characteristics of any process system. These arise due to the unpredictable and instantaneous variability of different process conditions, such as temperature and pressure of coupled operating units, market conditions, (recycle) flow rates and/or its composition, or due to certain model parameters such as kinetic constants or equilibrium parameters. These uncertainties or disturbances are often multivariate and correlated stochastic sequences which have a chain-effect to each unit operation of a production line. In industrial practice, uncertainties are usually compensated for by using conservative decisions like an over-design of process equipment and then retrofits to overcome operability bottlenecks, or an overestimation of operational parameters caused by worst case assumptions of the uncertain parameters, which leads to a significant deterioration of the objective function in an optimization problem. In other deterministic approaches, the expected values are used, which most likely leads to violations of the constraints when the decision variables are implemented on site. Moreover, the use of feedback control in order to compensate uncertainty can not ensure constraints on open-loop variables. Consequently, the consideration of uncertainties /disturbances and their stochastic properties in optimization approaches are necessary for robust process operation, and control.

During the past decades several approaches have been suggested to address these problems in a systematic manner (Sahinidis, 2004). These techniques mostly differ in how uncertainty is handled as well as in the objectives that may include process flexibility, profitability, and/or robustness. Nearly most of these approaches employed the two-stage programming method with the recourse formulation to handle inequality constraints. In this method, violation of the constraints is compensated for by some penalty terms in the objective function. This compensation, however, requires a common measurement to describe the objective function and constraint violations. In cases where this measurement is not available, the formulation of chance constraints with a user pre-defined probability limit of constraint compliance will be the most

suitable approach. Thus, in this work, we propose a systematic approach to solving chance constrained process optimization and control problems.

Decision making inherently involves consideration of uncertain outcomes. Thus, we are confronted with decisions a priori for the future operation. The decision should be taken before the realization of the random inputs. These uncertain variables can be constant or time-dependent in the future horizon. The stochastic distribution of the uncertain variables may feature different forms. The mean and variance values can be determined based on historical data analysis. However, stochastic optimization with even an approximated distribution is more reliable than a deterministic optimization. In this work, uncertainties are assumed to have a correlated multivariate normal distribution, but the presented approach does not depend on the distribution form.

2. CHANCE CONSTRAINED APPROACH

A general chance constrained optimization or control problem under uncertainty can be formulated as follows:

$$\begin{aligned} \min \quad & \mathrm{E}\left[f(\mathbf{x},\mathbf{u},\boldsymbol{\xi})\right] + \omega\, D\left[f(\mathbf{x},\mathbf{u},\boldsymbol{\xi})\right] \\ \text{s.t.} \quad & \mathbf{g}(\dot{\mathbf{x}},\mathbf{x},\mathbf{u},\boldsymbol{\xi}) = \mathbf{0},\ \mathbf{x}(t_0) = \mathbf{x}_0 \\ & \Pr\left\{\mathbf{h}(\dot{\mathbf{x}},\mathbf{x},\mathbf{u},\boldsymbol{\xi}) \geq \mathbf{0}\right\} \geq \alpha \\ & \mathbf{u}_{\min} \leq \mathbf{u} \leq \mathbf{u}_{\max},\ t_0 \leq t \leq t_f \end{aligned} \tag{1}$$

where f is the objective function, E and D are the operators of expectation and variation, respectively. ω is a weighting factor between the two terms. Here, $\mathbf{x}$, $\mathbf{u}$ and $\boldsymbol{\xi}$ are state, decision and random vectors, respectively. $\mathbf{g}$ represents the equality constraints (i.e model equations). The reliability or probability of complying with the inequality constraints is given by $\Pr\{\mathbf{h}(\dot{\mathbf{x}},\mathbf{x},\mathbf{u},\boldsymbol{\xi}) \geq \mathbf{0}\} \geq \alpha$. The value $\alpha\ (0 \leq \alpha \leq 1)$ represents the probability level. Since α can be defined by the user, it is possible to select different levels and make a compromise between the objective function value and the risk of constraint violation. The proposed approach relies on formulating output constraints as chance constraints which can be formulated in two different forms: single chance constraint where individual probabilities of ensuring each inequality will be held. In this form, different confidence levels can be assigned to different outputs based on their specifications. Another form is the joint chance constraint, where all inequalities are included in the probability computation i.e. they have to be satisfied simultaneously with the unique given confidence (probability) level.

The values of α are not given by an explicit formula, but rather defined as probabilities of some implicitly defined regions in the space of the random parameter ξ, i.e. the feasible region will shrink if the confidence level is increased, which implies a conservative decision. It has, however, the advantage of keeping a more stable operation, but it may be not flexible to the variations required. Thus, the main difference between single and joint constraints consists in their reliability. However, as shown in Fig. 1, such problems can be classified based on the properties of processes, uncertainties and constraint forms.

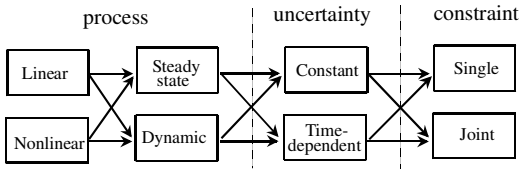

Fig. 1. Classification of chance constrained problems

The main challenge in chance constrained programming lies in calculating probability values, the gradients of the probability function to the controls and possibly Hessians. Different problems have different degrees of complexity for computing these values, which will be discussed in the next sections.

2.1 Monotonic relationship between constrained output and uncertain input

In systems where the relation between uncertain and constrained variables is nonlinear, the type of the probability distribution function of the uncertain input is not the same as the one of the constrained output. Thus, it is difficult to obtain the stochastic distribution of output variables. For this reason, nonlinear chance constrained programming remains an unresolved problem. Recently, a promising optimization framework for dynamic systems under uncertainty was introduced for the off-line optimization under probabilistic constraints and successfully applied to a large-scale nonlinear dynamic chemical process (Arellano-Garcia et al. 2003). The basic idea is to avoid directly computing the output probability distribution. Instead, an equivalent representation of the probability is derived by mapping the probabilistic constrained output region back to a bounded region of the uncertain inputs. Hence, the output probabilities and, simultaneously, their gradients can be calculated through multivariate integration of the density function of the uncertain inputs by collocation in finite elements (2). Since multiple time intervals are considered, the reverse projection of the output feasible region is not trivial. Thus, the approach also involves efficient algorithms for the computation of the required (mapping) reverse projection. The method relies upon the case of a monotonic relationship between the constrained output variables $y_i \in Y_i$ and at least one of the uncertain input variables $\xi_s \in \Xi_s$ where Ξ_s is a subspace of Ξ. So, for instance if $\xi_S \uparrow \Rightarrow y_i \uparrow$, then

$$\begin{aligned} \Pr\left\{y_i(\mathbf{u},\boldsymbol{\xi}) \leq y_i^{\max}\right\} &= \Pr\left\{\xi_S \leq \xi_S^{\max},\ \forall \xi_1,\cdots \xi_{S-1}\right\} \\ &= \int_{-\infty}^{\infty} \cdots \int_{-\infty}^{\xi_S^{\max}} \rho(\xi_1,\cdots,\xi_S)\mathrm{d}\xi_S \cdots \mathrm{d}\xi_1 \end{aligned} \tag{2}$$

where $\rho(\boldsymbol{\xi})$ is the joint distribution function of $\boldsymbol{\xi}$. The input boundary ξ_S^{max} is computed through reverse projection based on the output value of y_i^{max}. The boundaries of the infinite integrals in (2) are chosen as $[-3\sigma,3\sigma]$. In principle, the solution approach can be used to solve problems under uncertainties with any kind of joint correlated multivariate distribution function, provided that the density function is available or it can be approximated. However, the solution of a chance-constrained problem is only able to arrive at a maximum value α^{max} which is dependent on the properties of the uncertain inputs and the restriction of the controls and outputs. To address this issue, a preceding probability maximization step to find out the maximum probability value is set up. For this purpose, the original objective function is substituted and redefined as maximization of the achievable probability. The problem is then solved for the value of α^{max}. In some processes, where the control variable is strictly monotone w.r.t the constrained variable, α^{max} can be obtained through simulation, then α^{max} corresponds to the confidence level with the lower or upper bound of this control variable. This approach can basically be extended to multiple single probabilistic constraints. The application of the approach to a joint chance constrained problem is only related to those cases where an uncertain variable can be found, which is monotone to the joint probability. The approach has been applied to static and large-scale nonlinear dynamic processes. However, this approach can only be employed if the required monotony between constrained output and uncertain input exists.

2.2 *Non-monotonic relationship between constrained output and uncertain input*

There are, in fact, some stochastic optimization problems where no monotone relation between constrained output and any uncertain input variable can be assured. Especially, for those process systems where the decision variables are strongly critical to the question of whether there is a monotony or not. To address this problem, a novel efficient approach is proposed to chance constrained programming for process optimization and control under uncertainty with no warranty for a monotonic relation between constrained output and uncertain input. Thus, chance constrained nonlinear dynamic optimization can now also be realized efficiently even for those cases where the monotony can not be guaranteed.

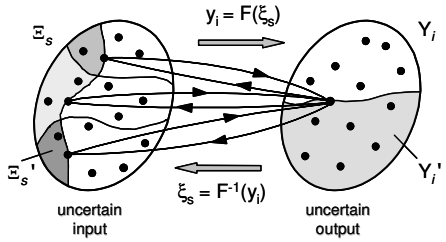

Fig. 2. Mapping feasible regions

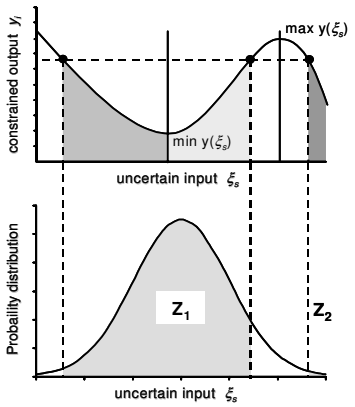

Fig. 3. Non-monotonous sections

The proposed approach uses a two-staged computation framework to decompose the problem. The upper stage is a superior optimizer following the sequential strategy, where the optimization generates the values of the decision variables and supplies those to a lower stage (simulation stage). This stage gives the values of the objective function, the deterministic and probabilistic constraints, as well as the gradients back to the superior optimizer.

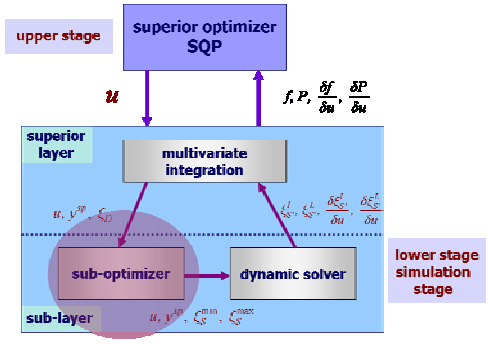

Fig. 4. Chance constrained optimization framework

Furthermore, there is a two-layer structure inside the simulation layer to compute the chance constraints. One is the superior layer, where the probabilities and their gradients are finally calculated by multivariate integration. The structure of the inferior layer is the key to the computation of the chance constraints with non-monotonic relation. The main principal of this section is that at temporarily given values of both the decision and uncertain variables the bounds of the constrained outputs **y** and those for the selected uncertain variables $\boldsymbol{\xi}$ reflecting the feasible area concerning **y** (Fig. 3), are computed for the multivariate integration. For this purpose, all local minima und maxima of the function reflecting **y** are first detected. This computation of the required points of [min **y**($\boldsymbol{\xi}$)] and [max **y**($\boldsymbol{\xi}$)] is achieved by an optimization step in the inferior layer (in case monotony exists, this optimization step can be neglected). However, with the help of those significant points, the entire space of $\boldsymbol{\xi}$ can be divided into sections in which the bounds of the subspaces of feasibility can be computed through a reverse projection by solving the model equations in the following step of this inferior layer. The bounds

of feasibility are supplied to the superior multivariate integration layer, where the necessary probabilities (Eq. 3, 4) and the gradients are computed by adding all those feasible fractions together (Fig. 3).

$$\Pr = \sum \Pr(z_i) \tag{3}$$

$$\Pr(z_i) = \int_{-\infty}^{\infty}\int_{-\infty}^{\infty}\ldots\int_{\xi_s^{\min,i}}^{\xi_s^{\max,i}} \varphi(\xi_i;\mathbf{R})\, d\xi_s\, d\xi_{s-1}\ldots d\xi_1 \tag{4}$$

In this work, a chance constrained programming framework and its applications to process optimization and control under uncertainty are discussed to demonstrate its potential.

3. CHANCE CONSTRAINED OPTIMAL PROCESS OPERATION

In the daily production of chemical industry numerous plant and units are operated to satisfy product requirements. Following the optimal operation planning, predefined steady-state operating points (point A in Fig. 5) for continuous processes are assigned to a process control system. The objective of a feedback control system is then to reject known or unknown disturbances so that the a priori setponits can be pursued. For several processes, however, productivity is optimal close to the inherent limitations or boundary of the equipment capacities. In the neighbourhood of such inherent limitations the process dynamics often exhibit a highly nonlinear behaviour. Furthermore, the constrained variables are often monitored for safety considerations but not close-loop controlled. The disturbances behave randomly and even measured disturbances are stochastic variables since their values can not be predicted for a future time point. Thus, it may be necessary to back off from the nominal optimal value of the constraints which are difficult to measure or to control due to the poor dynamics (Fig. 5). Since multivariate disturbances often exist in a large plant it is difficult to decide a proper value. However, the back off values are usually overestimated and thus leading to a conservative operation. For instance, it is well known that compositions are often non online measurable. Thus, temperatures are selected as reference variables for composition control. However, the specified points of temperature control does not necessarily guarantee the purity specifications (e.g. if the pressure of the plant swings). Consequently, because of the conservative decisions concerning the temperature setpoints (point B in Fig. 5), a much purer product than specified will be achieved which causes much more operating costs than needed.

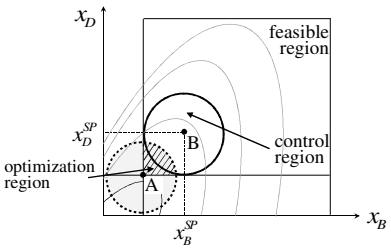

Fig. 5 Operating setpoints by feedback control

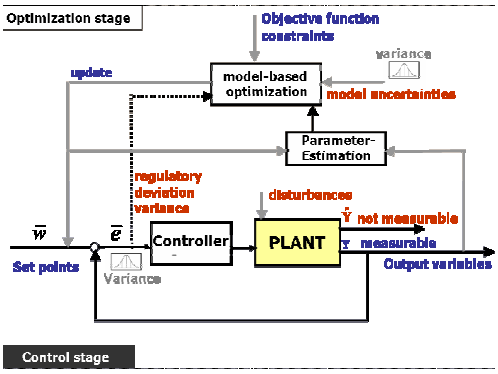

Fig. 6. Open-closed Framework

To overcome these problems, the chance constrained optimization approach is proposed in which the objective function will be improved while satisfying constraints to enforce product quality restrictions with a desired confidence level. This results in a new concept of control: to control open-loop processes by closed-loop control. Unlike the definition where controls are decision variables, in the proposed closed framework the set-points of the measurable outputs are defined as decision variables. Moreover, the controller performance based on the minimum variance control can be regarded as a random input, and thus is also included in the chance constrained formulation of the model-based stochastic optimization problem. The result is a cyclic adjustment of the operating point which guarantees the compliance with the product quality restrictions and assures the controller performance under parametric uncertainty, uncertain boundary conditions, and the random regulatory deviation.

The novel approach is applied to the optimal operation and control of one column embedded in a coupled two-pressure column system for the separation of an azeotropic mixture. The operating point is defined by the distillate and bottom product specifications, cooling outlet temperature limitations, as well as the maximum pressure of the considered high-pressure column. The expected disturbances and implementation errors concern the maximal allowable system pressure, the sensitive tray in the stripping column section as well as the feed flow rate and its composition. However, the values of the setpoints and controls are adjusted so that the target area in Fig. 7 will be tailored to the changing disturbances.

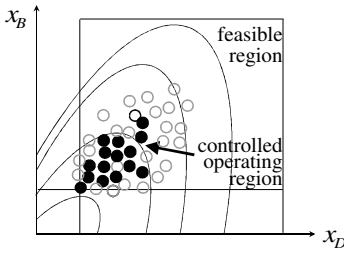

Fig. 7. Operating points of the high-pressure column by the open-closed framework based on the chance constrained approach

In Fig. 7 the black points represent the implemented operating points by feedback control with the open-closed framework. In comparison to the conventional feedback control shown in Fig. 5, the operating points are closer to the nominal point A which leads to a higher profit.

4. CHANCE CONSTRAINED NONLINEAR MODEL PREDICTIVE CONTROL

Since the prediction of future process outputs within an NMPC moving horizon is based on a process model involving the effects of manipulated inputs and disturbances on process outputs, the compliance with constraints on process outputs is more challenging than these on process inputs. Moreover, as the model involves uncertainty, process output predictions are also uncertain. This results in output constraints violation by the close-loop system, even though predicted outputs over the moving horizon might have been properly constrained. Consequently, a method of incorporating uncertainty into the output constraints of the online optimization is needed (Schwarm and Nikolau, 1999; Li et al., 2000).

In most of the previous work, successively updating of the control strategy based on actual measured values has commonly been applied in order to reject disturbances or to compensate for uncertainties. However, since the model mismatch is supposed to be unaltered within the prediction horizon, the control strategy will most likely lead to constraint violations. Another approach in robust MPC represents the assumption that uncertainty is bounded, or equivalently that it is random und uniformly distributed, and then to adopt a worst case contemplation (*min-max* approach) (Lee and Yu, 1997). In this work we propose a chance constrained nonlinear model predictive control. The general chance constrained NMPC problem which is solved at each sampling time k can be formulated as follows:

$$
\begin{aligned}
&\text{Min} \quad J = E\{f\} + \omega D\{f\} \\
&s.t. \\
&\mathbf{x}(k+i+1\,|\,k) = \mathbf{g}_1(\mathbf{x}(k+i\,|\,k), \mathbf{u}(k+i\,|\,k), \xi(k+i)) \\
&\mathbf{y}(k+i\,|\,k) = \mathbf{g}_2(\mathbf{x}(k+i\,|\,k), \mathbf{u}(k+i\,|\,k), \xi(k+i)) \\
&\mathbf{Pr}\{\mathbf{y}_{\min} \le \mathbf{y}(k+i\,|\,k) \le \mathbf{y}_{\max}\} \ge \boldsymbol{\alpha}, i = 1, \ldots, n \\
&\mathbf{u}_{\min} \le \mathbf{u}(k+i\,|\,k) \le \mathbf{u}_{\max}, i = 0, \ldots, m-1. \\
&\Delta\mathbf{u}_{\min} \le \Delta\mathbf{u}(k+i\,|\,k) = \mathbf{u}(k+i\,|\,k) - \mathbf{u}(k+i-1\,|\,k) \le \Delta\mathbf{u}_{\max}
\end{aligned}
$$

The solution of the above problem, however, is only able to arrive at a maximum value $\boldsymbol{\alpha}^{\max}$ which is dependent on the properties of the uncertain inputs and the restriction of the controls. The value of $\boldsymbol{\alpha}^{\max}$ can be computed through a previous probability maximization step. For this purpose, the original objective function is replaced and the following optimization problem will then be solved:

$$
\begin{aligned}
&\max \ \alpha \\
&\text{s.t.} \ \ \mathbf{g}(\dot{\mathbf{x}}, \mathbf{x}, \mathbf{y}, \mathbf{u}, \xi) = 0, \ \mathbf{x}(t_0) = \mathbf{x}_0 \\
&\qquad \Pr\{\, y_j \le y_j^{SP}, \ j = 1, \cdots, m\} \ge \alpha \\
&\qquad \mathbf{u}_{\min} \le \mathbf{u} \le \mathbf{u}_{\max}, \ t_0 \le t \le t_f
\end{aligned}
$$

Moreover, the relationship between the probability levels and the corresponding values of the objective function can be used for a suitable trade-off decision between profitability and robustness. Tuning the value of α is also an issue of the relation between feasibility and profitability. The resulting NMPC scheme is embedded in the on-line optimization framework (Fig. 8).

However, a strongly exothermic series reaction conducted in a non-isothermal batch reactor under safety restrictions is considered to demonstrate the efficiency of the proposed approach. The reaction kinetics are second-order for the first reaction producing B from A, and an undesirable consecutive first-order reaction converting B to C. The intermediate product B is deemed to be the desired product. Since the heat removal is limited, the temperature is controlled by the feed rate of the reactant A and the flow rate of the cooling liquid in the nominal operation. The reactor is equipped with a jacket cooling system. At the start, the reactor partly contains the total available amount of A. The remainder is then fed and its feed flow rate is optimized to maximize the yield. However, the accumulation of A at the start of the batch time must be prevented, otherwise, as the batch proceeds exhaustion of the cooling system capacity can not be avoided. Furthermore, whilst the reaction proceeds, the reactor's volume diminishes so that the computation of the corresponding cooling capacity is adapted according to the remaining cooling jacket area. The developed model considers both the reactor and the cooling jacket energy balance. Thus, the dynamic performance between the cooling medium flow rate as manipulated variable and the controlled reactor temperature is also included in the model equations. Thereby, it can be guaranteed that later the computed temperature trajectory can be implemented by the controller. Moreover, by this means the limitations of the cooling system (pump capacity) can explicitly be taken into account for the optimization.

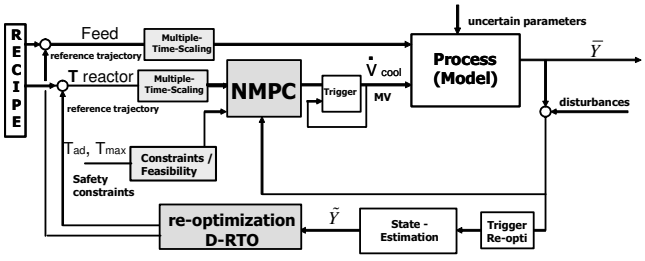

Fig. 8. On-line framework: integration of chance constrained NMPC and dynamic re-optimization.

There are path and end point constraints for the reaction process: first, a limited available amount of A to be converted by the final time is fixed. Furthermore, so as to consider the shut-down operation, the reactor temperature at the final batch time must not exceed a temperature limit. Additionally, there are path constraints for the reactor temperature, and the adiabatic end temperature which is used to determine the temperature after failure.

The decision variable is the cooling flow rate. In order to compare the performances of the open-loop nominal solution and the nominal NMPC with the proposed on-line framework under uncertainty, different disturbances have been considered, namely: catalyst activity mismatch and fluctuations of the reactor jacket cooling fluid temperature. Additionally, all measurements are corrupted with white noise e.g. component amount 8%, Temperature 2%.

While fast disturbances are efficiently rejected by the proposed regulatory NMPC-based approach, there are, on the other hand, in fact, slowly time-varying non-zero mean disturbances or drifting model parameters which change the plant optimum with time. Thus, a re-optimization i.e. dynamic real-time optimization (D-RTO) may be indispensable for an optimal operation (Fig. 8). When on-line measurement gives access to the system state, on-line re-optimization promises considerably improvement. Moreover, additional constraints can be formulated. In this work, we assume that the state information is available.

In order to compensate slow disturbances, the on-line re-optimization problem is automatically activated three times along the batch process time according to a trigger defined as the bounded above difference between the reactor temperature and the temperature reference trajectory. New recipes resulting from this are then updated as input to the on-line framework. Due to the different trigger time-points the current D-RTO problem progressively possesses a reduced number of variables within a shrinking horizon (Nagy and Braatz, 2003). As a result of this, and a catalyst contamination the total batch time increases. But, despite the large plant mismatch and the absence of kinetic knowledge nearly perfect control is accomplished.

5. CONCLUSIONS

The chance constrained optimization framework has been demonstrated to be promising to address optimization and control problems under uncertainties. Feasibility and robustness with respect to input and output constraints have been achieved by the proposed approach. The resulting NMPC scheme embedded in the on-line re-optimization framework is viable for the optimization of the semi-batch reactor recipe while simultaneously guaranteeing the constraints compliance, both for nominal operation as well as for cases of large disturbances e.g. failure situation. In fact, the approach is relevant to all cases when uncertainty can be described by any kind of joint correlated multivariate distribution function. The authors gratefully acknowledge the financial support of the Deutsche Forschungsgemeinschaft (DFG).

REFERENCES

Acevedo, J., and E. N. Pistikopoulos, “Stochastic Optimization Based Algorithms for Process Synthesis under Uncertainty,” *Comp. Chem. Eng.* 22, 647, (1998).

Arellano-Garcia, H., Martini, W., Wendt, M., Li, P., Wozny, G. (2003). Chance constrained batch distillation process optimization under uncertainty, FOCAPO2003, Florida, January 12-15, 2003.

Diwekar, U.M., Kalagnanam, J.R. (1997). Efficient sampling technique for optimization under uncertainty. *AIChE J.* 43, 440.

Kall, P., Wallace, S.W. (1994). Stochastic programming. New York: Wiley.

Lee. J. H., Yu, Z., (1997). Worst case formulations of model predictive control for systems with bounded parameters, *Automatica*, 33, 763-781.

Li, P., Wendt, M., Wozny, G. (2000). Robust model predictive control under chance constraints, *Comput. & Chem. Eng.*, 24, 829.

Li, P., Wendt, M., Arellano-Garcia, H., Wozny, G. (2002a) Optimal operation of distillation processes under uncertain inflows accumulated in a feed tank, *AIChE Journal*, 48, 1198.

Nagy, Z.K., and R.D. Braatz, (2003), *AIChE J.*, 49, 1776-1786.

Pistikopoulos, E. N., and M. G. Ierapetritou, “Novel Approach for Optimal Process Design under Uncertainty”, *Comp. Chem. Eng.*, 19, 1089 (1995).

Prékopa, A. (1995). Stochastic programming. Dordrecht: Kluwer.

Sahinidis, N. V., “Optimization under uncertainty: State-of-the-art and opportunities”, *Computers & Chemical Engineering*, 28(6-7), 971-983 (2004).

Samsatli, J.N., Papageorgiou, L. G., and Nilay Shah. (1998). Robustness Metrics for Dynamic Optimization Models under Parameter Uncertainty”, *AIChE J.*, 44, 1993-2006.

Schwarm, A.T., Nikolaou, M. (1999). Chance-constrained model predictive control, *AIChE J.,* 45, 1743.

Wendt, M., L, P., Wozny, G. (2002). Nonlinear chance constrained process optimization under uncertainty, *Ind. Eng. Chem. Res.*, 41, 3621.

ADCHEM 2006

International Symposium on Advanced Control of Chemical Processes
Gramado, Brazil – April 2-5, 2006

OPTIMAL GRADE TRANSITION IN POLYMERIZATION REACTORS:

A COMPARATIVE CASE STUDY

Nitin Padhiyar, Sharad Bhartiya[1], Ravindra D. Gudi

Department of Chemical Engineering, Indian Institute of Technology,
Bombay, Mumbai-400 076, India

A study of grade transitions as encountered in polymerization reactors is presented. The results underscore the need for global optimization algorithms to fully realize the benefits of grade transition that are necessarily non-convex. For comparison purposes we use a non-gradient, parallel search, stochastic method, namely differential evolution (DE). Our simulations indicate that while the DE solution is highly dependent on the algorithm parameters and mutation strategy, the SQP solution depends on the initial guess value and consistently provides faster convergence. Finally, we also explore the issue of evaluating the optimal grade changeover time. All of the above issues have been demonstrated for the grade transition of polymethyl methacrylate (PMMA) in a non-isothermal CSTR.

Keywords: gradient optimisation; genetic algorithm, nonlinear programming, dynamic programming, off-line programming, process model, time optimal control

1. INTRODUCTION

In the contemporary synthetic polymer-manufacturing environment, flexible operation holds the key towards processing of diverse product orders and maintaining profitable operation in the face of fluctuating market conditions. This has led to a shift from single polymer grade production in large continuous reactors to high quality, low volume, multiple grade manufacturing. Scheduling of various grades in continuous reactors necessitates grade transition, typically characterized by significant perturbations in the process operating conditions. Despite this, the polymer industry routinely performs grade transitions. In fact, as many as 30 to 40 different grades may be produced in a polyolefin plant (Chatzidoukas, et al., 2003). The ultimate incentive for such process upsets lies in transition from one grade to another in a safe and optimal fashion.

Complex kinetics as well as energy effects usually give rise to complex dynamic behavior. Such complex dynamics typically make grade transition a non-convex optimization problem having multiple optima.

Recipes of manipulated variables to achieve optimal grade transition are typically calculated using a dynamic model in conjunction with optimization. The optimization reflects minimization of off-specification material production, which is an essential ingredient of any profitability analysis. In literature, the dynamic optimization problem is converted to a standard NonLinear Program (NLP) using Control Vector Parameterisation (CVP) and then solved using various gradient-based methods, for which efficient solvers exist. (McAuley and MacGregor, 1992; Takeda and Ray, 1999; Seki, *et al.,* 2001). In each of these works, the resulting nonlinear program was solved using CVP followed by a nonlinear, gradient-based optimization method such as Sequential Quadratic Programming (SQP). Moreover, the gradients of objective function were computed using finite difference. Wang et al (2000) used sensitivity of the ODEs to determine gradient information.

It is likely that the nonlinear behavior, which is further accentuated during grade transition often leads to a non-convex optimization problems characterized by multiple optima. Conventional gradient-based nonlinear optimization methods such as SQP may at best lead to only a local optimum. In

[1] Correspondence should be addressed to Sharad Bhartiya at bhartiya@che.iitb.ac.in

such a case, the benefits of grade transition may not be fully realized. It is therefore important to analyze the structure of the nonlinear program encountered in grade transition control and quantify the impact of the optimization technique on the quality of the solution. To study this aspect, we compare the SQP optimization technique with a stochastic, direct parallel search method, namely Differential Evolution (DE), which is widely recognized for its ability to provide global solutions to optimization problems.

In this work, we use a model representing the non-isothermal polymerisation system for production of polymethyl methacrylate (PMMA). The model has been presented in Section 2. Our results in Section 3 present two case studies. Case Study I investigates presence of multiple optima in the PMMA grade transition problem. Using a fixed grade changeover time, we find that the gradient-based methods such as SQP are likely to yield only a locally optimal solution, whereas the DE method typically provides a superior optimal solution in terms of the objective function value. In Case Study II, we explore the benefits of optimal grade changeover time relative to fixed transition times used in Case Study I. Finally, the work is concluded in Section 4.

2. GRADE TRANSITION IN PMMA PRODUCTION

As a case study, we choose grade transitions encountered in a nonisothermal free-radical polymerization of methyl methacrylate (MMA) using azobisisobutyronitrile (AIBN) as initiator and toluene as solvent (Daoutidis *et al.*, 1990). The same non-isothermal version of this model has been adapted as a test bed in our study. The model equations consist of molar balances for the monomer and initiator, reactor temperature, jacket temperature, and the zeroth and first moment of dead chains and have been reproduced below,

$$\frac{dC_m}{dt} = -\left[Z_p \exp\left(\frac{-E_p}{RT}\right) + Z_{fm} \exp\left(\frac{-E_{fm}}{RT}\right)\right] C_m P_0(C_I, T) + \frac{F(C_{m_{in}} - C_m)}{V} \quad (1a)$$

$$\frac{dC_I}{dt} = -Z_I \exp\left(\frac{-E_I}{RT}\right) C_I + \frac{(F_I C_{I_{in}} - F C_I)}{V} \quad (1b)$$

$$\frac{dT}{dt} = Z_p \exp\left(\frac{-E_p}{RT}\right) Cm \frac{\left(-\Delta H_P\right)}{\rho c_p} P_0(C_I, T) - \frac{UA}{\rho C_p V}\left(T - T_j\right) + \frac{F}{V}\left(T_{in} - T\right) \quad (1c)$$

$$\frac{dD_0}{dt} = \left\{0.5 Z_{T_c} \exp\left(\frac{-E_{T_c}}{RT}\right) + Z_{T_d} \exp\left(\frac{-E_{T_d}}{RT}\right)\right\}\left[P_0(C_I, T)\right]^2 + Z_{f_m} \exp\left(\frac{-E_{f_m}}{RT}\right) C_m P_0(C_I, T) - \frac{FD_0}{V} \quad (1d)$$

$$\frac{dD_1}{dt} = M_m\left[(Z_p \exp\left(\frac{-E_p}{RT}\right) + (Z_{f_m} \exp\left(\frac{-E_{f_m}}{RT}\right)\right] C_m P_0(C_I, T) - \frac{FD_1}{V} \quad (1e)$$

$$\frac{dT_j}{dt} = \frac{F_{cw}}{V_o}\left(T_{w_o} - T_j\right) + \frac{UA}{\rho_w C_w V_o}\left(T - T_j\right) \quad (1f)$$

$$MW(t) = \frac{D_1(t)}{D_0(t)} \quad (1h)$$

where

$$P_0(C_I, T) = \left[\frac{2 f^* C_I Z_I \exp\left(\frac{-E_I}{RT}\right)}{Z_{T_d} \exp\left(\frac{-E_{T_d}}{RT}\right) + Z_{T_c} \exp\left(\frac{-E_{T_c}}{RT}\right)}\right]^{0.5} \quad (1g)$$

where C_m and C_I represent the molar concentrations of monomer and initiator, respectively. D_0, and D_1 represent the zeroth and first moments of the molecular weight distribution of the dead chains, respectively, and T, and T_j represent reactor and jacket temperatures, respectively. The process parameters values have been taken from Daoutidis *et al.* (1990). We consider a single grade change in the number average molecular weight MW_n of PMMA from 25,000 to 35,000 by manipulating initiator (F_I) and coolant (F_{cw}) flow rates. The steady-state operating conditions for the two grades were evaluated using the model in Equation 1 and are listed in Table 1. The SQP algorithm was implemented using the *fmincon* function in MATLAB's optimization toolbox, whereas the DE algorithm was coded in MATLAB.

Table 1. Steady state operating conditions for the initial and final grades

Grade indices	Initial Grade	Final Grade
Molecular weight	25000	35000
$\mathbf{F_{cw}}$, $\boldsymbol{m^3/hr}$	3.2636	9.2944×10^{-1}
F_I, m^3/hr	1.6883×10^{-2}	6.596×10^{-3}

3. RESULTS AND DISCUSSIONS

3.1. CASE I. Grade transition in PMMA shows multiple optima

We consider a grade transition in PMMA product from a grade characterized by molecular weight of 25,000 to a new grade with molecular weight of 35,000. The quantity of off-specification material produced and the grade changeover time may be represented by the following objective function,

$$J_1 = \int_{t_0}^{t_f} \left\| MW(t) - MW_{sp} \right\|_P^2 \, dt \quad (2a)$$

where $\left\| \cdot \right\|_P$ denotes the deviations form the target,

MW_{sp}, suitably weightedby P. Minimizing the objective function (Equation 2a) along with the process model (Equation 1) and following constraints (Equations 2b-2f) represent the optimization problem

$$MW_{\min} \le \max\left(MW(t)\right) \le MW_{\max} \quad (2b)$$

$$F_{cw,\,\min} \le F_{cw}(t) \le F_{cw,\,\max} \quad (2c)$$

$$F_{I,\min} \le F_I(t) \le F_{I,\max} \quad (2d)$$

$$\Delta t_{\min} \le \Delta t_{ij} \le \Delta t_{\max}\ ,\ \ i = 1,2\ ;\ \ j = 1,2,...,na \quad (2e)$$

$$\sum_{j=1}^{na} \Delta t_{ij} = t_f \quad (2f)$$

where Δt_{ij} represents the j^{th} switching interval of the i^{th} manipulated variable and na represents the number of times that the coolant flow rate (i=1) and the initiator flow rate (i=2) are switched during the transition horizon. The objective function penalizes squared deviations from the molecular weight of the new grade over the transition horizon, $t_f - t_o$. Equation 2b represents output constraints, i.e. the transients on the molecular weight, whereas Equations 2c,d represent constraints on the inputs. Equation 2e ensures that the switching interval is of an adequate size. Since in this case study, the grade changeover time is known a priori, we used the equality constraint Equation 2f to reduce one degree of freedom.

Equation 2 may be solved with a standard NLP solver through use of CVP, where manipulated variables are parameterised and approximated by a series of trial functions γ. Thus, for the i^{th} manipulated variable,

$$u_i(t) = \sum_{j=1}^{na} a_{ij}\gamma_{ij}(t - t_{ij}) \quad (3)$$

where t_{ij} is the j^{th} switching time of the i^{th} manipulated variable, na as explained above is the number of switching intervals, and a_{ij} represents the amplitude of the i^{th} manipulated variable at the switching time t_{ij}. We make use of a ramp trial function as shown in Fig. 1 since a ramp can approximate the optimal profile more closely relative to a zero order trial function. Gradient-based SQP further requires the gradient of the objective function and constraints. In this work we used sensitivity of the ODEs to evaluate the gradient of the objective function as follows (Leis and Kramer, 1988),

$$\dot{\mathbf{S}} = \frac{\partial \mathbf{f}}{\partial \mathbf{x}}\mathbf{S} + \frac{\partial \mathbf{f}}{\partial \mathbf{p}} \quad (4a)$$

where the (i,j) component of the sensitivity matrix is defined as follow,

$$S_{ij} = \frac{\partial x_i}{\partial p_j}\ \ ,\ \ S_{ij}(0) = 0\ \ ;i = 1,...,n; j = 1,2,...,m \quad (4b)$$

Where n and m represent the number of states, **x,** and the decision variables, **p**, respectively.

In the current section, the transition horizon is fixed at 4 hours. The constraint in Equation 2f ensures that the sum of the switching intervals equals the transition horizon. The constraint values are summarized in Table 2. All simulations presented in the current Case study use three optimized switching intervals. Thus the decision variables include two amplitude and two switching times for each manipulated variable, the coolant flowrate and initiator, thereby making a total of eight variables.

Table 2. Bound constraints for variables associated with the NLP of Equation 7.

	Minimum	Maximum
MW	24,800	35,200
Fcw, m^3/h	0.3	6
F_I, m^3/h	0.0007	0.1
Δt, h	0.016667	3.96
t_f, h	0.0501	4

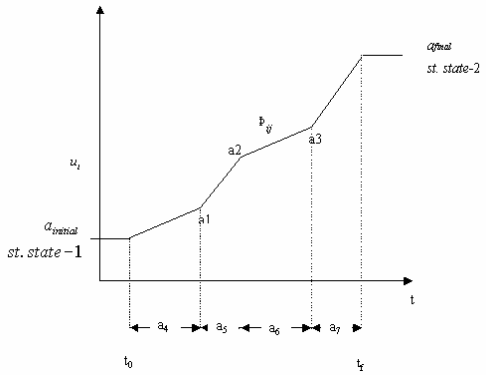

Fig. 1. Ramp trial function for parameterization of the manipulated variables

It is well known that gradient-based optimization methods such as SQP fail to provide the global optimum if the optimization problem has multiple optima. Dependence of the optimal solution on the choice of the initial guess value in a gradient-based algorithm such as SQP constitutes an empirical verification of the presence of multiple optima. Table 3 documents the values of the objective function J_1 for 10 different optimization runs using SQP each with a distinct initial guess of the decision variables. Simulation No. 5, 6, 7, and 8 yielded solutions that represent identical points in the decision space. The remaining simulations resulted in distinct solutions. Thus, the results indicate the presence of several optima. The tolerances used by the integrator and the optimizer in obtaining these solutions have been reported in Table 4. We have verified by varying the tolerance values that the difference between any two different optima is not due to a particular tolerance value used by the SQP solver. We also observed that use of perturbation methods to evaluate the gradient adversely affected the quality of the optimal solution in each of the 10 cases. For example, in simulation No. 10 in Table 3, use of finite difference to calculate gradients resulted in a minimum objective function value of 2.2533 x 10^7 as opposed to 1.1457 x 10^7 obtained when using sensitivity information (see Equation 4). Furthermore, solutions based on finite differences for

calculation of gradients were strongly dependent on the particular set of tolerance values used by the optimizer. The number of function evaluations required during optimization for each of the 10 simulations is also reported in Table 3. It has been widely claimed that the DE algorithm is a promising candidate for obtaining the global optimum in such cases. However, the quality of the solution and the computational expense is determined by the choice of its parameters such as the population size, the maximum number of generations as well as the mutation and crossover factors. To compare the relative performances of DE and SQP for grade transition from a steady molecular weight of 25,000 to 35,000, 10 optimization runs were performed using DE and the results documented in Table 3. In case of all DE based solutions, we utilized a population size of 40 members and the maximum number of generations was set to 200. Eight out of the 10 runs using DE were distinct from each other based on the choice of the members of the initial population. The mutation and crossover factors were decided by trial and error and were selected as 0.5 and 0.75, respectively. However, a subsequent study of the sensitivity of the optimal solutions using DE to the algorithm parameters shows that the value of 0.75 for both the factors is optimal. As noted from Table 3 we arrived at several DE solutions at the end of 200 generations. As can be seen from Table 3, the best solution using either DE or SQP corresponds to an objective function value of 1.0698 x 10^7. The subsequent six best solutions (simulation No. 2-7) obtained using the DE algorithm were very close to this best solution. The top seven SQP solutions showed a larger spread from this best solution. However, the last three simulation results using DE were worse than the worst SQP solution. This is due to the following mutation strategy used in this work

$$\hat{\mathbf{u}}_i^{g+1} = \mathbf{w}_b^g + F_m(\mathbf{w}_{r_1}^g - \mathbf{w}_{r_2}^g), \qquad i = 1,...N_p \qquad (5)$$

Since the mutated members represented perturbations around the best member of a given generation (based on elitism), it is likely that the members of the new generation were trapped in the vicinity of a local minimum. To verify this notion, we used a different mutation strategy for simulation No 10 as follows,

$$\hat{\mathbf{u}}_i^{g+1} = \mathbf{w}_{r_3}^g + F_m(\mathbf{w}_{r_1}^g - \mathbf{w}_{r_2}^g), \qquad i = 1,...N_p \qquad (6)$$

Since vectors $\mathbf{w}_{r_i}^g$ represent randomly selected and distinct members of generation *g*, the mutated members using this strategy enhance the diversity of the new generation relative to the mutation strategy used in Equation 5 where the mutated members represented perturbations around the best member of generation *g*. This mutation strategy was found to give substantial improvement to the solution when used alone; however when further accompanied with an increase in the number of generations from 200 to 300, the results for simulation No. 10 yielded a minimum objective function value of 1.10253 x 10^7.

We have used the number of objective function evaluations needed by the two methods as a measure of the computational expense. Although the best individual solutions yielded by SQP and DE have identical objective function values of J_1^*=1.0698 x 10^7 and represent an identical point in the decision space, the SQP algorithm is more computationally efficient by an average factor of 4.9. The number of function evaluations needed to obtain the best individual solution of SQP and DE were 1669 and 6331, respectively. All the 10 distinct solutions resulting from the different initial conditions used in SQP satisfy the KKT conditions for optimality and therefore confirm that grade transition in PMMA production exhibit multiple local optimal solutions. Figs. 2 and 3 show the transition profile of the molecular weight and the manipulated variables, respectively, using the best DE (solid line) and the best SQP (dash-dotted line) solutions. Since the two strategies yielded identical solutions, the lines are indistinguishable. We note that although we used a fixed changeover time of four hours, the integration necessary in computation of the objective function in Equation 9a is performed over six hours. The extra two hours enables penalizing deviation of the steady state output from the new grade properties. This feature of integration has been maintained in all subsequent results. The molecular weight profiles obtained using the best DE and best SQP solutions show identical rise times of 0.28 hr, and settle to within ± 100 Kg/Kmol limit of the steady state value in 1.37 hr. Fig. 2 also shows that the transition profile achieved by changing the two flow rates to their respective new grade steady state values in a step-like manner does not provide the optimal transition trajectory (see dotted line). Fig. 3 shows that the input recipes generated by the two methods make aggressive moves at the start of transition. However the lower bound on the size of switching intervals ensures that at least one minute elapses between two successive moves (see Table 2 for constraints values).

3.2. Grade changeover time as a decision variable

All simulations presented until now optimized switching time intervals but used a fixed time horizon of 4 hr. However, it is interesting to note that the defacto changeover times were less than the time horizon of 4 hr. For example, the best DE solution in Case Study I shows that the grade transition was accomplished in only 1.37 hr. (see Fig 2). One could also explicitly optimize the transition horizon by relaxing the equality constraint equation 2f and

Table 3. Summary of the objective function values and CPU times needed to perform 10 simulation runs for each of the two algorithms, namely SQP and DE

Sim No	SQP: Gradients using sensitivity equations		DE: Gradient free	
	J^* x 10^{-7}	No of function evaluations	J^* x 10^{-7},	No of function evaluat-ions
1	1.0698	1669	1.0698	6331
2	1.0818	1615	1.0708	6841
3	1.0991	1432	1.0945	7066
4	1.1011	2028	1.1016	6040
5	1.1313	586	1.1031	5804
6	1.1313	816	1.1045	6895
7	1.1313	881	1.1045	7109
8	1.1313	1303	1.1917	7597
9	1.1347	2056	1.2268	7373
10	1.1457	1437	1.2268	7373

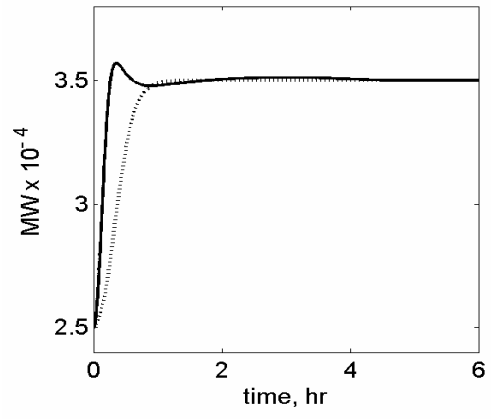

Fig. 2. CASE I: Optimal transition trajectory of molecular weight of PMMA, using DE (solid line) and SQP (dash dotted line) algorithms for solution of Equation 2. The dotted line represents the transition if the manipulated inputs corresponding to the new grade were implemented in a single step (non-optimal).A fixed time horizon of 4 hr is assumed. P = 1.

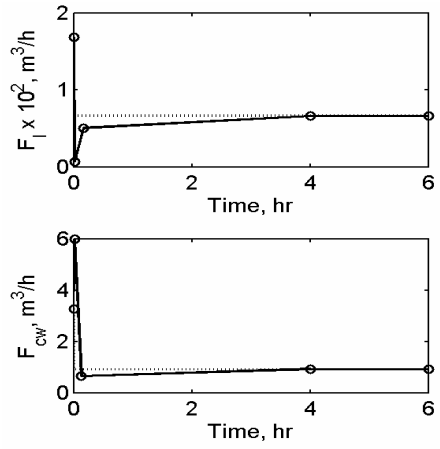

Fig. 3. CASE I. Optimal transition trajectory of manipulated inputs, namely initiator and coolant flow rate, using DE (solid line) and SQP (dash dotted line) algorithms.

adding t_f as an extra degree of freedom. The current case is similar to Case Study I in all respects except that in Equation 2f t_f is considered as a decision variable. Thus, we treat the *na*-1 switching intervals and t_f as the time related decision variables. As with the Case Study I, ten optimization runs starting with different initial guesses for SQP and 10 different initial populations for DE were performed. Figs. 4 and 5 show the molecular weight transition and the manipulated variable profiles, respectively, and represent the best of the ten runs for DE (solid line) and SQP (dashed line). The optimum transition horizons, t_f are 0.37 hr and 0.28 hr for DE and SQP, respectively. Although the grade changeover time is marginally higher when using DE, the rise time is same (0.23 hr). The settling times using the two methods are almost same (0.71 hr). The DE and SQP methods converge to the respective objective function values as J_1^*= 1.0189 x 10^7 and J_1^*=1.0419x 10^7. The lower values of objective functions obtained here relative to Case Study I (J_1^*=1.0698 x 10^7 for DE and SQP), indicate improved performance with both DE and SQP when the transition horizon is also optimized. Another unobvious advantage of optimization of transition horizon is observed upon comparing the manipulated variable profiles of Case Study I (Fig. 3) and the current case (Fig. 5). Optimizing the transition horizon results in achieving the new steady state for the manipulated variables faster (t_f =0.37 hr for DE and 0.28 hr for SQP) than for the case when the transition horizon is assumed fixed at 4 hr. This behavior would translate into benefits for grade transition and reduced transient operation and therefore tighter control on the product quality. Convergence of the SQP solution to a higher objective function value relative to DE demonstrates susceptibility of SQP to local minima, as also observed in Case Study I. In the current case study, both the standard deviation and average value of objective function for DE (J_{std}=2.44 x 10^5, J_{avg} =1.0446 x 10^7) were found to be lower than those for SQP (J_{std} = 8.8073 x 10^5, J_{avg} =1.13399 x 10^7). It is interesting to note that relaxation of the constraint of Equation 2f resulted in fewer number of function evaluations needed by SQP in the current Case Study relative to Case Study I. The average number of function evaluations was 569 as opposed to 1382 in Case Study I.

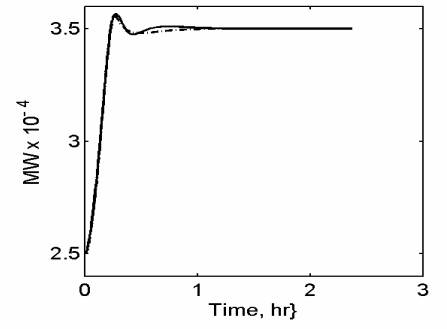

Fig. 4. CASE II. Optimal transition trajectory of molecular weight of PMMA, with DE (solid line) and SQP (dash dotted line) algorithms which optimized the transition times in addition

to the manipulated inputs and switching intervals. P = 1.

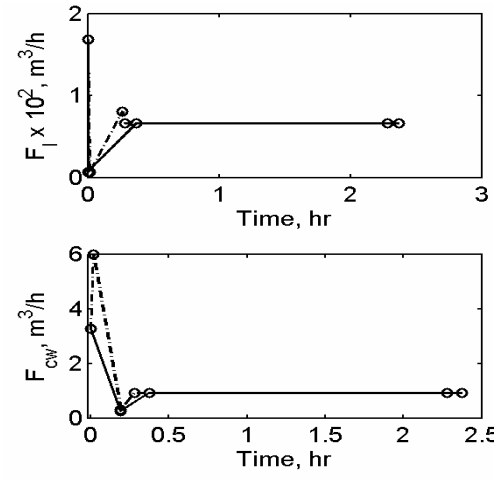

Fig. 5. CASE II. Optimal transition trajectory of manipulated inputs namely initiator and coolant flow rates, with DE (solid line) and SQP (dash dotted line) algorithms.

4. CONCLUSIONS

Optimal grade transition has emerged as a key strategy in the polymer industry, notably in gas-phase polymerization of olefins, to enable flexible operation. Our studies reveal that grade transition encountered during PMMA production results in a non-convex optimization problem having multiple optima. Thus, widely used solvers such as SQP may provide an inferior transition policy. Although DE has attributes consistent with global optimization, the DE solution is highly dependent on the mutation strategy as well as its parameters. Also, we demonstrate that explicit optimization of transition time yields solutions where the transition policies quickly converge to the new grade steady state values in addition to reducing the transition horizon.

Table 4: Tolerances used by the ODE solver (*ode15s* of MATLAB® 6.5) and the optimizer (*fmincon* in MATLAB® 6.5) in obtaining the SQP based solutions reported in Table 3.

Integration Tolerances	Absolute error	1×10^{-6}
	Relative error	1×10^{-10}
Termination Tolerances Used by Optimizer	Decision Variable	1×10^{-10}
	Constraint violation	1×10^{-9}
	Objective Function	1×10^{-8}

ACKNOWLEDGEMENTS

The authors acknowledge funding from the Department of Science and Technology, India, for financial assistance under SERC (Engg. Sciences) (#03DS015).

REFERENCES

Chatzidoukas C, Perkins JD, Pistikopoulos EN, Kiparissides C. Optimal grade transition and selection of closed-loop controllers in a gas-phase olefin polymerization fluidized bed reactor. Chemical Engineering Science. 2003;58:3643-3658.

McAuley KB, MacGregor JF. Optimal grade transition in a gas phase polyethylene reactor. AIChE J. 1992;38:1564-1576.

Takeda M, Ray WH. Optimal grade transition strategies for multistage polyolefin reactors. AIChE Journal. 1999;45:1776-1793.

Seki H, Ogawa M, Ooyama S, Akamatsu K, Ohshima M, Wang Y. Industrial application of a nonlinear model predictive control to polymerization reactors. Control Engineering Practice. 2001;8:819-828.

Wang Y, Seki H, Ohyama S, Akamatsu K, Ogawa M, Ohshima M. Optimal grade transition control for polymerization reactors. Computers and Chemical Engineering. 2000;24:1555-1561.

Daoutidis P, Soroush M, Kravaris C. Feedforward/Feedback Control of Multivariable Nonlinear Processes. AIChE Journal, 1990; 36:1471–1484.

Leis JR, Kramer MA. The simultaneous solution and sensitivity analysis of systems described by ordinary differntial equations. ACM Transactions on mathematical Software. 1988; **14**: 45-60.

Session 3.1

Batch Processes

ADCHEM 2006

International Symposium on Advanced Control of Chemical Processes
Gramado, Brazil – April 2-5, 2006

BATCH/SEMI-BATCH PROCESS FAULT DETECTION AND DIAGNOSIS USING ORTHOGONAL NONLINEAR MULTI-WAY PCA: Application to an emulsion co-polymerization process

A. Maulud[1] and J. Romagnoli[2]

[1]Depart. of Chemical Engineering, University of Sydney, NSW 2006, Australia
[2]Depart. of Chemical Engineering, Louisiana State University, Baton Rouge, LA 70803, USA

Abstract: In this paper, a fault detection and diagnosis for batch/semi-batch processes by utilizing the PCA scores subspace is proposed. To develop the diagnosis model, first the multi-way unfolding is utilised to transform 3-dimensional batches data onto 2-dimensional data. The process of extracting linear and nonlinear correlations from process data is performed by sequentially applying a linear PCA and an orthogonal nonlinear PCA. As a result the nonlinear structures become more apparent. In addition, the sequential approach reduces the complexity of nonlinear PCA development and compact the information to a very low dimension. The trajectory-boundary-limit crossing point discriminant analysis is proposed to diagnose the fault at the instance of being detected and to improve the diagnostic performance. The validity of the proposed strategy is demonstrated by application to the emulsion copolymerization of styrene/MMA semi-batch process.

Keywords: Fault detection and diagnosis, nonlinear systems, batch processes.

1. INTRODUCTION

Principal component analysis (PCA) has been recognized as important approach in multivariate statistical process monitoring. Its extension called a multi-way PCA (MPCA) has been successfully applied to monitor the batch/semi-batch processes (Nomikos and MacGregor 1994). MPCA allows detecting any deviation in current batch run by comparing to the reference model that has been developed from successful past batch runs. Although the approach is considerably simple, but it is powerful enough as many of its application in industrial batch monitoring had been reported (Kosanovich, Dahl et al. 1996; Lennox, Montague et al. 2001).

Batch/semi-batch processes are highly nonlinear in characteristic. The nonlinearity reduces the efficiency of the data compression which results more principal components are required to explain a certain percentage of the variance. This becomes a major disadvantage for a low-dimension process monitoring. For example, a single bi-variate plot of the first few principal components may not adequate to detect the fault. Despite multi-way unfolding is capable to remove major portion of nonlinearity among batch variables by subtracting the average trajectory from each variable (Nomikos and MacGregor 1994), some nonlinearity remains a problem (Dong and McAvoy 1996). In view this situation, incorporation of nonlinear PCA (NLPCA) into multi-way approach have been proposed (Dong and McAvoy 1996; Lee, Yoo et al. 2004). In the approaches, the nonlinear PCA is directly applied on unfolded data. This strategy requires extensive optimisation computation as the data is unfolded in multi-way approach, it results a very huge input dimension. Especially in neural network based model, if the ratio between the numbers of batches to variables (input dimension) is very low, to construct an optimal neural network model will be very difficult and cumbersome.

Despite significant advantages of PCA in detecting the faults, most of the application of scores plane for fault identification and diagnosis have been confined to continuous processes (Kresta, MacGregor et al. 1991; Raich and Cinar 1997; Dunia and Qin 1998). For a batch process, in early work, the identification and diagnosis are limited to the utilization of the contribution plots (Kourti, Nomikos et al. 1995). Although the contribution plot can be used to identify

which variable that contributes most to the out-of-control conditions, the actual cause is not directly diagnosed. Thus, the problem remains incompletely solved, in turns requires plant personnel to interrogate the variable further to diagnose the actual cause. In a typical continuous process, under a process upset, the scores are shifted to a new steady state which forming a new cluster. The classification of each fault cluster strongly relies on the assumption that the data is adequately represented by a normal distribution. However, as the batch/semi-batch process is continuously monitored, under a process upset, the scores do not form a new cluster instead they follow a certain trajectory. In this case, the normality assumption of the data distribution is clearly violated.

In this paper a fault detection and diagnosis for batch/semi-batch process based on the orthogonal nonlinear multi-way PCA is proposed. Rather than applying a nonlinear PCA directly onto unfolded data, a sequential application of a linear PCA and a nonlinear PCA is performed. The nonlinear PCA is applied only on selected principal components of the linear PCA. The main reason is since most of the nonlinearity has been removed, it is better to capture the remaining nonlinearity in more efficient manner. An improved nonlinear PCA called orthogonal nonlinear PCA is employed to improve the explained variance in the first few nonlinear principal components. For the fault diagnosis, a discriminant analysis based on the transient region is employed rather than out-of-boundary region. A single crossing point between the scores trajectory and boundary limit is used to classify the fault. It is expected that the proposed strategy is not only be able to maintain the diagnostic performance, but the foremost advantage is it provides a very fast diagnosis in view to a finite nature of the batch/semi-batch process.

The remaining of this paper is organized as follows. In the next section a brief overview on PCA and multi-way PCA is provided, followed by orthogonal NLPCA. Then, a complete framework for an orthogonal nonlinear multi-way PCA fault detection strategy is introduced. Finally, a discrimination analysis for fault diagnosis by using fault trajectory in the scores space is presented. An example is given to illustrate the performance of the proposed framework before concluding.

2. PRINCIPAL COMPONENTS ANALYSIS

2.1 Linear PCA.

Let X be a data matrix with n number of observations and m number of dimensions. The X matrix can be decomposed into two matrices as follows:

$$X = TP^T = \sum_{i=1}^{m} t_i p_i^T \qquad (1)$$

where T is called scores matrix and P is called loadings matrix. If the variables in X are collinear, the first f principal components can sufficiently explain the variability in data X. Thus, the data X can be written as follow in term of residual, E,

$$X = T_f P_f^T + E = \sum_{i=1}^{f} t_i p_i^T + E \qquad (2)$$

2.2 Multi-way PCA.

In typical batch processes, the process data is in the form of three-way matrix ($X(I\text{x}J\text{x}K)$). For a typical batch run, $j = 1, 2, \ldots, J$ variables are measured at $k = 1, 2, \ldots, K$ time intervals throughout the batch. There exists similar data on a number of batch run, $i = 1, 2, \ldots, I$. In MPCA strategy, this matrix must be unfolded into a two-way matrix before PCA can be performed. There are several possible ways to unfold the matrix. In this case, the matrix is unfolded onto matrix $X(I\text{x}JK)$ as shown in figure 1. This allows us to obtain some variability analysis among the batches. In batch processes, some variables follow certain trajectories rather than maintain around specific steady state conditions. Thus, the mean trajectory of each variable can be removed by subtracting the mean of each column of the unfolded matrix. This will remove major portion of nonlinearity among batch variables. PCA then can be performed in conventional way once the unfold matrix has been auto-scaled.

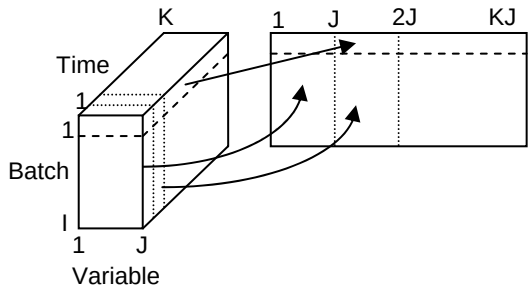

Fig. 1: Multi-way unfolding

One important performance of process monitoring is to detect the un-conformance condition as soon as possible by having on-line monitoring. However, the above unfolded matrix is not completed until the end of the batch. To handle the future missing data problem, a few suggestions have been proposed either by filling with zeros or using the current values, or using PCA projection (Nomikos and MacGregor 1995).

2.3 Nonlinear PCA.

For linearly correlated process data, linear PCA as mentioned above performs well to reduce the dimension of process data. For nonlinearly correlated process data Kramer has proposed a nonlinear PCA based on autoassociative neural network (Kramer 1991). The autoassociative neural network employs a feedforward structure with the bottleneck layer to represent the nonlinear principal components as shown in Figure 2. The overall structure consists of three hidden layers excluding input and output layers. A training procedure is conducted to perform identity

mapping by reproducing the network input at the output layer. The trained network is split into two networks, mapping network which consists of input, 1st hidden and bottleneck (2nd hidden) layers, and de-mapping network which consists of 3rd hidden and output layers. NLPCA will be represented by the output of the mapping network. If the network training is properly conducted and the reasonable approximation has been achieved, the data input features must be well represented by the bottleneck layer.

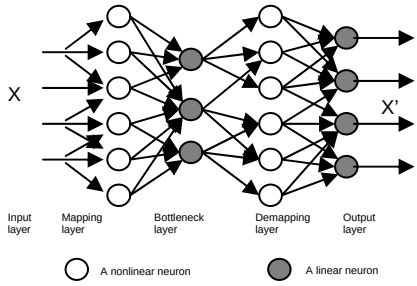

Fig. 2: Autoassociative NN Nonlinear PCA

2.4 Orthogonal Nonlinear PCA.

The NLPCA mentioned above shows one of the characteristics of linear PCA that it is capable of projecting the data to a lower dimension. Another important characteristic of linear PCA is that the first principal component always captures the highest variance of the input data followed by the second and so on. In NLPCA, the data information tends to be evenly distributed among the principal components (Chessari, Barton et al. 1995). In view of this drawback, a training algorithm using Gram-Schmidt process for NLPCA has been proposed in which the nonlinear scores produced are orthogonal at the end of training session(Chessari, Barton et al. 1995).

Although the Gram Schmidt scheme conceptually can provide some meaningful remedies for the orthogonality, in practice it suffers a constraint of trade-off between the main objective (overall convergence) and the secondary objective (orthogonal principal components). In the worst scenario, the orthogonal property may be severely affected as the main objective cannot be scarified at all. Otherwise, the network is not able to represent the data adequately. In view of orthogonal requirement and the drawbacks associated with the Gram-Schmidt approach, an alternative approach to orthogonal nonlinear principal component analysis is proposed. This approach utilizes the Hammerstein type model concept by incorporating a linear PCA model into the NLPCA strategy. In the proposed model formulation, the nonlinear and linear parts are separated into two blocks as shown in Figure 3.

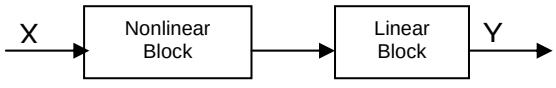

Fig. 3: Conceptual model architecture

In NLPCA, the bottleneck layer neurons are considered to be the principal components loadings, but they do not posses the orthogonal property. In order to build the orthogonal property on the model, a linear PCA module is incorporated as shown in Figure 4. In this case, the mapping network of NLPCA is the nonlinear block while the linear PCA is the linear block.

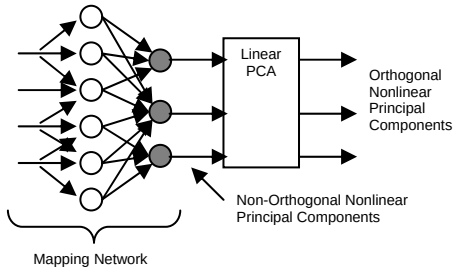

Fig. 4: Orthogonal Nonlinear PCA

In this proposal, the bottleneck layer nodes are called non-orthogonal nonlinear principal components and their outputs are called non-orthogonal scores. When linear PCA is applied on non-orthogonal score, it will produce orthogonal nonlinear principal components and orthogonal scores respectively. For the bottleneck layer in NLPCA, either a linear or nonlinear function can be used (Kramer 1991).

Let T be the non-orthogonal nonlinear scores matrix generated at the output of bottleneck layer. Thus, the non-orthogonal matrix T can be transformed into an orthogonal matrix U by

$$T = UP^T \tag{3}$$

where P is the eigenvector matrix.

An additional advantage of this approach compared to conventional NLPCA is that the specified number of bottleneck layer neurons can be relaxed as long as the number is reasonably selected. In a conventional NLPCA, it is necessary to optimize the number of neurons in bottleneck layer to the optimal minimum value.

3. FAULT DETECTION

In our proposed strategy, the monitoring is performed by sequentially performing the linear PCA followed by the nonlinear PCA. Only the first few linear principal components are utilised to develop the nonlinear PCA. The orthogonal nonlinear PCA is utilised to improve the distinct characteristics among the nonlinear principal components. The strategy is depicted in Figure 5.

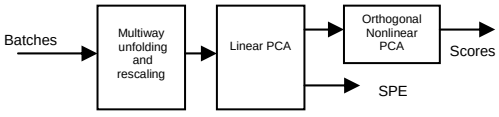

Fig. 5: Nonlinear Multi-way PCA Strategy

Using all retained principal components to develop nonlinear PCA model will not add any additional improvement. In spite it may over-shadow the remaining nonlinearity characteristics. There is no definite criterion on how few the number of principal components to be chosen. In this study, firstly we apply Jollife's approach (0.7 of average eigenvalues) to decide how many principal components to be retained for scores and squared prediction error (SPE) analysis (Jolliffe 1986). This is simply to screen unnecessary principal components since total principal components number is very large (equal to input dimension). Based on the retained principal components, the number of PC that explain 50~70% of data variability will be used to develop the nonlinear PCA model. Alternatively, a cross-validation approach can be used to decide the number of principal components used for nonlinear PCA modelling. With this approach, a ratio between the numbers of batches to variables (input dimension) will be tremendously improved for nonlinear PCA model development. For a SPE analysis (Q-Statistics) a similar approach and procedure in conventional MPCA approach is utilised. However, the significance of applying nonlinear PCA on the selected PC depends on the data variability distribution. If 50% explained variance constitutes a very small PC number, it clearly indicates that the nonlinearity is very minimal and the nonlinear PCA should not be applied.

Once appropriate model has been developed, the fault can be detected by testing the future data based on the Hotelling's T^2 statistics. Assuming that the multivariate normal distribution adequately represents the scores distribution, the confidence limits for T^2 can be calculated using *F*-distribution (Tracy, Young et al. 1992). For a SPE analysis (*Q*-Statistics) a similar approach and procedure in conventional MPCA approach is utilised. The critical value for *Q*-Statistic can be calculated by approximating the distribution as the quadratic form of a normal distribution (Jackson and Mudholkar 1979).

4. FAULT DIAGNOSIS

The orthogonal nonlinear multi-way PCA model developed in the previous section provides a good platform for fault diagnosis in the scores subspace. It provides low-dimensional principal components which are sensitive enough to faults.

The envelope of normal operating region (NOR) described by three principal components scores is illustrated in Figure 6. All points encapsulated by the sphere are considered statistically in-control with respect to scores space. For a continuous process, under a process upset, the scores are shifted to a new steady state which forming a new cluster as marked by the triangle (fault 1). Then the statistical analysis is performed on the new cluster to classify each different fault. The fault diagnosis can be performed by discriminating the test cluster mean against the known clusters mean.

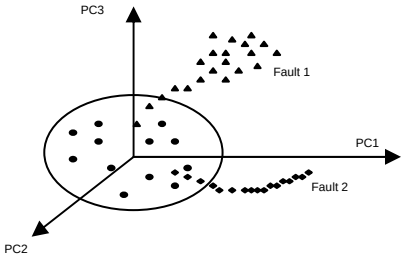

Fig. 6: Normal Operating Envelope

However, in on-line batch/semi-batch process monitoring, the fault is represented by a trajectory as marked by the diamond (fault 2). There is no new steady state cluster is attained in which it violates the vital assumption of the normality of the data distribution. As a result the cluster population mean approach will not work properly. The discriminant analysis must be performed on the trajectory rather than the cluster for batch/semi-batch processes. In this study, the crossing point between the trajectory of faulty batch and the boundary limits is proposed to perform the discriminant analysis. This representation is considerably acceptable because the same faults produce the same effects. Eventually, they will be characterized by the same trajectories in the scores subspace. Since the batch/semi-batch process is a finite process in nature, it is very essential to diagnose the problem as soon as the fault is detected. Thus examining the transient region will give much advantage rather than conducting an analysis on abnormal region. The process model and its boundary limit must be defined by using the reference data of past successful batches. The reference data must represent normal operating conditions and should be free from any fault or abnormality. Then each fault will be classified by the crossing point between its score trajectory and the boundary limit.

The crossing point can be determined when the calculated T^2 at time i is equal to the T^2-statistical threshold as calculated in the fault detection scheme. Then the future fault is diagnosed by discriminating its crossing point to the crossing points of known faults. The discriminant statement is minimizing the Euclidean distance between the two points of scaled scores as follows:

$$\min_j \left\| a - b_j \right\|_2 \qquad (4)$$

where a is the crossing test point and b is the reference crossing points of known fault j.

Since the boundary limits are utilised to represent the trajectory, the proposed discriminant approach inherits the good statistical properties itself. The fault diagnosis can be performed at different level of confidence limits. The lower limit gives a faster diagnosis with less confidence while the higher limit validates the lower limit observations. Although a

boundary limit less than 90% confidence is rarely used, but it is quite useful as a guideline to perform a routine preventive checking to ensure the process is adequately controlled and operated.

5. CASE STUDY

In order to demonstrate the proposed process monitoring strategy, a well developed mechanistic model of styrene/MMA emulsion copolymerisation semi-batch process is utilised (Alhamad, Romagnoli et al. 2005). There are 8 variables being measured and sampling is performed for every 30 sec (150 time intervals) of 4500 sec batch run. The process is seeded for 1500 sec before the continuous feeds are introduced. Autocorrelations are added to all system feeds and temperature. 30 good batches are simulated to create a reference batches to build the orthogonal nonlinear MPCA model. Variations are introduced in each good batch by random variations in initial charges within acceptable limits.

The main objective of this process is to produce a polymer product with a specific bi-modal particle size distribution (PSD). Any significant changes in monomers, surfactant and initiator conditions will distort the required bi-modal PSD. Two abnormal batches are created. For the first batch, the surfactant initial charge is set at 20% below the base recipe. As the process is under surfactant starvation, there are not enough micelles being produced for new nucleation. Thus most of the monomers favour in the particle growth rate in which it shifts the distribution to a higher particle size range. This eventually distorts the required bi-modal distribution. For the second batch, a 50% step drop in surfactant feed flow rate is simulated at the middle of the batch run.

In general, the overall monitoring is usually performed by using an adequate number of principal components regardless the strategies used. However, the significant advantage of the proposed strategy is in low-dimensional monitoring. If each principal component is individually sensitive enough to detect the fault, this advantage could be exploited to extract more information regarding the fault. One of important exploitations is in a fault diagnosis. Thus, the performance of proposed nonlinear strategy is evaluated by performing an on-line monitoring on a single principal component. For future data substitutions, the simplest approach (zero deviation) is utilised. The nonlinear MPCA strategy performance is compared with the conventional MPCA strategy for a comparison purpose. Solid line and dotted line in Figure 7 and 8 represent nonlinear and linear strategy respectively. All scores are scaled to zero means and unit variance. A simple 99% limit is calculated based on assumption the scaled scores follow the normal distribution.

Figure 7 shows a T^2 plot for the first fault batch. In this case, the linear strategy fails to detect the fault since it does not cross the limit. Whereas the proposed orthogonal nonlinear MPCA strategy depicts its superiority by crossing the 99% limit at the middle of batch run.

The T^2 plot for the second fault batch is illustrated in Figure 8. As the surfactant feed is reduced at the middle of the batch run, the nonlinear strategy responses faster than linear strategy and predicts that the product is off-specification by crossing the 99% limit before the batch run ends. Whereas the linear strategy response is much slower, resulting the off-specification in product cannot be highlighted.

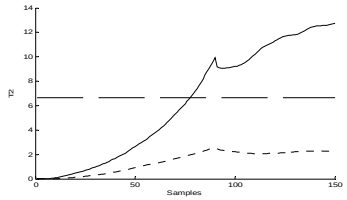

Fig. 6: T^2 plot for the first fault

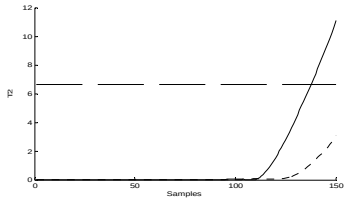

Fig. 7: T^2 plot for the second fault

To test the performance of the proposed framework of fault diagnosis for batch/semi-batch processes, the additional 25 abnormal batches are simulated. There are five fault classes (FA, FB, FC, FD and FE) and in each class contains five batches which have been numbered from 1 to 5. FA, FB and FC belong to initial condition problems while FD and FE belong to faults that occur in the middle of semi-batch run. Each batch is assigned with different common variation and fault magnitude which is randomly assigned. For fault FD and FE, the timing of fault occurrence is also randomly assigned. This setting is very important due to the fact that the faults in the same class occur at different magnitude and time. In general, each fault is considered unique although they belong to same category. The first batch of each fault class is considered as the fault reference set while the remaining four batches are considered as the test sets. Three principal components are utilised to build the discriminant model. Three different boundary levels (70%, 90% and 99%) are utilised to calculate the cross-point.

Table 1 shows the result of the diagnostic decision. In general the overall performance is satisfactory with an overall diagnosis success rate (DSR) is 82%. The diagnostic performances for 90% and 99% boundary limit are equal at 85% DSR. However as a lower boundary limit is being utilised (70%) the diagnostic performance is slightly degraded to 75% DSR. Despite this degradation, the performance is still considerably good. Therefore, the lower boundary limit can be utilised as a guideline to conduct a

routine preventive check list. Fault C has the best performance with 100% DSR, while fault D and E have the lowest performances. Since the magnitude and the timing of fault D and E are randomly assigned, this increases the complexity of the diagnosis.

Table 1: Diagnostic performance of trajectory-boundary-limit cross point approach

	Test Set												DSR			
	1			2			3			4						
Fault class	70%	90%	99%	70%	90%	99%	70%	90%	99%	70%	90%	99%	70%	90%	99%	Overall
FA	FE	FE	FE	✓	✓	✓	✓	✓	✓	✓	✓	✓	0.75	0.75	0.75	0.75
FB	✓	✓	FC	✓	✓	✓	✓	✓	✓	✓	✓	✓	1	1	0.75	0.92
FC	✓	✓	✓	✓	✓	✓	✓	✓	✓	✓	✓	✓	1	1	1	1
FD	FE	✓	✓	✓	✓	✓	FA	✓	✓	FB	FB	FB	0.25	0.75	0.75	0.58
FE	✓	✓	✓	✓	✓	✓	✓	✓	✓	FA	FE	✓	0.75	0.75	1	0.67
DSR	0.6	0.8	0.6	1	1	1	0.8	1	1	0.6	0.6	0.8	0.75	0.85	0.85	0.82

As the incorporation of O-NLPCA improves the fault detection sensitivity as has been illustrated in the above, the trajectory-boundary-limit cross point strategy improves the diagnostic effectiveness. To illustrate this advantage, a comparison study to the conventional PCA fault diagnosis approach is carried out. With the multi-way unfolding and orthogonal nonlinear PCA approaches are preserved, the diagnostic analysis is performed by discriminating between the populations means. Only the scores that exceeding the boundary limits are used to calculate the population mean. Each fault population mean is derived from the same model rather than being derived on its individual model. The single-model PCA can significantly outperform the multi-model PCA for diagnosing faults because it utilizes information from all fault classes and projects the data onto the same dimensions for each class (Chiang, Braatz et al. 2001). In this comparison, 90% boundary limit is utilised and the diagnostic is performed only after a complete run. Table 2 shows the diagnostic decision for the conventional PCA approach.

Table 2: Diagnostic performance of population means approach

Fault class	Test Set				DSR
	1	2	3	4	
FA	✓	✓	✓	✓	1
FB	FE	FE	✓	FE	0.25
FC	✓	✓	✓	✓	1
FD	✓	✓	FA	FB	0.5
FE	✓	✓	✓	✓	1
DSR	0.8	0.8	0.8	0.6	**0.75**

Comparing Table 2 content to Table 1 content (for 90% limit), the overall performance of proposed trajectory-boundary limit cross points is better with 85% overall DSR compared to conventional PCA with 75% overall DSR. For the proposed method, the diagnostic performance is considerably consistent through out the fault classes. For the conventional method, it has a bias superior performance towards particular faults where three fault classes (FA, FC and FE) have 100% DSR. However, the most significant advantage of the proposed discriminant approach is the faults are diagnosed as soon as they are being detected. Therefore, the operator will have an ample time to take a proper corrective action.

6. CONCLUSION

In this paper the framework of fault detection and diagnosis for batch/semi-batch processes has been presented. The strategy utilises a sequential application of PCA and orthogonal nonlinear PCA which captures the nonlinearity characteristic in an efficient manner. In addition, the sequential approach reduces the complexity of nonlinear PCA development and compact the information to a very low dimension. The trajectory-boundary limit crossing point discriminant analysis has been proposed to improve the diagnostic performance and foremost the fault is diagnosed as it is being detected.

REFERENCES

Alhamad, B., J. A. Romagnoli, et al. (2005). "Advanced modelling and optimal operating strategy in emulsion copolymerization: Application to styrene/MMA system." Chemical Engineering Science **60**(10): 2795-2813.

Chessari, C. J., G. W. Barton, et al. (1995). On the development of a neural network based orthogonal nonlinear principal component algorithm for process data analysis. Neural Networks, 1995. Proceedings., IEEE International Conference on.

Chiang, L. H., R. D. Braatz, et al. (2001). Fault Detection and Diagnosis in Industrial Systems. London, Springer.

Dong, D. and T. J. McAvoy (1996). "Batch tracking via nonlinear principal component analysis." Aiche Journal **42**(8): 2199-2208.

Dunia, R. and S. J. Qin (1998). "Subspace approach to multidimensional fault identification and reconstruction." AIChE Journal **44**(8): 1813-1831.

Jackson, J. E. and G. S. Mudholkar (1979). "Control procedures for residuals associated with principal components analysis." Technometrics **21**: 341-349.

Jolliffe, I. T. (1986). Principal components analysis. New York, USA, Springer-Verlag.

Kosanovich, K. A., K. S. Dahl, et al. (1996). "Improved process understanding using multiway principal component analysis." Industrial & Engineering Chemistry Research **35**(1): 138.

Kourti, T., P. Nomikos, et al. (1995). "Analysis, monitoring and fault diagnosis of batch processes using multiblock and multiway PLS." Journal of Process Control **5**(4): 277-284.

Kramer, M. A. (1991). "Nonlinear Principal Component Analysis Using Autoassociative Neural Networks." Aiche Journal **37**(2): 233-243.

Kresta, J. V., J. F. MacGregor, et al. (1991). "Multivariate Statistical Monitoring of Process Operating Performance." Canadian Journal of Chemical Engineering **69**: 35-47.

Lee, J.-M., C. Yoo, et al. (2004). "Fault detection of batch processes using multiway kernel principal component analysis." Computers & Chemical Engineering **28**(9): 1837-1847.

Lennox, B., G. A. Montague, et al. (2001). "Process monitoring of an industrial fed-batch fermentation." Biotechnology and Bioengineering **74**(2): 125-135.

Nomikos, P. and J. F. MacGregor (1994). "Monitoring Batch Processes Using Multiway Principal Component Analysis." Aiche Journal **40**(8): 1361-1375.

Nomikos, P. and J. F. MacGregor (1995). "Multivariate SPC charts for monitoring batch processes." Technometrics **37**: 41-59.

Raich, A. and A. Cinar (1997). "Diagnosis of process disturbances by statistical distance and angle measures." Computers & Chemical Engineering **21**(6): 661-673.

Tracy, N. D., J. C. Young, et al. (1992). "Multivariate control charts for individual observations." Journal of Quality Technology **24**: 88-95.

ADCHEM 2006

International Symposium on Advanced Control of Chemical Processes
Gramado, Brazil – April 2-5, 2006

AN ADJOINED MULTI-DPCA APPROACH FOR ONLINE MONITORING OF FED-BATCH PROCESSES

Ng Yew Seng and Rajagopalan Srinivasan*

Laboratory for Intelligent Applications in Chemical Engineering,
Department of Chemical and Biomolecular Engineering,
National University of Singapore, 10 Kent Ridge Crescent, Singapore 119260
**Email: chergs@nus.edu.sg; Tel: 65-68748041; Fax: 67791936*

Abstract: Batch processes are common in the manufacturing of high value-added products. Monitoring with the highly popular principal components analysis (PCA) approaches do not function adequately in the face of the sequential nature of batch processes, as the basic assumptions that its monitoring statistics (SPE and Hotelling's T^2) are developed upon – stationary, normal distribution of source data - are violated. Consequently, these monitoring techniques become prone to Type-I (false positives) and Type-II Errors (false negatives). In this article, an extension of PCA, called adjoined dynamic principal component analysis (ADPCA), is proposed for online monitoring of batch processes by using multiple dynamic-PCA (DPCA) models. The ADPCA models are developed by first clustering process data using fuzzy c-means algorithm and developing a DPCA model for each cluster. Each cluster is selected so that it satisfies the PCA's assumption. The problem of switching between the models which normally confounds multiple model-based approaches is overcome by allowing adjoining models to overlap and thus enabling smooth switching from one model to another during the course of batch operations. As shown in this paper, the proposed methodology reduces both Type-I and Type-II errors compared to single block methods.

Keywords: batch mode, batch control, fuzzy models, fault detection, non-stationary systems, non-linear systems.

1. INTRODUCTION

Batch/fed-batch operations are commonly used to manufacture high value-added products in the chemical, pharmaceutical, biological, and semi-conductor industries. The standard operating procedures (SOP) for fed-batch operations often occur in sequences specified in a recipe. Unlike continuous processes, batch processes have various characteristics that complicate process monitoring; these include finite time duration, nonlinearities, non-stationary (non-steady-state) behavior and run-to-run variations. Regulatory and supervisory control for batch operations is an open research area as most high-level automation applications are effective only during steady-states. Owing to the lack of effective automation and the high cognitive workload of plant operators, the occurrence of human errors during these operations is very likely (Ng and Srinivasan, 2004). A general feature of batch/fed-batch processes is that small changes in the operating conditions during critical periods may degrade the quality of the final product; this is especially obvious in biological processes. Due to the numerous complexities in these mode of operations, effective techniques for online monitoring is essential since timely corrective action may prevent fault propagation and allow a batch to be saved.

In this paper, a new monitoring technique, called adjoined dynamic principal component analysis (ADPCA), is proposed for online monitoring of fed-batch operations. ADPCA uses overlapping PCA models for monitoring batch trajectories and is inherently capable of modeling non-stationary processes more accurately. It is capable of overcoming both Type-I (false positives) and Type-II errors (false negatives) suffered by conventional single-block PCA techniques during batch operations. The organization of this article is as follows: Section 2 reviews PCA and its variants, and their shortcomings during online monitoring of batch operations. The proposed ADPCA methodology for online batch process monitoring is described in Section 3 while Section 4 presents the applications of the proposed method to a fed-batch penicillin cultivation process. Furthermore, a comparison of the proposed methodology with multiway-PCA and dynamic-PCA is also presented.

2. PCA-BASED PROCESS MONITORING : METHODS AND SHORTCOMINGS

Principal component analysis is a popular statistical technique for process monitoring (Kourti, 2002). Mathematically, PCA relies upon eigenvector decomposition of the covariance or correlation matrix to capture the major tendencies of process variables. Let $\boldsymbol{X} = \{\boldsymbol{x}^1, \boldsymbol{x}^2, \boldsymbol{x}^3, ..., \boldsymbol{x}^m\}^T$ with m rows and n columns. PCA linearly decomposes the data matrix $\boldsymbol{X}$ as the sum of scores, $\boldsymbol{t}$, loadings, $\boldsymbol{p}$, and a residual matrix $\boldsymbol{e}$ in the following way (Wise & Gallagher, 1996):

$$\boldsymbol{X} = \boldsymbol{t}_1\boldsymbol{p}_1^T + \boldsymbol{t}_2\boldsymbol{p}_2^T + ... + \boldsymbol{t}_i\boldsymbol{p}_i^T + ... + \boldsymbol{t}_k\boldsymbol{p}_k^T + \boldsymbol{e} \,. \quad (1)$$

Here, k is the number of principal components that a user wants to retain. The scores vector, $\boldsymbol{t}$ contains information on how the samples relate to each other,

while the loadings vector, $\boldsymbol{p}$ contains information regarding the correlation among the variables.

2.1 Fault detection with PCA approaches

Fault detection using PCA or its variants is usually performed through monitoring of the squared prediction error (SPE) and/or Hotelling's T^2 statistic. The *SPE* measures the variation of a sample $\boldsymbol{x}_i$ from the PCA model, i.e. lack-of-fit:

$$SPE_i = \boldsymbol{e}_i \boldsymbol{e}_i^T = \boldsymbol{x}_i (\boldsymbol{I} - \boldsymbol{p}_k \boldsymbol{p}_k^T) \boldsymbol{x}_i^T . \quad (2)$$

The process is considered normal if $SPE_i < Q_{1-\alpha}$, where $Q_{1-\alpha}$ denotes the upper control limit for confidence level at $1-\alpha$ percentile (Jackson and Mudholkar, 1979). The T^2 statistic measures the variation of the sample within the PCA model:

$$T_i^2 = \boldsymbol{t}_i \boldsymbol{\lambda}^{-1} \boldsymbol{t}_i^T = \boldsymbol{x}_i \boldsymbol{p} \boldsymbol{\lambda}^{-1} \boldsymbol{p}^T \boldsymbol{x}_i^T \quad (3)$$

where λ^{-1} is the diagonal matrix containing the inverse of the eigenvalues associated with k eigenvectors retained in the PCA model (Wise *et. al.,* 1990). An upper control limit $T^2_{k,m,\alpha}$ similar to $Q_{1-\alpha}$ can also be derived for the T^2 statistic (Jackson, 1991) by using a F-distribution of the training data. The *SPE* and T^2 monitoring statistics are complementary in nature, since the *SPE* measures the lack-of-fit while the T^2 statistic measures the variation of a sample within the model.

2.2 Type-I and Type-II Errors

Most of the statistical process control (SPC) literature has focused heavily on methods for handling data generated from normal distributions. The PCA-based techniques also assume that the training data follows a normal distribution. This assumption is not valid as for batch operations when analyzed *online*. There are two implications when the normal distribution assumption is used while monitoring batch processes *online*. First, the monitoring limits constructed using *SPE* and T^2 are prone to Type-II errors (false negatives), as the limits for monitoring statistics cover an unknown (possibly abnormal) operating region when a single model is used for online monitoring. Second, and perhaps the more common scenario, is the occurrence of Type-I errors (false positives). Even for a *perfectly normal* (data that are exactly normal distributed) process, the occurrence of Type-I errors are generally close to α (~50 false positives for 95% confidence limits with every 1000 samples analyzed) (Nomikos and MacGregor, 1994; Martin and Morris, 1996). Failure to account for the data distribution of the training data further increases the rate of false positives. The total rate of Type-I errors for a *non-normal* process, is thus equal to the sum of errors induced by the selected α, and the errors induced by the data distribution modeling process. As a result, the reliability of the supervision system is greatly reduced.

2.3 Multiway and Dynamic-PCA

PCA has been widely used for monitoring continuous operations (Kourti, 2002). However, there exist some limitations of the PCA approaches when they are used for monitoring batch processes (Nomikos and MacGregor, 1995). In practice, batch data are usually stored in a three dimensional data matrix. An extension of PCA called Multiway-PCA (Nomikos and MacGregor, 1995) was proposed for batch data analysis. MPCA organizes the batch data into time-ordered blocks by unfolding the three dimensional array into a large two dimensional matrix before they are decomposed into their corresponding principal components. In general, there exist three different ways (batch-wise unfolding; time-wise unfolding, and variable-wise unfolding) that a 3-Dimensional array $\boldsymbol{X}$ can be unfolded (Lee *et. al.,* 2004). The MPCA technique referred in this work is based on the time-wise unfolding. Such unfolding allows abnormal samples to be identified from a given batch trajectory.

PCA generates a linear static model of the data matrix $\boldsymbol{X}$. When the data contains dynamic information, as in the case with fed-batch operations, applying PCA/MPCA on the data does not capture the actual correlations between the variables, but only a linear static approximation. For most of the processes encountered, a dynamic-PCA is more appropriate (Ku *et. al*.,1995). For non-stationary systems, the current values of process variables will depend on the past values due to time-lag behavior of the chemical processes. $\boldsymbol{X(t)}$ can thus be augmented with previous observations, where

$$\boldsymbol{X}_D(t) = [\boldsymbol{X(t)} \;\; \boldsymbol{X(t-1)} \;\; \ldots \;\; \boldsymbol{X(t-l)}], \quad (4)$$

with l being the number of previous observations that are correlated to the current sample. The extracted dynamic model is implicitly multivariate autoregressive (AR) (Ljung and Glad, 1994) if process inputs are included (Ku et. al., 1995).

Previous literature on online monitoring based on MPCA/DPCA for transient operations normally require the batch-length to be equal in order to manipulate the monitoring limits at each time instant to reduce the occurrence of false positives, eg: Birol *et.al.* (2002), Lee *et. al*.(2004), Nomikos and MacGregor (1995), Rännar *et. al.* (1998), *etc*. Monitoring limits which are generated based on fixed time approach might give reasonable performance if the underlying events are highly synchronized, eg: activation of fed-batch at fixed time-point, all growth of microbiology to be consistent throughout, fixed duration of batch operation. However, run-to-run variations are often significant due to environmental or human factors. Such drastic behavior cannot be adequately modeled by MPCA and DPCA techniques. To overcome these shortcomings, multiple models are needed for a more flexible monitoring of batch processes.

2.4 Need for multiple adjoined models

The use of multiple models has been a popular approach in system identification (Böling *et. al*., 2004), advanced control (Palma and Magni, 2004), and monitoring (Bhagwat et.al., 2003). In this work, we use a *divide-and-conquer* strategy to overcome the shortcomings as outlined in the previous paragraph by using multiple PCA models for online monitoring. Though there exist several literatures (Hwang and Han,1999; Rännar *et. al.,* 1998) on performing batch monitoring with multiple models, the existing PCA approaches are limited by run-length, discontinuous in modeling, and prone to false

positives. This paper extends these methods by using overlapping models in order to be *robust to run length*, give *good monitoring resolution*, and *be sensitive to new operating region* (*i.e.* detect novel fault). When multiple models are used to model transient operation, false positives are often encountered in the *border* between two or more models. In Srinivasan *et. al*., (2005), it was reported that 50% of prediction errors occurred are attributed to state change when multiple sets of neural networks are used for temporal pattern recognition. The high level of errors during model switching, similarly in multiple PCA models approaches, is due to discontinuity in modeling transient operations. Fed-batch operations usually follow a trajectory on the PC subspace. If disjoint PCA models are used, the models constructed failed to incorporate all relevant normal operating region and thus result in oversensitivity in the bordering region of each model when future samples evolve through such sensitive region. These shortcomings can be overcome when the neighboring PCA models are allowed to overlap, since overlapping PCA models allow the modeling of the smooth evolution of the process trajectory in addition to any abrupt changes that occurred. As a result, the monitoring statistics constructed from each individual model cover all relevant normal operating regions and prevent false positives from occurring during model-switching / state change.

3. ADJOINED DPCA METHOD FOR ONLINE MONITORING OF FED-BATCH OPERATIONS

In this section, we propose an adjoined multi-model DPCA-based methodology for o*nline* monitoring and supervision of fed-batch processes. We term the proposed method as adjoined-DPCA (ADPCA) as the method is developed on the basis of multiple overlapping and connected DPCA models. The proposed methodology is based on the integration of fuzzy clustering methodology with dynamic-PCA monitoring approaches. As described in the earlier section, conventional single block MPCA or DPCA monitoring approaches fail to account for the non-stationary effects in temporal signals. Fuzzy clustering of process states based on historical data can thus be used to differentiate multiple modes of operations in these temporal signals for building different DPCA models for monitoring purposes. The additional membership information obtained through fuzzy clustering provides a means to construct overlapping DPCA models. Such membership information is often not available in crisp clustering algorithm such as *k*-means. The training data from different stages/phases can be extracted and reconstructed based on a proposed *fuzzy-data reconstruction approach*. The reconstructed data groups overlap with their neighboring groups, with a DPCA model constructed for each group reconstructed. At every instant, the best-fit DPCA model is selected for monitoring purposes. The offline ADPCA model construction is described next in Section 3.1 and the steps for online monitoring are presented in Section 3.2.

3.1 ADPCA model construction

The training algorithm is based on normal operating data only, which can be obtained from the plant historian directly. Process data are often corrupted with noise. In this work, a windowed finite impulse response (FIR) filter (IEEE, 1979) is implemented to eliminate high frequency noise. Let $\boldsymbol{Y}$ be the raw data collected from a plant historian. Variable unfolding is first carried out on the 3-dimensional dataset to reduce $\boldsymbol{Y}$ to a 2-dimensional dataset for analysis. Each variable of the training data, $\boldsymbol{y}_i$, is later normalized to eliminate the varying scales of the variables:

$$\boldsymbol{x}_i = \frac{\boldsymbol{y}_i - \boldsymbol{y}^{mean}}{\sigma_{\boldsymbol{y}}}. \tag{5}$$

The filtered signals, $\boldsymbol{X} = \{\boldsymbol{x}_1, \boldsymbol{x}_2, ... \boldsymbol{x}_i, ... \boldsymbol{x}_m\}$, is then partitioned into different clusters through fuzzy *c*-means clustering. Fuzzy *c*-means is a generalization of the *k*-means data clustering technique where each sample belongs to one or more clusters as per a membership grade. For a dataset consisting of *m* objects and a pre-specified *c* number of clusters, the fuzzy c-means algorithm computes the optimal memberships by minimizing (Hataway and Bezdeck, 1988):

$$obj = \sum_{j=1}^{c}\sum_{i=1}^{m} \boldsymbol{u}_{ij}^{v} d(\boldsymbol{x}_i, \boldsymbol{m}_j)^2 \tag{6}$$

where $\boldsymbol{m}_j$ is the centre of cluster c, $d(\boldsymbol{x}_i, \boldsymbol{m}_j)$ is the Euclidean distance between the data point and the cluster center, $\boldsymbol{u}_{ij} \geq 0$ for all *m*, and $\sum_{j=1}^{c} \boldsymbol{u}_{ij} = 1$, for each i^{th} sample. Here, *v* is called the fuzzifier and affects the final membership distribution. $v = 1$ leads to crisp clustering solution; a value of 2 is normally used. If $\boldsymbol{u}_{ic}$ is restricted to 0 or 1, the proposed algorithm reduces to the *k*-means algorithm. The fuzzy membership grade for any given sample indicates whether there is any other cluster that is comparable to the best cluster.

The samples are then stacked into different groups based on time-wise unfolding. Consider the training data $\boldsymbol{X}$ obtained together with its clustering information, $\boldsymbol{u}_{ij}$. $\boldsymbol{X}$ is now a two dimensional array obtained by stacking the training data of different runs through multi-way approaches, it is reorganized into *c* number of groups based on a *fuzzy-data reconstruction approach*. The data reconstruction process serves as a data preparation mode for constructing adjoined-DPCA models. At any instant, a sample (measurements) has a one-to-many relation with the data groups, which means a sample can be concurrently present in one or more data groups. Since

$$\boldsymbol{u}_{ij} = \frac{1}{\sum_{r=1}^{c}\left(\frac{d(\boldsymbol{x}_i, \boldsymbol{m}_j)}{d(\boldsymbol{x}_i, \boldsymbol{m}_r)}\right)^{2/v-1}}, \tag{7}$$

where $d(\boldsymbol{x}_i, \boldsymbol{m}_j)$ is the distance from point $\boldsymbol{x}_i$ to current cluster center $\boldsymbol{m}_j$, and $d(\boldsymbol{x}_i, \boldsymbol{m}_r)$ is the distance from $\boldsymbol{x}_i$ to other cluster center $\boldsymbol{m}_r$, the highest value of $\boldsymbol{u}_{ij}$ gives the cluster which is closest to $\boldsymbol{x}_i$. The best membership of $\boldsymbol{X}$ at every i^{th} instance, $\boldsymbol{x}_i$ is thus given by:

$$\boldsymbol{b}_i^{1st} = \arg\max(\boldsymbol{u}_{ij}), \ \forall j = \{1,2,...,c\}, \tag{8}$$

since $\boldsymbol{u}_{ij}$ is inversely proportional to the distance of $\boldsymbol{x}_i$ from j^{th} cluster centroid, $\boldsymbol{m}_j$, as shown in Equation 7. The subsequent layer of cluster membership function

$\boldsymbol{u}_{ij}$ is then analyzed iteratively following the general algorithm for *fuzzy-data reconstruction* to identify the existence of r^{th} best cluster:

$$\boldsymbol{b}_i^{rth} = \arg\max(\boldsymbol{u}_{ij}),\ \forall j = \{1,2,...,c\}, \tag{9}$$

subject to the following constraints:

$$\boldsymbol{b}_i^{rth} \neq \{\boldsymbol{b}_i^{(r-1)th}, \boldsymbol{b}_i^{(r-2)th}, ..., \boldsymbol{b}_i^{1st}\}\ \&\ exist(\boldsymbol{b}_i^{(r-1)th}, \boldsymbol{b}_i^{(r-2)th}, ..., \boldsymbol{b}_i^{1st})\ \&\ \boldsymbol{b}_i^{rth} - \boldsymbol{b}_i^{(r-1)th} < \delta. \tag{10}$$

The *association threshold*, δ defines the allowable regions to overlap when computing DPCA models from the reconstructed data. Here, δ is in the range of $[1\ 0]$. A large value of δ allows fully overlapped regions while setting $\delta = 0$ prohibits the spawning of $\boldsymbol{x}_i$ totally. Each sample $\boldsymbol{x}_i$, is then duplicated and placed within their corresponding groups of *reconstructed data*, $\boldsymbol{W}_j$, where $j \in \{\boldsymbol{b}\}$ identified from the algorithm for fuzzy-data reconstruction. Upon completion of the analysis of one sample, $\boldsymbol{x}_i$, i is incremented and the subsequent sample $\boldsymbol{x}_{i+1}$ is subjected to the same analysis as described in equation 10. The end results of the above algorithm is the creation of reconstructed cluster groups $\boldsymbol{W}_j$, $\forall j = \{1,2,...,c\}$ that overlaps with their proximity clusters. Such new clusters formation is deemed important especially when generating PCA models for monitoring fed-batch processes to avoid discontinuities in modeling the normal operating region. Failure to account for such discontinuities would make the monitoring system prone to Type-I errors when new process trajectory evolve through sensitive regions.

Subsequently, a total of c distinct DPCA models DPM_j, $j = \{1,2,...,c\}$ are constructed for process monitoring following (Equation 1 & Equation 4). Each DPM_j corresponds to a local DPCA model generated from the reconstructed dataset $\boldsymbol{W}$. At each instant of monitoring, the DPCA model that best describe the fed-batch processes, DPM_{opt} is selected and used for process monitoring. Multivariate statistical process control charts are based on the *SPE* and T^2 statistics of DPM_{opt}. With the proposed approach, the effect of false positives will become less severe as the data density for each of the PCA model is locally normal distributed. Additionally, the chances of having false negatives are also greatly reduced, as monitoring limits generated from the PC models do not cover the training subspace of unknown operating region compared to single block approaches.

3.2 Online fault detection

The algorithm for online fault detection is shown in Figure 1. The main challenge in the online monitoring using the proposed approach is to identify the best DPCA models at each point in time. New process measurements, designated here as $\boldsymbol{Y}$, is first filtered and autoscaled to $\boldsymbol{X}$ (Equation 5), before they are projected to the principal component subspace as scores, **t** and loadings, **p** (Equation 1). Its distance in the principal component subspace are then evaluated against all the DPCA models, DPM_j, $\forall j = \{1,2,...,c\}$. The distance between the sample $\boldsymbol{x}_i$ and each DPCA model, DPM_j is calculated based on a *adjoined discriminant similarity factor, $\boldsymbol{\Psi}'$*. The original proposal of $\boldsymbol{\Psi}$ (Raich and Çinar, 1996) is solely to facilitate human operators during process monitoring by combining the two separate monitoring statistics (SPE and T^2) into one uniformed, simple index. Here, we extend the discriminant similarity factor to the selection of best DPCA model for online applications. At every instance, the distance of $\boldsymbol{x}_i$ and all constructed DPCA models, DPM_j, $\forall j = \{1,2,...,c\}$ are evaluated through:

$$\boldsymbol{\Psi}'(DPM_j, \boldsymbol{x}_i) = \sqrt{\beta(SPE_{r,i}{}^2) + (1-\beta)(T_{r,i}{}^2)},\quad \forall j = \{1,2,...,c\}. \tag{11}$$

Here, $SPE_{r,i} = SPE_i / Q_{1-\alpha}$, $T_{r,i}{}^2 = T_i{}^2 / T^2_{k,m-k,\alpha}$, and $1-\alpha$ is the confidence level for limit evaluation. Here, β is a weighting factor between zero and one. Upon the absence of additional information, SPE and T^2 are weighted equally, where β is set to 0.5. The nearest PCA model to $\boldsymbol{x}_i$,

$$DPM_{opt} = \arg\min(\boldsymbol{\Psi}'(DPM_j, \boldsymbol{x}_i)),\quad \forall j = \{1,2,...,c\}, \tag{12}$$

is then selected for monitoring the current stage of the fed-batch operations. Monitoring statistics, *i.e.*: SPE and T^2, are generated based on DPM_{opt} and compared with their upper control limit, $Q_{1-\alpha}$ and $T^2_{k,m-k,\alpha}$ for anomaly detection.

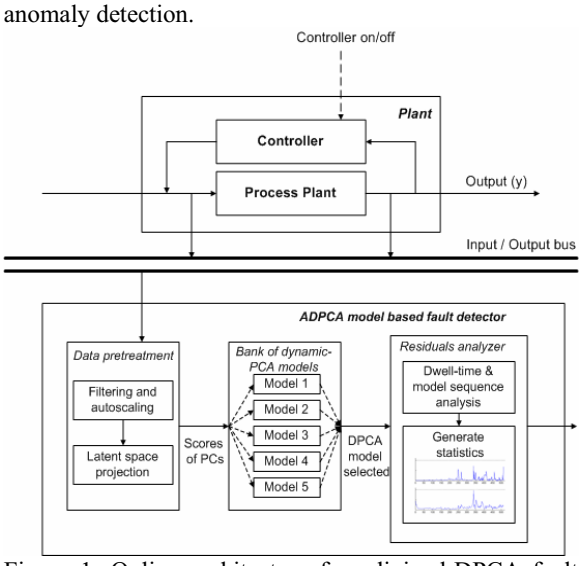

Figure 1: Online architecture for adjoined-DPCA fault detection

4. MONITORING OF FED-BATCH PENICILLIN CULTIVATION PROCESS

In this section, the proposed adjoined-DPCA (ADPCA) method is tested on a fed-batch penicillin cultivation process. In this work, we use the penicillin fed-batch simulator PenSim v2.0 (Birol *et. al.*, 2002a) that is based on the mathematical model of Bajpai and Reuss (1980). The simulator captures the dynamics in sixteen process variables, namely: flow rates of input streams, temperature, pH, heat generated, aeration rate of

fermenter, etc. The final quality and quantity of the final product is very much affected by pH and temperature. They are therefore controlled at specified setpoint. In our simulation, the pH was controlled at 5.0 and the temperature was maintained at 25°C to promote cell growth. In all runs, an initial batch culture is followed by a fed-batch operation based on the depletion of the carbon source (glucose). The process switches to the fed-batch mode when the level of glucose concentration reaches 0.3g/l. Detailed description of the fed-batch simulator including the state equations and simulation parameters is given by Birol *et. al.* (2002). In this work, a total of 50 normal batches were simulated to create the reference datasets, we have used an integration step size of 0.02h and a sampling interval of 0.5h.

The variables selected for the monitoring of penicillin cultivation process are similar to the study of (Lee *et al*., 2004). An association threshold, δ of 0.1 was chosen for constructing the adjoined-DPCA models. 10 adjoined-DPCA models were built based on the methods proposed in Section 3.1 by setting the time-lag parameters, l=0. By ignoring the time-lag behavior of the ADPCA, the method is actually reduced to adjoined-PCA approaches. The proposed technique is not prone to false positives as each of the PCA model constructed can model the different phases of the fed-batch process more accurately. Occasionally, more than one adjoined PCA models were used to monitor a single phase of the fermentation. The oscillatory nature of some process variables due to process controllers (pH and Temperature) caused some models to be used quite frequently throughout the cultivation period, eg: model 1 and model 5. On the other hand, the use of multiway-PCA and dynamic-PCA techniques, which are based on a single model, is prone to false positives at t~36.5. The results observed are consistent with the analysis of Lee *et. al.* (2004). Seven process disturbances have been tested as summarized in Table 1.

Table 1: Summary of fault scenarios considered

Case	Fault type	Occurrence time (h)
1.	pH controller failure	0.5
2.	Temperature controller failure	0.5
3.	-15% step in aeration rate	60
4.	-15% step in agitation power	30
5.	Ramp increase in aeration rate	70
6.	Ramp increase in agitation power	40
7.	Ramp increase in substrate feed rate	30

4.1 Monitoring of high agitation power

PEN06 corresponds to a ramp increase in agitation input power, P_w with a slope of +0.05. The increment in P_w results in positive deviation from nominal mass transfer rate and causes an over supply of oxygen to the biomass. Multiway-PCA technique detects the anomaly at t=252.0h (Figure 2) when the SPE exceeds the 99% confidence limit. Dynamic-PCA technique gives slightly better monitoring results by being able to detect the fault at t=241.0h when unusual variation are observed through T^2 statistic. The best result is observed from the proposed ADPCA technique (Figure 3) which detects the fault at t=233.0h, which is 19 hours (38 samples) earlier than multiway-PCA and 8 hours (16 samples) earlier than dynamic-PCA technique. The method is also not prone to false positives in comparison to multiway-PCA (11 false alarms) and dynamic-PCA techniques (19 false alarms). In general, dynamic-PCA is more sensitive in detecting process drift/ramp errors in comparison to multiway-PCA, as the method uses time-lag information from previous samples. However, the improvement in sensitivity of dynamic-PCA has been at the cost of having more false alarms since any misclassified samples are included as time-lag information in the future samples. These effects fade off with time. In contrast, with the proposed ADPCA technique, the improved fault detection sensitivity is not correlated with any increase in Type-I errors

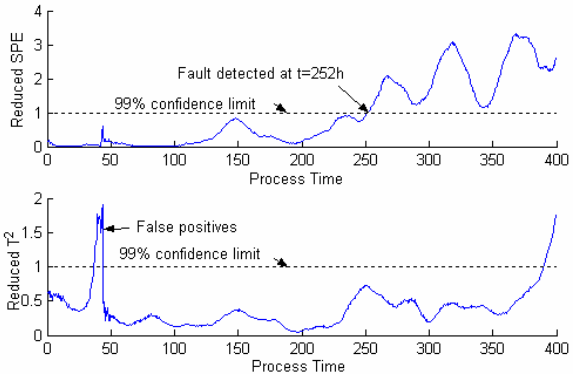

Figure 2: Monitoring results of PEN06 through MPCA

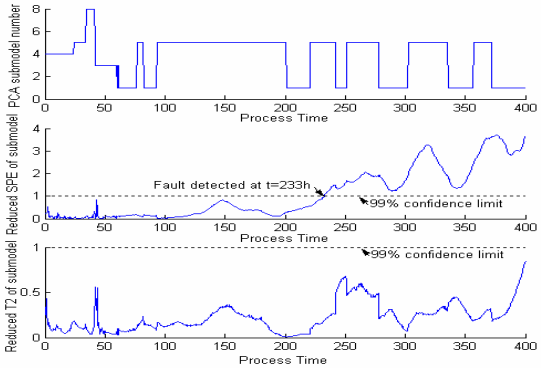

Figure 3: Monitoring results of PEN06 through ADPCA

4.2 Summary of monitoring

The summary of the monitoring results for all disturbances is presented in Table 2. All disturbances are successfully detected by all the methods utilized. Multiway-PCA and dynamic-PCA approaches are very prone to false positives. Multiway-PCA gives a total of 36 false alarms throughout the monitoring of 5600 samples (7 batches), and dynamic-PCA 75 false alarms. Dynamic-PCA gives better performance compared to multiway-PCA in terms of speed of detection as in cases PEN01 (-0.5h), PEN05(-4.0h), PEN06(-11.0h) and PEN07(-52.5h). As a whole, the proposed ADPCA technique gives the best monitoring resolution by being (1) able to detect all the disturbances in short duration (PEN01, PEN02, PEN05, PEN06), and (2) not prone to false positives. No false alarms is observed in all the fault cases studied. The ADPCA technique also offers the convenience of using lesser number of PCs to model batch operations. In this case study, 4 out of the 10 PCA models constructed used only 2 PCs to model a local phase of the fed-batch process (retaining > 95% variance of each of the local phase), with the rest ranging from 1

PC (min) to 5 PCs (max). On the other hand, the use of multiway-PCA technique requires 6 PCs to be retained while the number of PCs used is much higher in dynamic-PCA technique.

Table 2: Summary of monitoring results (Number of false alarms indicated in parenthesis)

Fault ID	Multiway-PCA	Dynamic-PCA	Adjoined-DPCA
	Time Fault Detected (hr)	Time Fault Detected (hr)	Time Fault Detected (hr)
PEN01	2.5 (0)	2.0 (0)	1.0 (0)
PEN02	4.0 (0)	4.0 (0)	2.0 (0)
PEN03	60.5 (10)	60.5 (24)	60.5 (0)
PEN04	30.5 (0)	30.5 (0)	30.5 (0)
PEN05	90.5 (10)	86.5 (24)	89.5 (0)
PEN06	252.0 (11)	241.0 (19)	233.0 (0)
PEN07	112.0 (5)	59.5 (8)	68.5 (0)

5. CONCLUSIONS AND DISCUSSIONS

In this paper, the shortcomings of MPCA and DPCA during online monitoring of batch processes are outlined and addressed. MPCA and DPCA are unable to adequately model fed-batch processes as they are based on the use of single block PCA for monitoring a transient trajectory. Such methods are usually prone to Type-I and Type-II errors as their applications violate the principle of *normal data distribution* based on which their monitoring limits (*SPE* and T^2) are developed upon. Exact estimation of the real distribution in multivariable system is difficult and multiple models could be used for modeling these transient, non-stationary and non-normal system. However, use of multiple PCA models are also prone to Type-I errors especially in the border region when model switching/ state change occurs as these models are discontinues whereas fed-batch operations are characterized by smooth evolution of process trajectories. In this article, we overcome these shortcomings through overlapping PCA models. The proposed adjoined-DPCA technique (ADPCA) uses multiple overlapping PCA models which allows the data densities in each DPCA model to be locally *normal distributed*. The overlap of neighboring DPCA models enforces continuity even when modeling batch-type operations. An optimal PCA model is selected at every instant for process monitoring during online application. Extensive testing of the proposed method shows its ability to reduce both Type-I and Type-II errors as it classifies the normal operating region more accurately in the principal component subspace. Such classification reduces the occurrence of Type-I errors as all relevant NOR is included in the model. Furthermore, the improvements in modeling also increases the methods sensitivity as unknown regions are also better excluded, subsequently reducing the chances of Type-II errors. Such performance is not achievable from the single block methods such as MPCA or DPCA where the well-known tradeoff between *selectivity and sensitivity* prevents their concurrent improvement. The automatic tracking of batch processes across phases based-on the criteria of *minimum-distance model selection* also allows the method to be applicable to operations of unequal batch length; with the most appropriate PCA models selected at each instant for process monitoring.

LITERATURE CITED

Bajpai, R., and Reuss, M., (1980). A mechanistic model for penicillin production, Journal of Chemical Technology and Biotechnology 30, 330-344.

Bhagwat, A., Srinivasan, R., Krishnaswamy, P.R., (2003). Multi-linear model-based fault detection during process transitions, Chemical Engineering Science 58, 1649-1670.

Birol, G., Ündey, C., Çinar, A., (2002). A modular simulation package for fed-batch fermentation: penicillin production, *Computers & Chemical Engineering 26*, 1553-1565.

Böling, J.M., Häggblom, K.E., Nyström, R.H., (2004). Multivariable uncertainty estimation based-on multi-model output matching, Journal of Process Control 14, 293-304.

Hathaway, R. J., and Bezdek, J.C., (1988). Recent convergence for the fuzzy c-means clustering algorithm, *Journal of Classification 5*, 237-247.

Hwang, D.H., Han, C, (1999). Real-time monitoring for a process with multiple operating modes, *Control Engineering Practice 7*, 891-902.

IEEE Digital Signal Processing Committee (eds), (1979). Programs for digital signal processing, IEEE Press, New York.

Jackson, J.E., (1991). A user's guide to principal components, Wiley Interscience, New York.

Jackson, J.E., and Mudholkar, G., (1979). Control procedures for residuals associated with principal component analysis, *Technometrics 21*, 341-349.

Kourti, T., (2002). Process analysis and abnormal situation detection: From theory to practice, IEEE Control System Magazine, October Issue 2002.

Ku, W., Storer, R.H., and Georgakis, (1995). Disturbance detection and isolation by dynamic principal component analysis, *Chemometrics and Intelligent Laboratory Systems 30*, 179-196.

Lee, J.M., Yoo, C.K., Lee, I.B., (2004). Enhanced process monitoring of fed-batch penicillin cultivation using time-varying and multivariate statistical analysis, *Journal of Biotechnology 110*, 119-136.

Ljung, L., and Glad, T., (1994). Modeling of dynamic systems, *Prentice Hall*, Englewood Cliffs.

Martin, E.B., and Morris, A.J., (1996). Non-parametric confidence bounds fro process performance monitoring charts, *Journal of Process Control 6(6),* 349-358.

Ng, Y.S, and Srinivasan, R., (2004). Transitions in the Process Industries: Opportunities and Prospective Solution, *IEEE International Symposium on Intelligent Control*, (Invited Paper), Taipei, Taiwan.

Nomikos, P., and MacGregor, J.F., (1994). Monitoring batch processes using multiway principal component analysis, *AIChE Journal 40*, 1361-1375.

Nomikos, P., and MacGregor, J.F., (1995). Multivariate SPC charts for monitoring batch processes, *Technometrics 37(1*), 41-59.

Palma, F.D., and Magni, L, (2004). A multi-model structure for model predictive control, Annual Reviews in Control 28, 47-52.

Raich, A.C., and Çinar, A., (1996). A statistical process monitoring and disturbance diagnosis in multivariate continuous processes, *AIChE Journal 42*, 995-1009.

Rännar S., MacGregor, J.F., Wold, S., (1998). Adaptive batch monitoring using hierarchical PCA, *Chemometrics and Intelligent Laboratory Systems 41*, 73-81.

Srinivasan, R., Wang, C., Ho, W. K., Lim, K. W., (2004). Dynamic PCA based methodology for clustering process states in agile chemical plants, *Industrial and Engineering Chemistry Research 43*, 2123 – 2139.

Wise, B.M., and Gallagher, B., (1996). The process chemometrics approach to process monitoring and fault detection, Journal of Process Control 6, No.6, 329-349.

Wise, B.M., Ricker, N.L., Veltkamp, D.J., and Kowalski, B.R., (1990). A theoretical basis for the use of principal components model for monitoring multivariate processes, *Process Control and Quality 1(1),* 41-51.

ADCHEM 2006

International Symposium on Advanced Control of Chemical Processes
Gramado, Brazil – April 2-5, 2006

PREDICTION OF RADICALS OF CRITICAL LENGTH IN EMULSION POLYMERIZATION PROCESSES

Mariano, Y.R.[2], **Casella, E.L.**[1], **Tvrzská de Gouvêa, M.**[1]

[1]*Universidade Presbiteriana Mackenzie, Department of Materials Engineering*
Rua da Consolação 896, 01302-907, São Paulo-SP, Brazil; miriamtg_br@yahoo.com
[2] *Universidade Presbiteriana Mackenzie, Department of Electrical Engineering*

Abstract: There is the need of a reliable process model of the emulsion polymerization so that process control and optimization may be adequately performed. Although process models for the emulsion polymerization have been proposed for over three decades, several discrepancies still exist. Here we discuss discrepancies that appear in the way the radicals of critical length are modeled in the literature. We show that the discrepancies cause significant deviations in the prediction of the behavior of the polymerization reactor.

Keywords: process models, polymerization, PVAC, dynamic behavior, mechanisms.

1. INTRODUCTION

Many important polymers are commercialy produced in batch or semi-batch reactors since they provide an efficient way to produce either high value-added products or products with specified properties. So, it is of interest to optimaly operate these reactors, which is, however, not a simple task, since optimal operating policies rely on model predictions. Although models for polymerization reactors have been proposed for many years, still many unsolved issues remain, particularly when it comes to the emulsion polymerization process, where dozens of different models exist, all being claimed to marvelously represent the polymerization process (Araújo and Giudici, 2003, Casella et al., 2003, Zubitur et al., 2003, Gao & Penlidis, 2002, Saldivar et al., 1998, Liotta et al., 1998, Dubé et al., 1997, Gilbert, 1995, Ray, 1972), which is accomplished by properly adjusting selected model parameters to particular reacting conditions. This is why models have been published where, e.g., the critical length for methyl methacrylate has been taken as 65 and nowadays it is known that the accepted value is about 10 (Forcada and Asua, 1990, Gilbert, 1995). Several discrepancies in modeling emulsion polymerization reactors are well known. Others are not explicitly discussed in the literature, like the ones related to the modeling of the mass balance for the radicals of critical length, i.e., radicals that become so large that get insoluble in the aqueous phase. So, in this paper we aim to discuss the several unsolved issues regarding the modeling of the radicals of critical length. We state that instead of ignoring the several discrepancies that exist among the different proposed models in the literature, effort should be made in unifying the phenomenological description of what happens with radicals of critical length, as is being performed for the establishment of propagating, chain transfer and termination rates (Van Berkel et al., 2005, Beuermann et al., 1997).

In section 2, a discussion on the current different available models for the mass balance for the radicals of critical length is provided and a unified general model is presented that is able to represent the main modeling tendencies in the literature, as well as some variations to them. In section 3, we discuss the different modeling possibilities. It seems clear for us that it is not acceptable that different assumptions be made to represent the same process, by just adjusting some parameters. In section 4, the paper is concluded and in appendix A, the remaining equations of the model with their parameters used for the simulations presented in this paper are given.

2. MATHEMATICAL MODELING OF EMULSION POLYMERIZATION REACTORS

As stated before, there is no definite model of the emulsion polymerization process. Different authors postulate different hypotheses and simply adjust some parameters so that experimental results are reproduced. It is known that some parameters should not depend on a particular system and universal values should be used like values for the propagation reactions (Gilbert, 1995), which are being established by a IUPAC party for several polymerization systems by the PLP technique (Van Berkel et al., 2005, Beuermann et al., 1997, Gilbert, 1995). Termination rates' coeficients should also not be adjusted to meet particular results, but still no definite values have been postulated for termination coefficients in spite of the several recent works (Van Berkel et al., 2005, Buback et al., 2003) on estimating them together with chain transfer rate coefficients. When it comes to modeling the capture of free-radicals in micelles and polymer particles, several discrepancies in the way of modeling emulsion polymerization reactors are well known and discussed in the literature (Herrera-Ordonez et al, 2004, Fitch, 2003, Gao and Penlidis, 2002) and no conclusion exists on how to proceed. The same is true when models are written for the prediction of particle nucleation. Other discrepancies in the existing models are more subtle and less commented, like the different approaches in modeling the mass balance for the free-radical of critical length in the aqueous phase, which will be considered in the next paragraphs.

In the literature, the mass balances for the oligomeric radicals in the aqueous phase are generally written assuming a pseudo-stationary condition. Some exceptions can be found, though (Casella et al., 2003). Here, non-stationary mass balances are considered for the radicals in the aqueous phase. The advantages of using dynamic equations instead of stationary ones to evaluate the concentrations of the radicals in the aqueous phase is the easiness of incorporating different hypotheses in the description of the equations making them more general. Moreover, the dynamic representation makes it easier to numerically solve a model constructed by the specifications of hypotheses made by the user. Because of the lack of space and in order to make the discussion clearer, we will restrict our attention in this section to reactors operated in batch mode. Moreover, the presentation here is restricted to the homopolymerization case, so that the equations become not too much visualy poluted.

Homogeneous nucleation occurs when radicals become insoluble in the aqueous phase, which occurs when radicals achieve the critical length *jcr*. Three distinct rates for predicting homogenous nucleation are most used in the literature, which are given in equations (1) to (3). One popular approach is to consider that the nucleation rate is proportional to the propagation rate of radical *jcr*-1 in case a partial solubility is assumed or equal to the propagation rate when radical *jcr* is assumed to be totally insoluble in the aqueous phase (Gao & Penlidis, 2002, Araújo and Giudici, 2003). In the former case $f_{ef,hom}$ in equation (1) may be adjusted (between 0 and 1) and in the latter case $f_{ef,hom}=1$. Equation (2) is also commonly used (Gilbert, 1995, Forcada and Asua, 1990, Abad et al., 1994). It is somewhat awkward, since it suggests that radicals of critical length are actually soluble in the aqueous phase and precipitate when they encounter a monomer. Again the parameter $f_{ef,hom}$ may be adjusted. Equation (3) may be used in two different contexts. In the first, it is a way to model the precipitated radicals and the constant k_h is set to 1 and $f_{ef,hom}$ is properly adjusted to experimental data or calculated from solubility considerations. The second interpretation for equation (3) is due to Fitch and Tsai (1971), who state that radicals of length *jcr* are not captured by either micelles and particles and the constant k_h is thus modeled accordingly to (4) (Dubé et al., 1997, Casella et al., 2003).

$$R_{\text{hom}} = f_{ef,\text{hom}} k_p [M]_w \left[R^{\bullet}_{j_{cr}-1}\right]_w V_w \qquad (1)$$

where, R_{hom} is the rate of nucleation, k_p is the propagation rate constant, $[M]_w$ is the concentration of monomer in the aqueous phase, $\left[R^{\bullet}_{j_{cr}-1}\right]_w$ is the concentration of radical of length j_{cr}-1, V_w is the volume of the aqueous phase and $f_{ef,hom}$ is a parameter as described above.

$$R_{\text{hom}} = f_{ef,\text{hom}} k_p [M]_w \left[R^{\bullet}_{j_{cr}}\right]_w V_w \qquad (2)$$

where, $\left[R^{\bullet}_{j_{cr}}\right]_w$ is the concentration of radical of length j_{cr}

$$R_{\text{hom}} = f_{ef,\text{hom}} k_h \left[R^{\bullet}_{j_{cr}}\right]_w V_w \qquad (3)$$

where, k_h is equal to 1 or obtained from equation (4).

$$k_h = k_{ho} e^{-E_{R,h}/T} \left(1 - \frac{A_p}{4V_w}\sqrt{\frac{2 j_{cr} \mathsf{A}^{\bullet}}{k_p [M]_w^{sat}}}\right) \qquad (4)$$

where, k_{ho}, $E_{R,h}$ are constants, T is the temperature of the reacting medium, A_p is the surface area of polymer particles, $[M]_w^{sat}$ is the saturation concentration of monomer in the aqueous phase and $\mathsf{A}^{\bullet}$ is the diffusivity of the radical.

Equation (5) describes the amount of radicals of critical length dissolved in the aqueous phase. No distinction is made between initiator originated radicals and monomeric radicals, i.e., radicals formed from the monomeric radical desorbed from the particles. This is generally the adopted strategy. Zubitur et al. (2003) are a noteworthy exception, except for the fact that the way they model the radicals not originated from the initiator is not presented. In the presentation of equation (5) four flags e_2 to e_5 are used in order to take into account variations in the models from the literature. If the radical of critical length is assumed to be totally insoluble in the aqueous phase, $e_3=e_4=0$, $e_5=1$ and $f_{ef,hom}=1$ (Gao and Penlidis, 2002, Araújo and Giudici, 2003). If absorption of the radical of length *jcr* is not possible, then e_2 must be set to zero. Some authors consider that the radical of length *jcr* may propagate

(Dubé et al., 1997, Gilbert, 1995) and even participate in termination reactions. The fate of the larger radicals and oligomers is however not discussed. Some authors claim that the radical of length *jcr* may participate in termination reactions but may not propagate. Each of these considerations may be taken into account by adequately selecting 0 or 1 values for the flags e_3 and e_4. Curiously, some authors do not include the precipitation term given by the homogeneous nucleation rate, as if it were possible that no radicals of length *jcr* were needed to generate polymer particles. That is why the flag e_5 appears in equation (5). One must just note that equation (2) corresponds to the propagation rate, so e_3 must be set to zero or e_5 to zero when equation (2) is used. So, equation (5) encompasses all the actual modeling approaches for describing the amount of radicals of length *jcr* in the reactor.

$$\frac{dR^{\bullet}_{j_{cr},w}}{dt} = k_p\left(\left[R^{\bullet}_{j_{cr}-1}\right]_w [M]_w - e_3\left[R^{\bullet}_{j_{cr}}\right]_w [M]_w\right)V_w - \\ - e_2\left(k_{a,m}\left[R^{\bullet}_{j_{cr}}\right]_w N_{mic} + k_{a,p}\left[R^{\bullet}_{j_{cr}}\right]_w N_p\right) - \\ - e_4\left(k_t^w\left[R^{\bullet}_{j_{cr}}\right]_w \left[R^{\bullet}\right]_w^{tot} + k_t^w\left[R^{\bullet}_{j_{cr}}\right]_w^2\right)V_w - \\ - e_5 R_{\hom} \qquad (5)$$

where, $k_{a,m}$ and $k_{a,p}$ are the absorption constants by micelles and polymer particles, respectively, N_{mic} and N_p, are respectively the number of micelles and polymer particles, k_t^w is the termination rate constant and $\left[R^{\bullet}\right]_w^{tot}$ is the total concentration of radicals in the aqueous phase.

As for the mechanism for capture of radicals, three major approaches are considered, presented in equations (6) to (8), which correspond to the propagation, diffusion and collision models. The latter equations are written for radical capture by micelles. For radical capture by particles, one just has to substitute the radius of micelles by the radius of the particles and $f_{abs,m}$ is substituted by $f_{abs,p}$. Further discussions regarding $f_{abs,m}$ and $f_{abs,p}$ are postponed to section 3.

$$k_{a,m} = f_{abs m} \qquad (6)$$

sendo, $f_{abs,m}$ is a constant.

$$k_{a,m} = f_{abs,m}\mathsf{A}_{M,w}N_{av}4\pi r_{mic} \qquad (7)$$

where, $\mathsf{A}_{M,w}$ is the diffusivity of monomer in the aqueous phase, N_{av} is the Avogadro number, r_{mic} is the micelle radius.

$$k_{a,m} = f_{abs,m}N_{av}4\pi r_{mic}^2 \qquad (8)$$

3. COMPARISON OF DIFFERENT MODEL PREDICTIONS

Table 1 summarizes the simulations performed in order to analyze the effect of different model formulations for the description of the radical of critical length. The simulations are referred to the homopolymerization of vinyl acetate with potassium persulfate used as initiator and sodium lauryl sulfate as emulsifier. The initial number of moles fed to the reactor of water, monomer, initiator and emulsifier are, respectively, 55.51, 3.44, 0.003124 and 0.0417. The simulations were carried for a temperature of 60°C.

Several situations were considered. For example, simulations were performed in order to analyze the effect of different modeling possibilities for capture of the radicals of critical length on the response of the reactor (cases a, b to e). Also some simulations were performed in order to analyze differences in the modeling of the homogeneous nucleation (cases a, b, f, g, h). Case b is considered as the base case for comparison purposes.

Table 1 Different model formulations for the radical of critical length

case	e_2	e_3 /e_4	e_5	R_{hom}	$f_{ef,hom}$ (%)	$k_{a,m/p}$	$f_{abs,m}$ (SI)	$f_{abs,p}$ (SI)
a	0	0	1	eq. 1	100	eq. 6	25	4000
b	1	1	1	eq. 1	80	eq. 6	25	4000
c	0	0	1	eq. 1	100	eq. 7	1.3e-5	1.3e-3
d	0	0	1	eq. 1	100	eq. 7	1.0e-4	1.0e-2
e	0	0	1	eq. 1	100	eq. 8	5.3e-7	1.3e-5
f	1	1	0	eq. 2	-//-	eq. 6	25	4000
g(*)	1	1	0	eq. 3	-//-	eq. 6	25	4000
h	1	1	0	eq. 3	-//-	eq. 6	25	4000

(*) for this case all radicals were assumed to be surface active in accordance to Casella's et al. (2003) model

In figures 1 to 4, the homogenous nucleation model was altered. The propagation micelar nucleation model was considered in these figures with the parameters presented in Casella et al. (2003). It is noteworthy to say that Casella's et al. (2003) model considers equation (3) for the homogeneous nucleation and assumes e_2=e_3=e_4=1, e_5=0 and k_h modeled as in (4), but they assume that all radicals are surface active. The response to their model is presented in case g. One can see that cases a and b behave in a similar way, which may signify that as long as the radical of critical length exhibits only a slight solubility in the aqueous phase, its propagation, termination with any radical and capture by particles or micelles is not very relevant. Case f shows a very slight deviation in respect to case a. This is because the numerical difference between the models of equations (1) and (2) is very little. Differences in the latter equations should therefore be regarded in terms of the physical meaning of the equations. Case h is the same as case g except that only the radicals that become surface active can be absorbed. As expected significant deviations are observed. So now attention must be turned towards the huge discrepancies in the responses between cases a and h. It becomes evident that completely different behaviors are observed and that the dynamic response of the reactor provides insights into what happens, i.e. by monitoring not only conversion, but the diameter of polymer particles as well as taking some measurements of the concentration of radicals, one might better devise what mechanism should be taking place.

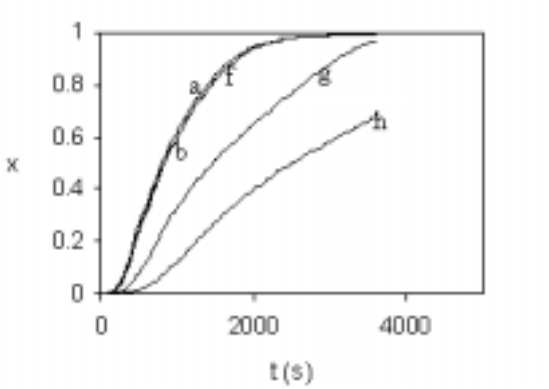

Fig. 1. Effect of the homogeneous nucleation model on the conversion.

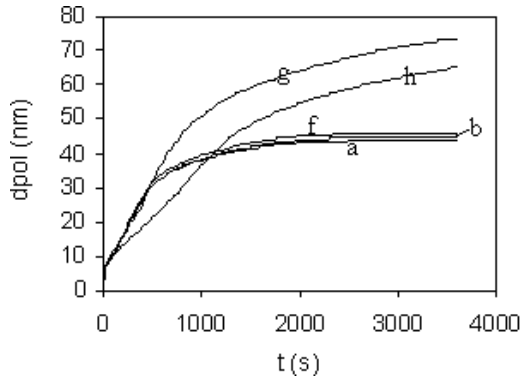

Fig. 2. Effect of the homogeneous nucleation model on the polymer diameter.

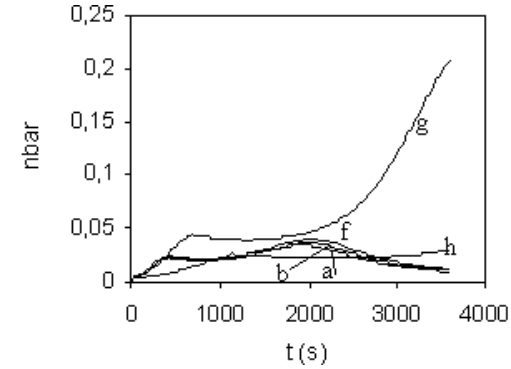

Fig. 3. Effect of the homogeneous nucleation model on means number of radicals in the particles.

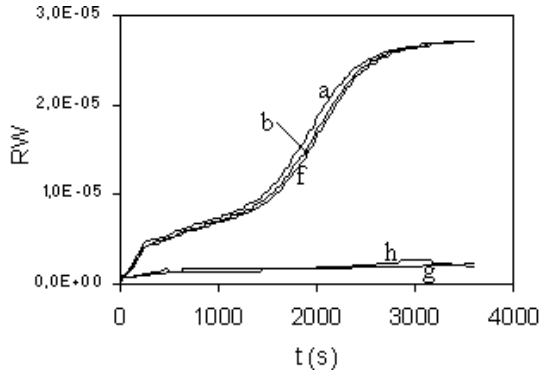

Fig. 4. Effect of the homogeneous nucleation model on the total concentration of radicals in the aqueous phase.

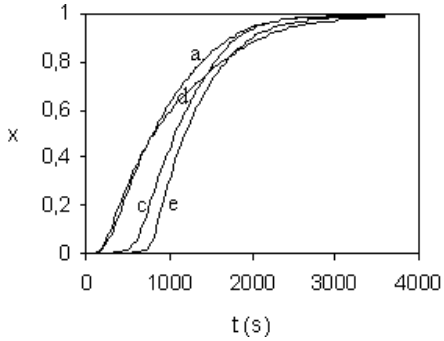

Fig. 5. Effect of the absorption model on the conversion.

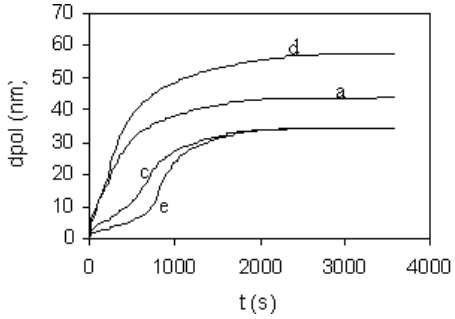

Fig. 6. Effect of the absorption model on the polymer diameter.

In figures 5 to 8 simulation responses are presented for different absorption models. As expected, great differences in the responses can be observed and one can clearly see how the process is dependent on the adjustment of the parameters $f_{abs,m}$ and $f_{abs,p}$. As already commented, the values in case b were simply taken from Casella et al. (2003). The parameters in cases c and e were calculated from the values presented in case a considering a particle diameter of about 10 nm and a micellar radius of 2.5 nm. The values in case d were taken arbitrary from several simulations performed in order to better adjust the parameters. One can see that it is not easy to adjust all curves. Moreover, the deviations to the base case, are very significant. So, it is clear that it is relevant that the real absorption model should be known. Figures 5 to 8 clearly show that the dynamic response is strongly affected by the choice of the model and that different models produce different dynamic responses for all four variables shown in figures 5 to 8. Lara (2005) has shown that reliable on-line monitoring of the diameter of polymer particles may be made by Raman and NIR spectrometry. Recently, the ESR technique has been routinely used to obtain information regarding the concentration of radicals. In spite of the fact that the latter technique is strongly dependent on the interpretation of the measured signals and relies on expensive equipment, not usually available in all research centers, one can see that measurements of the concentration of radicals will help to elucidate what absorption mechanism occurs. Moreover, measurements of the concentration of radicals and on-line monitoring of the polymer particle's diameter also help to clarify how homogenous nucleation may be modeled. We think that efforts towards the clarification of the absorption mechanism should be made as is being already

performed for the propagation and termination rate constants.

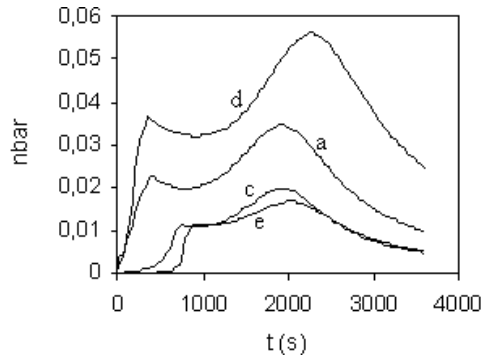

Fig. 7. Effect of the absorption model on means number of radicals in the particles.

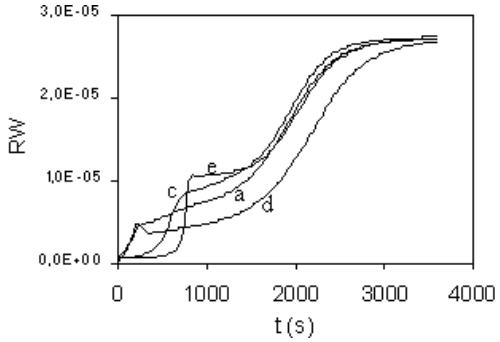

Fig. 8. Effect of the absorption model on the total concentration of radicals in the aqueous phase.

4. CONCLUDING REMARKS

In this paper we have shown that different modeling hypotheses regarding the fate of the radicals of critical length affect the dynamic behavior of the polymerization reactor. Moreover, we have stressed that is important to better understand the absorption mechanism, since the dynamic response of the reactor is strongly dependent on the adjustment of the absorption parameters. We have also shown that different models used to predict the homogenous nucleation rate also present large discrepancies. Hence, NIR, Raman and ESR measurements should be conducted in order to better clarify the really occurring mechanism.

ACKNOWLEDGMENT

Support from MACKPESQUISA under grant 1176 is gratefully acknowledged.

REFERENCES

Abad, C.; de La Cal, J.C.; Asua, J.M. (1994) Emulsion copolymerization in continuous loop reactors. *Chem. Engng. Sci.*, **49** (24B), p. 5025-5037

Araújo, P.H.H.; Giudici, R. Optimization of semicontinuous emulsion polymerization reactions by IDP procedure with variable time intervals. *Comput. Chem. Engng.*, v. 27, p. 1345-1360, 2003

Beuermann, S.; Buback, M.; Gilbert, R.G.; Hutchinson. R.A.; Klumperman, B.; Olaj, F.O.; Russel, G.T.; Schweer, J. Critically evaluated rate coefficients for free-radical polymerization, 2. Propagation rate coefficients for methyl methacrylate. *Macromol. Chem. Phys.*, v. 198, n.5, p. 1545-1560, 1997

Buback, M.; Egorov, M.; Gilbert, R.G.; Kaminsky, V.; Olaj, O.F.; Russel, G.T.; Vana, P.; Zifferer, G. Critically evaluated termination rate coefficients for free-radical polymerization, 1 - The current situation *Macromol. Chem. Phys.*, **203**, n. 18, p. 2570-2582, 2002

Casella, E.L.; Araujo, O.; Giudici, R. Mathematical modeling of batch emulsion copolymerization processes. *Polym. React. Engng.*, **11**, n.4, p. 869-910, 2003

Dubé, M.; Soares, J.B.P.; Penlidis, A.; Hamielec, A.E. Mathematical modeling of multicomponent chain-growth polymerization in batch, semibatch, and continous reactors: a review. *Ind. Eng. Chem. Res.*, **36**, p. 966-1015, 1997

Fitch, R.M. A personal history of chemically functional polymer colloids: formation, characterization and applications. *Polym. React. Engng.*, v. 11, n. 4, p. 911-954, 2003

Fitch, R.M., Tsai, C.H. (1971) Particle formation in polymer colloids. III: Prediction of the number of particles by a homogeneous nucleation theory. In Polymer Coloids; Fitch, R.M. editor, New York

Forcada, J. and Asua, J. (1990) Modeling of unseeded emulsion copolymerization of styrene and methyl methacrylate. *J. of Pol. Sci.*, **28**, 987-1009.

Gao, J.; Penlidis, A. Mathematical modeling and computer simulatior/database for emulsion polymerizations. *Prog. Polym Sci.*, v. 27, p. 403-535, 2002

Gilbert, R.G. *Emulsion Polymerization: a mechanistic approach*. Academic Press, 1995

Herrera-Ordonez, J.; Olayo, R.; Carro, S. The kinetics of emulsion polymerization: some controversial aspects. *J. of Macromol. Science – Polymers Reviews*, v. C44, n. 3, p. 207-230, 2004

Lara, D.C. (2005) *Monitoramento em linha da reação de co-polimerização de estireno e acrilato de butila em emulsão utilizndo a técnica de infravermelho próximo.* Master Dissertation. Universidade de São Paulo

Li, B.; Brooks, B. W. Modeling and Simulation of Semibatch Emulsion Polymerization. *J. Appl. Polym. Sci.* **40**, 1811, 1993

Liotta, V.; Sudol, E.D.; El-Aasser, M.S.; Georgakis, C. (1998) On-line monitoring, modeling, and model validation of semibatch emulsion polymerization in an automated reactor control facility. *J. of Pol. Sci.*, **36**, p. 1553-1571

Saldivar, E.; Dafniotis, P.; Ray, W.H. Mathematical modeling of emulsion copolymerizations reactors I. Model formulation and application to reactors operating with micellar nucleations. *J.*

Macromol. Sci. Rev. Macromol. Phys., C38, n.2, p. 207-325, 1998

Ray, W. H. (1972) On the mathematical modeling of polymerization reactors. *J. Macromol. Sci. Revs. Macromol. Chem.*, **CB(1)**, p. 1-56

Van Berkel, K.Y, Russel, G.T.; Gilbert, R.G. Molecular weight distributions and Chain-stopping events in the free-radical polymerization of methyl methacrylate. *Macromolecules*, v. 38, n. 8, p. 3214-3224, 2005

Zubitur, M.; Armitage, P.D.; Ben Amor, S.; Leiza, J.R.; Asua, J.M. Mathematical modeling of multimonomer (vynilic, divinylic, acidic) emulsion copolymerization systems. *Pol. React. Engng.*, v. 11, n. 4, p. 627-662, 2003

APPENDIX A

Here we present the other equations used to generate the simulation results presented in section 3. They are based on the following assumptions: (i) thermodynamic equilibrium is assumed to govern the partition of monomer between the aqueous and polymer phases and the term corresponding to the surface tension was neglected; (ii) the reactor is considered to be ideally mixed; (iii) the reacting medium is assumed to be monodisperse; (iv) additivity of volumes is assumed; (v) only radicals that become surface-active can be captured, i.e., only radicals with chains longer than Z-mer can be captured by either micelles or particles; (vi) emulsifier is added above the CMC; (vii) chemical initiation is used; (vii) particles may be formed by either micelar and homogeneous nucleation; (viii) monomeric radicals may be desorbed; (ix) the model of Li and Brooks (1993) was considered for predicting the average number of radicals inside the polymer particles.

$$\frac{dN_P}{dt} = k_{a,m} N_{mic} \left[R^{\bullet}\right]_w^{nu} + R_{\text{hom}} \tag{9}$$

where, $\left[R^{\bullet}\right]_w^{nu}$ is the concentration of all radicals that become surface active.

$$N_{mic} = \frac{\left(\left[E\right]_w - CMC\right) a_s V_w - A_p - A_d \dfrac{a_s}{a_{ms}}}{N_{av} 4\pi r_{mic}^2} \tag{10}$$

where, CMC=2.43 mol/m^3, a_s=3×10^{5}m^2/mol, A_d=0.

$$\frac{dN_M}{dt} = -N_P k_p \left[M\right]_P \bar{n} - k_p \left[M\right]_w \left[R^{\bullet}\right]_w^{tot} V_w \tag{11}$$

where, $k_p = 5.87\times10^4 e^{-3358.29/T}$.

$$\frac{dR_{1,w}^{\bullet}}{dt} = 2 f_{ef,I_r} k_I \left[I\right]_w V_w + k_{des} \bar{n} N_p - k_p \left[M\right]_w \left[R_1^{\bullet}\right]_w V_w - \\ - k_t^w V_w \left(\left[R_1^{\bullet}\right]_w \left[R^{\bullet}\right]_w^{tot} + \left[R_1^{\bullet}\right]_w^2\right) \tag{12}$$

where, $k_I = 1.8\times10^{17} e^{-17161.55/T}$ in SI units, $f_{ef,Ir}$=0.5, $k_t^w = 4.303\times10^6 e^{-1652.12/T}$ in SI units.

$$\frac{dR_{j,w}^{\bullet}}{dt} = k_p \left[R_{j-1}^{\bullet}\right]_w \left[M\right]_w V_w - k_p \left[R_j^{\bullet}\right]_w \left[M\right]_w V_w - \\ - k_t^w \left[R_j^{\bullet}\right]_w \left[R^{\bullet}\right]_w^{tot} V_w - k_t^w \left[R_j^{\bullet}\right]_w^2 V_w - \\ - e_2 \left(k_{a,m} N_{mic} \left[R_j^{\bullet}\right]_w + k_{a,p} N_P \left[R_j^{\bullet}\right]_w\right) \tag{13}$$

where, e_2=0 if $j < Z_{mer}$ and e_2=1 if $j \geq Z_{mer}$. For vynil acetate Z_{mer} = 8 and j_{cr} = 16.

$$k_{des} = k_{tsf} \left[M\right]_P \frac{k_o}{\beta k_o + k_p \left[M\right]_P} \tag{14}$$

where, $k_{tsf} = 693 e^{-4654.56/T}$, k_o is given in (17) and β in (18).

$$\frac{d\bar{n}}{dt} = k_{a,p} \left[R^{\bullet}\right]_w^{nu} - k_{des} \bar{n} - \gamma \frac{k_t^P}{N_{av} V_{1P}} \bar{n}^2 \tag{15}$$

$$\gamma = \frac{2\left(2k_{a,p}\left[R^{\bullet}\right]_w^{nu} + k_{des}\right)}{\left(2k_{a,p}\left[R^{\bullet}\right]_w^{nu} + k_{des}\right) + \dfrac{k_t^P}{N_{av} V_{1P}}} \tag{16}$$

$$k_o = \frac{\dfrac{12 \mathsf{A}_{M,w}}{K_M^P d_p^2}}{1 + \dfrac{2\mathsf{A}_{M,w}}{K_M^P \mathsf{A}_{M,p}}} \tag{17}$$

where, $\mathsf{A}_{M,w} = \mathsf{A}_{M,p} = 10^{-10}$ m^2/s.

$$\beta = \frac{k_p \left[M\right]_w + k_t^w \left[R^{\bullet}\right]_w^{tot_M}}{k_p \left[M\right]_w + k_t^w \left[R^{\bullet}\right]_w^{tot_M} + k_{a,p} \left[N_p\right]} \tag{18}$$

$$0 = 1 - \varphi_M^P + \ln \varphi_M^P + \psi_M \left(1 - \varphi_M^P\right)^2 - \ln \frac{\left[M\right]_w}{\left[M\right]_w^{sat}} \tag{19}$$

where, $\psi_M = 0.556$.

$$\left[M\right]_w = \frac{N_M - \varphi_M^P V_P \tilde{\rho}_M}{V_w} \tag{20}$$

$$V_p = \frac{\left(N_{M,o} - N_M\right) MM_M}{\varphi_p^P \rho_{pol}} \tag{18}$$

$$V_{1p} = \frac{V_P}{N_p N_{av}} \tag{19}$$

$$d_p = \sqrt[3]{\frac{6V_{1p}}{\pi}} \tag{20}$$

$$A_p = \pi d_p^2 N_p N_{av} \tag{21}$$

ADCHEM 2006

International Symposium on Advanced Control of Chemical Processes
Gramado, Brazil – April 2-5, 2006

A KINETIC MATHEMATICAL MODEL OF KRAFT PULPING PROCESS FOR CONTROL AND OPTIMIZATION APPLICATIONS

Natascha V. Polowski*, Eduardo C. Vasco de Toledo,
Rubens M. Filho

Laboratory of Optimization, Design and Advanced Control (LOPCA), Faculty of Chemical Engineering: State University of Campinas (Unicamp), P. O. Box 6066, 13081-970, Campinas, SP, Brasil, e-mail: polowski@terra.com.br, Phone: +55 – 19- 37883971, FAX: +55 – 19- 37883965

Abstract: Kraft wood pulping is the predominant process used in the pulp and paper industry for its versatility and insensitivity to variations of wood supply. In this work, a deterministic model has been developed for a Kraft Pulping Process of Eucalyptus by combining intrinsic kinetic equations (Lignin, Carbohydrates) and it is used to investigate the effects of process conditions on the extent of delignification. The aim of this work is to develop a mathematical model which at some time is able to represent the main phenomena taking place in the process and suitable to be used in control and optimization applications.

Keywords: Kraft pulping, kinetic equation, deterministic model and mass transfer equation.

1. INTRODUCTION

Chemical pulping includes all methods of pulp manufacture in which materials containing cellulose fibers are treated with aqueous alkaline or acidic solutions. The aim of chemical pulping is to remove enough lignin so that the fibers are free and give then the required characteristics at the lowest possible cost.

Two processes dominate chemical pulping: the Sulfate and the Sulfite process (Lemmetti et al., 1998). The Sulfate process is also known as Kraft Pulping where it is complex process which involves mass transfer of cooking chemical into wood structure, complex heterogeneous chemical reactions between wood components and the cooking chemicals. The Sulfite pulping derives its name from the use of a bissulfite solution as the delignifying medium. The cation used is usually calcium, magnesium, sodium, or ammonium. Sulfite pulping has also advantages over the Kraft process: easier pulp bleaching, higher carbohydrate yields, and the possibility of producing specialty pulps with high cellulose contents (Gullichsen, J.; Fogelbolm, C. J., 2000).

This work concentrates only on the Kraft process in which pulping liquor, mainly solution of sodium hydroxide (NaOH) and sodium sulfide (Na_2S), are used at controlled conditions to remove wood lignin. Wood chips are subjected to digestion in the pulping liquor at an elevated pressure and temperature (about 170^0C) in a pressure vessel (digester) to release cellulose fibers (Zhu et al., 2002).

The digestion process can be either batch or continuous. In batch cooking a pressured reactor is filled with chips and cooking liquor. The contents are heated under pressure according to a specified temperature-time program (H- Factor) and after that the digester is emptied.

Basically, there are two types of batch digesters to examine: those with direct steam heating and those with indirect steam heating. The second type is equipped with forced liquor circulation and a heat exchange in the circulation line (Yliniemi et al. (1995). In continuous cooking chips and cooking liquor are fed into the top of the digester in a co-current flow. The digester is a large, vertical pressurized tube. The chip column is heated up by various circulation systems as it moves downwards.

The cooked and partly washed pulp is fed out at the bottom in a uniform flow. In both cases, the cooking process is basically the same. The chips are impregnated with cooking liquor, heated under pressure and held at the certain temperature for some time. Then pressure and temperature are lowered and the cooked chips are blown or washed out of the digester. The chemical reactions which dissolve the

lignin take place mainly when the digester is at maximum pressure and fibers are released. The pulp is then washed, screened, cleaned and dried or pumped over to the paper mill (Lemmetti et al., 1998). The product of the digesting process is cellulose fibers, or pulp, which is used to make paper products (Al-Awami et al., 1999). Several different types of pressure vessel have been used for batch cooking over the years, including stationary horizontal and spherical configurations and rotating vertical digesters. Some factors favoring batch digesters may be pointed out: more reliable operation, greater operating flexibility (ability to change grades), ability to cook softwood and hardwood concurrently, easy to start-up and shut-down; and more efficient turpentine recovery. A simplified scheme is shown in Figure 01.

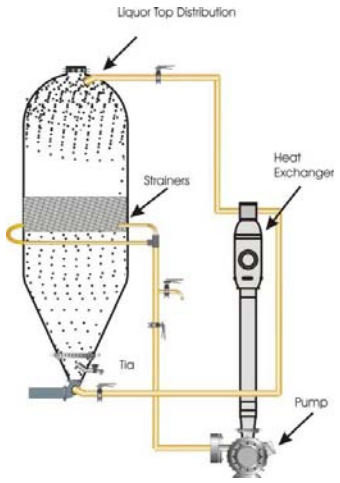

Figure 01: Batch Digester with Indirect Heating

The objective of this work is to present a deterministic model for batch pulp digester taking into account the main phenomena taking place in the process. It is considered that the reactions occur for lignin, hemicellulose, cellulose and extractive reactions with time.

An additional contribution of this paper is to develop a deterministic model for the *Eucalyptus* as a feedstock of cellulose. Most of papers in open literature deal with chips of pines but there exists an enormous advantage to use Eucalyptus since it grows up very much quicker and it is cheaper. Both woods have quite different structure in terms of fiber length so that an extensive analysis has to be made for the *Eucalyptus* in this work.

2. MODEL DESCRIPTION

In the digester, reaction start when chips are at the cooking temperature. The active chemicals in the cooking liquor react with lignin in chips and convert it chemically into compound that dissolves in the cooking liquor.

Lignin is the bonding material in chips that holds individual fibers together. Lignin is the "glue" of wood and it is a very complex three dimensional network polymer with hydroxyl phenyl propane groups as the basic units (Gullichsen et al., 2000). After dissolving the lignin, fibers are easily separated into the mass that is leaving the digester as pulp. Unfortunately the chemicals also react with fibrous material and break down the molecular bonds of them. These reactions have to be avoided as much as possible because they lead to losses in fiber yield and decrease the strength of pulp. Therefore cooking conditions that prefer lignin removal with the lower effect in the fibers should be preferred. Cooking models, with different approaches, can be found in literature.

One of the earliest kinetic models was developed by Vroom (1957), who used an Arrhenius type expression for the reaction rate temperature dependence to derive the "H-factor". H- Factor is regularly used in controlling the reaction end-point in batch digesting. It describes the combined effect of reaction temperature and reaction time. In practice it means that when longer reaction time is available the same cooking result can be obtained with a lower temperature. Equation (1) describes the delignification of Kraft pulping: $\frac{dL}{dt} = kCL$ (1) where L is the lignin content of chips, C is the effective alkali concentration of the liquor in the chips, k is the temperature dependent rate constant and t is the cooking time. The temperature dependency of the reaction rate constant k is usually presented by the means of Arrhenius equation $k = k_0 e^{B - E/RT}$ (2), where E is the activation energy, R is the universal gas constant, T is the absolute temperature and k_0 and B are constant. The parameters depend on wood species, cooking stage, etc. H-factor describes the joint effect of time and temperature and it is usually given as following integral: $H = \int_{t_0}^{t} k_r \, dt$ (3), where t_0 is the initial time for calculation, t is the actual time and kr is the relative reaction rate coefficient as defined bay the following equation: $k_r = e^{43{,}2 - 16113/T}$ (4), where T is the absolute temperature.

For the dissolution of high-reactivity lignin, cellulose, hemicelluloses and extractives the following kinetic equation will be used for each:

$$-\frac{dW}{dt} = \left[(k1[OH]^a + k2[OH]^b[HS]^c)(W - W\infty)\right]$$

(5), where W is the wood component concentration; k1, k2 are rate constants that are correlated as a function of temperature using the Arrhenius equation; W_∞ is the wood component after infinite time; a,b,c are the kinetic orders; $[OH^-]$ and $[HS^-]$ are

the OH- and HS^- concentrations, respectively and t is time.

The deterministic model equations can be written as follows:

- Lignin

$$\frac{dL_1}{dt} = k_{L_1} \exp(\frac{E_{L_1}}{RT})[OH]^a [HS]^b L_1 \quad (6)$$

$$\frac{dL_2}{dt} = k_{L_2} \exp(\frac{E_{L_2}}{RT})[OH]^a [HS]^b L_2 \quad (7)$$

$$\frac{dL}{dt} = \frac{dL_1}{dt} + \frac{dL_2}{dt} \quad (8)$$

- Cellulose

$$\frac{dC_1}{dt} = k_{C_1} \exp(\frac{E_{C_1}}{RT})[OH]^a C_1 \quad (9)$$

$$\frac{dC_2}{dt} = k_{C_2} \exp(\frac{E_{C_2}}{RT})[OH]^a C_2 \quad (10)$$

$$\frac{dC}{dt} = \frac{dC_1}{dt} + \frac{dC_2}{dt} \quad (11)$$

- Hemicelluloses

$$\frac{dH_1}{dt} = k_{H_1} \exp(\frac{E_{H_1}}{RT})[OH]^a H_1 \quad (12)$$

$$\frac{dH_2}{dt} = k_{H_2} \exp(\frac{E_{H_2}}{RT})[OH]^a H_2 \quad (13)$$

$$\frac{dH}{dt} = \frac{dH_1}{dt} + \frac{dH_2}{dt} \quad (14)$$

- Extractives

$$\frac{dE}{dt} = -0.6E \quad (15)$$

- Carbohydrates

$$\frac{dCT}{dt} = \left[\left(\frac{dC_1}{dt} + \frac{dC_2}{dt}\right) + \left(\frac{dH_1}{dt} + \frac{dH_2}{dt}\right)\right] \quad (16)$$

- Diffusion Coefficient

$$D = 60\times10^{-4}\sqrt{T}\exp(\frac{-22.3\times10^3}{RT})\times(1.24\times10^{-2} - 1.12\times10^{-4}\times[L+H+C+E] \quad (17)$$

- Hydroxide

$$\frac{\partial OH}{\partial t} = \frac{1}{X^2}\frac{\partial}{\partial x}\left(D\frac{\partial OH}{\partial x}\right) + \quad (18)$$
$$+\frac{\rho}{0.1\varepsilon}\left[3.2x10^{-3}\frac{dL}{dt} + 6.1x10^{-3}\left(\frac{dH}{dt} + \frac{dC}{dt}\right) + 7.0x10^{-3}\frac{dE}{dt}\right]$$

$$\frac{\partial HS}{\partial t} = \frac{1}{X^2}\frac{\partial}{\partial x}\left(D\frac{\partial HS}{\partial x}\right) \quad (19)$$

In the deterministic model the following considerations are made:

- The wood chips are treated as symmetrical plane sheets with only one important direction - the chip thickness (the chips are cut in such way that the thickness is the representative direction);
- The chips are fully impregnated with liquor before the heating period starts. This is a reasonable assumption, since the chips are exposed to the liquor for a long period prior to cooking;
- Heat transfer to and inside the wood chip is instantaneous and the heats of reaction are negligible;
- Mass transfer resistance between the bulk liquor and wood chip is negligible (no film theory is considered which is also reasonable due to agitation caused by the liquor forced flow along the vessel);
- The reactions are irreversible and the reaction products do not interfere in the pulping reactions.
- The concentration of hydroxide ions is equal to the effective alkali, the sum of the sodium hydroxide and half the sodium sulfide;
- The rate of sulfide ions diffusion is the same as for hydroxide ions.

The model has the following boundary conditions:

- The concentration gradient of each compound is zero at the center of the wood chip (symmetry condition);
- The concentrations of each compound at edge of the chip are equal to the concentrations in the bulk liquor surrounding the chip; the concentrations of hydroxide and hydrogen sulfide in bulk liquor are obtained by mass balances on the bulk liquor;

Some alternative models may be developed using hybrid approach, combining deterministic model and neural networks models as proposed by Aguiar and Maciel Filho (1998), but in any case they require a good deterministic description to be valid over a large operational range.

3. SOLUTION PROCEDURE

The model is a system of differential partial equations with the concentration of hydroxide varying with time. Note that the concentrations of lignin, hemicelluloses and cellulose impact the amount of hydroxide.

For lignin, it was assumed that the kinetic expression was the same as found by Mortha et al. (1992) and there are three types of lignin in proportions of 25.0, 73.8, 1.2 per cent. The third type

of lignin was estimated from the extended delignification results of Irvine et al. (1996), which showed that there was a small fraction of lignin that was no reactive. The rate of reaction of this lignin fraction was effectively zero. The proportions of the two types of hemicelluloses were calculated to be 36 and 64 per cent. For cellulose, the two reactions probably correspond to the different types of reaction - peeling and cleavage, and the proportions were calculated to be 17 and 83 per cent. In most models, the extractives are assumed to react instantaneously but the inclusion of a rate equation is more realistic and does not make the model much more difficult to solve. Available data on the rate of removal of extractives has been used in this study to calculate the rate constant, assuming that the reaction is first order. It was not possible to determine if the reaction rate depends on temperature or chemical concentration because it is a fast reaction compared to the reactions of other wood components. Only alkali diffusion was considered, and the same diffusivity coefficient is assumed for both sodium hydroxide and sulfide. In this model a proper energy balance was not developed. Flow characteristics, channeling, different wood compositions and other phenomena were not considered.

The equations describing the diffusion phenomena lead to a system of nonlinear partial differential equations, which are conveniently transformed by the orthogonal collocation method into a system of ordinary differential equation through the discretization of the spatial variable through the concept of the method of lines. The equations are integrated in respect to time by a LSODE integrator since stiffiness may occur.

To solve the model equations, the pulping conditions need to be specified along with various properties of wood. Some inputs terms are specified in Table 1:

Table 1: Pulping Conditions

Process Variable	Input Values
Thickness of Wood Chip (m)	0.003
Liquor to Wood Ratio (l/kg)	4.0
Initial Temperature (^{0}C)	80
Cooking Temperature (^{0}C)	170
Density (kg/dm^3)	0.6
Porosity	0.59
Heating time (min)	90
Cooking time (min)	180

4. RESULTS AND DISCUSSION

Wood chemistry and reaction mechanisms are not fully understood. In these studies the curves of lignin content and the carbohydrate (cellulose and hemicelluloses) content vs. time are presented in Figures 02 and 03. All the curves are simulated. The mathematical model was validated with experimental data from an industrial paper mill using *Eucalyptus* as feedstock. It use three different initials temperature (Tfo), in °C.

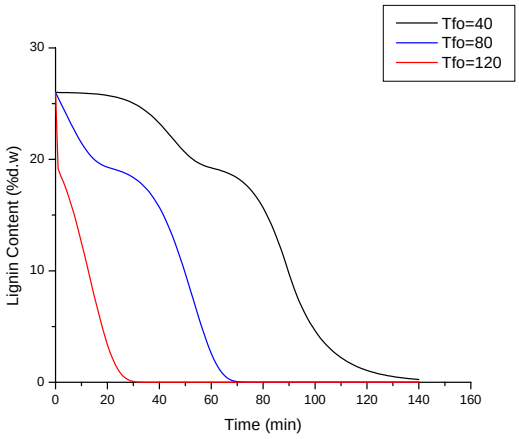

Figure 02: Lignin content vs. time

Lignin reactions in Kraft pulping can be divided in three phases: initial, bulk and residual delignification. Initial delignification occurs during the impregnation phase. About 20% of the total amount of lignin is dissolved in this stage. Another 70% of lignin is removed during bulk delignification when the cooking temperature is raised above 140^{0}C. The rate of bulk delignification depends on the alkali and hydrosulfide concentration as well as on the temperature in the digester. The final residual delignification proceeds very slowly.

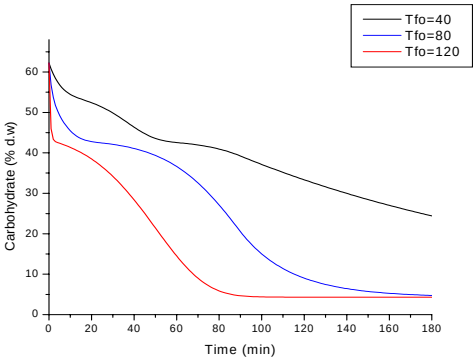

Figure 03: Carbohydrates vs. Time

Figure 03 shows the Carbohydrate reactions in Kraft pulping for the three phases (initial, bulk and residual) in three initials temperature (Tfo) in °C. During Kraft pulping not only delignification reactions occur but carbohydrate degradation also takes place. Carbohydrate degradation is not wanted because it results in pulp yield decrease and fiber strength loss during the pulping process.

In Figure 04, carbohydrate concentration is plotted against the lignin concentration.

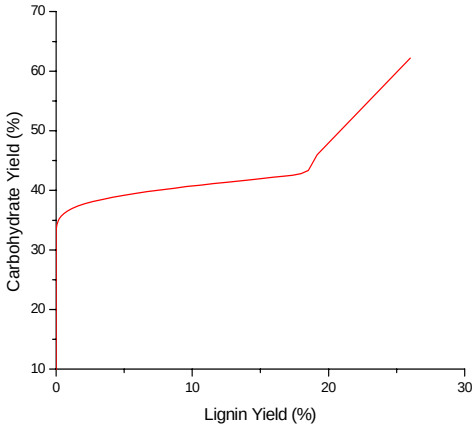

Figure 04: Yield of Carbohydrate material as a function of lignin yield for different parts of Eucalyptus wood

The carbohydrate removal is proportional to the rate of lignin removal. This is supported by the type of behavior shown in Figure 04. The three phases can be identified using plots of carbohydrate as a function of lignin. The initial phase lasts until the lignin concentration has decreased to about 18 per cent. The bulk phase continues until the lignin concentration has been reduced to about 3 per cent and this is followed by the residual phase.
Similar behavior for carbohydrate concentration can be found in Virkola (1983), in Figure 05.

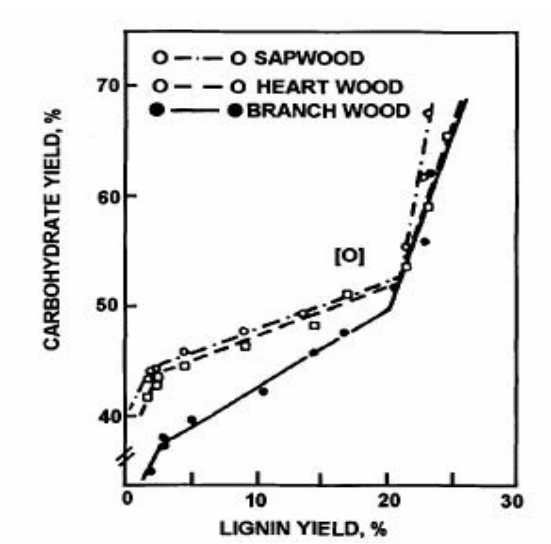

Figure 05: Yield of Carbohydrate as a function of lignin yield for different part of Pine wood (Virkola, 1983)

5. CONCLUSION

A deterministic model to describe Kraft pulping of Eucalypts has been developed. Most of the published papers deal with Kraft pulping of *Pines*, but the economic advantage in using *Eucalyptus* and the changes in digester behavior for both cellulose feedstocks has to be accounted for. The developed model was able to represent well the process theory. The model is used to investigate the effects of process conditions on the extent of delignification and it is a valuable tool to investigate the performance of control and optimization strategies...

REFERENCES

Aguiar, H.C. and Maciel Filho, R. (1997). Modelling and Optimization of Pulp and Paper Processes Using Neural Networks. *ESCAPE 8*, Bruges, Belgium.

Al-awami, L.; Sidrak, Y.; Bettayeb, M. (1999). Classical and Dynamic Matrix Control of Kamyr Digesters- A comparative study. *Ind. Eng. Chem. Res*. 38, 3950-3956.

Gullichsen, J.; Fogelbolm, C. J. (2000). Chemical Pulping, Papermaking Science and Technology, Book 6A, Tappi Press.

Yliniemi, L.; Alaimo, L.; Koskinen, J. (1995). Development and Tunin of a Fuzzy Controller for a Rotary Dryer. December.

Irvine, G., Clark, N.; Recupero, C., (1996). Extended Delignification of mature and Plantation Eucalypt Wood. Part I: The Principles of Extended Delignification. Proc. 48th Appita Conference, 49(4), 251 – 257.

Lemmetti, A.; Leiviska, K.; Sutinen, R. (1998). Kappa Number Prediction Based on Cooking Liquor Measurements. Control Engineering Laboratory, University of OULU, Report A No 5.

Mortha, G. Sarkanen, K. and Gustafson, (1992). R., *Tappi*, **75**(11), 99.

Virkola, N. E. (1983). Pauumassan valmistus. Suomen Paperi-insinoorien yhdistyksen oppi-ja kasikirija, Toinen uudistettu pianos.

Zhu, j. y.; Chai, X. S.; Pan, X. J.; Luo, Q.; Li, J. (2002). Quantification and Reduction of Organic Sulfur Compound Formation in a Commercial Word Pulping Process, Environ, Sci. Technol., 36, 2269-2272.

ADCHEM 2006

International Symposium on Advanced Control of Chemical Processes
Gramado, Brazil – April 2-5, 2006

DYNAMIC OPTIMIZATION OF MOLECULAR WEIGHT DISTRIBUTION IN BATCH POLYMERIZATION REACTORS

Krallis Apostolos; Meimaroglou Dimitris; Saliakas Vassilis; Chatzidoukas Christos; Kiparissides Costas

Department of Chemical Engineering and Chemical Process Engineering Research Institute, Aristotle University of Thessaloniki, P.O. Box 472, 54006 Thessaloniki, Greece

Abstract: This paper applies the orthogonal collocation on finite elements (OCFE) method and the fixed pivot (FP) technique for the prediction of the molecular weight distribution (MWD) for linear free-radical polymerization systems. It is shown that for linear polymers, the two methods result in similar molecular weight distributions for a bimodal MWD. An optimal operating policy that ensures the satisfaction of desired polymer quality specifications and process economics regulations is derived employing a performance index which penalizes the deviations of the MWD from specific desired values. Finally, the optimal trajectories were applied to a free-radical MMA batch pilot-scale polymerization reactor.

Keywords : optimization problems, optimal trajectory, distributions, finite method numerical algorithm, polymerization, cascade control

1. INTRODUCTION

Commonly employed polymer product quality indicators (e.g., mechanical strength, tear strength, rheological properties and so forth) are directly or indirectly linked with molecular structural properties of the polymer chains (e.g., molecular weight distribution (MWD), long-chain branching (LCD), copolymer composition distribution (CCD), chain sequence length distribution (CSD), and so forth). Hence, the ability of a model to predict accurately the molecular properties of polymers in a polymerization reactor is of profound interest to the polymer industry.

In the past a number of mathematical approaches have been proposed to describe the molecular weight developments in free-radical polymerization reactions. Crowley and Choi, (1997a) and Yoon, (1998), developed a kinetic lumping method in which the quasi steady state approximation (QSSA) for the "live" polymer chains holds true and the polymer chains population is divided into a specified number of "chain lump" domains where the resulting balance equations are solved numerically. Polynomial expansion methods of the MWD require the calculation of high-order moments and may lead to slow convergence (Tobita and Ito, 1993). Discrete weighted Galerkin formulation (Deuflhard and Wulkow, 1989; Wulkow, 1992), even though are computationally demanding, provide a useful tool for the prediction of the MWD in complex polymerization systems. However, the approximation of the infinite summation terms (e.g., resulting from termination by combination reactions), requires special treatment. The use of global orthogonal collocation methods for the prediction of the MWD in free-radical polymerization systems see (Nele et. al., 1999) was partially successful, because a single interpolation polynomial was employed for the entire domain. As a result, prior knowledge about the type of the approximated distribution is required. Kiparissides et. al., (2002), used the OCFE method assuming that the pseudo-steady-state approximation for "live" polymer chains of length "n" holds true, in order to calculate the MWD.

In operating a batch free-radical polymerization process, a typical task involves manipulation of reactant concentrations, reactor temperature and other variables in order to achieve a desired objective which can usually be expressed in terms of conversion, molecular weight distribution, polymerization time and so forth.

In the past, much attention has been given on control basically of the averages of the MWD (Ponnuswammy et. al., 1987; Kim and Choi, 1991; Kozub and MacGregor, 1992). However, for broad or bimodal distributions, the calculation of the number and weight average molecular weights does not uniquely characterize the MWD of the polymer (Ray, 1972).
Crowley and Choi, (1997b), applied a common method of controlling the MWD in batch free-radical polymerization reactors, by predetermining the optimal control variable trajectories, and then attempting to execute these trajectories during the batch. Clarke-Pringle and MacGregor, (1998) developed a batch-to-batch optimization methodology for producing a desired MWD using an approximate model.

In the present study the OCFE and FP methods are used to calculate the MWD for linear polymers. The rate equations for the "live" and "dead" polymer chains of length "n", derived from the mass balances, are solved

at specific discrete points, while no QSSA for the "live" polymer chains is assumed. Additionally the summation terms resulting from termination by combination reactions, are taken into account in both methods. A detailed polymerization model is used in conjunction with the FP and the OCFE methods to determine the MWD. Simulation results of the MWD calculations confirmed the validity and accuracy of both methods.

Finally, a model-based dynamic optimization approach was applied to optimally produce a specific desired MWD, calculated by the OCFE method. The calculation of the optimal trajectory of the reactor temperature set points was handled using sequential quadratic programming (SQP). The resulted model-based optimal set point sequence was subsequently imposed on the experimental pilot-scale reactor system which operates at our laboratory. The mathematical model closely describes the reactor unit, which consists of a well-mixed jacketed vessel. Stirring is provided by a flat-blade turbine, aided by four removable blade baffles. The reaction temperature is controlled by a cascade controller which manipulates the flows of two streams (e.g., a hot and a cold) entering the reactor jacket. The polymerization was highly exothermic and exhibited a strong acceleration in the polymerization rate due to the gel effect (e.g., the termination rate constant decreased with conversion).

2. FREE-RADICAL POLYMERIZATION MODEL

The kinetic scheme for the free-radical suspension polymerization of methyl methacrylate (MMA) is shown in Table 1. In this scheme the termination reactions include the combination and the disproportionation mechanisms.

Table 1: Kinetic mechanism for free-radical MMA polymerization.

Initiation:
$I \xrightarrow{k_d} 2PR^{\bullet}$
$PR^{\bullet} + M \xrightarrow{k_I} P_1^{\bullet}$
Propagation:
$P_n^{\bullet} + M \xrightarrow{k_p} P_{n+1}^{\bullet}$
Chain transfer to monomer:
$P_n^{\bullet} + M \xrightarrow{k_f} D_n + R_1^{\bullet}$
Termination by combination:
$P_n^{\bullet} + P_m^{\bullet} \xrightarrow{k_{tc}} D_{n+m}$
Termination by disproportionation
$P_n^{\bullet} + P_m^{\bullet} \xrightarrow{k_{td}} D_n + D_m$

To account for the effect of the diffusion-controlled phenomenon on the termination and propagation rate constants, the model of Chiu et. al. (1983), was employed. Given the above detailed kinetic mechanism, the following balances for the "live" and "dead" polymer chains of chain length "n" ($n \in [1,660000]$) are obtained:

$$\frac{dP_n}{dt} = 2 f_i k_d IV\delta(n-1) + kf\, M \sum_{m=1}^{\infty} P_m \delta(n-1) + k_p P_{n-1} M - k_p M P_n - kf\, M P_n - k_{td} P_n \sum_{m=1}^{\infty} P_m\left(\frac{1}{V}\right) - k_{tc} P_n \sum_{m=1}^{\infty} P_m\left(\frac{1}{V}\right) \quad (1)$$

$$\frac{dD_n}{dt} = kf\, M P_n + k_{td} P_n \sum_{m=1}^{\infty} P_m\left(\frac{1}{V}\right) + \frac{1}{2} k_{tc} \sum_{m=1}^{n-1} P_{n-m} P_m\left(\frac{1}{V}\right) \quad (2)$$

3. METHOD OF MOMENTS

The method of moments is based on the statistical representation of the average molecular properties of the polymer (e.g., number average, Mn, and weight average, Mw, molecular weights) in terms of the leading moments of the number chain length distributions (NCLDs) of "live" and "dead" polymer chains, defined by the following equations:

$$\lambda_k = \sum_{n=1}^{\infty} n^k R_n, \qquad \mu_k = \sum_{n=1}^{\infty} n^k P_n \quad , \quad k = 0, 1, 2 \quad (3)$$

The relevant rate functions for the moments of the NCLDs of the "live" and "dead" polymer chains can be obtained by multiplying each term of eqs (1)-(2) by n^k and summing up the resulting expressions over the total degree of polymerization, N∞. The resulting rate equations for the leading moments are see (Pladis et al., 1998):

$$\frac{d\lambda_k}{dt} = k_I [R^{\bullet}][M] + k_{fm}[M]\lambda_0 + k_p[M]\sum_{i=0}^{k}\binom{k}{i}\lambda_i - k_p[M]\lambda_k - k_{fm}[M]\lambda_k - k_t\lambda_0\lambda_k \quad (4)$$

$$\frac{d\mu_k}{dt} = k_{fm}[M]\lambda_k + \frac{1}{2}k_{tc}\sum_{i=0}^{k}\binom{k}{i}\lambda_i\lambda_{k-i} + k_{td}\lambda_0\lambda_k \quad (5)$$

where $[R^{\bullet}]$ and $[M]$ denote concentrations of the radicals and monomer, respectively. Usually, one needs to know the leading moments (i.e., λ_0, λ_1, λ_2 and μ_0, μ_1, μ_2) of the NCLDs of "live" and "dead" polymer chains to calculate the values of M_n and M_w.

4. FIXED PIVOT TECHNIQUE

The inherent limitations of the numerical solutions resulting from the discretization of the chain length, can be avoided in the more general formulations (i.e., fixed and moving pivot techniques) of Kumar and Ramkrishna (1996) and (1997). The last methods guarantee the correct calculation of any two moments of the distribution and are applicable to any type of discretization of the chain length.

The fixed pivot technique is a very efficient method for the calculation of the weight chain length distribution (WCLD). It assumes that the overall polymer chain population can be assigned to selected discrete lengths. Specific reaction steps (i.e., termination and propagation) leading to the formation of polymer chains other than the representative ones, are incorporated in the set of discrete equations in such a way that selected properties of the WCLD (i.e., total number, mass, etc.) corresponding to any two moments of the WCLD, are exactly preserved.

For the preservation of the zero and first moments of the WCLD, the assigned polymer chain fractions to the discrete lengths n_I and n_I+1 will be given by the following equation:

$$n_t = \begin{cases} \dfrac{n_{i+1}-n}{n_{i+1}-n_i} & n_i \le n \le n_{i+1} \\ \dfrac{n-n_{i-1}}{n_i-n_{i-1}} & n_{i-1} \le n \le n_i \end{cases} \quad (6)$$

5. ORTHOGONAL COLLOCATION ON FINITE ELEMENTS

A key characteristic of the OCFE method is the treatment of the discrete polymer chain length domain as a continuous one. Hence, the concentrations of "live" and "dead" polymer chains are handled as continuous variables. Accordingly, the chain length domain is divided into a number of finite elements, NE, with element boundaries at the points: ζ_0=1, ζ_1, ζ_2,…, ζ_{NE-1}, $\zeta_{NE} = S_f$, where S_f is the final degree of polymerization [S_f = 660000]. For each element a number of n interior collocation points, [s1, s2,…, sn] are specified. The concentrations of the "live" and "dead" polymer chains are then approximated by continuous low-order polynomial functions within each finite element. In the present study, Lagrange interpolation polynomials were used to approximate the concentrations of the "live" and "dead" polymer chains:

$$\widetilde{R}(s) = \sum_{i=0}^{n} W_{i,j}^{R}(s)\,\widetilde{R}(s_{i,j}) \qquad \zeta_{j-1} \le s \le \zeta_j \quad j = 1,\ldots,NE \quad (7)$$

$$\widetilde{P}(s) = \sum_{i=1}^{n} W_{i,j}^{P}(s)\,\widetilde{P}(s_{i,j}) \qquad \zeta_{j-1} \le s \le \zeta_j \quad j = 1,\ldots,NE \quad (8)$$

The tilde denotes approximation variables. The functions, $W_{i,j}^{R}(s)$ and $W_{i,j}^{P}(s)$ are Lagrange interpolation polynomials of order n+1 and n, respectively, given by the expressions:

$$W_{i,j}^{R}(s) = \prod_{\substack{k=0 \\ k\neq i}}^{n} \frac{s - s_{k,j}}{s_{i,j} - s_{k,j}} \qquad \zeta_{j-1} \le s \le \zeta_j \quad (9)$$

$$i = 0,\ldots,n \quad j = 1,\ldots,NE$$

$$W_{i,j}^{P}(s) = \prod_{\substack{k=1 \\ k\neq i}}^{n} \frac{s - s_{k,j}}{s_{i,j} - s_{k,j}} \qquad \zeta_{j-1} \le s \le \zeta_j \quad (10)$$

$$i = 1,\ldots,n \quad j = 1,\ldots,NE$$

The Lagrange polynomials $W_{i,j}^{R}(s)$ and $W_{i,j}^{P}(s)$ are equal to zero at the collocation points s_I,j, for k≠i and equal to unity for k=i. To take into account the concentration of "live" polymer chains at chain length x=1, the left boundary point of the first element was included as an interpolation point.

A set of residual equations was then derived, by substituting eqs (7)-(8) into the material balance equations. The main requirement of the OCFE formulation forces the residual balances to vanish at the selected collocation points, $s_{i,j}$.

The selection of the finite element boundaries controls the density of the collocation points in the overall chain length domain. Thus a high density of collocation points is usually required in chain length regions, where steep changes in the concentrations of "live" and "dead" polymer chains are foreseen. Therefore, the domain partition into finite elements can be performed either based on previous knowledge about the shape and characteristics of the weight chain length distribution (e.g., steep fronts and flat profiles in the WCLD) or based on the satisfaction of a certain error criterion (e.g., equidistribution of error throughout the domain). Extensive simulations showed that low-order interpolation polynomials predict the overall WCLD more accurately, compared to high-order polynomials for the same total number of collocation points. This was attributed to the oscillatory behavior of the high-order Langrange polynomials.

6. DYNAMIC OPTIMIZATION OF THE MWD

For the dynamic optimization of the molecular weight distribution of the free-radical MMA polymerization, the reactor temperature was chosen as manipulated variable, because it is a key process condition that has the greatest direct impact on the MWD. The optimal reactor temperature sequence can be used as temperature set points in order to control the MWD. A cascade control system was employed to drive the actual reactor temperature as close as possible to the optimal set point trajectory. The objective is to minimize the time required to produce a polymer with desired molecular properties. Thus, the objective function to be minimized, can be defined in terms of the final MWD and polymerization time:

$$\min J(T) = \sum_{i=1}^{N_d} w_i \left(\frac{MWD_i - MWD_{di}}{MWD_{di}} \right)^2 + w_{Nd+1}\, t_f \quad (11)$$

$$\text{subject to single bound constraints: } \quad l < T_i < u$$

where, MWD_{di} are the desired values of the MWD, N_d is the number of the desired values of the MWD, t_f is the final polymerization time and w_i are appropriate weights. l and u represent the lower and upper single bound constraints. The desired values of the MWD lie within a feasible domain of MWDs accounting for the capabilities of both the reactor control and heating systems. T stands for the vector of the sequence of the reactor temperature during the polymerization. Each element of the vector T represents a constant manipulated control variable during a specific time interval. The number of the elements j of the vector T is equal to the ratio of the final polymerization time over the number of time intervals selected by the user. All the time intervals have equal length. The objective function is minimized using NPSOL. The method of NPSOL is a sequential quadratic programming (SQP) method.

7. RESULTS

The predictive capabilities of the OCFE method and the FP technique on the MWD of linear polymers were

tested by direct comparison of the two methods for different values of monomer conversion see (Fig. 1). In the reported runs, the initiator (AIBN), monomer and water initial masses were 4 gr, 1.070 kg and 4.8 kg respectively. The reactor temperature was kept constant at 335 K during the whole polymerization horizon (isothermal operation). The continuous lines represent the simulation results derived from the application of the OCFE method while the discrete points represent the results from the FP technique. It is apparent that an excellent agreement between the two methods exists along the whole range of monomer conversion. Notice that both methods are capable to predict bimodal distributions.

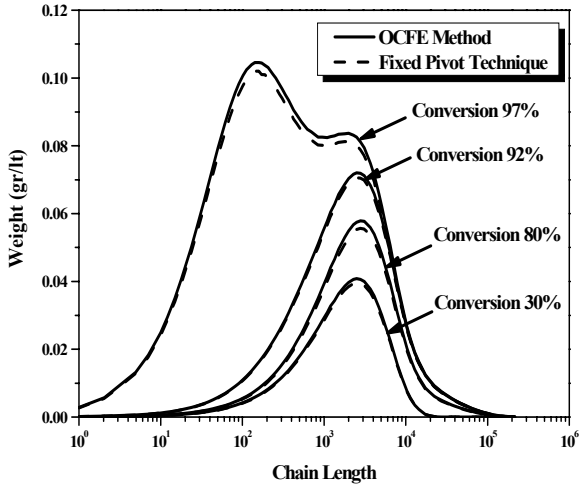

Fig. 1. Comparison of OCFE method and FP technique on the MWD at different monomer conversions

The reliability of the results derived from the application of the OCFE method and the FP technique was further tested by a direct comparison of the zero, first and second moments of the "live" and "dead" polymer chains derived from the predicted MWDs with the analogous ones derived from the application of the method of moments (Figures 2 and 3). Apparently, there is an excellent agreement among the predictions from all these methods.

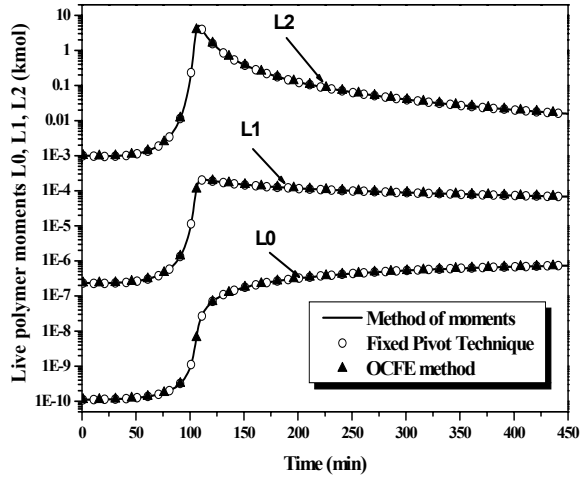

Fig. 2.Comparison of "live" polymer moments between the FP technique, the OCFE method and the method of moments

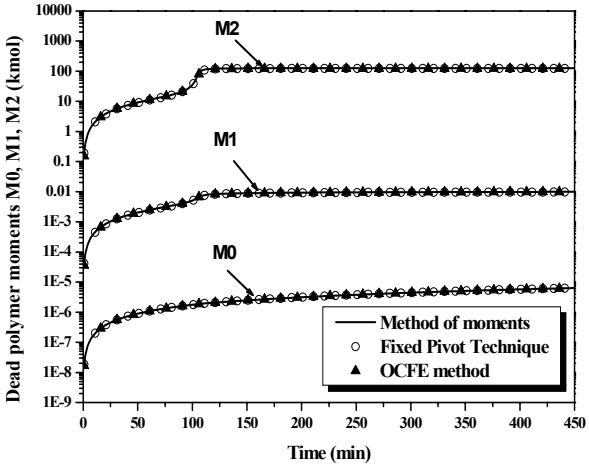

Fig 3.Comparison of "dead" polymer moments between the FP technique, the OCFE method and the method of moments

A model-based study of the optimization problem of a minimum-time production of polymer with a desired MWD is presented next, employing the OCFE method as a representative and reliable method for the MWD calculations. A bimodal MWD (i.e., PD $\approx$ 5) was selected as desired profile to be optimaly produced. An optimization policy, where the time domain was discretised into five intervals was selected. The optimization problem was solved for various initial guesses of the temperature set point profile. All these profiles exhibited a single step change in the area of the gel-effect phenomenon. The optimal results obtained by the different optimization runs were slightly different in terms of the time minimization and the shape of the final MWD, indicating low sensitivity on the initially guessed temperature set point profile.

The validity of the model was further tested by direct implementation of the model produced optimal temperature trajectory to a cascade control system of the pilot-scale batch polymerization reactor. The cascade control system consists of a primary proportional-integral-derivative (PID) and two secondary PI controllers.

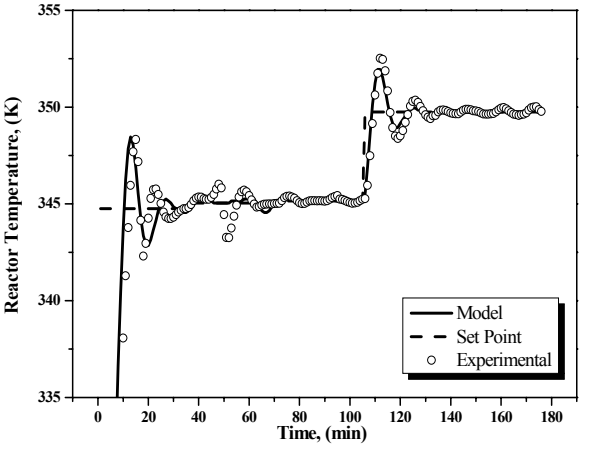

Fig. 4. Comparison between model predictions and experimental results on the reactor temperature (I_0=2 gr/kg of MMA).

Figure 4 depicts a comparison between model predictions and experimental results on the reactor temperature produced from the implementation of the optimal temperature trajectory as set points to the reactor's cascade control system. The optimal MWD in comparison with the desired MWD is shown in Figure 5. As can be seen from Figures 4 and 5, the optimizer, after the heat-up period, forces a low temperature in the reactor to restrain the polymerization, facilitating simultaneously the production of long polymer chains. At the onset of the gel effect and onwards a kick of the reactor temperature is necessary leading to the production of short polymer chains that result in the formation of a second peak in the MWD.

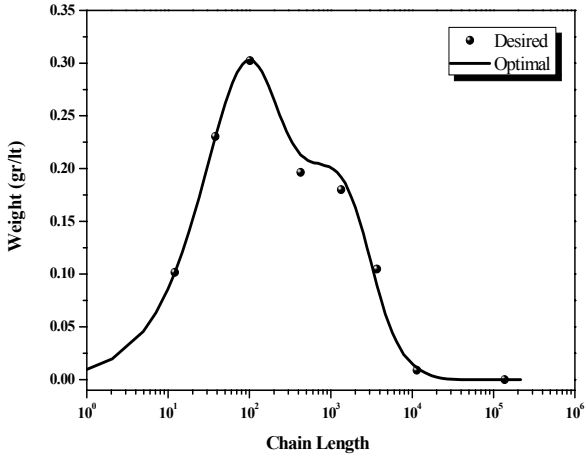

Fig. 5. Desired and optimal bimodal MWD using the OCFE method (I_0=2 g/kg of MMA).

Finally, in Figures 6, 7 and 8, model predictions on monomer conversion, average molecular weights and hot and cold water flowrates are compared with experimental data produced from the optimal temperature profiles depicted in Figure 4. It is apparent that a satisfactory agreement exists between model predictions and experimental results, proving the reliability of the proposed model to produce desired MWDs.

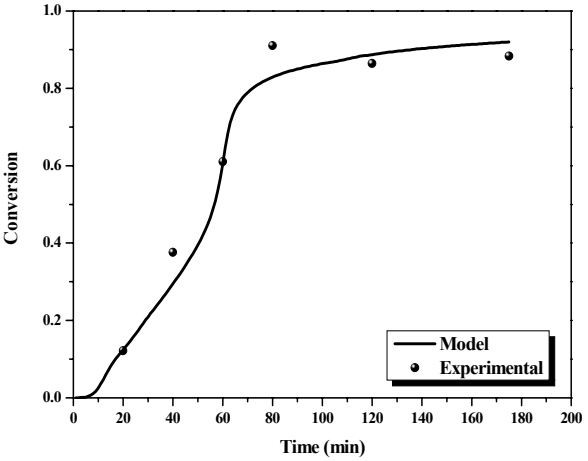

Fig. 6. Comparison of model predicted and experimental monomer conversion produced from the optimal temperature profile (I_0=2 g/kg of MMA).

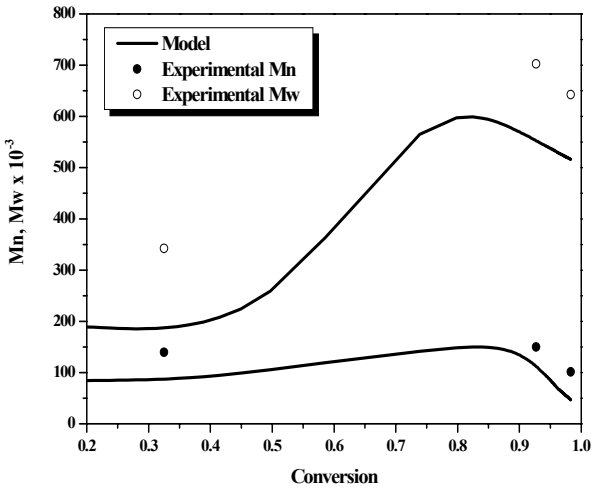

Fig. 7. Comparison of model predicted and experimental average molecular weights produced from the optimal temperature profile (I_0=2 g/kg of MMA).

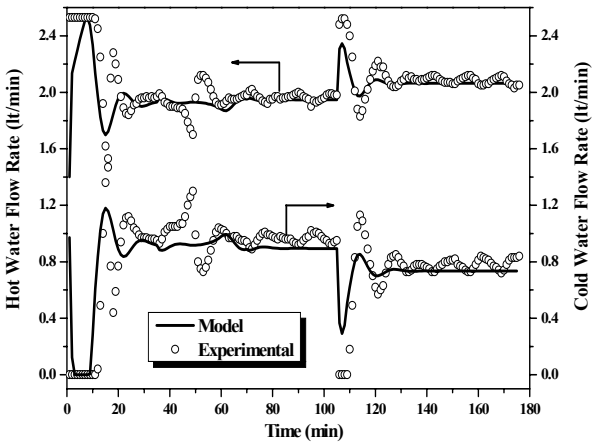

Fig. 8. Comparison of model predicted and experimental measurements on hot and cold water flowrates produced from the optimal temperature profile (I_0=2 g/kg of MMA).

REFERENCES

Chiu W.Y., G.M. Carratt, D.S. Soong (1983). A Computer Model for the Gel Effect in Free-Radical Polymerization, *Macromolecules*, **16**, 348-357.

Clarke-Pringle, T.L. and J.F. MacGregor (1998). Optimization of Molecular-Weight Distribution Using Batch-to-Batch Adjustments, *Industrial Engineering Chemistry Research*, **37**, 3660-3669.

Crowley, T.J. and K.Y. Choi (1997a). Calculation of Molecular Weight Distribution from Molecular Weight Moments in Free Radical Polymerization, *Industrial Engineering Chemistry Research*, **36**, 1419-1423.

Crowley, T.J. and K.Y. Choi (1997b). Discrete Optimal Control of Molecular Weight Distribution in a Batch Free Radical Polymerization Process, *Industrial Engineering Chemistry Research*, **36**, 3676-3684.

Deuflhard P. and M. Wulkow (1989). Computational treatment of polyreaction kinetics by orthogonal polynomials of a discrete variable, *Impact of Computing in Science and Engineering*, **1**, 269-276.

Kim, K.J. and K.Y. Choi (1991). On-line Estimation and Control of a Continuous Stirred Tank Polymerization Reactor, *Journal of Process Control*, **1**, 96-105.

Kiparissides, C., P. Seferlis, G. Mourikas, and A.J. Morris (2002). Online Optimizing Control of Molecular Weight Properties in Batch Free-Radical Polymerization Reactors, *Industrial Engineering Chemistry Research*, **41**, 6120-6131.

Kozub, D.J. and J.F. MacGregor (1992). Feedback Control of Polymer Quality in Semi-batch Copolymerization Reactors, *Chemical Engineering Science*, **47**, 929-942.

Kumar, S. and D. Ramkrishna (1996). On the Solution of Population Balance Equations by Discretization – I. A Fixed Pivot Technique. *Chemical Engineering Science*, **51**, 1311-1332

Kumar, S. and D. Ramkrishna (1997). On the Solution of Population Balance Equations by Discretization-II. Nucleation, Growth and Agregation of Particles, *Chemical Engineering Science*, **52**, 4659-4679.

Nele, M. C. Sayer, and J.C. Pinto (1999). Computation of Molecular Weight Distributions by Polynomial Approximation with Complete Adaptation Procedures, *Macromolecular Theory and Simulations*, **8**, 199-213.

Pladis, P. and C. Kiparissides (1998). A comprehensive model for the calculation of molecular weight-long-chain branching distribution in free-radical polymerizations, *Chemical Engineering Science*, **53**, 3315-3333.

Ponnuswamy, S.R., S.L. Shah, and C. Kiparissides (1987). Computer Optimal Control of Batch Polymerization Reactors, *Industrial Engineering Chemistry Research*, **26**, 2229-2236.

Ray, W.H. (1972). On the mathematical modeling of polymerization reactors, *J. Macromol. Sci.-Rev. Macromol. Chem.*, **C8(1)**, 1-13.

Tobita H. and K. Ito (1993). On the calculation of molecular weight distribution from the moments using Laguerre polynomials, *Polymer Reaction Engineering*, **1(3)**, 407-414.

Wulkow M. (1992). Adaptive treatment of polyreactions in weighted sequence spaces, *Impact of Computing in Science and Engineering*, **4**, 153-162.

Yoon W.J., J.H., Ryu, C., Cheong, and K.Y., Choi (1998). Calculation of Molecular Weight Distribution in a Batch Thermal Polymerization of Styrene, *Macromolecular Theory and Simulations*, **7**, 327-332.

Session 3.2

Model Based Control

Multivariable Control Strategy Based on Bifurcation Analysis of an Industrial Gas-Phase Polymerization Reactor

N. P. G. Salau, A. R. Secchi, J. O. Trierweiler and G. A. Neumann
Universidade Federal do Rio Grande do Sul

Predictive Control of Asymmetrical Processes

C. de Prada and S. Cristea
University of Valladolid

ADCHEM 2006

International Symposium on Advanced Control of Chemical Processes
Gramado, Brazil – April 2-5, 2006

ADAPTIVE ROBUST CONTROL FOR A CLASS OF UNCERTAIN TIME–DELAY SYSTEMS VIA OUTPUT FEEDBACK

Hansheng Wu *

* *Department of Information Science*
Hiroshima Prefectural University
Shobara–shi, Hiroshima 727–0023, Japan
Email: hansheng@pu–hiroshima.ac.jp

Abstract: The problem of robust stabilization is considered for a class of systems with the delayed state perturbations, uncertainties, and external disturbances. It is assumed that the upper bounds of the delayed state perturbations, uncertainties, and external disturbances, are unknown. An improved adaptation law with σ–modification is first introduced to estimate these unknown bounds. Then, by making use of the updated values of the unknown bounds, a class of adaptive robust output feedback controllers is proposed. On the basis of the strictly positive realness of the nominal system, it is also shown from the Kalman–Yakubovitch lemma that the solutions of the resulting adaptive closed–loop time-delay system can be guaranteed to be uniformly bounded, and the states decreases uniformly asymptotically to zero. Finally, a numerical example is given to demonstrate the validity of the results.

Keywords: Adaptive robust control, time–delay systems, asymptotic stability, output feedback.

1. INTRODUCTION

Many practical control problems, such as those arising in chemical processes, hydraulics and rolling mills, involve time–delay systems, connected with measurement of system variables, physical properties of the equipment, signal transmission, and so on. The existence of delay is frequently a source of instability.

On the other hand, it is well known that some uncertain parameters and disturbances are often included in practical control systems with time–delay due to modeling errors, measurement errors, linearization approximations, and so on. Therefore, the problem of robust stabilization of uncertain dynamical systems with time–delay has received considerable attention of many researchers (see, e.g., (Cheres *et al.*, 1989), (Wu and Mizukami, 1994), (Wu and Mizukami, 1996), and the references therein).

In the control literature, for dynamical systems with the delayed state perturbations, uncertainties, and external disturbances, where the system state vector is available, the upper bounds of the vector norms on the delayed state perturbations, uncertainties, and external disturbances, are generally supposed to be known, and such bounds are employed to construct some types of stabilizing state feedback controllers (see, e.g., (Cheres *et al.*, 1989), (Wu and Mizukami, 1996) for time–delay systems). However, in a number of practical control problems, such bounds may be unknown, or be partially known. Therefore, for such a class of uncertain time–delay systems whose uncertainty bounds are partially known, adaptive control schemes should be introduced to update these unknown bounds (see, e.g., (Wu, 2000), (Wu, 2002), (Wu, 2004) for time–delay systems). On the other hand, in many practical control problems, the states of the systems to be controlled may also be unknown or cannot be measured. Therefore, an output feedback controller should be designed to control such a class of dynamical systems.

In this paper, the problem of robust stabilization is considered for a class of systems with the delayed state perturbations, uncertainties, and ex-

ternal disturbances. It is assumed that the upper bounds of the delayed state perturbations, uncertainties, and external disturbances, are unknown, and that the states of the systems to be controlled are not measured. The purpose of the paper is to develop a stabilizing adaptive robust output feedback controller. For this, an improved adaptation law with σ–modification is employed to estimate the unknown bounds of the delayed state perturbations, uncertainties, and external disturbances. Then, by making use of the updated values of these unknown bounds, a class of output feedback controllers is constructed . On the basis of the strictly positive realness of the nominal system, it is shown from the Kalman–Yakubovitch lemma that by using the proposed adaptive robust output feedback controller, the solutions of the resulting adaptive closed–loop time–delay system can be guaranteed to be uniformly bounded, and the states decreases uniformly asymptotically to zero.

2. PROBLEM FORMULATION

Consider a class of uncertain time–delay systems described by

$$\begin{aligned}\frac{dx(t)}{dt} &= \Big[A + \Delta A(\upsilon,t)\Big]x(t) \\ &\quad + \sum_{j=1}^{r} \Delta E_j(\zeta,t)x(t-h_j) \\ &\quad + \Big[B + \Delta B(\xi,t)\Big]u(t) + q(\nu,t) \quad (1a)\end{aligned}$$

$$y(t) = Cx(t) \quad (1b)$$

where $t \in R$ is the "time", $x(t) \in R^n$ is the current value of the state, $u(t) \in R^m$ is the control input, $y(t) \in R^p$ is the output vector, A, B, C, are constant matrices of appropriate dimensions, $\Delta A(\cdot)$, $\Delta B(\cdot)$, $\Delta E_j(\cdot)$, $j = 1, 2, \ldots, r$, represent the system uncertainties and are assumed to be continuous in all their arguments, and the vector $q(\cdot)$ is the external disturbance, which is also assumed to be continuous in all their arguments. Moreover, the uncertain parameters $(\upsilon,\ \xi,\ \zeta,\ \nu) \in \Psi \subset R^L$ are Lebesgue measurable and take values in a known compact bounding set Ω. In addition, the time delays $h_j,\ j = 1, 2, \ldots, r$, are assumed to be any positive constants which are not required to be known for the system designer.

The initial condition for system (1) is given by

$$x(t) \ = \ \chi(t), \qquad t \in [t_0 - \bar{h},\ t_0] \quad (2)$$

where $\chi(t)$ is a continuous function on $[t_0 - \bar{h},\ t_0]$, and $\bar{h} := \max\big\{h_j,\ j = 1, 2, \ldots, r\big\}$.

Furthermore, a nominal system is described by

$$\frac{dx(t)}{dt} \ = \ Ax(t) + Bu(t), \quad y(t) \ = \ Cx(t) \quad (3)$$

For the uncertain time–delay systems described above, an output feedback controller $u(t)$ is introduced as follows.

$$u(t) \ = \ p(y(t),\ t) \quad (4)$$

where $p(\cdot) \ : \ R^p \times R \ \rightarrow \ R^m$ is a continuous function.

Now, the main objective of this paper is to synthesize an output feedback controller $u(t)$ that can guarantee the stability of system (1) in the presence of the delayed state perturbations, uncertainties, and external disturbances.

Assumption 2.1. The pair $\{A,\ B\}$ given in (1) is completely controllable.

Assumption 2.2. For all $(\upsilon,\ \xi,\ \zeta,\ \nu) \in \Psi$, there exist some continuous and bounded matrix functions $H(\cdot)$, $H_j(\cdot)$, $E(\cdot)$, $w(\cdot)$, of appropriate dimensions such that

$$\begin{aligned}\Delta A(\upsilon,t) &= B(t)H(\upsilon,t) \\ \Delta E_j(\zeta,t) &= B(t)H_j(\zeta,t), \quad j = 1, 2, \ldots, r \\ \Delta B(\xi,t) &= B(t)E(\xi,t) \\ q(\nu,t) &= B(t)w(\nu,t)\end{aligned}$$

For convenience, the following notations are introduced which represent the bounds of the uncertainties and external disturbances.

$$\begin{aligned}\rho(t) &:= \max_{\upsilon} \big\|H(\upsilon,t)\big\| \\ \rho_j(t) &:= \max_{\zeta} \big\|H_j(\zeta,t)\big\|, \quad j = 1, 2, \ldots, r \\ \mu(t) &:= \min_{\xi} \left[\ \frac{1}{2}\lambda_{\min}\left(E(\xi,t) + E^{\top}(\xi,t)\right)\ \right] \\ \rho_q(t) &:= \max_{\nu} \big\|w(\nu,t)\big\|\end{aligned}$$

In this paper, the functions $\rho(t)$, $\rho_j(t)$, $\mu(t)$, $\rho_q(t)$ assumed to be unknown. Moreover, the uncertain $\rho(t)$, $\rho_j(t)$, $\mu(t)$, $\rho_q(t)$ are also assumed, without loss of generality, to be uniformly continuous and bounded for any $t \in R^+$.

By employing the notations given above, for system (1), the following assumption is introduced.

Assumption 2.3. For every $t \geq t_0$, $\mu(t) \ > \ -1$.

Remark 2.1. It is well known that *Assumption 2.1* is standard and denotes the internally stabilizability of the nominal system, i.e., the system in the absence of uncertainties and external disturbances. *Assumption 2.2* defines the matching condition about the uncertainties and external disturbances, and is a rather standard assumption for robust control problem (see, e.g., (Cheres *et al.*, 1989), (Wu, 2000), (Wu and Mizukami, 1996), (Wu, 2002), (Choi and Kim, 1993)). On the other hand, Assumption 2.3 is also standard, and can be regarded as a necessary condition for robust stability of uncertain dynamical systems (see,

e.g., (Cheres *et al.*, 1989), (Wu, 2000), (Choi and Kim, 1993), and the references relative to robust stabilization of uncertain systems).

Moreover, for the nominal systems described by (3), the following assumption is also introduced.

Assumption 2.4. For the nominal system described by (3), there exists a matrix $F \in R^{m\times p}$ such that the transfer function matrix

$$T(s) \;=\; FC\big(sI - A\big)^{-1}B$$

is strictly feedback positive real (SFPR). Therefore, it follows from the Kalman–Yakubovitch lemma (see, e.g., (Narendra and Taylor, 1973), (Narendra and Annaswamy, 1989), (Khalil, 1996)) that there exist the matrices $P \in R^{n\times n}$, $Q \in R^{n\times n}$, $K \in R^{m\times n}$, $P = P^\top > 0$, $Q = Q^\top > 0$ satisfying

$$(A+BK)^\top P + P\,(A+BK) \;=\; -Q \tag{5}$$

$$\mathrm{Re}\Big[\,\lambda\,(A+BK)\,\Big] \;<\; 0 \tag{6}$$

such that

$$FC \;=\; B^\top P \tag{7}$$

Remark 2.2. Assumption 2.4 means that the nominal system is output feedback stabilizable. Indeed, in order to guarantee the stability of an uncertain system by the output feedback controllers, it is necessary that its nominal system can be stabilized by using uncorrupted output signal.

Remark 2.3. In a recent paper (Wu, 2000), a memoryless adaptive robust state feedback controller is proposed for a class of uncertain time–delay systems. It should be pointed out that the systems considered in (Wu, 2000) do not involve the uncertainty of input gain, and external disturbances, and the adaptive robust state feedback controllers proposed in (Wu, 2000) stabilize the systems only in the sense of uniform ultimate boundedness. In this paper, the purpose of the paper is to propose a class of adaptive robust output feedback controllers for system (1). It will be also shown that by employing the proposed controllers, one can guarantee the asymptotic stability, instead of the ultimate boundedness, of the considered systems.

On the other hand, it follows from Assumption 2.1 that there exists always a matrix K such that (6) holds. In particular, if one chooses K as

$$K \;=\; -\,\big(1\;/\;2\big)\;\eta\,B^\top P$$

where η is any positive constant, then the Lyapunov equation, described by (5), is reduced to the algebraic Riccati equation of the form

$$A^\top P + PA - \eta PBB^\top P \;=\; -Q \tag{8}$$

It is obvious from Assumption 2.1 that for any positive definite matrix $Q \in R^{n\times n}$, there exists an unique positive definite matrix $P \in R^{n\times n}$ as the solution of (8).

3. MAIN RESULTS

In this section, since the bounds $\rho(t)$, $\rho_j(t)$, $\mu(t)$, $\rho_q(t)$ have been assumed to be uniformly continuous and bounded for any $t \in R^+$, it can be supposed that there exist some positive constants ρ^*, ρ_j^*, μ^*, ρ_q^*, which are defined by

$$\rho^* := \max\big\{\;\rho(t)\;:\;\;t\in R^+\;\big\} \tag{9a}$$

$$\rho_j^* := \max\big\{\;\rho_j(t)\;:\;\;t\in R^+\;\big\} \tag{9b}$$

$$\mu^* := \min\big\{\;\mu(t)\;:\;\;t\in R^+\;\big\} \;>\; -1 \tag{9c}$$

$$\rho_q^* := \max\big\{\;\rho_q(t)\;:\;\;t\in R^+\;\big\} \tag{9d}$$

Here, it is worth pointing out that the constants ρ^*, ρ_j^*, μ^*, ρ_q^*, are still unknown. Therefore, such unknown bounds can not be directly employed to construct stabilizing output feedback controllers.

Without loss of generality, the following definition is also introduced :

$$\psi^* := \frac{1}{1+\mu^*}\left(1+\eta^{-1}\alpha\,(\rho^*)^2+\sum_{j=1}^{r}\eta^{-1}\alpha\,\big(\rho_j^*\big)^2\right) \tag{10a}$$

$$\phi^* := \frac{\rho_q^*}{1+\mu^*} \tag{10b}$$

where η are α are any positive constants. It is obvious from (10) that ψ^* and ϕ^* are two unknown positive constants.

Now, the following adaptive robust output feedback controller is proposed :

$$u(t) \;=\; p_1(y(t),\,t) + p_2(y(t),\,t) \tag{11a}$$

where $p_1(\cdot)$ and $p_2(\cdot)$ are given by

$$p_1(y(t),t) = -\frac{1}{2}\;\eta\hat{\psi}(t)Fy(t) \tag{11b}$$

$$p_2(y(t),t) = -\frac{\hat{\phi}^2(t)Fy(t)}{\|Fy(t)\|\,\hat{\phi}(t)\;+\;\sigma(t)} \tag{11c}$$

and where $\sigma(t) \in R^+$ is any positive uniform continuous and bounded function which satisfies

$$\lim_{t\to\infty}\int_{t_0}^{t}\sigma(\tau)d\tau \;\le\; \bar{\sigma} \;<\; \infty \tag{11d}$$

where $\bar{\sigma}$ is any constant. In addition, $F \in R^{m\times p}$ is the output feedback gain matrix.

In particular, $\hat{\psi}(t)$ and $\hat{\phi}(t)$ in (11) are, respectively, the estimates of the unknown ψ^* and ϕ^*, which are, respectively, updated by the following adaptive laws:

$$\frac{d\hat{\psi}(t)}{dt} = -\gamma_1\,\sigma(t)\hat{\psi}(t) + \gamma_1\eta\,\|Fy(t)\|^2 \tag{12a}$$

$$\frac{d\hat{\phi}(t)}{dt} = -\gamma_2\,\sigma(t)\hat{\phi}(t) + 2\gamma_2\,\|Fy(t)\| \tag{12b}$$

where γ_1 and γ_2 are any positive constants, and the initial conditions $\hat{\psi}(t_0)$, $\hat{\phi}(t_0)$ are finite.

Thus, applying the output feedback controller given in (11) to (1) yields an uncertain closed–loop time–delay system of the form:

$$\begin{aligned}\frac{dx(t)}{dt} \;=\; & [A+\Delta A(\upsilon,t)]\,x(t)\\ & +\sum_{j=1}^{r}\Delta E_j(\zeta,t)x(t-h_j)\\ & +\Big[B+\Delta B(\xi,t)\Big]p(y(t),\,t)+q(\nu,t) \qquad (13)\end{aligned}$$

where $p(\cdot)$ is given in (11).

On the other hand, letting

$$\tilde{\psi}(t) \;=\; \hat{\psi}(t)-\psi^*, \quad \tilde{\phi}(t) \;=\; \hat{\phi}(t)-\phi^*$$

one can rewrite (12) as the following error system

$$\begin{aligned}\frac{d\tilde{\psi}(t)}{dt} =& -\gamma_1\,\sigma(t)\tilde{\psi}(t)+\gamma_1\eta\,\|Fy(t)\|^2\\ & -\gamma_1\,\sigma(t)\psi^* \qquad (14a)\end{aligned}$$

$$\begin{aligned}\frac{d\tilde{\phi}(t)}{dt} =& -\gamma_2\,\sigma(t)\tilde{\phi}(t)+2\gamma_2\,\|Fy(t)\|\\ & -\gamma_2\,\sigma(t)\phi^* \qquad (14b)\end{aligned}$$

In the following, by $(x,\tilde{\psi},\tilde{\phi})(t)$ one denote a solution of the uncertain closed–loop time–delay system and the error system. Then, one can have the following theorem.

Theorem 3.1. Consider the adaptive closed–loop time–delay dynamical system, described by (13) and (14). Suppose that *Assumptions 2.1* to *2.4* are satisfied. Then, the solutions $(x,\tilde{\psi},\tilde{\phi})$ $(t;\,t_0,x(t_0),\tilde{\psi}(t_0),\tilde{\phi}(t_0))$ to the closed-loop time–delay system described by (13) and the error system described by (14) are uniformly bounded and

$$\lim_{t\to\infty}\; x(t;\,t_0,x(t_0)) \;=\; 0 \qquad (15)$$

Proof: For the adaptive closed–loop time–delay system described by (13) and (14), one first define a Lyapunov–Krasovskii functional candidate as follows.

$$\begin{aligned}V(x,\Psi) =& \,x^\top(t)Px(t)\\ & +\sum_{j=1}^{r}\alpha^{-1}\int_{t-h_j}^{t}\; x^\top(\tau)x(\tau)d\tau\\ & +\frac{1}{2}\big(1+\mu^*\big)\Psi^\top(t)\Gamma^{-1}\Psi(t) \qquad (16)\end{aligned}$$

where P is the solution to (8), $\Psi(\cdot):=[\psi(\cdot)\;\;\phi(\cdot)]^\top$, and $\Gamma^{-1}:=\mathrm{diag}\{\,\gamma_1^{-1},\;\gamma_2^{-1}\,\}$.

Let $(x(t),\Psi(t))$ be the solution to (13) and (14) for $t\geq t_0$. Then by taking the derivative of $V(\cdot)$ along the trajectories of (13) and (14) it is obtained that for $t\geq t_0$,

$$\begin{aligned}\frac{dV(x,\Psi)}{dt} \;=\; & x^\top(t)\left[A^\top P+PA\right]x(t)\\ & +2x^\top(t)P\sum_{j=1}^{r}\Delta E_j(\zeta,t)x(t-h_j)\\ & +2x^\top(t)P\Delta A(\upsilon,t)x(t)\\ & -\eta\hat{\psi}(t)x^\top(t)P\Big[B+\Delta B(\xi,t)\Big]Fy(t)\\ & -\frac{2\hat{\phi}^2(t)x^\top(t)P\Big[B+\Delta B(\xi,t)\Big]Fy(t)}{\|Fy(t)\|\,\hat{\phi}(t)\;+\;\sigma(t)}\\ & +2x^\top(t)Pq(\nu,t)\\ & +\sum_{j=1}^{r}\alpha^{-1}\Big[x^\top(t)x(t)-x^\top(t-h_j)x(t-h_j)\Big]\\ & +\big(1+\mu^*\big)\Psi^\top(t)\Gamma^{-1}\frac{d\Psi(t)}{dt} \qquad (17)\end{aligned}$$

From Assumption 2.4 and (7) one can obtain that

$$Fy(t) \;=\; FCx(t) \;=\; B^\top Px(t) \qquad (18)$$

Then, from Assumption 2.2, (17), and (18), by making use of some manipulations, one can obtain that for any $t\geq t_0$,

$$\begin{aligned}\frac{dV(x,\Psi)}{dt} \leq & -x^\top(t)\tilde{Q}x(t)+2\big(1+\mu^*\big)\sigma(t)\\ & +\frac{1}{4}\big(1+\mu^*\big)\sigma(t)\Big[|\psi^*|^2+|\phi^*|^2\Big] \qquad (19)\end{aligned}$$

where

$$\tilde{Q} \;:=\; Q-\alpha^{-1}(1+r)I \;>\; 0 \qquad (20)$$

Moreover, letting

$$\begin{aligned}\tilde{x}(t) :=& \big[\,x^\top(t)\quad\tilde{\psi}(t)\quad\tilde{\phi}(t)\,\big]^\top\\ \tilde{\varepsilon} :=& \frac{1}{4}\big(1+\mu^*\big)\left(8+|\psi^*|^2+|\phi^*|^2\right)\end{aligned}$$

one can obtain from (19) that for any $t\geq t_0$,

$$\frac{dV(\tilde{x}(t))}{dt} \;\leq\; -\lambda_{\min}(\tilde{Q})\|x(t)\|^2+\tilde{\varepsilon}\sigma(t) \qquad (21)$$

On the other hand, in the light of (16), there always exist two positive constants $\delta_{\min}$ and $\delta_{\max}$ such that for any $t\geq t_0$,

$$\tilde{\gamma}_1(\|\tilde{x}(t)\|) \;\leq\; V(\tilde{x}(t)) \;\leq\; \tilde{\gamma}_2(\|\tilde{x}(t)\|) \qquad (22)$$

where

$$\begin{aligned}\tilde{\gamma}_1(\|\tilde{x}(t)\|) :=& \,\delta_{\min}\,\|\tilde{x}(t)\|^2\\ \tilde{\gamma}_2(\|\tilde{x}(t)\|) :=& \,\delta_{\max}\,\|\tilde{x}(t)\|^2\\ & +\sum_{j=1}^{r}\alpha^{-1}h_j\sup_{\tau\in[t-h_j,\,t]}\|x_j(\tau)\|^2\end{aligned}$$

Now, from (21) and (22), one want to show that the solutions $\tilde{x}(t)$ of (13) and (14) are uniformly bounded, and that the state $x(t)$ converges asymptotically to zero.

By the continuity of the systems described by (13) and (14), it is obvious that any solution $(x, \tilde{\psi}, \tilde{\phi})(t;\, t_0, x(t_0), \tilde{\psi}(t_0), \tilde{\phi}(t_0))$ of the system is continuous.

It follows from (21) and (22) that for any $t \geq t_0$,

$$\begin{aligned} 0 \;\leq\; & \tilde{\gamma}_1(\|\tilde{x}(t)\|) \;\leq\; V(\tilde{x}(t)) \\ &= V(\tilde{x}(t_0)) + \int_{t_0}^{t} \dot{V}(\tilde{x}(\tau))d\tau \\ &\leq \tilde{\gamma}_2(\|\tilde{x}(t_0)\|) - \int_{t_0}^{t} \tilde{\gamma}_3(\|x(\tau)\|)d\tau + \int_{t_0}^{t} \tilde{\varepsilon}\sigma(\tau)d\tau \end{aligned} \quad (23)$$

where the scalar function $\tilde{\gamma}_3(\|x(t)\|)$ is defined as

$$\tilde{\gamma}_3(\|x(t)\|) := \lambda_{\min}(\tilde{Q})\, \|x(t)\|^2 \quad (24)$$

Therefore, from (23) one can obtain the following two results. First, taking the limit as t approaches infinity on both sides of inequality (23), one can obtain that

$$\lim_{t\to\infty} \int_{t_0}^{t} \tilde{\gamma}_3(\|x(\tau)\|)d\tau \;\leq\; \tilde{\gamma}_2(\|\tilde{x}(t_0)\|) + \tilde{\varepsilon}\bar{\sigma} \quad (25)$$

On the other hand, from (23) one also have

$$0 \;\leq\; \tilde{\gamma}_1(\|\tilde{x}(t)\|) \;\leq\; \tilde{\gamma}_2(\|\tilde{x}(t_0)\|) + \tilde{\varepsilon}\bar{\sigma} \quad (26)$$

which implies that $\tilde{x}(t)$ is uniformly bounded. Since $\tilde{x}(t)$ has been shown to be continuous, it follows that $\tilde{x}(t)$ is uniformly continuous, which implies that $x(t)$ is uniformly continuous. Therefore, it follows from the definition that $\tilde{\gamma}_3(\|x(t)\|)$ is also uniformly continuous. Applying the Barbalat lemma (Slotine and Li, 1991) to inequality (25) yields that

$$\lim_{t\to\infty} \tilde{\gamma}_3(\|x(t)\|) \;=\; 0 \quad (27)$$

Furthermore, since $\tilde{\gamma}_3(\cdot)$ is a positive definite scalar function, it is obvious from (27) that one can have (15). Thus, one can complete the proof of this theorem. $\nabla\nabla\nabla$

Remark 3.1. In the proof of *Theorem 3.1*, it is assumed for the constant α to satisfy (20). However, the adaptive output feedback controllers given in (11) with (12) are independent of this constant. Thus, it is not necessary for the designer to know or choose the constant α. In fact, the control gain adjusts automatically to counter the destabilizing effects of the delayed state perturbations, uncertainties, and disturbances.

Remark 3.2. The proposed robust output feedback control laws are memoryless, and the adaptive schemes given in (12) are independent of the time delays. Therefore, in the light of the proof given above, it can be known that the time–delay constants $h_j,\ j = 1, 2, \ldots, r$, are not required to be known for the system designer.

4. ILLUSTRATIVE EXAMPLE

Consider the following numerical example.

$$\begin{aligned} \frac{dx(t)}{dt} = & \left(\begin{bmatrix} 1 & 3 \\ 0 & 2 \end{bmatrix} + \Delta A(\upsilon, t) \right) x(t) \\ & + \left(\begin{bmatrix} 0 \\ 1 \end{bmatrix} + \Delta B(\xi, t) \right) u(t) \\ & + \sum_{j=1}^{3} \Delta E_j(\zeta, t) x(t - h_j) + q(\nu, t) \end{aligned} \quad (28a)$$

$$y(t) = \begin{bmatrix} 1 & 2 \end{bmatrix} x(t) \quad (28b)$$

where

$$\Delta A(\upsilon, t) = \begin{bmatrix} 0 & 0 \\ \upsilon(t) & 2\upsilon(t) \end{bmatrix}, \quad \Delta B(\xi, t) = \begin{bmatrix} 0 \\ \xi(t) \end{bmatrix}$$

$$\Delta E_1(\zeta, t) = \begin{bmatrix} 0 & 0 \\ 0.2\zeta(t) & 0.5\zeta(t) \end{bmatrix}$$

$$\Delta E_2(\zeta, t) = \begin{bmatrix} 0 & 0 \\ 0 & 0.3\zeta(t) \end{bmatrix}$$

$$\Delta E_3(\zeta, t) = \begin{bmatrix} 0 & 0 \\ 0.5\zeta(t) & 0 \end{bmatrix}, \quad q(\nu, t) = \begin{bmatrix} 0 \\ 0.5\nu(t) \end{bmatrix}$$

The problem is to determine a control law in the form (11) with (12), that will stabilizes the time–delay system described by (28) in the presence of the delayed state perturbations, uncertainties, and external disturbances.

It can known from (28) that if the output control gain matrix is given by

$$F \;=\; 2$$

then its transfer function matrix

$$T(s) \;=\; FC(sI - A)^{-1}B$$

is strictly positive real ((Narendra and Taylor, 1973), (Narendra and Annaswamy, 1989), (Khalil, 1996)).

Thus, one can construct an adaptive robust output feedback controller. In this numerical example, for the adaptation laws and output feedback controller, one select the following parameters:

$$\eta = 2, \qquad \gamma_1 = 0.5, \qquad \gamma_2 = 0.2$$

$$\sigma(t) = 20 \exp\{ -0.5t \}$$

Therefore, for uncertain time–delay system (28), from (11) with (12) one can obtain an adaptive robust output feedback controllers, by which the system state $x(t)$ can decrease uniformly asymptotically to zero.

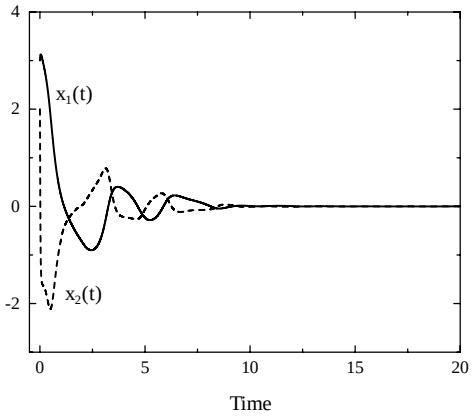

Fig. 1. Response of state variable $x(t)$.

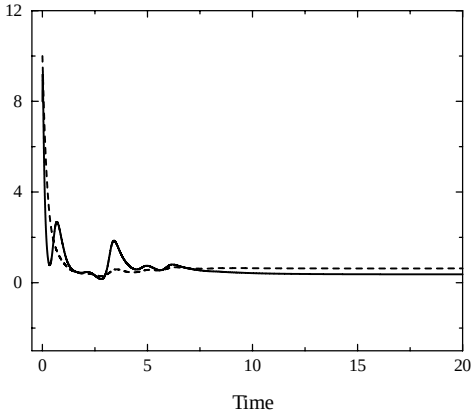

Fig. 2. History of the updating parameters $\hat{\psi}(t)$ (solid) and $\hat{\phi}(t)$ (dash).

For simulation, the uncertain parameters and initial conditions are given as follows.

$$\upsilon(t) = 0.2\sin(3t), \quad \xi = 0.3\cos(5t)$$
$$\zeta = 0.5\sin(2t), \quad \nu = 0.2\sin(3t)$$
$$h_1 = 1.0, \quad h_2 = 2.0, \quad h_3 = 3.0$$
$$x(t) = [3.0\cos(t) \;\; 2.0\cos(t)]^\top, \;\; t \in [-\bar{h},\, 0]$$
$$\hat{\psi}(0) = 8.0, \quad \hat{\phi}(0) = 10.0$$

With the chosen parameter settings, the results of simulation are shown in *Fig.1* and *Fig.2* for this numerical example.

It can be observed from *Fig.1* that the adaptive robust output feedback controllers can indeed stabilize system (34), and the states $x(t)$ decrease asymptotically to zero. On the other hand, it can be known from *Fig.2* that similar to the conventional adaptation laws with σ–modification, the improved ones make the estimate values of the unknown parameters decreasing.

5. CONCLUDING REMARKS

The problem of robust stabilization has been considered for a class of systems with the delayed state perturbations, uncertainties, and external disturbances. In this paper, It has been assumed that the upper bounds of the delayed state perturbations, uncertainties, and external disturbances, are unknown, and that the states of the systems to be controlled are not measured. An improved adaptation law with σ–modification have been introduced to estimate these unknown bounds. Then, by making use of the updated values of these unknown bounds. a class of adaptive robust output feedback controllers has been constructed. It has also been shown from the Kalman–Yakubovitch lemma that the solutions of the resulting adaptive closed–loop time-delay dynamical system can be guaranteed to be uniformly bounded, and the states decreases uniformly asymptotically to zero.

REFERENCES

Cheres, E., S. Gutman and Z. Palmor (1989). Stabilization of uncertain dynamic systems including state delay. *IEEE Trans. Automat. Contr.* **34**, 1199–1203.

Choi, C.H. and H.S. Kim (1993). Adaptive regulation for a class of uncertain systems with partial knowledge of uncertainty bounds. *IEEE Trans. Automat. Contr.* **38**, 1246–1250.

Khalil, H.K. (1996). *Nonlinear Systems*. Prentice–Hall. Upper Saddle River, NJ.

Narendra, K.S. and A.M. Annaswamy (1989). *Stable Adaptive Systems*. Prentice–Hall. Englewood Cliffs, NJ.

Narendra, K.S. and J.H. Taylor (1973). *Frequency Domain Criteria for Absolute Stability*. Academic Press. New York.

Slotine, J.J. and W. Li (1991). *Applied Nonlinear Control*. Prentice–Hall. Englewood Cliffs, NJ.

Wu, H. (2000). Adaptive stabilizing state feedback controllers of uncertain dynamical systems with multiple time delays. *IEEE Trans. Automat. Contr.* **45**, 1697–1701.

Wu, H. (2002). Decentralized adaptive robust control for a class of large–scale systems including delayed state perturbations in the interconnections. *IEEE Trans. Automat. Contr.* **47**, 1745–1751.

Wu, H. (2004). Adaptive robust tracking and model following of uncertain dynamical systems with multiple time delays. *IEEE Trans. Automat. Contr.* **49**, 611–616.

Wu, H. and K. Mizukami (1994). Robust stabilization of uncertain linear dynamical systems with time–varying delay. *J. Optimiz. Theory Appl.* **82**, pp.593–606.

Wu, H. and K. Mizukami (1996). Linear and nonlinear stabilizing continuous controllers of uncertain dynamical systems including state delay. *IEEE Trans. Automat. Contr.* **41**, 116–121.

ADCHEM 2006

International Symposium on Advanced Control of Chemical Processes
Gramado, Brazil – April 2-5, 2006

ADAPTIVE CONTROL OF A NEUTRALIZATION REACTOR

José Figueroa and Juan Cousseau [*,1]
Stefan Werner and Timo Laakso [**]

[*] *Departamento de Ingeniería Eléctrica y de Computadoras, Universidad Nacional del Sur, Av. Alem 1253; (8000) Bahía Blanca, Argentina*
[**] *Signal Processing Laboratory, Smart and Novel Radios (SMARAD) Center of Excellence, Helsinki University of Technology, P.O. BOX 3000, FIN-02015 HUT, Finland*

Abstract: In this paper the problem of on-line identification and adaptive control of Neutralization reactor is studied. It is used the fact that this process can be modeled as a Wiener type system. An recursive identification algorithm for Wiener systems is proposed whose linear and nonlinear parts are modeled using a Laguerre and Piecewise Linear basis functions, respectively. The model obtained is used to adapt the parameters of a controller designed for the specific structure of the model. The results show good performance when compared with other similar schemes found in the literature.

Keywords: Adaptive filtering, Nonlinear control, Adaptive Control.

1. INTRODUCTION

In the last decades, many contributions for controller design have been based on the linear model assumption. However, in some cases it is difficult to represent a given process using a linear model. This is the case when the system is highly nonlinear and the operating point changes along a wide region, or when the process is nonstationary, i.e., the characteristics change with time.

In these cases, the controller design can be performed using special techniques, such as exact linearization, nonlinear model predictive control, or other special purpose procedures (Ogunnaike and Ray, 1994).

One of the solutions to control such kind of systems is *adaptive control*, where the parameters of a linear controller are adjusted to follow the variations of the process behavior. Several control schemes assume a model structure whose parameters are identified on-line using an adaptive identification algorithm. The identified model parameters are then used to adjust the controller parameters.

It is well known that some systems can be described by a linear dynamic model followed by a static nonlinearity, i.e., a *Wiener system* (Pearson and Pottmann, 2000; Pearson, 2003). In this paper, an algorithm for adaptive control for Wiener models is presented.

The first step in the construction of an adaptive control algorithm is to obtain an efficient adaptive identification scheme. In this paper we use the identification methodology of block-oriented models introduced by Bai (1998). The algorithm is based on least-squares estimation (LSE) and singular value decomposition (SVD). The approach

[1] Corresponding author. Email: figueroa@uns.edu.ar. Phone: +54 291 4595101 ext. 3325. FAX: +54 291 4595154.

is useful only for the single input/single output (SISO) case due to the particular parameterization used. Gómez and Baeyens (2004) extended the results of Bai to include a more general parameterization that enables the use of multiple input/ multiple output (MIMO) systems.

In this paper we propose a new approach for adaptive control of Wiener type systems. In particular we propose the use of a Laguerre description for the linear part and a Piecewise Lineal description for the nonlinear gain. For this parametrization, an adaptive identification scheme is proposed extending the idea of Gómez and Baeyens (2004). Using this approach, the inverse of the nonlinearity is directly identified, avoiding the inversion problem. After that, the structure of the Wiener model is fully exploited to obtain all possible advantages.

The performance of the proposed algorithm is tested in the control of a neutralization reactor. It is well known that the control of a pH processes is particularly difficult. The main reason is the strong nonlinearity involved. The slope of a chemical system's titration curve can vary several orders of magnitude over a modest range of pH values, causing the overall process gain to change accordingly. The control of this kind of processes can be performed by several nonlinear schemes (Norquay *et al.*, 1998; Norquay *et al.*, 1999; Gerkšič *et al.*, 2000; Lussón *et al.*, 2003*a*; Biagiola *et al.*, 2004; Akesson *et al.*, 2005). The basic assumptions of these schemes are a fixed Wiener structure of the model and a fixed nonlinear controller. Several control strategies were used (including gain scheduling, model predictive control, H_∞, etc.).

However, when perturbations are applied to the process, a fixed Wiener model does not longer represents adequately the process. For example, the titration curve change drastically (Kalafatis *et al.*, 2005*b*). These move to some authors to include some robustness ideas in the controller design (Lussón *et al.*, 2003*b*), to use feedforward controllers (Kalafatis *et al.*, 2005*b*) or to use adaptive identification algorithms (Kalafatis *et al.*, 2005*a*). Pajunen (1987 and 1992) propose two adaptive control schemes for the control of Wiener systems. However, in the identification algorithms of these schemes, the Wiener structure is lost, resulting in a large number of parameters for the process model. In this paper we propose, as mentioned above, a more efficient algorithm to solve for adaptive control.

The paper is organized as follows. In Section 2 a description of model structure and adaptive identification procedure are presented. Section 3 describes the adaptive control algorithm and discusses some implementation details. A simulation example describing the application of this algorithm to control a pH neutralization reactor is detailed in Section 4. Finally, in Section 5 the conclusions are presented.

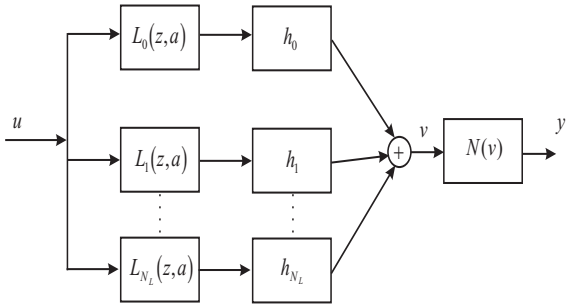

Fig. 1. Laguerre-PWL Wiener Model.

2. ADAPTIVE IDENTIFICATION SCHEME

2.1 Model Description

We propose in this paper a special description for the process, where the linear dynamic model is described by a Laguerre basis series and the nonlinear static block is modeled as a Piecewise Linear (PWL) model. This model is illustrated in Fig. 1. The Laguerre basis allows the use of prior knowledge about the dominant poles (Wahlberg, 1991; 1994; Lindskog, 1996). This model describes the linear model with the following basis function expansion

$$H(z) = \sum_{i=0}^{M} h_i L_i(z,a) \tag{1}$$

where

$$L_i(z,a) = \frac{\sqrt{1-a^2}}{z-a}\left(\frac{1-az}{z-a}\right)^{i-1} \tag{2}$$

and h_i are the parameters of the model, $a \in \Re$ is a filter coefficient chosen *a priori* (Wahlberg, 1991).

For the representation of the static nonlinear gain, $N(\cdot)$, we use a Piecewise Linear (PWL) description. In general $N(\cdot)$ is a real-valued function of one variable, i.e., $y = N(v) : \Re^1 \rightarrow \Re^1$, which we will assume to be invertible. This is a common assumption in the adaptive identification area (Wigren, 1994), often to allow a simplification in the feedback loop design (Lussón *et al.*, 2003*a*). For the specific control algorithm that we will use, we prefer to describe the inverse of this nonlinearity, i.e., $v = N^{-1}(y)$.

PWL functions have proven to be a very powerful tool in the modeling and analysis of nonlinear systems (Chua and Ying, 1983; Julián *et al.*, 1999). It can be proved (Julián *et al.*, 1999) that any continuous nonlinear function $f(v) : \Re^m \rightarrow \Re^1$ can be uniquely represented using PWL

functions. To express the nonlinear function, we will use a function expansion with basis functions and parameters

$$v = \mathbf{c}^T \mathbf{\Lambda}(y). \tag{3}$$

We will consider the case where the basis functions that are included in the matrix $\mathbf{\Lambda}$ have been predetermined, and the values of $\mathbf{c}$ are the parameters to be estimated. In this paper we use the orthogonal basis description proposed by Julián *et al.* (2000).

Since the basis functions $\mathbf{\Lambda}$ are fixed, the output is a linear function of the parameters. This allows us to use linear regression to estimate these parameters. The two basic advantages of this approach are its fast convergence and unique solution.

2.2 Adaptive implementation

Let us define an adaptive algorithm for the identification of the Wiener model described in previous section. As can be seen from Fig. 1, the signal $v(k)$ is given by

$$v(k) = \sum_{i=0}^{M} h_i L_i[u(k)] \tag{4}$$

and also

$$\begin{aligned} v(k) = N^{-1}[y(k)] &= \mathbf{c}^T \mathbf{\Lambda}[y(k)] \\ &= \sum_{i=0}^{N} c_i \Lambda_i[y(k)] \end{aligned} \tag{5}$$

By equaling both sides of (4) and (5) (including $\epsilon(k)$ to allow a modeling error), and fixing the parameter $h_0 = 1$ to overcome the well-known gain ambiguity in Wiener models, the following equation is obtained

$$\begin{aligned} \epsilon(k) = \sum_{i=0}^{N} c_i \Lambda_i[y(k)] - L_0[u(k)] - \\ \sum_{i=1}^{M} h_i L_i[u(k)] = \boldsymbol{\theta}^T(k)\boldsymbol{\phi}(k) - L_0[u(k)] \end{aligned} \tag{6}$$

where vectors $\boldsymbol{\theta}(k)$ and $\boldsymbol{\phi}(k)$ are defined as

$$\boldsymbol{\theta}(k) = [c_0, c_1, c_2, \cdots, c_N, h_1, h_2, \cdots, h_M]^T \tag{7}$$

$$\begin{aligned} \boldsymbol{\phi}(k) = [\Lambda_0[y(k)], \Lambda_1[y(k)], \cdots, \Lambda_N[y(k)], \\ -L_1[u(k)], -L_2[u(k)], \cdots, -L_M[u(k)]]^T. \end{aligned} \tag{8}$$

Next, we consider an stochastic gradient algorithm to estimate recursively the parameters of the model $\boldsymbol{\theta}$. For this purpose, we use as objective function $J_{\boldsymbol{\theta}}$, the instantaneous squared error, i.e.

$$J_{\boldsymbol{\theta}}[\epsilon(k)] = \epsilon^2(k) = \Big[\boldsymbol{\theta}^T(k)\boldsymbol{\phi}(k) - L_0[u(k)]\Big]^2 \tag{9}$$

The recursion of the stochastic gradient algorithm that minimizes the above objective function is given by

$$\boldsymbol{\theta}(k+1) = \boldsymbol{\theta}(k) + \mu\boldsymbol{\phi}(k)\epsilon(k). \tag{10}$$

where μ is the step size controlling the convergence and final error of $\boldsymbol{\theta}$. A bound on μ to ensure convergence and an analysis of convergence to a local stationary point can be found in Figueroa *et al.* (2004).

The identification algorithm is summarized in Table 1. From the implementation point of view, the initial condition for $\boldsymbol{h}$ is the vector zero and for $\boldsymbol{c}$ is the parameters that defines the identity nonlinear function.

Table 1. The adaptive identification algorithm.

Parameters:
M = number of $\boldsymbol{h}$ coefficients
N = number of $\boldsymbol{c}$ coefficients
μ = step size
Data:
$u(k)$ input signal at time k
$y(k)$ output signal at time k
Initialization
$\boldsymbol{h}(0) = \mathbf{0}$
$\boldsymbol{c}(0) = [-1\ 1\ 0\ \cdots\ 0\ -1]^T$
For each k,
$\boldsymbol{\theta}(k) = [c_0, \cdots, c_N, h_1, \cdots, h_M]^T$
$\boldsymbol{\phi}(k) = [\Lambda_0[y(k)], \cdots,$
$\Lambda_N[y(k)], -L_1[u(k)], \cdots, -L_M[u(k)]]^T$
$\boldsymbol{\epsilon}(k) = \boldsymbol{\theta}^T(k)\boldsymbol{\phi}(k) - L_0[u(k)]$
$\boldsymbol{\theta}(k+1) = \boldsymbol{\theta}(k) + \mu\boldsymbol{\phi}(k)\epsilon(k)$

3. CONTROLLER DESIGN

In the context of adaptive control, the essential idea is to identify a process and, based on the model obtained, adjust the controller parameters to improve the closed loop performance. For tuning the control parameters any classical strategy could be used, for example: minimum ITAE, retain constant loop gain, Ziegler-Nichols, Cohen-Coon, internal model control, etc. (Ogunnaike and Ray, 1994). In our particular application, we used a direct synthesis approach, which was modified to be applied to a Wiener model.

To design the controller, we will follow the principle of the nonlinear regulator as presented by Wigren (1999). Consider the closed-loop system of Fig. 2. The process is assumed to be represented by a Wiener model with a nonlinear gain $N(\cdot)$ that is invertible. We can use the inverse of this

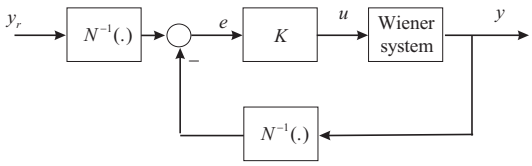

Fig. 2. The closed loop scheme for known Wiener Model.

block to extract the nonlinearities outside of the closed loop. In this way, a linear controller $K(z)$ should be designed to compensate the behaviour of the linear dynamic block of the process model.

In our case, the inverse of the nonlinearity is obtained directly from the identification process. To design the linear controller, we adopt the direct synthesis approach (Ogunnaike and Ray, 1994), applied to the Laguerre model of Eq. (4). The controller specification is to obtain a closed-loop pole in a_c without offset when the set point is changed in the form of steps. If the discrete transfer function of the linear model is called $H(z)$, and $H^{-1}(z)$ is stable and causal, then the controller can be defined as

$$K_{\boldsymbol{h}}(z) = \frac{a_c}{z-1}\frac{1}{H(z)}. \tag{11}$$

where the subscript $\boldsymbol{h}$ is included to remark the dependence of the controller with the parameters of the Laguerre model. The control algorithm is summarized in Table 2. A stability analysis for the fixed controller is similar to the one presented in Biagiola *et al.* (2004).

Table 2. The control algorithm.

Parameters:
Coefficients of Laguerre model $\boldsymbol{h}$.
Coefficients of PWL model $\boldsymbol{c}$.
Data:
$y_r(k)$ set point at time k
For each k,
Obtain $y(k)$ as measure from the process
Compute $v(k) = \mathbf{c}^T \mathbf{\Lambda}[y(k)]$
Compute $v_r(k) = \mathbf{c}^T \mathbf{\Lambda}[y_r(k)]$
Compute $e(k) = v_r(k) - v(k)$
Compute $u(k)$ by applying $e(k)$ to $K_{\boldsymbol{h}}(z)$
Applied $u(k)$ to the process.

Let us now consider the problem of controlling the process when the parameters of the Wiener model are unknown and varying along the operation. We can use the adaptive identification algorithm in Section 2 to obtain the parameters of the model, and use them to adapt the controller coefficients. This implies that each sample time, both algorithms (Table 1 and Table 2) are executed simultaneously. The complete adaptive scheme is illustrated in Fig. 3. The dotted lines denote the parameter information flow from the identification scheme to the compensator. In this formulation, the role of the measurement noise is essential in order to ensure the persistent excitation.

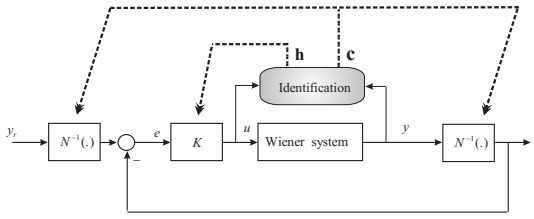

Fig. 3. The control adaptation scheme.

In the next section, this scheme is applied to the control of a pH neutralization reactor.

4. EXAMPLE: PH NEUTRALIZATION

In order to illustrate the design procedure and to evaluate the adaptive controller performance, simulation results were obtained. A chemical process with strong nonlinearity was selected. The example consists of the neutralization reaction between a strong acid (HA) and a strong base (BOH) in the presence of a buffer agent (BX) as described by Galán (2000). The neutralization takes place in a continuous stirred tank reactor (CSTR) with a constant volume V.

It is well known that the control of a pH processes is particularly difficult. The main reason is the high nonlinearity involved. The slope of the titration curve of the chemical system can vary several orders of magnitude over a modest range of pH values, causing the overall process gain to change accordingly. The regions of high and low slope on the titration curve correspond to conditions of high and low gain for a pH control loop, respectively.

In the continuous pH neutralization reactor an acidic solution, with a time-varying volumetric flow $q_A(t)$ of a composition $x_{1i}(t)$, is neutralized using an alkaline solution with volumetric flow $q_B(t)$ of known composition made up of base x_{2i} and buffer agent x_{3i}. Due to the high reaction rates of the acid-base neutralization, chemical equilibrium conditions are instantaneously achieved. Moreover, assuming that the acid, the base and the buffer are strong enough, the total dissociation of the three compounds takes place.

The process dynamics model can be obtained by considering the electroneutrality condition (which is always preserved) and through mass balances of equivalent chemical species (known as chemical invariants) that were introduced by Gustafsson and Waller (1983). For this specific case, under the previous assumptions, the dynamic behavior of the process can be described considering the following state variables:

$$x_1 = [A^-] \tag{12}$$

$$x_2 = [B^+] \tag{13}$$

$$x_3 = [X^-] \tag{14}$$

Therefore, the mathematical model of the process can be written in the following way (Galán, 2000):

$$\dot{x}_1 = 1/\eta\,(x_{1i} - x_1) - 1/V\,x_1 q_B \tag{15}$$

$$\dot{x}_2 = -1/\eta\,x_2 + 1/V\,(x_{2i} - x_2) q_B \tag{16}$$

$$\dot{x}_3 = -1/\eta\,x_3 + 1/V\,(x_{3i} - x_3) q_B \tag{17}$$

$$F(x,\xi) \equiv \xi + x_2 + x_3 - x_1 - K_w/\xi - x_3/[1 + (K_x\,\xi/K_w)] = 0 \tag{18}$$

where $\xi = 10^{-pH}$ and $\theta = V/q_A$. K_w and K_x are the dissociation constants of the buffer and the water, respectively. Note that this process is not strictly a Wiener process, however, it will be use to illustrate the proposed control. The parameters of the system represented by Eq. (15)–(18) are addressed in Table 3. Eq. (18) was deduced by McAvoy *et al.*, (1972) and takes the standard form of the widely used implicit expression that connects the pH value with the states of the process.

Table 3. Neutralization Parameters.

PARAMETER	VALUE
x_{1i}	0.0012 $mol\ HCL/l$
x_{2i}	0.0020 $mol\ NaOH/l$
x_{3i}	0.0025 $mol\ NaHCO_3/l$
K_x	$10^{-7}\ mol/l$
K_w	$10^{-14}\ mol^2/l^2$
q_A	$1\ l/m$
V	$2.5\ l$

A Wiener model describing this process has been presented for several control applications using q_B (manipulated variable) to control the pH (controlled variable), see, e.g., Lussón *et al.* (2003*a*) and Biagiola *et al.* (2004). However, when perturbations are present in the process ($q_A(t)$ and $x_{1i}(t)$), a simple Wiener model cannot provide an adequate representation of the plant.

The chosen parameters for our model are a third-order Laguerre basis with a pole at $a = 0.7$ to represent the linear dynamic model, /it i.e. $M = 2$. To represent the inverse of the nonlinear gain, the domain of the pH, the range $[3, 9.5]$, is divided in 10 regions, /it i.e. $N = 11$. The adaptation step size is $\mu = 0.015$.

In this particular application, the linear controller takes the form

$$K(z) = \frac{a_c\left(z^3 - 3az^2 + 3a^2z - a^3\right)}{\sqrt{1-a^2}\,(a_2z^2 + a_1z + a_0)\,(z-1)} \tag{19}$$

where $a_2 = 1 - ah_2 + a^2h_3$, $a_1 = h_2 - 2ah_3 + a^2 - 2a$, $a_0 = h_3 - ah_2 + a^2$ and the closed-loop pole is fixed at $a_c = 0.8$. In the adaptive adjustment of this controller, it is important to check the stability at every iteration. If a pole is outside the unit circle, it should be replaced by its stable reciprocal.

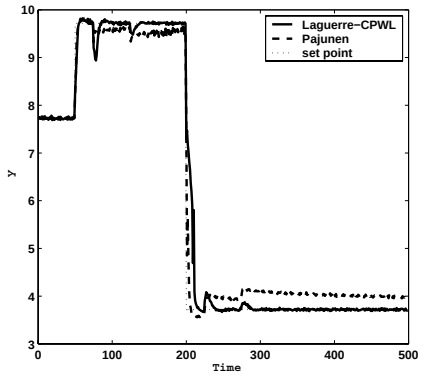

Fig. 4. Simulation results. $y = pH$ as function of time.

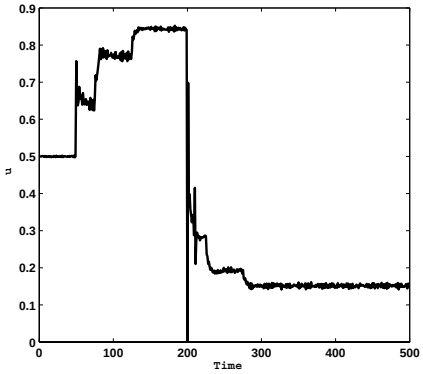

Fig. 5. Simulation results. $u = q_b$ as function of time.

Now, the results of the proposed adaptive controller are presented, and the performance is compared with that of the Model Reference Adaptive Technique proposed by Pajunen (1992).

The simulation involve a set point change from $pH_1 = 7.7182$ to $pH_2 = 9.7182$ at $t_2 = 25min$ and to $pH_3 = 5.7182$ at $t_3 = 100min$. Perturbations are applied in q_A (which is increased from 1 to 1.2 at $t = 38min$ and then reduced to 0.8 at $t = 113min$) and in x_{1i} (which increases 10 percent from the original value at $t = 63min$ and then is reduced 20 percent at $t = 138min$). In all cases a uniform noise in the range of ± 0.05 is considered.

Figure 4 illustrates the pH behaviour of the controllers. From this plot it is clear that the performance of the proposed Laguerre-PWL Wiener adaptive controller is better than the one proposed by Pajunen (1992). For example, our proposed remove completely the offset presented in the Pajunen scheme. Figure 5 depicts the manipulated variable q_B for the proposed algorithm.

An interesting point is to compare the number of the parameters involved in both approaches. While the identification of Laguerre-PWL involves 13 parameters, Pajunen's approach involves 23 parameters. This is because the Model Reference Adaptive Technique cannot take advantage of the Wiener structure of the model.

5. CONCLUSIONS

The problem of on-line identification and adaptive control of a neutralization reactor using a Wiener nonlinear system is studied. The linear and nonlinear parts are modeled using a Laguerre and Piecewise Linear basis functions, respectively. Then, since the fact that model error is linear in the parameters, an adaptive identification algorithm is presented based on a stochastic gradient algorithm. Information on the identified model is used to adjust the parameters of a controller online. The controller is designed based on the specific structure of the model. The complete scheme is successfully applied to a simulation example.

REFERENCES

Akesson, B.M., H.T. Toivonen, J.B. Waller and R.H. Nyström (2005). Neural network approximation of a nonlinear model predictive controller applied to a pH neutralization process. *Comp. and Chem. Eng.* **29**, 323–335.

Bai, E. (1998). An optimal two-stage identification algorithm for Hammerstein-Wiener nonlinear systems. *Automatica* **34, 3**, 333–338.

Biagiola, S.I., O.E. Agamennoni and J.L. Figueroa (2004). H_∞ control of a wiener type system. *Int. J. of Control* **77, 6**, 572–583.

Chua, L.O. and L.P. Ying (1983). Canonical piecewise-linear analysis. *IEEE Trans. on Circuits and Systems* **CAS-30**, 125–140.

Figueroa, J.L., J.E. Cousseau and R. J. P. de Figueiredo (2004). A simplicial canonical piecewise linear adaptive filter. *Circuits, System and Signal Processing* **23**, 365–386.

Galán, O. (2000). *Robust multi-linear model-based control for nonlinear plants*. PhD thesis. University of Sydney, Australia.

Gerkšič, S., D. Juričic, S. Strmčnic and D. Matko (2000). Wiener model based nonlinear predictive control. *Int. J. of Systems Science* **31**, 189–202.

Gómez, J.C. and E. Baeyens (2004). Identification of block-oriented nonlinear systems using orthonormal bases. *J. of Process Control* **14**, 685–697.

Gustafsson, T. and K. Waller (1983). Dynamic modelling and reaction invariant control of pH. *Chem. Eng. Science* **38**, 389–398.

Julián, P., A.C. Desages and M.B. D'Amicco (2000). Orthonormal high level canonical PWL functions with applications to model reduction. *IEEE Trans. on Circuits and Systems* **CAS-47, 5**, 702–712.

Julián, P., A.C. Desages and O.E. Agamennoni (1999). High level canonical piecewise linear representation using a simplicial partition. *IEEE Trans. on Circuits and Systems* **CAS-46**, 463–480.

Kalafatis, A., L. Wang and W.R. Cluett (2005*a*). Identification of time-varing ph processes using sinusoidal signals. *Automatica* **41**, 385–691.

Kalafatis, A., L. Wang and W.R. Cluett (2005*b*). Linearizing feedforward-feedback control of pH processes based on the wiener model. *J. of Process Control* **15**, 103–112.

Lindskog, P. (1996). *Methods, Algorithms and Tools for System Identification Based on Prior Knowledge*. PhD thesis. Linköping Universitet, Sweden.

Lussón, A., O. E. Agamennoni and J. L. Figueroa (2003*a*). A nonlinear model predictive control scheme based on Wiener piecewise linear models. *J. of Process Control* **13**, 655–666.

Lussón, A., O. E. Agamennoni and J. L. Figueroa (2003*b*). Robust identification of PWL-Wiener models: Use in model predictive control. *Latin Am. App. Res.* **33**, 435–442.

McAvoy, T., E. Hsu and S. Lowenthal (1972). Dynamics of pH in controlled stirred tank reactor. *Ind. Eng. and Chemistry Proc. Des. Dev.* **11, 1**, 68–70.

Norquay, S.J., A. Palazoglu and J.A. Romagnoli (1998). Model predictive control based on Wiener models. *Chem. Eng. Science* **53, 1**, 75–84.

Norquay, S.J., A. Palazoglu and J.A. Romagnoli (1999). Application of Wiener model predictive control (WMPC) to pH neutralization experiment. *IEEE Trans. Control System Technology* **7**, 437–445.

Ogunnaike, B.A. and W.R. Ray (1994). *Process Dynamics, Modeling and Control*. Oxford University. USA.

Pajunen, G.A. (1987). Comparison of linear and nonlinear adaptive control of a ph-process. *IEEE Control Syst. Magazine* **28**, 781–785.

Pajunen, G.A. (1992). Adaptive control of Wiener type nonlinear systems. *Automatica* **28, 4**, 781–785.

Pearson, R.K. (2003). Selecting nonlinear model structures for computer control. *J. of Process Control* **13**, 1–26.

Pearson, R.K. and M. Pottmann (2000). Gray-box identification of block-oriented nonlinear models. *J. of Process Control* **10**, 301–315.

Wahlberg, B. (1991). System identification using Laguerre models. *IEEE Transactions on Automatic Control* **36, 5**, 551–562.

Wahlberg, B. (1994). System identification using Kautz models. *IEEE Transactions on Automatic Control* **39, 6**, 1276–1282.

Wigren, T. (1994). Recursive prediction error identification using the nonlinear Wiener model. *Automatica* **29, 4**, 1011–1025.

Wigren, T. (1999). *Recursive Identification Based on The Nonlinear Wiener Model*. Prentice-Hall Inc.. Englewood Cliffs, NJ.

Robust MPC with Output Feedback and Realigned Model

J. M. Perez[1] and D. Odloak[2]

[1]*PETROBRAS – Cenpes*
e-mail: perez@petrobras.com.br
[2]*Chemical Engineering Department, University of São Paulo.*
C.P. 61548, 05424-970, São Paulo, Brazil.
e-mail: odloak@usp.br

Abstract: In this work, it is presented a contribution to the design of the robust MPC with output feedback and input constraints. This work extends existing approaches by considering a particular non-minimal state space model, which transforms the output feedback strategy into a state feedback strategy. The controller is developed to the case in which the system inputs may become saturated. We follow a two stages approach. In the off-line stage, a series of unconstrained robust MPCs is obtained by including in the control optimization problem, inequality constraints that force the state of the closed-loop system to contract along the time. Each of these controllers is associated to particular sets of manipulated inputs and controlled outputs. In the existing version of the method, the closed loop system involves a state observer that makes the solution to the robust MPC optimization problem a time consuming step. In the on-line step of the controller design proposed procedure, a sub optimal control law is obtained by combining control configurations that correspond to particular subsets of available manipulated inputs. The method is illustrated with a simulation example of the process industry.

Keyword: Model Predictive Control, Robust stability, Output feedback, Input constraints.

1. INTRODUCTION

Model predictive control has achieved a remarkable popularity in the process industry with thousands of practical applications (Qin and Badgwell, 2001). One of the reasons of this industrial acceptance is the ability of MPC to incorporate constraints in the inputs. However, one additional desirable characteristic still not attended by commercial MPC packages is closed loop stability in the presence of model uncertainty. When model uncertainty is considered in the synthesis of the predictive controller, the existing algorithms usually demand a computer effort that is prohibitive for practical implementation (Lee and Cooley, 2000). We could not find in the control literature a satisfactory solution, from the application viewpoint, to the robust MPC problem with output feedback and input constraints. Rodrigues and Odloak (2000) presented a formulation to the robust unconstrained MPC with output feedback where stability is achieved through the explicit inclusion of a Lyapunov inequality into the control optimization problem. Recently, Rodrigues & Odloak (2005) extended the method to include the switching of active input constraints during transient conditions. The controller is designed in two steps. The first step is developed off-line and results in a set of linear unconstrained MPCs each one corresponding to a controllable subsystem with previously defined inputs and outputs. The second step of the controller design procedure is performed on-line and involves the solution to an optimization problem that has the same objective function as the conventional MPC, but the control actions are computed as a convex combination of the linear controllers obtained in the first stage of design procedure. The main objective of this work is to improve the method of Rodrigues and Odloak (2005) by proposing an alternative solution to the off-line step of the synthesis of the robust MPC. The method proposed here is based on a non-minimal state space model formulation presented by Maciejowsky (2002) and designated by that author as realigned model. It will be shown here that the approach leads to a significant simplification in the off-line step of the design procedure. In the next section, the approach of Rodrigues and Odloak (2005) is briefly summarized. Then, the realigned model in the incremental form is introduced and the optimization problems of the off-line and on-line steps of the controller synthesis are presented. Next, a simulation example is used to illustrate the application potential of the new method and finally the paper is concluded.

2 A ROBUST UNCONSTRAINED MPC WITH OUTPUT FEEDBACK

We consider the following discrete time invariant model that is written in the incremental form:

$$[\tilde{x}]_{k+1|k} = \tilde{A}[\tilde{x}]_{k|k} + \tilde{B}\,\Delta u(k) \qquad (1)$$

$$[\tilde{y}]_{k|k} = \tilde{C}[\tilde{x}]_{k|k} \qquad (2)$$

where

$\tilde{x} \in \mathbb{R}^{nx}$ is the state of the predicting model, k is the present sampling instant, $u \in \mathbb{R}^{nu}$ is the input, $\Delta u(k) = u(k) - u(k-1)$ is the input increment, $y \in \mathbb{R}^{ny}$ is the output. $\tilde{A}$, $\tilde{B}$ and $\tilde{C}$ are matrices of appropriate dimensions.

As the state is not usually measured, they need to be updated with the output measurement as follows:

$$[\tilde{x}]_{k+1|k+1} = \tilde{A}[\tilde{x}]_{k|k} + \tilde{B}\,\Delta u(k) + \\ + K_F\{[y_p]_{k+1|k} - \tilde{C}[\tilde{x}]_{k+1|k}\} \quad (3)$$

where K_F is the gain of the observer that estimates the model states and y_p is the output of the true plant which is represented by a similar model as the one represented in Eqs (1) and (2) but with different coefficient matrices:

$$[x_p]_{k+1|k} = A_p[x_p]_{k|k} + B_p\Delta u(k) \quad (4)$$

$$[y_p]_{k+1|k} = C_p[x_p]_{k+1|k} \quad (5)$$

Assume now that related to the output reference vector y^{sp}, we can define a state reference v^{sp} for the plant and predicting model. Consequently, we can define errors for these states: $x_p^e = v^{sp} - x_p$ and $\tilde{x}^e = v^{sp} - \tilde{x}$.

Now, combining Eqs (3), (4) and (5) we obtain the plant plus observer model:

$$[x^e]_{k+1|k+1} = A[x^e]_{k|k} + B\,\Delta u(k) \quad (6)$$

where

$$x^e = \begin{bmatrix} \tilde{x}^e \\ x_p^e \end{bmatrix},\ x^e \in \mathbb{R}^{2nx},$$

$$A = \begin{bmatrix} (I - K_F\tilde{C})\tilde{A} & K_F C_p A_p \\ 0 & A_p \end{bmatrix},\ A \in \mathbb{R}^{2nx\times 2nx},$$

$$B = -\begin{bmatrix} (I - K_F\tilde{C})\tilde{B} + K_F C_p B_p \\ B_p \end{bmatrix},\ B \in \mathbb{C}^{2nx\times nu}$$

The cost function of the MPC considered here is defined as follows:

$$J_k = (\bar{A}[\tilde{x}^e]_{k|k} - \bar{B}\,\Delta u)^T Q(\bar{A}[\tilde{x}^e]_{k|k} - \bar{B}\Delta u) + \Delta u^T R\,\Delta u \quad (7)$$

where Q and R are weighting matrices and

$$\Delta u = \begin{bmatrix} \Delta u(k) \\ \vdots \\ \Delta u(k+m-1) \end{bmatrix},\quad \bar{A} = \begin{bmatrix} \tilde{C} \\ \tilde{C}\tilde{A} \\ \vdots \\ \tilde{C}\tilde{A}^p \end{bmatrix}$$

$$\bar{B} = \begin{bmatrix} 0 & 0 & 0 & \cdots & 0 \\ \tilde{C}\tilde{B} & 0 & 0 & \cdots & 0 \\ \tilde{C}\tilde{A}\tilde{B} & \tilde{C}\tilde{B} & 0 & \cdots & 0 \\ \vdots & \vdots & \vdots & \ddots & \vdots \\ \tilde{C}\tilde{A}^{p-1}\tilde{B} & \tilde{C}\tilde{A}^{p-2}\tilde{B} & & \cdots & \tilde{C}\tilde{A}^{p-m}\tilde{B} \end{bmatrix}$$

m and p are the input and output horizons.

The vector of future unconstrained control actions can be related to the error on the state of the prediction model as follows:

$$\Delta u = K_{MPC}[\tilde{x}^e]_{k|k},\quad K_{MPC} \in \mathbb{R}^{m.mu\times nx} \quad (8)$$

Substituting (8) in (6) produces

$$\left[x^e\right]_{k+1|k+1} = (A + B\tilde{K}_{MPC}\,N)\left[x^e\right]_{k|k} \quad (9)$$

where

$$\tilde{K}_{MPC} = C_K K_{MPC},\ C_K = [I_{nu}\quad 0],\ N = \begin{bmatrix} I_{nx} & 0 \end{bmatrix}$$

Consider also the following Lyapunov inequality:

$$\left(A + B\tilde{K}_{MPC}\,N\right)^T P^{-1}\left(A + B\tilde{K}_{MPC}N\right) - P^{-1} < 0 \quad (10)$$

with $P = P^T > 0$

Applying the Schur's complement to (10), results:

$$\begin{bmatrix} P & P\left(A + B\tilde{K}_{MPC}N\right) \\ \left(A + B\tilde{K}_{MPC}N\right)^T P^T & P \end{bmatrix} > 0 \quad (11)$$

A stable MPC would result from the minimization of the objective defined in (7) subject to the constraint defined in (11). However, to guarantee the contraction of the close-loop error vector, K_{MPC} and P should be fixed and so they need to be computed off-line and considering a fixed value for the error vector. For instance, they can be computed for an error $\tilde{x}_0^e$ that corresponds to a step change on the desired value of the output. The result is the following optimization problem:

Problem P1

$$\min_{\gamma, K_{MPC}, P}\ \gamma$$

subject to (11) and

$$\begin{bmatrix} (\bar{B}^T Q\bar{B} + R)^{-1} & K_{MPC}(\tilde{x}_0^e) \\ (\tilde{x}_0^e)^T K_{MPC}^T & \begin{bmatrix} \gamma - (\tilde{x}_0^e)^T \bar{A}^T Q\bar{A}\tilde{x}_0^e + \\ +(\tilde{x}_0^e)^T \bar{A}^T Q\bar{B}K_{MPC}\tilde{x}_0^e + \\ +(\tilde{x}_0^e)^T K_{MPC}^T \bar{B}^T Q\bar{A}\tilde{x}_0^e \end{bmatrix} \end{bmatrix} > 0 \quad (12)$$

where γ is a cost bound such $J_k \le \gamma$.

For the operating condition in which none of the input constraints becomes active, the control law obtained as the solution to Problem P1 results optimal and stability of the closed loop system is assured by the following theorem (Rodrigues and Odloak, 2000):

Theorem 1: Suppose that Problem P1 has a feasible solution. The resulting control law applied to the system defined in Eqs (4) and (5) will be asymptotic stable, as long as the system inputs do not become saturated.

Remark 1

As Inequality (11) is bilinear in the unknown variables P and K_{MPC}, Problem P1 has to be solved via an iterative algorithm that may be highly computer demanding for on-line implementation. Rodrigues and Odloak (2005) propose a two stages strategy to design and implement the stable MPC with output feedback and input saturation. The off-line synthesis is based on the solution to Problem P1. The on-line step is based on an optimization problem where the objective function is the same as the control objective used in the off-line step. The on-line controller is assumed to be a linear combination of the controllers obtained in the off-line step. The objective function of the on-line step is the true

control objective and the input constraints are included in the optimization problem.

To consider model uncertainty in the controller resulting from the solution to Problem P1, observe that in matrices A and B defined in Eq. (6), matrices A_p and B_p of the true plant are not usually known and they are not the same as matrices $\tilde{A}$ and $\tilde{B}$ of the predicting model. Note also that matrices A and B are affine in A_p and B_p respectively. The consequence of this observation is that, if model uncertainty concentrates on A_p and B_p, Problem P1 can be extended to produce a controller, which is robust to model uncertainty. For this purpose, we assume that state matrix A_p and input matrix B_p of the plant model defined in Eq. (4) are known to lie in the polytope defined in (13).

$$\left(A_p, B_p\right) = \sum_{i=1}^{L} \lambda_i \left(A_{p,i}, B_{p,i}\right),\ \sum_{i=1}^{L} \lambda_i = 1,\ \lambda_i \geq 0,\quad i = 1,\ldots,L \tag{13}$$

Also, let us define

$$A_i = \begin{bmatrix} (I - K_F\tilde{C})\tilde{A} & K_F C_p A_{p,i} \\ 0 & A_{p,i} \end{bmatrix}$$

$$B_i = -\begin{bmatrix} (I - K_F\tilde{C})\tilde{B} + K_F C_p B_{p,i} \\ B_{p,i} \end{bmatrix}$$

Next, consider the following off-line optimization problem

Problem P2

$$\min_{\gamma, K_{MPC}, P} \gamma$$

subject to (12) written for the nominal model and the following constraints

$$\begin{bmatrix} P & P\left(A_i + B_i C_K K_{MPC} N\right) \\ \left(A_i + B_i C_K K_{MPC} N\right)^T P^T & P \end{bmatrix} > 0 \quad i = 1,\ldots,L \tag{14}$$

In the above problem, each of the inequalities represented in Inequality (14) corresponds to one of the vertices of the polytope defined in (13). Stability of the uncertain closed-loop system with the output feedback controller defined by Problem P2 is ensured by the theorem below (Rodrigues and Odloak, 2000):

Theorem 2 Consider the system defined in Eqs (4) and (5), in which the true plant model matrices are unknown but defined by a polytope as in Eq. (13). Then, the closed loop system, with the control law obtained from the solution to Problem P2, will be asymptotically stable, as long as the system inputs do not become saturated.

Observe that in order to Problem P2 to have a feasible solution for the uncertain system, it is necessary that the system be observable and controllable. When one or more of the inputs become saturated, this condition may not be attained. Then, for the development that follows, it is assumed that the unstable and integrating modes of the system remains controllable after the saturation of one or more inputs.

3. ROBUST MPC WITH REALIGNED MODEL

Maciejowski (2002) shows that a suitable state space model to be used in the model predictive controller is the realigned model. Apart from the disadvantage of being a non-minimal representation of the system, this model form has the advantage that the state is composed of the inputs and outputs of the system at present and past time instants. Consequently, with this model form, the assumption that the state is perfectly known is always true. A consequence of this property of the model is that it is not necessary to include both the prediction model and the plant model in the closed loop representation of the system. To present the structure of the model as employed here, assume that the system is represented by the following equation:

$$y(k) + \sum_{i=1}^{na} a_i y(k-i) = \sum_{i=1}^{nb} b_i u(k-i)$$

It can be shown that this system can also be represented in the following state space form:

$$x(k+1) = \begin{bmatrix} I-a_1 & -a_2+a_1 & -a_3+a_2 & -a_4+a_3 & \ldots & -a_{na}+a_{na-1} & a_{na} & b_2 & b_3 & b_4 & \ldots & b_{nb} \\ I & 0 & 0 & 0 & \ldots & 0 & 0 & 0 & 0 & 0 & \ldots & 0 \\ 0 & I & 0 & 0 & \ldots & 0 & 0 & 0 & 0 & 0 & \ldots & 0 \\ 0 & 0 & I & 0 & \ldots & 0 & 0 & 0 & 0 & 0 & \ldots & 0 \\ \ldots & \ldots & \ldots & \ldots & \ldots & \ldots & \ldots & \ldots & \ldots & \ldots & \ldots & \ldots \\ 0 & 0 & 0 & 0 & \cdots & I & 0 & 0 & 0 & 0 & 0 & 0 \\ 0 & 0 & 0 & 0 & \cdots & 0 & 0 & 0 & 0 & 0 & 0 & 0 \\ 0 & 0 & 0 & 0 & \cdots & 0 & 0 & I & 0 & 0 & 0 & 0 \\ 0 & 0 & 0 & 0 & \cdots & 0 & 0 & 0 & I & 0 & 0 & 0 \\ 0 & 0 & 0 & 0 & \cdots & 0 & 0 & 0 & 0 & I & 0 & 0 \\ \ldots & \ldots & \ldots & \ldots & \ldots & \ldots & \ldots & \ldots & \ldots & \ldots & \ldots & \ldots \\ 0 & 0 & 0 & 0 & \cdots & 0 & 0 & 0 & 0 & 0 & I & 0 \end{bmatrix} x(k) + \begin{bmatrix} b_1 \\ 0 \\ 0 \\ 0 \\ \ldots \\ 0 \\ 0 \\ I \\ 0 \\ 0 \\ \ldots \\ 0 \end{bmatrix} \Delta u(k)$$

where

$$x(k) = \begin{bmatrix} y(k)^T & \cdots & y(k-na)^T & \Delta u(k-1)^T & \cdots & \Delta u(k-nb+1)^T \end{bmatrix}^T$$

The above model corresponds to the following general state space model form:

$$[x]_{k+1/k} = A[x]_{k/k} + B\,\Delta u(k) \tag{15}$$

$$[y]_{k/k} = C[x]_{k/k} \qquad C = \begin{bmatrix} I_{ny} & 0 & \cdots & 0 \end{bmatrix}$$

In the objective function defined in (7), the state error takes the following form

$$x^e = x^{sp}(k) - x(k) = \begin{bmatrix} y^{sp} - y(k) \\ \vdots \\ y^{sp} - y(k-na) \\ -\Delta u(k-1) \\ \vdots \\ -\Delta u(k-nb+1) \end{bmatrix}$$

Consider now the Lyapunov inequality presented in (10). In the realigned model case, matrix *N* becomes an identity matrix and (10) assumes the form:

$$\left(A + B\tilde{K}_{MPC}\right)^T P^{-1}\left(A + B\tilde{K}_{MPC}\right) - P^{-1} < 0$$

with $P = P^T > 0$

or

$$\begin{bmatrix} P & \left(A + B\tilde{K}_{MPC}\right)P \\ P^T\left(A + B\tilde{K}_{MPC}\right)^T & P \end{bmatrix} > 0 \quad (16)$$

Inequality (16) is still not a LMI as both $\tilde{K}_{MPC}$ and P are variables of the MPC optimization problem. However, in this case we can define a new variable $Y = \tilde{K}_{MPC}P$ and (16) is transformed into the following LMI:

$$\begin{bmatrix} P & AP + BY \\ P^T A^T + Y^T B^T & P \end{bmatrix} > 0$$

Observe that, as P is not singular, if Y and P are both known then $\tilde{K}_{MPC}$ can be computed by $\tilde{K}_{MPC} = Y P^{-1}$.

With these new variables, Problem P1 can be re-written as follows

Problem P3

$$\min_{\gamma, K_{MPC}, P, Y} \gamma$$

subject to

$$\begin{bmatrix} \left(\bar{B}^T Q \bar{B} + R\right)^{-1} & K_{MPC} x_0^e(k) \\ x_0^e(k)^T K_{MPC}^T & \begin{bmatrix} \gamma + x_0^e(k)^T \bar{A}^T Q \bar{B} K_{MPC} x_0^e(k) + \\ + x_0^e(k)^T K_{MPC}^T \bar{B}^T Q \bar{A} x_0^e(k) - \\ - x_0^e(k)^T \bar{A}^T Q \bar{A}\, x_0^e(k) \end{bmatrix} \end{bmatrix} > 0$$

$$\begin{bmatrix} P & AP + BY \\ P^T A^T + Y^T B^T & P \end{bmatrix} > 0$$

where

$$\tilde{K}_{MPC} = Y P^{-1}, \quad \tilde{K}_{MPC} = C_K\, K_{MPC} \qquad (17)$$

Problem P3 is not linear because of Eq. (17) and consequently, we cannot use the existing LMI packages to solve this problem. Thus, we propose a sub optimal solution that is based on the solution to two LMI sub problems:

Problem P3a

$$\max_{\alpha, P, Y} \alpha$$

subject to

$$\begin{bmatrix} P & AP + BY \\ P^T A^T + Y^T B^T & P - \alpha \end{bmatrix} > 0$$

$$\alpha \geq 0$$

Let us call the solution to this problem as α^*, Q^* and Y^*, and we can obtain the gain of the MPC controller as $\tilde{K}_{MPC}{}^* = Y^*(P^*)^{-1}$.

Problem P3b

$$\min_{K_{MPC}} J_k = x_0^e(k)^T K_{MPC}^T \left(\bar{B}^T Q \bar{B} + R\right) K_{MPC} x_0^e(k) - x_0^e(k)^T K_{MPC}^T \bar{B}^T Q \bar{A} x_0^e(k) - x_0^e(k)^T \bar{A}^T Q \bar{B} K_{MPC} x_0^e(k) + x_0^e(k)^T \bar{A}^T Q \bar{A} x_0^e(k)$$

subject to

$$\left(A + BC_K K_{MPC}\right)^T (P^*)^{-1}\left(A + BC_K K_{MPC}\right) - (P^*)^{-1} < 0 \qquad (18)$$

that can be transformed into the following LMI:

$$\begin{bmatrix} P^* & B\tilde{K}_{MPC} P^* \\ (P^*)^T \tilde{K}_{MPC}^T B^T & \begin{bmatrix} P^* + (P^*)^T A^T (P^*)^{-1} A P^* + \\ + (P^*)^T \tilde{K}_{MPC}^T B^T (P^*)^{-1} A P^* + \\ + (P^*)^T A^T (P^*)^{-1} B \tilde{K}_{MPC} P^* \end{bmatrix} \end{bmatrix} > 0$$

Problem P3a searches for a $\tilde{K}_{MPC}$ that maximizes α, which represents the distance the closed loop is from the stability limit. The purpose of Problem P3b is to improve the performance of the controller obtained in Problem P3a by minimizing the true objective function of the MPC while preserving stability, which is guaranteed by the presence of Inequality (18). It is easy to show that if Problem P3a is feasible then Problem P3b is also feasible as

$$K_{MPC} = \begin{bmatrix} \tilde{K}_{MPC}^{*\,T} & 0 & \cdots & 0 \end{bmatrix}^T$$

is a feasible solution to Problem P3b.

Assuming the same class of model uncertainty as the one defined in (13), Problems P3a and P3b can be extended to produce a new unconstrained robust MPC with output feedback, which is obtained from the solution of the following problems:

Problem P4a

$$\max_{\alpha, P, Y} \alpha$$

subject to

$$\begin{bmatrix} P & A_i P + B_i Y \\ P^T A_i^T + Y^T B_i^T & P - \alpha \end{bmatrix} > 0, \quad i = 1, \ldots, L$$
$$\alpha > 0$$

Problem P4b

$$\min_{K_{MPC}} J_k = x_0^e(k)^T K_{MPC}^T \left(\bar{B}^T Q \bar{B} + R\right) K_{MPC} x_0^e(k) -$$
$$- x_0^e(k)^T K_{MPC}^T \bar{B}^T Q \bar{A} x_0^e(k) - x_0^e(k)^T \bar{A}^T Q \bar{B} K_{MPC} x_0^e(k)$$
$$+ x_0^e(k)^T \bar{A}^T Q \bar{A} x_0^e(k)$$

subject to

$$\begin{bmatrix} P^* & B_i \tilde{K}_{MPC} P^* \\ (P^*)^T \tilde{K}_{MPC}^T B_i^T & \begin{bmatrix} P^* + (P^*)^T A_i^T (P^*)^{-1} A_i P^* + \\ + (P^*)^T \tilde{K}_{MPC}^T B_i^T (P^*)^{-1} A_i P^* + \\ + (P^*)^T A_i^T (P^*)^{-1} B_i \tilde{K}_{MPC} P^* \end{bmatrix} \end{bmatrix} > 0$$
$$i = 1, \ldots, L$$

Now, to obtain a new robust MPC with output feedback and input constraints, we propose the following algorithm:

Algorithm

Off-line step

Compute the output feedback gain K_{MPC} solving problems P4a and P4b considering the *nc* possible control configurations including the cases where one or more inputs become saturated. Each of these control configurations has a specific set of controlled outputs and unconstrained manipulated inputs. All the subsystems are assumed controllable. To stabilize all these subsystems that may result when one or more inputs become saturated, the following inequalities should be included in Problem P4a:

$$\begin{bmatrix} P & P\left(A_i + B_i \tilde{K}_{MPC}^j\right) \\ P^T \left(A_i + B_i \tilde{K}_{MPC}^j\right)^T & P \end{bmatrix} > 0$$
$$i = 1, \ldots, L, \quad j = 1, \ldots, nc$$

where matrix $\tilde{K}_{MPC}^j$ is obtained from $\tilde{K}_{MPC}$ by zeroing the terms related to the saturated inputs

On-line step

At each sampling step *k*, with the real output measurement compute the error on the state of the predicting model $[x^e]_{k|k}$ and solve the following problem:

Problem P5

$$\min_{\beta_0, \beta_1, \ldots, \beta_{nc}} J_k$$

Subject to

$$J_k = (\bar{A}[x^e]_{k|k} - \bar{B}\Delta u)^T Q (\bar{A}[x^e]_{k|k} - \bar{B}\Delta u) + \Delta u^T R \Delta u$$
$$\sum_{j=0}^{nc} \beta_j = 1$$
$$0 \le \beta_j \le 1 \qquad j = 0, 1 \ldots, nc$$
$$\Delta u = \left[\beta_0 K_{MPC} + \beta_1 K_{MPC}^1 + \cdots \beta_{nc} K_{MPC}^{nc}\right][x^e]_{k|k}$$
$$u_{\min} \le u(k+j) \le u_{\max} \qquad j = 1, \ldots, m-1$$

The successive application of the control law provided by the solution to Problem P5, for the uncertain system defined in Eq. (13), produces an asymptotically stable closed-loop system as shown in Theorem 3 below. The proof of this theorem can be obtained by following the same steps as in Rodrigues and Odloak (2005).

Theorem 3: Consider an uncertain system as defined in Eq. (13) and assume that this system remains controllable when one or more manipulated inputs become saturated. The closed loop system with the control strategy obtained by solving Problem P5 will remain stable when the system is moved from a point where none of the inputs is saturated to another point where one or more inputs become saturated. Stability is preserved in the reverse direction, when an input becomes available to be manipulated by the MPC.

4. EXAMPLE

The proposed control strategy was tested with a system of the process industry. The system is part of a distillation column where isobutene is separated from n-butane in an oil refinery. The controlled outputs are the level of liquid in the overhead drum (y_1) and the contents of isobutene in the distillate (y_2). The manipulated variables are the reboiler heat duty (u_1) and the distillate flow rate (u_2). From practical tests the following two models were obtained for different operating conditions:

$$G_1(s) = \begin{bmatrix} \frac{2.3}{s} & \frac{-0.7}{s} \\ \frac{-7e^{-7s}}{20s+1} & \frac{-1.8}{4s+1} \end{bmatrix}, G_2(s) = \begin{bmatrix} \frac{3}{s} & \frac{-0.5}{s} \\ \frac{-5e^{-5s}}{15s+1} & \frac{-2.5}{10s+1} \end{bmatrix}$$

In the simulation performed here, we study the set-point tracking problem where the desired value of isobutene in the distillate is increased by 1% and the desired value of the liquid level is not modified. The tuning parameters that were used in the off-line stage of the controller synthesis are the following: $T = 1$; $m = 3$; $p = 50$; $Q = \text{diag}[1\ 1]$; $R = diag[0.1\ 0.1]$. Related to the values the variables at the initial steady state of the system, the input limits are $u_{\max} = [0.2 \quad 2]$, $u_{\min} = [-0.2 \quad -2]$. The nominal model is represented by model 1 and the true plant can be either model 1 or model 2. Figure 1 shows the system responses for the nominally stable controller defined by problems 3a and 3b for three different cases. The first case corresponds to the ideal case where the predicting model and the true plant are represented by model 1. In Case 2, we have the same system as in Case 1 but the minimum bound for input u_1 was modified to –0.1 in order to force this input to become active during part of the simulation time.

From Fig. 1, we see that the controller stabilizes the true model without any problem and the performance of the controller is acceptable. However, in Case 3 where the controller is based in model 1 and the true plant is represented by model 2, the closed loop system becomes unstable.

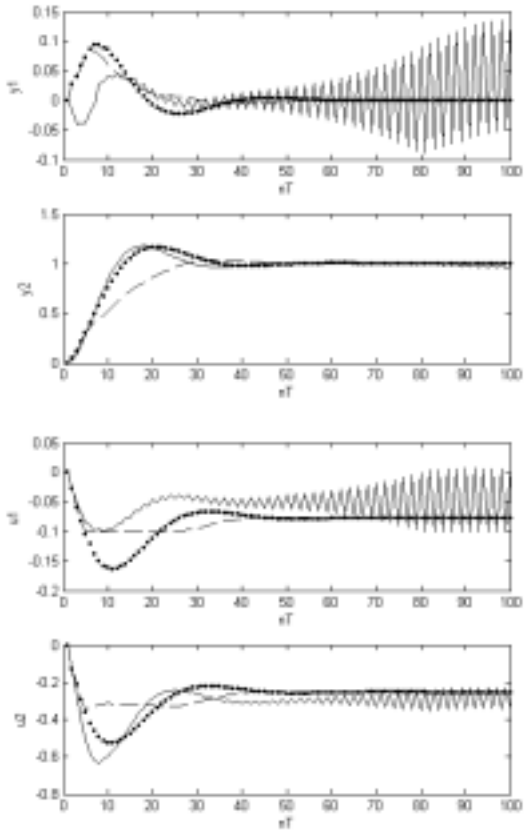

Figure 1. MPC with nominal model: Case 1 (….), Case 2 (- - - -) and Case 3 (——)

Fig.2 shows the closed loop responses with the robust MPC defined by Problems 4a and 4b considering models 1 and 2. In the two simulated cases plant is represented by model 2. In Case 4, the inputs do not saturate and the controller drives the two outputs to their desired values. The performance of the controller is slightly worse than in the ideal case as the output responses are slower than the responses for the nominal case. In Case 5, the minimum bound of input u_2 was modified to –0.2 in order to force this constraint to become active. We see from Fig. 2, that offset appears in both outputs because after saturation, the controller has only one manipulated input and two controlled outputs.

5. CONCLUSION

In this paper, it was developed a new version of the constrained robust MPC with output feedback. In the proposed method, assuming that controllability is preserved, stability is assured even when the system inputs become saturated at transient or equilibrium states. Polytopic model uncertainty is considered. Computer burden of the numerical methods involved in the practical synthesis of the controller is substantially reduced through the adoption of a simplified sub optimal solution to the control problem. On-line computation involves the search for the coefficients of a linear combination of previously defined MPC controllers. A simulation example shows that the implementation of the developed approach to real industrial systems may be achieved at least for systems of small to medium dimension.

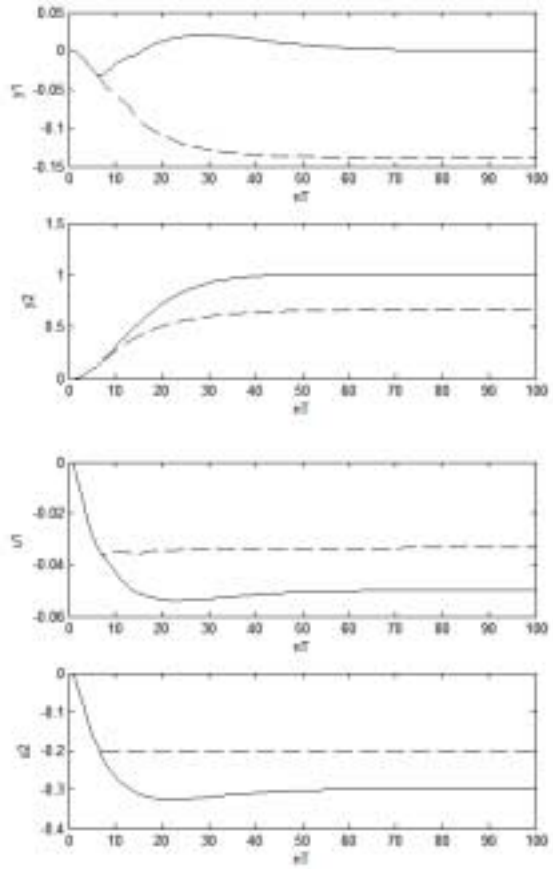

Fig.2. Robust MPC: Case 4 (——), Case 5 (- - - -)

ACKNOWLEDGMENTS

Support for this work was provided by CNPq under grants 300860/97-9 and 475893/2004-2.

REFERENCES

Lee, J. H. & B.L. Cooley (2000), Min-max predictive control techniques for linear system with bounded set of input matrices, *Automatica*, **36**, 463-473.

Maciejowski, J.M.(2002), *Predictive Control with Constraints*, Prentice Hall, London.

Qin, S.J. and T. A. Badgwell (2003), A survey of industrial model predictive control technology, *Control Eng. Practice*, **11** (7), 733-764.

Rodrigues, M.A. and D. Odloak (2000), Output feedback MPC with guaranteed robust stability, *Journal of Process Control*, **10** (6), 557-572.

Rodrigues, M.A. and D. Odloak (2005), Robust MPC for systems with output feedback and input saturation, *Journal of Process Control*, **15** (7), 837-846.

ADCHEM 2006

International Symposium on Advanced Control of Chemical Processes
Gramado, Brazil – April 2-5, 2006

DESIGN OF ROBUST GAIN-SCHEDULED MPC CONTROLLERS FOR NONLINEAR PROCESSES

Jianying Gao, Hector M. Budman*

Department of Chemical Engineering, University of Waterloo,
Waterloo, ON, Canada, N2L 3G1

Abstract**:** A methodology is proposed for the analysis and design of a robust gain-scheduled Model predictive Controllers (MPC) for nonlinear chemical processes. The stability and performance tests can be formulated as a finite set of linear matrix inequalities (LMI). A simulation study of a 2x2 system indicates that this approach can provide useful robust controllers, which guarantee closed-loop robust stability and performance. *Copyright © 2006 ADCHEM*

Keywords: robust control, nonlinear systems, model predictive control.

1. INTRODUCTION

MPC is a widely accepted control algorithm in the chemical industry. In most of industrial applications the design of the controller is based on a nominal linear model of the process. Such control systems that provide optimal performance for a particular linear model may perform poorly when implemented on a physical nonlinear system (Zheng and Morari, 1993).

Due to the process nonlinearity, a system behaves differently at different operating conditions. Therefore, controllers that are based on one single linear model have to be tuned for robustness to model errors or uncertainty between the nominal model and the actual process behavior.

The basic philosophy in the literature for optimizing the performance of MPC-based design algorithms that explicitly account for model-plant error is to modify the on-line minimization problem to a min-max problem, where the worst-case value of the objective function is minimized over the set of plants that account for the nominal model and uncertainty (Campo and Morari, 1987; Zheng and Morari, 1993).

This approach is clearly computationally much more demanding than solving it for a nominal plant. To simplify the computational complexity, one must choose simplistic, albeit unrealistic, model uncertainty descriptions, e.g., fewer impulse response coefficients. Also, controllers that are tuned for robustness to model errors between a nominal linear model and the actual nonlinear process output tend to have been proposed lately to address the nonlinearity of the process and to improve the closed loop performance (Allgower, *et al*., 2000). However, it is difficult to guarantee stability and performance for these controllers and they generally require a nonlinear mechanistic model of the process that is often difficult to obtain.

In this work, an alternative gain-scheduled MPC design approach is proposed, which allows explicit consideration of the nonlinear behavior of the process. To design this controller, instead of using one step response model for output prediction, several linear step models will be identified for different regions defined based on the values of the manipulated variable u. Then, for each of these models, a linear MPC calculation can be conducted based on the current value of u. Thus, the controller is referred to as a gain-scheduled MPC because the

*Corresponding author. Email: hbudman@engmail.uwaterloo.ca;
Phone: 519-888-4567 ext. 6980; Fax: 519-746 4979

MPC matrix gain changes as a function of the value of the manipulated variable *u*.

It is assumed in this work that a mechanistic model of the process is not available. Thus, for the purpose of controller design and robustness analysis, an empirical nonlinear state-affine model (Knapp and Budman, 2001) to be identified from experiments is used as follows:

$$\begin{aligned}
&\mathbf{x}(t+1) = \mathbf{F}(\mathbf{u})\mathbf{x}(t) + \mathbf{G}(\mathbf{u})\mathbf{u}(t) \\
&\mathbf{F}(\delta) = \{\mathbf{F}_0 + \sum_{i=1}^{K-1} \mathbf{F}_i u_{i,t}\} \\
&\mathbf{G}(\delta) = \{\mathbf{G}_1 + \sum_{i=1}^{K-1} \mathbf{G}_{i+1} u_{i,t}\} \\
&\mathbf{y}(t) = \mathbf{H}_0\mathbf{x}(t) + \mathbf{W}_\mathbf{f} d(t) \\
&d(t+1) = BW d(t) + (1-BW)v(t)
\end{aligned} \tag{1}$$

For a process given by the state-affine model , it is valid to assume that in a small neighborhood of a pre-selected nominal operating point, i.e. for $u(t) << 1$, the process can be accurately modeled by the linear part of the state-affine model. The uncertainty of the system will be assumed to be the difference between the nonlinear model and the nominal linear model. It is also assumed that all of the uncertainty in the state-affine model is due to the time-varying nonlinearity of the state-affine model around this operating point. It is therefore possible to describe the model uncertainty perturbation $\delta_{i,t}$ in the following form:

$$\delta_{i,t} = u(t)^i \tag{2}$$

Some of the advantages of this model for the purpose of analysis are: 1)-it can be easily identified from data, 2)- by considering the high order of *u* to be the uncertainty elements, it is easy to split the model above into a linear part and a nonlinear part and to formulate analysis tests for robust stability and performance (Budman and Knapp, 2001) and, 3)- the uncertainty elements can be easily bounded based on the limits of the manipulated variable *u*. Also, step models for designing the gain scheduled controller mentioned above can be easily extracted from the model given by (1).

The closed-loop system composed of the state-affine model combined with a state-space formulation of the gain-scheduled MPC controller is studied for robust stability and performance through LMI's tests. Thus, the proposed gain-scheduled MPC controller is designed to ensure closed-loop system robust stability and suitable performance.

This paper is organized as follows. Section 2 develops the state-space formulation of the unconstrained MPC control law. The closed-loop system equations, composed of the state-affine model and the MPC controller, are formulated as an affine parameter-dependent system. In Section 3, the procedures for the design and optimization of the robust gain-scheduled MPC are detailed. In Section 4, the above proposed approach is applied to a 2x2 system, leading to results and conclusions summarized in Section 5.

2. UNCONSTRAINED MPC ALGORITHM IN STATE-SPACE FORM

In order to formulate robust stability and robust performance tests, a state-space formulation of the MPC controller (Zanovello and Budman, 1999) is desired. A standard unconstrained MPC formulation is used. Consider a multiple-input-multiple-output (MIMO) system with n_u inputs and n_y outputs, to be controlled by a MPC controller, with prediction horizon *p* and control horizon *m*.

The model update vector is defined as follows:

$$\begin{aligned}
&\overline{\mathbf{Y}}(t) = \mathbf{M}_I \overline{\mathbf{Y}}(t-1) + \mathbf{s}^u \Delta\mathbf{u}(t-1) \\
&\mathbf{M}_I = \begin{bmatrix}
\mathbf{0}_{n_y\times n_y} & \mathbf{I}_{n_y} & \mathbf{0}_{n_y\times n_y} & . & \mathbf{0}_{n_y\times n_y} \\
\mathbf{0}_{n_y\times n_y} & \mathbf{0}_{n_y\times n_y} & \mathbf{I}_{n_y} & . & \mathbf{0}_{n_y\times n_y} \\
. & . & . & . & . \\
. & . & . & . & \mathbf{I}_{n_y} \\
\mathbf{0}_{n_y\times n_y} & \mathbf{0}_{n_y\times n_y} & . & \mathbf{0}_{n_y\times n_y} & \mathbf{I}_{n_y}
\end{bmatrix}_{nn_y\times mn_y}
\end{aligned} \tag{3}$$

The step response coefficient S_i^u and impulse response coefficient h_i are defined as follows:

$$\mathbf{S}_i^u = \begin{bmatrix}
S^u_{1,1,i} & S^u_{1,2,i} & . & S^u_{1,n_u,i} \\
S^u_{2,1,i} & . & . & 0 \\
. & . & . & . \\
S^u_{n_y,1,i} & S^u_{n_y,2,i} & . & S^u_{n_y,n_u,i}
\end{bmatrix}_{n_y\times n_u} \tag{4}$$

$$\mathbf{h}_i = \begin{bmatrix}
h_{1,1,i} & h_{1,2,i} & . & h_{1,n_u,i} \\
h_{2,1,i} & . & . & 0 \\
. & . & . & . \\
h_{n_y,1,i} & h_{n_y,2,i} & . & h_{n_y,n_u,i}
\end{bmatrix}_{n_y\times n_u}$$

where $S^u_{l,k,i}$ and $\mathbf{h}_{l,k,i}$ are the i^{th} response coefficient describing the effect of k^{th} input on l^{th} output. The step response vector $\mathbf{s}^u$ and the step response matrix $\mathbf{S}^u$ are given as follows:

$$\begin{aligned}
&\mathbf{s}^u = \begin{bmatrix} \mathbf{S}_1^u & \cdots & \mathbf{S}_n^u \end{bmatrix}^T \\
&\mathbf{S}^u = \begin{bmatrix}
\mathbf{S}_1^u & 0 & . & 0 \\
\mathbf{S}_2^u & \mathbf{S}_1^u & . & 0 \\
. & . & . & . \\
\mathbf{S}_n^u & \mathbf{S}_{n-1}^u & . & \mathbf{S}_{n-m+1}^u
\end{bmatrix}_{nn_y\times mn_u}
\end{aligned} \tag{5}$$

where *m* is referred to as the control horizon. The *p*-step-ahead prediction vector $\overline{\mathbf{Y}}(t+1/t)$ is defined as follows:

$$\overline{\mathbf{Y}}(t+1/t) = \mathbf{M}_p \overline{\mathbf{Y}}(t) + \mathbf{W}(t+1/t) + \mathbf{S}_p^u \Delta \mathbf{U}(t)$$
$$\mathbf{M}_p = \begin{bmatrix} \mathbf{I}_{pn_y \times pn_y} & 0 \end{bmatrix}_{pn_y \times nn_y} \mathbf{M}_I \quad (6)$$

$\mathbf{S}_p^u$ is the sub-matrix of the first p rows of $\mathbf{S}^u$ and p is the prediction horizon. The vector $\mathbf{W}(t+1/t)$ is defined to represent the unmeasured disturbance and model/plant mismatch. Making the common assumption that the disturbances are step-like, the disturbance vector $\mathbf{W}(t+1/t)$ is given as follows:

$$\mathbf{W}(t+1/t) = \mathbf{N}_2[\mathbf{y}(t) - \overline{\mathbf{y}}(t)]$$
$$\mathbf{N}_2 = \begin{bmatrix} \mathbf{I}_{n_y} & . & \mathbf{I}_{n_y} \end{bmatrix}^T_{n_y \times pn_y} \quad (7)$$

where $\mathbf{y}(t)$ is the vector of the n_y measured values, and $\overline{\mathbf{y}}(t)$ is the vector composed of the first n_y elements of the vector $\overline{\mathbf{Y}}(t)$.

The objective function is given as follows:

$$\min_{\Delta \mathbf{u}(t)} \frac{1}{2} \{ \left\| \mathbf{\Gamma}[\overline{\mathbf{Y}}(t+1|t) - \mathbf{R}(t+1)] \right\|^2 + \left\| \mathbf{\Lambda} \Delta \mathbf{U} \right\|^2 \} \quad (8)$$

where $\mathbf{\Lambda}, \mathbf{\Gamma}$ are positive-definite weighting matrices for the manipulated and controlled variables respectively. Then, the least squares solution of the minimization problem with the cost function given by (8) is given as follows:

$$\Delta \mathbf{u}(t) = \mathbf{K}_{MPC} \boldsymbol{\varepsilon}(t+1|t)$$
$$\mathbf{K}_{MPC} = \mathbf{e}(\mathbf{S}_p^{u\,T} \mathbf{\Gamma}^T \mathbf{\Gamma} \mathbf{S}_p^u + \mathbf{\Lambda}^T \mathbf{\Lambda})^{-1} \mathbf{S}_p^{u\,T} \mathbf{\Gamma}^T \mathbf{\Gamma} \quad (9)$$
$$\mathbf{e} = \begin{bmatrix} \mathbf{I}_{n_u} & \mathbf{0}_{n_u} & \cdots & \mathbf{0}_{n_u} \end{bmatrix}_{n_u \times mn_u}$$

$\boldsymbol{\varepsilon}(t+1|t)$ is the feedback error vector defined as follows:

$$\boldsymbol{\varepsilon}(t+1|t) = \mathbf{R}(t+1) - \mathbf{M}_p \overline{\mathbf{Y}}(t) - \mathbf{W}(t+1|t) \quad (10)$$

The controller state vector $\mathbf{U}(t-1)$ is defined as follows:

$$\mathbf{U}^T(t-1) = \begin{bmatrix} \mathbf{u}(t-1) & \ldots & \mathbf{u}(t-n) \end{bmatrix}_{1 \times nn_u} \quad (11)$$

Assuming $\mathrm{R} = 0$ without loss of generality, the following is obtained from (11), (9) and (10):

$$\mathbf{U}(t) = \mathbf{T}_2 \mathbf{U}(t-1) +$$
$$\mathbf{T}_1 \mathbf{K}_{MPC}[-\mathbf{M}_p \overline{\mathbf{Y}}(t) - \mathbf{W}(t+1|t)] \quad (12)$$
$$\mathbf{T}_1 = \begin{bmatrix} \mathbf{I}_{n_u} \\ \mathbf{0} \\ . \\ . \\ \mathbf{0} \end{bmatrix} \mathbf{T}_2 = \begin{bmatrix} \mathbf{I}_{n_u} & \mathbf{0} & \mathbf{0} & . & \mathbf{0} \\ \mathbf{I}_{n_u} & \mathbf{0} & \mathbf{0} & . & \mathbf{0} \\ \mathbf{0} & \mathbf{I}_{n_u} & \mathbf{0} & . & . \\ . & . & . & . & . \\ \mathbf{0} & . & . & \mathbf{I}_{n_u} & \mathbf{0} \end{bmatrix}$$

The controller output $\mathrm{u}(\mathrm{t})$ is defined as follows:

$$\mathbf{u}(t) = \mathbf{e}_1 \mathbf{U}(t-1) + \Delta \mathbf{u}(t)$$
$$\mathbf{e}_1 = \begin{bmatrix} \mathbf{I}_{n_u} & \mathbf{0}_{n_u \times n_u} & . & \mathbf{0}_{n_u \times n_u} \end{bmatrix}_{n_u \times nn_u} \quad (13)$$

Using the relation $\mathbf{S}_{l,k,j} = \sum_{i=1}^{j} \mathbf{h}_{l,k,i}, j = 1,2,\ldots,n$, the model update vector $\overline{\mathbf{Y}}(t)$ is also given by:

$$\overline{\mathbf{Y}}(t) = \begin{bmatrix} \overline{\mathbf{y}}(t) & \cdots & \overline{\mathbf{y}}(t+n-1) \end{bmatrix}^T$$
$$= \begin{bmatrix} \mathbf{S}_1^u & \mathbf{h}_2 & . & . & \mathbf{h}_n \\ \mathbf{S}_2^u & \mathbf{h}_3 & . & \mathbf{h}_n & \mathbf{0} \\ . & . & . & . & . \\ . & . & . & . & . \\ \mathbf{S}_n^u & \mathbf{0} & . & . & \mathbf{0} \end{bmatrix} \begin{bmatrix} \mathbf{u}(t-1) \\ \mathbf{u}(t-2) \\ . \\ . \\ \mathbf{u}(t-n) \end{bmatrix} \quad (14)$$
$$\overline{\mathbf{Y}}(t) = \mathbf{H}_{nn_y \times nn_u} \mathbf{U}(t-1)$$

The predicted output is given as follows:

$$\overline{\mathbf{y}}(t) = \begin{bmatrix} \mathbf{I}_{n_y} & \mathbf{0}_{n_y \times n_y} & . & \mathbf{0}_{n_y \times n_y} \end{bmatrix}_{n_y \times nn_y} \overline{\mathbf{Y}}(t) \quad (15)$$
$$= \mathbf{e}_2 \mathbf{H} \mathbf{U}(t-1)$$

To analyze the robustness of the closed loop system the state affine model given in equation 1 is used to model the process. This model (Knapp and Budman, 2001; Gao and Budman, 2005) has been shown to correctly describe the nonlinear behavior of the process.

From (14), (7) and (15), equation (12) can be rewritten as:

$$\mathbf{U}(t) = \mathbf{E}_2 \mathbf{U}(t-1) - \mathbf{T}_1 \mathbf{K}_{MPC} \mathbf{N}_2 (\mathbf{H}_0 \mathbf{x}(t) + \mathbf{W}_\mathbf{f} d(t)) \quad (16)$$
$$\mathbf{E}_2 = \mathbf{T}_2 - \mathbf{T}_1 \mathbf{K}_{MPC} (\mathbf{M}_p \mathbf{H} - \mathbf{N}_2 \mathbf{e}_2 \mathbf{H})$$

The control action can be calculated from the following expression:

$$\mathbf{u}(t) = \mathbf{C}_{u1} \mathbf{U}(t-1) - \mathbf{K}_{MPC} \mathbf{N}_2 (\mathbf{H}_0 \mathbf{x}(t) + \mathbf{W}_\mathbf{f} d(t)) \quad (17)$$
$$\mathbf{C}_{u1} = \mathbf{e}_1 - \mathbf{K}_{MPC} (\mathbf{M}_p \mathbf{H} - \mathbf{N}_2 \mathbf{e}_2 \mathbf{H})$$

Then, a state-space representation of the MPC controller can be obtained by combining (16) and (17) as follows:

$$\begin{bmatrix} \mathbf{U}(t) \\ \hline \mathbf{u}(t) \end{bmatrix} = \begin{bmatrix} \mathbf{E}_2 & -\mathbf{T}_1\mathbf{K}_{mpc}\mathbf{N}_2 \\ \mathbf{C}_{u1} & -\mathbf{K}_{mpc}\mathbf{N}_2 \end{bmatrix} \begin{bmatrix} \mathbf{U}(t-1) \\ \hline \mathbf{y}(t) \end{bmatrix} \quad (18)$$

From (1) and (18), the closed-loop system is obtained by combining the state-affine model and the MPC controller equations into the following equation:

$$\begin{bmatrix} \mathbf{x}(t+1) \\ \mathbf{U}(t) \\ \hline d(t+1) \\ \mathbf{y}(t) \end{bmatrix} = \begin{bmatrix} \mathbf{A}(\boldsymbol{\delta}_t) & \mathbf{B} \\ \mathbf{C} & \mathbf{D} \end{bmatrix} \begin{bmatrix} \mathbf{x}(t) \\ \mathbf{U}(t-1) \\ \hline d(t) \\ \nu(t) \end{bmatrix}$$

$$\mathbf{A}(\boldsymbol{\delta}_t) = \begin{bmatrix} \mathbf{A}_{11} & \mathbf{A}_{12} & \mathbf{A}_{13} \\ -\mathbf{T}_1\mathbf{K}_{MPC}\mathbf{N}_2\mathbf{H}_0 & \mathbf{E}_2 & -\mathbf{T}_1\mathbf{K}_{MPC}\mathbf{N}_2\mathbf{W}_\mathbf{f} \\ \mathbf{0} & \mathbf{0} & BW \end{bmatrix} \quad (19)$$

$$\mathbf{A}_{11} = \mathbf{F}(\delta) - \mathbf{G}(\delta)\mathbf{K}_{MPC}\mathbf{N}_2\mathbf{H}_0, \mathbf{A}_{12} = \mathbf{G}(\delta)\mathbf{C}_{u1}$$

$$\mathbf{A}_{13} = -\mathbf{G}(\delta)\mathbf{K}_{MPC}\mathbf{N}_2\mathbf{W}_\mathbf{f}$$

$$\mathbf{B} = \begin{bmatrix} \mathbf{0} \\ \mathbf{0} \\ 1-BW \end{bmatrix}, \mathbf{C} = \begin{bmatrix} \mathbf{H}_0^T \\ \mathbf{0}^T \\ \mathbf{W}_\mathbf{f}^\mathbf{T} \end{bmatrix}^T, \mathbf{D} = [\mathbf{0}]$$

The above state-space system representation is used for robust stability and performance analysis as described in the next section.

3. ROBUST GAIN-SCHEDULED MPC DESIGN

For open-loop stable plants, the stability and performance of the closed-loop system depends on the MPC design parameters, *m*, *p*, Λ and Γ, and step response coefficients. In this work, for simplicity, Λ is the only parameter considered for tuning whereas the other parameters are assumed constant.

For the design of a gain-scheduled MPC controller for a MIMO system with n_u inputs, the overall range of change of each input variable $u_i(t), i = 1,2,\ldots,n_u$ is discretized into $k_i, i = 1,2,\cdots,n_u$ regions. The impulse model H(u) is identified in each of these sub-ranges from equation (1). An optimal value of the input weight matrix $\boldsymbol{\Lambda}$ is selected for each one of these sub-ranges resulting in a gain-scheduled MPC algorithm.

The closed-loop system given by (19) has affine-parameter dependence with respect to the uncertain parameters $\delta_{i,t}$'s, and this allows the formulation of the robust stability and performance conditions developed by Gao and Budman (2005) to the design of MPC controllers given by (18). The robust stability condition (Gao and Budman, 2005) is:

$$\mathbf{A}(\omega)^T \mathbf{P}\mathbf{A}(\omega) - \mathbf{P} < 0 \quad \textit{for all } \omega \in \Re \quad (20)$$

where $\Re$ denotes the vertices or corners of the parameter box. For robust performance analysis, the system performance index is defined from the ratio between the error to disturbances: $\|\mathbf{e}\|_{\ell_2} < \gamma \|\mathbf{v}\|_{\ell_2}$. The objective of the controller optimization problem is to minimize the parameter γ according to a GEVP (Generalized Eigenvalue Problem) that can be formulated and solved using MATLAB as follows:

$$\min_{\mathbf{P}} \gamma^2$$

$$s.t. \quad \mathbf{K}(\omega, \mathbf{P}) < \gamma^2 \mathbf{L}, \textit{for all} \quad \omega \in \Re$$

$$\mathbf{K} = \begin{bmatrix} \mathbf{A}(\omega)^T \mathbf{P}\mathbf{A}(\omega) - \mathbf{P} & \mathbf{A}(\omega)^T \mathbf{P}\mathbf{B} & \mathbf{C}^T \\ \mathbf{B}^T \mathbf{P}\mathbf{A}(\omega) & \mathbf{B}^T \mathbf{P}\mathbf{B} & \mathbf{D}^T \\ \mathbf{C} & \mathbf{D} & -\mathbf{I} \end{bmatrix} \quad (21)$$

$$\mathbf{L} = \begin{bmatrix} 0 & 0 & 0 \\ 0 & \mathbf{I} & 0 \\ 0 & 0 & 0 \end{bmatrix}$$

4. DESIGN CASE STUDY

To illustrate the design technique, a simple 2-input-2-output example is used. The state-affine model has the form of with $\delta_{1,t} = u_1(t), \delta_{2,t} = u_2(t)$, and the model coefficient matrices are as follows:

$$\mathbf{F}_0 = \begin{bmatrix} 0.1188 & -0.0346 \\ -2.3416 & 0.0937 \end{bmatrix}, \mathbf{F}_1 = \begin{bmatrix} 0.1076 & 0 \\ 1.2289 & 0 \end{bmatrix}$$

$$\mathbf{G}_1 = \begin{bmatrix} 1 & 0 \\ 0 & 1 \end{bmatrix}, \mathbf{G}_2 = \begin{bmatrix} 0 & 0.1 \\ 0.1 & 0 \end{bmatrix}, \quad (22)$$

$$\mathbf{G}_3 = \begin{bmatrix} -0.01 & -0.0159 \\ -0.0508 & -0.0928 \end{bmatrix}$$

$$\mathbf{H}_0 = \begin{bmatrix} 0.1755 & -0.0382 \\ 0 & 0.1 \end{bmatrix}, \mathbf{W}_\mathbf{f} = [1 \quad 0]^T, \; BW = 0.8$$

Assuming even discretization of each one of the manipulated variables u into two regions, the following controller, referred to as GSMPC, is proposed for a total of four operating regions:

$$\begin{aligned} &I \quad \begin{bmatrix} -0.3 \le u_1 \le 0 \\ -0.3 \le u_2 \le 0 \end{bmatrix} \quad MPC_{11}(\mathbf{K}_{MPC11}, \boldsymbol{\Lambda}_{11}) \\ &II \quad \begin{bmatrix} -0.3 \le u_1 \le 0 \\ 0 < u_2 \le 0.3 \end{bmatrix} \quad MPC_{12}(\mathbf{K}_{MPC12}, \boldsymbol{\Lambda}_{12}) \\ &III \quad \begin{bmatrix} 0 < u_1 \le 0.3 \\ -0.3 \le u_2 \le 0 \end{bmatrix} \quad MPC_{21}(\mathbf{K}_{MPC21}, \boldsymbol{\Lambda}_{21}) \\ &IV \quad \begin{bmatrix} 0 < u_1 \le 0.3 \\ 0 < u_2 \le 0.3 \end{bmatrix} \quad MPC_{22}(\mathbf{K}_{MPC22}, \boldsymbol{\Lambda}_{22}) \end{aligned} \quad (23)$$

where $\mathrm{MPC_{ij}}(\mathrm{K_{MPCij}}, \Lambda_{\mathrm{ij}})$ refers to the *ij*th MPC controller, where u_1 evolves within the *i*th region, and u_2 evolves within the *j*th region. Each Λ_{ij} is of the following form:

$$\boldsymbol{\Lambda}_{ij} = \begin{bmatrix} \lambda_{1i} & \\ & \lambda_{2j} \end{bmatrix} \begin{matrix} i = 1,2 \\ j = 1,2 \end{matrix} \quad (24)$$

K_{MPCij} is calculated based on the step response conducted between the extreme values of u of each of the regions defined in (23) in terms of u. For example, K_{MPC12} will be calculated using a step response corresponding to

$$\left[-0.3 \le u_1 \le 0, \quad 0 < u_2 \le 0.3\right].$$

For comparison, a linear MPC controller, referred to as LMPC in the sequel, will be designed with the following form:

$$for \quad \begin{bmatrix} -0.3 \le u_1 \le 0.3 \\ -0.3 \le u_2 \le 0.3 \end{bmatrix} \quad MPC(\mathbf{K}_{MPC}, \mathbf{\Lambda}(\lambda_{11}, \lambda_{22})) \quad (25)$$

where, λ_{11} and λ_{22} are the weights of the manipulated variables u_1 and u_2 respectively. For this linear controller, K_{MPC} is calculated based on step responses carried out between the limits -1 to 1 for each u.

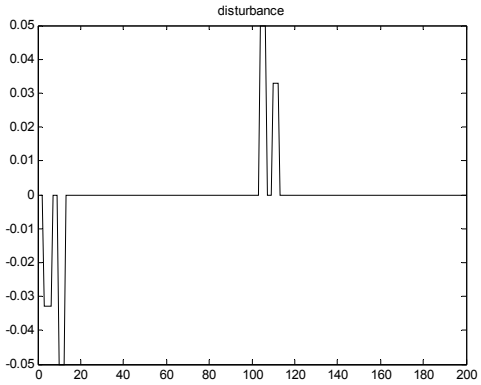

Fig. 1. Disturbance signal for the simulation

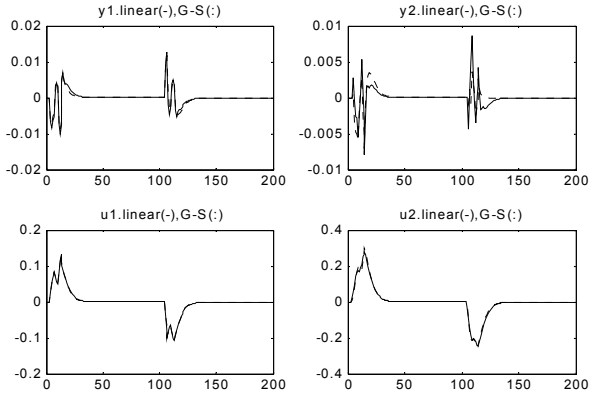

Fig. 2. Comparison of the LMPC (solid line) and GSMPC (dotted line) controllers designed based on the minimization of $\bar{\gamma}_{\text{local}}$.

The input weights of the GSMPC and LMPC controllers are optimized to minimize the performance index γ calculated according to the GEVP problem given by (21). The calculation includes 16 LMI's according to all the vertices ω defined by (23) and the resulting optimal γ will be referred to as γ_{global}.

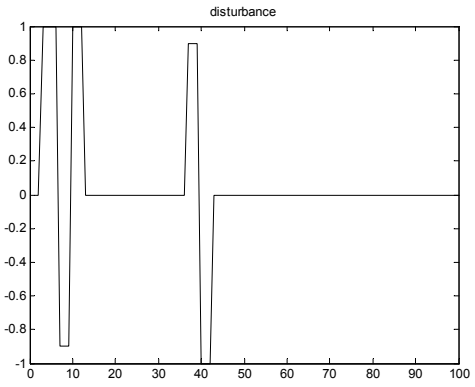

Fig. 3. Disturbance signal for the simulation

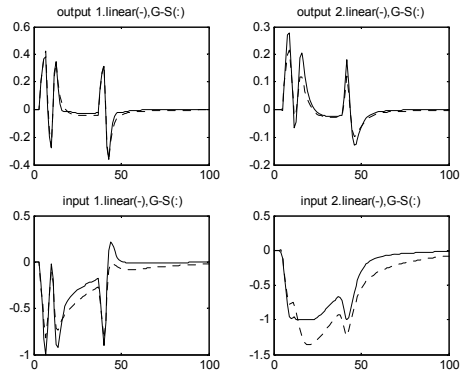

Fig. 4 Comparison of the LMPC (solid line) and GSMPC (dotted line) controllers designed based on the minimization of γ_{global}.

The robust performance analysis and simulation results of the gain scheduled and linear MPC controllers for the MIMO process are summarized in Table 1. It can be seen from Table 1 that the performance index γ_{global} for GSMPC controllers is 0.8494, larger than the value of 0.7472 for γ_{global} obtained for LMPC. This seems to indicate that a better performance can be achieved with LMPC. This result is not completely surprising since the gain scheduling controller is not necessarily better when large changes in u values occurred during dynamic transitions between the different regions defined in (23). One way to improve the GSMPC is by optimizing further the step response models used to calculate the controllers. However, this is a difficult optimization problem and it is beyond the scope of this study.

On the other hand, a scenario where GSMPC is expected to perform better than the LMPC is when the process is operated within each of the regions described by (23) for long periods of time. This is due to the fact that the GSMPC is based on "local" step response models identified in each of these regions. This scenario can be assessed by computing a value of γ for each of the regions given in (23) by using the corresponding set of 4 LMI's for each one of the

combinations of u values in each of these 4 regions. An overall performance index, to be referred as $\bar{\gamma}_{local}$, can be obtained by calculating the average of the four resulting γ 's. Then, LMPC and GSMPC controllers that minimize $\bar{\gamma}_{local}$ can be designed. The results, shown in Table 1, confirm that the GSMPC is better than the LMPC when the controllers are designed based on this $\bar{\gamma}_{local}$ index, instead of the global performance index γ_{global} calculated for the whole range of operation.

Table 1 MPC controller optimization

based on γ_{global}	LMPC	GSMPC
$[\lambda_{11},\lambda_{12},\lambda_{21},\lambda_{22}]$	[0.5009,-,-,0.4983]	[0.5164,0.5029, 0.4980,0.5034]
γ_{global} at optimum	0.7472	0.8694
$\gamma_{simulation}$	0.3396	0.3238
based on $\bar{\gamma}_{\text{local}}$	LMPC	GSMPC
$[\lambda_{11},\lambda_{12},\lambda_{21},\lambda_{22}]$	[0.1054,-,-,0.0958]	[0.0988,0.1006, 0.1044, 0.1006]
$\bar{\gamma}_{local}$ at optimum	0.4765	0.4021
$\gamma_{simulation}$	0.2524	0.2490

To assess the correctness of the analysis, a large number of disturbances were simulated for the controllers described above. Ideally, the disturbances that lead to the worst γ values are sought. However, this is a very difficult optimization problem and therefore the γ values calculated from simulations and shown in Table 1 as $\gamma_{simulation}$, are the largest found during the simulations but not necessarily the largest possible. The worst disturbances found in the simulations are given in Fig. 1 and Fig.3, for the controllers based on $\bar{\gamma}_{local}$ and γ_{global} respectively.

Both GSMPC, based on γ_{global} and $\bar{\gamma}_{local}$, showed improvement in terms of $\gamma_{simulation}$ compared to the LMPC. Fig. 2 and Fig.4 show the results for the simulations carried out to compute $\gamma_{\text{simulation}}$ for controllers that are designed based on the minimization of $\bar{\gamma}_{local}$ and γ_{global} respectively. It should be noticed in Fig.2 that corresponds to the design based on $\bar{\gamma}_{local}$ that during $0<t<100$ the *u's* are evolving within region I described in (23) and during $100<t<200$ the *u's* are within region IV in (23). The analytical γ_{global} and $\bar{\gamma}_{local}$ are clearly larger than the $\gamma_{simulation}$ indicating that the analytical bounds may be conservative but they can still be useful as an indicator of the relative performance of the controllers described above.

5. CONCLUSIONS

An approach is proposed to design gain-scheduled MPC controllers for nonlinear processes using process data. It is based on empirical state-affine models of the process. Gain-scheduled MPC controllers are obtained using a GEVP based optimization algorithm. The analysis show that the gain scheduled MPC performs better than the linear MPC when the local performance in small regions of operation is considered.

REFERENCES

Allgower, F., R. Findeisen, Z. Nagy, M. Diehl, H.G. Bock, and J.P. Schloder (2000). Efficient nonlinear model predictive control for large scale constrained processes. In *Proceedings of the 6th International Conference on Methods and Models in Automation and Robotics*, pp. 43–54.

Budman, H.M. and T.D. Knapp (2001). Stability analysis of nonlinear processes using empirical state-affine models and LMIs. *Journal of Process Control,* **vol. 11**, pp. 375-386.

Campo, P.J. and M. Morari (1987). Robust Model Predictive Control. *Proceedings of American Control Conference*. v**ol.2**, pp. 1021-1026.

Doyle III, F.J., A. Packard, and M. Morari (1989). Robust Controller Design for a Nonlinear CSTR. *Chemical Engineering Science*, **vol. 44**, pp. 1929-1947.

Gao, J. and H.M. Budman (2004). Reducing conservatism in the design of a robust gain-scheduled controller for nonlinear chemical processes. *International Journal of Control*, **vol.77**, No.11, pp.1050-1061.

Gao, J. and H.M. Budman (2005). Design of robust gain-scheduled PI controllers. *Journal of Process Control*. (accepted for publication).

Zafiriou, E. (1990). Robust Model Predictive Control of Processes with Hard Constraints. *Computers and Chemical Engineering*. **vol.14**, No.4/5, pp. 359-371.

Zanovello, R. and H.M. Budman (1999). Model predictive control with soft constraints with application to lime kiln control. *Computers and Chemical Engineering*. **23**. pp. 791-806.

Zheng, A. and M. Morari (1993). Robust Stability of Constrained Model Predictive Control. *Proceedings of American Control Conference*. **vol.1**, San Francisco, CA. pp. 379-383.

ADCHEM 2006

International Symposium on Advanced Control of Chemical Processes
Gramado, Brazil – April 2-5, 2006

TOWARDS ROBUST DESIGN OF CLOSED-LOOP NONLINEAR SYSTEMS WITH INPUT AND STATE CONSTRAINTS

Johannes Gerhard, Wolfgang Marquardt, Martin Mönnigmann

Lehrstuhl für Prozesstechnik, RWTH Aachen University
Turmstr. 46, D-52064 Aachen, Germany

Abstract: In this paper we address the task of finding a robust process and control design for nonlinear systems with uncertainties and disturbances such that bounds on inputs and outputs are not violated. The solution of this task is approached by Constructive Nonlinear Dynamics (CNLD), an optimization based method developed by the authors in recent years. CNLD guarantees robustness by backing off a nominal point of operation from critical manifolds. Critical manifolds are boundaries in the space of system and controller parameters that separate regions with qualitatively different system behavior, such as a region with stable operating points from a region with unstable system behavior. In this work, CNLD is adopted and extended to account for bounds and constraints on trajectories of inputs and states. Critical boundaries in the parameter space are presented that separate a region where all trajectories stay within the bounds from a region where trajectories violate the constraints. Constraints ensuring a minimal back off from this new type of critical manifold are derived. Application to an illustrative case study demonstrates the feasibility of the approach.

Keywords: robust nonlinear control, disturbances, constraints

1. INTRODUCTION

In most process systems, bounds on inputs and states must not be violated for safety reasons or because of product specifications even in the presence of process uncertainties and disturbances. A large number of articles addresses the task of process and control design to guarantee that constraints on inputs and outputs hold in the presence of disturbances. Nonlinear model predictive control is widely used for systems with constraints, including robust control with min-max formulations in the presence of uncertainties, see e. g. the survey paper (Mayne *et al.*, 2000). Other approaches that address constrained robust nonlinear control include Lyapunov based techniques (El-Farra and Christofides, 2001) or the combination of feedback linearizing control and linear model predictive control (Kurtz and Henson, 1997).

In this work, we address the integration of robust process and control design from a different perspective with optimization based *Constructive Nonlinear Dynamics* (CNLD). CNLD has originally been developed by the authors for the robust design of nonlinear process systems for which stability and feasibility in the presence of parametric uncertainty must be guaranteed (Mönnigmann and Marquardt, 2002). With some extensions, however, this method has also successfully been applied to the robust design of closed-loop systems (Mönnigmann and Marquardt, 2005). The method is based on imposing additional constraints on the system to guarantee a specified distance from critical boundaries in the space of

uncertain parameters. These boundaries separate those designs in the parameter space that exhibit desired properties from those which do not satisfy the desired properties. The general concept of critical boundaries allows to consider robust stability, feasibility, as well as robust performance of closed loop systems. One drawback of this versatile method so far, however, is the limitation to steady states and quasi-statically varying parameters (Mönnigmann and Marquardt, 2005). This is quite a severe restriction in a closed-loop control context as disturbances are generally fast compared to the system dynamics. In this paper an extension of CNLD is discussed to incorporate fast disturbances.

2. CRITICAL MANIFOLDS

Assume that a process model can be written as a system of nonlinear ordinary differential equations,

$$\dot{x} = f(x, p, d(\alpha, t)), \quad x(t_0) = x_0, \tag{1}$$

with states $x \in \mathbb{R}^{n_x}$, initial conditions $x_0 \in \mathbb{R}^{n_x}$, constant process parameters $p \in \mathbb{R}^{n_p}$, which are known or can be set to a specified value, and time-varying disturbances $d \in \mathbb{R}^{n_d}$ parameterized by a set of uncertain parameters $\alpha \in \mathbb{R}^{n_\alpha}$. The right hand side, f, maps from $\mathbb{R}^{1+n_x+n_p+n_\alpha} \rightarrow \mathbb{R}^{n_x}$.

In the framework of CNLD, the structure of the disturbances has to be known except for the exact values of the uncertain parameters α. We assume that all α vary around a nominal value $\alpha^{(0)}$ by the uncertainty $\Delta\alpha$ according to

$$\alpha \in [\alpha^{(0)} - \Delta\alpha, \alpha^{(0)} + \Delta\alpha]. \tag{2}$$

A simple example of a disturbance $d(\alpha, t)$ is a step disturbance triggered at t_0,

$$d(\alpha, t) = \begin{cases} 0, & t \leq t_0 \\ \alpha, & t > t_0 \end{cases}, \tag{3}$$

with α parameterizing the height of the disturbance. In the following we will replace disturbances $d(\alpha, t)$ by their parameterization t and α.

The system class (1) includes open-loop systems as well as closed-loop systems with specified control structure. In the latter case, system and control parameters are concatenated together in the parameter vector p. The flow of the nonlinear system (1) is given by

$$\begin{aligned} x &= \chi(x_0, p, \alpha, t), \\ \chi(x_0, p, \alpha, t_0) &= x_0. \end{aligned} \tag{4}$$

For nonlinear systems, the flow χ is generally not available in an analytical form but has to be evaluated by numerical integration. Let

$$0 < h(x, p, \alpha, t), \quad h \in \mathbb{R}, \quad t \in [t_0, t^e] \tag{5}$$

denote some time-varying bound on the trajectories of the process model which must not be violated at any time $t < t^e$. In the simplest case $h = x_{1b} - x_1$ represents a constant upper bound for one of the state variables. Then the bound h is a straight line in the (x_1, t)-plane, which unfolds into a hyperplane in the space (x, α, t) of states, parameters, and time as shown in Fig. 1 (left).

Given the constraint (5), we can define two different kinds of critical manifolds. The first one is characterized by the set of trajectories which tangentially touch the hypersurface spanned by (5). The second one is defined by the set of trajectories where the constraint exactly holds at a specified final time t^e. The first type of points is closely related to the phenomena of grazing bifurcation of hybrid systems (Nordmark, 1991) where hitting the boundary h triggers a discrete event, e. g. the impact of a periodically forced oscillator on a solid wall. The grazing point corresponds to the trajectory where the system hits the boundary with zero velocity. Donde and Hiskens (2004) use manifolds of grazing bifurcations to calculate the closest grazing bifurcation from a nominal trajectory of a hybrid system. In this paper, however, boundaries (5) do not trigger a discrete event but are specified for safety reasons or product specifications.

2.1 Critical manifold of grazing points

Consider a realization x^* of the flow $\chi(x_0, p, \alpha, t)$ at t^* satisfying the constraint (5):

$$\begin{aligned} x^* - \chi(x_0, p, \alpha, t^*) &= 0, \\ h(x^*, p, \alpha, t^*) &= 0. \end{aligned} \tag{6}$$

Eq. (6) defines the time t^* and states x^* at which the trajectory corresponding to x_0, p, and α crosses the constraint (5). Assume that the system is subject to a step disturbance at t_0 with magnitude α_1. As can be inferred from Fig. 1 (left) a curve of points satisfying (6) unfolds in the (t, α_1)-plane by continuously varying α_1.

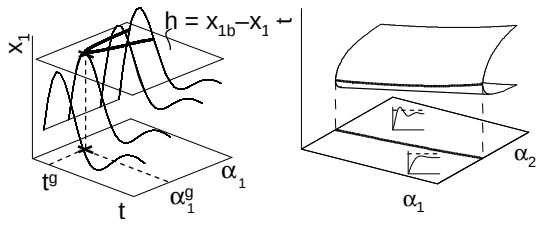

Fig. 1. Left: trajectories for different values of α_1 and curve (thick line) connecting points where trajectories cross the constraint $h = 0$. The grazing point is marked by $\times$. Right: manifold of grazing points. Trajectory sketches show on which side specified boundary $h = 0$ is not crossed.

The point (t^g, α_1^g) in Fig. 1 (left) marks the grazing point at which a trajectory touches tangentially the surface of the constraint. The tangent space of the hypersurface defined by constraint

(5) in the space (x,t), is spanned by the vector $[v^T,\tilde{v}]^T$ with $v\in\mathbb{R}^{n_x}$ and $\tilde{v}\in\mathbb{R}$ satisfying

$$\begin{aligned}\left[h_x^T,h_t\right]\begin{bmatrix}v\\ \tilde{v}\end{bmatrix}&=0,\\ v^Tv+\tilde{v}^2&\neq 0.\end{aligned}\tag{7}$$

h_x and h_t are the partial derivatives of the constraint h with respect to the state variables and time, respectively. At (x^g,t^g) the tangent space of the trajectory spanned by $[\dot{\chi}(x_0,p,\alpha,t)^T,1]^T$ must satisfy (7). The deriviative of the flow with respect to time $\dot{\chi}$ is the right hand side f of the nonlinear system (1). The augmented system $M^{(g)}$ for a grazing point can therefore be written as

$$M^{(g)}=\begin{pmatrix}h(x,p,\alpha,t)\\ h_xf(x,p,\alpha,t)+h_t\end{pmatrix}=0,\tag{8}$$

with the flow $x=\chi$ as defined in (4). These two equations determine the time t^g, and one parameter α_1^g at which the grazing point occurs.

Assume that there is a second disturbance at t_0 with magnitude α_2. The grazing point then unfolds to a curve (and the curve of crossing points into a two dimensional surface) in the three dimensional space (t,α_1,α_2) as shown in Fig. 1 (right). The curve of grazing points divides the parameter space into system designs with qualitative different behavior with respect to the constraint (5). In Fig. 1 (right) trajectories located on one side of this curve will not cross the constraint $h=0$ for all times t, while transients of the system located on the other side of the critical manifold will always cross the boundary at some point after the step disturbances.

Note, that more than one critical manifold may exist for a constraint (5) in general if the trajectory touches or crosses the boundary several times. The region in the parameter space where the constraint is not violated is then the intersection of the regions devised by all critical manifolds.

2.2 Critical manifolds of endpoints

A second type of critical manifold can be defined for a bound on a trajectory by specifying a final time t^e at which the constraint must be exactly fulfilled as shown in Fig. 2 (left). Responses of system (1) after a step disturbance, parameterized by α_1 are shown together with the curve where the constraint h is crossed.

The trajectory with disturbance parameter $\alpha_1=\alpha_1^e$ crosses the boundary at the specified time t^e. The augmented system defining the endpoint condition is given by

$$M^{(e)}=\begin{pmatrix}h(x,p,\alpha,t)\\ t-t^e\end{pmatrix}=0.\tag{9}$$

These two equations determine the time t^e, and one parameter α_1^e.

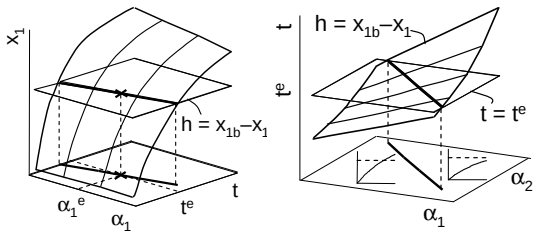

Fig. 2. Left: trajectories for different values of disturbance parameter α_1 and curve (thick line) connecting points where trajectories cross the boundary $h=0$. Critical point at t^e,α_1^e is marked by $\times$. Right: manifold of trajectories which fulfill constraint $h=0$ at t^e after step disturbances of magnitude α_1 and α_2. Sketches of trajectories show in which region $h=0$ is crossed or not.

By taking into account a second disturbance parameterized by α_2, the critical crossing point unfolds into a curve in the space (t,α_1,α_2) as shown in Fig. 2 (right). This curve separates a region in the parameter space (α_1,α_2) where the boundary is not touched or crossed until the specified time t^e is reached from a region where the constraint is always violated for $t<t^e$. This type of critical manifold is particularly useful for bounds on strictly monotonously increasing states or outputs where grazing points cannot occur.

3. NORMAL VECTORS ON CRITICAL MANIFOLDS

The basic idea of CNLD (Mönnigmann and Marquardt, 2002) is to utilize critical manifolds as defined in the previous section for the robust design of nonlinear systems. The approach enforces a lower bound on the parametric distance between a nominal operating point $\alpha^{(0)}$ and the nearest point $\alpha^{(c)}$ on the critical boundary. This lower bound ensures that the complete range of uncertain parameters is at a safe distance from the critical boundary as will be shown below.

The scaling of the parameters $\alpha_i\rightarrow\alpha_i/\Delta\alpha_i$, $\alpha_i^{(0)}\rightarrow\alpha_i^{(0)}/\Delta\alpha_i$ gives the dimensionless parameters

$$\alpha_i\in\left[\alpha_i^{(0)}-1,\alpha_i^{(0)}+1\right].\tag{10}$$

In this case the minimal distance is equal to the radius $\sqrt{n_\alpha}$ of the n_α-dimensional ball enclosing the n_α-dimensional cube of sidelength 2 defined by (10). In Fig. 3, a robust operating point is shown for $n_\alpha=2$. The shortest distance between $\alpha^{(0)}$ and $\alpha^{(c)}$ occurs along the direction of the normal vector r to the critical manifold (Dobson, 1993). The minimal back off constraints can be stated as

$$\begin{aligned}\alpha^{(0)}&=\alpha^{(c)}+l\frac{r}{\|r\|},\\ l&\geq\sqrt{n_\alpha}.\end{aligned}\tag{11}$$

The normal vector of critical manifolds can be calculated from the defining augmented systems

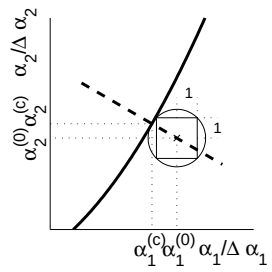

Fig. 3. Robust operating point $\alpha^{(0)}$ with critical manifold (thick line) and normal vector direction r (dashed thick line).

(8) and (9) following the scheme of derivation developed by Mönnigmann and Marquardt (2002). As parameters p and initial conditions x_0 are known, and because the states x are defined by the flow (4), the remaining variables are time t and uncertain parameters α. The normal space of the hypersurface defined by an augmented system $M^{(c)}$, $c \in \{g, e\}$ in the (t, α)-space is spanned by the Jacobian matrix of the partial derivatives $\nabla M^{(c)}$. The normal space of the augmented systems (8) and (9) is a $(n_\alpha + 1) \times (n_\alpha + 1)$ matrix

$$B = \begin{bmatrix} \nabla_t M_1^{(c)} & \nabla_t M_2^{(c)} \\ \nabla_\alpha M_1^{(c)} & \nabla_\alpha M_2^{(c)} \end{bmatrix}, c \in \{g, e\}. \quad (12)$$

For the augemented system of the grazing point (8), the entries of B are defined by

$$\begin{aligned} \nabla_t M_1^{(g)} &= h_x f + h_t, \\ \nabla_t M_2^{(g)} &= h_{xx} f f + h_x f_x f + h_x f_t + 2 h_{xt} f + h_{tt}, \\ \nabla_\alpha M_1^{(g)} &= h_x \chi_\alpha + h_\alpha, \\ \nabla_\alpha M_2^{(g)} &= h_{xx} f \chi_\alpha + h_{x\alpha} f + h_x f_\alpha + h_x f_x \chi_\alpha + \\ &\quad h_{tx} \chi_\alpha + h_{t\alpha}. \end{aligned}$$

The entries of B for the endpoint system (9) are

$$\begin{aligned} \nabla_t M_1^{(e)} &= h_x f + h_t, \\ \nabla_t M_2^{(e)} &= 1, \\ \nabla_\alpha M_1^{(e)} &= h_x \chi_\alpha + h_\alpha, \\ \nabla_\alpha M_2^{(e)} &= 0. \end{aligned}$$

Note that the gradients include sensitivities χ_α of the flow with respect to the uncertain parameters α. Sensitivity equations are obtained by differentiating the dynamic system (1) with respect to α

$$\dot{\chi}_\alpha = f_x \chi_\alpha + f_\alpha.$$

A number of numerical integrators supports efficient evaluation of the sensitivity equations (e. g. Schlegel *et al.* (2004)).

The minimal distance in the space of the uncertain parameters α is in the direction of a vector $r \in \mathbb{R}^{n_\alpha}$ in the normal space (12) which has no contribution along the variable t. This vector is obtained by choosing an appropriate vector $\kappa \in \mathbb{R}^2$ such that

$$B\kappa = \begin{bmatrix} 0 \\ r \end{bmatrix} \in \mathbb{R}^{n_\alpha + 1}. \quad (13)$$

Together with the condition $\kappa^T z - 1 = 0$ with $z \in \mathbb{R}^2$ not normal to κ the two entries of κ are defined by the equations

$$\begin{bmatrix} \nabla_t M_1^{(c)} & \nabla_t M_2^{(c)} \end{bmatrix} \kappa = 0, \\ \kappa^T z - 1 = 0. \quad , c \in g, e \quad (14)$$

For the grazing point, i. e. $c = g$, this system of equations is solved by choosing $\kappa = [1, 0]^T$ and $z = \kappa$. The trailing n_α elements of (13) then give the n_α equations defining the normal vector r. The normal vector r can be calculated by combining the system of the normal vector equations with the augmented system defining the critical manifold (8) to result in

$$G^{(g)} = \begin{pmatrix} h(x, p, \alpha, t) \\ h_x f + h_t \\ h_x \chi_\alpha + h_\alpha - r \end{pmatrix} = 0. \quad (15)$$

For the endpoint constraint the system of equations (14) is solved by choosing $\kappa = [1, -(h_x f + h_t)]$ and $z = [1, 0]$. The augmented system of equations defining the normal vector direction for the endpoint constraint (9) then reads

$$G^{(e)} = \begin{pmatrix} h(x, p, \alpha, t) \\ t - t^e \\ h_x \chi_\alpha + h_\alpha - r \end{pmatrix} = 0. \quad (16)$$

The task of finding a system and control design minimizing an objective ϕ and guaranteeing that specified constraints (5) are never violated despite disturbances is addressed by solving the following constrained nonlinear program (NLP)

$$\min \phi(x^{(0)}, p^{(0)}, \alpha^{(0)}, t^{(0)}) \quad (17a)$$

$$\begin{aligned} \text{s. t. } x^{(0)} &= \chi(x_0^{(0)}, p^{(0)}, \alpha^{(0)}, t^{(0)}), \\ 0 &< h^{(i)}(x^{(0)}, p^{(0)}, \alpha^{(0)}, t^{(0)}), \end{aligned} \quad (17b)$$

$$\begin{aligned} x^{(i,j)} &= \chi(x_0^{(0)}, p^{(0)}, \alpha^{(i,j)}, t^{(i,j)}), \\ 0 &= G^{(c,i,j)}(p^{(0)}, \alpha^{(i,j)}, t^{(i,j)}, r^{(i,j)}), \end{aligned} \quad (17c)$$

$$\begin{aligned} 0 &= \alpha^{(i,j)} - \alpha^{(0)} + l^{(i,j)} \frac{r^{(i,j)}}{\|r^{(i,j)}\|}, \\ 0 &\leq l^{(i,j)} - \sqrt{n_\alpha}. \end{aligned} \quad (17d)$$

Eqs. (17b) define the states $x^{(0)}$ and constraints of the nominal system with upper index $i = 1 \ldots I$ enumerating the constraints. Eqs. (17c) define the states and augmented normal vector systems of the critical points. The superscript c denotes the type of critical manifold (grazing point or endpoint) and the index $j = 1 \ldots J_i$ enumerates the nearest critical manifolds for constraint i. Eqs. (17d) enforce the minimal back off between the nominal point and the critical manifold (i, j). The degrees of freedom of the NLP (17) are $p^{(0)}$, $\alpha^{(0)}$, $x_0^{(0)}$, $t^{(i,j)}$, $\alpha^{(i,j)}$, $r^{(i,j)}$, and $l^{(i,j)}$.

Note that the location of the critical manifolds corresponding to endpoints and grazing points are not known beforehand. Therefore the algorithm of Mönnigmann and Marquardt (2005) has to be employed where critical manifolds are detected as the optimization proceeds. If none of the determining critical manifolds is known a priori, optimization has to start without any robustness constraints (17c)-(17d). Detection of unknown critical points is implemented by numerical integration of system (1). The detection of critical points must therefore be realized on a finite time horizon with the length of the time horizon being a degree of freedom. Specification of the horizon length is a compromise between computational costs on the one hand and the risk of missing constraint violations after the time horizon on the other hand. Minimal distance constraints for the new detected manifolds are added to (17). By repeatedly solving the optimization problem and monitoring for new critical points, the set of known critical manifolds can be built up iteratively. If no further critical manifolds are detected along the optimization path, the robustness region has to be examined for critical manifolds which were not crossed by the nominal operating point during optimization, but which nevertheless might exist inside the robustness region. In this work this test is employed on a grid of points of the uncertainty region, e. g., on the corner or center points of the hypercube (2). A rigorous search for critical points within the uncertainty region can be implemented with interval arithmetics (Mönnigmann and Marquardt, 2005). Such a rigorous search is, however, computationally expensive and therefore only feasible for problems with a few uncertain parameters. If the tests reveal no further critical manifolds, an optimal operating point that is robust with respect to the specified parametric uncertainty is found and the algorithm terminates.

4. ILLUSTRATIVE CASE STUDY

Consider a continuous fermenter model with three nonlinear ODEs (c. f. Henson and Seborg (1992) for details on the model):

$$\begin{aligned}\dot{X} &= -DX + \mu X,\\ \dot{S} &= D(S_f - S) - \frac{\mu}{Y_{X/S}}X,\\ \dot{P} &= -DP + (\alpha\mu + \beta)X.\end{aligned} \tag{18}$$

Here X, S, and P denote the three states biomass, substrate, and product concentration, μ is the growth rate:

$$\mu = \frac{\mu_m\left(1 - \frac{P}{P_m}\right)S}{K_m + S + \frac{S^2}{K_i}}.$$

The dilution rate D is the manipulated variable and the biomass concentration X the variable to be controlled with a PI controller

$$D = D_0 + K_c\left(X_{\mathrm{sp}} - X + \frac{1}{\tau_i}\int_0^t (X_{\mathrm{sp}} - X)d\tau\right),$$

with tuning parameters K_c and τ_i. The parameter values of the model are summarized in Table 1. According to Henson and Seborg (1992) the yield

Table 1. Parameter values

Parameter	Value	Parameter	Value
$Y_{X/S}^{(0)}$	0.4	$\mu_m^{(0)}$	$0.48\,\frac{1}{\mathrm{h}}$
α	2.2	β	$0.2\,\frac{1}{\mathrm{h}}$
P_m	$50\,\frac{\mathrm{g}}{\mathrm{L}}$	K_m	$1.2\,\frac{\mathrm{g}}{\mathrm{L}}$
K_i	$22\,\frac{\mathrm{g}}{\mathrm{L}}$	S_f	$20\,\frac{\mathrm{g}}{\mathrm{L}}$

$Y_{X/S}$ and the maximum specific growth rate μ_m may exhibit significant uncertainty. We assume therefore that both are subject to disturbances for $t > t_0$:

$$\begin{aligned}Y_{X/S} &= Y_{X/S}^{(0)} + \tilde{Y}_{X/S},\\ \tilde{Y}_{X/S} &= \begin{cases} 0, & t \le t_0,\\ \Delta Y_{X/S}\left(1 - \exp\left((t-t_0)/\tau\right)\right), & t > t_0,\end{cases}\\ \mu_m &= \mu_m^{(0)} + \tilde{\mu}_m,\\ \tilde{\mu}_m &= \begin{cases} 0, & t \le t_0,\\ \Delta\mu_m \sin(\omega(t-t_0)), & t > t_0.\end{cases}\end{aligned}$$

The disturbance $\tilde{Y}_{X/S}$ is parameterized by the magnitude $\Delta Y_{X/S} \in [-0.05, 0.05]$ and the time constant set to $\tau = 2\,\mathrm{h}$. The sinusoidal disturbance $\tilde{\mu}_m$ is parameterized by the amplitude $\Delta\mu_m \in [-0.05, 0.05]$ and the frequency set to $\omega = 1\,\mathrm{h}^{-1}$.

We want to find an optimal operating point which minimizes the economic objective $\phi = -(10P - S_f)D$ for the undisturbed nominal case and a controller design that guarantees that the following constraints hold for all time even in the presence of disturbances $\tilde{\mu}_m$ and $\tilde{Y}_{X/S}$:

$$\begin{aligned}0 &< h_1 = PD - 3.0\left[\mathrm{g\,(Lh)^{-1}}\right],\\ 0 &< h_2 = 6.5\left[\mathrm{g\,L^{-1}}\right] - S,\\ 0 &< h_3 = 1.25\left[\mathrm{hg^2L^{-2}}\right] - \int_0^t (X_{\mathrm{sp}} - X)^2 d\tau.\end{aligned} \tag{19}$$

The first two constraints guarantee a minimal reactor yield and an upper bound on the substrate concentration in the product stream. The upper bound on the integrated squared tracking error (ISE) guarantees a minimal performance of the closed loop. Constraints h_1 and h_2 are implemented as minimal back off from critical manifolds of grazing points. For the ISE criterion, however, a grazing point cannot occur as the ISE increases monotonically and complete supression of the sinusoidal disturbance cannot be expected. Therefore, a minimal distance constraint to an endpoint condition (16) is established. The end time is set to $t^e = 200\,\mathrm{h}$ which is roughly 30 times the time constant of the open loop process. The length of the time horizon for the detection of critical points is chosen accordingly to 200 h.

For the nominal operating point steady state constraints $0 = f^{(0)}$ are employed replacing the flow in (17b). For the nominal point the ISE constraint h_3 of (19) is therefore automatically fulfilled. The initial values of the critical trajectories (i, j) are set to the nominal steady states $x_0^{(i,j)} = x^{(0)}$. In this scenario the fermentor runs at its steady state operating point $x^{(0)}$ with disturbances $\tilde{Y}_{X/S}$ and $\tilde{\mu}_m$ starting at t_0. The control design and operating point obtained by solving the NLP (17) guarantees that all possible trajectories resulting from these disturbances starting from initial conditions $x_0^{(i,j)} = x^{(0)}$ do not cross the specified constraints (19). Free optimization variables are the tuning parameters K_c, τ_i, the nominal dilution rate D_0, the set point of the biomass concentration X_{sp}, the substrate feed concentration S_f and the steady state variables of the nominal system $X^{(0)}, S^{(0)}, P^{(0)}$.

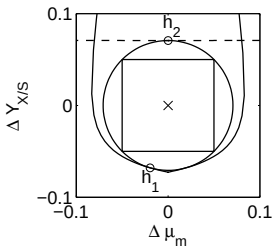

Fig. 4. Robustness ellipse in the plane of the uncertain disturbance parameters. Two constraints h_1 (continuous line) and h_2 (dashed line) are active for the robustly optimal process and control design.

Optimization starts without robustness constraints. Unknown critical manifolds are detected by numerical integration and repeated optimization steps. Each detected critical manifold adds a normal vector constraint with four new variables $t^{(i,j)}$, $l^{(i,j)}$, $\Delta\mu_m^{(i,j)}$, $\Delta Y_{X/S}^{(i,j)}$ to the NLP. At the robust optimum, two minimal distance constraints are active for bounds h_1 and h_2 with $l^{(i,j)} = \sqrt{2}$ as shown in Fig. 4. This guarantees that the specified bounds hold despite the disturbances. The resulting design is summarized in Table 2.

Table 2. Optimal operating point

Parameter	Value	Parameter	Value
S_f	$17.82\ \frac{\mathrm{g}}{\mathrm{L}}$	D_0	$0.218\ \frac{1}{\mathrm{h}}$
$X^{(0)}$	$5.33\ \frac{\mathrm{g}}{\mathrm{L}}$	$S^{(0)}$	$4.50\ \frac{\mathrm{g}}{\mathrm{L}}$
$P^{(0)}$	$16.61\ \frac{\mathrm{g}}{\mathrm{L}}$	K_c	-7.19
τ_i	0.1098h		

5. CONCLUSIONS

In this paper an extension to the method of Constructive Nonlinear Dynamics has been presented. This approach enables the robust optimization of nonlinear systems such that specified dynamics or feasibility can be guaranteed even in the presence of uncertainty. Here, the idea of backing off from critical manifolds is extended from steady state design to constraints on trajectories of nonlinear systems. Minimal distance constraints based on normal vector directions to critical manifolds of grazing points and endpoints guarantee that bounds on states and inputs hold for all times even in the presence of fast disturbances. For closed loop systems, this method can be used for the simultaneous system and control design. The case study presented in this paper shows the feasibility of the approach for robust control and process design in the presence of fast disturbances. In this study only simple disturbance signals were considered. In the future, therefore the influence of more complex disturbances will be investigated.

Acknowledgement: This work has been partially supported by the Deutsche Forschungsgemeinschaft (DFG) under grant no. MA1188/22-1.

REFERENCES

Dobson, I. (1993). Computing a closest bifurcation instability in multidimensional parameter space. *J. Nonlinear Sc.* **3**, 307–327.

Donde, V. and I.A. Hiskens (2004). Guaranteeing performance in nonlinear non-smooth power systems. In: *Preprints Volume 1-3 of NOLCOS 2004, Stuttgart.* pp. 1331–1336.

El-Farra, N.H. and P.D. Christofides (2001). Integrating robustness and constraints in control of nonlinear processes. *Chem. Eng. Sci.* **56**, 1841–1868.

Henson, M.A. and D.E. Seborg (1992). Nonlinear control strategies for continuous fermenters. *Chem. Eng. Sci.* **47**, 821–835.

Kurtz, M.J. and M.A. Henson (1997). Input-output linearizing control of constrained nonlinear processes. *J. Process Contr.* **7**, 3–17.

Mayne, D.Q. J.B. Rawlings, C.V. Rao and P.O.M. Scokaert (2000). Constrained model predictive control: Stability and optimality. *Automatica* **36**, 789–814.

Mönnigmann, M. and W. Marquardt (2002). Normal vectors on manifolds of critical points for parametric robustness of equilibrium solutions of ODE systems. *J. Nonlinear Sc.* **12**, 85–112.

Mönnigmann, M. and W. Marquardt (2005). Steady state process optimization with guaranteed robust stability and flexibility: Application to HDA reaction section. *Ind. Eng. Chem. Res.* **44**, 2737–2753.

Nordmark, A.P. (1991). Nonperiodic motion caused by grazing-incidence in an impact oscillator. *J. Sound Vib.* **145**, 279–297.

Schlegel, M., W. Marquardt, R. Ehrig and U. Nowak (2004). Sensitivity analysis of linearly-implicit differential-algebraic systems by one-step extrapolation. *Appl. Num. Math.* **48**(1), 83–102.

ADCHEM 2006

International Symposium on Advanced Control of Chemical Processes
Gramado, Brazil – April 2-5, 2006

A CONTROL STRATEGY USING A CPWL NOE STRUCTURE

L.R. Castro [*,1] **J. L. Figueroa** [**,1,2]
O. E. Agamennoni [***,1,3]

[*] *Dto. de Matemática, Univ. Nac. del Sur, B8000CPB Bahía Blanca,Argentina*
[**] *Dto. de Ing. Eléctrica y de Computadoras, CONICET - Univ. Nac. del Sur, B8000CPB Bahía Blanca, Argentina*
[***] *Dto. de Ing. Eléctrica y de Computadoras, CIC - Univ. Nac. del Sur, B8000CPB Bahía Blanca, Argentina*

Abstract: In this paper we develop a nonlinear control strategy based on a Nonlinear Output Error (NOE) model structure that uses Canonical High Level Piecewise Linear (HL CPWL) functions to approximate the nonlinear system. This model structure allows the implementation of identification and control algorithms that allows to increase or decrease very easily the complexity of the model during the identification process. This property is very attractive because it allows to find the appropriate NOE model without overfitting. Using this CPWL NOE model structure, we define a simple local linear control scheme.

Keywords: Nonlinear systems, identification, piecewise linear techniques.

1. INTRODUCTION

There exist a set of very well known techniques to design and analyze feedback control strategies for linear systems. If the system under consideration is nonlinear and important performance requirements are imposed, nonlinear control design tools must be used. Canonical Piecewise Linear (CPWL) approximation in the context of Nonlinear Output Error (NOE) model structure allows a systematic multilinear or Linear Parameter Varying (LPV) consideration of a nonlinear dynamical systems. The High Level CPWL (HL CPWL) formulation used in this paper (Julián *et al.*, 1999) is based on a simplicial partition of the input domain such that the system has a linear affine formulation in each simplex which is continuous on the boundaries.

Under slowly varying assumptions, different linear controller scheduling techniques have been proposed in the literature ((Rugh and Shamma, 2000), (Shamma and Athans, 1991), (Shamma and Athans, 1992), (Galán *et al.*, 2004)).

Within the context of fuzzy logic and neural networks, the controller scheduling idea has received the attention of researchers ((Palm and Stutz, 2003), (Chen and Huang, 2004)) as well.

In the framework of these ideas, in this paper we present a new local linear control strategy of a nonlinear system based on a CPWL NOE model description. In ((Castro *et al.*, 2005*b*), (Castro *et al.*, 2005*a*)) a CPWL Nonlinear Output Error (NOE) model structure and an identification algorithm were presented. This structure is similar to the one proposed by Narendra and Parthasarathy

[1] Partially supported by the ANPCyT
[2] Partially supported by CONICET
[3] Partially supported by CIC

(Narendra and Parthasarathy, 1990) in the context of Neural Networks. The CPWL NOE structure uses HL CPWL functions to develop an identification algorithm that offers a simple mechanism for increasing the model approximation capabilities, retaining the approximation achieved when moving from a coarse grid to a finer one. In this way, it is possible to start the identification with a linear approximation and then increase the model's degrees of freedom progressively in order to reduce the mismatch up to an acceptable value. On the other hand, a reduced model may be evaluated to alleviate overfitting. It is also important to remark that the NOE algorithm assures minimum noise effect in the identified model.

The HL CPWL formulation of the NOE model allows to follow in real time the simplex where the system is actually situated. Each simplex is directly related with the corresponding linear model. Then, under invertibility assumptions, *i.e.* minimum phase assumption of all linear models, a simple controller composed of the local inverse linear model in cascade with a filter to tune the performance, is considered. The minimum phase assumption can be relaxed since special consideration may be applied to guarantee stability of the closed loop system. The particular controller formulation is used only to present a general idea of controller scheduling using CPWL NOE model formulation.

The paper is organized as follows. In Section 2 the identification algorithm (Castro *et al.*, 2005*a*) is reviewed. In Section 3 the proposed control scheme is discussed; in Section 4 we develop an example using the proposed methodology. Finally, in Section 5 we draw some conclusions.

2. IDENTIFICATION METHODOLOGY

Let $(\mathbf{u}, \mathbf{y})$ the input/output available data of length L corresponding to a given Lipschitz continuous, SISO system. If $\tilde{\mathbf{y}}$ is the estimated value corresponding to the input $\mathbf{u}$, and

$$\mathbf{u}^{k,M+1} = [u_k, \ldots, u_{k-M}] \tag{1}$$
$$\tilde{\mathbf{y}}^{k-1,N} = [\tilde{y}_{k-1}, \ldots, \tilde{y}_{k-N}], \tag{2}$$

we propose the following black-box identification structure

$$\begin{aligned}\tilde{y}_k &= f_{pwl}(u_k, \ldots, u_{k-M}, \tilde{y}_{k-1}, \ldots, \tilde{y}_{k-N}) \\ &= \mathbf{c}\Lambda\left([\mathbf{u}^{k,M+1}, \tilde{\mathbf{y}}^{k-1,N}]\right).\end{aligned} \tag{3}$$

where the the HL CPWL function $f_{pwl}(\mathbf{x}) = \mathbf{c}\Lambda(\mathbf{x})$ is defined as in (Julián *et al.*, 1999), (Julián, 2000) and the model orders M and N are given. This identification structure, pictured in Fig. 1, can be considered a black box model where the regression vector noted by $\boldsymbol{\varphi}^k$ is taken as $\boldsymbol{\varphi}^k = \left[\mathbf{u}^{k,M+1}, \tilde{\mathbf{y}}^{k-1,N}\right]$ see (Sjöberg *et al.*, 1995), for example). It is worth to mention that a linear model is a particular case of f_{pwl}. Finally, let us note

$$\mathbf{z}^k = \left[\, \mathbf{u}^{k,M+1},\ \tilde{\mathbf{y}}^{k-1,N} \,\right]. \tag{4}$$

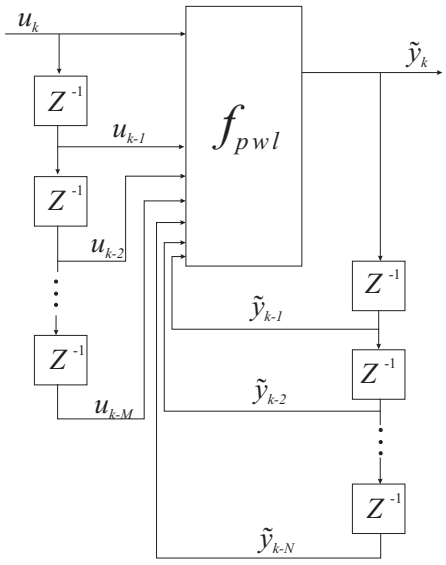

Fig. 1. CPWL NOE model

The domain of the function f_{pwl} is a compact set $\mathbf{S} \subset \mathbb{R}^m, m = M + N + 1$, defined as follows

$$\begin{aligned}\mathbf{S} = \{\mathbf{z} \in \mathbb{R}^m : \underline{z}_i \le z_i \le \overline{z}_i;\ \ \overline{z}_i = \underline{z}_i + \delta.ndiv, \\ i = 1, 2, \ldots, m\},\end{aligned} \tag{5}$$

being δ the fixed grid size, $\underline{z}_i = \min z_i$ and $\overline{z}_i = \max z_i$ over the entire input/output set with $\mathbf{z}$ defined in (4).

According to ((Julián *et al.*, 1999), (Julián, 1999)), the set defined by (5) is partitioned into polyhedral regions using a simplicial boundary configuration and f_{pwl} is linear on each simplex and continuous on the adjacent boundaries of the simplices.

Taking into account Eq. (5) each dimension is divided into a number of subintervals of equal length δ. Then, when the grid size δ decreases, the number of divisions $ndiv$ on each direction increases. As a consequence, using HL CPWL functions for the nonlinear approximation, $ndiv$ allows to go from a linear model ($ndiv = 1$) with a coarse partition of the domain to a nonlinear one with a finer partition of $\mathbf{S}$. The advantages of using this kind of models is pointed out in (Sjöberg and Ngia, 1998, Ch.1).

According to the proposed methodology we write the identification algorithm using the following notation.

Notation

$ndiv = 2^d, d \geq 0$: number of divisions of the region $\mathbf{S}$. Equal number of divisions in each dimension is assumed.
V^d: the set of vertices of the simplicial partition of the set $\mathbf{S}$ with $ndiv = 2^d$ number of divisions.
Λ^d: The HL CPWL basis defined on $\mathbf{S}$ with vertices belonging to V^d.
$\mathbf{c}^{d,*}$: the row vector of parameters associated with the basis Λ^d. The number of parameters is $(ndiv+1)^{M+1+N}$ ((Julián *et al.*, 1999), (Julián, 1999)).
$(A)_j$: the j-th row of a matrix A.
$Niter \in \mathbb{R}$: maximum number of iterations of the optimization algorithm.
$Maxerror$: maximum allowable approximation error.
$\mathbf{lr}$: learning rate, $lr_i > 0 \, \forall i$ ($lr_i = 0.001$).
mom: momentum, $mom > 0$ ($mom = 0.9$).
lr_{inc}: learning rate increment, $lr_{inc} > 1$ (typically, $lr_{inc} = 1.05$).
lr_{dec}: learning rate decrement, $0 < lr_{dec} < 1$ (typically, $lr_{dec} = 0.3$).
η: constant update, $0 \leq \eta \leq 1$.

Identification Algorithm

Step 1. $d = 0$**:** *Linear Approximation.*
Compute the set of parameters $\mathbf{c}^{d,*}$ of the linear model solving the following LS problem

$$\begin{aligned}\mathbf{c}^{d,*} &= \min\left(\|\mathbf{y} - \tilde{\mathbf{y}}\|^2\right) \\ &= \arg\left\{\min_{\mathbf{c}^d}\left\{\frac{1}{2}\sum_{i=1}^{L}[y_i - \right.\right. \\ &\qquad \left.\left.\mathbf{c}^d\Lambda^d\left([\mathbf{u}^{i,M+1}, \tilde{\mathbf{y}}^{i-1,N}]\right)\right]^2\right\}\right\}.\end{aligned}$$

Step 2. $d \leftarrow d+1$**:** . Set $r = 0$. Evaluate the initial condition $\mathbf{c}^{d,*}$ for the new d according to the algorithm given in (Castro *et al.*, 2005*a*). Set

$r = 0$, $\mathbf{c}^{d,r} = \mathbf{c}^{d,*}$, $\eta = 0$,
$\Delta\mathbf{c}^{d,r} = [0, \ldots, 0]$ $lr_i^0 = 0.001 \, \forall i$.

Step 3. $r \leftarrow r+1$**:** *Error and gradient evaluation.*

$$E^r = \frac{1}{2}\sum_{i=1}^{L}\left[y_i - \mathbf{c}^{d,r-1}\Lambda^d\left([\mathbf{u}^{i,M+1}, \tilde{\mathbf{y}}^{i-1,N}]\right)\right]^2 \tag{6}$$

$$\begin{aligned}\nabla E_j^r &= \frac{\partial E^r}{\partial c_j^{d,r-1}} \\ &= -\sum_{i=1}^{L}\left[y_i - \mathbf{c}^{d,r-1}\Lambda^d\left([\mathbf{u}^{i,M+1}, \tilde{\mathbf{y}}^{i-1,N}]\right)\right] . \\ &\qquad \left.\left(\Lambda^d\left([\mathbf{u}^{i,M+1}, \tilde{\mathbf{y}}^{i-1,N}]\right)\right)_j .\right.\end{aligned}$$

Step 4. Parameter update. If $E^r \leq Maxerror$ then STOP; otherwise

$$\Delta c_j^{d,r} = \eta\left(-\nabla E_j^r lr_j^r + \Delta c_j^{d,r-1} mom\right), \tag{7}$$

$$\mathbf{c}^{d,r} = \mathbf{c}^{d,r-1} + \Delta\mathbf{c}^{d,r}, \tag{8}$$

where the constant η is precisely defined in Appendix B and the components of the learning rate vector $\mathbf{lr}^r$ are modified as described below.

$$lr_j^r = \begin{cases} lr_j^{r-1} \times lr_{inc} \text{ if sign}\left(\nabla E_j^r\right) = \text{sign}\left(\nabla E_j^{r-1}\right) \\ lr_j^{r-1} \times lr_{dec} \text{ if sign}\left(\nabla E_j^r\right) \neq \text{sign}\left(\nabla E_j^{r-1}\right). \end{cases}$$

If $r < Niter$ go to Step 3.
else
$\mathbf{c}^{d,*} = \mathbf{c}^{d,r}$, go to Step 2.

Remark 1. In order to improve the algorithm performance, any of the well known stop conditions based on the error evolution, may be applied in Step 4.

Remark 2. The described algorithm could be modified to reduce the order of the model. Then, the solution at any level could be found backwards. If only the solution before the last one must be recovered, other possibility would be to retain that vector of parameters and reconstruct the solution using the expression $\tilde{}_k = \mathbf{c}^{d,r}\Lambda^d\left([\mathbf{u}^{k,M+1}, \tilde{\mathbf{y}}^{k-1,N}]\right)$ for all k, $1 \leq k \leq L$.

The advantages and drawbacks of this algorithm have been pointed out in ((Castro *et al.*, 2005*b*), (Castro *et al.*, 2005*a*)).

3. CONTROLLER DESIGN

In order to design the controller, we use the fact that in each sector of the domain, the CPWL NOE structure behaves as a linear model. Then, we will use a linear controller for each one of these sectors.

To design these linear controllers, we adopt the direct synthesis approach (Ogunnaike and Ray, 1994). The controller specification produces a feedback system with a closed-loop pole in a_c without offset, when the set point is changed in the form of steps. If the discrete transfer function of the linear model is called $H(z)$, and $H^{-1}(z)$ is stable and causal, then the controller can be described as

$$K(z) = \frac{a_c}{z-1}\frac{1}{H(z)}. \tag{9}$$

Then, the controller algorithm involves two steps, first it is necessary to extract the linear model valid for the current operating point; then, with this model, a controller is designed.

Let us consider that the process is actually in a given operating point described by the vector $\left[\mathbf{u}^{k,M+1}, \tilde{\mathbf{y}}^{k-1,N}\right]$. Then it is simple to determine the simplex $R^{(i)}$ that contains this point, for example using the PWL Toolbox of MATLAB

(Julián, 2000). Note that if the dimension of the domain is $m = N + M + 1$ each simplex is defined by their $m + 1$ vertices. Then the gradient $J^{(i)}$ in this simplex can be easily evaluated using the values of f_{pwl} at its vertices (see Appendix A). The parameters of the linear model at the region are the entries of this gradient vector. Then it is possible to implement the control algorithm (see Fig. 2) as follows.

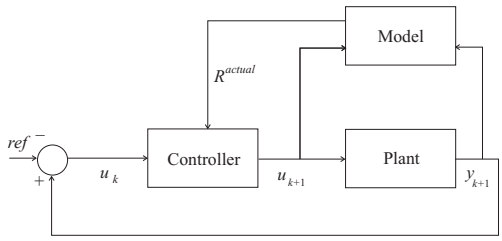

Fig. 2. Control scheme.

Control Model Algorithm

Data. At time k, the past values of the measured and controlled variables to form $\mathbf{x} = \left[\mathbf{u}^{k,M+1}, \tilde{\mathbf{y}}^{k-1,N}\right]$. The desired closed loop time constant (a_c).

Step 1. Determine the sector R^{old} in which is operating the process, the linear model corresponding to this sector (using the algorithm of Appendix B) and the linear controller K^{actual} of Eq. (9).

Step 2. Determine the actual sector R^{actual}.

Step 3. If R^{actual} is not equal to R^{old}, compute the actual linear model, the new controller K^{actual} and make $R^{old} = R^{actual}$.

Step 4. Apply the corresponding manipulated variable u_k to the process, and measure y_k.

Step 5. Compute the new manipulated variable u_{k+1} (computed using K^{actual} and y_k). Make $k \leftarrow k + 1$.

Step 6. Update $\mathbf{x} = \left[\mathbf{u}^{k-M}, \mathbf{y}^{k-N}\right]$ using u_{k+1} and y_k and return to Step 2.

Remark 3. It is obvious that the performance of this control algorithm depends on the quality of the model. In this case, we consider that each simplex in the partition of the domain have enough data to allow a good quality model. In this way, it is possible to improve the robustness of the control algorithm by relaxing the control specification *i.e.* the time constant when the number of data in a given region is small.

4. EXAMPLE

In this example we model the neutralization reaction between a strong acid and a strong base in the presence of a buffer agent as described by (Galán, 2001) (for a complete description of this process and a first principles models see (Biagiola *et al.*, 2004)).

The goal is to control the output pH, by manipulating the alkaline solution flow rate q_B. The operating point for the neutralization is $q_B = 0.5$ and $pH = 7.7182$.

In order to identify the system, q_B is excited by a random signal with uniform distribution between 0 and 1, the limits of the physical variable. Time simulation is performed for a 250 seconds for a sample time of 0.25 sec. The regression vector of the CPWL NOE model is taken as $\varphi_k = [u_k, \tilde{y}_{k-1}, \tilde{y}_{k-2}]$ and the number of divisions for each variable are two, four and eight, giving a total number of parameters equal to 27, 125 and 729, respectively. The parameters of the algorithm for adjusting the vector of parameters are taken as $\mathbf{lr}^0 = 0.0002$, $mom = 0.9$, $inc = 1.05$ and $dec = 0.3$.

In Fig. 3 the error is displayed as a function of the iterations; the number of divisions of the simplices increases every 1000 iterations.

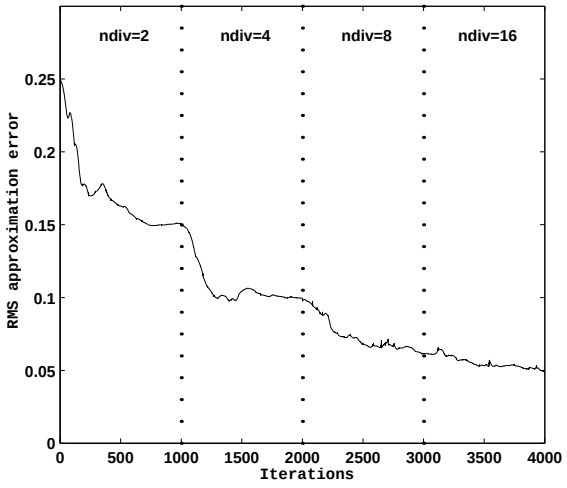

Fig. 3. RMS error for pH neutralization.

The controller is used to follow a set point change. The controller parameter is set at $a_c = 0.5$. The simulation for this control is shown in Fig. 4. In this figure, the system response for the controller with $ndiv = 2, 4$ and 8, $ndiv = 4$ are shown. Again, from these plots it is clear that the controller performance improves when the number of divisions increase.

5. CONCLUSIONS

In this paper, a NOE identification algorithm based on HL CPWL functions approximation method is reviewed, and an algorithm to control this model structure is presented. The identification methodology allows to approximate a NOE

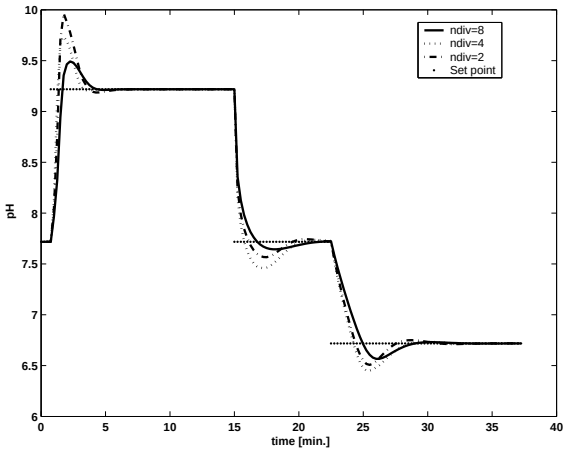

Fig. 4. Simulation for pH neutralization control.

model from a linear one, and the control scheme uses the linear information in each region of operation to design a simple controller. The main feature of this process is that it enables to go from a linear model to a nonlinear one straightforwardly. Finally, the potentials of our approach have been illustrated with two examples.

REFERENCES

Biagiola, S.I., O.E. Agamennoni and J.L. Figueroa (2004). H_∞ control of a Wiener type system. *International Journal of Control* **77**(6), 572–583.

Castro, L.R., J.L. Figueroa and O.E. Agamennoni (2005*a*). BIBO stability for NOE model structure using HL CPWL functions. In: *Proc. of the 24th IASTED Int. Conf., MIC 2005.* Univ. California, Berkeley. pp. 91–96.

Castro, L.R., J.L. Figueroa and O.E. Agamennoni (2005*b*). An NIIR structure using HL CPWL functions. *Latin Amer. Appl. Res.* **35**, 161–166.

Chen, J. and T-C. Huang (2004). Applying neural networks to on-line updated PID controllers for nonlinear process control. *Joural of Process Control* **14**, 211–230.

Galán, O. (2001). Robust multi-linear model*-based control for nonlinear plants. PhD thesis. The University of Sydney. Sydney, Australia.

Galán, O., J.A. Romagnoli and A. Palazoglu (2004). Real-time implementation of multi-linear model-based control strategies: an application to a bench-scale pH neutralization reactor. *Journal of Process Control* **14**, 571–579.

Julián, P. (2000). A toolbox for the piecewise linear approximation of multidimensional functions. http://www.pedrojulian.com.

Julián, P., A. Desages and O. Agamennoni (1999). High level canonical piecewise linear representation using a simplicial partition. *IEEE Trans. on Circ. and Syst.* **44**, 463–480.

Julián, Pedro M. (1999). A High Level Canonical Piecewise Linear Representation: Theory and Applications. PhD thesis. Universidad Nacional del Sur, Bahía Blanca, Argentina. UMI Dissertation Services, Michigan, USA.

Narendra, K. S. and K. Parthasarathy (1990). Identification and control of dynamical systems using neural networks. *IEEE Trans. on Neural Networks* **1**, 4–27.

Ogunnaike, B.A. and W.R. Ray (1994). *Process Dynamics, Modeling and Control.* Oxford University.

Palm, R. and C. Stutz (2003). Open loop dynamic trajectory generator for a fuzzy gain scheduler. *Engineering Applications of Artificial Intelligence* **16**, 213–225.

Rugh, W. and J. Shamma (2000). Research on gain scheduling. *Automatica* **36**, 1401–1425.

Shamma, J. and M. Athans (1991). Guaranteed properties of gain scheduled control for linear parameter-varying plants. *Automatica* **27**, 559–564.

Shamma, J. and M. Athans (1992). Gain scheduling: potential hazards and possible remedies. *IEEE Control Systems Magazine* **12**, 101–107.

Sjöberg, J. and L. S. H. Ngia (1998). *Neural Nets and Related Model Structures for Nonlinear System Identification.* pp. 1–28. Nonlinear Modeling: Advanced Black-Box Techniques. J. A. K. Suykens and J. Vandevalle, Eds.. Kluwer Academic Publishers.

Sjöberg, J., Q. Zhang, L. Ljung, A. Beneviste, B. Delyon, P. Glorennec, H. Hjalmarsson and A. Juditsky (1995). Nonlinear black-box modeling in system identification: a unified overview. *Automatica* **35**(12), 1691–1724.

Appendix A. LINEAR MODEL FROM CPWL FUNCTIONS

Let us consider a HL CPWL function $f_{pwl} : \mathbf{S} \subset \mathbb{R}^m \rightarrow \mathbb{R}^1$ and a vector $\mathbf{x}$ at a given region $R^{(k)}$, *i.e.* $\mathbf{x} \in R^{(k)} \subset \mathbf{S}$. This region $R^{(k)} \in \mathbb{R}^m$ is uniquely defined by its $m+1$ vertices $V^{(j)}, j = 1, \ldots, m+1$. Once that these vertices are computed [4], it is possible to obtain the linear model $J^{(j)} \in \mathbb{R}^m$ that represents the process at this region. An algorithm to perform the linear model can be written as follows.

Linear Model Algorithm

Step 1. Compute the value of f_{pwl} at vertices,

[4] This is trivial using the function *vertices.m* from (Julián, 2000)

for $i = 1$ to $m+1$

$(z)_i = \mathbf{c}\Lambda\left(V^{(i)}\right)$,

end

Step 2. From the vector and matrix,

for $i = 1$ to m

$(\Gamma)_i = (z)_i - (z)_{m+1}$,

$\Theta(:,i) = V^{(i)} - V^{(m+1)}$,

end

where $\Theta(:,i)$ represents the i^{th} column of the Θ matrix.

Step 3. Compute the gain vector J ,

$J = \Theta^{-1}\Gamma$

Appendix B. BIBO STABILITY

Let us suppose that $\mathbf{u} \in U \subset \mathbb{R}^{M+1}$, $\mathbf{y} \in O \subset \mathbb{R}^N$, U and O given compact sets, $Q \subset U \times O$, Q compact and $I = \left[\underline{y}, \overline{y}\right] \subset \mathbb{R}$, with $\underline{y} = \min \mathbf{y}, \overline{y} = \max \mathbf{y}$.

Definition 4. We say that the model defined by (3) is BIBO stable if $f_{pwl}(Q) \subset I$.

This definition means that the model output remains within the output values when the input is any signal $\mathbf{u} \in U$.

The expression (3) defines a mapping $f_{pwl} : Q \to I$. As Q is a compact set and f_{pwl} is continuous on Q, then it attains its maximum and minimum values on Q. Moreover, since f_{pwl} is linear on each simplex, the extreme values are attained on V_Q, the set of vertices of Q. Then the NOE identification structure given by (3) will be BIBO stable if the minimization problem

$$\min_{\mathbf{c}^d} E^r \quad \text{s.t.} \quad \max_{\substack{\mathbf{z}^k \in Q \\ 1 \le k \le L}} f_{pwl}\left(\mathbf{z}^k\right) = \max_{\mathbf{v} \in V^d} \left|\mathbf{c}^d \Lambda(\mathbf{v})\right| \subset I,$$

where E^r is given by equation Eq. (6) and V^d is defined in Section 2, is solvable. This minimization problem is equivalent to

$$\min_{\mathbf{c}^d} E^r \text{ s.t. } \begin{cases} \max\limits_{\mathbf{v} \in V^d} \left(\left|\mathbf{c}^d \Lambda(\mathbf{v})\right|\right) \le \overline{y} \\ \min\limits_{\mathbf{v} \in V^d} \left(\left|\mathbf{c}^d \Lambda(\mathbf{v})\right|\right) \ge \underline{y}. \end{cases} \quad \text{(B.1)}$$

Remark 5. Considering a 10.000-length input vector, it takes around $16\mu s$ of CPU to solve the minimization problem with restrictions given by (B.1) in the MATLAB environment, with a Pentium IV, 512Mb RAM computer.

Once we have found $\mathbf{c}^d$ that satisfies (B.1), we must guarantee that, for any r with d fixed, is $\tilde{\mathbf{y}}_k = \mathbf{c}^{d,r}\Lambda\left(\mathbf{z}^k\right) \in I, 1 \le k \le L$, where $\mathbf{c}^{d,r}$ is obtained from Step 4 of the identification algorithm described in Section 2.

We can state the following sufficient condition.

Proposition 1. Let us suppose that, for d and $r-1$ fixed, the model is BIBO stable. Then the model will be BIBO stable for d and r if the following condition is satisfied

$$\underline{y} - \min_{\mathbf{v} \in V_d} \left(\mathbf{c}^{d,r-1}\Lambda(\mathbf{v})\right) \le \Delta\mathbf{c}^{d,r}\Lambda(\mathbf{v}) \le \overline{y} - \max_{\mathbf{v} \in V_d} \left(\mathbf{c}^{d,r-1}\Lambda(\mathbf{v})\right), \quad \text{(B.2)}$$

where $\Delta\mathbf{c}^{d,r}$ is given by equation Eq. (8) and $\mathbf{v} \in V^d$.

Proof. See (Castro *et al.*, 2005*a*).

Corollary 2. With the hypothesis of Proposition 1, let us note $a = \underline{y} - \min_{\mathbf{v} \in V^d}\left(\mathbf{c}^{d,r-1}\Lambda(\mathbf{v})\right)$, $b = \overline{y} - \max_{\mathbf{v} \in V^d}\left(\mathbf{c}^{d,r-1}\Lambda(\mathbf{v})\right)$. Then

$$\eta \ge \frac{a}{\min_{\mathbf{v} \in V^d}\left[\left(-\nabla E_j^r lr_j^r + \Delta c_j^{d,r-1} mom\right)\Lambda(\mathbf{v})\right]} \quad \text{(B.3)}$$

$$\eta \le \frac{b}{\max_{\mathbf{v} \in V^d}\left[\left(-\nabla E_j^r lr_j^r + \Delta c_j^{d,r-1} mom\right)\Lambda(\mathbf{v})\right]} \quad \text{(B.4)}$$

simultaneously.

Proof. See (Castro *et al.*, 2005*a*).

Remark 6. From both bounds for η given by Eq. B.3 and B.4, the only one with practical interest is the least positive one and is the bound used in Step 4 of the identification algorithm.

ADCHEM 2006

International Symposium on Advanced Control of Chemical Processes
Gramado, Brazil – April 2-5, 2006

A STATE SPACE APPROACH FOR BOUNDARY CONTROL OF DISTRIBUTED PARAMETER SYSTEMS

Megan Dillabough * **Huilan Shang** *,[1] **P. James McLellan** **

* *School of Engineering, Laurentian University, Sudbury, ON, Canada P3E 2C6*
** *Department of Chemical Engineering, Queen's University, Kingston, ON, Canada K7L 3N6*

Abstract: Many industrial processes exhibit spatially distributed behaviour and are distributed parameter systems (DPS). Much of the current literature has focused on the control of specific types of DPS, such as those modelled by hyperbolic or parabolic partial differential equations (PDEs). State space models for these systems (termed as 2-D systems) have also been studied extensively, however additional techniques are required to deal with boundary conditions. In this paper, general boundary conditions for discretized 2-D state space models are formulated in the state space domain. A controller is developed for boundary control problems using the discretized state space method. Simulation results indicate that the resulting boundary controller can achieve desirable performance for setpoint tracking.

Keywords: Boundary Control, Distributed Parameter Systems, State Space Model, Partial Differential Equations, Linear systems, Discretized models

1. INTRODUCTION

Distributed parameter systems (DPS), in which the state variables change with space and time, are common in industry. Examples include sheet forming, fixed bed reactor, and metallurgical processes. DPS models can be obtained by application of mass and energy conservation laws and often take the form of partial differential equations (PDEs). Active research has been focused on control development for DPS based on PDE models (Christofides, 2000; Neittaanmaki and Tiba, 1994; Godasi *et al.*, 2002; Shang *et al.*, 2005). Most of these PDE-based controllers address specific classes of PDE systems (*e.g.*, hyperbolic or parabolic). Owing to lack of a general model structure and their continuous nature in both dimensions (*e.g.*, time and space), PDE models can hardly be used for model identification when first principal modelling cannot be achieved.

Research into the use of state space models for DPS started in the mid-1970s. It is noted that DPS have been termed as infinite dimensional systems for researchers using PDE model based approaches while the community using state space approaches has used the term 2-D system to represent DPS that has two independent variables. In this paper, we follow the convention of using the term 2-D systems in state space approaches. Roesser (1975) extended the state space model for lumped parameter systems (LPS) (1-D) to a 2-D discrete, linear time invariant state space model with potential applications in image processing (Roesser, 1975). Almost simultaneously, Fornasini and Marchesini also proposed a state space model for 2-D systems (Fornasini and Marchesini, 1976). It was shown that the Roesser model was more general, as the Fornasini and Marchesini model could be rewritten in the Roesser model form (Kung *et al.*, 1977). The limitations of the Roesser model are that it requires causality of the state variables in the spatial direction as

[1] Corresponding Author: hshang@laurentian.ca

well as in time, and it can only represent systems with unilateral boundary conditions due to the assumption of causality in space (Marszalek, 1984). In the following years, the Roesser model was studied extensively (Kaczorek, 1985; Chen and Tsai, 2002; Hernández and Arkun, 1992) and its application extended to various fields (Wellstead *et al.*, 2000; Galkowski *et al.*, 2000). More recently, a multi-dimensional state space model that does not require causality in space was presented (D'Andrea, 1998; D'Andrea and Chandra, 2002); thus, it has the potential to represent those DPS with bilateral boundary conditions. The model has been used for formulating distributed control problems for spatially interconnected systems (D'Andrea and Dullerud, 2003), vehicle formation (Fowler and D'Andrea, 2002), and sheet forming processes (Stewart, 2000). Existing state space models and control developments have mainly addressed DPS with distributed input and distributed output where the effect of boundary conditions has been simplified.

Although distributed control is becoming more practical with continuing advances in the technology of sensors and actuators (D'Andrea and Dullerud, 2003), for many systems, control actions cannot be performed at every point. An example is a boundary control system, where manipulated variables can only be implemented at the boundaries (Abu-Hamdeh, 2002). The importance of boundary control problems is well recognized and boundary controllers have been developed for systems described by PDEs or integral equation models (Chakravarti and Ray, 1999; Alvarez-Ramirez, 2001).

In this paper, a discretized 2-D state space model with general boundary conditions is formulated, and the resulting framework is used to develop a boundary controller. Simulations are performed to examine the effectiveness of the resulting boundary controller, and indicate that the developed boundary controller can generate a desirable output response to setpoint changes.

2. 2-D STATE SPACE MODELS

DPS can commonly be classified into systems with distributed inputs and distributed outputs, and those with boundary inputs and boundary or spatially uniform outputs.

2.1 Distributed Input

The discretized state space model of a DPS with distributed input and distributed output is composed of state equations, boundary conditions and an output equation:

state equations

$$\begin{bmatrix} x^L(i+1,j) \\ x^R(i-1,j) \\ x^V(i,j+1) \end{bmatrix} = \begin{bmatrix} A_{11} & A_{12} & A_{13} \\ A_{21} & A_{22} & A_{23} \\ A_{31} & A_{32} & A_{33} \end{bmatrix} \begin{bmatrix} x^L(i,j) \\ x^R(i,j) \\ x^V(i,j) \end{bmatrix} + \begin{bmatrix} B_1 \\ B_2 \\ B_3 \end{bmatrix} u(i,j), \quad (1)$$

boundary conditions

$$\begin{aligned} x^L(1,j) &= \alpha_{11}x^R(1,j) + \alpha_{12}x^V(1,j), \\ x^R(N,j) &= \alpha_{21}x^L(N,j) + \alpha_{22}x^V(N,j), \end{aligned} \quad (2)$$

output equation

$$y(i,j) = C_1x^L(i,j) + C_2x^R(i,j) + C_3x^V(i,j), \quad (3)$$

where i indicates the spatial index and j indicates the time index, $x^L(i,j) \in R^{m_1}$ is the distributed state variable evolving horizontally (or spatially) in one direction, $x^R(i,j) \in R^{m_2}$ is the state variable evolving horizontally (or spatially) in the opposite direction, $x^V(i,j) \in R^{m_3}$ is the state variable evolving vertically (or in time), $u(i,j) \in R$ is the distributed input and $y(i,j) \in R$ is the distributed output. In the above equations, all As, Bs, Cs and αs are constant matrices with proper dimensions. Equations (1) to (3) represent a DPS with a finite range and $i \in [1, N]$.

In the existing literature, the systems addressed were assumed to be of infinite extent or periodic, meaning boundary conditions were not imposed. Recently, systems of finite extent possessing a certain symmetry structure were addressed (Langbort and D'Andrea, 2005). For PDE systems, boundary conditions play an important role in the solution technique and the process dynamics. Equation (2) provides a general formulation for boundary conditions in DPS since it can describe any linear boundary condition for PDE systems.

2.2 Boundary Input

In many DPS, the manipulated input is located on a boundary. Without loss of generality, it is assumed that the input variable appears on the boundary $x^L(1,j)$. The state space model can be described as:

state equations

$$\begin{bmatrix} x^L(i+1,j) \\ x^R(i-1,j) \\ x^V(i,j+1) \end{bmatrix} = \begin{bmatrix} A_{11} & A_{12} & A_{13} \\ A_{21} & A_{22} & A_{23} \\ A_{31} & A_{32} & A_{33} \end{bmatrix} \begin{bmatrix} x^L(i,j) \\ x^R(i,j) \\ x^V(i,j) \end{bmatrix}, \quad (4)$$

boundary conditions

$$\begin{aligned} x^L(1,j) &= \alpha_{11}x^R(1,j) + \alpha_{12}x^V(1,j) \\ &\quad + \beta u(j), \\ x^R(N,j) &= \alpha_{21}x^L(N,j) + \alpha_{22}x^V(N,j), \end{aligned} \quad (5)$$

output equation

$$y(j) = \sum_{i=1}^{N} c_{1i} x^L(i,j) + \sum_{i=1}^{N} c_{2i} x^R(i,j) + \sum_{i=1}^{N} c_{3i} x^V(i,j). \quad (6)$$

Equation (6) is a general output representation including the value of the state variables on one boundary or any other spatial point, or the weighted average of the state variables. In this paper, the case when $u(j) \in R$ and $y(j) \in R$ are scalars is considered.

The state space model in Equations (4) to (6) describes the general boundary control problem when the manipulated input appears on one boundary. Physically meaningful boundary conditions, such as Dirichlet, Neumann or mixed boundary conditions for PDEs, can be written in the form of Equation (5). Most available studies on boundary control have focused on specific types of PDE systems and specific boundary conditions (*e.g.*, boundary value of the state variables is equal to the input). Equations (4) to (6) provide a general state space framework for boundary control problems which can be used in control development, model identification as well as and system studies.

3. BOUNDARY CONTROL

In this section, a boundary controller is developed for systems modelled by Equations (4) to (6).

From Equation (4), x^L can be expanded to yield:

$$\begin{aligned} x^L(i,j) = {} & A_{11}^{i-1} x^L(1,j) + A_{11}^{i-2} A_{12} x^R(1,j) \\ & + \cdots + A_{12} x^R(i-1,j) + A_{11}^{i-2} A_{13} x^V(1,j) \\ & + \cdots + A_{13} x^V(i-1,j). \end{aligned} \quad (7)$$

The state variables in an extended vector form are defined as follows:

$$\begin{aligned} \mathbf{x}^L(j) &= \left[x^L(1,j)\; x^L(2,j) \cdots x^L(N,j)\right]^T, \\ \mathbf{x}^R(j) &= \left[x^R(1,j)\; x^R(2,j) \cdots x^R(N,j)\right]^T, \\ \mathbf{x}^V(j) &= \left[x^V(1,j)\; x^V(2,j) \cdots x^V(N,j)\right]^T. \end{aligned} \quad (8)$$

Applying the boundary conditions (5), Equation (7) can be expressed as:

$$\mathbf{x}^L(j) = \mathbf{\Phi} \mathbf{x}^R(j) + \mathbf{\Gamma} \mathbf{x}^V(j) + \theta u(j) \quad (9)$$

where $\mathbf{\Phi} = [\phi_{kl}],\ \phi_{kl} \in R^{m_1 \times m_2}$, $\mathbf{\Gamma} = [\gamma_{kl}], \gamma_{kl} \in R^{m_1 \times m_3}$, $\theta = [\theta_k], \theta_k \in R^{m_1 \times 1},\ k = 1, \cdots, N,\ l = 1, \cdots, N$, and

$$\phi_{kl} = \begin{cases} A_{11}^{k-1}\alpha_{11} + A_{11}^{k-2} A_{12}, k = 1, \cdots, N, l = 1, \\ A_{11}^{k-l-1} A_{12},\ k = 3, \cdots, N,\ 1 < l < k, \\ 0,\ \text{else}, \end{cases}$$

$$\gamma_{kl} = \begin{cases} A_{11}^{k-1}\alpha_{12} + A_{11}^{k-2} A_{13},\ k = 1, \cdots, N, l = 1, \\ A_{11}^{k-l-1} A_{13},\ k = 3, \cdots, N,\ 1 < l < k, \\ 0,\ \text{else}, \end{cases}$$

$$\theta_k = A_{11}^{k-1}\beta,\ k = 1, \cdots, N. \quad (10)$$

Substituting Equation (9) and boundary conditions (5) into Equation (4), the expression for x^R in an extended matrix form is obtained:

$$\mathbf{x}^R(j) = \mathbf{\Psi} \mathbf{x}^R(j) + \mathbf{\Xi} \mathbf{x}^V(j) + \zeta u(j) \quad (11)$$

where $\mathbf{\Psi} = [\psi_{kl}],\ \psi_{kl} \in R^{m_2 \times m_2}$,$\mathbf{\Xi} = [\xi_{kl}], \xi_{kl} \in R^{m_2 \times m_3}$, $\zeta = [\zeta_k], \zeta_k \in R^{m_2 \times 1}$ and

$$\psi_{kl} = \begin{cases} A_{21} A_{11}^{k} \alpha_{11} + A_{21} A_{11}^{k-1} A_{12}, \\ \qquad k = 1, \cdots, N-1, l = 1, \\ A_{21} A_{11}^{k-l} A_{12}, \\ \qquad k = 2, \cdots, N-1, 1 < l \le k, \\ A_{22},\ k = 1, \cdots, N-1, l = k+1, \\ \alpha_{21} A_{11}^{k-1} \alpha_{11} + \alpha_{21} A_{11}^{k-2} A_{12}, k = N, l = 1 \\ \alpha_{21} A_{11}^{k-l-1} A_{12}, k = N, l = 2, \cdots, N-1, \\ 0,\ \text{else}, \end{cases}$$

$$\xi_{kl} = \begin{cases} A_{21} A_{11}^{k} \alpha_{12} + A_{21} A_{11}^{k-1} A_{13}, \\ \qquad k = 1, \cdots, N-1, l = 1, \\ A_{21} A_{11}^{k-l} A_{13}, \\ \qquad k = 2, \cdots, N-1, 1 < l < k, \\ A_{23}, k = 1, \cdots, N-1, l = k+1, \\ \alpha_{21} A_{11}^{k-1} \alpha_{12} + \alpha_{21} A_{11}^{k-2} A_{13}, k = N, l = 1 \\ \alpha_{21} A_{11}^{k-l-1} A_{13}, k = N, l = 2, \cdots, N-1, \\ \alpha_{22}, k = N, L = N, \\ 0,\ \text{else}, \end{cases}$$

$$\zeta_k = \begin{cases} A_{21} A_{11}^{k} \beta,\ k = 1, \cdots, N-1 \\ \alpha_{21} A_{11}^{k-1} \beta, k = N \end{cases} \quad (12)$$

From the state equation in (4), the extended matrix form of $x^V(j+1)$ can be written as:

$$\mathbf{x}^V(j+1) = \mathbf{Q}_1 \mathbf{x}^L(j) + \mathbf{Q}_2 \mathbf{x}^R(j) + \mathbf{Q}_3 \mathbf{x}^v(j) \quad (13)$$

where $\mathbf{Q}_1 = \text{diag}[A_{31}] \in R^{m_3 N \times m_1 N}$, $\mathbf{Q}_2 = \text{diag}[A_{32}] \in R^{m_3 N \times m_2 N}$ and $\mathbf{Q}_3 = \text{diag}[A_{33}] \in R^{m_3 N \times m_3 N}$.

From Equations (9) and (11), $\mathbf{x}^L$ and $\mathbf{x}^R$ can be rewritten:

$$\begin{aligned} \mathbf{x}^R(j) = {} & (\mathbf{I}_{m_2 N \times m_2 N} - \mathbf{\Psi})^{-1} \mathbf{\Xi} \mathbf{x}^V(j) \\ & + (\mathbf{I}_{m_2 N \times m_2 N} - \mathbf{\Psi})^{-1} \zeta u(j), \\ \mathbf{x}^L(j) = {} & (\mathbf{\Phi}(\mathbf{I}_{m_2 N \times m_2 N} - \mathbf{\Psi})^{-1} \mathbf{\Xi} + \mathbf{\Gamma}) \mathbf{x}^V(j) \\ & + (\mathbf{\Phi}(\mathbf{I}_{m_2 N \times m_2 N} - \mathbf{\Psi})^{-1} \zeta + \theta) u(j), \end{aligned} \quad (14)$$

where $\mathbf{I}_{m_2 N \times m_2 N}$ is an identity matrix of dimension $m_2 N$ by $m_2 N$. Well-posedness of the systems requires that $(\mathbf{I}_{m_2 N \times m_2 N} - \mathbf{\Psi})$ be invertible. The output equation in (6) can be written in matrix form:

$$y(j) = \mathbf{C}_1 \mathbf{x}^L(j) + \mathbf{C}_2 \mathbf{x}^R(j) + \mathbf{C}_3 \mathbf{x}^V(j), \quad (15)$$

where $\mathbf{C}_1 = [c_{11}, c_{12}, \cdots, c_{1N}]$, $\mathbf{C}_2 = [c_{21}, c_{22}, \cdots, c_{2N}]$, and $\mathbf{C}_3 = [c_{31}, c_{32}, \cdots, c_{3N}]$.

Substituting Equation (14) into Equations (13) and (15) yields:

$$\begin{aligned} \mathbf{x}^V(j+1) &= \mathbf{\Omega}\mathbf{x}^V(j) + \varphi u(j), \\ y(j) &= \mathbf{F}\mathbf{x}^V(j) + Du(j), \end{aligned} \tag{16}$$

where

$$\begin{aligned} \Omega &= \mathbf{Q}_1(\mathbf{\Phi}(\mathbf{I}_{m_2N\times m_2N} - \mathbf{\Psi})^{-1}\mathbf{\Xi} + \mathbf{\Gamma}) \\ &\quad + \mathbf{Q}_2(\mathbf{I}_{m_2N\times m_2N} - \mathbf{\Psi})^{-1}\mathbf{\Xi}) + \mathbf{Q}_3, \\ \varphi &= \mathbf{Q}_1(\mathbf{\Phi}(\mathbf{I}_{m_2N\times m_2N} - \mathbf{\Psi})^{-1}\zeta + \theta) \\ &\quad + \mathbf{Q}_2(\mathbf{I}_{m_2N\times m_2N} - \mathbf{\Psi})^{-1}\zeta \\ \mathbf{F} &= \mathbf{C}_1(\mathbf{\Phi}(\mathbf{I}_{m_2N\times m_2N} - \mathbf{\Psi})^{-1}\mathbf{\Xi} + \mathbf{\Gamma}) \\ &\quad + \mathbf{C}_2(\mathbf{I}_{m_2N\times m_2N} - \mathbf{\Psi})^{-1}\mathbf{\Xi}) + \mathbf{C}_3, \\ D &= \mathbf{C}_1(\mathbf{\Phi}(\mathbf{I}_{m_2N\times m_2N} - \mathbf{\Psi})^{-1}\zeta + \theta) \\ &\quad + \mathbf{C}_2(\mathbf{I}_{m_2N\times m_2N} - \mathbf{\Psi})^{-1}\zeta. \end{aligned} \tag{17}$$

Note that Equation (16) takes the same form as a state space model for LPS. If the setpoint profiles for the state variables $\mathbf{x}^V$ could be calculated for any output setpoint changes, the abundance of existing control theory and techniques for LPS could be applied to the control of DPS. The boundary control design presented in this paper is focused on convergence of the output to the setpoint. An alternative design problem would examine convergence of the state variables to the origin, incorporating the problem of state estimation using output measurements. This problem will be examined in future research.

Assume that $D = 0$ in Equation (17), meaning that at least one sampling time is needed for the input to affect the output. In fact, the time required for the impact of the input to reach the output can be significant for boundary control problems, especially when the input is at one boundary and the output at the opposite boundary. The delay phenomenon in boundary control problems can be systematically defined by a time delay index, k_d, such that

$$\begin{aligned} \mathbf{F}\mathbf{\Omega}^l\phi = 0,\ l = 1, \cdots, k_d - 2, \\ \mathbf{F}\mathbf{\Omega}^{k_d-1}\phi \neq 0. \end{aligned} \tag{18}$$

When the conditions in Equation (18) hold, the system is called to have a time delay of k_d. The future output in the next k_d steps can be written:

$$\begin{aligned} y(j+l) &= \mathbf{F}\mathbf{\Omega}^l\mathbf{x}^V(j),\ l = 0, 1, \cdots, k_d - 1, \\ y(j+k_d) &= \mathbf{F}\mathbf{\Omega}^{k_d}\mathbf{x}^V(j) + \mathbf{F}\mathbf{\Omega}^{k_d-1}\phi u(j). \end{aligned} \tag{19}$$

Then control can be developed such that

$$(y(j+k_d) - r) = \sum_{l=0}^{k_d-1} \lambda_l (y(j+l) - r), \tag{20}$$

where r is the setpoint for the output y, λ_l are tuning parameters that should satisfy $\lambda_l > 0$, $l = 0, 1, \cdots, k_d - 1$ and $\sum_{l=0}^{k_d-1} \lambda_l < 1$ for stability of the tracking error dynamics. One choice of tuning parameters is $\lambda_0 = \lambda_1 = \cdots = \lambda_{k_d-1} < \frac{1}{k_d}$. From Equation (20), the boundary controller can be formulated as:

$$u(j) = \frac{\sum_{l=0}^{k_d-1} \lambda_l (\mathbf{F}\mathbf{\Omega}^l\mathbf{x}^V(j) - r) - (\mathbf{F}\mathbf{\Omega}^{k_d}\mathbf{x}^V(j) - r)}{\mathbf{F}\mathbf{\Omega}^{k_d-1}\phi}. \tag{21}$$

The controller described in Equation (21) can drive the output to the setpoint, with its behaviour depending on the choice of the tuning parameters λ_l. The time delay index is usually $k_d \geq 1$. When the input is on one boundary and the output on the opposite boundary, the time delay index is greatest and could be close to or greater than the residence time. In this case, the boundary control input in Equation (21) is a function of the state variables at all spatial points. The performance of the controlled output can be improved because the controller takes into account the response of the current output and future outputs (within the delay horizon). An additional advantage of this control method is that the resulting control is robust to sensor failures at some spatial points.

4. SIMULATIONS

The boundary controller developed above is evaluated using two examples: a second order parabolic PDE system and a hyperbolic countercurrent heat exchanger.

4.1 Parabolic PDE

Consider a system described by

$$\frac{\partial s(z,t)}{\partial t} = a\frac{\partial s(z,t)}{\partial z} + b\frac{\partial^2 s(z,t)}{\partial z^2} - cs(z,t) \tag{22}$$

with boundary conditions

$$\begin{aligned} s(0,t) &= u(t), \\ \frac{\partial s(z,t)}{\partial z}\Big|_{z=L} &= 0, \end{aligned} \tag{23}$$

where t indicates time, z indicates the spatial coordinate, $s(z,t)$ is the distributed state variable, and a=0.005, b=0.1, c=0.05. The manipulated input $u(t)$ is the inlet value of the state variable $s(z,t)$. The controlled output is the outlet value of the state variable $s(z,t)$, *i.e.*, $y(t) = s(L,t)$. The parabolic system described here may represent an isothermal tubular reactor with diffusion and convection.

A state space model for the system described by (22) and (23) can be derived using different approaches

(*e.g.*, numerical discretization, state space identification, analytical solutions). For the sake of simplicity, the finite difference method is applied to the PDE system and yield the state space model:

$$\begin{bmatrix} x^L(i+1,j) \\ x^R(i-1,j) \\ x^V(i,j+1) \end{bmatrix} = \begin{bmatrix} 0 & 0 & 1 \\ 0 & 0 & 1 \\ \eta_1 & \eta_2 & \eta_3 \end{bmatrix} \begin{bmatrix} x^L(i,j) \\ x^R(i,j) \\ x^V(i,j) \end{bmatrix} \quad (24)$$

$$\begin{aligned} x^L(1,j) &= u(j), \\ x^R(N,j) &= x^V(N,j), \\ y(j) &= x^V(N,j). \end{aligned} \quad (25)$$

Using the controller in (21), it is found that the system has a time delay of $k_d = N = 6$. The tuning parameters used are $\lambda = [\,0\ 0.01\ 0.15\ 0.12\ 0.21\ 0.5\,]$. Figure (1) shows the closed-loop response to setpoint changes. It is observed that the output reaches the setpoint quickly with smooth control action.

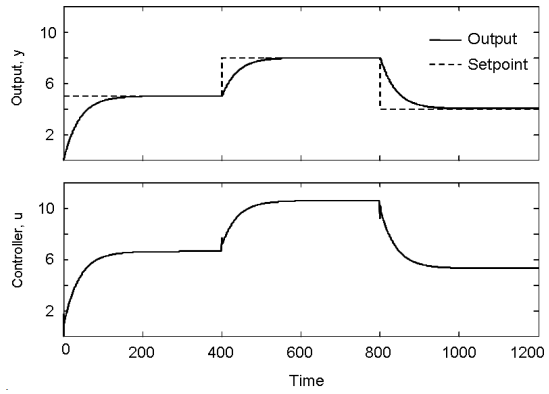

Fig. 1. Response of the parabolic PDE with boundary control to setpoint changes

4.2 Countercurrent Heat Exchanger

This example shows the application of the developed boundary controller to a countercurrent heat exchanger. Figure (2) shows the diagram of the system. The controller is designed to regulate the outlet temperature of the cold water by manipulating the inlet temperature of the hot water. Assuming that heat transfer to the environment is negligible, the system can be modelled as follows (Abdelghani-Idrissi *et al.*, 2001):

$$\begin{aligned} \frac{\partial T_h}{\partial t} &= -V_h \frac{\partial T_h}{\partial z} + V_h N_h (T_w - T_h), \\ \frac{\partial T_c}{\partial t} &= V_c \frac{\partial T_c}{\partial z} + V_c N_c (T_w - T_c), \\ \frac{\partial T_w}{\partial t} &= V_h C_h N_h (T_h - T_w) \\ &\quad + V_c C_c N_c (T_w - T_c), \end{aligned} \quad (26)$$

with boundary conditions

$$\begin{aligned} T_h(0,t) &= u(t), \\ T_c(L,t) &= T_{co} \end{aligned} \quad (27)$$

where subscripts h, c, and w refer to hot stream, cold stream, and wall temperatures respectively.

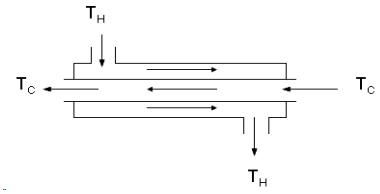

Fig. 2. Diagram of the countercurrent heat exchanger

The state space model of the system takes the form of:

$$\begin{bmatrix} x_h^L(i+1,j) \\ x_c^R(i-1,j) \\ x_w^V(i,j+1) \\ x_h^V(i,j+1) \\ x_c^V(i,j+1) \end{bmatrix} = \left[\begin{array}{cc|ccc} 0 & 0 & 0 & 1 & 0 \\ 0 & 0 & 0 & 0 & 1 \\ \hline 0 & 0 & \alpha_1 & \alpha_2 & \alpha_3 \\ \alpha_4 & 0 & \alpha_5 & \alpha_6 & 0 \\ 0 & \alpha_7 & \alpha_8 & 0 & \alpha_9 \end{array}\right] \begin{bmatrix} x_h^L(i,j) \\ x_c^R(i,j) \\ x_w^V(i,j) \\ x_h^V(i,j) \\ x_c^V(i,j) \end{bmatrix}$$
$$y(j) = K_1 x^V(j) \quad (28)$$

with boundary conditions:

$$\begin{aligned} x_h^L(1,j) &= u(j) \\ x_c^R(N,j) &= T_{co} \end{aligned} \quad (29)$$

The boundary control performance was evaluated by examining the closed-loop output response to changes in the setpoint. Using the developed control method, the delay time was calculated to be 3 time units. Figure (3) shows that the outlet cold-water temperature displays a stable response and quick convergence to the setpoint under the boundary controller with $\lambda = [\,0\ 0.3\ 0.6\,]$.

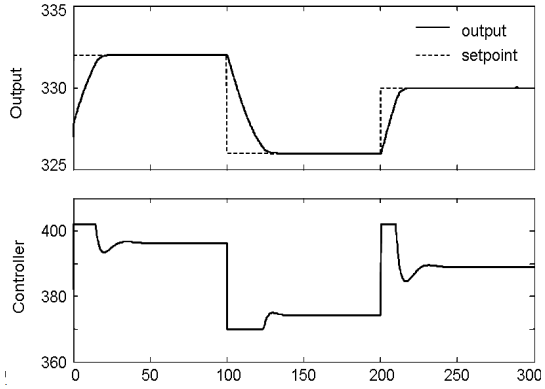

Fig. 3. Response of the heat exchanger with boundary control to changes in setpoint

5. CONCLUSIONS

This work has demonstrated how boundary conditions can be incorporated and used for controller design in discretized 2-D state space models for distributed

parameter systems. State space models with general boundary conditions are formulated for systems with either distributed or boundary inputs. The controller design approach is presented for systems with boundary input. Time delay can arise because of the spatially distributed nature of the process, and is defined in terms of the state space model parameters. The resulting controller demonstrates good performance for systems with a significant time delay because the controller determines the control input taking into account the projected behaviour of the output over the time delay horizon.The developed boundary controller was evaluated by simulation using both a parabolic system and a countercurrent hyperbolic system. The results show that, under the boundary controller, the output converges to the setpoint in a quick and smooth way without aggressive control action.

6. ACKNOWLEDGEMENTS

The financial support from Natural Sciences and Engineering Research Council of Canada is gratefully appreciated.

REFERENCES

Abdelghani-Idrissi, M.A., F. Bagui and L. Estel (2001). Analytical and experimental response time to flow rate step along a counter flow double pipe heat exchanger. *International Journal of Heat and Mass Transfer* **44**, 3721–3730.

Abu-Hamdeh, N.H. (2002). Control of a liquid-liquid heat exchanger. *Heat and Mass Transfer* **38**, 687–693.

Alvarez-Ramirez, J. (2001). Linear boundary control for a class of nonlinear pde processes. *Systems and Control Letters* **44**, 395–403.

Chakravarti, S. and W. H. Ray (1999). Boundary identification and control of distributed parameter systems using singular functions. *Chemical Engineering Science* (54), 1181–1204.

Chen, C.W. and J.S.H. Tsai (2002). Modeling and Optimal Control of Multi-Dimensional Systems. PhD thesis. National Cheng Kung University, Taiwan.

Christofides, P.D. (2000). *Nonlinear and Robust Control of PDE Systems*. Birkhauser Boston.

D'Andrea, R. (1998). A linear matrix inequality approach to decentralized control of distributed parameter systems. Proceedings of the American Control Conference. pp. 1350 – 1354.

D'Andrea, R. and G. E. Dullerud (2003). Distributed control design for spatially interconnected systems. *IEEE Transactions on Automatic Control* **48**(9), 1478–1495.

D'Andrea, R. and R. S. Chandra (2002). Control of spatially interconnected discrete-time systems. Proceedings of the 41st IEEE Conference on Decision and Control. pp. 240 – 245.

Fornasini, E. and G. Marchesini (1976). State-space realization theory of two-dimensional filters. *IEEE Transactions on Automatic Control* **AC-21**(4), 484–492.

Fowler, J. M. and R. D'Andrea (2002). Distributed control of close formation flight. Proceedings of the 41st IEEE Conference on Decision and Control. pp. 2972 – 2977.

Galkowski, K., E. Rogers, A. Gramacki, J. Gramacki and D. Owens (2000). Strong practical stability for a class of 2d linear systems. IEEE International Symposium on Circuits and Systems. pp. I–404–I–406.

Godasi, S., A. Karakas and A. Palazoglu (2002). Control of nonlinear distributed parameter processes using symmetry groups and invariance conditions. *Computers & Chemical Engineering* **26**(7-8), 1023–1036.

Hernández, E. and Y. Arkun (1992). Design of pole placement controllers for systems described by two-dimensional models. *Chemical Engineering Science* **47**(2), 297–310.

Hollis, S. (2002). *Differential Equations with Boundary Value Problems*. Prentice Hall. Upper Saddle River, NJ.

Kaczorek, T. (1985). *Lecture Notes in Control and Information Sciences: Two-Dimensional Linear Systems*. Springer-Verlag. New York.

Kung, S.Y., B.C. Levy, M. Morf and T. Kailath (1977). New results in 2-d systems theory, part ii: 2-d state-space models—realization and the notions of controllability, observability, and minimality. *Proceedings of the IEEE* **65**(6), 945–961.

Langbort, C. and R. D'Andrea (2005). Distributed control of spatially reversible interconnected systems with boundary conditions. *SIAM Journal of Control and Optimization* **44**, 1–28.

Marszalek, W. (1984). Two-dimensional state-space discrete models for hyperbolic partial differential equations. *Applied Mathematical Modelling* **8**, 11–14.

Neittaanmaki, P. and D. Tiba (1994). *Optimal Control of Nonlinear Parabolic Systems: Theory, Algorithms and Applications*. Marcel Dekker Inc.

Roesser, R. P. (1975). A discrete state-space model for linear image processing. *IEEE Transactions on Automatic Control* **AC-20**(1), 1–10.

Shang, H., J. F. Forbes and M. Guay (2005). Feedback control of hyperbolic distributed parameter systems. *Chemical Engineering Science* **60**, 969–980.

Stewart, G. E. (2000). Two Dimensional Loop Shaping Controller Design for Paper Machine Cross-Directional Processes. PhD thesis. University of British Columbia.

Wellstead, P.E., M.B. Zarrop and S.R. Duncan (2000). Signal processing and control paradigms for industrial web and sheet manufacturing. *International Journal of Adaptive Control and Signal Processing* **14**, 51–76.

ADCHEM 2006

International Symposium on Advanced Control of Chemical Processes
Gramado, Brazil – April 2-5, 2006

CONTROL OF A FEDBATCH BIOPROCESS USING NONLINEAR MODEL PREDICTIVE CONTROL

L. Álvarez, J. García and D. Urrego

National University of Colombia. Faculty of Mines. Medellín.
Research Group in Automatic (GAUNAL). e-mail: jfgarciat@unalmed.edu.co

Abstract: This paper presents an explorative work about a Model Predictive Control (MPC) technique. A nonlinear model predictive controller was designed and applied to a fedbatch bioprocess. First, bioprocess and its model are described. Then, a controller based in a nonlinear MPC scheme (Dual Fuzzy Model Predictive Control DF-MPC) is proposed with the aim to test the control of substrate concentration in simulation and to conclude about its ability to tackle the difficulties inherited from the bioprocess batch operation mode. In addition, different kinds of disturbances were applied showing the powerful disturbance rejection of the controller. *Copyright © 2002 IFAC*

Keywords: model based control, batch mode, nonlinearity, biotechnology, fuzzy sets.

1. INTRODUCTION

Despite most theoretical advances in process control are focused on continuous operations, batch processes have an important role in industrial field. Their inherent nonlinear nature and time variability increase complexity and make difficult the control tasks (Gutiérrez, Rincón and Alvarez, 2005).

In the last years, it is particularly amazing the introduction of biotechnological processes into the industrial field. Many commercial products like foods, pharmaceuticals and insecticides are produced by processes that involve living organisms. The increment of biotechnology-based products introduces new necessities in the industrial scope. The development of the biotechnological industry has still many challenges to affront. One of them is associated with control, mainly because most of bioprocesses operate in batch or fedbatch mode.

Controlling a bioprocess is not an easy work. Batch nature of most of bioprocesses produces difficulties when control is intended. In general, batch processes have some particularities that complicate control tasks. The major difficulty is associated with time-varying operating point. Along a batch run the transformations proceeds from an initial state to a final state under quite different conditions, therefore all process variables and some parameters are in permanent change. Such parameters time variation can generate nonlinearities. Therefore, control problem cannot be attacked using conventional linearization model techniques. In addition, the inherently transitory behavior of the variables and parameters generates internal disturbances (Gutiérrez, Rincón and Alvarez, 2004), e.g., the cells growth kinetics in bioprocesses.

Model Predictive Control (MPC) is an attractive technique to achieve a desired process behavior despite the difficulties mentioned previously. Its ability to predict future process behavior allows the controller to select the best control action according the designer criteria. Nonlinear formulation of MPC is even more attractive because the bioprocess model used here is highly nonlinear.

The aim of this work is the design of a controller for a bioprocess, able to affront difficulties inherited from batch operation mode. Additionally, a nonlinear controller is proposed making use of a restrictive enumerative optimization technique to generate a set of control policies (Alvarez, 2000), i.e., the set of possible control actions to evaluate in the cost functional.

2. BIOPROCESS MODEL

The bioprocess chosen for this work is a Fedbatch Fermentation of *Bacillus thuringiensis (Bt)*. This microorganism has been widely used to produce biologic pesticides over the world. *Bt* is specie **I** from *Bacillus* genre. Species from this group are sporulated and Gram positive bacterias.

Bacillus thuringiensis biological cycle is illustrated in Fig. 1. During vegetative stage, cellular reproduction occurs by binary fission. When vegetative cells stop growing the sporulation stage begins. Inside the cell a spore and a crystal are formed. Sporulation process finishes with the breaking of cellular wall and spore and crystal are released to the environment. This process is named cellular lysis. Finally, the spore can be isolated and prepared for its germination becoming a new vegetative cell and completing *Bt* biological cycle. Notice that *Bt* produces one or more crystalline bodies during sporulation process. Such crystals are named delta endotoxins, some of them are toxic for a variety of insect species and this property makes *Bt* an important microorganism in biological pesticides industry.

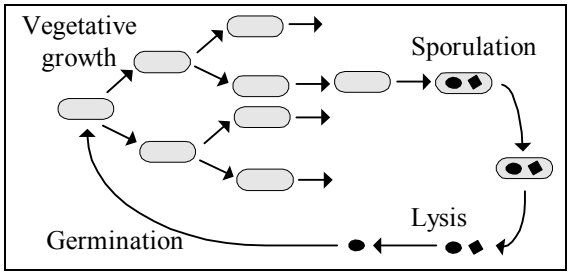

Fig. 1. Biological cycle of *Bacillus thuringiensis*

The model used in this work (Atehortúa, 2004) describes growth, sporulation, death and lysis. Other factors in *Bt* fermentation process are the dissolved oxygen, pH and temperature. The model does not include such dynamics, i.e, and suppose them to be controlled. Consider the bioprocess flow diagram in Fig. 2. Feed flow contains only substrate for cellular growth. The phenomenological model contains four states: volume *V*, vegetative cells concentration *Xv*, sporulated cells concentration *Xs*, and primary substrate concentration *Sp*.

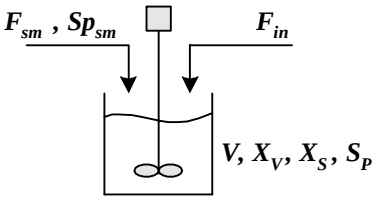

Fig. 2. Bioprocess flow diagram, the subindex *sm* indicates substrate medium feeding to the system.

The model is defined by the following differential equations:

$$\frac{dV}{dt} = F_{in} + F_{sm} \tag{1}$$

$$\frac{dX_v}{dt} = -\left(\frac{F_{in}+F_{sm}}{V}\right)X_v + (\mu - k_s - k_e)X_v \tag{2}$$

$$\frac{dX_s}{dt} = -\left(\frac{F_{in}+F_{sm}}{V}\right)X_s + k_s X_v - k_l X_s \tag{3}$$

$$\frac{dS_p}{dt} = -\left(\frac{F_{in}+F_{sm}}{V}\right)S_p + \left(\frac{F_{sm}}{V}\right)S_{p,fm} - \left(\frac{\mu}{Y_{X/S}} + m_s\right)X_v \tag{4}$$

F_{in} is the inlet flow of pH control reactants and antifoaming agent. F_{sm} is the feed flow of substrate medium, $S_{p,sm}$ is the substrate concentration in the feed flow. $Y_{X/S}$ denotes biomass-substrate yielding coefficient and m_s is the maintenance coefficient. k_s, k_e, k_l and μ are kinetic parameters defined as follows:

$$k_s = k_{s,fix}\left(\frac{1}{1+e^{a(Sp-aa)}}\right) - k_{s,fix}\left(\frac{1}{1+e^{a(Sp,ini-aa)}}\right) \tag{5}$$

$$k_e = k_{e,fix}\left(\frac{1}{1+e^{-b(t-c)}}\right) - k_{e,fix}\left(\frac{1}{1+e^{-b(t_{ini}-c)}}\right) \tag{6}$$

$$k_l = k_{l,fix}\left(\frac{1}{1+e^{d(X_v-e)}}\right) - k_{l,fix}\left(\frac{1}{1+e^{d(X_{v,ini}-e)}}\right) \tag{7}$$

$$\mu = \frac{\mu_{\max} S_p}{K_s + S_p} \tag{8}$$

Where k_s denotes the specific velocity of cellular sporulation, k_e denotes the specific velocity of natural death of vegetative cells, k_l is the lysis specific velocity of sporulated cells and μ is the specific velocity of vegetative growth. μ is given by the Monod growth model where $\mu_{\max}$ is the maximum specific velocity of cellular growth and *Ks* is the substrate saturation constant. The subindex *fix* indicates constant or fixed parameter. *a*, *aa*, *b*, *c* and *e* are constants values identified for this particular bioprocess. Notice that the equations describing the specific velocities k_s, k_e, and k_l are sigmoids in function of substrate concentration, time and vegetative cells concentration respectively, and show high nonlinearities associated to bioprocess model.

3. NONLINEAR MODEL PREDICTIVE CONTROL USING POLICIES GENERATION

MPC is an advanced control strategy that integrates many tools and fundamentals from other control techniques. The use of a process model in order to predict the plant immediate future is the main feature. MPC takes into account the feedforward and feedback control actions and integrates input and state constraints (process, economics, safety, environmentals, etc).

The NMPC (Nonlinear Model Predictive Controller) designed in this work must search for the best control action generating control policies. In order to obtain the best control policy, many works have focused on a solution through gradient based techniques (Boyd and Vandenberghe, 1996). On the other hand, there are some techniques named enumerative techniques

(ET) that require heavy computational demand but they offer more feasible control policies than others.

When ET are used, the best control policy is found by solving a programming or numeric problem. One of the difficulties of solving the numerical problem is to find a feasible control action before each sample time. When the model is nonlinear, the solution of the optimization algorithm loses convexity. Thus, finding the best solution is difficult and when it is found, the global minimum can not be guaranteed. Hence, in order to get a good control policy, the optimizer must evaluate quickly and repeatedly the cost beginning from a set of generated control policies and at each evaluation the nonlinear differential system must be solved. With the values obtained from iterations of numerical algorithm, optimizer calculates the numerical value of cost.

These tasks take more time and computation than linear case. It is important to take into account that the "optimality degree" of the problem depends on the amount of generated policies (Np). Restricted Enumerative Optimization with Control Horizon equal to three (REO3) is an evolution of Restricted Enumerative Optimization with control horizon equal to one (REO1) (Álvarez, 2000). REO1 procedure is as follows: first the controller explores all the valve possible movements, taking into account its spam and sample time constraint. When the controller selects a valve position, it maintains this value until the end of prediction horizon. Despite REO1 is a powerful policies generator, MPC needs that dynamical information delivered to the prediction model be as variable as possible. Hence REO3 generates $(Np)^3$ policies regarding all the variation possibilities with a control horizon equal to three. Notice that if the initial amount of policies Np is equal to 36 then the total policies generated $(Np)^3$ is 46.656. The next procedure of REO3 is the evaluation of each policy in the prediction model. It is computationally hard for the controller. In order to affront this difficulty, REO3 reduces the computational load applying important criteria based on control theory. The idea is to reduce the policies number to $(Np/4)^3$, e.g., $(Np/4)^3 = 729$.

4. DUAL FUZZY MODEL PREDICTIVE CONTROLLER

In this section the design of a nonlinear model predictive controller is presented: dual model predictive controller with fuzzy terminal region, **DF-MPC** (**D**ual **F**uzzy **M**odel **P**redictive **C**ontrol). The suggested control scheme has Dual Mode Controller (Mayne and Michalska, 1993), where a terminal region is defined around the set point. One disadvantage of a Dual Mode Controller is an abrupt commutation between the MPC and a linear controller tuned inside a terminal region (Ω). An important feature of DF-MPC is doing a soft transition through a Fuzzy Set that commutates step by step the controllers. Another feature that differences DF-MPC from Dual Mode Controller is that MPC is not replaced by linear controller inside the terminal region, but the controller is gradually transformed into a PI controller, i.e., there is a cost term, whose weight parameter is a Fuzzy Set that penalizes the difference between the MPC and a well tuned PI Controller. Notice that if the MPC is similar to a PI controller, such a cost tends to its minimization.

This Controller uses Restricted Enumerative Optimization with H_c=3 (REO3) and a Fuzzy region, such that the transition between the controllers (MPC → PI y PI → MPC) be soft. This is accomplished through a set point proximity criterion instead an abrupt or hard commutation in a region that is mathematically hard to define in most of cases. That is, the Dual Mode Controller is similar to Gain Scheduling Adaptive Controller (Aström and Wittenmark, 1989), its stability can't be guaranteed due to hard commutation between the regions. Finally, PI controller is used as linear controller inside Ω because driving the nonlinear process model to a standard form (local linear state feedback) is so difficult.

DF-MPC is based on the state location in the state-space. The fuzzy region (conformed by Ω and a neighborhood around it) is a Z Fuzzy Set, where there are four tuning parameters: α and β usually employed in MPC and the new ones γ and λ inside the cost functional. In Fig. 3 a two-variable state-space is depicted. $\mathbf{X_1}$ and $\mathbf{X_2}$ are the states, **Ω** is the linear region where **PI** controller operates, **SP** is the Set Point, **TR** is the Transition Region where the fuzzy commutation between the controllers (MPC to PI and PI to MPC) is effectuated.

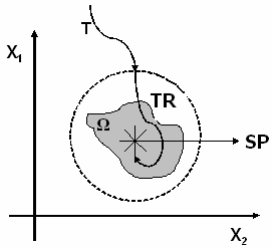

Fig. 3. Two-Variable State Space. $\mathbf{X_1}$ and $\mathbf{X_2}$ are the states. **SP** is the Set Point. **Ω** is the linear region. **TR** is the Transition Region

In other words, controller operation is as follows: When the state is outside of transition region a pure MPC operates, that is, α, β and γ take an initial values and the fuzzy parameter λ is zero. After crossing the boundary of **TR** the controller begins to change its parameters α, β and γ according λ changes. That is, λ parameter tends to one and α, β and γ tends to zero while the state approaches to Ω. This allows operating only with the cost term related to λ and canceling the cost terms related with α, β and γ. The last idea can be shown explaining the cost functional inside DF-MPC. In this work, the cost functional is a topic that differs from the MPC regular approaches. The DF-MPC cost functional penalizes the output error and the manipulated input changes between consecutive steps. It also penalizes the output

changes and the difference between the MPC and the PI Controller. The Cost Functional is:

$$J = \sum_{j=1}^{H_P} \alpha(k) * [\hat{y}(t+j/t) - y\_SP(t+j)]^2 + \sum_{i=1}^{H_C} \beta(k) * [\Delta u(t+j-1)]^2 + \sum_{j=1}^{H_P} \gamma(k) * [\Delta y(t+j-1)]^2 + \sum_{j=1}^{H_P} \lambda(k) * [u_{PI} - u_{MPC}]^2 \quad (9)$$

Notice that the parameters change in each step of the algorithm when the state is inside the TR. H_c is the control horizon and H_p is the prediction horizon. From the cost functional, α parameter penalizes the error between output with respect to the set point. Tuning of β parameter tries to avoid the hard movements of the control final element between two consecutive steps and γ parameter executes the same task than β, but on output. γ tries to soft the output response compensating the process inertia. λ parameter looks for the MPC emulates to a PI controller on the linear region Ω. Here, the technique has a benefit in comparison to the original approach (Mayne and Michalska, 1993) because DF-MPC does not commutate the controllers. Furthermore, inside Ω the cost functional is transformed to:

$$J = \sum_{j=1}^{H_P} \lambda(k) * [u_{PI} - u_{MPC}]^2 \quad (10)$$

That is, on Ω, λ tends to one and α, β and γ tend to zero while the output error tends to zero. Notice that in TR the MPC turns softly into a PI controller, because the difference among controllers weight (MPC and PI) has more relevance than the other weights. The Fig. 4 shows how λ changes while the output error tends to zero. The length of the transition zone is modified by a designer criterion.

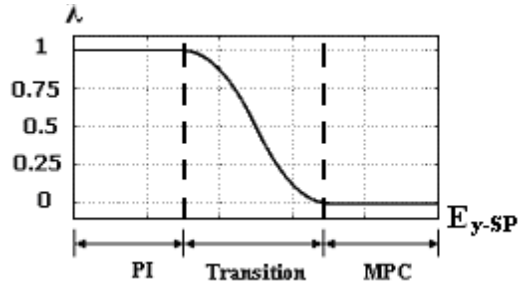

Fig 4. **Z** Fuzzy Set of the λ parameter. Lambda (λ) variates from zero to one according to the error position $E_{y\text{-}SP}$.

Finally, cost functional parameters are defined as follows:

$$\alpha(k) = [1 - \lambda(k)] * \alpha(1) \quad (11)$$

$$\beta(k) = [1 - \lambda(k)] * \beta(1) \quad (12)$$

$$\gamma(k) = [1 - \lambda(k)] * \gamma(1) \quad (13)$$

Notice that α, β and γ varies at each iteration (k) and the variation depends on its initial conditions and the λ value in each sample time.

5. APPLICATION OF DF-MPC TO THE BIOPROCESS.

In this point a DF-MPC Controller for substrate regulation in a *Bt* fedbatch culture is presented. Despite the bioprocess is effectuated in a fedbatch mode, notice that the process is continuous for the substrate (defining substrate inside the bioreactor as a system) because it is being permanently fed to the bioreactor and simultaneously cells consume it. Another significant issue is: why substrate regulation? The basic idea is controlling substrate concentration inside the bioreactor, and the way is manipulating the substrate inlet flow to the bioreactor. The biotechnological knowledge about fedbatch cultures indicates that substrate concentration is one of the most influential conditions for an adequate bacterial growth.

The values used in simulation for the controller designed are the followings: **Initial values**: substrate concentration Sp=9.718g/l, vegetative cells concentration Xv=0.645g/l, volume V=11.0l and fresh medium flow F_{fm}=0. **Tuning parameters** of the DF-MPC are α=100, β=8, γ=10. Control horizon Hc=3 because REO3 is used, prediction horizon Hp=10. The amount of policies generated is Np=32. It implies the total evaluation of 512 policies on each sample time. Notice that REO3 makes a reduction of the possibilities. Such trim reduces the policies from 32768 to 512. **Operation conditions:** Set point is fixed in SP=10g/l, linear region Ω is defined around the SP value after 0.02 g/l and transition region TR is between 0.02g/l and 0.1g/l around the SP value. The valve span is the maximum value that the valve opens in each sample time, and it is 5%. It is important to regard that the Ω and TR values are not implementable physically, but in simulation such implementation is possible.

6. RESULTS

In this section, simulation results for the designed controller are presented. Some plots about process performance, response to external and internal disturbances are shown. A purpose is to expose how the designed controller (DF-MPC) handles the fedbatch process even when disturbances occur. First result is the performance of DF-MPC without disturbances. Cellular growth is shown in Fig. 5, notice that vegetative cells reach a maximum value when sporulation begins. Fig. 6 shows the substrate concentration during the first 7 hours until the valve saturation, as it is shown in Fig. 7. When vegetative cells reach a maximum value, the valve closes immediately to stop substrate flow. So the process evolves naturally to obtain the maximum crystal concentration (Atehortúa, 2004).

However, performance of the controller designed for regulation must be also proven with respect to

disturbances. In this work, an analysis about internal and external disturbances is made. External disturbance is defined as substrate concentration of inlet flow ($S_{p,sm}$). In addition, the batch process has particular disturbances called internal disturbances, i.e., unexpected changes into the bioreactor that are not totally known. Furthermore there are disturbances that the prediction model does not take into account. Another kind of internal disturbances are the dynamical effect of uncontrolled states (*Xv, Xs, V*) into the controlled state *Sp* in the fedbatch run. This type of disturbance is named fundamentally internal disturbance (Gutiérrez, Rincón and Alvarez, 2005). In the present work an applied internal disturbance is an unexpected consumption of substrate by other microorganism into the bioreactor for an instant.

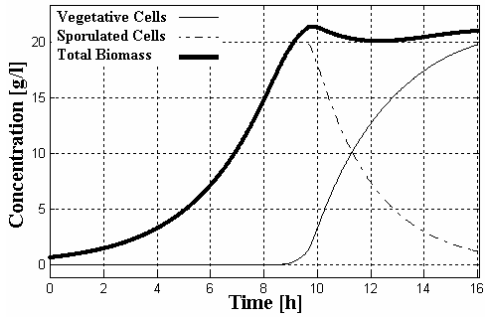

Fig. 5. Cellular Growth (Total batch run)

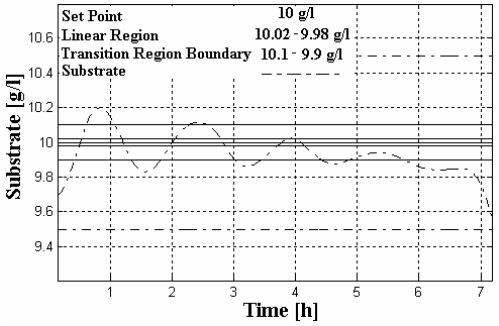

Fig. 6. Substrate Regulation (Zoom).

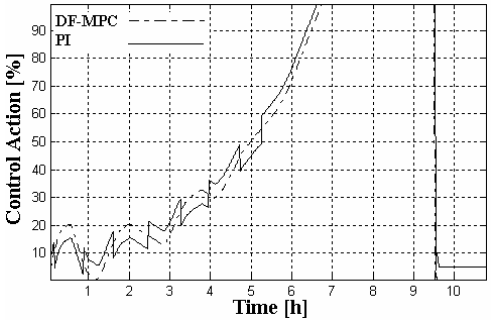

Fig. 7. DF-MPC Control Action (Zoom)

6.1. External Disturbances

DF-MPC rejects correctly the external disturbances when the substrate concentration in the feed $S_{p,fm}$ changes positively, even a high one is well tackled (100% from the original concentration). When the external disturbances are negative, the DF-MPC must saturate the valve while the substrate is consumed. Fig. 8 shows the output response to multiple disturbances with different amplitudes at different times (10%, 20%, 30% and 40% at one, two, three and four hours respectively). An important feature that difficult batch process control is the instant of the batch run when disturbance appears, that is, because disturbance effects change with time, even if the disturbance amplitude is the same.

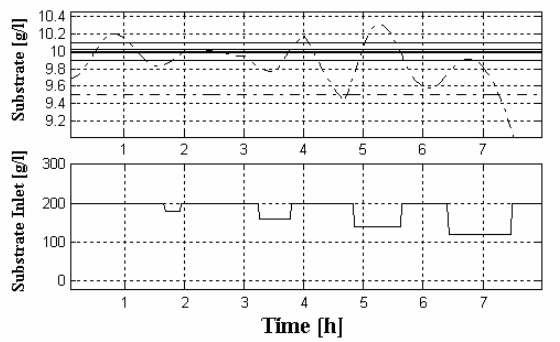

Fig. 8. Substrate Regulation with External Disturbances (Zoom).

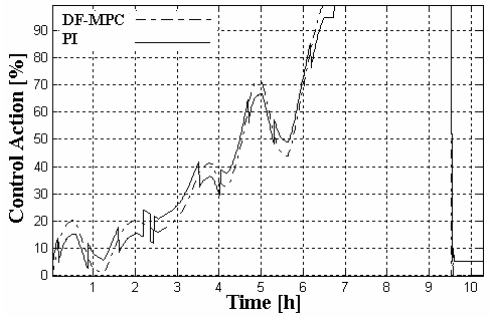

Fig. 9. Control Action when External Disturbances are applied to the Bioprocess (Zoom).

6.2. Internal Disturbances

This kind of disturbances is well rejected depending on its application instant and its amplitude. It is essential to remark that some internal disturbances occur during all the process: those produced by non controlled states, i.e, vegetative cells (X_v) are consuming substrate (*Sp*), so the state *Xv* is changing permanently. The other internal disturbances are applied to the process in two times: at the beginning of the batch run (first hour) and at the end of the controllable process phase (fifth hour). It is important to remark that internal disturbances applied are negative in sign with respect to the set point, that is, there is a substrate disappearance inside the bioreactor. If these disturbances are positive the MPC would not act because substrate would be exceeded and cells would eat with their natural dynamics. The results of internal disturbances applied at the first hour are shown in Figs. 10 and 11 for a maximum disturbance percent (80%). Notice that, the substrate concentration is also drastically reduced inside the bioreactor and the DF-MPC drives the process to the set point again. In addition, DF-MPC operates in all

the state-space because it was designed to operate in a nonlinear way, that is, a linear MPC controller cannot operate as good as a nonlinear one. The Fig. 11 shows how the final control element (a valve) moves under DF-MPC orders. Likewise, internal disturbances applied in the fifth hour are shown in Figs. 12 and 13 with a maximum disturbance (60%). Observe an important result: In this fedbatch process, disturbances are more harmful at the end of the process than the beginning. Notice that before the internal disturbance occurs, DF-MPC regulates the substrate in the set point and control actions are soft as it is shown in Fig. 13. In the same figure it can be seen that DF-MPC tries to drive the process to the set point, but in such point controllability is lost again.

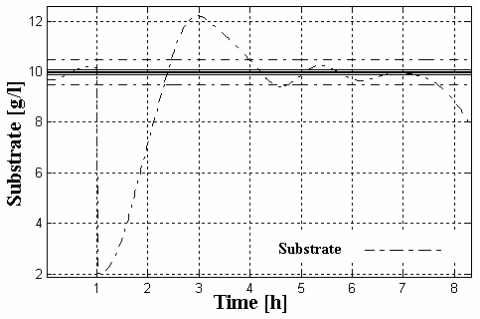

Fig. 10. Substrate Regulation with Internal Disturbance applied at the first hour (Zoom).

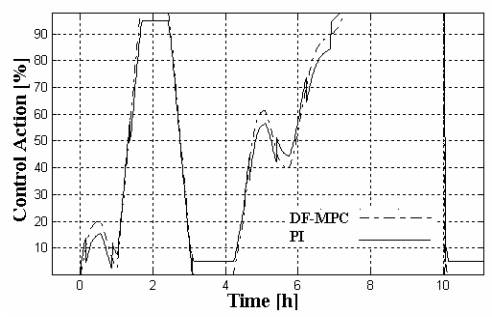

Fig. 11. Control Action when Maximal Internal Disturbance is applied at the first hour.

7. CONCLUSIONS

As it was mentioned above, this work is an exploration about a new MPC technique. A nonlinear MPC controller with dual fuzzy set strategy was designed. One of the aims of this work is verifying how the controller designed could affront the particularities that difficult the bioprocess control, specially the difficulties inherited from its batch nature (Gutiérrez, Rincón and Alvarez, 2005). Regulation was made to guarantee a maximum growth of vegetative cells. The main problem associated to regulation was the fundamentally internal disturbances, when substrate tries to maintain in the set point, the other states are permanently changing. These changes disturb the regulated substrate value. The use of a MPC technique based in Dual Mode (Michalska and Mayne, 1993) could affront the fundamentally internal disturbances, the internal (eventual) and external disturbances. In this work, PI parameters used for the DF-MPC could not be calculated to guarantee stability. Future works must explore issues like parameter tuning of PI and MPC controllers for batch process. An interesting suggestion is making multivariable control based on the design presented in this work.

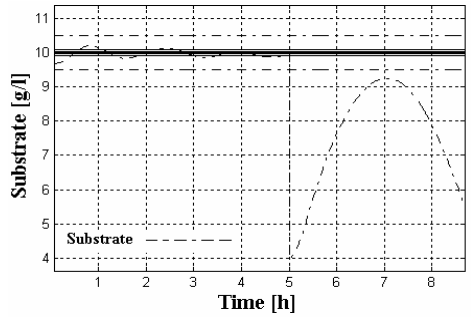

Fig. 12. Substrate Regulation with Internal Disturbance applied at the fifth hour (Zoom).

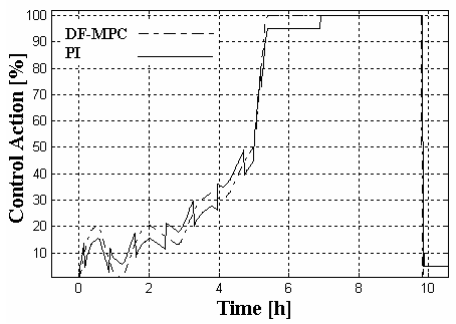

Fig 13. Control Action when Maximal Internal Disturbance is applied at the fifth hour (Zoom)

REFERENCES

Alvarez, H (2000). Control predictivo basado en modelo borroso para el control de pH. Ph.D. Thesis. Universidad Nacional de San Juan. San Juan, Argentina.

Alvarez, L., García, J. and Urrego, D. (2005) Control Predictivo Basado en Modelo No Lineal aplicado a un Bioproceso. Universidad Nacional de Colombia. Medellín, Colombia.

Aström and Wittenmark (1989). Adaptive Control. Addison-Wesley.

Atehortúa, P. (2004) Modelado del proceso de producción de δ-endotoxinas de *Bacillus thuringiensis* en un reactor discontinuo alimentado a pulsos con retención celular completa. M.Sc. Thesis. Universidad Nacional de Colombia. Medellín, Colombia.

Boyd, S and Vandenberghe, L (1996). Convex optimization, a course reader. Stanford university press.

Gutiérrez, L., Rincón, M. and Alvarez, H. (2005) Control Difficulties in bioprocesses inherited from their batch conditions. XI RPIC. Río Cuarto, Argentina.

Michalska, H. And Mayne, D.Q. (1993) *"Robust Receding Horizon Control of Constrained Nonlinear Systems"*. IEEE Transactions on Automatic Control, vol. 38, pp. 1623-1633.

ADCHEM 2006

International Symposium on Advanced Control of Chemical Processes
Gramado, Brazil – April 2-5, 2006

MULTIVARIABLE CONTROL STRATEGY BASED ON BIFURCATION ANALYSIS OF AN INDUSTRIAL GAS-PHASE POLYMERIZATION REACTOR

Nina P. G. Salau[1], Argimiro R. Secchi[2], Jorge O. Trierweiler[3], Gustavo A. Neumann[4]

[1,2,3]Group of Integration, Modelling, Simulation, Control and Optimization of Processes (GIMSCOP)
Department of Chemical Engineering, Universidade Federal do Rio Grande do Sul (UFRGS), Brazil
[4]*BRASKEM S. A.- Brazil*
{[1]ninas, [2]arge, [3]jorge}@enq.ufrgs.br , [4]gustavo.neumann@braskem.com.br

Abstract: In an industrial gas-phase polyethylene reactor, the safe operating range of temperature is rather narrow. Even within this temperature range, temperature excursions must be avoided because they can result in low catalyst productivity and significant changes in product properties. In previous work, using a first-principles model, including the recycle stream and the heat exchange system, a PID temperature controller with robust performance was designed via optimization in the frequency domain for different operating points. For the reactor total pressure, ethylene partial pressure, H2/C2 and C4/C2 molar ratios, PI controllers were designed. In the PID temperature controller, if the manipulated variable (cooling water valve opening) saturates then the reactor operates without a feedback temperature controller, leading to oscillatory behaviour and limit cycles. It has been demonstrated that the manipulated variable saturation and the nonlinear dynamic behaviour are removed when auxiliary manipulated variables, obtained by bifurcation analysis, are used in a multivariable control strategy for the reactor temperature control. In this work, two control structures are compared to define the most suitable proposal for implementation in an industrial reactor and the impact of these control structures in the reactor production and in the polymer melt index are analyzed. The first control structure considers the control problem using the designed PID controller for the reactor temperature and includes a switching strategy with a PI controller for the auxiliary manipulated variables. The second control structure considers the control problem also using the designed PID controller for the reactor temperature, however including a MPC controller for the auxiliary manipulated variables.

Keywords: Multivariable Control Strategy, Bifurcation Analysis, Polymerization Reactor, and Stability.

1. INTRODUCTION

Stabilization of polyethylene reactors is a challenging problem and needs to be addressed through a good control. Dadebo et al. (1997) have demonstrated that without feedback control, industrial gas-phase polyethylene reactors are prone to unstable steady states, limit cycles and excursions toward unacceptable high temperature steady states. In their work, the ability of the controllers to stabilize desired setpoints of industrial interest is evaluated using a bifurcation approach. Seki et al. (2001) have studied the stabilization of gas-phase polyethylene reactors through an adequate tuning of PID controller, which is applicable regardless of the pole locations of the transfer function and have been proposed a retuning method of a PID controller, which can be performed at the onset of closed-loop instability.

In their paper, Ali et al. (2003) have investigated a multivariable control problem of an industrial gas-phase polyethylene reactor, where are considered the two time-scale of the process and the multi-rate sampling of the process variable control. Specially, the control of the reactor temperature and pressure in addition to the gas partial pressures is considered in their paper. Two control scheme and two algorithms are tested and compared.

All of aforementioned studies dealt only with the tight regulation of the bed temperature to ensure reactor stability in an operating condition where the

saturation does not occur. In this work, a more comprehensive model is used to reproduce the process of an industrial gas-phase polyethylene reactor. In this model, the manipulated variable of bed temperature reactor controller is the control valve opening (the real situation in the industrial reactor), instead of the cooling water temperature. Thus, the saturation of this valve can be accounted for. Besides, in the practical point of view, if the control valve saturates, then the reactor operates without a feedback temperature controller, leading to oscillatory behaviour and limit cycles. Therefore, the manipulated variable saturation and the nonlinear dynamic behaviours should be removed from the system by using auxiliary manipulated variables. In this work, these variables are determined by bifurcation analysis, and then two multivariable control structures for the reactor temperature control are tested and compared to define the best proposal for implementation in industrial reactors.

2. PROCESS MODEL

A fluidized-bed zone and a disengagement zone compose the reactor, as shown in Figure 1. A heat exchanger is used to remove the reaction heat from the compressed recycle stream, and then the cooled gas is mixed with the feed stream to be re-injected in the base of the reactor. The solid catalyst (chromium based) is fed in a stream of nitrogen and then dragged to the fluidized-bed. The product is removed from the reactor by a discharge system operating in cycles determined by the production rate. In the disengagement zone the gas composition is analyzed by chromatography.

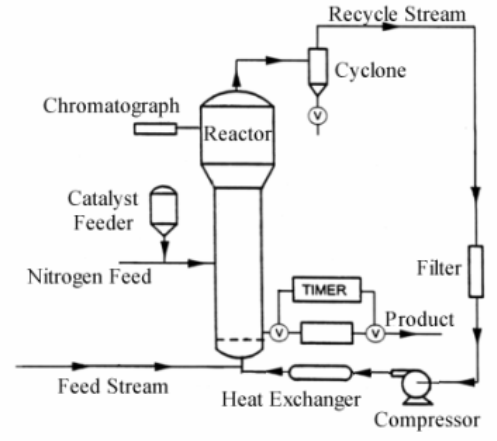

Fig. 1. UNIPOL® process.

The UNIPOL® process model is shown in Figure 2. McAuley et al. (1995) have demonstrated that the additions of the recycle stream and the external cooler models to the reactor model make possible the study of complex dynamics and location of bifurcation points, which could not be reproduced just by the reactor model. Besides, the addition of the heat exchange system, including all their equipments, makes possible an optimal design for the reactor temperature controller, using the cooling water valve opening as manipulated variable. The equations of the model used in this work are detailed in Salau et al. (2005).

3. DYNAMIC BEHAVIOUR ANALYSIS

The effects of the reactor operating conditions on the process dynamics and stability were analysed using the reactor model, including the recycle stream and the external cooler. The developed model was implemented in AUTO®, software for continuation and bifurcation problems in ordinary differential equations. Unstable steady states, limit cycles, and excursions toward unacceptably high-temperature steady states arise during the model simulation, when supposing the reactor operation with open-loop temperature control and the addition of a reactor total pressure controller to the system, whose manipulated variable is the ethylene feed flow rate. These non-linear dynamic behaviours, as shown in Figure 3, can be explained by positive feedback between the reactor temperature and the reaction rate.

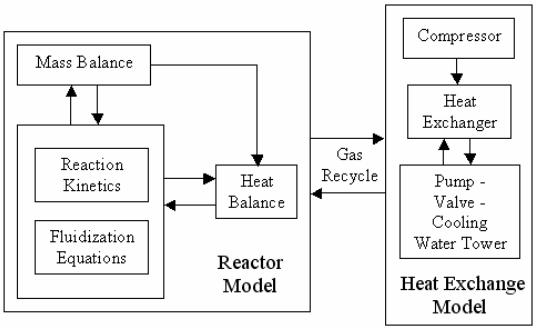

Fig. 2. UNIPOL® process model.

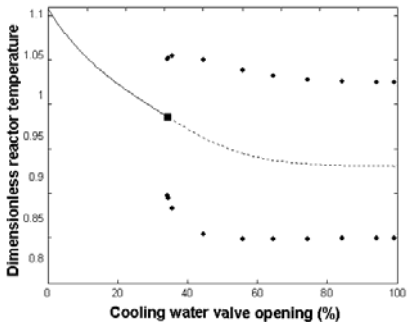

Fig. 3. The effect of cooling water valve opening on stability: — stable steady state; --- unstable steady state; ■ Hopf bifurcation; • stable limit cycles.

If the reactor temperature is above the unstable steady-state temperature, then the heat removal in the heat exchanger is larger than the steady-state heat-generation rate (McAuley et al., 1995). As result, the reactor temperature begins to decrease, decreasing the rate of reaction and the product outflow rate, thereby reducing the rate at which catalyst flows from the reactor. Thus, catalyst and monomer begin to accumulate in the reactor, increasing the temperature, the rate of reaction, and the product outflow rate, resuming the limit cycle.

4. PROPOSED SOLUTION FOR THE REGULATORY TEMPERATURE CONTROL PROBLEM

The reactor system is easily stabilized with a proportional controller. However, the addition of

integral and derivative action eliminates offset and leads to faster controller performance (Dadebo et al., 1997). The advantages of a PID controller in this case are the speed and thereby the sample time, the rejecting disturbances, the robustness and the trustworthiness.

Due to high non-linearity between the reactor temperature and cooling water valve opening, the relation between these variables were characterized by a multi-model system (many representative linear models of different operating region). The linear models used to design a robust PID controller were built at the points that belong to the unstable regions of valve opening, shown in Figure 3. Thus, the PID temperature controller was designed using the SIOM-MMA (Sequential Iterative Optimization Method - Multi-Model Approach, Faccin and Trierweiler, 2004), based on a frequency domain optimization problem for a given desired performance. The method is able to design a PID controller for different operating points with robust performance, as shown in Figure 4.

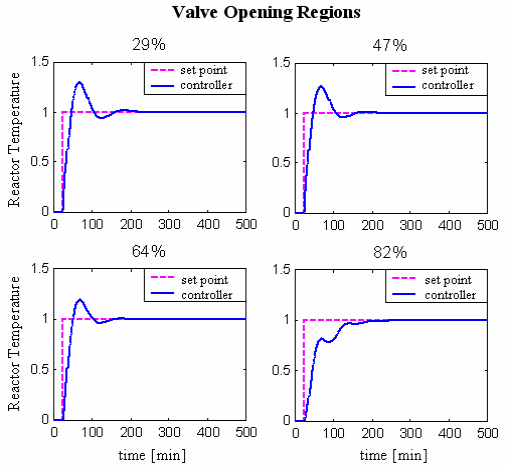

Fig. 4. Temperature response for a step setpoint change using the robust PID controller.

For better representation of industrial plant operation conditions, PI controllers were designed to reactor total pressure, ethylene partial pressure, H2/C2 and C4/C2 molar ratios, whose manipulated variables are, respectively, ethylene, nitrogen, hydrogen and butene feed flow rate. A MPC temperature controller also was designed in order to obtain a similar performance of the PID temperature controller. Thus, some tests were carried out, using the linear and the non-linear model, to demonstrate the controllers' performance in regions where the valve operates in a nominal condition and where the valve moves in the fully open direction, in other words, operates in a saturation condition. The controllers' performances for a step setpoint change and a step disturbance in the reactor temperature using the linear model (of a nominal operating condition of valve opening) is shown in the Figure 5 and using the non-linear model is shown in Figure 6. According to Figure 5, the MPC temperature controller presents a better performance for a step setpoint change and a worst performance for an unmeasured disturbance rejection (presenting an oscillatory behaviour) than the PID temperature controller. However, in the industrial plant there are many unmeasured disturbances, which cannot be modelled and, according to Figure 6, the MPC temperature controller fails for a step setpoint change when subject to unmodelled disturbances, causing oscillatory behaviour and leading the reactor operation to a limit cycle. On the other hand, satisfactory results were obtained for a step setpoint change and for unmeasured disturbance rejection using the non-linear model in a nominal operating condition with the designed PID temperature controller.

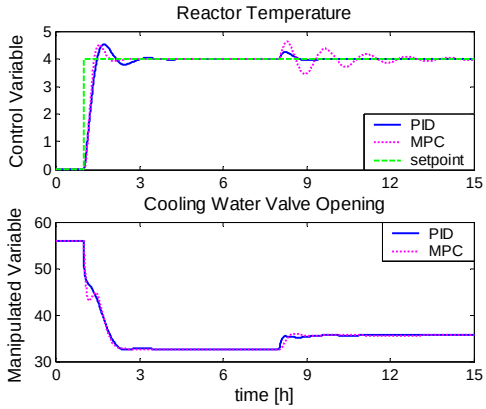

Fig. 5. Reactor temperature and valve opening cooling water responses for a step setpoint change at time of 1 hour and for a step disturbance at time of 8 hours with the PID and the MPC controller using the linear model.

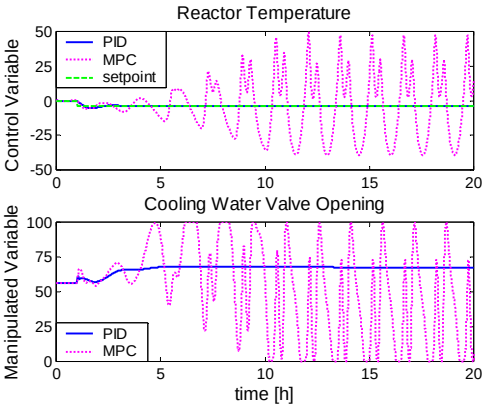

Fig. 6. Reactor temperature and valve opening cooling water responses for a step setpoint change at time of 1 hour with the PID and the MPC controller using the non-linear model.

It is shown in Figure 4 that as the valve moves in the fully open direction, the controller performance degrades. A better controller performance could be achieved using a gain-scheduling strategy. However, according to Figure 3, the gain in the reactor temperature as the valve moves after an opening of 80% in the fully open direction is practically ineffective because, in these conditions, the heat exchange does not occur due to the system thermal limitation. Besides, if the control valve saturates (a common situation in the industrial reactor), then the reactor operates without a feedback temperature controller, leading to oscillatory behaviour and limit cycles, as shown in Figure 7. Thus, the use of gain-scheduling strategy was ruled out. Therefore,

manipulation of valve opening alone may not be sufficient to bring the temperature back to the desired level. Thus, auxiliary manipulated variables need to be determined in order to move the reactor away from region where the limit cycles occur.

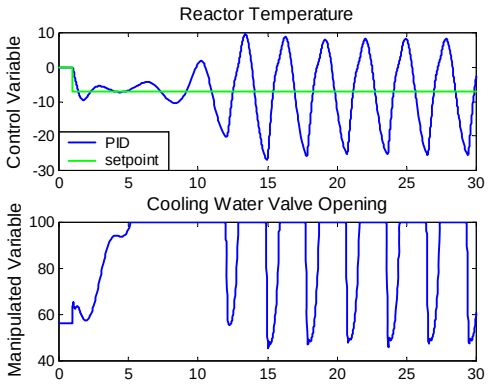

Fig. 7. Reactor temperature and valve opening cooling water responses for a step setpoint change at time of 1 hour with the PID controller using the non-linear model in a saturation operating condition.

5. FEASIBLE OPERATING REGIONS

Candidate auxiliary manipulated variables, that can be manipulated to reduce the reactor temperature, are catalyst feed rate, inert saturated organic feed rate, and ethylene partial-pressure controller setpoint. All these variables can stabilize the reactor temperature controller in the desired setpoint by reducing the rate of heat generation or increasing the heat transfer capacity (Salau, 2004). However, all of these variables reduce the production rate and other problems may arise with their use, some of them are shown in Table 1.

Table 1. Problems in using auxiliary manipulated variables to help control the reactor temperature.

Variables	Problems
Catalyst feed rate	It is difficult to determinate the flow rate in the feeder due to its small sensibility. High impact in the reactor production.
Inert saturated organic feed rate (low boiling point)	If the gas mixture dew point is achieved, the distributed plate of gas in the reactor will block. To prevent accumulation, the inert has to be removed from the reactor through the product or purge streams.
Ethylene partial-pressure controller setpoint	It causes a decrease in the recycle heat exchange capacity, by increasing the nitrogen/ethylene concentration ratio.

In the industrial unit, due to the high correlation between the reactor total pressure and the ethylene partial pressure, the operator manually controls the last one through the nitrogen feed rate or the bleed stream. As the reactor total pressure is controlled through the ethylene flow rate manipulation, to use the ethylene partial-pressure controller setpoint in the multivariable control strategy would be necessary to design a controller strategy for the reactor using the total pressure and the ethylene partial pressure, simultaneously. Thus, only the catalyst and the inert saturated organic feed rate were used in this work.

To prove the potentiality in using auxiliary manipulated variables to help control the reactor temperature, it was made a bifurcation study in open loop where the evaluated state variable is the reactor temperature and the bifurcation parameters are: valve opening cooling water (the manipulated variable of the PID temperature controller), and catalyst feed rate and inert saturated organic feed rate (the auxiliary manipulated variables to be used in the reactor temperature control). In Figure 8 is shown the effect of two different values of inert saturated organic feed rate on stability with valve opening cooling water and catalyst feed rate as bifurcation parameters. In Figure 9 is shown the effect of two different values of catalyst feed rate on stability with valve opening cooling water and inert saturated organic feed rate as bifurcation parameters.

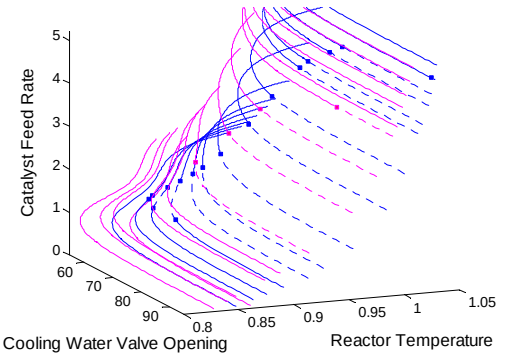

Fig. 8. The effect of a lower (in blue) and a higher (in magenta) inert saturated organic feed rate on stability: — stable steady state; --- unstable steady state; ■ Hopf bifurcation.

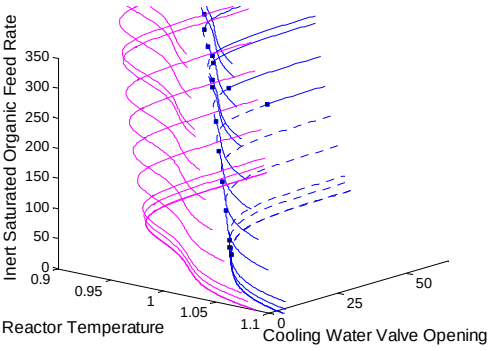

Fig. 9. The effect of a higher (in blue) and a lower (in magenta) catalyst feed rate on stability: — stable steady state; --- unstable steady state; ■ Hopf bifurcation.

According to Figure 8, if the inert saturated organic feed rate is increased, the region of stability for different catalyst feed rates increases, reducing the reactor temperature and the valve opening cooling water. In Figure 9, it is shown that if the catalyst feed rate is reduced, the region of stability for different inert saturated organic feed rates also increases, reducing the reactor temperature and the valve

opening cooling water. As a small reduction in the catalyst feed rate has a negative large impact in the reactor production, and the increase in the inert saturated organic feed rate enlarge the stability region keeping the catalyst feed rate at the nominal operating point, the best strategy is the use of inert as auxiliary manipulated variable as much as possible.

6. PROPOSED SOLUTION FOR THE SUPERVISORY CONTROL PROBLEM

In the supervisory control problem, the reactor temperature PID controller, designed using the SIOM-MMA method, was maintained and the valve opening, which is the manipulated variable of this controller, becomes the controlled variable in two different control structures within a multivariable strategy: a sequential PI switch controller and a model predictive controller (MPC). The idea of these control structures is open the control valve through the reactor temperature PID controller, until achieving a region where the gain between the valve opening and the cooling water becomes low. When a pre-determinate value of the valve opening is achieved, the inert saturated organic feed rate, with high specific heat capacity, is increased to improve the heat exchange between the recycle gas and the cooling water. Thereby, more reaction heat is removed from the reactor, decreasing the reactor temperature back to the setpoint. However, the maximum amount of this inert saturated organic feed rate is limited by the gas mixture dew point. When this upper bound is achieved without stabilizing the reactor temperature in the setpoint, the catalyst feed rate is reduced to decrease the reactor temperature.
The first control structure considers the control problem using the designed PID controller for the reactor temperature and includes a switching strategy with a sequential PI controller for the auxiliary manipulated variables. The second control structure considers the control problem also using the designed PID controller for the reactor temperature, however, including a MPC controller for the auxiliary manipulated variables. The responses of both sequential PI switch controller and MPC are compared to define the most suitable proposal for implementation in an industrial reactor.

6.1 Results for a Nominal Operating Condition

It was chosen a nominal operating condition to compare the control problem using only the reactor temperature PID controller (Figure 6) and the control problem using the two proposed multivariable control structures (Figures 10 and 11). In the multivariable control structures, the inert saturated organic feed rate is increased after the valve opening achieves 60%, and the catalyst feed rate is decreased after the inert saturated organic feed rate increases 3 dimensionless units. According to Figures 10 and 11, the performances of both proposed control structures to stabilize the reactor temperature in the desired setpoint are similar. Thus, both controllers are able to get quickly the new polymer melt index, avoiding off-specification product. However, the MPC controller presents a better result than the sequential PI switch controller for a nominal operating condition, because this controller is able to achieve the maximum quantity of the inert saturated organic feed rate before to manipulate the catalyst feed rate and, thereby, reducing production loss.

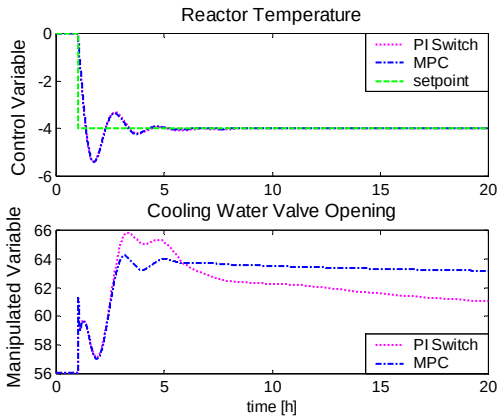

Fig. 10. Reactor temperature and valve opening cooling water response to a step change in reactor temperature setpoint with the multivariable strategy (sequential PI switch and MPC).

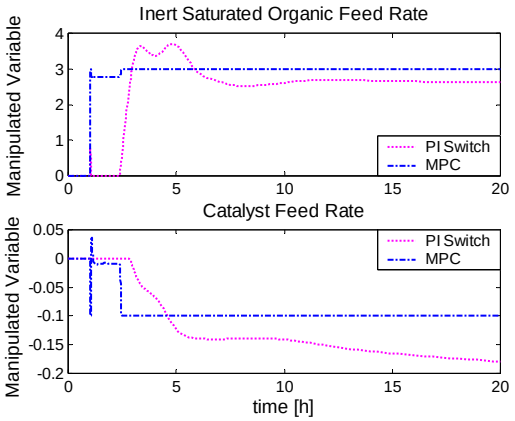

Fig. 11. Inert saturated organic feed rate and catalyst feed rate manipulation with the multivariable strategy (sequential PI switch and MPC).

6.2 Results for a Saturation Condition

It was chosen a valve opening saturation condition to compare the control problem using only the reactor temperature PID controller (Figure 7) and the control problem using the two proposed multivariable control structures (Figures 12 and 13). In the multivariable control structures, the inert saturated organic feed rate is increased after the valve opening achieves 75%, and the catalyst feed rate is decreased after the inert saturated organic feed rate increases 6 dimensionless units. In a valve opening saturation condition, the results for the proposed strategies are similar to the results obtained in a nominal operating condition. Without the multivariable strategies the oscillatory behaviour leads to a limit cycle (Figure 7). In this condition, the MPC controller also is able to achieve the maximum amount of inert saturated organic feed rate before manipulating the catalyst feed rate. Therefore, the MPC controller is more sensitive to the oscillations in the valve opening than the sequential PI switch controller, because the reactor temperature PID

controller is operating in a region where the PID performance is poor, according to Figure 4. In this case, a better MPC controller performance can be achieved using a gain-scheduling strategy in the PID temperature controller. The responses of both sequential PI switch controller and MPC with and without a gain-scheduling strategy in the PID temperature controller are compared in Figure 14.

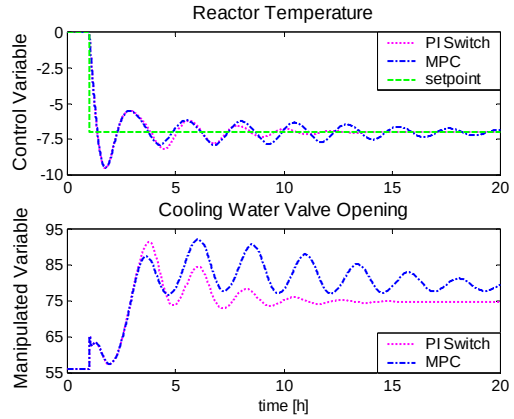

Fig. 12. Reactor temperature and valve opening cooling water response to a step change in reactor temperature setpoint with the multivariable strategy (sequential PI switch and MPC).

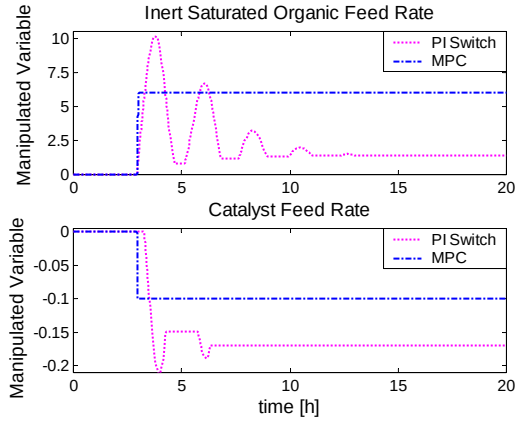

Fig. 13. Inert saturated organic feed rate and catalyst feed rate manipulation with the multivariable strategy (sequential PI switch and MPC).

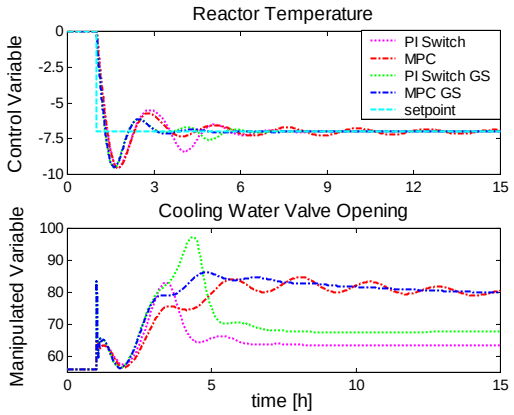

Fig. 14. Reactor temperature and valve opening cooling water response to a step change in reactor temperature setpoint with the multivariable strategy (sequential PI switch and MPC, with and without gain-scheduling).

7. CONCLUSION

It was shown that control of gas-phase polymerization reactors is a difficult task due to high non-linearity of the system and the strong interaction of the process variables. For this challenging control problem, a PID temperature controller with robust performance was designed via optimization in the frequency domain for different operating points. However, when the manipulation of valve opening alone is not sufficient to bring the temperature back to the desired level and this equipment saturates, limit cycles arises in the system. Thus, the use of auxiliary manipulated variables, determined by bifurcation analysis, can stabilize the reactor temperature controller in the desired setpoint by reducing the rate of heat generation or increasing the heat transfer capacity. However, if not properly used, these variables may reduce the production rate and other problems may arise with their manipulation and, consequently, limiting the use of these variables in a multivariable control strategy. The results of this work suggest that the use of gain-scheduling strategy in the PID temperature controller including a MPC controller for the auxiliary manipulated variables for closing the reactor temperature control loop avoids the saturation of manipulated variable and, hence, the undesired non-linear dynamic behaviour. Besides, this controller reduces the production loss and improves the product quality because of its ability to stabilize the reactor temperature in the setpoint with good performance. In order to obtain a better performance of the MPC controller in regions where the control valve moves in the fully open direction, a gain-scheduling in the reactor temperature PID controller, based on the SIOM-MMA approach, showed to be a good choice.

REFERENCES

Ali, E., Al-Humaizi, K., Abjar, A. (2003). Multivariable Control of a Simulated Industrial Gas-Phase Polyethylene Reactor. Ind. Eng. Chem. Res., 42, 2349-2364.

Dadedo, S.A., Bell, M.L., McLellan, P.J. McAuley, K.B. (1997). Temperature Control of Industrial Gas-Phase Polyethylene Reactors. J. Proc. Cont., 7(2), 83-95.

Faccin, F. and Trierweiler, J. O. (2004). A Novel Tool for Multi-Model PID Controller Design. In Proceedings of the 7th DYCOPS, Cambridge.

McAuley, K.B., McDonald, D. A., McLellan, P.J. (1995). Effects of Operating Conditions on Stability of Gas-Phase Polyethylene Reactors. AIChE Journal, 41(4), 868-879.

Salau, N. P. G., Secchi, A. R., Trierweiler, J. O., Neumann, G. A. (2005). Dynamic Behavior and Control of an Industrial Fluidized-Bed Polymerization Reactor. In Proceedings of the 15th ESCAPE Symposium, Barcelona.

Salau, N. P. G. (2004). Controle de Temperatura em Reatores de Polimerização em Fase Gasosa. Master Thesis, CPGEQ, UFRGS (in portuguese).

Seki, H., Ogawa, M., Oshima M. (2001). PID Temperature Control of an Unstable Gas-Phase Polyolefin Reactor. J.Chem. Eng. Jpn, 42 (11), 1415-1422.

ADCHEM 2006

International Symposium on Advanced Control of Chemical Processes
Gramado, Brazil – April 2-5, 2006

PREDICTIVE CONTROL OF ASYMMETRICAL PROCESSES

César de Prada, Smaranda Cristea

Department of Systems Engineering and Automatic Control,
University of Valladolid, Spain
prada@autom.uva.es, smaranda@autom.uva.es

Abstract: This paper deals with the control of processes that present different dynamic responses for equal increments and decrements of its manipulate variable, showing a non symmetric response. Being non-linear systems, instead of using non linear general methods directly, the paper explores two alternative formulations based on an MPC approach that take advantage of its structure. An application example is provided showing the behaviour of the proposed methods. *Copyright © 2006 IFAC*

Keywords: asymmetrical processes, predictive control, non linear programming, MIQP problem

1. INTRODUCTION

There are many processes in which, when a positive change in the manipulated variable is performed, one obtains a dynamic response that is quite different, either in shape or magnitude, to the one that can be obtained with a similar, but opposite change in the same manipulated variable (Fig.1).

We will denote these kind of processes as asymmetric. Examples of them can be found in several processes due, for instance, to different heating/cooling systems in chemical reactors. Other examples include the relation between the gas phase concentration and the pressure in a flash tank, or the one between head temperature and reflux flow in a distillation column. Clearly, they are non-linear and, as such, they pose a challenging problem to the control engineer. If tuned according to the "slow" response, they will present oscillations and overshoots in some operating conditions and if tuned according to the "fast" response, the closed loop will be also very slow in other cases.

The answer is, of course, to take into account the non-linear characteristic of the process and to design a controller applying general methods for this type of systems. Nevertheless, one can ask himself if it is possible to gain advantage of the special structure of the system in order to obtain easier solutions, either in terms of modeling or in the controller.

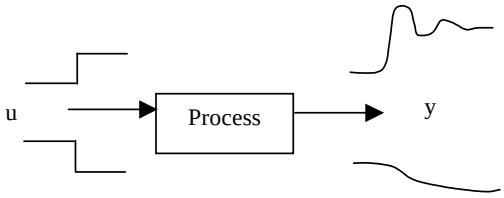

Fig. 1 Typical response of an asymmetric process to positive and negative steps inputs

A control technique that has gained wide acceptance in industry is model predictive control (MPC). As it is well known, it is based in the use of an internal model for computing predictions of the model responses, over a given time horizon, as functions of the present and future values of the manipulated variables (Fig. 2).

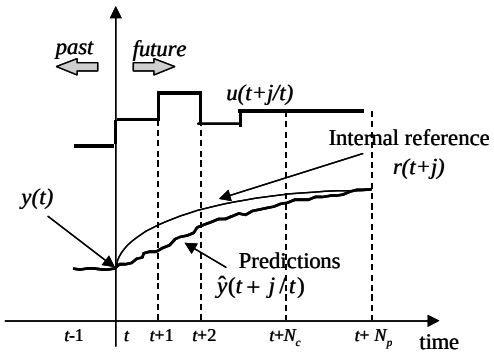

Fig. 2 MBPC strategy

The manipulated variables are chosen by minimization of a cost function of the quadratic errors between the output predictions and a desired internal reference, under the constraint imposed by the model prediction equations. Usually, other additional constraints are included on the range and speed of the manipulated inputs, as well as on the admissible range of the outputs, and, perhaps, some others in order to guarantee some stability properties.

If the internal model is linear, than the solution is obtained solving a QP optimization problem every sampling time. If not, the solution of a NLP problem is usually required, which increased considerably the complexity and computation time of the controller.
In the literature, very few contributions can be found devoted specifically to this topic. Previous contributions to the mentioned problem appear for instance in (Doyle *et al*., 1995) and (Camacho and Bordons, 2000) but only from the point of view of general non-linear systems. In (Tan *et al*., 1998) the use of PID controller has focused on the control of processes with severe asymmetry where an automatic tuning procedure for gain-scheduled is described.

This paper follows the non-linear MPC approach, but, at the same time, tries to re-formulate the model and the solution, in such way that, and this is the main contribution of the paper, for this particular kind of problems, an alternative and efficient formulation is obtained. The main point of the proposed method is the direct use of the linear models that could represent each of the two asymmetric dynamics of the process, instead of a more complex, perhaps first principles, non-linear model that could explain the whole system behavior, or the use of multiple linear models characteristic of other approaches. Using this internal model, two optimization algorithms are proposed that exploit its structure.

The paper is organized as follows: after the introduction, section II describes the internal model of the controller, then section III gives the first algorithm that includes a non-linear constraint. Section IV describes an alternative that leads to a mix integer algorithm. Finally, section V provides an application example showing the advantages of the proposed approach.

2. INTERNAL PROCESS MODEL

The use of linear models or a combination of them for representing a non-linear process is always an attractive approach because it leads very often to less complex controllers. In the so-called multi-model representation, a collection of linear models, each of which describing an operating point, are combined according to some fuzzy rules. The control action is computed for each of the models and the actual control applied to the process is a combination of the control actions computed from the different models.

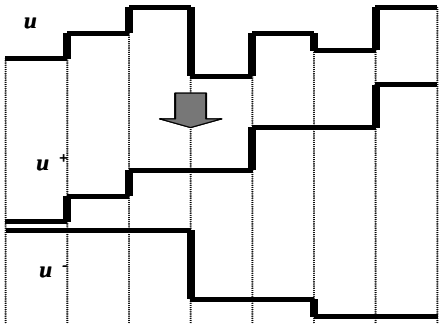

Fig. 3 Signal u(t) decomposed as u^+(t) and u^-(t)

Existing methods can differ in implementation details. One of the main problems of this approach is how to establish the partitions between the different operating regimes.
In our case, the nature of the problem is a different one, where the source of non-linearity is not the operating point but the direction of the changes in the manipulated input. It is assumed that the system responses to both, positive and negative inputs, can be characterized by discrete transfer functions that will be denoted as $G^+(q^{-1})$ and $G^-(q^{-1})$ respectively, as in Fig.1.
The key modeling idea for combining both models is depicted in Fig. 3, where the discrete control signal $u(t)$ being applied to a process can always be considered as the sum of two sequences $u^+(t)$ and $u^-(t)$, that have only increasing or decreasing changes correspondingly.

Every positive or negative change in $u(t)$ at a sampling time, is translated into the same change in $u^+(t)$ or $u^-(t)$ with the condition that they can not take place simultaneously. In this way, the moves in the control signal can be written as:

$$\begin{aligned} &\Delta u(t+j) = \Delta u^+(t+j) + \Delta u^-(t+j) \\ &\begin{cases} \Delta u^+(t+j) \geq 0 \\ \Delta u^-(t+j) \leq 0 \\ \Delta u^+(t+j) \cdot \Delta u^-(t+j) = 0 \end{cases} \end{aligned} \quad (1)$$

Now the model output can be formulated as:

$$y(t) = G^+(q^{-1})u^+(t)(q^{-1}) + G^-(q^{-1})u^-(t) + v(t) \quad (2)$$

where $v(t)$ represents a non-stationary stochastic disturbance, or alternatively as:

$$\begin{aligned} A(q^{-1})y(t) = B^+(q^{-1})u^+(t) + B^-(q^{-1})u^-(t) \\ + \frac{T(q^{-1})}{\Delta}\xi(t) \end{aligned} \quad (3)$$

where $\Delta = 1-q^{-1}$, A, B^+, B^-, T are polynomials in the backward operator q^{-1}, $\xi(t)$ is a zero-mean white noise signal and u^+, u^- are constrained by (1).

3. MPC CONTROLLER

Model (3), even if constrained by (1), has a nice structure that allows us to formulate closed expressions for the predictions of the process outputs. Taking into account that (1) refers only to the inputs, we can apply the superposition principle with our model (3) and develop prediction equations in the usual way in linear MPC.

Future values of the output at times $t+j$, $(j=1,\ldots,N_2$ sampling periods) can be considered as the sum of two terms: the so called free and forced responses:

$$y(t+j) = y_f(t+j) + y_c(t+j) \tag{4}$$

where the free response corresponds to:

$$y_f(t+j) = \frac{B^+}{A}u_f^+(t+j) + \frac{B^-}{A}u_f^-(t+j) + \frac{T}{A\Delta}\xi(t+j) \tag{5}$$

and u^+_f and u^-_f can be computed according to:

$$\begin{aligned} &\text{if } u(t-1)-u(t-2)>0 \quad \begin{cases} u_f^+(t+j) = u(t-1) \\ u_f^-(t+j) = 0 \end{cases} \\ &\text{if } u(t-1)-u(t-2)<0 \quad \begin{cases} u_f^+(t+j) = 0 \\ u_f^-(t+j) = u(t-1) \end{cases} \end{aligned} \tag{6}$$

so they are known variables at time t. Then, the predictions are obtained using the usual procedures, either based on filters or in Diophantic equations. As they are well known, they will not be repeated here. See for instance (Clarke, 1987).

On the other hand, the forced response can be computed using:

$$\begin{aligned} &y_c(t+j) = G_j^+(q^{-1})\Delta u_c^+(t+j) + G_j^-(q^{-1})\Delta u_c^-(t+j) \\ &G_j^+(q^{-1}) = g_1^+q^{-1} + \ldots + g_j^+q^{-j} \\ &G_j^-(q^{-1}) = g_1^-q^{-1} + \ldots + g_j^-q^{-j} \end{aligned} \tag{7}$$

with g_j being the step response coefficients of each transfer functions and

$$\begin{aligned} \Delta u_c^+(t+j) &= \Delta u^+(t+j) \geq 0 \\ \Delta u_c^-(t+j) &= \Delta u^-(t+j) \leq 0 \end{aligned} \tag{8}$$

Once output predictions are available, the optimal control actions of our MPC controller can be obtained as the ones that minimize a cost function (9) of the squared errors between these predictions and a desired set point, including a penalty on the control moves, along a given time horizon:

$$I(t) = \sum_{j=N1}^{N2}\left(r(t+j) - \hat{y}(t+j)\right)^2 + \beta\sum_{j=1}^{Nu}\left(\Delta u(t+j-1)\right)^2 \tag{9}$$

Notice that (1) allow us to write the equivalent problem:

$$\min_{\substack{\Delta u^+(t),\ldots,\Delta u^+(t+Nu-1),\\ \Delta u^-(t),\ldots,\Delta u^-(t+Nu-1)}} I(t) = \sum_{j=N_1}^{N_2}\left(r(t+j) - \hat{y}(t+j)\right)^2 + \beta_1\sum_{j=1}^{Nu}\left(\Delta u^+(t+j-1)\right)^2 + \beta_2\sum_{j=1}^{Nu}\left(\Delta u^-(t+j-1)\right)^2 \tag{10}$$

$$\begin{aligned} &\hat{y}(t+j) = \hat{y}_f(t+j) + \\ &+ G_j^+(q^{-1})\Delta u^+(t+j) + G_j^-(q^{-1})\Delta u^-(t+j) \end{aligned} \tag{11}$$

where we take advantage of the cost function structure that allows different weighting of the positive and negative moves.

Defining the matrices:

$$\mathbf{G}^+ = \begin{bmatrix} g^+_{N_1} & g^+_{N_1-1} & \ldots & g^+_1 & 0 & \ldots & 0 \\ g^+_{N_1+1} & g^+_{N_1} & \ldots & \ldots & g^+_1 & \ldots & 0 \\ \vdots & \vdots & \ldots & \ldots & \vdots & \ldots & \vdots \\ g^+_{N_2} & g^+_{N_2-1} & \ldots & \ldots & \ldots & \ldots & g^+_{N_2-Nu+1} \end{bmatrix} \tag{12}$$

$$\mathbf{G}^- = \begin{bmatrix} g^-_{N_1} & g^-_{N_1-1} & \ldots & g^-_1 & 0 & \ldots & 0 \\ g^-_{N_1+1} & g^-_{N_1} & \ldots & \ldots & g^-_1 & \ldots & 0 \\ \vdots & \vdots & \ldots & \ldots & \vdots & \ldots & \vdots \\ g^-_{N_2} & g^-_{N_2-1} & \ldots & \ldots & \ldots & \ldots & g^-_{N_2-Nu+1} \end{bmatrix} \tag{13}$$

and the vectors:

$$\mathbf{u}^+ = \begin{bmatrix} \Delta u^+(t) & \Delta u^+(t+1) & \ldots & \Delta u^+(t+Nu-1) \end{bmatrix}^T \tag{14}$$

$$\mathbf{u}^- = \begin{bmatrix} \Delta u^-(t) & \Delta u^-(t+1) & \ldots & \Delta u^-(t+Nu-1) \end{bmatrix}^T \tag{15}$$

$$\mathbf{E_0} = \begin{bmatrix} e_0(t+N_1) & e_0(t+N_1+1) & \ldots & e_0(t+N_2) \end{bmatrix}^T \tag{16}$$

where

$$e_0(t+j) = r(t+j) - \hat{y}(t+j) \tag{17}$$

it is possible to reformulate $I(t)$ as a quadratic function that the controller solves:

$$\min_{\mathbf{x}} I(t) = \min_{\mathbf{x}}\left(\frac{1}{2}\mathbf{x}^T\mathbf{H}\mathbf{x} + \mathbf{c}^T\mathbf{x}\right) \tag{18}$$

with

$$\mathbf{H} = \left[\begin{array}{c:c} \mathbf{G}^{+T}\mathbf{G}^+ + \beta_1\mathbf{I} & \mathbf{G}^{+T}\mathbf{G}^- \\ \hdashline \mathbf{G}^{-T}\mathbf{G}^+ & \mathbf{G}^{-T}\mathbf{G}^- + \beta_2\mathbf{I} \end{array}\right] \tag{19}$$

$$\mathbf{c}^T = \left[-\mathbf{E_0}^T\mathbf{G}^+ \;\vdots\; -\mathbf{E_0}^T\mathbf{G}^-\right] \tag{20}$$

$$\mathbf{x}^T = \left[\mathbf{u}^+ \quad \mathbf{u}^-\right] \tag{21}$$

and the constraints (1) every sampling time. Due to constraint

$$\Delta u^+(t+j)\cdot\Delta u^-(t+j)=0\,, \qquad (22)$$

a non-linear programming problem with $2N_u$ decision variables, a quadratic cost function and the linear constraints (8) has to be solved. Notice that adding additional constraints on the manipulated and controlled variables, or on their speed of change, this assertion does not modify.

$$\begin{aligned} &U_{\min}\le\sum_{i=0}^{j}\Delta u^+(t+j)+\sum_{i=0}^{j}\Delta u^-(t+j)\le U_{\max}\\ &U_{\min}=U_m-u(t-1)\ \text{ and }\ U_{\max}=U_M-u(t-1)\\ &0\le j\le Nu-1 \end{aligned} \qquad (23)$$

$$D_m\le\Delta u(t+j)=\Delta u^+(t+j)+\Delta u^-(t+j)\le D_M \qquad (24)$$

$$\begin{aligned} &L_m-\hat{y}_f(t+j)\le\sum_{i=0}^{\min(j,Nu-1)}g^+_{j-i}\Delta u^+(t+i)+\\ &+\sum_{i=0}^{\min(j,Nu-1)}g^-_{j-i}\Delta u^-(t+i)\le L_M-\hat{y}_f(t+j)\\ &N_3\le j\le N_4 \end{aligned} \qquad (25)$$

where U_x, D_x, L_x, refers to the low and upper limits of these variables.

As such, it must be solved with an appropriate NLP solver. The fact that the cost function, with adequate values of β, is convex and the most of the equations are linear, can help in finding the optimal solution, but there is no way to avoid the non-convex constraint (22).

4. A HYBRID PREDICTIVE CONTROL ALTERNATIVE

Because of this difficulty, an alternative solution to the problem described by (1), (18), (23)-(25) is proposed, in the form of a hybrid MPC problem.

With this purpose, we have introduced N_u new binary variables z_j, $j = 1,\ldots, N_u\text{-}1$. It is not difficult to realize that the set of constraints (1) is equivalent to

$$\begin{aligned} 0\le\Delta u^+(t+j)&\le D\,z_j\\ (z_j-1)D\le\Delta u^-(t+j)&\le 0 \end{aligned} \qquad (26)$$

where D is a large positive number and the variable z_j has 0/1 value. Notice that $z_j = 1$ means that a positive change will be implemented at time instant $t+j$ and $z_j = 0$ means that a negative change will be the one implemented at that time instant.

The interest of substituting the set of constraints (1) by (26) is that, even if new binary variables z_j are introduced, the set (26) is a linear one, eliminating the non-convex equations (22), which facilitates the finding of the optimal control moves.

Now, the associated controller optimization problem can be formulated as an MIQP problem considering the cost index (18), the definitions (19)-(21) and the constraints (26). The optimization problem is solved every sampling period, for which efficient algorithms as Branch & Bound can be found.

5. APPLICATION EXAMPLE

In order to test the proposed method, an asymmetric process like the one depicted in Fig. 4 was considered. The two dynamics have been identified and the corresponding transfer functions are given by:

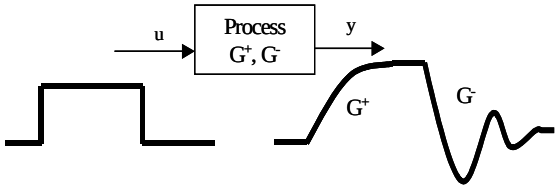

Fig. 4 Asymmetric process of our example

$$G^+(s)=\frac{2}{5s+1}\qquad\text{and}\qquad G^-(s)=\frac{0.5}{s^2+0.6s+1} \qquad (27)$$

with the step responses like the ones shown in Fig. 5 and 6.

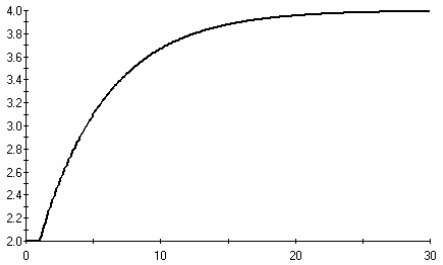

Fig. 5. Step response of $G^+(s)$

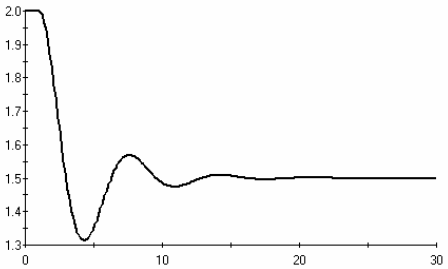

Fig. 6. Step response of $G^-(s)$

The proposed hybrid controller was applied to this asymmetric process and a series of experiments were performed.

The controller had the following parameters: $N_1 = 1$, $N_2 = 15$, $N_u = 2$, and, initially, the same control weights $\beta_1 = 0.1$, $\beta_2 = 0.1$, were applied to each positive or negative movements of the control variable u. The experiments consist of several step changes in the set point of the controller. Fig. 7 shows the process response and the set point in the lower graph as well as the control signal in the upper one. As we can see it behaves very well following the reference and with sensible control efforts.

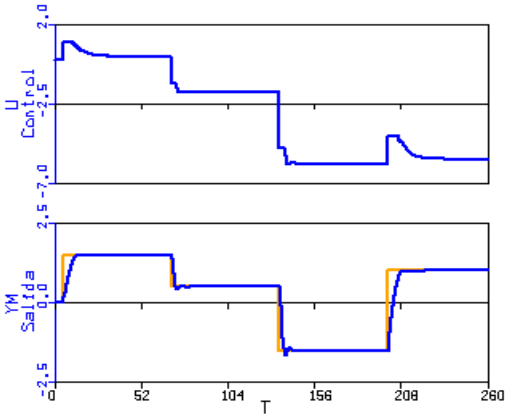

Fig. 7. Closed loop response of the asymmetric process to several step changes in the set point. Upper graph: control signal. Lower graph: set point and process output.

A more symmetric process response can be obtained weighting the control moves differently. For instance, with β_1 = 0.1, β_2 = 10, it is possible to obtain the response of Fig. 8.

Additional constraints in both inputs and outputs can be added easily. Fig. 9 and 10 show responses of the process when the control signal was constraint to be in the range [-1, 0.7] (Fig. 9.) and the process output was constraint also to be in the range [-1, 1] (Fig. 10). Notice that the set point is outside this range.

In order to test the advantages of the proposed controller, it was compared with a linear MPC using a fix internal model. Fig. 11 shows the case where the internal model is given by $G^{+}(s)$ with the same tuning parameters as in the hybrid controller. As we can see, the response is very poor, with high control moves and oscillatory process output. This response can be improved by tuning of the control weights, compromising between the positive and negative responses. For instance, with β = 5, it is possible to obtain the responses of Fig. 12, which is still not very good.

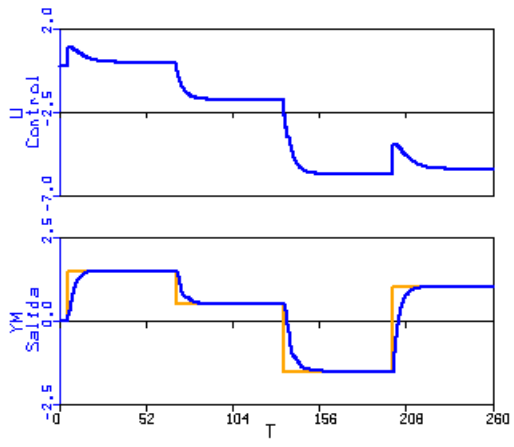

Fig. 8. Closed loop response of the asymmetric process to several step changes in the set point with different weights. Upper graph: control signal. Lower graph: set point and process output.

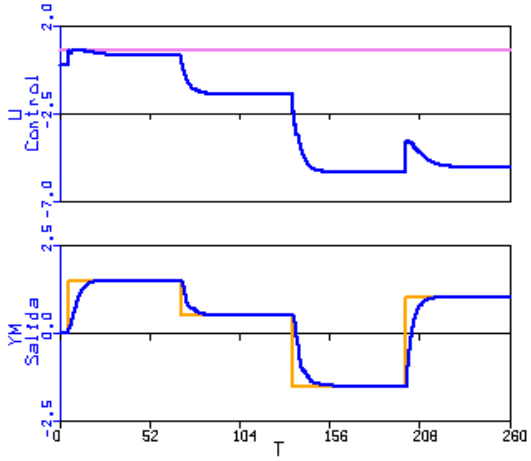

Fig. 9. Closed loop response of the asymmetric process to several step changes in the set point. Limits on *u*. Upper graph: control signal. Lower graph: set point and process output.

In the same way, Fig. 13 shows the case where the internal model is given by $G^{-}(s)$ with the same tuning parameters as in the hybrid controller. Similar conclusions can be obtained. Moreover the computation time for the whole experiment is only a bit smaller (0.313 seconds) than the case of the hybrid control (0.344 seconds). The both experiments were computed in a Pentium 2.53 GHz and 524 kB RAM.

As a final test, we compared the hybrid and the non-linear MPC model. The responses were very similar to the ones of Fig. 7, but the computation time was almost five times faster in the case of the hybrid controller and moreover the guarantee of optimality is given by the fact that the hybrid problem is convex.

For save of simplicity, no terminal penalty term has been added to the cost functions but it could be easily included in order to stabilize the closed system.

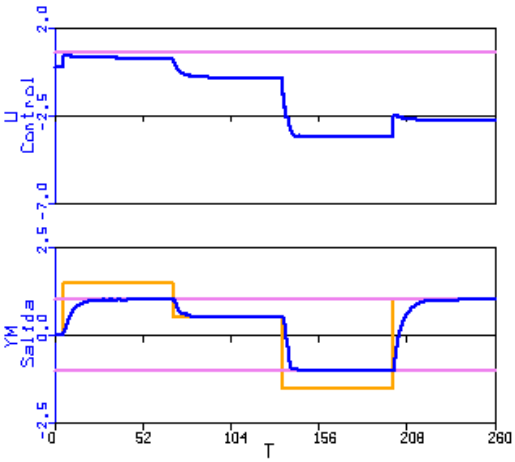

Fig. 10. Closed loop response of the asymmetric process to several step changes in the set point. Limits on *u* and *y*. Upper graph: control signal. Lower graph: set point and process output.

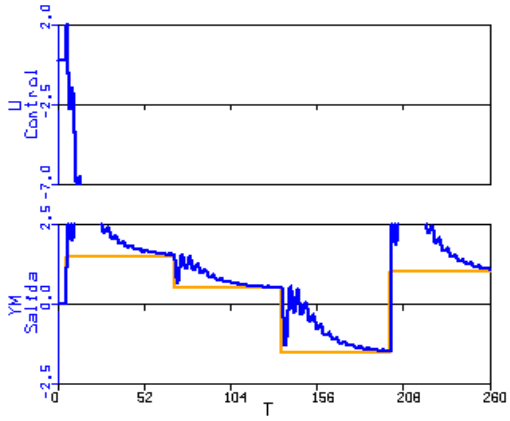

Fig. 11. Closed loop response of the asymmetric process to several step changes in the set point. Internal model G^+. Upper graph: control signal. Lower graph: set point and process output.

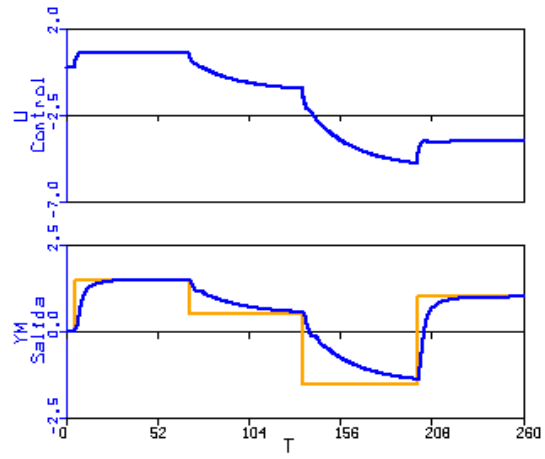

Fig. 12. Closed loop response of the asymmetric process to several step changes in the set point. Internal model G^+ and $\beta = 5$. Upper graph: control signal. Lower graph: set point and process output.

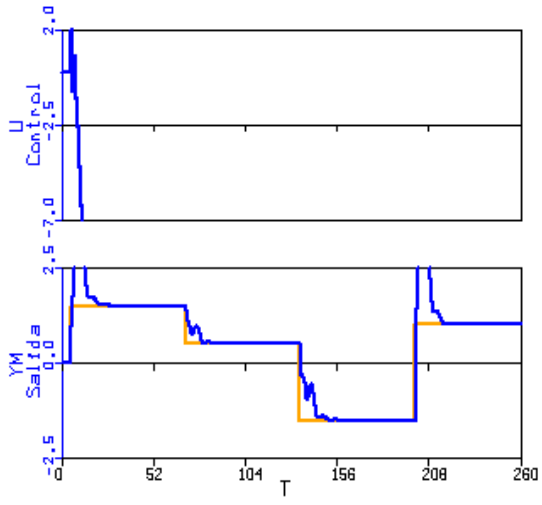

Fig. 13. Closed loop response of the asymmetric process to several step changes in the set point. Internal model G^- , $\beta = 0.1$. Upper graph: control signal. Lower graph: set point and process output.

6. CONCLUSIONS

In this paper two alternative formulations for a MPC algorithm to deal with asymmetrical processes are presented instead of using a full non linear model strategy. Both algorithms take advantage of the use of two linear internal models and a quadratic cost function in spite of the non linearity of the process. The first proposed method involves NLP because of the constraints and the second one has the form of a hybrid MPC problem with only linear constraints, some of them including binary variables, leading to a MIQP problem.

Simulations using an example of a process with severe asymmetry were performed. Comparing with a linear MPC using a fix internal model, the new controllers show a better performance and an important advantage raises with the hybrid one where the computation time is similar to a classic linear MPC.

ACKNOWLEDGEMENT

This work was supported in part by the Spanish Department of Science and Technology under Project "Técnicas de control predictivo no-lineal y Supervisión de controladores", DPI2003-0013 as well as the EU NoE HYCON.

REFERENCES

Bemporad, A. and M. Morari (1999). Control of systems integrating logic, dynamics , and constraints. *Automatica*, **35**, 407-427.

Camacho E. and C. Bordons (2000). *Model Predictive* Control. Springer-Verlag, , Great Britain.

Clarke D. W. (1987). Generalized Predictive Control. *Automatica*, **23**, 137-160.

Doyle F. J., B. A. Ogunnaike and R. K. Pearson (1995). Nonlinear Model-based Control using second-order Volterra Models. *Automatica*, **31**, 697-714.

Prada C. de, S. Cristea, D. Megías and J. Serrano (2004). Hybrid control of a four tanks system. *7th International Symposium on Advanced Control of Chemical Processes (ADCHEM'2004)*, Hong Kong.

Prada C. De and S. Cristea (2004). Controlador predictivo para procesos con dos dinámicas diferentes. *Workshop "Identificación, optimización y control de procesos híbridos"*, Valencia.

Tan K.K., Q.-G. Wang, T.H. Lee and C.H. Gan (1998). Automatic tuning of gain-scheduled control for asymmetrical processes. *Control Engineering Practice*, **6**, 1353-1363.

Session 3.3

Process Control Applications

Constrained Nonlinear Model Predictive Control for Practical Application

A. G. Montandon1, R. M. Borges and H. M. Henrique
Federal University of Uberlândia

Multivariable Subspace Identification and Predictive Control of a Heat-Integrated Superfractionator

G. Pannocchia A. Micchi, R. Bulleri, A. Brambilla, and G. Marchetti
University of Pisa

Control Strategies Evaluation for a Three-Phase Hydrogenation Catalytic Reactor

D. N. C. Melo, E. C. Vasco de Toledo, M. M. Santos and R. M. Filho
State University of Campinas

On Input-Output Selection for Multiloop Control: from RGA to ROMA

A. Balestrino, A. Landi
University of Pisa

Design and Control of a Power Generation System for a Fuel-Cell Powered Automobile

P. K. Kolavennu, S. Palanki, and J. C. Telotte
Florida State University

Output-Feedback Control of Continuous Polymer Reactors with Continuous and Discrete Measurements,

P. Gonzalez and J. Alvarez
Universidad Autonoma Metropolitana-Iztapalapa

Auto-Tuning of PID Controllers for MIMO Processes by Relay Feedback

L. Campestrini, P. R. Barros and A. S. Bazanella
Universidade Federal do Rio Grande do Sul

Regulatory Control of a Pilot Rotary Kiln for Activated Carbon Production

O. A. Ortiz, N. Aros and I. G. Suarez
Universidad Nacional de San Juan

Development of an Extruder Based Melt Index Soft Sensor

I. R. Alleyne, S. Shah, U. Sundararaj and B. West
University of Alberta

ADCHEM 2006

International Symposium on Advanced Control of Chemical Processes
Gramado, Brazil – April 2-5, 2006

ADAPTIVE CONTROL OF THREE – TANK - SYSTEM: POLYNOMIAL APPROACH

Marek Kubalčík, Vladimír Bobál

Department of Process Control, Faculty of Applied Informatics,
Tomas Bata University in Zlin, Mostní 5139, 760 01, Zlín, Czech Republic,
Tel.: +420 57 603 5198, Fax: +420 57 603 5279, E-mail: kubalcik@ft.utb.cz

Abstract: Control of a three – tank - system laboratory model as a two inputs – two outputs system is presented. The objective laboratory model is a multivariable nonlinear system. It is based on experience with authentic industrial control applications. Two control algorithms utilizing polynomial theory and pole – placement are proposed. Particular controllers are based on various configuration of the closed loop. The algorithms in adaptive version are then used for control of the model. The results of the real-time experiments are also included. Quality of control achieved by both methods is compared and discussed.

Key words: Polynomial methods, Nonlinear system, Self-tuning control, Multivariable control, Real-time control.

1. INTRODUCTION

Many technological processes require a simultaneous control of several variables related to one system. Each input may influence all system outputs. The three – tank - system in Fig. 1 is a typical multivariable nonlinear system with significant cross – coupling. The design of a controller able to cope with such a system must be quite sophisticated. There are many different methods of controlling MIMO (multi input – multi output) systems. Several of these use decentralized PID controllers (Luyben, 1986), others apply single input-single-output (SISO) methods extended to cover multiple inputs (Chien *et al.*, 1987).

Here polynomial theory approach (Kučera 1980, Kučera, 1991, Skogestad and Postlethwaite, 1996) is used for the design of multivariable controllers. Two controllers are presented. The first one is based on traditional 1DOF (one degree of freedom) configuration of the closed loop, the second one applies 2DOF configuration proposed in (Ortega and Kelly, 1984) for SISO control loop. Application of the designed methods for adaptive control of the three – tank - system is then presented. The algorithms were applied as self – tuning controllers. It was assumed, that the dynamic behaviour of the system could be described in the neighbourhood of a steady state by a discrete linear model. The recursive least squares method with the directional forgetting was used for the identification part of the self – tuning controllers.

This paper is organised as follows: Section 2 contains description of the three – tank - system; Section 3 presents a mathematical model of the system which was used for the controllers design; Sections 4 and 5 describes designs of the 1DOF and 2DOF controllers; Section 6 describes the system identification method; Section 7 contains the experimental results; finally, Section 8 concludes the paper.

2. THREE – TANK – SYSTEM

The experiments were carried out with an experimental laboratory model three – tank – system. Such a system can be viewed as a prototype of many industrial applications in process industry, such as chemical and petrochemical plants, oil and gas systems. The typical control issue involved in the system is how to keep the desired liquid level in each tank. The principle scheme of the model is shown in Fig 1. The basic apparatus consists of three plexiglass tanks numbered from left to right as T1, T3 and T2. These are connected serially with each other by cylindrical pipes. Liquid, which is collected in a reservoir, is pumped into the first and the third

tanks to maintain their levels. The level in the tank T3 is a response which is uncontrollable. It affects the level in the two end tanks. Each tank is equipped with a static pressure sensor, which gives a voltage output proportional to the level of liquid in the tank. Hmax denotes the highest possible liquid level. In case the liquid level of T1 and T2 exceeds this value the corresponding pump will be switched off automatically. Q_1 and Q_2 are the flow rates of the pumps 1 and 2. Two variable speed pumps driven by DC motor are used in this apparatus. These pumps are designed to give an accurate well defined flow per rotation. Thus, the flow rate provided by each pump is proportional to the voltage applied to its DC motor.

There are six manual valves v1, v2...v6 that can be used to vary the configuration of the process or to introduce disturbances or faults.

The pump flow rates Q_1 and Q_2 denote the input signals, the liquid levels of T1 and T2 are the output signals.

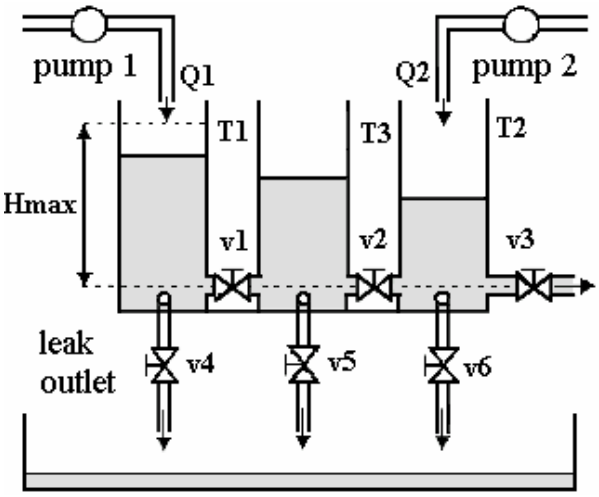

Fig. 1. Principal scheme of three – tank - system

3. MATHEMATICAL MODEL OF THE APPARATUS

An analytical model of the three – tank - system based on physics and the equipment construction is presented in (AMIRA, 1996). All the parameters in this model have a particular physical denotation. The apparatus is a nonlinear system, as it was mentioned above. A possible method for control of nonlinear systems is using of self – tuning controllers. A suitable model for adaptive control of the real object is an input – output model ("black box model"). This is a standard approach in self tuning controller area. Instead of often tedious construction of a model from first principles and then calculating its parameters from plant dimensions and physical constants, general type of model is chosen (here it is in fact transfer function (1)) and its parameters are identified from data. It is a model of the system behaviour and its parameters do not have a particular physical denotation. Of course, not all properties of the plant can be extracted from the data in this way but as a rule dominant properties are modelled, which is sufficient for a controller design. Advantages of this kind of model are its simplicity and accuracy in an operational range in which the input – output dependence is measured. In the framework of adaptive controllers it was chosen this kind of model. It was necessary to determine its structure in advance. The aim here was to find experimentally as simple structure of the model as possible, as it is mentioned bellow. The parameters are identified during the process of the recursive identification in virtue of the measured input and output signals.

A general transfer matrix of a two inputs – two outputs system with cross coupling is expressed as

$$\boldsymbol{G}(z)=\begin{bmatrix} G_{11}(z) & G_{12}(z) \\ G_{21}(z) & G_{22}(z) \end{bmatrix} \tag{1}$$

$$\boldsymbol{Y}(z)=\boldsymbol{G}(z)\boldsymbol{U}(z) \tag{2}$$

Where $\boldsymbol{U}(z)$ and $\boldsymbol{Y}(z)$ are vectors of the manipulated variables (flow rates of liquid into tanks T1 and T2) and the controlled variables (liquid levels of T1 and T2).

$$\boldsymbol{U}(z)=[u_1(z),u_2(z)]^T \qquad \boldsymbol{Y}(z)=[y_1(z),y_2(z)]^T \tag{3}$$

It is possible to assume that the dynamic behaviour of the system can be described in the neighbourhood of a steady state by a discrete linear model in the following form of the matrix fraction

$$\boldsymbol{G}(z)=\boldsymbol{A}^{-1}(z^{-1})\boldsymbol{B}(z^{-1})=\boldsymbol{B}_1(z^{-1})\boldsymbol{A}_1^{-1}(z^{-1}) \tag{4}$$

Where polynomial matrices $\boldsymbol{A}\in R_{22}[z^{-1}], \boldsymbol{B}\in R_{22}[z^{-1}]$ are the left coprime factorization of matrix $\boldsymbol{G}(z)$ and matrices $\boldsymbol{A}_1\in R_{22}[z^{-1}], \boldsymbol{B}_1\in R_{22}[z^{-1}]$ are the right coprime factorization of $\boldsymbol{G}(z)$.

At first, the algorithms described bellow were designed for a model with polynomials of the first order. This model proved to be unsuitable for the process and the control algorithms failed. Consequently, the polynomial orders were increased and the algorithms were designed for a model with second order polynomials. This model proved to be effective. The model has sixteen parameters:

$$\boldsymbol{A}(z^{-1})=\begin{bmatrix} 1+a_1z^{-1}+a_2z^{-2} & a_3z^{-1}+a_4z^{-2} \\ a_5z^{-1}+a_6z^{-2} & 1+a_7z^{-1}+a_8z^{-2} \end{bmatrix} \tag{5}$$

$$\boldsymbol{B}(z^{-1})=\begin{bmatrix} b_1z^{-1}+b_2z^{-2} & b_3z^{-1}+b_4z^{-2} \\ b_5z^{-1}+b_6z^{-2} & b_7z^{-1}+b_8z^{-2} \end{bmatrix} \tag{6}$$

Polynomial matrices of the right matrix fraction of the system are defined in the following form

$$\boldsymbol{A}_1(z^{-1})=\begin{bmatrix} 1+a_9z^{-1}+a_{10}z^{-2} & a_{11}z^{-1}+a_{12}z^{-2} \\ a_{13}z^{-1}+a_{14}z^{-2} & 1+a_{15}z^{-1}+a_{16}z^{-2} \end{bmatrix} \tag{7}$$

$$\boldsymbol{B}_1\left(z^{-1}\right)=\begin{bmatrix} b_9 z^{-1}+b_{10}z^{-2} & b_{11}z^{-1}+b_{12}z^{-2} \\ b_{13}z^{-1}+b_{14}z^{-2} & b_{15}z^{-1}+b_{16}z^{-2} \end{bmatrix} \quad (8)$$

The coefficients of the matrices are given by solving the matrix equation

$$\boldsymbol{B}\left(z^{-1}\right)\boldsymbol{A}_1\left(z^{-1}\right)-\boldsymbol{A}\left(z^{-1}\right)\boldsymbol{B}_1\left(z^{-1}\right)=0 \quad (9)$$

4. DESIGN OF 1DOF CONTROLLER

The 1DOF control configuration is depicted in Fig. 2.

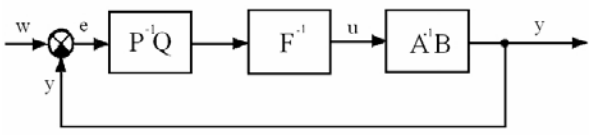

Fig. 2. Block diagram of 1DOF configuration

Similarly as it was for the controlled system, the transfer matrix of the controller takes the form of the following matrix fraction

$$\boldsymbol{G}_R\left(z\right)=\boldsymbol{P}^{-1}\left(z^{-1}\right)\boldsymbol{Q}\left(z^{-1}\right)=\boldsymbol{Q}_1\left(z^{-1}\right)\boldsymbol{P}_1^{-1}\left(z^{-1}\right) \quad (10)$$

Generally, the vector $\boldsymbol{W}\left(z^{-1}\right)$ of input reference signals is specified as

$$\boldsymbol{W}\left(z\right)=\boldsymbol{F}_w^{-1}\left(z^{-1}\right)\boldsymbol{h}\left(z^{-1}\right) \quad (11)$$

In case of control of the three – tank - system, the reference signals were considered as a class of step functions. In this case $\boldsymbol{h}\left(z^{-1}\right)$ is a vector of constants and $\boldsymbol{F}_w\left(z^{-1}\right)$ is expressed as

$$\boldsymbol{F}_w\left(z^{-1}\right)=\begin{bmatrix} 1-z^{-1} & 0 \\ 0 & 1-z^{-1} \end{bmatrix} \quad (12)$$

The compensator $\boldsymbol{F}\left(z^{-1}\right)$ is a component formally separated from the controller. It has to be included in the controller to fulfil the requirement on the asymptotic tracking. If the reference signals are step functions, then $\boldsymbol{F}\left(z^{-1}\right)$ is an integrator.

The control law in the block diagram in Fig. 2 (operator z^{-1} will be omitted from some operations for the purpose of simplification) is defined as

$$\boldsymbol{U}=\boldsymbol{F}^{-1}\boldsymbol{Q}_1\boldsymbol{P}_1^{-1}\boldsymbol{E} \quad (13)$$

where $\boldsymbol{E}$ is a vector of control errors. Using matrix operations it is possible to modify this vector as

$$\boldsymbol{E}=\boldsymbol{W}-\boldsymbol{Y}=\boldsymbol{P}_1\left(\boldsymbol{AFP}_1+\boldsymbol{BQ}_1\right)^{-1}\boldsymbol{AW} \quad (14)$$

Asymptotic tracking of the reference signals is then fulfilled if $\boldsymbol{FP}_1$ is divisible by $\boldsymbol{F}_w$.

It is possible to derive the following equation for the system output

$$\boldsymbol{Y}=\boldsymbol{A}^{-1}\boldsymbol{BF}^{-1}\boldsymbol{P}^{-1}\boldsymbol{QE}=\boldsymbol{A}^{-1}\boldsymbol{BF}^{-1}\boldsymbol{P}^{-1}\boldsymbol{Q}\left(\boldsymbol{W}-\boldsymbol{Y}\right) \quad (15)$$

and this can be modified

$$\boldsymbol{Y}=\boldsymbol{P}_1\left(\boldsymbol{AFP}_1+\boldsymbol{BQ}_1\right)^{-1}\boldsymbol{BQ}_1\boldsymbol{P}_1^{-1}\boldsymbol{W} \quad (16)$$

It is apparent, that the elements of the vector of the output signal have in their denominators the determinant of the matrix $\boldsymbol{AFP}_1+\boldsymbol{BQ}_1$. This determinant is the characteristic polynomial of a MIMO system. The roots of this polynomial matrix are the ruling factors for the behaviour of a closed loop system. The roots must be inside the unit circle (of the Gauss complex plain), in order for the system to be stable. Conditions of BIBO (bounded input bounded output) stability can be defined by the following diophantine equation

$$\boldsymbol{AF}\,\boldsymbol{P}_1+\boldsymbol{BQ}_1=\boldsymbol{M} \quad (17)$$

Where $\boldsymbol{M}\in R_{22}\left[z^{-1}\right]$ is a stable diagonal polynomial matrix.

$$\boldsymbol{M}\left(z^{-1}\right)=\begin{bmatrix} 1+m_1z^{-1}+m_2z^{-2}+ & 0 \\ +m_3z^{-3}+m_4z^{-4} & \\ 0 & 1+m_1z^{-1}+m_2z^{-2}+ \\ & +m_3z^{-3}+m_4z^{-4} \end{bmatrix} \quad (18)$$

The degree of the controller polynomial matrices depends on the internal properness of the closed loop. The structure of matrices $\boldsymbol{P}_1$ and $\boldsymbol{Q}_1$ was chosen so that the number of unknown controller parameters equals the number of algebraic equations resulting from the solution of the diophantine equation. The method of the uncertain coefficients was used to solve the diophantine equation.

$$\boldsymbol{P}_1\left(z^{-1}\right)=\begin{bmatrix} 1+p_1z^{-1} & p_2z^{-1} \\ p_3z^{-1} & 1+p_4z^{-1} \end{bmatrix} \quad (19)$$

$$\boldsymbol{Q}_1\left(z^{-1}\right)=\begin{bmatrix} q_1+q_2z^{-1}+q_3z^{-2} & q_4+q_5z^{-1}+q_6z^{-2} \\ q_7+q_8z^{-1}+q_9z^{-2} & q_{10}+q_{11}z^{-1}+q_{12}z^{-2} \end{bmatrix} \quad (20)$$

The solution of the diophantine equation results in a set of sixteen algebraic equations with unknown controller parameters. Using matrix notation the algebraic equations can be expressed in the following form

$$\begin{bmatrix} -a_2 & -a_4 & 0 & 0 & b_2 & 0 & 0 & b_4 \\ a_2-a_1 & a_4-a_3 & 0 & b_2 & b_1 & 0 & b_4 & b_3 \\ a_1-1 & a_3 & b_2 & b_1 & 0 & b_4 & b_3 & 0 \\ 1 & 0 & b_1 & 0 & 0 & b_3 & 0 & 0 \\ -a_6 & -a_8 & 0 & 0 & b_6 & 0 & 0 & b_8 \\ a_6-a_5 & a_8-a_7 & 0 & b_6 & b_5 & 0 & b_8 & b_7 \\ a_5 & a_7-1 & b_6 & b_5 & 0 & b_8 & b_7 & 0 \\ 0 & 1 & b_5 & 0 & 0 & b_7 & 0 & 0 \end{bmatrix}\begin{bmatrix} p_1 \\ p_3 \\ q_1 \\ q_2 \\ q_3 \\ q_7 \\ q_8 \\ q_9 \end{bmatrix}=\begin{bmatrix} m_4 \\ m_3+a_2 \\ m_2-a_2+a_1 \\ m_1-a_1+1 \\ 0 \\ a_6 \\ a_5-a_6 \\ -a_5 \end{bmatrix}$$

$$\begin{bmatrix} -a_2 & -a_4 & 0 & 0 & b_2 & 0 & 0 & b_4 \\ a_2-a_1 & a_4-a_3 & 0 & b_2 & b_1 & 0 & b_4 & b_3 \\ a_1-1 & a_3 & b_2 & b_1 & 0 & b_4 & b_3 & 0 \\ 1 & 0 & b_1 & 0 & 0 & b_3 & 0 & 0 \\ -a_6 & -a_8 & 0 & 0 & b_6 & 0 & 0 & b_8 \\ a_6-a_5 & a_8-a_7 & 0 & b_6 & b_5 & 0 & b_8 & b_7 \\ a_5 & a_7-1 & b_6 & b_5 & 0 & b_8 & b_7 & 0 \\ 0 & 1 & b_5 & 0 & 0 & b_7 & 0 & 0 \end{bmatrix} \begin{bmatrix} p_2 \\ p_4 \\ q_5 \\ q_6 \\ q_7 \\ q_{10} \\ q_{11} \\ q_{12} \end{bmatrix} = \begin{bmatrix} 0 \\ a_4 \\ a_3-a_4 \\ -a_3 \\ m_4 \\ m_3+m_4 \\ m_2-a_4+a_7 \\ m_1-a_3+1 \end{bmatrix} \quad (21)$$

The controller parameters are obtained by solving these equations.

5. DESIGN OF 2DOF CONTROLLER

The configuration of the closed loop, shown in Fig. 3, was presented in (Ortega and Kelly, 1984) for SISO control loop.

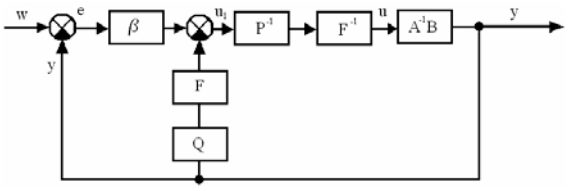

Fig. 3. Block diagram of 2DOF configuration

It is possible to derive the following equation for the system output

$$\boldsymbol{Y} = \boldsymbol{A}^{-1}\boldsymbol{B}\boldsymbol{U} = \boldsymbol{A}^{-1}\boldsymbol{B}\boldsymbol{F}^{-1}\boldsymbol{P}^{-1}\boldsymbol{U}_1 \quad (22)$$

Where

$$\boldsymbol{U}_1 = \boldsymbol{\beta}(\boldsymbol{W}-\boldsymbol{Y}) - \boldsymbol{Q}\boldsymbol{F}\boldsymbol{Y} \quad (23)$$

The corresponding equation for the controller's output, as shown in the block diagram in Fig. 3, follows as

$$\boldsymbol{U} = \boldsymbol{F}^{-1}\boldsymbol{P}^{-1}\boldsymbol{U}_1 \quad (24)$$

The substitution of $\boldsymbol{U}_1$ and $\boldsymbol{Y}$ results in

$$\boldsymbol{U} = \boldsymbol{F}^{-1}\boldsymbol{P}^{-1}\left[\boldsymbol{\beta}(\boldsymbol{W}-\boldsymbol{A}^{-1}\boldsymbol{B}\boldsymbol{U}) - \boldsymbol{Q}\boldsymbol{F}\boldsymbol{A}^{-1}\boldsymbol{B}\boldsymbol{U}\right] \quad (25)$$

The equation (25) can be modified using the right matrix fraction of the controlled system into the form

$$\boldsymbol{U} = \boldsymbol{A}_1\left[\boldsymbol{P}\boldsymbol{F}\boldsymbol{A}_1 + (\boldsymbol{\beta}+\boldsymbol{F}\boldsymbol{Q})\boldsymbol{B}_1\right]\boldsymbol{\beta}\boldsymbol{W} \quad (26)$$

The closed loop system is stable when the following diophantine equation is satisfied

$$\boldsymbol{P}\boldsymbol{F}\boldsymbol{A}_1 + (\boldsymbol{\beta}+\boldsymbol{F}\boldsymbol{Q})\boldsymbol{B}_1 = \boldsymbol{M} \quad (27)$$

Where $\boldsymbol{M}$ is defined by expression (18) and the structure of the matrices $\boldsymbol{P}$, $\boldsymbol{Q}$ and $\boldsymbol{\beta}$ were chosen according to the same rules that are presented in the previous section. The matrices $\boldsymbol{P}$, $\boldsymbol{Q}$ and $\boldsymbol{\beta}$ are the matrices of the controller.

$$\boldsymbol{P}(z^{-1}) = \begin{bmatrix} 1+p_1z^{-1} & p_2z^{-1} \\ p_3z^{-1} & 1+p_4z^{-1} \end{bmatrix} \quad (28)$$

$$\boldsymbol{Q}(z^{-1}) = \begin{bmatrix} q_1+q_2z^{-1} & q_3+q_4z^{-1} \\ q_5+q_6z^{-1} & q_7+q_8z^{-1} \end{bmatrix} \quad (29)$$

$$\boldsymbol{\beta}(z^{-1}) = \begin{bmatrix} \beta_1 & \beta_2 \\ \beta_3 & \beta_4 \end{bmatrix} \quad (30)$$

A set of algebraic equations, that is used to obtain the unknown controller parameters, is defined by solving the diophantine equation (27). The algebraic equations in the matrix form are specified by the following expressions:

$$\begin{bmatrix} 1 & 0 & b_9 & 0 & b_{13} & 0 & b_9 & b_{13} \\ a_9-1 & a_{13} & b_{10}-b_9 & b_9 & b_{14}-b_{13} & b_{13} & b_{10} & b_{14} \\ a_{10}-a_9 & a_{14}-a_{13} & -b_{10} & b_{10}-b_9 & -b_{14} & b_{14}-b_{13} & 0 & 0 \\ -a_{10} & -a_{14} & 0 & -b_{10} & 0 & -b_{14} & 0 & 0 \\ 0 & 1 & b_{11} & 0 & b_{15} & 0 & b_{11} & b_{15} \\ a_{11} & a_{15}-1 & b_{12}-b_{11} & b_{11} & b_{16}-b_{15} & b_{15} & b_{12} & b_{16} \\ a_{12}-a_{11} & a_{16}-a_{15} & -b_{12} & b_{12}-b_{11} & -b_{16} & b_{16}-b_{15} & 0 & 0 \\ -a_{12} & -a_{16} & 0 & -b_{12} & 0 & -b_{16} & 0 & 0 \end{bmatrix} \begin{bmatrix} p_1 \\ p_2 \\ q_1 \\ q_2 \\ q_3 \\ q_4 \\ \beta_1 \\ \beta_2 \end{bmatrix} = \begin{bmatrix} m_1-a_9+1 \\ m_2+a_9-a_{10} \\ m_3+a_{10} \\ m_4 \\ -a_{11} \\ a_{11}-a_{12} \\ a_{12} \\ 0 \end{bmatrix}$$

$$\begin{bmatrix} 1 & 0 & b_9 & 0 & b_{13} & 0 & b_9 & b_{13} \\ a_9-1 & a_{13} & b_{10}-b_9 & b_9 & b_{14}-b_{13} & b_{13} & b_{10} & b_{14} \\ a_{10}-a_9 & a_{14}-a_{13} & -b_{10} & b_{10}-b_9 & -b_{14} & b_{14}-b_{13} & 0 & 0 \\ -a_{10} & -a_{14} & 0 & -b_{10} & 0 & -b_{14} & 0 & 0 \\ 0 & 1 & b_{11} & 0 & b_{15} & 0 & b_{11} & b_{15} \\ a_{11} & a_{15}-1 & b_{12}-b_{11} & b_{11} & b_{16}-b_{15} & b_{15} & b_{12} & b_{16} \\ a_{12}-a_{11} & a_{16}-a_{15} & -b_{12} & b_{12}-b_{11} & -b_{16} & b_{16}-b_{15} & 0 & 0 \\ -a_{12} & -a_{16} & 0 & -b_{12} & 0 & -b_{16} & 0 & 0 \end{bmatrix} \begin{bmatrix} p_3 \\ p_4 \\ q_5 \\ q_6 \\ q_7 \\ q_8 \\ \beta_3 \\ \beta_4 \end{bmatrix} = \begin{bmatrix} -a_{13} \\ a_{13}-a_{14} \\ a_{14} \\ 0 \\ m_5-a_{15}+1 \\ m_6+a_{15}-a_{16} \\ m_7+a_{16} \\ m_8 \end{bmatrix} \quad (31)$$

The controller parameters are derived by solving these equations. The control law apparent from the block diagram is defined as

$$\boldsymbol{F}\boldsymbol{P}\boldsymbol{U} = \boldsymbol{\beta}\boldsymbol{E} - \boldsymbol{F}\boldsymbol{Q}\boldsymbol{Y} \quad (32)$$

6. SYSTEM IDENTIFICATION

For control of the three – tank – system, the control algorithms were applied as self tuning controllers. They were incorporated into an adaptive control system with recursive identification. The recursive least square method proved to be effective for self-tuning controllers (Kulhavý, 1987; Bittanti *et al.*, 1990) and was used as the basis for our algorithm. For our two-variable example it was considered the disintegration of the identification into two independent parts.

Difference equations describing the models in a vector form are as follows:

$$\begin{aligned} y_1(k) &= \boldsymbol{\Theta}_1^T(k)\boldsymbol{\varphi}_1(k-1) + n_1(k) \\ y_2(k) &= \boldsymbol{\Theta}_2^T(k)\boldsymbol{\varphi}_2(k-1) + n_2(k) \end{aligned} \quad (33)$$

where $n_1(k)$, $n_2(k)$ are unmeasurable random signals.

The parameter vectors are specified as shown below:

$$\begin{aligned} \boldsymbol{\Theta}_1^T(k) &= [a_1,a_2,a_3,a_4,b_1,b_2,b_3,b_4] \\ \boldsymbol{\Theta}_2^T(k) &= [a_5,a_6,a_7,a_8,b_5,b_6,b_7,b_8] \end{aligned} \quad (34)$$

The data vector is

$$\begin{aligned} \boldsymbol{\varphi}_{1,2}^T(k-1) = [&-y_1(k-1),-y_1(k-2),-y_2(k-1), \\ &-y_2(k-2),u_1(k-1),u_1(k-2),u_2(k-1),u_2(k-2)] \end{aligned} \quad (35)$$

The parameter estimates are updated using the recursive least squares method with adaptive directional forgetting.

7. EXPERIMENTAL EXAMPLES

The model was connected with a PC equipped with a control and measurement PC card. The Matlab and the Real Time Toolbox were used to control the system.

For the experiments presented in this paper, the three – tank – system was configured in such a way that the valves v3 and v5 were closed and the remaining valves were open.

The best sampling period T_0=5 *s* was found in virtue of many experiments. Another problem was finding of suitable poles of the characteristic polynomial. In comparison with controllers for SISO control loops, where it is often possible to assume influence of particular poles to behaviour of the closed loop, pole – placement of multivariable controllers is much more complicated. Pole – placement applicable for both controllers was obtained from a number of experiments as follows:

$$\boldsymbol{M}\left(z^{-1}\right)=\begin{bmatrix} 1-0{,}9z^{-1}+0{,}19z^{-2}- & 0 \\ -0{,}009z^{-3}-0{,}002z^{-4} & \\ 0 & 1-0{,}9z^{-1}+0{,}19z^{-2}- \\ & -0{,}009z^{-3}-0{,}002z^{-4} \end{bmatrix} \quad (36)$$

In Fig. 4 and Fig. 5 are shown time responses of the control when the initial parameter estimates were chosen without any a-priori information:

$$\boldsymbol{\Theta}_1^T(0)=[0.1,0.2,0.3,0.4,0.1,0.2,0.3,0.4] \quad (37)$$
$$\boldsymbol{\Theta}_2^T(0)=[0.5,0.6,0.7,0.8,0.5,0.6,0.7,0.8]$$

The reference signals contain frequent step changes in the beginning of experiments to activate input and output signals and improve the identification. The controlled variables y_1 and y_2 are liquid levels of tanks T1 and T2. The manipulated variables u_1 and u_2 are flow rates of liquid into the tanks. As w_1 and w_2 are denoted desired liquid levels in particular tanks (reference signals).

Subsequent experiments were carried out in such a way that initial parameter estimates were set as the last parameter estimates obtained in the ends of the previous experiments. The initial conditions of the recursive identification were also modified by reducing of diagonal elements of the square covariance matrix from 1000 to 10. Because the system is nonlinear and the identified parameters were valid only for particular steady states, the reference signals were set to the same values as it was in the ends of the previous experiments. Time responses of these experiments are shown in Fig. 6 and Fig. 7.

Tables 1 and 2 contain values of control quality criterions. The criterions are sum of powers of tracking errors and sum of increments of manipulated variables. The table 1 contains values obtained from the experiments, when the initial parameter estimates were chosen without a-priori information. The table 2 relates to the experiments with steady parameters.

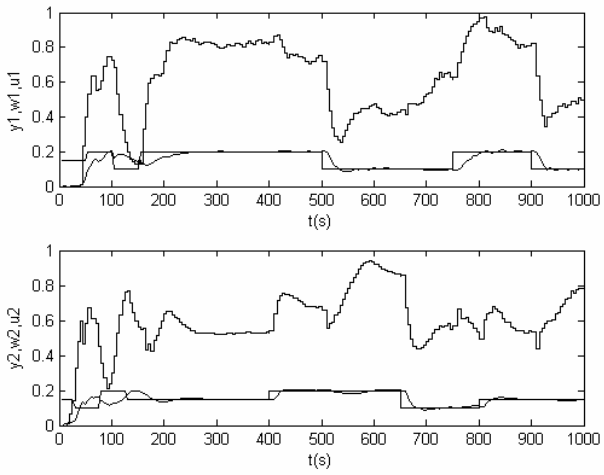

Fig. 4. Control of the laboratory model using 1DOF controller

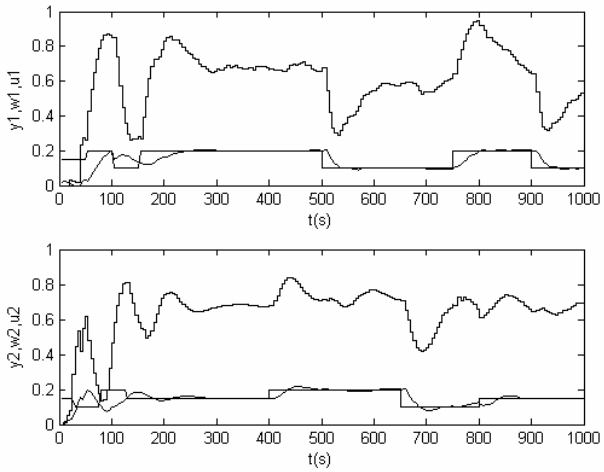

Fig. 5. Control of the laboratory model using 2DOF controller

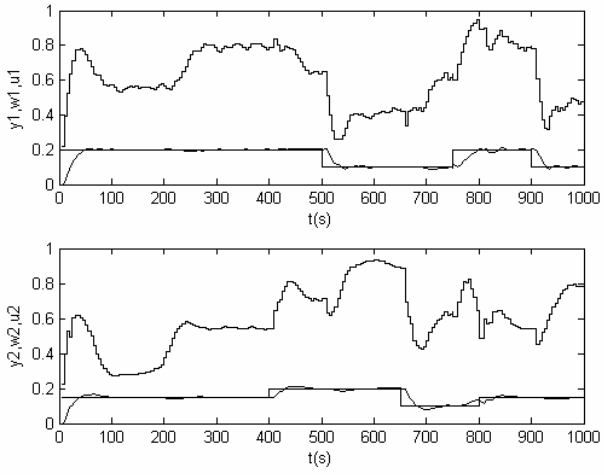

Fig. 6. Control of the laboratory model using 1DOF controller – experiment with steady parameters

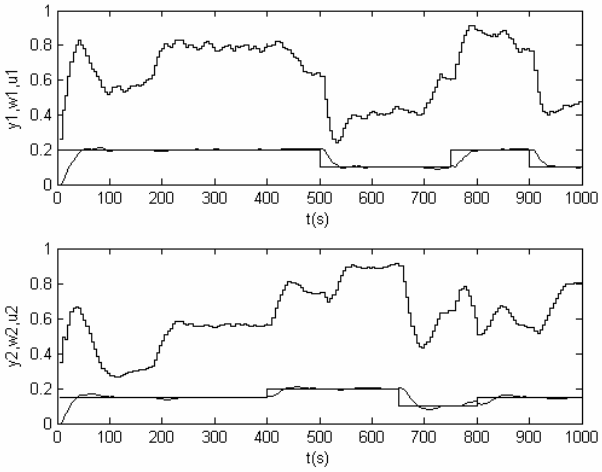

Fig. 7. Control of the laboratory model using 2DOF controller – experiment with steady parameters

Table 1 Control quality criterions

Controller	$\sum e_1^2$	$\sum e_2^2$	$\sum \Delta u_1^2$	$\sum \Delta u_2^2$
1DOF	0,2181	0,1185	3,9846	4,6327
2DOF	0,2204	0,1262	1,7375	1,3647

Table 2 Control quality criterions – experiments with steady parameters

Controller	$\sum e_1^2$	$\sum e_2^2$	$\sum \Delta u_1^2$	$\sum \Delta u_2^2$
1DOF	0,4059	0,2195	5,5649	8,2888
2DOF	0,4472	0,2810	4,1135	4,1825

8. CONCLUSIONS

It is possible to derive several conclusions from the values of the control quality criterions obtained during experiments with particular controllers. If the first criterion (powers of tracking errors) is considered, comparable results were achieved with both controllers. According to the second criterion (increments of manipulated variables) the 2DOF controller performed significantly better. This fact is also evident from the courses in Figs. 4 – 7.

The control tests executed on the laboratory model provide very satisfactory results, despite of the fact, that the non–linear dynamics was described by a linear model. The objective laboratory model simulates technological processes, which frequently occur in industry. The laboratory tests proved that the examined methods could be implemented and used successfully to control such processes.

ACKNOWLEDGEMENTS

This work was supported in part by the Grant Agency of the Czech Republic under grants No.102/05/0271, 102/04/P244 and in part by the Ministry of Education of the Czech Republic under grant MSM 7088352101.

REFERENCES

AMIRA-DTS2000 (1996). Laboratory setup three tank system. Amira Gmbh, Duisburg.

Bittanti, S., Bolzern, P., Campi, M. (1990). Convergence and Exponential Convergence of Identification Algorithms with Directional Forgetting Factor. *Automatica*, 26, 5, pp. 929 – 932.

Chien, I.L., Seborg, D.E., Mellichamp, D. A. (1987). Self-Tuning Control with Decoupling. *AIChE* J., 33, 7, pp. 1079 – 1088.

Kučera, V. (1980). Stochastic Multivariable Control: a Polynomial approach. *IEEE Trans. of Automatic Control* , 5, pp. 913 – 919.

Kučera, V. (1991). *Analysis and Design of Discrete Linear Control Systems*. Academia, Prague.

Kulhavý, R. (1987). Restricted exponencial forgetting in real – time identification. *Automatica*, 23, pp. 589 – 600.

Luyben, W. L. (1986). Simple Method for Tuning SISO Controllers in Multivariable Systems. *Ing. Eng. Chem. Process Des. Dev.*, 25, pp. 654 – 660.

Ortega, V., and Kelly R.: (1984). PID self – tuners: Some theoretical and practical aspects. *IEEE Trans. Ind. Electron.*, IE - 3, 332 – 338.

Skogestad, S., Postlethwaite, J. (1996). *Multivariable Fedback Control - Analysis and Design.* New York, J. Willey.

ADCHEM 2006

International Symposium on Advanced Control of Chemical Processes
Gramado, Brazil – April 2-5, 2006

ADAPTIVE AGENT-BASED CONTROL OF PRODUCT GRADE TRANSITIONS IN REACTOR NETWORKS

Eric Tatara, Cindy Hood, Fouad Teymour and Ali Cinar [*]
Michael North [**]

[*] *Illinois Institute of Technology, Chicago, IL*
[**] *Argonne National Lab, Argonne, IL*

Abstract: Large-scale spatially distributed systems provide control challenges because of their nonlinearity, spatial distribution and generally high order. The control structure for these systems tend to be both discrete and distributed. A layered control structure interfaced with complex arrays of sensors and actuators provides a flexible supervision and control system that can deal with local and global challenges. An adaptive agent-based control structure is presented whereby local control objectives may be changed in order to achieve the global control objective. Information is shared through a global knowledge environment that promotes the distribution of ideas through reinforcement. The performance of the agent-based control approach is illustrated in a case study where the interaction front between two competing autocatalytic species is moved from one spatial configuration to another. The multi-agent control system is able to effectively explore the parameter space of the network and intelligently manipulate the network flow rates such that the desired spatial distribution of species is achieved.

Keywords: Agent-based control, distributed systems.

1. INTRODUCTION

Large-scale spatially distributed systems provide a difficult control challenge because of their nonlinearity, spatial distribution and generally high order.

The control structure for these systems tend to be distributed and contain discrete and continuous elements. Hybrid control systems that combine process dynamics and discrete control elements and include multiple models for different operating points are one way to develop control systems for spatially distributed systems (Morari *et al.*, 2003; Christofides and El-Farra, 2005). An alternative approach is based on a hierarchical agent-based system with local and global control structures (Tatara *et al.*, 2005*c*; Tatara *et al.*, 2005*b*) that has been demonstrated on a network of interconnected continuous stirred tank reactors (CSTRs). Reactor networks exhibit highly complex behavior with multiple steady state operating regimes and have a large pool of candidates for manipulated variables (Tatara *et al.*, 2004).

The operation of highly nonlinear systems like autocatalytic replicator networks may benefit from evolutionary self-organizing control because the optimal operating regime and the required control strategies may not be known a priori. Agent-based control systems provide the capability for localized and global control strategies that are both reactive in controlling disturbances and proactive in searching for better operational solutions (Jennings and Bussmann, 2003). An adaptive agent-based control system for a CSTR network

is proposed. The performance of the agent-based control approach is illustrated in a case study where the interaction front between competing autocatalytic species is moved from one spatial configuration to another.

2. AGENT-BASED CONTROL FRAMEWORK

Multi-agent control system architectures have several properties that make them particularly attractive for use in supervising large, complex systems (Lesser, 1999). The first, and usually most important in critical systems, is a high level of reliability. Modularity, scalability and adaptability are also attractive features of multi-agent systems. The adaptive and self-regulatory nature of agent systems has only recently been investigated for solving control problems that are normally solved with traditional methods.

2.1 Design Process

The design procedure used is a derivative of recent agent design methodologies based on the concept of the agent-services-acquaintance model (Wooldridge *et al.*, 1999) and the application to manufacturing control (Brueckner *et al.*, 1998). The goal of the design process is to develop an agent-based control system for physically distributed industrial processes. Certain parts of the agent-based control system are generic because they are based on general concepts of industrial control systems and operation of distributed processes.

Comprehensive studies of the physical process domain provide information regarding the expected normal operating conditions of the the processes, types of faults and disturbances that may occur, and control strategies. Additionally, the desired process operation and/or optimal conditions are expected to be known by the designers. Required agent types and roles are identified based on the requirements for controlling the physical system. The details of the hierarchical agent-based architecture (Tatara *et al.*, 2005*b*; Tatara *et al.*, 2005*a*) will not be repeated in detail here. The focus will rather be on the specific agent synthesis and instantiation for the presented examples.

2.2 Agent synthesis

There is nearly a one-to-one mapping of roles to agent types. The number of control agents is variable, depending on the number of reactors (I) in the network, as well as the complexity of the control actions being performed. Generally, a single control agent can be used for controlling each reactor. While multiple control agents can be applied to each reactor, from a software design point of view, it makes more sense to encapsulate the functionality of several control concepts (ie, temperature, level, etc.) into a single software agent, as long as the control algorithms are not extraordinarily complex.

The number of arbitration agents is probably the most flexible variable in the agent model. As with the control agents, the run time environment will set the number of arbitrators required. Larger networks with more control agents will subsequently require more arbitrators to handle the setpoint change requests coming from the controllers. Ultimately, the number of realized arbiters will be determined by the supervisory level agents.

The simplest implementation will have at least one supervisory level agent to coordinate efforts between the control and arbitration agents. While local interactions between agents are intended to serve as the primary driving force in the control system, the supervisor needs to maintain an overview at all times. More complex control schemes can include multiple supervisors for each high-level function such as help in mediating disputes, setting spatial concentration patterns, and supervising process recovery from disturbances that are too complex for the local controllers.

Finally, there will be exactly one instance each of the data collection and data acquisition agents. The data acquisition essentially functions as a bridge between the agent system and the physical domain. The acquisition agent will read values from either a simulator or a hardware data acquisition system and write the numeric values to objects that can be read and manipulated by the control and arbitration agents. The data collection agent encapsulates the roles for both data collection and file I/O since these roles share very similar tasks. Any agent in the system will likely have a small memory space for storing local information relative its specific tasks. The data collection agent will, however, be responsible for cataloging relevant data for the entire network, such as average concentrations, or possible even the concentration histories in each reactor. This data will be written to a file stream in chunks at some variable rate.

2.3 Global Knowledge Environment

Considering the nonlinearity of reactor networks, it is difficult to predict how the behavior of the system changes when the system parameters are manipulated. Consequently, one cannot easily predict how to change operating conditions of the network by manipulating the flow rates nor what

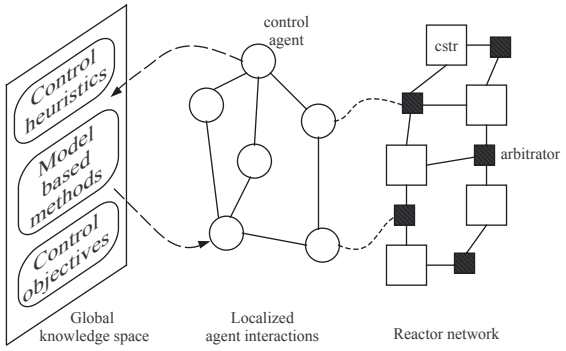

Fig. 1. Coupling of control agents with global knowledge space.

the localized operating conditions should be, in order to satisfy a global objective. Several methods can be used to guide the decision agents in planning their control strategies including dynamic exploration of the parameter space, rule-based heuristic models, or first-principles based models.

Although information is exchanged between agents via arbitrators, these interactions are local and limit the amount and quality that can propagate through the system. The global knowledge representation (Figure 1) serves as an environment for indirect communication between agents. This concept builds upon the hierarchical structuring of the control system by adding a mechanism for communication and reinforcement of ideas. The information in the knowledge space is divided into categories including local control objectives, control heuristics, and data-based models.

Information exchange occurs indirectly between agents because agents asynchronously read/write information from/to the knowledge space. For example, a particular agent may discover a local control strategy that works particularly well in meeting an objective set by a supervisor. This strategy is cataloged in the knowledge space by the originating agent. Other agents may read this strategy from the knowledge space and implement it to satisfy their particular control objective. The value of the strategy is then rated by the agents that adopt this new strategy such that its value relative to others is promoted. Similarly, outdated information in the knowledge space continuously decreases in value and eventually may be deleted from the knowledge space.

Although the stability of the agent dynamics cannot be guaranteed for every scenario, this methodology helps to reduce or prevent the emergence of dysfunctional agent dynamics by reinforcing "good" agent behavior, while punishing undesirable agent behavior. Furthermore, the agent system has been designed with the assumption that the agents' decision delays are small compared to the time scale of the physical process. The importance of this assumption becomes apparent when examining the consequences of its impact on process performance. If the agents' computing time is very long with respect to the process time scale, control of a continuous process becomes difficult due to the reduced data acquisition, control action computation and implementation rates. This assumption generally holds for chemical processes in which operating changes are introduced infrequently and process dynamics are represented with time scales of tens of minutes or even hours. Traditional controllers are normally used in the event of very rapid localized dynamics and, while the agents may modify the setpoints of such controllers, the time-critical (first response) control actions are strictly outside the domain of the higher-level decision making agents.

3. PRODUCT GRADE TRANSITION IN A CHEMICAL REACTOR NETWORK

Product grade transitions may be used to schedule the production of various composite compounds at different points in time. The overall product quality is determined by selecting one or more exit streams from the network and mixing them in the desired proportions. Therefore, if one would like to produce a grade consisting of the majority of one chemical species and only a small amount of another, it makes sense to mirror this grade composition in the network.

The supervisory level agent sets the grade composition by specifying the fraction of each species desired in the network. The composition is then transformed into a set of behaviors via the utility function that determines each control agent's goal. The fraction of desired species determines the agent's willingness to change or remain the same. If the agent's average composition value is set very high, and it surrounded by competitor agents, then its desire to remain unchanged is high. Conversely, if the agent's composition value is set very low and it is surrounded by cooperator agents, its desire to remain unchanged is low. This behavioral programming results in the network self-organizing to meet the global composition goal. A few isolated agents controlling reactors with a trace compound will contribute a lesser amount of their species to the product grade, while many closely clustered groups of the majority will contribute to the primary product in the desired grade. This self-organizing behavior arises from some aspects of the rules governing the local interactions as well as the open loop behavior or the network, since local clusters of one autocatalytic species will be more stable than single isolated reactors.

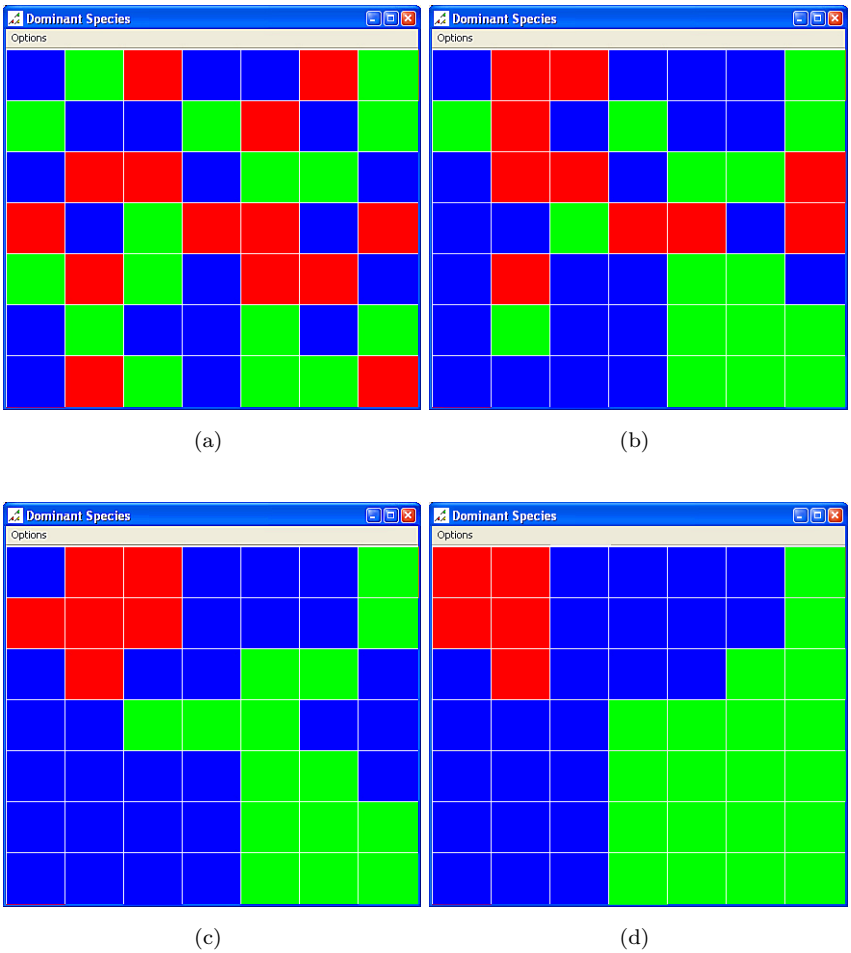

Fig. 2. Evolution of 2D spatial concentration profile of the dominant species in each reactor, with red (dark gray) representing species 1, blue (black) species 2, and green (light gray) species 3.

The performance of the agent-based control architecture is demonstrated in a case study to control the distribution of autocatalytic species in a network model (Tatara *et al.*, 2004) of 49 (7x7 grid) reactors hosting three autocatalytic species using the interaction flow rates as the manipulated variables. The species that populate the reactor network are characterized by identical growth and death rates, such that one species does not have an unfair advantage over the others. The reactor network model and agent-based control system is implemented with the open source Java agent modeling and simulation environment RePast (Collier *et al.*, 2003; Tatara *et al.*, 2005*a*).

The map of the dominant species in each reactor, with red (dark gray) representing species 1, blue (black) species 2, and green (light gray) species 3. The map shows the distribution of each species in the network as is updated whenever the state of one of the reactors change, ie the dominant species switches from one species to another.

The spatial distribution of autocatalytic species shown in Figure 2a shows the open loop behavior of the system following the temporal evolution from a randomly generated set of initial conditions. The supervisory agent responsible for the product grade composition of the network sets the grade for species (1,2,3) = (0.1,0.5,0.4); Once the control agents receive the specification for the grade composition (instantaneously, unless a higher priority action exists), they initiate the routine for determining the species setpoint based on their neighborhood and grade information. Figure 2b shows the temporal evolution of the network after 20 time (dimensionless) steps. Species 2 and 3 begin to form clusters at the bottom of the network. The aggregation of species in clusters occurs due to the natural open-loop behavior of the network in addition to the control agents, which reinforce the species robustness in a given reactor when surrounded by like species. After 40 time steps (Figure 2c), the network grade composition begins to approach the setpoint and finally arrives to the desired grade after 100 time steps (Figure 2d). The exact spatial boundaries between the species clusters may fluctuate with time if the network displays oscillatory behavior or is subjected to a disturbance. However, the network average values for the species concentrations will

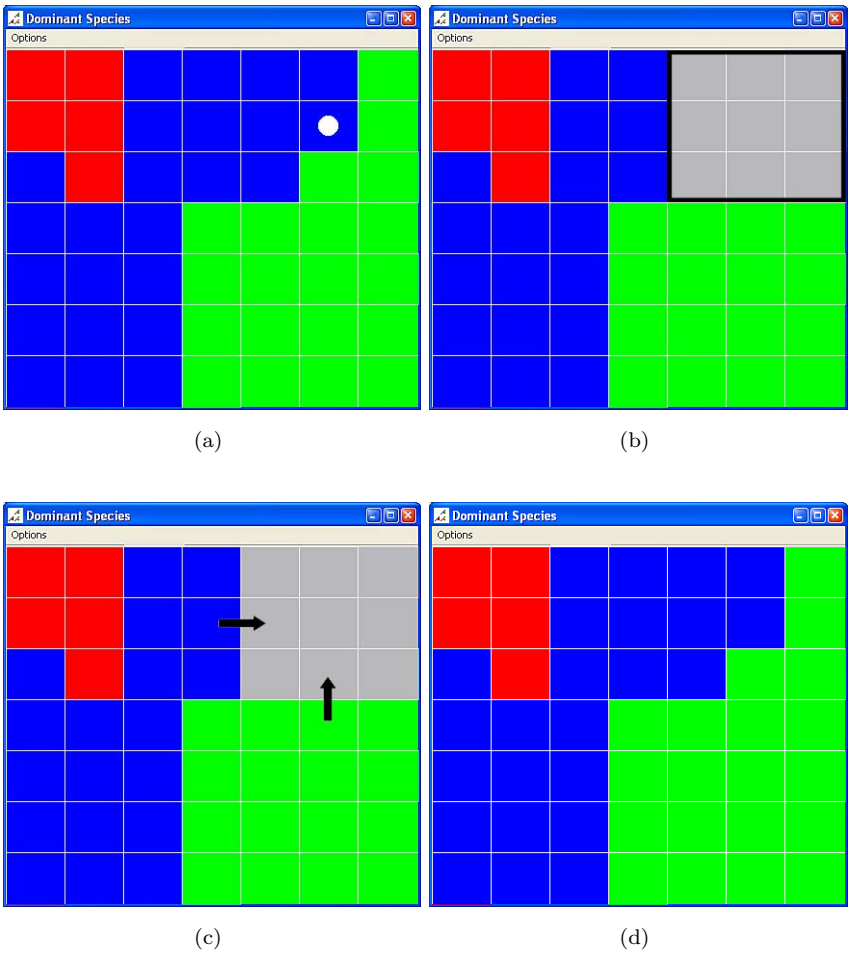

Fig. 3. Agent response to species invasion in reactor marked with white circle, with red (dark gray) representing species 1, blue (black) species 2, green (light gray) species 3, and very light gray representing an unpopulated reactor.

remain constant due to local spatial reconfigurations, thereby meeting the grade specification.

4. DISTURBANCE REJECTION

Figure 3 shows a 7x7 grid of reactors hosting three autocatalytic species. The spatial distribution of species is an arbitrary choice, but is treated as the desired operating condition for the network. Therefore, the control agent for each reactor should prevent the invasion of the reactor for which it is responsible. For neighboring competitors, this control function can be achieved by the previously detailed methods of local agent control via the interaction rates (Tatara *et al.*, 2005*b*). However, in the case where a new, more aggressive autocatalytic species is introduced to the network, these methods may fail. A species with a higher ratio of growth to death rates than those of pre-existing species will quickly dominate a contaminated reactor and spread throughout the network, effectively eliminating all other species.

A method for containment of aggressive invading species is modeled after the concept of programmed cell death (PCD) in plants (Liu *et al.*, 2005), in which cells that are infected with viruses die to prevent the infection from spreading to the rest of the plant. The immune system in plants is sensitive to invading species, namely viruses, which causes a chemical reaction in the infected plant cells resulting in their death. The PCD mechanism is encapsulated in the genetics for each cell, yet is only activated when the cells become infected. The mechanism is sufficiently robust to quickly contain infections, yet not so sensitive as to be pathological.

The application to disturbance rejection in the reactor network is straightforward. When a control agent detects the presence of an unknown species above some minimal concentration threshold (for example reactor (2,6) of Figure 3a, it isolates itself from neighboring reactors to prevent the spread of the invading species (Figure 3b). The controller manipulates the residence time of the reactor such that the invading species is washed out below the detection threshold. This procedure may in

fact result in the other species being completely washed out as well. However, the containment of the invading species takes precedence to maintaining the original control objective, once the reactor has been compromised. After the invader has been washed out, the reactor can be reconnected to the network and the autocatalytic species can be repopulated using the feed stream or, preferably, resources from adjacent reactors (Figure 3c), such that the original spatial configuration is restored (Figure 3d).

5. CONCLUSIONS

An adaptable, intelligent agent-based control system has been implemented to control the product grade transitions via spatial distribution of autocatalytic species in a reactor network. This methodology has been proposed as a real-time alternative to traditional nonlinear control schemes involving predetermined controller configurations or computationally expensive optimization techniques.

Controlling the overall spatial distribution of autocatalytic species in a network of reactors requires a coordinated effort between local control agents. The practical application of this control scheme is in managing the composition of a product composition. From a production standpoint, the net feed flow rate through the network, that is the total sum of all feed flow and exit flow rates, should be kept constant. Therefore, there is a constraint on the total network inflow and outflow. However, the distribution of interconnection flow rates may be distributed as necessary, as long as the volume constraints are maintained. The distribution of interconnection flows will not be set by a supervisory level agent, since the agent's control algorithm performance would deteriorate quickly as the network is scaled up. Therefore, the set point changes for the interconnection flow rates will be determined by coordination of the local control agents.

In addition to case studies demonstrating the behavior of the agent-based control system under normal operating conditions, methods were designed and implemented to allow the framework to correct disturbances in the form of invading species or reactor malfunction. The disturbance rejection behavior was based on the immune system response of plant species to viral infections. The control agents were successfully able to detect invading autocatalytic species and isolate infected reactors to prevent the invading species from spreading through the network. The infected reactors can be repopulated with the desired species once the invader is washed out of the network.

6. ACKNOWLEDGMENT

This material is based upon work supported by the National Science Foundation under Grant No. CTS-0325378 of the ITR program.

REFERENCES

Brueckner, S., J. Wyns, P. Peeters and M. Kollingbaum (1998). Designing agents for manufacturing control. In: *Proceedings of the 2nd AI & Manufacturing Research Planning Workshop*. Albuquerque, NM.

Christofides, P. and N. El-Farra (2005). *Control of Nonlinear and Hybrid Process Systems*. Springer-Verlag: Berlin.

Collier, N., T. Howe, and M. North (2003). Onward and upward: The transition to repast 2.0. In: *First Annual North American Association for Computational Social and Organizational Science Conference, Pittsburgh, PA*.

Jennings, N.R. and S Bussmann (2003). Agent-based control systems. *IEEE Control Systems* **23**, 61–73.

Lesser, V.R. (1999). Cooperative multiagent systems: A personal view of the state of the art. *IEEE Transactions on Knowledge and Data Engineering* **11**(1), 133–142.

Liu, Y., M. Schiff, K. Czymmek, Talloczy Z., B. Levine and S.P. Dinesh-Kumar (2005). Autophagy regulates programmed cell death during the plant innate immune response. *Cell* **121**, 567–577.

Morari, M., M. Baotic and F. Borrelli (2003). Hybrid systems modeling and control. *European Journal of Control* **9**(2–3), 177–189.

Tatara, E., F. Teymour and A. Cinar (2005*a*). Control of complex distributed systems with distributed intelligent agents. *submitted to Journal of Process Control*.

Tatara, E., I. Birol, F. Teymour and A. Cinar (2004). Static and dynamic behavior of autocatalytic replicators in reactor networks. *Industrial and Engineering Chemistry Research* **43**, 3972–3993.

Tatara, E., I. Birol, F. Teymour and A. Cinar (2005*b*). Agent-based control of autocatalytic replicators in networks of reactors. *Computers & Chemical Engineering* **29**, 807–815.

Tatara, E., I. Birol, F. Teymour and A. Cinar (2005*c*). Measuring complexity in reactor networks with cubic autocatalytic reactions. *Industrial and Engineering Chemistry Research* **44**, 2781–2791.

Wooldridge, M., N.R. Jennings and D. Kinny (1999). A methodology for agent-oriented analysis and design. In: *Proceedings of the Third International Conference on Autonomous Agents (Agents'99)*. Seattle, WA.

ADCHEM 2006

International Symposium on Advanced Control of Chemical Processes
Gramado, Brazil – April 2-5, 2006

CONTROL OF LIQUID TANKS USING DECENTRALIZED APPROACH WITH LOGICAL SUPERVISOR

Petr Chalupa*, Vladimír Bobál**

Tomas Bata University in Zlín
Faculty of Applied Informatics
Department of Process Control
fax: +420 57603 5279
**email: chalupa@ft.utb.cz*
***email: bobal@ft.utb.cz*

Abstract: The paper deals with decentralized control with logical supervisor. The decentralized control is an approach of controlling multi input multi output systems with the same number of inputs as the number of outputs. The logical supervisor was proposed as a possible way of improving the stability and the quality of control courses. The theoretical results are applied to a real-time laboratory control system – DTS200 Three Tank System.

Keywords: decentralized control, logical supervisor, self-tuning control, on-line identification

1. INTRODUCTION

Problem of control of liquid level of interconnected tanks is very common in many industrial areas, especially in chemical industry. The controlled plats often perform nonlinear and sometimes even time-varying behaviour and thus usage of classical control approaches does not reach desired performance in many cases. Different techniques such as adaptive generic model control (Wang *at al.*, 2004) or fuzzy adaptive control (Blažič *at al.*, 2003) have been developed to cope with this problem. From the control theory point of view, the problem of control of multi input multi output (MIMO) system is to be solved.

The classical approach to the control of MIMO systems is based on the design of a matrix controller to control all system outputs at one time. Computation of the matrix controller is realized by one central computer. The basic advantage of this approach is the possibility of achieving optimal control performance because the controller can use all information known about the controlled system. The disadvantage of using a central matrix controller is its demand on computer resources because the number of operations and required memory depend on the square of the number of controlled signals.

Nowadays this problem is reduced thanks to great progress in the development of computer hardware; this, however, increases the price of the control system. Another disadvantage is the influence central controller faults on the controlled system. If the central controller fails, all the controlled signals are affected; thus the reliability of the controller is fundamental. Ensuring the required reliability can be unbearable from the financial point of view, especially in critical applications.

2. DECENTRALIZED CONTROL

An alternative solution to the control of MIMO systems is a decentralized approach. In this case, the system is considered as a set of interconnected subsystems and the output of each subsystem is influenced not only by the input to this subsystem but also by the input to the other subsystems (Aoki,

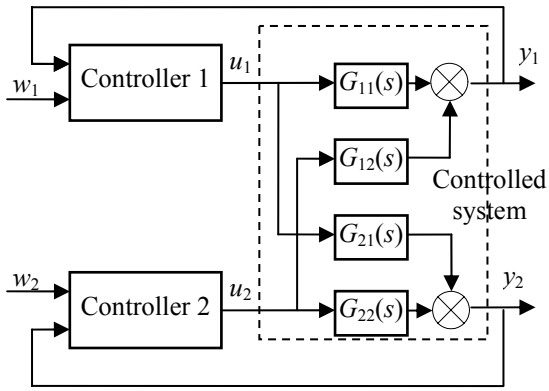

Fig. 1. Decentralized control of TITO system

1972). Each subsystem is controlled by a stand-alone controller. The simplest case of control circuit of two input two output (TITO) system is shown in Fig. 1.

Thus, decentralized control is based on decomposition of the MIMO system to subsystems, and the design of a controller for each subsystem (Cui and Jacobsen, 2002). Another advantage of the decentralized approach is that it is a lot easier to set controller parameters (e.g. choice of poles of the characteristic polynomial) for SISO control loops than for MIMO control loops. On the other hand, the control performance of a decentralized control system is suboptimal because controllers do not use information from the other subsystems. A further disadvantage is the limited applicability of the decentralized control to symmetric systems (systems with an equal number of inputs and outputs).

Each output of a multivariable controlled system can be affected by each system input. The strength of the effect is determined not only by internal transfers of the MIMO system but also by the evolution of the system input signals. When the decentralized approach is used to control such a system then, from the point of view of a controller of a particular subsystem, the transfer function varies in time even if the MIMO system is linear and stable.

The presence of subsystem interconnections is the main reason for using self-tuning controllers (Bobál *at al.*, 2005) in a decentralized approach to ensure the required course of controlled variables. Identification algorithms suitable for use in decentralized control must include weighting of identification data such that new data affect model parameters estimation more than older data. This requirement is a consequence of the time-varying influences of other subsystems on the identified subsystem. The influence of control variable (u_i) on the corresponding controlled variable (y_i) decreases with increasing gain of subsystem interconnections. This could lead to an unstable process of recursive parameter estimates.

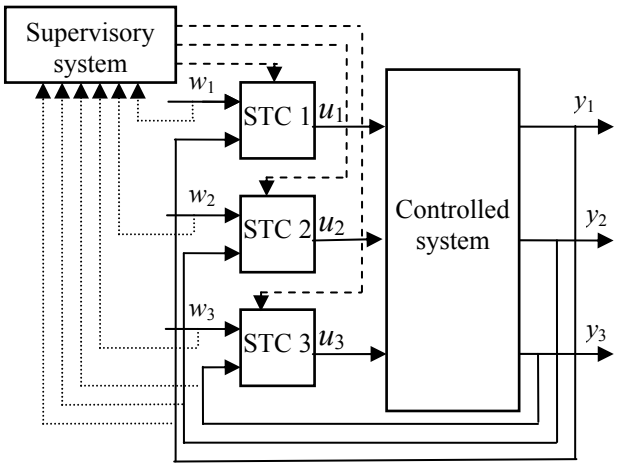

Fig. 2. Decentralized control circuit with supervisory system

3. SUPERVISORY SYSTEM

The stability of recursive identification can be increased by ensuring that just one of the controllers connected to the multivariable systems works in an adaptive regime at a particular time. Recursive identification parts of other controllers are suspended and parameter model estimates are constant for that time.

The process of switching on and off recursive identification is controlled by a new part of the control circuit – the supervisory system. Switching the identification on and off can be described as a process of transferring tokens among subsystems where only the controller, which currently has a token, can perform recursive identification. The token is moved to an other subsystem when a selected criterion is used.

The supervisory system represents a second level of control and thus a control circuit with supervisory system has a hierarchical control structure. An example of a control circuit scheme with supervisory system is shown in Fig. 2. The first (lowest) level of hierarchy contains individual self-tuning controllers (STC 1, STC 2 and STC 3 in Fig. 2) and the second level (superior) is represented by a supervisory system, which controls individual self-tuning controllers. The supervisory system analyses particular values from the control circuit and on the basis of these analyses moves the identification token among subsystems. In the case shown in Fig. 2, the analysis is performed on the basis of reference values and controlled values (dotted lines) and the process of transferring token is represented by dashed lines.

4. LOGICAL SUPERVISOR

A logical supervisor has been proposed to utilize and simplify the design of a supervisory system. This approach is suitable for use in real-time industrial

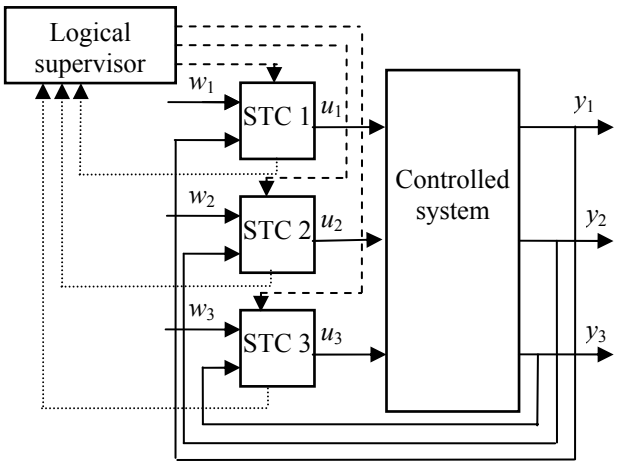

Key:
Real signals
Adaptation required
Adaptation enabled
boolean signals

Fig. 3. Decentralized control circuit with logical supervisor

applications. The idea of a logical supervisor is based on the following two principles:

- assigning priorities to individual subsystems;
- on-line evaluation of criteria for each subsystem.

The situation that reaching the reference value is more important for some subsystems than for others is very common, especially in industrial applications. It is thus possible to assign a unique priority to each subsystem. The priority corresponds to the importance of the subsystem's output. The numbering of subsystems is just a formal problem and thus the subsystems can be numbered according to priorities. The first subsystem has the highest priority; the second subsystem has the second highest priority and so on.
Further, for each subsystem, a criterion which determines whether the subsystem requires switching to adaptive mode or not, is calculated. The criterion can be designed with respect to particular properties of the subsystem. The block responsible for computing the criterion can be encapsulated with the self-tuning controllers and the output, which is sent to the logical supervisor, is a Boolean value determining whether or not the subsystem requires adaptation.

The last part of the logical supervisor approach is a superior logic determining which of subsystems requiring adaptation will be switched to adaptive mode. The decision-making is based on priorities assigned to individual subsystems. If the first subsystem requires switching to adaptive mode it is always satisfied; if the second subsystem requires switching to adaptive mode, it is satisfied only if the first subsystem does not require switching to adaptive mode, etc. The control circuit schema with logical supervisor approach and a controlled system of three inputs and three outputs is shown in Fig. 3 when only one of the dashed signals, "Adaptation enabled", is switched on at a time.

The logical supervisor uses only the logical values on its input and provides logical values on its output. In addition, the relations between inputs and outputs are simple logical functions. The transfer function between the input and output signals of the logical supervisor can be arranged as a table of logical values. This situation is shown in Table 1 for the MIMO system of three inputs and three outputs.

Table 1 Relation between inputs and outputs of logical supervisor

Adaptation required (inputs)			Adaptation enabled (outputs)		
Subsystem 1	Subsystem 2	Subsystem 3	Subsystem 1	Subsystem 2	Subsystem 3
R_1	R_2	R_3	E_1	E_2	E_3
0	0	0	0	0	0
0	0	1	0	0	1
0	1	0	0	1	0
0	1	1	0	1	0
1	0	0	1	0	0
1	0	1	1	0	0
1	1	0	1	0	0
1	1	1	1	0	0

It is also possible to rewrite the relation between inputs (R_k) and outputs (E_k) using logical operators:

$$\begin{aligned} E_1 &= R_1 \\ E_2 &= \overline{R_1}\ \text{AND}\ R_2 \\ E_3 &= \overline{R_1}\ \text{AND}\ \overline{R_2}\ \text{AND}\ R_3 \end{aligned} \tag{1}$$

where the bar denotes negation of a variable and function AND represents logic product.

When determining signal "Adaptation enabled" for general controlled MIMO system, the following relation is valid:

$$E_k = \prod_{i=1}^{k-1} \overline{R_i}\ \text{AND}\ R_k \tag{2}$$

where Π stands for logic product.

The logical supervisor represents a reliable approach to design of supervisory logic for decentralized control. The advantage of this approach is its simplicity of implementation and small number of signals that are transferred from subsystems to supervisory system and back.

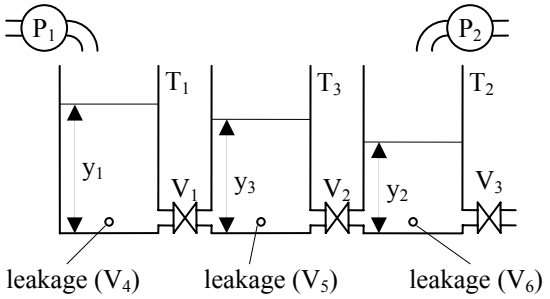

Fig. 4. Schema of three-tank system

5. THREE TANK SYSTEM

The logical supervisor approach was verified by the control of laboratory model DTS200 "Three-Tank-System" by Amira.

The system consists of three interconnected cylindrical tanks, two pumps, six valves, pipes, measurement of liquid levels and other elements. The schema of the system is shown in Fig. 4. The pump P_1 controls the inflow to tank T_1 while the pump P_2 controls the liquid inflow to tank T_2. There is no pump connected to tank T_3. The characteristic of the flow between tank T_1 and tank T_3 can be affected by valve V_1, flow between tanks T_3 and T_2 can be affected by the valve V_2 and the outflow of the tank T_2 is can be affected by valve V_3. The system also provides the capability of simulating leakage from individual tanks by opening the valves V_4, V_5 and V_6.

The valve states didn't change during the experiments and were positioned as follows: valves V_1 and V_2 were fully opened, valves V_5 and V_6 were fully closed and valves V_3 (outflow) and V_4 (leakage of tank T_1) were approximately in the midpoint of their control range.

The controlled values during the experiments were liquid levels of tanks T_1 and T_2. The control signals were voltages of the motors of the pumps P_1 and P_2. Decomposition of this TITO system into subsystems

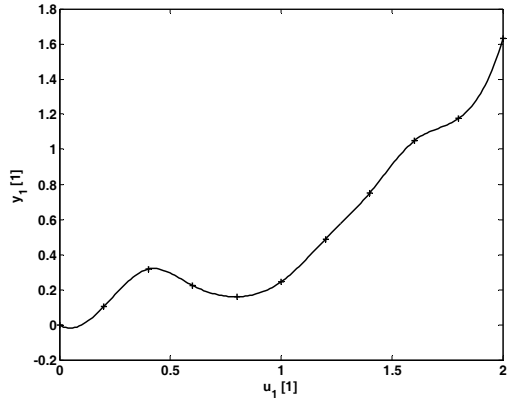

Fig. 5. Static characteristic of the first subsystem while second input of the plant is zero (u_2=0)

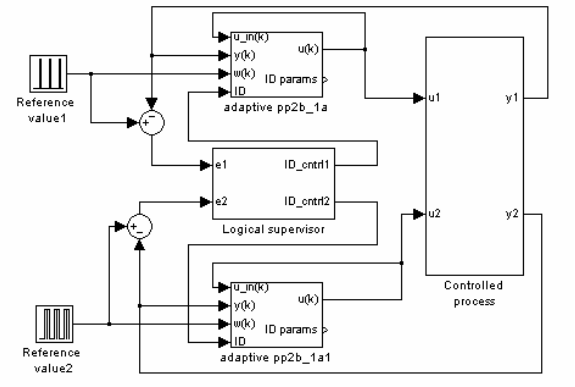

Fig 6. Simulink schema of control circuit

for application of decentralized control is straightforward in this case. The pump P_1 is used to control level in the tank T_1 and the pump P_2 controls the level in the tank T_2. The Non-linear behaviour of the plant can be seen from static characteristic of the first subsystem in Fig 5.

Simulink control circuit with the logical supervisor is shown in Fig 6. Pole placement self-tuning controllers *pp2b_1* from the Self-tuning Controllers Simulink Library (Bobál and Chalupa 2002) were used. The self-tuning controllers use second order models of controlled processes. The transfer function of the model is stated by the equation 3.

$$G\left(z^{-1}\right)=\frac{b_1 z^{-1}+b_2 z^{-2}}{1+a_1 z^{-1}+a_2 z^{-2}} \tag{3}$$

The initial parameter estimations were set without using any a priori information of the system. Initial estimations according to equation 4 were used in both controllers in all experiments.

$$\hat{\boldsymbol{\Theta}}(0)=\left[\hat{a}_1,\hat{a}_2,\hat{b}_1,\hat{b}_2\right]=\left[0.1,0.2,0.3,0.4\right] \tag{4}$$

The least squares method with adaptive directional forgetting (Kulhavý, 1987) was used for on-line calculation model parameters.

Control laws of used pole placement controllers *pp2_b1*and *pp2_b1a* (see Fig. 6) are determined by the equation 5.

$$\begin{aligned} u(k)=-\left[(q_0'+\beta)y(k)-(q_0'+q_2')y(k-1)+q_2'y(k-2)\right]- \\ -(\gamma-1)u(k-1)+\gamma u(k-2)+\beta w(k) \end{aligned} \tag{5}$$

Controller parameters are computed to make the dynamic behaviour of the closed loop similar to the continuous second order model with characteristic polynomial:

$$s^2+2\xi\omega s+\omega^2 \tag{6}$$

The damping factor of ξ=1, the natural frequency of ω=0.1 and the sample time of T_0=2s was used for both controllers. The request of on-line identification

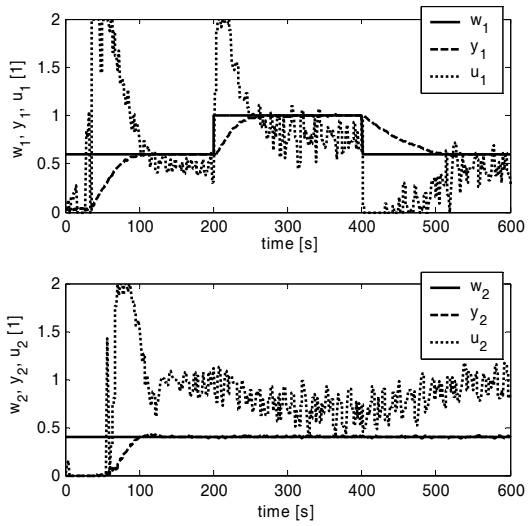

Fig. 7. Control courses without logical supervisor

was calculated on base of course of control error in this case.

5.1 Control courses without logical supervisor

The control without the logical supervisor was performed first to obtain base data for comparison of the effect of the incorporation of logical supervisor into control circuit.

The courses of reference value, control value and controlled value are shown in Fig. 7. The first subsystem consists of the control voltage of pump P_1 as an input (u_1) and the height of liquid level in tank T_1 as an output (y_1). The second subsystem consists of the control voltage of the pump P_2 as an input and the height of liquid level in tank T_2 as an output (y_2). The set point of the second subsystem (w_2) was constant during the control process to make easier the control of liquid level in tank T_1 in desired range. The control signals are limited to the range from 0 to 2. Where the value of zero corresponds to zero

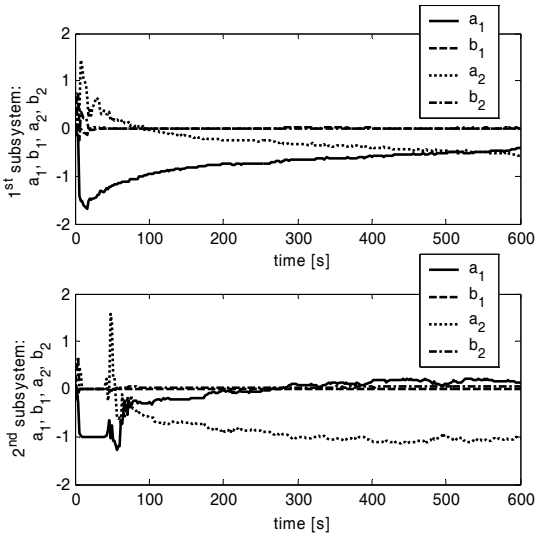

Fig. 8. Course of identification parameters during the control process without using logical supervisor

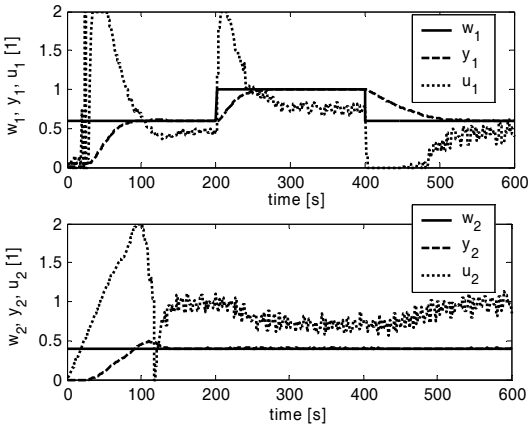

Fig. 9. Control courses with logical supervisor

inflow and the value of 2 corresponds to maximal inflow. The courses of estimations of parameters of these models are shown in Fig. 8.

5.2 Control courses with logical supervisor

The same course of reference signal was used also for the control with logical supervisor incorporated into control circuit. The priority of identification request of second subsystem is lower then the priority of the first subsystem.

The courses of reference signal, controlled signal and control signal are shown in Fig. 9. The courses of identification parameters are shown in Fig. 10. The values of identification request and identification enabled signals was also recorded for this control process. The results are presented in Fig. 11. Simple method of generating identification requests was used. The boolean value of identification request signal is determined just by the absolute value the current control error. It can be seen that both subsystems requested identification in the beginning of control process. But just the request of the first subsystem was satisfied.

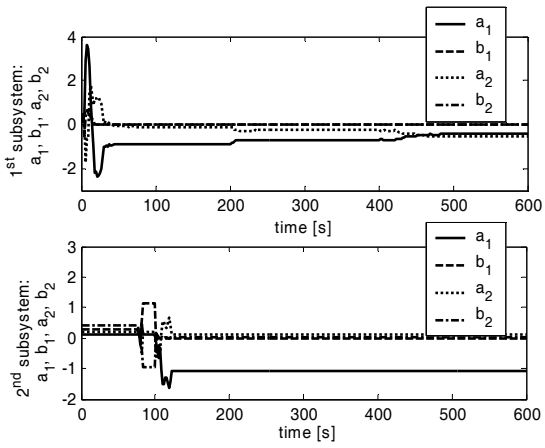

Fig. 10. Course of identification parameters during the control process with using logical supervisor

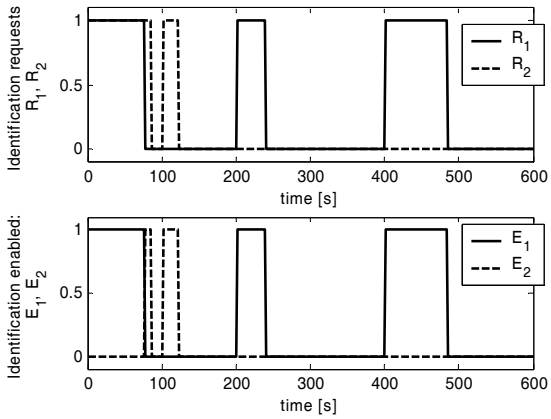

Fig. 11. Course of identification requests and identification enabled signals

5.3 Comparison of control results with and without logical supervisor

Figures 7 and 9 contain control courses of the systems without and with logical supervisor respectively. It can be seen from the Fig. 8 that the on-line identification of the second subsystem was not accurate in the first approximately 50 seconds. The control process remained stable just because the saturation of the control signal while the controller itself produced negative outputs. The small overshoot of the second subsystem in the Fig. 9 is caused by insufficient time for the identification of this subsystem and very simple method of generating identification request signals. Described method of generating identification requests led to the situation in time of about 100s where the absolute value of the control error of the second subsystem was close to zero and thus identification was not requested although on-line identification of this subsystem had not been finished yet.

By comparing courses of model parameter estimations in Fig. 8 and 10 can be seen that the system with logical supervisor does not suffer from the drift of parameters. This drift can be observed especially in the course of parameters a_1 and a_2 of the first subsystem in Fig. 8.

The control courses were also compared by calculating the two quadratic criterions of quality of controlled process. The first criterion used evaluates control error and is determined by equation 5.

$$S_e = \sum_{k=0}^{N} \left[w(k) - y(k) \right]^2; \quad N = 300 \qquad (5)$$

The second criterion used is based on differences of control signal and is determined by equation 6.

$$S_u = \sum_{k=1}^{N} \left[u(k) - u(k-1) \right]^2; \quad N = 300 \qquad (6)$$

The results for both control circuit and both subsystem are arranged in table 2.

Table 2 Comparison by quadratic criterions

		subsystem 1st	subsystem 2nd	total
without logical supervisor	S_y	11.64	5.84	17.48
	S_u	14.76	10.08	24.84
with logical supervisor	S_y	11.04	4.55	16.59
	S_u	13.39	4.87	18.26

It can be calculated that the system with logical supervisor produced better results. The difference was in range of tens of percent.

6. CONCLUSION

Logical supervisor as a hierarchical element in the decentralized control circuit was presented in this paper. The logical supervisor is responsible for enabling just one self-tuning controller to be in the adaptation phase at a particular time. Real-time experiments demonstrated that usage of logical supervisor can improve stability and accuracy of controlled process.

7. ACKNOWLEDGMENT

This work was supported in part by the Ministry of Education of the Czech Republic under grants MSM 7088352101, 1M0567, and in part by the Grant Agency of the Czech Republic under grants No.102/05/0271 and 102/06/P286.

REFERENCES

Aoki, M. (1972). On feedback stabilizability of decentralized dynamic systems, *Automatica*, **8**, Issue 2, pp. 163-173.

Blažič, S, I. Skrjanc and D. Matko (2003). Globally stable direct fuzzy model reference adaptive control, *Fuzzy Sets and Systems* **139**, pp 3 – 33.

Bobál, V., J. Böhm, J. Fessl and J. Macháček (2005). Digital Self-tuning Controllers: Algorithms, Implementation and Applications, Springer, Berlin.

Bobál, V. and P. Chalupa (2002): *Self-Tuning Controllers Simulink Library*, http://www.utb.cz/stctool/

Cui H. and E. W. Jacobsen (2002). Performance limitations in decentralized control, *Journal of Process Control*, **12**, pp. 485–494.

Kulhavý, R. (1987). Restricted exponential forgetting in real time identification, *Automatica* **23**, pp. 586 – 600.

Wang, D., D.H. Zhou, Y.H. Jin, S.J. Qin (2004). Adaptive generic model control for a class of nonlinear time-varying processes with input time delay, *Journal of Process Control* **14**, pp.517-531

ADCHEM 2006

International Symposium on Advanced Control of Chemical Processes
Gramado, Brazil – April 2-5, 2006

INJECTION VELOCITY CONTROL BASED-ON AN ITERATIVE LEARNING AND FEEDBACK COMBINED CONTROLLER

Yi Yang and Furong Gao*
Department of Chemical Engineering
Hong Kong University of Science and Technology
Hong Kong, China

Abstract: Injection velocity is a key variable in injection molding process. The dynamics of injection velocity is largely affected by the control valves used in the hydraulic system. Previously, it has been controlled precisely using advanced control algorithms based on servo-valves. However, this increased significantly the capital and maintenance costs. In this paper, the injection velocity was controlled using economical but slow response proportional valves. Iterative learning control is adopted to exploit the repetitive nature of the process for control performance improvement with the slow valves. Most nonlinearity is handled by the ILC control, with a simple feedback control incorporated to provide within-cycle disturbance rejection. Experiments show that the proposed method can work well over a wide range of operating conditions.

Keywords: Injection moulding, iterative methods, feedback control, nonlinear systems, control valves.

1. INTRODUCTION

Injection molding, a major polymer processing technique, is a typical multi-stage batch process consists of filling, packing-holding and cooling three main stages. Filling is the first stage of the molding. During filling, the polymer melt is forced into a mold cavity through the nozzle and runner system by a screw forward motion until the mold cavity is completely filled. The nature of the melt flow entering the cavity influences strongly the quality of the molded part, particularly the mechanical properties, such as tensile strength, impact strength and dimension stability. Polymer flow rate inside the mold cavity is not directly controlled due to the lack of a practical measurement. It is common to control melt pressure or ram injection velocity in filling stage, as they can be correlated well to the filling rate.

Ram injection velocity, often referred simply as injection velocity, approximates but not equal to the polymer filling rate entering a mold cavity due to the melt compressibility and the plastic leakage through the check ring valve. Despite the fact that injection velocity differs from the polymer filling rate, it is still widely used as a controlled variable during injection phase, as it provides a better approximation than the other variables such as cavity pressure or nozzle pressure. A proper setting and good control of injection velocity can achieve an evenly distributed flow pattern, avoid over-pressurization, high thermal stresses, and high residual flow stresses (Boldizar *et al.*, 1990).

Like any process control, a dynamic model is required for the injection velocity control. The modelling of injection velocity based on servo-valve controlled hydraulic systems has been studied by Davis (1976), Abu Fara (1984) and Wang *et al.* (1985).

Pandelidis and Agrawal (1987, 1988) conducted a series of control simulations for injection velocity control. Their simulation results using a self-tuning controller showed a better control performance than a traditional PID controller. However, none of their work was tested experimentally. The non-linear and time-varying characteristics of the injection velocity during the filling phase were ignored.

Extensive experimental control applications have been conducted by Gao's group. A model-free fuzzy controller was first designed by Tsoi and Gao (1999) for injection velocity control. Non-linear and time-varying characteristics of the velocity were reported. The controller rules were determined by a phase plane analysis. The controller was tested and found to work reasonably well under different molding conditions. However, this design requires the user to have extensive experience with the process, which may be not available in certain cases. Later, Yang and Gao (1999, 2000)

*-To whom correspondence should be addressed. Tel: (852) 23587139, Fax:(852)23580054, Email: kefgao@ust.hk.

adopted an adaptive self-tuning scheme for injection velocity control which includes a process model, an online model identification module and a feedback controller. They first implemented a pole-placement design as the feedback controller. Good experimental control results have been achieved for a wide range of operating conditions by incorporating some enhancements such as adaptive feedforward control and cycle-to-cycle learning. They improved the robustness of this adaptive self-tuning regulator by introducing a generalized predictive control (GPC) design. The adaptive GPC controller not only has an inherent good performance on set point tracking, but also exhibits good robustness against model mismatch. Further improvement has been focused on the process model (Li *et al.*, 2001). A fuzzy multi-model has been proposed and implemented for the injection velocity control with good experimental results.

In all the above works, the velocity control was based on servo-valves. In the current molding industry, there are two types of commonly used control valves providing directional and flow control of the hydraulic system, i.e. the servo-valve and proportional valve. A servo-valve is a device, which converts a low power electrical input signal into a proportionally higher hydraulic output with high accuracy. Servo-valve normally has complicated structure including a torque motor, a flapper valve, a spool valve for the second hydraulic stage, and an internal feedback mechanism (Rohner, 1995). Using servo-valve as the actuator for the closed-loop control produces a good control performance with fast response. However, it not only increases the capital cost but also operation cost, for example, it requires a much more sophisticated oil filtration system. The proportional valve is another type of control valves developed to fill the wide gap between simple on/off valves and sophisticated servo-valves. Corresponding to the control signal, its proportional solenoid produces a proportional spool shift for flow controls. The proportional valves have simpler structures and are much less expensive than the servo-valves. It also has good tolerance of small oil contamination. For these reasons, they are widely used in molding industry. Compared to the servo-valve, the disadvantages of the proportional valve are obvious. It has a relatively slower response, resulting in a large time constant of the hydraulic system. The input-output linearity of proportional valves is also not as good as that of the servo-valve, and severe nonlinear behavior can be observed especially during the transient stages.

In summary, though many research efforts have been put on the injection velocity control, they were mostly based on the fast response servo-valves. In practice, when slow response proportional valves are adopted to control the injection velocity, the performance is deteriorated significantly. The objective of this paper is to develop a practical robust control scheme for injection velocity using proportional valves, taking the repetitive nature of the injection molding process into account.

2. CONTROL BACKGROUND

Injection molding is a cyclic process typically lasts for several seconds to minutes. The control of such a batch process, unlike that of the continuous processes, involves keeping a defined sequence of operations. At the same time, the control system must also control the key process variables to follow certain profiles repetitively and accurately to ensure a good part quality. The disturbances can come from the materials being processed, molding machine itself, environments and human interferences. Most disturbances cause the process to drift slowly over cycles instead of abrupt changes. For example, mold temperature may increase from cycle to cycle during the warm-up stage as a result of the continuous molding operation. These disturbances are typically difficult to be accurately represented by mathematical models, but their impacts on the control system can be reflected by the change of the manipulated variables. Injection molding is a repetitive process, information of past controls may be explored for improvement of the current and future cycles. Iterative learning control, a control algorithm taking advantage of the repetitive nature of the process, can deal with the nonlinear properties of the process and slow response of the actuators therefore is a good candidate to control the injection velocity.

Iterative learning control is motivated to mimic human learning process. It is originally developed for the manipulation of industrial robots, in which it is required to repeat a given task with high precision. By using the repetitive nature of the processes, ILC progressively and iteratively improves the control accuracy along two time dimensions for control input, that is the trial (or batch) direction from trial to trial, and the elapsed time direction during a trial from step to step. This two-dimensional learning results in advantages over the conventional feedback control techniques where only one time dimensional control actions are made along the time axis. The key for a learning control design is to find an algorithm to ensure that the control input is generated for next trial in such a way that the performance is improved for each successive trial. The concept of iterative learning for generating such an input was first introduced by Uchiyama (1978) and was later mathematically formulated by Arimoto *et al.* (1984). Since then, considerable efforts have been made on the development and analysis of iterative learning control. Recently, ILC has been applied to some repetitive processes, such as batch reactor (Lee *et al.*, 1996), batch distillation, and injection molding (Havlicsek *et al.*, 1999).

The conventional ILC scheme works as an open-loop feed-forward compensator. It generates the control signals of the future cycle u_{k+1} by using the input, output, and the desired trajectory of the current cycle, u_k , y_k and r , respectively. Over past a few decades ILC has made a good advance, most practical research has focused on the P-type, D-type and modified PD-type or PID-type learning algorithms. These learning have good physical insight, and they are relatively easy to be

implemented. It has been found, however, that an ILC not using within cycle feedback tends to be sensitive to perturbation, and tends to be slow in system convergence (Bien *et al.*, 1998). Feedback combination is thus considered in this paper.

A simple but effective P-type iterative learning algorithm is adopted in this paper to control the injection velocity. It updates the control signal of the complete injection stage $[0, \ N]$ for the next cycle based on the error profile of the current cycle, as shown below:

$$u_{k+1}(t) = u_k(t) + L_p e_k(t) \qquad (1)$$

where $e_k(t) = r(t) - y_k(t)$ is the tracking error of current cycle k, and L_p is the learning rate.

3. EXPERIMENTAL SETUP

The molding machine used is a Chen-Hsong reciprocating screw injection molding machine, model JM88MKIII. The maximum machine clamping force is 88 ton, and the maximum shot weight is 128 g. A Temposonics series III displacement/velocity transducer, type RH-N-0200M, is installed to measure the injection displacement and velocity. The hydraulic system is fitted with two Bosch proportional valves, type PV-60 and QV45-RGC1, to control the hydraulic pressure and flow rate, respectively. An industrial PC was used as the control platform for the control of the injection molding machine. Two National Instruments data acquisition cards mounted in the PC are used to provide interface to the molding machine. All the programs are developed using C language under a real-time multi-task operating system, the QNX. There are two molds used in the experiments, as shown in Figure 1.

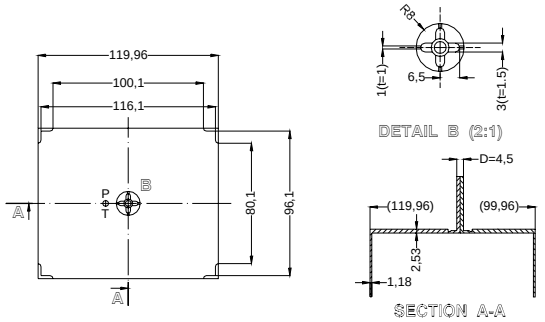

(a) Mold 1 geometry

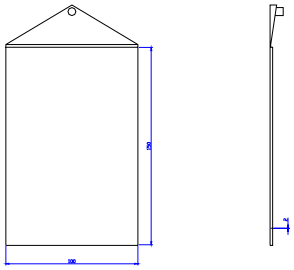

(b) Mold 2 geometry

Figure 1: Geometry of molds used in injection molding experiments.

All the experiments were conducted using material of high-density polyethylene (HDPE) unless otherwise specified.

4. RESULTS & DISCUSSIONS

4.1 Open loop tests

Some open loop experiments were conducted first for the observation of the dynamic characteristics of injection velocity, with a sampling rate of 5 millisecond. The Mold 1 shown in Figure 1(a) was used first with the proportional valve opening step-up change from 42% to 48% at 600ms of injection time. The results are shown in Figure 2(a) where dot line shows the valve opening and the solid line indicates the corresponding injection velocity response. It is obvious that the injection velocity exhibits large over-shoot in the initial stage of filling. When a valve opening step change was applied, the injection velocity has a relatively slow response with large over-shoot. The nonlinear response of the injection velocity is mainly due to the hydraulic system and complicated rheological properties of the polymer melt. The nonlinear and time-varying characteristics of injection velocity have been analyzed extensively in References (Tsoi *et al.*, 1999 and Yang *et al.*, 2000). With the replacement of the control actuators from the servo-valves to proportional valves, the nonlinearity has become even severe.

Another open loop experiment was conducted using the Mold 2 shown in Figure 1(b). The results are plotted in Figure 2(b). A constant valve opening of 60%, significantly larger than the opening used in Mold 1, has been applied, as indicated by the dot line in Figure 2(b). The corresponding injection velocity response, as shown by the solid line, is significantly different from that of Mold 1. This result not only proves the nonlinear characteristics but also shows that the injection velocity dynamics changes significantly with different molds used in the experiments.

4.2 Determination of delay and sampling rate

A P-type learning algorithm has been selected to control the injection velocity in this paper, as formulated in Equation (1). The advantage of using P-type learning is that it is a simple and effective ILC method, and the design of P-type learning does not require any process model, hence be beneficial to industrial implementation. However, Equation (1) cannot be applied to injection velocity control directly, due to the process delay. It must be modified to take the delay into consideration, as shown in the following:

$$u_{k+1}(t) = u_k(t) + L_p e_k(t + t_d) \qquad (2)$$

where t_d is the time delay of injection velocity. It has been observed that the order of t_d is important for the successful implementation of ILC. A delay mismatch may cause the accumulation of control errors and results in an oscillatory control after several cycles. It is therefore decided to use the open loop velocity response to identify the delay orders first.

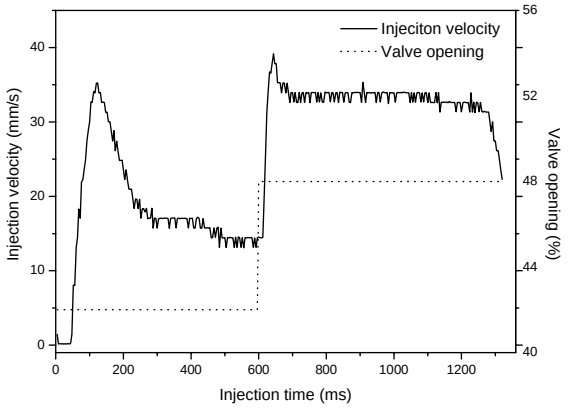

(a) Mold 1 open loop test

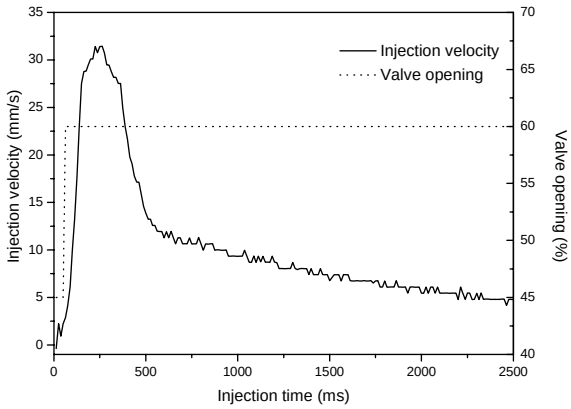

(b) Mold 2 open loop test

Figure 2: Open loop injection velocity response of two molds

The injection velocity response to the process input, the proportional valve opening, is represented by a discrete z-transform equation:

$$A(z)y(t) = B(z)u(t - n_d) + e(t) \quad (3)$$

where y is the velocity output, u is the control action (the proportional valve opening), and:

$$A(z) = 1 + a_1 z^{-1} + ... + a_{na} z^{-na},$$

$$B(z) = (b_0 + b_1 z^{-1} + ... + b_{nb-1} z^{-nb+1}) \cdot z^{-nd} \quad (4)$$

Na and nb are the orders of A and B polynomials, nd represents the delay order of the process. Equation 3 is the velocity model in AutoRegressive with eXternal input (ARX) form. The open loop response of Mold 1 was used for the model identification. To identify the delay order accurately, this open loop response was fitted into the ARX model with same na and nb values but different delay order. The na and nb were determined both to be 3, as the process is unlikely to be a higher order system. The model prediction loss function as well as the Akaike's Final Predictive Errors (FPE) are used to determine the degree of model matching (Ljung, 1987). The resulted loss functions and FPE values with respect to different delay orders are plotted in Figure 3. It is clearly shown that the prediction reaches its best performance when nd=5, i.e. 25 millisecond. The sampling rate is thus decided to be 12.5, half of the process delay.

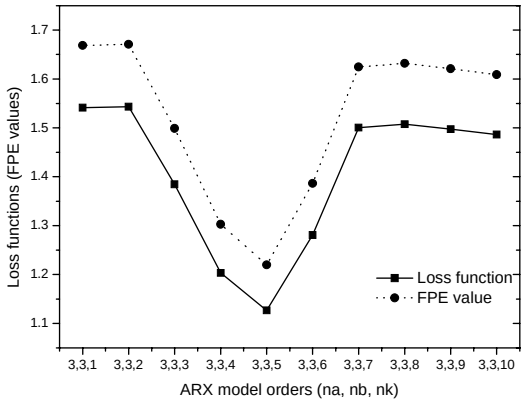

Figure 3: Determination of delay orders using loss functions and FPE values

4.3 Incorporation of feedback control

The ILC law as formulated by Equation (2) was thus implemented to control injection velocity with a sampling rate of 12.5 ms, and delay order of 2. The learning rate is determined to be 0.025 through inversion of the process gain. The experimental results with Mold 1 and material of HDPE are shown in Figure 4, where Figure 4a plots the injection velocity measurements and Figure 4b plots the corresponding proportional valve opening. A step down velocity profile was selected, as shown by the solid gray line in Figure 4a. The first cycle, as indicated by the dash line, was open loop controlled with an arbitrary constant valve opening of 46%. The second cycle's injection velocity, shown by the dash-dot line, quickly approaches to the set point. The velocity response of the 10th cycle, plotted by the solid line, is very close to the set point profile. The control results prove the learning capability of ILC scheme. Notice that the valve opening was adjusted before the set point step change, thus the injection velocity can follow the set point profile closely without delay. This observation shows the inherent advantage of ILC. However, there are several problems in this result. First the initial stage control is still oscillatory and steady state noisy result is still obvious. These problems are mainly due to the lack of within cycle feedback control. It has been reported that ILC without feedback action tends to be susceptible to the process noise and hence to be unstable. Therefore, a simple integral feedback control is added to the original ILC to enhance the noise rejection capability of the velocity controller and eliminate the steady-state errors. The ILC incorporated with the I-type feedback control can be written as follows,

$$u_k(t) = u_{k-ff}(t) + u_{k-fb}(t) \quad (5)$$

where $u_{k-ff}(t)$ is the feedforward or learning control action calculated using Equation (2) and $u_{k-fb}(t)$ is the feedback control action calculated as below,

$$u_{k-fb}(t) = u_{k-fb}(t-1) + k_i \cdot e_k(t) \quad (6)$$

The proportional control gain ki is tuned using trial and error method, and determined to be 0.005.

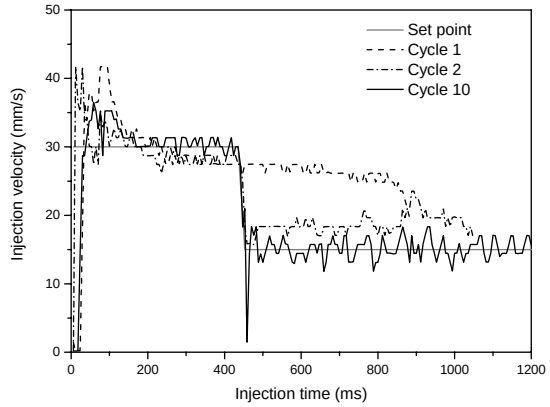

(a) Injection velocity measurements

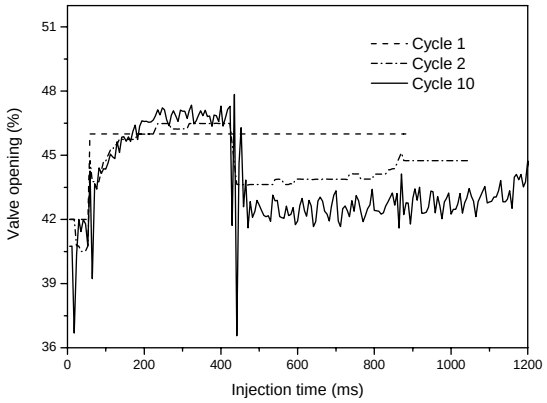

(b) Corresponding valve opening

Figure 4: Injection velocity iterative learning control without feedback enhancement

The control results with ILC and I-type feedback control are shown in Figure 5. The injection velocity measurements are shown in Figure 5a, and zoomed-in plot around the set point step change is shown in Figure 5b. All the other experimental conditions are the same as previous. Due to space limitation, the corresponding valve openings are not shown in this paper. It is clearly shown that with the incorporation of the feedback control, the control performance is improved throughout the filling stage and the steady state responses are smoother than before. It is also clearly shown in Figure 5b that in the 10th cycle the set point step change has been closely followed, despite the slow response of the proportional valves.

4.4 Different operation conditions

The designed ILC controller with I-type feedback has been tested with different operating conditions to evaluate the control performance. As the injection velocity varies significantly with mold geometry, a different mold, Mold 2, was tested first. The injection velocity control results are shown in Figure 6. The valve opening of the first cycle was arbitrarily set to be 60%. It is shown in Figure 6 that although the control converges to the constant set point value eventually, i.e. after 17 cycles, the convergence rate is too slow. This slow convergence rate is undesirable in industry. There are mainly two methods to speed up the convergence, to increase the learning rate, or to improve the first cycle's control performance. A conservative PI controller was tuned to control the injection velocity in the first cycle, and the same learning rate was used for the rest of cycles. The control results are shown in Figure 7. This time the control only takes about 5 cycles to converge, hence proves the effectiveness of this improvement.

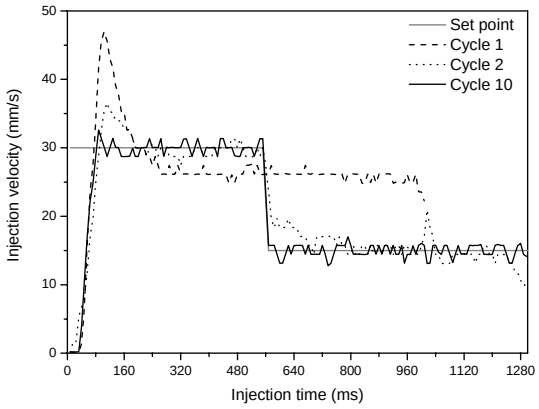

(a) Injection velocity measurements

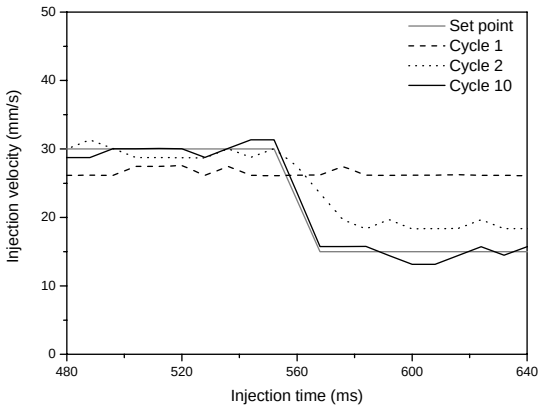

(b) Zoomed-in plot around step change

Figure 5: Injection velocity iterative learning control with feedback enhancement

Different material, namely polypropylene (PP) was also tested experimentally. The injection velocity control results using PP were shown in Figure 8. The control quickly converges to the set point, which is a step down profile. The 10th cycle's injection velocity measurement is the fastest response without overshoot and it almost overlaps with the set point despite the slow response of the proportional valves, indicating the good performance of the control system.

5. CONCLUSIONS

An iterative learning control system has been adopted in this paper to control the injection velocity. Open loop tests have demonstrated the nonlinearity and slow response of the velocity dynamics. By proper selection of the sampling time and delay order, the ILC, enhanced with an integral feedback control, can effectively control the injection velocity. The designed system has been experimentally tested to work well for a wide range of operating conditions.

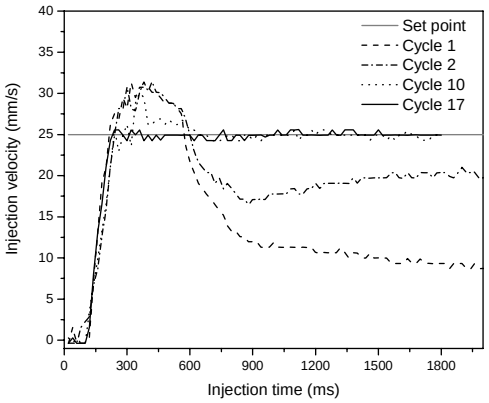

Figure 6: Injection velocity iterative learning control using Mold 2, 1st cycle opening loop control

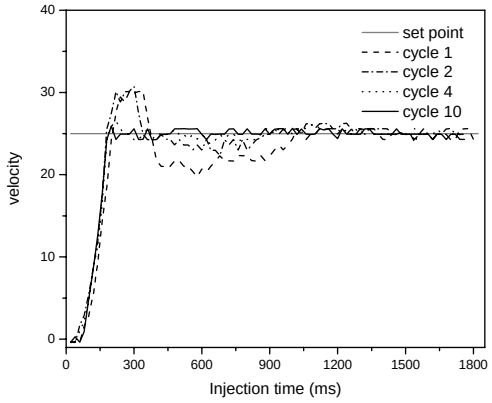

Figure 7: Injection velocity iterative learning control using Mold 2, 1st cycle closed-loop control

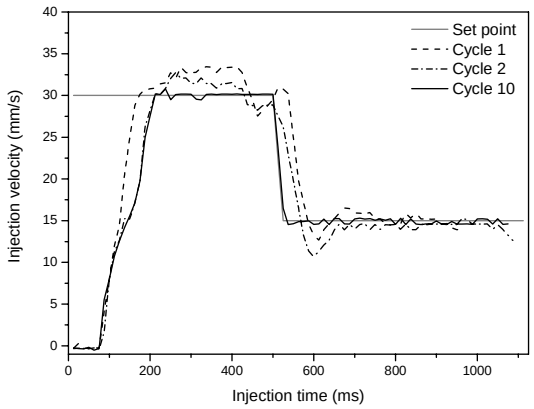

Figure 8: Injection velocity iterative learning control using PP

REFERENCES

Abu Fara D. (1984). *M.Eng. Thesis.* McGill University, Montreal, Canada.

Arimoto S., Kawamura S. and Miyazaki F. (1984). Bettering operation of robots by learning. *Journal of Robotic Systems*, **1**, 123.

Bien Z. and Xu J.-X. (1998). *Iterative Learning Control: Analysis, Design, Integration and Applications.* Kluwer Academic Publishers, Boston /Dordrecht/ London.

Boldizar A., Kubat J. and Rigdahl M. (1990). Influence of mold filling rate and gate geometry on the modulus of high pressure injection-molded polyethylene. *Journal of Applied Polymer Science*, **39**, 63.

Davis M. A. (1976). Servocontrolled injection molding. *SPE Annual Technical Conference Paper*, **22**, 618.

Havlicsek H., and Alleyne A. (1999). Nonlinear control of an electrohydraulic injection molding machine via iterative adaptive learning. *IEEE/ASME Transactions on Mechatronics*, **4**, 312.

Lee K. S., Bang S. H., Yi S., Son J. S. and Yoon S. C. (1996). Iterative learning control of heat up phase for a batch polymerization reactor. *Journal of Process Control*, **6**(4), 255.

Li M. Z., Yang Y., Gao F., Wang F. L. (2001). Fuzzy Multi-Model Based Adaptive Predictive Control and Its Application to Thermoplastic Injection Molding. *Canadian Journal of Chemical Engineering*, **79**, 263.

Ljung L. (1987). *System identification: theory for the user*. Englewood Cliffs, NJ: Prentice-Hall, New Jersey, U. S. A.

Pandelidis I. O. and Agrawal A. R. (1987). Self-tuning control of ram velocity in injection molding. *SPE Annual Technical Conference Paper*, **33**, 235.

Pandelidis I. O. and Agrawal A. R. (1988). Optimal anticipatory control of ram velocity in injection molding. *Polymer Engineering and Science*, **28**, 147.

Rohner P. (1995). *Industrial Hydraulic Control (4th Edition)*. John Wiley & Sons, Milton, Australia.

Tsoi H.-P. and Gao F.-R. (1999). Control of injection velocity using a fuzzy logic rule-based controller for thermoplastics injection molding. *Polymer Engineering and Science*, **39**, 3.

Uchiyama M. (1978). Formation of high-speed motion pattern of a mechanical arm by trial. *Transactions of SICE (Society for Implementation and Control Engineers) (in Japanese)*, **14**, 706.

Wang K. K., Shen S. F., Cohen C., Hieber A. C., Kwon T. H. and Ricketson R. C. (1985). *Progress Report No. 11*. Cornell University, Ithaca, New York, U.S.A.

Yang Y. and Gao F.-R., (1999). Injection velocity control using a self-tuning controller for thermoplastic injection molding. *International Polymer Processing*, **XIV**, 196.

Yang Y. and Gao F. (2000). Adaptive Control of the Filling Velocity of Thermoplastics Injection Molding. *Control Engineering Practice*, **8**, 1285.

ADCHEM 2006

International Symposium on Advanced Control of Chemical Processes
Gramado, Brazil – April 2-5, 2006

CONTROLLING THE PERFORMANCE OF A CYCLONIC OIL-WATER SEPARATION SYSTEM

Giovani Cavalcanti Nunes[1*], Magno Antonio Calil[2], Enrique Luis Lima[2]

[1]*Research Centre of PETROBRAS-CENPES*
22411.001-Rio de Janeiro-RJ-Brazil
E-mail: giovanicn@.petrobras.com.br

[2] *Chemical Engineering Program, COPPE-UFRJ*
BOX 68502-21945.970- Rio de Janeiro-RJ-Brazil
E-mail: magno,enrique@peq.coppe.ufrj.br

Abstract: This work analyzes various configurations for the control of a recently developed compact oil-water separation process for offshore production platforms consisting of a gravity separator and a sequence of three modules of hydrocyclones. Three different control algorithms were compared for interface level control in the separator: proportional and integral, band and linear model predictive control. These algorithms were combined with a classical differential pressure ratio (DPR) control for the modules of hydrocyclones. Results have shown that band control is a promising approach for the interface level and that the DPR control is better if only used in the last module of the sequence of hydrocyclones.

Keywords: Process control, control algorithms, load regulation, level control, process models.

1. INTRODUCTION

In petroleum production plants, gravity separators are used for three-phase separation of gas, oil and water. Its inflow is oscillatory, frequently characterized by slugs of liquid and gas coming from the wells, a flow regime generically named slug flow. Proportional and integral (PI) controllers are used for level and pressure control. Precise load regulation is adopted to avoid upsets such as liquid carry over, gas carry under, etc. As the integral mode guarantees an offset free response for the controlled variables - level and pressure - flow perturbations are not filtered and oscillations are propagated to the downstream equipments.

Recently flow conditions in offshore platforms are becoming more stringent and higher amplitude slugs have achieved frequencies that result in significant degradation of performance of such plants. Furthermore, in a move to reduce dimensions of offshore platforms, very compact equipments are increasingly more used for water and oil treatment. One such case is the development of a more efficient water treatment system, based on hydrocyclone technology. A sequence of three different types of hydrocyclones, designed for very high oil concentration streams, is being researched. Although the resulting unit is very small its reduced volume makes it extremely sensitive to oscillations. In this case a control algorithm that is able to dampen the outflow of gravity separators should be crucial.

This is known as the problem of level control for surge tanks and has been studied extensively since the 1960s (Buckley, 1964; Shinskey, 1967). The objective is to use the vessels capacity to filter inlet flow disturbances, reducing its propagation to downstream equipments. As level constraints limit the tanks usable inventory, a trade off must be met between filtering capacity and allowable – within bounds - performance. For this purpose innumerous control strategies, from linear to non-linear, have been proposed and analyzed (Cheung and Luyben, l979 (a), l979 (b) and l980; McDonald and McAvoy,

*Corresponding author

l986; Campo and Morari, l989; Friedman, l999; Bequette, l998; Nunes, 2005).

Over the last two years Petrobras has implemented what has been named “band control” in the gravity separators of several of its platforms (Nunes, 2005). Its simplicity has attracted operators and helped popularize the algorithm in Petrobras. However its application has been restricted to the level control of two phase (gas-liquid) separators. For the oil-water interface no application has yet been reported.

In this article three different control (PI, band and linear model predictive - MPC) strategies are studied for the control of the oil-water interface level in a separation system made up of a three-phase gravity separator and three modules of hydrocyclones.

2. SYSTEM DESCRIPTION

In offshore production plants, Figure 1, gravity separators, compressors, hydrocyclones (de-oilers) and electrostatic treaters are used to specify oil, gas and water for exportation. Electrostatic treaters execute the de-hydration of oil and hydrocyclones de-oil the water. As no recycling occurs a simple structure of vessels in series results. Although this sequence of accumulation vessels indicate that substantial attenuation of feed can be obtained if proper control is done, fast acting loops designed for disturbance rejection propagate the disturbances of flow rate.

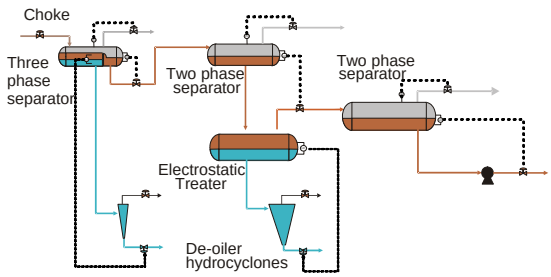

Fig. 1. Offshore process plant

Typically the water discharged by the three phase separator has a concentration of oil of approximately 0.1 % (1000 ppm). Hydrocyclones known as “de-oilers” execute further treatment of such streams reducing the oil concentration to approximately 200 ppm after which it is sent to flotation units for final specification at 20 ppm.

Recently Petrobras has been investigating the use of high oil concentration hydrocyclones in what is expected to be a more compact water treatment system able to debottleneck existing plants by discharging more water from the three phase separators. The proposed configuration, Figure 2, is made up of a sequence of three modules of hydrocyclones able to treat water streams with very high oil concentrations (as much as 30% of oil). The first hydrocyclone, known as BOW (for bulk oil-water cyclone) reduces the oil concentration to approximately 15%. The second is the PDC (pre de-oiler cyclone), which extracts most of the oil in order to specify the water at the 1000 ppm required by the de-oilers. The oily water is then sent to the third cyclone, which is the DC (de-oiler cyclone itself).

Typically hydrocyclones are controlled to maintain a certain ratio of pressure drops (DPR) between the overflow and underflow, which results in a constant ratio of flow rates. This strategy assumes constant oil concentration in the outflow of the separator. This is achieved by adopting a (oil-water interface) level regulator designed for disturbance rejection – a proportional and integral controller with high gain. As a drawback to this approach flow rate disturbances are propagated to the hydrocyclones.

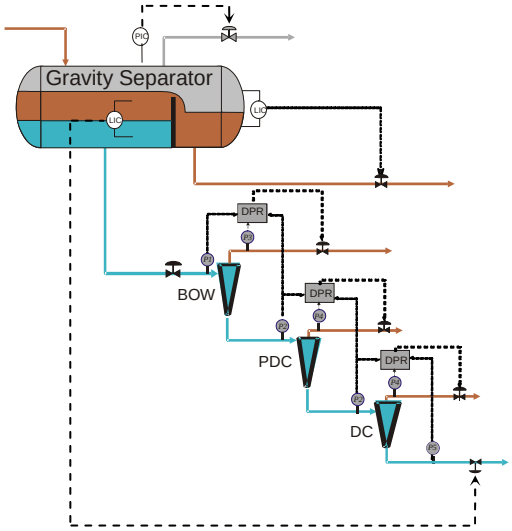

Figure 2 Cyclonic water treatment unit

Thus a good control strategy should try to maintain flowrate and oil concentration both as constant as possible. The ultimate goal is to achieve maximum oil-water separation performance for the whole water treatment system, under periodical oscillations in the feed of the gravity separator.

3. SYSTEM MODELING

The three phase gravity separator is described by a simplified dynamic phenomenological model (Nunes, 2001), based on mass balances in three regions, easily identified in Figure 2: separation chamber, oil chamber and gas space. Dispersed droplets trajectories are calculated and a population balance is done to estimate the oil-water separation efficiency. This model is able to correctly predict the trends in oil-water separation under dynamic changes.

For this investigation it was considered a 5.4m long horizontal cylindrical separator, with a diameter of 1.8m. The separation chamber is 4.4m long and is separated from the oil chamber by a 1m weir. The average values of the liquid (oil and water) and gas feed flow rates were, respectively, 1.962 and 7.8 m^3/min.

Due to negligible residence time ($\approx$ 2s), compared to separators ($\approx$ 600s) hydrocyclones can be considered

in quasi-steady state. They are modeled following a phenomenological approach relating oil separation efficiency with input flow rate and oil concentration (Moraes, l994, Wolbert et al., l995). Efficiency is calculated based on the oil droplets trajectories in the system; droplets bellow a certain size leave the hydrocyclones through the underflow.
For the high oil concentration hydrocyclones – BOW and PDC - no phenomenological models, which could be useful for control analysis, have been reported. This is a consequence of the very complex nature of the two-phase (oil and water emulsions) flow. Thus field experiments were executed to generate the required empirical models (Moraes, 2005).

In this work six BOW hydrocyclones were used in the first module, six PDC in the second module and five DC in the last one.

4. CONTROL STRATEGIES AND RESULTS

The main control objective for the system depicted in Figure 2 is to maintain the quality of the water phase leaving the underflow of the DC module, rejecting the negative effect of a periodical slug water flow fed to the separator, shown in Figure 3.

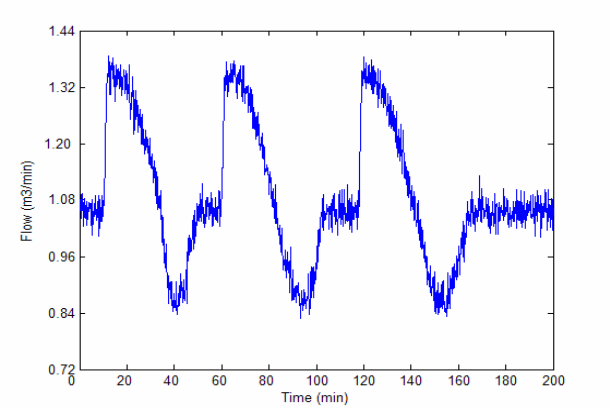

Fig. 3. Periodic input slug water flow

As shown in Figure 2, the controlled variables of the system are the oil-water interface level in the separation chamber, the level in the oil chamber, the separator pressure and the oil concentration in the DC module underflow stream. The manipulated variables are the flow rate of the DC underflow (water phase), the oil outlet flow rate of the separator, the gas outlet flow rate of the separator and the flow rates of the overflow of the hydrocyclones.

Because of one-way interaction a decentralized control scheme was adopted for the separator, with PI controllers for separator pressure and oil chamber level. For these controllers the following tuning was used: oil level, T_I (reset time) = 0.5 min, K_c (proportional gain) = -390 %/m; pressure, T_I = 1,65min, K_c = -24 %/kg_f/cm^2. It should be noted that tuning values for all control strategies used in this work were obtained by a trial and error approach.

As already mention, for the interface level in the separation chamber three different control strategies were tried: PI, band and MPC.

The first one was used as a reference, taking into account that it is the most popular approach for surge tank level control (Friedman, l999).

Band control strategy considers two different control laws depending on the interface level position. When this level is between certain limits of a band, the control action is a combination of two signals, one proportional to the measured error and the other an average of the manipulated variable, in this case inferred from the valve position. The average value is calculated along the period of the slug flow. This control law can be explained as follows.

Due to high operation pressure ($\approx$ 10 kg_f/cm^2) the separation chamber behaves almost as a surge tank (an integrator). Consider a simplified model of this system

$$\frac{dy}{dt} = d - u \tag{1}$$

where y represents volume, d the input flow and u the output flow.

For a periodic perturbation a smooth output requires $u = \bar{d}$, where $\bar{d}$ is the average value of the perturbation. Using Equation (1), this value can be inferred from

$$\bar{d} = \bar{u} + \frac{d\bar{y}}{dt} \tag{2}$$

$$\bar{d} = \frac{1}{T}\left[\int_{t-T}^{t} u \cdot d\tau + y(t) - y(t-T)\right] \tag{3}$$

To simplify this approach, and to follow variations of the input average value, it was proposed the following modification (Nunes et al., 2005)

$$\bar{d} = \frac{1}{T}\int_{t-T}^{t} u \cdot d\tau + K(r - y) \tag{4}$$

where r is the reference value for y.

The transfer function of the resulting control law is

$$u(s) = \frac{KTs}{Ts - 1 + e^{-Ts}}\left[r(s) - y(s)\right] \tag{5}$$

This control law is similar to the PI, with the advantage that the average operation produces smoothing effect on the control signal.

When the band limits are exceeded a stronger PI control law (K_{cout}, T_{Iout}) takes action to return the level to these limits, and to recover the surge capacity of the separator.

Predictive control (McDonald and McAvoy, l986) was selected because, although more complex than the other two algorithms, it allows a direct weighting of two desired but opposite objectives: constant level - implying in constant composition - and constant output rate flow.

Initially the three modules of hydrocyclones were controlled using a DPR scheme, as shown in Figure 2. This scheme keeps a constant ratio between the two pressure drops: the inlet-overflow, and the inlet-underflow pressure drops. Depending on the oil concentration of the input flow, BOW and PDC hydrocyclones have an ideal DPR value that results in the best separation performance. These ideal values were adaptively inferred using correlations built from field experimental data. For all the simulations the DPR for DC hydrocyclones was fixed at the design value, 2.5. To keep these DPR values at the desired setpoint, PI controllers were used to manipulate the overflow flow rates for any change in the underflow flow rates.

Results obtained when controllers were tuned for the best performance for each separator interface level control strategy, PI, band, and MPC, are presented in Figures 4-6. The tuning parameters are listed in Table 1 in terms of the corresponding control loops: BOW overflow, PDC overflow, DC overflow and DC underflow. Recall that DPR control schemes are based on PI controllers.

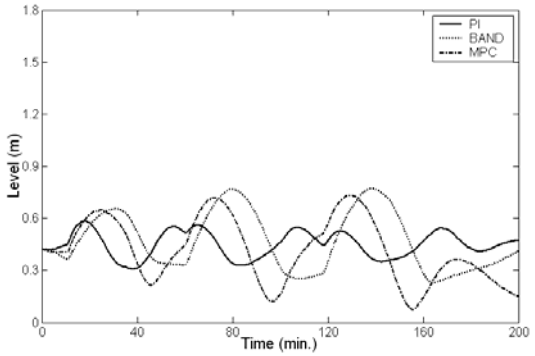

Fig. 4. Oil-water interface level in the separator

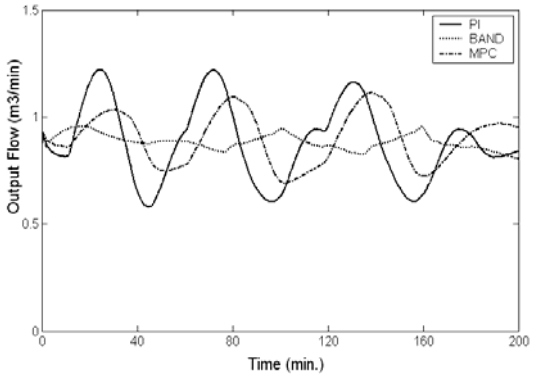

Fig. 5. Water outlet flow rate from the separator

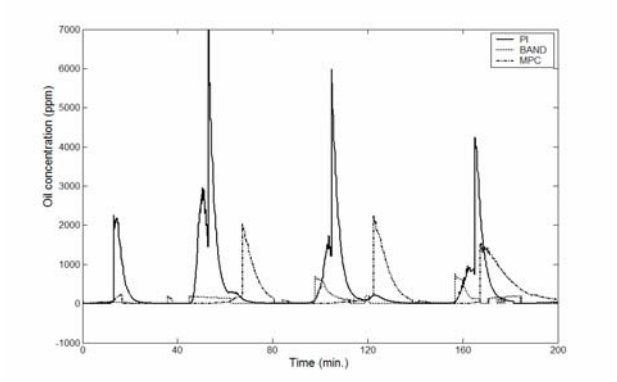

Fig. 6. DC underflow oil concentrations

It can be seen in Figures 4 and 5 that all three controllers manage to maintain the interface level out of the dangerous regions (0.1-0.9m). Although MPC control produces the oscillations of biggest magnitude in the interface level, it was the band control that results in smoother variations of the output flow rate. This is a good result for a surge tank but it should be noted that oscillations of the level produce oscillations of the oil concentration that can modify the separation efficiency of the downstream hydrocyclones.

Figure 6 shows an irregular behavior for the main controlled variable. Again it is clear that the band strategy presents the better performance, but also in this case the system shows significant sensibility to interface level and flow rate variations

The reason for this behavior could be related to the use of DPR control strategies for the three cyclones modules. Although the interface level controller acts directly on the underflow rate flow of the DC module, the DPR strategies indirectly modified the overflow flow rate of each module, not always resulting in a smooth rate flow from the separator.

Table 1 Controllers tuning parameters when using DPR control for all hydrocyclones modules

Loop	PI	Band	MPC
BOW	K_c=3.5	4.0	3.5
overflow	T_I=0.8	0.8	0.8
PDC	K_c=4.0	1.0	2.0
overflow	T_I=0.8	0.8	0.8
DC	K_c=8.0	8.0	8.0
overflow	T_I=0.8	0.8	0.8
DC	K_c=-200	K=-0.2	P=10
underflow	T_I=15	T=13	M=1
		K_{cout}=-180	γ=60
		T_{Iout}=50	λ=30

overflow: K_c[=]%/kg$_f$/cm^2, T_I[=]min; underflow: K_c[=]%/m, T_I[=]min, T[=]min; P: prediction horizon; M: control horizon;γ: controlled variable weight;λ: control variable change weight.

To investigate this behavior a new control configuration was used manipulating the flow rates of the DC module underflow, and the BOW and PDC modules overflows to control the separator interface level. DPR was controlled only for the DC module.

Results of this new strategy can be seen in Figures 7-9, for the same variables of Figures 4-6. The tuning parameters of the controllers for this case are listed in Table 2.

From these figures it can be seen that the new control configuration has produced better results, especially with respect to the main controlled variable, the oil concentration at the DC module underflow. Comparing Figures 6 and 9 it is clear that all three algorithms produce acceptable results for the interface level control, although the band strategy again shows to be slightly better than the other two.

Table 2 Controllers tuning parameters when using DPR control only for DC module

Loop	PI	Band	MPC
BOW overflow	K_c=-10.0 T_I=3	-10.0 4	-10.0 4
PDC overflow	K_c=-10.0 T_I=3	-10.0 4	-10.0 4
DC overflow	K_c=6.0 T_I=0.8	8.0 0.8	6.0 3
DC underflow	K_c=-50.0 T_I=15	K=-0.2 T=13 K_{cout}=-180.0 T_{Iout}=50	P=10 M=1 γ=80 λ=5

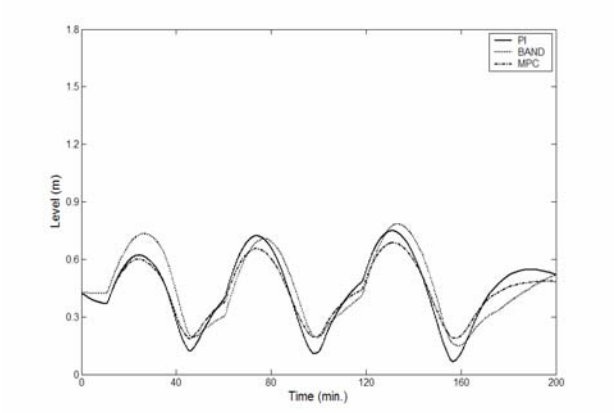

Fig. 7. Interface level without DPR control in BOW and PDC hydrocyclones modules

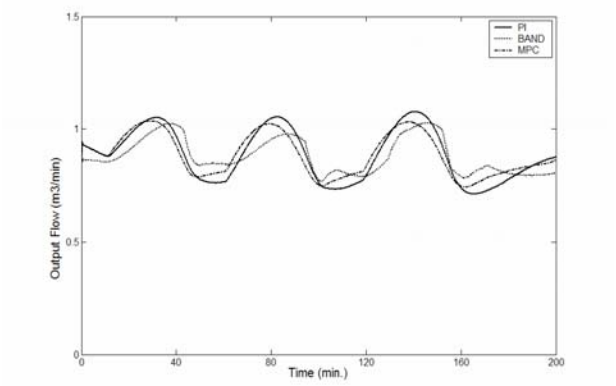

Fig. 8. Output flow rate without DPR control in BOW and PDC hydrocyclones modules

The nice results produced by the new cocntrol configuration are mainly the consequence of a better efficiency in the PDC module. This can be clearly observed comparing results in Figures 10 and 11, representing this efficiency for the original and the new control configurations, respectively. Note the difference of scales in these figures, necessary due to the high regular efficiency in the second case.

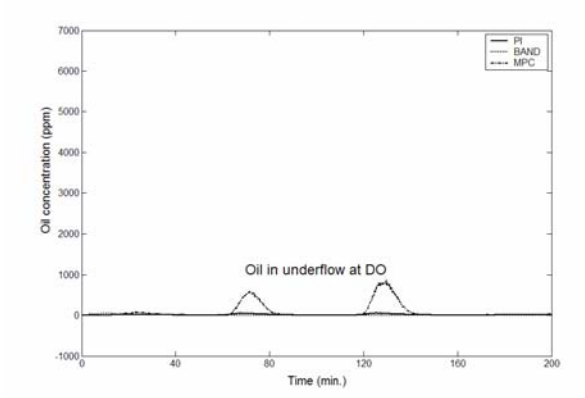

Fig. 9. Oil concentration without DPR control in BOW and PDC hydrocyclones modules

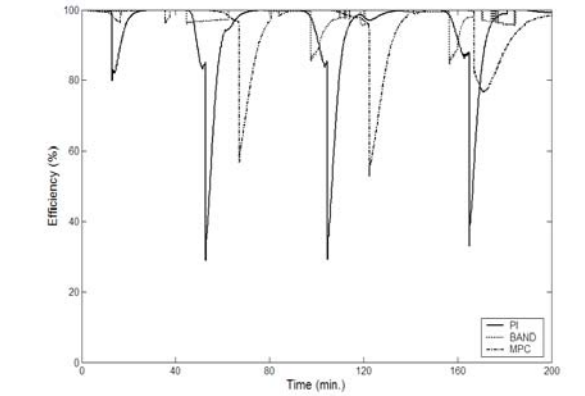

Fig. 10. PDC module efficiency with DPR control in BOW, PDC and DC hydrocyclones modules

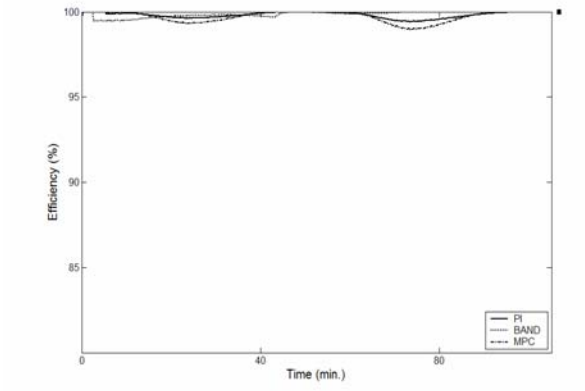

Fig. 11. PDC module efficiency without DPR control in BOW and PDC hydrocyclones modules

5. CONCLUSIONS

This work analyzes some preliminary control aspects of a new configuration for the primary treatment in offshore platforms. Although this configuration will

reduce the size of primary treatment units, it presents important operational constraints associated with the fast dynamic behavior of the hydrocyclones. The classical DPR control strategy seems to be of limited use if applied to a sequence of modules of hydrocyclones. When this strategy was applied only to the last module of the sequence the performance of the global system was significantly better than when it was used for all the cyclones modules. Another result of this analysis was that the band controller represents a satisfactory solution for the interface level control problem, especially considering that it is very simple to be implemented in commercial hardware.

We consider that these are preliminary results for the solution of a problem that deserves more investigation, as it is just one part of a more complex system that certainly will require optimization and multivariable control approaches. These problems are nowadays under investigation

ACKNOWLEDGMENT

The authors would like to thank CNPq and PETROBRAS for financial and technical support.

REFERENCES

Bequette, B. W. (1998). Practical Approaches in Nonlinear Control. In: *Nonlinear Model Based Control* (R. Berber and C. Kravaris. (Ed)), 3-32. Kluwer Academic Publisher, Netherlands.

Bukley, P. S. (1964). *Techniques of Process Control*, p. 167, Wiley, New York.

Campo, P. J. and M. Morari (1989). Model Predictive Optimal Averaging Level Control. *AIChE Journal*, **35**, 579-591.

Cheung, T. and W. L. Luyben (1979a). Liquid-Level Control in Single Tanks and Cascades of Tanks with Proportional-Only and Proportional-Integral Feedback Controllers. *Ind. Eng. Chem. Fundam.*, **18**, 15-21.

Cheung, T. and W. L. Luyben (1979b). A Further Study of the PL Level Controller. *ISA Transactions*, **18**, 73-77.

Cheung, T. and W. L. Luyben (1980). Nonlinear and Nonconventional Liquid Level Controllers. *Ind. Eng. Chem. Fundam.*, **19**, 93-98.

Friedman, Y. Z. (1999). Tuning Averaging Level Controllers. In: *Advanced Process Control and Information Systems for the Process Industries* (L. A. Kane. (Ed.)), 302-310. Gulf Publishing Company, Houston, Texas.

McDonald, K. A. and T. J. McAvoy (1986). Optimal Averaging Level Control. *AIChE Journal*, **32**, 75-86.

Moraes, C. A. C. (1994). Hydrodynamic Model for Efficiency Estimation in Hydrocyclones for Oily Water (in portuguese). *MSc. Thesis*, Federal University of Rio de Janeiro, Brazil.

Moraes, C. A. C. and Nunes, G. C. (2005). Technical Report RT-TE 003/2005, CENPES, Petrobras, Brazil.

Nunes, G. C. (2001). Design and Analysis of Multivariable Predictive Control Applied to an Oil-Water-Gas Separator. *PhD Dissertation*, University of Florida.

Nunes, G. C., Coelho, A. A. R., Sumar, R. R. and R. I. G. Mejín (2005). Band Control: Concepts and Application in Dampening Oscillations of Feed of Petroleum Production Units. *16th IFAC WORLD CONGRESS*, Prague, July 3-8.

Shinskey, F. G. (1967). *Process Control Systems*, p. 147, McGraw-Hill, New York.

Wolber, D., Ma, F. and Y. Aurelle (l995). Efficiency Estimation of Liquid-Liquid Hydrocyclones Using Trajectory Analysis. *AIChE Journal*, **41**, 1395-14

ADCHEM 2006

International Symposium on Advanced Control of Chemical Processes
Gramado, Brazil – April 2-5, 2006

ROBUST MPC OF THE REFINING STAGE OF AN ELECTRIC ARC FURNACE

L.C. Coetzee * **I.K. Craig** **

* *Department of Electrical, Electronic and Computer Engineering, University of Pretoria, Pretoria, 0002, South Africa. Tel. +27 12 998 9853 Fax.+27 82 131 558 2699*
Email: loutjie@tuks.co.za
** *Email: icraig@postino.up.ac.za*

Abstract: In this article a robust MPC controller is presented for the refining stage of an electric arc furnace. A reduced version of a generic EAF model will be used - it simplifies the controller. The controller's objective is to steer the temperature to the desired value before the carbon content reaches its target value. The controller design is verified through a simulation study. The controller behaves well even under extreme model mismatch when full state feedback is used, but is high dependent on the accuracy of the predictor under limited feedback conditions. With timely measurement, the error can be contained and even reduced if the predictor's parameters are adjusted when measurements are taken.

Keywords: Robust model predictive control, RMPC, electric arc furnace, EAF, steel making

1. INTRODUCTION

At the heart of recycling scrap metal into steel is the electric arc furnace (EAF). The electric arc furnace primarily uses an electric arc to generate the heat required to melt the scrap metal and refine it to steel. The process is still dominantly operator controlled, often resulting in suboptimal and inconsistent steel quality. The use of electric arc furnaces is growing world wide, and the process can benefit from increased automation in improving overall steel quality as well as improving the economics of the process. Automation could also improve the safety of this dangerous process, as well as reduce its negative effects on the environment (Bekker *et al.*, 2000).

In order to design and implement control, a suitable mathematical model is needed. There are different approaches to model the electric arc furnace process. The one approach is to model the process as containing equilibrium zones with mass transport transport between the zones (Cameron *et al.*, 1998; Matson and Ramirez, 1999; Modigell *et al.*, 2001). Some models tend to be proprietary (Morales *et al.*, 1997). An alternate approach was taken by Bekker *et al.* (1999) who derived a model from fundamental thermodynamic and kinetic relationships that resulted in a generic nonlinear model consisting of 17 ordinary differential equations (ODE). This generic model was then fitted to actual plant data by Rathaba (2004).

The following stage was to investigate the feasibility of control on this model. First efforts focused on the off-gas subsystem (Bekker *et al.*, 2000) by controlling the relative furnace pressure, CO emissions as well as the off-gas temperature. Oosthuizen *et al.* (2004) extended the scope by

incorporating economic objectives into the control strategy.

The EAF process consists of three phases, the first two are meltdown phases and the last phase is called the refining phase, where the final grade of the steel is determined. During the refining stage, certain simplifying assumptions can be made with regards to the model in order to reduce it to only 5 ODEs (Rathaba, 2004). The reduced model is better suited for control, because it reduces the computational burden. Coetzee *et al.* (2005) applied nominal MPC to the reduced model, but the modelling effort by Rathaba (2004) revealed model uncertainties that could not be explicitly incorporated into the controller design.

The application of robust MPC to this problem was therefore investigated, as discussed in this paper. Two robust MPC methods were investigated for this paper. Firstly, a linear matrix inequalities (LMI) based robust MPC technique has been developed by Kothare *et al.* (1996). The technique was improved by Cuzzola *et al.* (2002) and Ding *et al.* (2004). This technique is limited to symmetric constraints on the inputs and use ellipsoid invariant sets, that makes it conservative. The on-line optimization is based on semi-definite programming (SDP) and is very slow compared to quadratic programming (QP). Secondly, a technique by Pluymers *et al.* (2005*b*,*a*) constructs a robust invariant set, that can accommodate asymmetric constraints and has a much bigger feasible are than their ellipsoid counterparts. This method uses a simple MPC algorithm similar to nominal MPC that is based on QP rather than SDP.

2. REDUCED EAF MODEL

The MPC controller uses an optimization algorithm to calculate the future control sequence. This requires a number of iterations to be done on the internal model. If the model is complex, as in the case of the generic EAF model (Bekker *et al.*, 1999), this will result in a large computation time. The reduced model reduces the computational burden in the refining stage where certain assumptions can be made to simplify the model.

The generic model (Bekker *et al.*, 1999) was reduced by Rathaba (2004) for the refining stage. During the first sixty to eighty percent of a tap, the process is often unpredictable due to delays, breakdowns and maintenance that invalidate the modelling assumption of process continuity. The advantage of using the refining stage for control is that after the initial measurement, except for deslagging, the process is mostly uninterrupted until the final measurement is made. This is typically a flat bath stage when all melting has occurred; the modeling assumption of homogeneity (Bekker *et al.*, 1999) is also valid. The bath temperature and carbon content become especially important during the refining stage just before tapping.

Process variables that undergo significant change during refining are bath temperature, carbon and silicon concentrations (masses), masses of SiO_2 and FeO in slag and all free-board gases. All masses of the bath and composite slag are at steady state - they can be treated as constants.

The reduced model (Rathaba, 2004) is given by

$$\dot{x_3} = -k_{dC}\left(X_C - X_C^{eq}\right) \tag{1}$$

$$\dot{x_4} = -k_{dSi}\left(X_{Si} - X_{Si}^{eq}\right) \tag{2}$$

$$\dot{x_7} = \frac{2M_{FeO}d_1}{M_{O_2}} - \frac{x_7 k_{gr} M_{Fe} d_5}{\left(m_{T(slag)} + x_7 + x_8\right) M_C} + 0.13 d_2 \tag{3}$$

$$\dot{x_8} = \frac{M_{SiO_2}}{M_{Si}} k_{dSi}\left(X_{Si} - X_{Si}^{eq}\right) + 0.045 d_2 \tag{4}$$

$$\dot{x_{12}} = \left(p_t + \eta_{ARC} d_4 - k_{VT}(x_{12} - T_{air})\right) / \left[\frac{m_{T(Fe)} C_{p(FeL)}}{M_{Fe}} + \frac{2m_{T(slag)} + 2x_7 + 3x_8}{M_{slag}} C_{p(slag_{(L)})}\right] \tag{5}$$

where the molar concentrations are given by

$$X_c = \frac{x_3/M_C}{m_{T(Fe)}/M_{Fe} + x_3/M_C + x_4/M_{Si}} \tag{6}$$

$$X_{FeO} = \frac{x_7/M_{FeO}}{m_{T(slag)}/M_{slag} + x_7/M_{FeO} + x_8/M_{SiO_2}} \tag{7}$$

$$X_C^{eq} = k_{XC}\left(\frac{m_{T(slag)} M_{FeO}}{x_7 M_{slag}} + \frac{x_8 M_{FeO}}{x_7 M_{SiO_2}} + 1\right) \tag{8}$$

$$X_{Si} = \frac{x_4/M_{Si}}{m_{T(Fe)}/M_{Fe} + x_3/M_{Si} + x_4/M_{Si}} \tag{9}$$

$$X_{Si}^{eq} = k_{XSi}\left(\frac{m_{T(slag)} M_{FeO}}{x_7 M_{slag}} + \frac{x_8 M_{FeO}}{x_7 M_{SiO_2}} + 1\right)^2 \tag{10}$$

The reduced equations for the heat balance are:

$$p_2 = \left(-2H_{FeO} d_1 / M_{O_2}\right)\eta_{FeO} \tag{11}$$

$$p_5 = \frac{d_1}{M_{O_2}}\left(x_{12} - T_{O_2}\right) C_{P(O_2)} \tag{12}$$

$$p_{11} = \frac{x_7 k_{gr} d_5 (\Delta H_{FeO} - \Delta H_{CO})}{\left(m_{T(slag)} + x_7 + x_8\right) M_C} \tag{13}$$

$$p_t = p_2 + p_5 + p_{11} \tag{14}$$

where k_{dC} and k_{dSi} are the constants for removal of carbon and silicon from the bath; k_{gr} is the graphite reactivity constant; η_{ARC} and η_{FeO} are the efficiencies of arc energy input and bath oxidation; $m_{T(Fe)}$ and $m_{T(slag)}$ are the total masses of the slag formers and bath - both are assumed constant; M_C, M_{Fe}, M_{FeO}, M_{Si}, M_{SiO_2} and M_{slag} are the molar masses of the different elements. The states and inputs are described in table 1.

3. LINEARIZED MODEL

For the robust MPC controller (Pluymers *et al.*, 2005*b*,*a*), linear models are required to describe

the uncertain polytope. The reduced model of section 2 was fitted to actual plant data (Rathaba, 2004), with resulting confidence intervals on the parameter values. The parameters were varied to determine the extreme deviations from the nominal plant. The reduced model was linearized with different parameter values, resulting in different linear models that form the polytopic uncertainty description used to synthesise the robust MPC controller. In order to reduce complexity of the controller, only the most significant uncertainties were included in the uncertainty description. The nominal model is shown below with the maximum variation of the input matrix. The states of the linear models were reduced to 2 (Temperature and FeO), because these are the states that are of primary interest. The inputs were reduced to three (oxygen injection rate, electric power and graphite injection rate). Slag and DRI are not added during the refining stage and therefor removed from the model. To compensate for the reduced dynamics in the linearised model, the controller uses the full nonlinear model of section 2 as a predictor. The operating point around which the linearization is done is the average values from measured tap data as summarized in table 1. The total iron mass $m_{T(Fe)}$ is 80000 kg and the slag mass $m_{T(slag)}$ is 6917.8 kg.

The linearized model is described as a nominal model, or a model with values in the middle of the uncertainty interval, and matrices that describes the extreme deviations, found using Monte Carlo type simulations, from the nominal model. The notation used is as in MATLAB, where 3.03e-6 represents 3.03×10^{-6}. The nominal linear model is

$$
\begin{aligned}
A_{nominal} &= \begin{bmatrix} 9.99e{-}1 & 0 \\ -7.87e{-}6 & 1.00 \end{bmatrix} \\
B_{nominal} &= \begin{bmatrix} 11.99 & 0 & -1.17 \\ 0.41 & 6.07e{-}6 & -1.67e{-}2 \end{bmatrix} \\
C_{nominal} &= \begin{bmatrix} 1 & 0 \\ 0 & 1 \end{bmatrix} \\
D_{nominal} &= \begin{bmatrix} 0 & 0 & 0 \\ 0 & 0 & 0 \end{bmatrix}
\end{aligned} \tag{15}
$$

with extreme deviations from nominal on the inputs

$$
B_{dev} = \begin{bmatrix} 0 & 0 & 0 \\ 0.11 & 3.03e{-}6 & 1.42e{-}2 \end{bmatrix} \tag{16}
$$

The polytopic uncertainty produces a total of eight linear models used to construct the robust invariant set for the controller as described in section 4.1.

4. CONTROL STRATEGY

In general, the steel grade is determined by the carbon content. It is desirable to have the steel at a specific tap temperature for down-stream processing. The carbon content and temperature should be controlled without creating too much undesirable material such as FeO in the slag. The controller should contain the FeO content, controllable through the oxygen injection rate, to less than 40% of the total slag mass. Oxygen injection influences the decarburization rate depending on the level of the bath carbon. Under high bath carbon levels, oxygen injection leads to high decarburization, while only a limited influence is observed in the late stages of refining. The speed of the reaction cannot be accelerated through control, because of the carbon content being weakly controllable. (The carbon content is controllable, but the constraints on the inputs limit the influence over the decarburization rate to practically none.) The aim of the controller would therefore be to steer the temperature to the desired value before the carbon reaches its target.

4.1 Robust model predictive controller

The controller proposed by Pluymers *et al.* (2005*b*) uses an optimized control sequence over the prediction horizon N after which a global stabilizing state feedback gain K is used. The system $\tilde{x}(k+1) = \Phi(k)\tilde{x}(k)$ uses an augmented description with vertices of the uncertainty polytope given by:

$$
\Phi_i = \begin{bmatrix} A_i - B_i K & B_i & 0 \\ 0 & 0 & I_{((N-1).n_u,(N-1).n_u)} \\ 0 & 0 & 0 \end{bmatrix} \tag{17}
$$

for $i = 1, 2, \ldots, L$, where L is the number of models, subject to constraints $A_{\tilde{x}}\tilde{x}(k) \leq b_{\tilde{x}}, k = 0, ..., \infty$ with $A_{\tilde{x}}$ and $b_{\tilde{x}}$ defined as:

$$
A_{\tilde{x}} = \begin{bmatrix} A_x & 0 & 0 \\ -A_u K & A_u & 0 \end{bmatrix} \quad b_{\tilde{x}} = \begin{bmatrix} b_x \\ b_u \end{bmatrix} \tag{18}
$$

where the state constraints are $A_x x \leq b_x$ and the input constraints are $A_u u \leq b_u$.

To calculate the robust invariant set from $A_{\tilde{x}}$ and $b_{\tilde{x}}$ the algorithm from Pluymers *et al.* (2005*a*) is used to construct $S_{aug} = \{\tilde{x} | A_S \tilde{x} \leq b_S\}$.

The implemented input vector is the combination of the state feedback gain and the first block of the optimized sequence of free control moves.

$$
u(k) = -Kx(k) + c^o(k|k) \tag{19}
$$

The optimized sequence of free control moves $c_N^o(k)$ are determined from a quadratic program

Table 1. States, inputs and operating point.

State	Operating point	Input	Operating point
x_3 Dissolved Carbon	480 kg	d_1 Oxygen injection rate	1 kg/s
x_4 Dissolved Silicon	24 kg	d_2 DRI addition rate	0 kg/s
x_7 FeO in bath	4250.6 kg	d_3 Slag addition rate	0 kg/s
x_8 SiO_2 in bath	1405 kg	d_4 Arc power	40000 kW
x_{12} Bath temperature	1600 ^0C	d_5 Graphite injection rate	0.5 kg/s

subject to the polyhedral set constraints of the form $A_S\tilde{x} \leq b_S$ that form S_{aug}.

$$\min_{c_N(k)} J(x(k),c_N(k)) \tag{20}$$

subject to

$$\left[\, x(k)^T \;\; c_N(k)^T \,\right]^T \in S_{aug} \tag{21}$$

where the objective function is

$$\begin{aligned} J(x(k),c_N(k)) \;=\; & \left[\, x(k)^T \;\; c_N(k)^T \,\right] P \\ & \times \left[\, x(k)^T \;\; c_N(k)^T \,\right]^T \end{aligned} \tag{22}$$

with

$$P = P^T \in \Re^{(n_x+N.n_u)\times(n_x+N.n_u)} \tag{23}$$

satisfying

$$P - \Phi_i^T P \Phi_i > \Gamma_x^T Q \Gamma_x + \Gamma_u^T R \Gamma_u,\; i=1,...,L \tag{24}$$

where $\Gamma_x = \left[\, I_{(n_x,n_x)} \;\; 0 \,\right]$, $\Gamma_u = \left[\, -K \;\; I_{(n_u,n_u)} \;\; 0 \,\right]$ and $\Phi_i,\; i = 1, ..., L$. The R matrix is the weighting on the inputs and Q the weighting on the states. The P matrix can be obtained by doing convex optimization

$$\min_{P=P^T>0} \text{trace}(P) \tag{25}$$

subject to (24).

4.2 Controller design

There are a few parameters that have to be chosen in order to construct the controller. These are the prediction horizon, weights on the state deviation, and the weights on the control actions. The constraints on the input and states are determined by the process and actuator limitations as summarized in table 2. The dimension of the constraint set grows exponentially with the prediction horizon. A prediction horizon of 4 gives adequate forward prediction, without resulting in an excessively large constraint set. The aim is to control the temperature of the bath without any penalty on the FeO content, except when it reaches the constraint. The weighting is expressed in the Q value of table 3. The FeO content in the slag should be kept below 40% of the total slag mass. This requirement is enforced by a state constraint on FeO as stipulated in table 2. In order for the process to reach the desired set-point as fast as possible and reduce the steady-state offset, cheap control is used, as expressed in the R value of table 3. The structure of the Q and R matrices are diagonal, because only the individual states and inputs are penalized.

Table 2. Constraints on manipulated and controlled variables.

Variable	Minimum	Maximum
Oxygen injection rate	0 kg/s	1 kg/s
Power	0 kW	40 000 kW
Graphite injection rate	0 kg/s	1 kg/s
FeO amount	0% of Slag	40% of Slag

Table 3. Controller parameters

Parameter	Value
N	4
Q	$\begin{bmatrix} 0 & 0 \\ 0 & 1 \end{bmatrix}$
R	$\begin{bmatrix} 0.1 & 0 & 0 \\ 0 & 0.1 & 0 \\ 0 & 0 & 0.1 \end{bmatrix}$

5. SIMULATION AND RESULTS

In this section, a simulation study is done to determine the effectiveness of the control on the system. For these simulations a predictor, the reduced nonlinear model of section 2, is used to interpolate the missing state-data and a second nonlinear model is used to represent the actual plant. Model mismatches are introduced between the predictor and real plant, by manipulating the parameters of the "real" plant. The model mismatch has the greatest influence on the temperature, because of the uncertainty in the effectivity coefficients (ECs), η_{ARC} of equation (5) and η_{FeO} of equation (11). The ECs will be used to describe the parameter set being used.

In the first scenario, full state feedback is assumed, and the parameters of the "real" plant are set to the two extreme points of the uncertainty intervals. The controller is able to handle the extreme cases of model mismatches as seen in figure 1. In the scenario where the ECs are lower

than nominal, the rate of change in temperature decreases because the FeO constraint was met; oxygen could no longer be used as an energy source.

In the second scenario, a more practical approach is taken. In the real process, it is difficult to get measurements. Each time a temperature measurement is taken, the slag layer must be removed from the metal through a process called deslagging. For deslagging, the electrical power is reduced and a probe is dropped into the molten metal by an operator. The probe is burnt away as part of the measurement process, making measurements costly. Only one measurement is available for feedback from the real plant during the refining stage. A predictor, the reduced nonlinear model of section 2, is used to interpolate the missing process state-data between measurements. For this scenario, nominal plant parameters are assumed for the predictor, while the real plant uses the extreme points as before. In this case (figure 2), the controller was not able to steer the temperature to the desired set-point and could not even steer it to within 10 degrees of the set-point, which is an acceptable temperature variation. In practice this variation is often much larger.

In the third scenario, the predictor parameters, that have the greatest influence on the temperature response, are manipulated with the difference in predicted and measured temperature, to better approximate the real plant. With the corrections to the predictor, the controller is able to steer the process closer to the desired set-point (figure 2). For this simulation, the model mismatch was assumed to be constant, but unknown. The predictor was initiated with nominal plant parameters.

From this results we see that robust MPC does not guarantee offset free tracking. Integral action or robust MPC techniques that specifically address this problem (Pannocchia, 2004; Wang and Rawlings, 2004*a*,*b*) will remedy the problem and will be considered for future work. The third scenario where corrections are made to the predictor, show optimistic results. The assumption of unknown but constant model mismatch might not be valid. All these scenarios investigate the worst case where the model mismatch between the predictor and actual plant is at the extreme. The performance of the controller should yield better results if the actual plant behaviour is closer to the nominal case.

6. CONCLUSION

This paper, through a simulation study, found robust model predictive control feasible to improve the quality of the steel produced in an EAF. This is provided that the predictor is a suitably accurate predictor of the real process. The robust model predictive controller could explicitly take the model uncertainties into account as part of the synthesis process. The focus was on the refining stage, because it allowed for the use of the reduced model of the process, which is better suited for on-line calculations. The speed of the process could not be increased, because the carbon is only weakly controllable. The only improvement possible is to control the temperature to the desired set-point before the carbon reaches its target value. This will result in fewer delays attributed to incorrect tap temperature. The controller performed well with full state feedback, but in practice, the performance is dependant on the accuracy of the predictor.

An ad-hoc method was used to update the parameters of the predictor in order to determine if it will yield better results than a predictor without parameter update. The updating of the parameters of the predictor show promise, but further study is needed where a more systematic method is followed.

REFERENCES

Bekker, J.G., I.K. Craig and P.C. Pistorius (1999). Modelling and simulation of an electric arc furnace process. *ISIJ International* **39**(1), 23–32.

Bekker, J.G., I.K. Craig and P.C. Pistorius (2000). Model predictive control of an electric arc furnace off-gas process. *Control Engineering Practice* **8**, 445–455.

Cameron, A., N. Saxena and K. Broome (1998). Optimizing EAF operations by dynamic process simulation. In: 56^{th} *Electric Furnace Conference Proceedings*. ISS Publishers. Warrendale, Pennsylvania. pp. 689–696.

Coetzee, L.C., I.K. Craig and P.L. Rathaba (2005). MPC control of the refining stage of an electric arc furnace. In: *Procedings of the 16th IFAC World Congress*. IFAC. Prague, Czech Republic.

Cuzzola, F. A., J. C. Geromel and M. Morari (2002). An improved approach for constrained robust model predictive control. *Automatica* **38**, 1183–1189.

Ding, B., Y. Xi and S. Li (2004). A synthesis approach of on-line constrained robust model predictive control. *Automatica* **40**, 163–167.

Kothare, M. V., V. Balakrishnan and M. Morari (1996). Robust constrained model predictive control using linear matrix inequalities. *Automatica* **32**, 1361–1379.

Matson, S. and W.F. Ramirez (1999). Optimal Operation of an Electric Arc Furnace. In: 57^{th} *Electric Furnace Conference Proceedings*. ISS

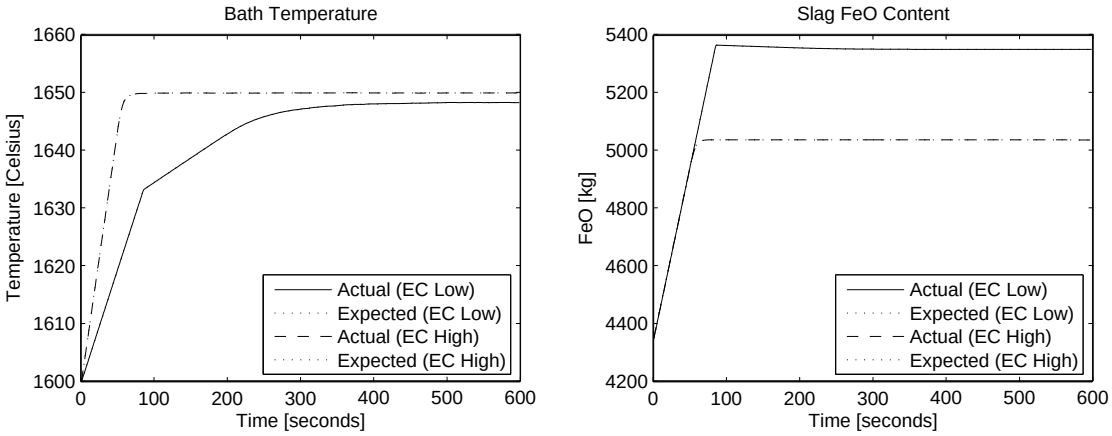

(a) Temperature (b) FeO Content

Fig. 1. Process with full state feedback

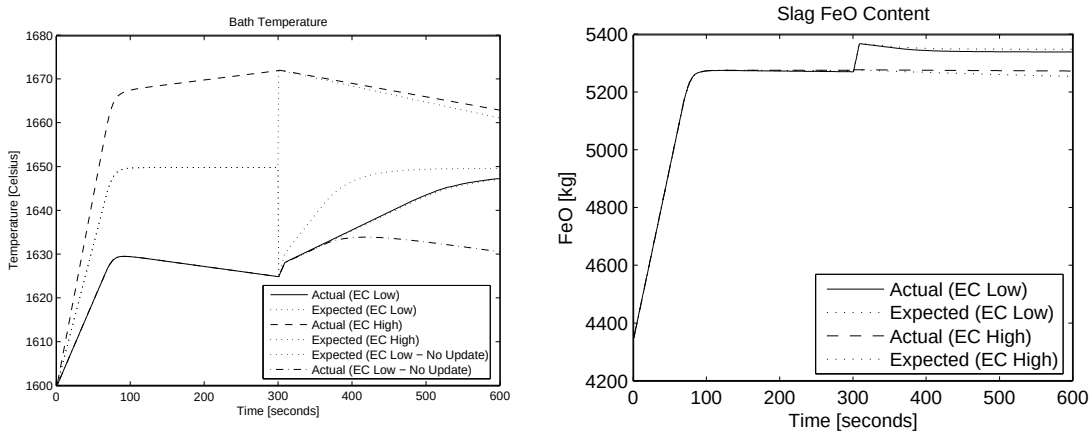

(a) Temperature (b) FeO Content

Fig. 2. Process with one measurement at time $t = 300s$

Publishers. Warrendale, Pennsylvania. pp. 719–728.

Modigell, M., A. Traebert, P. Monheim, S. Peterson and U. Pickartz (2001). A new tool for process modeling of metallurgical processes. *Computers & Chemical Engineering* **25**, 723–727.

Morales, R.D., H. Rodriguez-Hernandez, P. Garnica-Conzalez and J.A. Romero-Serrano (1997). A Mathematical Model for the Reduction Kinetics of Iron Oxide in Electric Furnace Slags by Graphite Injection. *ISIJ International* **37**(11), 1072–1080.

Oosthuizen, D.J., I.K. Craig and P.C. Pistorius (2004). Economic evaluation and design of an electric arc furnace controller based on economic objectives. *Control Engineering Practice* **12**, 253–265.

Pannocchia, G. (2004). Robust model predictive control with guaranteed setpoint tracking. *Journal of Process Control* **14**, 927–937.

Pluymers, B., J.A. Rossiter, J. Suykens and B. De Moor (2005*a*). The efficient computation of polyhedral invariant sets for linear systems with polytopic uncertainty. In: *Proceedings of the American Control Conference 2005,*. Portland, USA. pp. 804–809.

Pluymers, B., J.A. Rossiter, J.A.K. Suykens and B. De Moor (2005*b*). A simple algorithm for robust MPC. In: *Procedings of the 16th IFAC World Congress*. Prague, Czech Republic.

Rathaba, P.L. (2004). Model fitting for an electric arc furnace refining. Master's thesis. University of Pretoria. Pretoria, South Africa.

Wang, Y. J. and J. B. Rawlings (2004*a*). A new robust model predictive control method I: Theory and computation. *Journal of Process Control* **14**, 231–247.

Wang, Y. J. and J. B. Rawlings (2004*b*). A new robust model predictive control method II: Examples. *Journal of Process Control* **14**(3), 249–262.

Dynamics and Control of Reactive Distillation Configurations for Acetic Acid Esterification

Shih-Bo Hung[2], Yeong-Tarng Tang[1], Yi-Wei Chen[1], I-Kuan Lai[1], Wan-Jen Hung[1], Hsiao-Ping Huang[1], Ming-Jer Lee[2], and Cheng-Ching Yu[*1]

Dept. of Chem. Eng., National Taiwan University[1]
Taipei 106-17, TAIWAN
Dept. of Chem. Eng., National Taiwan University of Sci. Tech.[2]
Taipei 106-07, TAIWAN

Abstract: Three different flowsheets have been proposed for acetic acid esterification of acetic acid with alcohols ranging from C_1 to C_5 according to the ranking of normal boiling points and immiscibility. This work explores the similarities and differences in the dynamics and control of these three types of flowsheets. The degree of process nonlinearity can be computed quantitatively based on the fraction of "sign reversal" for all tray temperatures or based on Allgower's nonlinearity measure. These measures provide useful information to the potential problems in closed-loop control. Next, a systematic design procedure is proposed to devise control structures for all three types of flowsheets for these five esterification systems. The simulation results reveal that reasonable control can be achieved for all five systems with different degrees of asymmetry in closed-loop responses as predicted by the nonlinearity measures. Simulation results clearly show that the simple decentralized control provides a workable solution for highly nonlinear reactive distillation columns under various flowsheet configurations.

Keywords: reactive distillation, esterification, process control, temperature control, nonlinearity.

1. Introduction

Reactive distillation combines reaction and separation in a single unit which provides substantial economic incentives for some chemical processes. The literature and patents in reactive distillation have grown rapidly in recent years as surveyed by Malone and (Doherty, 2000). The books by (Doherty and Malone, 2001) and (Sundmacher and Kienle, 2003) give updated summaries in the field. The review paper of (Taylor and Krishna, 2000) describes potential advantages, modeling, simulation, and hardware configurations of reactive distillation. However, the multifunctional nature of the reactive distillation complicates already very nonlinear dynamics of either reactors or separators. Thus, the dynamics and control of reactive distillation are less obvious as compared to its single unit counterparts. Last decade has seen a steady growth in the number of papers that deal with control of reactive distillation column, from mere a handful to over a dozen. (Roat et al., 1986), among the first, propose a two-temperature control structure for an industrial column in which two fresh feeds are manipulated by two tray temperatures. This is a rather "unconventional" control structure as far as the distillation control is concerned. The reaction considered is the methyl acetate production with a reversible reaction with two reactants and two products (i.e., A + B $\leftrightarrow$ C + D). Moreover, the esterification is carried out in a "neat", i.e., no excess reactant flowsheet as opposed to an "excess-reactant" flowsheet as defined by (Luyben and co-workers, 2000~2005). The "excess-reactant" flowsheet requires two columns to achieve high purity product and is, therefore, more expensive. The "neat" flowsheet has a greater economical potential because only one column is needed. However, it is more difficult to control because two reactants must be fed in the "exact" amount to satisfy the stoichiometry down to the last molecule. Luyben is, among the first, to recognize this fact and, therefore, not so conventional control structures results. Luyben and co-workers propose eight control structures for the "neat" reactive distillation (CS1- CS6 in (Al-Arfaj, 2000) and (Luyben, 2002) ; CS6-CS7 in (Al-Arfaj and Luyben, 2002) ; CS7-CS8 in (Kaymak and Luyben, 2005)). Typically, a generic distillation column with a second order reversible reaction is investigated. In addition to the control of continuous reactive distillation for A + B $\leftrightarrow$ C + D systems, control of reactive distillations for fuel ether (MTBE, ETBE,TAME) has been studied by (Sneesby et al, 1999). This corresponds to a reactive kinetics of two reactants and one product, i.e., A + B $\leftrightarrow$ C. Linear and nonlinear control of semi-batch reactive distillation for ethyl acetate production has been explored by (Engell and Fernholz, 2003). Nonlinear estimation and control of a two-stage reaction has been studied by (Grüner et al, 2003). Because of the difference in the mode of operation (batch versus continuous) and in the reaction kinetics (A + B $\leftrightarrow$ C + D versus A + B $\leftrightarrow$ C), the potential problems of the "neat" flowsheet have not been emphasized. This

work continues the earlier effort to explore the control of acetic acid esterification with different alcohols (ranging from C1 to C5; (Tang et al., 2005)). The esterifications lead to three different types of flowsheets (category I ~ III) with different economical potentials (Tang et al., 2005). The esterification processes explored share a common characteristic, "neat" flowsheet, while maintaining their own process configuration and the object of this work is to devise control structures for these three different categories of reactive distillation. A systematic procedure is proposed for the control structure design which is applicable to all three process configurations. Temperature as well as composition controls are explored and interaction between design and control is discussed.

2. Process Characteristics

2.1 Process Studies

As pointed out by (Tang et al., 2005), the esterification of acetic acid with different types of alcohols (ranging from C1 to C5) can be classified into three flowsheets, type I, type II, and type III, as shown in figure 1. Steady-state analysis indicates that the type I and type III systems are more economical than the type II system. Here we would like to explore the dynamical controllability of these three flowsheets. More importantly, we would like to devise a systematic approach to the control of these three types of reactive distillations.

(A)

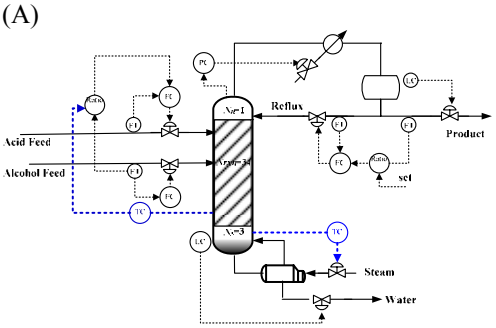

(B)

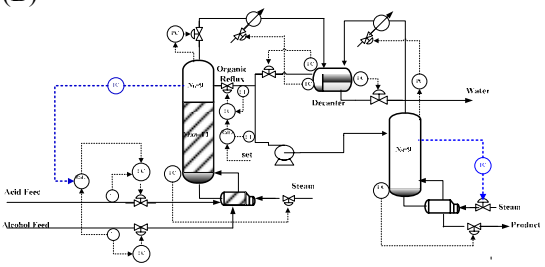

(C)

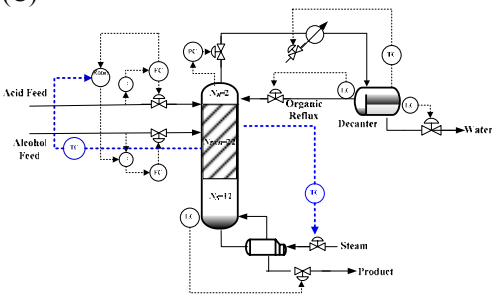

Figure 1. Process flowsheets for temperature control configurations for type I (A), II (B), and III (C) systems

2.2 Quantitative Analysis

Before getting into detailed quantitative analysis, we need to identify manipulated variables for these three different types of processes. As pointed out by (Luyben,) it is important to maintain the stoichiometric balance for the "neat" reactive distillation. (Al-Arfaj and Luyben, 2002) choose to use one of the feed rate and, here, the feed ratio (FR) is used as the manipulated variable. In addition to hold the stoichiometric balance, in theory, we need to control two product compositions using two manipulated variables. However, for reactions such as A + B ↔ C + D, if the conversion is properly maintained and the product flow rate are equally distributed, one-end composition control will do a fairly good job. For type I flowsheet of MeAc production, following Al-Arfaj and Luyben, we choose to control the bottoms composition using vapor boilup while fixing the reflux ratio. For type II flowsheet, the product composition of water from the first column (RD column) is determined by liquid-liquid equilibrium, so no composition control is necessary. However, the reflux ratio of the RD column is fixed. The acetate production is withdrawn from the stripper and the composition is controlled by manipulating the vapor boilup as shown in Figure 1. Similar to the type II flowsheet, a decanter is used for type III flowsheets to separate the water from column overhead and, therefore, composition control is not necessary and the origin phase is totally refluxed back to the column. This is similar to the configuration studied by (Huang et al, 2004). and (Chiang et al., 2003) . The bottoms acetate composition is, however, controlled by changing the reboiler duty. In summary, the manipulated variables are:

Type I: feed ratio, and reboiler duty (fixing reflux ratio)

Type II: feed ratio and reboiler duty in the stripper (fixed organic reflux ratio in RD)

Type III: feed ratio and reboiler duty (organic phase totally refluxed)

3. Nonlinearity

Once the manipulated variables are determined, we could like to evaluate process nonlinearity for these 3 different types of flowsheets. The tray temperatures are treated as the state variables. The manipulated variables are the heat input Q_R and feed ratio FR, respectively. First, the upper and lower bounds of the steady-state gains between the tray temperatures and the manipulated variables (Q_R and FR) are obtained for a range of input variations. In this work, -5% to +5% changes in the heat input (Q_R) and -1% to +1% changes in the feed ratio are made. Note that, for a truly linear system, the upper and lower bounds should coincide with each other. Figure 2 clearly shows that the reactive distillation columns exhibit

strong nonlinearity for all 5 systems studied, despite showing different degrees of severity. Moreover, the "sign reversal" is also observed for all 5 systems under either Q_R or FR change. The results presented here are rather unconventional, because chemical processes are known to be quite nonlinear, but not to this degree in such a consistent manner. Two measures are used to differentiate the degree of nonlinearity for these three types of reactive distillation. One obvious choice is the faction of sign reversal for all tray temperatures. In this aspect, the AmAc system (Figure 2) indicates that more than half of the trays show sign reversal followed by the MeAc system (category I) in which almost half of the tray temperatures exhibit the "sign reversal". The category II system (EtAc and IPAc) show that almost 1/3 of the tray temperatures exhibit the "sign reversal" and the BuAc system is the system with the least sign changes in the tray temperatures. Table 1

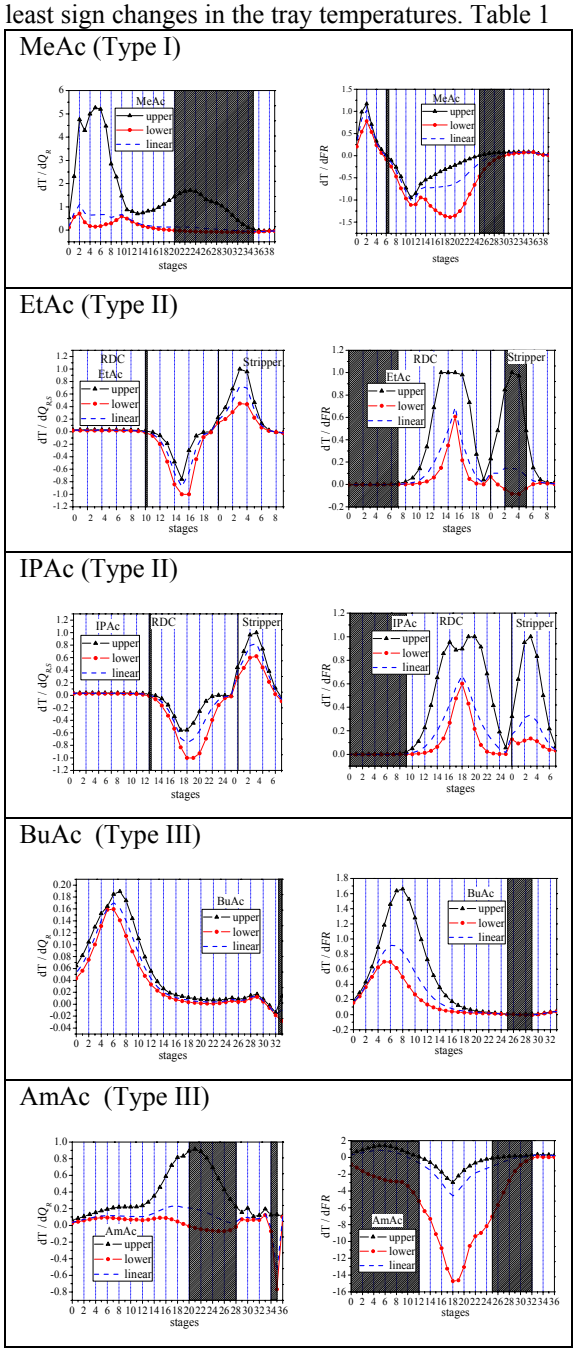

Figure 2. Upper and lower bounds of steady-state gains of all tray temperatures for ±5% reboiler duty and ±1% feed ratio changes and the sign reversal indicated as shaded areas.

summarizes the fraction of a sign changes for all five systems. The second nonlinearity indicator is ϕ^N which is first proposed by (Allgower, 1997) for general dynamic systems and further studied by (Hernjak and Doyle, 2003) for systems under feedback. (Schweickhardt and Allgower, 2004) give an updated summary on the nonlinearity measure. Here, we only consider the steady-state aspect (e.g., can be viewed as the nonlinearity measure for a static function) and the approach of (Schweickhardt and Allgower, 2004) is taken here. In this work, the 2-norm is used to compute ϕ^N and each manipulated variable is considered separately. The measure is defined as:

$$\phi^N = \inf_{G\in\mathbb{G}} \sup_{\boldsymbol{u}\in\mathbb{U}} \frac{\|G(\boldsymbol{u}) - N(\boldsymbol{u})\|_2}{\|N(\boldsymbol{u})\|_2} \tag{1}$$

Where G is a linear operator, N is a nonlinear static function, $\mathbb{U}$ is the input set, $\mathbb{G}$ is a set of all linear operators. Physically, this can be viewed as the relative deviation of a linear (static) transfer function to the nonlinear function in a normalized sense. The measure ϕ^N ranges form 0 to 1 and ϕ^N=0 indicates a linear system and ϕ^N increases toward 1 as the nonlinearity becomes more severe. For static functions with the upper and lower bounds available, the solution to the optimization problem is simply:

$$\frac{\|\overline{G} - G_+\|_2}{\|G_+\|_2} = \frac{\|\overline{G} - G_-\|_2}{\|G_-\|_2} \tag{2}$$

Where G_+ is the upper bound of $N(\boldsymbol{u})/\boldsymbol{u}$, G_- is the lower bound of $N(\boldsymbol{u})/\boldsymbol{u}$, and the nonlinear measure can be computed as:

$$\phi^N = \frac{\|\overline{G} - G_+\|_2}{\|G_+\|_2} = \frac{\|\overline{G} - G_-\|_2}{\|G_-\|_2} \tag{3}$$

Because we treat two manipulated inputs separately, two ϕ^N's are available for a given system. Table 1 gives the nonlinearity measures for all 5 systems with two different inputs. Qualitatively, the results of ϕ^N are consistent with the fractions of sign reversal as shown in Table 1. The 2-norm is employed for overall nonlinearity assessment based on ϕ^N and the results are consistent with the previous "sign reversal" analysis. The ranking of the processes from linear to nonlinear becomes: BuAc (Type III) → IPAc (Type II) → EtAc (Type II) → MeAc (Type I) → AmAc (Type III).

Flow sheet Type	System	Fraction of sign reversal			Nonlinearity measure (Schweickhardt and Allgower)			Overall Assessment ***
		Q_R	*FR*	Overall*	Q_R	*FR*	Overall**	
I	MeAc	0.40	0.18	0.43	0.84	0.44	0.67	H
II	EtAc	0.03	0.40	0.43	0.34	0.70	0.55	M
	IPAc	0.03	0.29	0.32	0.32	0.60	0.48	M
III	BuAc	0.03	0.15	0.18	0.16	0.46	0.34	L
	AmAc	0.30	0.57	0.76	0.78	0.79	0.79	H

Table 1 Fractions of sign reversal and nonlinearity measures for all five esterification systems.
* delete overlapping (from each input) trays
** taking as 2-norm of two inputs divided by two
***High (if the averaged value exceeds 0.5), Medium (if the averaged value exceeds 0.3), and Low (if the averaged value less than 0.3),

3. Control Structure Design

In this section, a systematic approach is proposed to the control structure design for these three types of reactive distillation flowsheets. In this work, the feed ratio (*FR*) is adjusted to prevent accumulation of unreacted reactants, stoichiometric imbalance. The next issue is: how many product compositions or inferred product purities should be controlled? For the esterification reactions with A + B ↔ C + D under the "neat" flowsheet, controlling one-end product purity implied a similar purity level on the other end, provided with equally distributed product flow rates. So, a single-end composition (or temperature control) is preferred. This leads to 2×2 multivariable control, as opposed to a 3×3 multiple input- multiple- output (MIMO) system. The next problem is more of the robustness consideration. Because of input multiplicities and potential sign reversals, the decentralized control is preferred over the inverse-based control. The reason is quite obvious: we are not even sure of the sign in some entries of a process transfer function. The decentralized control is more likely to work than an inversed-based multivariable controller. In summary, the following principles are recommended:
(1) Maintain the stoichiometric balance using the feed ratio.
(2) Prefer to control only one-end composition (or temperature).
(3) Use decentralized control to maintain robust stability.
This leads to the following design procedure for temperature control of reactive distillation systems.
(1) Select an additional manipulated variable. Typically, the other manipulated input is the heat input or the reflux ratio.
(2) Use the non-square relative gain (NRG; Chang and Yu[23]) to select temperature control trays. The larger row sums of the NRG indicate potential temperature control tray. Note that the temperatures with the "sign reversal" (Figure 2) cannot be used as controlled variable.
(3) Use the relative gain array (RGA) for variable pairing, once the inputs and outputs are determined.
(4) Performance sequential relay feedback test (Shen and Yu) to find the ultimate gain (K_u) and ultimate period (P_u).

Use the Tyreus-Luyben tuning to set the tuning constant for the PI controllers. A simple version is:

$K_c = K_u/3$ and $\tau_I = 2\ P_u$.

3.1 Selection of Temperature Control Trays

The non-square relative gain (NRG) of Chang and (Yu) is used to find the temperature control trays. The NRG (Λ^N) is defined as:

$$\Lambda^N = K_p \otimes (K_p^+)^T \qquad (3)$$

where K_p is the steady-state gain matrix, $\otimes$ denotes the element-by-element multiplication, the superscript + is the pseudo-inverse, and the superscript *T* means the transpose. The largest row sum of the NRG is selected as the temperature control trays. The controlled variables are:
MeAc : T_2 and T_{11}
EtAc : $T_{RDC,15}$ and $T_{STR,3}$
IPAc : $T_{RDC,18}$ and $T_{STR,3}$
BuAc : T_6 and T_{29}
AmAc : T_{11} and T_{33}
The "sign reversal" areas of Figure 2 are used to check potential sign changes in the selected tray temperatures. For these five systems, the temperature control trays do not exhibit sign reversal in the ranges (±5% for heat input and ±1% for *FR*) of manipulated variable variations. Note that if the NRG selected temperature falls within the "sign reversal" area, alternative temperature should be sought.

	Controlled Variables	Manipulated Variables	Steady State Gain	RGA	Tuning Parameter
MeAc	T_2 T_{11}	F_{Acid}/F_{MeOH} Q_R	$\begin{bmatrix} T_{11} \\ T_2 \end{bmatrix} = \begin{bmatrix} 1.839 & -1.522 \\ 4.802 & 3.659 \end{bmatrix} \begin{bmatrix} Q_R \\ F_{Acid}/F_{MeOH} \end{bmatrix}$	$\Lambda = \begin{matrix} Q_R & F_{Acid}/F_{MeOH} \\ \begin{bmatrix} 0.479 & 0.520 \\ 0.520 & 0.479 \end{bmatrix} & \begin{matrix} T_{11} \\ T_2 \end{matrix} \end{matrix}$	Q_R - T_2 : Kc= 0.464 τ_I = 0.333(hr) F_{Acid}/F_{MeOH} - T_{11} : Kc= 1.237 τ_I = 1.98(hr)
EtAc	$T_{STR,3}$ $T_{RDC,15}$	F_{Acid}/F_{EtOH} $Q_{R,S}$	$\begin{bmatrix} T_{STR,3} \\ T_{RDC,15} \end{bmatrix} = \begin{bmatrix} 0.087 & 1.967 \\ -4.26 & 102.57 \end{bmatrix} \begin{bmatrix} Q_{R,S} \\ F_{Acid}/F_{EtOH} \end{bmatrix}$	$\Lambda = \begin{matrix} Q_{R,S} & F_{Acid}/F_{EtOH} \\ \begin{bmatrix} 0.517 & 0.482 \\ 0.482 & 0.517 \end{bmatrix} & \begin{matrix} T_{STR,3} \\ T_{RDC,15} \end{matrix} \end{matrix}$	$Q_{R,S}$ - $T_{STR,3}$: Kc= 22.65 τ_I = 0.018(hr) F_{Acid}/F_{EtOH} - $T_{RDC,15}$: Kc= 0.755 τ_I = 2.069(hr)
IPAc	$T_{STR,3}$ $T_{RDC,18}$	F_{Acid}/F_{IPOH} $Q_{R,S}$	$\begin{bmatrix} T_{STR,3} \\ T_{RDC,18} \end{bmatrix} = \begin{bmatrix} 0.227 & 1.574 \\ -2.336 & 70.439 \end{bmatrix} \begin{bmatrix} Q_{R,S} \\ F_{Acid}/F_{IPOH} \end{bmatrix}$	$\Lambda = \begin{matrix} Q_{R,S} & F_{Acid}/F_{IPOH} \\ \begin{bmatrix} 0.812 & 0.187 \\ 0.187 & 0.812 \end{bmatrix} & \begin{matrix} T_{STR,3} \\ T_{RDC,18} \end{matrix} \end{matrix}$	$Q_{R,S}$ - $T_{STR,3}$: Kc= 25.5 τ_I = 0.08(hr) F_{Acid}/F_{IPOH} - $T_{RDC,18}$: Kc= 3.92 τ_I =2.66(hr)
BuAc	T_{29} T_6	F_{BuOH}/F_{Acid} Q_R	$\begin{bmatrix} T_{29} \\ T_6 \end{bmatrix} = \begin{bmatrix} 0.026 & -0.007 \\ 0.299 & -2.127 \end{bmatrix} \begin{bmatrix} Q_R \\ F_{BuOH}/F_{Acid} \end{bmatrix}$	$\Lambda = \begin{matrix} Q_R & F_{BuOH}/F_{Acid} \\ \begin{bmatrix} 1.041 & -0.041 \\ -0.041 & 1.041 \end{bmatrix} & \begin{matrix} T_{29} \\ T_6 \end{matrix} \end{matrix}$	Q_R - T_{29} : Kc = 38.86 τ_I = 0.06(hr) F_{BuOH}/F_{Acid} - T_6 : Kc= 5.16 τ_I = 0.9(hr)
AmAc	T_{33} T_{16}	F_{AmOH}/F_{Acid} Q_R	$\begin{bmatrix} T_{33} \\ T_{16} \end{bmatrix} = \begin{bmatrix} 0.29 & -0.059 \\ 0.31 & 15.995 \end{bmatrix} \begin{bmatrix} Q_R \\ F_{AmOH}/F_{Acid} \end{bmatrix}$	$\Lambda = \begin{matrix} Q_R & F_{AmOH}/F_{Acid} \\ \begin{bmatrix} 0.961 & 0.038 \\ 0.038 & 0.961 \end{bmatrix} & \begin{matrix} T_{33} \\ T_{16} \end{matrix} \end{matrix}$	Q_R - T_{33} : Kc= 29.72 τ_I = 0.08(hr) F_{AmOH}/F_{Acid} - T_{16} : Kc= 9.1 τ_I = 1.2(hr)

Table 2. Controlled variables , manipulated variables, process gain matrices, relative gain array, and tuning parameters for these five esterification systems under temperature control.

4. Perormance

Feed flow and feed ratio disturbances are used to evaluate the control performance of the temperature control for these five esterification systems. Recall

that these reactive distillation systems are highly nonlinear (Figure 2) with significant "sign reversal" and input multiplicity. Figure 3 shows that the simple PI temperature control actually works quite well for all 5 systems.

For the MeAc system, the product composition, $X_{D,acetate}$ in particular, does not settle down 15 hours after the 20% feed flow rate change is introduced. Asymmetrical responses are observed for most of the process variable and steady-state offsets (~ 0.02 m.f.) exist (Figure 3A). For the type II flowsheets, faster responses and much symmetrical responses can be obtained as shown in Figure 3B and 3C. The product composition settles in the less than 10 hours and much smaller offsets in the acetate composition can be achieved (~0.002 m.f. for EtAc and nil for IPAc). For the type III flowsheets, two different dynamics are observed which can be foreseen from nonlinear analysis (Table 1). For the BuAc system, the product composition dynamics settles in less than 5 hours (the fastest response) and symmetrical responses can also been seen for most of the process variables except the trace acid concentration (Figure 3D). Steady-state offsets are also observed, but error is around 0.02 m.f. for ±20% feed flow changes. For the AmAc system, again, fast dynamics is attainable, but the responses are asymmetrical especially for the product compositions ($X_{B,acetate}$ and X_{D,H_2O}). Large steady-state offset (~0.02 m.f.) is also observed for the acetate composition.

Despite the strong nonlinearity, workable temperature control of esterification reactive distillation systems can be obtained using a systematic design procedure with rather simple control structure. It should be emphasized that the selections of controlled and manipulated variables (control structure design) play a crucial role for these highly nonlinear processes and the decentralized control provides a better structure to cope with steady-state gain variations. As expected, MeAc system (type I flowsheet) exhibits relatively poor control performance as can be seen early from quantitative nonlinearity measures. The closed-loop behavior of the EtAc and IPAc (type II flowsheet) is not as quite nonlinear as the steady-state measures predict. Relatively fast and symmetrical dynamics can be obtained as shown in Figures 3B, 3C. One reason for this is that the type II flowsheet has a two-column configuration (Figure 1) and they are separated by a decanter with typically a 20 minutes holdup. In other words, a large surge tank is placed between these two units and they are somewhat decoupled dynamically. As predicted, the BuAc system should be an easy one to control and the closed-loop responses confirmed that (Figure 3D). the other type III flowsheet, the AmAc system, on the other hand, gives significantly different closed-loop performance. Less symmetrical responses are observed as predicted by the nonlinearity measures and a large composition offset results for feed flow rate changes (Figure 3E). However, similar to the BuAc system, the type III flowsheet generally gives fast closed-loop dynamics.

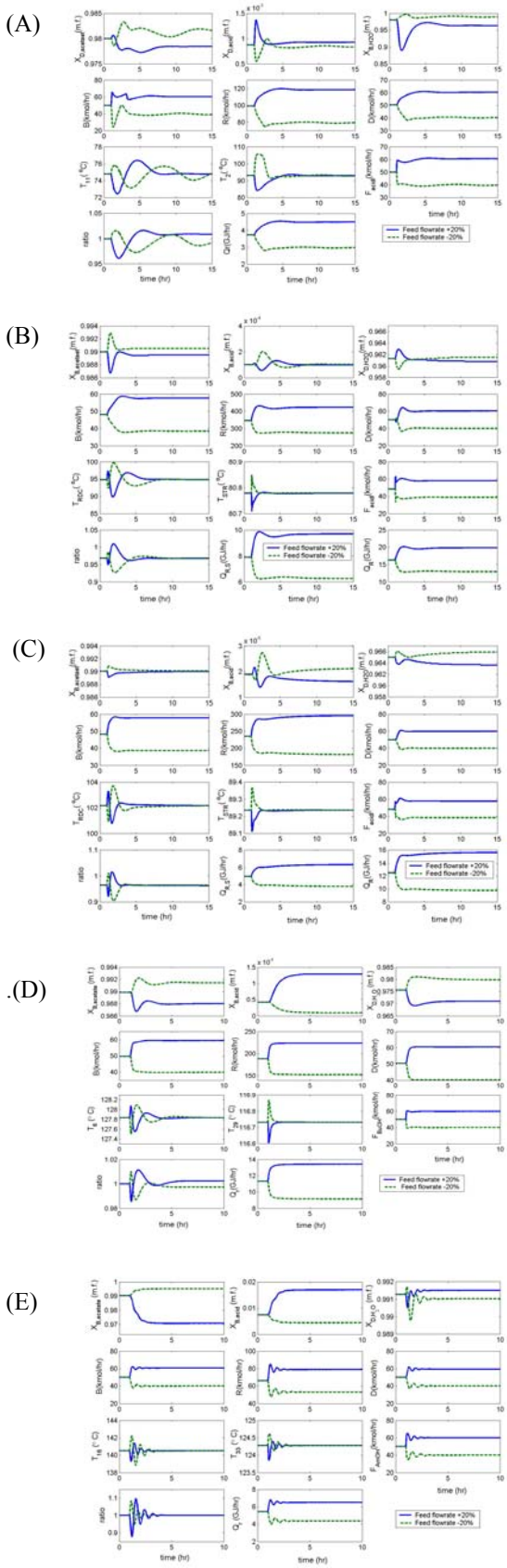

Figure 3. Temperature control responses for ±20% production rate changes for MeAc (A), EtAc (B), IPAc (C), BuAc(D), and AmAc (E) systems.

5. Conclusion

The dynamics and control for three different types of reactive distillation flowsheets (type I, II, and III) are

explored. This covers acetic acid esterification with different alcohols ranging from C_1 (MeOH) to C_5 (AmOH). Simultaneous reaction and separation leads to strongly nonlinearity to all five systems studied. However, the degree of nonlinearity can be analyzed qualitatively or computed quantitatively. A systematic design procedure is proposed to devise the control structures for all three types of flowsheets. The simulation results reveal that workable temperature control can be obtained for these highly nonlinear processes with simple control. Moreover, the closed-loop systems do behave as the preliminary nonlinear analyses predict and inherent strong nonlinearity does lead to asymmetrical responses, especially for the MeAc and AmAc systems. As far as the flowsheet is concerned, the type II flowsheet (EtAc and IPAc) is divided into two units separated by a large decanter. This somewhat damps out the disturbance between the RDC and the stripper which subsequently leads to a more controllable process. The flowsheet (BuAc and AmAc) where a decanter is used to provide a natural one-end composition control via liquid-liquid equilibrium. Interaction between top and bottom composition control can, thus, be alleviated. Finally, the type I flowsheet cannot escape from either the inherent nonlinearity or the dynamic interactions. The nonlinearity and strong interactions lead to a very difficult process to control.

Acknowledgement

This work was supported by the Ministry of Economic Affairs under grant 92-EC-17-A-09-S1-019.

REFERENCES

Al-Arfaj MA, Luyben WL. Comparison of Alternative Control Structures for an ideal Two-product Reactive Distillation Column. *Ind. Eng. Chem. Res.* 2000; 39:3298-3307.

Chiang SF, Kuo CL, Yu CC, David SHW. Design Alternatives for the Amyl Acetate Process: Coupled Reactor/Column and Reactive Distillation. *Ind. Eng. Chem. Res.* 2002;41:3233-4246.

Chang JW, Yu CC. The Relative Gain for Non-square Multivariable Systems. *Chem. Eng. Sci.* 1990;45:1309.

Doherty MF, Malone MF. Conceptual Design of Distillation System. New York: McGraw-Hill, USA 2001.

Engell S, Fernholz G. Control of a Reactive Separation Process. *Chemical Engineering and Processing*. 2003;42:201-210.

Grüner S, Mohl KD, Kienle A, Gilles ED, Fernholz G, Fredrich M. Nonlinear Control of a Reactive Distillation Column. *Control Engineering Practice*, 2003;11: 915-925.

Huang SG., Kuo CL, Hung SB, Chen YW, Yu CC. Temperature Control of Heterogeneous Reactive Distillation. *AIChE J.* 2004;50:2203-2216.

Hernjak N, Doyle III FJ. Correlation of Process Nonlinearity with Closed-Loop Disturbance Rejection. *Ind. Eng. Chem. Res.* 2003;42:4611-4619.

Kaymak DB, Luyben WL. Quantitative Comparison of Reactive Distillation with Conventional Multiunit Reactor/Column/Recycle Systems for Different Chemical Equilibrium Constants. *Ind. Eng. Chem. Res.* 2004;43:2493-2507.

Kaymak DB, Luyben WL. Comparison of Two Types of Two-Temperature Control Structures for Reactive Distillation Columns. submitted to *Ind. Eng. Chem. Res* (2005).

Kaymak DB, Luyben WL. Evaluation of a Two-Temperature Control Structure for a Two-Reactant/Two-Product Type of Reactive Distillation Column. submitted to *Ind. Eng. Chem. Res* (2005).

Luyben WL. Practical Distillation Control. New York: Van Nostrand Reinhold Ed, 1992.

Luyben WL. Economic and Dynamic Impact of the Use of Excess Reactant in Reactive Distillation Systems. *Ind. Eng. Chem. Res.* 2000;39:2935-2946.

Malone MF, Doherty MF. Reactive Distillation. *Ind. Eng. Chem. Res.* 2000;39:3953.

Sundmacher K, Kienle A. Reactive Distillation: Status and Future Directions. Germany: Wiley-VCH Verlag GmbH & Co. KGaA, Weinheim, 2003.

Menold PH, Allgöwer F, Pearson RK. Nonlinear Structure Identification of Chemical Processes. *Computers Chem. Eng*. 1997;21:S137-S142.

Roat S, Downs J, Vogel E, Doss J. Integration of Rigorous Dynamic Modeling and Control System Synthesis for Distillation Columns. in Chemical process Control- CPC III; Elsevier, Amsterdam,1986;99-138.

Sneesby MG., Tade MO, Smith TN. Two-Point Control of a Reactive Distillation Column for Composition and Conversion. *J. Process Control*. 1999;9:19-31.

Schweickhardt T, Allgower F. Quantitative Nonlinearity Assessment: An Introduction to Nonlinearity Measure. Integration of Process Design and Control. Amsterdam: Seferlis, P. and Georgiadis, M. C. Eds., Elsevier,2004.

Schweickhardt T, Allgower F. Linear Modeling Error and Steady-state Behaviour of Nonlinear Dynamical Systems. Internal Report, Institute of System Theory in Engineering, University of Stuttgart (2005).

Shen SH, Yu CC. Use of Relay-Feedback Test for Automatic Tuning of Multivariable Systems. *AIChE J.* 1994;40:627-646.

Tang YT, Hung SB, Chen YW, Huang HP, Lee MJ, Yu CC. Design of Reactive Distillations for Acetic Acid Esterification with Different Alcohols. *AIChE J.* 2005;51:1683-1699

ADCHEM 2006

International Symposium on Advanced Control of Chemical Processes
Gramado, Brazil – April 2-5, 2006

A WAVELET FILTERING APPLICATION FOR ON-LINE DYNAMIC DATA RECONCILIATION

Kuo-Yuan Luo, Hsiao-Ping Huang[1]

Department of Chemical Engineering,
National Taiwan University,
Taipei, Taiwan, R.O.C.

Abstract: Discrete wavelet transform (DWT) is known for its signal processing ability. In the recent researches, DWT is adopted for signal filtering before executing dynamic data reconciliation. While on-line dynamic data reconciliation is concerned, the computation is heavy duo to the filtering in every time instant. In this article, a shift property of the DWT is indicated and is applied to reduce the computation duty. The efficiency of this application is also discussed.

Keywords: filtering technique, data processing, dicsrete wavelets transform, integral method

1. INTRODUCTION[1]

Data reconciliation can be used to reduce the measurement errors which come from imperfect instrument measurements. In this way, the adjusted data obey the natural laws. Measurement redundancies, which include functional and temporal redundancy, are the first important consideration in processing data reconciliation. Measurements are functionally redundant if there are more than enough data to completely define the process model at any time instant in time. Measurements are temporally redundant if past measurements are available to reconcile the measurements. Then the data reconciliation problem is defined as a constrained, weighted, least-squares optimization problem.

The steady-state data reconciliation is well-documented (Narasimhan and Jordache, 2000; Romagnoli and Sanchez, 2000) and have applications in industrial processes (Crowe, 1996). However, dynamic data reconciliation is better to deal with this kind of problem in the real conditions.The formulation of the dynamic data reconciliation can be written in Eqs. (1)-(4).

$$\min \ \phi[y,\ \hat{y};\ \Sigma] \tag{1}$$

$$g_1\left(\frac{\mathrm{d}\hat{y}(t)}{\mathrm{d}t},\hat{y}(t)\right)=0 \tag{2}$$

$$g_2\left(\hat{y}(t)\right)=0 \tag{3}$$

$$g_3\left(\hat{y}(t)\right)\geq 0 \tag{4}$$

Where, ϕ is the objective function, g_1 is the differential equation constraint, g_2 is the algebraic equality constraint, g_3 is the inequality constraint, y is the measurement variable, $\hat{y}$ is the reconciled variable and Σ is the covariance matrix. A general data reconciliation problem is thus formulated as minimizing an object function of Eq. (1) subjected to equality and inequality constraints of Eqs. (2)-(4).

There have been different kinds of solutions to the optimization problems. The discretization-based methods solve the problems by transforming the differential equations into algebraic equations (Liebman *et al.*, 1992; Rollins and Devanathan, 1993; Albuquerque and Biegler, 1996). But discretization increases the number of variables and equations, which increase the computation effort, and is impractical for applications in the real process. Dynamic data reconciliation methods by pre-treating the variables with wavelets analysis are also proposed (Kong *et al.*, 2000; Luo and Huang, 2005; Tona *et al.*, 2005).

[1] Author to whom all correspondence should be addressed.
E-mail: huanghpc@ntu.edu.tw;
Tel: 886-2-2363-8999,
Fax: 886-2-2362-3935.

If these methods are used in the on-line application, the algorithms need to be executed in every time instant which leads to a lot of computation duties. In this article, an integral approach method for dynamic data reconciliation with wavelets pre-treatment of the measurement signals is proposed. A shift property of the discrete wavelet transform (DWT) is also addressed. Based on this property, a method is proposed which can reduce the computation duties of the traditional DWT. The analysis of the efficiencies is also discussed. Finally, a four-tank process is taken to testify the proposed method.

2. FILTERING BY WAVELETS

Wavelets are families of mathematical functions, which have been applied widely for signal and image processing. Wavelets theories are introduced friendly in the text book (Burrus *et al.*, 1998) and some simple application examples are illustrated in the Matlab® user guide for wavelet toolbox (Misiti *et al.*, 1997). In practice, the wavelets analysis is accomplished by discrete wavelet transform (DWT), whose algorithm is well matched to the digital computer. The DWT is commonly employed using dyadic filter banks, which are sets of filters that divide a signal frequency band into sub-bands. These filter banks are comprised of low-pass, high-pass filters and the outputs are the approximation coefficients and the detail coefficients. The process of obtaining the approximation and detail coefficients is called decomposition. This process can be repeated with successive approximations (the output of the low-pass filter in the first bank) being decomposed in turn, called multilevel decomposition, so that one signal is broken down into a number of components. The inverse discrete wavelet transform (IDWT) reconstructs a signal from the approximation and detail coefficients derived from decomposition at certain level. And the filtering is accomplished by omitting the detail coefficients at the proper decomposition level (Luo and Huang, 2005). The details of the proposed are described in the following article.

2.1 Moving-Horizon Filtering

As carrying out data reconciliation on-line, the filtering is repeated at every time instant with a finite length. The choices of the wavelets and the length of the moving-horizon are discussed in the following part of this section.

2.2 Shift Property of DWT

In mathematics, the DWT decomposition includes two procedures: 1. convolution, 2. down-sampling.
The two procedures can be expressed by Eq. (5) (Jensen and Cour-Harbo, 2001).

$$c_0[k] = \sum_f h_0[2k-f]X[f] = \sum_f h_0[f]X[2k-f] \qquad (5)$$

C_0 is the 'approximate' coefficient, h_0 is the low pass filter, f is the length of the filter and X is the original signal. The procedure is shown in the Figure 1 and constant padding is used to solve the problems of end distortion. In order to simplify the condition, n is set to be even. And assuming that the previous moving-horizon, X_1, is represented by Eq. (6) and the instant moving-horizon, X_2, is represented by Eq. (7).

$$X_1 = [x_1 \quad x_2 \quad \cdots \quad x_n] \quad (6)$$

$$X_2 = [x_3 \quad x_4 \quad \cdots \quad x_{n+2}] \quad (7)$$

According to the Eq. (5), as the moving-horizon moving by two points at a time, some coefficients of this window are identical with some coefficients of the previous window. So the DWT decomposition can be executed by just calculating some coefficients on two sides and shifting some coefficients of the previous window. Precisely, the shift relation can be expressed as Eq. (8).

$$\tilde{c}_{i/2} = c_{(i+2)/2} \qquad (8)$$

$\tilde{c}$ is the coefficient of the present moving-horizon and c is the coefficient of the previous moving-horizon. The corrected terms of both sides are calculated by Eqs. (9) and (10). In this manner, the DWT procedure is accomplished in another way but the computation is saved.

$$\begin{bmatrix} \tilde{c}_1 \\ \tilde{c}_2 \\ \vdots \\ \tilde{c}_{(f-2)/2} \end{bmatrix}_{\frac{f-2}{2}} = \begin{bmatrix} h_2+\cdots+h_f & h_1 & 0 & \cdots & & & 0 \\ h_4+\cdots+h_f & h_3 & h_2 & h_1 & 0 & \cdots & 0 \\ \vdots & & & & \ddots & & 0 \\ h_{f-2}+\cdots+h_f & \cdots & & & & \cdots & h_2 \quad h_1 \end{bmatrix}_{\frac{f-2}{2}\times f-2} \begin{bmatrix} x_3 \\ x_4 \\ \vdots \\ x_f \end{bmatrix}_{f-2} \qquad (9)$$

$$\begin{bmatrix} \tilde{c}_{n/2} \\ \tilde{c}_{n/2+1} \\ \vdots \\ \tilde{c}_{(n+f-2)/2} \end{bmatrix}_{f/2} = \begin{bmatrix} h_f & h_{f-1} & \cdots & & & \cdots & h_2 & h_1 \\ & & \ddots & & & & & \vdots \\ & & \cdots & 0 & h_f & h_{f-1} & h_{f-2} & h_1+\cdots+h_{f-3} \\ & & & & \cdots & 0 & h_f & h_1+\cdots+h_{f-1} \end{bmatrix}_{(f/2)\times(f)} \begin{bmatrix} x_{n+2-f+1} \\ \vdots \\ x_{n+1} \\ x_{n+2} \end{bmatrix}_f \qquad (10)$$

2.3 Applying the Shift Property to Multilevel DWT Decomposition

The shift property described in the previous article can be revealed in the multilevel decomposition if the following two conditions are held.

1. The length of the coefficients of different levels must be even (identical to the original assumption).
2. The coefficients must be moved by two points compared with the previous moving-horizon.

Duo to the first reason, as processing multilevel DWT decomposition, the length of the moving-horizon must be with a specific length according the types of the wavelets. In order words, there are specific lengths of the chosen wavelets to satisfy this condition. Some specific lengths of the Daubechies wavelets are listed in Table 1. For example, if five-level DWT decomposition is desired, the smallest length of the moving-horizon will be the number at the column No. 5 at Table 1 to make sure the length of different level to be even.

The second condition is that coefficients at the different DWT decomposition level must be moved by two points compared with the certain previous moving-horizon.
A phenomenon of DWT is described firstly.
From Eq. (8) (disregard the corrected terms), it is known that the 1st level coefficients are shifted by

one point if the 0^{th} level coefficients (i.e., original signal) are moved by two points. The 2^{nd} level coefficients are shifted by one point if the 1^{st} level coefficients are moved by two points or the 0^{th} coefficients are moved by four points. In this manner, the shift property holds at level m if the original moving-horizon is moved by 2^m points, which restricts the application for on-line filtering that needs to execute at every time instant (if m level DWT decomposition is desired). But this can be solved by setting a dataset containing the information of different levels coefficients shown in the Figure 3. In Figure 3, the moving-horizon is represented by a solid line. The moving-horizon in the time instant is the line on the rightest. The size of dataset is determined by the chosen DWT level. If the desired multilevel DWT is m , then 2^m moving-horizons need to be built. Furthermore, the first level coefficients can be obtained by calculation from the current moving-horizon and shifting some coefficients from the first level coefficients of the previous two moving-horizons. The second level coefficients can be obtained by calculation from the current first level coefficients and shifting some coefficients from the second level coefficients of the previous four moving-horizon. And the corrected terms at each level are listed in Table 2. In this manner, the on-line filtering by DWT using shift property can be executed at each time instant. In Figure 1, which illustrate just one of the moving-horizon in the test signals, the results are identical between direct DWT decomposition and proposed method. (In the following examples, wavelets Daubechies 6 is adopted and the length f is equal to 12.)

Table 1 Specific length of different Daubechies wavelets

wavelets	Filter length	1	2	3	4	5	6	7	
db02	4	4	6	10	18	34	66	130	…
db04	8	8	10	14	22	38	70	134	…
db06	12	12	14	18	26	42	74	138	…
db08	16	16	18	22	30	46	78	142	…
db10	20	20	22	26	34	50	82	146	…
db12	24	24	26	30	38	54	86	150	…
db14	28	28	30	34	42	58	90	154	…
db16	32	32	34	38	46	62	94	158	…
db18	36	36	38	42	50	66	98	162	…
db20	40	40	42	46	54	70	102	166	…

2.4 Modified Application

The shift property can save the computations compared with the original DWT algorithm. In order to obtain larger computation efficiency, a modified application is also proposed.

As on-line application, not all of the data in filtered signal in the moving-horizon is needed. Filtered data near the time instant is desired in the application, so the correction action on the right side is executed and the right side result of reconstruction is consistent with the right side result of the direct IDWT. The number of the identical data depends on which level is chosen. The larger chosen level leads to less identical terms. Further, as reconstruction, it can just focus on the desired terms. Not all of the filtered data needs to be reconstructed. It can reconstruct the data with certain points at each level. For example, if the last 12 terms of the filtered data are needed, then the reconstruction at each level can be set to 12 terms to obtain the final 12 terms. In this way, the computation is saved more.

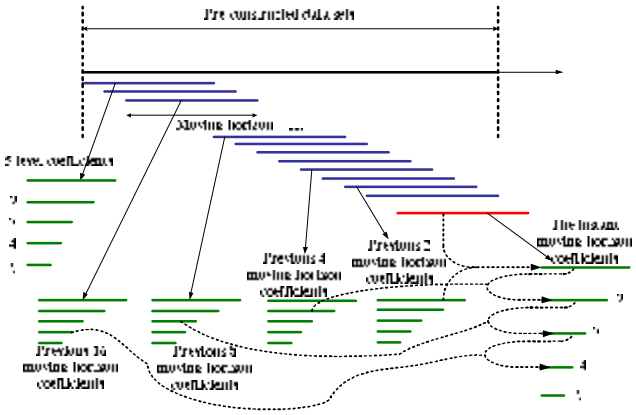

Fig. 1. on-line filtering application

Table 2 Corrected terms at each level

level	Left side	Right side
1	$(f\text{-}2)/2$ (l_1)	$f/2$ (r_1)
2	$floor\{(l_1+f\text{-}1)/2\}(l_2)$	$ceil\{(r_1+1)/2\}+floor\{(f\text{-}1)/2\}(r_2)$
3	$floor\{(l_2+f\text{-}1)/2\}(l_3)$	$ceil\{(r_2+1)/2\}+floor\{(f\text{-}1)/2\}(r_3)$
4	…	…

*"*floor*" rounds the elements of X to the nearest integers towards minus infinity.
*"*ceil*" rounds the elements of X to the nearest integers towards infinity.

2.5 Determination of DWT Level

Determination of the DWT level is accomplished by the method proposed by Luo and Huang (2005). From DWT and IDWT procedure, the signal is decomposed into various parts, i.e., high frequency (detail) and low frequency (approximate) part. Like shown in Figure 2, A_i is the approximate of the signal and D_i is the detail of the signal. The relation between A_i and D_i is expressed in Eq. (11).

$$A_i = A_{i+1} + D_{i+1} \tag{11}$$

The square errors of D_i , i.e. the energy of the detail part, represent the removed energy after decomposition at the level i. The energy of D_i should be decreases as i increases duo to the narrower band-pass region. If the energy of D_i increases suddenly at certain level, which means some dominated low frequency signal is filtered, then the decomposition level is determined at the previous level.

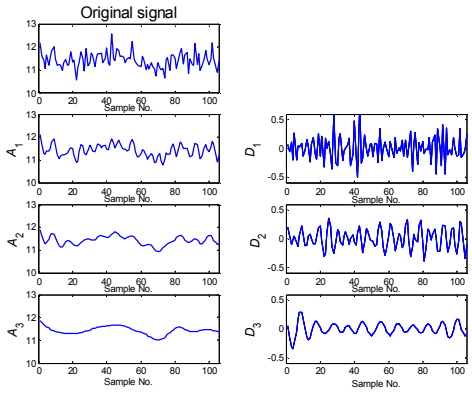

Fig. 2. DWT analysis and IDWT synthesis

2.6 The Efficiency Analysis

In this section, the efficiency is discussed. In order to discuss the efficiency of the proposed algorithm, it is assumed that a convolution calculation is viewed as a computation unit. For traditional DWT, the computation unit of different level can be calculated by Eq. (12) which means the length after convolution. And s_1 can be the length of the signal or coefficients at different level. The coefficient at different level can be calculated by Eq. (13). s_2 is the length of the coefficients of the previous level.

$$s_1 + f - 1 \tag{12}$$

$$(s_2 + f - 2)/2 \tag{13}$$

If the length of the signal is n and the length of the filter is f, then the convolution leads to a signal with length equal to $n + f - 1$. After down-sampling, the length of 1st level coefficients is equal to $(n + f - 2)/2$. In Table 3, the computation units of direct DWT are listed. As IDWT reconstruction, the procedure includes firstly up-sampling and then convolution. The computation unit can be calculated by Eq. (14) which means the length after convolution the up-sampling sequences, where s_3 is the length of the signal or coefficient at different level and the results are listed in Table 4.

$$(2 * s_3 - 1) + f - 1 \tag{14}$$

For the DWT decomposition of the proposed modified method, the computation unit of different level is the same and is equal to the corrected terms at the right side, $f/2$. For IDWT reconstruction, the computation unit is also calculated by Eq. (14) but s_3 keeps constant at the different level and usually s_3 is set to the length of the coefficients at the desired level. While application, two points are considered: 1. length of the moving-horizon, 2. selection of the filter.

Selection of the filter Different wavelets show different filter bands in the frequency domain but the differences are quite small. The mean square errors for the reconstruction signals, which have the same original signal with random noises of fixed standard deviation, from different level of different Daubechies wavelets are plotted in the Figure 3. From the figure, it tells that the performances are almost the same except the first two wavelets. So it can select the wavelets freely after Daubechies 6, but it does matters if the efficiency is considered.

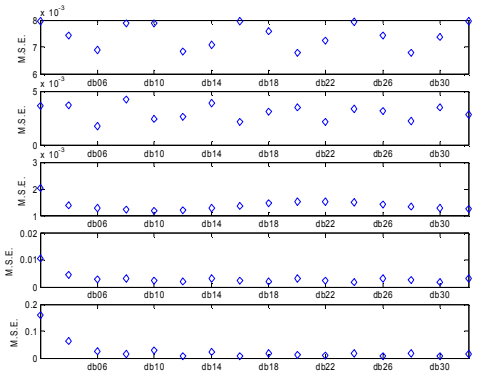

Fig. 3. The mean square errors after different level IDWT reconstruction for different Daubechies wavelets

Table 3 The computation units of direct DWT

DWT decomposition	Computation unit
0-th level to 1st level	$n + f - 1$
1st level to 2nd level	$(n + 3f - 4)/2$
2nd level to 3rd level	$(n + 7f - 7)/4$
3rd level to 4th level	$(n + 15f - 22)/8$
…	…

Table 4 The computation units of direct IDWT

IDWT reconstruction	Computation unit
…	…
4th level to 3rd level	$(n + 23f - 46)/8$
3rd level to 2nd level	$(n + 11f - 22)/4$
2nd level to 1st level	$(n + 5f - 10)/2$
1st level to 0th level	$n + 2f - 4$

Length of the moving-horizon According to Table 3 and Table 4, assuming that four-level of DWT decomposition is chosen, then the total computation units of direct DWT is equal to $(15n + 65f - 114)/4$. For the proposed method, the total computation units is $(15n + 97f - 162)/8$ (s_3 in Eq. (14) is equal the length of the 4th level coefficients). Then the efficiencies of different Daubechies wavelets with corresponding lengths in the Table 2 are calculated and the results are listed in Table 5. If the computation units are normalized, then the efficiencies are shown as Figure 4. It can see from the figure that at certain length there exist the best benefits.

3. INTEGRAL APPROACH RECONCILIATION

Applying the integral approach reconciliation method (Luo and Huang, 2005) to the filtered signal, the algorithms are described briefly in the following article.

Table 5 Efficiencies of different length of the moving horizon respect to different Daubechies wavelets

	5	6	7	8
db02	0.5738	0.6703	0.7483	0.8007
db04	0.5062	0.6036	0.6959	0.7663
db06	0.4653	0.5573	0.6545	0.7363
db08	0.438	0.5232	0.6209	0.71
db10	0.4184	0.4971	0.5931	0.6866
db12	0.4037	0.4764	0.5697	0.6658
db14	0.3923	0.4597	0.5498	0.6471

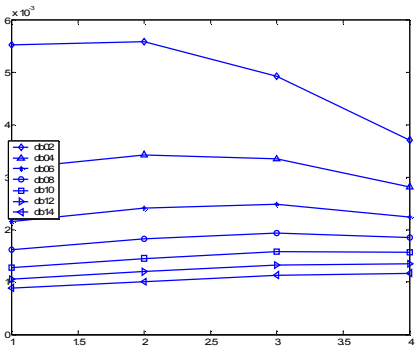

Fig. 4. Efficiencies with normalized computation units

By integrating differential-algebraic (DAE) equations of a linear dynamic system between some time t_0 and t_n, we can get the following algebraic Equations (i.e. Eqs. (15) and (16)). ***h*** is the vector of state variables, ***f*** is the vector of non-state variables, ***A*** and ***C*** are constant matrices from the algebraic part of the DAE.

$$\int_{t_0}^{t_n} \frac{\mathrm{d}h}{\mathrm{d}t} dt = A \int_{t_0}^{t_n} f \,\mathrm{d}t \tag{15}$$

$$C \int_{t_0}^{t_n} f \mathrm{d}t = 0 \tag{16}$$

Let $Z_1 = \int_{t_0}^{t_n} \frac{\mathrm{d}h}{\mathrm{d}t}\,\mathrm{d}t$, $Z_2 = \int_{t_0}^{t_n} f\,\mathrm{d}t$, and we can rearrange the integrations and get the following matrix form in Eq. (17).

$$\begin{bmatrix} A & -I \\ C & 0 \end{bmatrix} \begin{bmatrix} Z_2 \\ Z_1 \end{bmatrix} = 0 \tag{17}$$

It shows that the result is an algebraic constraint. In the following, the reconciliation procedure is to incorporate the integrating part by Simpson's rule for numerical integration. Then the algebraic equations can be expressed as Eqs. (18) and (19).

$$Z_1 = Q_1 * F \tag{18}$$

$$Z_2 = Q_2 * H \tag{19}$$

Define new variable ***H*** and ***F*** which represent the collections of all measurements of all instruments during the integrating time interval t_0 to t_n. Finally, we obtain the algebraic constraint equation (Eq. 20) represented by ***H*** and ***F*** from the original DAE.

$$\begin{bmatrix} A & -I \\ C & 0 \end{bmatrix} \begin{bmatrix} Q_1 & 0 \\ 0 & Q_2 \end{bmatrix} \begin{bmatrix} F \\ H \end{bmatrix} = 0 \tag{20}$$

With the equality constraint, the reconciliation problem can be solved. As on-line reconciliation, one reconciled point is obtained in one moving-horizon.

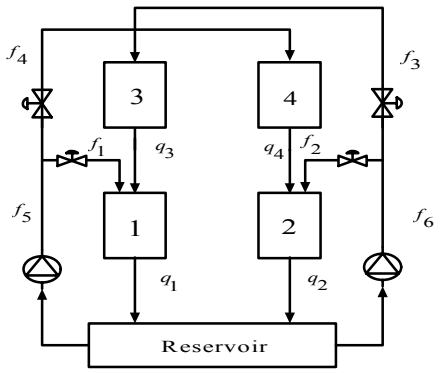

Fig. 5 A four-tank system

4. EXAMPLE

A four-tank system shown in Figure 5 is illustrated as an example. The differential algebraic equation of this example is showed in Eq. (21). There are two main flows f_5, f_6 split into two branches apiece. The four branches, f_1, f_2, f_3, f_4, flow into four tanks respectively. Each tank has flow, q_1, q_2, q_3, q_4, out of it. The flow out of tank 3 is fed into tank 1 and the one out of tank 4 is fed into tank 2. Parameters of the process are listed in Table 6. From the analysis in section 2, wavelets "Daubechies 6" is selected and the moving-horizon is 74.The results are shown in Figures (6)-(8).

$$\begin{aligned} A r_1 \frac{\mathrm{d}h_1}{\mathrm{d}t} &= -q_1 + q_3 + f_1 \\ A r_2 \frac{\mathrm{d}h_2}{\mathrm{d}t} &= -q_2 + q_4 + f_2 \\ A r_3 \frac{\mathrm{d}h_3}{\mathrm{d}t} &= -q_3 + f_3 \\ A r_4 \frac{\mathrm{d}h_4}{\mathrm{d}t} &= -q_4 + f_4 \\ f_5 &= f_1 + f_4 \\ f_6 &= f_2 + f_3 \end{aligned} \tag{21}$$

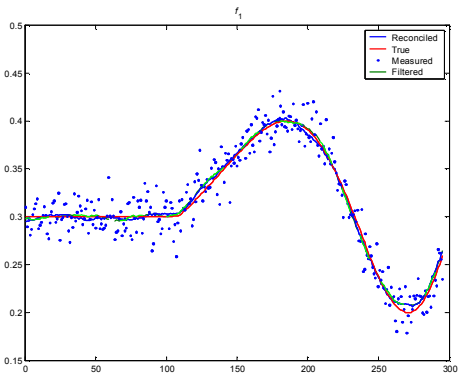

Fig. 6 Reconciled result of f_1

CONCLUSIONS

In this research, the wavelet filtering is used to apply in the on-line dynamic data reconciliation. In the theory, the shift property of the DWT is the basic idea to establish the method whose main purpose is to save the DWT computation efforts. A modified method is actually being applied which can save more computation efforts. The efficiencies of different Daubechies wavelets are discussed in order to decide the best performance match-up. The reconciliation performances are good.

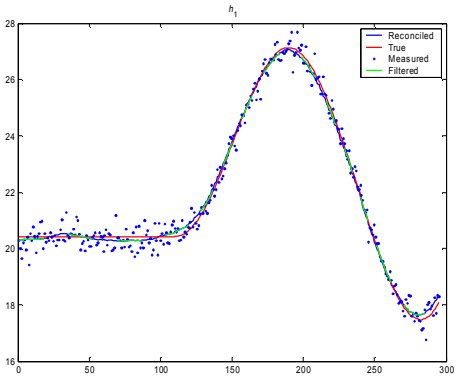

Fig. 7 Reconciled result of h_1

Table 6 Parameters of the four-tank system

Symbol	State/Parameter	Value	Dimension
h_0	Nominal levels	[20.4; 20.4; 11.5; 11.5]	cm
a_i	Area of the drain	[3; 3; 2 ;2]	cm^2
Ar_i	Area of tank *i*	1000	cm^2
f_i	flow into the tank *i*	[0.3; 0.3; 0.3; 0.3; 0.6; 0.6]	cm^3/S
T_i	Time constants	[68; 68; 76.5; 76.5]	S
g	Gravitation constant	981	cm/S^2
σ_f	Standard deviation of flow	0.015	cm^3/S
σ_h	Standard deviation of level	0.6	cm

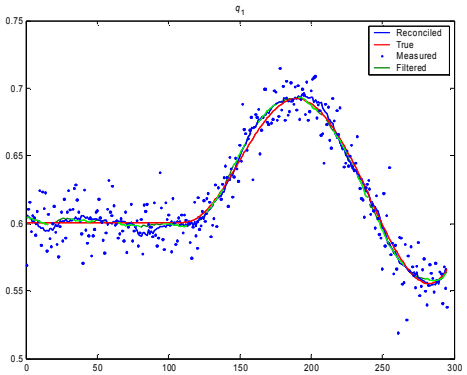

Fig. 8 Reconciled result of q_1

REFERENNCE

Albuquerque, J. S. and L. T. Biegler (1996). Data reconciliation and gross-error detection for dynamic systems. *AIChE J.*, **42**, 2841-2856.

Burrus, C. S., R. A. Gopinath and H. Guo (1998). *Introduction to Wavelets and Wavelet Transformations- A Primer*. Prentice-Hall, Upper Saddle River, U.S.A.

Crowe, C. M. (1996). Data reconciliation – progress and challenges. *J. Proc. Cont.* **6,** 89-98.

Jensen, A. and A. Cour-Harbo (2001). *Ripples in mathematics-the discrete wavelet transform*. Springer-Verlag, Berkin Heidelberg, Germany.

Kong, M., B. Chen and X. He (2002). Wavelet-based regulation of dynamic data reconciliation. *Ind. Eng. Chem. Res.,* **41**, 3405-3412.

Liebman, M. J., T. F. Edgar and L. S. Lasdon (1992). Efficient data reconliliation for dynamic processes using nonlinear programming techniques. *Comput. Chem. Eng.*, **16**, 963-986.

Luo, K. and H. Huang (2005). A wavelet enhanced integral approach to linear dynamic data reconciliation. *Proceedings of 16th IFAC World Congress.*

Misiti, M., Y. Misiti, G. Oppenheim and J. M. Poggi (1997). *Wavelet Toolbox for Use with MATLAB® :User's Guide Version 2*. The MathWorks, Inc., Apple Hill Drive Natick, MA.

Narasimhan, S. and C. Jordache (2000). *Data reconciliation and gross error detection-an intelligent use of process data*, Gulf Publishing Company, Houston, U.S.A.

Rollins, D. K. and S. Devanathan (1993). Unbised estimation in dynamic data reconciliation. *AIChE J.*, **39,** 1330-1334.

Romagnoli, J. A. and M. C. Sanchez (2000). *Data processing and reconciliation for chemical process operations*, Academic Press, San Diego, U.S.A.

Tona, R. V., C. Benqlilou, A. Espuna and L. Puigjaner (2005). Dynamic data reconciliation based on wavelet trend analysis. *Ind. Eng. Chem. Res.,* 44, 4323-4335

CONSTRAINED NONLINEAR MODEL PREDICTIVE CONTROL FOR PRACTICAL APPLICATION

A. G. Montandon[1], R. M. Borges[2] , H. M. Henrique[3]

School of Chemical Engineering/Federal University of Uberlandia
Av. João Naves de Ávila, 2160
Phone number: +55-34-3239-4292 Fax number: +55-34-3239-4188
POB 38400-100 Uberlandia - MG, Brazil
E-mails: amanda.montandon@bra.xerox.com.br[1], raquel.borges@ele.ufes.br[2], humberto@ufu.br[3]

Abstract: The proposed MPC is based on a successive linearization of the model at each sampling time and a formulation of a MPC. The cost function of the MPC problem is subject to a reference system as equality constraint and to upper and lower limits in the input variables. In order to satisfy both constraints simultaneously it is needed to include a slack variable in the equality constraint. This slack variable provides more flexibility in the control moves so that the solution of the optimization problem becomes feasible. Proposed controller was implemented to an experimental neutralization pH plant. Results showed a very satisfactory performance of the proposed strategy. *Copyright © 2006 IFAC*

Keywords: Dynamic systems, MPC, Reference System, Constrained nonlinear control, Neural network, pH neutralization process.

1. INTRODUCTION

Process control is concerned to application of automatic control principles for industrial processes. The effect of the global competition in industries has caused the perception of the importance of the product quality in the profitability. Because of this control strategies are used to assure a satisfactory product quality and to decrease raw and energy cost.
However, even though the vast majority of chemical processes are inherently nonlinear, these processes have been controlled by linear controllers. The advantage of this approach is that an easy analytical solution of control problem can be found and a low computational effort is demanded by them. However, the linear approach can be very limiting for highly nonlinear processes and it can lead to unstable solution. The use of nonlinear process models within the control strategy has been shown to provide the potential for significant improvement over linear controllers for nonlinear processes (Bequette, 1991; Henson and Seborg, 1997). Nonlinear model predictive control (NMPC) (Garcia and Morshedi, 1986; Garcia *et al.*, 1989; Gattu and Zafiriou, 1992) and input-output linearizing control (IOLC) are the most widely studied nonlinear control techniques for process control problems. NMPC offers many of the appealing features of linear model predictive control, including explicit compensation for input and output constraints (Meadows et al., 1995). As compared to NMPC, IOLC offers several important advantages including transparent controller tuning and low computational requirements (Kravaris and Kantor, 1990). However, conventional feedback linearization techniques have neither constraint handling (Rawlings et al., 1994) nor predictive capabilities. This has motivated the development of several modifications of the basic input-output linearization approach (Balchen and Sandrib, 1995; Kendi and Doyle, 1995).

On the other hand, the nonlinear approach can result in a large computational effort what turn its use is limited for practical applications. The aim of this work is to present a nonlinear control technique which is computationally feasible for industrial implementation. The proposed strategy is a predictive control technique (MPC) based on a successive linearization of the model via Taylor's series expansion at each sampling time. The cost function of the optimization problem is subject to a first order reference system as a constraint together with upper and lower limits in the inputs. In order to satisfy both constraints simultaneously and to provide a feasible solution, it is necessary to include a slack variable (λ) in the cost function of the optimization problem. The advantage of the proposed algorithm is that it does not need be re-tuned for different operating points. An experimental study was carried out in a pH neutralization plant.

2. THE DYNAMIC SYSTEM

Consider a general dynamic system described by:

$$\frac{d\mathbf{x}}{dt} = \mathbf{f}(\mathbf{x},\mathbf{u}) \qquad \mathbf{y} = \mathbf{h}(\mathbf{x}) \tag{1}$$

Where $\mathbf{u} \in \mathbb{R}^n$ is the vector of manipulated variables, $\mathbf{x} \in \mathbb{R}^m$ is the state vector and $\mathbf{y} \in \mathbb{R}^n$ is the output vector. Linearizing Eq. (1) via Taylor's series expansion around the point immediately earlier to the current point of operation, the following equation is obtained:

$$\frac{d\mathbf{x}}{dt} = \mathbf{A}_{k-1}\mathbf{x} + \mathbf{B}_{k-1}\mathbf{u} + \mathbf{f}_{k-1} \qquad \mathbf{y} = \mathbf{C}_{k-1}\mathbf{x} + \mathbf{h}_{k-1} \quad (2)$$

Where $\mathbf{A}_{k-1} \in \mathbb{R}^{m\times m}$, $\mathbf{B}_{k-1} \in \mathbb{R}^{n\times n}$, $\mathbf{C}_{k-1} \in \mathbb{R}^{n\times m}$, $\mathbf{f}_{k-1}$: $\mathbb{R}^{n+m} \to \mathbb{R}^n$ and $\mathbf{h}_{k-1}$: $\mathbb{R}^m \to \mathbb{R}^n$ are given by:

$$\mathbf{A}_{k-1} = \left(\partial \mathbf{f} / \partial \mathbf{x}\right)\Big|_{\mathbf{x}=\mathbf{x}(k-1),\mathbf{u}=\mathbf{u}(k-1)}$$
$$\mathbf{B}_{k-1} = \left(\partial \mathbf{f} / \partial \mathbf{u}\right)\Big|_{\mathbf{x}=\mathbf{x}(k-1),\mathbf{u}=\mathbf{u}(k-1)}$$
$$\mathbf{C}_{k-1} = \left(\partial \mathbf{h} / \partial \mathbf{x}\right)\Big|_{\mathbf{x}=\mathbf{x}(k-1)}$$
$$\mathbf{f}_{k-1} = \mathbf{f}(\mathbf{x},\mathbf{u})\Big|_{\mathbf{x}=\mathbf{x}(k-1),\mathbf{u}=\mathbf{u}(k-1)}$$
$$\mathbf{h}_{k-1} = \mathbf{h}(\mathbf{x})\Big|_{\mathbf{x}=\mathbf{x}(k-1)}$$

Eq.(2) is integrated from t to t+Δt assuming $\mathbf{u}(k)$ constant during sampling instant:

$$\begin{aligned} \hat{\mathbf{x}}(k+1) &= \boldsymbol{\Phi}\,\mathbf{x}(k) + \boldsymbol{\Psi}\,\mathbf{u}(k) + \boldsymbol{\Omega}\mathbf{f}_{k-1} \\ \hat{\mathbf{y}}(k) &= \mathbf{C}\,\mathbf{x}(k) + \mathbf{h}_{k-1} \end{aligned} \quad (3)$$

Where $\boldsymbol{\Phi} \in \mathbb{R}^{m\times m}$, $\boldsymbol{\Psi} \in \mathbb{R}^{m\times n}$, $\boldsymbol{\Omega} \in \mathbb{R}^{m\times m}$ are:

$$\boldsymbol{\Phi} = e^{\mathbf{A}\Delta t}, \quad \boldsymbol{\Psi} = \mathbf{A}^{-1}\left(e^{\mathbf{A}\Delta t} - \mathbf{I}\right)\mathbf{B}, \quad \boldsymbol{\Omega} = \mathbf{A}^{-1}\left(e^{\mathbf{A}\Delta t} - \mathbf{I}\right)$$

Since $\mathbf{A}$ is nonsingular. Eq.(3) can be written for each prediction instant from k = 1 to k = P where P is a prediction horizon and M control horizon with $P \geq M$ and $\Delta\mathbf{u}(k + j) = \mathbf{0}$ to $M < j \leq P$. The resulting set of equations can be put in a matrix form:

$$\hat{\mathbf{y}} = \boldsymbol{\Gamma} \cdot \Delta\mathbf{u} + \boldsymbol{\gamma} \quad (4)$$

Where:

$$\hat{\mathbf{y}} = \left[\hat{\mathbf{y}}(k+1) \quad \hat{\mathbf{y}}(k+2) \quad \cdots \quad \hat{\mathbf{y}}(k+M) \quad \cdots \quad \hat{\mathbf{y}}(k+P)\right]^T$$
$$\Delta\mathbf{u} = \left[\Delta\mathbf{u}(k) \quad \Delta\mathbf{u}(k+1) \quad \cdots \quad \Delta\mathbf{u}(k+M)\right]^T$$

$$\boldsymbol{\Gamma} = \begin{bmatrix} \mathbf{C}\boldsymbol{\Psi} & [\mathbf{0}] & \cdots & [\mathbf{0}] \\ \mathbf{C}(\boldsymbol{\Phi}+\mathbf{I})\boldsymbol{\Psi} & \mathbf{C}\boldsymbol{\Psi} & \cdots & [\mathbf{0}] \\ \vdots & \vdots & \cdots & \vdots \\ \mathbf{C}\left(\sum_{i=1}^{M}\boldsymbol{\Phi}^{i-1}\right)\boldsymbol{\Psi} & \mathbf{C}\left(\sum_{i=1}^{M-1}\boldsymbol{\Phi}^{i-1}\right)\boldsymbol{\Psi} & \cdots & \mathbf{C}\boldsymbol{\Psi} \\ \vdots & \vdots & \cdots & \vdots \\ \mathbf{C}\left(\sum_{i=1}^{P}\boldsymbol{\Phi}^{i-1}\right)\boldsymbol{\Psi} & \mathbf{C}\left(\sum_{i=1}^{P-1}\boldsymbol{\Phi}^{i-1}\right)\boldsymbol{\Psi} & \cdots & \mathbf{C}\left(\sum_{i=1}^{P-M}\boldsymbol{\Phi}^{i-1}\right)\boldsymbol{\Psi} \end{bmatrix}$$

$$\boldsymbol{\gamma} = \begin{bmatrix} \mathbf{y}(k) + \mathbf{C}\boldsymbol{\Phi}\Delta\mathbf{x}(k) \\ \mathbf{y}(k) + \mathbf{C}\left(\sum_{i=1}^{2}\boldsymbol{\Phi}^{i}\right)\Delta\mathbf{x}(k) \\ \vdots \\ \mathbf{y}(k) + \mathbf{C}\left(\sum_{i=1}^{M}\boldsymbol{\Phi}^{i}\right)\Delta\mathbf{x}(k) \\ \vdots \\ \mathbf{y}(k) + \mathbf{C}\left(\sum_{i=1}^{P}\boldsymbol{\Phi}^{i}\right)\Delta\mathbf{x}(k) \end{bmatrix}$$

2.1 The Reference System

The controller is designed in order to transform the closed loop system in a first order system:

$$\frac{d\mathbf{y}^*}{dt} = \mathbf{K}\left(\mathbf{y}^{SP} - \mathbf{y}\right) \quad (5)$$

Where $\mathbf{K} \in \mathbb{R}^{n\times n}$ is tuning parameter, $\mathbf{y}^{SP}$ are the setpoints and $\mathbf{y}^*$ are the reference output trajectories. The controller must satisfy the following reference system:

$$\frac{d\mathbf{y}}{dt} = \frac{d\mathbf{y}^*}{dt} \quad (6)$$

Infeasible solutions of the MPC optimization problem can occur when equality constraints represented by Eq.(6) and hard constraints (upper and lower bounds for inputs) must be satisfied simultaneously. To overcome this problem, a slack variable ($\boldsymbol{\lambda}$) is introduced into Eq.(6) in order to allow the system to deviate from reference system and to satisfy the hard constraints. Therefore, introducing slack variable $\boldsymbol{\lambda} \in \mathbb{R}^n$ into Eq. (6) and substituting Eq. (2) into Eq. (6) we obtain:

$$\mathbf{C}\,\mathbf{f}_{k-1} + \mathbf{C}\mathbf{A}_{k-1}\mathbf{x}(k) + \mathbf{C}\mathbf{B}_{k-1}\mathbf{u}(k) + \boldsymbol{\lambda}(k) = \mathbf{K}\left(\mathbf{y}^{SP}(k) - \mathbf{y}(k)\right) \quad (7)$$

Eq. (7) can be written for each prediction instant and it can be put in a matrix form:

$$\mathbf{D}\;\mathbf{z} = \mathbf{b} \quad (8)$$

Where:

$$\mathbf{D} = \begin{bmatrix} \mathbf{CB} & [\mathbf{0}] & \cdots & [\mathbf{0}] & [\mathbf{I}] & [\mathbf{0}] & [\mathbf{0}] & [\mathbf{0}] & \cdots & [\mathbf{0}] \\ (\mathbf{CA}+\mathbf{KC})\boldsymbol{\Psi} & \mathbf{CB} & \cdots & [\mathbf{0}] & [-\mathbf{I}] & [\mathbf{I}] & [\mathbf{0}] & [\mathbf{0}] & \cdots & [\mathbf{0}] \\ (\mathbf{CA}+\mathbf{KC})\boldsymbol{\Phi}\mathbf{C} & (\mathbf{CA}+\mathbf{KC})\boldsymbol{\Psi} & \cdots & [\mathbf{0}] & [\mathbf{0}] & [-\mathbf{I}] & [\mathbf{I}] & [\mathbf{0}] & \cdots & [\mathbf{0}] \\ \vdots & \vdots & \ddots & \vdots & \vdots & \vdots & \vdots & \vdots & \ddots & \vdots \\ (\mathbf{CA}+\mathbf{KC})\boldsymbol{\Phi}^{P-1}\boldsymbol{\Psi} & (\mathbf{CA}+\mathbf{KC})\boldsymbol{\Phi}^{P-2}\boldsymbol{\Psi} & \cdots & (\mathbf{CA}+\mathbf{KC})\boldsymbol{\Phi}^{P-M-1}\boldsymbol{\Psi} & [\mathbf{0}] & [\mathbf{0}] & [\mathbf{0}] & [\mathbf{0}] & \cdots & [\mathbf{I}] \end{bmatrix}$$

$$\mathbf{b} = \begin{bmatrix} \mathbf{K}\mathbf{y}^{SP}(k) - (\mathbf{CA}+\mathbf{KC})\mathbf{x}(k) - \mathbf{C}\mathbf{f}_{k-1} \\ \mathbf{K}\Delta\mathbf{y}^{SP}(k+1) - (\mathbf{CA}+\mathbf{KC})\boldsymbol{\Phi}\mathbf{x}(k) \\ \mathbf{K}\Delta\mathbf{y}^{SP}(k+2) - (\mathbf{CA}+\mathbf{KC})\boldsymbol{\Phi}^2\mathbf{x}(k) \\ \vdots \\ \mathbf{K}\Delta\mathbf{y}^{SP}(k+P) - (\mathbf{CA}+\mathbf{KC})\boldsymbol{\Phi}^P\mathbf{x}(k) \end{bmatrix}$$

$$\mathbf{z} = \left[\Delta\mathbf{u}(k) \quad \cdots \quad \Delta\mathbf{u}(k+M) \quad \boldsymbol{\lambda}(k) \quad \cdots \quad \boldsymbol{\lambda}(k+P)\right]^T \tag{9}$$

2.2 The proposed MPC Design

The cost function of the MPC problem is defined as:

$$\min_{\Delta\mathbf{u}(k),\ldots,\Delta\mathbf{u}(k+M),\,\boldsymbol{\lambda}(k),\ldots,\boldsymbol{\lambda}(k+P)} \mathbf{J} = \frac{1}{2}\left(\Delta\mathbf{u}^T\mathbf{R}\,\Delta\mathbf{u} + \boldsymbol{\lambda}^T\mathbf{S}\boldsymbol{\lambda}\right) \tag{10}$$

and also reorganized as a cost function of a quadratic programming problem:

$$\begin{aligned} &\min_{\mathbf{z}(k),\ldots,\mathbf{z}(k+M+P+2)} \ \mathbf{J} = \frac{1}{2}\mathbf{z}^T\mathbf{H}\,\mathbf{z} \\ &\text{subject to:} \\ &\mathbf{D}\,\mathbf{z} = \mathbf{b} \\ &\mathbf{u}_{min}(k+j) \le \mathbf{u}(k+j) \le \mathbf{u}_{max}(k+j) \\ &-\left|\Delta\mathbf{u}_{max}(k+j)\right| \le \Delta\mathbf{u}(k+j) \le \left|\Delta\mathbf{u}_{max}(k+j)\right| \\ &j = 0,\cdots,P \end{aligned} \tag{11}$$

Where $\mathbf{z}$ is given by Eq.(9) and matrix $\mathbf{H} \in \mathbb{R}^{(P+M+2)\times(P+M+2)}$ is:

$$\mathbf{H} = \begin{bmatrix} \mathbf{R} & [\mathbf{0}] \\ [\mathbf{0}] & \mathbf{S} \end{bmatrix}$$

Borges (2001) showed the proposed controller as presented here can not eliminate offset. Borges (2001) unless that the following change in Eq. (8) is made:

$$\mathbf{f}_{k-1} \approx \frac{\mathbf{y}_k - \mathbf{y}_{k-1}}{\Delta t} \tag{12}$$

Where $\mathbf{y}_k$ and $\mathbf{y}_{k-1}$ are the system outputs at k^{th} and $(k-1)^{th}$ sampling instants respectively. Both vectors are available at k^{th} sampling instant.

2.3 The MPC design

A classical MPC is designed in order to compare results. The following classical MPC is defined:

$$\begin{aligned} &\min_{\Delta\mathbf{u}(k),\ldots,\Delta\mathbf{u}(k+M)} \mathrm{J} = \frac{1}{2}\left(\mathbf{e}^T\mathbf{Q}\mathbf{e} + \Delta\mathbf{u}^T\mathbf{R}\Delta\mathbf{u}\right) \\ &\mathbf{u}_{min}(k+j) \le \mathbf{u}(k+j) \le \mathbf{u}_{max}(k+j) \quad (j = 0,\ldots,M) \\ &-\left|\Delta\mathbf{u}_{max}(k+j)\right| \le \Delta\mathbf{u}(k+j) \le \left|\Delta\mathbf{u}_{max}(k+j)\right| \\ &j = 0,\cdots,P \end{aligned} \tag{13}$$

Where $\mathbf{e}$ represents the setpoint deviation vector and it is given by $\mathbf{e} = -\boldsymbol{\Gamma}\Delta\mathbf{u} + \mathbf{e}'$ where $\mathbf{e}' = (\mathbf{y}^{SP} - \boldsymbol{\gamma})$. The optimization problem represented by Eq. (13) can also be put as a quadratic programming problem.

3. EXPERIMENTAL APPLICATION

3.1 The system

Consider a neutralization process that occurs in the CSTR shown in Fig.1. The system involves the dynamic behavior of pH and contains two inputs, an acid stream (HNO_3), Q_1, a base stream (NaOH), Q_2, and a single output, pH. The liquid level is constant and the chemical reactions involved are:

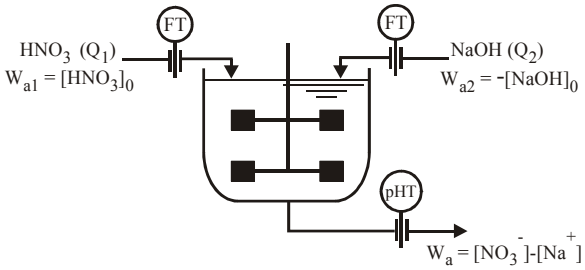

Fig. 1. Experimental setup

$$\begin{aligned} &H_2O \Leftrightarrow OH^- + H^+ \\ &H_2CO_3 \Leftrightarrow HCO_3^- + H^+ \\ &HCO_3^- \Leftrightarrow CO_3^{=} + H^+ \end{aligned} \tag{14}$$

The dynamic of the process is given by the following physical model (Montandon, 2005):

$$V\frac{d(W_a)}{dt} = Q_1(W_{a1} - W_a) + Q_2(W_{a2} - W_a) \tag{15}$$

$$W_a(0) = \overline{W}_a \tag{16}$$

where $W_a = [NO_3^-] - [Na^+]$ is a reaction invariant because it is not affect by extension of the reaction. Eq.(16) represents initial condition for the reactor:

$$\overline{W}_a = \frac{(Q_1 W_{a1} + Q_2 W_{a2})}{(Q_1 + Q_2)} \tag{17}$$

$W_a(t)$ can be obtained by integrating of Eq.(15), $[H^+]$ is obtained by substituting $W_a(t)$ into Eq.(18) and pH(t) is obtained by substituting $[H^+]$ into Eq. (19):

$$W_a = [H^+] - \frac{K_W}{[H^+]} \tag{18}$$

$$pH = -\log[H^+] \tag{19}$$

Table 1 gives the nominal values of system parameters. This system is interesting from control point of view because it is strongly nonlinear as it can be seen in Fig. 2.

Table 1. Nominal values of the system parameters.

Variable	Symbol	Nominal values
Volume	V	4459,94 cm3
Acid flowrate	Q_1	12,0 mL/s
Base flowrate	Q_2	12,0 mL/s
pH	pH	7,0
Acid conc. in Q_1	$[HNO3]_0$	3,611e-03 M
Base conc. in Q_2	$[NaOH]_0$	3,611e-03 M
W_a in Q_1	W_{a1}	3,611e-03 M
W_a in Q_2	W_{a2}	-3,611e-03 M
W_a in output	W_a	0,0

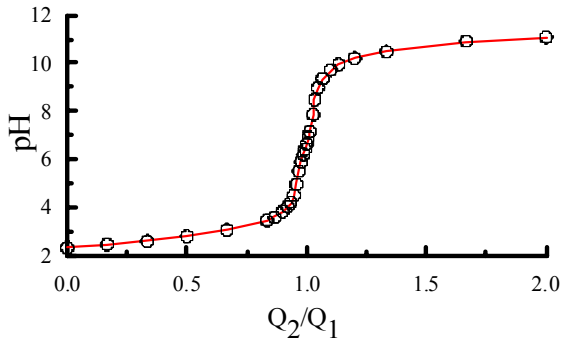

Fig. 2. Experimental Titration curve.

3.2 The neural network model

The problem of using physical model is that it can be quite difficult to get or insufficiently accurate to be used in a MPC. In addition, input/output data are generally available in industrial application. To take advantage of this fact, it was developed a version of proposed controlled based on a neural network models. Before introducing NN models, it is convenient to discuss some practical aspects of the representation of these types of dynamic systems. The natural way to represent the dynamic system represented by Eq. 1 is to use neural networks with neurons with dynamic characteristics (You and Nikolaou, l993). This approach has the advantage of producing models of small dimension. For a single input single output system (SISO), the resulting neural network will have only one input. The main disadvantage of these types of neural networks is the training phase. It is very time consuming and hard to converge. A popular alternative is to consider a neural network with static neurons representing a discrete approximation of the dynamic system in the form of a NARX model (Su *et al*, l992). In this case, the main advantage is associated with the simplicity of the training phase. The disadvantage is that the number of required network inputs increases with input and output lags causing a huge increase in network structure. Another problem is that the determination of the input and output lags requires very often a tedious iterative process. For these reasons, in this work we consider a different alternative that consists of the direct representation of Eq.(1) with a static neural network followed by a numerical integration to recover **y**(t+1).

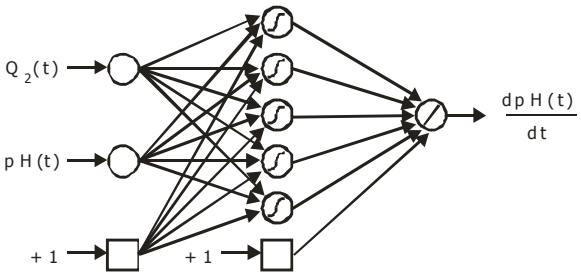

Fig. 3. Neural network topology used.

The Fig. 3 shows the neural network topology schematically. If the value of **y**(t) from plant is used as initial condition for obtaining **y**(t+1) by integration then an one step ahead prediction is obtained, but if the value of **y**(t) is obtained from previous integration step then a multiple step ahead prediction is obtained. For pH neutralization process, the FNN model predicts the time derivatives of pH as a function of the base flow rate and the system pH. The system was excited using a random uniform step sequence for base flow rate Q_2 with a step probability (probability of a step change occurring at any given sampling instant) equal to 0.8 (Bomberger and Seborg, 1997). Q_1 was kept constant in its nominal value. Fig. 4 shows the experimental input and output and the one step ahead prediction performed by the neural model. A sampling period of 10s was used. Data from the time interval [0 to 256 min] were used to the FNN training phase and from the interval [256 to 400 min] to the validation phase. The network inputs were $Q_3(t)$, pH(t) and the network output was d[pH(t)]/dt. The derivatives of pH were calculated numerically by finite difference schemes of filtered pH values. After a cross validation procedure a neural network with five nonlinear hidden neurons (hyperbolic tangent activation function) and one linear output neuron was selected and trained until convergence using the Levenberg-Marquardt method.

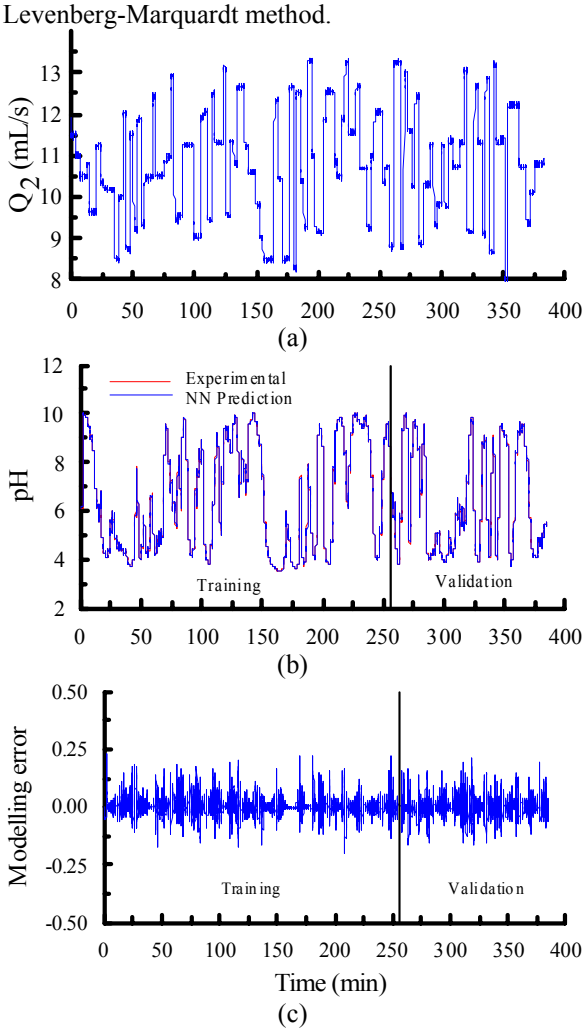

Fig. 4. Experimental data: a). Input sequence for Q_2. b). System output and one step ahead NN prediction. c). Modelling error using NN model.

Fig. 4 shows the data used for training and validation phases and the NN prediction. Prediction results by using physical model were not accurate and this

model was not used in MPC calculation. These results were not shown here to save space. In order to illustrate the advantage of proposed technique over classical PID and MPC technique, a digital PID and a constrained predictive controller (Eq. 13) were implemented experimentally and compared to the proposed controller (Eq. 11) for servo and regulator problems (unmeasured perturbation). All controllers were first tuned by simulation tests using the NN model to represent the real system. In following field tuning were performed for three controllers using preliminary parameters in order to get the best controller parameters experimentally adjusted. The tuned PID parameters are $\Delta t = 10$ s, $K_c = 0.5$ s/mL, $\tau_I = 90$ s and $\tau_D = 0$ s. For classical MPC the tuned parameters are $\Delta t = 10$ s, M = 10, P = 20, Q = 1, R = 150, $|\Delta Q_{3\,max}| = 1$ mL/s, $Q_{3\,max} = 30$ mL/s and $Q_{3\,min} = 5$ mL/s. For proposed MPC the tuned parameters are $\Delta t = 10$ s, K=5e-03 s^{-1}, M = 10, P = 20, R = 1, S = 100, $|\Delta Q_{3\,max}| = 1$ mL/s, $Q_{3\,max} = 30$ mL/s, $Q_{3\,min} = 5$ mL/s. Fig. 5 and Fig. 6 show results of the controllers in servo problems.

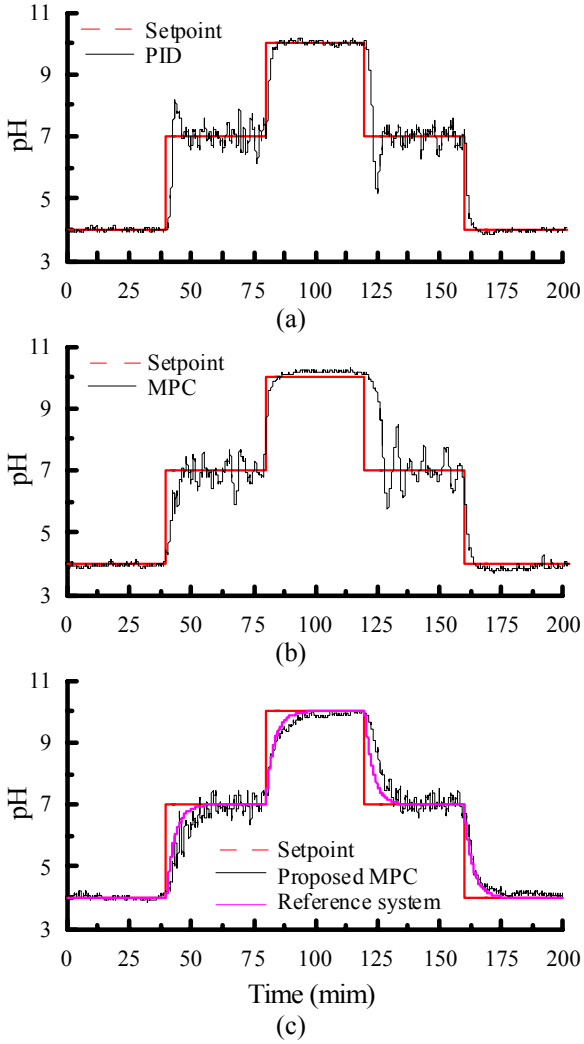

Fig. 5. Closed loop responses for setpoint changes: a). PID, b). Classical MPC, c). Proposed MPC.

Results from Fig. 5 reveal that the proposed MPC yielded a symmetric response for setpoint changes. This result is a consequence of the system reference put as an equality constraint in the quadratic programming of the control problem. As a consequence of this the closed loop response of the real system is basically a first order response. Therefore, controller re-tuning was not needed when new operation points are required. On the other hand, the Fig. 5 shows also that the PID and classical MPC performance are acceptable for system operation at low and high pH values, but the responses deteriorated considerably for system operation around of pH = 7. Consequently, a different set of the controller parameters must be required for good performance at different operational conditions. This is clearly not a desirable situation in any application since it greatly increases the maintenance needs of the controller. Fig. 6 shows the control actions for the three controllers. This Figure reveals that the PID yielded more aggressive control moves than MPC approaches. The more conservative control moves obtained by MPC approaches are because of the presence of hard constraints in the manipulated variable.

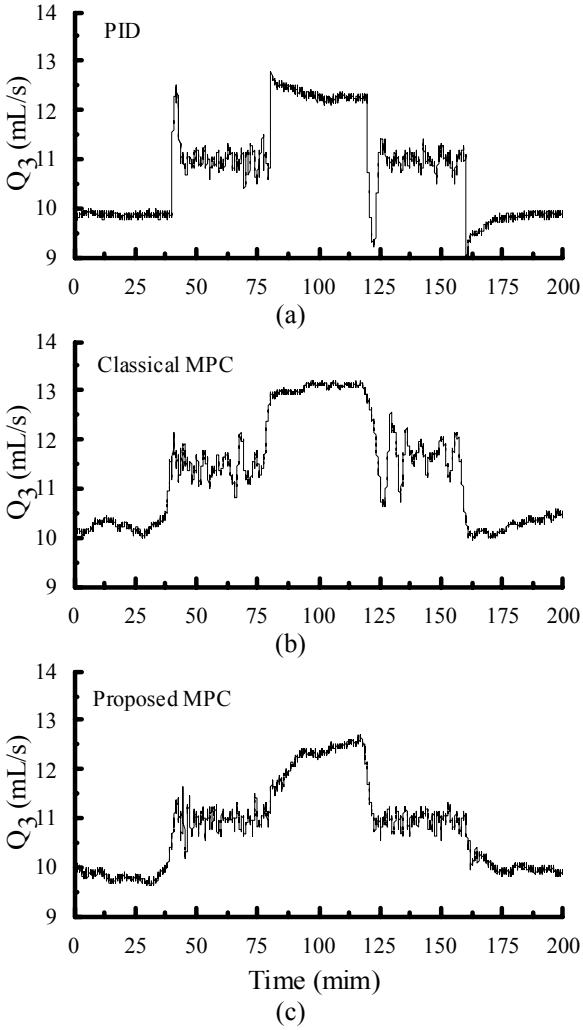

Fig. 6. Control actions: a). PID, b). Classical MPC, c). Proposed MPC.

Next, the capacity of unmeasured perturbation rejection of the controllers was tested. Acid flowrate was chosen as system load and the controller parameters were kept the same for all controllers. The run was started with $Q_1 = 12$ mL/s, it was changed to $Q_1 = 13.5$ mL/s at instant t = 40 min, to $Q_1 = 12$ mL/s

at instant t = 80 min, to Q_1 = 10.5 mL/s at instant t = 120 min and to Q_1 = 12 mL/s at instant t = 160 min. After t = 160 min the acid flowrate was kept in its initial value Q_1 = 12 mL/s. The initial condition of the system is pH =7. In this region the magnitude of the change in Q_1 are too severe because of the high value of the system static gain. Fig. 7 shows the controller performances for load changes.

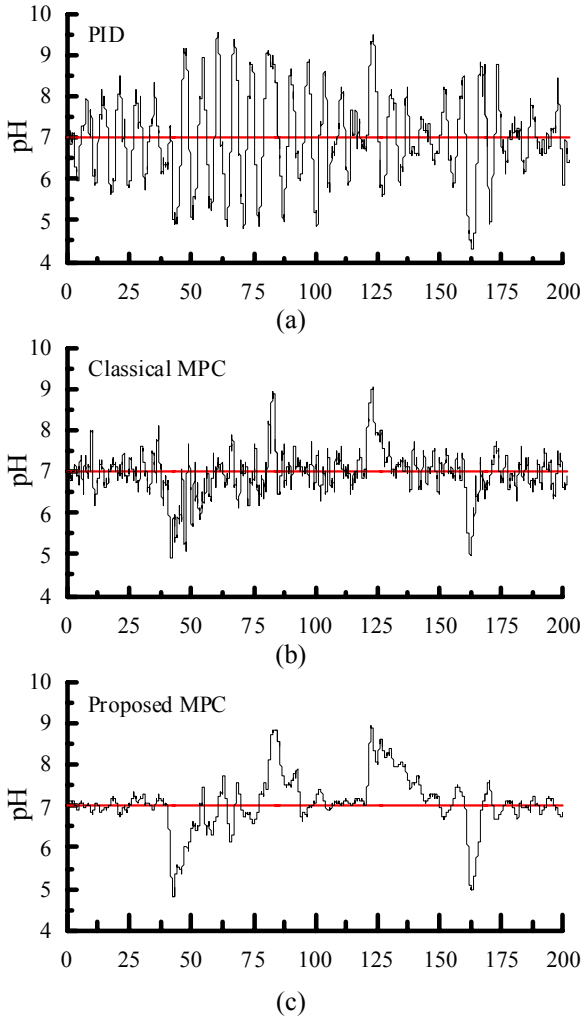

Fig. 7. Closed loop responses for load changes: a). PID, b). Classical MPC, c). Proposed MPC.

Fig. 7 reveals that the PID controller yielded unstable response, very oscillatory with increasing amplitudes. The MPC approaches yielded stable and acceptable responses around of the operation point (pH = 7). These behaviors are remarkable because of the NN network was just trained to Q_1 = 12 mL/s. Due to high sensitivity of the static gain of the system around of pH =7 (see Fig. 2) these changes in Q_1 have a drastic impact in accuracy of the NN model. In spite of this the MPCs controlled the system in a stable fashion. The PID control moves were very aggressive and the MPC control moves were acceptable and no violation of the limits occurred. Results for control moves were not shown here because of slack of space.

4. CONCLUSION

This paper introduces a new MPC strategy based on a first order reference system. The proposed control algorithm was developed and implemented experimentally. Results of a pH neutralization process showed the proposed controller was clearly superior to PID and classical MPC for servo and regulator problem. The proposed method retains the computational simplicity while providing some desirable features from model predictive control, such as constraint handling, incorporating future setpoint changes, penalizing large control move increments by selecting appropriate weighting parameters in the objective function. It was also verified the proposed technique yielded promising results in a real control problem confirming its good potential for practical implementation due to low computational requirements, good closed loop performance as well as transparent controller tuning.

REFERENCES

Balchen, J. G. and Sandrib, B. (1995). Input saturation in nonlinear multivariable processes resolved by nonlinear decoupling. *Model. Ident. Control*, **Volume 16**, 95-106.

Bequette, B. W. (1991). Nonlinear Control of Chemical Process: A Review. *Ind. Eng. Chem. Res,* **Volume 30**, 1391-1413.

Borges, R. M. (2001). Controle Preditivo Basedo em Sistema de Referência. *M. Sc. Thesis*. Uberlandia, Brazil. *(in Portuguese)*

Garcia, C. E., Morshedi, A.M. (1986). Quadratic Programming Solution of Dynamic Matrix Control (QDMC). *Chem. Engng.Commun*, **Volume 46**, 73-87.

Garcia, C.E. , Prett, D.M. and Morari, M. (1989). Model Predictive Control – A Survey. Automatica **Volume 25**, 335-348.

Gattu, G. and Zafiriou, E. (1992). Nonlinear Quadratic Dynamic Matrix Control With State Estimation. *Ind. and Eng. Chem. Res,* **Volume 31**, 1096-1104.

Henson, M. A., Seborg, D. E.(1997). *Nonlinear Process Control*. Prentice Hall, New Jersey.

Kendi, T. A. and Doyle, F. J.(1995). An anti-windup scheme for input-output linearization. *Proc. European Control Conf.*, Rome, Italy.

Kravaris, C. and Kantor, J. C. (1990). Geometric methods for nonlinear process control: 2. controller synthesis. *Ind. Eng. Chem. Res.*, **Volume 29**, 2310-2323.

Meadows, E. S., Henson M. A., Eaton, J. W. and Rawlings, J. B. (1995). Recending horizon control and discontinuous state feedback stabilization. *Int. J. Control*, **Volume 62**, 1217-1229.

Montandon, A. G. (2005). Controle Preditivo em Tempo Real com Trajetória de Referência Baseado em Modelo Neural para Reator de Neutralização. *M. Sc. Thesis*. Uberlandia, Brazil. *(in Portuguese)*

Rawlings, J. B., Meadows, E. S. and Muske, K. R. (1994). Nonlinear model predictive control: A tutorial and survey. *Proc. IFAC Symposium on Advanced Control of Chemical Processes*, Kyoto, Japan, pp. 203-214.

ADCHEM 2006

International Symposium on Advanced Control of Chemical Processes
Gramado, Brazil – April 2-5, 2006

MULTIVARIABLE SUBSPACE IDENTIFICATION AND PREDICTIVE CONTROL OF A HEAT-INTEGRATED SUPERFRACTIONATOR RIGOROUS MODEL

Gabriele Pannocchia [*,1] **Andrea Micchi** [*] **Rachele Bulleri** [*]
Alessandro Brambilla [*] **Gabriele Marchetti** [**]

[*] *Department of Chemical Engineering, Industrial Chemistry and Science of Materials – University of Pisa*
Via Diotisalvi 2, 56126 Pisa (Italy)
[**] *AspenTech S.r.l*
Lungarno Pacinotti 47, 56126 Pisa (Italy)

Abstract: The control of a heat-integrated superfractionator is addressed in this paper. A multivariable subspace identification method is proposed to overcome the difficulties associated to the large time constants of the process and identify a linear process model, upon which a constrained predictive controller is developed. The effectiveness of the proposed identification and control algorithm is shown by means of closed-loop rigorous dynamic simulation results. *Copyright 2006 IFAC* ©

Keywords: Multivariable subspace identification, heat-integrated distillation, predictive control, test design, rigorous simulators.

1. INTRODUCTION

In the process industries, Advanced Process Control (APC) plays a fundamental role for the achievement of economical benefits with respect of safety and quality constraints. APC systems perform multivariable model-based control and require, therefore, a model of the process to be controlled. For simple (small) processes this model can be derived from fundamental equations, but in most cases a (linear) model is identified from data, either collected during specific tests or historical one. Model Predictive Control (MPC) algorithms are the kinds of APC systems most widely used in the process industries, especially in refinery and petrochemical plants (Qin and Badgwell, 2003).

Traditionally, model identification for MPC design is conducted in an "open-loop" fashion, i.e. starting from some steady state, each manipulated variable is varied, usually once at a time according to some pattern (often sequences of steps, from which the usual name of "step tests"), and data of all output variables are collected. Then, using identification techniques, a multiple-input single-output (MISO) model is obtained for each output variable. This step test MISO identification approach has several drawbacks:

(1) The time required to complete step tests in all variables can be very long, since one typically waits until all controlled variables reach a steady state (so that the model gains can be obtained) before introducing a new step. For some processes, like superfractionators, waiting for a new steady state can be "impractical" (times-to-steady-state are of the order of several days), and some modifications may be necessary (Pannocchia and Brambilla, 2005).
(2) The quality of the obtained model can be poor because open-loop uncorrelated input signals may not excite the process dynamics in all relevant "directions" (Koung and MacGregor, 1994; Zhu, 2001). Moreover MISO identification of ill-conditioned processes can result in erroneous models (Dayal and MacGregor, 1997).
(3) Open-loop unstable or integrating processes cannot be handled with open-loop tests.

Mainly for these reasons, open-loop identification methods based on different multivariable input sig-

[1] Corresponding author. Email: g.pannocchia@ing.unipi.it, Fax: +39 050 511266.

nals and/or closed-loop identification methods have become more popular during the last decade [see e.g. Hjalmarsson *et al.* (1996), Forssell and Ljung (1999), Zhu (2001), Zhu and Butoyi (2002) and references therein]. With regards of methods for computing the model parameters it is remarkable to notice that most of current research is focused on subspace methods (Verhaegen and Dewilde, 1992*a*; Verhaegen and Dewilde, 1992*b*; Van Overschee and De Moor, 1994; Favoreel *et al.*, 2000; Wang and Qin, 2002; Huang *et al.*, 2005). The strength of these methods is due to their numerical robustness, applicability to both open-loop and closed-loop data (with some extra care), and the fact that they directly generate state-space models which are becoming the standard models in industrial MPC algorithms (Qin and Badgwell, 2003).

In the present paper, a rigorously simulated heat-integrated distillation process is studied to evaluate the effectiveness of subspace identification techniques for the design of constrained multivariable predictive control algorithms. As well-known, distillation (the separation method most widely used in the process industries) is particularly energy consuming. It is estimated that 3% of energy consumption of the world is due to distillation processes (Engelian *et al.*, 2003), and therefore a natural interest in heat-integrated processes is justified. However, heat integration introduces a number of issues, especially from a control point of view [see e.g. (Ding and Luyben, 1990; Hansen *et al.*, 1998; Engelian *et al.*, 2003; Engelian and Skogestad, 2004) and references therein], mainly due to relevant interactions among process variables. Therefore, these characteristics along with the presence of dynamics with large time constants make multivariable model identification and control particularly suited for these processes. The process model used by the controller is obtained by means of a subspace multivariable identification, and closed-loop results are presented to show to achievable benefits.

2. MULTIVARIABLE SUBSPACE IDENTIFICATION

2.1 Overview of subspace identification methods

Discrete linear time-invariant systems are considered in this paper, in the following form:

$$\begin{aligned} x_{k+1} &= A_p x_k + B_p u_k + w_k \\ y_k &= C_p x_k + v_k \end{aligned} \tag{1}$$

in which $x \in \mathbb{R}^{n_p}$ is the state vector, $u \in \mathbb{R}^m$ is the input vector, $y \in \mathbb{R}^p$ is the output (measured) vector, the (true) system matrices (A_p, B_p, C_p) have appropriate dimensions, $w \in \mathbb{R}^{n_p}$ and $v \in \mathbb{R}^p$ are (unmeasured) noise vectors. The basic identification problem is to find estimates of the system matrices (A, B, C) and order n, and possibly of the statistical properties, i.e. the covariance, of w and v. Notice that the feed-through from u to y is omitted in (1) because this is the typical case of most processes. If necessary, one can add the appropriate term and estimate the corresponding matrix (typically denoted with D).

Subspace identification methods achieve these goals by starting from the Kalman predictor:

$$\begin{aligned} \hat{x}_{k+1} &= A\hat{x}_k + Bu_k + Ke_k \\ y_k &= C\hat{x}_k + e_k \end{aligned} \tag{2}$$

in which $\hat{x} \in \mathbb{R}^n$ is the predicted state, $e \in \mathbb{R}^p$ is noise, (A, B, C) are the model matrices and $K \in \mathbb{R}^{n \times p}$ is the Kalman predictor gain matrix (to be determined). Given an arbitrary time-point k, the vector of future outputs can be constructed as:

$$y_k^f = \begin{bmatrix} y_k \\ y_{k+1} \\ \vdots \\ y_{k+r-1} \end{bmatrix} \tag{3}$$

in which r is a positive integer. A similar straightforward definition can be made for the vectors of future inputs and noise, denoted with u_k^f and e_k^f, respectively. From (2), one can write

$$y_k^f = \Gamma_r \hat{x}_k + H_r^u u_k^f + H_r^e e_k^f \tag{4}$$

in which Γ_r is the extended observability matrix, H_r^u and H_r^e are lower block-triangular Toeplitz matrices associated to inputs and noise:

$$\begin{aligned} \Gamma_r &= \begin{bmatrix} C \\ CA \\ CA^2 \\ \vdots \\ CA^{r-1} \end{bmatrix} \\ H_r^u &= \begin{bmatrix} 0 & 0 & \cdots & \cdots & 0 \\ CB & \ddots & \ddots & & \vdots \\ CAB & \ddots & \ddots & & \\ \vdots & & \ddots & \ddots & \\ CA^{r-2}B & \cdots & CAB & CB & 0 \end{bmatrix} \\ H_r^e &= \begin{bmatrix} I & 0 & \cdots & \cdots & 0 \\ CK & \ddots & \ddots & & \vdots \\ CAK & \ddots & \ddots & & \\ \vdots & & \ddots & \ddots & \\ CA^{r-2}K & \cdots & CAK & CK & I \end{bmatrix} \end{aligned} \tag{5}$$

Then, one can rewrite the basic relation (4) for N time-points as:

$$Y^f = \Gamma_r \hat{X} + H_r^u U^f + H_r^e E^f \tag{6}$$

in which

$$\begin{aligned} Y^f &= \begin{bmatrix} y_1^f & y_2^f & \cdots & y_N^f \end{bmatrix} \\ U^f &= \begin{bmatrix} u_1^f & u_2^f & \cdots & u_N^f \end{bmatrix} \\ E^f &= \begin{bmatrix} e_1^f & e_2^f & \cdots & e_N^f \end{bmatrix} \\ \hat{X} &= \begin{bmatrix} \hat{x}_1 & \hat{x}_2 & \cdots & \hat{x}_N \end{bmatrix} \end{aligned} \tag{7}$$

Starting from (6), subspace methods obtain an estimate of Γ_r and H_r^u (from which the model matrices can be calculated) by removing the noise and/or the future input terms with appropriate matrix multiplications, i.e. by projection onto some subspaces. Each method differs from the others in the matrices used

to perform these projections and in the way the final model matrices are obtained from Γ_r and H_r^u. In the next sections the orthogonal projection approach (Huang *et al.*, 2005; Wang and Qin, 2002) is reviewed, and a modification used in this work is proposed.

2.2 Orthogonal projection method (modified)

The key idea is to use instrumental variables to remove the noise from (6), i.e. to multiply (6) by a matrix W^T such that $\lim_{N\to\infty} \frac{1}{N} E_f W^T$. Thus, one can write

$$\begin{bmatrix} I & -H_r^u \end{bmatrix} Z_f W^T = \Gamma_r \hat{X} W^T \tag{8}$$

in which

$$Z_f = \begin{bmatrix} Y_f \\ U_f \end{bmatrix} \tag{9}$$

Then, multiplying (8) on the left by a matrix $\Gamma_r^\perp$ such that $\Gamma_r^\perp \Gamma_r = 0$, permits one to obtain:

$$\Gamma_r^\perp \begin{bmatrix} I & -H_r^u \end{bmatrix} Z_f W^T = \Gamma_r^\perp \begin{bmatrix} I & -H_r^u \end{bmatrix} Z = 0 \tag{10}$$

in which $Z = Z_f W^T$.

Wang and Qin (2002) chose $W = Z_p$, which is the matrix of past outputs and inputs, whose definition is straightforward. This serves as a good instrument because E_f (future noise) is independent of Z_p (past outputs and inputs). Huang *et al.* (2005) instead propose using $W = Z_p^T (Z_p Z_p)^{-1} Z_p$, which performs an orthogonal projection onto the row space of Z_p. This latter method is used in this work. Performing an SVD of Z leads to

$$Z = \begin{bmatrix} U_1 & U_2 \end{bmatrix} \begin{bmatrix} \Sigma_1 & 0 \\ 0 & 0 \end{bmatrix} \begin{bmatrix} V_1^T \\ V_2^T \end{bmatrix} \tag{11}$$

in which the dimension of Σ_1, i.e. the rank of Z, should be equal to $mr + n$ (Wang and Qin, 2002, Lemma 1). In practice, the rank and consequently the order n are determined from the singular values, using e.g. an Akaike Information Criterion as in (Wang and Qin, 2002) or using a heuristic PCA approach (Micchi, 2005). From (11), one obtains that (10) is satisfied if

$$\Gamma_r^\perp \begin{bmatrix} I & -H_r^u \end{bmatrix} = M U_2^T \tag{12}$$

in which M is an arbitrary non-singular matrix of dimension $pr - n$ (usually chosen equal to the identity matrix). Finally, by partitioning

$$M U_2^T = \begin{bmatrix} P_1^T & P_2^T \end{bmatrix} \tag{13}$$

in which $P_1 \in \mathbb{R}^{pr \times (pr-n)}$, it follows from (12) that

$$P_1^T \Gamma_r = 0 \tag{14}$$

$$-P_1^T H_r^u = P_2^T \tag{15}$$

which can be easily solved to compute Γ_r and H_r^u, from which it is possible to obtain the system matrices as described next.

Given the computed estimate of the extended observability matrix $\hat{\Gamma}_r$, it is straightforward to compute A and C from the following relations:

$$C = \hat{\Gamma}_r(1:p,:) \tag{16}$$

$$\hat{\Gamma}_r(p+1:pr,:) = \hat{\Gamma}_r(1:p,:) A \tag{17}$$

in which a MATLAB notation is used and the last equation is solved for A in a least-square sense. Wang and Qin (2002) and Huang *et al.* (2005) propose using the first block column of H_r^u to compute B (and D if appropriate) with a least-square equation. This method was investigated in (Micchi, 2005) who found that poor estimation of B (and D) is obtained in a number of cases. Therefore a different approach is used in this work. Given A and C, let $\hat{y}_{k|B}$ denote the estimate of y_k given past inputs and a generic matrix B, i.e.

$$\hat{y}_{k|B} = C \sum_{j=0}^{k-1} A^j B u_j \tag{18}$$

By differentiating $\hat{y}_{k|B}$ with respect to the elements of B, (18) can be rewritten as follows:

$$\hat{y}_{k|B} = \varphi_k \operatorname{Vec} B \tag{19}$$

where $\varphi_k \in \mathbb{R}^{p \times nm}$ is the corresponding Jacobian matrix and Vec is the operator that builds a vector from a matrix by stacking its columns on top of each other. Then, given N measured output vectors $y_1, \ldots, y_N$, the following least-square regression problem can be posed:

$$\underset{\operatorname{Vec} B}{\operatorname{argmin}} \sum_{k=1}^{N} \|y_k - \hat{y}_{k|B}\|_2^2 \tag{20}$$

whose solution is

$$\operatorname{Vec} B = (\Phi^T \Phi)^{-1} \Phi^T Y_N \tag{21}$$

in which

$$\Phi = \begin{bmatrix} \varphi_1 \\ \varphi_2 \\ \vdots \\ \varphi_N \end{bmatrix}, \qquad Y_N = \begin{bmatrix} y_1 \\ y_2 \\ \vdots \\ y_N \end{bmatrix} \tag{22}$$

Notice that in these formulae a zero initial condition is assumed; but the initial state x_0 can be estimated with straightforward extensions. Also notice that existence of $(\Phi^T \Phi)^{-1}$ depends on the input signal being sufficiently exciting.

3. PREDICTIVE CONTROL

The model predictive control algorithm used in this work is based on three modules: a state and disturbance estimator, a steady-state target optimizer and a dynamic input sequence optimizer, which are executed at each sampling time, as described next.

3.1 State and disturbance estimation

Given the (identified) state-space matrices (A, B, C), the system model is augmented with fictitious disturbances to guarantee offset-free control (Pannocchia and Rawlings, 2003), as follows:

$$\begin{aligned} \begin{bmatrix} x_{k+1} \\ d_{k+1} \end{bmatrix} &= \begin{bmatrix} A & B_d \\ 0 & I \end{bmatrix} \begin{bmatrix} x_k \\ d_k \end{bmatrix} + \begin{bmatrix} B \\ 0 \end{bmatrix} u_k \\ y_k &= \begin{bmatrix} C & D_d \end{bmatrix} \begin{bmatrix} x_k \\ d_k \end{bmatrix} \end{aligned} \tag{23}$$

in which $d \in \mathbb{R}^p$ is the integrating disturbance, (B_d, D_d) are matrices of suitable dimensions, chosen to satisfy an appropriate detectability condition (Pannocchia and Rawlings, 2003). The augmented state is estimated, at each sampling time, from the measured output vector y_k by using a steady-state Kalman filter:

$$\begin{aligned} \hat{x}_{k|k} &= \hat{x}_{k|k-1} + L_x e_k \\ \hat{d}_{k|k} &= \hat{d}_{k|k-1} + L_d e_k \end{aligned} \tag{24}$$

in which $e_k = y_k - (C\hat{x}_{k|k-1} + D_d\hat{d}_{k|k-1})$, while $\hat{x}_{k|k-1}$ and $\hat{d}_{k|k-1}$ are the state and disturbance vectors predicted at the previous sampling time, as discussed at the end of Section 3.3.

3.2 Steady-state target calculation

Using the disturbance estimate $\hat{d}_{k|k}$, a steady-state optimization problem is solved to find the current targets for states and inputs such that offset in (some) controlled variables is (possibly) removed and the constraints satisfied. To this aim, it is assumed that a subset of the measured output vector, $z = H_z y$ has a known setpoint vector $\bar{z}$, and the following quadratic program (QP) is considered:

$$(\bar{x}_k, \bar{u}_k) = \underset{x_s, u_s}{\operatorname{argmin}}\ u_s^T \bar{R} u_s \tag{25a}$$

subject to:

$$x_s = Ax_s + Bu_s + B_d\hat{d}_{k|k} \tag{25b}$$

$$\bar{z} = H_z(Cx_s + D_d\hat{d}_{k|k}) \tag{25c}$$

$$u_{\min} \le u_s \le u_{\max} \tag{25d}$$

$$y_{\min} \le Cx_s + D_d\hat{d}_{k|k} \le y_{\max} \tag{25e}$$

in which $\bar{R}$ is a symmetric positive definite matrix, $u_{\min}$ ($u_{\max}$) and $y_{\min}$ ($y_{\max}$) are vectors which contain the minimum (maximum) limits for inputs and outputs, respectively. If, for a given disturbance estimate $\hat{d}_{k|k}$, the problem (25) turns out to be infeasible, a second QP is posed by softening setpoint constraints (25c) and output constraints (25e), i.e. by solving

$$\min_{x_s, u_s, \eta_s, \epsilon_s}\ u_s^T \bar{R} u_s + \eta_s^T \bar{Q} \eta_s + \epsilon_s^T \bar{P} \epsilon_s \tag{26a}$$

subject to:

$$x_s = Ax_s + Bu_s + B_d\hat{d}_{k|k} \tag{26b}$$

$$\bar{z} = H_z(Cx_s + D_d\hat{d}_{k|k}) + \eta_s \tag{26c}$$

$$u_{\min} \le u_s \le u_{\max} \tag{26d}$$

$$y_{\min} - \epsilon_s \le Cx_s + D_d\hat{d}_{k|k} \le y_{\max} + \epsilon_s \tag{26e}$$

in which $\bar{Q}$ and $\bar{P}$ are positive definite matrices.

3.3 Optimal input sequence calculation

Having computed the state and input targets, and defined the corresponding output target vector as $\bar{y}_k = C\bar{x}_k + D_d\hat{d}_{k|k}$, an optimal input sequence vector $\mathbf{v}_k = \begin{bmatrix} v_{0,k}^T & v_{1,k}^T & \cdots & v_{N-1,k}^T \end{bmatrix}^T$, is computed (along with a corresponding vector of slacks for output constraints, ϵ_k) from the following optimization problem:

$$(\mathbf{v}_k, \epsilon_k) = \underset{\mathbf{v}, \epsilon}{\operatorname{argmin}}\ (\bar{x}_k - w_N)^T P (\bar{x}_k - w_N) + \sum_{j=0}^{N-1} \left\{ \Delta v_j^T S \Delta v_j + r_j^T Q r_j + \epsilon_j^T Q^\epsilon \epsilon_j \right\} \tag{27a}$$

subject to:

$$w_0 = \hat{x}_{k|k}, \quad v_{-1} = u_{k-1} \tag{27b}$$

$$w_{j+1} = Aw_j + Bv_j + B_d\hat{d}_{k|k} \tag{27c}$$

$$r_j = \bar{y}_k - (Cw_j + D_d\hat{d}_{k|k}) \tag{27d}$$

$$u_{\min} \le v_j \le u_{\max} \tag{27e}$$

$$y_{\min} - \epsilon_j \le Cw_j + D_d\hat{d}_{k|k} \le y_{\max} + \epsilon_j \tag{27f}$$

in which N is a positive integer (referred to as horizon), $\Delta v_j = v_j - v_{j-1}$, the matrices S, Q, Q^ϵ are symmetric positive definite and the symmetric positive semidefinite matrix P is computed from an appropriate Riccati equation associated to (27). Given the optimal input vector $\mathbf{v}_k$, only the first component is injected into the plant, i.e.

$$u_k = v_{0,k} \tag{28}$$

and the predicted state and disturbance vectors for the next sampling time are accordingly defined:

$$\begin{aligned} \hat{x}_{k+1|k} &= A\hat{x}_{k|k} + Bu_k + B_d\hat{d}_{k|k} \\ \hat{d}_{k+1|k} &= \hat{d}_{k|k} \end{aligned} \tag{29}$$

4. CASE STUDY

4.1 Process description

The separation of propane and propylene is considered as a case study. Due to the very low relative volatility, this separation is conducted in superfractionators, i.e. columns with large number of trays and high reflux ratios, and is therefore particularly suited for heat-integration via thermo-compression because of the small difference in boiling temperature between top and bottom products.

The process layout is depicted in Figure 1 along with the regulatory PID control loops. Due too the high reflux ratios, reflux rate is used to control the condenser drum, which is common practice in superfractionator columns. The column has 210 stages, it operates at a top pressure of 9.5 bar (bottom pressure is 10.6 bar) and the vapor phase feed enters the column at stage 166. The top stage vapor is compressed at a pressure of 19 bar and then it is partially condensed in a heat exchanger (condenser/reboiler), whose cold fluid is the liquid draw from the bottom of the column, which is consequently vaporized to generate the boil-up flow returned to the last stage of the column. The condenser/reboiler operates with an average ΔT of $25 \div 30^{\circ}$C, and the vapor/liquid stream leaving this exchanger is totally condensed and sub-cooled in a trim cooler. Details of the main operating variables are reported in Table 1. Further details regarding this study can be found in (Bulleri, 2005).

Table 1. Main operating variables

Feed rate (tonne/hr)	Feed propylene fraction	Internal reflux ratio	Distillate rate (tonne/hr)	Distillate propylene fraction	Bottom propane fraction
20.0	0.70	12.1	13.3	0.9955	0.9162

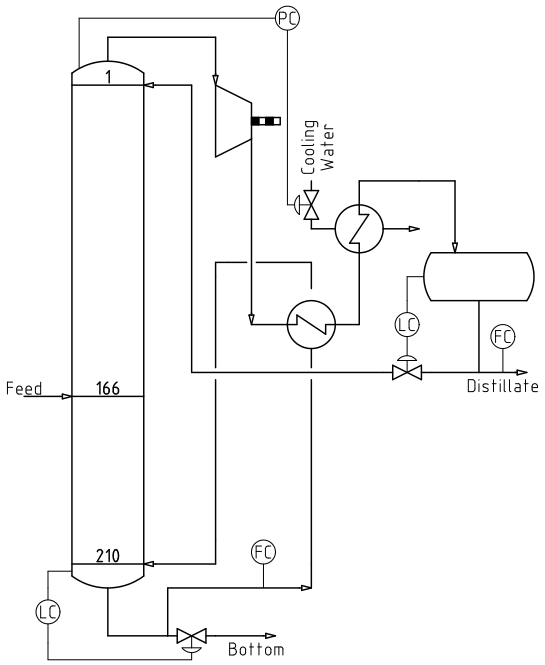

Fig. 1. Heat-integrated distillation process layout

The process is simulated using the rigorous dynamic simulator HYSYS™ (version 3.2), while the predictive controller is implemented in MATLAB (version 7.0.1). Dynamic communication between the two environments is achieved using appropriate exchange spreadsheet modules. The predictive controller, at each sampling time, reads the values of all controlled variables from the process simulator, performs its internal calculations and returns the value of the manipulated variables (i.e. the setpoints of regulatory PID controllers) to the process simulator.

4.2 Identification and control results

Three manipulated variables and seven controlled variables are considered for design of the predictive controller. The manipulated variables are the setpoints of distillate and boil-up flow-rate controllers and of the column pressure controller. The controlled variables are the opening percents of all control valves and the distillate propylene fraction and bottom product propane fraction. For these latter variables desired setpoints are defined, while all control valves are only required to meet inequality constraints, as shown in Table 2.

Data for identification are obtained by perturbing the reference value of the manipulated variables with Generalized Binary Noise [GBN, see e.g. (Zhu, 2001)] signals. Notice that these input signals affect all manipulated variables simultaneously and independently of the controlled variables, i.e. a multivariable open-loop test design is performed. [2] Compared to traditional step tests, these signals usually have shorter duration; moreover, they excite the process dynamics much more thoroughly, thus allowing a more effective model identification. For the present application, a traditional step approach would have required an overall plant testing time at least $20 \div 30$ times larger than that required using multivariable GBN signals. Using these data, the orthogonal projection method is applied and a (stable) state-space linear model of order $n = 12$ is obtained and used to implement the predictive controller described in Section 3.

Table 2. Upper and lower limits (and reference setpoints) for MVs and CVs.

Variable	Lower	Setpoint	Upper
Dist. rate (tonne/hr)	12.6	–	14.0
Boilup rate (tonne/hr)	150	–	173
Pressure (bar)	9.4	–	9.6
Boilup OP (%)	10	–	90
Reflux OP (%)	10	–	90
Bottom OP (%)	10	–	90
Distillate OP (%)	10	–	90
Cool. Water OP (%)	10	–	90
Dist. propyl. frac.	0.97	0.9955	0.9984
Bottom propane frac.	0.85	0.9162	0.982

For comparison with the proposed MPC regulator, two decentralized (PI controllers cascaded on corresponding flow-rate controllers) quality control schemes are considered: DV (distillate rate controls the distillate composition, boil-up rate controls the bottom composition) and VD (vice-versa). As an example, closed-loop simulation results of a setpoint change in the compositions of the products are reported. Due too space limitations, closed-loop results for disturbance changes, as well as specific robustness analysis results are not presented. It should, however, be mentioned that since the plant is simulated with a rigorous nonlinear model, an intrinsic mismatch exists between the plant and the linear model used in the MPC regulator. The controllers are required to reduce the purity of both products: the distillate propylene fraction changes from 0.9955 to 0.993 while the bottom product propane fraction changes from 0.9162 to 0.913. In Figure 2 the behavior of the products' compositions is reported for each controller, while in Figure 3 the behavior of distillate and boil-up rate is reported for each controller. From these figures, the benefits of using a multivariable constrained control algorithm are evident, since the products' compositions reach their setpoint much more quickly (notice the large time scale) due a more coordinate action of the manipulated

[2] Closed-loop tests, other signals (PRBS, steps, ...) and several subspace and prediction error methods were studied and compared in (Micchi, 2005).

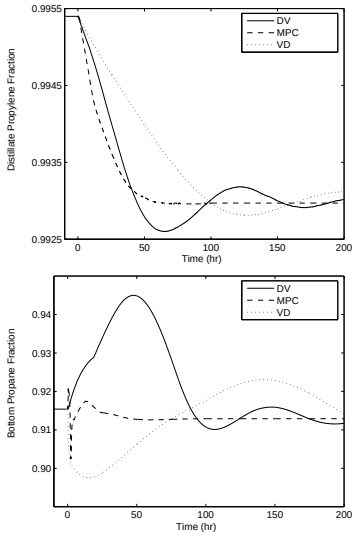

Fig. 2. Products' composition for three controllers.

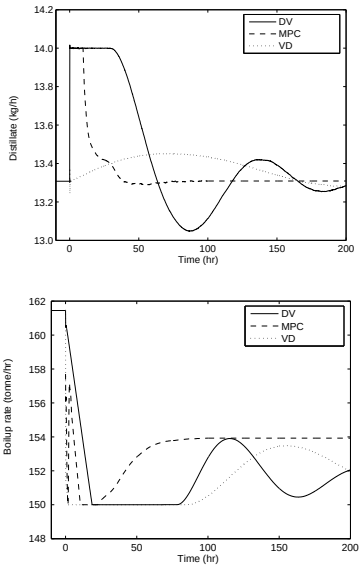

Fig. 3. Distillate and boilup rate for three controllers.

variables and an appropriate saturation of the constraints when necessary. These results also indicates that multivariable subspace identification methods are effective for superfractionators, which present large time constants and for which traditional step tests are, therefore, impractical.

5. CONCLUSIONS

In this paper the effectiveness of subspace multivariable identification techniques was studied for a heat-integrated distillation process simulated with a rigorous dynamic simulator model. This process is characterized by large time constants and hence traditional step tests are undesirable and impractical. Generalized Binary Noise signals were successfully used to obtain informative input/output data. A (modified) orthogonal projection algorithm was implemented to identify a state-space model used to build a constrained multivariable predictive controller, whose effectiveness was tested in closed-loop simulations.

A final remark concerns the potential benefits and flexibility of using rigorous simulators, which can prove useful for shortening the model identification and controller design/commissioning phases in APC projects, especially for processes with large number of variables (Pannocchia *et al.*, 2005) and/or slow processes like the one considered in this paper.

REFERENCES

Bulleri, R. (2005). Controllability of heat-integrated distillation systems (in italian). Master's thesis. Chemical Engineering, University of Pisa.

Dayal, B. S. and J. F. MacGregor (1997). Multi-output process identification. *J. Proc. Cont.* **7**, 269–282.

Ding, S. S. and W. L. Luyben (1990). Control of a heat-integrated complex distillation configuration. *Ind. Eng. Chem. Res.* **29**, 1240–1249.

Engelian, H. K. and S. Skogestad (2004). Selecting appropriate control variables for a heat-integrated distillation system with prefractionator. *Comput. Chem. Eng.* **28**, 683–691.

Engelian, H. K., T. Larsson and S. Skogestad (2003). Implementation of optimal operation for heat integrated distillation columns. *Chem. Eng. Res. Des.* **81**, 277–281.

Favoreel, W., B. De Moor and P. Van Overschee (2000). Subspace state space system identification for industrial processes. *J. Proc. Cont.* **10**, 149–155.

Forssell, U. and L. Ljung (1999). Closed-loop identification revisited. *Automatica* **7**, 1215–1241.

Hansen, J. E., S. B. Jorgensen, J. Heath and J. D. Perkins (1998). Control structure selection for energy distillation columns. *J. Proc. Cont.* **8**, 185–195.

Hjalmarsson, H., M. Gevers and F. de Bruyne (1996). For model-based control design, closed-loop identification gives better performance. *Automatica* **32**, 1659–1673.

Huang, B., S. X. Ding and S. J. Qin (2005). Closed-loop subspace identification: an orthogonal projection approach. *J. Proc. Cont.* **15**, 53–66.

Koung, C. W. and J. F. MacGregor (1994). Identification for robust multivariable control: the design of experiments. *Automatica* **30**, 1541–1554.

Micchi, A. (2005). Multivariable identification techniques and predictive control of distillation processes (in italian). Master's thesis. Chemical Engineering, University of Pisa.

Pannocchia, G. and A. Brambilla (2005). How to use simplified dynamics in model predictive control of superfractionators. *Ind. Eng. Chem. Res.* **44**, 2687–2696.

Pannocchia, G. and J. B. Rawlings (2003). Disturbance models for offset-free model predictive control. *AIChE J.* **49**, 426–437.

Pannocchia, G., L. Gallinelli, G. Marchetti, F. Trivella and A. Brambilla (2005). Rigorous simulation and model predictive control of a crude distillation unit. Submitted for presentation in ADCHEM 2006.

Qin, S. J. and T. A. Badgwell (2003). A survey of industrial model predictive control technology. *Cont. Eng. Pract.* **11**, 733–764.

Van Overschee, P. and B. De Moor (1994). N4SID: Subspace algorithms for the identification of combined deterministic stochastic systems. *Automatica* **30**, 75–93.

Verhaegen, M. and P. Dewilde (1992*a*). Subspace model identification. part 1. the output-error state-space model identification class of algorithms. *Int. J. Control* **56**, 1187–1210.

Verhaegen, M. and P. Dewilde (1992*b*). Subspace model identification. part 2. analysis of the elementary output-error state-space model identification algorithm. *Int. J. Control* **56**, 1211–1241.

Wang, J. and S. J. Qin (2002). A new subspace identification approach based on principal component analysis. *J. Proc. Cont.* **12**, 841–855.

Zhu, Y. (2001). *Multivariable System Identification for Process Control*. Springer.

Zhu, Y. and F. Butoyi (2002). Case studies on closed-loop identification for MPC. *Cont. Eng. Pract.* **10**, 403–417.

ADCHEM 2006

International Symposium on Advanced Control of Chemical Processes
Gramado, Brazil – April 2-5, 2006

Control Strategies Evaluation for a Three-Phase Hydrogenation Catalytic Reactor

Delba N. C. Melo, Eduardo C. Vasco de Toledo, Marcela M. Santos, Rubens Maciel Filho.

Laboratory of Optimization, Design and Advanced Control (LOPCA). Faculty of Chemical Engineering. State University of Campinas (Unicamp)

P.O. Box 6066, 13081-970, Campinas, SP, Brazil

email:delba@lopca.feq.unicamp.br, Tel.:+55-19-37883971; Fax: +55-19-37883965

Abstract: Hydrogenation reactions are widely applied industrially, and reactors have been designed for this purpose. It is a highly non-linear process, multivariable, with exothermic reaction. The model formulation was made focusing on the hydrogenation reaction of o-cresol to obtain the 2-methil-cyclohexanol, in the presence of a Ni/SiO_2 catalyst. A competitive advantage in such kind of system (a commodity with large production scale) is to operate an optimal level of performance under control. The present work introduces an optimization problem and control in a simulation study of the reactor. The model allowed to reproduce the main characteristics of its dynamic, as well as the evaluation of the performance of different control strategies (Feedback, Feedforward or both strategies). The analysed controller was the linear model predictive (QDMC), and extensive analysis allow to identify which control strategy was more suitable to operate the reactor in an efficient and safe way. These informations are important for the real time integration implementation procedure. *Copyright © 2006 IFAC*

Keywords: hydrogenation, dynamic modelling, simulation, optimization, advanced controller.

1. INTRODUCTION

The control of many chemical processes like tubular reactors, with or without catalytic bed, is complicated by problems associated with the on-line measurements of desired control objectives, especially those concerned with concentrations. For the tubular reactors, the primary control objective is usually the regulation of the outlet concentration at optimum levels, while attention is paid to a safe operation and reactor temperatures that do not exceed some pre-specified maximum value. The outlet concentration cannot be easily measured on-line, so it must be inferred (estimated) from the available temperature measurements along the reactor.

Therefore, for the establishment of the control strategy of a chemical reactor, it is necessary to define its operational objective as well as to develop a model that predicts the main characteristics of the dynamic behaviour of this reactor. In this work, the priority of the control is not directly related to the outlet concentration, but the problem is seen as the thermal control of the reactor, making indirectly the control of the concentration. Therefore, the controllers were evaluated in order to absorb disturbances, which alter the thermal profile of the reactor. This is not a trivial task, and in fact, it is one of the most difficult and dangerous operations in the chemical industry, especially when large scale industrial reactors are considered. Another important objective, in the implementation of the control loop, is to know the physical and operational limitations of the manipulated and controlled variables of the reactor. This information is essential to have a suitable and feasible control strategy.

2. CONTROL

The system used as case of study is a multiphase reactor, where the hydrogenation reactor of o-cresol takes place. The deterministic model takes into account the heterogeneous dynamic behaviour of the system, and the model basically consists of mass and energy balance equations for the reactants as well as for the catalyst particles. The kinetic law considers the hydrogenation reaction of o-cresol to obtain the 2-methil-cyclo-hexanol, in the presence of the catalyst Ni/SiO_2. The utilized scheme to

represent the reactor is shown in Figure 1 (Vasco de Toledo et al., 2001).

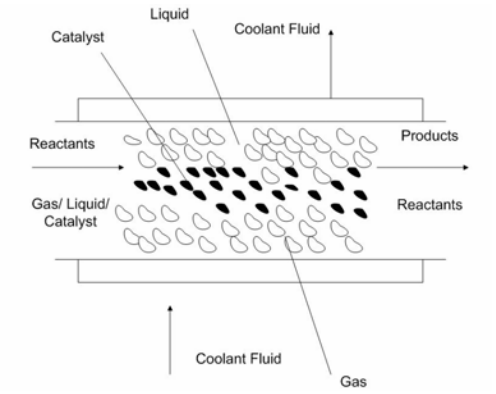

Figure 1 - Three-phase reactor.

The following hypothesis were adopted for the model development (Vasco de Toledo et al., 2001, Vasco de Toledo and Maciel Filho, 2004): a) negligible pressure variations; b) reaction of the type: A (g) + νB (l) → νC (l), occurring at the catalyst and with a kinetic that is dependent on the concentrations of A and B; c) no phase exchange in the system. The operational parameters of the reactor, mass and energy balance coefficients, and physical properties have been considered as constant. Some of these parameters were generated by empirical correlations (Mariano et al., 2004).

Very Few attentions have been paid for the control of this type of reactors, Resende et al., 2004 investigated the DMC performance on the control of the multi-phase reactor but only a superficial analysis was considered out.In this work, it was carried out the performance analysis of different control strategies (feedback, feedforward or both strategies), as it can be seen in the diagram represented in the figure 2. The feedforward strategy design frequently suffers from several inherent difficulties: it requires the identification of the disturbance, and a very good model of the process, something quite difficult for many systems in the chemical industry and the changes in the process parameters cannot be compensated unless a reliable estimation procedure is incorporated.

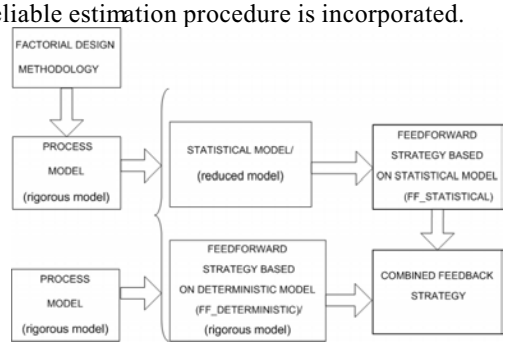

Figure 2- Schematic diagram of the strategies control

The objective of a feedforward controller is basically to generate anticipated corrective actions to compensate measured input disturbances. The control action of the feedforward strategy was generated by a deterministic model and a parametric model of the controlled and manipulated variables, which was developed by the application of the full factorial design method. The application of the factorial design to generate a working model for control purposes is a new procedure introduced in this work and seems to be powerful procedure due to its simplicity and predictions capabilities.

The performance of advanced controller and different control strategies for the thermal control of the reactor were extensively carried out and analysed. The control evaluation consists on problems of set point changes (servo control) and disturbance in the operational parameters of the reactor (regulatory control). These strategies and controller make use of advanced numerical techniques that allow an effective control of the process, due mainly to the several parameters adjustments procedure implemented.

2.1. Feedback Strategy

In the context of feedback strategy, it was used the predictive QDMC (*Quadratic Dynamic Matrix Control*), that is a model predictive controls (MPC) with constraints through the implementation of a optimization routine based on the method of Successive Quadratic Programming (SQP), Garcia and Morshedi, 1986; Zafiriou and Marchal, 1991; and Vasco de Toledo et al., 2004. Among the digital controllers, the QDMC was chosen by its robustness and flexibility to tune due to the presence of several parameters.

The QDMC algorithm predicts the performance of the controlled variables over a prediction horizon, by solving an optimization problem using a quadratic programming (QP) approach to find out the controller actions to a control horizon (smaller or equal to the prediction horizon) (Mayne et al., 2000). The predicted behaviour is calculated using a process model (convolution models). The projected errors, between the desired trajectory and the predicted response, are used to determine future control actions. Only the first control action is implemented. At the next sampling instance, the real plant measurement is used to correct for any plant/model mismatch and the optimization is repeated to find out the next optimal control solution.

When criteria of high level complexity are proposed to obtain the control action, considering restrictions in the controlled and manipulated variables it is necessary to use optimisation

algorithms, because, in this case, there is no possibility of analytical solutions. In this work, the performance criterion, optimised via the SQP algorithm, is expressed as:

$$
\begin{aligned}
&J = \min_{\Delta u} \phi = \frac{1}{2}\Delta u^T H \Delta u + c^T \Delta u \\
&\text{where :} \\
&H = A^T W^T W A \\
&c^T = -E'^T W^T W A \\
&\text{subjected to the following operational constraints :} \\
&y_{min} \le y \le y_{max} \\
&u_{min} \le u \le u_{max},\ \Delta u_{min} \le \Delta u \le \Delta u_{max}
\end{aligned}
\qquad (1)
$$

In these equations W is the weighting factor matrix (adjustable parameters that allow to penalize the control actions); A is the dynamic matrix of the system; E' is the array that stores the differences between past predictions and reference values; Δu is the array with the incremental of the manipulated variables and y is the controlled variable, u is the manipulated variable with maximum and minimum values, $y_{max,}$, y_{min}, u_{max} and u_{min}, respectively.

Although this controller, associated to optimisation algorithm, is able to consider more sophisticated control problems, the benefits obtained in this approach must justify the inherent increase of complexity (computational efforts for instance) when it is compared to analytical methods of solution.

2.2. Feedforward Strategy

The feedforward strategy was developed using two methodologies. In the first one, the deterministic model is used in an optimization problem in which the manipulated variable T_{fo} is used as optimization parameter, seeking to minimize the objective function specified by equation (2). The function may be written as:

$$
\begin{aligned}
&\min_{Tfo} \left((T - Tsetpoint)^2\right) \\
&\text{s.t. } Tfo_{min} \le Tfo \le Tfo_{max} \\
&\text{or} \\
&\min_{Tr} \left((T - Tsetpoint)^2\right) \\
&\text{s.t. } Tr_{min} \le Tr \le Tr_{max}
\end{aligned}
\qquad (2)
$$

The objective was to minimize the difference of the square between the temperature of exit of the reactor and the calculated temperature of the new set point starting from the disturbances for T_{fo} and T_r. T is the exit temperature of the reactor.

Through the Levenberg-Marquardt algorithm was possible to implement this methodology, which allows to find out the value of the manipulated variable, knowing the desired set point and the disturbances of the process.

In the second methodology, the feedforward strategy was developed using a reduced model (statistical model) obtained through the full factorial design method**.** The factorial design was carried out in order to study the effects of some variables of the mathematical model in significant responses and with such information to develop the statistical model for exit temperature of the reactor. The runs were planned to obtain a model, with temperature as response. The central points provide additional degrees of freedom for pure error estimating, but in this case is not possible to calculate it because the responses were determined by simulation. The distance of the axial points was ±2.38, calculated from Eq. (3) (Khuri and Cornell, 1987), where a is the distance of the axial points and n is the number of independent variables. These independent variables and their levels are presented in Table 1. The software Statistical (Statsoft, v. 7) was used to analyse the results.

$$\alpha = \left(2^n\right)^{1/4} \qquad \textbf{(3)}$$

The estimated effects of variables, as well the interactions between them, on each response were determined for a 95% confidence level. To confirm the significance and influence of the studied factors were used statistical parameters. For example, $p < 0.05$, suggests significance at the 0.05 level (Box et al., 1978).

In estimated effects the variables that present statistically significant main effects in the temperature are the o-cresol and hydrogen concentrations in the liquid phase, and the both temperatures (T_{fo} and T_r). For the responses, the most significant variables are the temperatures (T_{fo} and T_r). However, it should be observed that the feed reactant temperature was disturbed in ±5% and the refrigerant one, as well as the other independent variables, in ±10%. Thus, when the main effects were analysed, initially the refrigerant temperature is presumed as the variable that has larger impact on the conversion as well as on the reactor exit temperature. In fact, the variable of larger impact is the feed reactant temperature due to its smaller disturbance. Therefore, as it will be seen later, this variable (T_{fo}) introduces great potential to be used as manipulated variable in the control layer, when compared to the refrigerant temperature (T_r). At this point it is worthwhile mentioning that for practical implementation changes in the refrigerant temperature are difficult to be used since usually thermal fluids have as characteristic present high heat capacity. This

means that a large effort, in terms of heat exchanger designs and operation have to be made to change the temperature of large amount of fluid in a reasonable time interval.

The R-square value provided a measure of how much of the variability in the observed response values could be explained by the factors and their interactions. A good model (values above 0.9 are considered good) explains most of the variation in the model response. In fact, a way to obtain a reduced model using such approach to an existing process may be to carry out perturbation in the real plant (what is not always possible), otherwise, to develop a mathematical (deterministic) model, do a proper validation and then use such model in the proposed procedure. Based on the *F*-test, the model is predictive, since its calculated *F*-value is higher than the critical *F* value and the regression coefficient is close to unity, for the temperature. The developed statistical model for the temperature exit was used to solve the control problem.
The statistical analysis was used to obtain the empirical equation that describes the feed reactant temperature (T_{fo}) and the cooling temperature (T_r) as manipulated variables. The empirical equations are presented as a function of the exit reactor temperature (*Tset point*), the feed reactant temperature (when the manipulated variable is T_r), the cooling temperature (when the manipulated variable is T_{fo}), the o-cresol (B_{lfo}) and the hydrogen (A_{gfo} and A_{lfo}, gas and liquid phase, respectively) feed concentration. The linear empirical equations are given by equations (4) and (5), which were obtained from of the full factorial design. The statistical models are:

-feedforward strategy when T_{fo} as manipulated variable:

$$\begin{aligned} Tfo = {} & Tset\ point - (-62.50498252 + \\ & + 355.6215012 * Agfo + 3.836649024 * Alfo \\ & + 143.4758567 * Blfo + 0.428379079 * Tr) / 0.67691109 \end{aligned} \quad (4)$$

-feedforward strategy when T_r as manipulated variable:

$$\begin{aligned} Tr = {} & Tset\ point - (-62.50498252 + 355.6215012 * Agfo + \\ & + 3.836649024 * Alfo + 143.4758567 * Blfo + \\ & 0.67691109 * Tfo) / 0.428379079 \end{aligned} \quad (5)$$

Table 1 – Variables and levels for central composite design.

	-2.38*	-1	0	+1	+2.38*
A_{gfo} (± 10%)	1.14E-02	1.35E-02	1.50E-02	1.65E-02	1.86E-02
A_{lfo} (± 10%)	8.38E-03	9.90E-03	1.10E-02	1.21E-02	1.36E-02
B_{lfo} (± 10%)	1.83E-01	2.16E-01	2.40E-01	2.64E-01	2.97E-01
T_{fo} (± 5%)	476.00	513.00	540.00	567.00	604.00
T_r (± 10%)	381.00	450.00	500.00	550.00	619.00
$\pm 2.38^* = (2^5)^{1/4}$ (star point)					

2.3. Feedforward-Feedback Strategy

The basic concept of this strategy is to couple both feedback and feedforward approaches aiming to take advantage of each one of the strategies simultaneously.

The feedforward strategy makes possible an increase in the velocity of the three-phase reactor control, and when it is associated to the feedback control, the result is a powerful plan of control, represented by equation (6), which was, among the control strategies studied, the most efficient, as it will be seen later.

$$\begin{aligned} & u\_(feedback + feedforward) = \beta\, u\_feedforward + \\ & + (1-\beta)\, u\_feedback \qquad \text{where } 0 \le \beta \le 1 \end{aligned} \quad (6)$$

Therefore, the performance of five different strategies were analysed, to know: feedback strategy (FB), feedforward strategy based on deterministic model (FF_deterministic) and on statistical model (FF_statistical), combined feedback strategy and feedforward strategy based on deterministic model (FF_deterministic +FB) and combined feedback strategy and feedforward strategy based on statistical model (FF_statistical + FB).

3. RESULTS AND DISCUSSIONS

The open-loop dynamic behaviour of multiphase reactor was observed by Vasco de Toledo et al. (2001).The comparison of the performance for the studied strategies (feedback, feedforward and mixed feedforward and feedback) is shown in Figures 3 to 7.

In order to evaluate the feedforward-feedback strategy (FF and FB), with both types of model (deterministic and statistical), tests were performed for values of β (eq.6) equal to 0.1, 0.3, 0.5, 0.7 and 0.9. The best profiles for both cases (FF_deterministic + FB and FF_statistical + FB) were found when β =0.7, which is the value used in this work.

As expected, the feedforward strategy, using the deterministic model as well as the statistical model was more efficient to reach the desired set-points.

Care has to be taken for the variation of the manipulated variables which was in most of the cases, the abrupt and this may cause difficulties to the practical implementation of this strategy. The performance analysis of the feedback strategy for the controllers QDMC was considered for typical operating conditions. The SISO regulatory control with T_{fo} as manipulated variable (Figures 3, 4 (for example, the Figure 4 making indirectly the control of the concentration of the o-cresol) and 5) and the SISO servo control with T_r as manipulated variable (Figures 6 and 7) are depicted with a good controller performance.

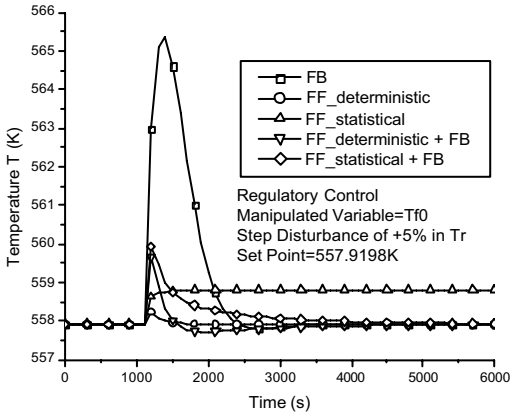

Figure 3. Regulatory SISO control of the reactor – controlled variable

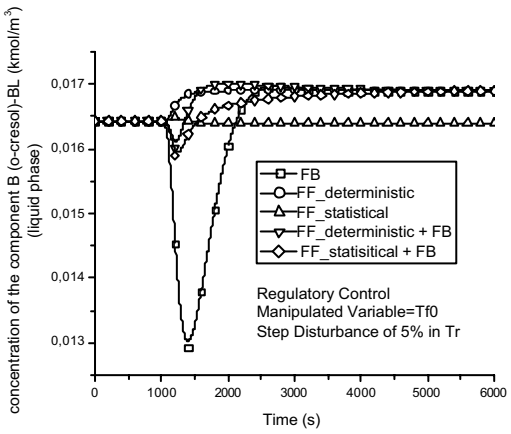

Figure 4. Regulatory SISO control of the reactor – controlled variable

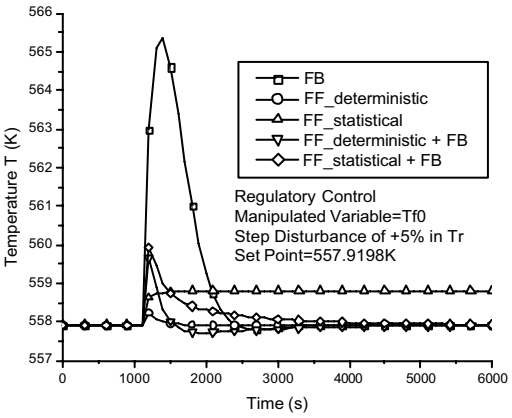

Figure 5. Regulatory SISO control of the reactor - manipulated variable.

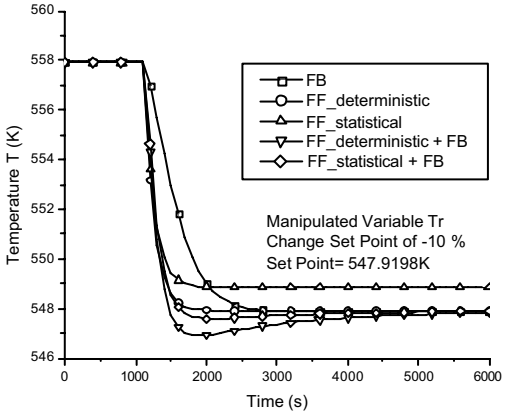

Figure 6. Servo SISO control of the reactor – controlled variable.

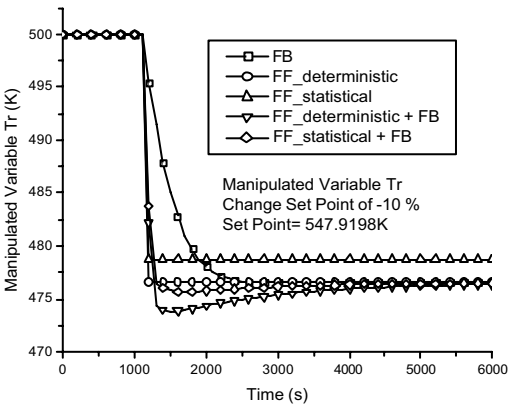

Figure 7. Servo SISO control of the reactor – manipulated variable

The feedforward strategy based on statistical model presented significant off-sets due, mainly, to its sensitivity and inherent errors, which do not allow to represent the dynamic behaviour of the process for the whole operating conditions. The use of statistical based model is a good approach to speed up the

calculations but care has to be taken to the model representativity for all possible operation range.

The mixed strategy (Feedforward and feedback) using feedforward based on the statistical model did not present off set as in the case for the conventional feedforward, because the feedback strategy eliminates the off sets. This strategy has good performance and the mixed strategy (FF_deterministic + FB) is even better due to the prediction capabilities of the deterministic model when compared to statistical one.

Nevertheless, the feedforward with statistical model (FF_statistical) and the mixed configuration (FF_statistical + FB), presents advantage since its solution is more rapid, although for the case of the control feedforward (FF_statistical), it was generated off set in comparison with the control feedforward (FF_deterministic). Therefore, depending upon the objectives and operational constraints of the system, some particular strategy can be the most appropriate. For the case of this work, the mixed strategy feedforward-feedback was that presented the better performance.

Finally, the mixed configuration (feedforward + feedback) was able to conciliate quickness to reach the desired set-points with smooth changes in the manipulated variable, which is desired characteristic for an industrial implementation.

4. CONCLUSIONS

The results showed that was possible to evaluate different control strategies for the solution of the multiphase reactor control. This understanding made possible the elaboration of an efficient and safe control strategy with desirable characteristics for an industrial implementation, mixed configuration (feedforward + feedback).

This control strategy should conciliate quickness to reach the desired objectives (set-points) and generate smooth changes in the manipulated variable.

ACKNOWLEDGEMENTS

The authors are grateful to the Fundação de Amparo à Pesquisa do Estado de São Paulo - FAPESP and to the Conselho Nacional de Desenvolvimento Científico e Tecnológico - CNPq for their financial support.

REFERENCES

Box, G.E.P., Hunter W.G., Hunter, J.S. (1978). Statistics for Experiments – An introduction to design, data analysis and model building, New York, John Wiley.

Garcia, C. E., Morshedi, A. M. (1986). Quadratic Programming Solution of Dynamic Matrix Control (QDMC), Chem. Eng. Comun., **46**, 73-87.

Khuri, A.I., Cornell, J.A. (1987). Response surface design and analyses , New York, Marcel Dekker Inc.

Mayne, D. Q., Rawlings, J. B., Rao, C. V., & Scokaert, P. O. M. (2000). Constrained model predictive control: Stability and optimality. Automatica, ***36***, 789–814.

Rezende, M. C. A. F., A. C. Costa and Maciel Filho, R. (2004). Control and Optimization of a Three Phase Industrial Hydrogenation Reactor. International Journal of Chemical Reactor Engineering,**2**,A21.

Vasco de Toledo, E.C., Maciel Filho, R. (2004). Detailed Deterministic Dynamic Models for Computer Aided Design of Multiphase Slurry Catalytic Reactor, European Symposium on Computer-Aided Process Engineering **14**, 18, 823-828.

Vasco de Toledo, E.C., Mariano, A.P., Stremel, D. P., Maciel Filho, R. (2004). Advanced Control of a Three-Phase Slurry Catalytic Reactor, European Symposium on Computer-Aided Process Engineering **14**, 18, in CD.

Vasco de Toledo, E.C.., Santana, P.L., Wolf-Maciel, M.R., Maciel Filho, R. (2001). Dynamic modelling of a three-phase catalytic slurry reactor, Chem. Eng. Sci., **56**, 6055-6061.

Zafiriou, E., Marchal, A. (1991). Stability of SISO Quadratic Dynamic Matrix Control with Hard Output Constraints", AIChE Journal, **37,**10, 1550–1560.

ADCHEM 2006

International Symposium on Advanced Control of Chemical Processes
Gramado, Brazil – April 2-5, 2006

ON INPUT-OUTPUT SELECTION FOR MULTILOOP CONTROL: FROM RGA TO ROMA

Aldo Balestrino, Alberto Landi

Dipartimento di Sistemi Elettrici e Automazione, Università di Pisa, Italy

Abstract: A new tool for selecting the right pairing between inputs and outputs in a multiloop system is introduced. Similar in structure to the classical RGA the new array, called a Relative Omega Array, is based on the characteristic frequencies in open and closed loop under perfect control, as eventually detected by a classical relay test. This way the dynamic properties of the system are simply taken into account. Some examples show that the new tool is effective, giving the correct pairing also when the RGA approach fails. *Copyright © 2006 IFAC*

Keywords: Multivariable control, RGA, interaction, auto-tuning, integrity.

1. SELECTION OF PAIRING INPUT AND OUTPUT VARIABLES IN DECENTRALIZED CONTROL SCHEMES

In multi-loop industrial control systems decentralised multi-loop SISO controllers are widely used, despite the interactions between the input/output variables (Luyben, 1997, Ogunnaike, 1994, Mayne, 1973). A decentralised structure is usually preferred for large scale industrial processes, since its simplicity, especially in case of sensor or actuator failures, where a process engineer can easily modify the controller parameters in order to counteract the abnormal operating condition. Experience show that usually performance of decentralised control structures meets satisfactory process design requirements. Performance improvements obtained adopting more refined (and complex) controllers are not usually so relevant to justify additional costs for their implementation and maintenance. Before developing a control structure design for a multivariable process, some basic question must be answered (Havre, 1996):

- What outputs must be controlled?
- How to select the control variables?
- How to pair input and output variables?
- How to tune the controllers?

The selection of controlled outputs essentially depends on the decision of the expert and on the physical insight of the process. In the selection it will be necessary to keep into account costs of production, safety in terms of protecting plant personnel and plant investments, physical limitations, availability and reliability of the sensors.
It can be required to control simultaneously levels of liquids, pressures, temperatures, positions, speed, product quality, production rates. In real plants often the choice of the variable to be controlled is clear, but not always such variables are directly measurable and they must be estimated from other measures. The problem of loop pairing between controlled and manipulated variables was usually solved by the relative gain array (RGA) method, introduced in 1966 by Bristol, and its several extensions. Suppose for simplicity to consider a multi-variable system with an equal number of controlled and manipulated variables, described by the matrix of transfer functions G(s). In the classic formulation due to Bristol, it is considered the matrix of the steady-state process gains of the system A = G(0) and it is defined the Relative Gain Array (RGA) as:

$$\Lambda = A \otimes (A^T)^{-1} = A \otimes A^{-T} \qquad (1)$$

where ⊗ denotes element-by-element product.

Definition: the RGA matrix $\Lambda = \{ \lambda_{ij} \}$ is formed by the generic λ_{ij} element which corresponds to the ratio of the open loop and closed loop gains between input j and output i, representing first the process gain in an isolated loop and, second, the apparent process gain in that same loop when all other control loops

are closed. Two main hypotheses are posed: matrix Λ is evaluated at steady-state and the control is perfect, i.e., the closed loop gains are evaluated when all other outputs h ≠ i are ideally regulated to zero.
RGA matrix (1) has several properties: the more relevant for following developments (Ogunnaike, 1994, Skogestad, 1997) are:

1) Any row or column sums to one.
2) The relative gain is invariant under scaling, i.e., $\Lambda(M) = \Lambda(PMQ)$, where P and Q are arbitrary diagonal matrices.
3) The only effect of altering the order of rows or columns in K is to introduce the same alteration of order in Λ.

The meaning of the relative gains λ_{ij} is that for ideal decentralised control the pairing should have a value of $\lambda_{ij} = 1$.
If $\lambda_{ij} = 0$, it implies that the steady-state gain of a single loop is zero, or that the interaction is so high that the behaviour of the loop is totally affected by the other loops. Such interaction has opposite effects if λ_{ij} is negative: in this case the open and closed loop gains have opposite signs, that is the closed loop multiloop process is unstable, or the single loops with negative λ_{ij}'s are unstable if the remaining loops are turned off, or the multiloop process is unstable if the loops with negative λ_{ij}'s are turned off (e.g., in case of failure in the i-j loop (Grosdidier, 1986)).
Based on the previous properties a suitable use of RGA matrix leads to an easy and practical rule for selecting the less interacting pairings: the variable pairings corresponding to positive relative gains λ_{ij} as close to unity as possible are preferred.

To illustrate the use of the RGA method and its limitations, consider the following examples:

Example 1.

Wood and Berry process (Ogunnaike, 1994):

$$P_1(s)=\begin{bmatrix} \dfrac{12.8e^{-s}}{16.7s+1} & \dfrac{-18.9e^{-3s}}{21s+1} \\ \dfrac{6.6e^{-7s}}{10.9s+1} & \dfrac{-19.4e^{-3s}}{14.4s+1} \end{bmatrix}$$

The steady-state RGA is:

$$\Lambda_1 = \begin{pmatrix} 2.0094 & -1.0094 \\ -1.0094 & 2.0094 \end{pmatrix}$$

It suggests the use of a diagonal pairing (y_1-u_1, y_2-u_2) in a good agreement the physical behaviour of the process.

Example 2.

Process described by the following matrix transfer function (Meeuse, 2002):

$$P_2(s)=\begin{pmatrix} \dfrac{e^{-s}}{1+s} & \dfrac{1}{1+s} \\ \dfrac{-1}{1+s} & \dfrac{e^{-2s}}{1+s} \end{pmatrix}$$

The steady-state RGA is:

$$\Lambda_2 = \begin{pmatrix} 0.5 & 0.5 \\ 0.5 & 0.5 \end{pmatrix}$$

In this example the steady-state RGA does not suggest any preferential pairing.

Example 3.

Process described by the following matrix transfer function (Seider, 1999):

$$P_3(s)=\begin{pmatrix} \dfrac{2.5e^{-5s}}{(1+15s)(1+2s)} & \dfrac{1}{1+4s} \\ \dfrac{1}{1+3s} & \dfrac{-4e^{-5s}}{1+20s} \end{pmatrix}$$

The steady-state RGA is:

$$\Lambda_3 = \begin{pmatrix} 0.9091 & 0.0909 \\ 0.0909 & 0.9091 \end{pmatrix}$$

It suggests the use of a diagonal pairing (y_1-u_1, y_2-u_2), but a practical implementation based on dynamical considerations leads to off-diagonal pairing (y_1-u_2, y_2-u_1). In this example the static RGA fails.

2. A CRITICAL REVIEW

As suggested from the previous examples a simple application of the steady-state RGA can lead to wrong pairings or may not help the designer. The most important limitations of the static RGA can be summarized as:

- it doesn't include dynamics and a correct pairing should be frequency-dependent
- an optimal pairings may vary with the structure of the SISO controllers adopted
- RGA cannot discriminate diagonal processes from processes with triangular structure
- it does not consider disturbances.

Anyway, a primary advantage of RGA is that it requires only minimal process information; it relies on the knowledge of the steady-state gain matrix, very simple to measure.
Therefore in literature many researchers tried to extend the basic RGA definition, with several modifications.

A frequency-dependent RGA matrix can be introduced as (Grosdidier, 1986, Witcher, 1977):

$$\Lambda(s)=P(s)\otimes(P(s)^T)^{-1}=P\otimes P^{-T} \qquad (2)$$

Unfortunately, there are some arguments against the use of this frequency-dependent RGA: an ideal mathematical model of the process is usually unknown and it is very sensitive to modelling errors. Furthermore a classical frequency-based analysis will require to consider and analyse n(n+1) Bode plots, which is very time-consuming.

A different approach (Karlsmose, 1994) combines the frequency-dependent RGA method with the singular value decomposition of the transfer matrix representing the process, for a quantitative analysis of the results in the frequency domain.

A different method for measuring interaction is based on the Niederlinski index (Bristol, 1966, Niederlinski, 1971, Chiu, 1991), defined as:

$$N(s)=\frac{\prod_{i=1}^{n} P_{ii}(s)}{\det P(s)} \qquad (3)$$

This index is unitary, if P(s) is diagonal or triangular; an application of (3) to example 3 is able to select the correct pairing. Niederlinski index cannot discriminate the correct pairing in the case of example 2.
In practice it is possible to use more criteria sequentially, for selecting correct pairings; for example a first analysis can be performed using the classic RGA method, then the Niederlinski index can be applied, after discarding the negative pairings. If necessary it can be used a singular value decomposition.
In industrial applications seldom process engineers cope with so complex and unusual problems, with a high number of input/output variables. Furthermore the knowledge of the process at a physical-chemical level suggests often in a natural way the selection of the pairing between controlled and manipulated variables. Nevertheless the problem of the pairing maintains a remarkable interest, both from a theoretical point of view and in practice.
In the following section a different solution of this problem is addressed, suggesting a new index of dominance and the method for its practical application.

3. ROmA INDEX

In the design of a decentralized control system, standard proportional-integral-derivative (PID) controllers have remained the most popular ones in the industry since the 1950s, due to their simplicity and immediate way of operation. Relay feedbacks and auto-tuning techniques (Semino, 1998) are simple, powerful, and commonly used methods of finding system parameters useful for designing and tuning PID controllers: their parameters can be easily set from the knowledge of the ultimate gains (k_{ij}'s) and frequencies (ω_{ij}'s) (Loh, 1993, Dhen, 1994). The auto-tuning method ATLS of Loh and Shen ranks the loops according to their speed and the fastest loop is to be tuned first (Toh, 2002).
This procedure is in a good agreement (Leonhard, 2001) with the practice of the experts of cascade-control, especially in the field of high-performance electrical drives, where the synthesis proceeds closing first the inner faster loop and proceeding toward the slowest outer loops.
If we consider the generic loop between the i-th output variable and the j-th input variable, it will be described by the $P_{ij}(s)$ transfer function; if we consider the insertion of a standard $C_{ij}(s)$ controller, the open loop transfer function is $G_{ij}(s) = P_{ij}(s)\, C_{ij}(s)$.
The ideal closed loop transfer function, keeping all other loops open is:

$$W_{ij} = G_{ij}(s)/(1+ G_{ij}(s)) \qquad (4)$$

At the critical frequency ω_{ij}, we obtain:

$G_{ij}(\omega_{ij}) = -m_{ij}$,

and

$W_{ij}(\omega_{ij}) = -m_{ij}/(1-m_{ij})$.

In single-input single-output systems the critical frequency ω_{ij} remains unchanged in the passage from open loop to closed loop; m_{ij} represents the relative gain margin, strictly less than one for guaranteeing the loop stability. Of course this property holds also for multi-input multi-output systems if the systems are decoupled.
Consider now the introduction of a new interaction measure, taking into account dynamics. It relies on the classic definition RGA-like, where the measure is expressed as the ratio of a variable correlated to a single loop of the process under test with all other outputs uncontrolled, and the same variable when all other outputs are perfectly controlled. In this last situation the transfer function between the i-th output variable and the j-th input variable is modified, due to the interaction of all other control loops. For RGA case the variable under test is the steady-state gain, but in our proposal we consider the critical frequencies ω_{ij}.
Define $\hat{W}_{ij}(s)$ as the new transfer function in case of perfect control and $\hat{\omega}_{ij}$ the corresponding new critical frequency. For non interacting systems, $\hat{\omega}_{ij} = \omega_{ij}$ so that, by mimicking the RGA procedure, the ratios $\omega_{ij}/\hat{\omega}_{ij}$ are considered for creating a new matrix $F = \{\omega_{ij}/\hat{\omega}_{ij}\}$, as a different dominance index.
Dominance is guaranteed if a ratio $\omega_{ij}/\hat{\omega}_{ij}$ tends to one. The pairings can be easily verified introducing

the matrix ROmA (Relative Omega Array), in a way analogous to the RGA definition:

$$\Psi = F \otimes F^{-T} \tag{5}$$

Note that the ROmA matrix retains all the properties of the RGA matrix.

Example 1: Wood and Berry process (Ogunnaike, 1994):

$$P_1(s) = \begin{bmatrix} \dfrac{12.8e^{-s}}{16.7s+1} & \dfrac{-18.9e^{-3s}}{21s+1} \\ \dfrac{6.6e^{-7s}}{10.9s+1} & \dfrac{-19.4e^{-3s}}{14.4s+1} \end{bmatrix}$$

Operating conditions: a relay and a fixed delay of 4 s are inserted in the control loop. The delay is inserted for maintaining physical causality in all following tests. In plain words all other loops are open, only the loop under test is closed for detecting its critical frequency.

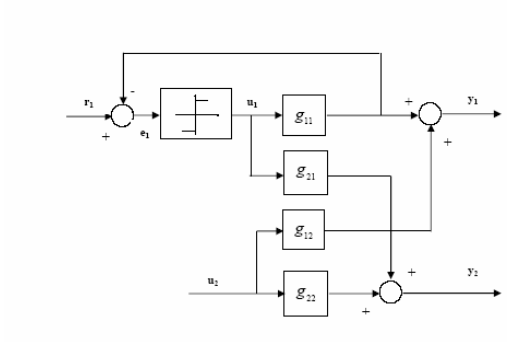

Fig. 1. A 2x2 system with a relay test in the first loop.

Results of the tests are:
A) closing the first loop y_1-u_1 the critical frequency is ω_{11}=0.3553 rad/s.
B) closing the second loop y_2-u_2 the critical frequency is ω_{22}=0.2688 rad/s.
Note that to induce a stable oscillation in the second loop the sign of the input u_2 has to be inverted.
This means that pairing is possible only by changing sign to u_2 ; therefore the test procedure continues inverting the sign of this input.
The system under test considering the added delay and the correct signs becomes:

$$P_1'(s) = \begin{bmatrix} \dfrac{12.8e^{-s}}{16.7s+1} & \dfrac{18.9e^{-3s}}{21s+1} \\ \dfrac{6.6e^{-7s}}{10.9s+1} & \dfrac{19.4e^{-s}}{14.4s+1} \end{bmatrix} e^{-4s}$$

C) closing the loop y_1-u_2 the critical frequency is ω_{12}=0.192 rad/s
D) closing the loop y_2-u_1 the critical frequency is ω_{21}=0.2567 rad/s

Consider now the oscillating conditions in the hypothesis of a perfect control.
A1) the loop y_1-u_1 is closed in the hypothesis the an ideal controller in the other loop may guarantee y_2 = 0. Then:

$$\begin{cases} y_{1CL} = \left(g_{11} - \dfrac{g_{12}g_{21}}{g_{22}} \right) u_1 \\ y_{1OL} = g_{11}u_1 \end{cases}$$

and, after simple computations:

$$y_{11CL} = \left(12.8\frac{e^{-s}}{(16.7s+1)} - 6.43\frac{(1+14.4s)e^{-7s}}{(1+10.9s)(1+21s)} \right) u_1$$

Pre-multiplying by e^{4s}:

$$y_{11CL} = \left(12.8\frac{e^{-5s}}{(16.7s+1)} - 6.43\frac{(1+14.4s)e^{-11s}}{(1+10.9s)(1+21s)} \right) u_1$$

The critical frequency $\hat{\omega}_{11}$=0.4012 rad/s is detected.

B1) In a similar way the loop 2-2 is closed:

$$\begin{cases} y_{2CL} = \left(g_{22} - \dfrac{g_{12}g_{21}}{g_{11}} \right) u_2 \\ y_{2OL} = g_{22}u_2 \end{cases}$$

$$y_{22CL} = \left(-19.4\frac{e^{-3s}}{(14.4s+1)} + 9.7453\frac{(1+16.7s)e^{-9s}}{(1+10.9s)(1+21s)} \right) u_2$$

.

Pre-multiplying by e^{4s}:

$$y_{22CL} = \left(-19.4\frac{e^{-7s}}{(14.4s+1)} + 9.7453\frac{(1+16.7s)e^{-13s}}{(1+10.9s)(1+21s)} \right) u_2$$

The critical frequency $\hat{\omega}_{22}$=0.3185 rad/s is measured.

C1) For the loop 1-2:

$$y_{12CL} = \left(-18.9\frac{e^{-3s}}{(21s+1)} + 37.6242\frac{(1+10.9s)e^{3s}}{(1+16.7s)(1+14.4s)} \right) u_1$$

Pre-multiplying by e^{4s}:

$$y_{12CL} = \left(-18.9\frac{e^{-7s}}{(21s+1)} + 37.6242\frac{(1+10.9s)e^{-s}}{(1+16.7s)(1+14.4s)} \right) u_1$$

The critical frequency $\hat{\omega}_{12}$=1.582 rad/s is measured.

D1) For the loop 2-1:

$$y_{21CL} = \left(6.6\frac{e^{-7s}}{(10.9s+1)} - 13.1386\frac{(1+21s)e^{-s}}{(1+16.7s)(1+14.4s)} \right) u_2$$

Pre-multiplying by e^{4s}:

$$y_{21CL}=\left(6.6\frac{e^{-11s}}{(10.9s+1)}-13.1386\frac{(1+21s)e^{-5s}}{(1+16.7s)(1+14.4s)}\right)u_2$$

The critical frequency $\hat{\omega}_{21}=0.4095$ rad/s is measured.

Therefore the matrix of the relative frequencies is:

$$F=\frac{\omega_{OL}}{\omega_{CL}}=\begin{pmatrix}\frac{0.3553}{0.4012} & \frac{0.192}{1.582}\\ \frac{0.2567}{0.4095} & \frac{0.2688}{0.3185}\end{pmatrix}$$

The relative omega array (ROmA) index is:

$$\Psi=F\otimes F^{-T}=\begin{bmatrix}1.1133 & -0.1133\\ -0.1133 & 1.1133\end{bmatrix}=ROmA$$

Pairing suggested by the ROmA matrix is in a perfect agreement with the RGA rule:

$$\Lambda=A\otimes A^{-T}=\begin{bmatrix}2.0094 & -1.0094\\ -1.0094 & 2.0094\end{bmatrix}=RGA\ .$$

Example 2. Consider now the process (Meeuse, 2002):

$$P_2(s)=\begin{pmatrix}\frac{e^{-s}}{1+s} & \frac{1}{1+s}\\ \frac{-1}{1+s} & \frac{e^{-2s}}{1+s}\end{pmatrix}$$

Introducing the new scaled input variables $v_1 = u_2$, $v_2 = - u_1$ the new matrix under test is:

$$P_2^{'}=\begin{bmatrix}\frac{1}{1+s} & -\frac{e^{-s}}{1+s}\\ \frac{e^{-2s}}{1+s} & \frac{1}{1+s}\end{bmatrix}$$

Adding a common delay in all loops, e.g., e^{-3s} for guaranteeing the oscillations, the new matrix under test is:

$$P_2^{''}=\begin{bmatrix}\frac{1}{1+s} & -\frac{e^{-s}}{1+s}\\ \frac{e^{-2s}}{1+s} & \frac{1}{1+s}\end{bmatrix}e^{-3s}$$

Note that all operations introduced do not vary the results of the RGA or ROmA analysis, because of its invariance property under scaling.
The matrix of relative critical frequencies is now:

$$F=\frac{\omega_{OL}}{\omega_{CL}}=\begin{pmatrix}\frac{0.67}{2.101} & \frac{0.8566}{0.5196}\\ \frac{0.8566}{0.5196} & \frac{0.5522}{1.471}\end{pmatrix}$$

The ROmA index is:

$$\Psi=F\otimes F^{-T}=\begin{pmatrix}-0.0461 & 1.0461\\ 1.0461 & -0.0461\end{pmatrix}=\text{ROmA}$$

By comparing this matrix with the traditional RGA matrix:

$$RGA=\begin{pmatrix}0.5 & 0.5\\ 0.5 & 0.5\end{pmatrix}$$

It may be observed that the suggested pairings is the off-diagonal one: y_1-u_2, y_2-u_1. This result is in a good agreement with the results of Meeuse [8], in a critical case where steady-state RGA does not prefer any pairing.

Example 3. Consider the process studied in (Seider, 1999):

$$P_3(s)=\begin{pmatrix}\frac{2.5e^{-5s}}{(1+15s)(1+2s)} & \frac{1}{1+4s}\\ \frac{1}{1+3s} & \frac{-4e^{-5s}}{1+20s}\end{pmatrix}$$

In this case the common delay chosen is 6 s.
The matrix of relative critical frequencies is now:

$$F=\frac{\omega_{OL}}{\omega_{CL}}=\begin{pmatrix}\frac{0.1573}{1.823} & \frac{0.3786}{0.09454}\\ \frac{0.3992}{0.4133} & \frac{0.174}{3.143}\end{pmatrix}$$

Matrix ROmA is:

$$\Psi=F\otimes F^{-T}=\begin{pmatrix}-0.0012 & 1.0012\\ 1.0012 & -0.0012\end{pmatrix}$$

An off-diagonal pairing is suggested, opposite to the wrong pairing given by the steady-state RGA:

$$RGA=\begin{pmatrix}0.9091 & 0.0909\\ 0.0909 & 0.9091\end{pmatrix}.$$

4. SENSITIVITY

In the previous examples an additional delay has been introduced in order to assure the oscillating conditions in presence of a relay. Indeed for a given matrix of transfer function it is possible that no oscillation occurs. In practice if the control is networked or is remote we must always take into account some delay. In the previous examples the amount of delay introduced is somewhat arbitrary. Of course if the oscillations are obtained on the field by suitable relay testing, we must consider that greater is the delay more expensive and time consuming are the tests; by reducing the delay there may occur a limiting value leading to a non-oscillating condition.

It is interesting to evaluate the sensitivity of the proposed procedure to the amount of delay θ introduced.

By computing for different delays the ROmA array for Wood and Berry process we get the following results, where λ is the element 1-1 of the ROmA matrix:

Table 1 . Element 1-1 of the ROmA matrix varying the introduced delay θ.

Θ (s)	4	5	6	7	8	50	100
λ	1.113	1.31	1.398	1.496	1.580	8.656	15.545

The results displayed in the Table show that the information given by ROmA are quite insensitive to the delay; of course for very large delay the pairing suggested is still correct but the larger value of λ denote a possible greater difficulty in control.

4. CONCLUSIONS

In this work a new approach for the selection of the pairings between input and output variables in decentralized MIMO control schemes. The ROmA index is based on the ratio between the critical frequencies of the loops closed with a relay, keeping all other loops open and the critical frequencies of the loops closed with a relay, in case of a perfect control on the other loops. It maintains all properties of static RGA index, but it considers dynamics of the process under test with simple autotuning tests. All critical frequencies can be measured from autotuning tests, they may be easily performed on line and the knowledge of the model of the process in not necessary. Examples of applications were selected to illustrate the effectiveness of the new indicator in different critical cases, also in presence of different delays; other examples of applications to MIMO processes have always shown the capability of the new approach in choosing the correct pairing.

REFERENCES

Bristol, E. H. (1966). On a new measure of interaction for multivariable process control. *IEEE Transactions on Automatic Control*, **11**, 133-134.

Chiu M.-S. and Y. Arkun. (1991). A new result on relative gain array, Niederlinski index and decentralized stability condition: 2x2 plant case. *Automatica*, **27** (2), 419-421.

Grosdidier, P. and M. Morari (1986). Interaction measures for systems under decentralized control. *Automatica*, **22** (3), 309-319.

Havre K. and S. Skogestad (1996). Input/output selection and partial control. *13th IFAC World Congress*, San Francisco, 181-186.

Karlsmose, J., A. Koggersbol, N. Jensen and S. B. Jorgensen. (1994). A two stage procedure for control structure analysis and design. *Computers Chem. Engng*., **18**, S465-S470.

Leonhard, W. (2001). *Control of Electrical Drives*. Springer-Verlag, Berlin.

Loh, A.P., C.C.Hang, C.K.Quek and V.U. Vasnani (1993). Autotuning of Multiloop Proportional-Integral Controllers Using Relay Feedback. *Ind. Eng. Chem. Res*., **32** (6), 1102-1107.

Luyben, W.L. and M.L. Luyben (1997). *Essentials of Process Control*. McGraw-Hill, New York.

Mayne, D.Q. (1973). The design of linear multivariable systems. *Automatica*, **9**, 201-207.

Meeuse, F.M. and A. E. M. Huesman. (2002). Analyzing Dynamic Interaction of Control Loops in the Time Domain. *Ind. Eng. Chem. Res*, **41**, 4585-4590.

Niederlinski, A. (1971). A Heuristic Approach to the Design of Linear Multivariable Interacting Control Systems. *Automatica*, **7**, 691-701.

Ogunnaike B.A. and W. Harmon Ray (1994). *Process Dynamics, Modeling, and Control*. Oxford University Press.

Seider, W.D., J.D.Seader and D.R. Lewin. (1999). *Process design principles*. John Wiley & Sons: New York.

Semino D. and C. Scali (1998). Improved Identification and Autotuning of PI Controllers for MIMO Processes by Relay Techniques. *J. Process Control*, **8** (3), 219-227.

Shen, S.H. and C.C. Yu. (1994). Use of Relay-Feedback Test for Automatic Tuning of Multivariable Systems. *AIChE J*., **40** (4), 627-646.

Skogestad, S. and I. Postlethwaite. (1997). *Multivariable Feedback Control.* J.Wiley, New York.

Toh, W.K., and G.P. Rangaiah. (2002). A Metodology for Autotuning of Multivariable Systems. *Ind. Eng. Chem. Res*., **41**, 4605-4615.

Witcher, M. F. and T. J. McAvoy. (1977). Interacting control systems: Steady-state and dynamic measurement of interaction. *ISA Transactions*, **16** (3):35-41.

ADCHEM 2006

International Symposium on Advanced Control of Chemical Processes
Gramado, Brazil – April 2-5, 2006

DESIGN AND CONTROL OF A POWER GENERATION SYSTEM FOR A FUEL-CELL POWERED AUTOMOBILE

Panini K. Kolavennu, Srinivas Palanki [1]
John C. Telotte

Department of Chemical and Biomedical Engineering, FAMU-FSU College of Engineering, Florida State University, Tallahassee, FL 32310-6046, USA

Abstract: In this paper, we consider design and control issues in a fuel-cell powered automobile that utilizes methane as a source of hydrogen. A power generation system is designed based on a steady state model of a PEM fuel cell that is capable of generating 50 kW of power. The transient behavior of the fuel cell is captured via a transfer function model and an appropriate adaptive controller is tuned to follow a time varying power profile that mimics realistic road conditions. Finally, a logic-based controller is designed and tested that switches to a battery backup that provides power to the electric motor when the fuel cell is unable to meet the necessary power demand.

Keywords: fuel processor, PEM fuel cell, power generation system

1. INTRODUCTION

Fuel cell power systems for automotive applications have received increased attention in recent years because of their potential for high fuel efficiency and lower emissions [Zalc and Loffler, 2002]. In particular, a fuel cell converts hydrogen and oxygen into water, directly generating electrical energy from chemical energy without being restricted by efficiency limits of the Carnot thermal cycle [Larminie and Dicks, 2000]. This interest in automotive applications has primarily been the result of the breakthroughs made in polymer electrolyte membrane (PEM) fuel cells which have several attractive features such as low operating temperatures (around 80 ^{o}C), relatively low cost, simple maintenance requirements, and high efficiency.

While there have been significant advances in fuel cell technology, one reason this technology has not seen wide-spread applications in the automotive industry has been the lack of an efficient hydrogen distribution center and the difficulties associated with storing hydrogen onboard an automobile [Lovins and Williams, 1999]. One option to alleviate these problems is to develop a system that utilizes a commonly available carbon-based hydrogenous fuel such as gasoline or methane to generate the necessary hydrogen *in situ* on an "as needed" basis. Hydrocarbon fuels are relatively easy to store onboard a vehicle and a nationwide infrastructure to supply these fuels already exists. In this paper, we consider the design of a fuel-cell powered automobile that utilizes methane as a source of hydrogen.

[1] Corresponding author: palanki@eng.fsu.edu

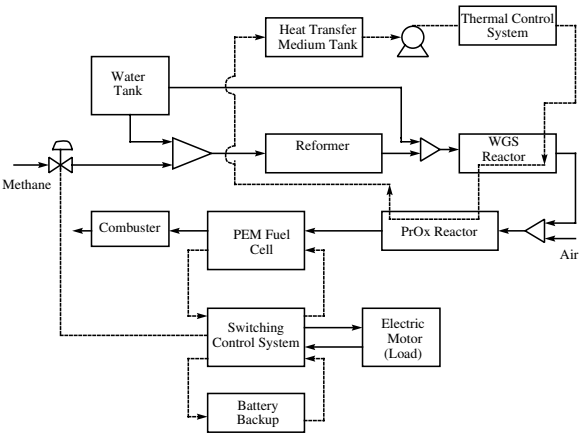

Fig. 1. Schematic of Fuel Cell System

2. SYSTEM DESIGN CONSIDERATIONS

A schematic of the fuel cell system under consideration is shown in Fig. 1. The two main components of the overall system are (1) the fuel processing subsystem and (2) the power generation subsystem. Methane enters the fuel processing subsystem and is converted to hydrogen. Hydrogen enters the fuel cell where it mixes with oxygen to generate electrical power which drives an electric motor.

In addition to the fuel cell, there is a battery backup that the electric motor switches to when the hydrogen delivered to the fuel cell is insufficient to meet the *instantaneous* power demands of the electric motor. This battery backup is essential because significant load transitions occur frequently as a result of sudden acceleration on highway ramps as well as terrain changes [Zalc and Loffler, 2002].

In an earlier paper [Kolavennu *et al.*, 2004], the primary components of a fuel cell power system, that utilizes methane to generate hydrogen, were analyzed. In particular, basic chemical engineering principles were utilized to design a reactor train that converts methane to hydrogen of the desired purity. The relation between power produced by a PEM fuel cell and methane entering the reactor train *at steady state* was calculated. However, a typical automobile does not operate at steady state. The power demand for an automobile motor undergoes significant variations due to acceleration, changes in road surface and traffic conditions.

In this paper, we analyze the power generation subsystem in the face of fluctuating power demand. In particular, we design a controller that adjusts the hydrogen flow into the fuel cell in response to changing power demand. When power demand goes down, the excess hydrogen can be diverted from the fuel cell. However, a sudden *increase* in power demand requires an instantaneous increase in hydrogen flow rate into the fuel cell. However, the conversion of methane to hydrogen takes several seconds which leads to an unacceptable lag between power demand of the motor and the power supplied by the fuel cell. For this reason, a backup battery is required that takes over this power load during the time it takes for the fuel cell to generate the necessary power. In this paper, a logic-based switching controller is designed that switches to the battery backup when the fuel cell is unable to provide the necessary power to the motor. This design is tested via simulations for a typical power profile of an automobile motor.

Reactor Name	T(K)	P (atm)	Size (l)
Steam Reformer	1000	5	10
Water-Gas Shift	700 (HT)	2	41.8
	490 (LT)		
Preferential Oxidation	473	2	0.35

Table 1. Fuel Processing Subsystem

2.1 Fuel Processing Subsystem

In this subsystem, methane is converted to hydrogen. In a previous publication [Kolavennu *et al.*, 2004], we utilized basic chemical engineering principles to design a reactor train that produced hydrogen of the desired purity. The design operating conditions of this series of reactors are summarized in Table 1.

The steam reformer operates at 1000 K and 5 atm and utilizes a steam to carbon ratio of 3:1. The water gas shift reactor operates at 2 atm and has two temperature zones. The initial 1 liter is operated at 700 K (HT) to promote high reaction rate and the remaining 40.8 liters are operated at 490 K (LT) to promote high conversion. The preferential oxidation reactor operates at 473 K and 2 atm. It was shown [Kolavennu *et al.*, 2004] that the relation between methane utilized and hydrogen produced was linear and could be represented by the following relation:

$$F_{H_2} = 3.12 F_{CH_4} \tag{1}$$

2.2 Design of Power Generation Subsystem

The current generated by the fuel cell stack is directly proportional to the hydrogen consumption rate. The voltage generated by a cell depends on the current density in the cell, thermodynamic parameters (temperature and partial pressures) and the cell materials and design. For a given cell design and thermodynamic state a detailed calculation of the voltage versus current density can be performed. In this work we have utilized a semi-theoretical model first proposed by Larminie and

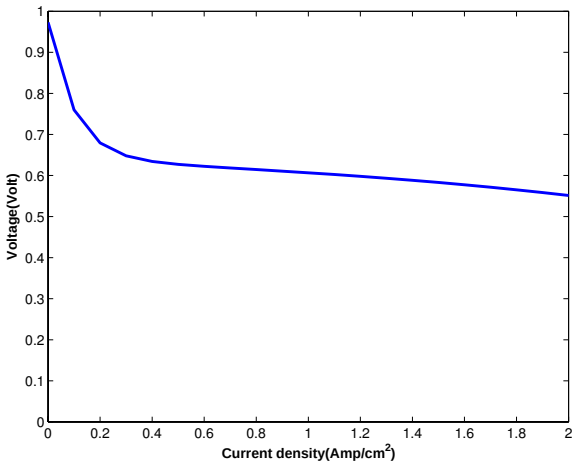

Fig. 2. Voltage vs. Current Density

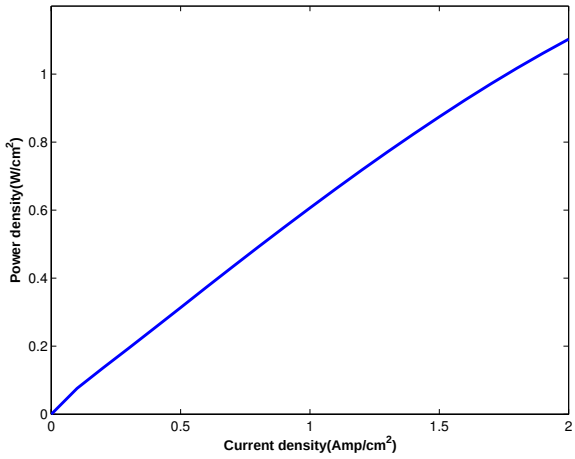

Fig. 3. Power Density vs. Current density

Dicks [2000] and later parameterized by Pukrushpan [2003]. For a fuel cell operating at 353 K with an anode partial pressure of hydrogen of 3 atm and air fed to the cathode at 5 atm, the following cell polarization curve is obtained:

$$V = 0.6405 + 0.3325e^{-10i} - 0.03036i - 0.00355i^3 \quad (2)$$

For these conditions that there is a sharp drop-off in cell voltage at small current densities but a very flat region to the polarization curve with cell voltages being nearly 0.6 V over a wide range of current densities as shown in Figure 2. This is desirable characteristic as this produces a power density that varies nearly linearly with current density, as seen in Figure 3.

The design objective for this project has been for a 50 kW fuel cell stack. We have based our design on a cell voltage of 0.6 V. This occurs for a current density of 1.15 A/cm^2. If one desires a system with a 300 volt output [Pukrushpan, 2003], then 500 cells in series are required. To generate 50 kW of power then requires 166.67 A of current which requires an active cell area of 145 cm^2. The required hydrogen flow per cell is calculate from

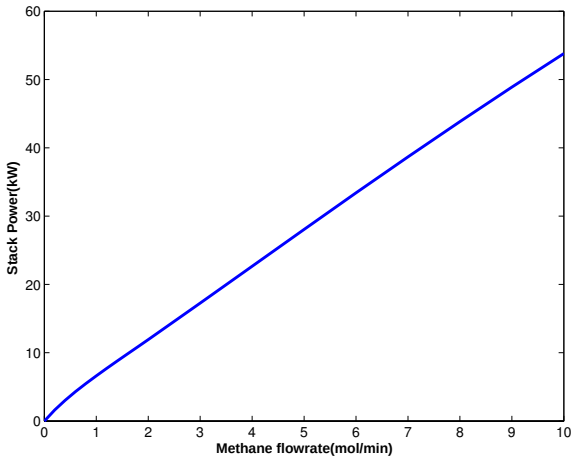

Fig. 4. Effect of Methane Flow on Power Generated

$$I = 2FX\dot{N}_{H_2} \quad (3)$$

The conversion is assumed to be 90%, which yields a maximum required hydrogen flow of 0.001 moles/sec/cell. This corresponds to a total required methane flow of 9.2 moles/min. The power curve for the combined fuel processor and fuel cell stack system is shown in Figure 4. To construct this curve a methane flow rate was selected and the resultant hydrogen flow from the fuel processor was calculated using equation (1). Using equation (3), the cell current was then determined. With the cell area specified at 145 cm^2, the current density could then be found and the stack power was finally calculated using equation (2).

3. CONTROLLER DESIGN FOR POWER GENERATION SUBSYSTEM

For the fuel cell systems to operate at levels comparable to existing internal combustion engines, the key issue that should be addressed is the *transient* behavior of fuel cell systems. Automobiles are subjected to significant load transitions during operation and the fuel cell system should be able to produce power which can follow this varying load profile. Hydrogen from the fuel processing subsystem comes at the anode and splits into hydrogen ions and electrons. The electrons pass through an external circuit towards the cathode thereby producing the current. The whole process involves electrochemical, mass and heat transport phenomena and there has been considerable research effort in modeling fuel cells to capture this phenomena [Nguyen and White, 1993; Kim et al, 1995]. Power produced by the fuel cell is dependent on the voltage current characteristics. Hence for control related studies a dynamic model which can mimic the voltage-current characteristics of the fuel cell system is required. Pukrushpan [2003] proposed a dynamic nonlinear model which can be

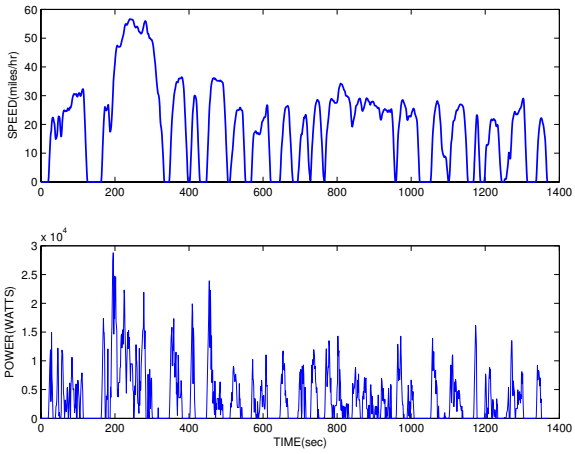

Fig. 5. Speed and Power Profile for UDDS

used for this purpose. For a given current demand the model calculates the voltage produced and thereby the power output of the fuel cell. The model also takes into account the effects of humidity on cell performance. The transient response data from the nonlinear model was generated by subjecting the nonlinear system to a series of step inputs in the current around the 100 Amperes operating point. Utilizing this input output data from the nonlinear model system identification techniques were employed to derive a linear second order model was fit between the current demand and the voltage produced by the fuel cell stack. The transfer function G_p is given below

$$G_p = \frac{-390.78}{s^2 + 27.291s + 2068.8} \tag{4}$$

This transfer function is used in this paper to design a controller to regulate the power output of the fuel cell to the power demand. The control problem is to track the power demand of the motor using current as the manipulated variable.

To get a more realistic power vs time profile we obtained the power profile for a small car from an existing speed vs time profile using ADVISOR software package [NREL, 2002] as shown in Figure 5. The Urban Dynamometer Driving schedule(UDDS) which is designed for light duty vehicle testing in city driving conditions was used.

4. MODEL REFERENCE ADAPTIVE CONTROLLER

Model reference adaptive control (MRAC) is derived from the model reference control (MRC) problem. The objective of MRC is to find the feedback control law that changes the structure and dynamics of the plant so that its I/O properties are exactly the same as those of a reference model. The structure of an MRC scheme for a

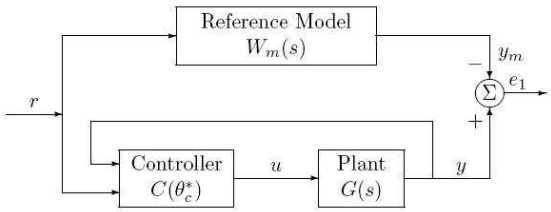

Fig. 6. Model Reference Adaptive Control

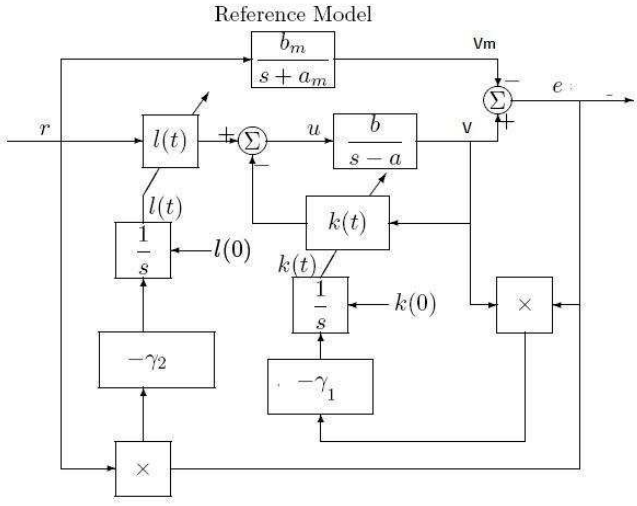

Fig. 7. Implementation of Model Reference Adaptive Control

LTI, SISO plant is shown in Fig. 6 [Ioannou and Sun, 1996]. Here, $W_m(s)$ is the transfer function of the reference model, $r(t)$ a given reference input signal, $y_m(t)$ the output of the reference model and $y(t)$ is the plant output. The feedback controller, denoted by $C(\Theta_c)$, is designed so that all signals are bounded and the closed-loop plant transfer function from r to y is equal to $W_m(s)$. This transfer function matching guarantees that for any given reference input $r(t)$, the tracking error $e = y - y_m$, which represents the deviation of the plant output from the desired trajectory ym, converges to zero with time.

The MRAC control law equation can be implemented as shown in Fig. 7. The initial conditions $l(0)$; $k(0)$ are chosen by an *a priori* guess of the unknown parameters k and l respectively.

To make a quantitative comparison between the adaptive controller and a PID controller, the Integrated Time Averaged Error (ITAE) is calculated by the following equation.

$$ITAE = \sum_{i=0}^{n} \frac{t_i |e_i(t)|}{n} \tag{5}$$

where n stands for the number of time steps. e_i is the error at time t_i.

Table 2. Average ITAE error in kW obtained for the nonlinear model

Controller	UDDS	US HWY
PID	91.46	unstable
Adaptive	40.5	55.6

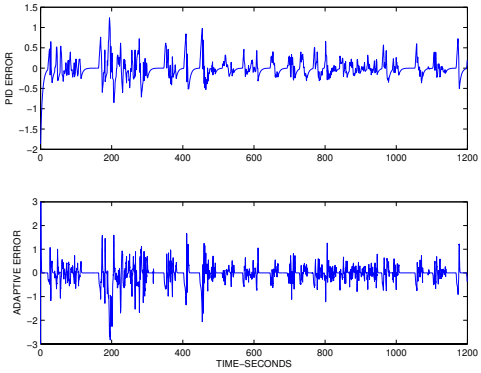

Fig. 8. Error obtained for the PID and Adaptive controllers implemented on the nonlinear model

After designing the controllers for the linear model it was implemented on the nonlinear model. The PID controller and the adaptive controller were fine-tuned for the nonlinear model and the errors obtained for the UDDS profile are shown in Fig. 8. The adaptive controller error has a larger overshoot compared to the PID controller but the error comes back to zero quickly when compared with the PID controller. An important aspect of designing a controller for an automotive purpose is we do not know the trajectory of the power profile *a priori* and so the controller tuned for one profile should work for several other typical road profiles. This is where the adaptive controller scores over the PID controller. The PID controller has to be retuned for each different power profile to meet the performance specifications whereas the adaptive controller can adapt to the new power profile. To test this the controller designed for the UDDS profile was implemented on a US06-HWY profile which simulates highway driving instead of city driving represented by UDDS. When the US06-HWY profile is used on the controllers designed for the UDDS profile the PID controller failed as the system became unstable whereas the adaptive controller works well as shown in Table 2.

4.1 Switching to Battery Backup

When the power demand increases suddenly (e.g. due to sudden acceleration), this requires an instantaneous increase in hydrogen. However, since it takes time for reactants and products to go through the reactor train, there is a time delay in producing the hydrogen. If the reactions are not kinetically limited, this time delay can be estimated from the space time of the reactor train

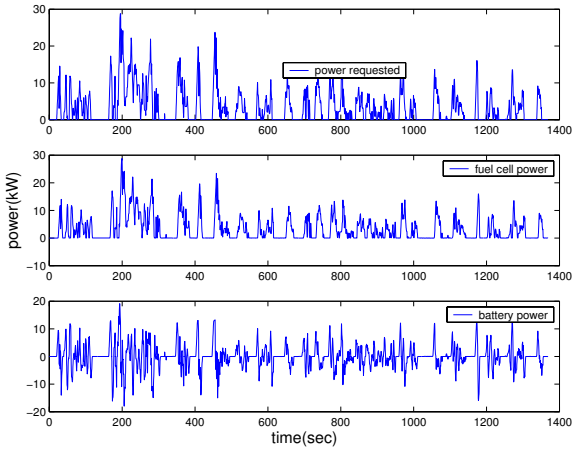

Fig. 9. Power Profiles for the UDDS

which was estimated to be about 4 seconds based on the maximum flow rate of 10 moles/min of methane. Thus, it is necessary to have a battery backup that provides power to the motor during this time lag while sufficient hydrogen is generated. Since the battery is charged and discharged continuously, knowledge of the transient behavior of the batteries is very important. Dynamic modeling of batteries is a major concern for electric vehicles and fuel cell hybrid vehicles. For control oriented studies we require models which can be simulated quickly and so in this paper we utilize an equivalent electric circuit model developed along the lines of [He and Hodgson, 2002] which gives an accurate prediction of state-of-charge (SOC) of the battery.

The switching controller is a logic based on-off controller that switches back and forth between the fuel cell and the battery to meet the power demand. The logic controller addresses the following issues:

- The power produced by the fuel cell comes with a certain time delay and hence any deficit in power demand is handled by switching to the battery until the fuel cell can produce sufficient power.
- The excess power produced by the fuel cell during deceleration or decrease in power demand should be routed to the battery.
- When the SOC of the battery falls below a specified target the controller should direct the fuel cell to produce power to charge the battery in addition to the power demand.
- Since the fuel processor and the fuel cell system were designed for a maximum power output of 50 kW. The controller should make sure that the power demand is not greater than 50 kW.

The time profiles of power requested, fuel cell power and battery power are plotted in Fig. 9. The power supplied by the battery also depends on

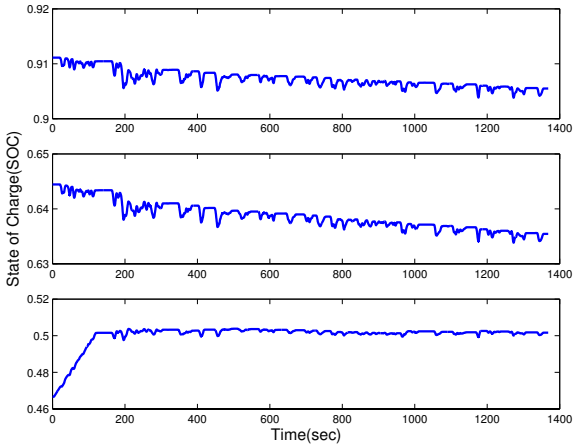

Fig. 10. State of Charge for Different Initial Conditions

the initial SOC of the battery. For the same cycle the system was simulated for different initial SOC as shown in Fig. 10. The controller was designed to maintain the SOC above 0.5. For the initial conditions where the battery is almost charged (SOC=0.9) and semi charged (SOC=0.64) the profiles look similar. But for the case where the initial SOC is less than 0.5 the controller is activated and brings the SOC level to above 0.5.

5. CONCLUSIONS

A power generation system for a methane-powered automobile is designed that consists of a fuel cell and a battery backup. The hydrogen flow to the fuel cell is adjusted via an adaptive controller depending on the power demand of the electric motor. A logic-based controller switches to the battery backup when the fuel cell is unable to meet the power demand. These controllers are tested via simulation on realistic power demand profiles.

Currently, the effect of thermal transients on the fuel processor and the power generation system are being studied.

ACKNOWLEDGMENTS

Funding from Pharogen Inc. as well as Florida State University is gratefully acknowledged.

REFERENCES

[1] He, X. and Hodgson, J.W., " Modeling and simulation for hybrid electric vehicles. i. modeling." *Intelligent Transportation Systems*, volume 3, 235-243, (2002)

[2] Ioannou P. and J. Sun, *Robust Adaptive Control*, Prentice Hall, Inc., 1996

[3] Kim, J., Lee, S.M., Srinivasan, S., "Modeling of Proton Exchange Membrane Fuel Cell Performance with an Empirical Equation," *J. Electrochem. Soc.*, 142, 8, 2670 (1995)

[4] Kolavennu, P.K., Telotte, J.C., and Palanki, S., "Modeling and Control of a Fuel Cell Power System for Automotive Applications," *European Symposium for Computer Aided Process Engineering-14*, Lisbon, Portugal, May 16-19, 2004

[5] Larminie, J., and Dicks, A., *Fuel Cell Systems*, Wiley, New York, 2000

[6] Lovins, A.B., and Williams, B.D., "A strategy for the hydrogen transition," *10th Annual U.S. Hydrogen Meeting*, Vienna, Virginia, April 1999

[7] National Renewable Energy Laboratory, "ADVISOR (Advanced Vehicle Simulator)", 2002

[8] Nguyen, T.V., and White, R.E., "A water and heat management model for proton-exchange-membrane fuel cells," *J. Electrochem. Soc.*, 140, 8, 2178-2186 (1993)

[9] Pukrushpan, J. T., *Modeling and Control of Fuel Cell Systems and Fuel Processors*, PhD thesis, The University of Michigan, Ann Arbor, 2003

[10] Zalc, J.M., and Loffler, D.G., "Fuel processing for PEM fuel cells: transport and kinetic issues of system design," *J. Power Sources*, 111, 58-64 (2002)

ADCHEM 2006

International Symposium on Advanced Control of Chemical Processes
Gramado, Brazil – April 2-5, 2006

OUTPUT-FEEDBACK CONTROL OF CONTINUOUS POLYMER REACTORS WITH CONTINUOUS AND DISCRETE MEASUREMENTS

Pablo González and Jesús Alvarez

Universidad Autónoma Metropolitana-Iztapalapa
Depto. de Ingeniería de Procesos e Hidráulica
Apdo. 55534, 09340 México D.F, MÉXICO

Abstract: An output-feedback (OF) control to stabilize continuous free-radical solution polymer reactors is presented, on the basis of continuous measurements of temperatures, level and flows, and discrete-delayed measurements of molecular-weight (MW). First, the state-feedback controller is presented, and its behavior is the recovery target for the OF design. The OF control consists of continuous linear PI-type decentralized volume and cascade temperature controllers, a continuous material-balance monomer controller, and a discrete MW controller. The temperature controller requires two approximate static parameters, the monomer controller requires the heat capacity function, and the MW controller requires one static parameter and initiation constants (pre-exponential factor and activation energy), which are fewer modeling requirements than the ones of the case without MW measurements. The proposed control technique has a systematic construction and simple tuning guidelines, and is tested with an industrial size reactor through simulations.

Keywords: Polymerization reactor control, decentralized control, discrete measurements, discrete estimator, chemical process control, continuous process control.

1. INTRODUCTION

In the last two decades the polymerization reactor problem has been the subject of extensive theoretical, simulation and experimental studies, given the demand of processes with better compromises between safety, productivity and quality, and the development of control methods. In a typical industrial setting, the volume and temperature are controlled with decentralized linear PI controllers, and the conversion and molecular weight (MW) are feedback and/or feedforward controlled with inferential, advisory, or supervisory control schemes. On the other hand, in the academic field a diversity of control techniques have been employed, such as nonlinear geometric (Soroush and Kravaris, 1993; Alvarez, 1996; Gauthier and Kupka, 2001), MPC (Mutha et al., 1997), and calorimetric (Alvarez et al., 2004) control techniques; these controllers have been implemented with open-loop (Soroush and Kravaris, 1993), extended Kalman filter (EKF) (Mutha et al, 1997), and Luenberger (Alvarez, 1996; Gauthier and Kupka, 2001) nonlinear observers. Despite valuable insight has been gained in the understanding of the polymer reactor control problem, the resulting nonlinear controllers are strongly interactive and model dependent, signifying complexity and reliability drawbacks for industrial applicability.

Recently, González and Alvarez (2005) presented a PI-inventory controller which: (i) combines the simplicity features (linearity, decentralization, and modeling dependency) of the PI and inventory industrial controllers (Shinskey, 1988; Luyben, 1990) with the structure and robustness design tools offered by the nonlinear geometric (Isidori, 1995) and constructive (Sepulchre et al., 1997) control approaches, (ii) recovers the behavior of an exact model-based nonlinear state-feedback (SF) passive controller, (iii) employs continuous-instantaneous (CI) measurements of volume, temperatures and flows, (iv) doubles the molecular-weight (MW)

response speed in comparison with the MW open-loop mode, and (v) regulates the MW with an offset whose size depends on the accuracy of the initiation rate and transfer models.

These observations rise the issue that constitutes the motivation of the present work: the incorporation of discrete-delayed (DD) MW measurements to speed-up the response and eliminate the asymptotic offset of the MW output.

In this work, an output-feedback (OF) controller to regulate a (possibly open-loop unstable) polymerization reactor is presented, on the basis of: (i) continuous level, temperature and flow measurements, (ii) discrete-delayed MW measurements, and (iii) mass-energy balances. For applicability purposes, the quest of linearity, decentralization and reduced model dependency features as well as the derivation of conventional-like tuning guidelines are important design objectives.

2. CONTROL PROBLEM

Consider a CSTR where an exothermic free-radical solution homopolymer reaction takes place. Monomer, solvent and initiator are fed to the tank, and heat exchange is enabled by a cooling jacket. Due to the gel effect (Chiu et al, 1983), the reactor can have multiple steady-states (Hamer et al., 1981). From standard free-radical polymerization kinetics (Hamer et al., 1981), and viscous heat exchange considerations (Alvarez et al., 1996), the reactor dynamics are given by the following energy and material balances:

$$\dot{T} = \{\Delta r - U(T - T_j) + (\rho_m q_m c_m + \rho_s q_s c_s)(T_e - T)\}/C := f_T, \qquad y_T(t) = T \tag{1a}$$

$$\dot{T}_j = \{U(T - T_j) + \rho_j q_j c_j (T_{je} - T_j)\}/C_J := f_j, \qquad y_j(t) = T_j \tag{1b}$$

$$\dot{V} = q_m + q_s - (\varepsilon_m/\rho_m) r - q := f_V, \quad y_V(t) = V \tag{1c}$$

$$\dot{m} = - r + \rho_m q_m - (m/V) q := f_m \tag{1d}$$

$$\dot{\pi} = (r - \pi r_0)\pi/(V\rho - m - s) := f_\pi, \quad y_\pi(t_k) = \pi(t_{k-1}) \tag{1e}$$

$$\dot{I} = - r_i + w_i - (I/V) q := f_i \tag{1f}$$

$$\dot{s} = \rho_s q_s - (s/V) q := f_s \tag{1g}$$

$$\dot{\mu}_2 = r_2 - (\mu_2/V) q := f_{\mu 2} \tag{1h}$$

$$z_T = T, \; z_V = V, \; z_m = m, \; z_\pi = \pi$$

$$u_j = q_j, \; u_V = q, \; u_m = q_m, \; u_i = w_i$$

$$r = f_r(T, V, m, I, s), \qquad Q = \Delta r \tag{2a}$$

$$U = f_U(T, T_j, V, m, s), \qquad H = U(T - T_j) \tag{2b}$$

$$C = f_C(V, m, s), \qquad \rho = f_\rho(V, m, s) \tag{2c}$$

$$r_i = f_{ri}(T, I), \quad (r_0, r_2)' = (f_0, f_2)'(T, V, m, I, s) \tag{2d, e}$$

$$\theta = W_m \mu_2/[(V\rho - m - s)\pi] \tag{2f}$$

The *states* (x) are: the reactor (T) and jacket (T_j) temperatures, the volume (V), the free (i.e., unreacted) monomer (m), solvent (s) and initiator (I) masses, as well as the (number-average) molecular weight (π) and second moment (μ_2) of the MW distribution. The *measured exogenous inputs* (d) are: the reactor (T_e) and jacket (T_{je}) feed temperatures, and the solvent (q_s) volumetric flowrate. The *regulated outputs* (z) are: the temperature (T), the volume (V), the monomer content (m), and the (number-average) molecular weight (π). The *continuous-instantaneous measured outputs* (y_c) are: the temperature (y_T), the volume (y_V), and the jacket temperature (y_j). The *discrete-delayed measured output* (y_d) is the molecular weight (y_π). The *control inputs* (u) are: the coolant volumetric flowrate (q_j) through the jacket circuit, the exit flowrate (q), the monomer flowrate (q_m) and the initiator mass feedrate (w_i). Δ is the heat of polymerization per unit monomer mass, W_m is the monomer molecular weight, ε_m is the monomer contraction factor, ρ_m (or c_m), ρ_s (or c_s) and ρ_j (or c_j) are the monomer, solvent and coolant fluid densities (or specific heat capacities), C and C_J are the reacting mixture and cooling system heat capacities; U, ρ, r, r_i, r_0, and r_2 are the heat transfer coefficient, the reacting mixture density and the rates of polymerization, initiator decomposition, and change of the zeroth and second moments (Hamer et al., 1981); θ is the MW polydispersity. The moment rates r_0 and r_2 can be expressed in terms of initiation and monomer and solvent transfer rates (Flory, 1953).

In vector notation, the reactor model (1) is given by:

$$\dot{x} = f(x, d, u), \qquad y = C_y x, \qquad z = C_z x \tag{3}$$

$$x = (T, T_j, V, m, \pi, I, s, \mu_2)'$$

$$f = (f_T, f_j, f_V, f_m, f_\pi, f_i, f_s, f_2)', \quad d = (T_e, T_{je}, q_s)'$$

$$y = (y_c', y_d)', \qquad y_c = (y_T, y_j, y_V)', \qquad y_d = (y_\pi)$$

$$u = (q_j, q, q_m, w_i)', \; z = (z_T, z_V, z_m, z_\pi)'$$

In a previous study (González and Alvarez, 2005), the behavior of an exact model-based MIMO nonlinear passive SF controller was recovered by means of a measurement-driven controller with: linear-decentralized volume and cascade temperature PI-controllers, as well as feedforward-like monomer and MW controllers. Having this study as a point of departure, in this work is addressed the case of controlling the (possibly open-loop unstable) reactor (3) with DD MW measurements. In particular, we are interested in redesigning the nonlinear MW control component of the abovementioned study (González and Alvarez, 2005): (i) in the light of the linearity, decentralization and reduced model dependency features that underlie the functioning of the CI measurement-driven volume and temperature PI components, and (ii) with conventional-like tuning guidelines that account for the DD nature of the MW measurement.

3. BEHAVIOR RECOVERY TARGET

From the development of a previous work (González and Alvarez, 2005), in this section an exact model-based nonlinear SF passive controller is presented, whose behavior is the recovery target of the proposed OF controller. Since the following solvability conditions

$$\text{(i) } f_U > (T_j - T)\partial_{T_j} f_U, \qquad \text{(ii) } V f_\rho > m + s \qquad (4)$$
$$\text{(iii) } \partial_I f_r > \pi\, \partial_I f_0$$
$$\text{(iv) Stable (solvent- MW second moment) zero-dynamics: } \dot{x}_I = \phi_I(x_I, d), \quad x_I(0) = x_{Io}$$

are met by the reactor class (4), the *cascade (passive) SF controller*

$$u_p = \eta_p(x, d, K_p, p), \qquad u_p = (q, q_m)' \qquad (5a)$$
$$u_s = \eta_s(x, d, \dot{d}, K_s, p), \qquad u_s = (q_j, w_i)' \qquad (5b)$$

yields a closed-loop stable operation. Here, u_p (or u_s) is the primary (or secondary) controller, K_p (or K_s) is the primary (or secondary) control gain matrix, and η_p, η_s, and ϕ_I are nonlinear maps (defined in González and Alvarez, 2005) determined by the kinetics (f_r, f_0), heat exchange (f_U), and heat capacity (f_C) functions (2) as well as some of their partial derivatives. The regulated outputs (z) converge to their nominal values as with adjustable rates (k_V, k_T, k_m, k_π):

$$z_V(t) \xrightarrow{\sim k_V} \bar{z}_V, \qquad z_T(t) \xrightarrow{\sim k_T} \bar{z}_T \qquad (6a, b)$$
$$z_m(t) \xrightarrow{\sim k_m} \bar{z}_m, \qquad z_\pi(t) \xrightarrow{\sim k_V} \bar{z}_\pi \qquad (6c, d)$$

The last controller (5) sets the limiting behavior (6) attainable by feedback control with maximum robustness and LNPA output dynamics, and such behavior is regarded as the recovery target for the development of the related measurement-driven controller.

4. OUTPUT-FEEDBACK CONTROL

As shown in our previous study (González and Alvarez, 2005), the direct (Luenberger or EKF) estimator-based implementation of the preceding nonlinear passive SF controller (5) is unduly complex and modeling dependent, and the same control task can be performed, in a simpler way, by means of a combination of (volume and temperature) PI decentralized feedback controllers with monomer and MW material-balance-based feedforward components that require initiation and transfer function models (2d, e). Since we are looking at a MW control redesign given the availability of DD MW measurements and the quest of linearity, decentralization and model independency features, let us recall the control model employed in the abovementioned study (González and Alvarez, 2005), now with DD MW measurements:

$$\dot{V} = b_V - q, \qquad y_V(t) = V \qquad (7a)$$
$$\dot{T} = a_T T_j + b_T, \qquad y_T(t) = T \qquad (7b)$$
$$\dot{T}_j = a_j q_j + b_j, \qquad y_j(t) = T_j \qquad (7c)$$
$$\dot{\pi} = a_\pi I + b_\pi, \qquad y_\pi(t_k) = \pi(t_{k-1}) \qquad (7d)$$
$$\dot{I}^* = v_i^*, \qquad y_i^*(t_k) = I^*(t_k) \qquad (7e)$$
$$(b_V, b_T, b_j, b_\pi)' = \beta(x, d, u, p) \qquad (7f)$$

where the nonlinear maps (b_V, b_T, b_j) and the static parameters (a_T, a_j) are defined by González and Alvarez (2005), and (a_π, b_π) are given by

$$a_\pi = -2\bar{\pi}^2 \hat{f}_d \hat{k}_{d0} e^{-E_d/RT}/[\bar{V} f_\rho(\bar{V}, \bar{m}, \bar{s}) - \bar{m} - \bar{s}]$$
$$b_\pi = \{\pi f_r(T, V, m, I, s) - V\pi^2 \kappa(T, m, s) - 2\pi^2 f_d f_{r_i}(T, I)\}/[V f_\rho(V, m, s) - m - s] - a_\pi I$$

Equation (7a-d) [or (7f)] is a linear-decentralized dynamic (or nonlinear, interactive and static) component, and (7) is an (exact) b-parametric representation of the actual reactor model (1). I^* is the initiator content regarded as a "virtual control input" in a cascade configuration, and $\dot{I}^* = v_i^*$ is its time derivative. The MW measurement (y_π) available at k-th time (t_k) is the value of the MW sampled at the time t_{k-1}. In other words, the MW measurement involves a delay of one sampling period.

Observe that b_V, b_T, b_V, and b_π are unknown inputs that are determined by the measurements (u, y, $\dot{y}$), and consequently, can be quickly reconstructed by means of a set of linear, decentralized observers, one for each (b_i-y_i) pair. Since the construction of the CI measurements-based observers and their corresponding feedback controllers are given in a previous study (González and Alvarez, 2005), here it suffices to address the development of a suitable discrete observer for the MW measurement and the construction of the related controller.

4.1 MW estimator

To handle the DD nature of the MW measurement, a discrete state estimator must be employed, and the load disturbance b_π (8) can be estimated from the DD MW measurement (y_π) in conjunction with the MW balance (7d). To construct the discrete estimator, let us make the standard estimation assumptions $\dot{b}_\pi \approx 0$, $\dot{v}_i^* \approx 0$, and write the Euler discrete version of these equations in conjunction with the discrete approximations of the MW balance (7d) and the initiator set point derivative (7e), and obtain the discrete model of the MW balance and of the initiator set point filter:

$$\pi(t_k) = \pi(t_{k-1}) + [a_\pi I(t_{k-1}) + b_\pi(t_{k-1})]\,\delta \qquad (8a)$$
$$b_\pi(t_k) = b_\pi(t_{k-1}) \qquad y_\pi(t_k) = \pi(t_{k-1}) \qquad (8b)$$

$$I^*(t_{k+1}) = I^*(t_k) + v_i^*(t_k)\,\delta \quad (9a)$$
$$v_i^*(t_{k+1}) = v_i^*(t_k) \qquad y_i^*(t_k) = I^*(t_k) \quad (9b)$$

The application of the geometric discrete estimation technique (Hernández and Alvarez, 2003) yields the MW estimator (10) and initiator setpoint filter (11):

$$\hat{\pi}(t_k) = \hat{\pi}(t_{k-1}) + [a_\pi \hat{I}(t_{k-1}) + \hat{b}_\pi(t_{k-1})]\,\delta + k_{D_1}[y_\pi(t_k) - \hat{\pi}(t_{k-1})] \quad (10a)$$
$$\hat{b}_\pi(t_k) = \hat{b}_\pi(t_{k-1}) + k_{D_2}[y_\pi(t_k) - \hat{\pi}(t_{k-1})] \quad (10b)$$
$$\hat{I}^*(t_{k+1}) = \hat{I}^*(t_k) + \hat{v}_i^*(t_k)\,\delta + k_{D_1}[y_i^*(t_k) - \hat{I}^*(t_k)] \quad (11a)$$
$$\hat{v}_i^*(t_{k+1}) = \hat{v}_i^*(t_k) + k_{D_2}[y_i^*(t_k) - \hat{I}^*(t_k)] \quad (11b)$$

where the (k_{D_1}, k_{D_2}) are the discrete estimator gains according to the following expressions

$$k_{D_1} = 2 - 2\,e^{-\zeta\omega\delta}\cos[\omega\delta(1-\zeta^2)^{1/2}], \qquad \delta = t_k - t_{k-1}$$
$$k_{D_2}(\zeta, \omega, \delta) = 1 + e^{-2\zeta\omega\delta} - 2\,e^{-\zeta\omega\delta}\cos[\omega\delta(1-\zeta^2)^{1/2}]$$

δ is the sampling period, and ω (or ζ) is the characteristic frequency (or damping factor) associated to the mappings of the estimator design poles into the continuous representation in the LHS of the complex plane (Hernández and Alvarez, 2003).
Observe that, due to the discrete nature of the MW (8) and initiator setpoint (9) models and the DD feature of the MW measurement: (i) the initiator setpoint filter (11) is a one-step-ahead predictor, and (ii) the MW estimator (10) yields the present estimate on the basis of the actual MW value one-step-behind.

4.2 MW SF controller

Recall the discrete MW balance (8a), regard the initiator content (I) as a virtual controller (I^*), impose the closed-loop discrete dynamics (with gain k_π) for the MW, this is,

$$a_\pi I^*(t_k) + b_\pi(t_k)] = -\,k_\pi[\pi(t_k) - \bar{z}_\pi]$$

solve this equation for I^* to obtain the primary MW SF controller (12a), and combine this primary controller with the initiator balance (1f) to obtain the secondary controller (12b). Thus, the result is the *cascade MW SF controller*

$$I^*(t_k) = \{b_\pi(t_k) + k_\pi[\pi(t_k) - \bar{z}_\pi]\}/a_\pi \quad (12a)$$
$$w_i = v_i^*(t_{k+1}) + f_{r_i}[T, I^*(t_k)] + [I^*(t_k)/V]q \quad (12b)$$

driven by discrete $[\pi(t_k)]$ and continuous (V, T, q) measurements.

4.3 Output-feedback reactor controller

The combination of the MW SF controller (12) with the MW estimator (10) and initiator setpoint filter (11) yields our DD MW measurement-driven controller (13c), and the volume, temperature and monomer controllers are the ones presented in a previous study. Thus, the entire *OF reactor controller* is given by:

Volume and temperature controllers (13a)

$$\dot{\hat{V}} = \hat{b}_V - q + 2\zeta\omega(y_V - \hat{V}), \qquad \dot{\hat{b}}_V = \omega^2(y_V - \hat{V})$$
$$\dot{\hat{T}} = a_T\hat{T}_j + \hat{b}_T + 2\zeta\omega(y_T - \hat{T}), \qquad \dot{\hat{b}}_T = \omega^2(y_T - \hat{T})$$
$$\dot{\hat{T}}_j = a_j q_j + \hat{b}_j + 2\zeta\omega(y_j - \hat{T}_j), \qquad \dot{\hat{b}}_j = \omega^2(y_j - \hat{T}_j)$$
$$q = \hat{b}_V + k_V(\hat{V} - \bar{z}_V)$$
$$T_j^* = -\,[(\hat{b}_T + k_T(\hat{T} - \bar{z}_T)]/a_T$$
$$\dot{T}_j^* = -\,\{\omega^2(y_T - \hat{T}) + k_T[a_T\hat{T}_j + \hat{b}_T + 2\zeta\omega(y_T - \hat{T})]\}/a_T$$
$$q_j = [\dot{T}_j^* - \hat{b}_j - k_j(\hat{T}_j - T_j^*)]/a_j$$

Monomer controller (13b)

$$\dot{\hat{m}} = -\,\hat{r} + \rho_m q_m - (\hat{m}/\hat{V})\,q, \qquad \dot{\hat{s}} = \rho_s q_s - (\hat{s}/\hat{V})\,q$$
$$\hat{r} = [f_C(\hat{V}, \hat{m}, \hat{s})(a_T\hat{T}_j + \hat{b}_T) + C_J\hat{b}_j)]/\Delta$$
$$q_m = [-\,k_m(\hat{m} - \bar{z}_m) + \hat{r} + (\hat{m}/\hat{V})\,q]/\rho_m$$

MW controller (13c)

$$\dot{\hat{I}} = -\,f_{r_i}(\hat{T}, \hat{I}) + w_i - (\hat{I}/\hat{V})\,q$$
$$\hat{\pi}(t_k) = \hat{\pi}(t_{k-1}) + [a_\pi\hat{I}(t_{k-1}) + \hat{b}_\pi(t_{k-1})]\,\delta + k_{D_1}[y_\pi(t_k) - \hat{\pi}(t_{k-1})]$$
$$\hat{b}_\pi(t_k) = \hat{b}_\pi(t_{k-1}) + k_{D_2}[y_\pi(t_k) - \hat{\pi}(t_{k-1})]$$
$$\hat{I}^*(t_{k+1}) = \hat{I}^*(t_k) + \hat{v}_i^*(t_k)\,\delta + k_{D_1}[y_i^*(t_k) - \hat{I}^*(t_k)]$$
$$\hat{v}_i^*(t_{k+1}) = \hat{v}_i^*(t_k) + k_{D_2}[y_i^*(t_k) - \hat{I}^*(t_k)]$$
$$I^*(t_k) = \{\hat{b}_\pi(t_k) + k_\pi[\hat{\pi}(t_k) - \bar{z}_\pi]\}/a_\pi$$
$$w_i(t_k) = \hat{v}_i^*(t_{k+1}) + f_{r_i}[\hat{T}, \hat{I}^*(t_k)] + [\hat{I}^*(t_k)/\hat{V}]\,q$$

This OF controller (13) consists of linear PI-type decentralized volume and cascade temperature controllers (13a), linear and decentralized cascade MW controller (13c), and a material-balance monomer controller (13b). Comparing with the case without MW measurements (González and Alvarez, 2005), the OF controller (13) has: (i) a linear discrete estimator with MW measurements (10), coordinated with a linear discrete estimator (11) for the initiator set point (I^*), and (ii) an initiator feedrate input (12b) from a material balance, without feedback term. The discrete estimator (10) replaces the continuous MW estimator without MW injection of the abovementioned work, and has fewer modeling requirements.

Model requirements. The modeling requirements of the proposed OF controller (13) are the following: (i) the temperature controller requires two approximate static parameters (a_T, a_j), (ii) the MW controller requires one static parameter (a_π) and initiation constants [pre-exponential factor and activation energy in the function f_{r_i} of (12b)], and (iii) the monomer controller requires the heat capacity function (f_C) and the related calorimetric parameters.

Comparing with the modeling requirements of the case without MW measurements (González and Alvarez, 2005), the proposed controller (13) does not need the transfer function model, and this is so because of the DD MW measurement introduced in the primary control part. On the other hand, these modeling requirements are considerably smaller than the ones of the estimator-based nonlinear controllers employed in previous polymer reactor studies (Soroush and Kravaris, 1993; Alvarez, 1996; Mutha et al., 1997; Gauthier and Kupka, 2001).

Closed-loop dynamics and tuning. The rigorous assessment of the robust closed-loop behavior goes beyond the scope of the present work, and here it suffices to state that: (i) such assessment can be performed with a suitable extension (Hernández and Alvarez, 2003) of the nonlocal input-to-state stability framework employed in the case without MW measurements (González and Alvarez, 2005), and (ii) the related tuning guidelines amount to the ones given in the last work for the CI measurements and to the ones given by Hernández and Alvarez (2003) for a discrete estimator. Next are given the tuning guidelines for the present case:

1. Choose the sampling period δ (equal to the measurement delay) to be from 1/10th to 1/20th of reactor residence time, according to the well known sampling theorem-based criterion (Stephanopoulos, 1984) employed in control designs.
2. Set the MW control gain at the inverse of the nominal residence time, $k_\pi = 1/\tau_R$ and set the estimator frequency parameter (ω) about three times faster, $\omega = 3/\tau_R$.
3. Increase the estimator parameter ω up to its ultimate value ω^+, where the response becomes oscillatory, and backoff until a satisfactory response is attained, say at $\omega \leq \omega^+/3$.
4. Increase the MW gain k_π up to its ultimate value k_π^+, and then back off until a satisfactory response is attained, say $k_\pi \leq k_\pi^+/3$.

This tuning should yield a closed-loop stable reactor where the discrete-delayed measured MW is regulated asymptotically with almost linear error dynamics and adjustable convergence rate, depending on modeling errors, measurement noise, measurements sampling period and delay, and natural reactor dynamics.

5. APPLICATION EXAMPLE

To subject the OF controller to an extreme industrial situation, let us consider (via numerical simulations) the operation of a reactor about an open-loop unstable steady-state, at high-solid fraction with the potentially destabilizing gel-effect at play. The system is methyl methacrylate (monomer)-ethyl acetate (solvent)-AIBN (initiator). The residence time is $\tau_R = 220$ minutes with a nominal volume $\bar{z}_V \approx$ 2000 L. The operating conditions are given by González and Alvarez (2005), and the reactor has three steady states $\bar{x} = [\bar{T}(K), \bar{m}(Kg), \bar{\pi}(Kg/Kmol)]'$:

$\bar{x}_1$: (373.88, 312.7, 29395.15)'

$\bar{x}_2$: (351.62, 660.1, 110384.75)'

$\bar{x}_3$: (329.72, 1361.1, 399149.03)'

The second steady-state ($\bar{x}_2$) is open-loop unstable and was chosen as the control setpoint. Following the tuning guidelines of section 4 and the ones from González and Alvarez (2005), the observer and control gains were set as follows:

$\delta = 15$ min, $\zeta = 0.71$, $\omega = (1/5)$ min^{-1}
$k_j = k_V = \omega/4$, $k_T = k_\pi = \omega/8$, $k_m = 1/\tau_R$

with a MW sampling period (δ) that is feasible according to experimental works (Mutha et al., 1997), and an observer damping factor (ζ) that was set according to a Butterworth criterion (Alvarez and López, 1999).

In Fig. 1, three closed-loop responses are shown with (i) the cascade SF controller (5), (ii) the proposed OF controller (13) with CI and DD measurements, and (iii) the proposed OF controller with CI and DD measurements and a typical - 20 % error in the frequency factor (k_{d0}) of the initiation rate.

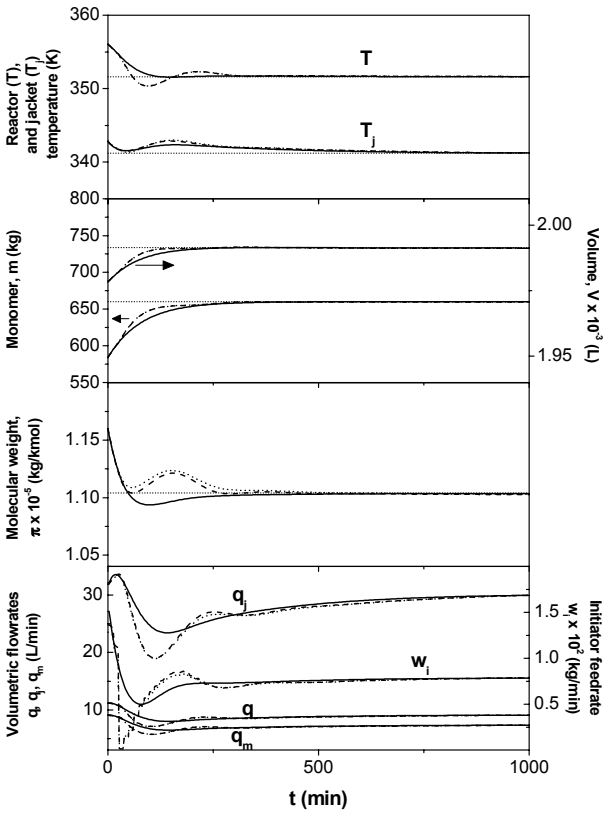

Fig. 1. Reactor behavior with the model-based cascade SF control (──), the proposed OF control with CI and DD measurements, with (· · · ·) and without (- - -) parameter error, and setpoints (····).

Figure 1 shows that the proposed OF controller with CI and DD measurements: (i) stabilizes the volume, temperature and monomer (related to the stability and the production rate level) in about 1 residence time; (ii) regulates the MW also in about 1.2 residence time, or in other words, the MW response is almost twice faster than the response of the PI-inventory without MW measurements (González and Alvarez, 2005), and 3.5 times faster than an open-loop response (with a settling time of 4 residence times); (iii) regulates the outputs with similar times that the ones of the exact model-based SF controller (5); and (iv) is not affected by presence of the parameter error, yielding a MW response without offset.

6. CONCLUSIONS

An output-feedback controller to continuous free-radical polymer reactor was presented, driven by continuous-instantaneous volume, temperature and flows measurements, and discrete-delayed molecular weight measurements. The measurement-driven controller consists of: (i) linear PI-type decentralized volume and cascade temperatures, (ii) a linear and decentralized cascade MW controller, and (ii) a material-balance monomer controller. The temperature controller requires two approximate static parameters, the monomer controller requires the heat capacity function, and both controllers are based on a continuous estimator. The MW controller is based on a discrete estimator, and requires one static parameter and initiation constants (pre-exponential factor and activation energy), which are fewer modeling requirements than the ones of the case without MW measurements. The proposed control technique has a systematic construction and simple tuning guidelines, and the solution polymerization of MMA in an open-loop unstable industrial size reactor was considered as application example with numerical simulations, yielding: (i) output responses with convergence times similar to the ones of an exact model-based state-feedback cascade control, (ii) a MW response that is almost twice faster than the response of a PI-inventory controller without MW measurements, and (iii) a MW response without offset, showing that the controller is not affected by parameter errors.

Acknowledgements. The authors gratefully acknowledge the support from the Mexican National Council for Research and Technology (CONACyT Scholarship 118632) and from CIP-COMEX graduate student award for P. González, as well as the CIP Faculty award for J. Alvarez.

REFERENCES

Alvarez J. (1996). Output-feedback control of nonlinear Plants. *AIChE J.*, 42(9), 2540.

Alvarez, J. and T. López (1999). Dynamic robust state estimation of nonlinear plants, *AIChE J.*, 45 (1), 107.

Alvarez, J., F. Zaldo and G. Oaxaca (2004). *The Integration of Process Design and Control*. Chapter: Towards a joint process and control design framework for batch processes: application to semibatch polymer reactors. Seferlis, P. and M. C. Georgiadis (Eds.), Elsevier, Amsterdam, The Netherlands.

Chiu, W. Y., G. M. Carratt and D. S. Soong (1983). A computer model for the gel effect in free-radical polymerization, *Macromolecules*, 16 (3) 348.

Flory, P. J. (1953). *Principles of Polymer Chemistry*. Cornell University Press, New York.

Gauthier, J. P. and I. Kupka (2001). *Deterministic observation theory and applications*. Cambridge University Press, UK.

González, P. and J. Alvarez (2005). Combined proportional/integral-inventory control of solution homopolymerization reactors. *Ind. Eng. Chem. Res*. 44, 7147.

Hamer, J.W., T.A. Akramov and W.H. Ray (1981). The dynamic behavior of continuous polymerization reactors - II. Nonisothermal solution homopolymerization and copolymerization in a CSTR, *Chem. Eng. Sci.*, 36(12), 1897.

Hernandez, H., and J. Alvarez (2003). Robust estimation of continuous nonlinear plants with discrete measurements. *J. Proc. Cont.* 13, 69.

Isidori, A. (1995). *Nonlinear Control Systems (3rd ed.)*. McGraw-Hill, Springer-Verlag, New York.

Luyben, W. L. (1990) *Process Modeling, Simulation and Control for Chemical Engineers (2nd ed.)*. McGraw-Hill, Singapore.

Mutha, R. K., W. R. Cluett, and A. Penlidis (1997). On-line nonlinear model-based estimation and control of a polymer reactor, *AIChE J.*, 43(11), 3042.

Sepulchre, R., M. Jankovic and P. Kokotovic (1997). *Constructive Nonlinear Control*, Springer-Verlag, NY.

Shinskey, F. G. (1988). *Process Control Systems (3rd ed.)*. McGraw-Hill, New York.

Soroush M. and C. Kravaris (1993). Multivariable nonlinear control of a continuous polymerization reactor: an experimental study. *AIChE J.*, 39(12), 1920.

Stephanoupoulos, G. (1984). *Chemical Process Control*. Prentice-Hall, Englewood Cliffs, NJ.

ADCHEM 2006

International Symposium on Advanced Control of Chemical Processes
Gramado, Brazil – April 2-5, 2006

AUTO-TUNING OF PID CONTROLLERS FOR MIMO PROCESSES BY RELAY FEEDBACK

Lucíola Campestrini [**] **Péricles Rezende Barros** [*]
Alexandre Sanfelice Bazanella [**]

[*] *Universidade Federal de Campina Grande, Campina Grande, PB, Brazil*
[**] *Universidade Federal do Rio Grande do Sul, Porto Alegre, RS, Brazil*

Abstract: In this paper, the auto-tuning of decentralized PID controllers for MIMO processes using different relay feedback experiments is studied. These methods consist in identifying the ultimate point of the process, using relay feedback and applying Ziegler-Nichols-like formulae in order to tune the controllers. A benchmark illustrates the benefits and drawbacks of each approach.

Keywords: Process control, PID control, Multivariable feedback control, Relay control, Sequential control, Decentralized control

1. INTRODUCTION

Relay feedback is widely applied as a tuning method for single-input-single-output (SISO) processes. The most usual applications are based on Ziegler-Nichols and related tuning formulae, in which the tuning is performed based on the identification of one point of the process' frequency response - the ultimate point (Astrom and Hagglund, 1995). More sophisticated tuning, providing better robustness and performance, can also be achieved by relay feedback, using different experiments which identify several points of the frequency response (Arruda, 2003), (Johansson *et al.*, 1998), (Arruda *et al.*, 2002), (Goncalves, 2001). Such methods have shown to be quite effective for many years, and many auto-tuning techniques and commercial products are based on them.

Attempts to generalize relay-feedback tuning methods to the tuning of multiple-input-multiple-output (MIMO) plants have been described recently. Two forms of generalization have been studied: Decentralized Relay Feedback (DRF) and Sequential Relay Feedback (SRF). In this paper we review the theory on these different approaches, discuss some results, present and illustrate these ideas by means of a case study.

In this paper, the processes to be considered are MIMO square processes, described by a transfer matrix

$$Y(s) = G(s)U(s) \tag{1}$$

with $Y(s), U(s) \in \Re^m$. The processes are assumed to be BIBO-stable. The aim is to design decentralized PID controllers

$$U(s) = C(s)Y(s) \tag{2}$$
$$= \begin{bmatrix} p_1(s) & 0 & 0 \dots & 0 \\ 0 & p_2(s) & 0 \dots & 0 \\ \vdots & \vdots & \ddots & \\ 0 & 0 & 0 \dots & p_m(s) \end{bmatrix} \begin{bmatrix} y_1(s) \\ y_2(s) \\ \vdots \\ y_m(s) \end{bmatrix}$$

where $p_i(s) = k_{pi} + \frac{k_{ii}}{s} + k_{di}s$.

2. SISO RELAY FEEDBACK

The PID design based on the identification of one point of the frequency response is considered.

This design approach relies on the application of simple formulae to tune the parameters of the PID. These formulae are given in terms of the process' ultimate quantities. Hence, the method consists simply in identifying somehow these characteristics and then applying the formulae. This method is usually referred to in the literature as the closed-loop Ziegler-Nichols method. Different formulae have been proposed over the years, after the pioneer work by Ziegler and Nichols. Given these variations in the method, in which the same procedure is applied but with different formulae, this tuning method will be refered as the *ultimate quantities* method in order to avoid confusion.

The ultimate quantities are the ultimate frequency ω_c and the ultimate gain K_c and, for SISO process, are defined as follows.

Definition 1. Let a BIBO-stable SISO process be controlled by purely proportional controller $u = -Ky$, with gain $K \in [0, \infty)$. Since the process is stable, the feedback system is stable for sufficiently small K. Assume that there exists a value K_c such that the closed-loop system is stable $\forall 0 \leq K < K_c$ and unstable for $K = K_c + \epsilon$, for ϵ an arbitrarily small positive scalar; this value K_c is the *ultimate gain* of the process. On the other hand, for $K = K_c$ the closed-loop system is on the verge of stability and hence a sustained oscillation will be observed; the frequency of this oscillation is called the ultimate frequency ω_c.

Fact 1. The ultimate gain K_c exists if and only if there exists a frequency ω_π, such that $\arg G(j\omega_\pi) = -\pi$. Furthermore, in this case $\omega_c = \omega_\pi$. (Astrom and Hagglund, 1995).

Different formulae have been proposed, with different ranges of application. Clearly, none of these formulae can be guaranteed to provide specified performance or even closed-loop stability. Yet, for a wide range of processes, they provide successful tuning.

Ziegler-Nichols PID formulae, which are used in this paper, are $k_p = 0.6K_c$, $k_i = k_p/T_i = k_p/(T_c/2)$ and $k_d = k_p T_d = k_p T_c/8$, where $T_c = 2\pi/\omega_c$.

2.1 The relay experiment

A convenient procedure to determine the ultimate quantities is the relay experiment. This experiment consists in putting the process under *relay feedback*. The relay function $\eta(\cdot)$ is described as

$$\eta(e) = -dsign(e) + bias \tag{3}$$

where $bias = r/G(0)$. Then, if the process satisfies the assumptions in Fact 1, a symmetric oscillation is observed, and this oscillation satisfies the statements below.

Fact 2. Let ω_{osc} be the frequency of the oscillation observed in the relay experiment and A_{osc} be its amplitude at the relay input. Then

$$\omega_\pi = \omega_{osc} \tag{4}$$

$$K_c = \frac{4d}{\pi A_{osc}} \tag{5}$$

Since the ultimate frequency is such that $G(j\omega_c) = -\pi$, $\omega_{osc} = \omega_\pi$ gives an estimate for the ultimate frequency, so that both ultimate quantities can be obtained by means of the relay experiment.

More complex phenomena can occur in relay feedback systems, such as multiple limit cycles, multimodal limit cycles, and even chaotic behavior (Arruda, 2003), (Goncalves, 2001) and (Johansson *et al.*, 1998), which complicates and sometimes invalidates the relay experiment as a means to determine the ultimate quantities of the process. Safeguards against these phenomena and/or further signal processing to extract the ultimate quantities even in their presence must be provided in PID auto-tuning with relay feedback. Still, the relay experiment has been largely and successfully applied to SISO processes (Astrom and Hagglund, 1995).

3. SEQUENTIAL RELAY FEEDBACK

In Sequential Relay Feedback (SRF), the control loops are put under relay feedback one at a time, sequentially, and m relay experiments are performed. After the relay experiment is applied to a given loop, the loop is closed with the tuned PID before applying the relay experiment to the next loop.

At each step of the SRF procedure, one PID controller is applied to an input-output pair for which a SISO relay experiment has been performed. The input-output relationship "seen" by the controller is the same one that was identified by the relay experiment. So, from the point of view of closed-loop stability, the SRF procedure is as safe as a SISO tuning.

However, each controller is tuned taking into consideration only the dynamics of the previously tuned loops. Indeed, at the $i-th$ step, all the loops indexed from $i+1$ until m are open and therefore have no influence on the system behavior. To correct this drawback, an iterative procedure can be performed: after closing all the loops the procedure is repeated for all the loops. In this

second time the loops are closed, so that all the couplings are observed in the relay experiments. Although good results are usually obtained with this iterative procedure, convergence of the tuning parameters is not guaranteed, and - most important - the total number of experiments is large; if k iterations are to be performed, km relay experiments are necessary.

4. DECENTRALIZED RELAY FEEDBACK

In Decentralized Relay Feedback (DRF) only one experiment is performed, with all control loops in relay feedback, that is $u_i = \eta(e_i)\ \forall i$. Since all the input-output pairs are connected, the behavior of the whole multivariable system is observed at this one experiment.

However, the theoretical analysis necessary to the correct application of this procedure is by necessity of a MIMO nature. The SISO reasoning and theoretical analysis do not apply in this case, and can only be usefull as intuitive guidelines. The current understanding of DRF is far from complete, so it is not clear how to make the best use of the information provided by it.

4.1 Theoretical Analysis

The relay experiment in the SISO case serves to identify the ultimate quantities of the process: the ultimate gain K_c and the ultimate frequency ω_c. Based solely on these ultimate quantities the PID tuning is determined. The definitions of ultimate quantities can be made *mutatis mutandis* for MIMO systems.

Definition 2. Let a BIBO-stable square process with m inputs be controlled by purely proportional controller $u = -Ky$, with gain $K = diag\{k_1\ k_2\ \dots\ k_m\}$, $k_i \in [0, \infty)$. Since the process is stable, the feedback system is stable for sufficiently small K. Assume that there exists a value K_c such that the closed-loop system is stable $\forall K = \alpha K_c,\ 0 < \alpha < 1$ and unstable for $K = K_c(1+\epsilon)$, with ϵ an arbitrarily small positive scalar; this value K_c is called an *ultimate gain* of the process. On the other hand, for $K = K_c$ the closed-loop system is on the verge of stability and hence a sustained oscillation will be observed; the frequency of this oscillation is called an *ultimate frequency* ω_c.

As discussed in Section 2, the ultimate quantities are usually unique in the SISO case; even when they are not unique, they are countable. The situation is quite different in the MIMO case, since the gain K can be increased from 0 in infinite

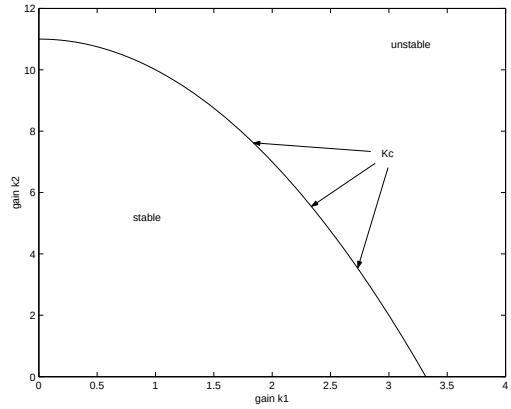

Fig. 1. MIMO case

different directions in the parameter space. It can be expected that a different K_c and ω_c will be found for each different direction, as depicted in Fig. 1 The ultimate gains form a curve in the parameter space. In the more general ($m > 2$) case these gains will form a surface of dimension $m-1$; this surface will be called the *ultimate surface.*

If PID tuning is determined based on the ultimate quantities, using Ziegler-Nichols like formulae, then two things must be realized. First, all PID's will be tuned based on the same ultimate frequency. Second, the tuning will be dependent on which of the ultimate quantities has been identified.

For simplicity, let $m = 2$. Consider that the gain K is increased in the direction $K = diag\{k_1\ 0\}$, that is, the second loop is kept open, and the proportional gain in loop 1 is increased. The ultimate gain that will be obtained in this experiment is the SISO ultimate gain k_{c1} of the first loop. Then, if the PID's are tuned according to these ultimate quantities, this tuning is the "correct" one for the first SISO loop. On the other hand, if the gain K as $K = diag\{0\ k_2\}$ is increased then the "correct" SISO tuning for the second loop is obtained. If a different direction in the parameter space is picked to increase the gain K, then it is expected to find a tuning that will not be optimal for any of the two loops, but will represent some sort of "average" of the two. The closer this direction is to either one of the two SISO directions defined above, the closer the tuning will be to the corresponding "correct" SISO tuning for that loop (Halevi *et al.*, 1997).

Let r_i be the relative importance given by the designer to the $i-th$ loop, so that $\sum_{i=1}^{m} r_i = 1$. Then the desired ultimate point is the one that is in the direction of the vector $K_d = diag\{g_{11}(0)r_1\ g_{22}(0)r_2\ \dots g_{mm}(0)r_m\}$, where g_{ii}'s are the diagonal terms of $G(s)$.

Once the ultimate quantities are identified, a gain sufficiently smaller than the ultimate one should guarantee stability and enough stability margins.

This is the reasoning in the SISO case, and also the reasoning justifying ZN-like formulae. However, this is not necessarily true in the MIMO case. If the ultimate curve in the parameter space is convex, then adequate stability margins are guaranteed by taking a gain $K = \alpha K_c$ for sufficiently small α. However, it is not possible to guarantee that the ultimate surface is convex, or even smooth. As a matter of fact, there are cases in which the ultimate surface is not convex, like in the benchmark studied in the sequel.

5. CASE STUDY - DISTILLATION COLUMN

Aiming to demonstrate the use of SRF and DRF methods, this section presents some results obtained for the control of the Wood and Berry distillation column, whose transfer matrix is presented in (6). This process has been widely used as a benchmark (Loh and Vasnani, 1994) and (Wang *et al.*, 1997). It is hard to control since it has significant transport delay and strong coupling.

$$G(s) = \begin{bmatrix} \dfrac{12.8e^{-s}}{16.7s+1} & \dfrac{-18.9e^{-3s}}{21s+1} \\ \dfrac{6.6e^{-7s}}{10.9s+1} & \dfrac{-19.4e^{-3s}}{14.4s+1} \end{bmatrix} \qquad (6)$$

5.1 Real × Estimated Ultimate Surface

The ultimate surface of a process can be obtained from the very definition of ultimate quantities, that is, by applying increasing gains to the inputs of the plant until a sustained oscillation is obtained. When a sustained oscillation is presented, the "gains" applied in the plant are one ultimate point of the surface. The ultimate gains are then determined within a certain precision, which is given by the size of the steps used to increase the gains. So, although this curve is still an approximation to the actual ultimate surface, we will refer to it as the "real ultimate surface"; the estimate obtained by DRF will be referred to as the "estimated ultimate surface".

Fig. 2 shows two ultimate surfaces of the Wood and Berry distillation column: the estimated one, obtained by Decentralized Relay Feedback (doted curve), and the real one (solid curve). It is clear from the figure that the DRF experiment does not always provide good estimates of the ultimate quantities.

As described in section 4.1, the closer the direction of the ultimate point is to either one of the two directions in the parameter space (k_1 or k_2), the closer the tuning will be to the corresponding "correct" SISO tuning for that loop. So, it is expected to find a point in the ultimate surface

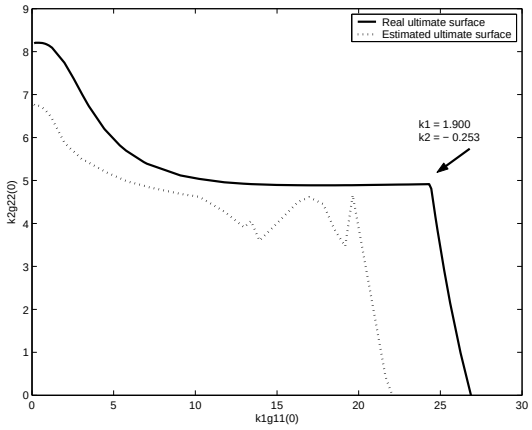

Fig. 2. Real and estimated ultimate surfaces of the Wood and Berry distillation column.

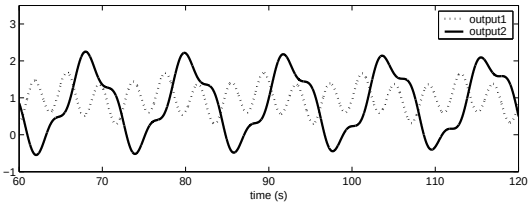

Fig. 3. Plant's outputs when a proportional controller $K = diag\{1.9 \ -0.2533\}$ is applied.

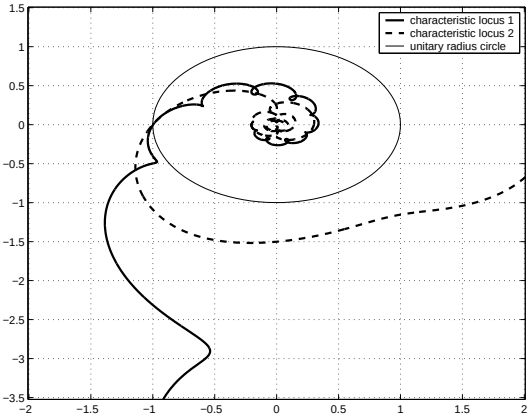

Fig. 4. Characteristic loci of the distillation column with a proportional controller $K = diag\{1.9 \ -0.2533\}$.

where information about both loops can be found. Hence, with this ultimate point, it is expected a better tunning of the PID controllers.

In fact, there is a point at the distillation column's ultimate surface for which the system presents multimodal oscillations, as presented in Fig. 3. This ultimate point is given by $k_1 = 1.9$ and $k_2 = -0.2533$. When this ultimate gain is applied on the plant, both characteristic loci cross the point -1, as shown in Fig. 4.

Fig. 5 shows the response of the system controlled by PIs obtained with ultimate values $k_1 = 1.9$, $k_2 = -0.2533$ and $t = 12$ from the real ultimate surface and Ziegler-Nichols like formulae. It can be

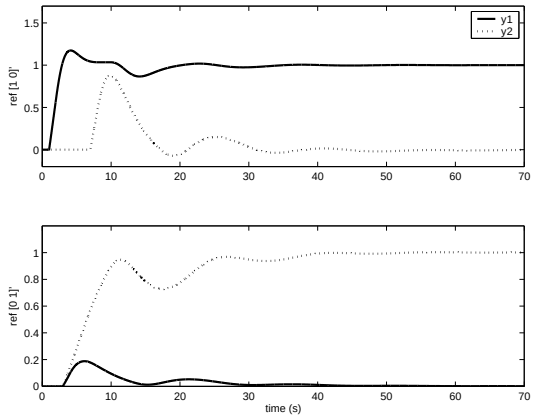

Fig. 5. Response of the system controlled by PI - Ziegler-Nichols like formulae - obtained with ultimate point $k_1 = 1.9$ and $k_2 = -0.2533$.

Table 1. Ultimate values and PID controller's gains obtained from SRF (1^{st} iteration: detuning and 2^{nd} iteration: Ziegler-Nichols).

	1^{st} iter.		2^{nd} iter.	
	loop 1	loop 2	loop 1	loop 2
K_c	1.72	-0.27	1.59	-0.19
T_c	3.90	12.37	3.80	12.27
k_p	0.342	-0.163	0.955	-0.112
k_i	0.058	-0.026	0.503	-0.018
k_d	0.500	-0.252	0.454	-0.172

seen that, choosing the "right point", the relative controller provides a good performance to the system. Unfortunatelly, this point cannot be reached with relay experiment, because it presents multimodal oscillations and the ultimate quantities cannot be taken from it. Indeed, there is a region around this point in which the relay experiment does not work, as can be seeing in the estimated ultimate surface from Fig. 2.

5.2 PID Tuning

5.2.1. Sequential Relay Feedback A sequential relay feedback was performed in the distillation column. The results are shown in Table 1 and Figs. 6 and 7. Table 1 presents the ultimate quantities obtained for each loop and the related gains of the PID controllers. Besides, these values were obtained twice, for first and second iterations.

The results are satisfactory, suggesting that this method can be used in order to find the ultimate quantities for further PID tuning. The system presents a considerable overshoot for reference $r = [1\ 0]'$ because Ziegler-Nichols like formulae are used. On the other hand, the disturbance rejection is strongly enhanced from first to second iteration in the second loop.

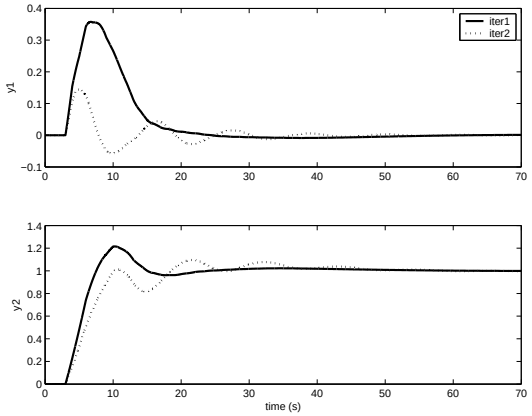

Fig. 6. Response of the system controlled by PID obtained from SRF and $r = [0\ 1]'$.

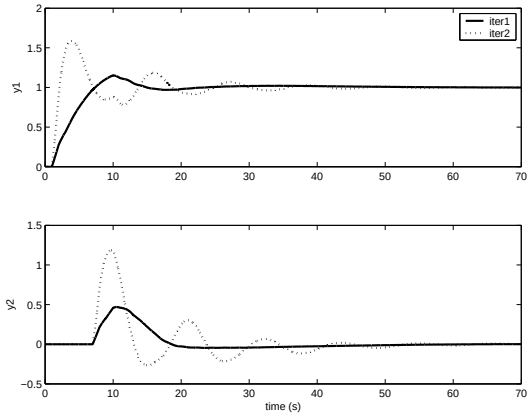

Fig. 7. Response of the system controlled by PID obtained from SRF and $r = [1\ 0]'$.

5.2.2. Decentralized Relay Feedback In order to identify the ultimate surface, several decentralized relay feedback experiments were performed in the system, in which different relay amplitude ratios d_2/d_1 were set. Hence, different ratios d_2/d_1 correspond to different weights $k_2 g_{22}(0)/k_1 g_{11}(0)$.

As can be seen in Fig. 2, the estimated surface with DRF is non-smooth for a wide range of gains. Within this range, the system presents multimodal limit cycles. So, it is only safe to tune PID controllers based on information taken from unimodal oscillations. Table 2 and Figs. 8 and 9 show the results obtained for different weights.

Fig. 8 shows the response of the system controlled by PID obtained from DRF and reference $r = [0\ 1]'$. It shows that, the higher the weight $k_2 g_{22}(0)/k_1 g_{11}(0)$, the larger is the overshoot of the system. However, for a reference equal to $r = [0\ 1]'$, the higher the weight $k_2 g_{22}(0)/k_1 g_{11}(0)$, the smaller is the overshoot of the system, as shown in Fig. 9. Thus, the hard task is to find a weight that will yield an ultimate point that provides good performance of both loops.

Table 2. Ultimate values and PID controller's gains obtained from DRF for different weights ($k_2 g_{22}(0)/k_1 g_{11}(0)$).

$k_2 g_{22}(0)/k_1 g_{11}(0)$		loop 1	loop 2
10.44	K_c	0.050	-0.345
	T_c	11.2	11.2
	k_p	0.029	-0.203
	k_i	0.005	-0.036
	k_d	0.041	-0.285
2.96	K_c	0.155	-0.303
	T_c	12.4	12.4
	k_p	0.091	-0.178
	k_i	0.015	-0.029
	k_d	0.142	-0.276
0.52	K_c	0.707	-0.241
	T_c	12.7	12.7
	k_p	0.416	-0.142
	k_i	0.065	-0.022
	k_d	0.660	-0.226

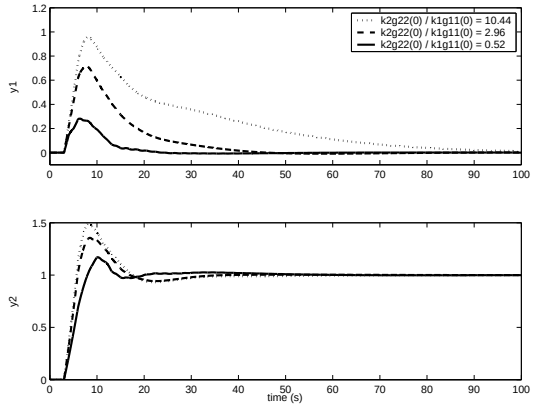

Fig. 8. Response of the process controlled by PID obtained from DRF, reference $r = [0\ 1]'$ and different weights.

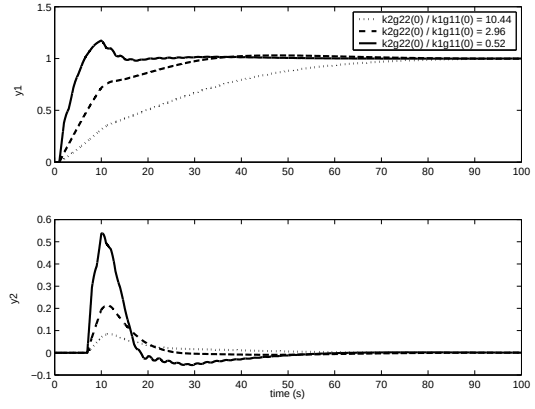

Fig. 9. Response of the process controlled by PID obtained from DRF, reference $r = [1\ 0]'$ and different weights.

6. CONCLUDING REMARKS

In this paper, two forms of generalization of relay feedback tuning to multivariable processes are studied: Sequential and Decentralized Relay Feedback. These "multivariable" methods extend the SISO relay feedback to MIMO processes and uses given formulae in order to tune the PID controllers.

The decentralized relay experiment seems to be the best way to obtain the ultimate quantities of the process, since it observes the behavior of the whole multivariable system and requires only one experiment. However, it can present multimodal oscillations, in which case the oscillations are not representative of the ultimate quantities. Hence, it is still a risky approach to tuning. Even if it is expected that this oscillation presents more information about the process, it is still not known how to get them from the experiment. Indeed, the point $k_1 = 1.9$, $k_2 = -0.2533$ of the real ultimate surface, seems to be the point that intersects both loops surface, and more characteristics of the process are expected to be obtained in this point.

On the other hand, the Sequential Relay Feedback requires more time to get the "right" controller parameters. However, as only one relay is applied at a time, it is a safer experiment because multimodal oscillations are not troublesome.

REFERENCES

Arruda, G. H. M., Barros P. R. (2003). Relay-based closed loop transfer function frequency points estimation. *Automatica* **39**(2), 309–315.

Arruda, G. H. M., P. R. Barros and A. S. Bazanella (2002). Dynamics of a relay based frequency response estimator. In: *Proc. 15th Triennial World Congress*. Barcelona, Spain.

Astrom, K.J. and T. Hagglund (1995). *PID Controllers: Theory, Design and Tuning*. Instrument Society of America. Research Triangle Park, N.C.

Goncalves, J.M., Megretski A. Dahleh M.A. (2001). Global stability of relay feedback systems. *IEEE Transactions on Automatic Control* **46**(4), 550–562.

Halevi, Y., Zalman J. Palmor and T. Efrati (1997). Automatic tuning of decentralized PID controllers for MIMO processes. *Journal of Process Control* **7**(2), 119–128.

Johansson, Karl Henrik, B. James, G. F. Bryant and Karl Johan Åström (1998). Multivariable controller tuning. In: *Proc. 17th American Control Conference*. Philadelphia, Pennsylvania.

Loh, A. P. and V. U. Vasnani (1994). Describing function matrix for multivariable systems and its use in multiloop PI design. *Journal of Process Control* **4**(3), 115–120.

Wang, Qing-Guo, Biao Zou, Tong-Heng Lee and Qiang Bi (1997). Auto-tuning of multivariable PID controllers from decentralized relay feedback. *Automatica* **33**(3), 319–330.

ADCHEM 2006

International Symposium on Advanced Control of Chemical Processes
Gramado, Brazil – April 2-5, 2006

REGULATORY CONTROL OF A PILOT ROTARY KILN FOR ACTIVATED CARBON PRODUCTION

Nelson Aros[a], Graciela I. Suarez[b], Oscar A. Ortiz[b*]

[a] Universidad de La Frontera, Avenida Francisco Salazar 01145, Temuco – Chile
[b] Universidad Nacional de San Juan, Libertador San Martín 1109 Oeste, San Juan Argentina [*] E-mail: rortiz@unsj.edu.ar

Abstract: The design of a regulatory control strategy for a pilot rotary kiln to produce activated carbon is presented. A complex dynamic behavior with high non-linearity and an important dead time characterizes the rotary kiln operation. The main control objective of the process is to maintain the solid temperature profile inside of a narrow limit in order to produce an activated carbon with acceptable adsorbent properties. The manipulated variables are the temperature and the mass flow rate of the heating gas. The control scheme proposed consists of a conventional PID controller with Smith predictor in order to compensate the time delay. The control scheme is tested by means of simulation with a dynamic model previously developed in Matlab. The results are satisfactory and constitute a reference point to develop other advanced control strategies.

Keywords: Chemical Industry; Process control; Time delay; Conventional control

1. INTRODUCTION

The rotary kiln is the main process equipment in the activated carbon production by means of physical activation of charcoal with water vapor. In the last time, a complete study about the operation of a pilot rotary kiln for such process has been performed in our laboratory (Ortiz et al., 2003a, b; Ortiz et al., 2005). The activation process in the rotary kiln is inherently difficult to operate efficiently because of complex dynamics and multi-variable process with non-linear reaction kinetics, and long time delays. During its operation many interconnected variables must be considered and control actions must be designed to meet multiple and sometimes conflicting objectives, and changing operating conditions. Some measurements are unreliable, and the kiln characteristics may change during a long run. The operation may also be upset by disturbances such as changes in the mass flow rate and properties of the charcoal fed. In this context, the solid temperature inside the kiln must be maintained within predefined constraints in order to assure an acceptable product quality from its adsorbent properties point of view.
The control of rotary kilns, particularly in the field of the calcination and incineration processes, has been studied since the early 70`s and, very different schemes have been proposed. Such schemes varies since conventional controller based on phenomenological and empirical models to diverse approximations using artificial intelligence tools such as rule based expert systems, fuzzy logic and neural networks. Also, some applications based on model predictive control have been reported.

Despite the advent of many complicated control theories and techniques, more than 95% of the control loops based on proportional-Integral-Derivative (PID) controllers are still being used in the industrial processes. This is because PID controllers have a well and robust performance for a wide class of processes and for a wide range of operating conditions. Furthermore, engineers have expertise in PID tuning running in stand alone, in PLC or in SCADA systems (Astrom, 1995; Kaya, 2003). Other important advantage of PID controllers is its good performance in different configurations such as cascade PID control scheme, feedforward PID, Predictive Smith loops and antiwindup feedback loops (Kaya, 1998). In addition, the most controllers used really in the industry are of PID family type.

This work presents the design of a regulatory control for the operation of a pilot rotary kiln used in the charcoal activation process. The main control objective is to maintain the solid temperature profile inside of pre-specified constrains manipulating the temperature and mass flow rate of the heating gas. Due to the PID controllers have a variety of advantages; such as easiness to tuning, extensive use and familiarity in the industry, they have been adopted as a first approach to develop an adequate control scheme for the process. For the process identification, the Strejc method have been used and, taking account that the process presents a considerable time delay (Ortiz et al., 2005), the Smith predictor has been considered. For this proposes, a SISO controller is proposed. The design procedure must be made taking into account all the constraints imposed for the whole temperature profile. The performance of the control scheme proposed has been tested by means of simulation with the Matlab/Simulink tool.

2. PROCESS DYNAMIC MODEL

A pilot rotary kiln is a cylinder that rotates around its longitudinal axis and operates essentially as a heat exchanger. The cylinder is lightly inclined (i.e., slope about 2–6%) to facilitate the axial displacement of the solid bed, which moves towards the discharge end as the hot gases circulate countercurrent mode. The solid feed is a carbonized matter obtained from a variety of raw materials (e.g., eucalyptus wood). The hot gases originated by the combustion of natural gas arise from a central burner; supply the necessary energy for the activation reaction. Water vapor is injected as the activation agent in cocurrent mode.

The dynamic mathematical model developed includes the heat and mass balance equations for the three phases within the rotary kiln: freeboard gas, solid bed and wall. In order to model the transfer phenomena for the three phases the differential mass and energy balances, which include the chemical reaction is posed in cylindrical coordinates. Because of the main operating variables such as temperature and mass flow rate change along the axial axis, a distributed parameter system (DPS) is obtained. Therefore, the dynamic model is constituted by a set of algebraic and partial differential equations with boundary conditions. More details about the rotary kiln scheme with input and output streams, the model and its solution may be found in Ortiz et al., (2005). In that work a complete dynamic study is presented for three different operation modes; start up, shut down and normal operation with disturbances. Finally, is important to point out that the solid temperature profile inside the kiln must be maintained within narrow bounds in order to produce a high quality product.

2.1 Process identification

The required model type and its precision, as well as the identification method to use depend on which objective it is needed to complete.

In this case, the process dynamic is knows by means of simulation, hence, an identification method that takes into account the system characteristics has been selected (Strejc, 1960). The used method is that of graphic identification of non-periodic systems of high order (Aguado, 2000), which is based on the graphic construction of a reaction curve of a high order system. In this one, a non-periodic system with n different time constants may be approximate adequately by means of a transfer function that represents n identical time constant, as the following:

$$G(s) = \frac{K}{(T_1 s + 1)(T_2 s + 1)\ldots(T_n s + 1)} \cong \frac{K}{(\tau \cdot s + 1)^n} \qquad (1)$$

where K represents the gain in steady state. Generally, the industrial processes are non-linear, though is possible approximate it through linear mathematical models plus a time delay (Ogata, 1998). For these one, it is possible to develop one or more control methods, where the determined performance specifications for the system suggest the class of method to use and, in addition the type of wanted system response.

3. PROPOSED CONTROL SCHEME

3.1 Controller design for systems with time delay

Among the main troubles in classical controllers as PID, it can be mentioned its bad performance in plants with a considerable time delay. In these cases, it is necessary to consider a Smith predictor in order to compensate the time delay. Basically, the main idea is based on to previous knowledge of time delay in order to compensate its effect. In other words, it is based on the prediction of the future process behaviour (Smith, 1959). Based on such idea the proposed control scheme for the studied rotary kiln is shown in figure 1, where the regulation is obtained adjusting the process loop without delay.

4. SYSTEM IMPLEMENTATION

4.1 Plant model

From the system reaction curve an incremental linear model has been determined, see figure 2. Thus, from the reaction curve for the output temperature that corresponds to a change of 10 % in the input temperature in open loop and in accordance with the identification method (Strejc, 1960), the following model is obtained (the time constants are in [min]):

$$G_p(s) = \frac{0{,}6038}{(5{,}53 \cdot s + 1)^4} \qquad (2)$$

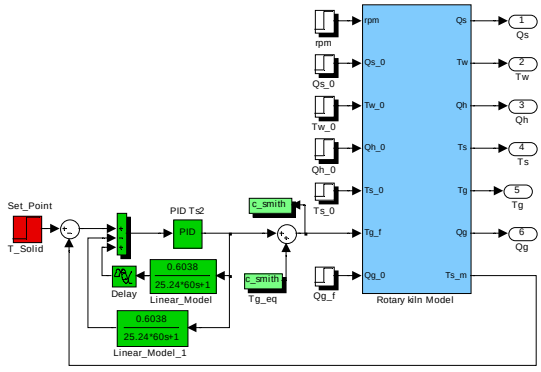

Fig. 1. Smith configuration for the rotary kiln control

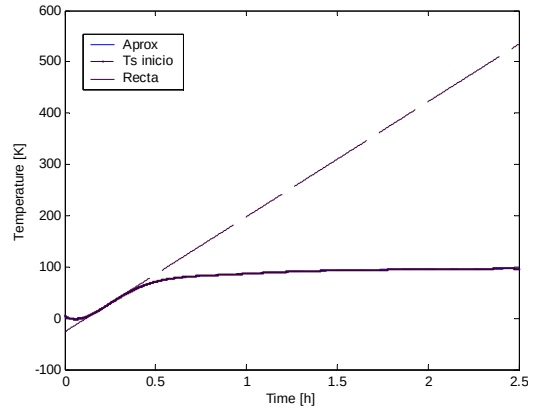

Fig. 2. Plant reaction and approximation curves (overlapped) and the straight line that cross the inflexion point

4.2 Controller tuning

For the tuning of the solid temperature controller an open loop is utilized. In this sense, a first order model with delay of the process is required. Using an approximation from the model in Eq. (2), the following model is derived:

$$G_p(s) = \frac{0{,}6038}{25{,}83 \cdot s + 1} \cdot e^{-7{,}24 \cdot s} \tag{3}$$

The controller parameters are obtained from the Cohen Coon tuning, corresponding to: $K_c = 8.29$, $t_r = 16$ [min] and $t_d = 2.51$ [min].

As the time delay is big in comparison with the time constant, the feedback control with Smith predictor is used (Kaya, 1998). The model in Eq. (2) is utilized for tuning the PID controller parameters.

5. PERFORMANCE OF THE CONTROL SYSTEM

In order to test the proposed control strategy the dynamic simulator implemented by Ortiz et al., (2005) has been used as actual plant. First, the performance of the feedback control to change in the set point and in presence of disturbances is presented. Second, the performance of the feedback control with Smith predictor to similar changes is analyzed and compared with the first scheme.

5.1 Performance of feedback control system to change in the set point

In this section, the behaviour of the feedback system tuning a PID controller is analyzed. Firstly, the regulatory system is tested in the face of a set point change. Therefore, the desired solid temperature is changed as a step signal equal to 1100 ± 55 [K] (± 5% of steady state operation value) in a time of 16.67 [min]. Three points to register the temperature inside the kiln are considered, which correspond to three zones within the kiln: inlet zone ($z = 0.05L$), middle zone ($z = 0.5L$) and outlet zone ($z = 0.95L$). L represents the axial length of the kiln.

Figure 3a depicts the wall temperature behaviour, where it is appreciated that the maximum time to reach the steady state is approximately 2.5 [h] and, shows an overshoot of 25 %. On the other hand, the wall temperature in the inlet zone presents a delay of 0.2 [h], 20 % of overshoot and it require 2 [h] to reach the steady state. The responses to changes in the reference signal, increment or decrement, are symmetric.

Figure 3b shows the behaviour of solid temperature. Particularly, the curve denominated as “z input” corresponds to the temperature controlled by the system. It is appreciated that the new steady state is reached after to 2.5 [hs]. Also, a delay and an overshoot of 20 % can be appreciated. However, at the outlet zone “z output curve”, the solid temperature presents a great overshoot of 25 % approximately. It must emphasize that exists a small asymmetry due to the non-linearity of the process.
Figure 3c shows the gas temperature behaviour, which presents the same tendency that the wall and solid temperature. The gas temperature at the outlet zone, “z output curve”, indirectly represents the system control action.

The solid mass flow rate, non-controlled process variable, presents an increment of 39 % respect of the nominal value at the outlet zone. In consequence, a decrement in the temperature reference value produces an apparent increment in the production yield. Such circumstance cause a diminution in the “burn off “ and hence a loss in the product quality. An increment in the temperature reference value causes the opposite effect. The necessary time to reach the new steady state is around 2.2 [h] (fig. 4a). As it was expected, see fig. 4b, the gas flow rate which is a controlled process variable not shows any variation at the outlet zone, “z output curve”, to a step change in the solid temperature reference value. Such behaviour shows clearly the efficiency of the gas flow rate controller.

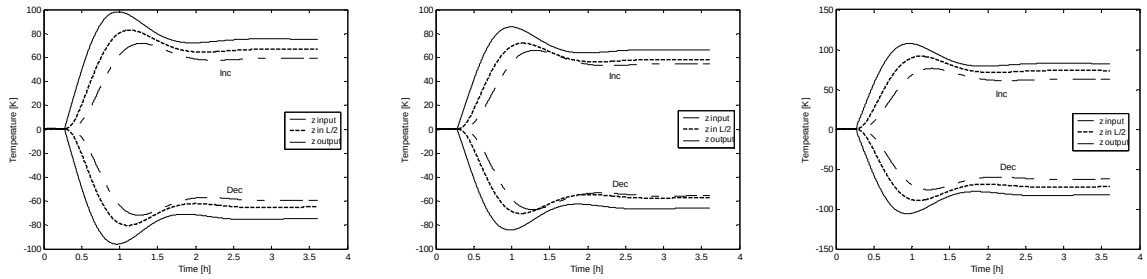

Fig. 3. Temperatures behaviour (a) wall, (b) solid y (c) gas.

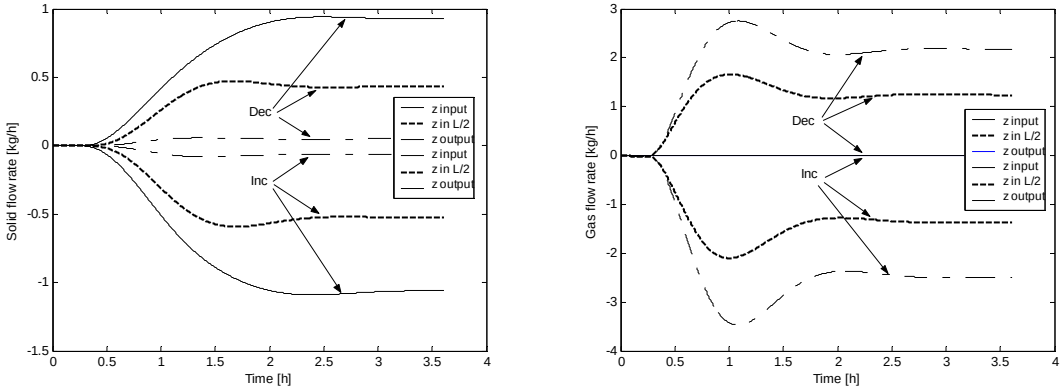

Fig. 4. Flow rate behaviour (a) solid y (b) gas.

5.2 Performance of feedback control system in presence of disturbances

Change in the rotary kiln speed. Figures 5, and 6 show the operation variables response to a step change in rotary kiln speed of 2.0±0.5 [rpm]. An asymmetry in the curves of fig. 5 after an increment or decrement in the rotation speed can be observed. Particularly the solid temperature response, which is a controlled variable, presents an inverse performance. However, a tendency to reach its nominal value can be appreciated. Such behaviour may be explained by the sudden change in the rotary speed, which causes a sliding effect between the solid bed and the rotary kiln wall and, in consequence a decrease in the heat transfer by conduction between the solid and the wall. In addition, the before mentioned change mainly alter the regenerative effect that occur between the solid bed and the wall.

In fig. 6a, an appreciable difference in the variables behaviour may be observed when the rotary speed it is increased o decreased. Therefore, after a diminution in the rotary speed, a greatest control effort must be done. Such difference may be attributed to high non-linearity of the system. The same effect in the behaviour of gas mass flow rate in fig. 6b is appreciated.

Change in the solid fed. Figure 7 shows the response of the operation variables to a step change (±10%) in the reference point of the mass flow rate of solid fed. As can be seen from fig. 7b the controlled variable, solid temperature, presents a maximum variation of 5 [K] (0.5 % on set point). Also, the high non-linearity of the system may be appreciated.

5.3 Performance of feedback control system with Smith predictor

In this section, the performance of the Smith predictor system tuning a PID controller is analyzed. Also, as in paragraph 5.1, the system is tested to a change in the set point.
In fig. 8a, the wall temperature shows a settling time of 1 [h] approximately with an overshoot smaller than that the obtained in paragraph 5.1. The controlled solid temperature, “z input”, reaches the desired value faster that without Smith predictor and, the asymmetry for the increment and decrement is also less important (fig. 8b). On the other hand, the curve “z output” in fig. 8c, which indirectly represents the control action, shows that to achieve an improvement in the controlled system a smaller energy is required.

The asymmetry shown by the curves of mass flows rate (not showed due space reason) represent the high non-linearity of the system. In addition, an increment in the product mass flow rate may be appreciated when the set point temperature is diminished. This behaviour corresponds to an apparent growth in the production yield, because it occurs at the expense of the product quality.

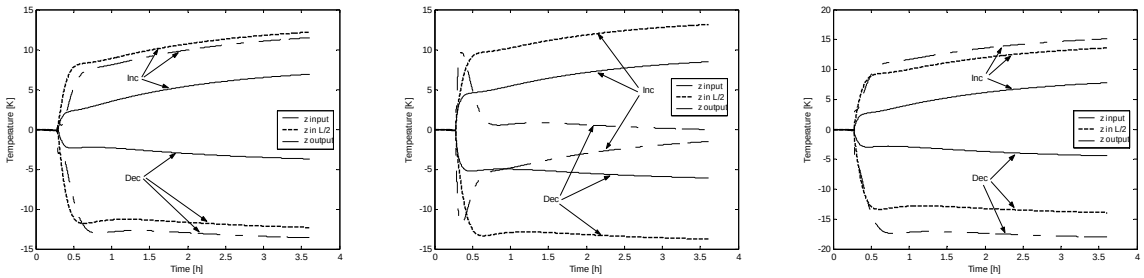

Fig. 5. Temperatures behaviour (a) wall, (b) solid bed (c) gas.

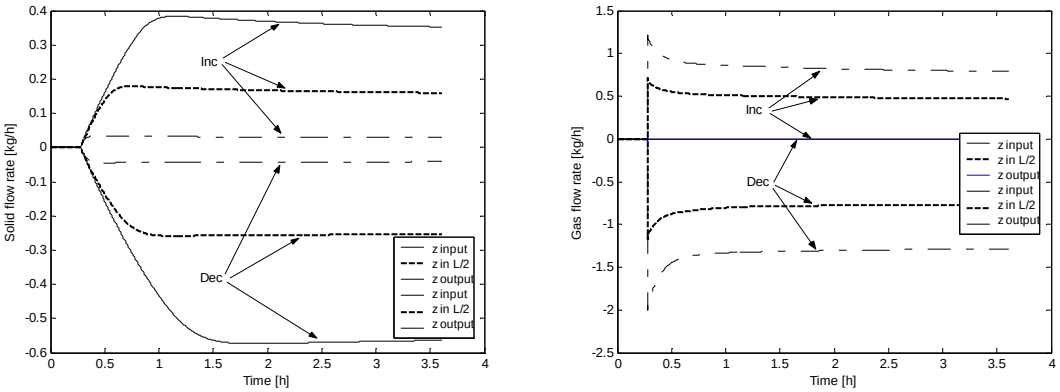

Fig. 6. Mass flows rate performance (a) solid (b) gas.

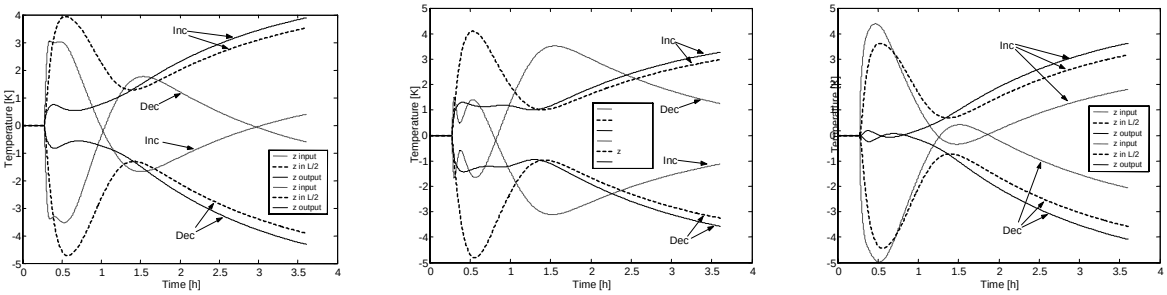

Fig. 7 Temperatures response to a step change in the solid mass flow rate fed (a) wall, (b) solid, (c) gas.

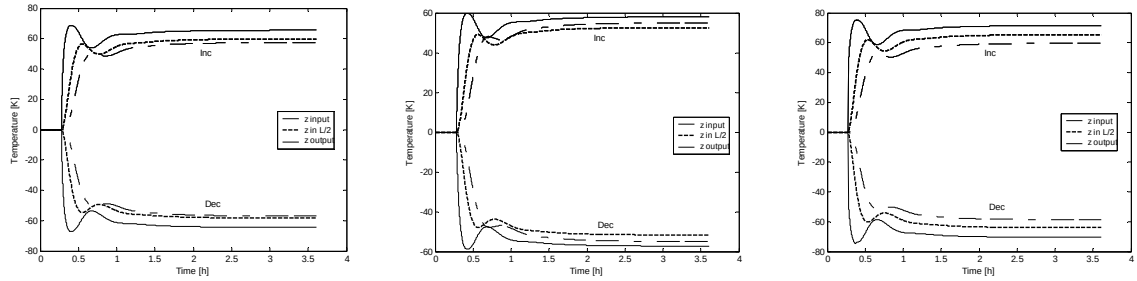

Fig. 8 Temperatures behaviour (a) wall, (b) solid (c) gas.

5.4 Performance of the control system with Smith Predictor in presence of disturbances

Change in the rotary kiln speed. Figure 9 shows the response of the control system to variations in rotary kiln speed, which is considered as one of the more frequent disturbance during the steady state operation.

Figure 9a shows that the controlled variable, corresponding to the "z input" curve, attain the new set point equivalent to the step change when the steady state is reached. Such behaviour is observed for an increment or a decrement in rotary kiln speed. As can be observed the system with the Smith predictor have a more faster response that with the traditional PID. In addition, fig. 9b shows that the settling time is lower, 43.4 [min] approximately. Also, the non-linear characteristic of the system may be appreciated in the curve corresponding to solid mass flow rate vs. time (not showed), where the response to an increase and decrease do not show symmetry around the set point. For a change in the solid mass flow rate fed, the control system exhibits a notable improvement in its performance regarding the conventional PID.

6. CONCLUSIONS

The control of the solid temperature profile inside of a pilot rotary kiln for activated carbon production has been studied and a control scheme constituted by a conventional PID controller with Smith predictor was satisfactory tested. Taking into account that the studied system have special constraints such as: high non-linearity, variation of its main operation variables along the axial direction (distributed parameters system) and, an inherent time delay; we can assert that the control strategy proposed has been satisfactory. On the other hand, due to the conventional PID controller may be easily tuned, the same has been considered as a reference point for any other control strategy that it can be proposed.

The use of a control scheme such as a PID controller with a Smith predictor has allowed us to obtain a better system response, because that configuration permit to compensate the time delay in the process and, at the same time increase the speed of the closed-loop retaining its robustness. In addition, its performance in the presence of disturbances in rotary kiln speed and solid mass flow rate fed is excellent, because shows a stabilizing effect on the closed-loop response of the process. It can be affirm that the overshoots, settling times and frequency of oscillation are within acceptable limits.

The proposed control scheme constitutes the first approach to control the operation of the pilot rotary kiln in the activation process. Although the first results are promissory, an extensive work must be carried out. Though the dynamic model has been tested with experimental data is necessary to implement the control system in the actual plant in order to check its performance. Not always the phenomenological or empirical model have been adequate for control purpose (Barreto, 1997). In addition, different advanced control alternatives must be explored, especially those based on artificial intelligence tools such as rule-based expert systems, neural networks and fuzzy logic; which had have very acceptable performance in rotary kilns for calcinations and incineration processes. Finally, the model predictive control approach, widely used in other fields of the industry, also must be considered.

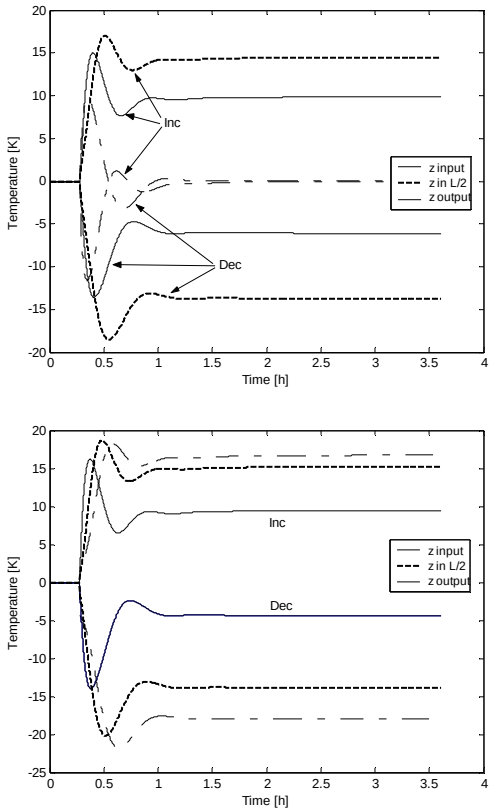

Fig. 9 Temperatures response to step change in rotary kiln speed (a) solid, (b) gas.

REFERENCES

Aguado A, (2000). Temas de identificación y Control Adaptable. La Habana, Cuba.

Astrom K. J. y Hagglund T., (1995). PID Controllers: Theory, Desing and Tuning, 2nd Edition, ISA Research Park, NC.

Barreto, A.G. (1997) Lime kiln hybrid control system. Proceeding of the IEEE workshop on dynamic modelling control applications for industry. New York, USA, 44-50

Kaya A.y Scheib T. I., (1998). Tuning of PID control of different structures. Control Engineering, pp. 60

Kaya, Ibahim (2003). Obtaining controller parameters for a new PI-PD Smith predictor using autotuning. Journal of Process Control 13 465-47

Ogata K, (1998) Ingeniería de Control Moderna Prentice-Hall Hispanoamericana, Naucalpan de Juárez, México

Ortiz, O. A., N. D. Martínez, C. A. Mengual and L.M. Petkovic (2003 b). Performance Analysis of Pilot Rotary Kiln for Activated Carbon Manufacture Using a Steady State Mathematical Model. Latin American Applied Research, 33: No. 3, 295-300

Ortiz, O. A., S. E. Noriega, C. A. Mengual and N. D. Martínez (2003 a). Steady State Simulation of a Rotary Kiln for Charcoal Activation. Latin American Applied Research, 33: 51-57

Ortiz, O.A., G.I. Suarez and N. Aros (2005). Dynamic simulation of a rotary kiln for charcoal activation. Computer and Chemical Engineering 29 1837-1848

Smith, O. J. (1959). A controller to overcome dead time. ISA Journal, 6 (2), 28–33.

Strejc R. (1960) Aproximate determination of the control characteristics of an aperiodic response process. Automatisme.

ADCHEM 2006

International Symposium on Advanced Control of Chemical Processes
Gramado, Brazil – April 2-5, 2006

DEVELOPMENT OF AN EXTRUDER BASED MELT INDEX SOFT SENSOR

Ian R. Alleyne[1], Sirish L. Shah[1], Uttandaraman Sundararaj[1], Brent West[2]

[1]Department of Chemical and Materials Engineering,
University of Alberta
[2]AT Plastics Inc., Edmonton, Alberta

Abstract: The control of polymer quality has become increasingly important as the production of polymer grades has increased in quantity and diversity. On a typical polymerization plant there is an extruder downstream of the reactor. This paper provides details on the use of the operating variables of such an extruder as an empirical sensor for the melt flow index, an important indicator of polymer quality. An empirical model was built in several stages. First a simple model was built which related the melt index with the extruder pressure. After many iterations a model which also included extruder speed and temperature compensation and a bias updating procedure was developed. The final bias updated model has been installed at the plant and detects a change in the melt index nine (9) minutes before the online instrument. The end goal is to use this soft sensor to build a data based plant model, and subsequently use this model to compute optimal grade transition trajectories in the plant. *Copyright © 2005 IFAC*

Keywords: Polymer Reactor control, Soft sensing, Trajectories, Polymerization, Predictive control, Optimal Trajectory, System Identification.

1. INTORDUCTION

The increased reliance on polymers with specifically tailored properties for different applications has been documented extensively (Alperowicz 2005). Previously the specifications for polymer grades and products were very relaxed. However, with the advent of much larger capacity plants; many smaller plants are moving from commodity to speciality polymers which have higher profit margins. These products however have tighter specifications. Thus variability which was acceptable before is no longer tolerable. This implies online properties of polymers need to be controlled more tightly. The more diverse, lower volume product requirements by speciality customers forces the product specification required from the plant to change regularly. Therefore reliable online polymer quality measurements are very critical.

This research was undertaken in collaboration between industry and academia. The plant in this study was the AT Plastics EVA high pressure polymerization plant in Edmonton, Canada. The main polymer quality variable on the plant was the melt index. This plant ran approximately twenty grades of polymer regularly in the 1 – 1000 gm/min. melt index range. The online reading for this melt index was determined by an online rheometer. This instrument gave an update every six (6) minutes and was subject to transport lags. These two problems were not significant as there are system identification algorithms which can compensate for these issues. However, a more significant issue, because of the large range of melt index measurement required, was that the rheometer used several models and die sizes. Each die has a manufacturer's recommended pressure range for which the readings are very close to linear. However, once the instrument gets close to one of the limits, i.e. the polymer is too hard or soft for the particular die and measurement temperature, the readings become unreliable. This is acceptable if the plant is running a grade campaign which does not have a significant change in melt index. Therefore, the goal of modelling the grade transitions was severely hampered because the rheometer data during the grade transitions were plagued with issues such as the unit having to be switched off or becoming unreliable, as it needed die changes or gave inaccurate results because it was at the end of its linear range. It was clear that some new variable was required to give online polymer melt index values.

The measurement of polymer quality through the use of indirect variables (soft sensors) has been the subject of much research. Ohshima and Tanigaki 2000 gave a comprehensive review of property estimation methods published for different polymerization processes. The typical design of these

soft sensors involves building relationships between the process control variables, such as the reactor, pressure and temperature and the polymer property to be controlled. The method of building this relationship typically involves methods such as linear observers (Lines et al. 1993), extended Kalman Filters (Scali et al. 1997), nonlinear parameter estimation (Kiparissides et al. 1996), neural networks (Chan and Nascimento 1994) and partial least squares (Han et al. 2005). Here a different approach is taken; after the reactor there is an extruder, in which many variables are monitored. The identification of the relationship between these and the polymer properties is the main subject of this paper.

Watari et al. 2004 and Nagata et al. 2000 independently used measurements from an extruder estimating the properties of molten polyethylene. However, their methods required the installation of a fibre optic sensor at the end of the extruder to obtain NIR (near infra-red) readings. The method proposed here uses the raw data which is commonly measured and monitored on extruders to give an indication of the melt index of the polymer produced on the reactor.

1.1 Outline

The plant at which this project was undertaken is described next followed by a description of the procedure for development of the melt index soft sensor. This includes the method for selection and lag times of the extruder variables. More details on the modelling of the errors and the significant disturbances that were the cause of these errors are then given. Methods for reducing these errors are also detailed.

1.2 Process Description

The plant considered is an EVA polymerization plant. The plant has the ability to manufacture polymers over a wide range of melt indices and vinyl acetate (VA) content. The flow sheet for the plant is shown in Figure 1.

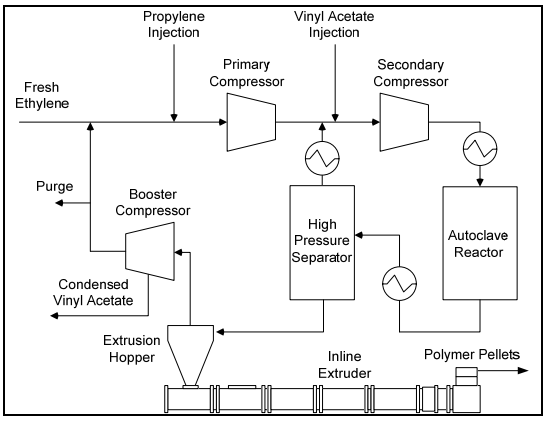

Figure 1 – Process Flowsheet

The monomers used are ethylene, vinyl acetate and propylene (used as a modifier). These are compressed to supercritical conditions and then mixed with peroxide-based initiators in a multi-zone autoclave reactor. An exothermic polymerization reaction occurs in the autoclave, and about twenty percent of the monomer is polymerized in a single-pass. The autoclave product is cooled and then goes through two separation stages where the unconverted monomers are recycled. The polymer product is then compounded with additives in the extruder before it is pelletized. There can be a build-up of inert components and unwanted propylene in the recycle loop and a purge stream is used to control this. At the booster compressor the majority of the Vinyl Acetate (VA) condenses. This is collected, refined, and then reused with fresh VA. There are three main heat exchangers (coolers) shown. These are the feed gas coolers, product coolers and return gas coolers. These become fouled over time with polymer. When this occurs, the pressure drop across the cooler becomes significant and the process efficiency is compromised. This fouling over time causes a drift in the pressures at the extruder. An operator controlled "cooler cook" is usually performed to remove the fouling. This involves increasing the temperature of the contents of the heat exchanger to remove the polymer lining from the heat exchanger inner wall.

2. MELT INDEX SOFT SENSOR

The steps in building the soft sensor for the melt index are detailed here. It was observed that the plant operators relied on the extruder pressure to give them an indication of the melt index of the polymer whenever the online reading was offline.

2.1 The Extruder

A schematic of the extruder is shown in Figure 2. Several pressures and temperatures are monitored. The extruder screw is driven by a motor. The motor's frequency is modulated (thus screw speed) to maintain a constant level in the extruder feed hopper. There is a mesh screen pack between the last two pressure sensors on the extruder. This mesh is very fine and becomes clogged with solids and gel particles over time. This causes the extruder variables, predominantly the upstream pressure, to change even if the flow rate and other conditions are constant. All the pressures at the extruder drift due to cooler fouling; while the pressures just before the screen pack have an even more significant drift because the screen pack becomes clogged.

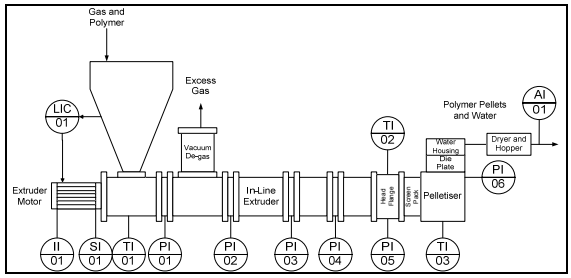

Figure 2– Extruder Schematic

After the extruder there is a pelletizer. The polymer pellets are dried, and then pass through a hopper

before a side stream is used to measure the melt index with the online rheometer.
The extruder is downstream of the reactor thus changes in the melt index of the polymer would occur first at the reactor and its effect felt at the extruder. Clearly, the online rheometer being down stream of the extruder detects changes in the melt index much later than the extruder would.

2.2 Variable correlation and lags

All of the variables shown were correlated with the polymer's melt index. It has been shown(McAuley and MacGregor 1991) that the melt index has significant log-linear relationship with plant process variables such as temperature and pressure. The same relationship was noticed in the data reported here and therefore log-transformed variables were used in the analysis. Table 1 shows a summary of the correlation of the extruder variables with the log of the melt index.
The variable used for fitting and validation of the soft sensor was the online rheometer. It was expected that these readings would be delayed. Thus a delay estimation algorithm and cross-validation via visual inspection were used to estimate the time delays between the variables. The lags between the extruder variables and the online rheometer are also shown in Table 1.

Table 1 Extruder variables correlation and lag with log of rheometer measured melt index

Variable	Correlation	Lag (min.)
PI-01	-0.742	13.92
PI-02	-0.799	13.50
PI-03	-0.881	12.08
PI-04	-0.712	10.08
PI-05	-0.917	10.00
PI-06	-0.981	9.92
TI-01	-0.887	7.83
TI-02	-0.705	5.33
TI-03	-0.947	4.91
SI-01	0.922	10.25
II-01	-0.863	10.33

The correlation between the variables was found using standard correlation analysis.
The data set used to calculate the correlation comprised 16340 one minute samples form fifteen (15) different grades with melt indices ranging from 1.7 to 870 gm/min.
Figure 3 shows one of the plots used to determine the time delay between the signals based on visual inspection. The most significant deviations in the data (large peaks) were used to visually confirm the time delay.

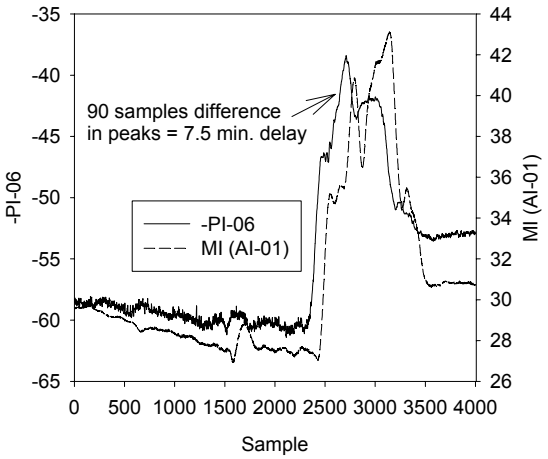

Figure 3 – Visual inspection plot for time delay

The delay estimation algorithm used was defined by (Moddemeijer 1988). It is a relatively old algorithm, it is available online and it was simple to use. The algorithm requires no apriori information about the signals; however, it assumes the signals to be stochastic and stationary. These assumptions are not fully true for the signals being considered here. As mentioned before, the extruder variables drift with time. However, over relatively short times, they can be considered stationary. This method involves splitting the two signals into a past and future vector. Then the capture of information between the concatenated past and future vectors is calculated. A function which continuously splits the data series into the past and future vectors is used to find which split gives the maximum common information. The capture of information is stored in a variable pair called the criterion. The maximum value of the criterion gives the number of sample times which correspond to the estimated time delay between the two signals.

Figure 4 shows the criterion plotted against sample intervals for two of the extruder variables (sample time = 5 seconds).

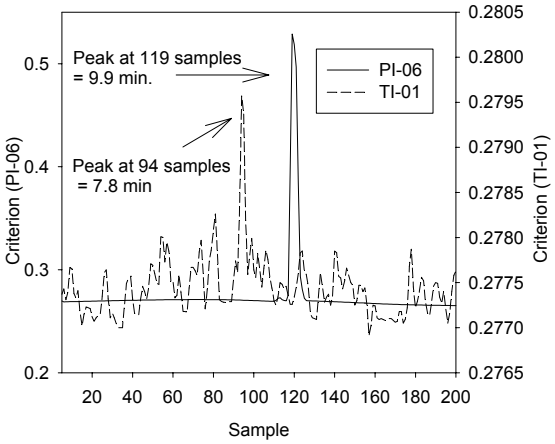

Figure 4 – Delay estimation algorithm for two extruder variables

2.3 Soft sensor models

The selection of plant variables which comprise the soft sensor was based on the correlation with the melt index, time delays and lack of disturbances. The main disturbances affecting the extruder variables are the screen pack fouling and cooler fouling. The typical disturbances caused by these are shown in Figure 5. This figure clearly shows that a screen pack change causes a significant change in the operating pressure for PI-05. A cooler cook event causes a change in the pressure and melt index, however the steady state melt index after the event is the same while the corresponding steady state pressures are not.

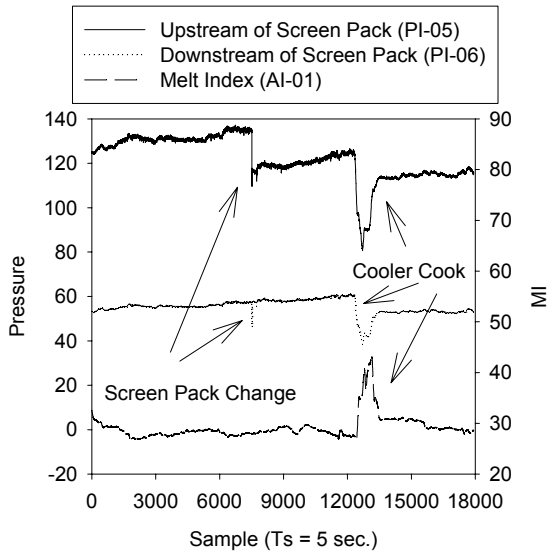

Figure 5 – Disturbances effecting extruder variables

The most important variables were chosen based on the physics and rheology of the extruder and the correlation. As described, the melt index range for products produced by this facility is very large. Initially, one simple model was developed which covered the entire product range. However, during events such as cooler cooks and grade changes, the melt index for each grade showed an exaggerated change. Thus, a speed and temperature modified model was developed.

The Basic Model. This model was built using least squares regression. It was based on Equation(1).

$$MI = f\left(P\right) \tag{1}$$

where

MI is the melt index.

P is the pressure at PI-06 (the variable with the highest correlation).

$$MI = \exp\left(a + b\left(P^{\alpha}\right)\right) \tag{2}$$

Equation(2) was implemented, where a, b and α were constants found using regression. This was found useful to give an idea of the relative behaviour of the melt index (increasing or decreasing and rate of change). However, the absolute value was found to contain errors; due to the speed of the extruder being controlled by the hopper level controller and the fouling of the coolers and screen pack.

S and T Compensated Model. This model was based on equation 2 but includes some more information about the physics of the extruder. Equation(3) shows the basis of the model.

$$MI_{T_r,S_r} = f\left(P_{T_r,S_r}\right) \tag{3}$$

where

MI_{T_r,S_r} is the melt index at a reference temperature, T_r and reference speed S_r.

P_{T_r,S_r} is the pressure at a reference temperature, T_r and reference speed S_r.

In this application the extruder can be viewed as a pseudo melt indexer. With a typical melt index instrument, melt index is measured by applying a fixed pressure to the polymer at a fixed temperature. For the melt index measurement, the polymer is forced through a die, and the weight of polymer which flows through the die in a fixed time interval is the melt index. With the extruder, the pressure applied to the polymer depends on the extruder speed and temperature. This gives the relationship shown in Equation(4).

$$MI_{T,S} = f\left(P_{T,S}\right) \tag{4}$$

where

$MI_{T,S}$ is the melt index at a operating temperature, T and operating speed S.

$P_{T,S}$ is the pressure at a operating temperature, T and operating speed S.

This equation can be modified to give Equation(5); which compensates for the change in temperature and speed.

$$MI_{T_r,S_r} = f\left(P_{T,S}\right) + f(T - T_r) + f(S - S_r) \tag{5}$$

Equation(5) reports a melt index similar to that measured by the rheometer.

The relationships internal to these functions are not exactly known, but based on the high correlations observed, a relationship was assumed. The relationship which included the speed compensation was of the form shown in Equation (6).

$$MI_{T,S_r} = \exp\left(a + b\left(P^{\alpha}\right)\right)\left(c + d\left(S\right)\right) \tag{6}$$

This was expressed in the form shown in equation(7).

$$MI_{T,S_r} = \exp\left(a + b\left(S\right) + c\left(SP^{\beta}\right) + d\left(P^{\alpha}\right)\right) \tag{7}$$

The relationship shown in equation(8) was found after the initial regression.

$$\beta = -\alpha \tag{8}$$

Thus equation(9).

$$MI_{T,S_r} = \exp\left(a + b\left(S\right) + c\left(\frac{S}{P^{\alpha}}\right) + d\left(P^{\alpha}\right)\right) \tag{9}$$

Where a, b, c, d and α are constants fit using least squares regression.

A relationship between the melt index and temperature (TI-03) was found by manipulation of the

variables and observing the correlation. The relationship found is shown in equation(10).

$$MI \propto \frac{1}{T^2} \tag{10}$$

Thus equation(9) was extended to equation(11) which included both speed and temperature compensation.

$$MI_{T_r,S_r} = \frac{\exp\left(a + b(S) + c\left(\frac{S}{P^{\alpha}}\right) + d\left(P^{\alpha}\right)\right)}{T^2} \tag{11}$$

The model with and without the temperature compensation are shown in Figure 6. It was noticed that without the temperature compensation there was a significant overshoot during the dynamic periods (such as cooler cook events and grade transitions) and the model was more susceptible to the fouling errors. The temperature compensation alleviated the majority of the overshoot and some of the offset due to fouling; this is as shown during a typical cooler cook in Figure 6.

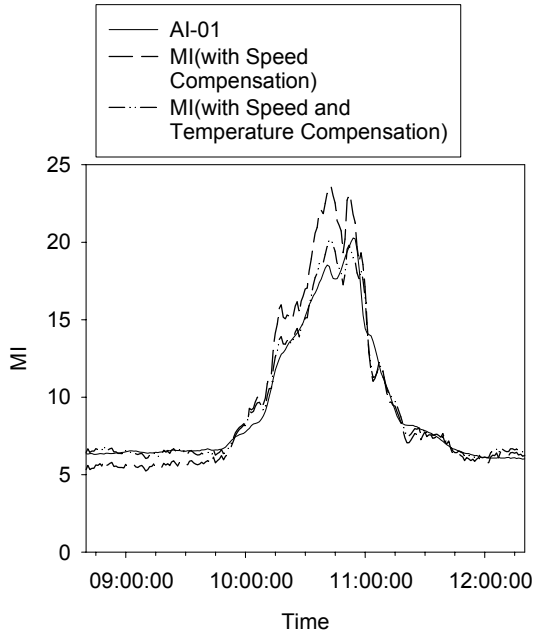

Figure 6 – Cooler Cook Event

The model was modified during the fitting process. This included lagging the independent variables to take advantage of the time delay information found previously. It was found that use of the lagged data did not give any significant gains. Upon implementation it was found using the most current data available for all independent variables gave a value for the melt index nine (9) minutes ahead of the online rheometer.

Figure 7 shows the validation data for a dynamic run. It can be seen the model captured the dynamics of the melt index change well.

Figure 8 shows the validation data for the model. It can be seen the model showed an excellent fit for the full range of product produced by the plant (these products were produced over a four month period).

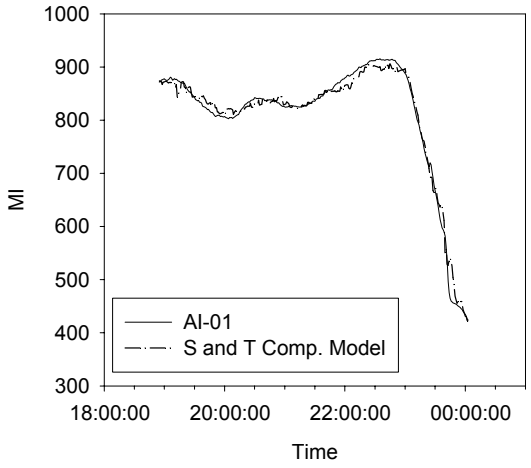

Figure 7 – S and T Compensated Model Dynamic Validation Plot

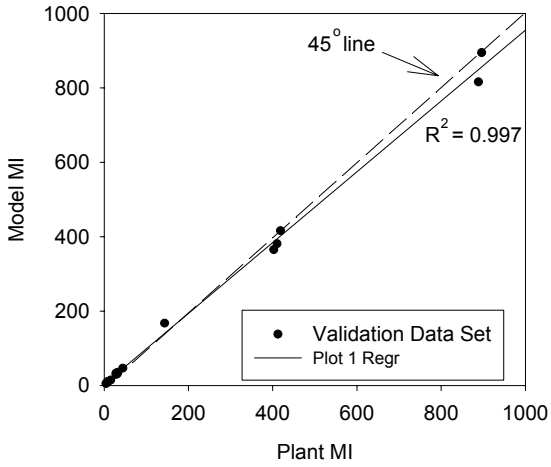

Figure 8 - S and T Compensated Model Validation Plot (several grades)

Bias Updating of the Model. The compensated model built was found to operate well for a certain period of time and at certain grades, then drifting occurred. This was attributed to the significant changes in the extruder operating conditions due to the fouling. In order to compensate for this characteristic of the process a bias updating scheme for the model was implemented. The bias was applied to the constant a in equation(11). Equation(12) shows how the new a_{Calc} was found.

$$a_{Calc} = \ln\left(MI_{Avg} \times T^2\right) - b(S) - c\left(\frac{S}{P^{\alpha}}\right) - d\left(P^{\alpha}\right) \tag{12}$$

The bias which is calculated in equation(13) was stored in the historian.

$$bias = a_{Calc} - a \tag{13}$$

Equation(14) shows how a_{Calc} was used to calculate the new melt index.

$$MI_{Bias} = \frac{\exp\left(a_{Calc} + b(S) + c\left(\frac{S}{P^{\alpha}}\right) + d\left(P^{\alpha}\right)\right)}{T^2} \tag{14}$$

Figure 9 shows the flow sheet of the procedure developed for implementing the bias updating scheme.

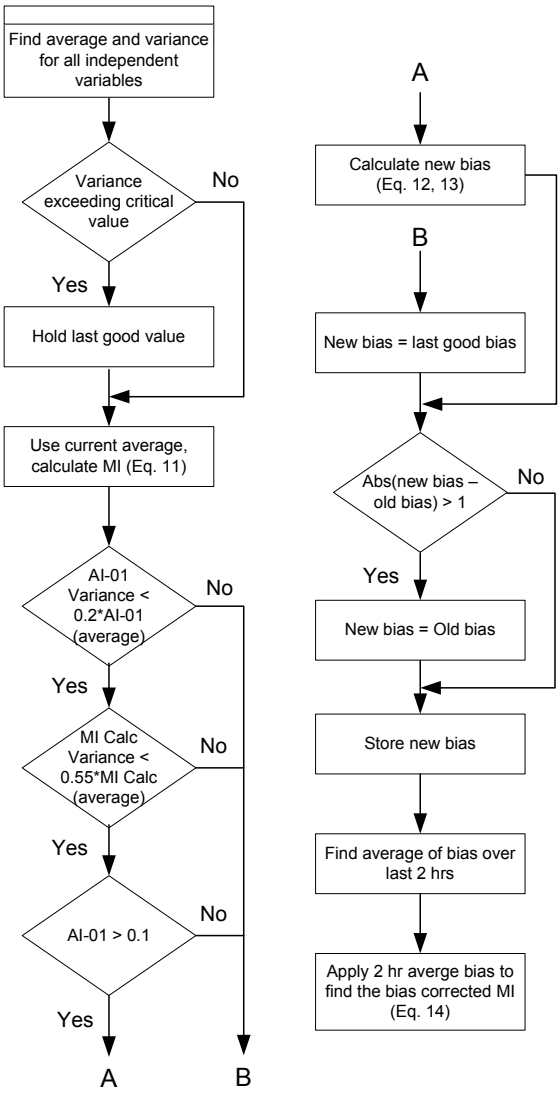

Figure 9 – Bias updating flowsheet (30 min. execution period)

3. CONCLUSION

A soft sensor model for the melt index of EVA copolymer was built and has been implemented at AT Plastics Inc (Edmonton, Canada). This soft sensor was built at different stages to handle different problems. The soft sensor used variables from the plant extruder (pressure, speed and temperature) to calculate the melt index. Biased nonlinear least squares regression was used to calculate the parameters in the soft sensor model. To compensate for drifts due to fouling, bias correction was added. It was also found that it would require some time for the parameters in the bias to update after the plant had gone through a grade transition or a cooler cook.

The main goal of this soft sensor was to have a reliable reading for the melt index during the grade transitions to build a model of the process. The compensated model with bias updates fits this application well. The next step will be to use this soft sensor to model the plant and produce optimal grade transitions and compare them with those produced by a first principles model.

4. ACKNOWLEDGEMENTS

This work was financially supported by AT Plastics Inc and NSERC through an Industrial Post Graduate Scholarship. We would like to thank the staff at AT Plastics Inc., the Computer Process Control Group and Polymer Group at the University of Alberta for their support.

REFERENCES

Alperowicz, N. (2005). "A changing lineup." Chemical Week **167**(27): 26-31.

Chan, W.-M. and C. A. O. Nascimento (1994). "Use of neural networks for modeling of olefin polymerization in high pressure tubular reactors." Journal of Applied Polymer Science **53**(10): 1277-1289.

Han, I.-S., C. Han, et al. (2005). "Melt index modeling with support vector machines, partial least squares, and artificial neural networks." Journal of Applied Polymer Science **95**(4): 967-974.

Kiparissides, C., G. Verros, et al. (1996). "On-line parameter estimation in a high-pressure low-density polyethylene tubular reactor." AIChE Journal **42**(2): 440-454.

Lines, B., D. Hartlen, et al. (1993). "Polyethylene reactor modeling and control design." Hydrocarbon Processing **72**(6): 4.

McAuley, K. B. and J. F. MacGregor (1991). "On-line inference of polymer properties in an industrial polyethylene reactor." AIChE Journal **37**(6): 825-835.

Moddemeijer, R. (1988). An information theoretical delay estimator. Ninth Symposium. on Information Theory in the Benelux, Mierlo, The Netherlands, Enschede.

Nagata, T., M. Ohshima, et al. (2000). "In-line monitoring of polyethylene density using near infrared (nir) spectroscopy." Polymer Engineering and Science **40**(5): 1107-1113.

Ohshima, M. and M. Tanigaki (2000). "Quality control of polymer production processes." Journal of Process Control **10**(2): 135-148.

Scali, C., M. Morretta, et al. (1997). "Control of the quality of polymer products in continuous reactors: Comparison of performance of state estimators with and without updating of parameters." Journal of Process Control **7**(5): 357-369.

Watari, M., H. Higashiyama, et al. (2004). "On-line monitoring of the density of linear low-density polyethylene in a real plant by near-infrared spectroscopy and chemometrics." Applied Spectroscopy **58**(2): 248-255.

AUTHOR INDEX